

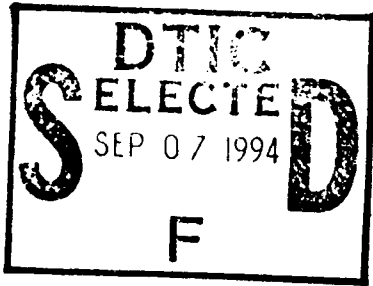
AD-A284 096



Report No. CG-D-16-94

1

VALIDATION OF FULL ROOM INVOLVEMENT TIME CORRELATION
APPLICABLE TO STEEL SHIP COMPARTMENTS



Michelle J. Peatross
Craig L. Beyler
Gerard G. Back

Hughes Associates, Inc.
Columbia, MD 21045



FINAL REPORT
NOVEMBER 1993

This document has been approved
for public release and sale; its
distribution is unlimited.

This document is available to the U.S. public through the
National Technical Information Service, Springfield, Virginia 22161

Prepared for

U.S. Coast Guard
Research and Development Center
1082 Shennecossett Road
Groton, Connecticut 06340-6096

and

U.S. Department of Transportation
United States Coast Guard
Office of Engineering, Logistics, and Development
Washington, DC 20593-0001

434 120
94-29088

NOTICE

This document is disseminated under the sponsorship of the Department of Transportation in the interest of information exchange. The United States Government assumes no liability for its contents or use thereof.

The United States Government does not endorse products or manufacturers. Trade or manufacturers' names appear herein solely because they are considered essential to the object of this report.

The contents of this report reflect the views of the Coast Guard Research & Development Center. This report does not constitute a standard, specification, or regulation.



D. L. Motherway
D. L. Motherway
Technical Director, Acting
United States Coast Guard
Research & Development Center
1082 Shennecossett Road
Groton, CT 06340-6096

1. Report No. CG-D-16-94		2. Government Accession No.		3. Recipient's Catalog No.	
4. Title and Subtitle Validation of Full Room Involvement Time Correlation Applicable to Steel Ship Compartments				5. Report Date November 1993	
				6. Performing Organization Code WPI HAL 1117-004-93	
7. Author(s) Michelle J. Peatross, Craig L. Beyler, and Gerard G. Back				8. Performing Organization Report No. R&DC 26/93	
				10. Work Unit No. (TRAIS)	
9. Performing Organization Name and Address Hughes Associates, Inc. 6770 Oak Hall Lane, Suite 125 Columbia, Maryland 21045 Worcester Polytechnic Institute 100 Institute Road Worcester, MA 01609				11. Contract No. DTCG 39-92-D-E38K37 Delivery Order No. DTCG39-F-E99043	
				13. Type of Report and Period Covered Final Report October 1992-November 1993	
12. Sponsoring Agency Name and Address Department of Transportation U.S. Coast Guard Office of Engineering, Logistics, and Development Washington, DC 20593-0001 U.S. Coast Guard Research and Development Center 1082 Shennecossett Road Groton, CT 06340-6096				14. Sponsoring Agency Code	
15. Supplementary Notes The WPI Senior Technical Representative is Dr. Robert Zalosh. The Coast Guard technical contact and COTR is Mr. Dave Beene of the U.S. Coast Guard R&D Center. The Headquarters Project Officer is LCDR J. Hautala of the Office of Engineering, Logistics, and Development.					
16. Abstract The Ship Fire Safety Engineering Methodology (SFSEM) requires a submodel for the prediction of the time to full room involvement (FRI) in compartment fires. In order to validate a temperature correlation for compartments with conductive barriers, preflashover fire tests were conducted in a steel compartment on the test vessel, MAYO LYKES. Fifteen of these tests used natural ventilation, and twelve tests used forced ventilation. In addition to validating a temperature correlation using measured vent flows, the use of predicted vent flows was investigated. The MQH Temperature Prediction Method was compared with these results. The compartment was instrumented with thermocouple trees and a gas sampling tree. Vertical oxygen and temperature profiles are discussed and compared to ventilation configurations.					
17. Key Words preflashover, compartment fire, forced ventilation, natural ventilation, temperature prediction, full room involvement, Ship Fire Safety Engineering Methodology			18. Distribution Statement Document is available to the U.S. Public through the National Technical Information Service, Springfield, VA 22161.		
19. Security Classif. (of this report) UNCLASSIFIED		20. SECURITY CLASSIF. (of this page) UNCLASSIFIED		21. No. of Pages	
				22. Price	

METRIC CONVERSION FACTORS

Approximate Conversions to Metric Measures

Symbol	When You Know	Multiply By	To Find	Symbol
LENGTH				
in	inches	* 2.5	centimeters	cm
ft	feet	30	centimeters	cm
yd	yards	0.9	meters	m
mi	miles	1.6	kilometers	km
AREA				
in ²	square inches	6.5	square centimeters	cm ²
ft ²	square feet	0.09	square meters	m ²
yd ²	square yards	0.8	square meters	m ²
mi ²	square miles	2.6	square kilometers	km ²
	acres	0.4	hectares	ha
MASS (WEIGHT)				
oz	ounces	28	grams	g
lb	pounds	0.45	kilograms	kg
	short tons (2000 lb)	0.9	tonnes	t
VOLUME				
tsp	teaspoons	5	milliliters	ml
tbsp	tablespoons	15	milliliters	ml
fl oz	fluid ounces	30	milliliters	ml
c	cups	0.24	liters	l
pt	pints	0.47	liters	l
qt	quarts	0.95	liters	l
gal	gallons	3.8	liters	l
ft ³	cubic feet	0.03	cubic meters	m ³
yd ³	cubic yards	0.76	cubic meters	m ³
TEMPERATURE (EXACT)				
°F	Fahrenheit temperature	5/9 (after subtracting 32)	Celsius temperature	°C

* 1 in = 2.54 (exactly).

Approximate Conversions from Metric Measures

Symbol	When You Know	Multiply By	To Find	Symbol
LENGTH				
mm	millimeters	0.04	inches	in
cm	centimeters	0.4	inches	in
m	meters	3.3	feet	ft
m	meters	1.1	yards	yd
km	kilometers	0.6	miles	mi
AREA				
cm ²	square centimeters	0.16	square inches	in ²
m ²	square meters	1.2	square yards	yd ²
km ²	square kilometers	0.4	square miles	mi ²
ha	hectares (10,000 m ²)	2.5	acres	
MASS (WEIGHT)				
g	grams	0.035	ounces	oz
kg	kilograms	2.2	pounds	lb
t	tonnes (1000 kg)	1.1	short tons	
VOLUME				
ml	milliliters	0.03	fluid ounces	fl oz
l	liters	0.125	cups	c
l	liters	2.1	pints	pt
l	liters	1.06	quarts	qt
l	liters	0.26	gallons	gal
m ³	cubic meters	35	cubic feet	ft ³
m ³	cubic meters	1.3	cubic yards	yd ³
TEMPERATURE (EXACT)				
°C	Celsius temperature	9/5 (then add 32)	Fahrenheit temperature	°F

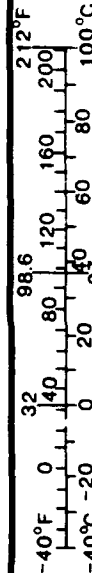


Table of Contents

	Page
1.0 Introduction	1
1.1 Background	1
1.2 Objectives	1
2.0 Approach	2
3.0 Experimental Setup	2
3.1 Fire Room Construction	2
3.2 Ventilation	4
3.2.1 Natural Ventilation Tests	4
3.2.2 Forced Ventilation Tests	4
3.3 Instrumentation	9
3.3.1 Air Flow Rate Measurements	9
3.3.2 Temperature Measurements	9
3.3.2.1 Gas Temperatures	9
3.3.2.2 Surface Temperatures	9
3.3.3 Incident Heat Flux Measurements	13
3.3.4 Gas Species Measurements	13
3.3.5 Fuel Mass Loss Measurements	13
3.3.6 Pressure Measurements	15
3.3.7 Video Cameras	15
4.0 Test Procedures	15
4.1 Test Description	15
4.2 Additional Tests	17
5.0 Data Analysis Methods	17
6.0 Results	21
6.1 Series 1 - Natural Ventilation Tests	21
6.1.1 Overview	21
6.1.2 Diesel Pan Fires	25
6.1.2.1 62 cm Diameter Pan (S101, S105, S111)	25
6.1.2.2 84 cm Diameter Pan (S102, S107, S112)	32
6.1.3 Wood Crib Fires (S103, S106, S110)	32
6.1.4 Polyurethane Fires (S104, S108, S109)	39
6.1.5 Additional Tests - Diesel Pan Fires (ADD1, ADD2, ADD3)	48

Table of Contents (Continued)

	Page
6.2 Series 2 - Forced Ventilation Tests	52
6.2.1 Overview	52
6.2.2 Diesel Pan Fires	57
6.2.2.1 62 cm Diameter Pan (S201, S207, S210)	57
6.2.2.2 84 cm Diameter Pan (S203, S208, S211)	57
6.2.3 Wood Crib Fires (S202, S206, S209)	57
6.2.4 Polyurethane Fires (S204, S205, S212)	70
7.0 Discussion	70
7.1 Temperature Predictions	70
7.1.1 Peatross/Beyler Method	79
7.1.1.1 Deal/Beyler Layer Driven Method for Determining Vent Flow Rates	83
7.1.1.2 Mowrer Method for Determining Vent Flow Rates	87
7.1.2 McCaffrey, Quintiere, and Harkleroad (MQH) Method	90
7.1.3 Comparison of Temperature Prediction Methods ...	92
7.2 Barrier Temperature Predictions	92
7.3 Compartment Fire Analysis	94
7.3.1 Natural Ventilation Tests	94
7.3.2 Forced Ventilation Tests	94
8.0 Conclusions	96
9.0 References	98
10.0 Acknowledgements	101
Appendix A: Series 1 Test Results	A-1
Appendix B: Series 2 Test Results	B-1
Appendix C: Series 1 - Peatross/Beyler Temperature Prediction Method Results	C-1

Table of Contents (Continued)

	Page
Appendix D: Series 2 - Peatross/Beyler Temperature Prediction Method Results	D-1
Appendix E: Deal/Beyler Layer Driven Vent Flow Rate Prediction Method Results	E-1
Appendix F: Mowrer Vent Flow Rate Prediction Method Results	F-1
Appendix G: MQH Temperature Prediction Method Results	G-1
Appendix H: Barrier Temperature Predictions Using Peatross/Beyler Method	H-1

Accession For	
NTIS	<input checked="" type="checkbox"/>
CRA&I	<input type="checkbox"/>
DTIC	<input type="checkbox"/>
TAB	<input type="checkbox"/>
Unannounced	<input type="checkbox"/>
Justification	
By	
Distribution/	
Availability Codes	
Dist	Avail and/or Special
A-1	

List of Figures

	Page
Figure 1. Overview of Test Deck on MAYO LYKES	3
Figure 2. Fuel Cradle Configuration	5
Figure 3. Vent Configurations for Natural Ventilation Tests	6
Figure 4. Forced Ventilation Setup - Elevation View	7
Figure 5. Exhaust Vent Configuration for Forced Ventilation Tests	8
Figure 6. Temperature and Air Velocity Instrumentation - Side View	10
Figure 7. Elevation View of Instrumentation	11
Figure 8. Schematic of Surface Thermocouples	12
Figure 9. Gas Species Instrumentation - Side View	14
Figure 10. Example of Gas Sampling System Time Delay (S112) Gas Concentrations Corrected for Time Delay	22
Figure 11. Mass Loss Rate and Temperature-Time Histories for 62 cm Diameter Pan (S101)	26
Figure 12. Mass Loss Rate and Temperature vs. Ventilation Rate for 62 cm Diameter Pan Tests (Series 1)	27
Figure 13. Minimum Oxygen Concentration vs. Ventilation Rate for 62 cm Diameter Pan Tests (Series 1)	28
Figure 14. Vertical Oxygen Concentration and Temperature Profiles for S101 ..	30
Figure 15. Vertical Oxygen Concentration and Temperature Profiles for S105 ..	31
Figure 16. Vertical Oxygen Concentration and Temperature Profiles for S116 ..	32
Figure 17. Mass Loss Rate and Temperature vs. Ventilation Rate for 84 cm Diameter Pan Tests (Series 1)	33
Figure 18. Minimum Oxygen Concentration vs. Ventilation Rate for 84 cm Diameter Pan Tests (Series 1)	34

List of Figures (Continued)

	Page
Figure 19. Vertical Oxygen Concentration and Temperature Profiles for S102 . .	35
Figure 20. Vertical Oxygen Concentration and Temperature Profiles for S107 . .	36
Figure 21. Vertical Oxygen Concentration and Temperature Profiles for S112 . .	37
Figure 22. Mass Loss Rate and Oxygen Concentration-Time Histories for S110 .	38
Figure 23. Mass Loss Rate and Temperature vs. Ventilation Rate for Wood Crib Tests (Series 1)	40
Figure 24. Minimum Oxygen Concentration vs. Ventilation Rate for Wood Crib Tests (Series 1)	41
Figure 25. Vertical Oxygen Concentration and Temperature Profiles for S103 . .	42
Figure 26. Vertical Oxygen Concentration and Temperature Profiles for S106 . .	43
Figure 27. Vertical Oxygen Concentration and Temperature Profiles for S110 . .	44
Figure 28. Mass Loss Rate and Upper Layer Temperature-Time Histories for S104	45
Figure 29. Mass Loss Rate and Temperature vs. Ventilation Rate for Polyurethane Tests (Series 1)	46
Figure 30. Minimum Oxygen Concentration vs. Ventilation Rate for Polyurethane Tests (Series 1)	47
Figure 31. Vertical Oxygen Concentration and Temperature Profiles for S104	49
Figure 32. Vertical Oxygen Concentration and Temperature Profiles for S108 . .	50
Figure 33. Vertical Oxygen Concentration and Temperature Profiles for S109 . .	51
Figure 34. Vertical Oxygen Concentration and Temperature Profiles for ADD1 .	53
Figure 35. Vertical Oxygen Concentration and Temperature Profiles for ADD2 .	54
Figure 36. Vertical Oxygen Concentration and Temperature Profiles for ADD3 .	55

List of Figures (Continued)

	Page
Figure 37. Mass Loss Rate and Temperature vs. Ventilation Rate for 62 cm Diameter Pan Tests (Series 2)	58
Figure 38. Minimum Oxygen Concentration vs. Ventilation Rate for 62 cm Diameter Pan Tests (Series 2)	59
Figure 39. Vertical Oxygen Concentration and Temperature Profiles for S201	60
Figure 40. Vertical Oxygen Concentration and Temperature Profiles for S207 ..	61
Figure 41. Vertical Oxygen Concentration and Temperature Profiles for S210 ..	62
Figure 42. Mass Loss Rate and Temperature vs. Ventilation Rate for 84 cm Diameter Pan Tests (Series 2)	63
Figure 43. Minimum Oxygen Concentration vs. Ventilation Rate for 84 cm Diameter Pan Tests (Series 2)	64
Figure 44. Vertical Oxygen Concentration and Temperature Profiles for S203 ..	65
Figure 45. Vertical Oxygen Concentration and Temperature Profiles for S208 ..	66
Figure 46. Vertical Oxygen Concentration and Temperature Profiles for S211 ..	67
Figure 47. Mass Loss Rate and Temperature vs. Ventilation Rate for Wood Crib Tests (Series 2)	68
Figure 48. Minimum Oxygen Concentration vs. Ventilation Rate for Wood Crib Tests (Series 2)	69
Figure 49. Vertical Oxygen Concentration and Temperature Profiles for S202	71
Figure 50. Vertical Oxygen Concentration and Temperature Profiles for S206 ..	72
Figure 51. Vertical Oxygen Concentration and Temperature Profiles for S209 ..	73
Figure 52. Mass Loss Rate and Temperature vs. Ventilation Rate for Polyurethane Tests (Series 2)	74
Figure 53. Minimum Oxygen Concentration vs. Ventilation Rate for Polyurethane Tests (Series 2)	75

List of Figures (Continued)

	Page
Figure 54. Vertical Oxygen Concentration and Temperature Profiles for S204 ..	76
Figure 55. Vertical Oxygen Concentration and Temperature Profiles for S205 ..	77
Figure 56. Vertical Oxygen Concentration and Temperature Profiles for S212 ..	78
Figure 57. Temperature Prediction Results Using Peatross/Beyler Method for S104	81
Figure 58. Temperature Prediction Results Using Peatross/Beyler Method for S106	82
Figure 59. Summary of Temperature Prediction Results Using Peatross/Beyler Temperature Prediction Method (Series 1)	84
Figure 60. Summary of Temperature Prediction Results Using Peatross/Beyler Temperature Prediction Method (Series 2) ..	85
Figure 61. Mass Loss Rate and Temperature Prediction-Time Histories for S103	86
Figure 62. Vent Flow Rate and Temperature Prediction-Time Histories for S101	88
Figure 63. Summary of Temperature Prediction Results Using Deal/Beyler Layer Driven Method to Predict Vent Flow Rates ...	89
Figure 64. Summary of Temperature Prediction Results Using Mowrer Method to Predict Vent Flow Rates	91
Figure 65. Summary of Temperature Prediction Results Using MQH Temperature Prediction Method	93
Figure 66. Typical Predicted Barrier Temperature-Time Histories	95

List of Tables

	Page
Table 1. Series 1: Natural Ventilation Tests	16
Table 2. Series 2: Forced Ventilation Tests	16
Table 3. Fuel Properties	18
Table 4. Series 1 - Summary of Results	24
Table 5. Series 2 - Summary of Results	56
Table 6. Comparison of Temperature Prediction Methods	92

1.0 INTRODUCTION

1.1 Background

The Ship Fire Safety Engineering Methodology (SFSEM), developed by the USCG and WPI, requires a submodel for the prediction of the time to full room involvement (FRI) in compartment fires. In the application of the SFSEM to the Polar Icebreaker Replacement design, attempts to use existing methods for predicting FRI time were unsuccessful for compartments with highly conductive barriers and for forced ventilation scenarios [1]. These difficulties were addressed theoretically in a subsequent analysis and a method for FRI prediction was developed [2,3,4]. This method was validated only with minimal forced ventilation data. Data were not available, however, for compartment fires with conductive barriers for either natural or forced ventilation scenarios. Clearly, steel barriers are of great importance for marine applications, and model validation for this barrier type is essential. This validation can be achieved by comparing model predictions with the results from a series of experiments.

1.2 Objectives

The main objective of these experiments was to provide experimental data to validate the FRI time correlation for both forced and natural ventilation compartment fires with conductive barriers. A post-test analysis of the data was performed to determine whether the heat transfer coefficients developed in [2] needed to be changed in the SFSEM submodel. Additional objectives were to investigate the robustness of the FRI time correlation for different fire growth rate curves (i.e., examine different fuels) and to gain a better understanding of forced ventilation compartment fires so that their behavior may be more accurately modeled.

2.0 APPROACH

In order to achieve these goals, a steel-bounded compartment was constructed and instrumented on board the Coast Guard Test Vessel MAYO LYKES for the purpose of performing compartment fire experiments. Measurements included gas and bulkhead surface temperatures, mass loss, heat fluxes, gas species concentrations, and air velocities.

3.0 EXPERIMENTAL SETUP

A portion of the third deck of the Test Vessel MAYO LYKES consisted of a corridor, 37.6 m long, surrounded by 21 staterooms. One of these rooms was modified to serve as the fire room and is labeled "2" in Figure 1.

3.1 Fire Room Construction

The fire room was approximately 3.4 m wide by 3.3 m deep by 3.05 m high. All bulkheads, with the exception of the port bulkhead, were 12.7 mm steel with vertical stiffeners. The port bulkhead was 15.9 mm thick. There were two door openings, measuring 0.9 m wide by 2 m high, in the bulkheads: one to serve as the exhaust vent and one to be used to access the room before and after the test. The access door was located in the horizontal center of the aft bulkhead. It remained closed during all tests. The second door opening was centered horizontally in the starboard bulkhead and was modified to simulate three separate exhaust vents. Section 4.2 details these modifications.

Two 30 cm by 30 cm viewing ports of 3 mm furnace glass were installed in the bulkheads. The first port was located beside the opening in the starboard bulkhead, and the second port was located in the aft bulkhead. The tests were videotaped through these ports.

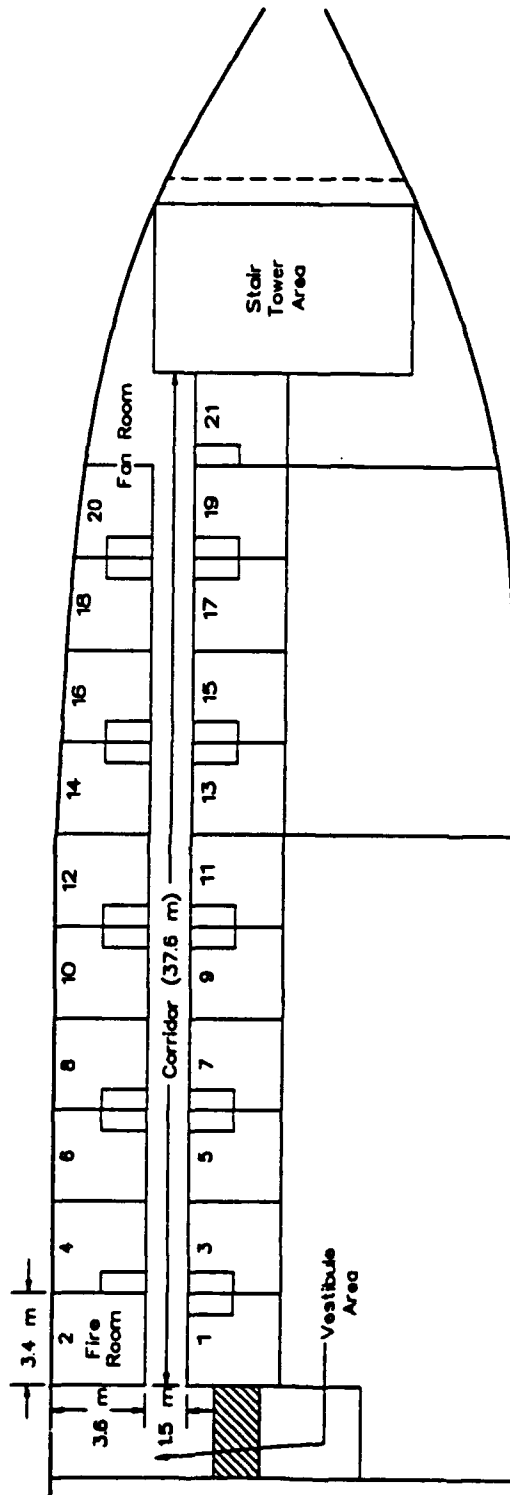


Figure 1. Overview of Test Deck on MAYO LYKES

A fuel cradle, 2 m by 2 m, was suspended in the center of the compartment by a cable extending through the upper deck (Figure 2). The cradle was constructed of a square frame of 8 cm angle iron with supports inside the frame. It was suspended approximately 30 cm above the ground. A load cell was attached to the cable so the mass loss could be monitored. A second hole was also located in the upper deck for the carbon dioxide extinguishing system.

3.2 Ventilation

3.2.1 Natural Ventilation Tests

Three vent configurations were used in the natural ventilation test series. These vents represented an open door, a quarter door, and an open window as illustrated in Figure 3. The quarter door and window vents were simulated by using steel plates to cover the appropriate portion of the doorway. The door vent was 0.9 m wide by 2 m high, the quarter door vent was 0.225 m wide by 2 m high and the window vent was 0.9 m wide by 0.8 m high. Both the door vent and quarter door vent were flush with the floor while the window vent had a sill of 1.2 m.

3.2.2 Forced Ventilation Tests

Ventilation for these fires was supplied to the fire room via 30 cm diameter ductwork which extended from a supply fan (Dayton Model 4C259). The supply duct discharged through the upper deck of the Fire Room at a location 30 cm starboard of the port bulkhead and 24 cm forward of the aft bulkhead (Figure 4). A 42 cm by 42 cm diffuser was attached to the discharge hole to help disperse the air. In the ductwork, there was a damper used to vary the air supply rate. Exhaust products exited through a vent created by covering a portion of the doorway with a steel cover as in Series 1. This vent opening was 28 cm by 28 cm, flush with the deck (Figure 5).

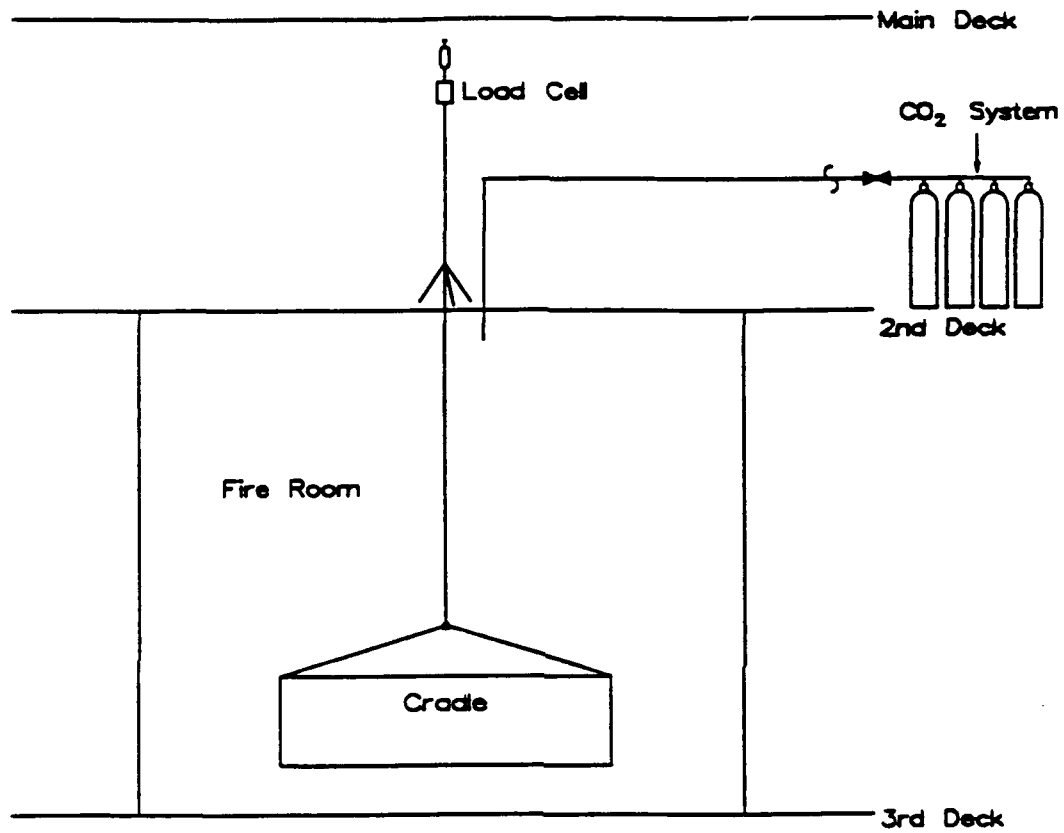


Figure 2. Fuel Cradle Configuration

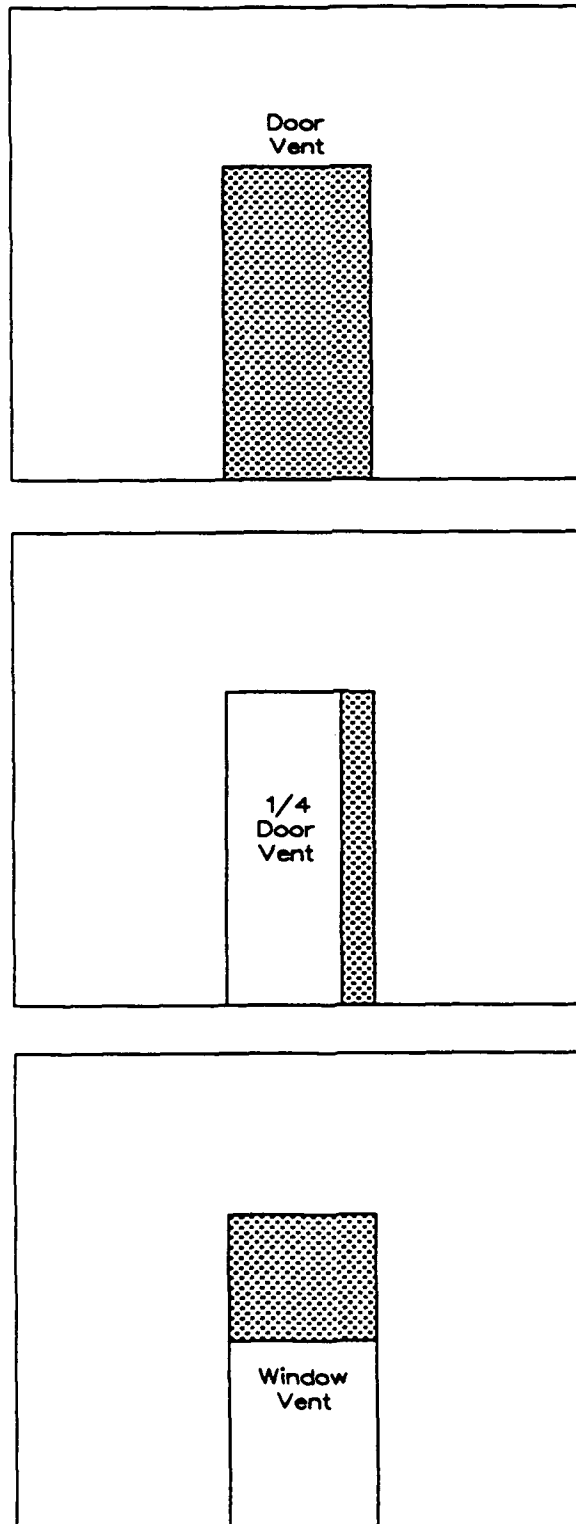


Figure 3. Vent Configurations for Natural Ventilation Tests

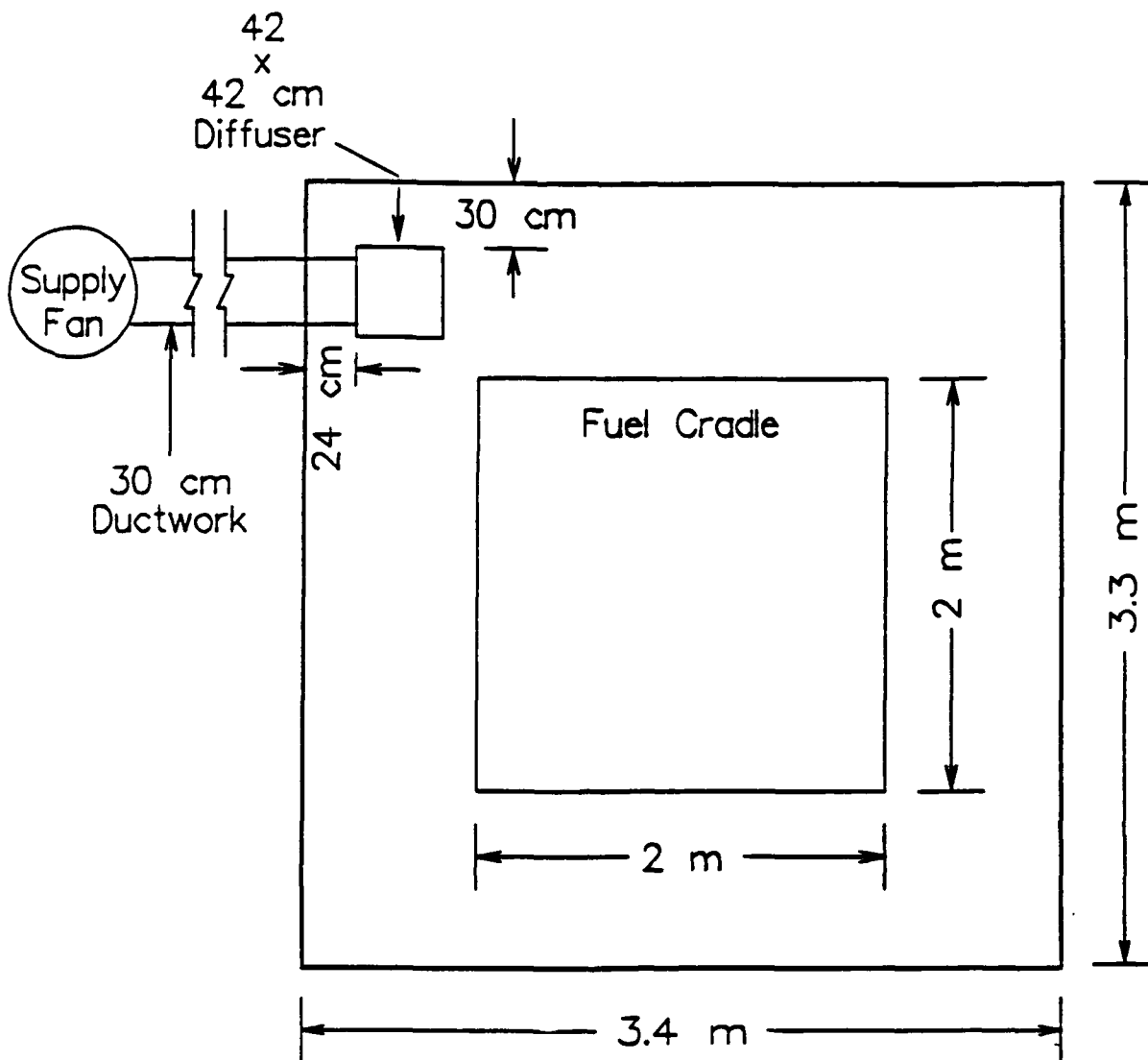


Figure 4. Forced Ventilation Setup - Elevation View

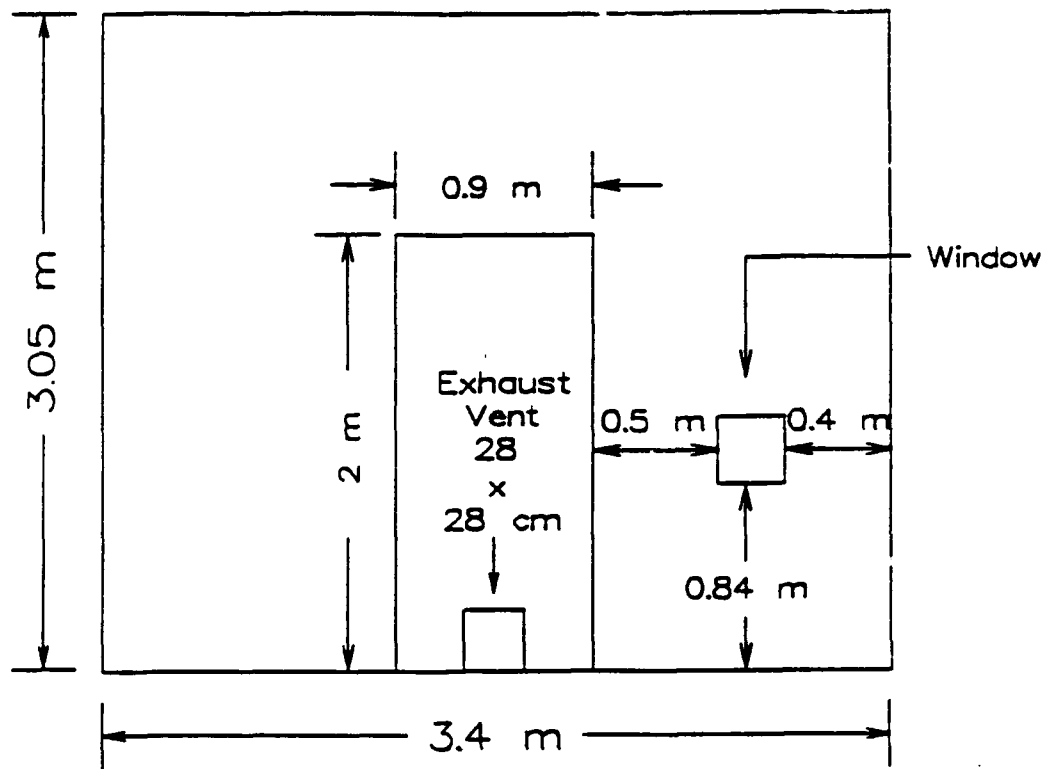


Figure 5. Exhaust Vent Configuration for Forced Ventilation Tests

3.3 Instrumentation

3.3.1 Air Flow Rate Measurements

Bi-directional probes were used to measure the air velocity in the exhaust vent in all tests and in the supply duct in the forced ventilation tests. Probes were spaced 15 cm apart vertically on the centerline of the vent with a total of 13 probes in the full and quarter door vent experiments and 5 probes in the window vent experiments (Figure 6). In the forced ventilation experiments, there was one probe located in the middle of the exhaust vent.

3.3.2 Temperature Measurements

3.3.2.1 Gas Temperatures

Three thermocouple trees were used to measure gas temperatures. Two of these trees were located in corners of the fire room and consisted of 10 branches spaced 30 cm apart (Figures 6 and 7). These thermocouples were 20 gage, Type K with high temperature CEFIR insulation. The third tree accompanied the bidirectional probes in the vent and were necessary for calculation of the density. Vent tree thermocouples were Type K, 3.2 mm Inconel sheathed.

3.3.2.2 Surface Thermocouples

Thermocouples were welded to the upper deck and to the bulkheads at three heights to measure barrier temperatures. These thermocouples were also 20 gage, Type K with CEFIR insulation and were attached as shown in Figure 8. Figures 6 and 7 show the locations of these measurements.

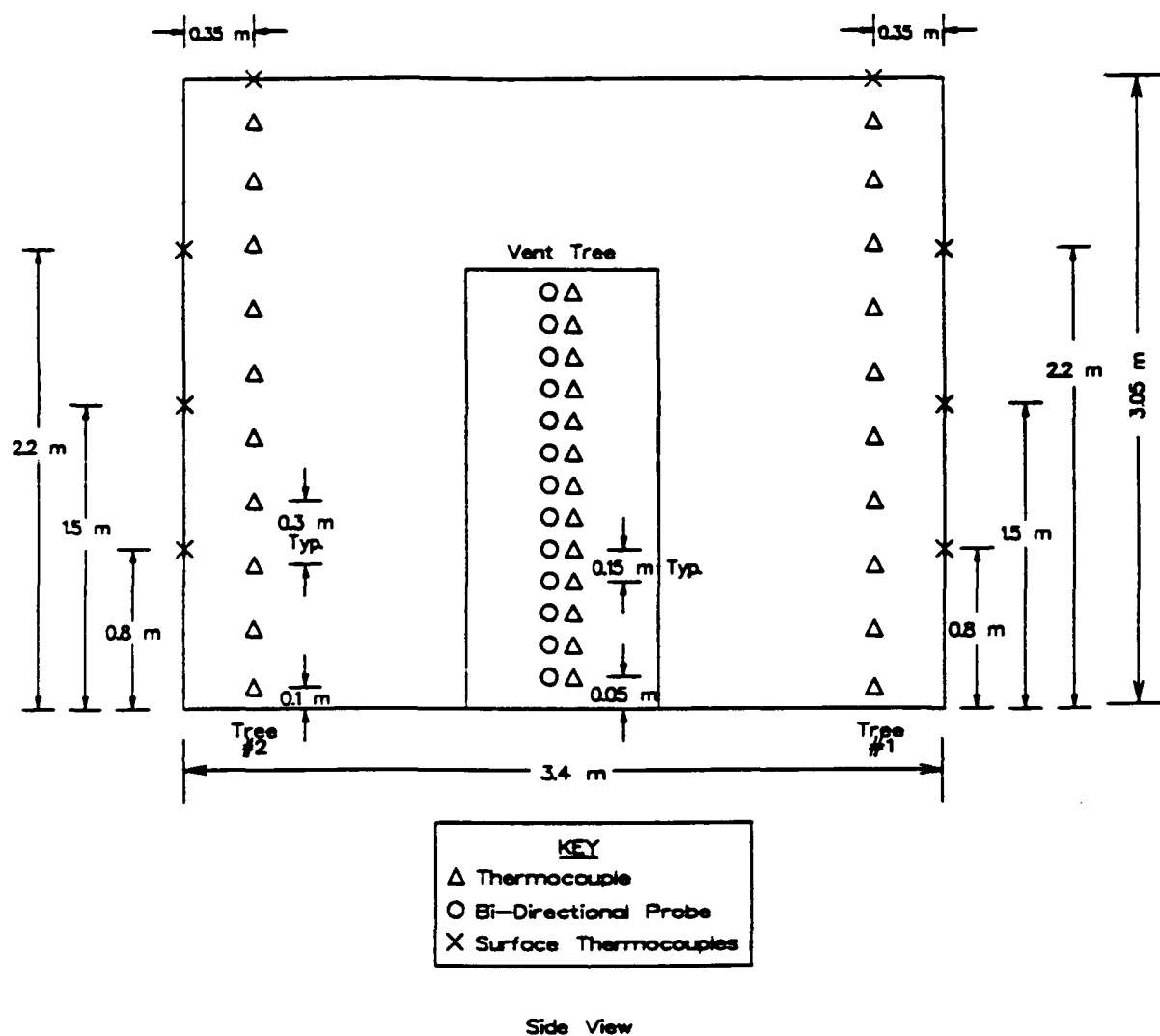
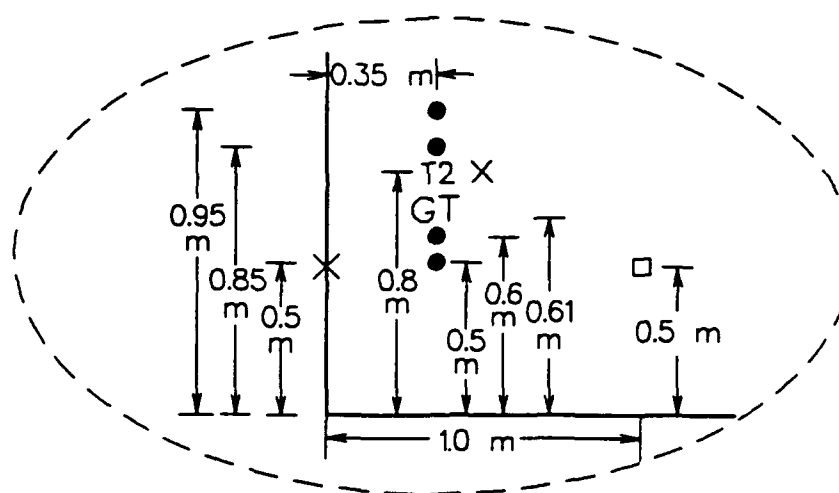
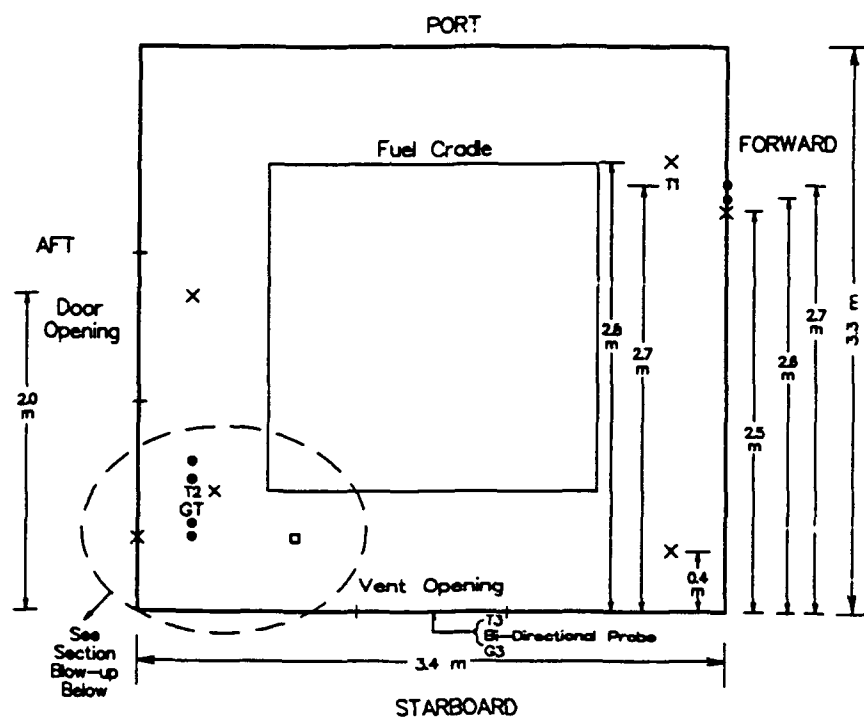


Figure 6. Temperature and Air Velocity Instrumentation - Side View



KEY	
X	Surface Thermocouples
□	Pressure Transducer
●	Heat Flux Transducer
G3	CO, CO ₂ , O ₂ , UHC
GT	Gas Tree
T1	Thermocouple Tree #1
T2	Thermocouple Tree #2
T3	Thermocouple Tree #3

Figure 7. Elevation View of Instrumentation

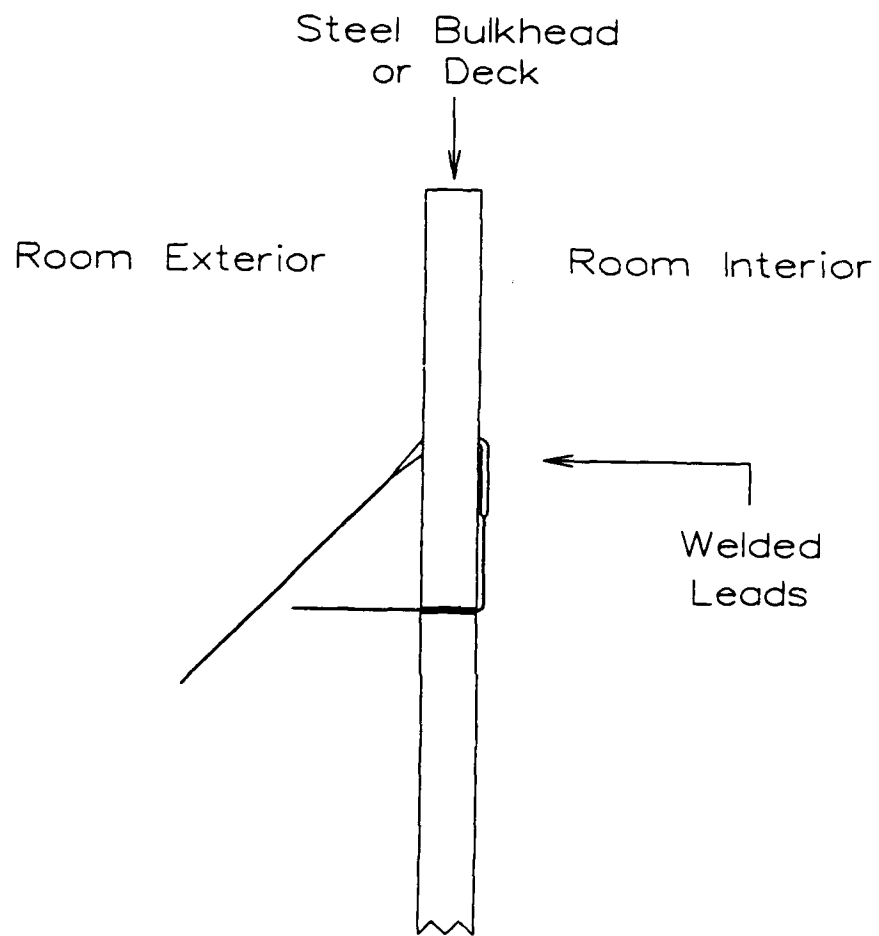


Figure 8. Schematic of Surface Thermocouples

3.3.3 Incident Heat Flux Measurements

Pairs of Medtherm radiometers and calorimeters were located in the floor, bulkhead and upper deck. All transducers had a range of 0-50 kW/m². Specific transducer locations can be found in Figure 7.

3.3.4 Gas Species Measurements

A vertical tree consisting of 7 branches was used for gas analysis (Figure 9). Branches were spaced 41 cm apart beginning 36 cm from the ceiling. Oxygen concentration was measured at each location. The second branch, 77 cm from the ceiling, was also instrumented to measure carbon monoxide, carbon dioxide, and unburned hydrocarbons. In addition to oxygen, the lowest branch measured carbon monoxide and carbon dioxide.

A gas sampling tube was located in the exhaust vent. In Series 1 tests, it was positioned near the top of the vent so that it was in the exhaust portion of the flow field. The probe was placed in the center of the exhaust vent for Series 2 tests. Measurements consisted of O₂, CO, CO₂, and unburned hydrocarbons (UHC).

Water was removed from all gas samples by passing them through Drierite filters. Thus, all recorded concentrations were "dry" concentrations.

3.3.5 Fuel Mass Loss Measurements

A 0-200 kg load cell with a resolution of 0.1 kg was used to record the mass loss. As shown in Figure 2, it was attached to the cable which supported the fuel cradle. The cradle weighed 72 kg.

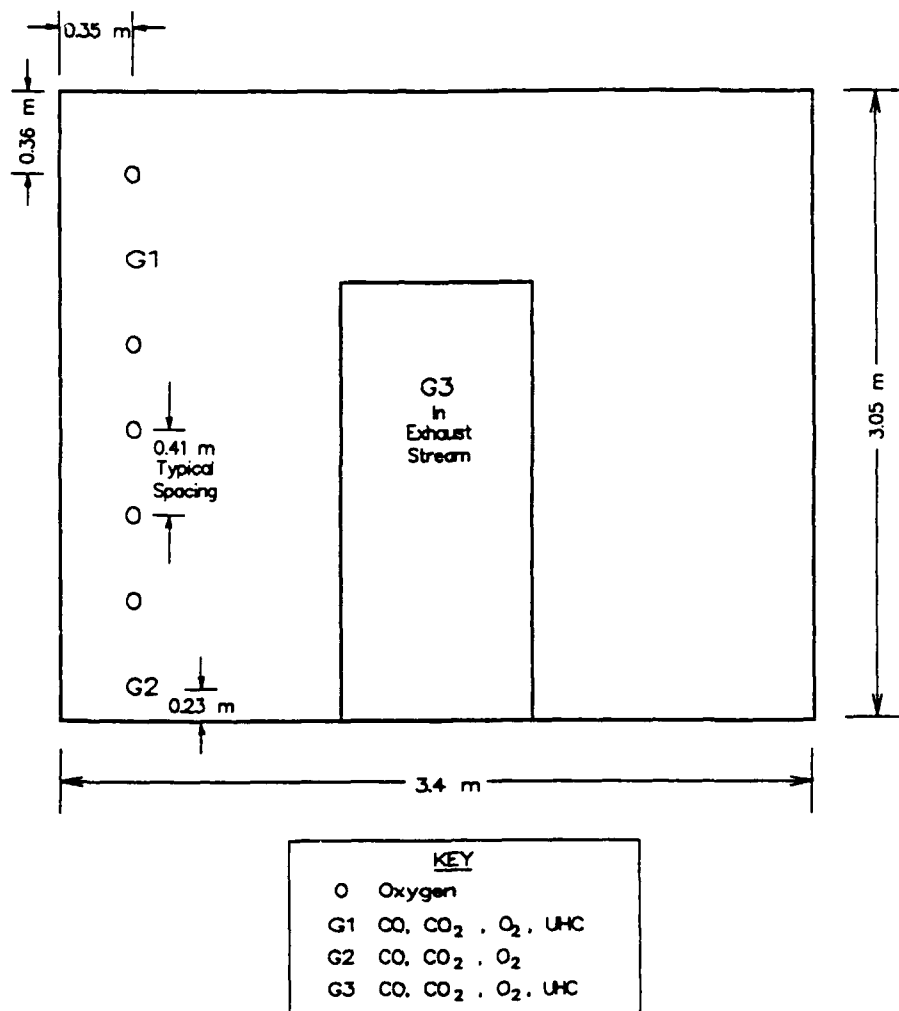


Figure 9. Gas Species Instrumentation - Side View

3.3.6 Pressure Measurements

A 0-250 Pa pressure transducer was located in the floor of the compartment between the fuel cradle and the vent (Figure 7). This pressure measurement was used as one means of determining the neutral plane location.

3.3.7 Video Cameras

Each test was videotaped from three locations. Two of these views were through the portholes and recorded the fire development. In most tests, vision through the portholes was quickly obscured by soot. The third camera was located in the corridor so that it monitored the air flow through the vent.

4.0 TEST PROCEDURES

4.1 Test Description

Tests were divided into two series, each consisting of 12 tests. Series 1 tests used natural ventilation while Series 2 tests used forced ventilation. Within each series, three different vent sizes or ventilation rates were examined in conjunction with four fuel configurations. Fuel types included diesel pans, wood cribs, and polyurethane slabs. Two pan diameters, 84 cm and 62 cm, were used for the diesel pan fires. All wood cribs were 1.9 by 1.9 m and consisted of 6 layers of 28 3.8 cm members spaced 3.1 cm apart. Polyurethane slabs measuring 1.8 m by 1.8 m by 0.15 m were burned in the last fuel configuration. Tables 1 and 2 provide the test sequence with a brief test description.

Table 1. Series 1: Natural Ventilation Tests

Ventilation	62 cm Pan Steady Fire	84 cm Pan Steady Fire	Wood Crib, Growing Fire	PU, Growing Fire
Full Door	1	2	3	4
Window	5	7	6	8
Quarter Door	11	12	10	9

Table 2. Series 2: Forced Ventilation Tests

Ventilation	62 cm Pan Steady Fire	84 cm Pan Steady Fire	Wood Crib, Growing Fire	PU, Growing Fire
0.38 m ³ /sec	1	3	2	4
0.61 m ³ /sec	7	8	6	5
0.25 m ³ /sec	10	11	9	12

Ignition was initiated in the diesel pan fires by pouring 350 ml of gasoline on top of the diesel fuel. The wood cribs were ignited by placing a 0.305 m square pan underneath the crib. This pan was filled with diesel fuel 1 cm deep and a thin layer of gasoline on the top. This arrangement was used to ensure that the crib was burning before the initiator had burned out. Polyurethane slabs were ignited by soaking a rag approximately 0.305 m by 0.305 m in gasoline and laying it in the center of the slab. The goal in the wood crib and polyurethane fires was to ignite the fuel so that the flame would spread radially from the center in a uniform manner. It is believed that with each ignition technique, the ignition source disappeared early in the transient portion of the test, before steady-state conditions were achieved.

4.2 Additional Tests

The tests described above were designed to span an upper layer temperature increase between 0 and 600 °C though a temperature of 600 °C was not reached in any of the tests. In an effort to achieve higher upper layer temperatures, three additional tests were conducted following Series 1 and 2 tests and were named ADD1, ADD2, and ADD3. These tests were naturally ventilated and used the full door vent. In each test, the fuel load consisted of three pans having dimensions of 62 cm diameter, 84 cm diameter, and 46 cm by 92 cm. Each pan was filled with a layer of diesel fuel 1.9 cm deep. As with the other diesel pan fires, gasoline was used as an initiator. 700 ml of gasoline was divided between the three pans prior to ignition.

These three tests differed by the remote ventilation configuration. ADD1 was conducted with the door at the top of the stairtower open, as was the case in most of the other tests. The second test, ADD2, was conducted with the door at the top of the stairtower and the door at the end of the passageway closed. The last test, ADD3, was performed with these doors open with an addition of an open window. Specifically, this window was located in the skin of the ship in the room adjacent to the fire room (Room 4 in Figure 1). Also, in this test, the smoke extraction fan was used with only two of the four vents open. The two vents closest to the fire room remained closed since high temperature air could damage the extraction fan. These additional ventilation measures were used in ADD3 to assess the effect that variable ship ventilation outside the fire compartment may have on fire compartment behavior.

5.0 DATA ANALYSIS METHODS

Experimental data were reduced to determine mass loss rates, supply and exhaust air flow rates, hot and cold layer temperatures and depths, wet gas concentrations, and heat release rates. In order to perform some of these calculations, molecular formulas of the fuel and their heats of combustion had to be estimated. Table 3 lists the values used [5,6,7,8].

It should be noted that values used for wood reflect the composition of the volatiles burning during the flaming stage of the fire.

Table 3. Fuel Properties

Fuel Type	Molecular Formula	Heat of Combustion (kJ/g)
Diesel	$C_{10}H_{19}$	45
Wood (Fir)	$CH_{3.584}O_{1.55}$	13
Polyurethane	$C_{18.7}H_{33.4}O_{5.5}N$	26

Mass loss rates were calculated using a one minute running average of the mass loss divided by the time elapsed.

Air velocities (m/s) were calculated using Bernoulli's equation:

$$V(z) = \pm C \sqrt{\frac{2\Delta p(z)}{\rho_d(z)}} \quad (1)$$

where C is the flow coefficient which was taken as 1.08 [9], $\Delta p(z)$ is the pressure difference across the bi-directional probe (Pa), and ρ_d is the density of the gases in the doorway (kg/m^3). Then, the exhaust and supply flow rates were determined by integrating the air velocity profile in the doorway [10].

$$\dot{m}_{ex} = C_o W_d \int_{z_a}^{z_d} \rho_d(z') V(z') dz' \quad (2)$$

$$\dot{m}_i = C_i W_d \int_{z_b}^{z_n} \rho_d(z') V(z') dz' \quad (3)$$

C_o and C_i are the out and in flow coefficients, respectively, and were taken to be 0.73 and 0.68 [11], w_v is the width of the vent, z_t and z_b are the location of the top and bottom of the vent (m), respectively, and z_n is the height of the neutral plane (m). The neutral plane is the location where there is no pressure change across the vent. This location was determined by finding the height where the pressure differential readings changed signs. This value was verified with two other methods. The first method was to find the location where the temperature gradient in the vent tree was the highest. The other method used the pressure reading at the floor and the temperature profile in the compartment [10]. Generally, the values determined with these methods were within 15 cm of each other, which is the distance between bi-directional probes.

Hot and cold layer temperatures were calculated differently for natural and forced ventilation tests. Natural ventilation tests produced two-layer systems which allowed for a determination of the layer interface. The layer interface was taken as the point where the temperature gradient was highest. Temperatures from both thermocouple trees above this point were averaged for the hot layer temperature and below this point for the cold layer temperature. In general, forced ventilation tests did not produce two-layer systems. The upper layer temperature was calculated both by averaging the temperatures over the entire compartment height and by averaging the temperatures over the top half of the compartment. These values did not differ by more than 30 °C in smaller fires and 45 °C in larger fires. The value determined by averaging over the entire compartment will be reported here and compared to the predictive methods.

It should be noted that other common methods of layer interface determination were implemented for Series 1 tests and found to yield unrealistic results. These methods included the Cold Layer Temperature Method, the Hot Layer Temperature Method, and the Layer Interface Method [4]. In each method, there are two equations and three unknowns: the upper and lower layer temperatures and the interface height. A different variable is assumed in each method so that the equations can be solved. In most cases, each method gave results which were questionable. As an example, the interface location would be at a point which was in the middle of the upper or lower layer based on the temperature

profiles. These methods may not have been successful since the difference between the upper and lower layer temperatures was small.

Overhead temperatures were averaged over the four locations for the interior side of the barrier. One of the exterior measurements was faulty so that the exterior value was only averaged over three locations. In the same manner, the interior and exterior bulkhead temperature was determined by averaging the values at the highest position on the forward and aft bulkheads.

Since water was trapped out of the gas samples before the concentration was determined, the gas concentration measurements were corrected to represent "wet concentrations." The water concentration was estimated by assuming that the ratio of water to carbon dioxide production remained the same as the stoichiometric ratio. This assumption is good in situations where carbon monoxide concentrations are minimal as is the case in most of these tests. This correction is typically performed for analyses involving gas species yields. Data from these tests were used to calculate gas species yields, but the results were not presented due to measurement problems which are discussed in Section 6.1.1. The wet oxygen concentration is not reduced by more than 10% from the dry oxygen concentration in these tests.

The response time of each analyzer was measured and then used to adjust the readings so that the delay in response was removed from the results. These delay times ranged from 24 to 138 seconds.

Heat release rate calculations were performed by multiplying the mass loss rate and the heat of combustion. This method may overestimate the heat release rate because it assumes that all fuel is burned to completion (i.e., all exhaust products are water and carbon dioxide). Heat release rates based on oxygen depletion were attempted [12], but uncertainties in transient concentration measurements reduced the confidence in these results. However, these heat release rates calculated during steady periods were used to verify the heats of combustion in Table 3.

6.0 RESULTS

6.1 Series 1 Tests: Natural-Ventilation Fires

6.1.1 Overview

The measured air flow rates remained relatively constant during the fires and did not fluctuate considerably from test to test for a given vent size. The measured inflow and outflow rates were not consistent with one another in all cases. Since they should differ only by the fuel mass loss rate, the inflow and outflow were averaged and used in subsequent calculations. As expected, their values were less than the maximum air flow rate based on choked flow [13]. For the door vent, the average air flow rate was 0.9 kg/sec compared to a choked flow rate of 1.27 kg/sec. The window and quarter door vents both had an average flow rate of 0.28 kg/sec. The maximum choked flow rate is 0.32 kg/sec for each of these vents.

Although gas concentrations were adjusted for the sampling system transport times, they did not correspond properly to the mass loss rate and temperature time histories in the diesel and polyurethane fires. Figure 10 shows upper layer temperature, mass loss rate, carbon dioxide concentration, and oxygen concentration-time histories for test S112, an 84 cm diameter diesel pan fire. The oxygen concentration reflects the measurement at the top of the gas sampling tree and the carbon dioxide concentration reflects the measurement at the second tree branch. Both graphs have been corrected for the transport time. An arrow has been placed on each graph indicating the point where it appears steady-state conditions have been achieved based on that particular measurement. As shown in this figure, there were some tests where as much as a two-minute time shift was present between the rise in mass loss rate and temperature and the depletion in oxygen concentration and rise in carbon dioxide concentration even after correction for sample transport delays. This discrepancy made analysis which involved both mass loss rate and gas species measurements (i.e., CO yield, heat release rate based on oxygen depletion, etc.) unreliable. The magnitude of the

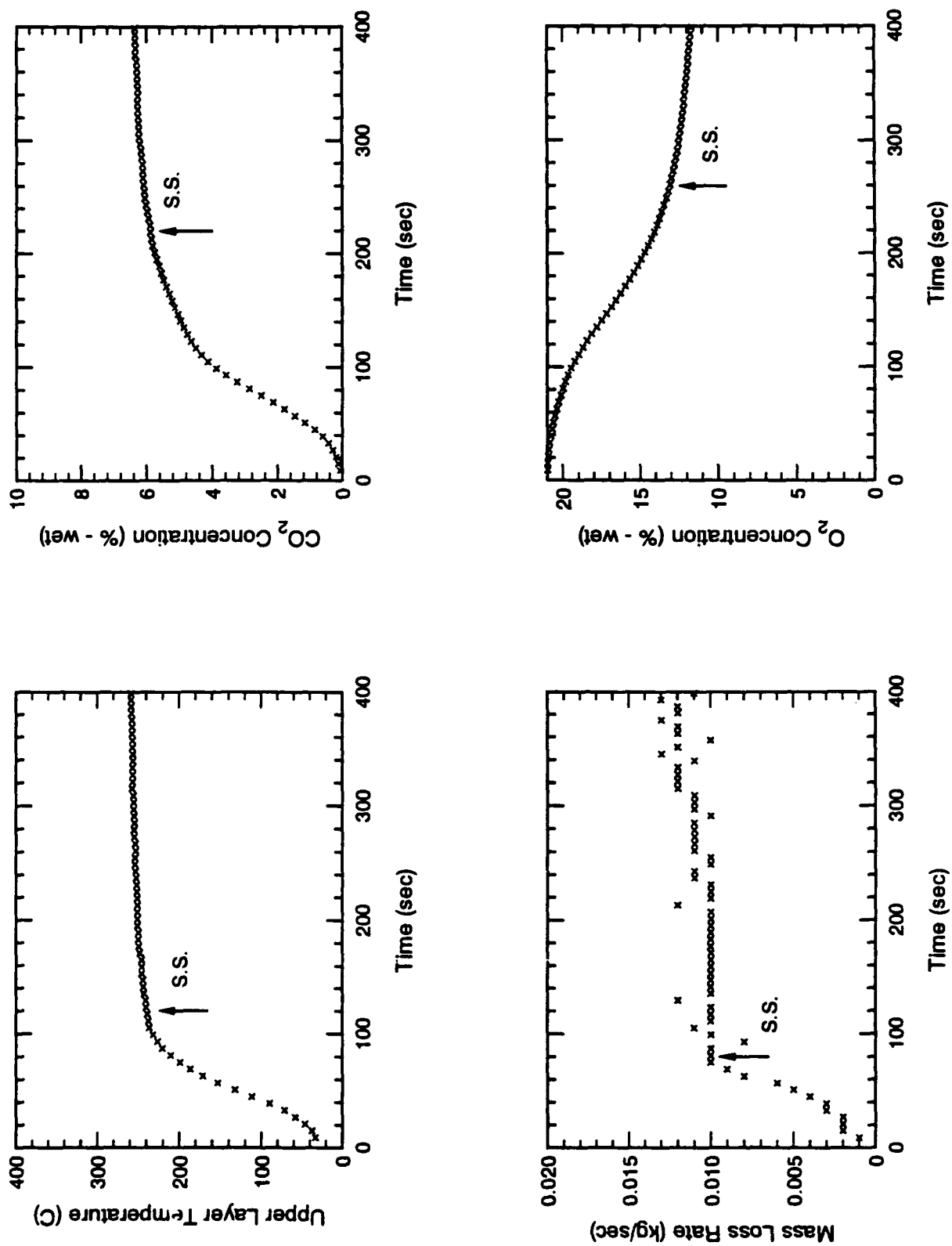


Figure 10. Example of Gas Sampling System Time Delay (S112) - Gas Concentrations Corrected for Time Delay

transient measurement problems varied from test to test and sample line to sample line. No source of the problem was identified.

The oxygen measurements on Branch 2 were usually lower than those on the other branches. One would expect that the concentration on Branch 1 would be the lowest since it is the highest sampling point in the compartment. Nonetheless, due to the fact that this reading showed 4% less oxygen than on the other branches, well out of the experimental error limits, it was plotted but not used in calculations. It was also disregarded when determining the minimum oxygen concentrations in each test since no explanation could be offered for the behavior. Since the gas concentrations measured in the vent exhaust were also not usable due to measurement problems, exhaust oxygen concentrations were assumed to be the same as those recorded on Branch 1 of the gas sampling tree.

Vertical temperature and oxygen profiles plotted at steady-state conditions showed that most of these fires produced environments which were contaminated, two-layer systems. Some tests were well-mixed based on the oxygen concentrations but showed some thermal stratification. Only two of the Series 1 tests had ambient oxygen concentrations at the base. These tests were the diesel pan full door vent tests.

A summary of results is provided in Table 4 where \dot{m}_f represents the mass loss rate, \dot{Q}_{th} represents the theoretical heat release rate, T_H and T_C represent the hot and cold layer temperatures, respectively, T_{OH} and T_{BULK} represent the upper deck and bulkhead temperatures, respectively, and O_2 represents the lowest oxygen concentration recorded on the gas sampling tree during the test (discounting Branch 2). These values were taken as the average over the steady-state portion of the test with the exception of polyurethane tests where values were taken at the initial peak. Barrier temperatures were taken as the maximum temperature achieved during the test.

Trends in fire behavior were not necessarily consistent between fuels. Therefore, further results are described below for each fuel type. Plots of the time histories for mass

Table 4. Series 1 – Summary of Results

Test	Fuel Type	Vent Type	\dot{m}_t (kg/s)	\dot{Q}_{th} (kW)	T_H (°C)	T_c (°C)	T_{CEIL} (°C)		T_{BULK} (°C)		O_2 (%-wet)
							INT	EXT	INT	EXT	
S101	62 cm Pan	Door	0.007	315	165	60	60	55	70	60	17.5
S102	84 cm Pan	Door	0.018	810	260	90	75	70	87	75	14
S103	Wood Crib	Door	0.1	1300	520	300	300	280	350	320	9
S104	Polyurethane	Door	0.04	1050	280	100	45	37	60	40	11
S105	62 cm Pan	Window	0.0075	340	195	95	65	60	80	70	14.5
S106	Wood Crib	Window	0.03	390	380	250	225	220	250	225	7
S107	84 cm Pan	Window	0.0085	380	230	125	90	84	100	85	13
S108	Polyurethane	Window	0.02	520	360	150	64	60	70	60	10
S109	Polyurethane	Quarter Door	0.025	700	340	115	64	60	70	63	8
S110	Wood Crib	Quarter Door	0.04	780	400	300	265	250	250	240	1.5
S111	62 cm Pan	Quarter Door	0.005	230	190	70	60	55	80	68	14
S112	84 cm Pan	Quarter Door	0.011	500	260	110	90	84	95	90	10
ADD1	3 Pan Combo.	Door	0.032	1440	440	150	135	120	160	145	11
ADD2	3 Pan Combo.	Door	0.032	1440	410	160	160	145	170	150	10.5
ADD3	3 Pan Combo.	Door	0.032	1440	440	180	170	160	180	160	11.5

\dot{m}_t = Mass Loss Rate
 \dot{Q}_{th} = Theoretical Heat Release Rate
 T_H = Upper Layer Temperature
 T_c = Lower Layer Temperature
 T_{OH} = Overhead Temperature
 T_{BULK} = Bulkhead Temperature (85 cm below overhead deck)
 O_2 = Minimum Oxygen Concentration
 INT = Interior Surface
 EXT = Exterior Surface

loss rate, temperature profiles, average hot and cold layer temperatures, wet gas concentrations, and heat release rates are included in Appendix A. Since the additional tests performed (ADD1, ADD2, and ADD3) were also natural ventilation tests, they will be presented in this section. In cases where it was determined that particular measurements were bad, they were not plotted.

6.1.2 Diesel Pan Fires

6.1.2.1 62 cm Diameter Pan (S101, S105, S111)

These fires had a relatively steady mass loss rate and temperature-time history. A typical mass loss rate-time history is shown in Figure 11. Discretization in mass loss rate values resulted from poor load cell resolution.

Figures 12 and 13 provide a comparison of the mass loss rate, upper layer temperature, and minimum oxygen concentration as a function of the ventilation rate. From Figure 12, there appears to be no direct relationship between the ventilation rate and the mass loss rate. The window vent had the highest mass loss rate while the quarter door vent had the lowest rate. Figure 12 also demonstrates that the upper layer temperature in the door vent test is lower than with the other two vents as expected for an overventilated fire. The larger vent allowed air to flow through the compartment and remove heat without participating in combustion. The increasing oxygen concentrations further show that the air supply is excessive (Fig. 13).

Vertical oxygen and temperature profiles for each test recorded at steady-state conditions can be found in Figures 14-16. The temperatures plotted reflect an average of the two thermocouple trees. Two-layer characteristics are most prominent in the full door vent test (S101). It is interesting to note that this test is one of the two Series 1 tests where an ambient oxygen concentration was recorded at the fire base. The quarter door vent test shows more stratification than the window vent tests indicating that more mixing is occurring with the window vent.

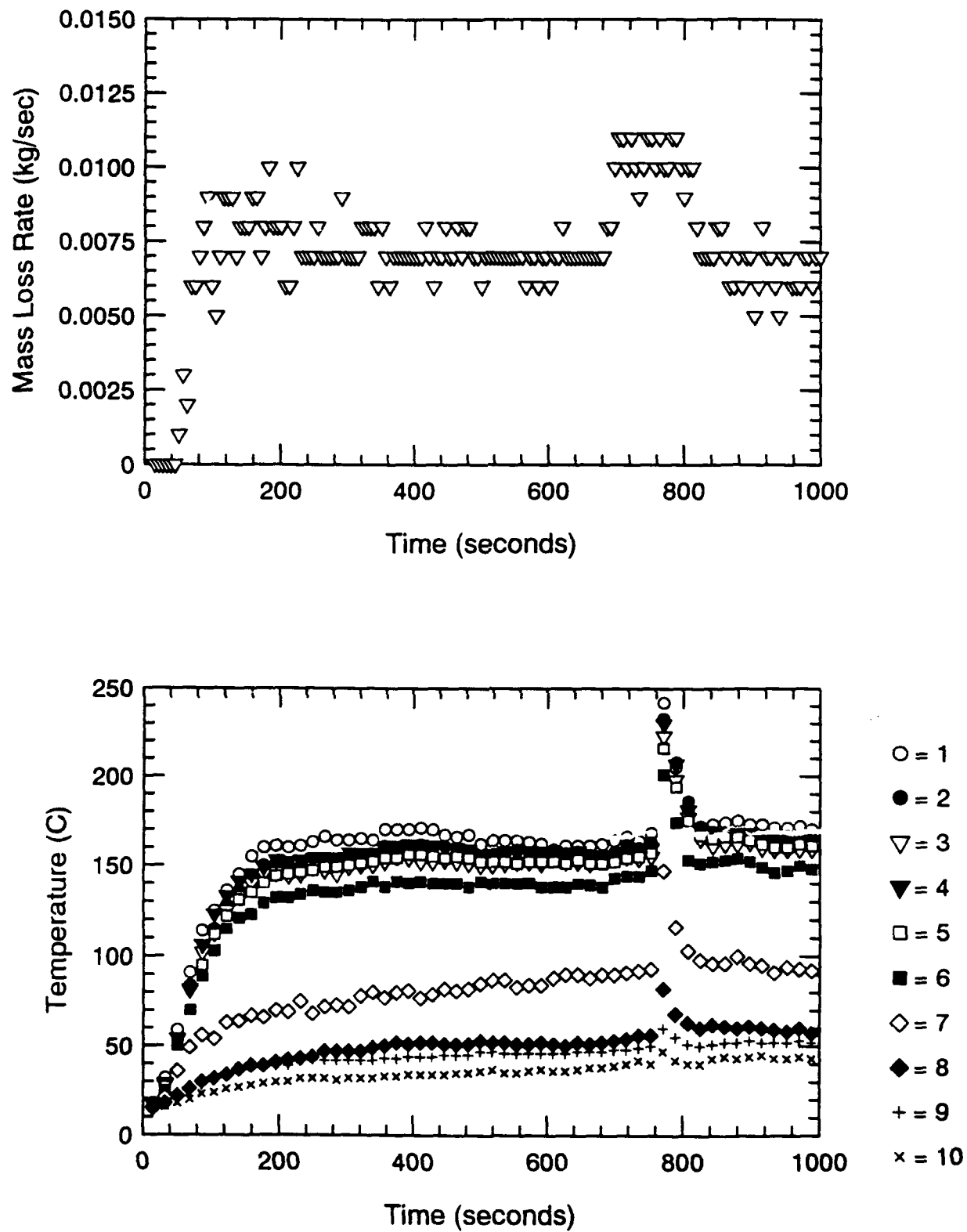


Figure 11. Mass Loss Rate and Temperature-Time Histories for 62 cm Diameter Pan (S101)

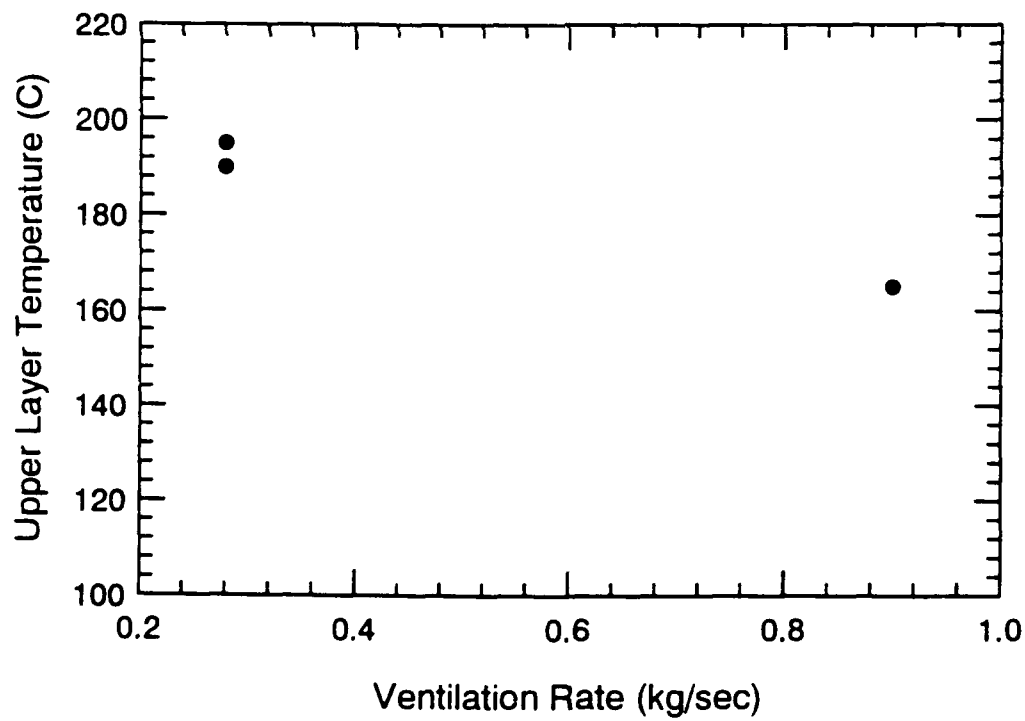
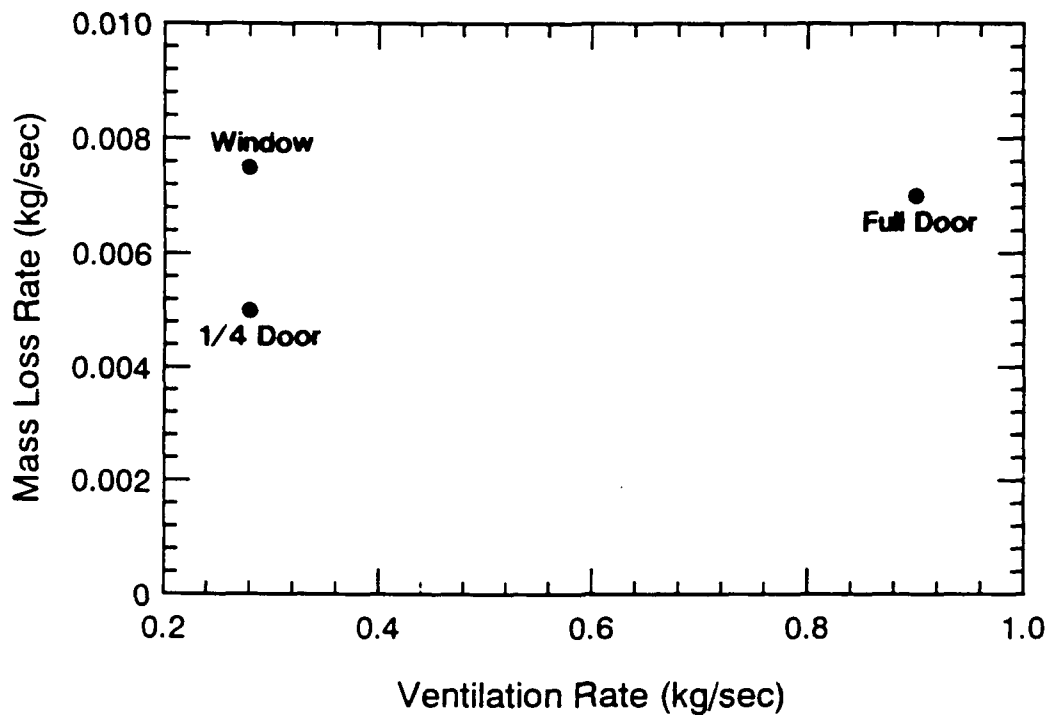


Figure 12. Mass Loss Rate and Temperature vs. Ventilation Rate for 62 cm Diameter Pan Tests (Series 1)

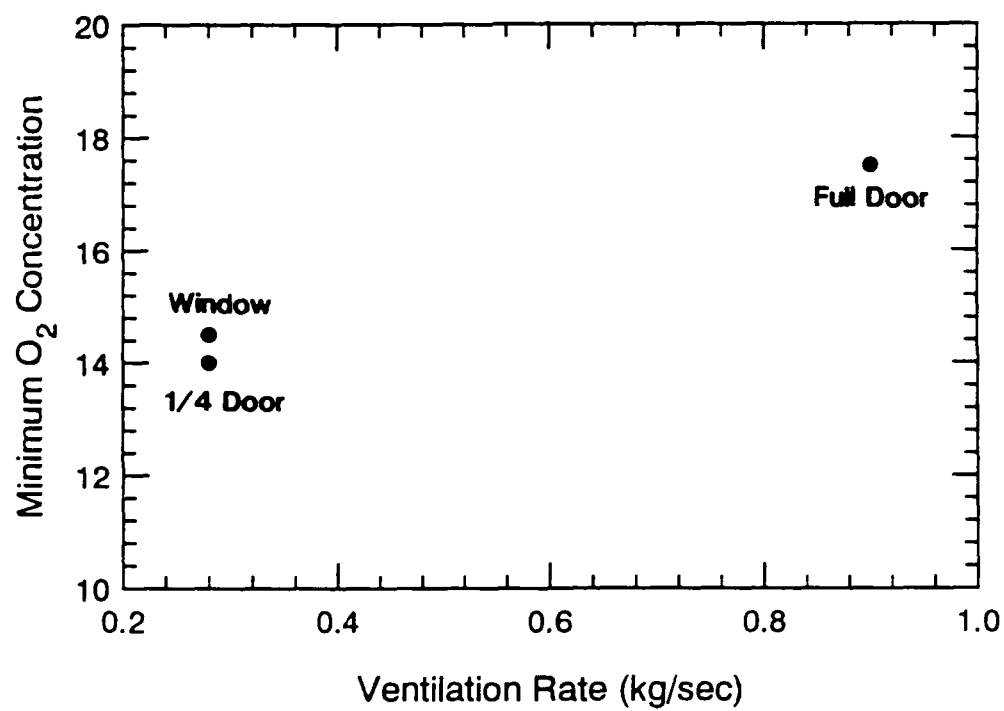


Figure 13. Minimum Oxygen Concentration vs. Ventilation Rate for 62 cm Diameter Pan Tests (Series 1)

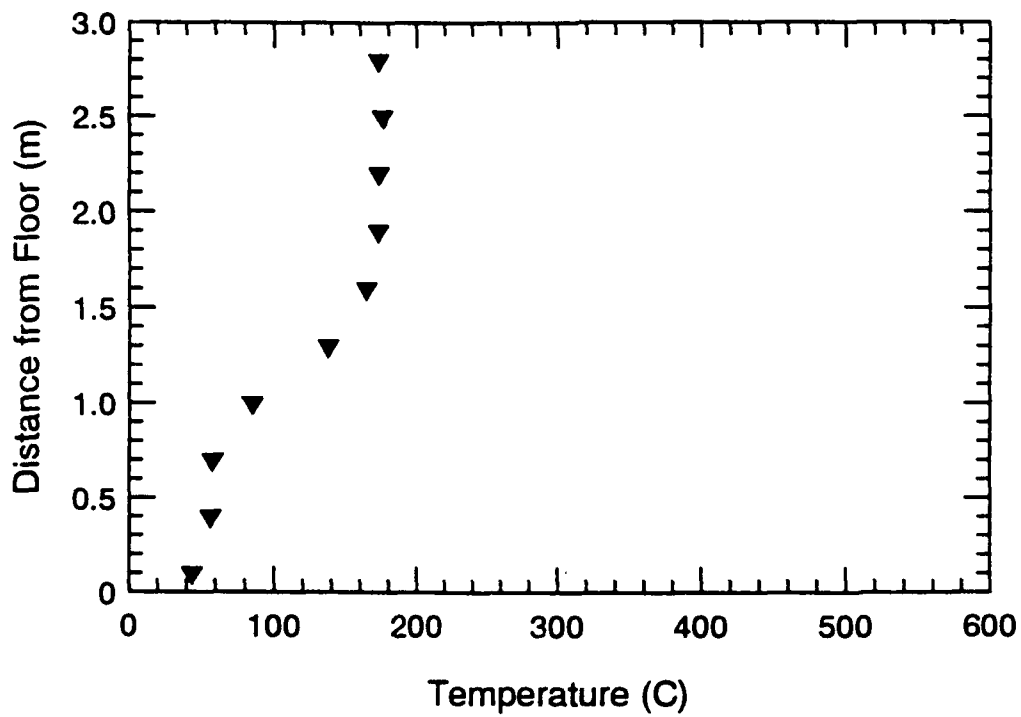
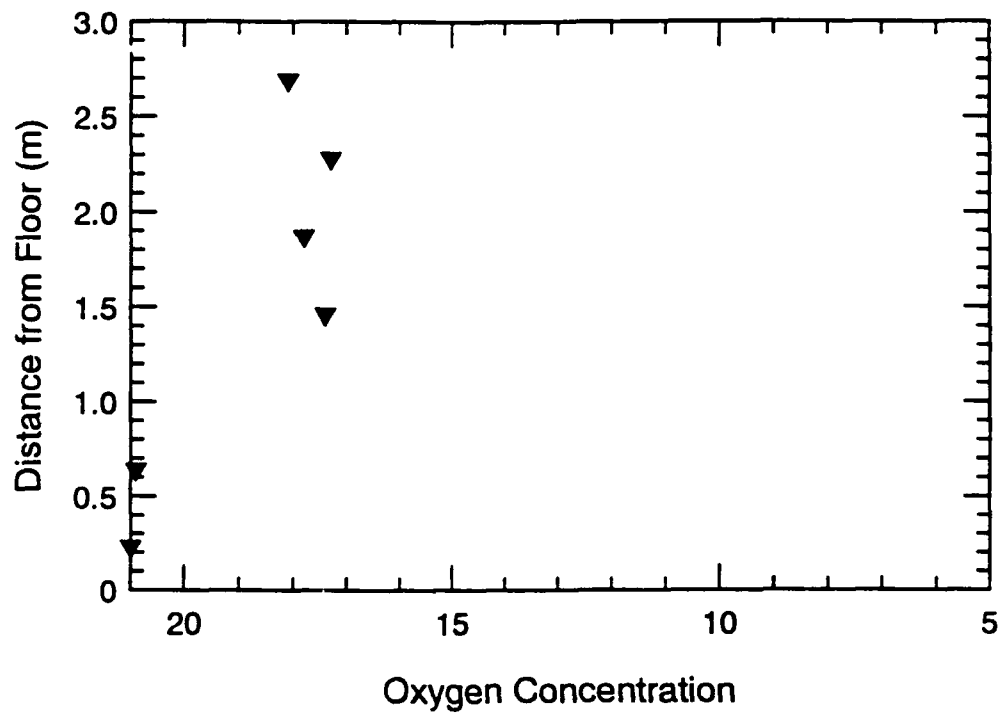


Figure 14. Vertical Oxygen Concentration and Temperature Profiles for S101 (Door Vent)

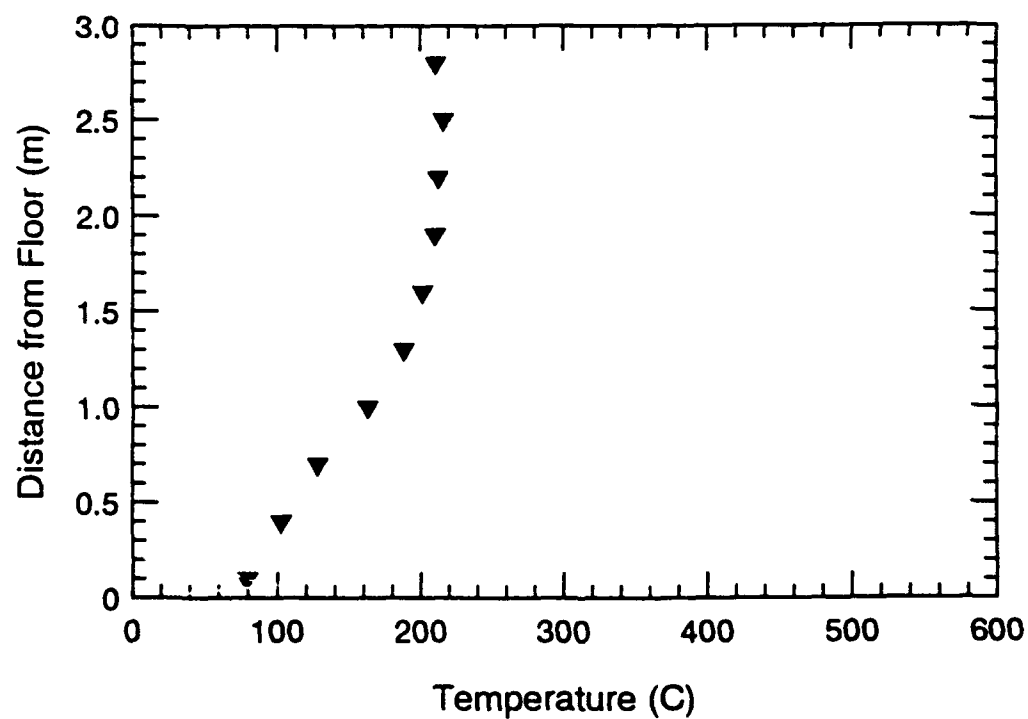
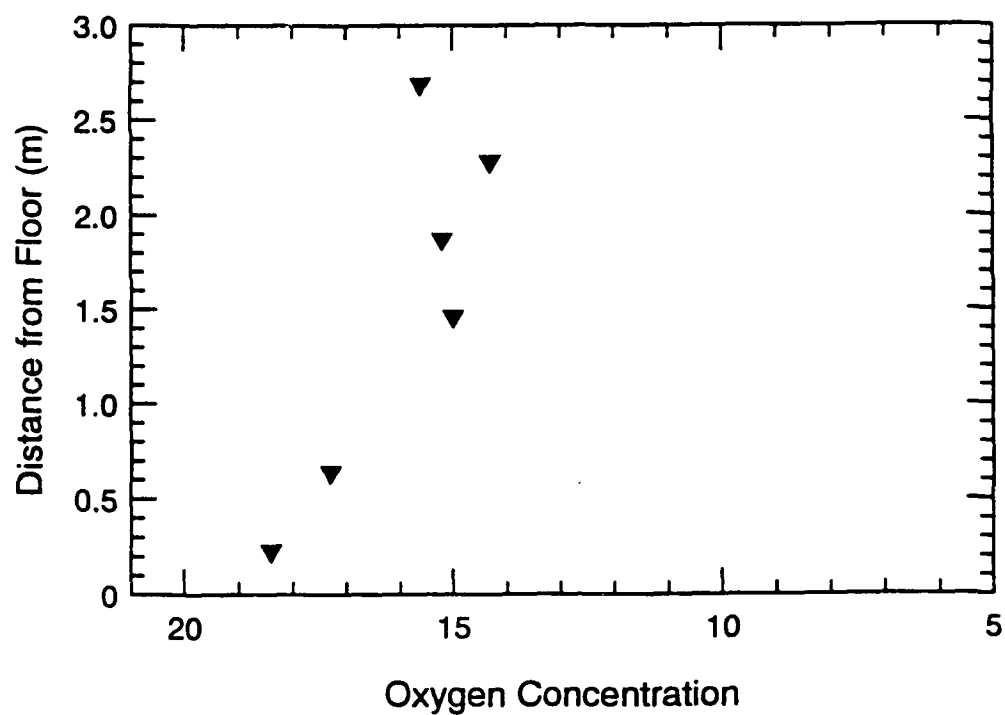


Figure 15. Vertical Oxygen Concentration and Temperature Profiles for S105 (Window Vent)

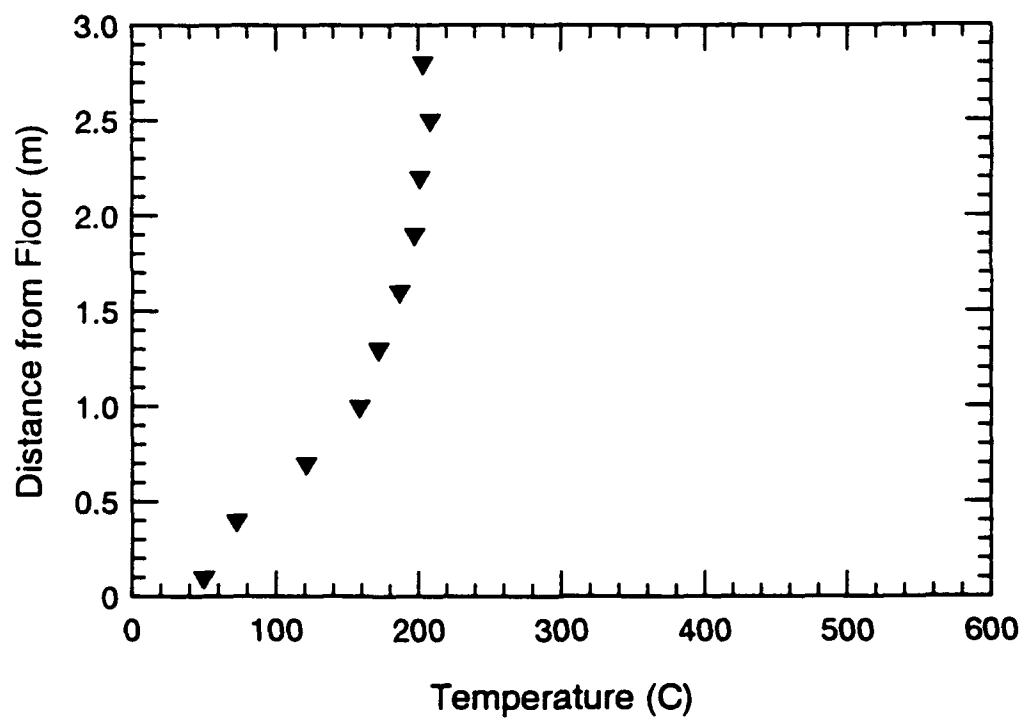
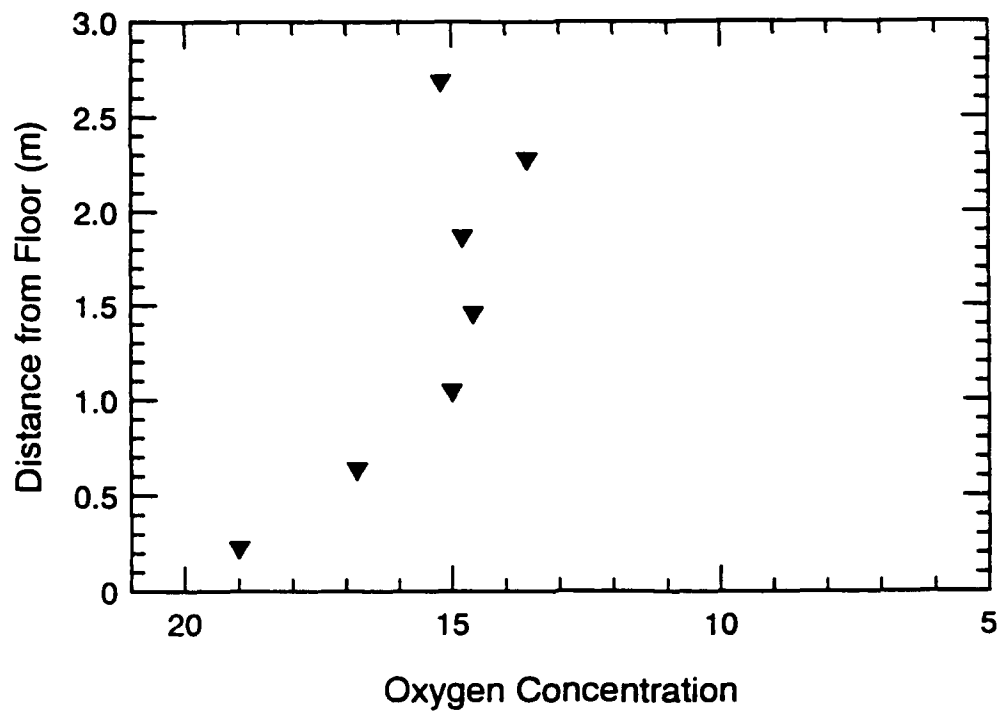


Figure 16. Vertical Oxygen Concentration and Temperature Profiles for S116 (Quarter Door Vent)

6.1.2.2 84 cm Diameter Pan (S102, S107, S112)

As with the 62 cm pan fires, the mass loss rate and temperature-time histories for these tests were quite steady. From Figure 17, the mass loss rate increases with the ventilation rate. However, when comparing the temperatures, the ventilation does not seem to affect the values. This trend suggests that the added ventilation is removing enough heat to compensate for the higher heat release rate. In Figure 18, the minimum oxygen concentration increases with the ventilation rate. The quarter door vent test has a concentration 3% lower than the window vent test.

The vertical oxygen and temperature profiles for the door vent test indicate a two-layer system (Figure 19). The other tests show some two-layer qualities (Figures 20-21). These qualities are less evident in the window vent test where well-mixed, one layer characteristics are beginning to be favored.

6.1.3 Wood Crib Fires (S103, S106, S110)

These fires were very slow growing. At the beginning of the test, the flame spread slowly from the center. Burning occurred in a localized area and the entire crib was never involved. In each test, the compartment temperatures were still rising after 1000 seconds. The latter two tests, S106 and S110, were terminated before all fuel was consumed due to the test length.

In both tests S106 and S110, a distinctive peak in mass loss rate and gas species concentrations occurs near 1000 seconds. An example of this behavior is shown in Figure 22 which represents test S110, the quarter door vent test. After this time, the mass loss rate decreases and levels off while the oxygen concentrations rise and also level off. This drop in oxygen concentration is particularly interesting in the quarter door vent test where it reaches a low of 1.5% in the upper layer before it begins to rise. At this time, a carbon monoxide concentration of 3% was measured. This is the only time during all tests that the

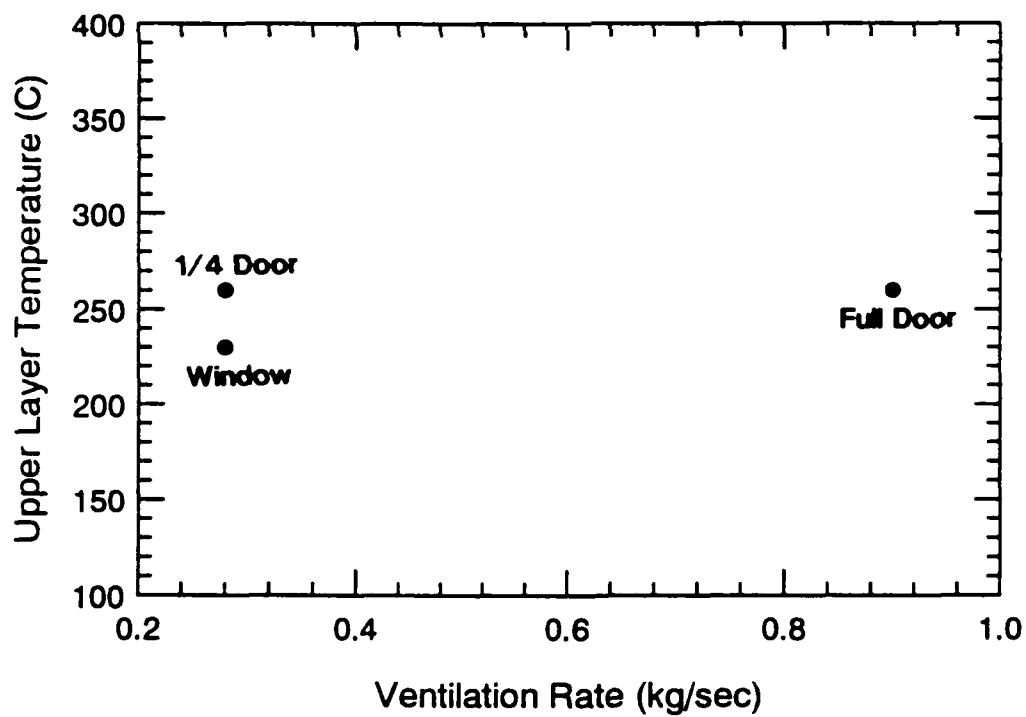
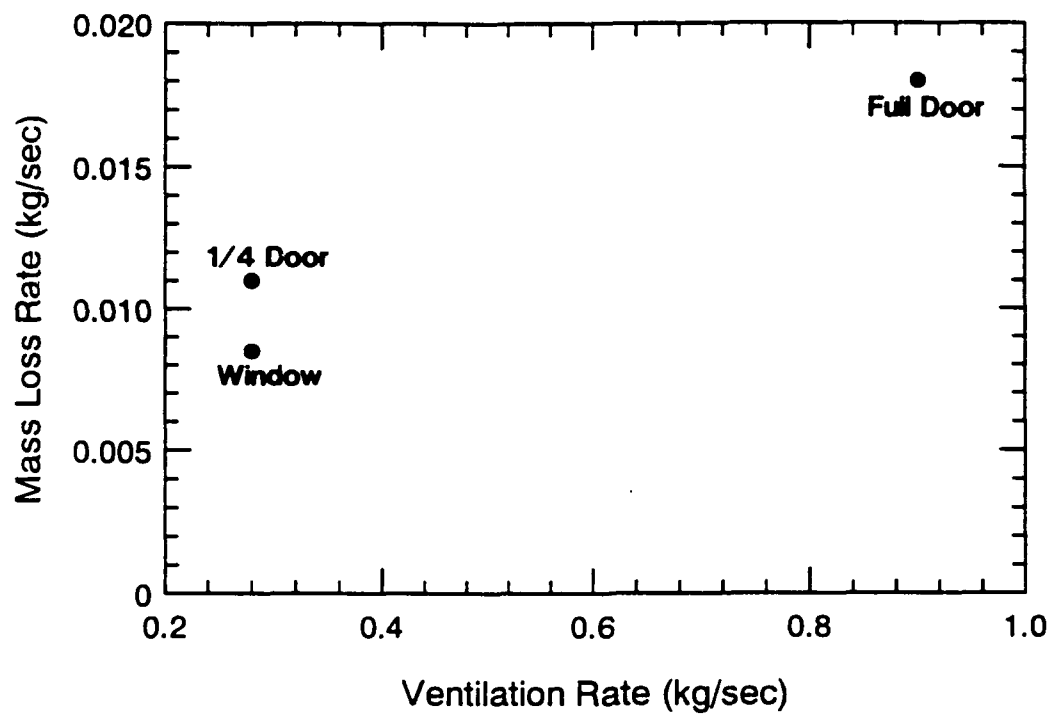


Figure 17. Mass Loss Rate and Temperature vs. Ventilation Rate for 84 cm Diameter Pan Tests (Series 1)

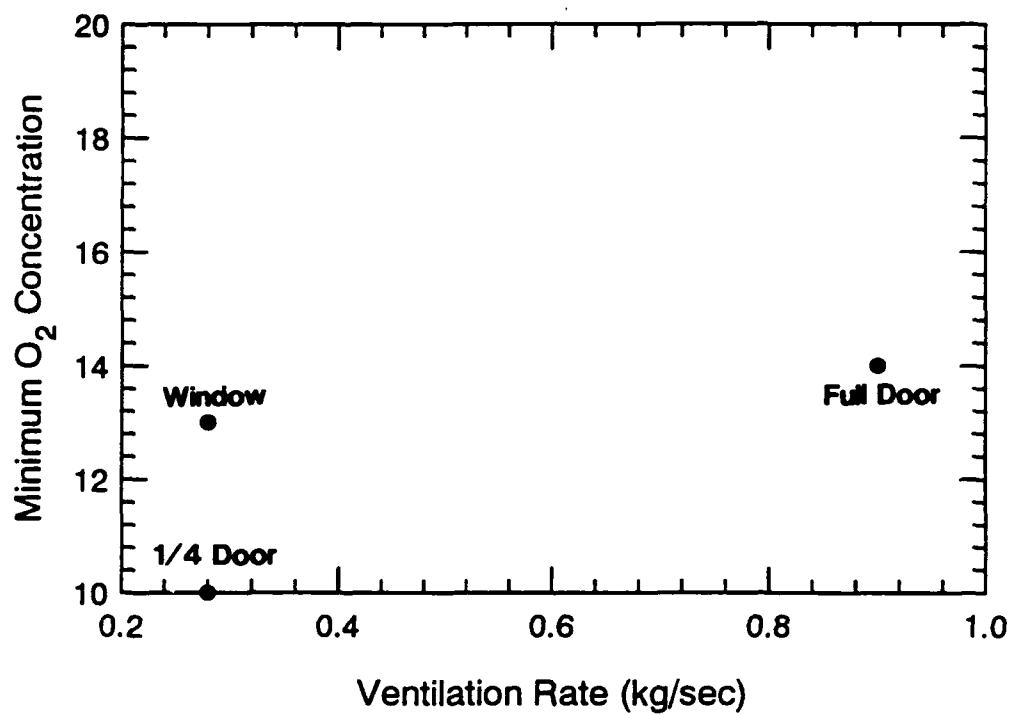


Figure 18. Minimum Oxygen Concentration vs. Ventilation Rate for 84 cm Diameter Pan Tests (Series 1)

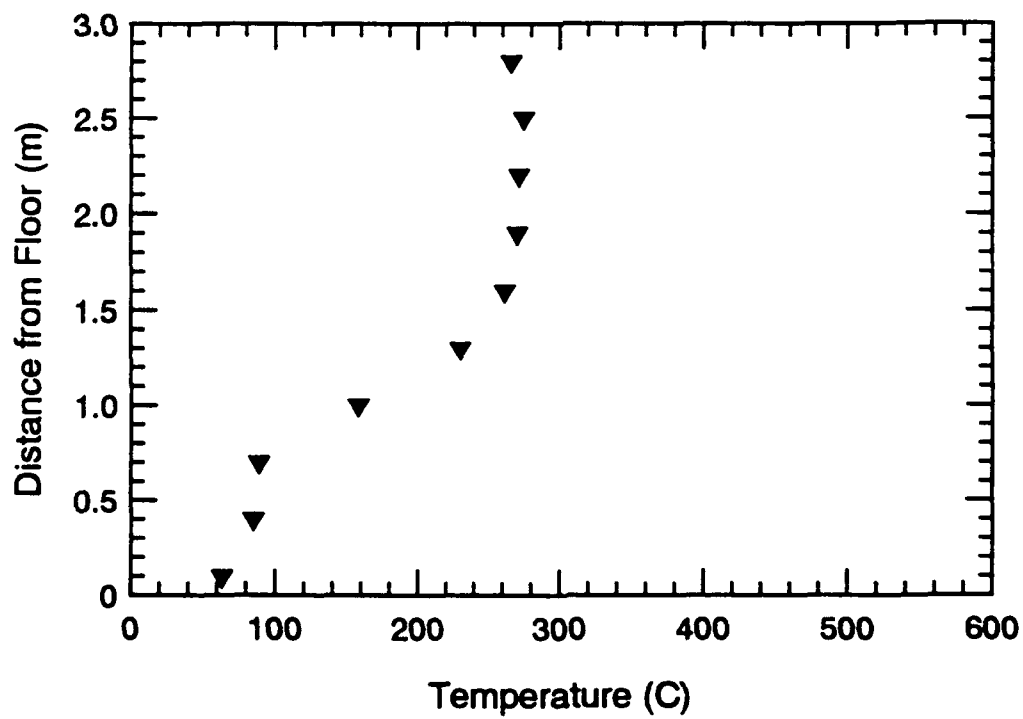
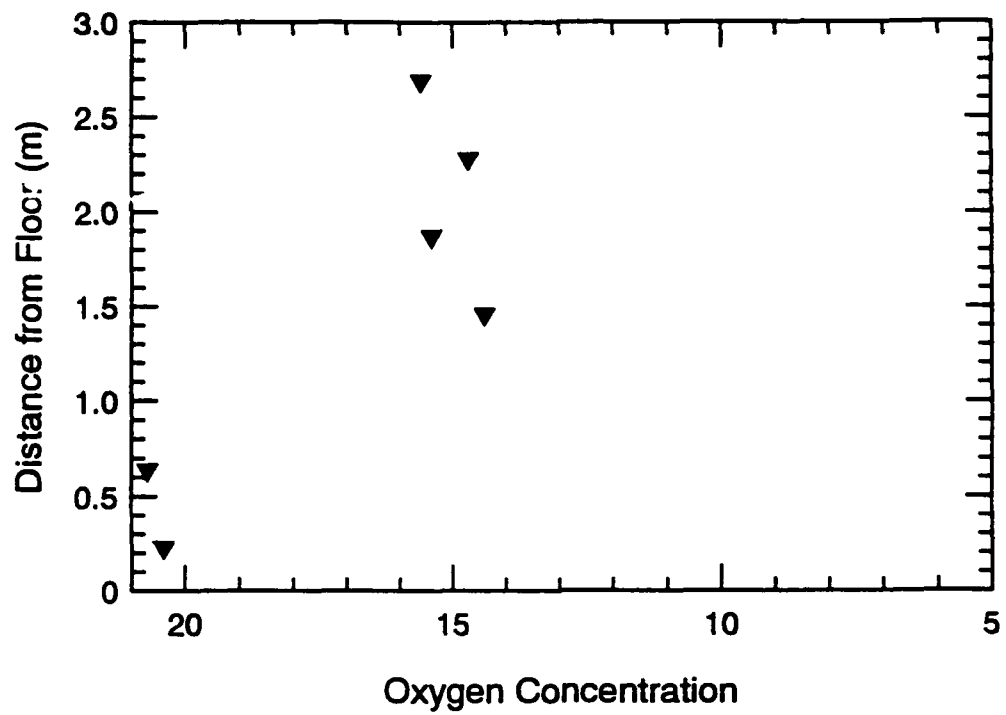


Figure 19. Vertical Oxygen Concentration and Temperature Profiles for S102 (Door Vent)

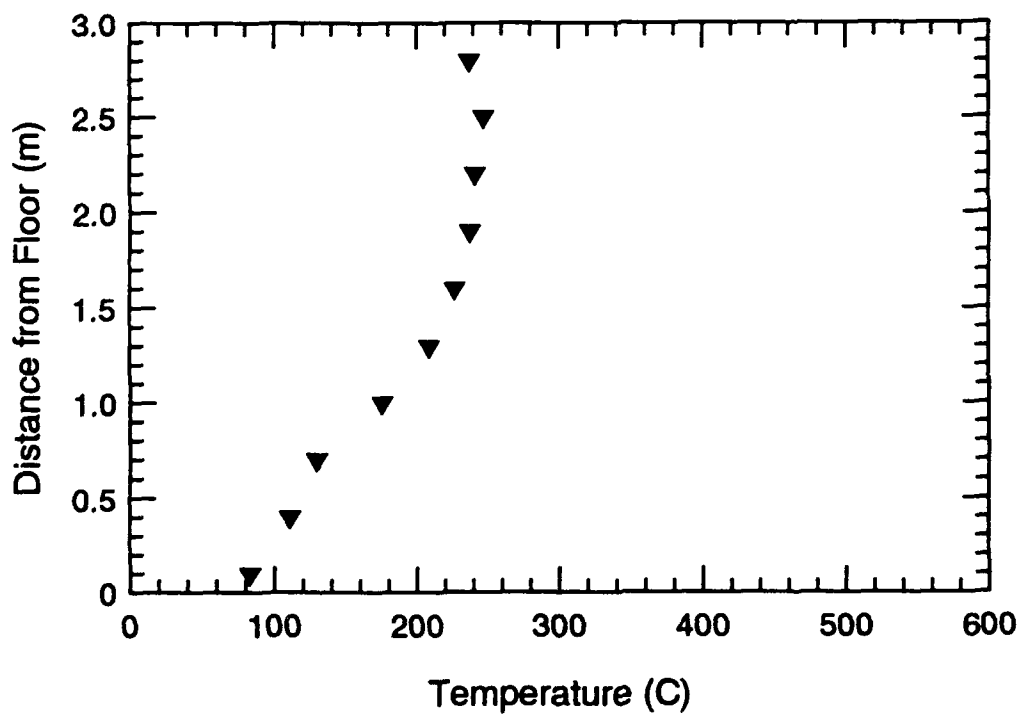
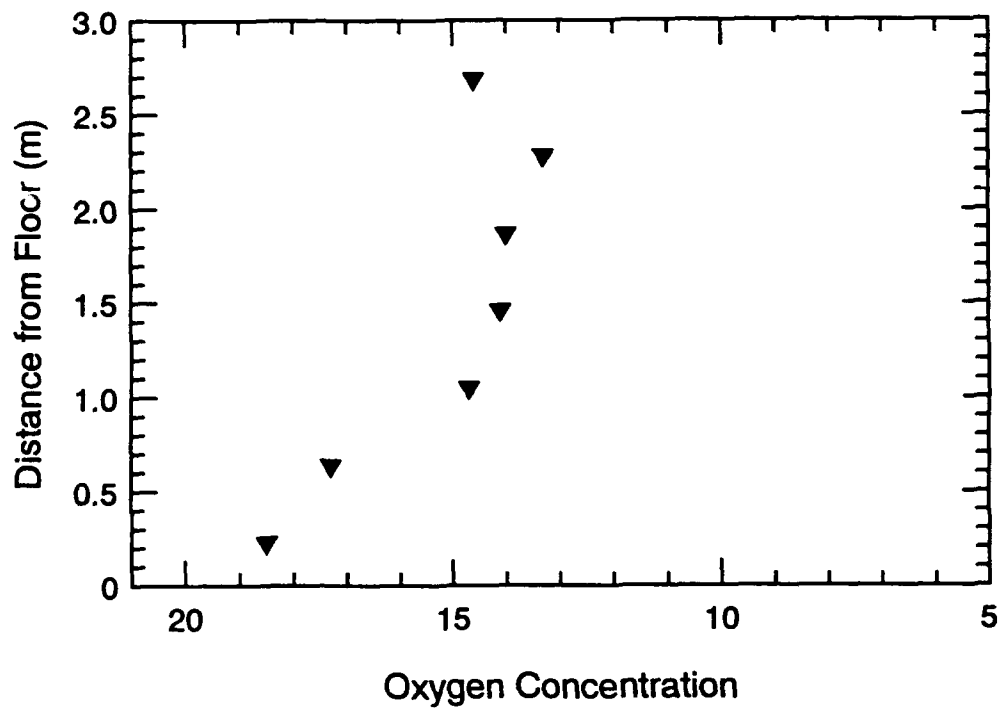


Figure 20. Vertical Oxygen Concentration and Temperature Profiles for S107 (Window Vent)

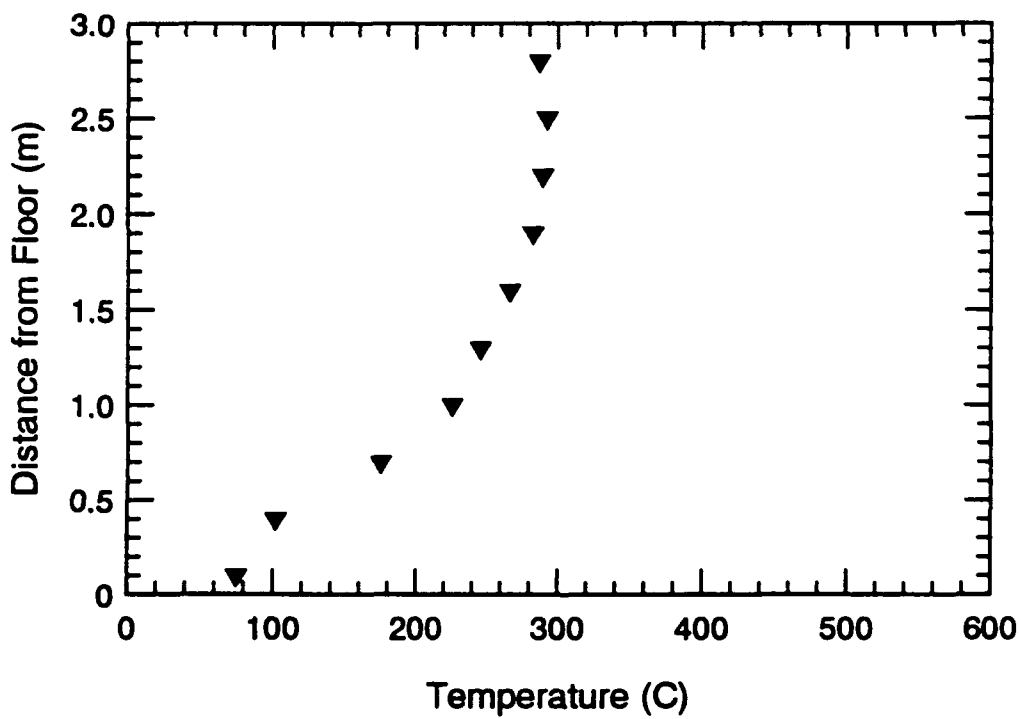
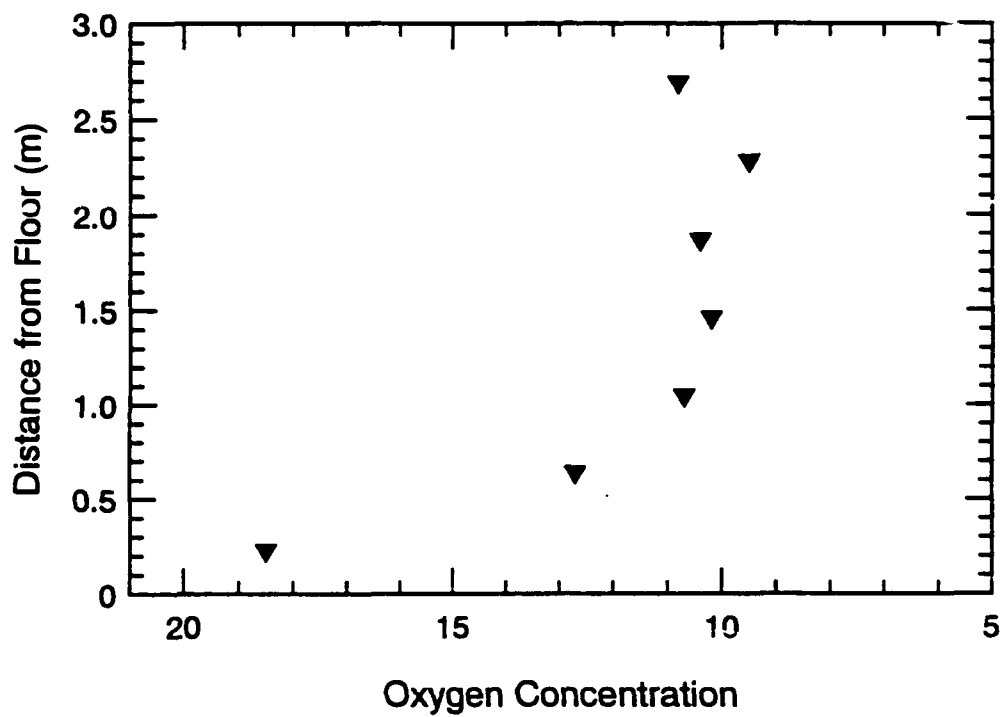


Figure 21. Vertical Oxygen Concentration and Temperature Profiles for S112 (Quarter Door Vent)

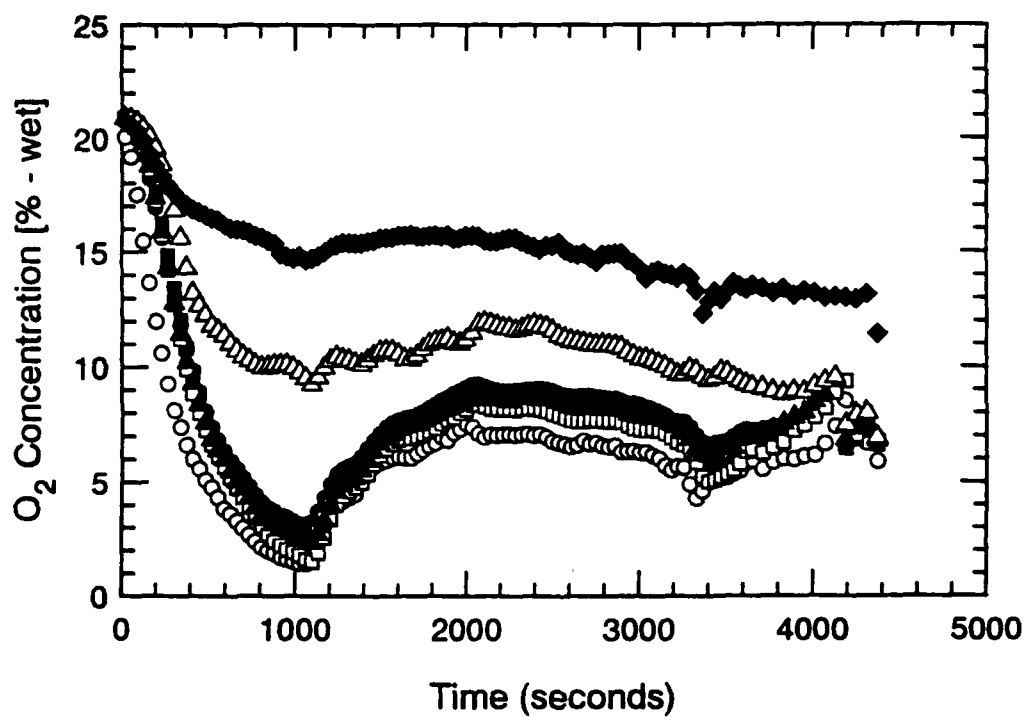
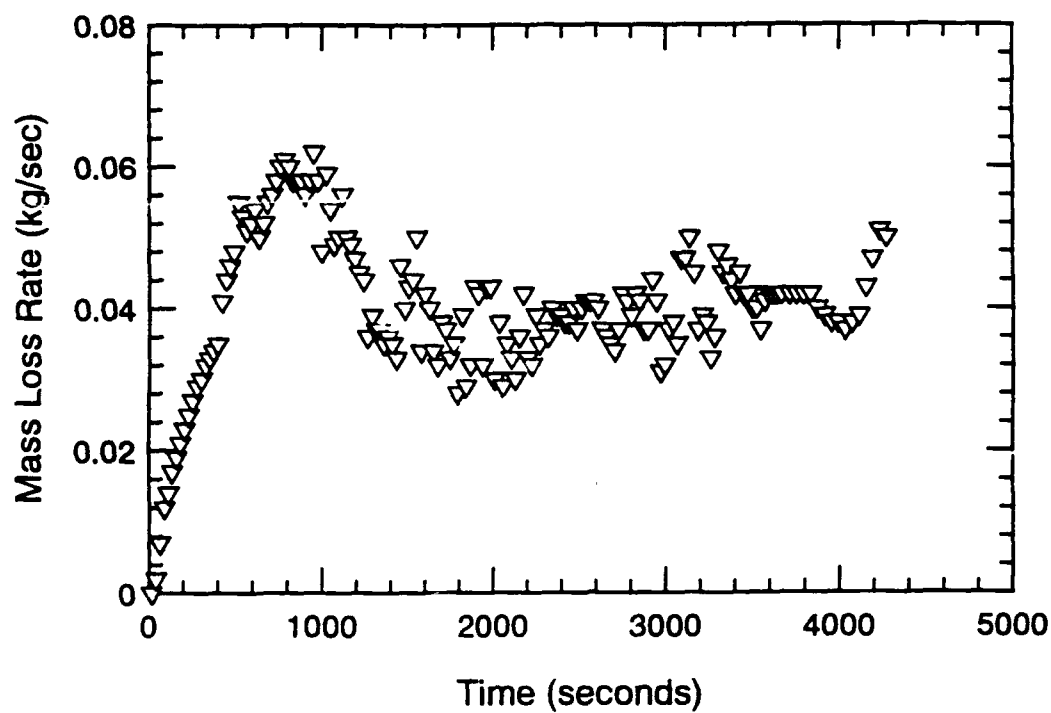


Figure 22. Mass Loss Rate and Oxygen Concentration-Time Histories for S110

fire appears to have been oxygen starved. This behavior could be indicative of wood's tendency to be self-regulating. The fire will grow to a point where it cannot sustain itself and then choke back to conditions where it can be sustained.

Figure 23 shows a dramatic increase in mass loss rate with ventilation rate as well as a significant increase in temperature. A notable increase in the minimum oxygen concentration is observed between the quarter and full door vent tests in Figure 24. However, the increase is much smaller between the window and full door vent tests.

Figures 25-27 show the vertical oxygen and temperature profiles for these tests. These profiles represent a time in the fire where the oxygen concentrations are steady. Therefore, the low concentrations shown in Figure 24 are not reflected in the profiles. Each test has two-layer characteristics both thermally and chemically; however, the window vent test presents the scenario closest to a one-layer, well-mixed system. The largest amount of oxygen stratification occurs in the quarter door vent test while the largest amount in temperature occurs in the full door vent test.

6.1.4 Polyurethane Fires (S104, S108, S109)

These fires are characterized by an initial peak in temperature and heat release rate. Referring to Figure 28 which represents test S106, this peak occurs in the first 200 seconds of the fire after which the mass loss rate remains at a low, steady value. Once ignition occurred, the entire slab was involved before this peak in mass loss rate. It appeared as though the fire grew to such magnitude that it had to choke itself back to avoid extinction.

In Figure 29, it is demonstrated that the mass loss rate increases with ventilation rate while the temperature decreases. An increase in mass loss rate is expected for increasing ventilation rate since there is more air available for combustion. However, it would also be expected that the temperature would increase with ventilation rate since the heat release rate is increasing with vent size. Figure 30 shows an increase in oxygen concentration with

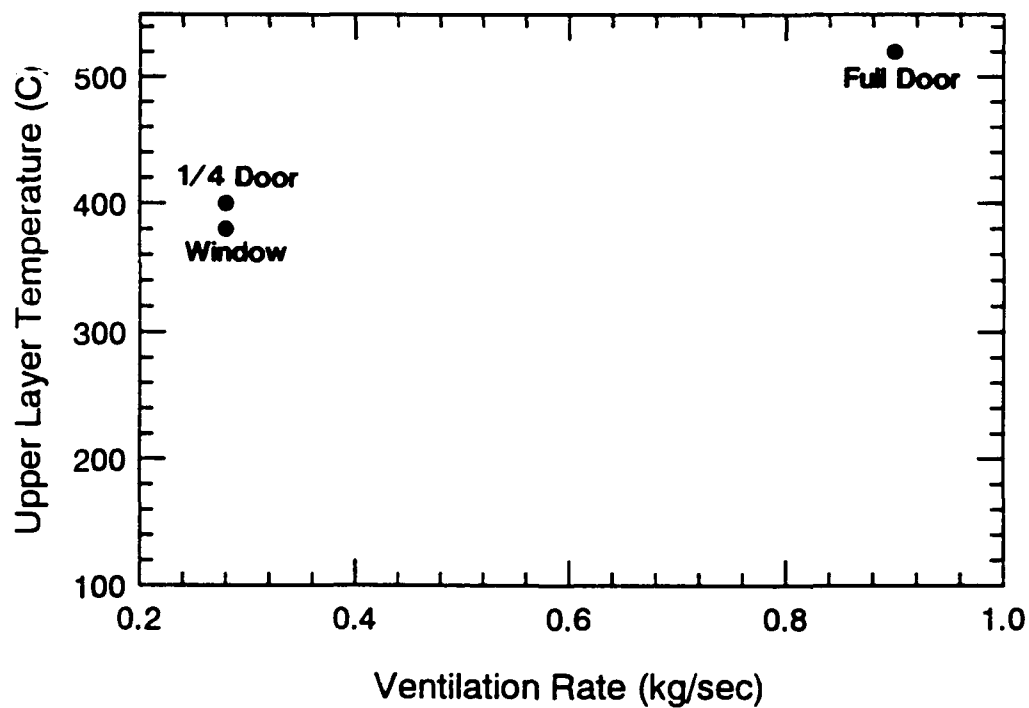
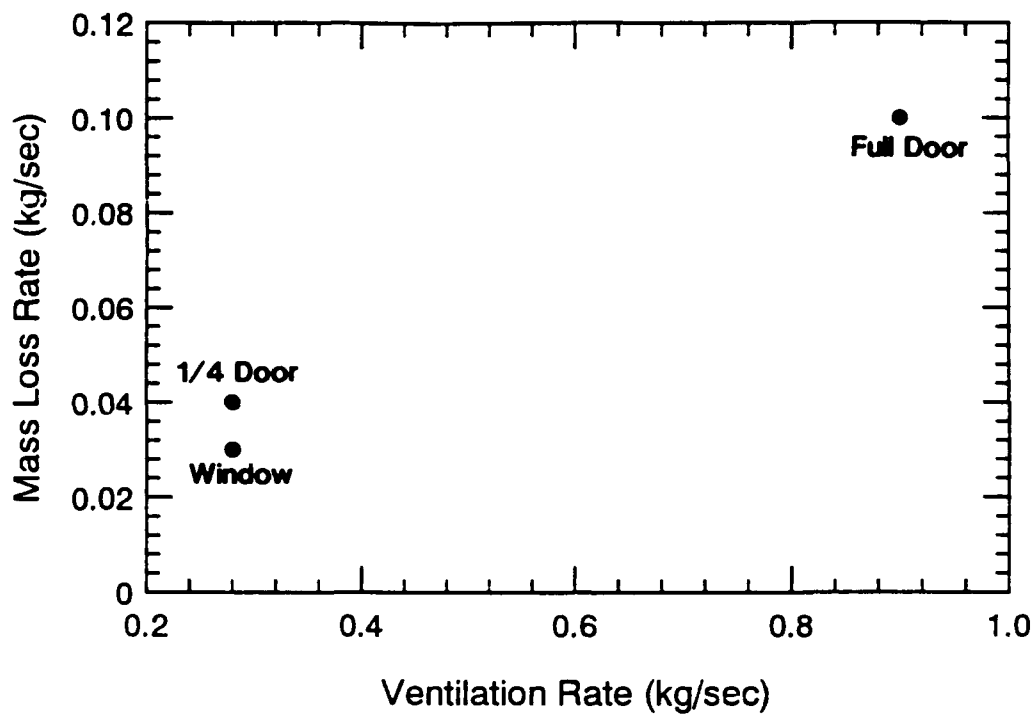


Figure 23. Mass Loss Rate and Temperature vs. Ventilation Rate for Wood Crib Tests (Series 1)

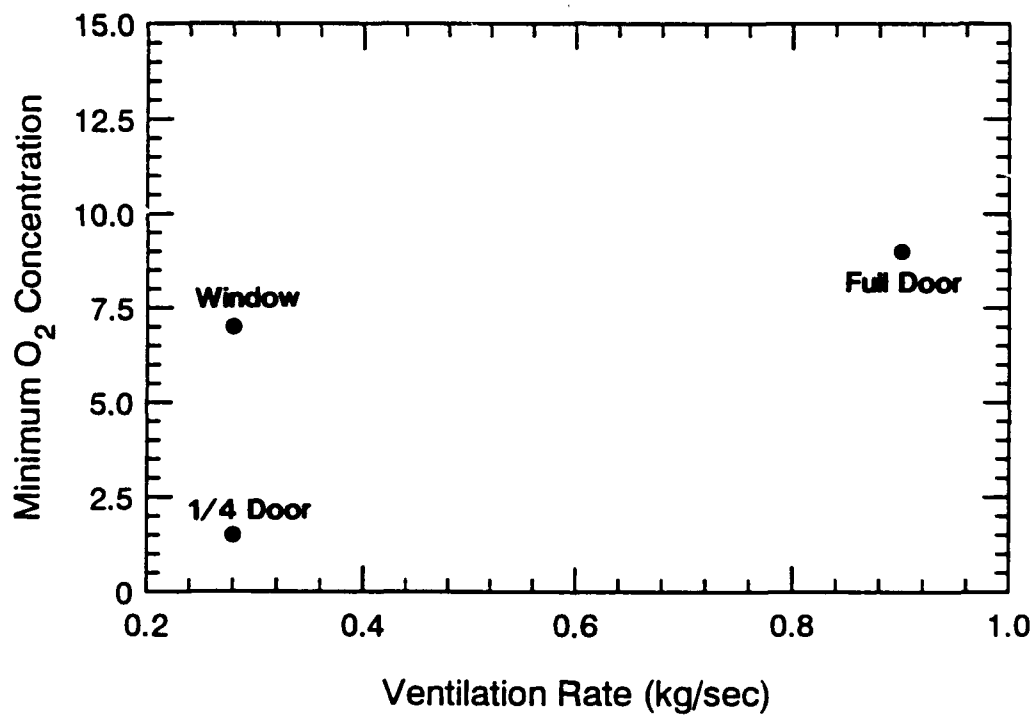


Figure 24. Minimum Oxygen Concentration vs. Ventilation Rate for Wood Crib Tests (Series 1)

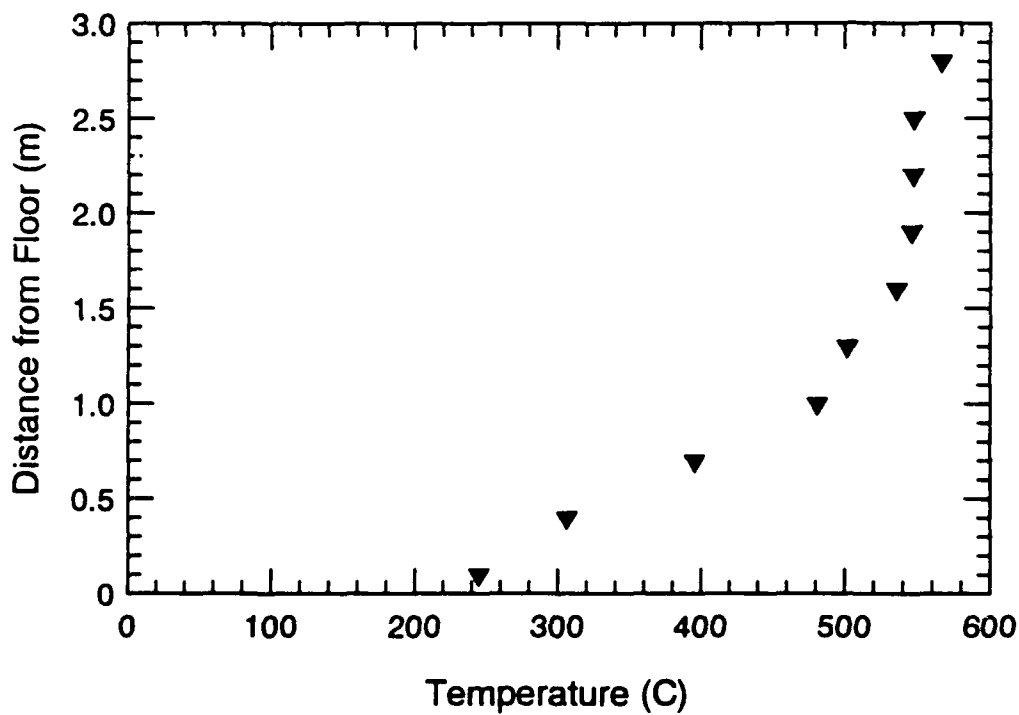
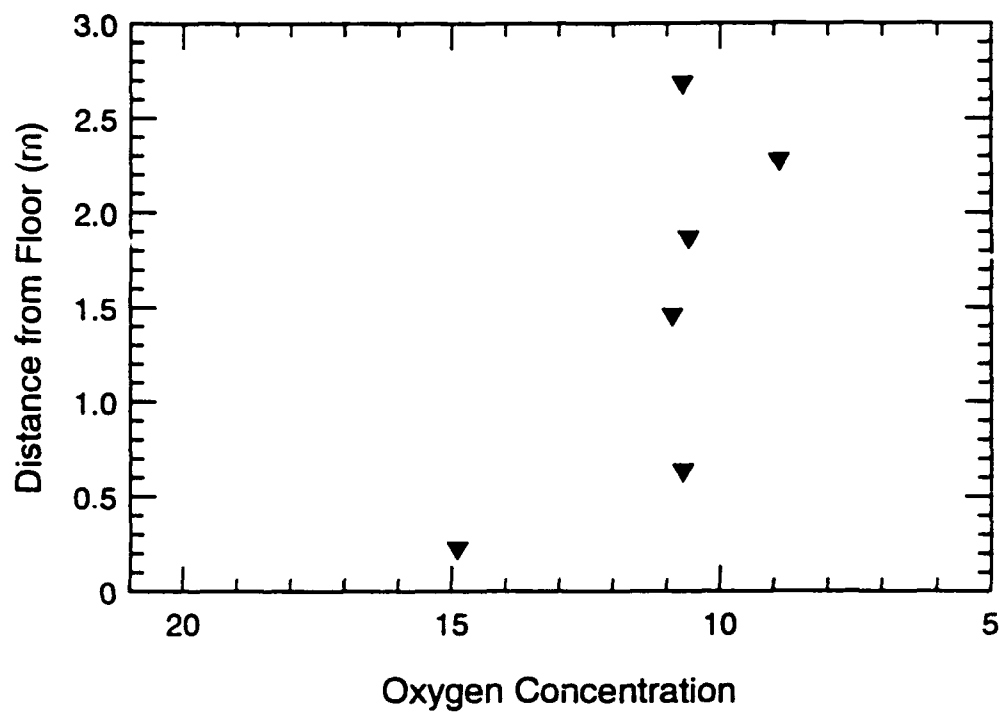


Figure 25. Vertical Oxygen Concentration and Temperature Profiles for S103

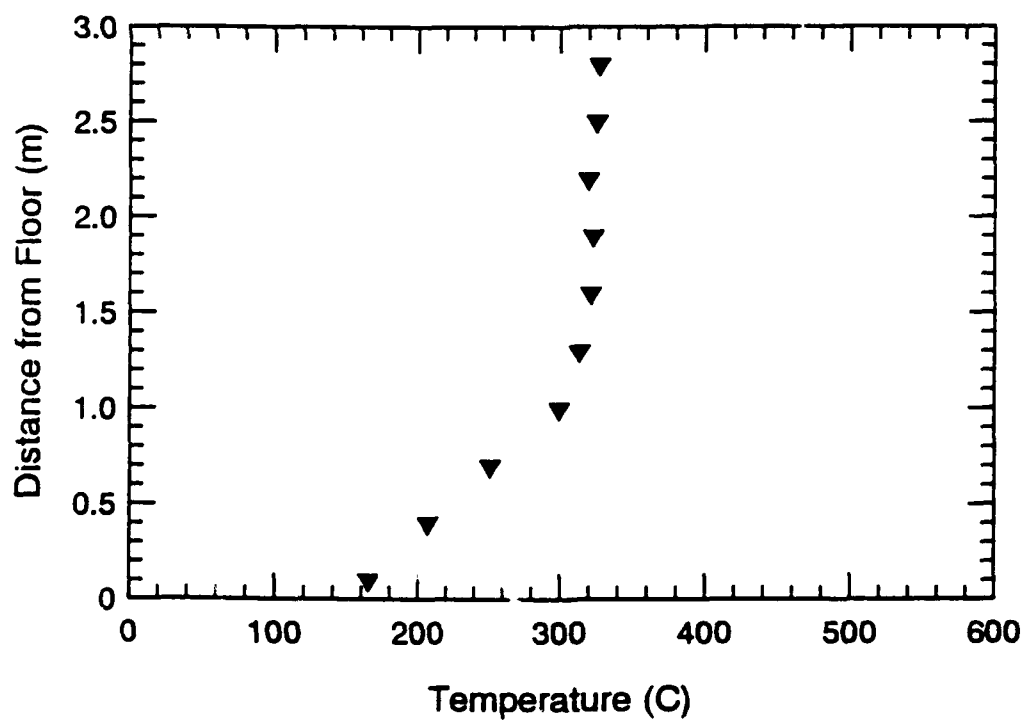
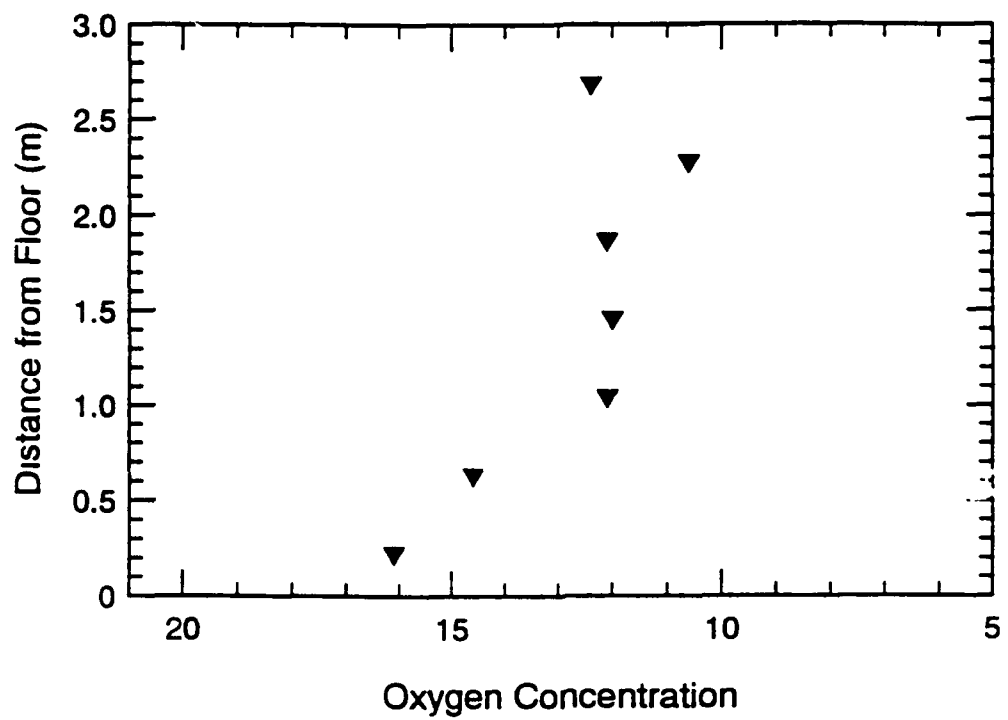


Figure 26. Vertical Oxygen Concentration and Temperature Profiles for S106

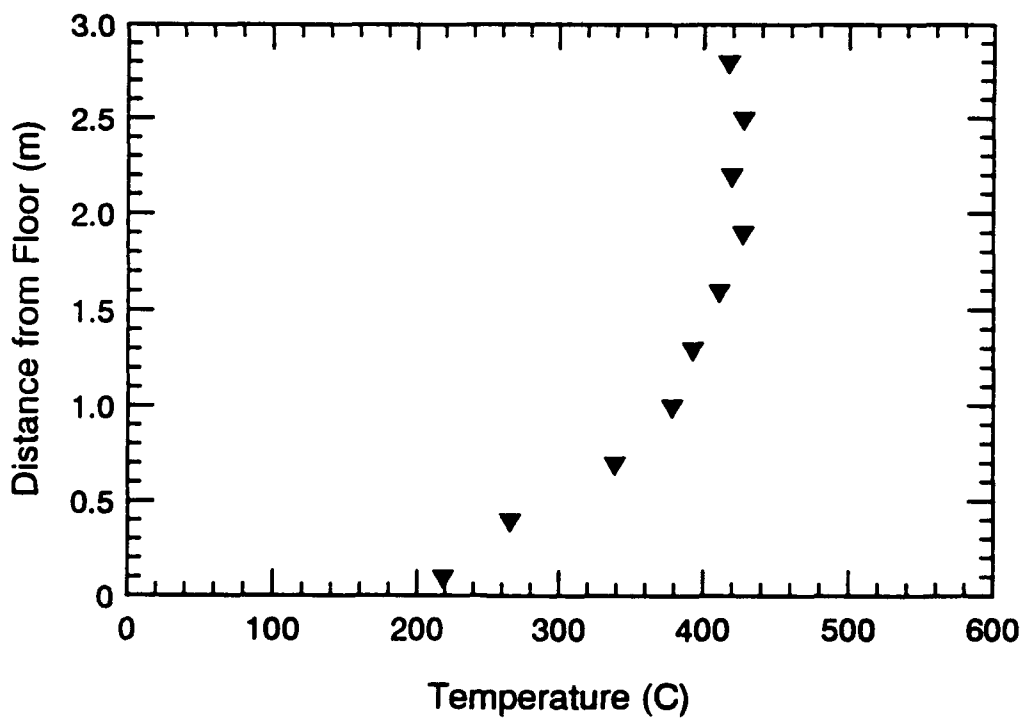
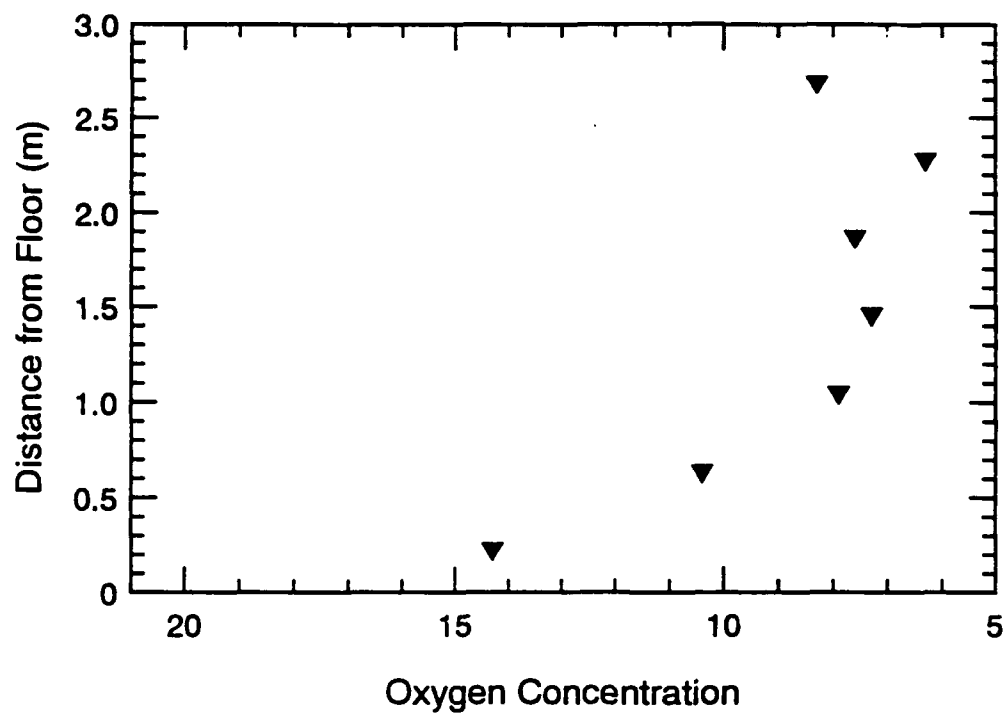


Figure 27. Vertical Oxygen Concentration and Temperature Profiles for S110

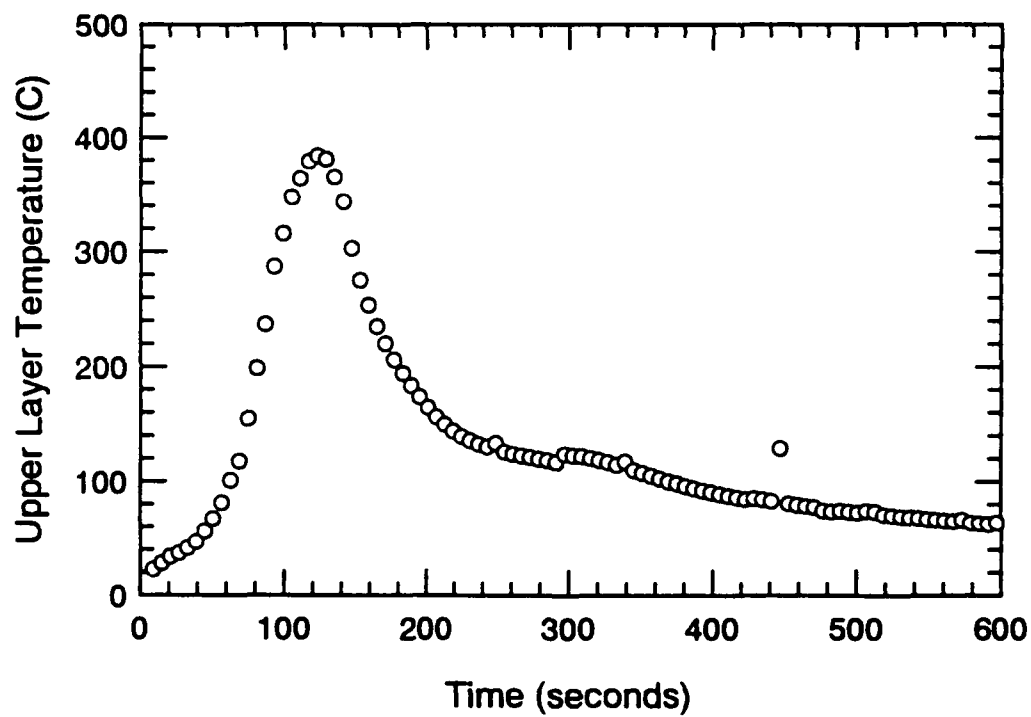
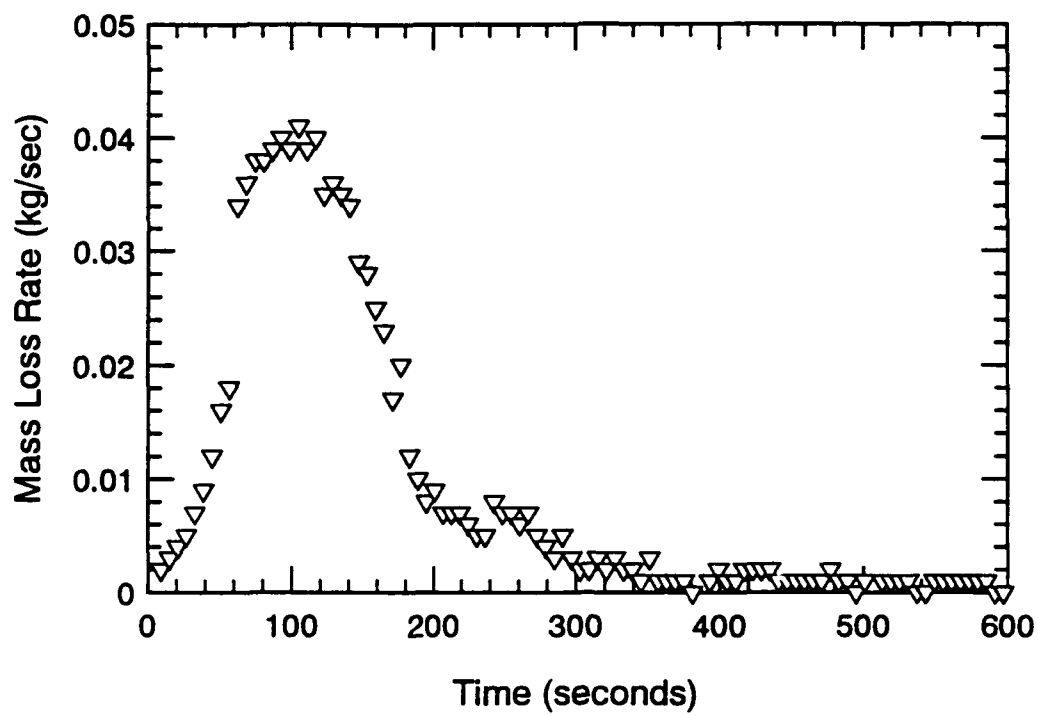


Figure 28. Mass Loss Rate and Upper Layer Temperature-Time Histories for S104

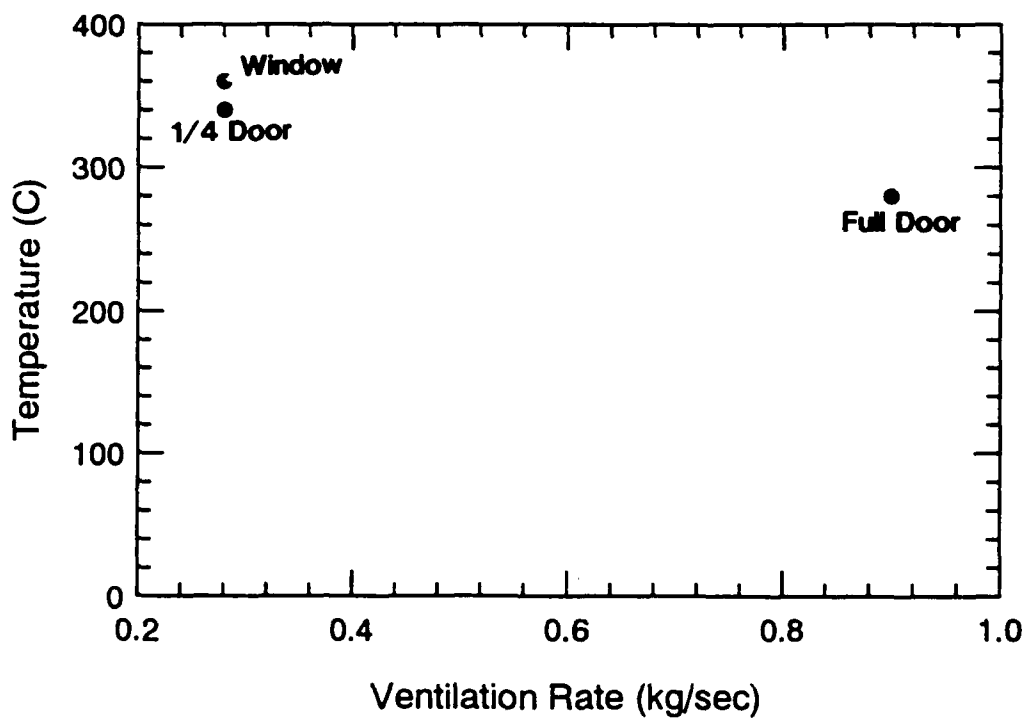
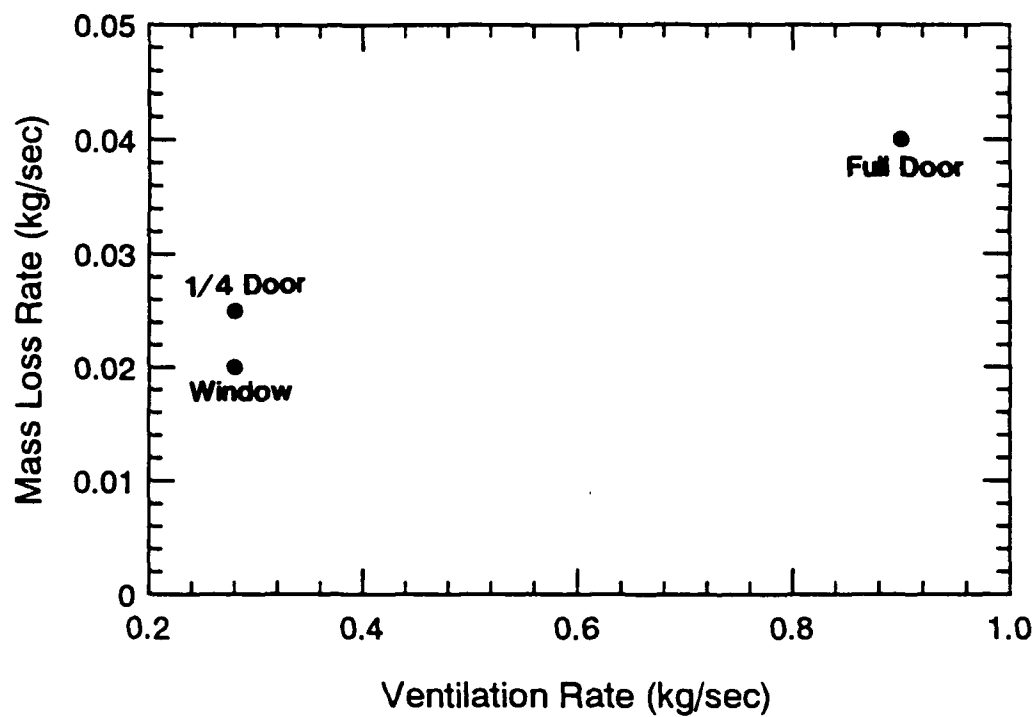


Figure 29. Mass Loss Rate and Temperature vs. Ventilation Rate for Polyurethane Tests (Series 1)

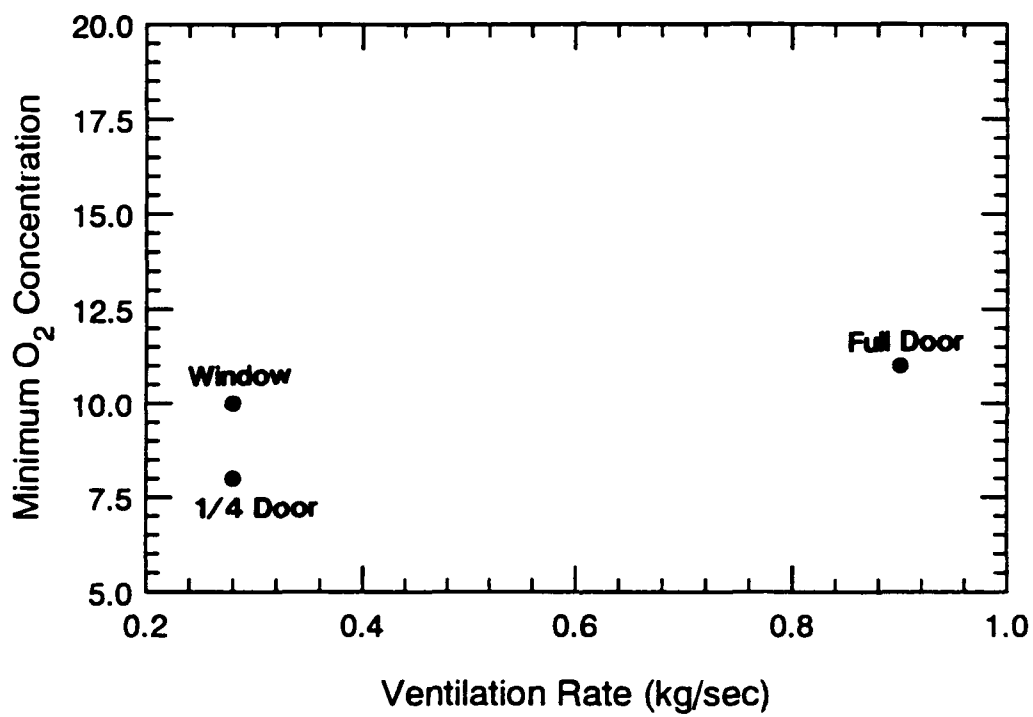


Figure 30. Minimum Oxygen Concentration vs. Ventilation Rate for Polyurethane Tests (Series 1)

ventilation rate. The lowest mass loss rate and highest temperature occurred with the window vent test.

Figures 31-33 show vertical oxygen and temperature profiles which represent the time where the mass loss rate and temperature peaked. The most striking characteristic of these plots is the oxygen concentration at 2.3 m. In each test, this concentration is at least 4% lower than on any other branch. No explanation can be offered for this behavior. The calibration of the analyzer was checked, and there was no justification for disqualifying these measurements. Ignoring these points, stratification in oxygen concentration is seen between the lowest and second lowest branch. This separation is the most pronounced in Figure 33 (quarter door vent) where the oxygen concentration increases from 13% to 19% at the base. The window vent test appears to be the most well-mixed while the cleanest layer division occurred in the quarter door vent test.

Temperature profiles all show a similar shape which favors a two layer system. Each test exhibits an upper layer which is nearly uniform thermally. At a height near 1 m above the floor, this uniform profile changes as it begins to gradually decrease in a linear fashion to the floor. This flat slope probably occurs because the temperature rise period is too short for the entire compartment to be heated.

6.1.5 Additional Tests - Diesel Pan Fires (ADD1, ADD2, ADD3)

As explained previously, the purpose of these tests was to generate upper layer temperatures closer to 600 °C since there was a lack of data in this area. This effort was unsuccessful as the highest temperature was 440 °C.

Air flow rates in these tests were higher than those measured in previous door vent tests. An average value of 1.25 kg/sec was measured compared to 0.9 kg/sec which was measured in earlier tests. This value did not change significantly for the three tests where the remote ventilation (i.e. corridor door, stairtower door, etc.) was changed suggesting that it was not a large factor.

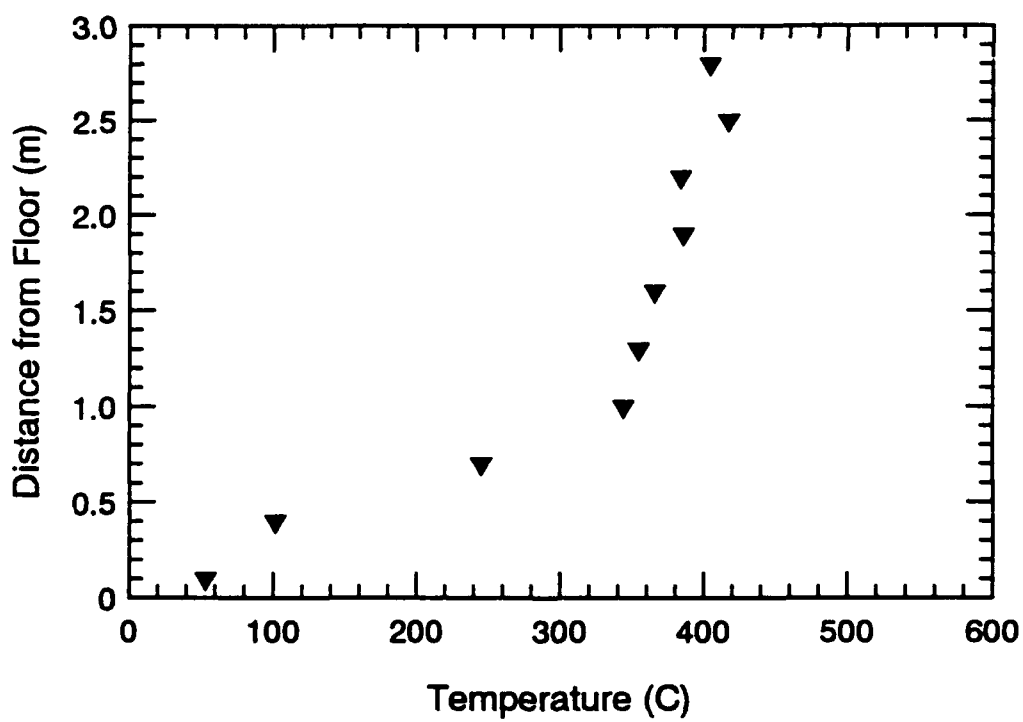
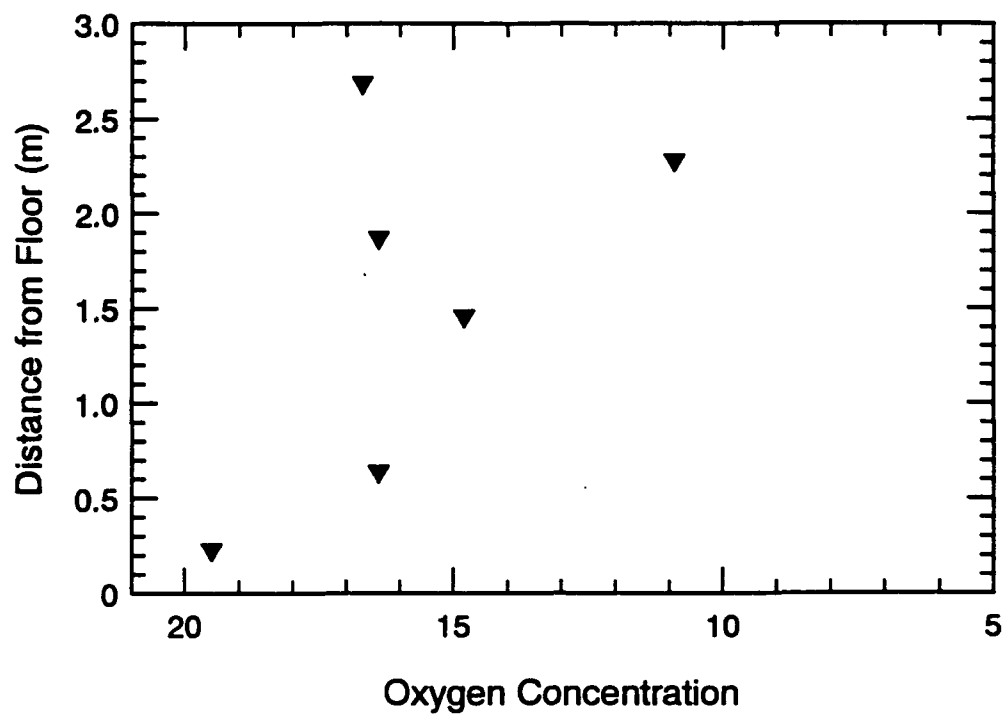


Figure 31. Vertical Oxygen Concentration and Temperature Profiles for S104

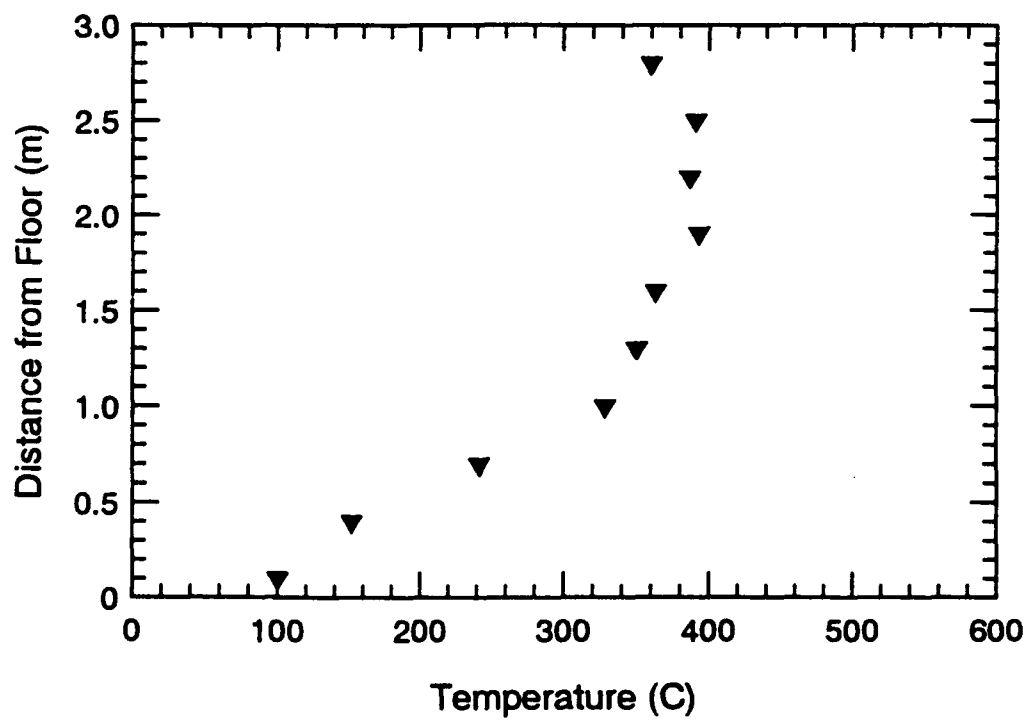
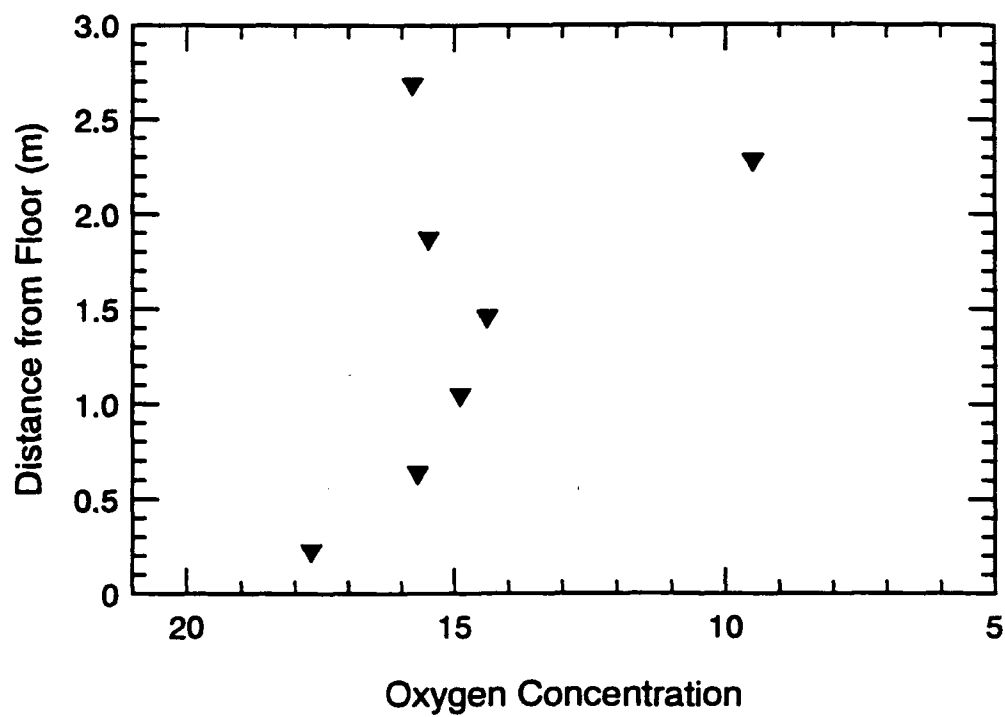


Figure 32. Vertical Oxygen Concentration and Temperature Profiles for S108

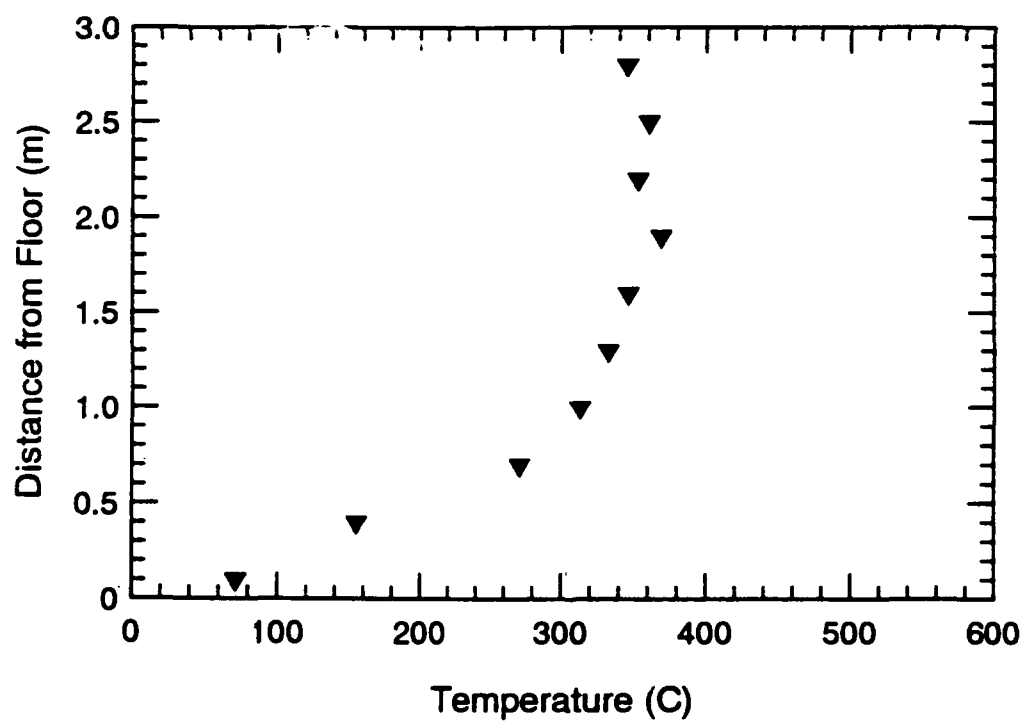
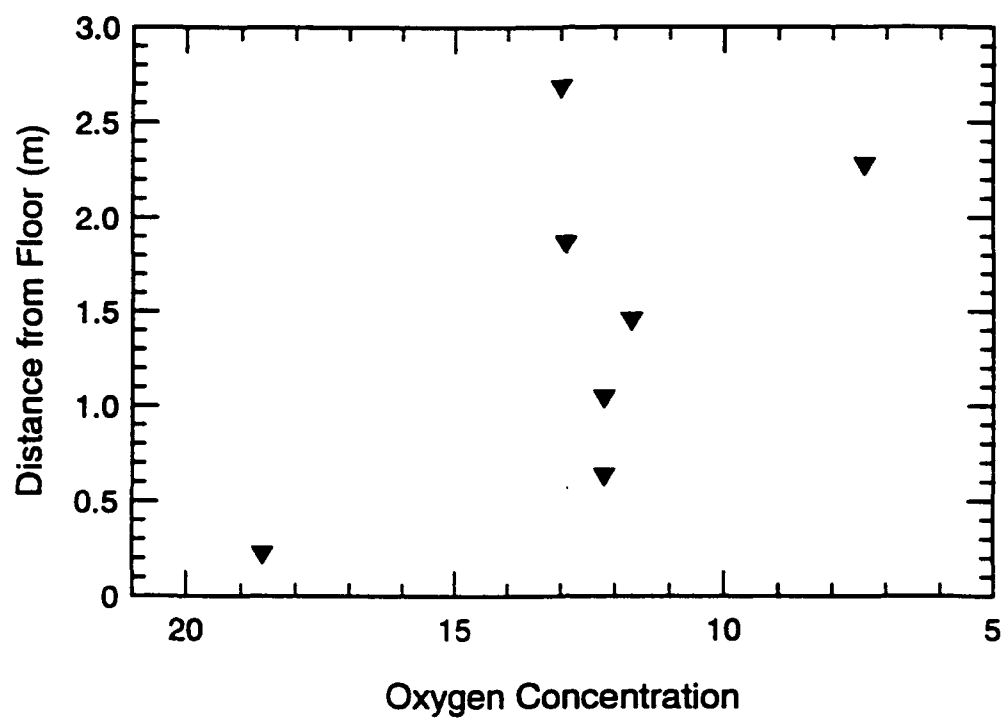


Figure 33. Vertical Oxygen Concentration and Temperature Profiles for S109

The mass loss rate, minimum oxygen concentration, and upper layer temperature were very similar between tests. The temperature was slightly higher, and the minimum oxygen concentration was slightly lower in ADD2 which may be attributed to closing off the remote ventilation.

Vertical oxygen and temperature profiles are nearly identical for each test (Figures 34-36). Each test shows some thermal stratification and a gradient in oxygen concentration near the fire base.

6.2 Series 2 Tests - Forced Ventilation Fires

6.2.1 Overview

In general, these fires produced environments which showed no clear thermal interface. In addition, the tests appeared well-mixed from a gas species standpoint.

Air flow measurements showed significant differences in the supply and exhaust rate during testing. Prior to testing, air velocities were recorded at each damper position using a hot wire anemometer. The supply rates agreed more closely with these values so the exhaust rate measurements were not used in the analysis.

A summary of these tests is provided in Table 5. The values listed are the same as those in Table 4 except the cold layer temperature is not listed since there was only one thermal layer. Appendix B includes the time histories which summarize these tests.

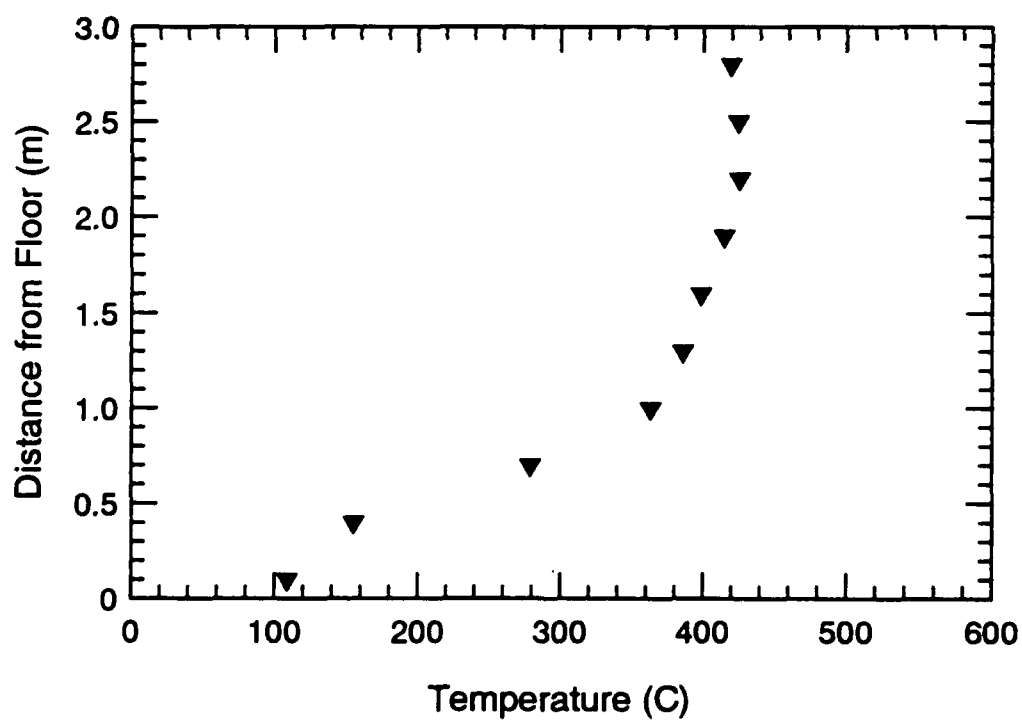
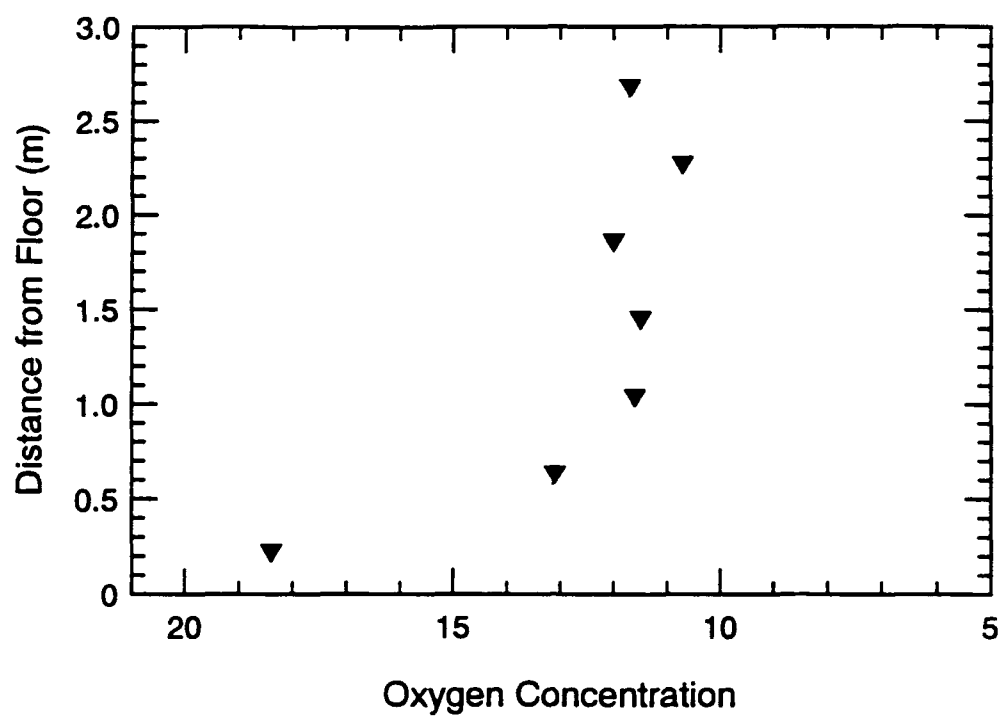


Figure 34. Vertical Oxygen Concentration and Temperature Profiles for ADD1

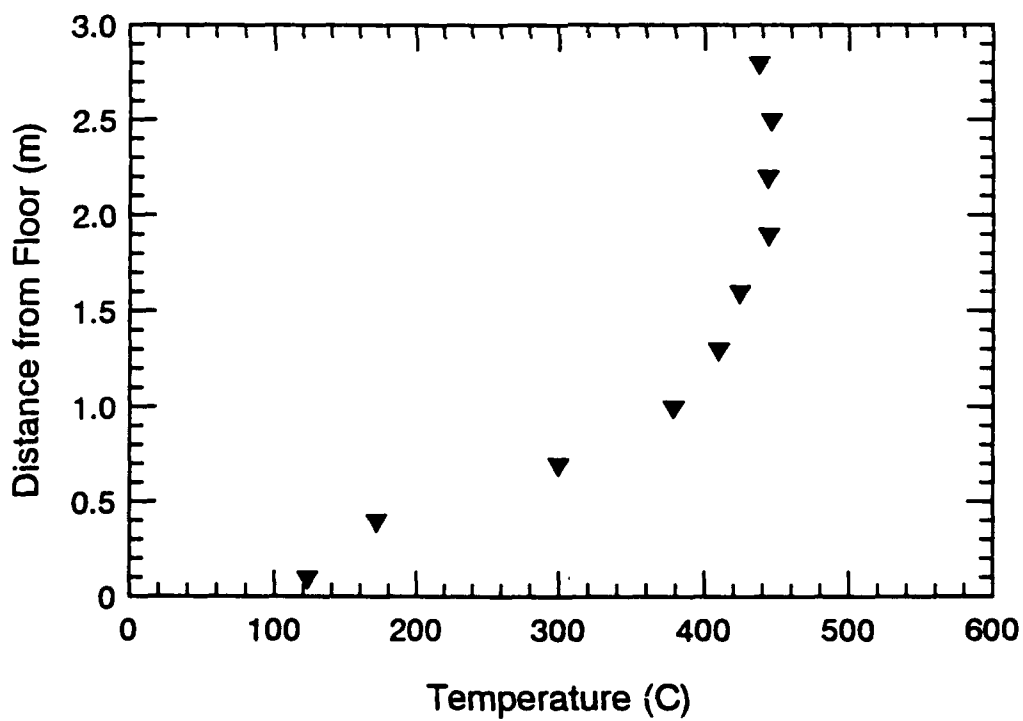
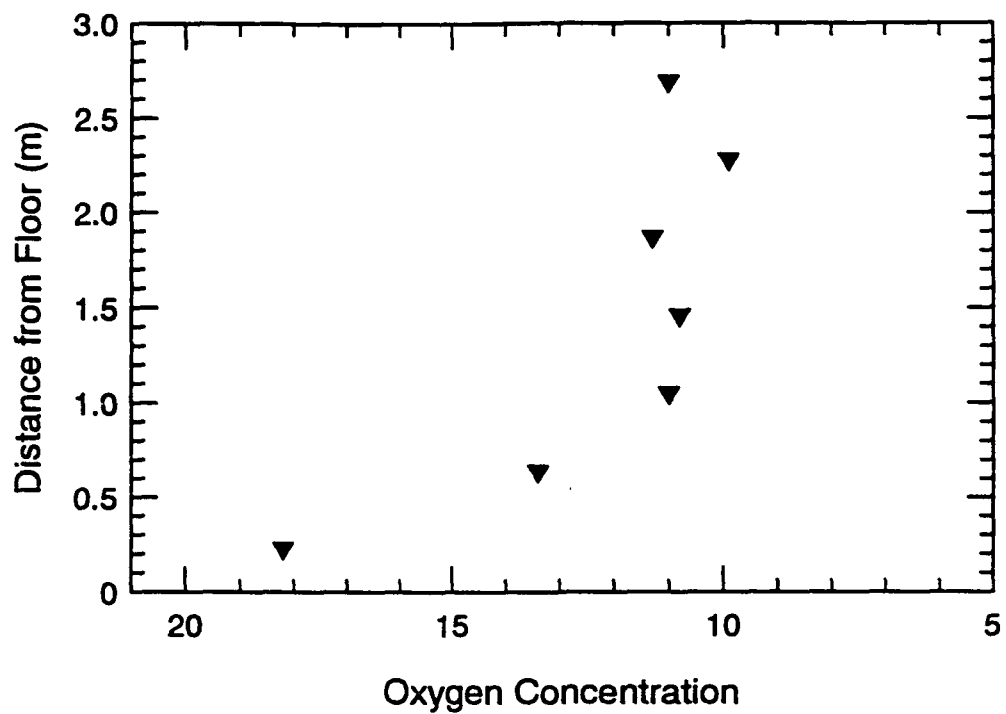


Figure 35. Vertical Oxygen Concentration and Temperature Profiles for ADD2

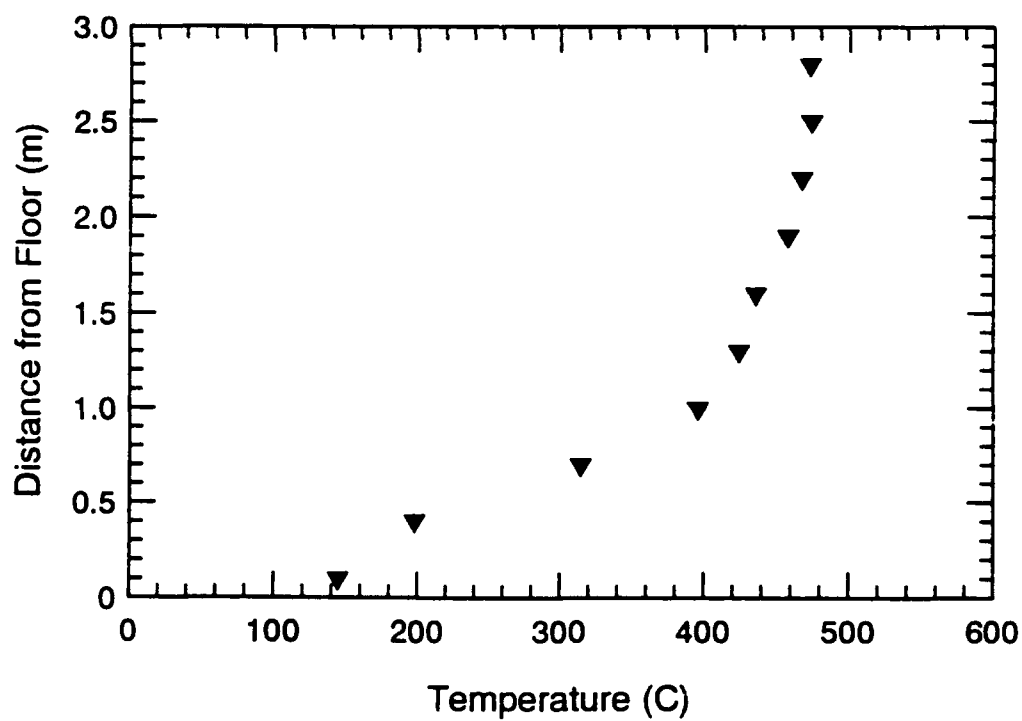
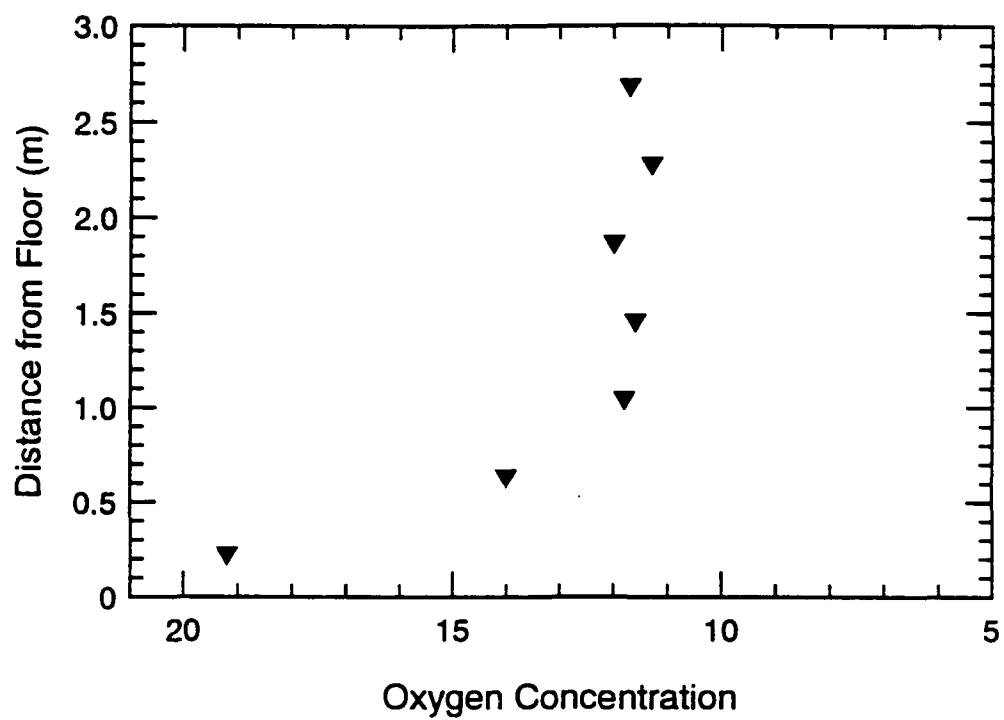


Figure 36. Vertical Oxygen Concentration and Temperature Profiles for ADD3

Table 5. Series 2 - Summary of Results

Test	Fuel Type	Ventilation Rate (m ³ /sec)	\dot{m}_f (kg/s)	\dot{Q}_{Tb} (kW)	T_H (°C)	T_{OH} (°C)		T_{BULK} (°C)		O_2 (%-wet)
						INT	EXT	INT	EXT	
S201	62 cm Pan	0.38	0.005	225	160	60	55	80	70	17
S202	Wood Crib	0.38	0.036	470	360	220	210	260	240	11.5
S203	84 cm Pan	0.38	0.008	360	215	90	85	120	110	13.5
S204	Polyurethane	0.38	0.014	360	250	60	60	73	68	14
S205	Polyurethane	0.61	0.02	520	260	55	55	62	58	15
S206	Wood Crib	0.61	0.07	900	515	290	270	330	300	9.5
S207	62 cm Pan	0.61	0.006	270	160	55	55	60	57	18
S208	84 cm Pan	0.61	0.0095	430	225	93	90	110	105	15
S209	Wood Crib	0.25	0.018	270	270	162	158	180	150	12
S210	62 cm Pan	0.25	0.004	180	155	50	50	70	62	15
S211	84 cm Pan	0.25	0.006	270	220	75	75	105	95	12
S212	Polyurethane	0.25	0.01	300	260	68	63	80	70	15

\dot{m}_f = Mass Loss Rate
 \dot{Q}_{Tb} = Theoretical Heat Release Rate
 T_H = Upper Layer Temperature
 T_{OH} = Overhead Temperature
 T_{BULK} = Bulkhead Temperature (85 cm below overhead deck)
 O_2 = Minimum Oxygen Concentration
 INT = Interior Surface
 EXT = Exterior Surface

6.2.2 Diesel Pan Fires

6.2.2.1 62 cm Diameter Pan (S201, S207, S210)

From Figures 37 and 38, it is seen that the mass loss rate and the minimum oxygen concentration increase with increasing ventilation rate. The upper layer temperatures seem to be unaffected by the ventilation rate suggesting that the added ventilation is cooling the compartment, so no net temperature rise is measured.

Examination of the vertical temperature and oxygen profiles in Figures 39-41 suggests that the environments were well-mixed and one-layer. This linearity is most clear with the highest ventilation rate test (S207).

6.2.2.2 84 cm Diameter Pan (S203, S208, S211)

The same trends with the mass loss rate, minimum oxygen concentration, and upper layer temperature are apparent in these tests as for the 62 cm diameter pan tests. The mass loss rate and minimum oxygen concentration increase with ventilation rate while the temperature is not affected (Figures 42-43). In Figures 44-46, there is no clear interface seen in the temperature profiles. The oxygen concentrations, however, increase as they get closer to the floor until a height of 0.6 m where they level off. This behavior suggests that a small amount of stratification is present.

6.2.3 Wood Crib Fires (S202, S206, S209)

It is clear from Figure 47 that the mass loss rate and upper layer temperature are affected considerably by the ventilation rate. Despite the added ventilation, though, the minimum oxygen concentration decreases (Figure 48).

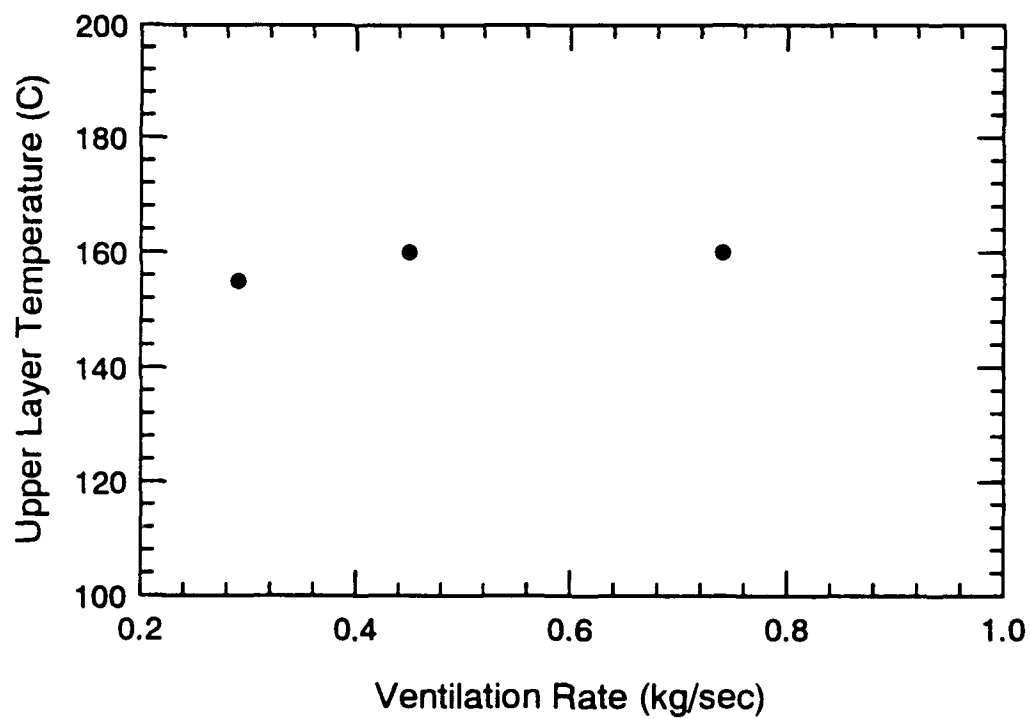
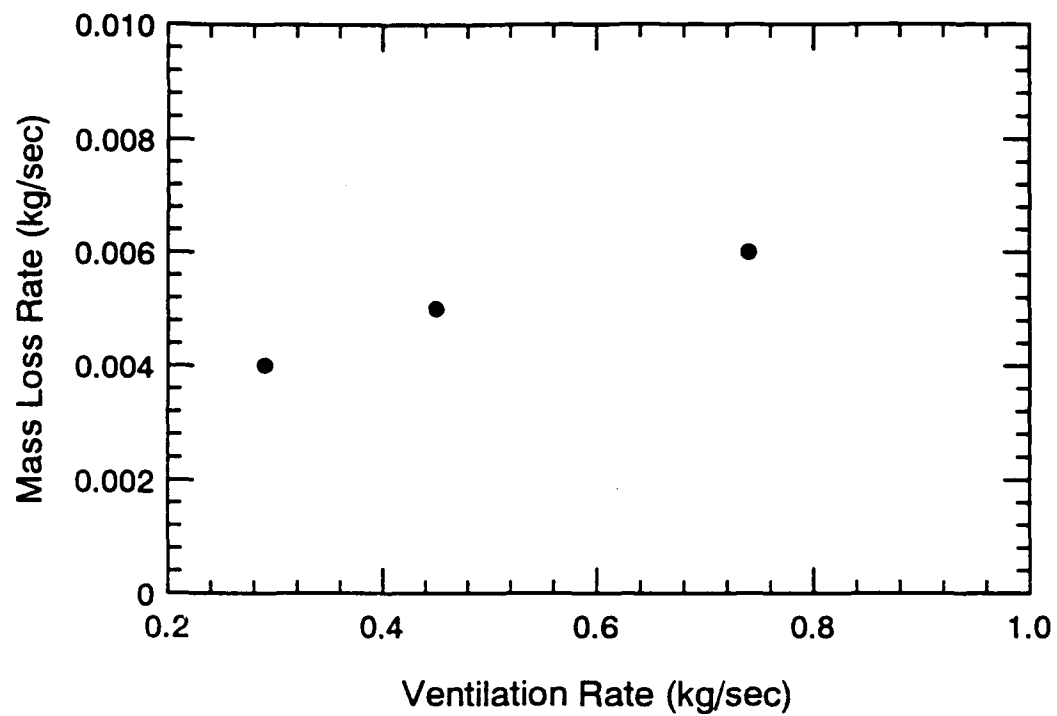


Figure 37. Mass Loss Rate and Temperature vs. Ventilation Rate for 62 cm Diameter Pan Tests (Series 2)

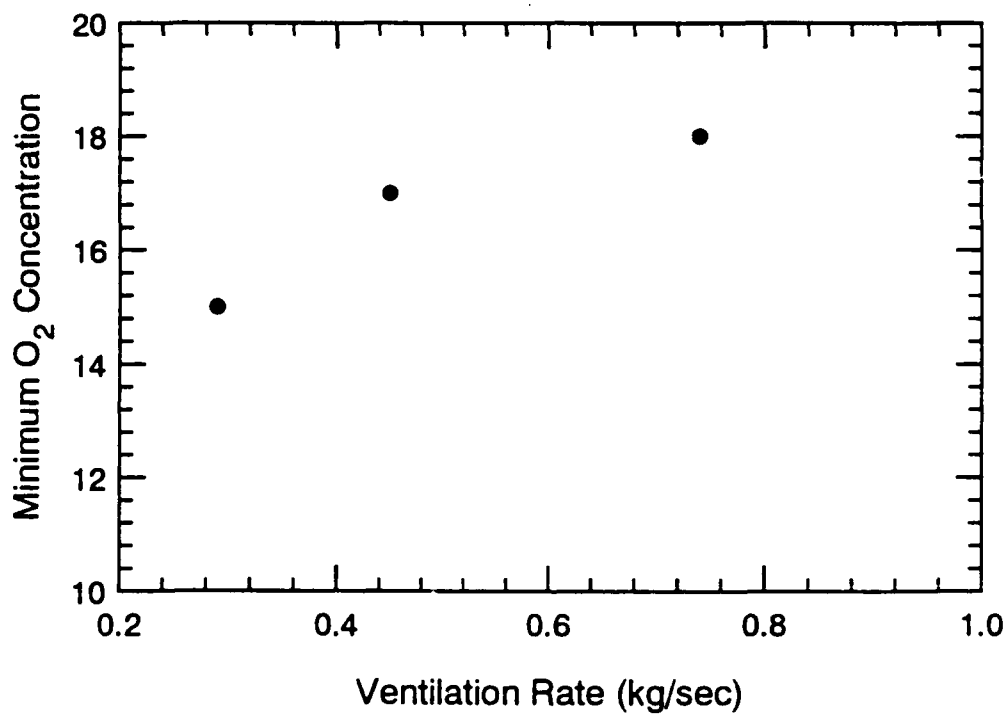


Figure 38. Minimum Oxygen Concentration vs. Ventilation Rate for 62 cm Diameter Pan Tests (Series 2)

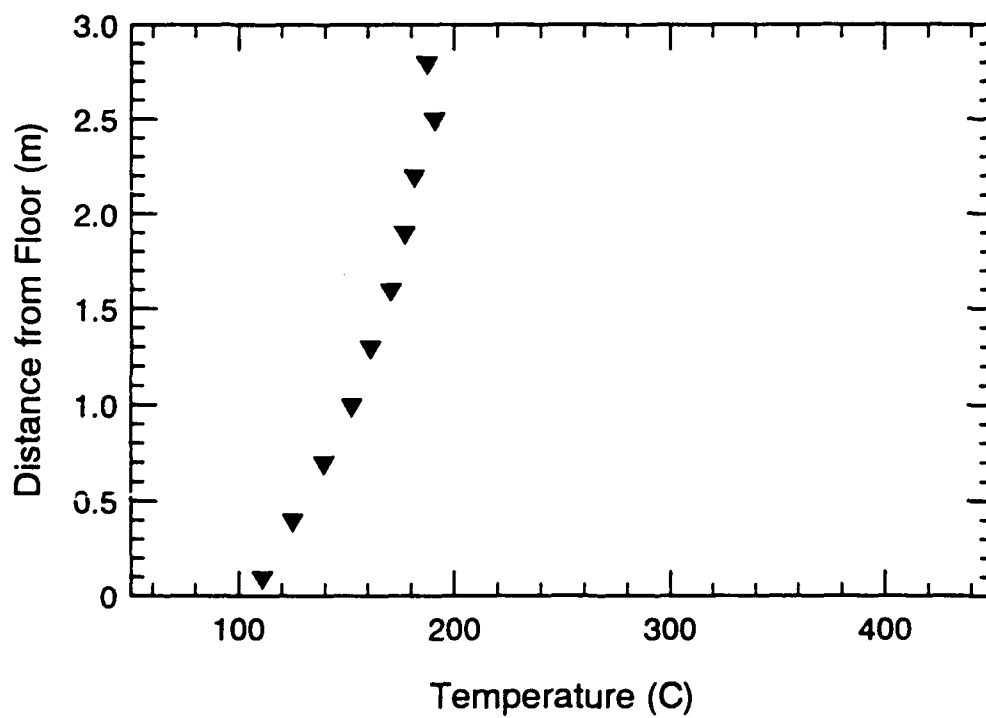
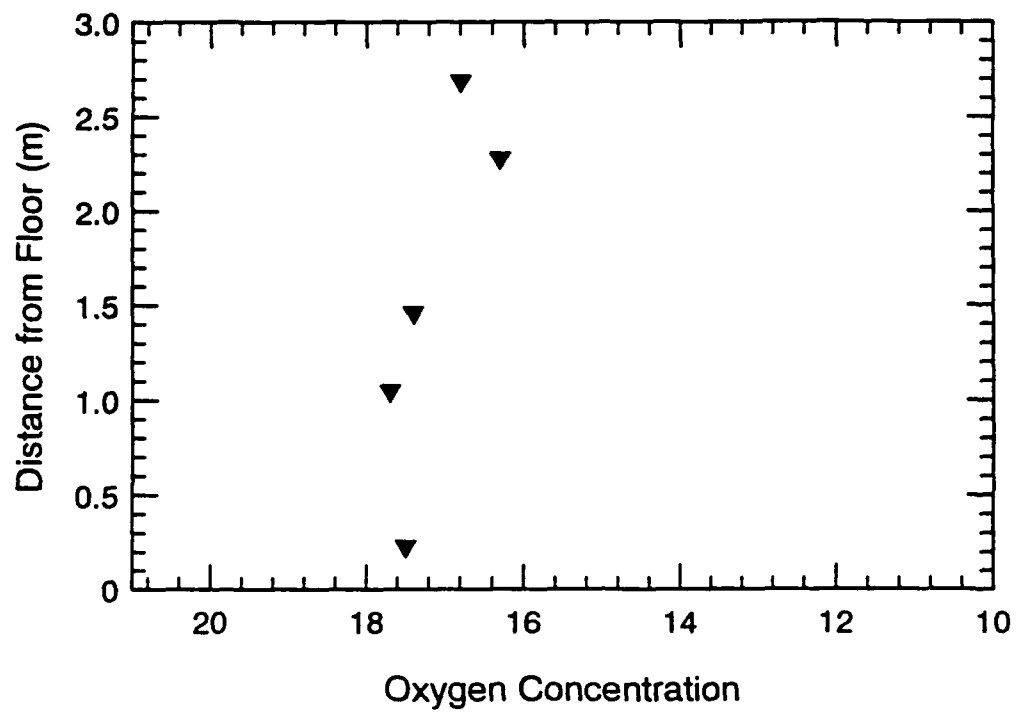


Figure 39. Vertical Oxygen Concentration and Temperature Profiles for S201

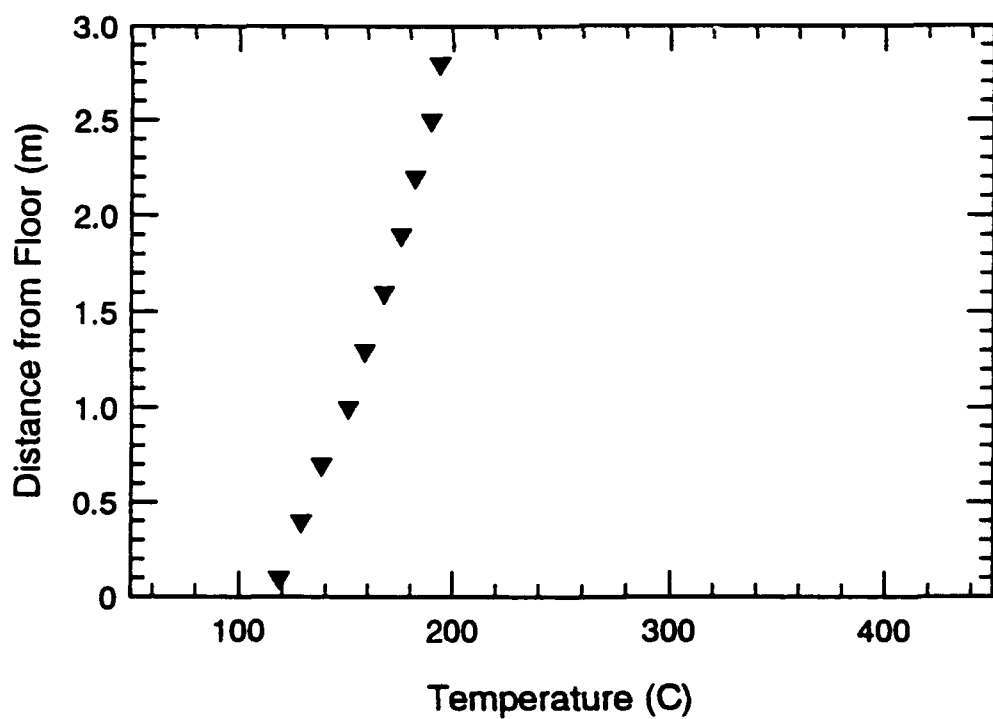
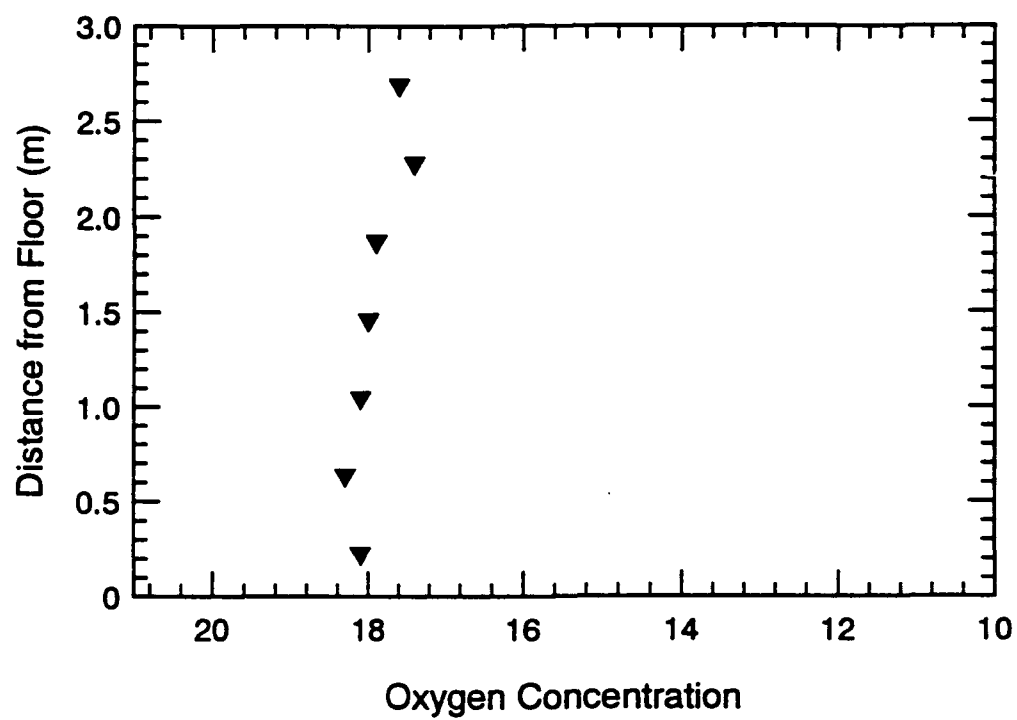


Figure 40. Vertical Oxygen Concentration and Temperature Profiles for S207

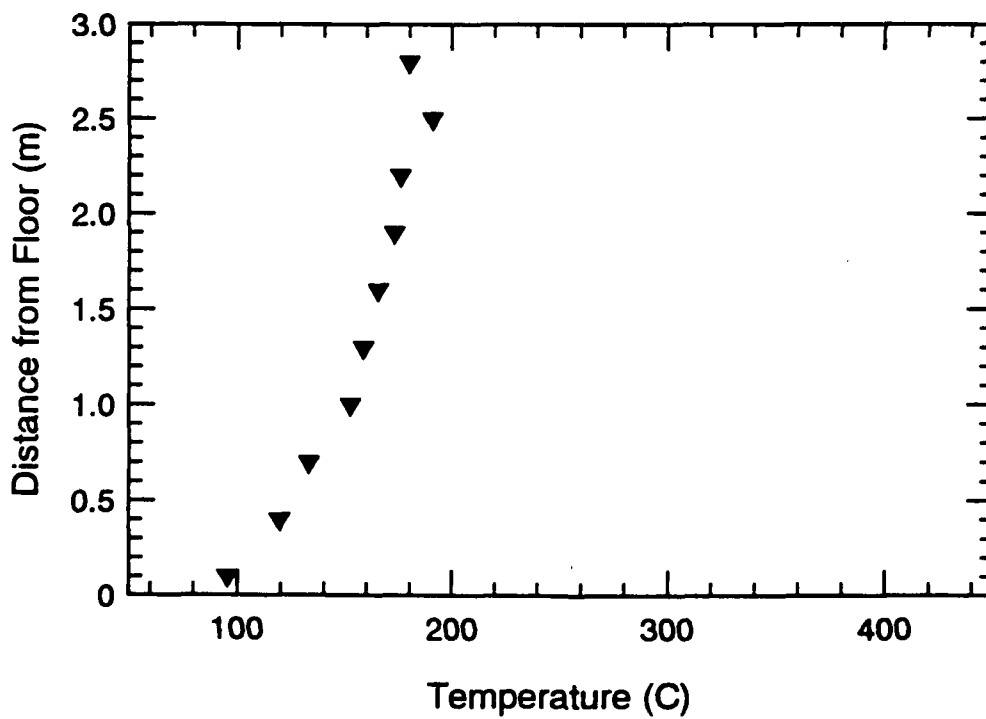
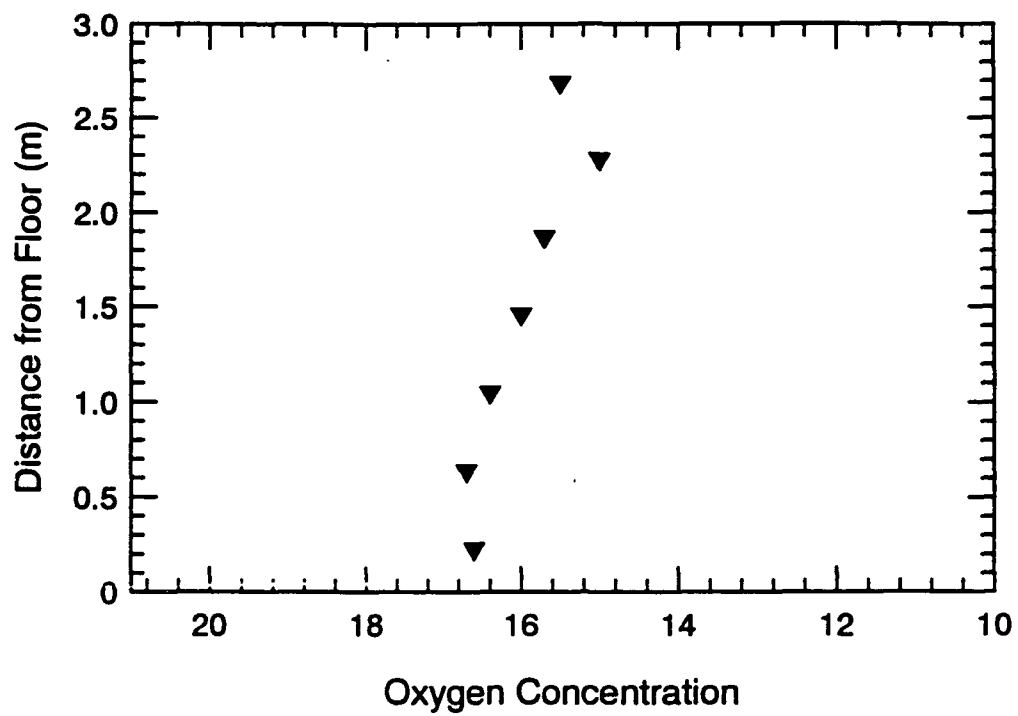


Figure 41. Vertical Oxygen Concentration and Temperature Profiles for S210

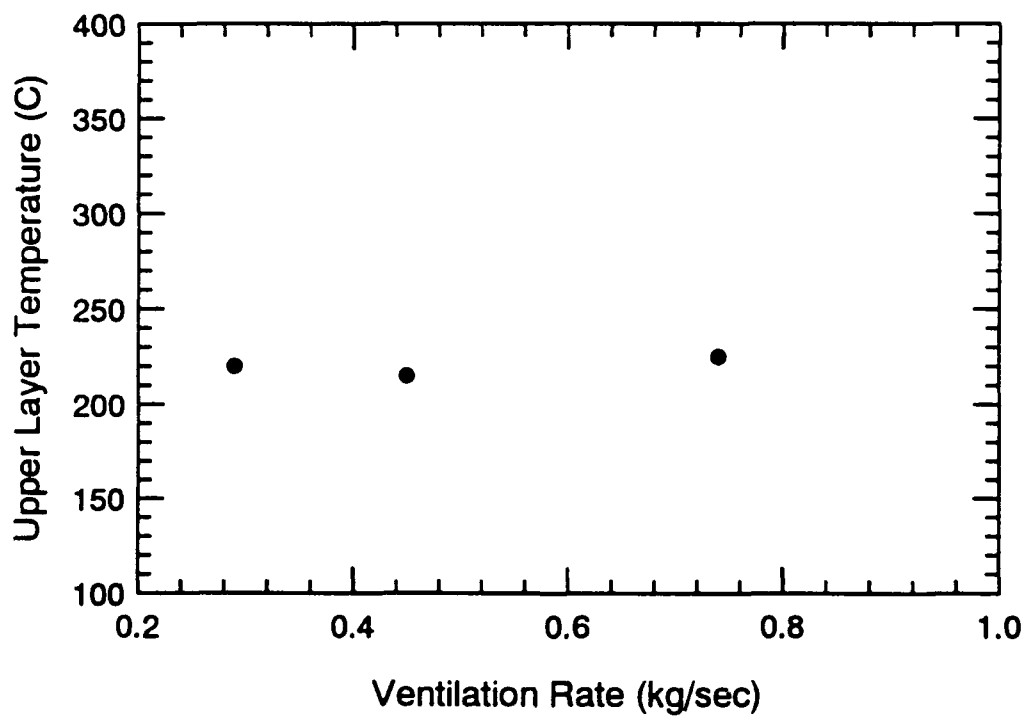
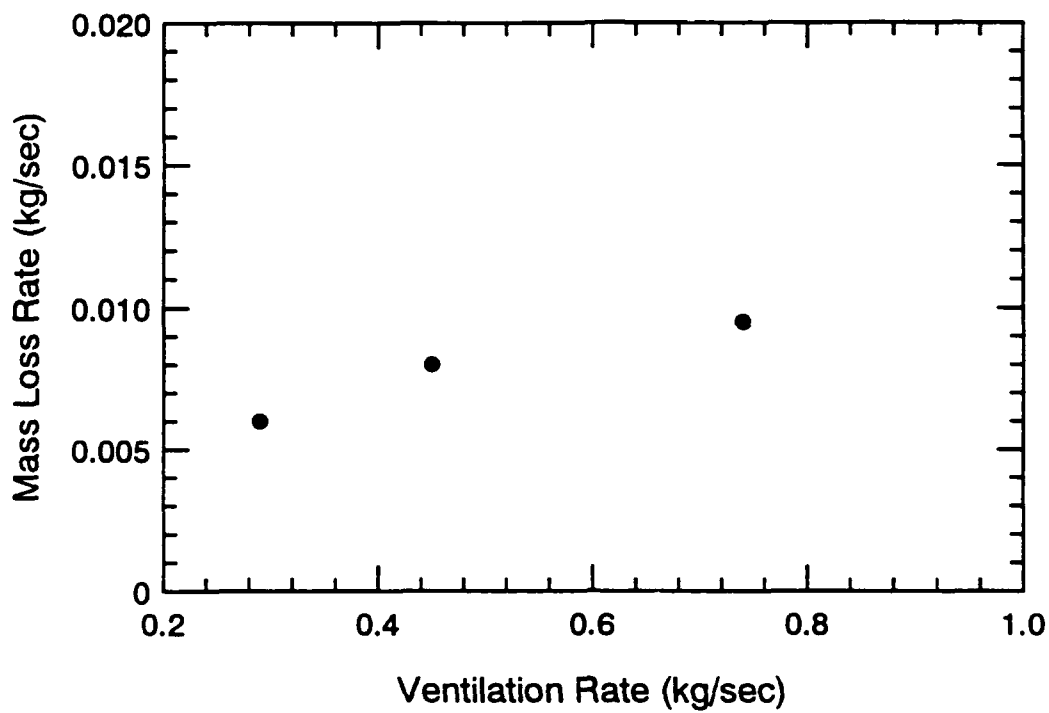


Figure 42. Mass Loss Rate and Temperature vs. Ventilation Rate for 84 cm Diameter Pan Tests (Series 2)

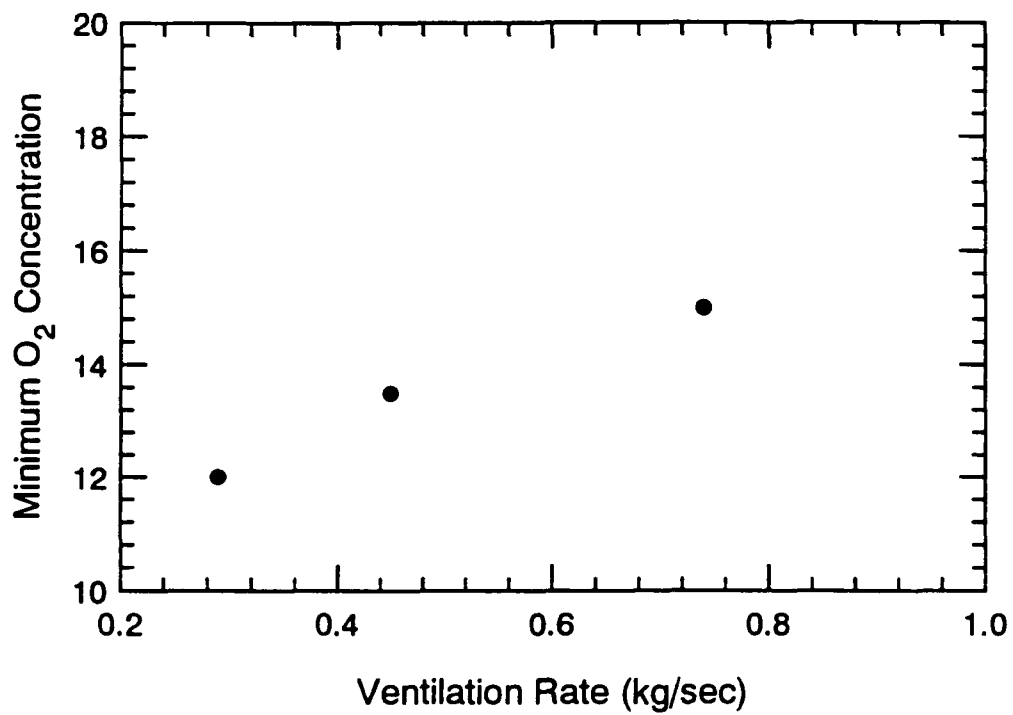


Figure 43. Minimum Oxygen Concentration vs. Ventilation Rate for 84 cm Diameter Pan Tests (Series 2)

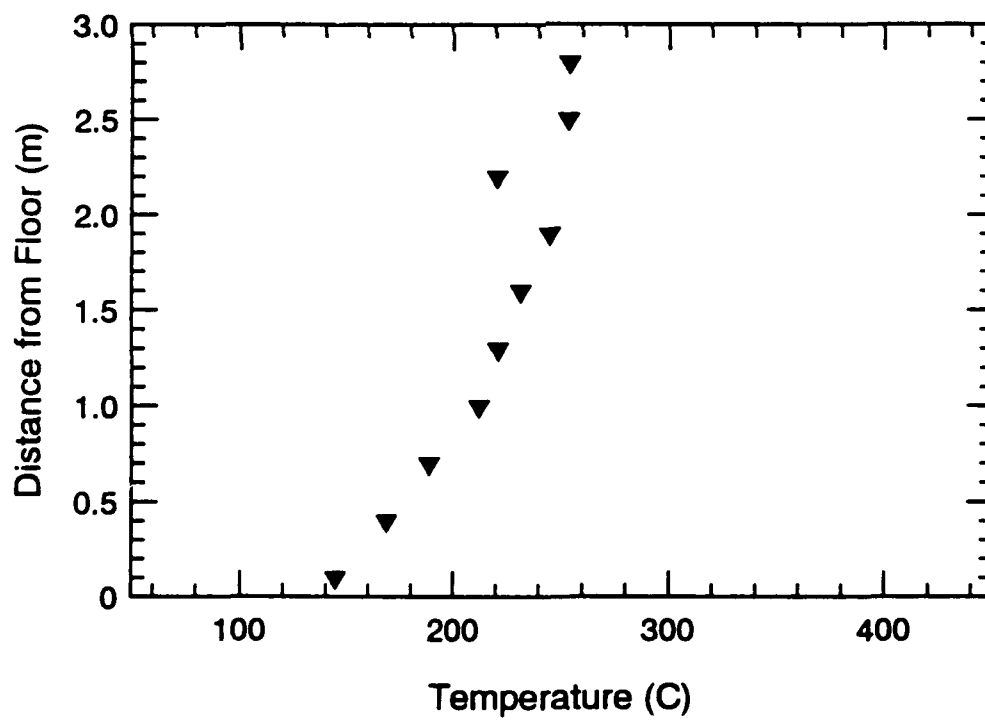
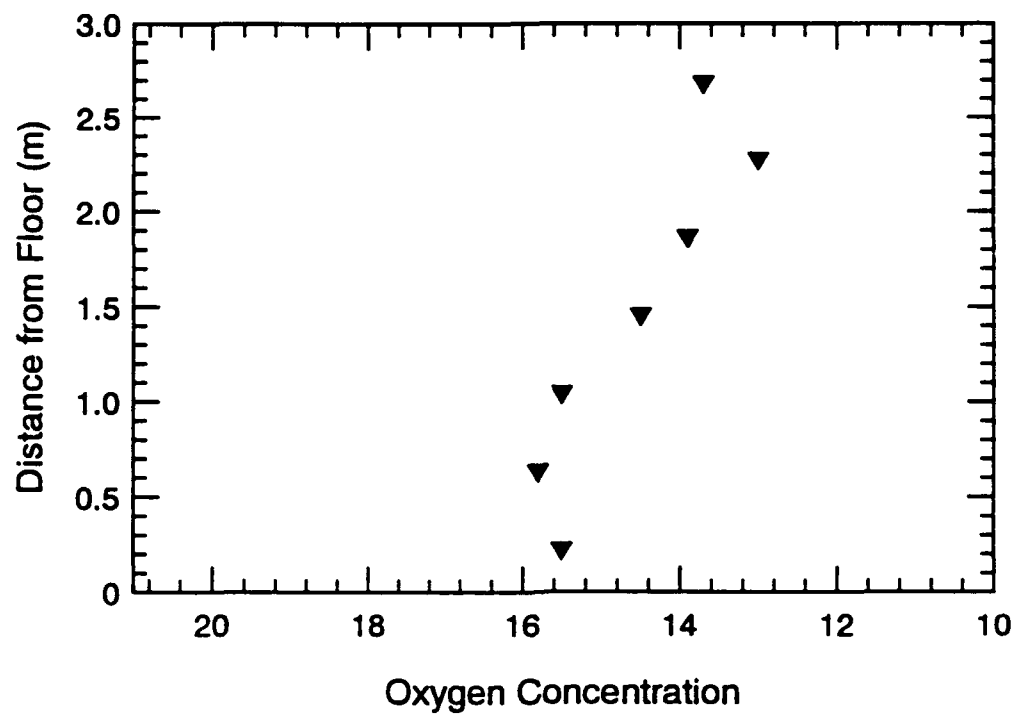


Figure 44. Vertical Oxygen Concentration and Temperature Profiles for S203

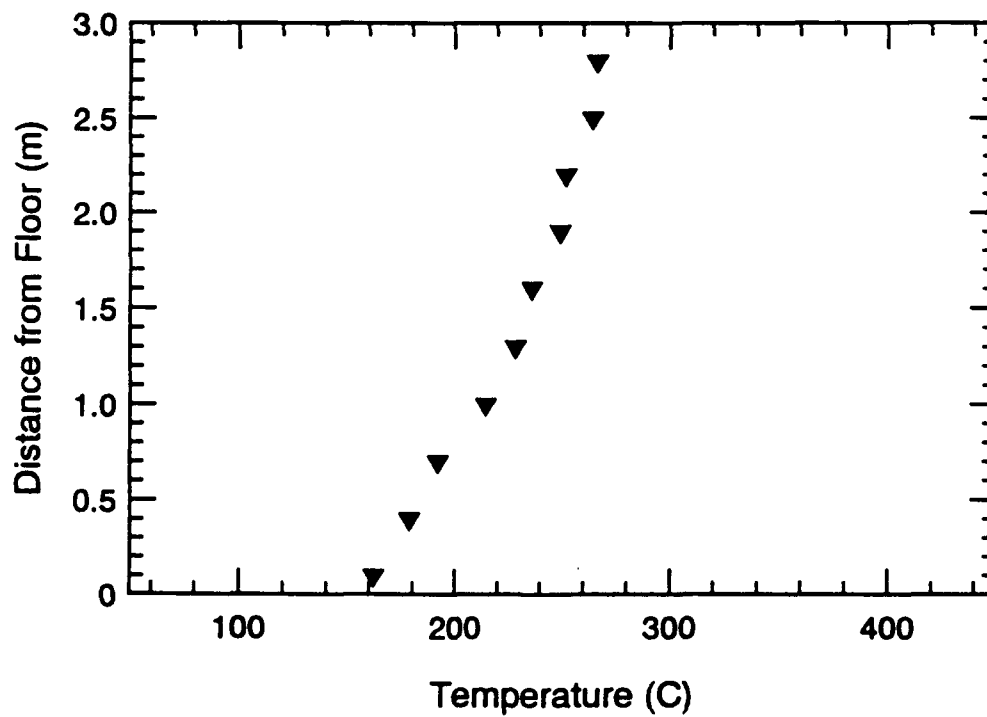
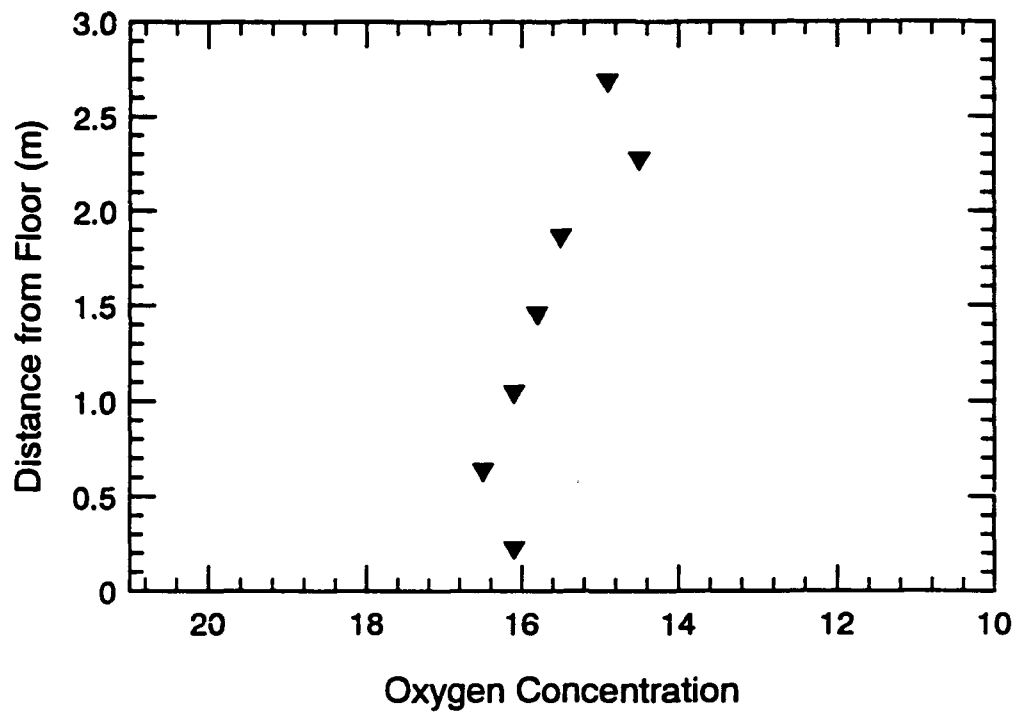


Figure 45. Vertical Oxygen Concentration and Temperature Profiles for S208

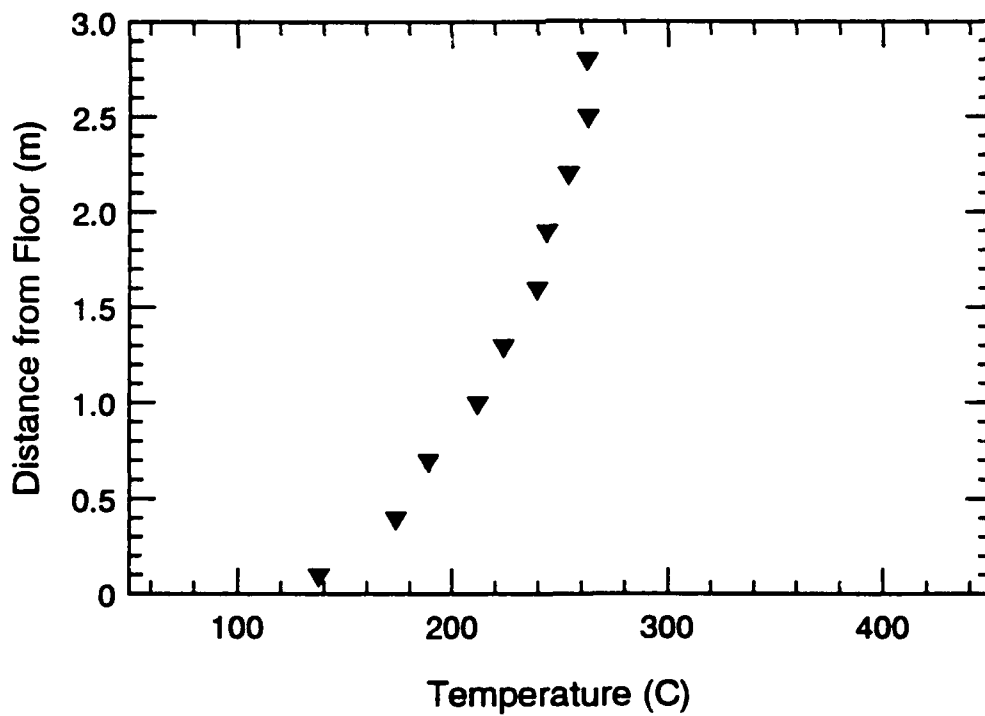
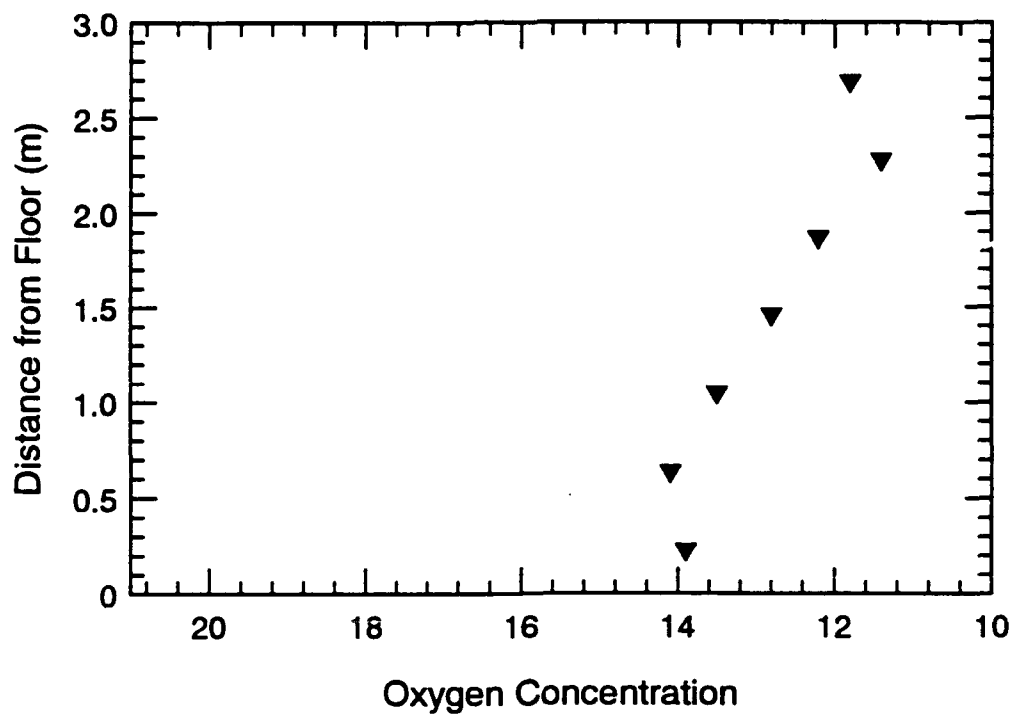


Figure 46. Vertical Oxygen Concentration and Temperature Profiles for S211

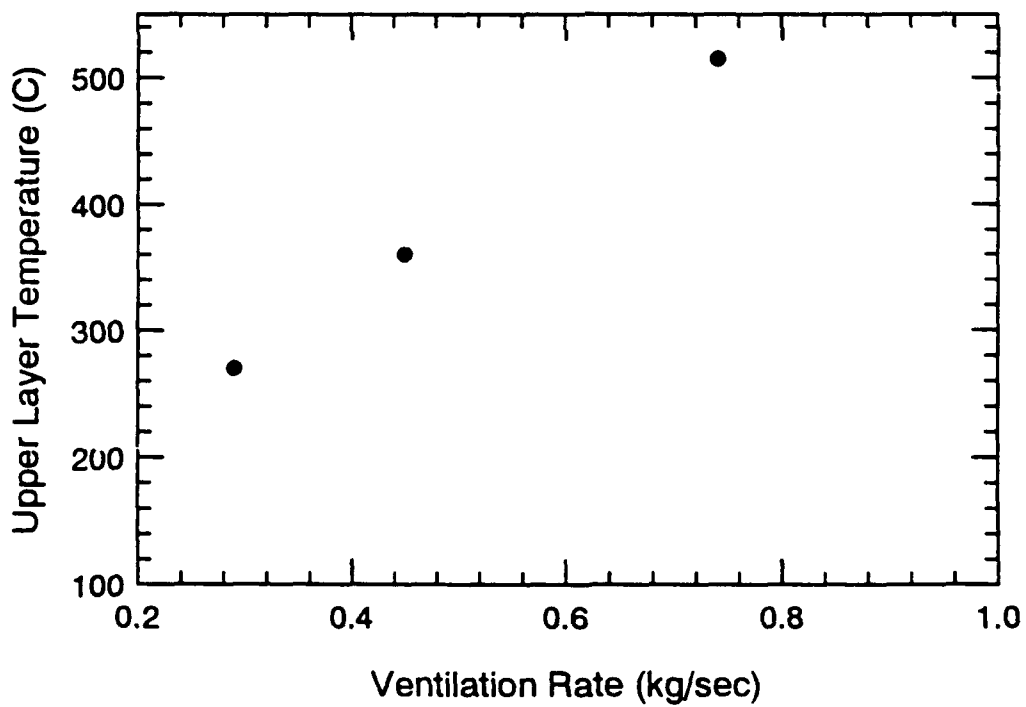
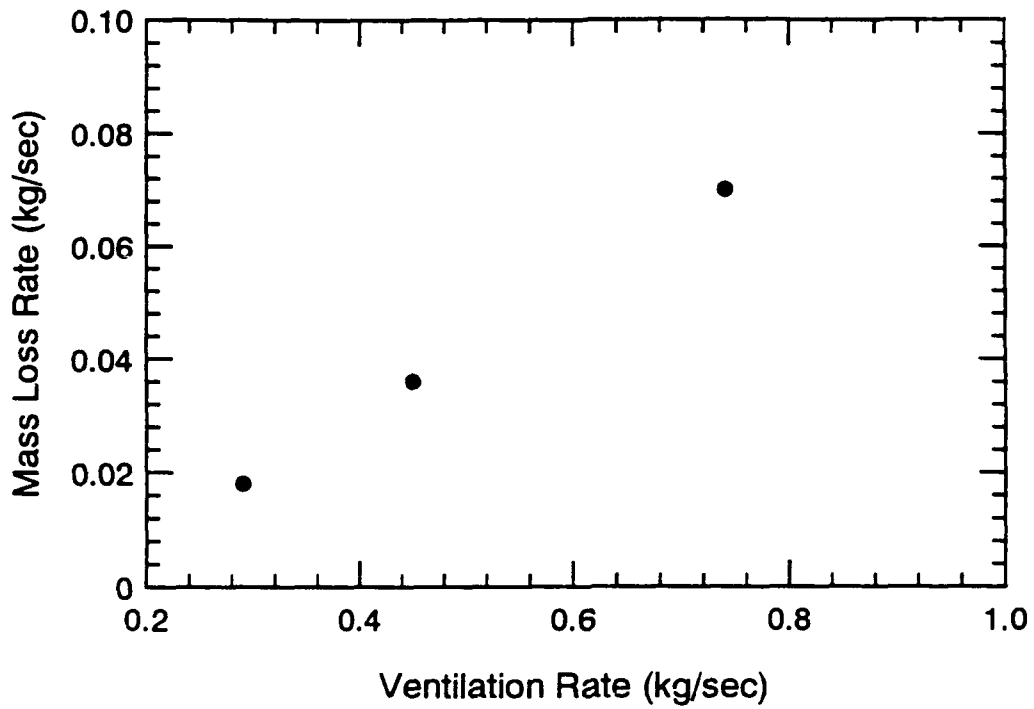


Figure 47. Mass Loss Rate and Temperature vs. Ventilation Rate for Wood Crib Tests (Series 2)

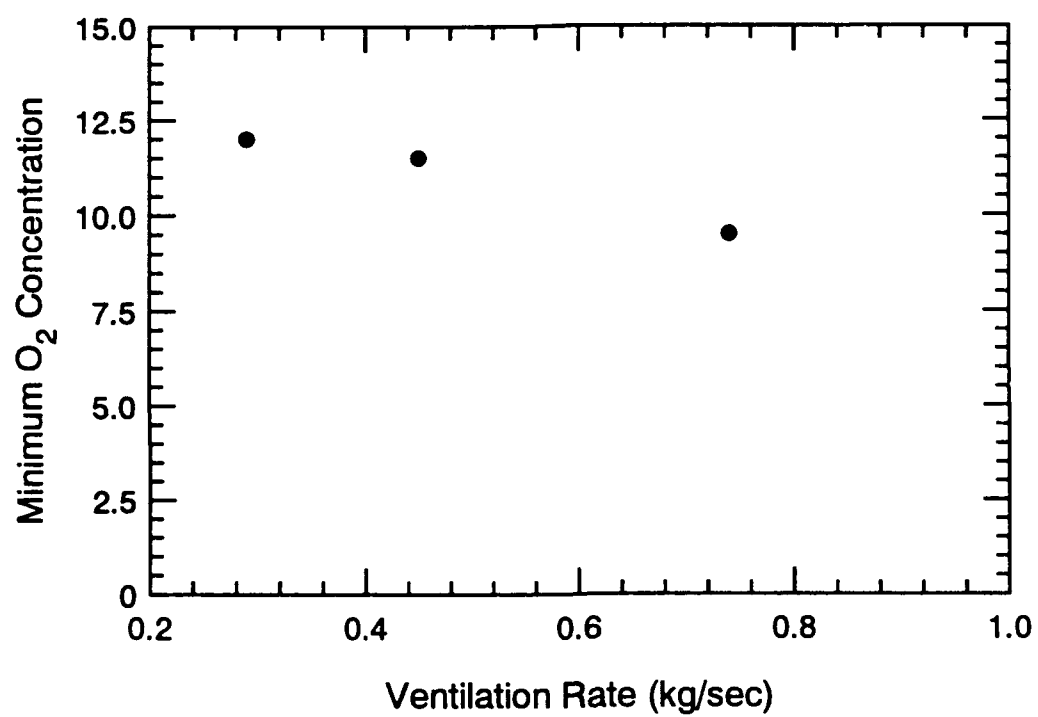


Figure 48. Minimum Oxygen Concentration vs. Ventilation Rate for Wood Crib Tests (Series 2)

Oxygen concentration profiles shown in Figures 49-51 show environments which are well-mixed (within 2%). For an unknown reason, a decrease in oxygen concentration is noticed near the fire base. The temperature profile for the highest ventilation rate test appears linear (Figure 50) while the profiles for the other two tests show a gradient change near 1.5 m (Figures 49 and 51).

6.2.4 Polyurethane Fires (S204, S205, S212)

From Figures 52 and 53, it is concluded that the mass loss rate is the only quantity directly affected by the ventilation rate. The temperatures and oxygen concentrations do not follow a clear trend.

The vertical oxygen profiles are nearly well-mixed as seen in Figures 54-56. The temperature profiles show more stratification than was present with the other fuels. A nearly uniform upper region is seen with a gradual decline in temperature near the fire base. As mentioned in Section 6.1.4, this effect could be a result of the quick peak in temperature which is not reflected low in the compartment.

7.0 DISCUSSION

7.1 Temperature Predictions

Experimental results were compared to temperatures predicted using measured vent flow rates. However, since the vent flow rates are often not known, two methods of predicting the vent flow rate were used and compared with the measured values. Also, the MQH method was examined using an overall heat transfer coefficient calculated using Beyler's equation.

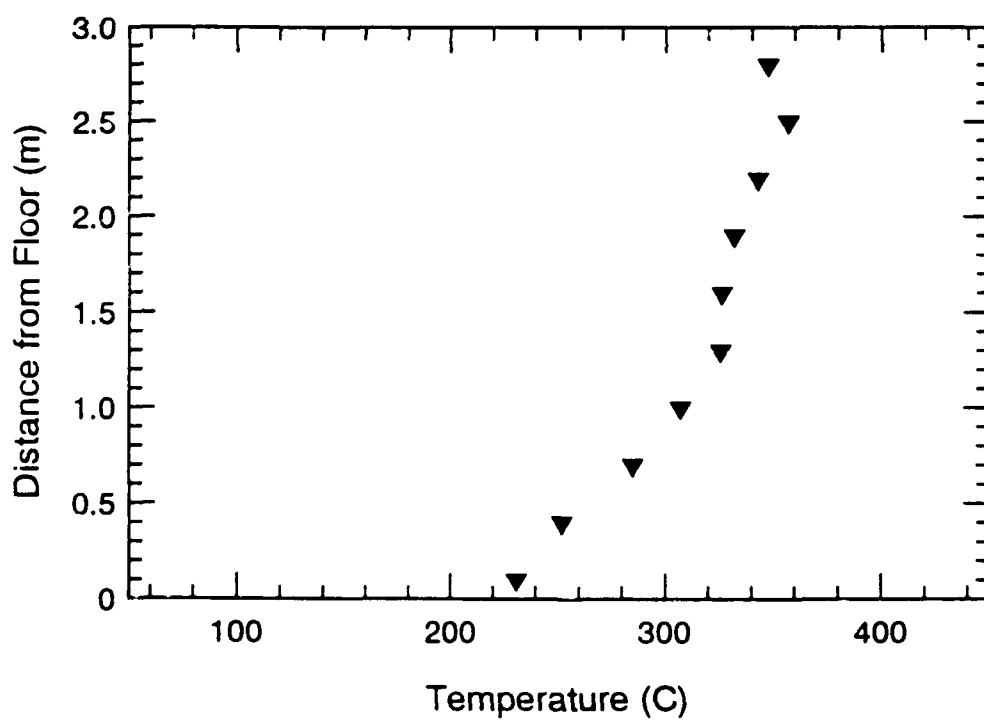
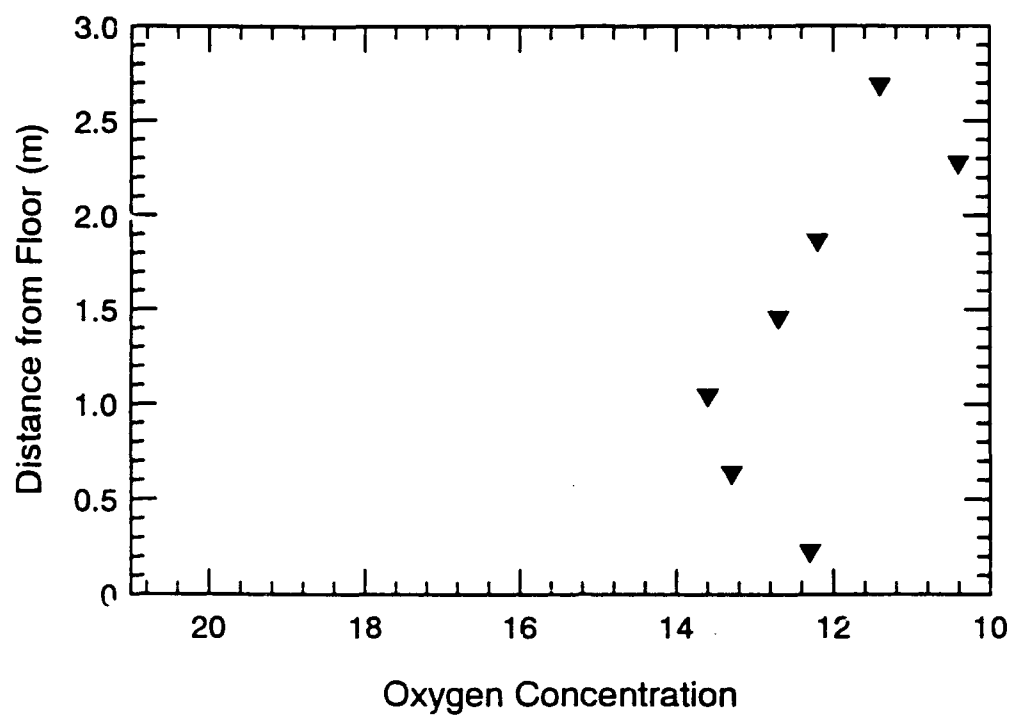


Figure 49. Vertical Oxygen Concentration and Temperature Profiles for S202

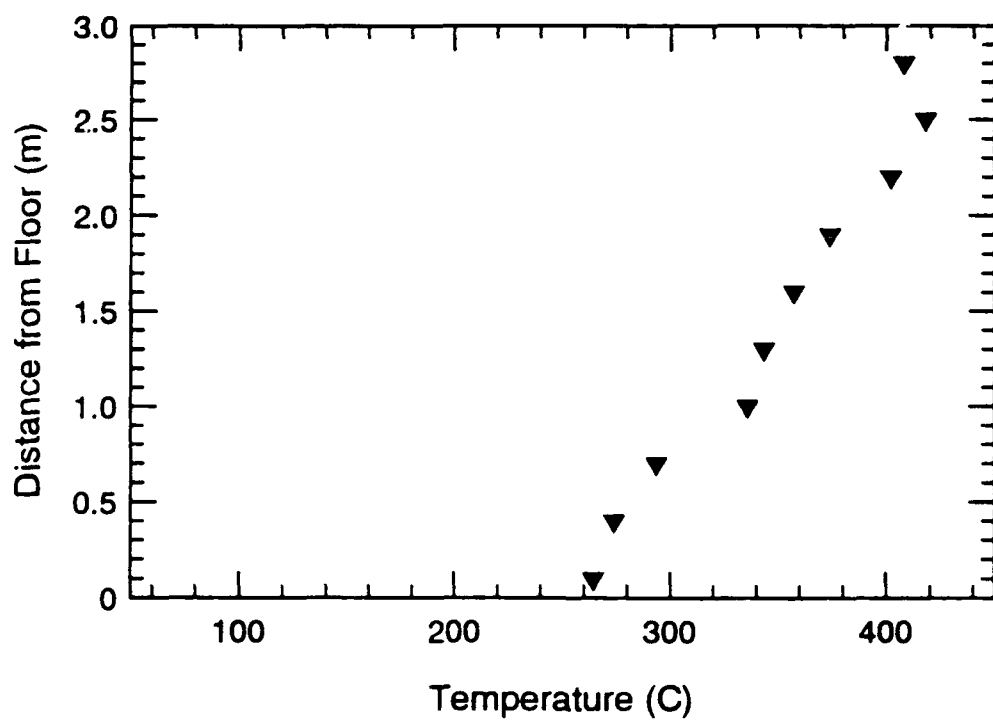
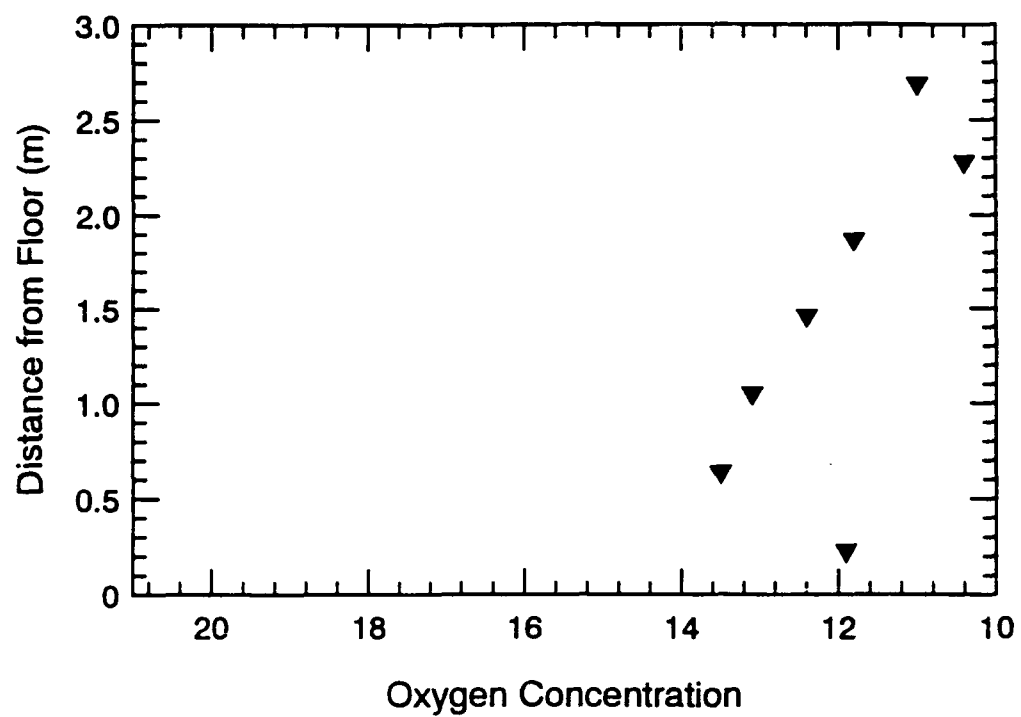


Figure 50. Vertical Oxygen Concentration and Temperature Profiles for S206

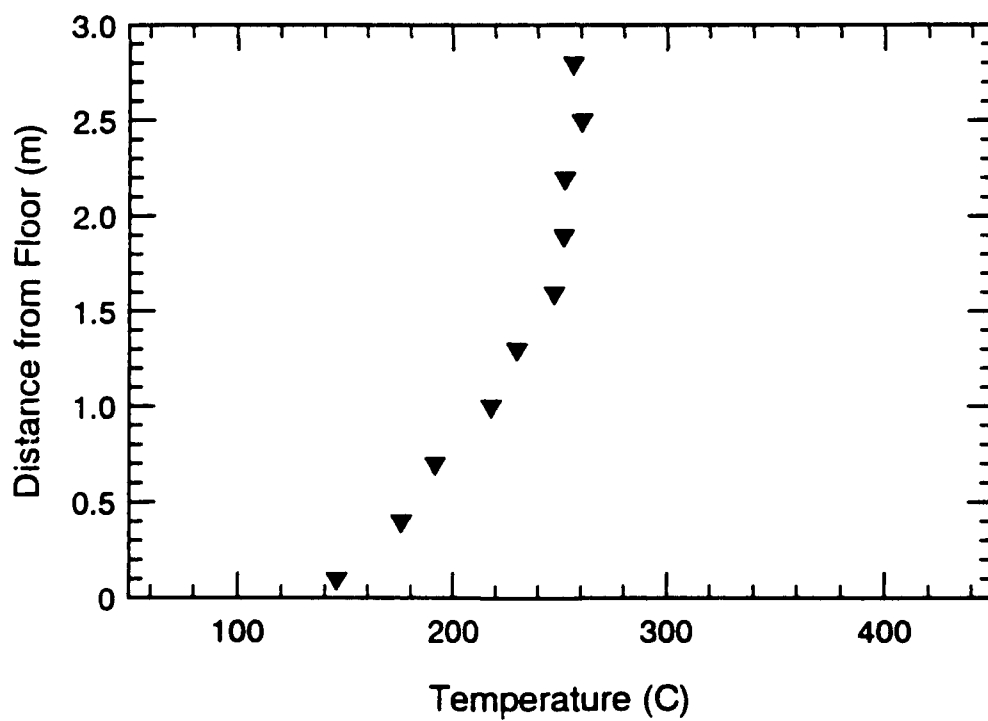
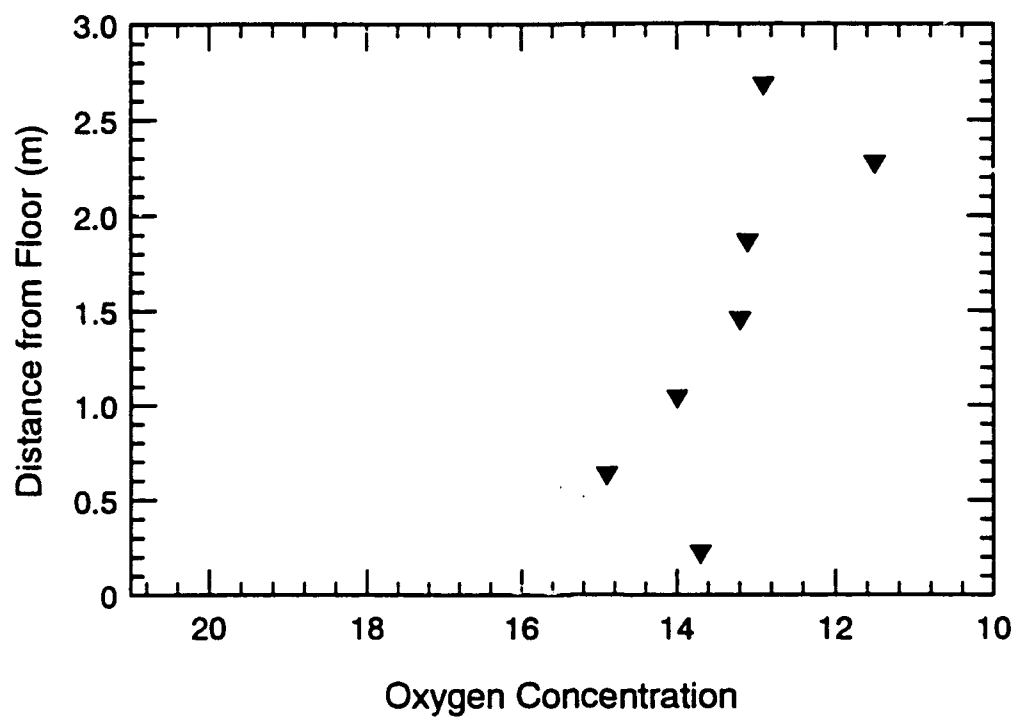


Figure 51. Vertical Oxygen Concentration and Temperature Profiles for S209

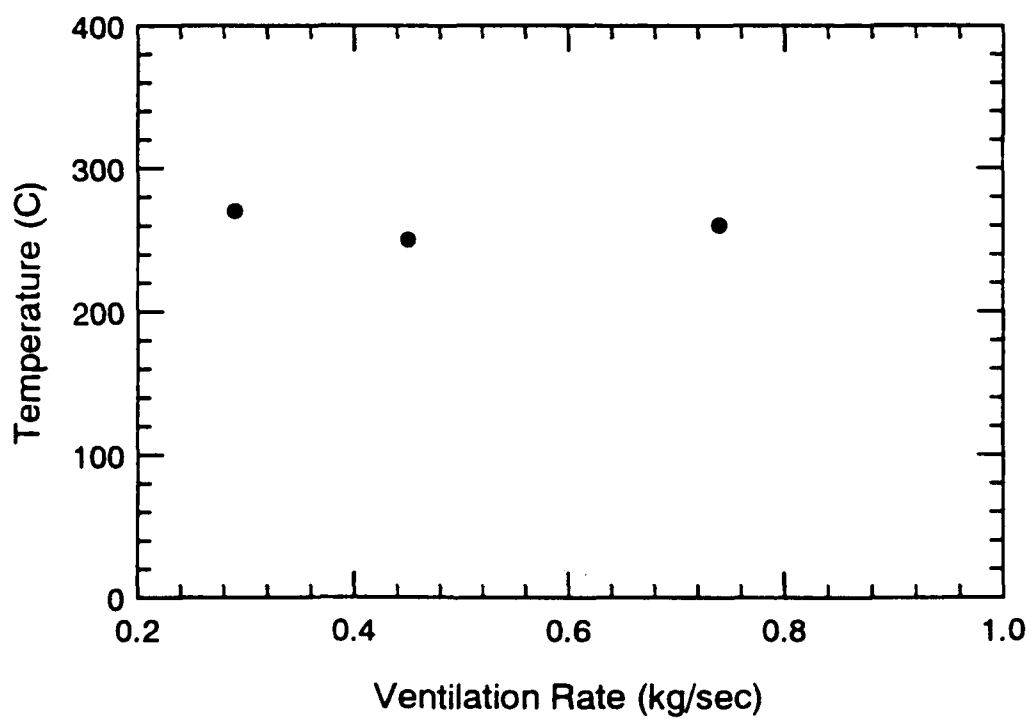
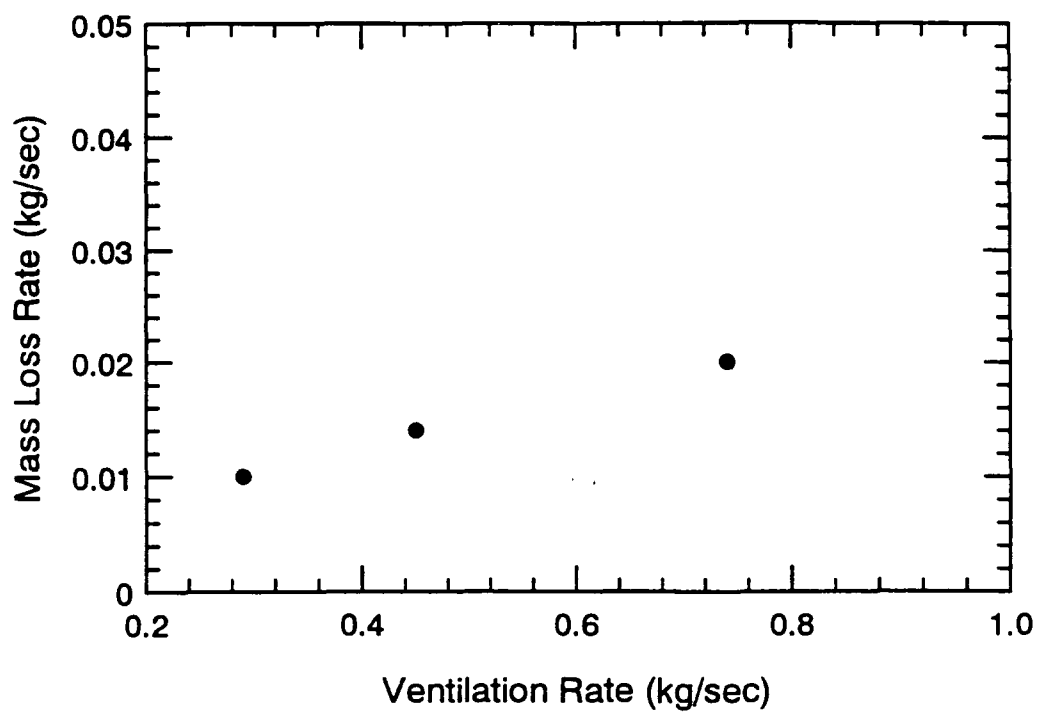


Figure 52. Mass Loss Rate and Temperature vs. Ventilation Rate for Polyurethane Tests (Series 2)

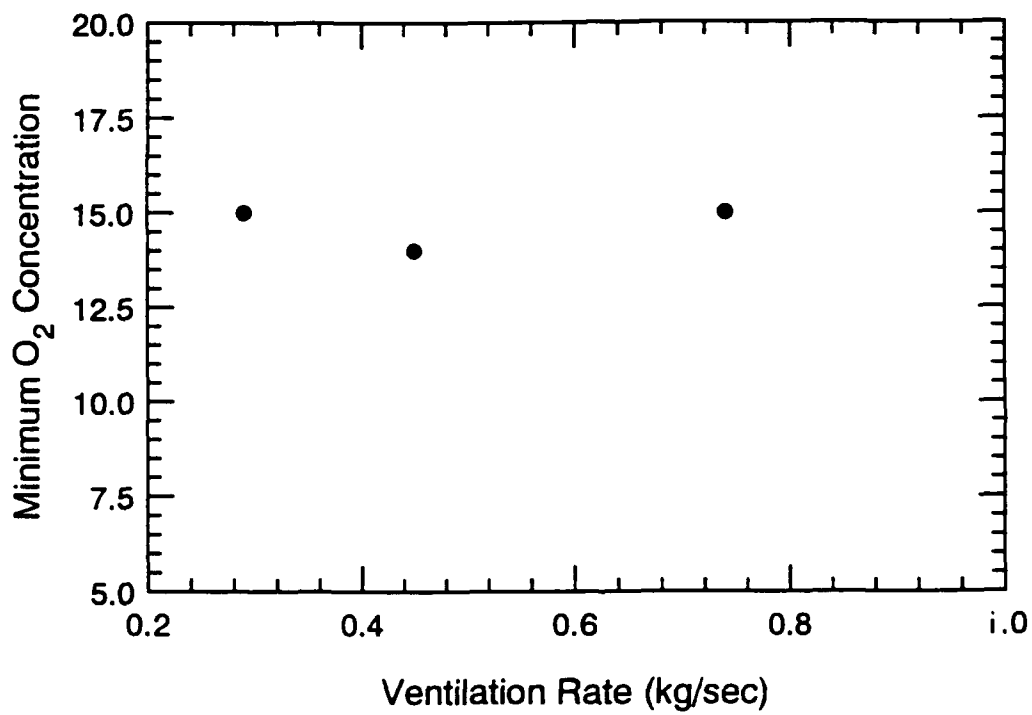


Figure 53. Minimum Oxygen Concentration vs. Ventilation Rate for Polyurethane Tests (Series 2)

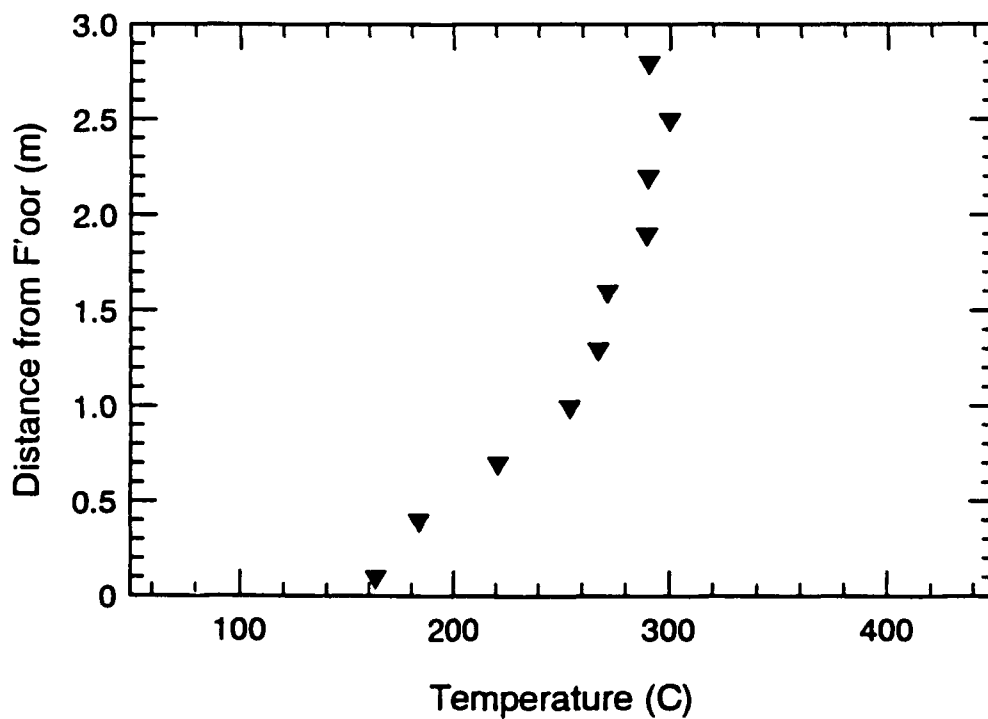
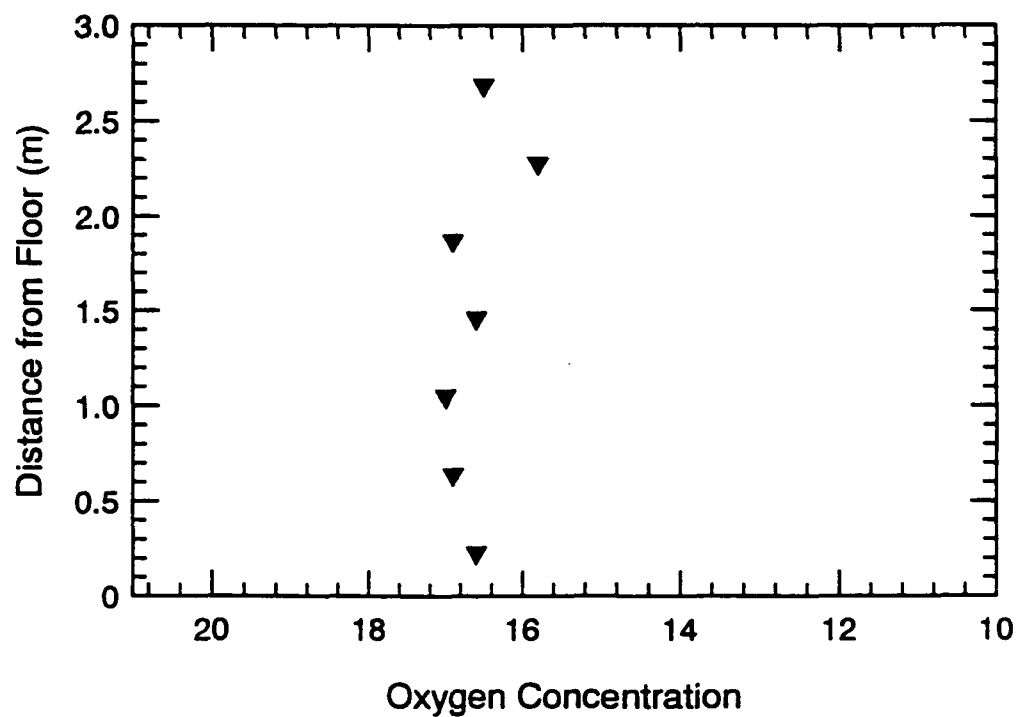


Figure 54. Vertical Oxygen Concentration and Temperature Profiles for S204

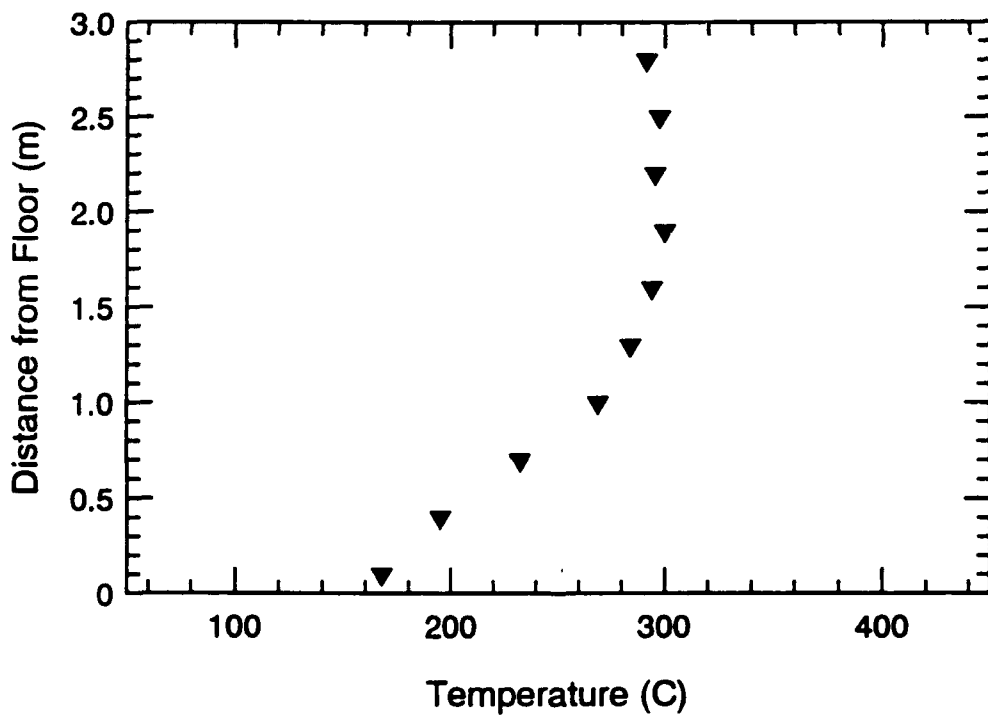
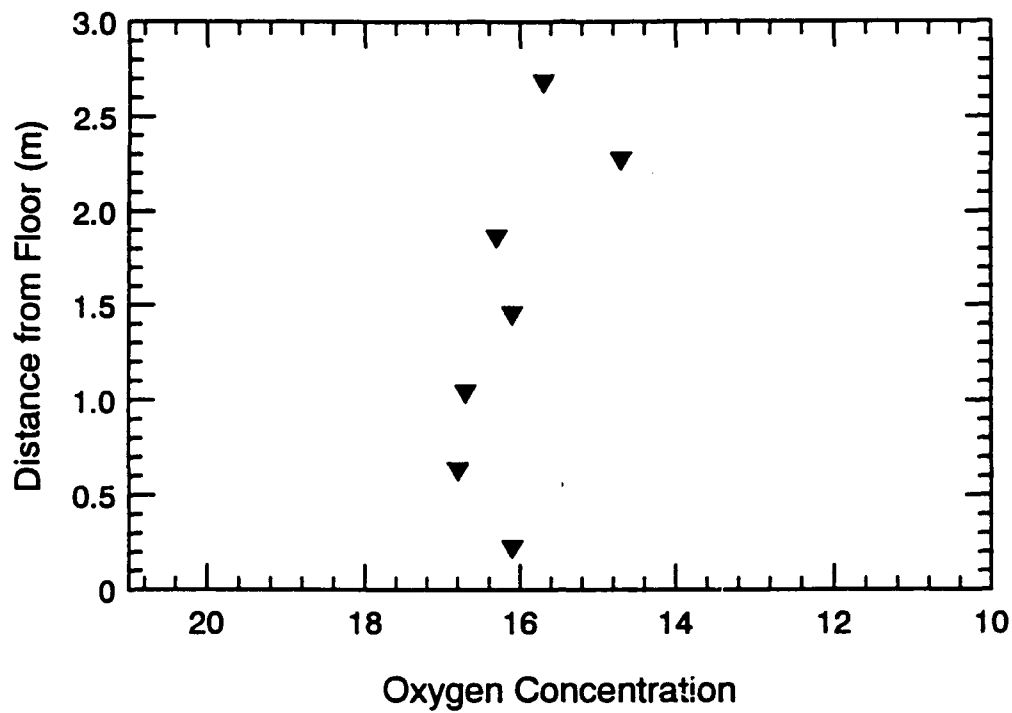


Figure 55. Vertical Oxygen Concentration and Temperature Profiles for S205

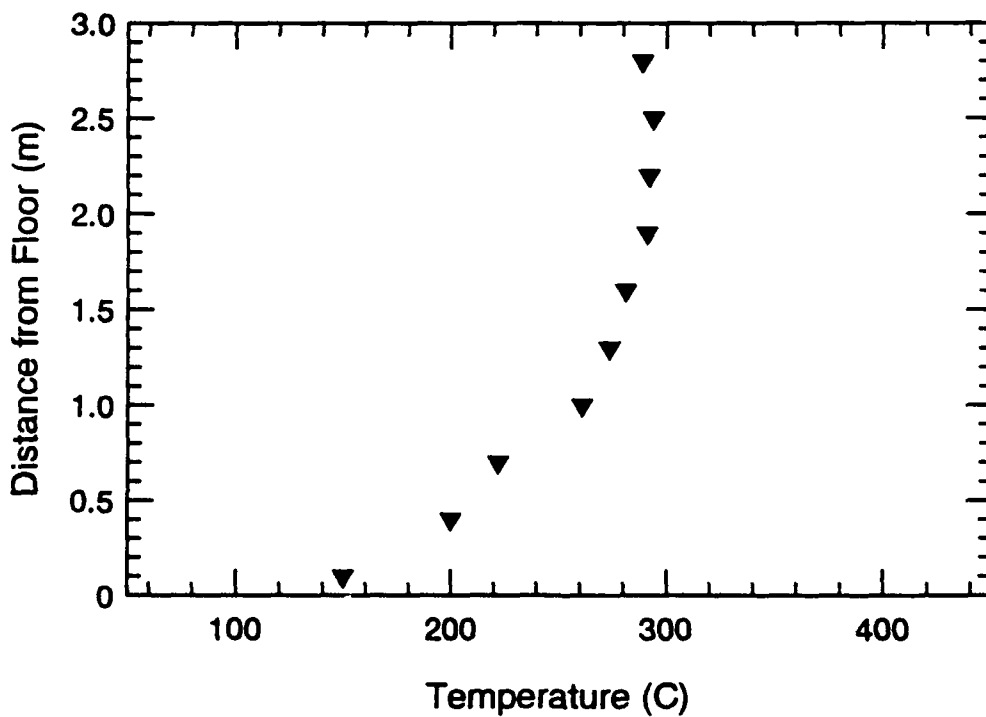
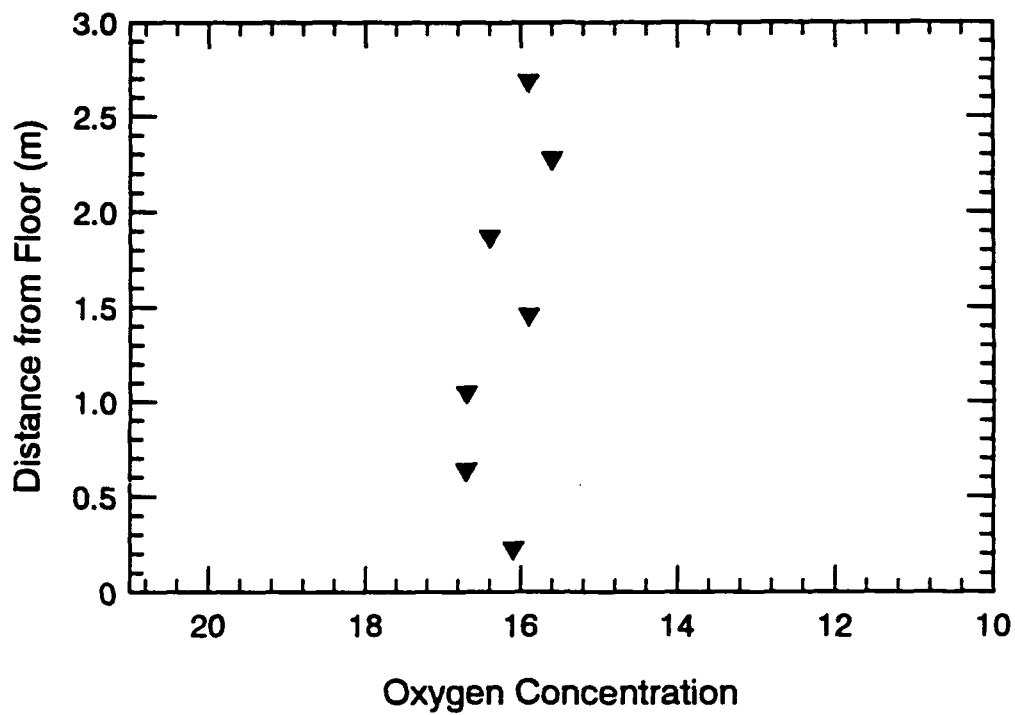


Figure 56. Vertical Oxygen Concentration and Temperature Profiles for S212

7.1.1 Peatross/Beyler Method

A correlation for temperature rise was developed by Deal and Beyler based on an energy balance across the compartment [4].

$$\Delta T = \frac{\dot{Q}}{\dot{m}c_p + h_k A_t} \quad (4)$$

where \dot{Q} is the heat release rate (W), \dot{m} is the compartment exhaust rate (kg/sec), c_p is the heat capacity of the exhaust gases (J/kgK), A_t is the barrier surface area (m²), and h_k is the overall heat transfer coefficient (W/m²K). The barrier surface area is taken as the interior surface area of the compartment, including the floor.

The challenge with this expression lies in the determination of the heat transfer coefficient. Assuming that the compartment temperature is uniform at T_h and using a lumped mass analysis to look at the barrier, the energy equation becomes

$$m''c_p \frac{dT}{dt} = h_h(T_h - T) - h_o(T - T_o) \quad (5)$$

where T is the barrier temperature, T_h is the temperature of the hot gas layer, T_o is the ambient temperature, m'' is the mass per unit area of the barrier, c_p is the barrier's specific heat, and h_h and h_o are the heat transfer coefficients on the hot and ambient sides of the barrier, respectively. Using an ambient temperature of zero and the initial conditions of $T = 0$ at $t = 0$, the following expression results

$$T = \frac{h_h T_h}{h_h + h_o} \left(1 - \exp\left(-\frac{h_h + h_o}{m''c_p} t\right) \right) \quad (6)$$

The overall heat transfer coefficient, h_o , may be expressed by

$$\dot{q}'' = h_h(T_h - T) = h_k(T_h - T_o) \quad (7)$$

so that solving for h_k yields

$$h_k = h_h - \frac{h_h^2}{h_h + h_o} * \left(1 - \exp \left(- \frac{h_h + h_o}{\rho * \delta * c_p} t \right) \right) \quad (8)$$

Looking at the behavior of this equation, it is found that

$$h_k = h_h \quad \text{at } t = 0 \quad (9)$$

$$h_k = \frac{h_h h_o}{h_h + h_o} \quad \text{at } t = \infty \quad (10)$$

Since time is a variable used to calculate the overall heat transfer coefficient, the FRI time may be determined by looking at the time which corresponds to a ΔT of 500 to 600 °C.

Based on a simple analysis, Beyler estimated values of h_h and h_o as 91 W/m²K and 45 W/m²K, respectively [2]. These values result in an overall heat transfer coefficient which begins at 91 and is lowered to 30 W/m²K as time reaches infinity.

Preliminary comparisons of the experimental results with this correlation indicated that Beyler's proposed heat transfer coefficients, h_h and h_o , were too large. As a result, too much heat was lost through the walls so that temperatures were underpredicted. In both natural and forced ventilation tests, the most suitable values for h_h and h_o were 30 and 20 W/m²K, respectively. Therefore, the current heat transfer coefficients used in the SFSEM submodel are inappropriate for predicting temperature rise in compartment fires with highly conductive barriers and these new coefficients should be used.

Figures 57 and 58 show plots of the actual and predicted temperature-time histories and of the predicted temperature versus the actual temperature for Tests S104 and S106 respectively. Figure 57, which represents a polyurethane fire, shows excellent prediction of

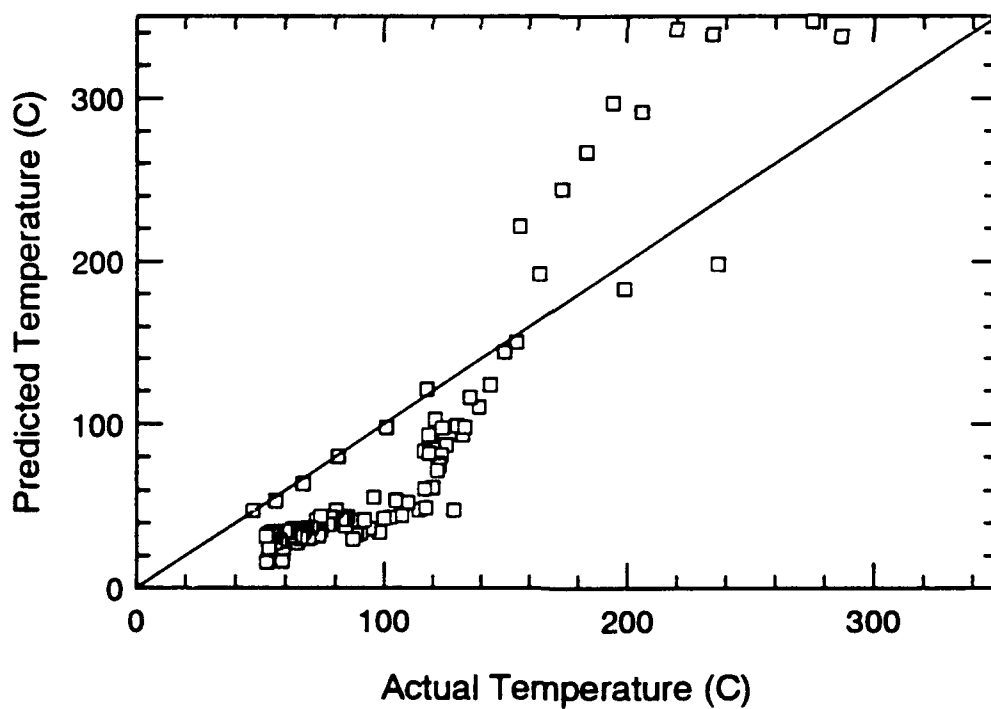
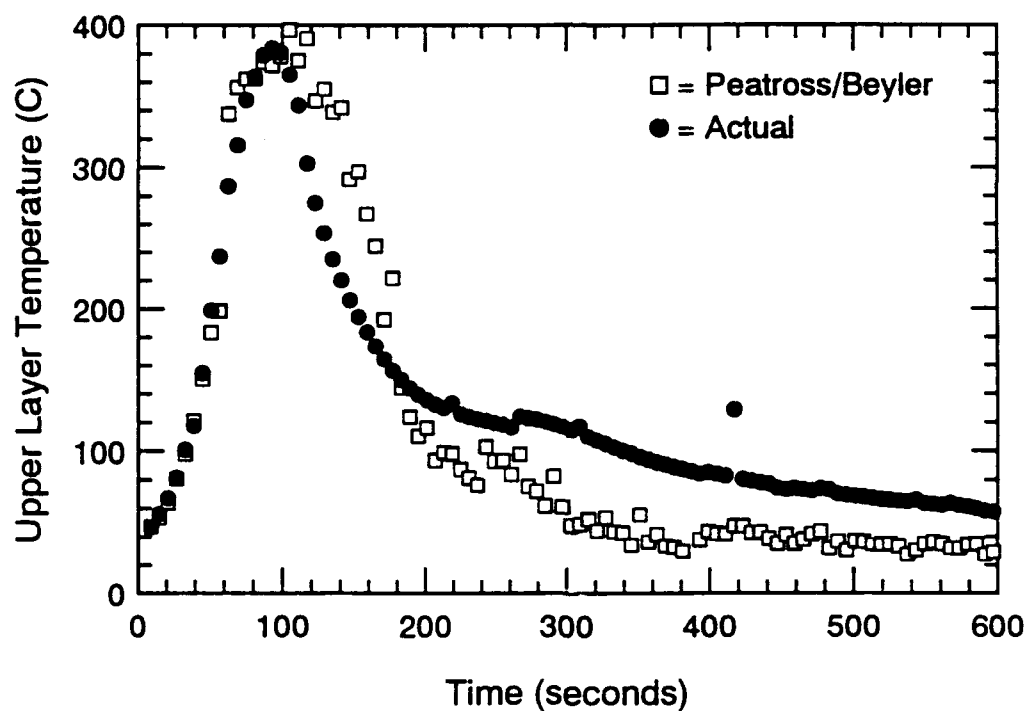


Figure 57. Temperature Prediction Results Using Peatross/Beyler Method for S104

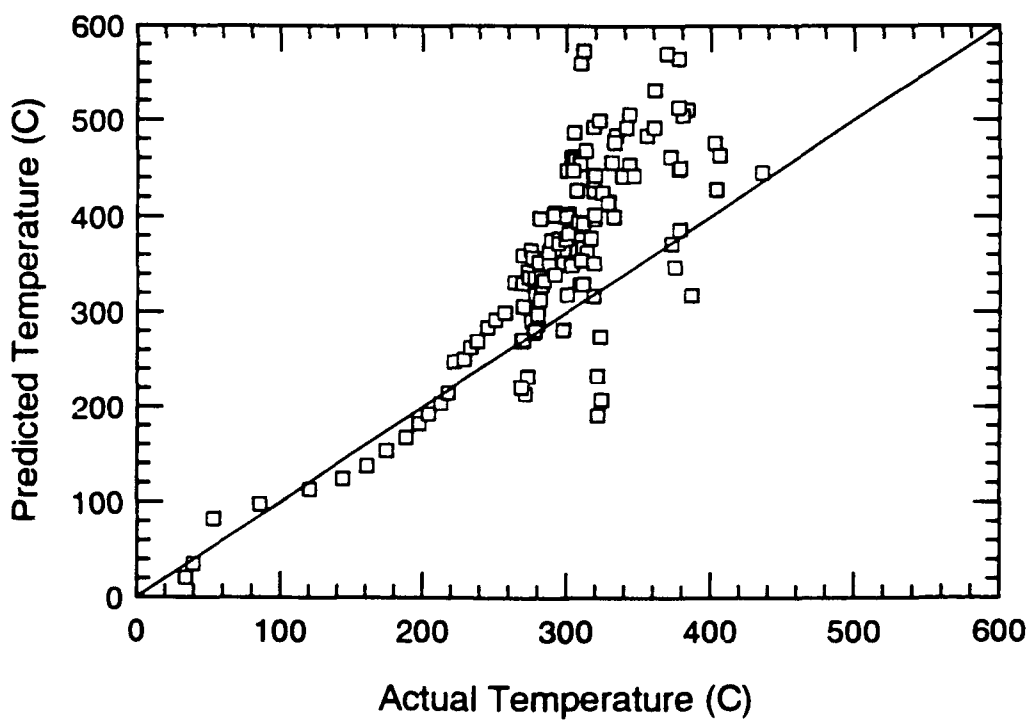
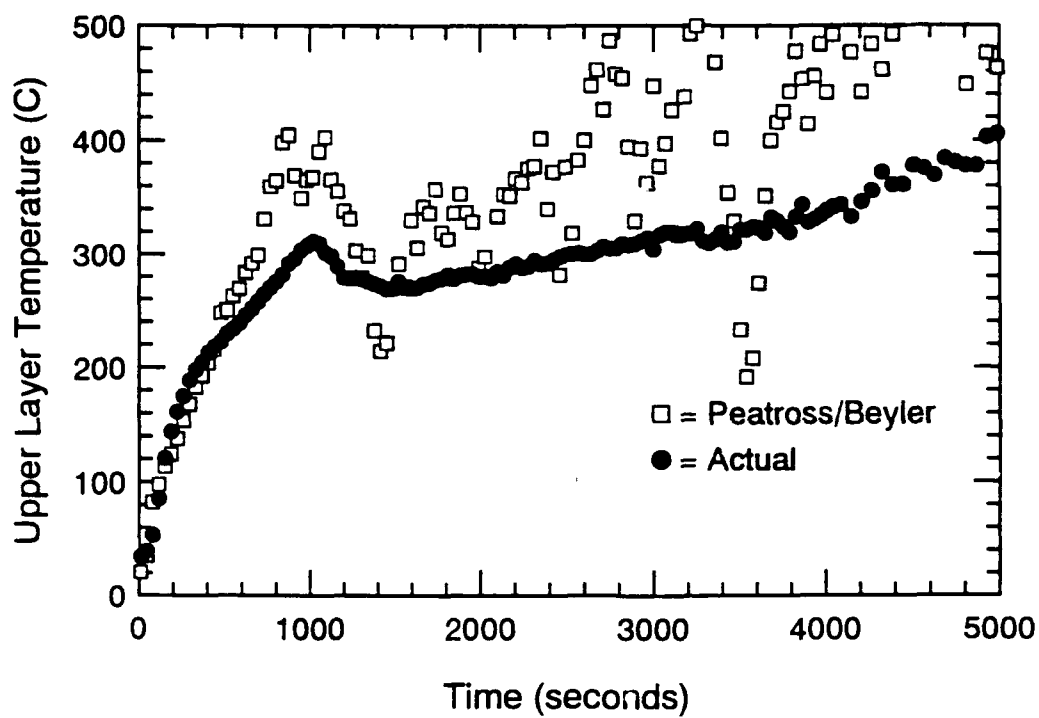


Figure 58. Temperature Prediction Results Using Peatross/Beyler Method for S106

the temperature peak. Figure 58 corresponds to a wood fire and shows poorer agreement than Figure 57 with a tendency to overpredict the temperature. Plots of this format are included in Appendix C for all natural ventilation tests.

Figure 59 displays the upper layer temperature prediction results from all Series 1 tests. In order to obtain the data points, four points were taken from each test during the growth and steady-state period. Summary plots for other methods use this same procedure to obtain points to plot. In situations where the predictions were noisy, care was taken to pick average temperature values. Agreement is excellent. The average difference between the predicted and actual values used in this graph was calculated as 18 °C.

Forced ventilation fire temperatures were predicted less reliably. A plot summarizing the forced ventilation tests is shown in Figure 60. The mean difference between the experimental and predicted results was 30 °C, almost twice that of the natural ventilation results. Individual test results from this analysis can be found in Appendix D.

It is important to identify the sources of error in these predictions. To begin with, some of the tests have predictions which reflect a lot of noise. This is primarily due to noisy mass loss measurements since this measurement is used to determine the heat release rate. This noise is notably worse for wood crib fires as is shown in Figure 61. Another source of error in this analysis lies in the estimation of the heat of combustion for each fuel. Since the theoretical heat release rate was used in the calculations, an overestimation of the heat of combustion could lead to overprediction of the temperatures.

7.1.1.1 Deal/Beyler Layer Driven Method for Determining Vent Flow Rates

When the vent flow rate is not known, vent flow dynamics and plume entrainment may be used to estimate the flow rate. This approach assumes that the entrained air flow rate is equal to the exhaust flow rate. Since plume entrainment is a complex problem, several models have been developed. This report discusses two of these models.

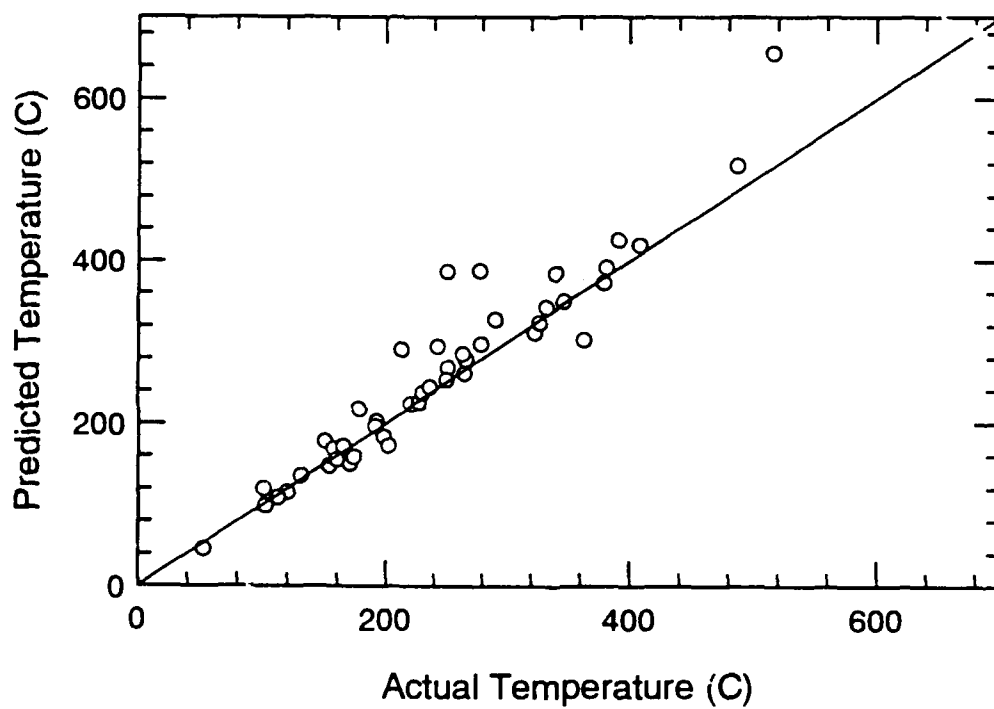


Figure 59. Summary of Temperature Prediction Results Using Peatross/Beyler Temperature Prediction Method (Series 1)

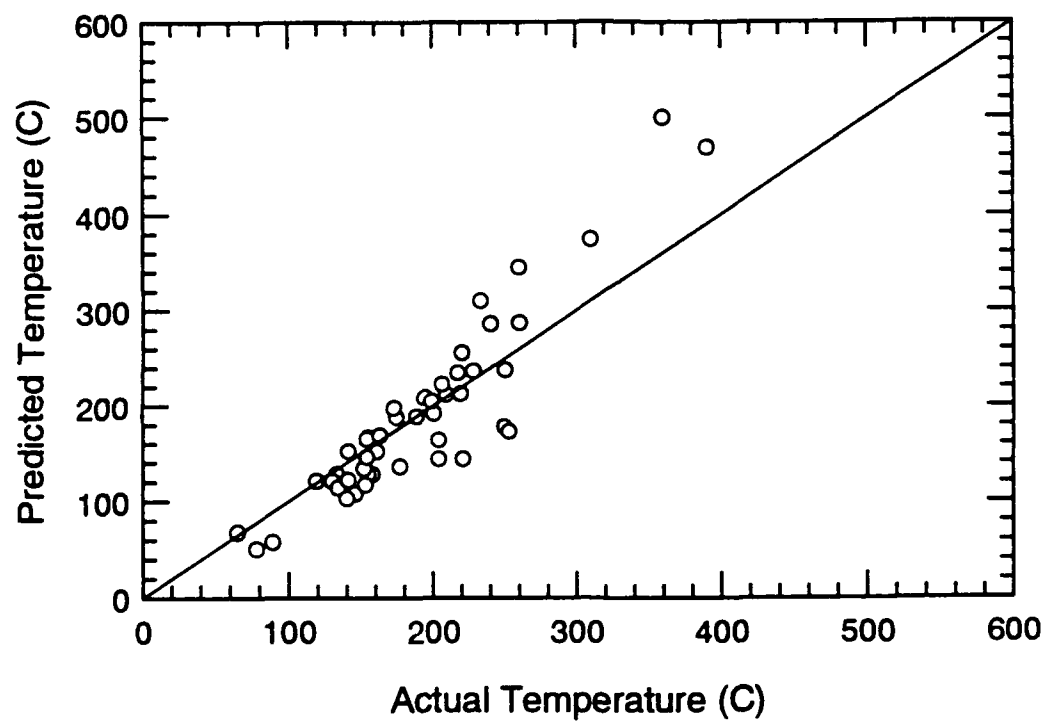


Figure 60. Summary of Temperature Prediction Results Using Peatross/Beyler Temperature Prediction Method (Series 2)

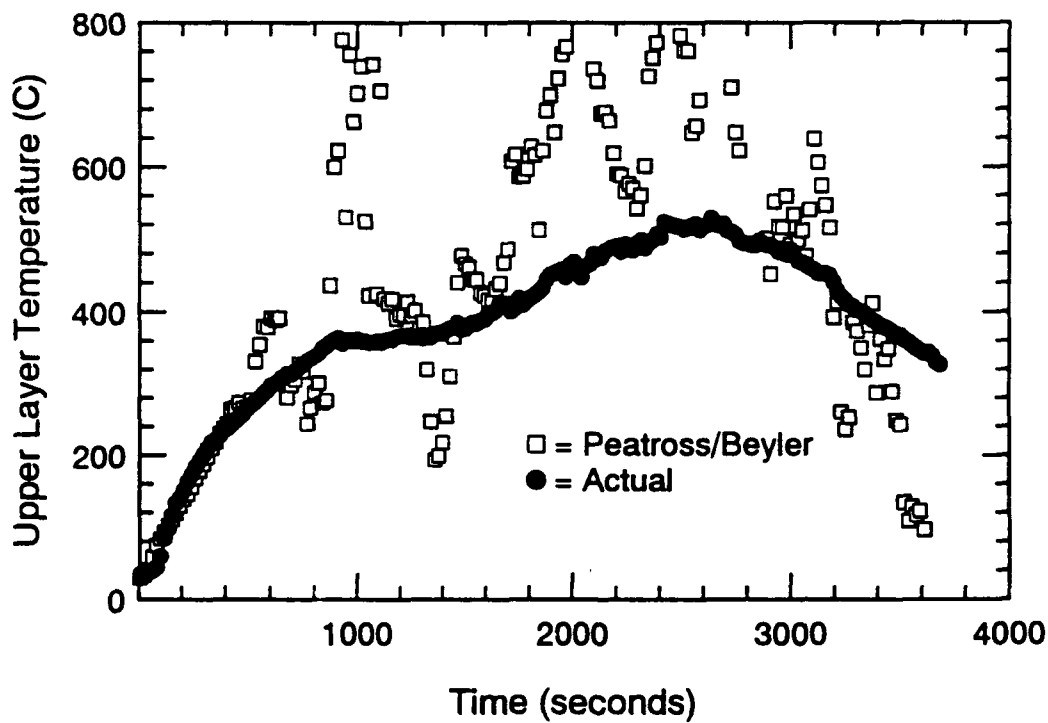
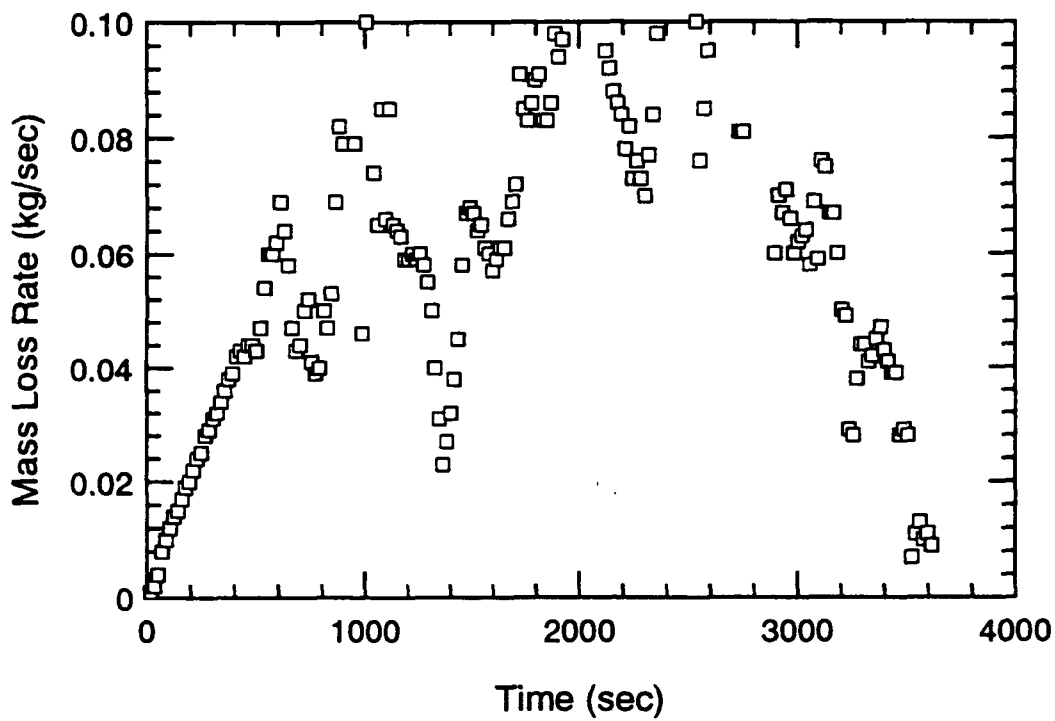


Figure 61. Mass Loss Rate and Temperature Prediction-Time Histories for S103

Rockett expressed the vent flow rate for a 2 layer compartment fire as

$$\dot{m}_{out} = \frac{2\sqrt{2g}}{3} C_D \rho_a A_o \sqrt{A_o} \sqrt{\frac{T_a}{T_h} \left[1 - \frac{T_a}{T_h} \right]} (1 - N)^{\frac{3}{2}} \quad (11)$$

where C_D is the discharge coefficient (0.68), ρ_a is the ambient density (1.2 kg/m³), A_o is the vent area, H_o is the vent height, T_a is the ambient temperature, T_h is the hot layer temperature, and N is the height of the neutral plane above the base of the vent normalized by the height of the vent [14].

Deal and Beyler's Layer Driven Method uses Zukowski's correlation for plume entrainment [15]. A comparison of this method with experimental results was performed using equations 25-27 in reference [4]. As seen in Figure 62, this method underpredicts the vent flow rate. A complete set of results can be found in Appendix E. In some tests, the predicted values are underpredicted by as much as 33%. However, since the temperature correlation equation is relatively insensitive to the exhaust rate, the predictions were not shifted significantly from those using the measured vent flow rate. Figure 63 presents a comparison of this model with the experimental results. The mean difference in the predictions and the actual values was 54 °C.

7.1.1.2 Mowrer Method for Determining Vent Flow Rates

Mowrer's Method employs Heskestad's correlation for fire plume entrainment, neglecting the virtual origin offset [16]. Mowrer determined that the correlation was better when this offset was ignored. This correlation differs from Zukowski's in that it is for entrainment at the fire base instead of along the flame height.

Vent flow rates were calculated using simplifications and assumptions detailed by Mowrer's equations 15, 21, and 23 [17]. In contrast to the Deal/Beyler Layer Driven Method, exhaust flow rates were overpredicted. Due to the small area of the window and quarter door vents, the predicted exhaust flow rate for these tests was based on the ventilation factor. Results for these tests are in Appendix F.

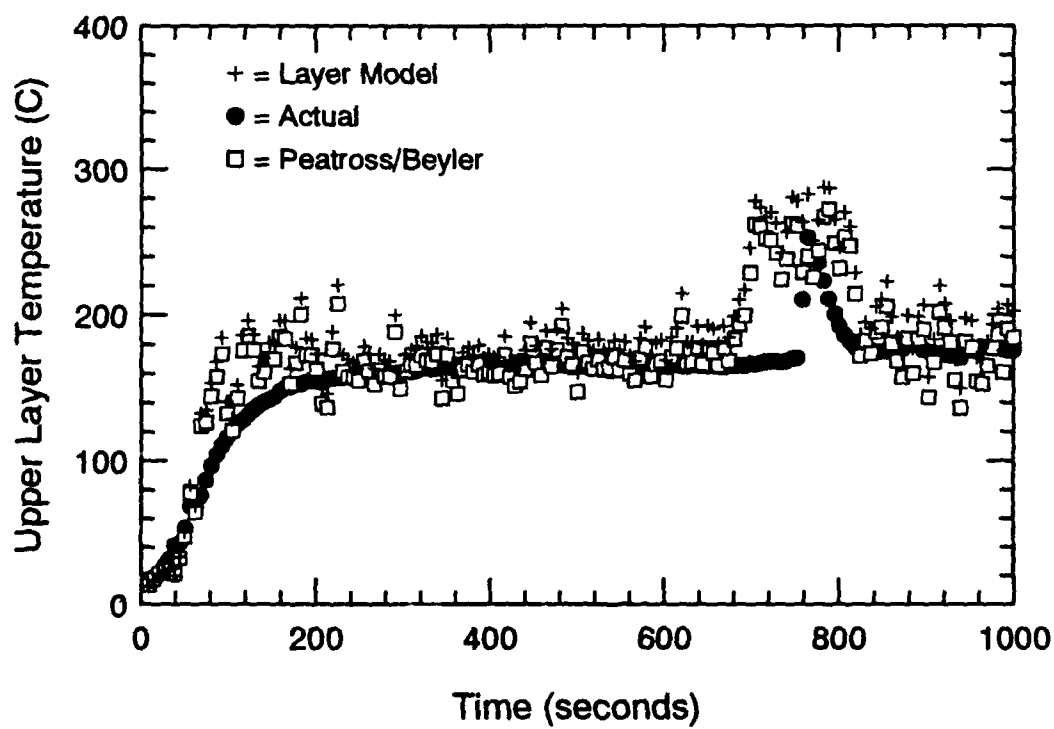
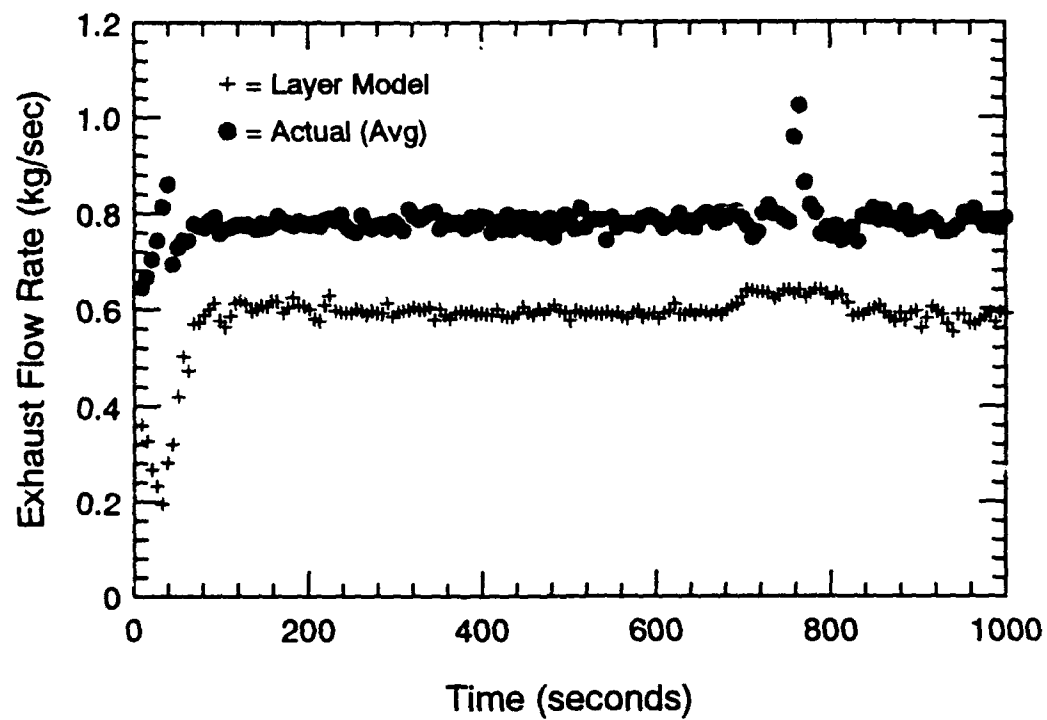


Figure 62. Vent Flow Rate and Temperature Prediction-Time Histories for S101

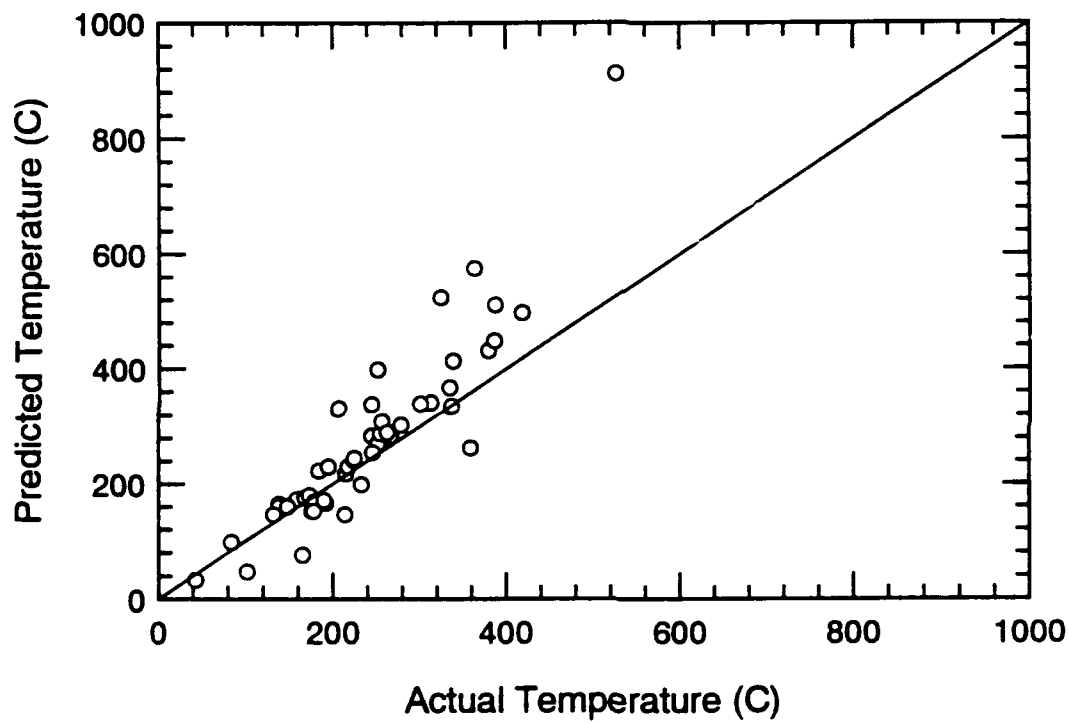


Figure 63. Summary of Temperature Prediction Results Using Deal/Beyler Layer Driven Method to Predict Vent Flow Rates

As was the case with the Deal/Beyler Layer Driven Model, the inaccuracies in the vent flow prediction did not affect the temperature predictions. A summary plot including points from each test is shown in Figure 64. A mean difference of 46°C was calculated. In general, these predictions were better than those resulting from the Deal/Beyler Layer Driven Model.

7.1.2 McCaffrey, Quintiere, and Harkleroad (MQH) Method

The motivation for a temperature correlation which could handle highly conductive barriers resulted from the shortcomings of the relationship developed by McCaffrey et al. They expressed the temperature rise using the following relationship [18]

$$\frac{\Delta T}{T_{\infty}} = C \left(\frac{\dot{Q}}{c_p \rho_{\infty} A_o \sqrt{g H_o}} \right)^m \left(\frac{h_k A_T}{c_p \rho_{\infty} A_o \sqrt{g H_o}} \right)^n \quad (12)$$

This equation can be simplified further using ambient conditions and best fit values:

$$\Delta T = 6.85 \left(\frac{\dot{Q}^2}{h_k A_T A_o \sqrt{H_o}} \right)^{\frac{1}{3}} \quad (13)$$

Their suggested values for h_k are expressed by

$$h_k = \max \left(\sqrt{\frac{k \rho c_p}{t}}, \frac{k}{\delta} \right) \quad (14)$$

However, this expression of the heat transfer coefficient is inappropriate for thermally conductive boundaries. In previous work by Deal and Beyler [4], it was found that the overall heat transfer coefficients used in the MQH Method differed by a factor of 2.5 from those used in the Deal/Beyler Method. Consequently, the overall heat transfer coefficient was calculated using Beyler's equation and then multiplied by 2.5.

The results from this analysis can be found in Appendix E. In most cases, these predictions are somewhat higher than the data and the temperatures predicted with the

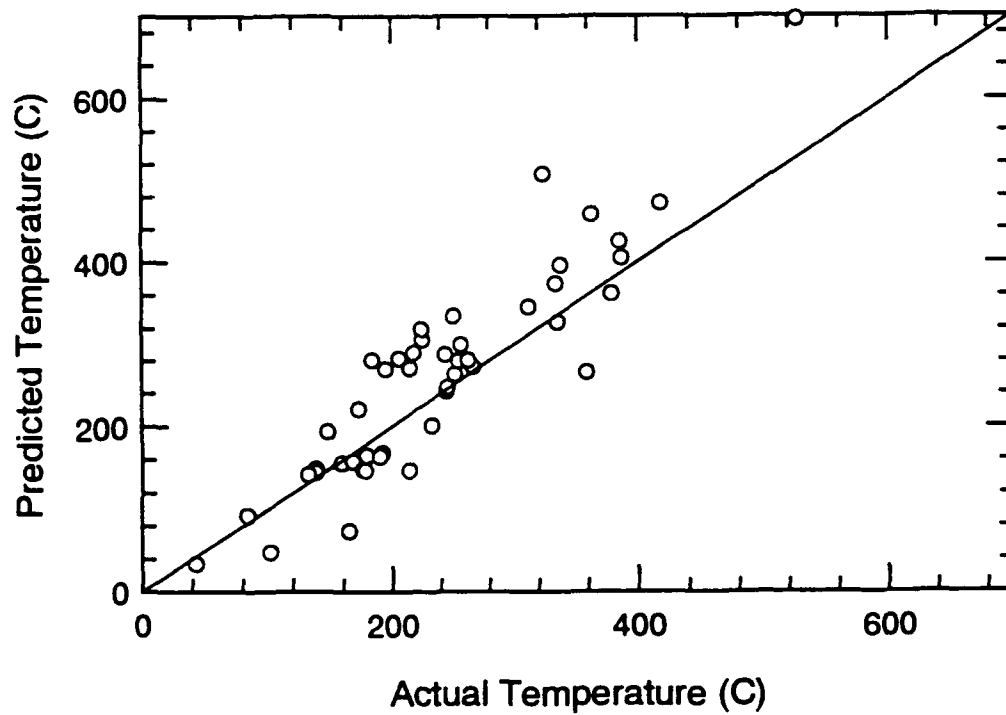


Figure 64. Summary of Temperature Prediction Results Using Mowrer Method to Predict Vent Flows Rates

Deal/Beyler Method. A comparison of these results with the actual temperatures is presented in Figure 65. A mean difference of 47 °C was calculated for these data points.

7.1.3 Comparison of Temperature Prediction Methods

Based on these experimental results, each method of temperature prediction investigated was successful. A table of the mean differences and standard deviations calculated for the data points used in the summary plots is included below. The Peatross/Beyler Method performs well for fires with known ventilation rates. Furthermore, the MQH Method is more reliable than vent flow rate prediction methods in situations where the vent flow rate is not known.

Table 6. Comparison of Temperature Prediction Methods

Ventilation Type	Thermal Model (Vent Flow Rate)	Mean (°C)	Standard Deviation (°C)
Natural	Peatross/Beyler (measured)	18	36
Natural	Peatross/Beyler (Deal/Beyler Layer Driven Method)	54	68
Natural	Peatross/Beyler (Mowrer Method)	46	41
Natural	MQH Method (none)	47	28
Forced	Peatross/Beyler (measured)	30	29

7.2 Barrier Temperature Predictions

In addition to upper layer temperature prediction, it is useful to predict barrier temperatures since they are indicative of when a fire will spread to adjacent spaces.

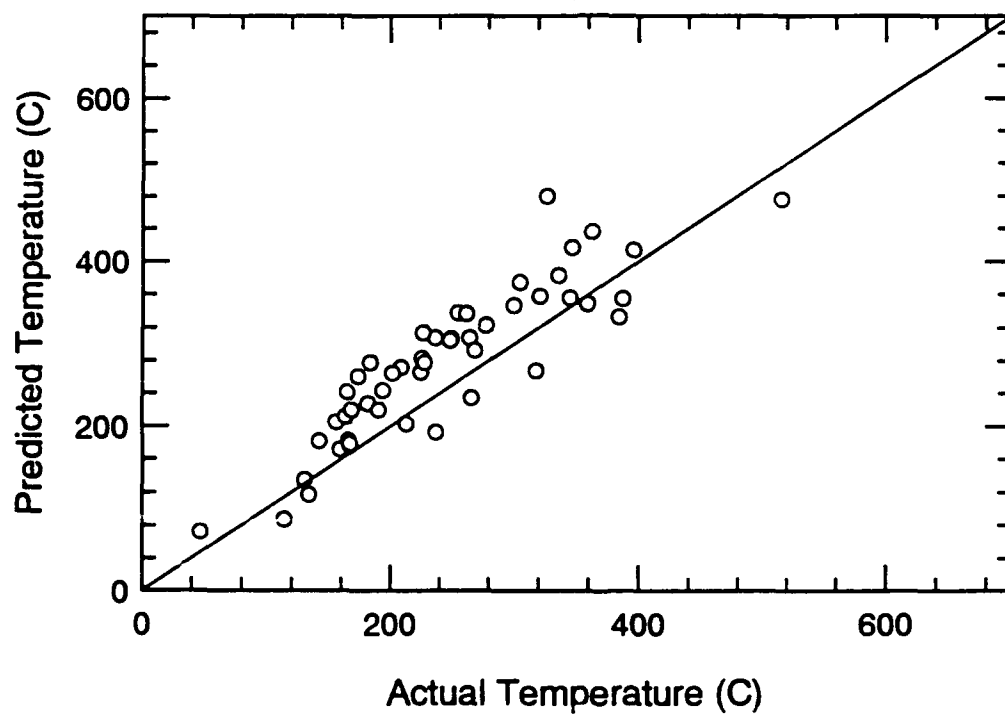


Figure 65. Summary of Temperature Prediction Results Using MQH Temperature Prediction Method

Equation 6 expresses this temperature. Figure 66 shows typical time histories for both natural and forced ventilation tests. Measured barrier temperatures on both the interior and exterior surfaces are included.

7.3 Compartment Fire Analysis

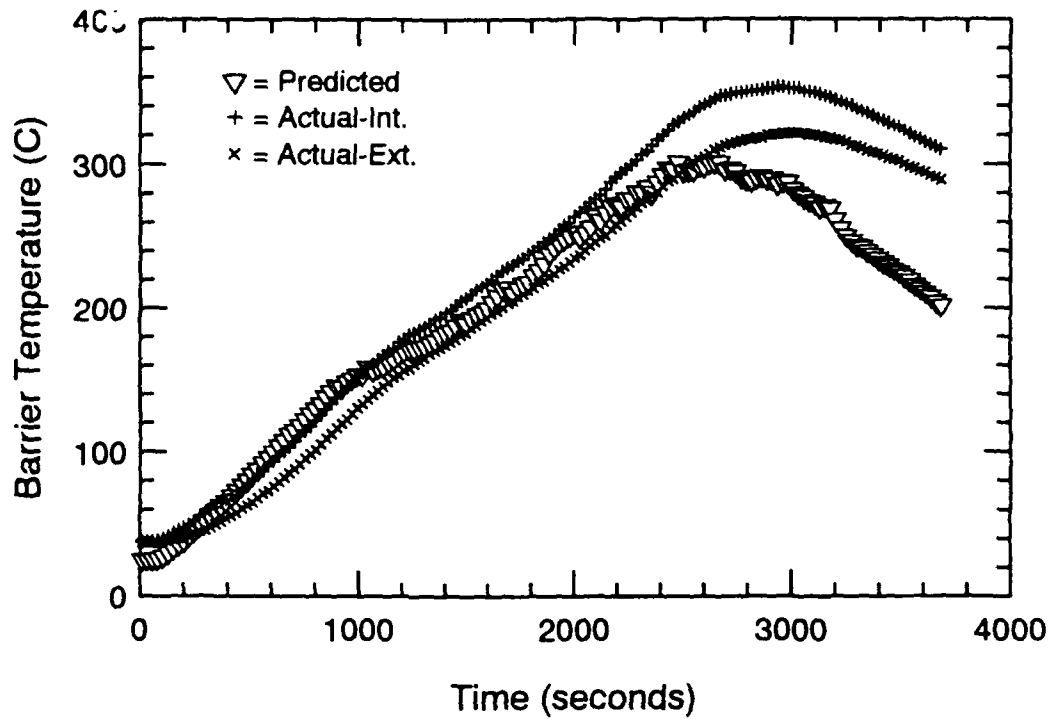
7.3.1 Natural Ventilation Tests

In all but two of these tests, it is indicated by the oxygen concentrations that contaminated air was being entrained into the fire plume. The two fires which reported ambient concentrations at the fire base had the two smallest fuel loads and the door vent. While it is possible that exhaust gases were mixed with fresh air in the corridor before the air flowed in through the vent, one would expect this effect to occur later in the fire after most of the fresh air in the corridor has been entrained. This explanation is questionable though since the entrained air was contaminated even in shorter fires. Given the correlation of floor level oxygen concentration with the smaller vents, it is likely that the gases are mixing within the compartment due to wall flows or vent mixing.

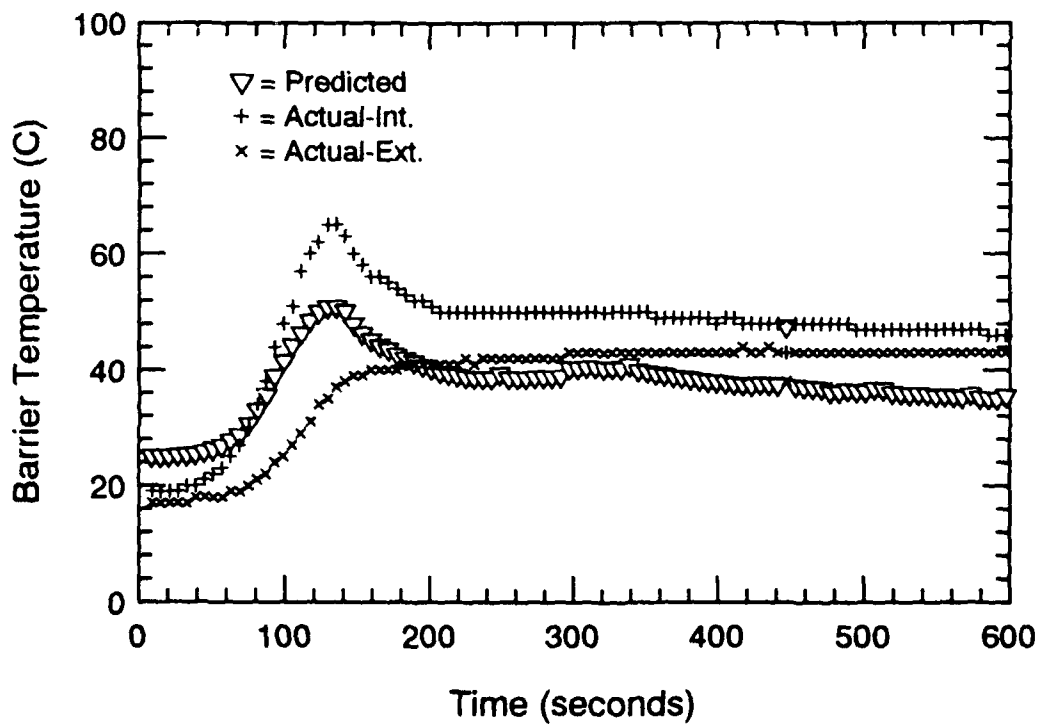
Window vent tests were least likely to have two-layer characteristics. These results suggest that there is a significant amount of mixing occurring after air is entrained through the window. As the air moves toward the fire base, it is mixed with exhaust gases so that the temperature profile in the compartment becomes more uniform vertically. The oxygen concentrations follow this same trend.

7.3.2 Forced Ventilation Tests

Forced ventilation tests generally exhibited one layer as well as well-stirred characteristics as indicated by the vertical temperature and oxygen concentration profiles.



S103



S104

Figure 66. Typical Predicted Barrier Temperature-Time Histories

These experiments can be compared to those conducted by Foote et al. at Lawrence Livermore National Laboratory [19]. In their tests which had forced ventilation from above, they found that the temperature profiles were linear regardless of the ventilation rate. Foote's results agree with these forced ventilation tests since temperature profiles were linear, and the ventilation rate did not affect this linearity. Since they did not measure the vertical oxygen concentration profile, they could not conclude whether their fires were well-mixed. The gas species profile is an important consideration when modelling these fires. Beyler assumed these fires were well-mixed and was able to successfully predict the extinction time that Foote observed [3]. These tests show for the first time that linear temperature profiles can occur in experiments in which gas concentrations are relatively uniform over height thereby representing well-stirred conditions.

8.0 CONCLUSIONS

A correlation (Eqs. 4 and 8) to predict the time to full room involvement suitable for compartment fires with conductive barriers has been validated for both natural and forced ventilation scenarios. Appropriate heat transfer coefficients for the hot and ambient sides of the barrier are lower than those reported in Beyler's analysis [2]. New values were determined experimentally as $h_h = 30$ and $h_a = 20$ W/m²K. These values correspond to an overall coefficient starting at 30 and decaying to 12 W/m²K. Consequently, these changes should be reflected in the SFSEM submodel for predicting FRI time.

Two vent flow rate prediction methods, the Deal/Beyler Layer Driven Method and the Mowrer Method, were used to determine the exhaust rate to be used in the Peatross/Beyler temperature prediction equation. These methods were not extremely reliable for predicting the vent flow rate; however, since the Peatross/Beyler correlation is not very sensitive to changes in the exhaust rate, temperature predictions were good. The McCaffrey, Harkleroad, and Quintiere Method was also used to predict upper layer temperatures. Using Beyler's equation of the overall heat transfer coefficient multiplied by a factor of 2.5, excellent results were obtained.

In summary, the Peatross/Beyler Method is preferred in situations where the vent flow rates are known. In cases where the vent flow rate is not known, the MQH Method presents a better prediction of temperature than vent flow rate prediction techniques.

9.0 REFERENCES

1. Richards, R.C., "Fire Safety Analysis of the Polar Icebreaker Replacement Design," U.S. Coast Guard Report, CG-M-04-88, 1987.
2. Beyler, C., "Effects of ceiling ventilation on the time to full room involvement," Task 5 Report, DTCG 39-87-D-80559, Worcester Polytechnic Institute, Worcester, MA, 1989.
3. Beyler, C.L., "Analysis of Compartment Fires with Overhead Forced Ventilation," *Proceedings of the Third International Symposium on Fire Safety Science*, 1992, pp. 291-300.
4. Deal, S., and Beyler, C., "Correlating Preflashover Room Fire Temperatures," *Journal of Fire Protection Engineering*, 2 (2), 1990, pp. 33-48.
5. Personal Communications with Richard J. Roby.
6. Babrauskas, V., "Burning Rates," *SFPE Handbook of Fire Protection Engineering*, P.J. DiNenno, ed., 1990.
7. Gottuk, D.T., "Generation of Carbon Monoxide in Compartment Fires," NIST-GCR-92-619, National Institute of Standards and Technology, 1992.
8. "Special Reference Material Report GM 21 and GM 22," Materials Bank Compendium of Fire Property Data, Product Research Committee, 1980.
9. McCaffrey, B.J., and Heskestad, G., "A Robust Bidirectional Low-Velocity Probe for Flame and Fire Application," Brief Communication, *Combustion and Flame*, 26, 1976, pp. 125-127.

10. Janssens, M., and Tran, H.C., "Data Reduction of Room Tests for Zone Model Validation," *Journal of Fire Sciences*, 10, Nov.-Dec. 1992, pp. 528-555.
11. Steckler, K.D., Quintiere, J.G., and Rinkinen, W.J., "Fire Induced Flows Through Room Openings - Flow Coefficients," *Twentieth Symposium on Combustion*, The Combustion Institute, 1984, pp. 1591-1600.
12. Janssens, M., and Parker, W.J., "Oxygen Consumption Calorimetry," *Heat Release in Fires*, V. Babrauskas and S. J. Grayson, ed., Elsevier Applied Science, NY, 1992
13. Prahl, J. and Emmons, H.W., "Fire Induced Flow Through an Opening," *Combustion and Flame*, 25, 369-385.
14. Rockett, J.A., "Fire Induced Gas Flow in an Enclosure," *Combustion Science and Technology*, 12, 1976, pp. 165-175.
15. Zukoski, E., Kubota, T., and Cetegen, B., "Entrainment in Fire Plumes," *Fire Safety Journal*, 3, 1981, pp. 107-121.
16. Heskestad, G., "Engineering Relations for Fire Plumes," *Fire Safety Journal*, 7, 1984, pp. 25-32.
17. Mowrer, F.W., "A Closed-Form Estimate of Fire-Induced Ventilation Through Single Rectangular Wall Openings," *Journal of Fire Protection Engineering*, 4 (3), 1992, pp. 105-114.
18. McCaffrey, B., Quintiere, J., Harkleroad, M., "Estimating Room Fire Temperature and the Likelihood of Flashover using Fire Test Data Correlations," *Fire Technology*, 17 (2), 1981, pp. 133-145.

19. Backovsky, J., Foote, K.L., and Alvares, N.J., "Temperature Profiles in Forced-Ventilation Enclosure Fires," *Proceedings of the Second International Symposium on Fire Safety Science*, Hemisphere Publishing Corp., New York, pp. 315-324, 1989.

10. ACKNOWLEDGEMENTS

The authors wish to thank Rob Richards, Dave Beene, and Mark Cummings of the Marine Fire and Safety Research Division in Groton, CT for their support on this project. Also, they would like to express their appreciation to the personnel at the Fire and Safety Test Detachment in Mobile, AL for their tremendous amount of hard work and cooperation which allowed this test series to be a success. The assistance of Worcester Polytechnic Institute in providing technical review is gratefully acknowledged.

APPENDIX A. Series 1 Test Results

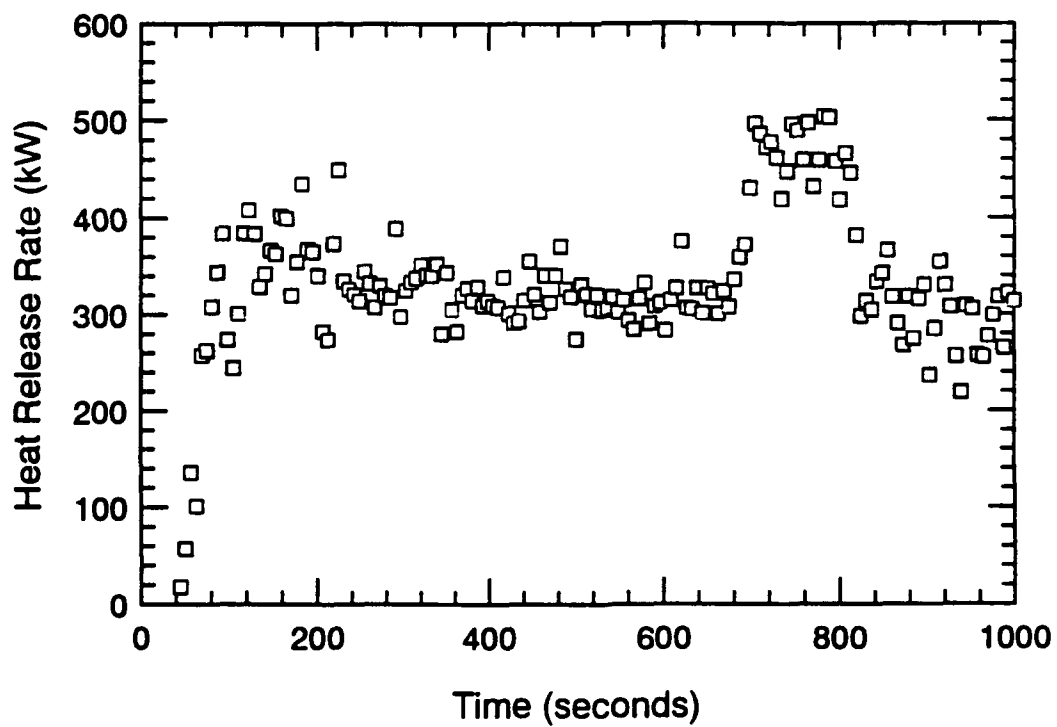
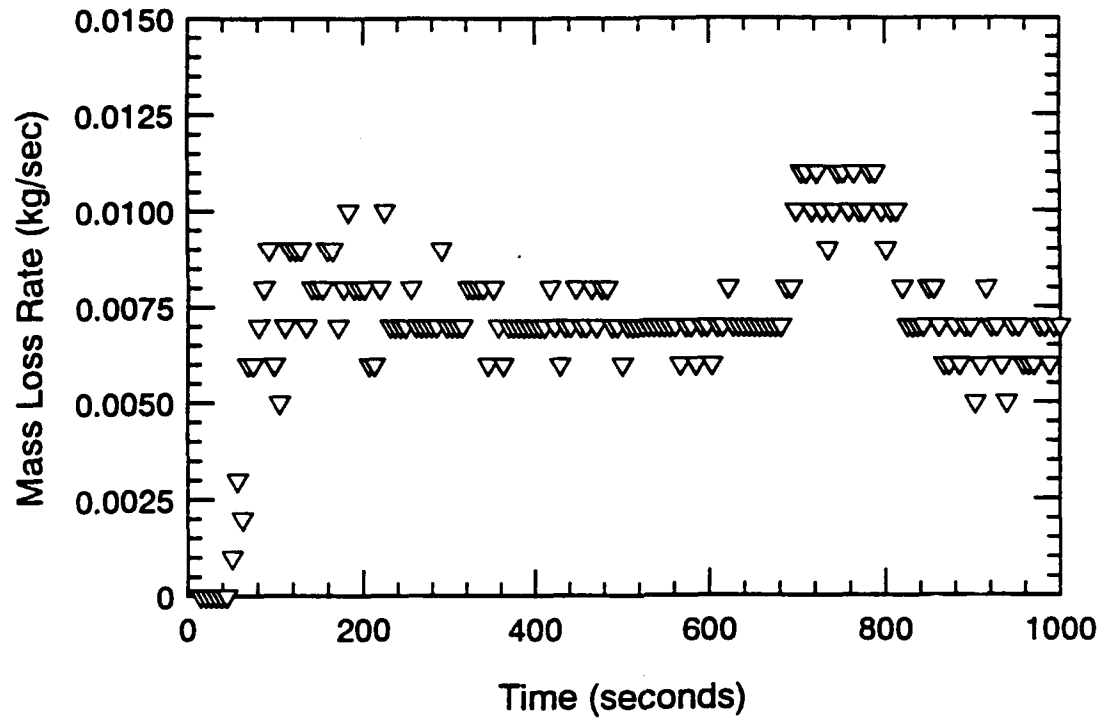


Figure A.1 Mass Loss Rate and Heat Release Rate-Time Histories - S101

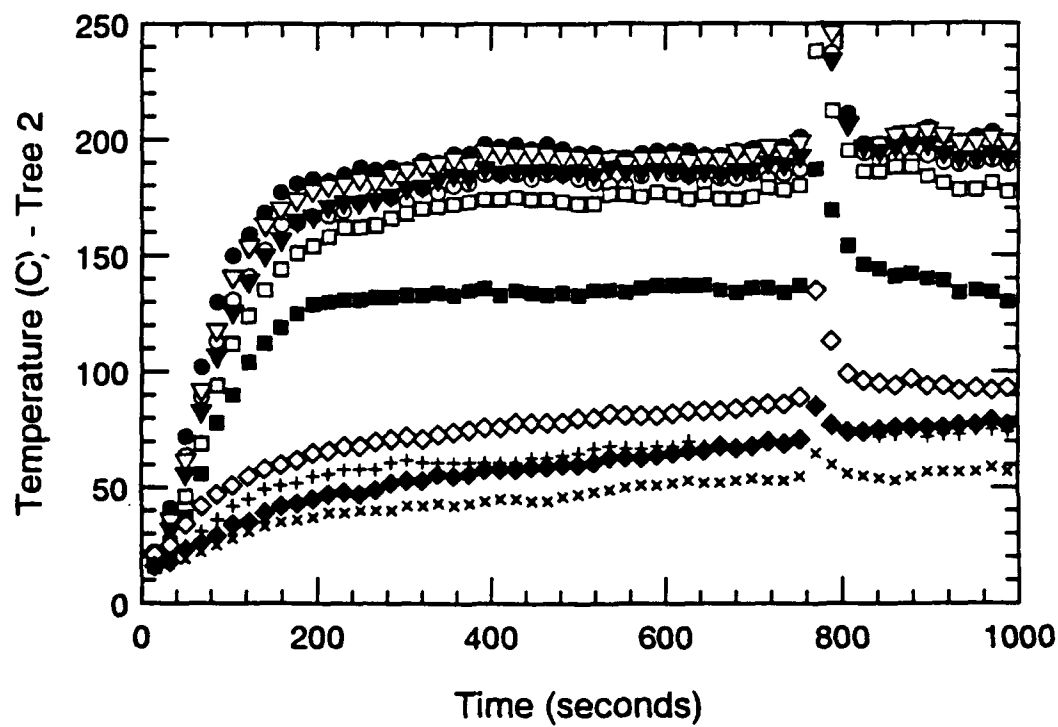
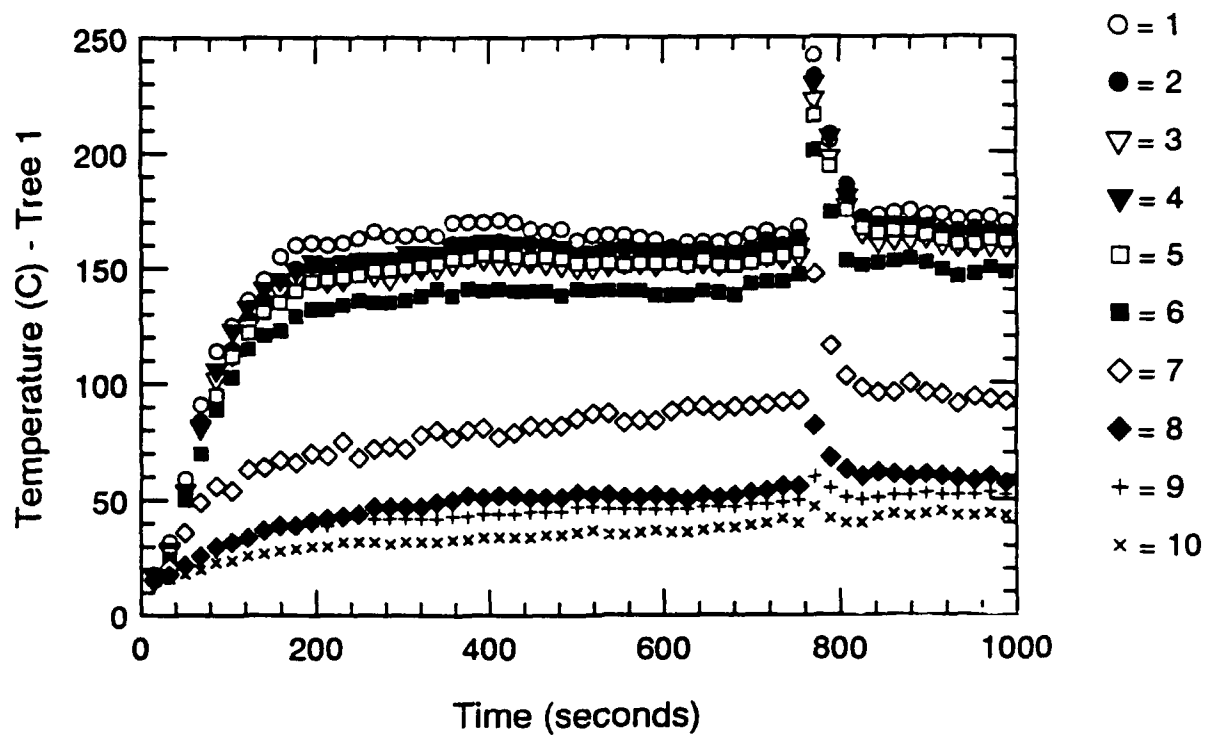


Figure A.2 Thermocouple Trees 1 & 2-Time Histories - S101

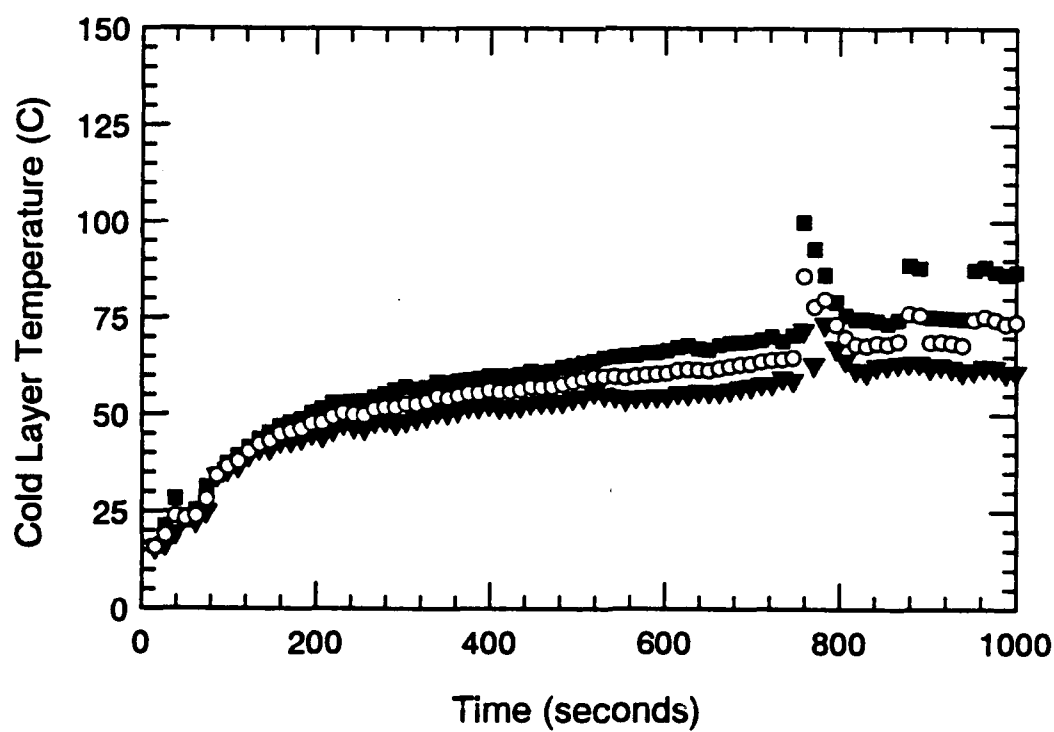
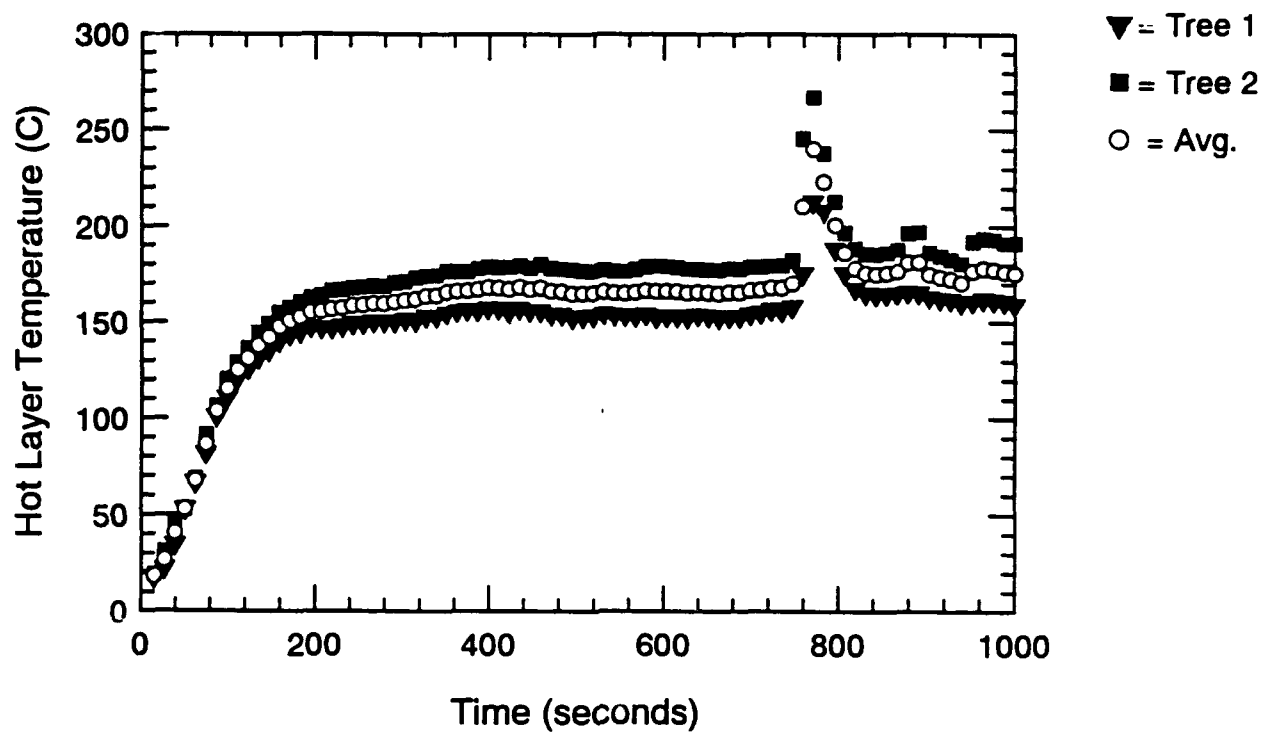


Figure A.3 Hot and Cold Layer Temperature-Time Histories - S101

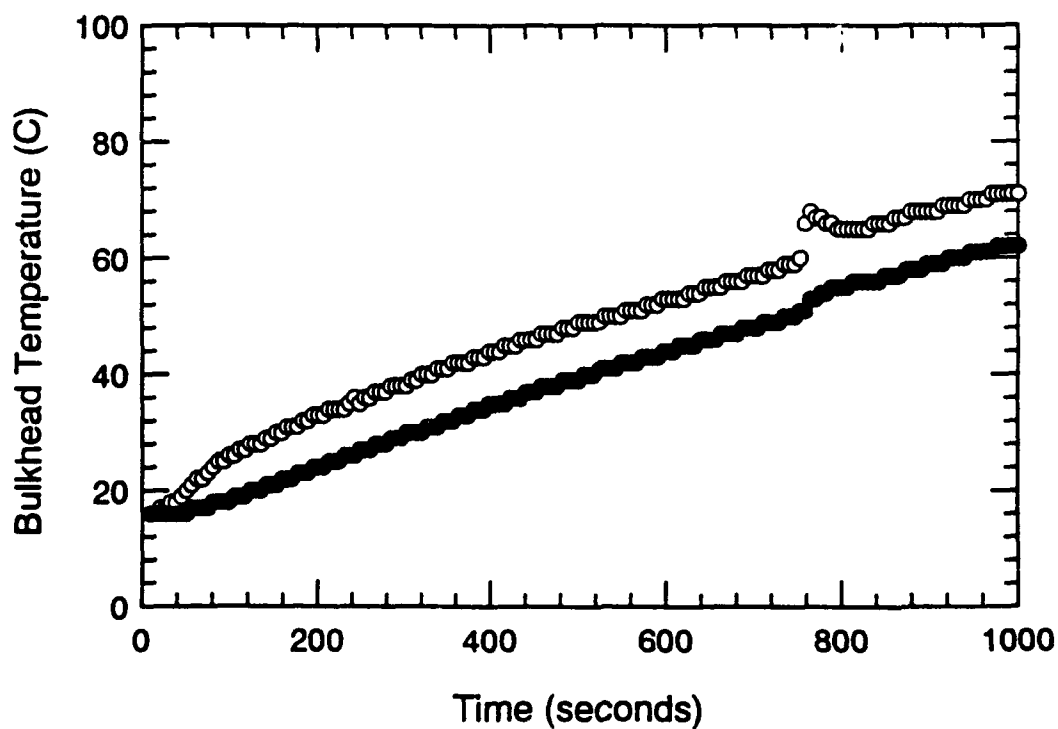
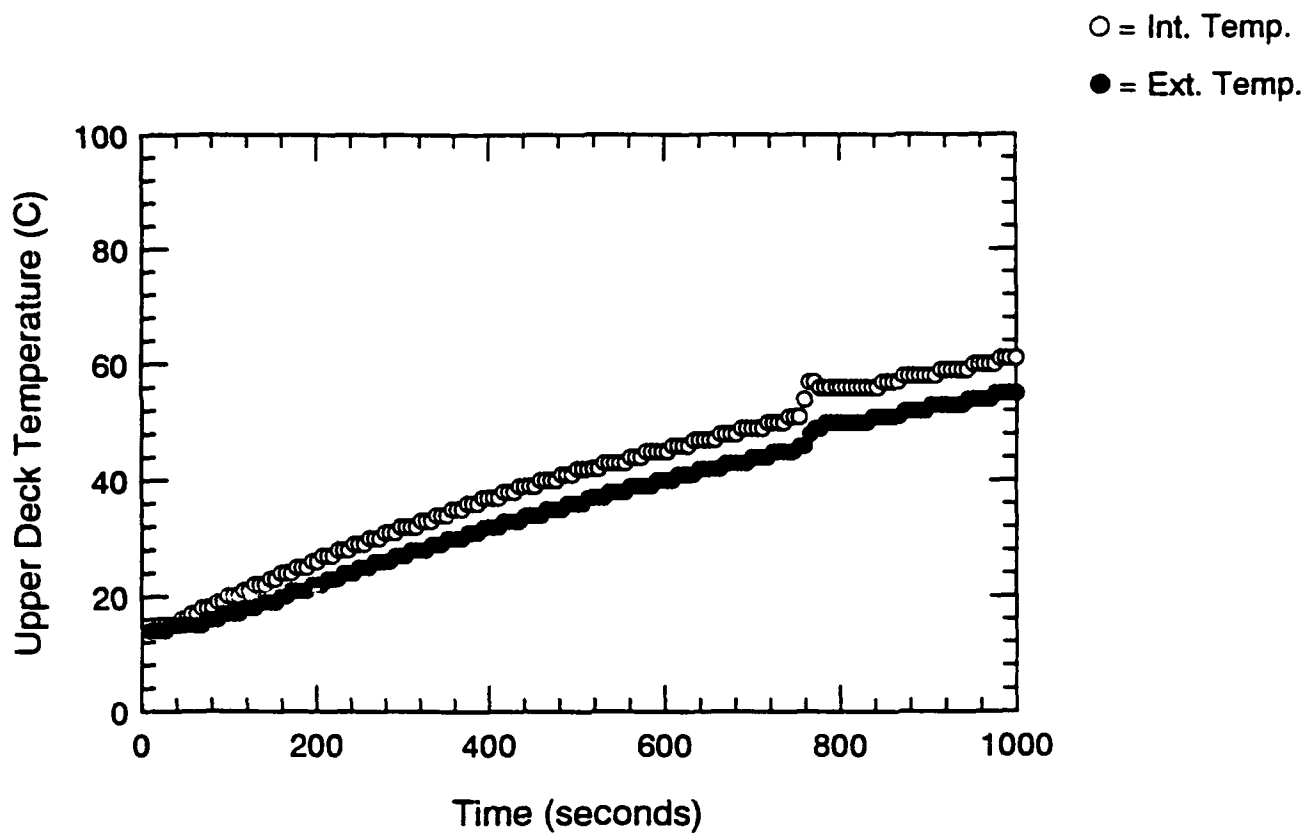


Figure A.4 Surface Thermocouple-Time Histories - S101

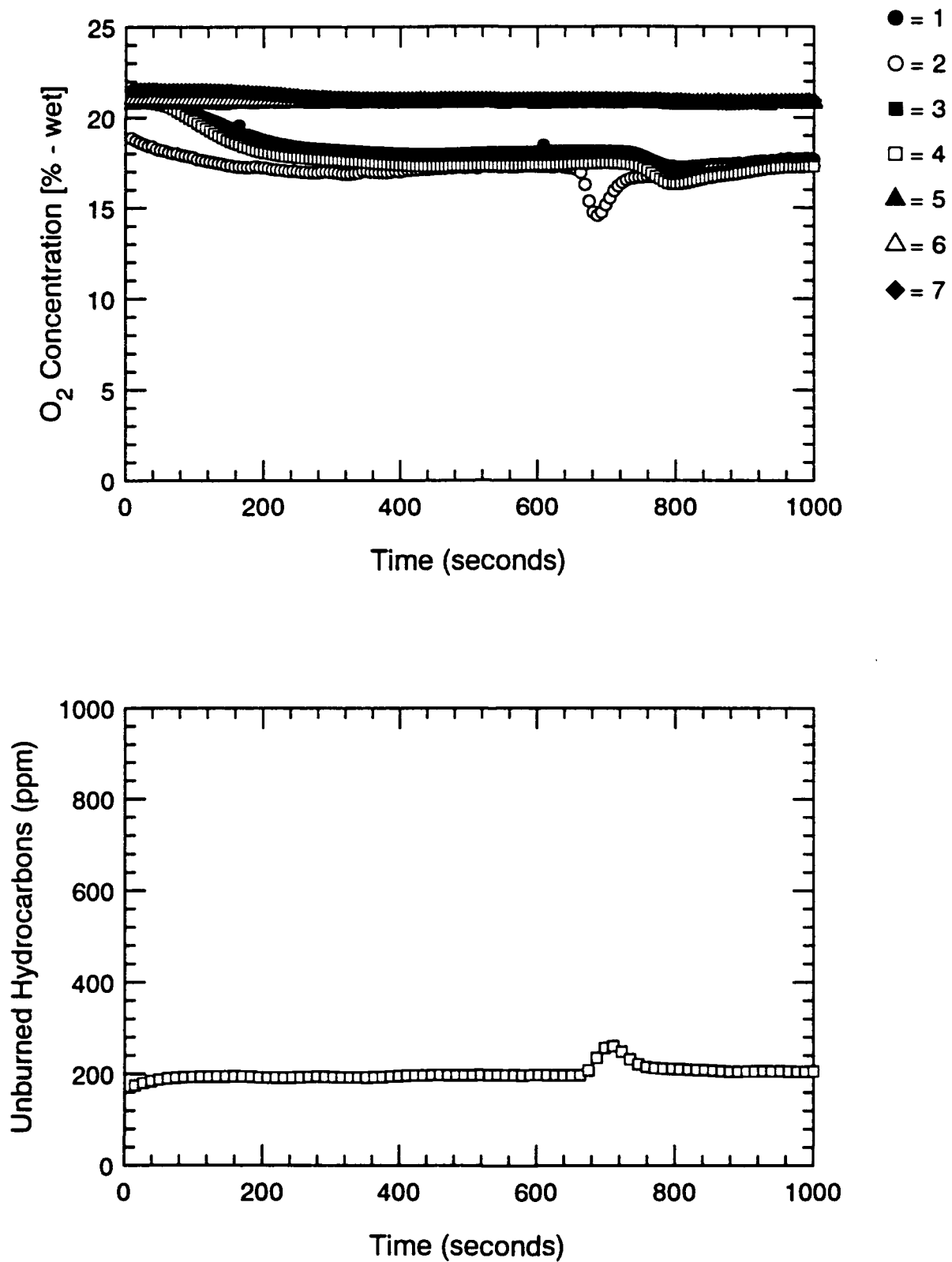


Figure A.5 Oxygen and Unburned HC Concentration-Time Histories - S101

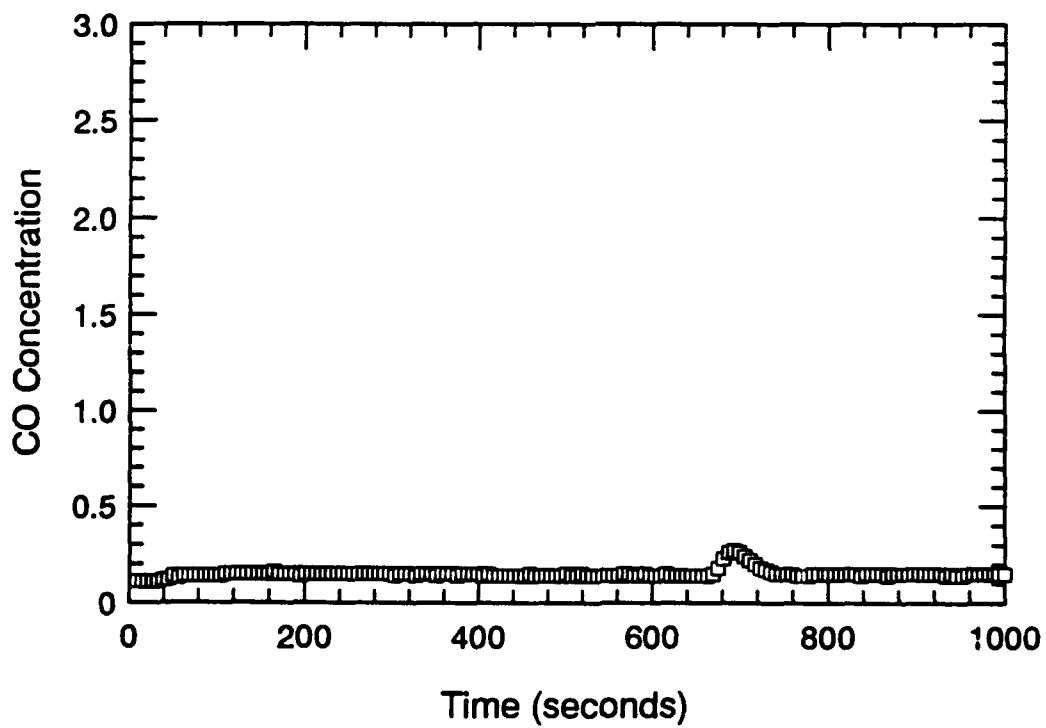
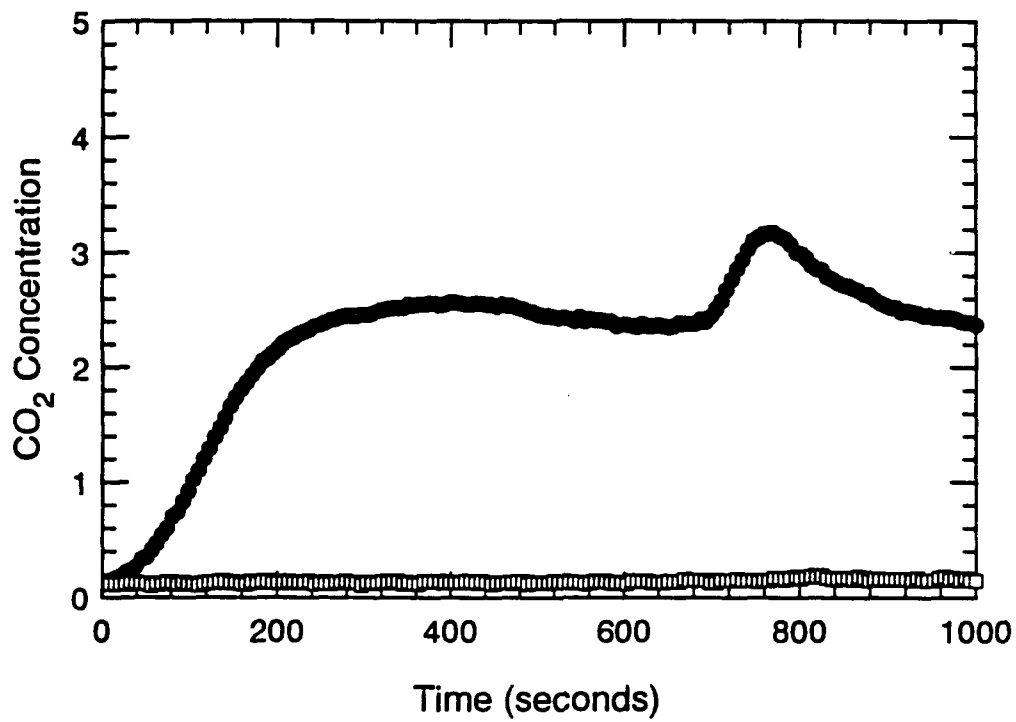


Figure A.6 CO₂ and CO Concentration-Time Histories - S101

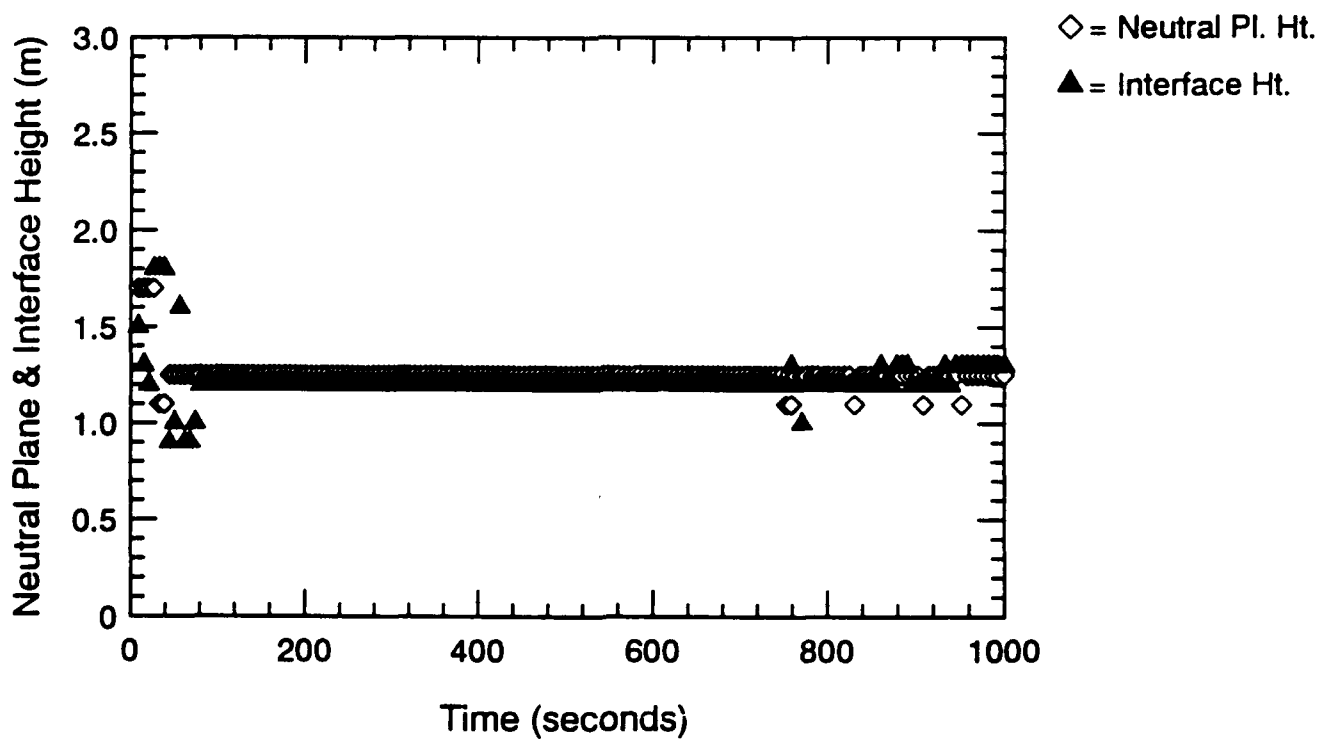
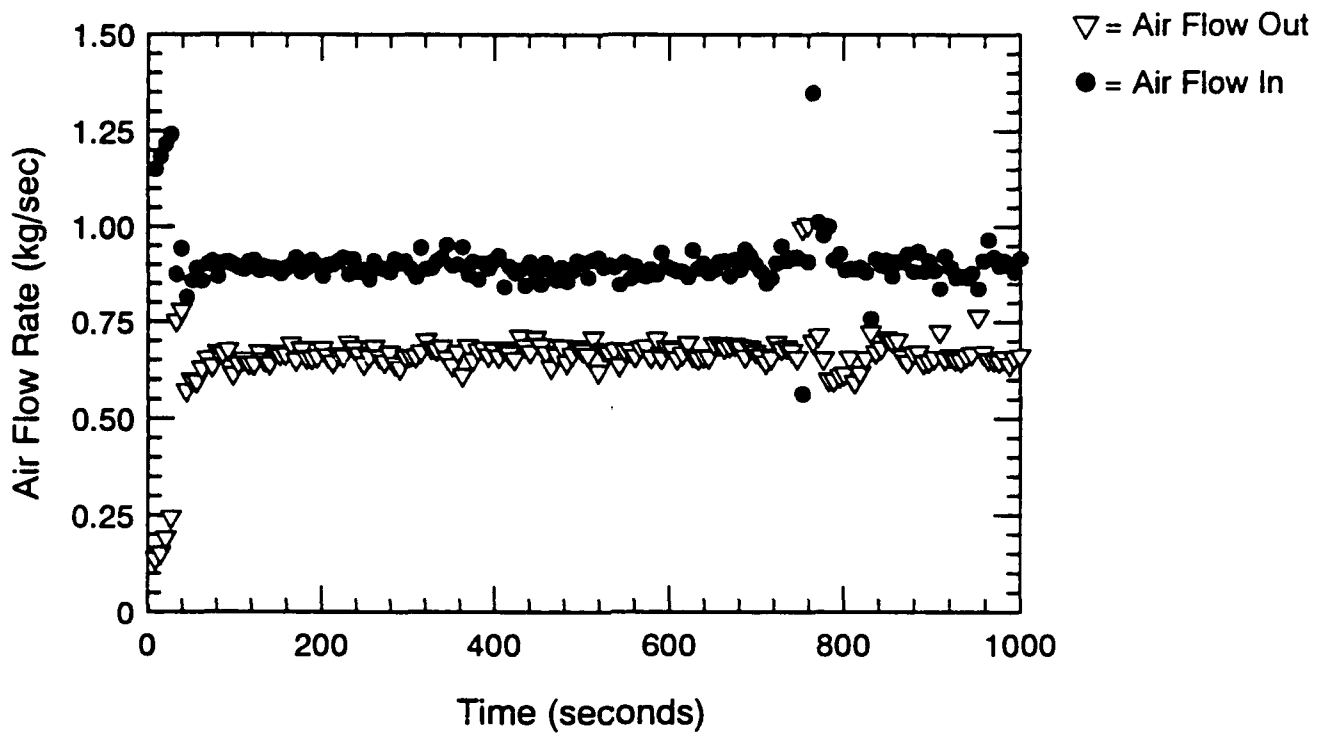


Figure A.7 Air Flow Rate, Neutral Plane & Interface Ht.-Time Histories - S101

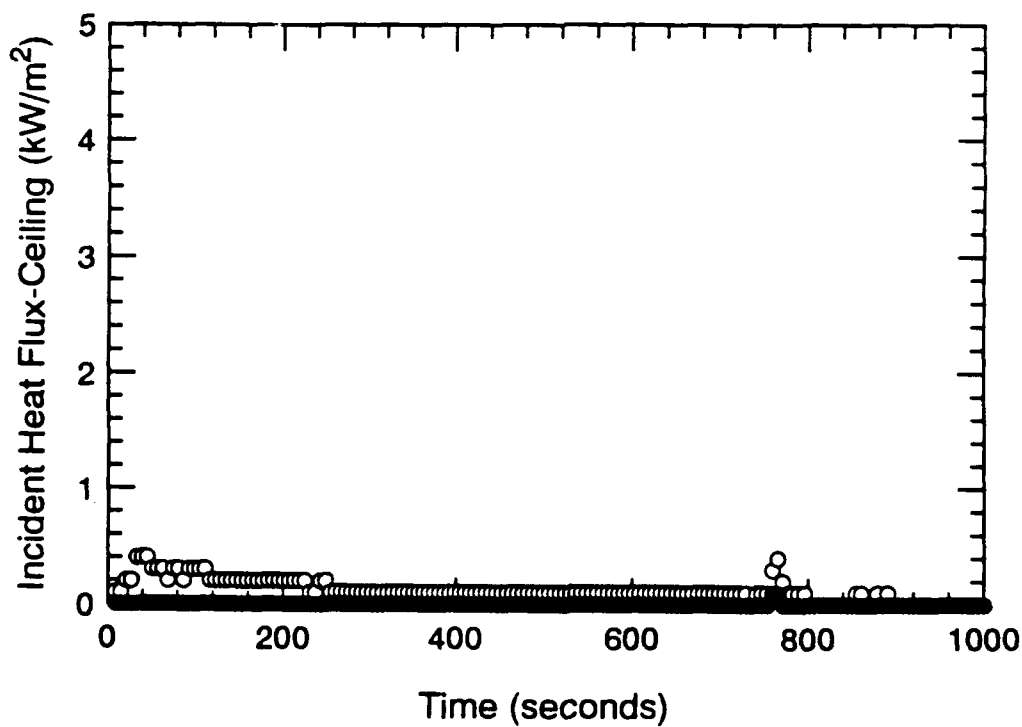
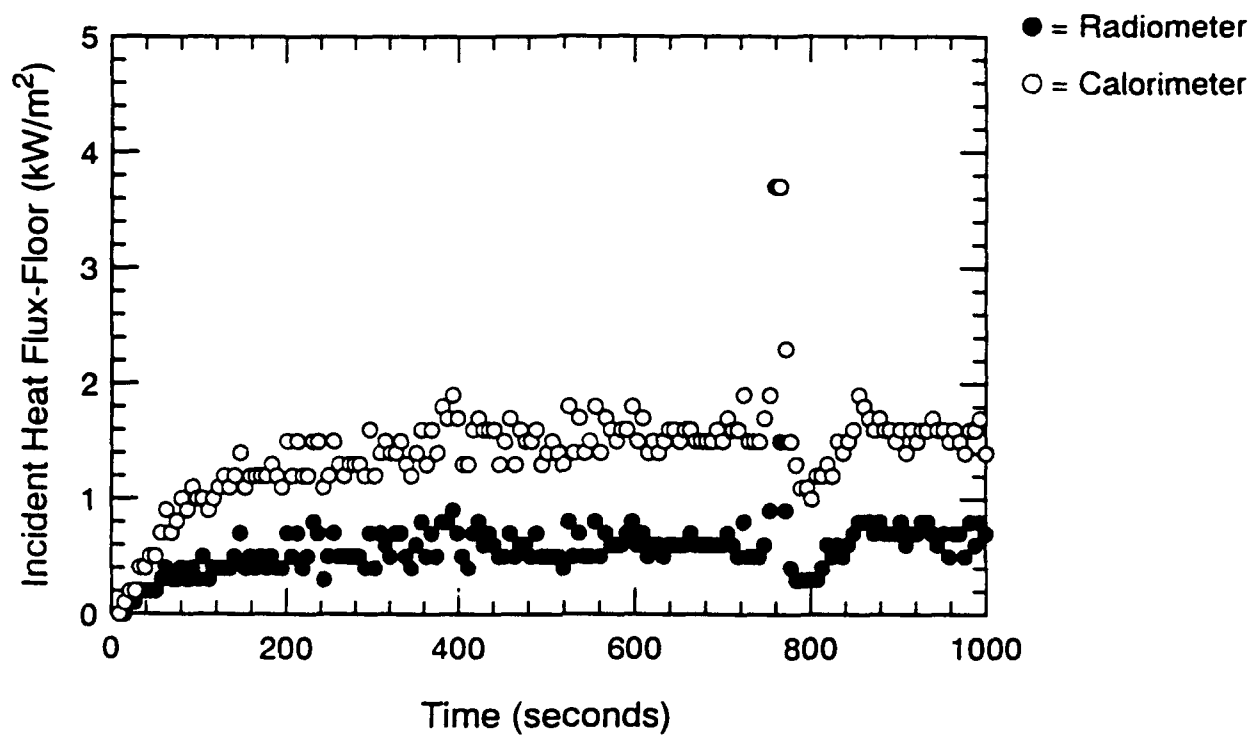


Figure A.8 Incident Heat Flux at Floor and Ceiling-Time Histories - S101

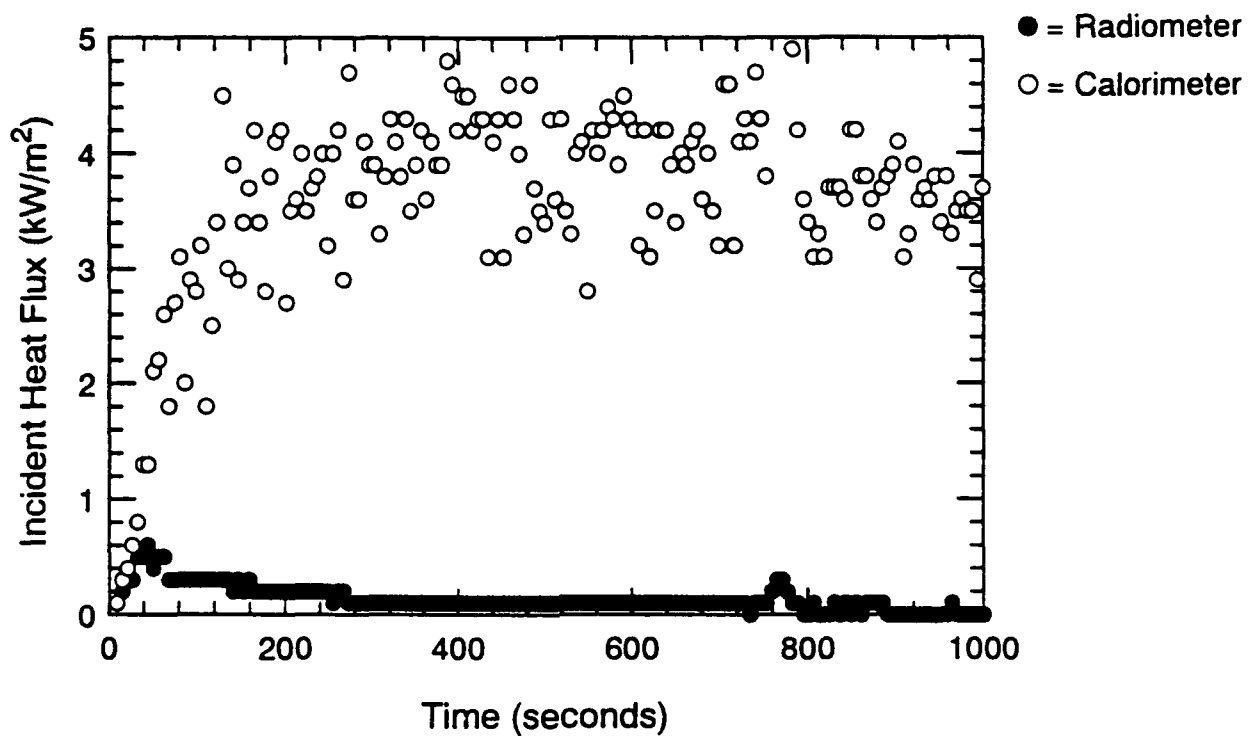


Figure A.9 Incident Heat Flux at Fwd. Bulkhead-Time Histories - S101

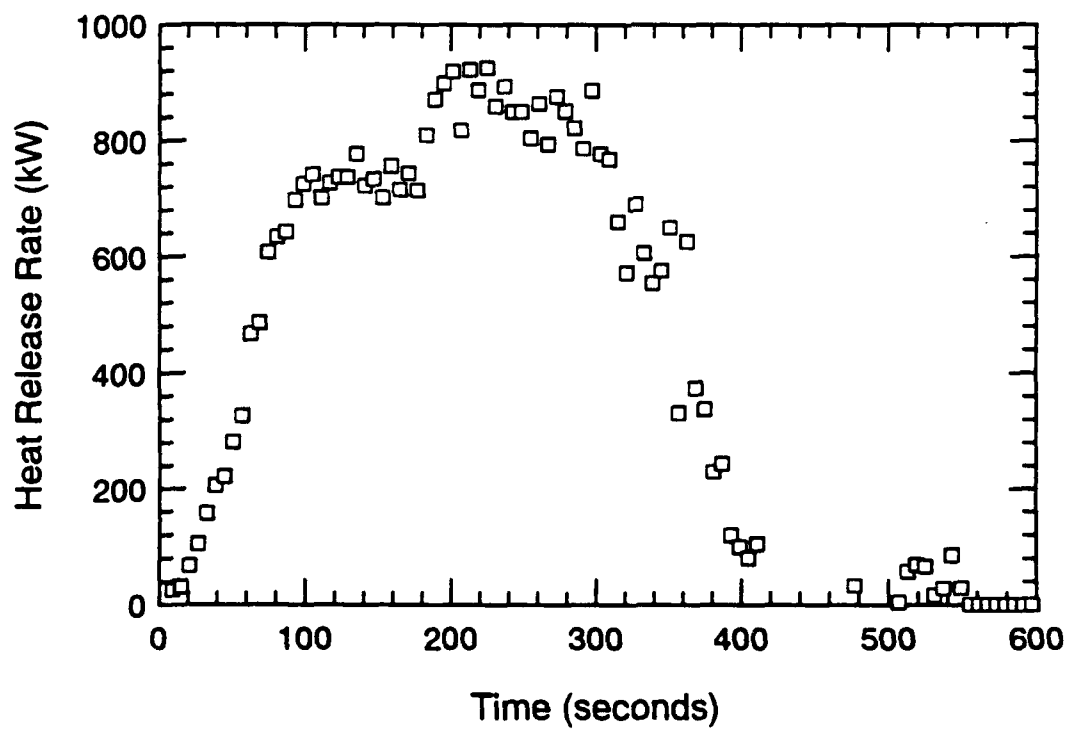
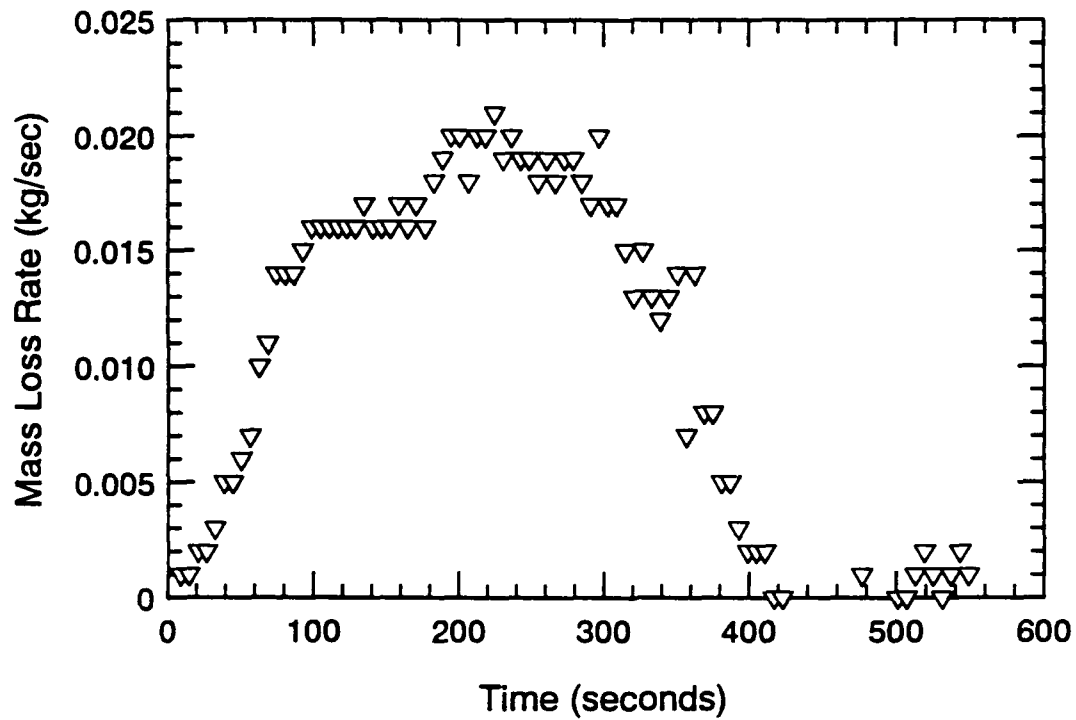


Figure A.10 Mass Loss Rate and Heat Release Rate-Time Histories - S102

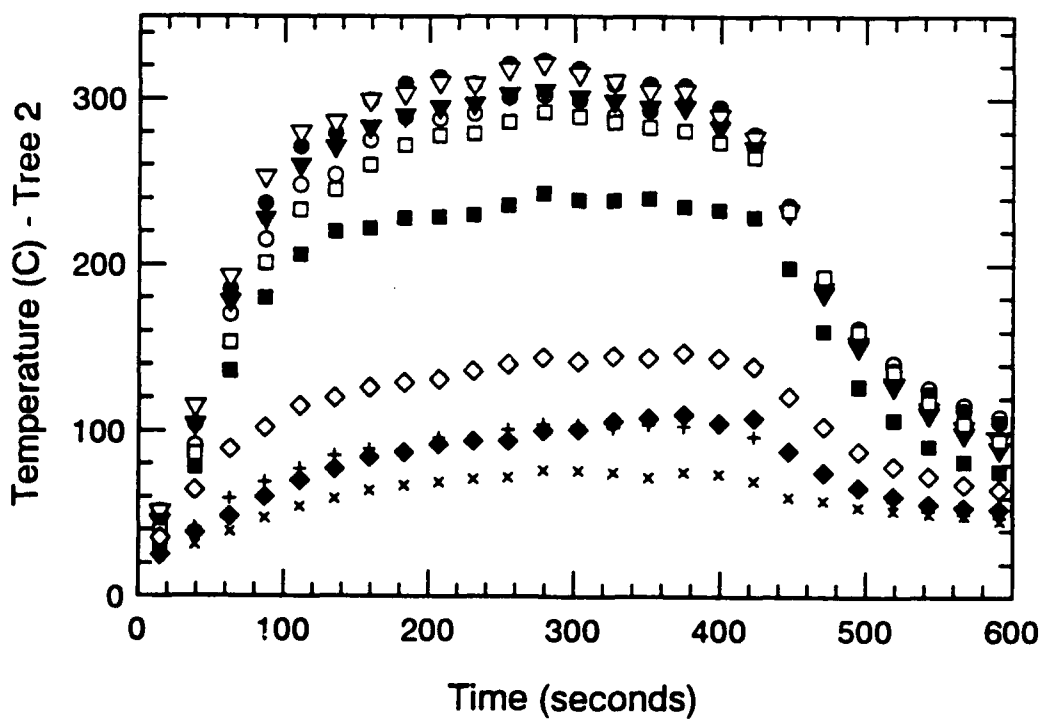
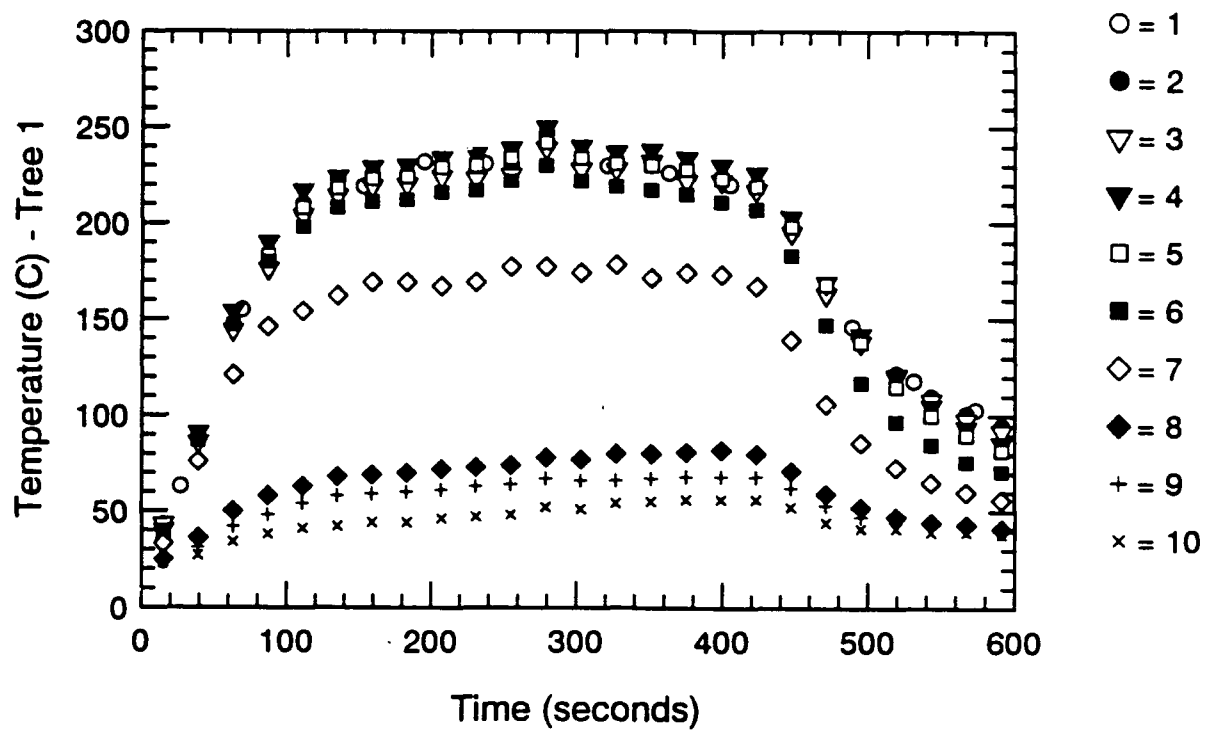


Figure A.11 Thermocouple Trees 1 & 2-Time Histories - S102

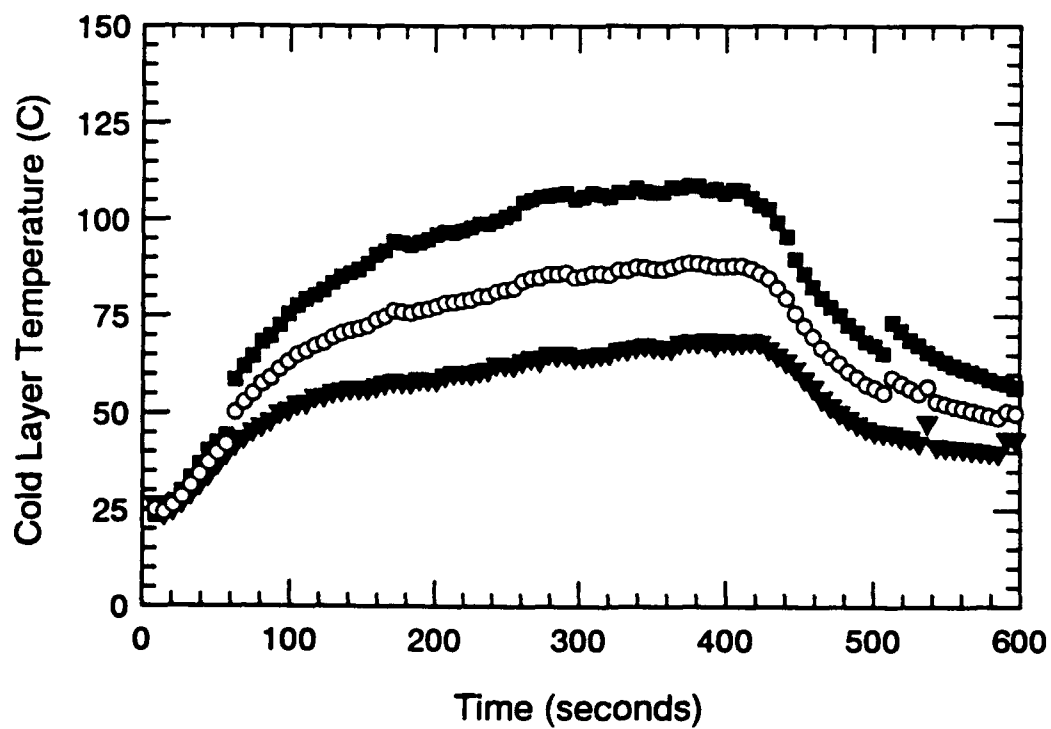
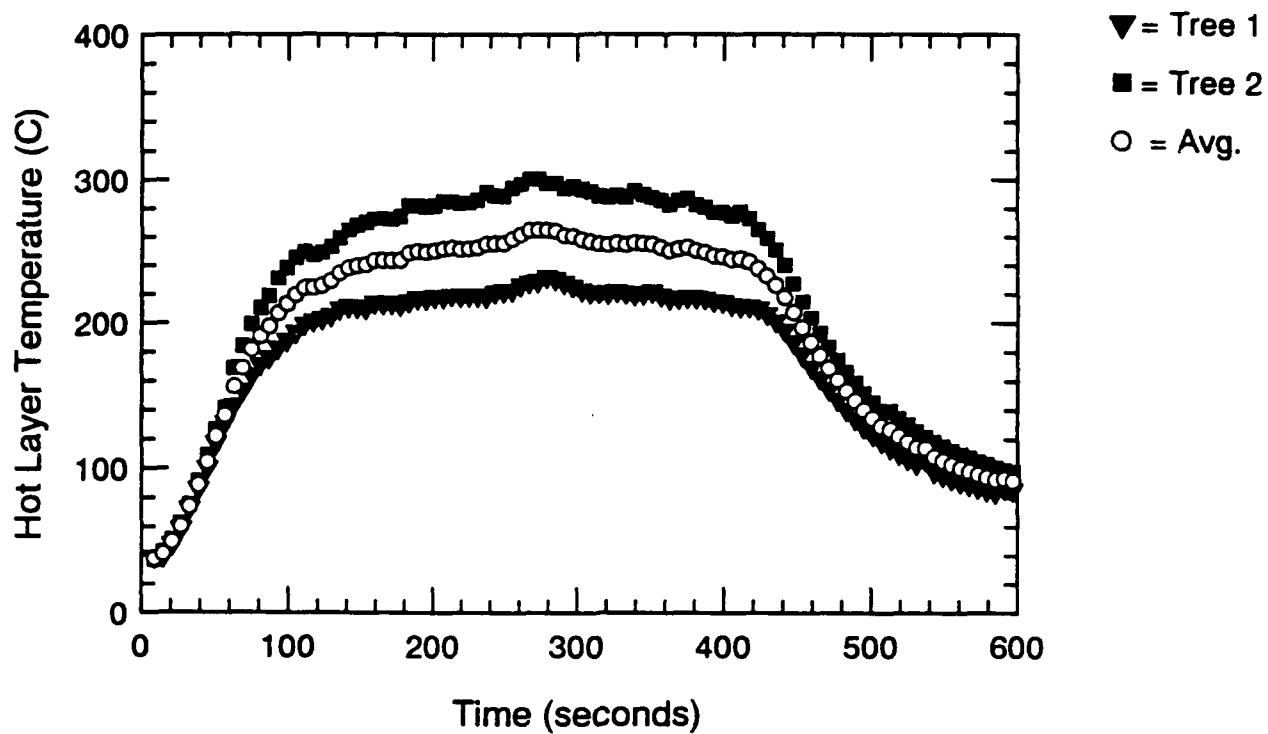


Figure A.12 Hot and Cold Layer Temperature-Time Histories - S102

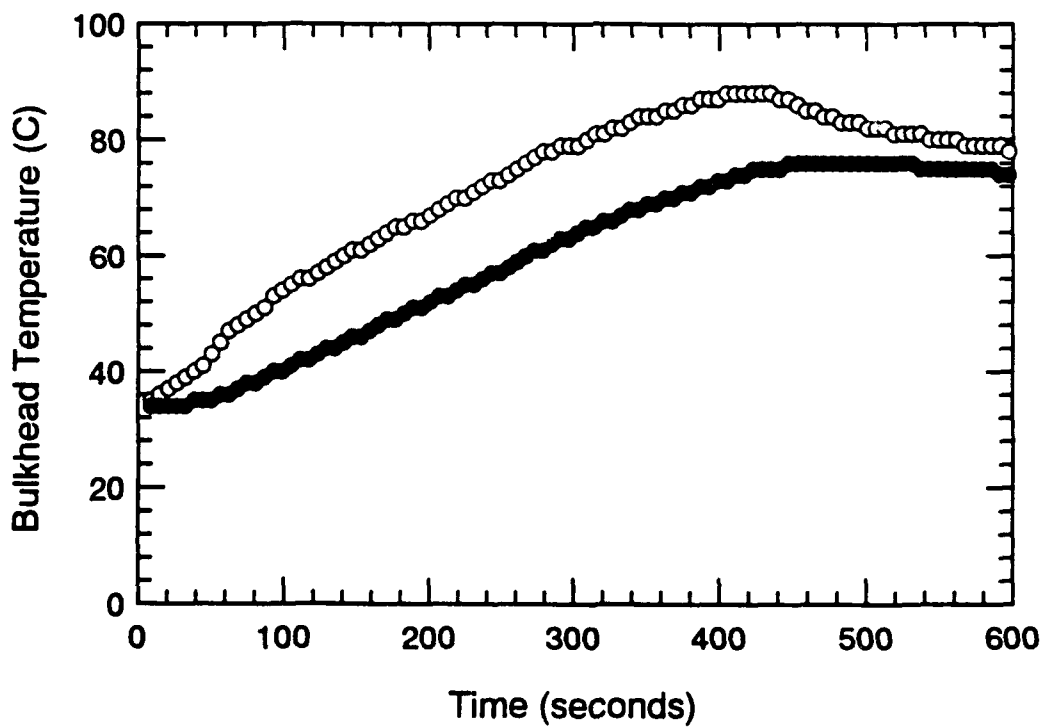
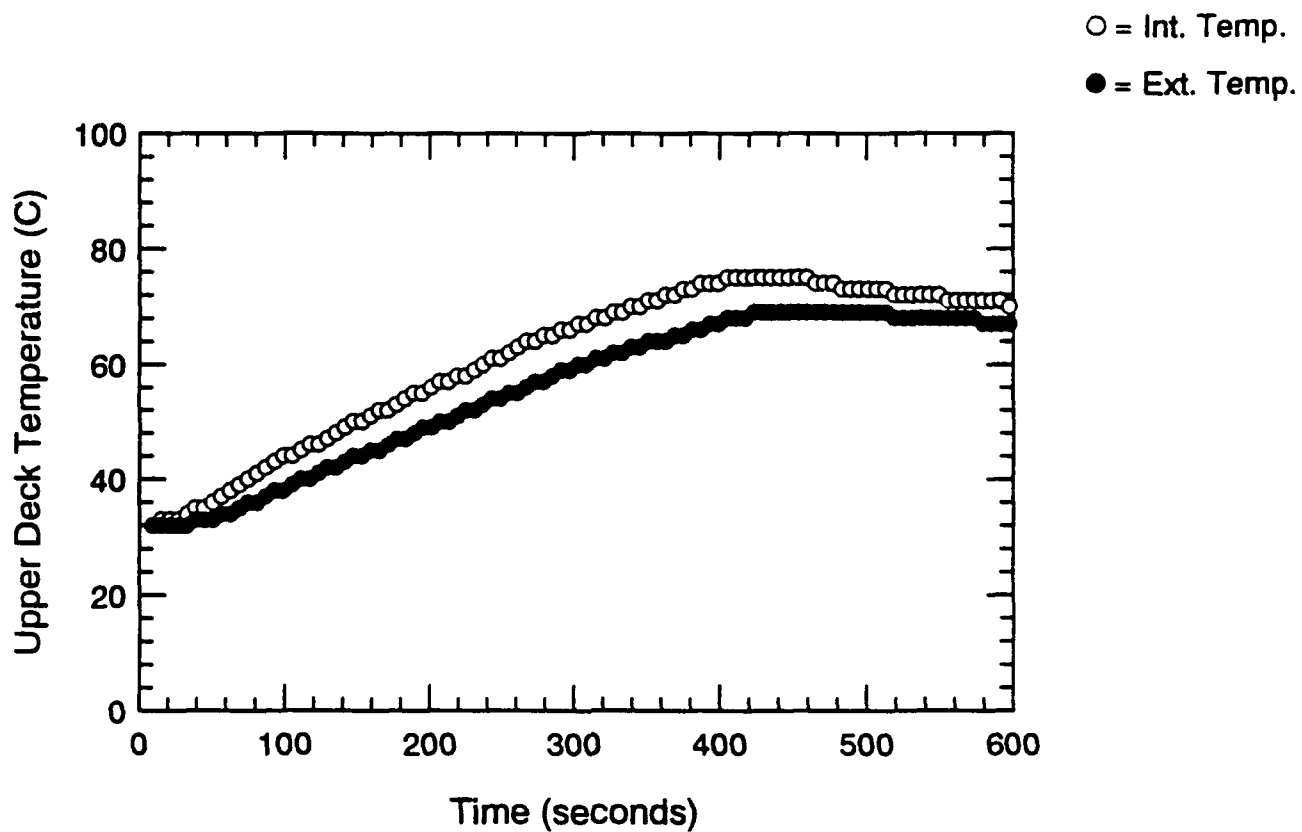


Figure A.13 Surface Thermocouple-Time Histories - S102

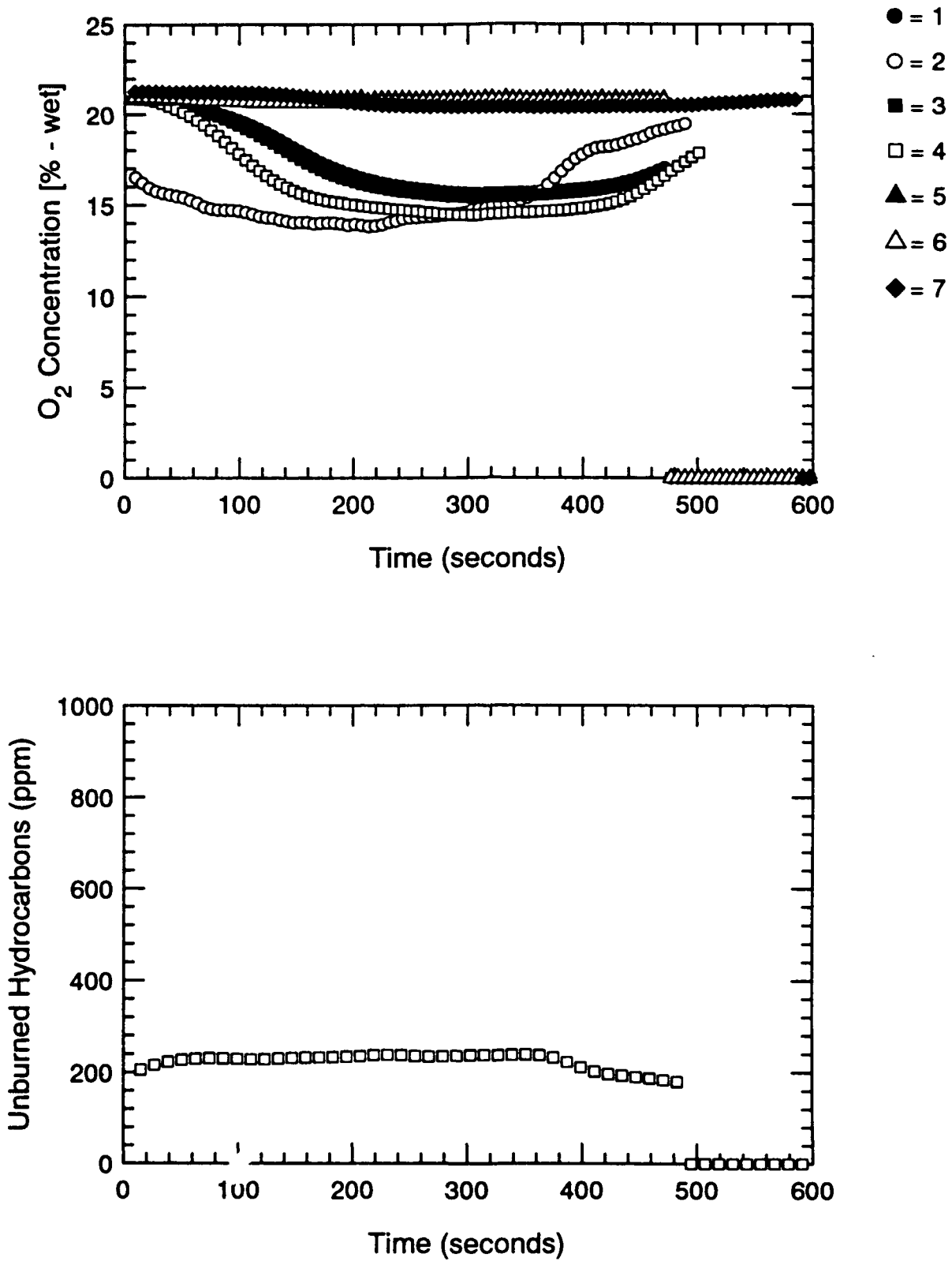


Figure A.14 Oxygen and Unburned HC Concentration-Time Histories - S102

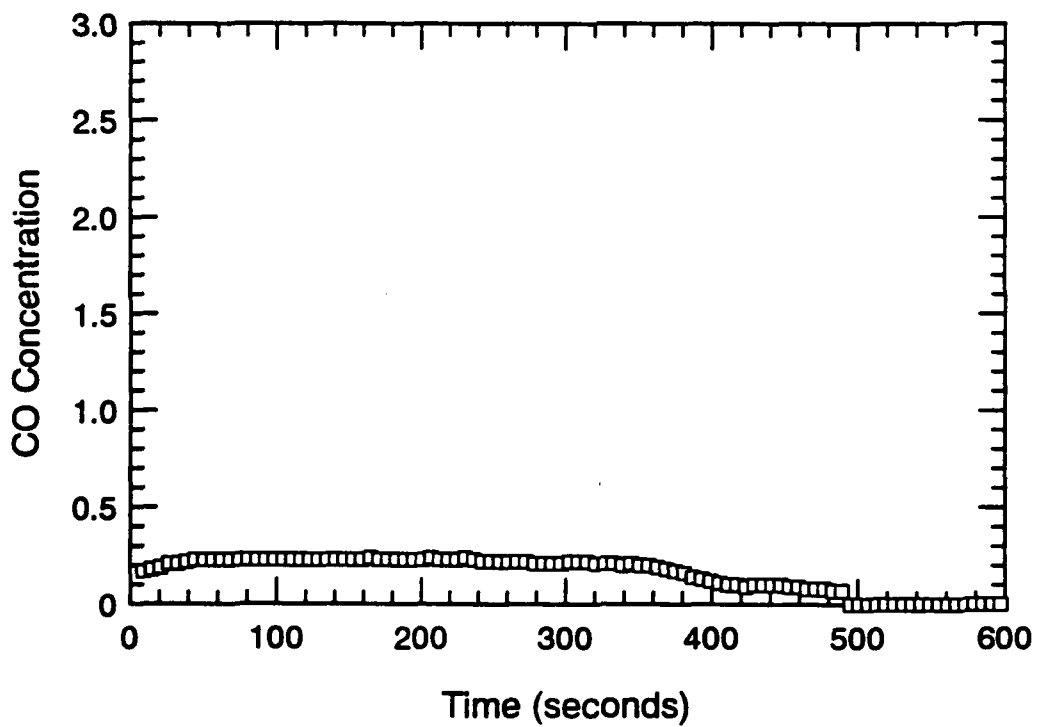
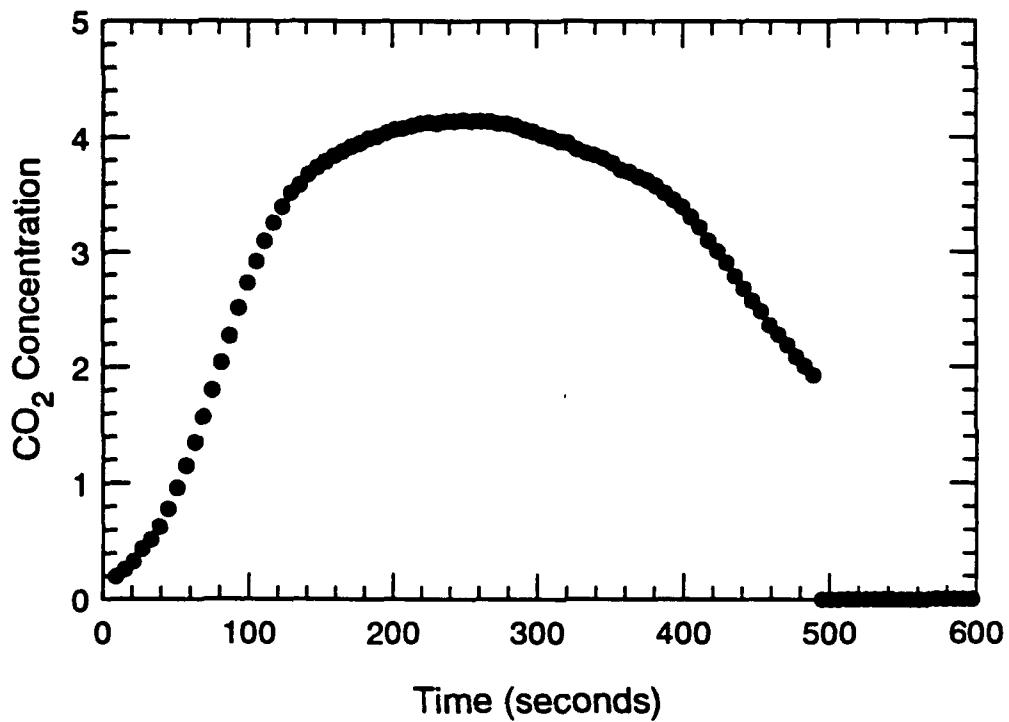


Figure A.15 CO₂ and CO Concentration-Time Histories - S102

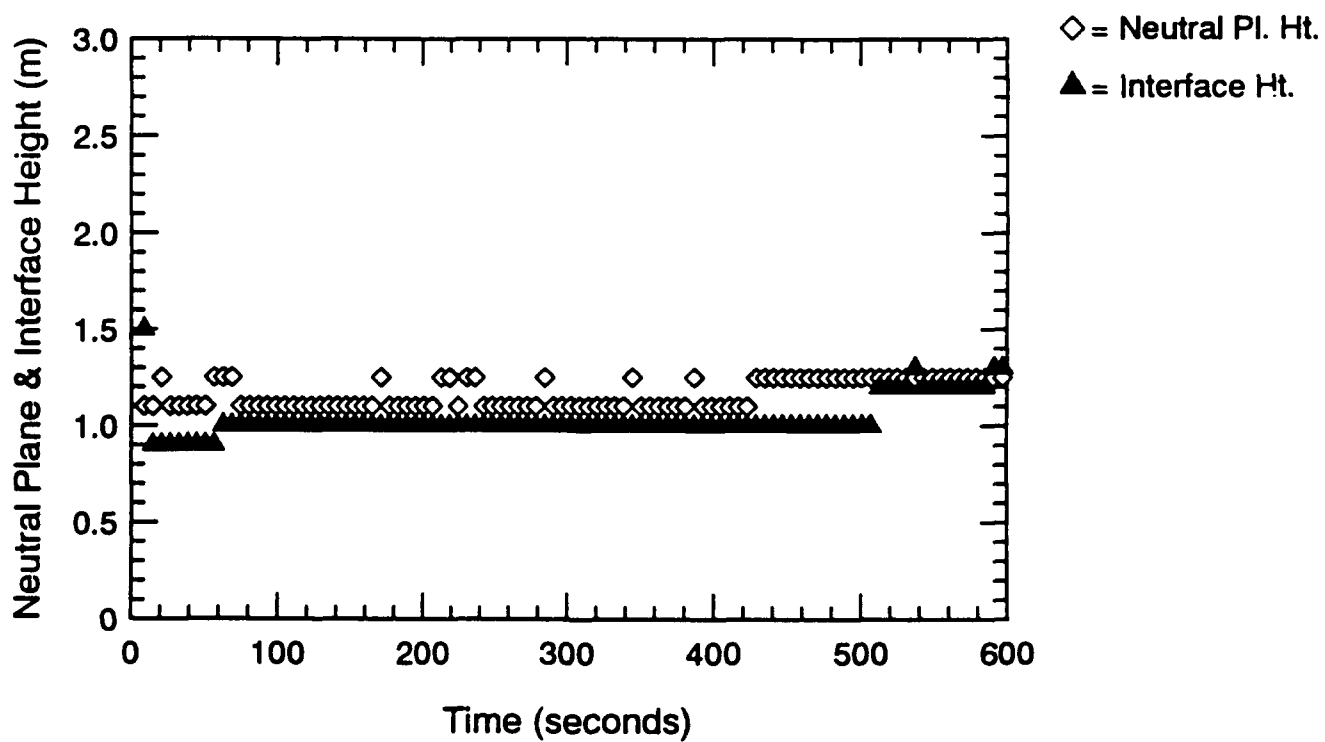
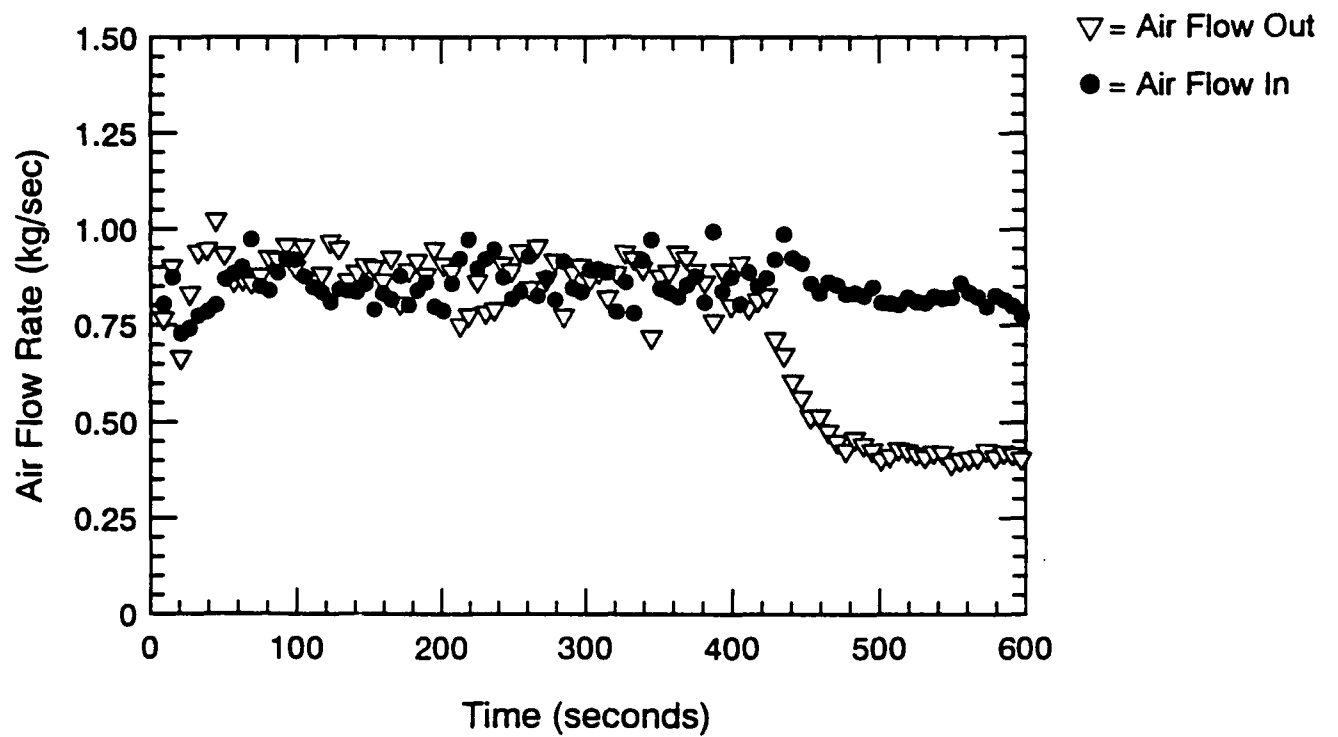


Figure A.16 Air Flow Rate, Neutral Plane & Interface Ht.-Time Histories - S102

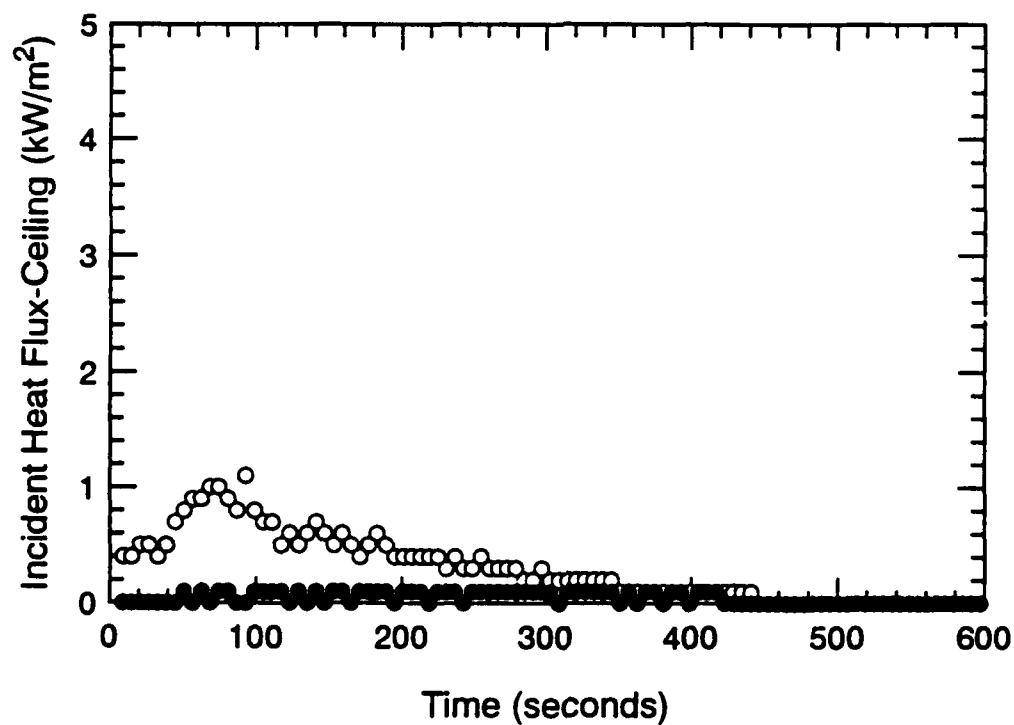
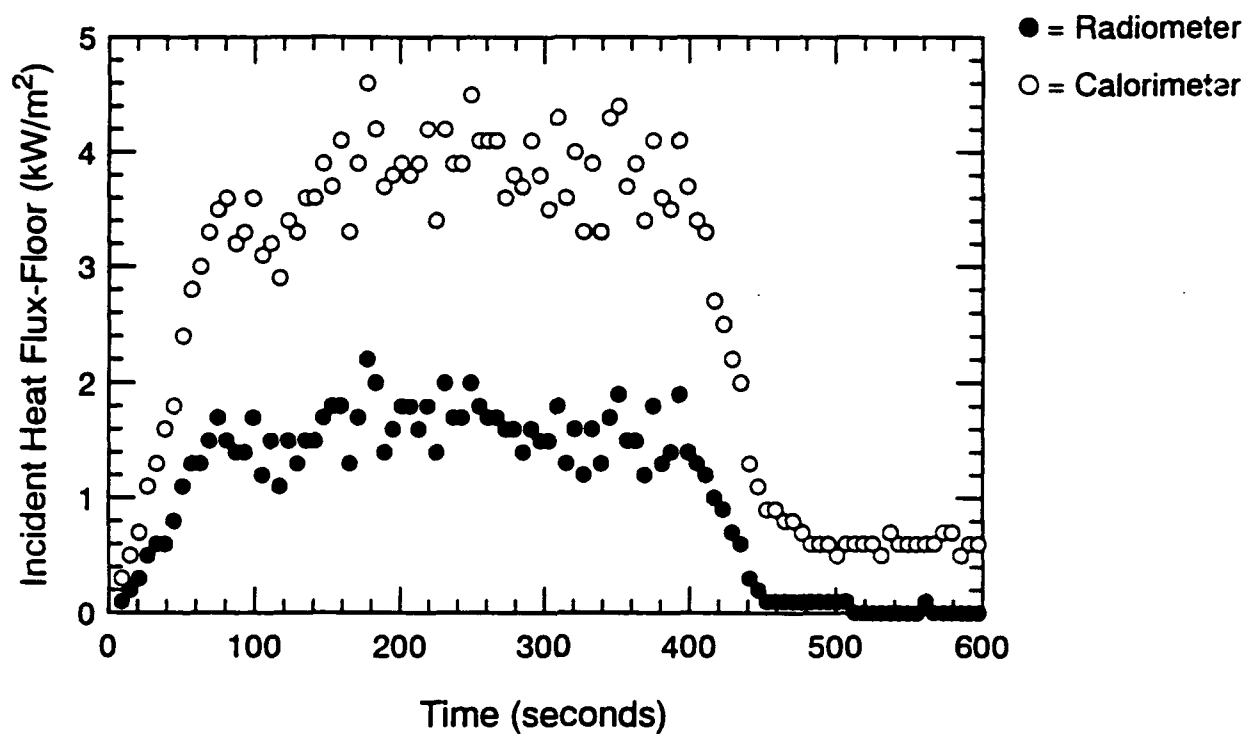


Figure A.17 Incident Heat Flux at Floor and Ceiling-Time Histories - S102

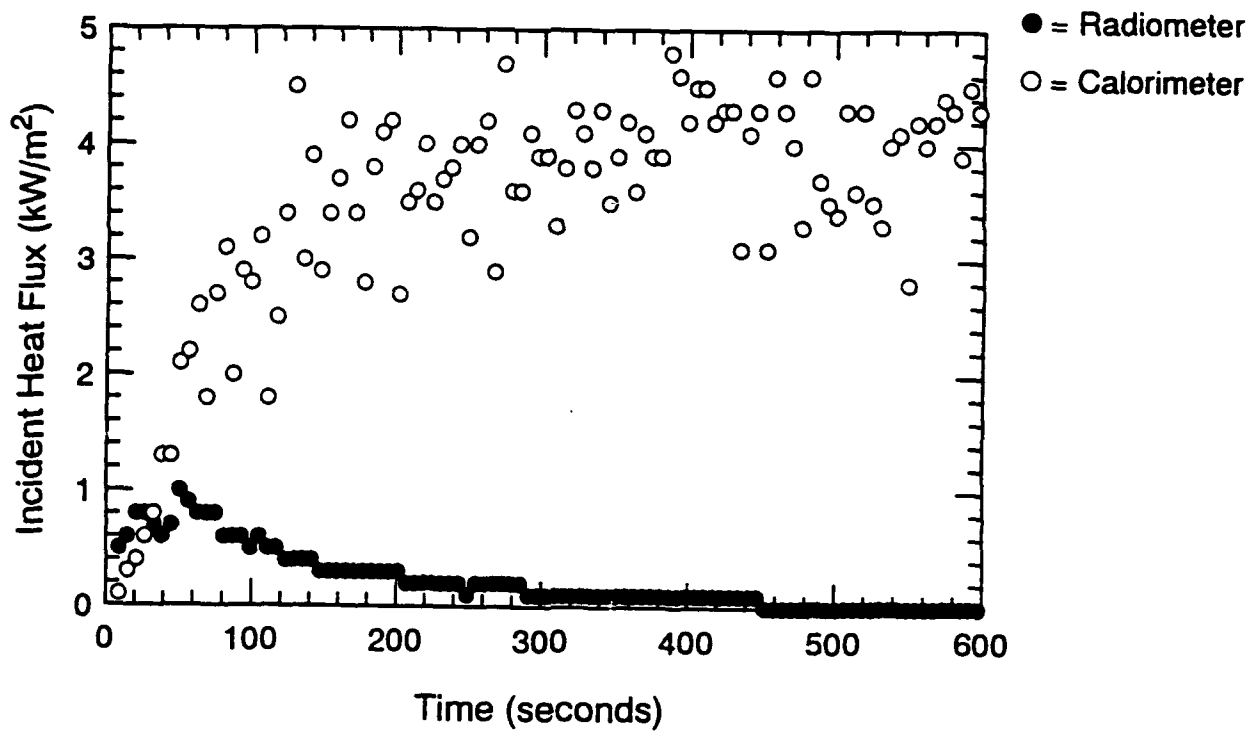


Figure A.18 Incident Heat Flux at Fwd. Bulkhead-Time Histories - S102

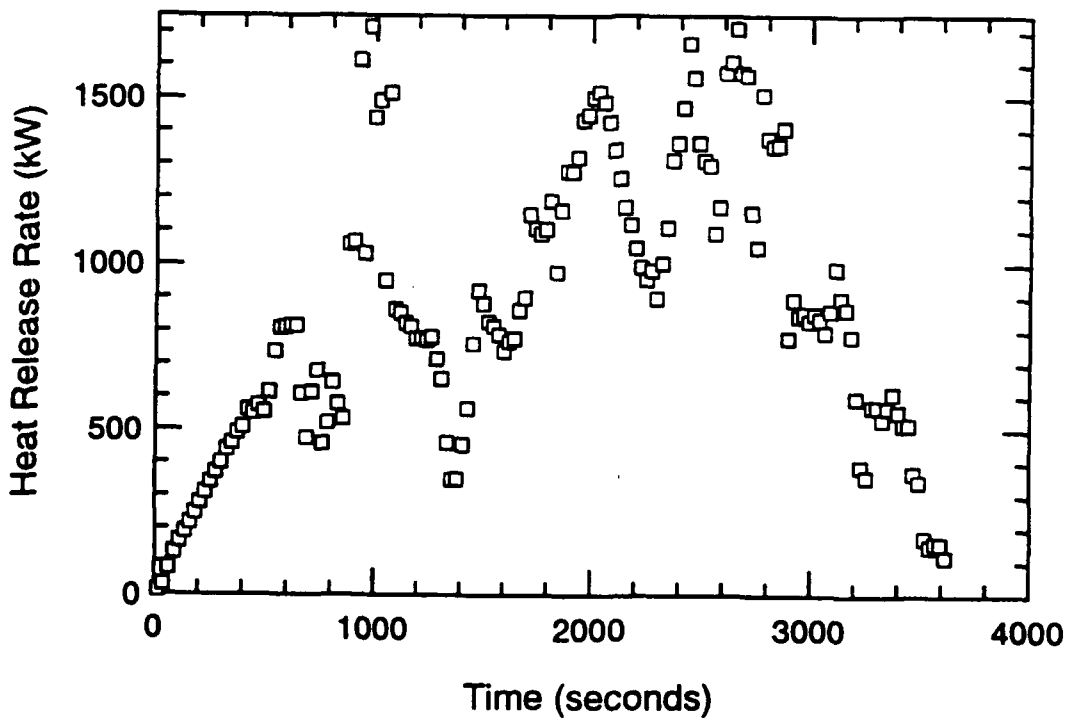
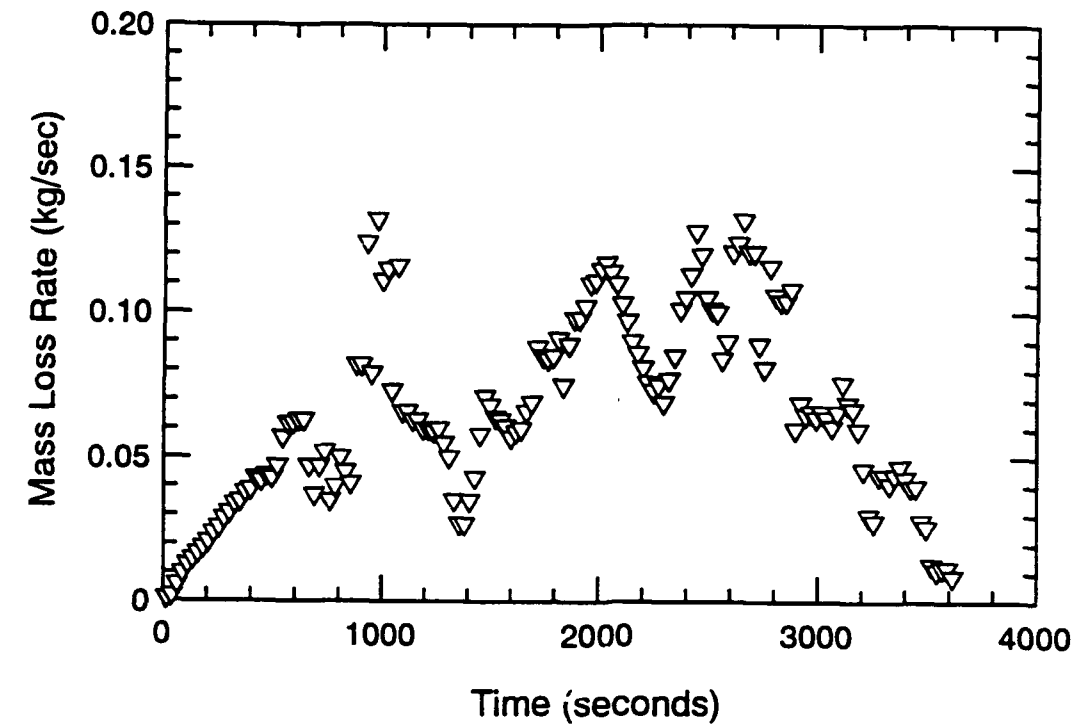


Figure A.19 Mass Loss Rate and Heat Release Rate-Time Histories - S103

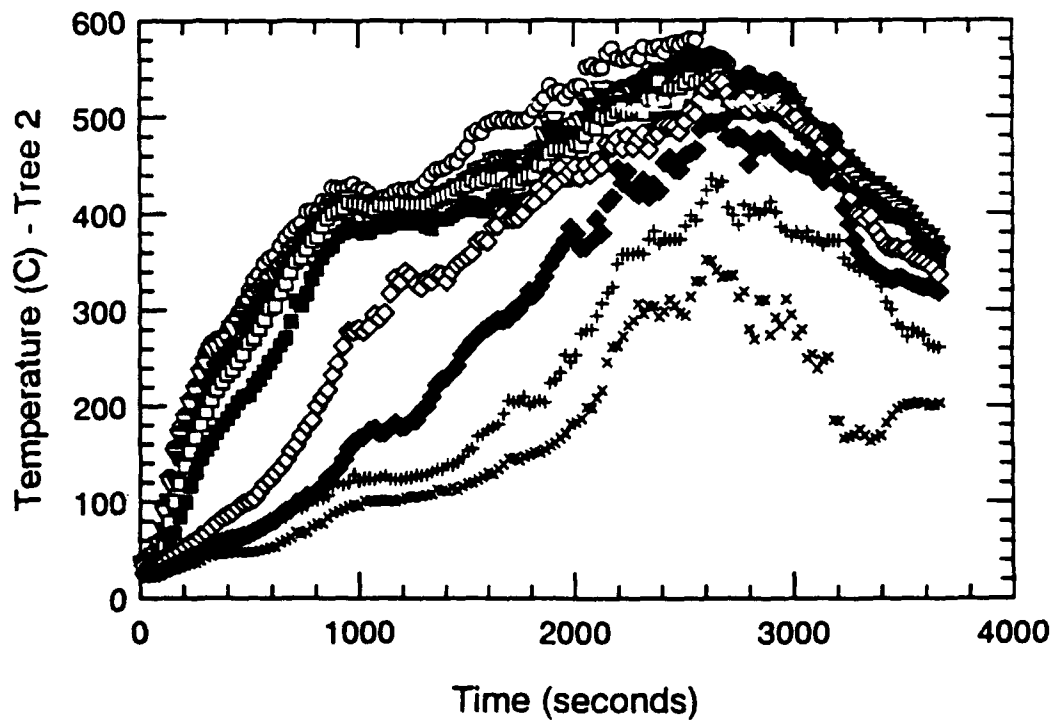
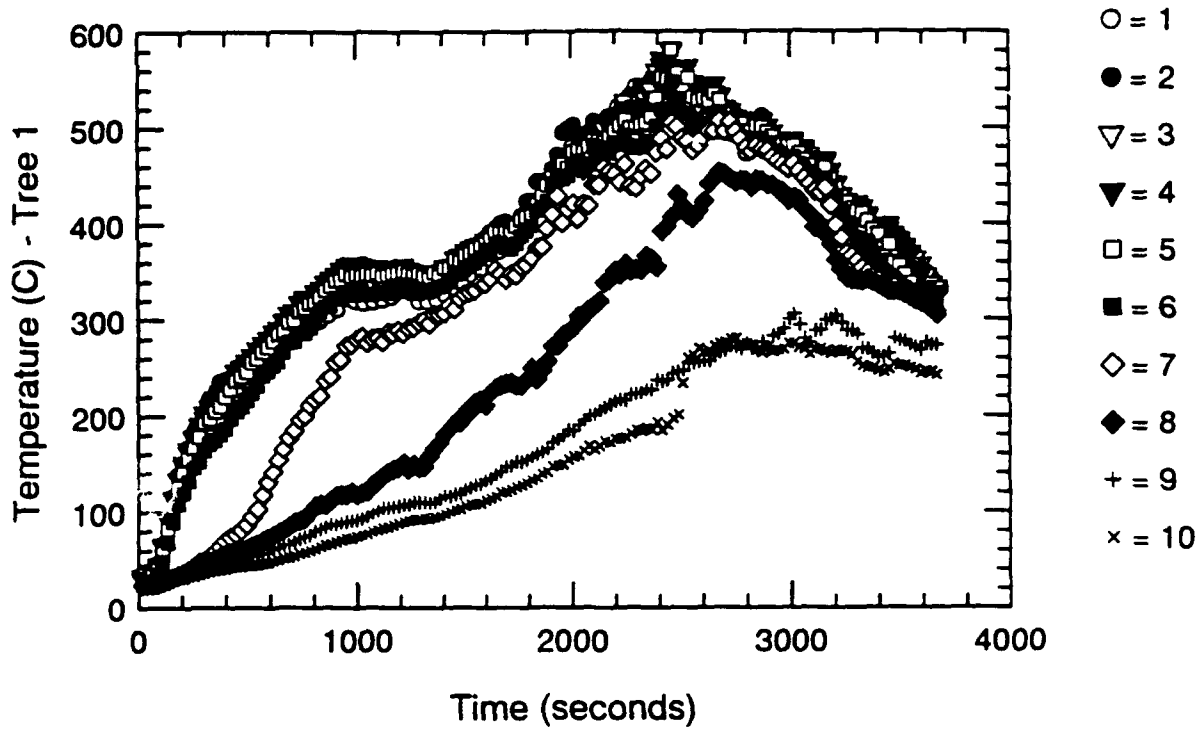


Figure A.20 Thermocouple Trees 1 & 2-Time Histories - S103

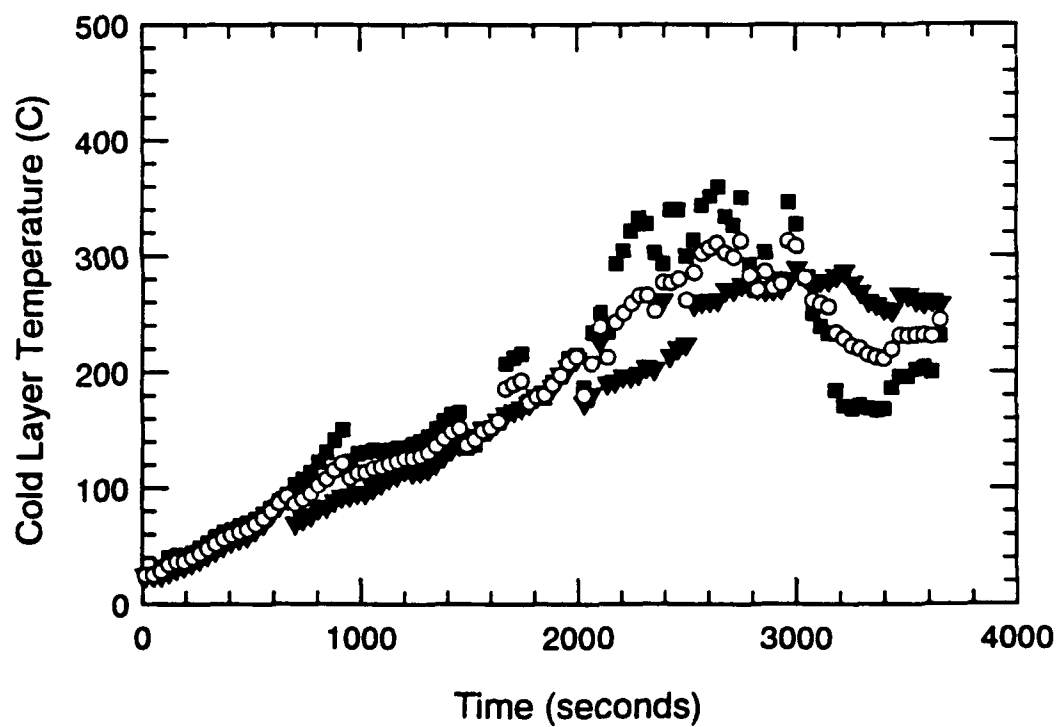
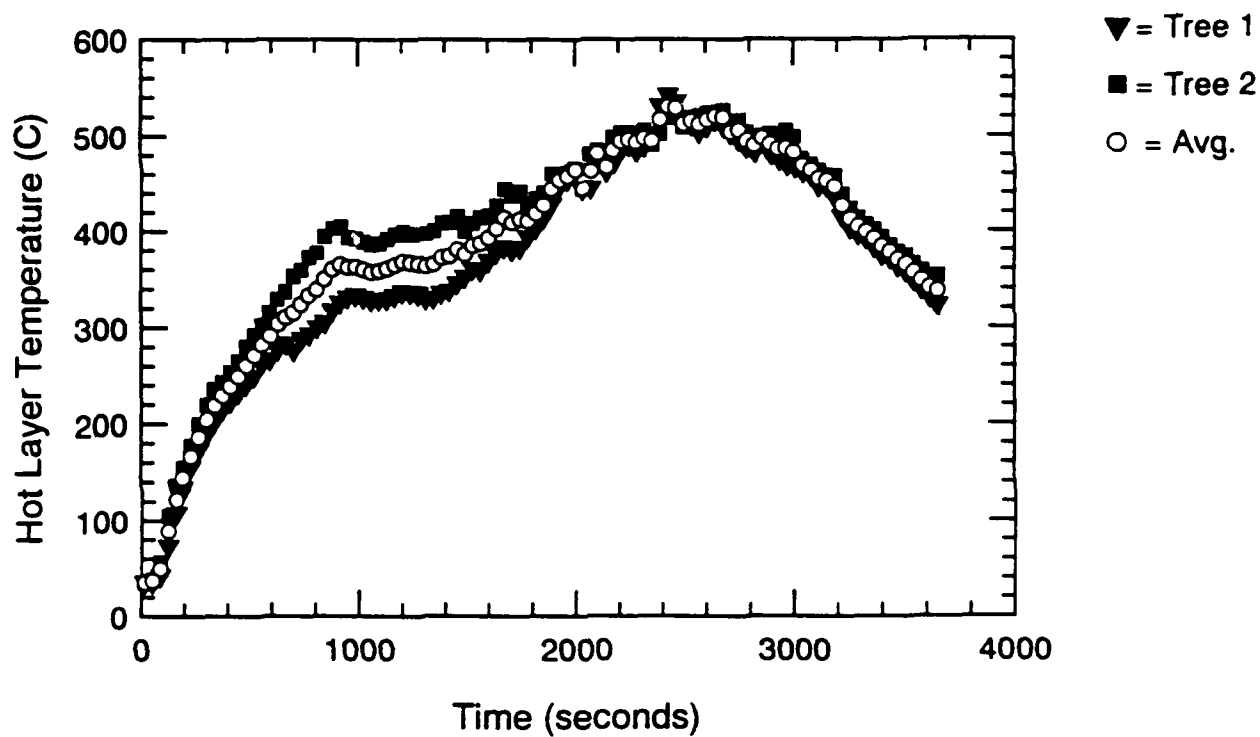


Figure A.21 Hot and Cold Layer Temperature-Time Histories - S103

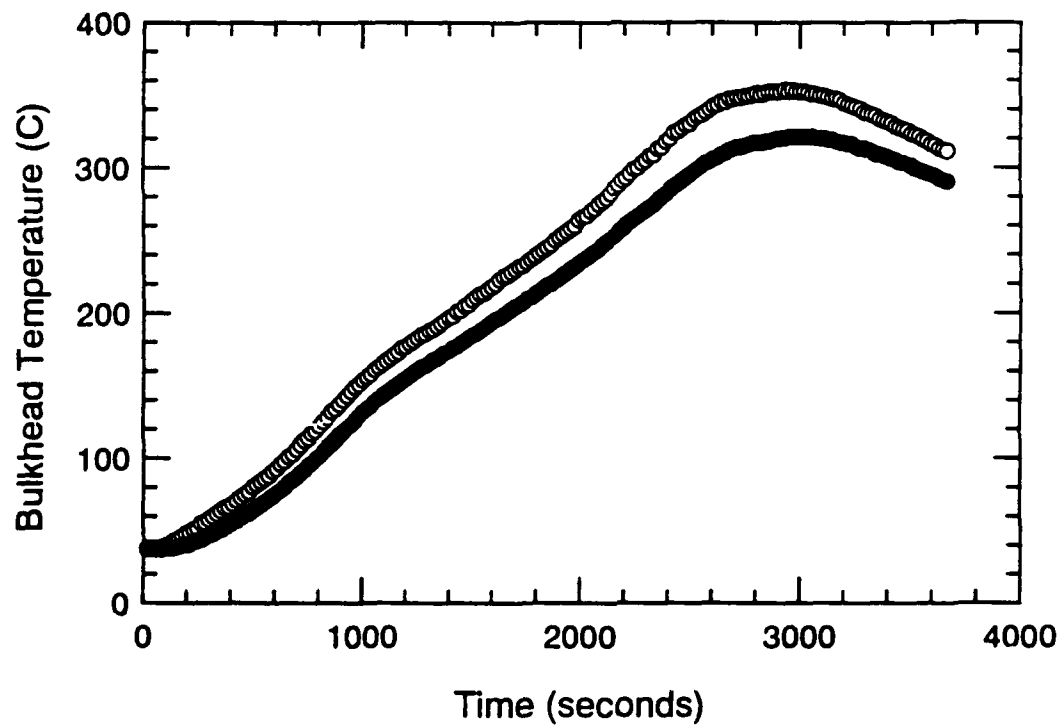
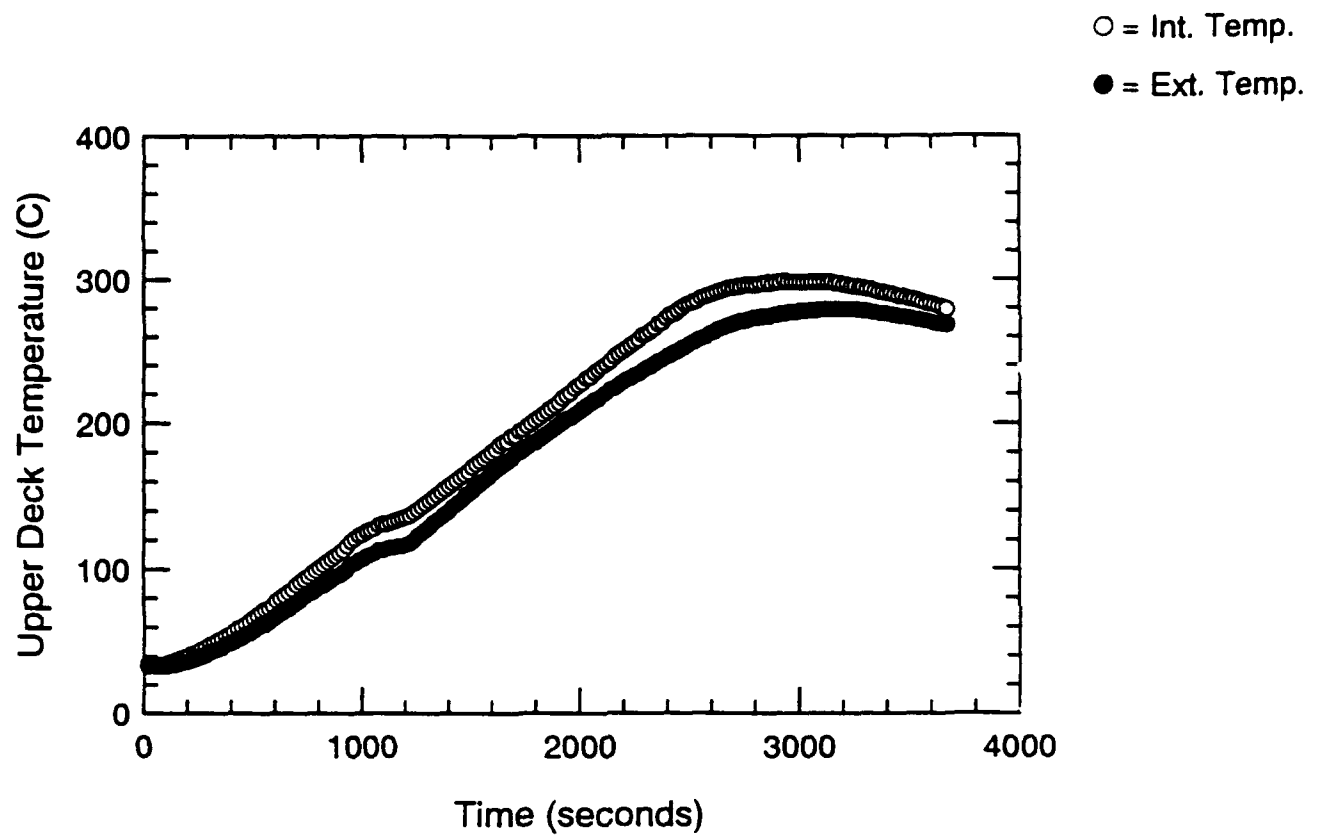


Figure A.22 Surface Thermocouple-Time Histories - S103

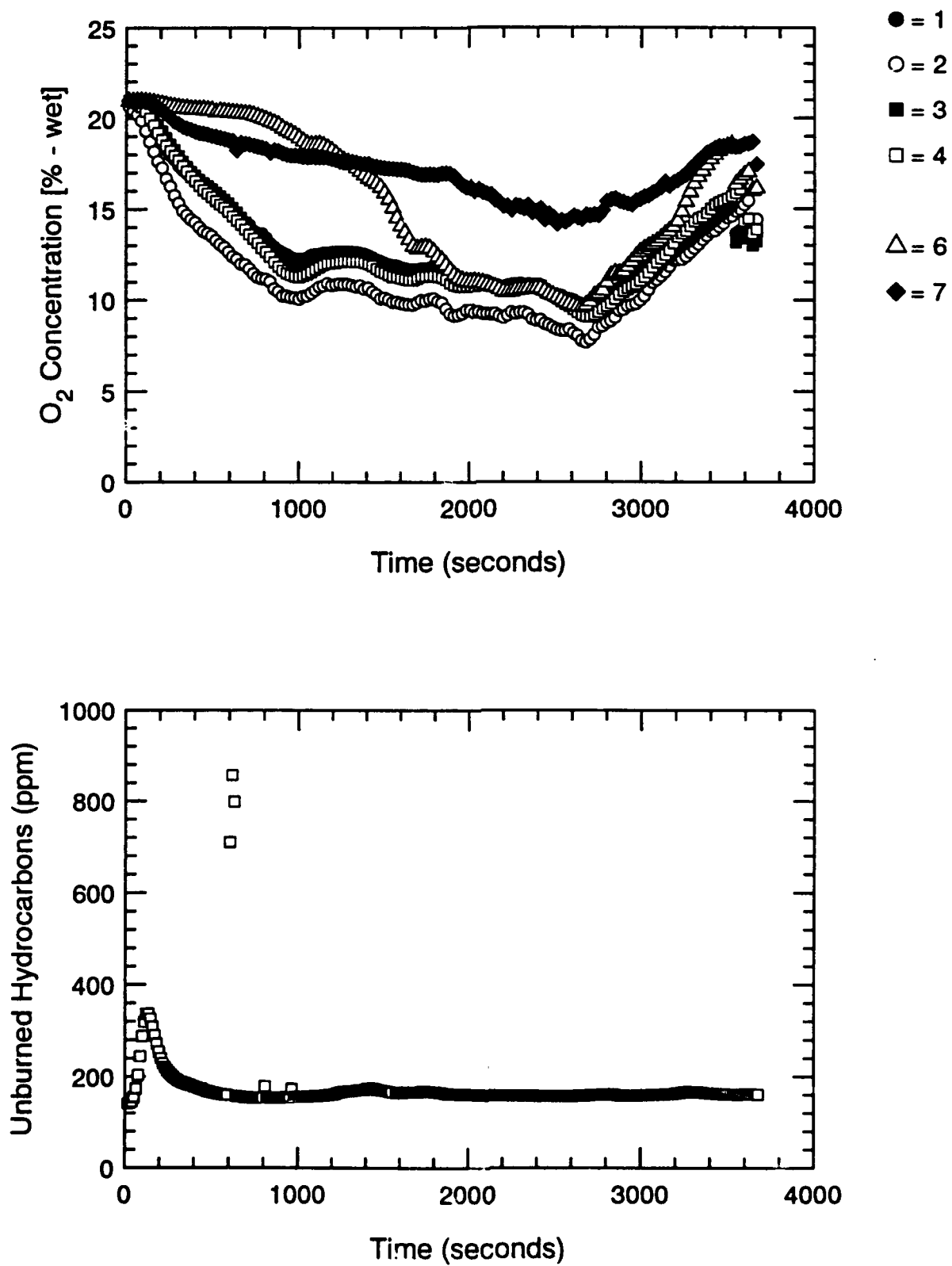


Figure A.23 Oxygen and Unburned HC Concentration-Time Histories - S103

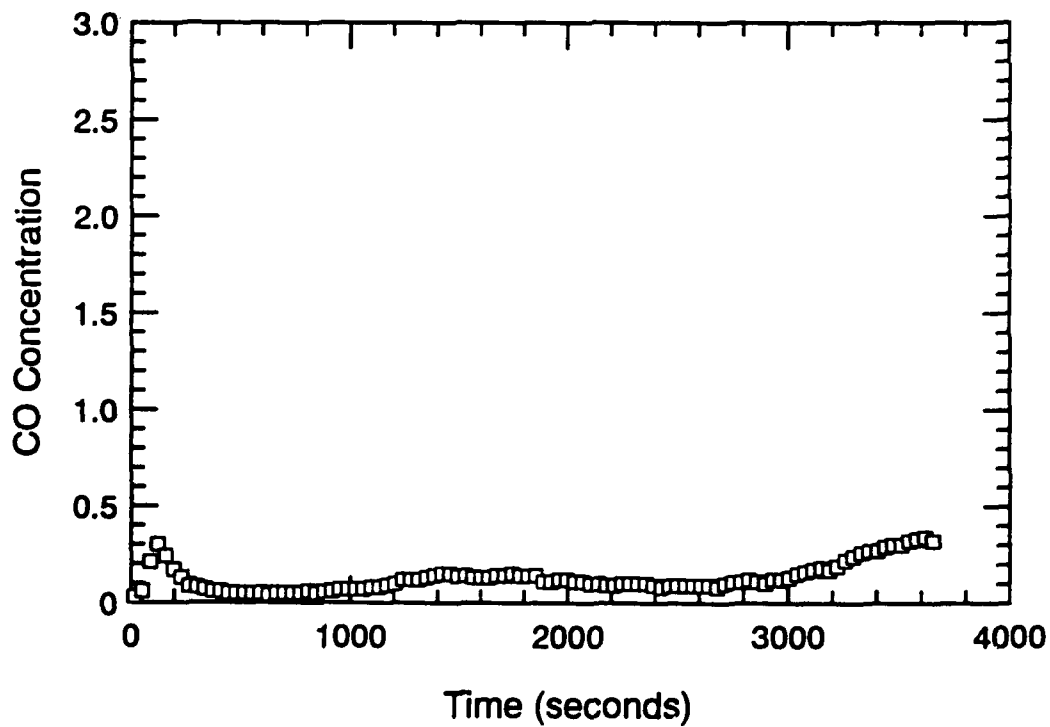
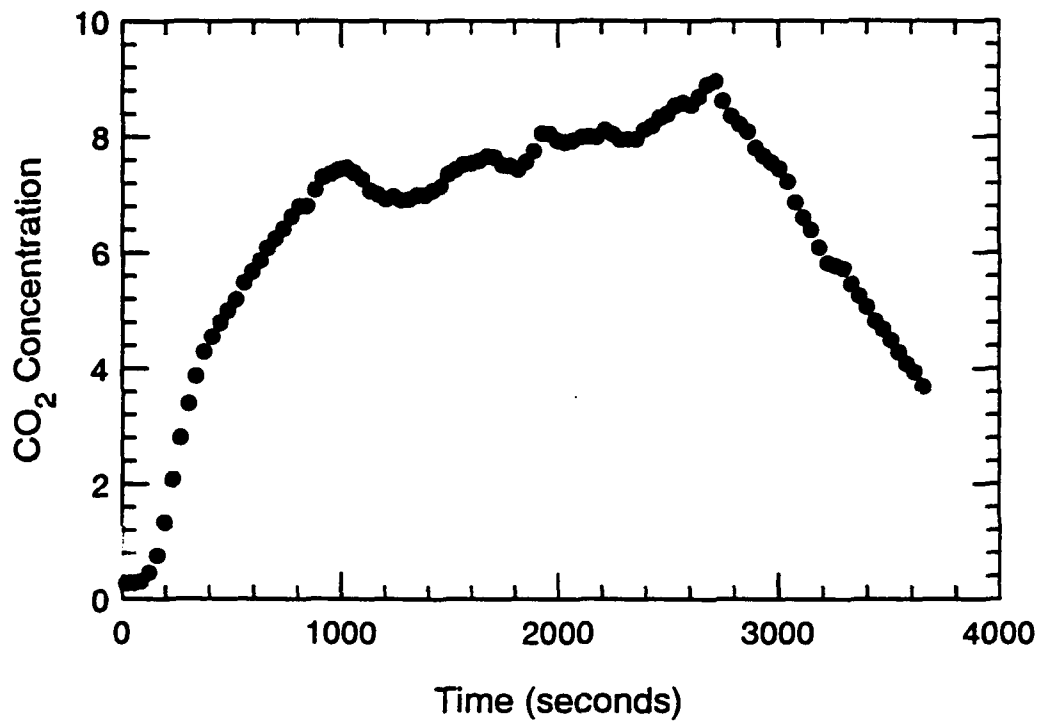


Figure A.24 CO₂ and CO Concentration-Time Histories - S103

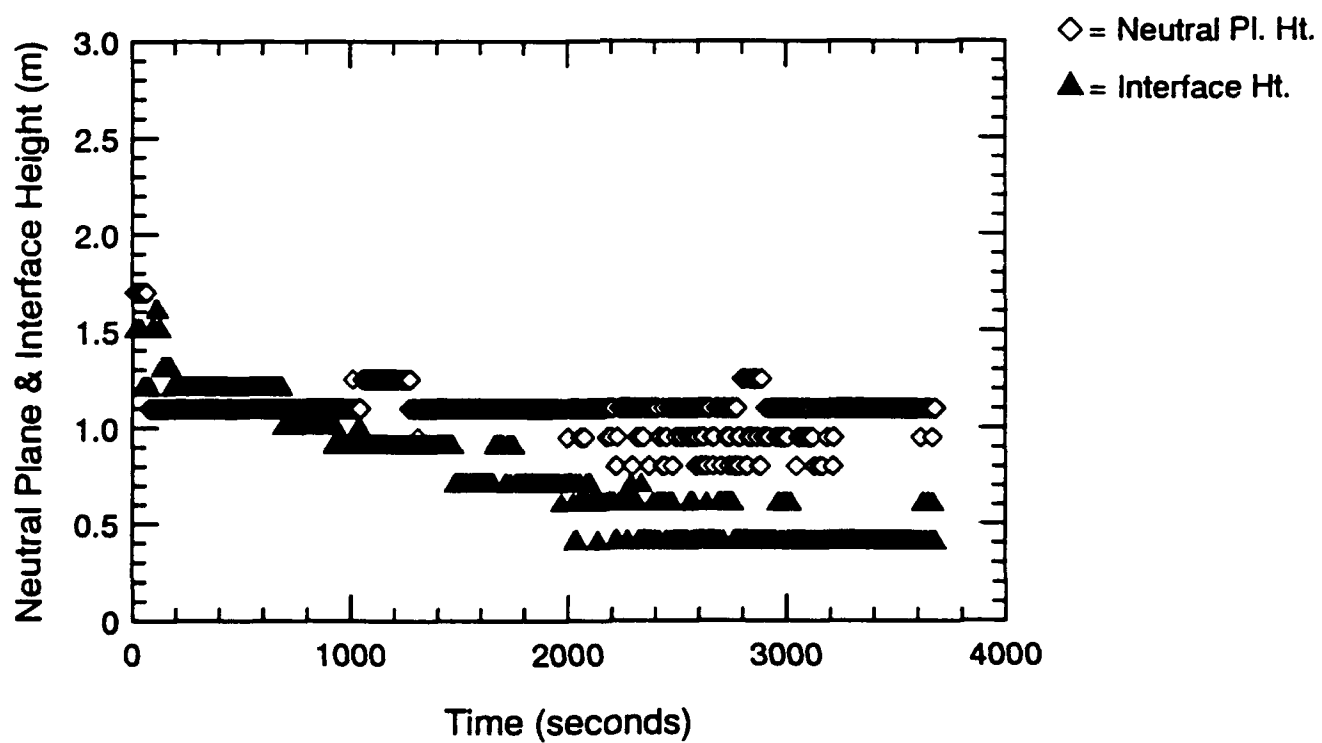
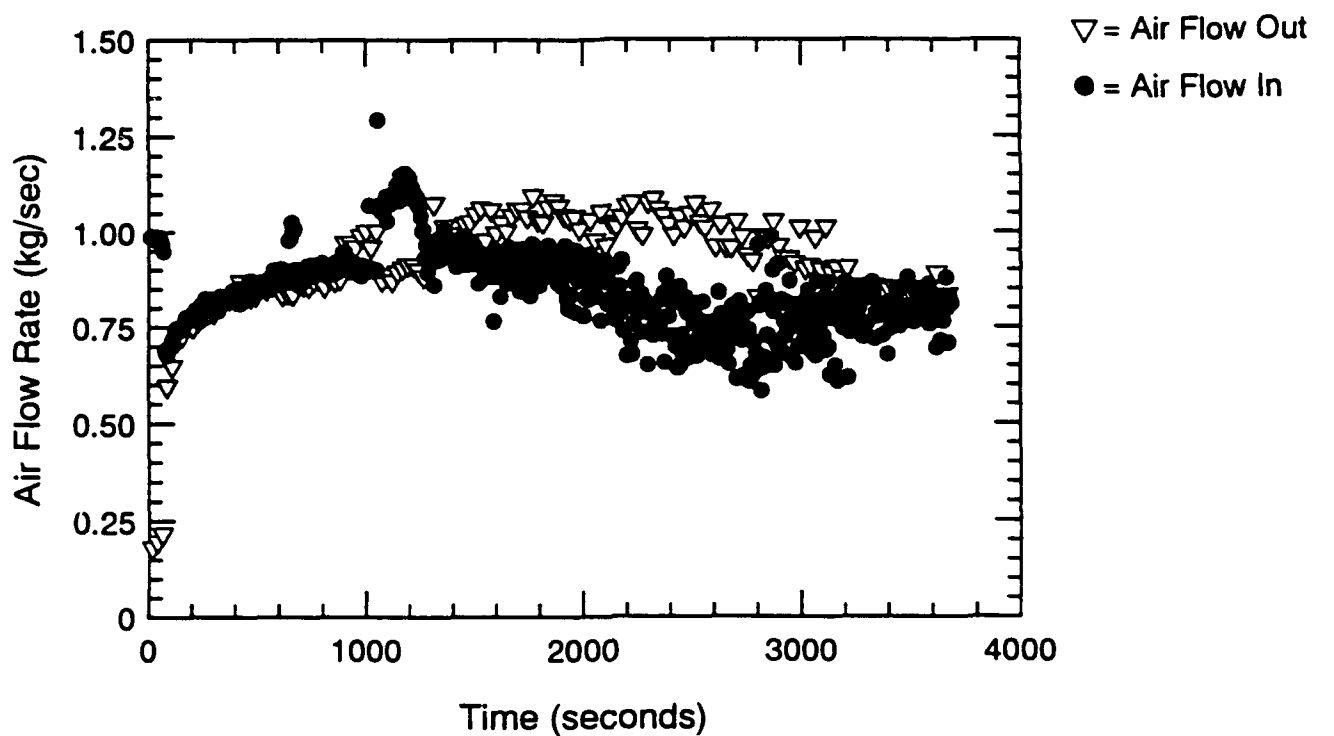


Figure A.25 Air Flow Rate, Neutral Plane & Interface Ht.-Time Histories - S103

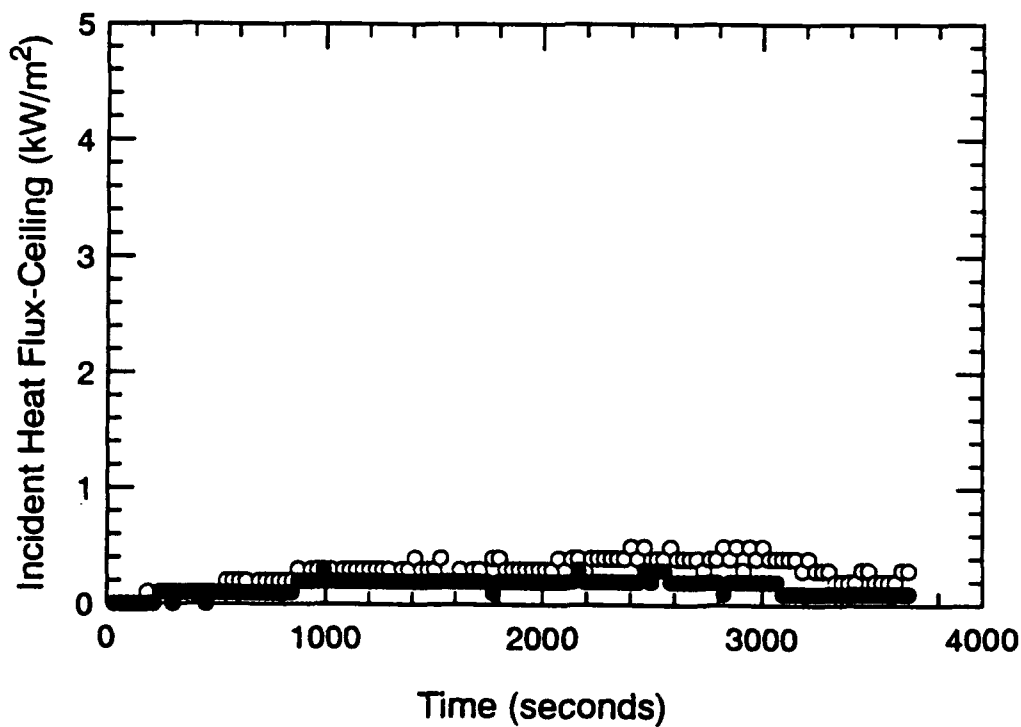
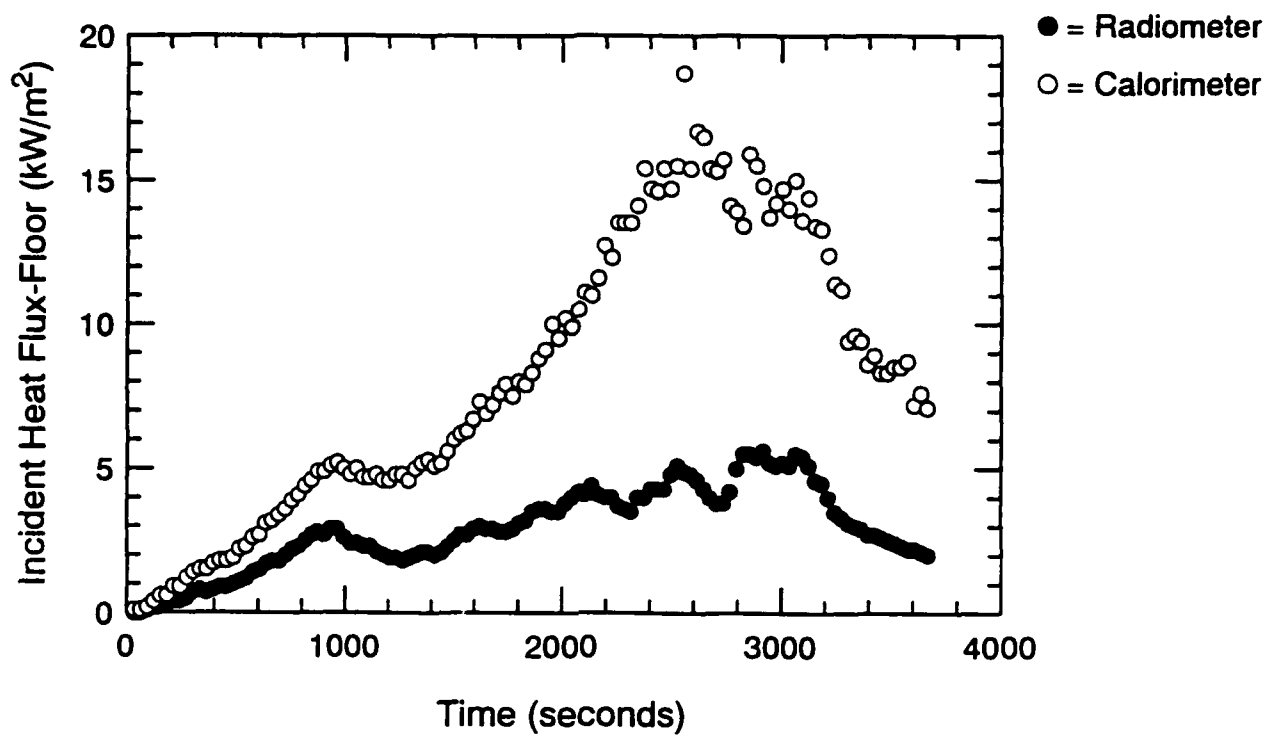


Figure A.26 Incident Heat Flux at Floor and Ceiling-Time Histories - S103

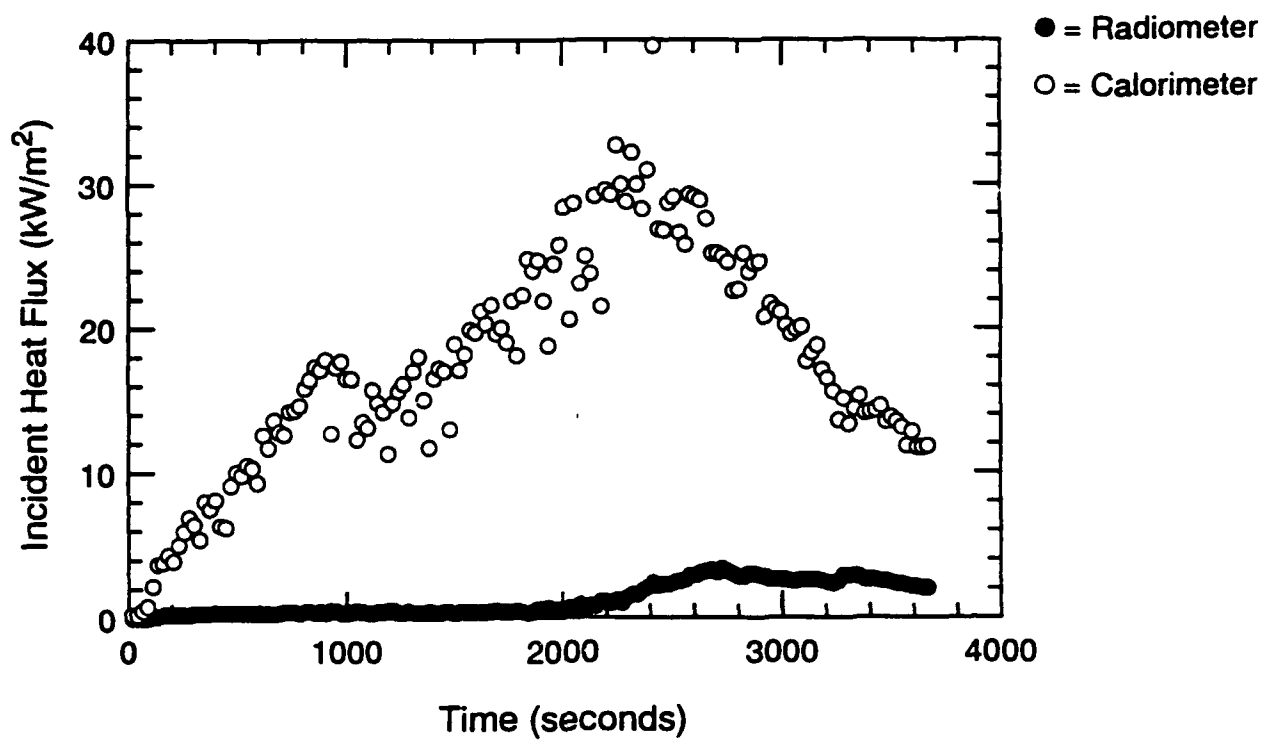


Figure A.27 Incident Heat Flux at Fwd. Bulkhead-Time Histories - S103

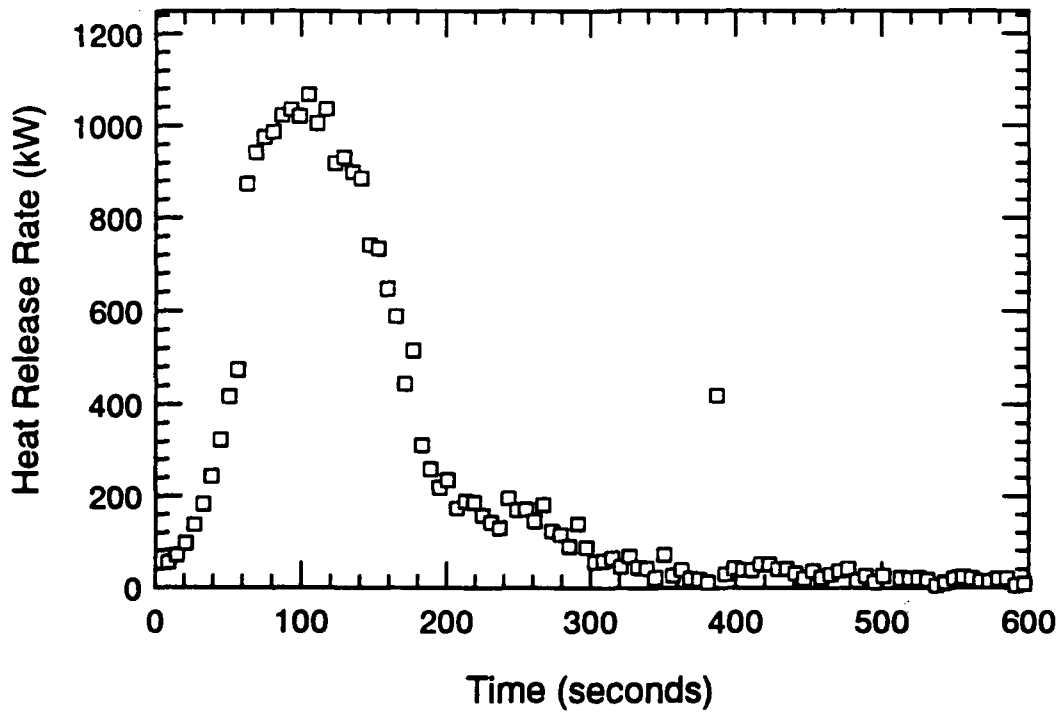
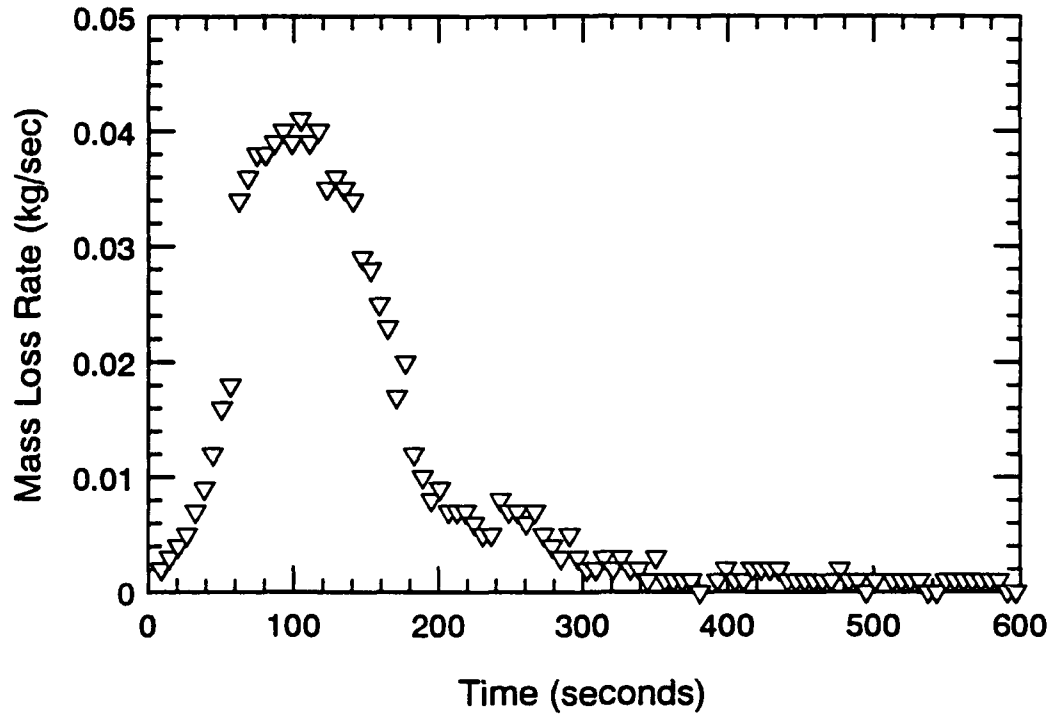


Figure A.28 Mass Loss Rate and Heat Release Rate-Time Histories - S104

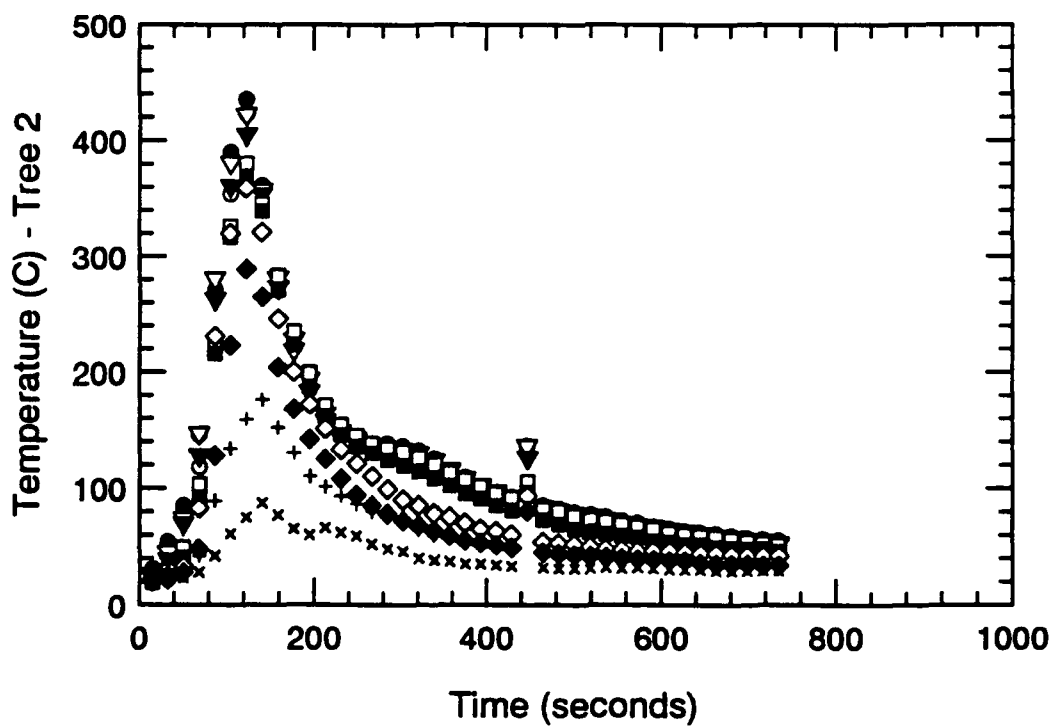
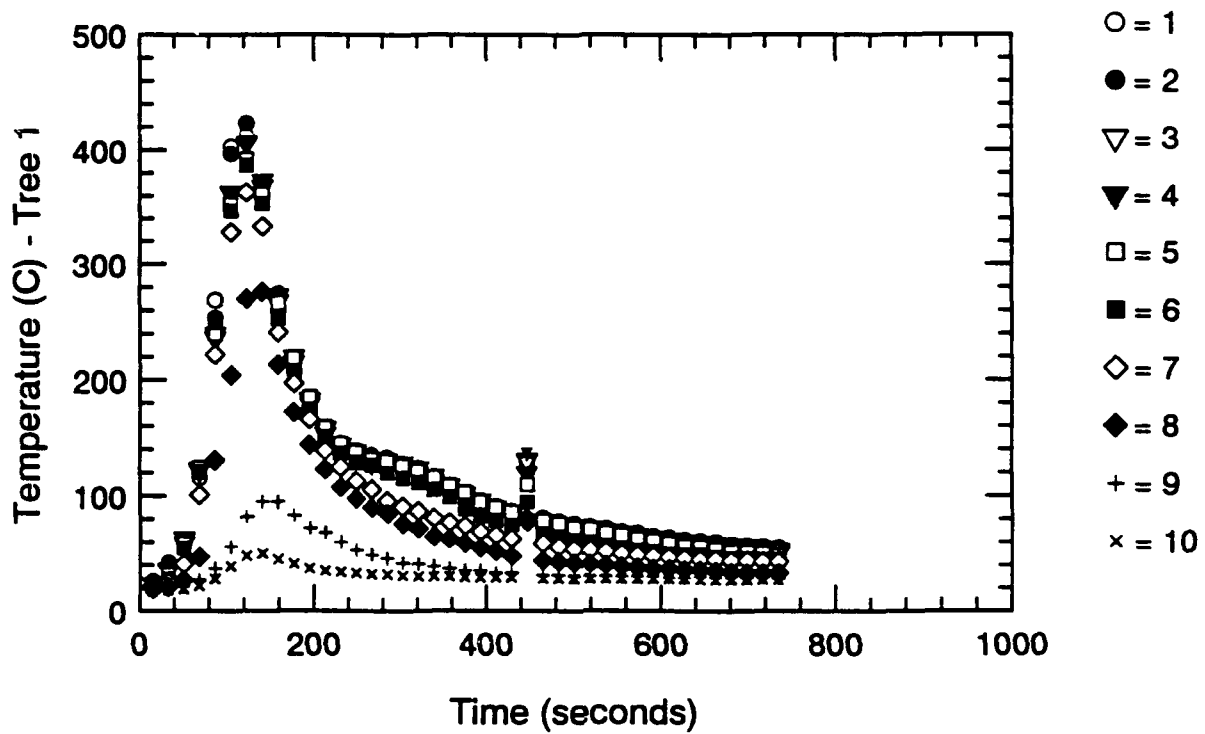


Figure A.29 Thermocouple Trees 1 & 2-Time Histories - S104

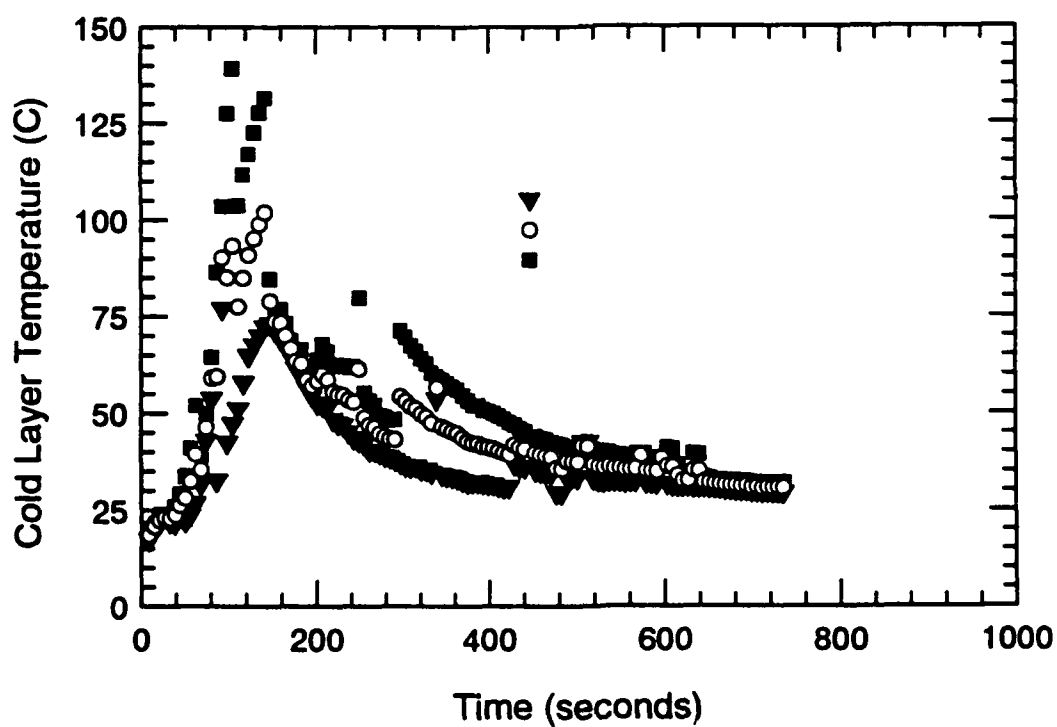
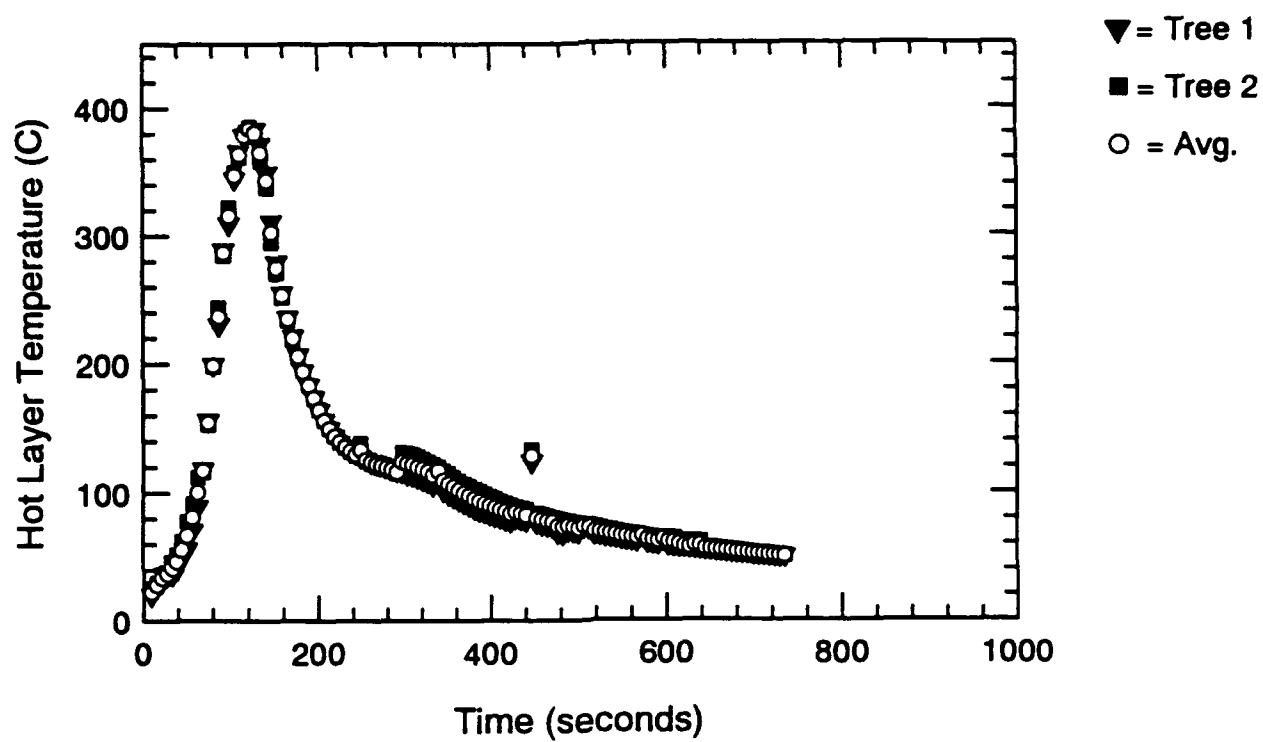


Figure A.30 Hot and Cold Layer Temperature-Time Histories - S104

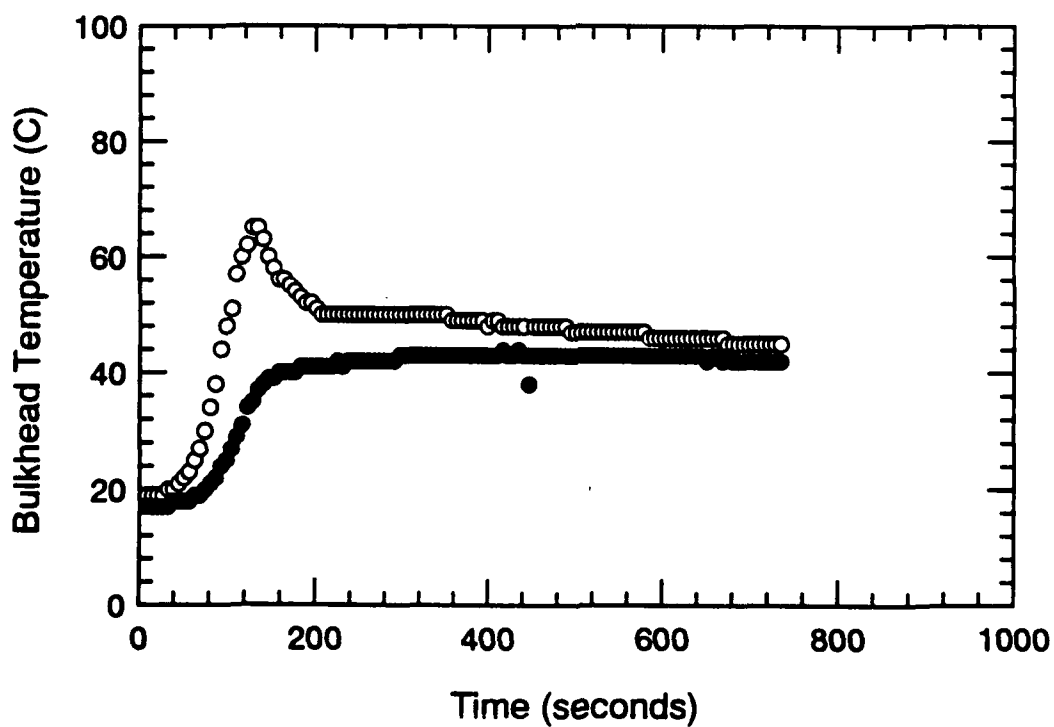
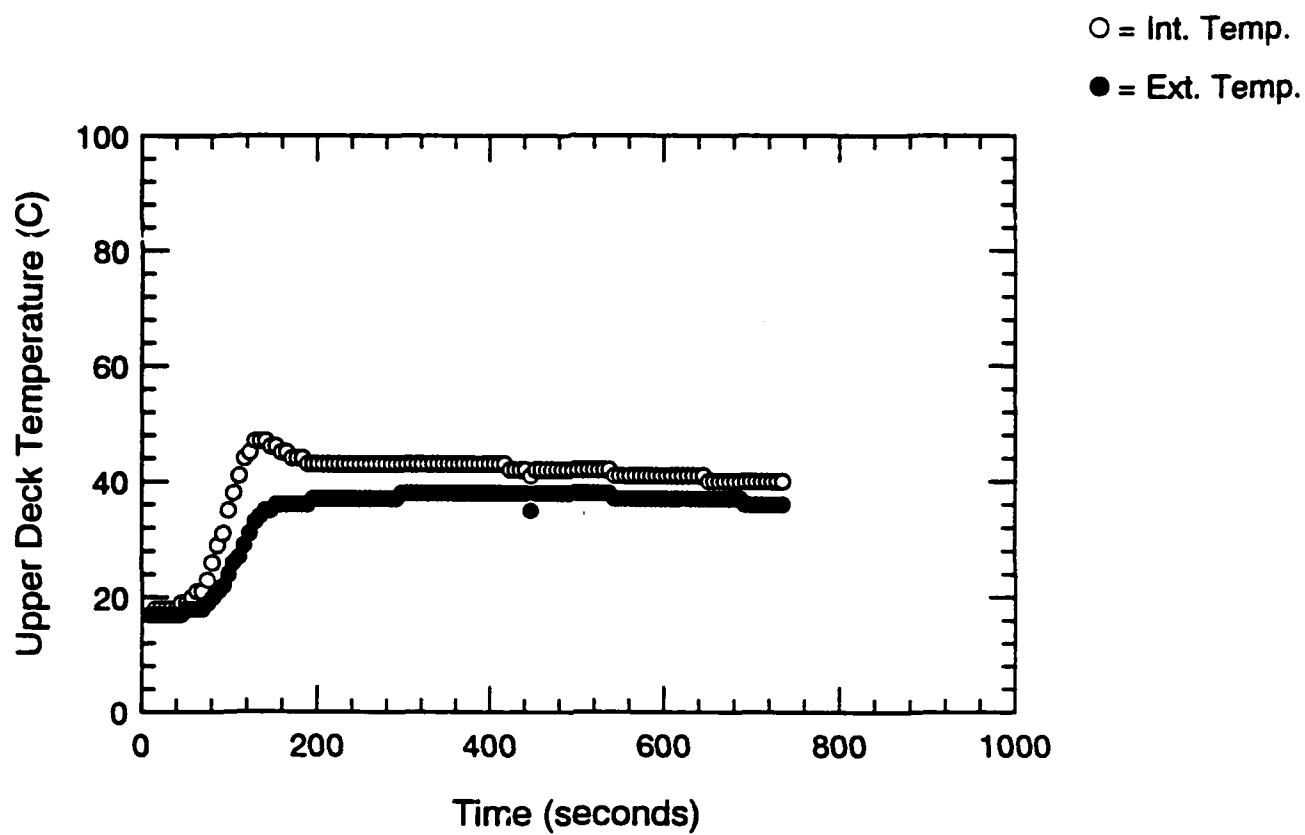


Figure A.31 Surface Thermocouple-Time Histories - S104

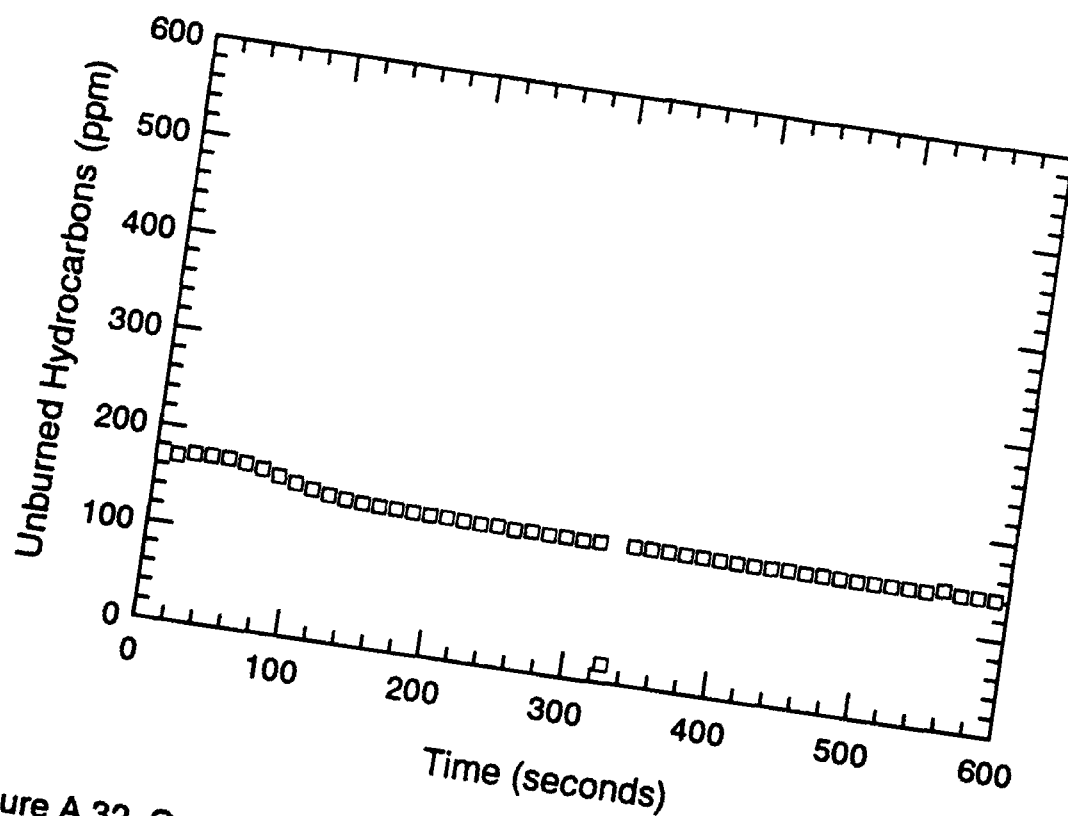
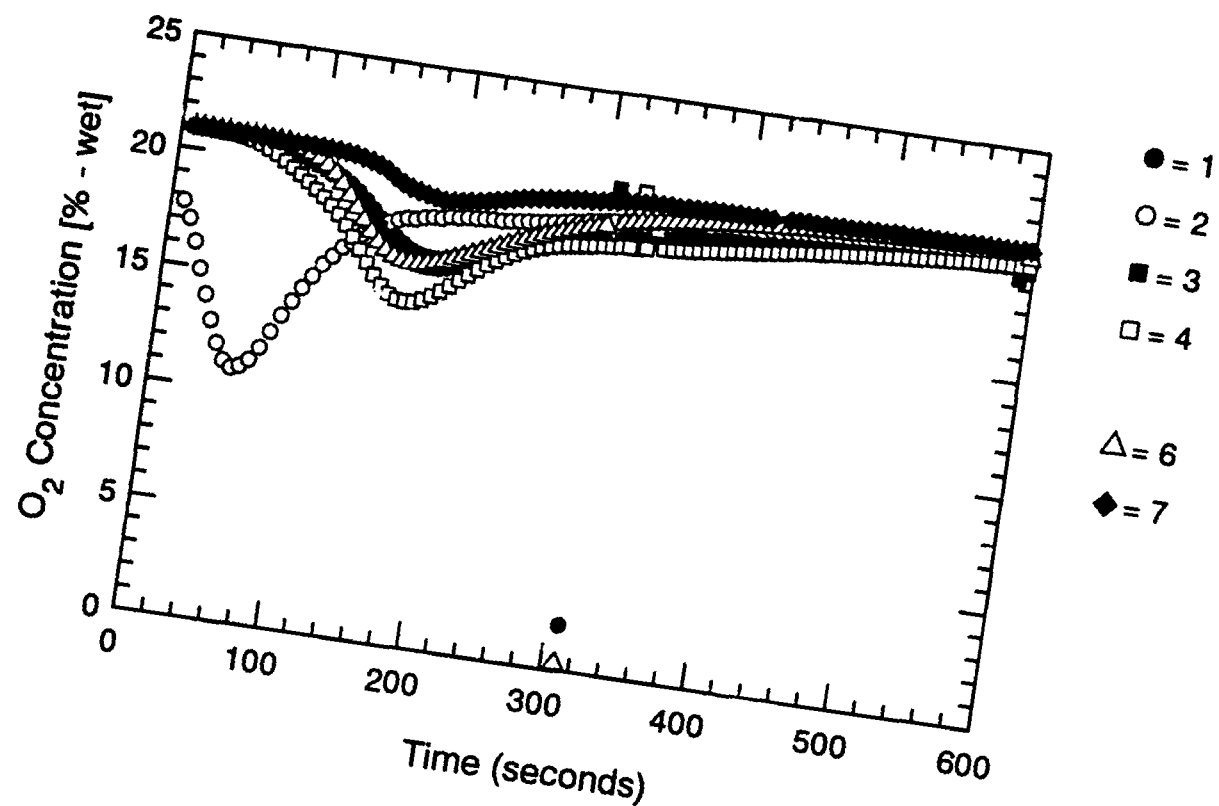


Figure A.32 Oxygen and Unburned HC Concentration-Time Histories - S104

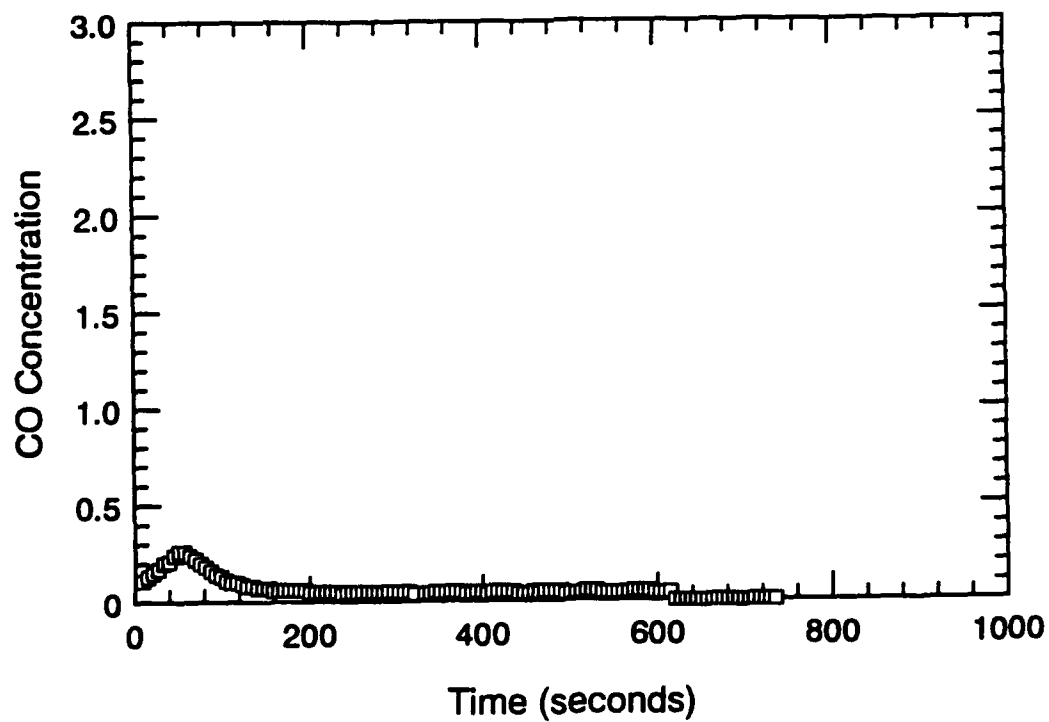
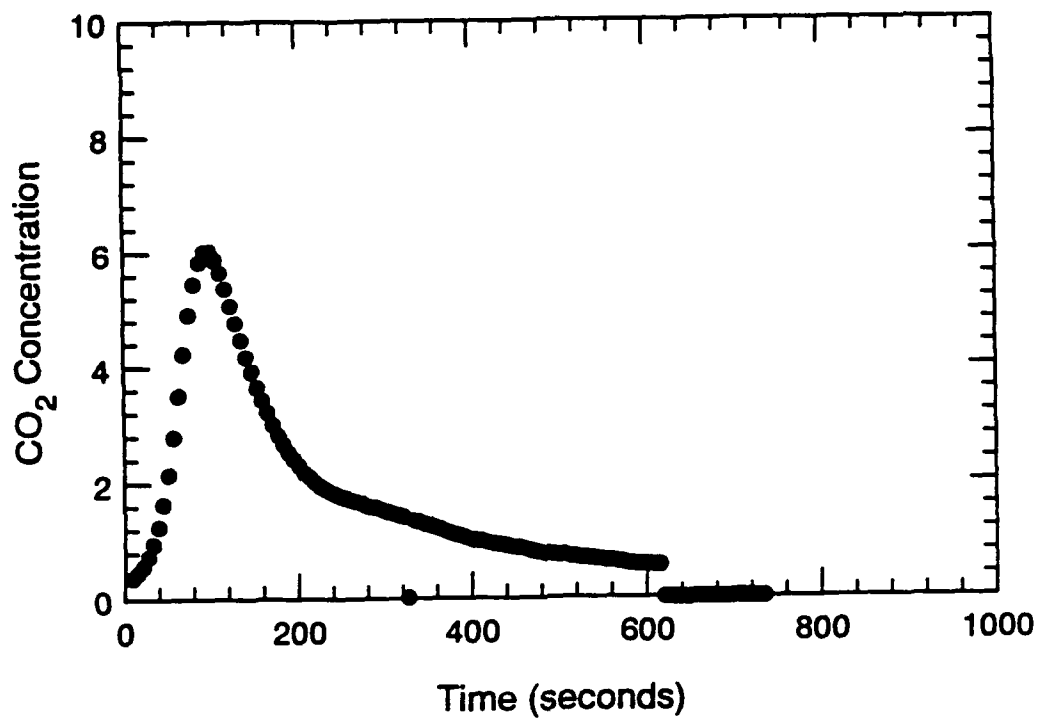


Figure A.33 CO₂ and CO Concentration-Time Histories - S104

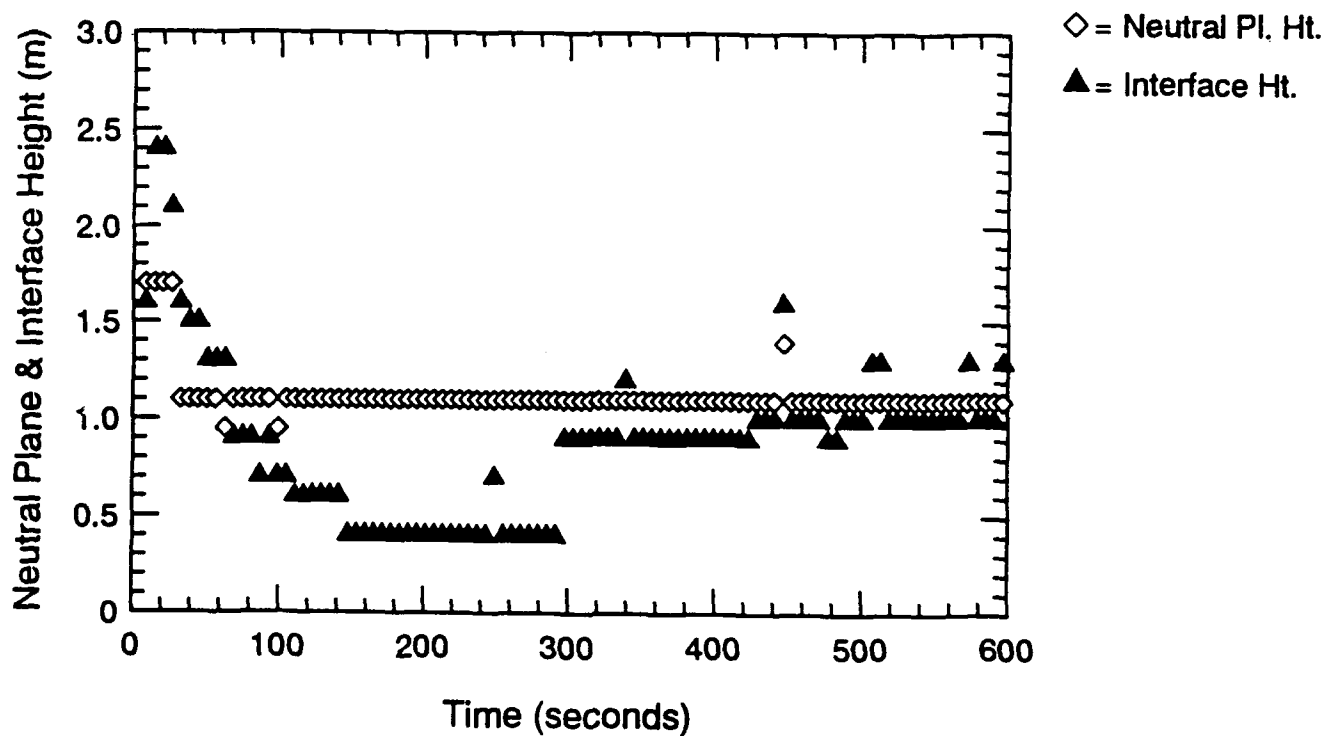
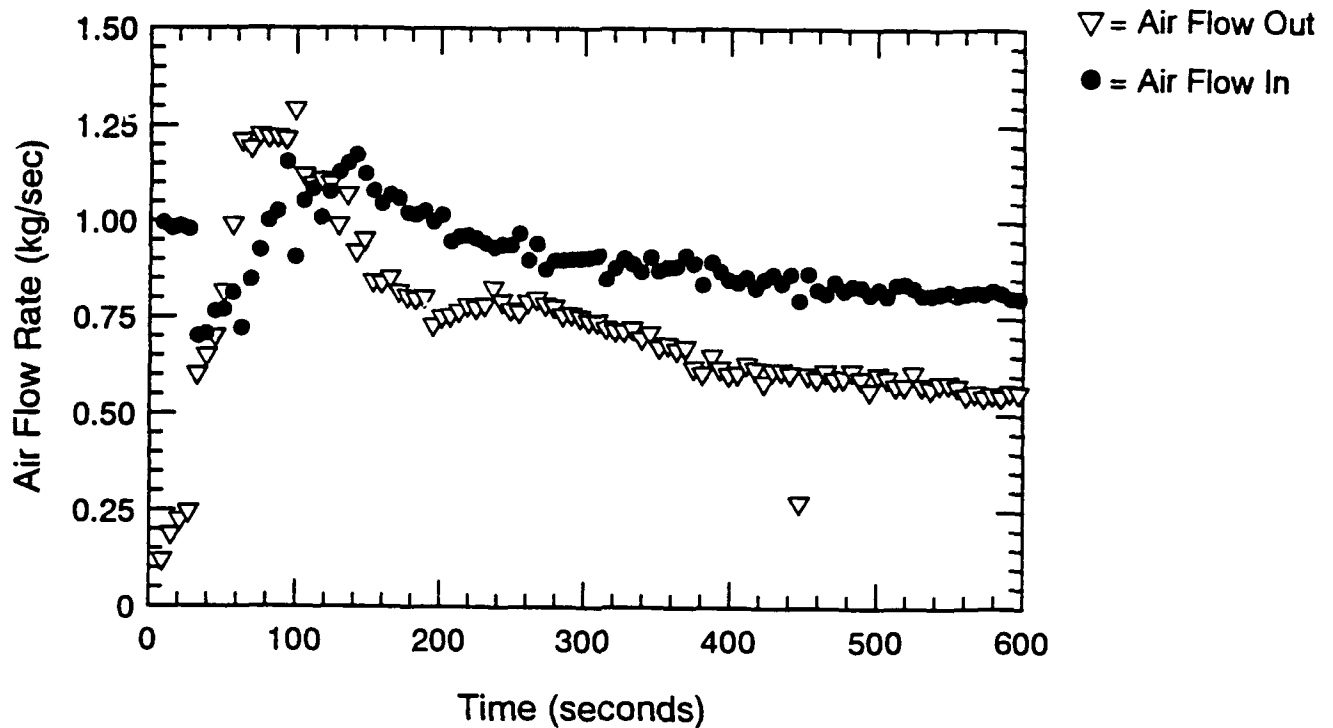


Figure A.34 Air Flow Rate, Neutral Plane & Interface Ht.-Time Histories - S104

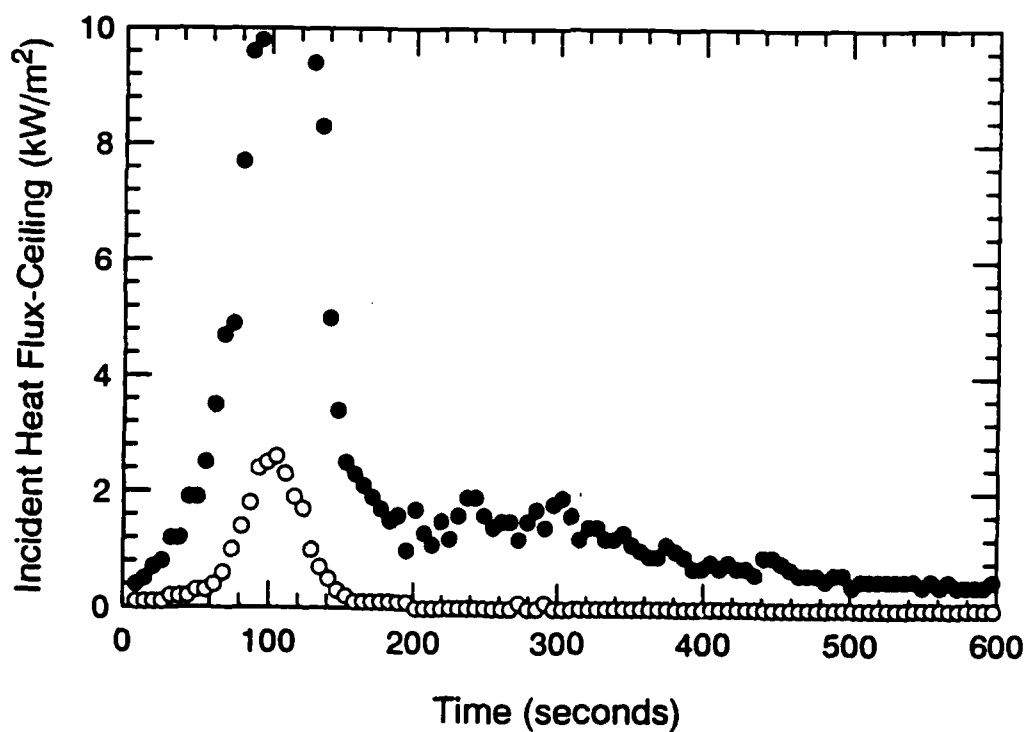
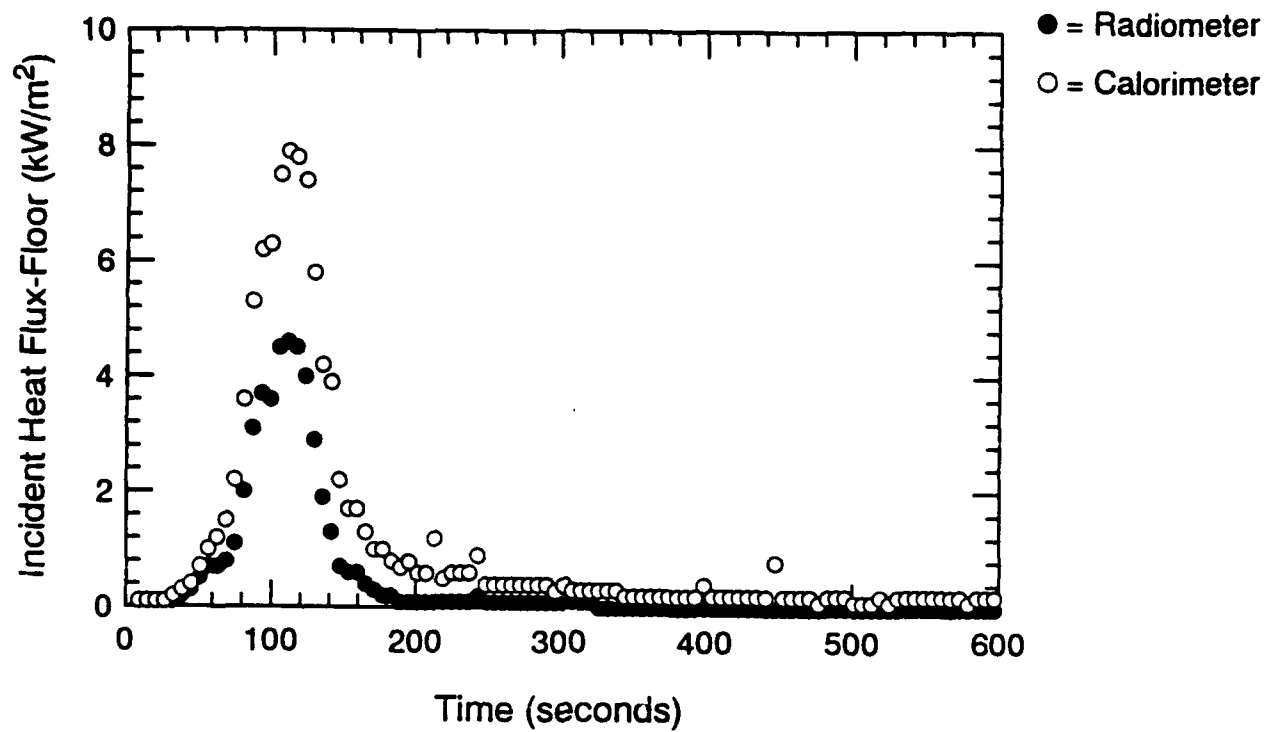


Figure A.35 Incident Heat Flux at Floor and Ceiling-Time Histories - S104

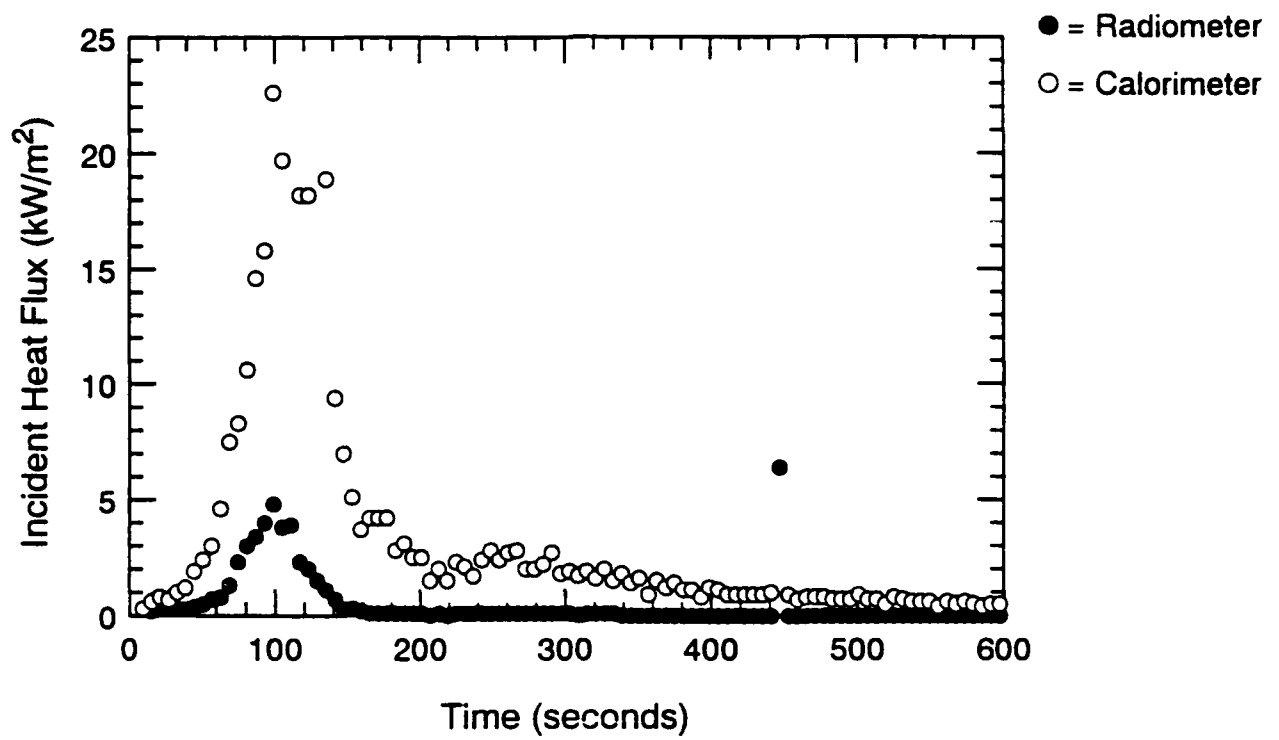


Figure A.36 Incident Heat Flux at Fwd. Bulkhead-Time Histories - S104

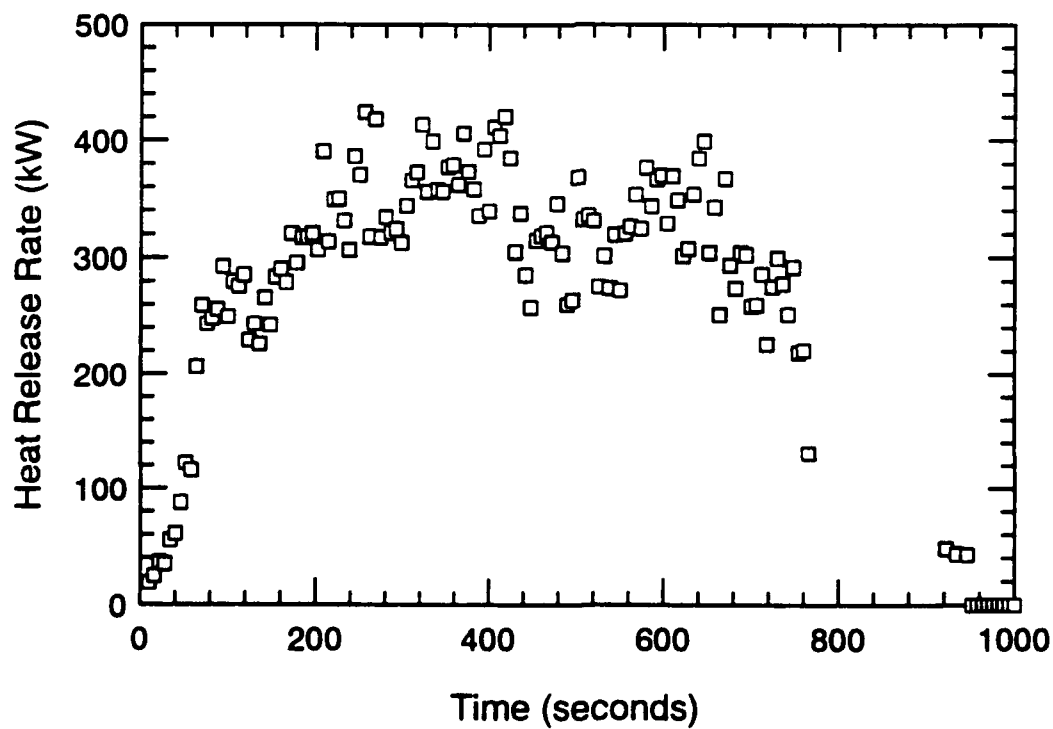
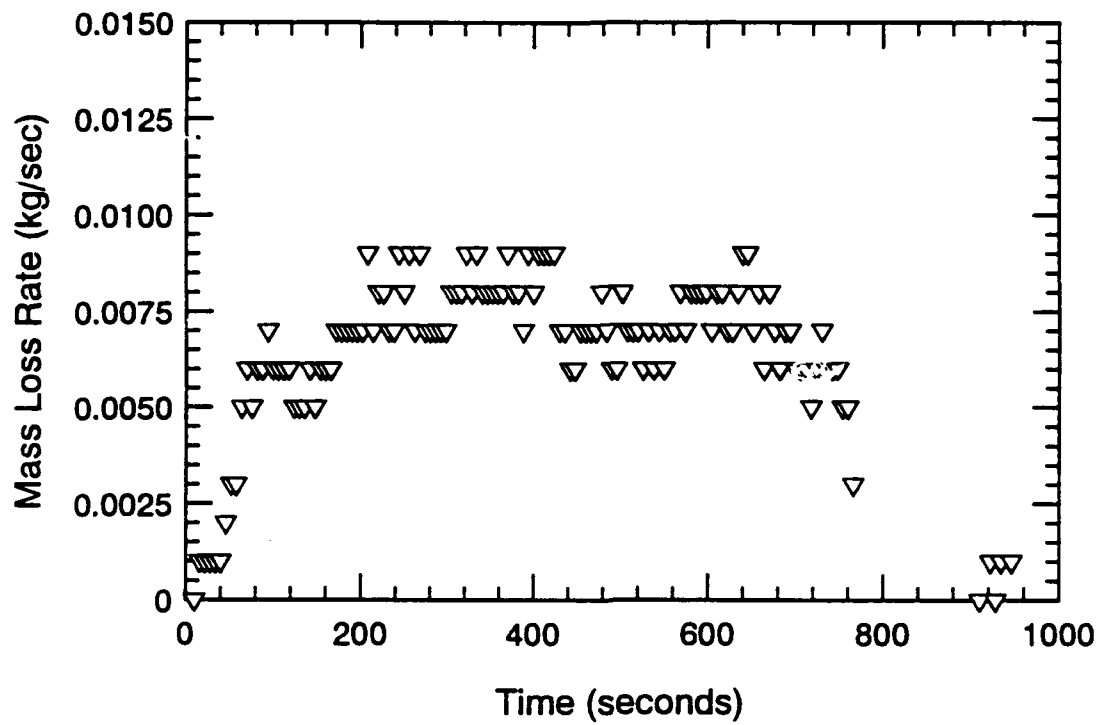


Figure A.37 Mass Loss Rate and Heat Release Rate-Time Histories - S105

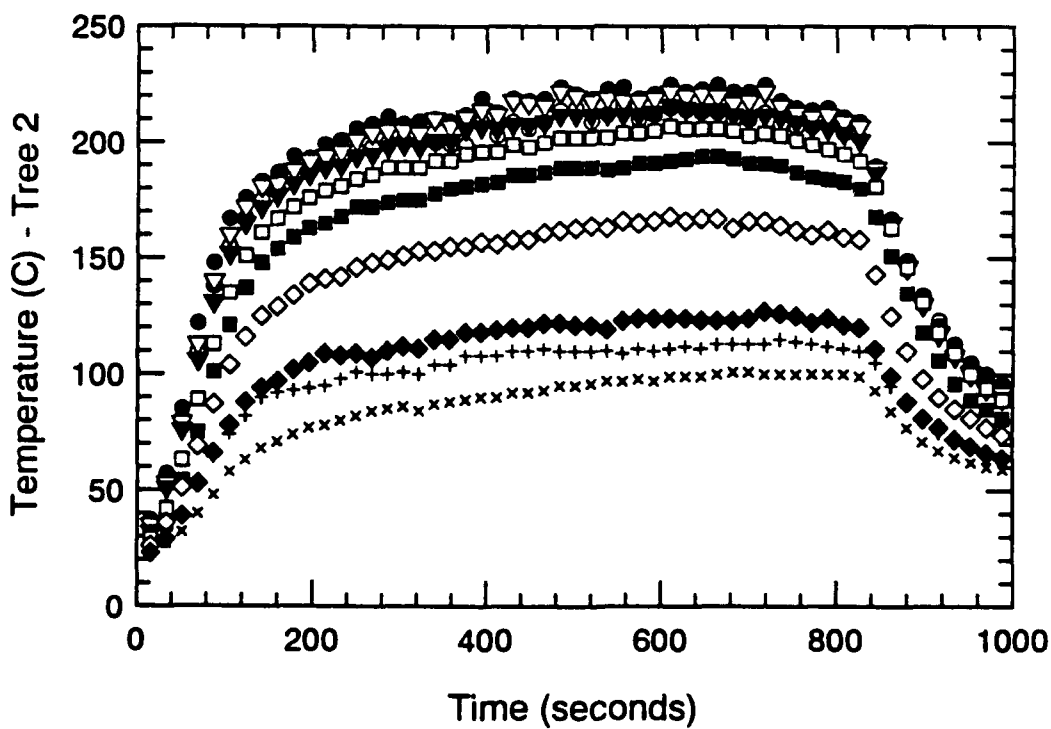
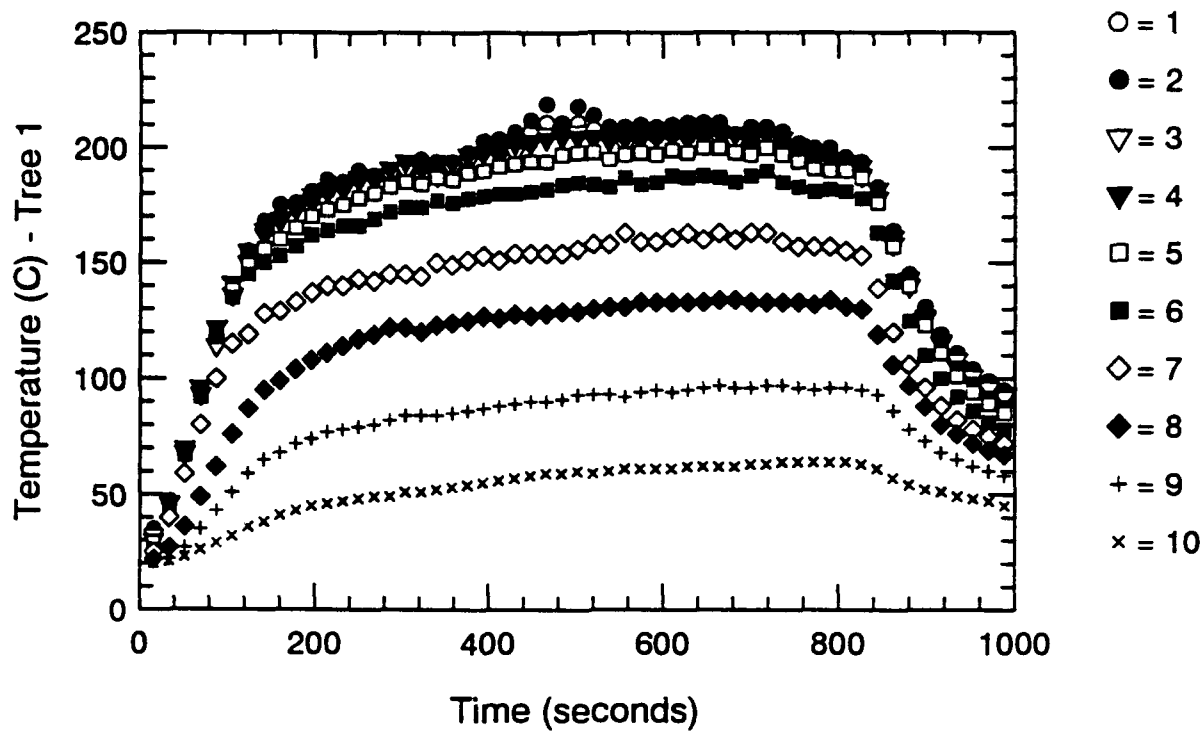


Figure A.38 Thermocouple Trees 1 & 2-Time Histories - S105

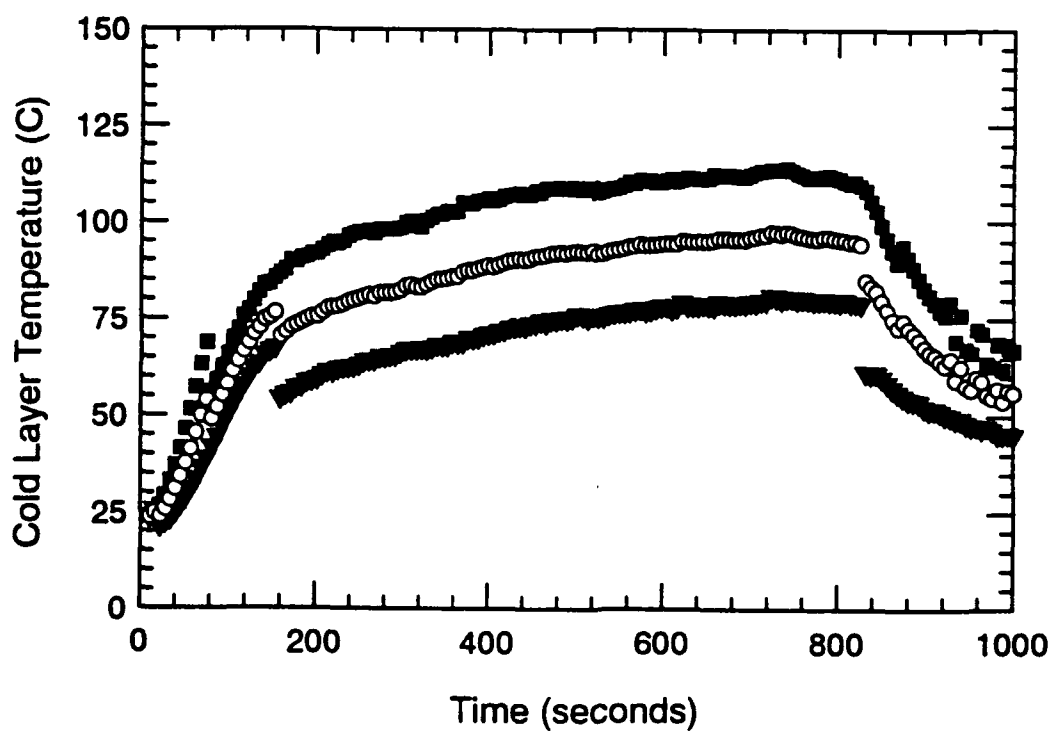
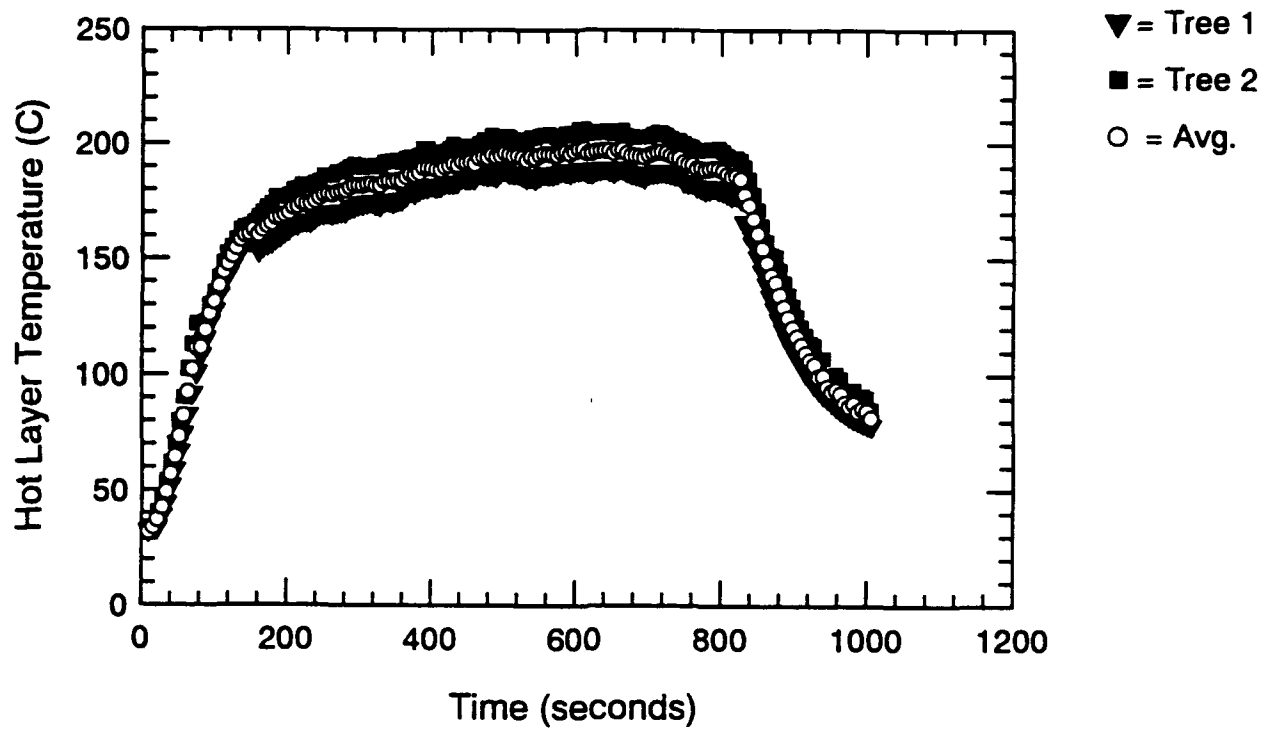


Figure A.39 Hot and Cold Layer Temperature-Time Histories - S105

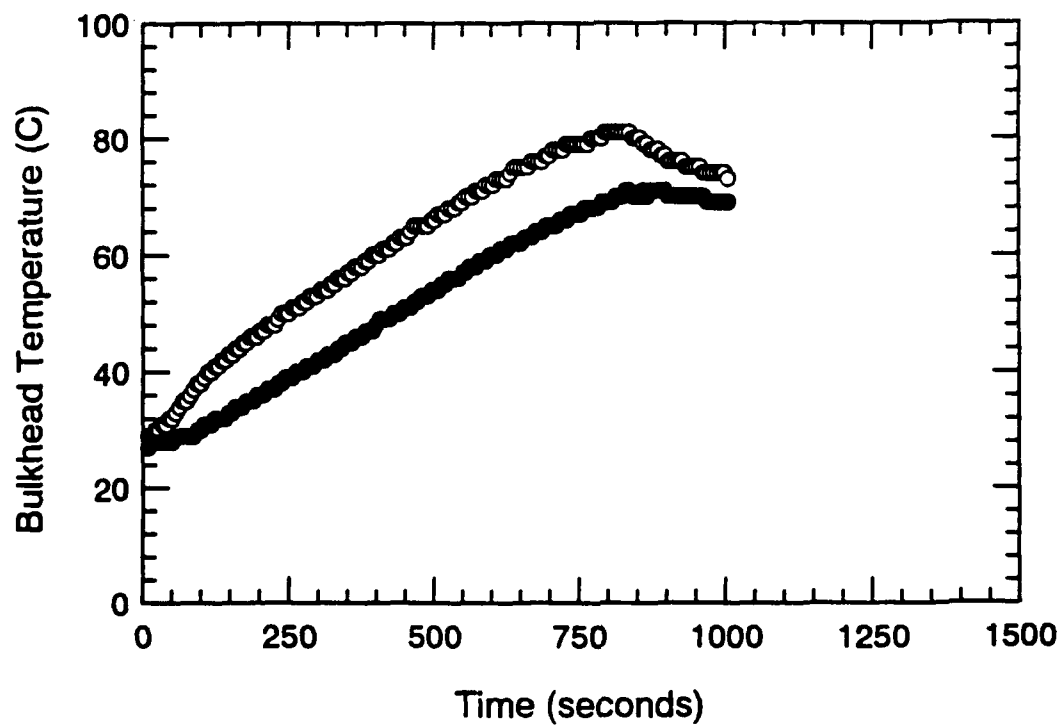
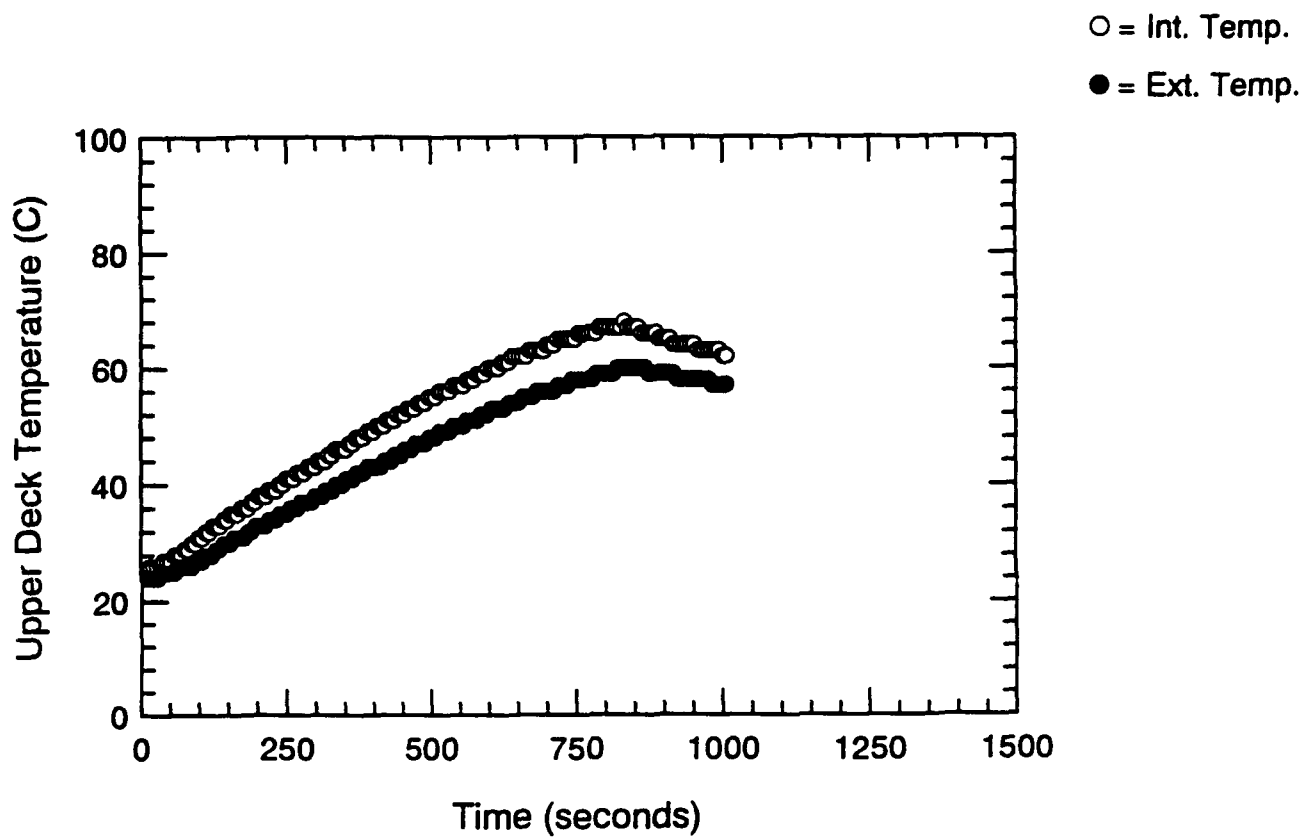


Figure A.40 Surface Thermocouple-Time Histories - S105

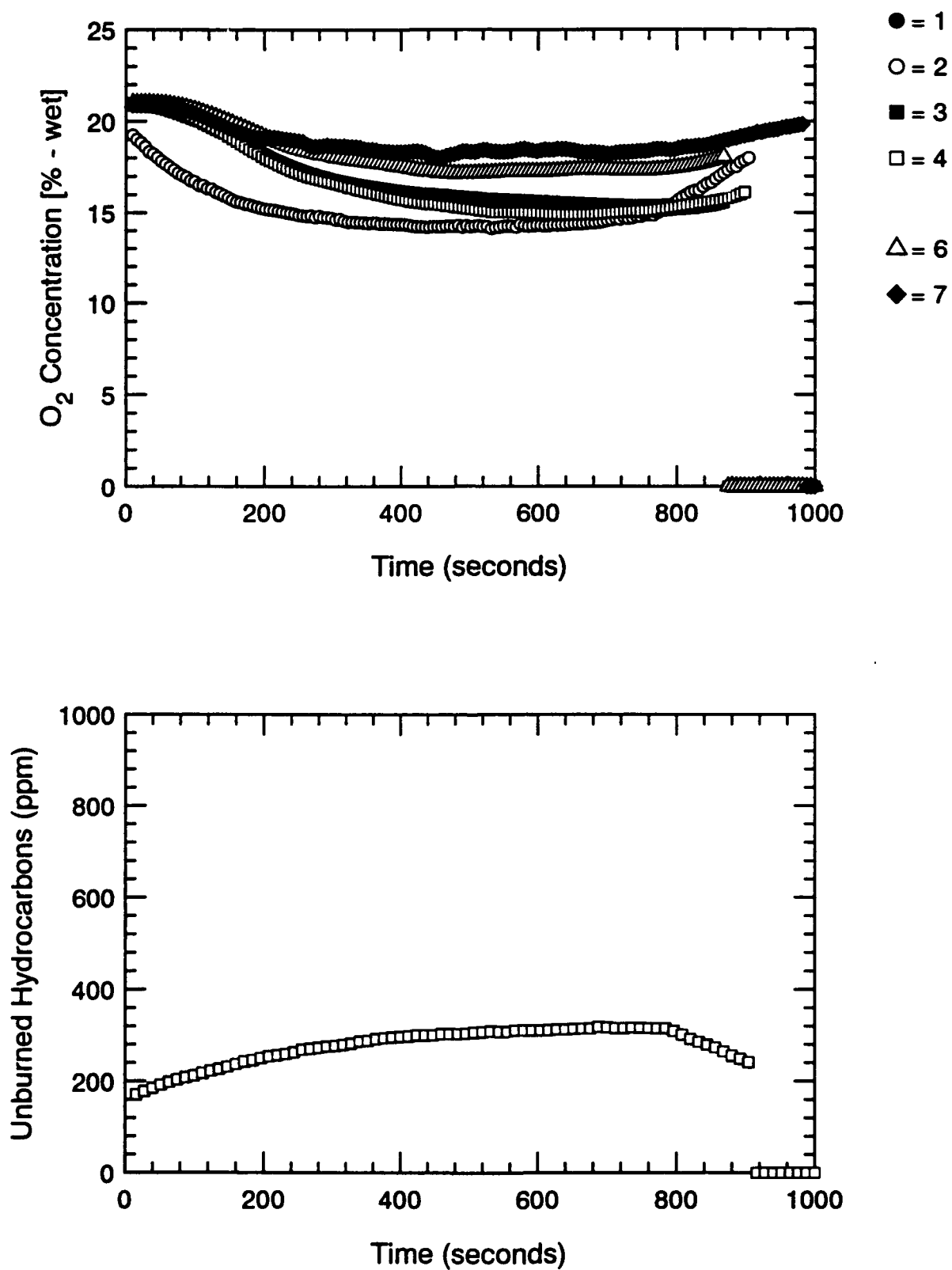


Figure A.41 Oxygen and Unburned HC Concentration-Time Histories - S105

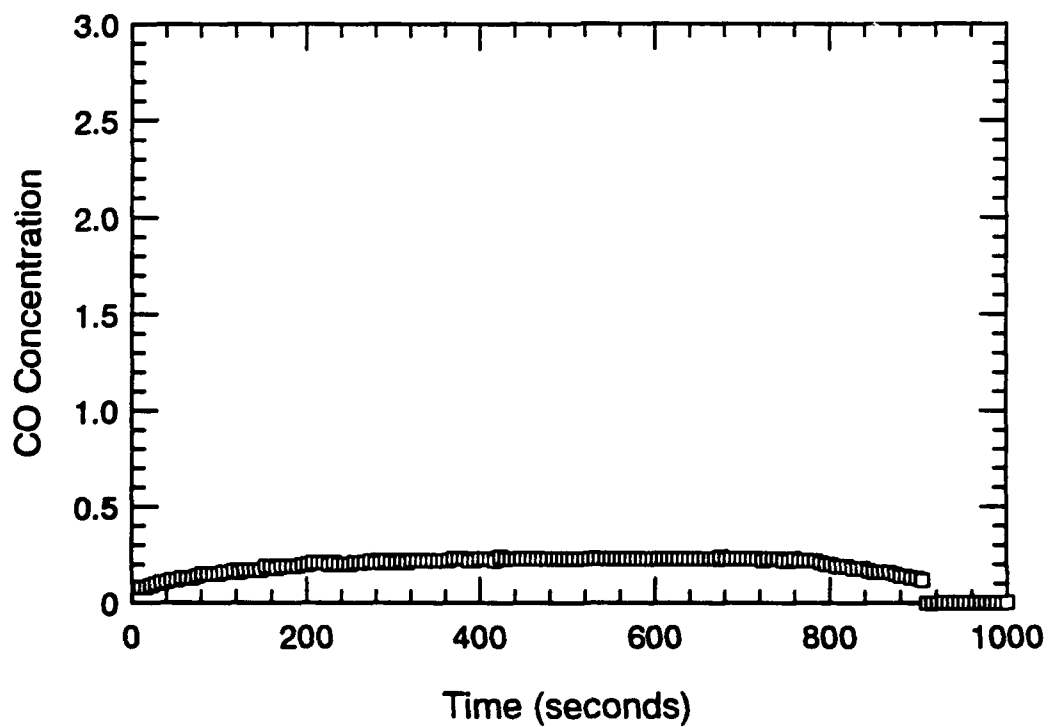
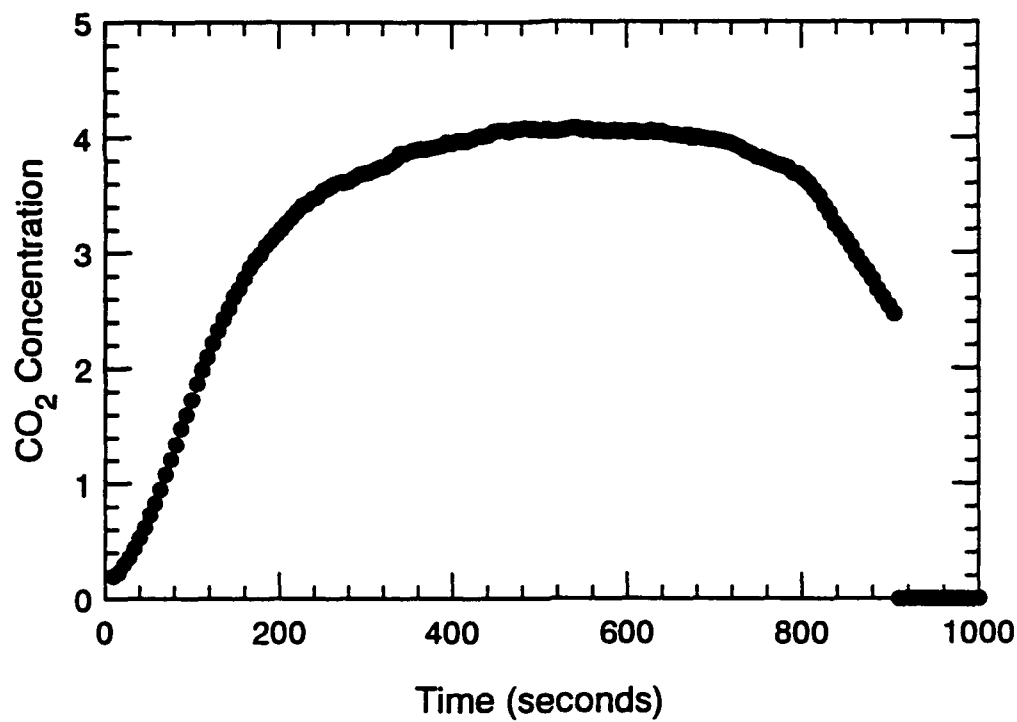


Figure A.42 CO₂ and CO Concentration-Time Histories - S105

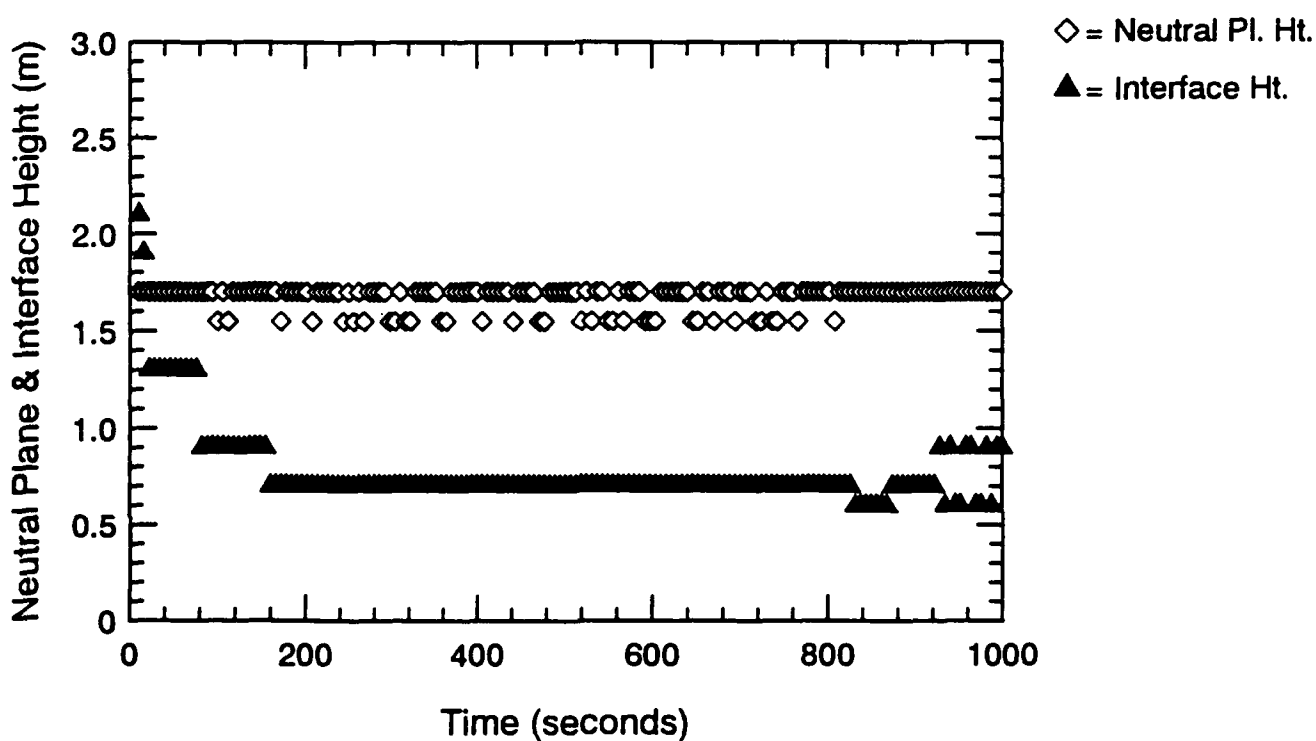
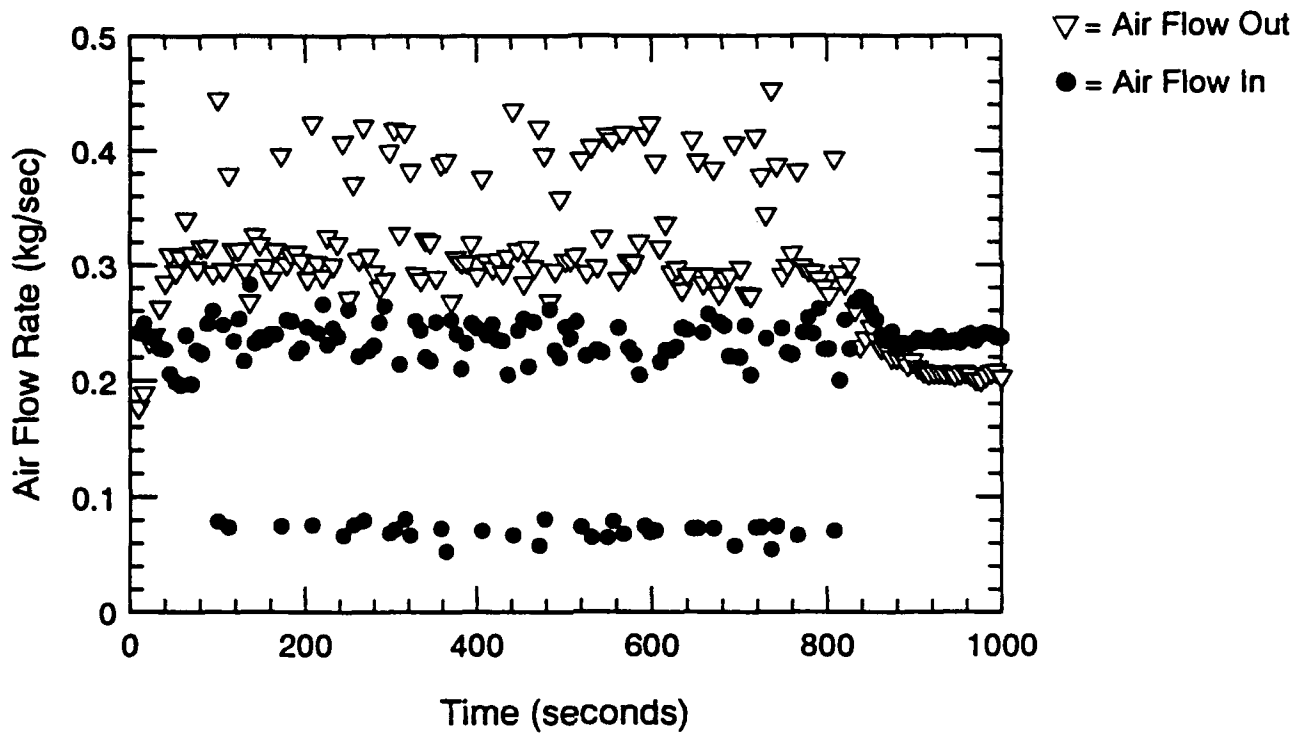


Figure A.43 Air Flow Rate, Neutral Plane & Interface Ht.-Time Histories - S105

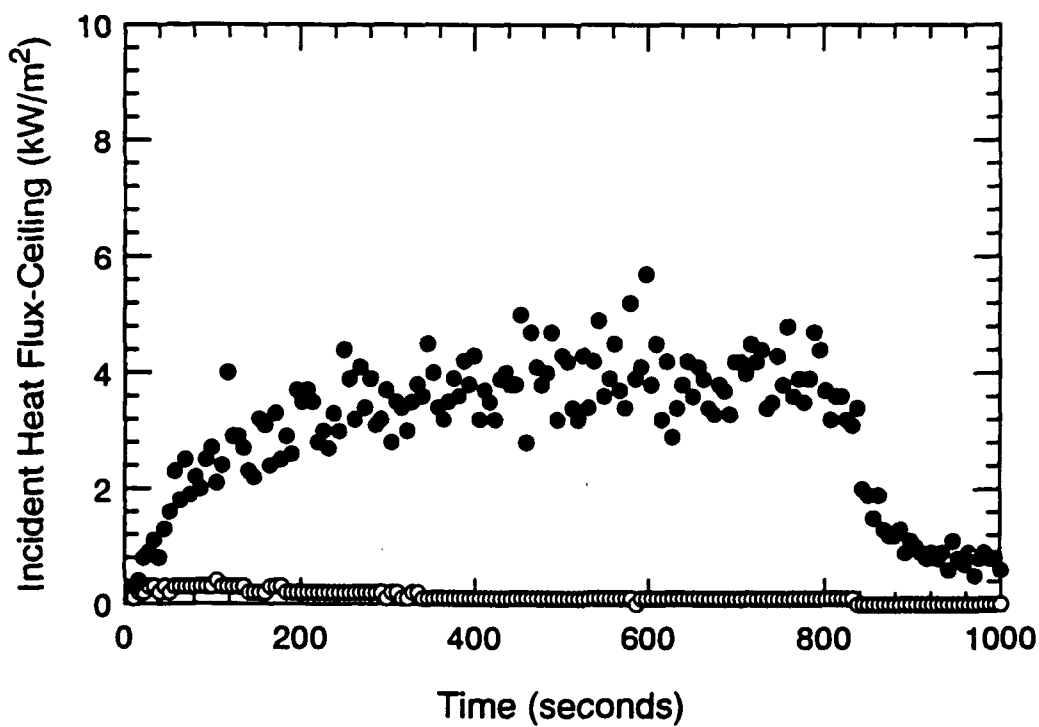
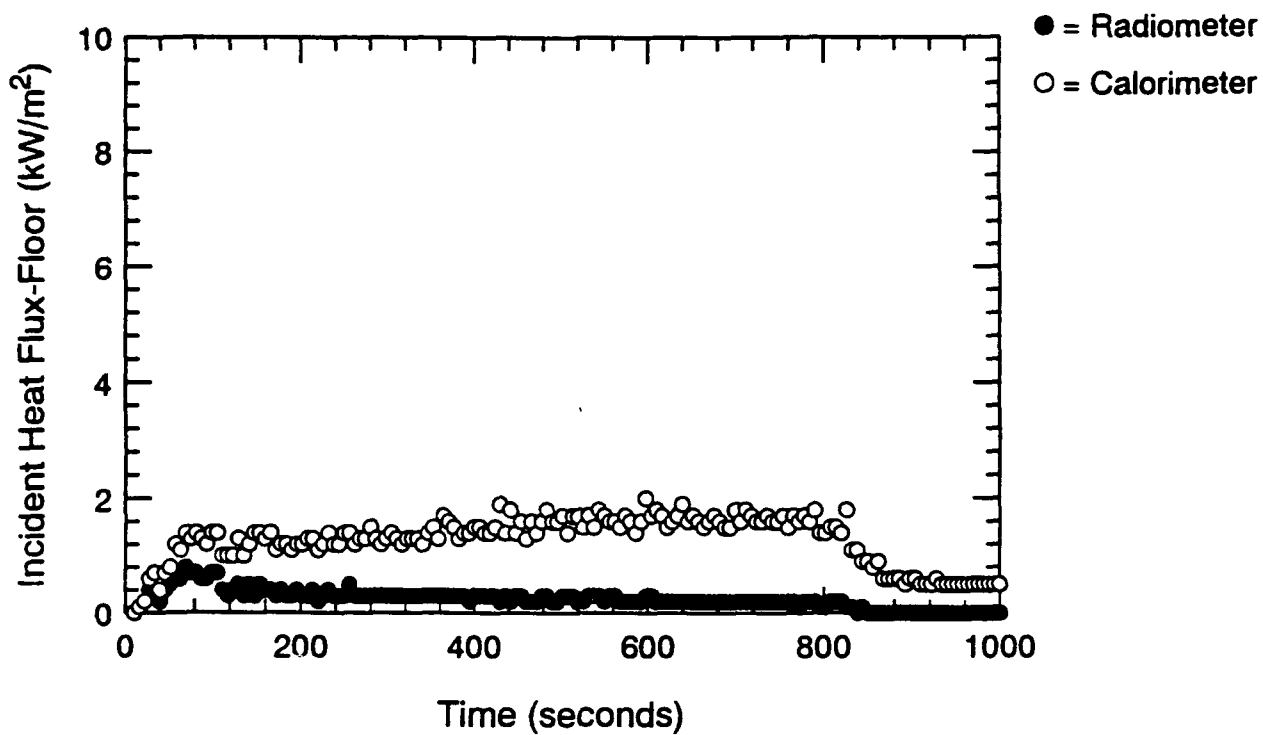


Figure A.44 Incident Heat Flux at Floor and Ceiling-Time Histories - S105

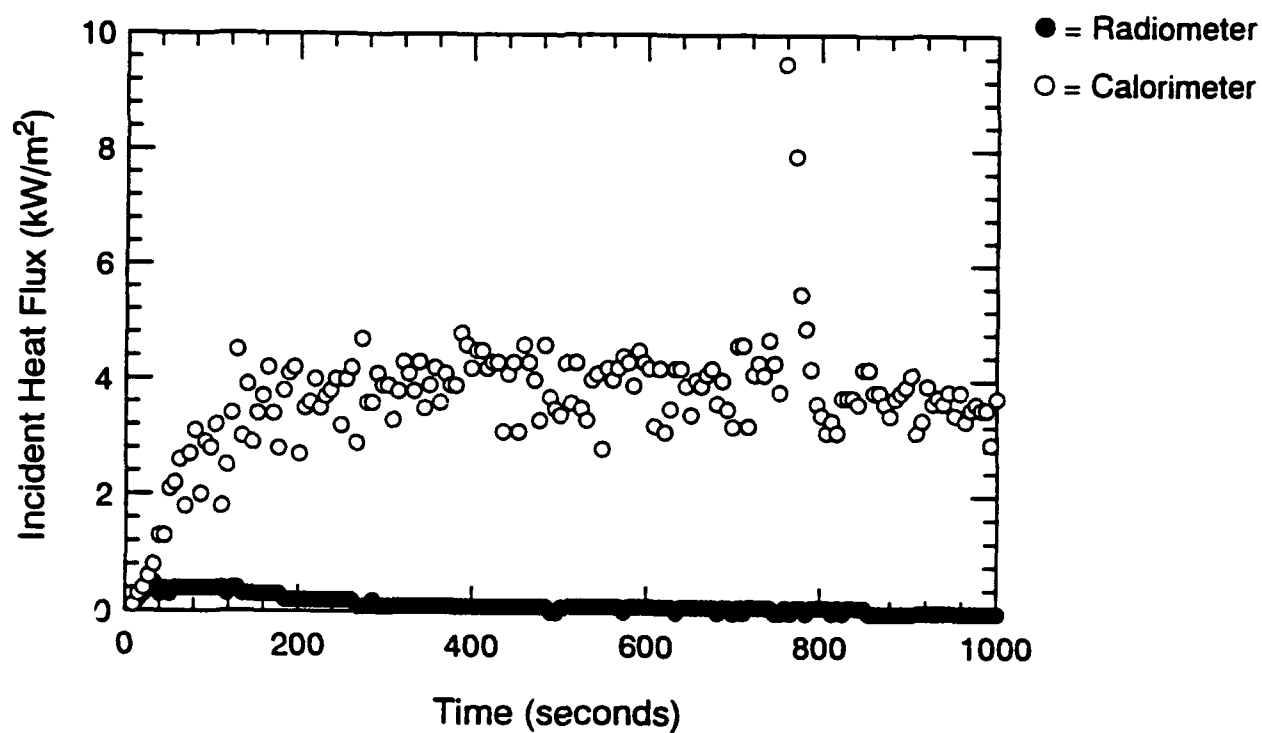


Figure A.45 Incident Heat Flux at Fwd. Bulkhead-Time Histories - S105

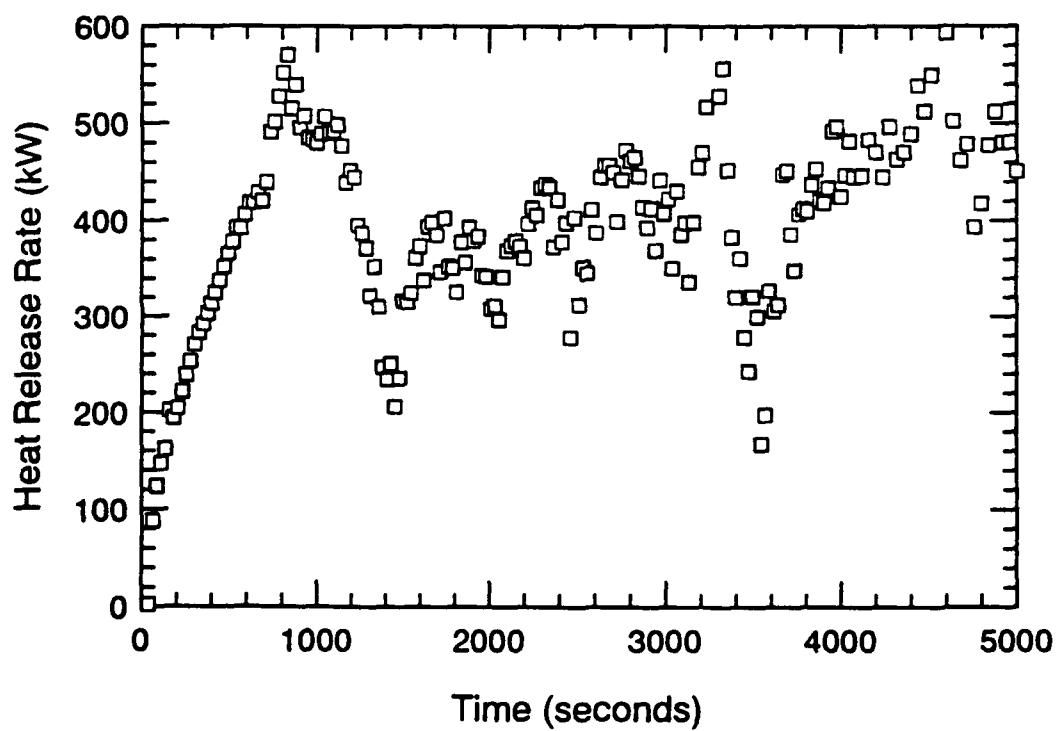
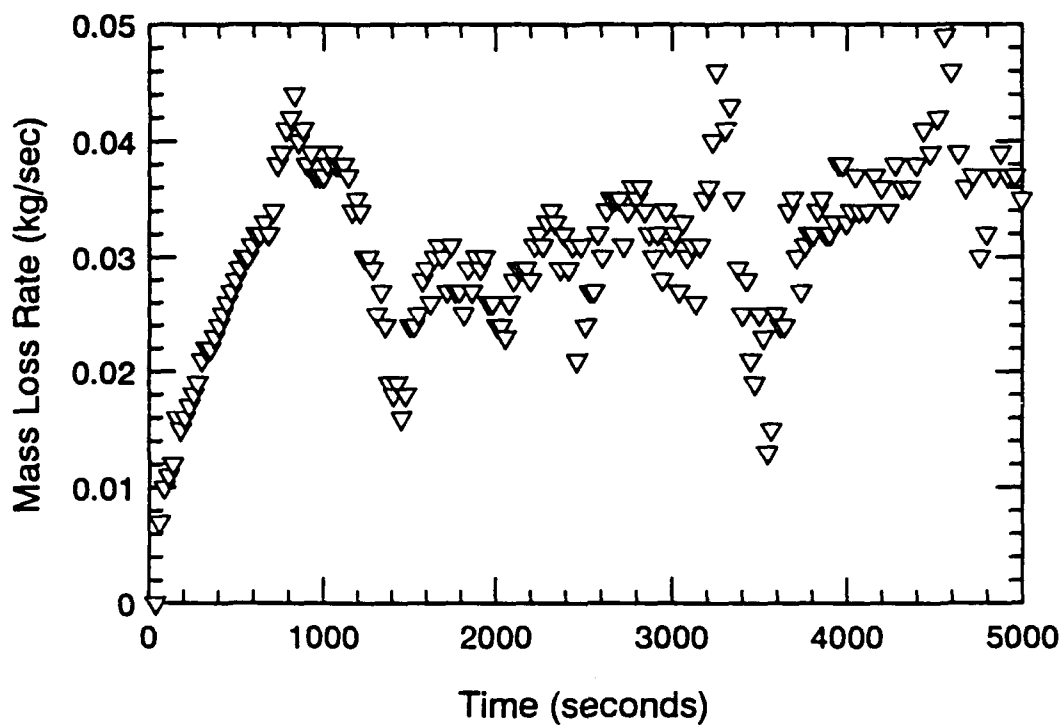


Figure A.46 Mass Loss Rate and Heat Release Rate-Time Histories - S106

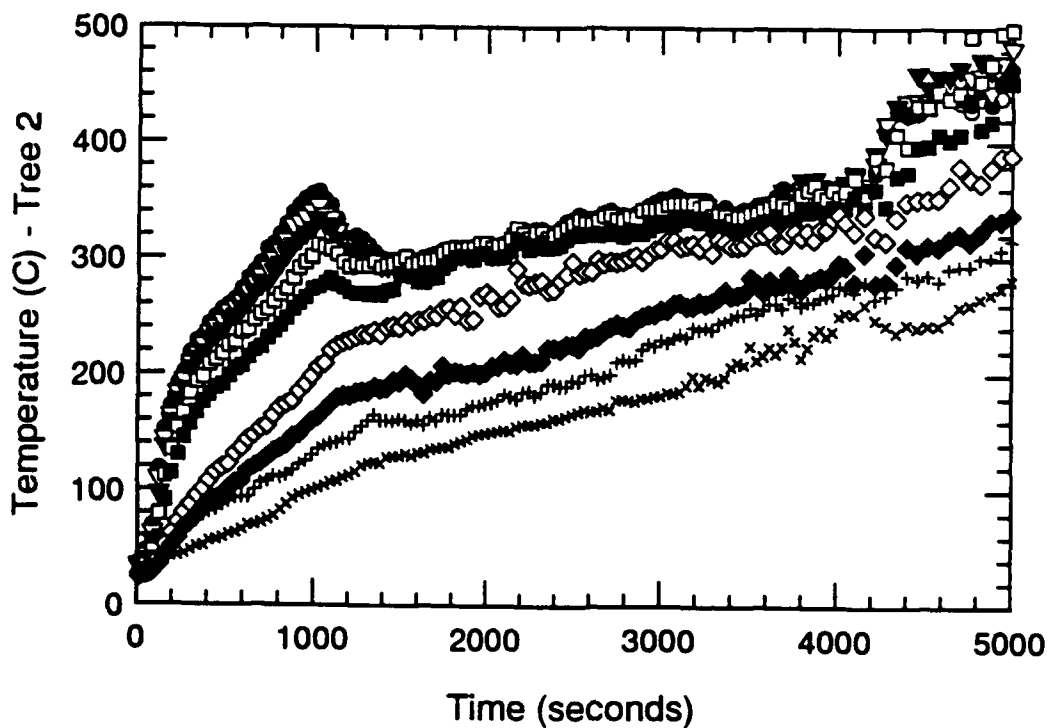
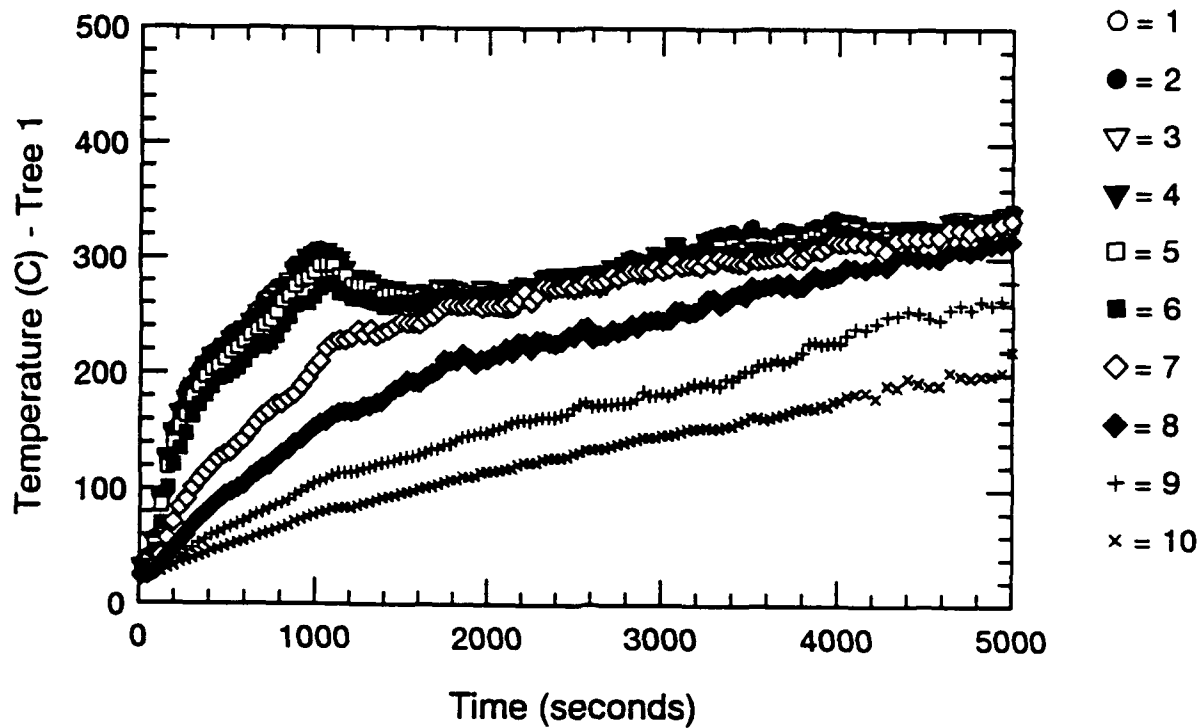


Figure A.47 Thermocouple Trees 1 & 2-Time Histories - S106

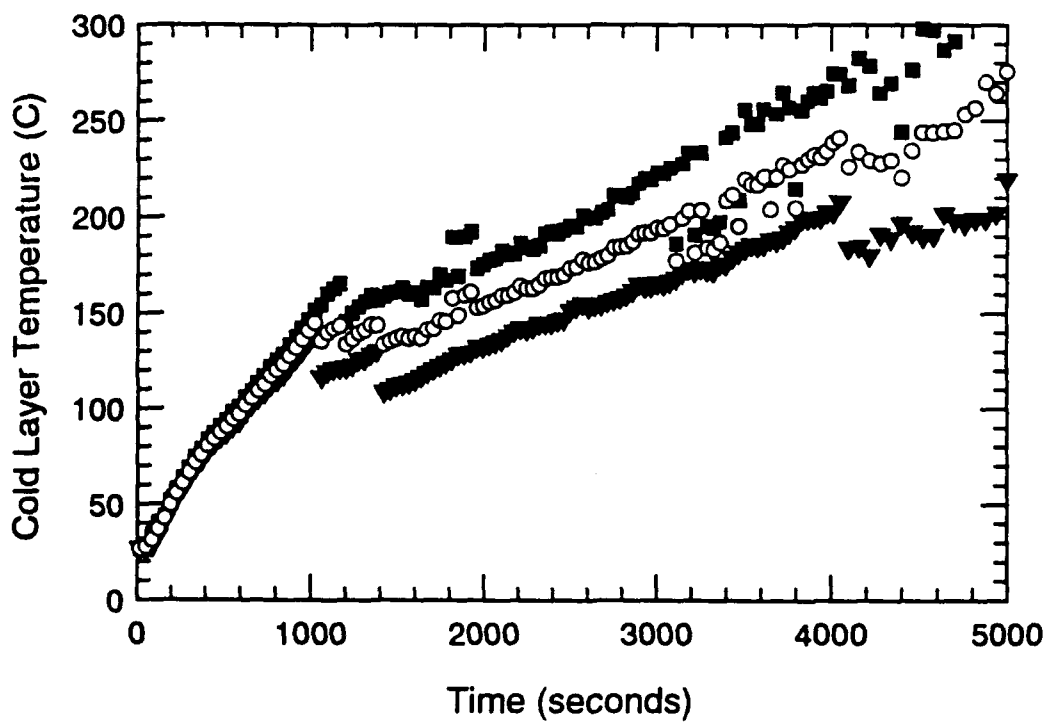
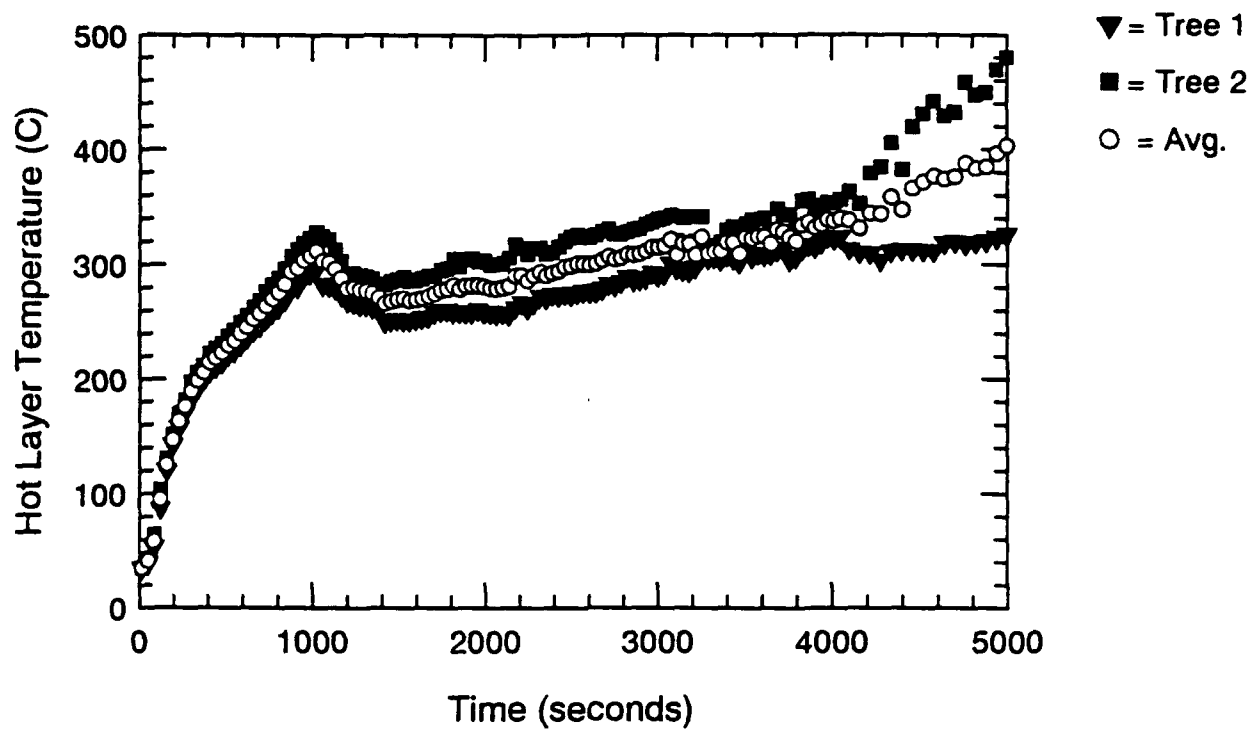


Figure A.48 Hot and Cold Layer Temperature-Time Histories - S106

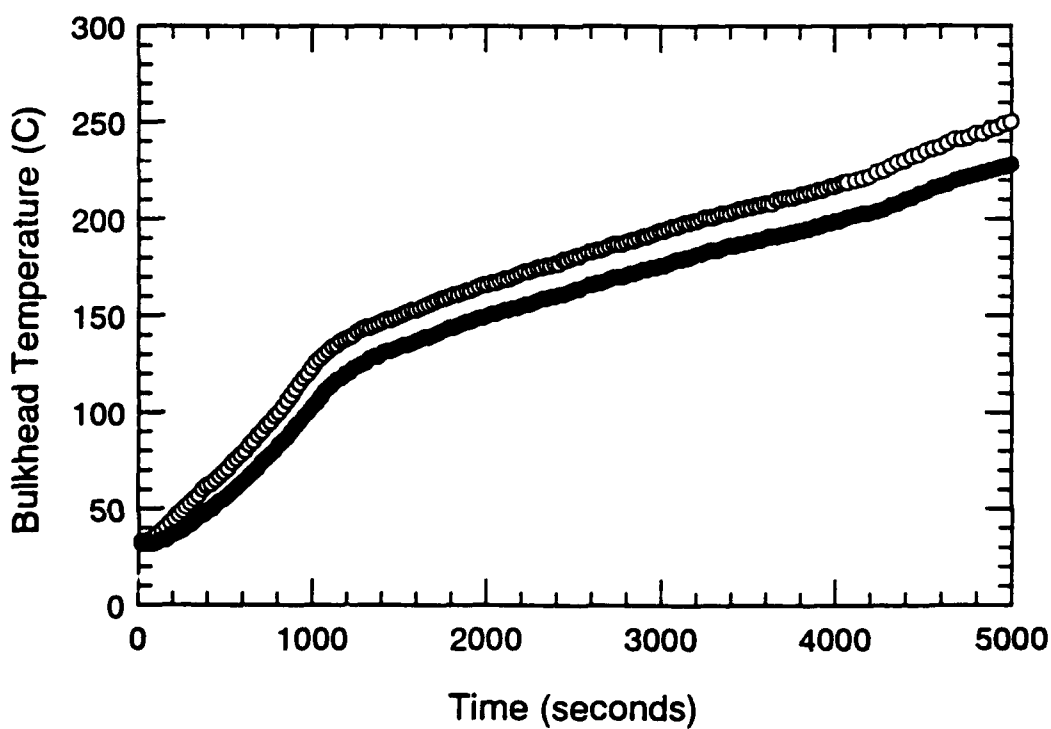
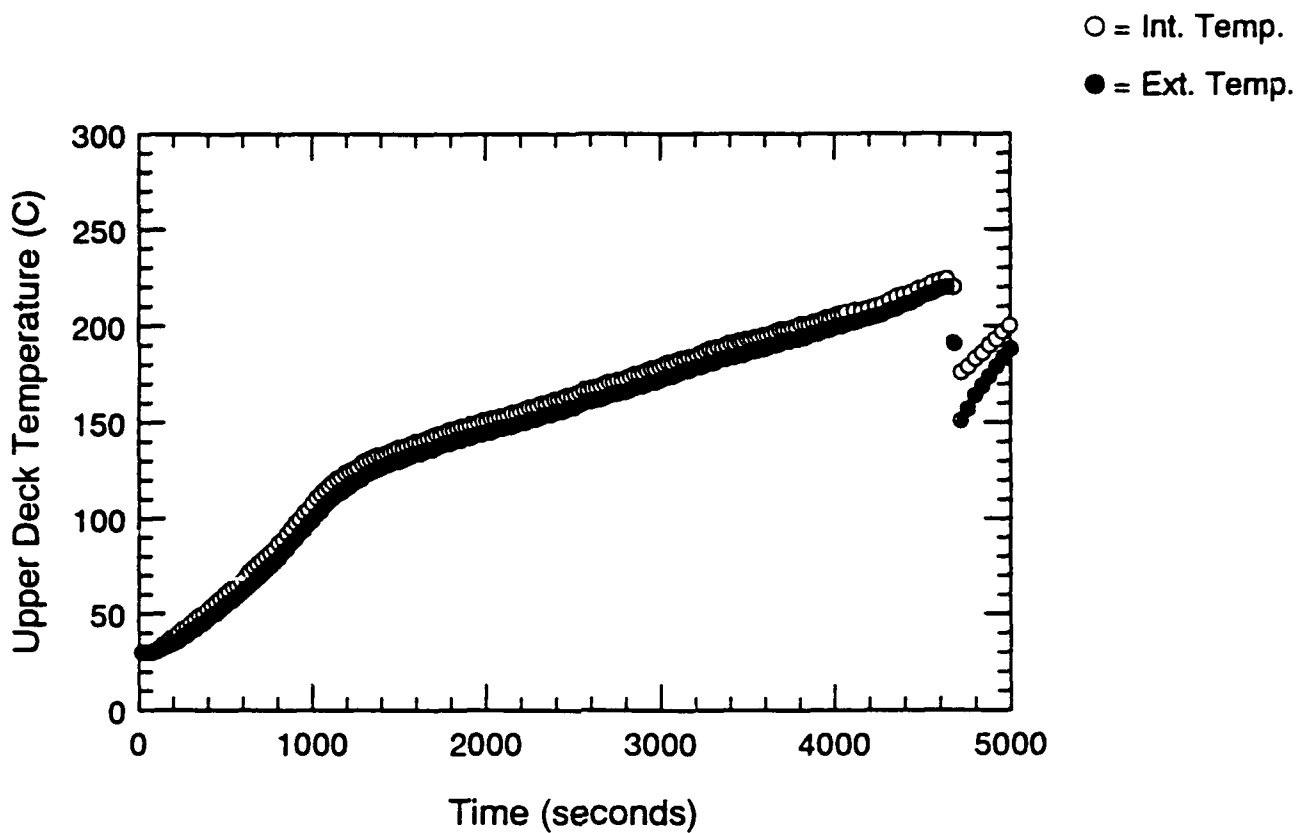


Figure A.49 Surface Thermocouple-Time Histories - S106

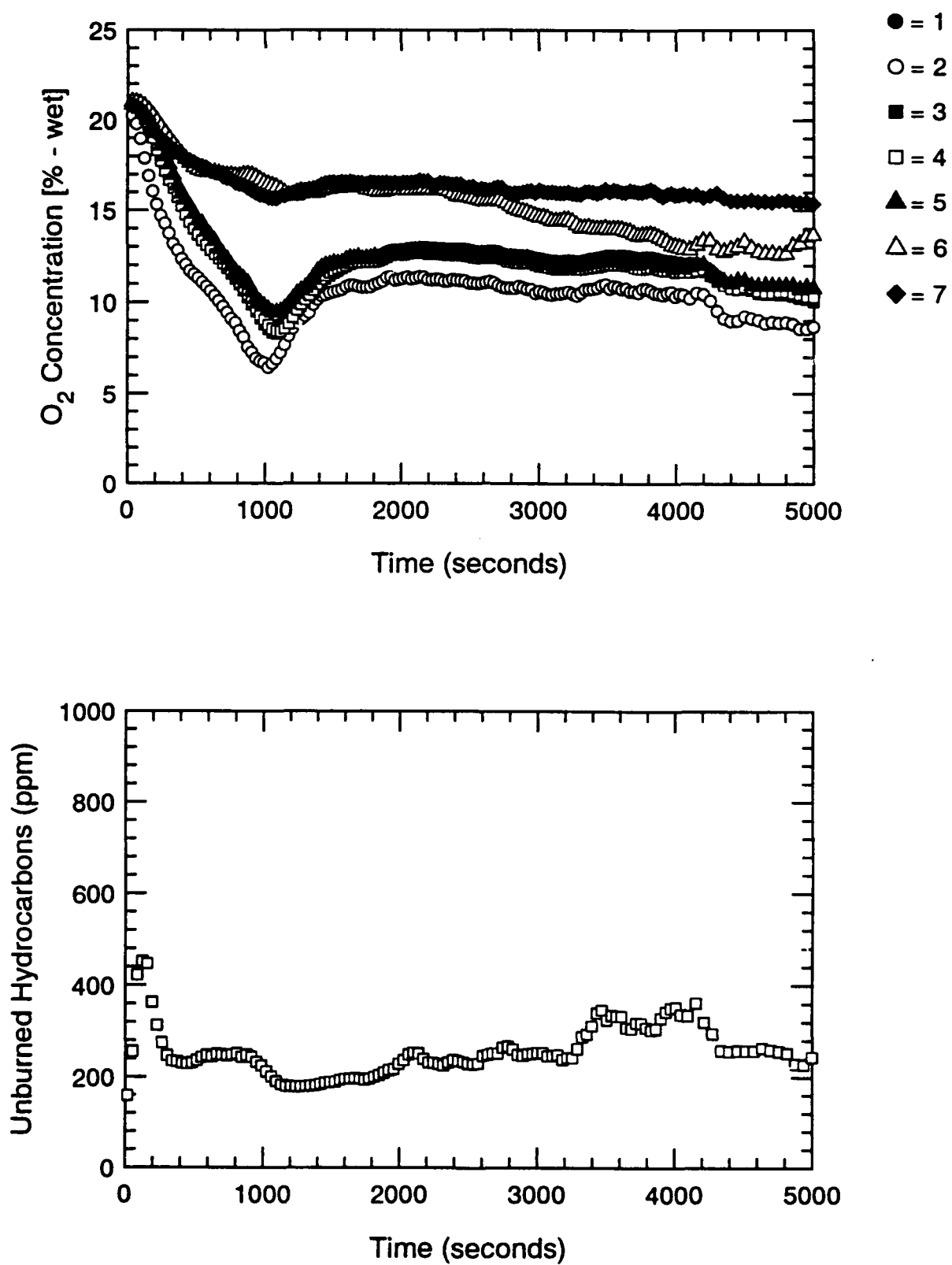


Figure A.50 Oxygen and Unburned HC Concentration-Time Histories - S106

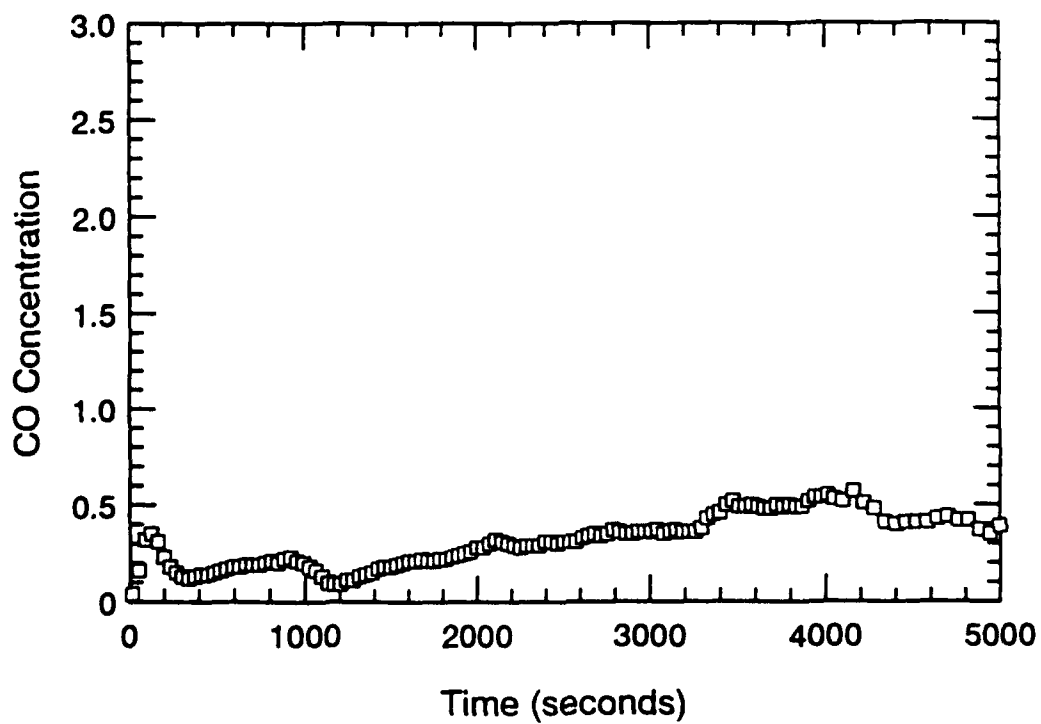
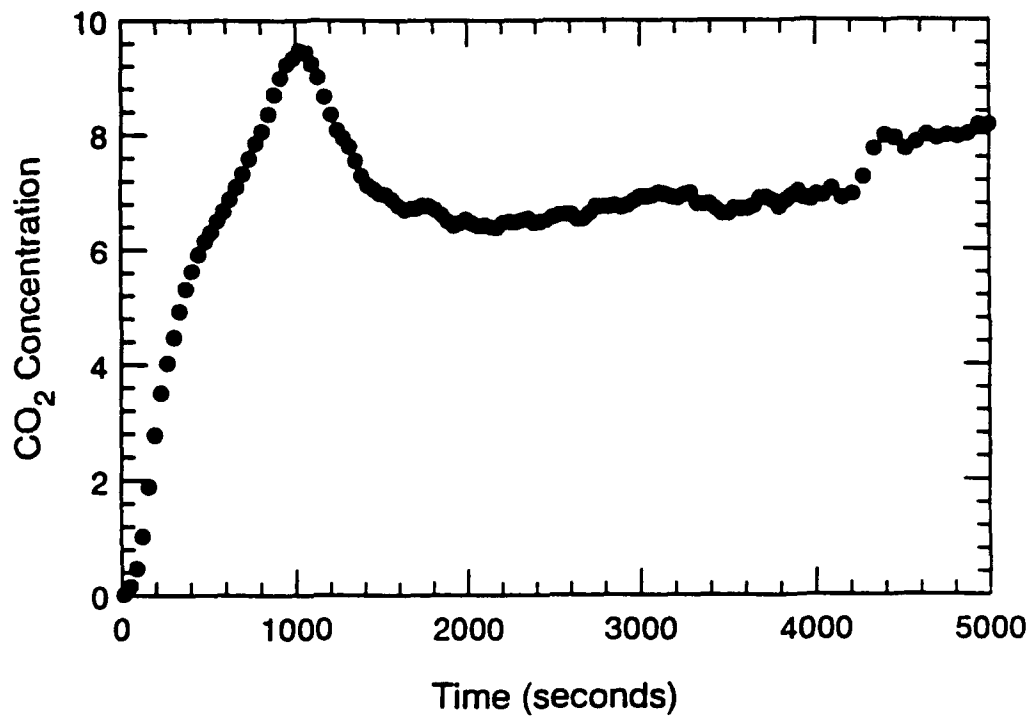


Figure A.51 CO₂ and CO Concentration-Time Histories - S106

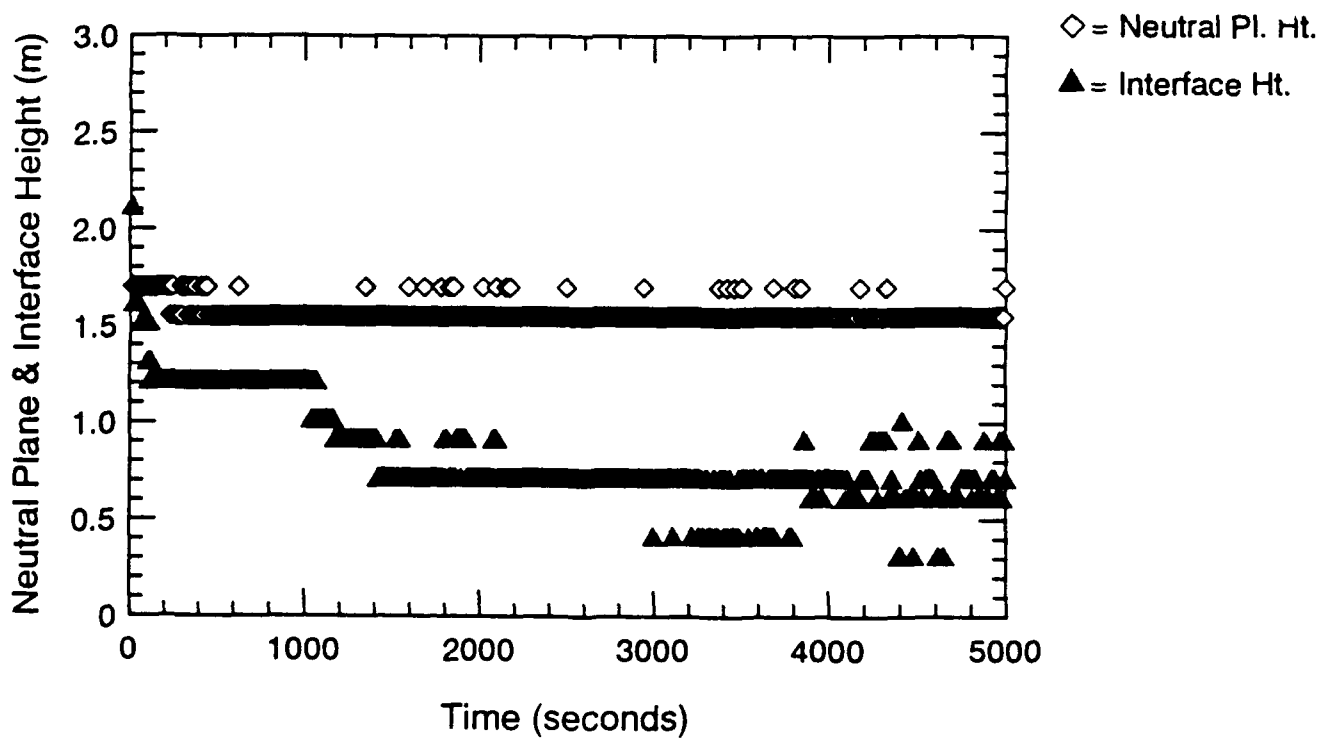
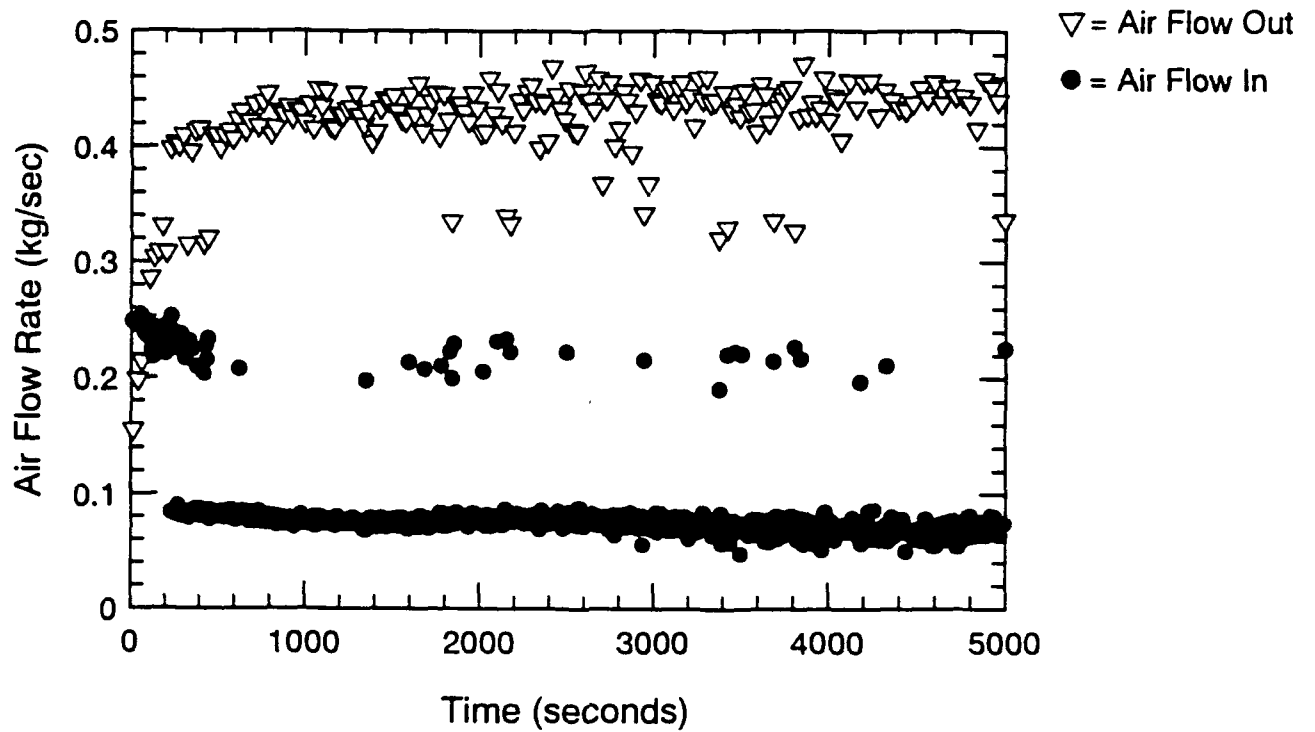


Figure A.52 Air Flow Rate, Neutral Plane & Interface Ht.-Time Histories - S106

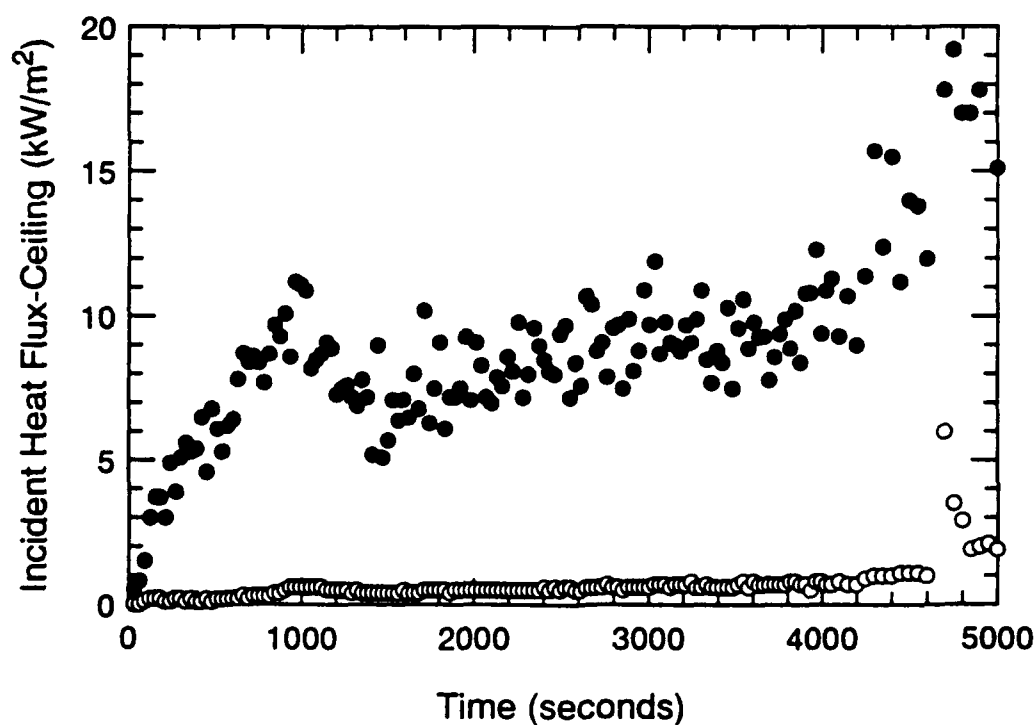
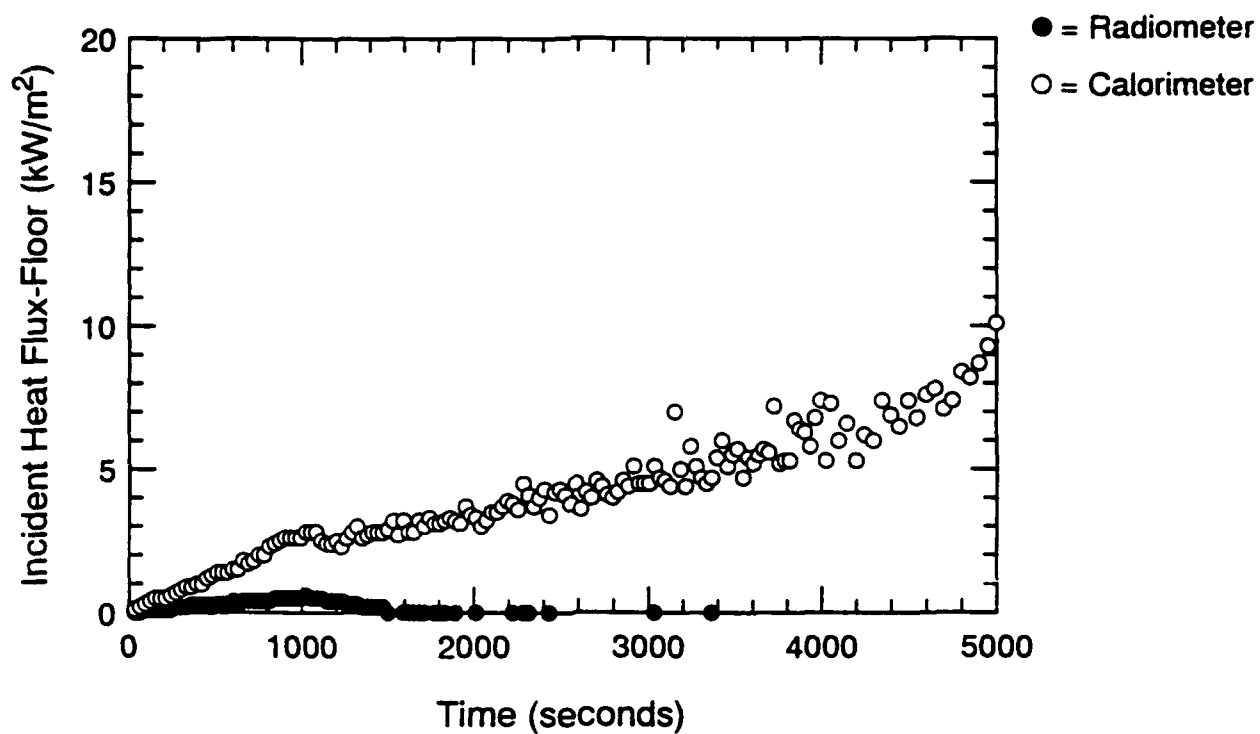


Figure A.53 Incident Heat Flux at Floor and Ceiling-Time Histories - S106

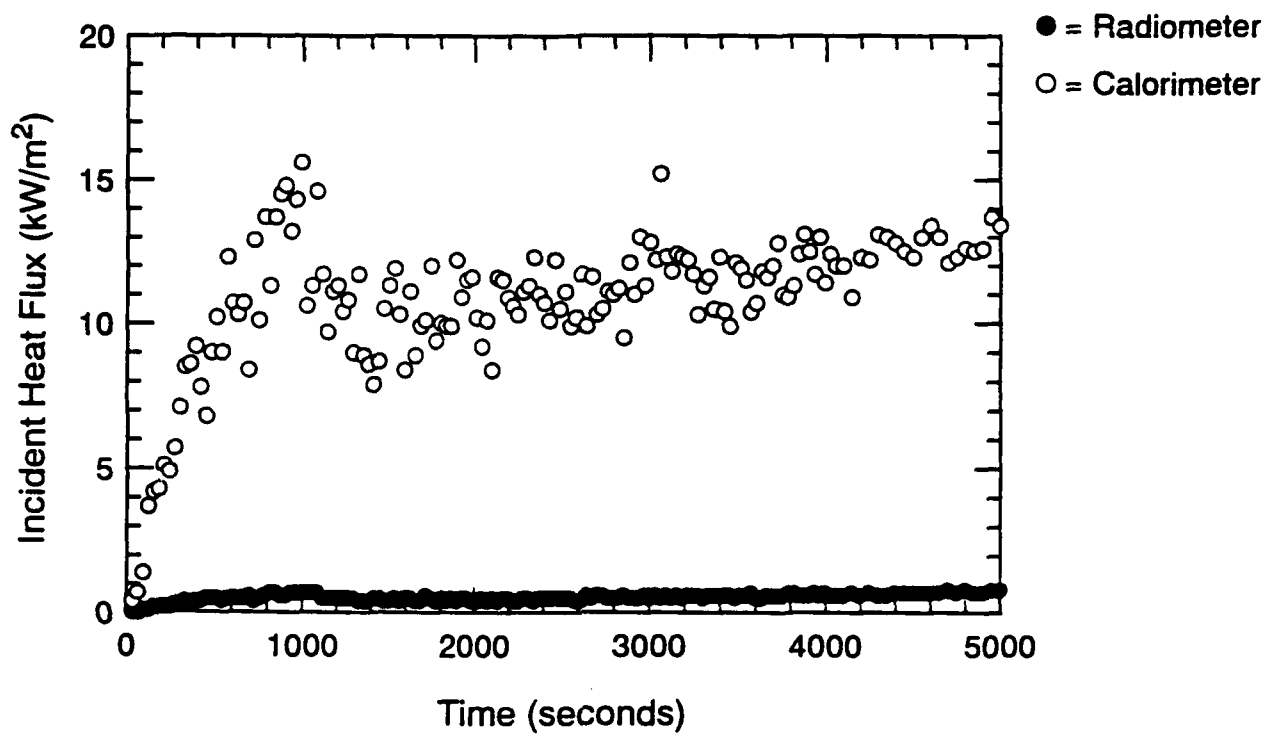


Figure A.54 Incident Heat Flux at Fwd. Bulkhead-Time Histories - S106

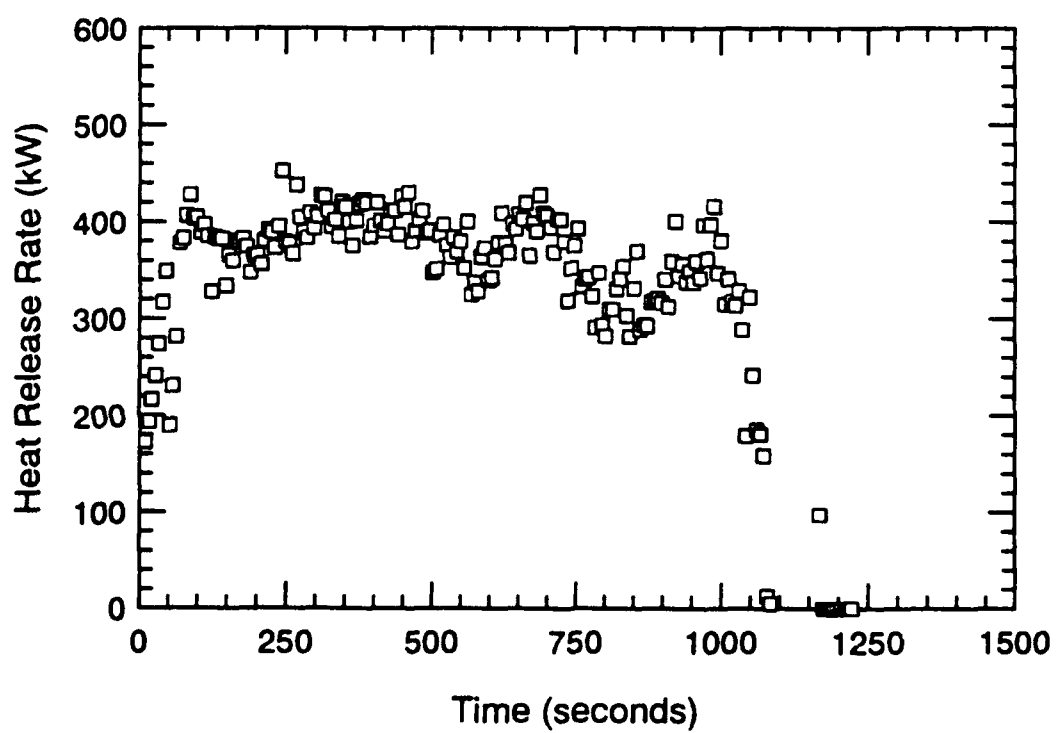
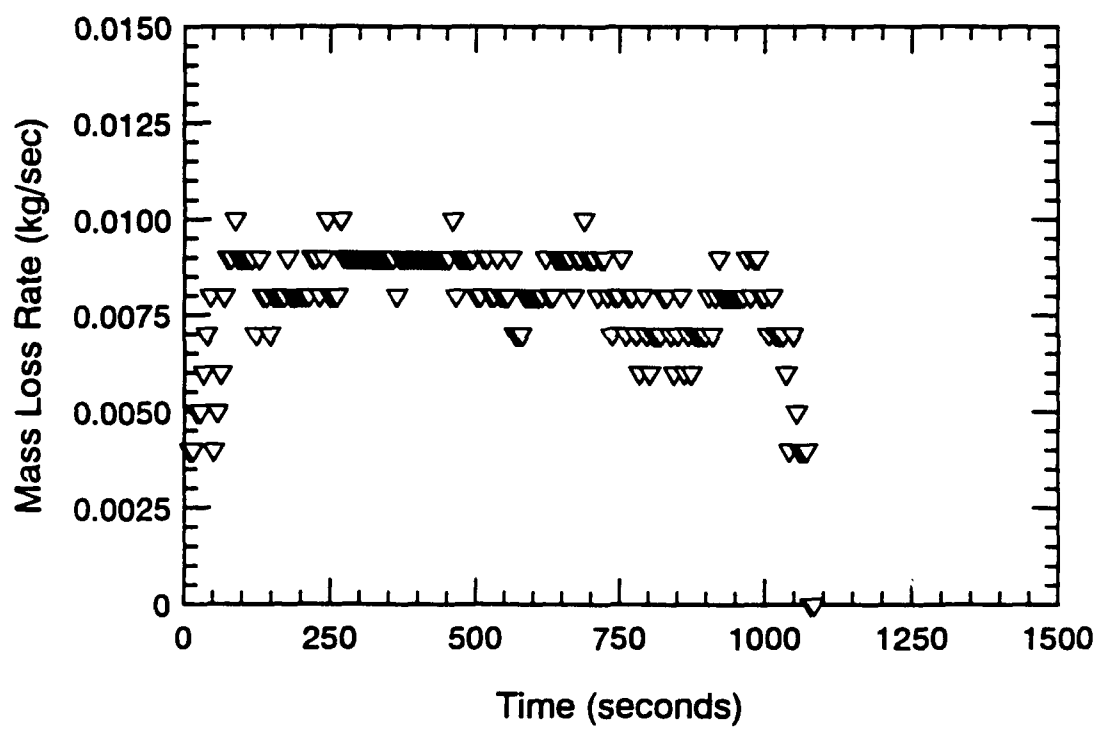


Figure A.55 Mass Loss Rate and Heat Release Rate-Time Histories - S107

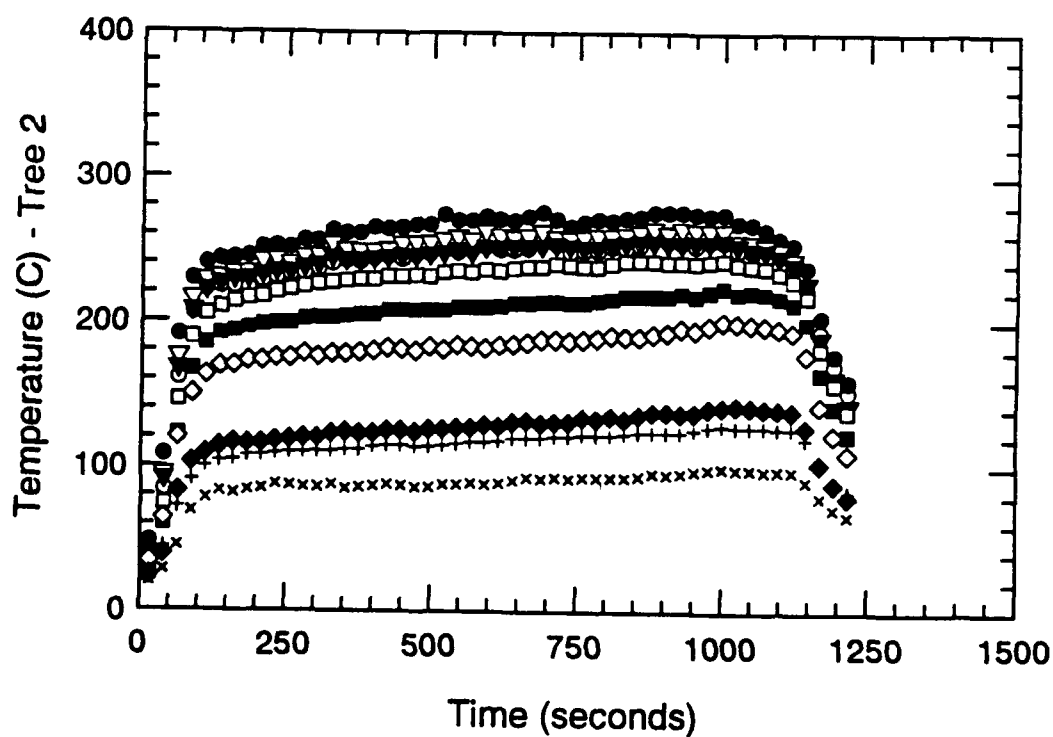
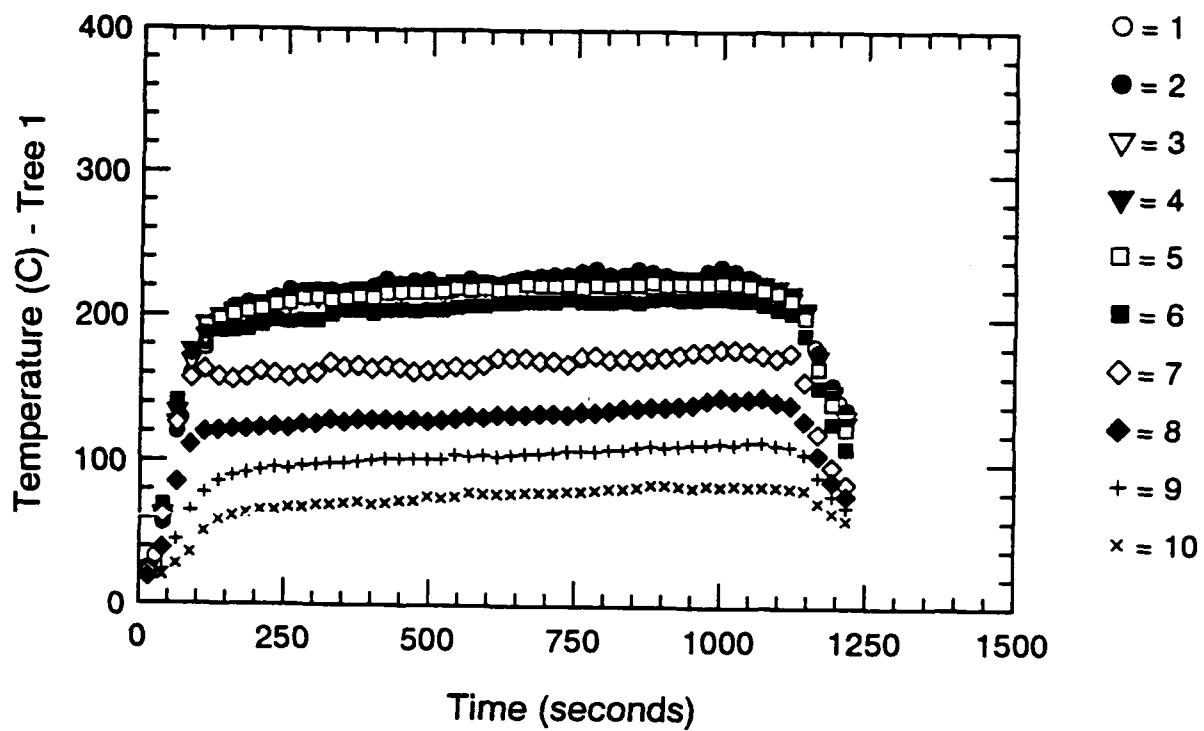


Figure A.56 Thermocouple Trees 1 & 2-Time Histories - S107

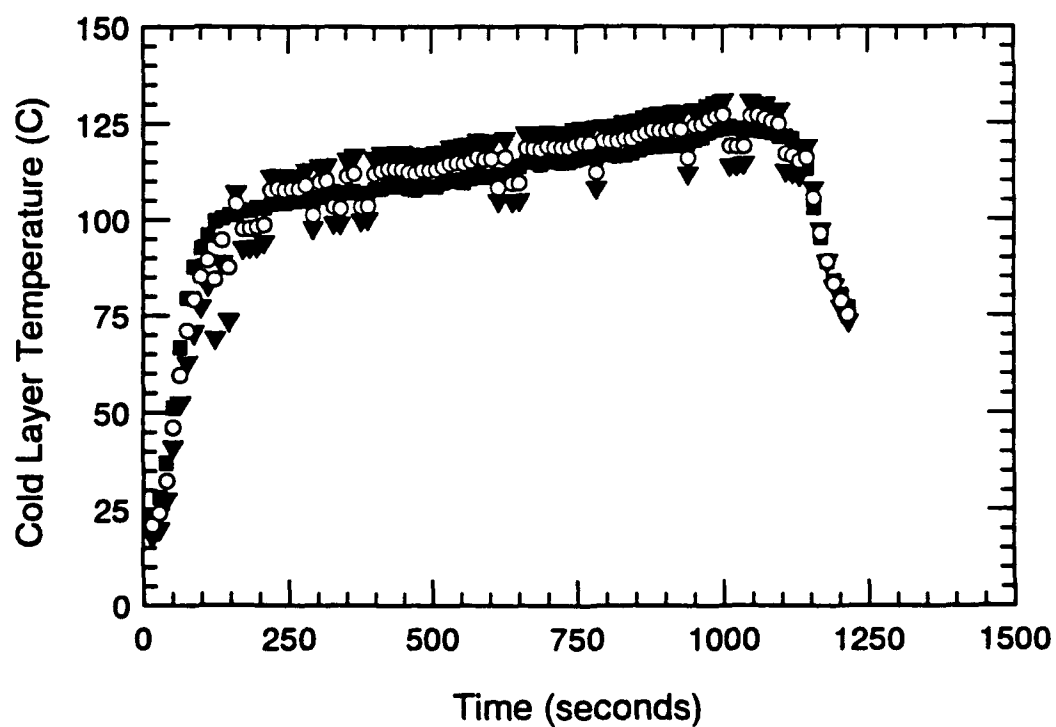
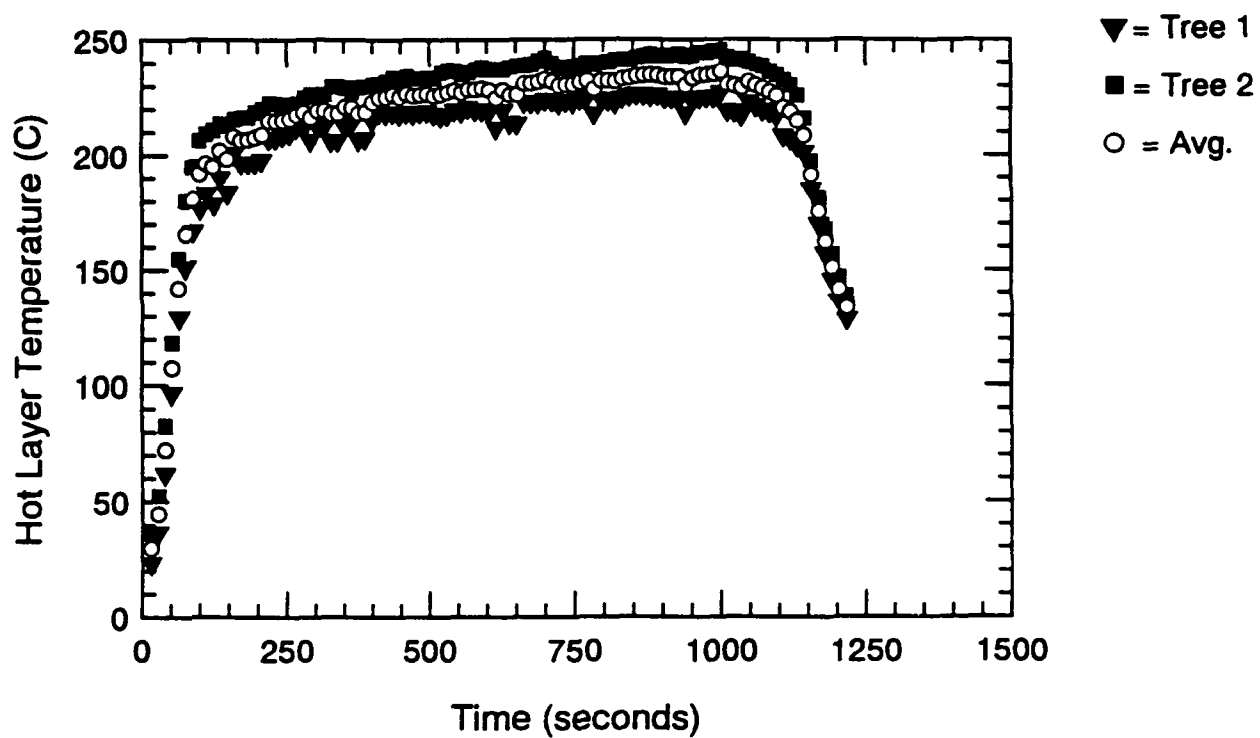


Figure A.57 Hot and Cold Layer Temperature-Time Histories - S107

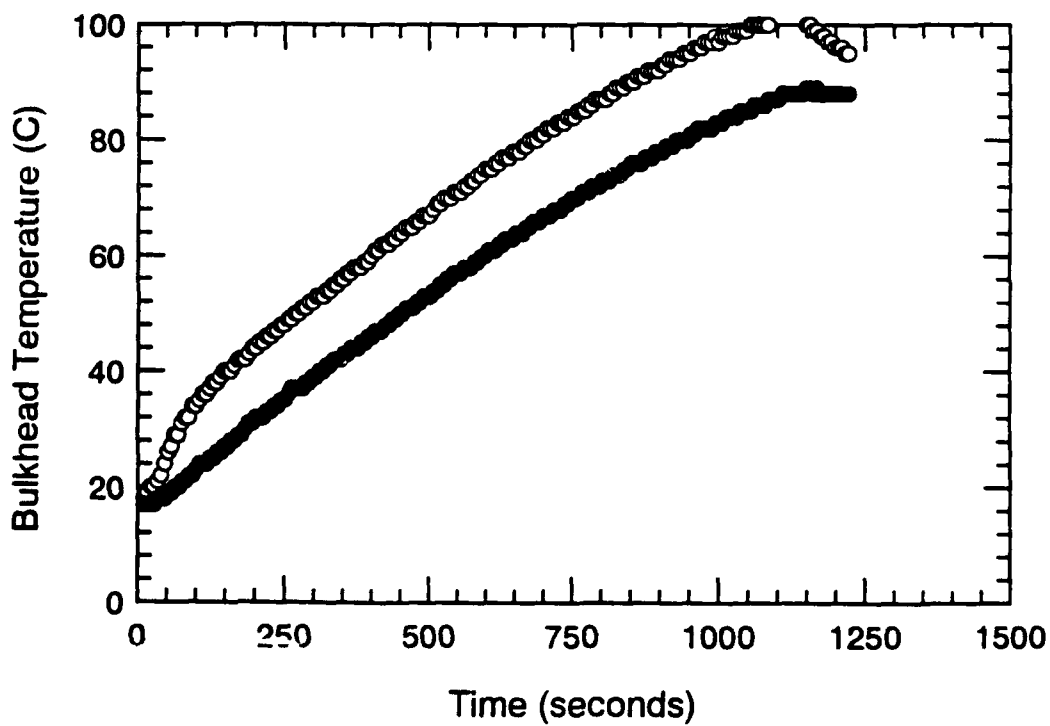
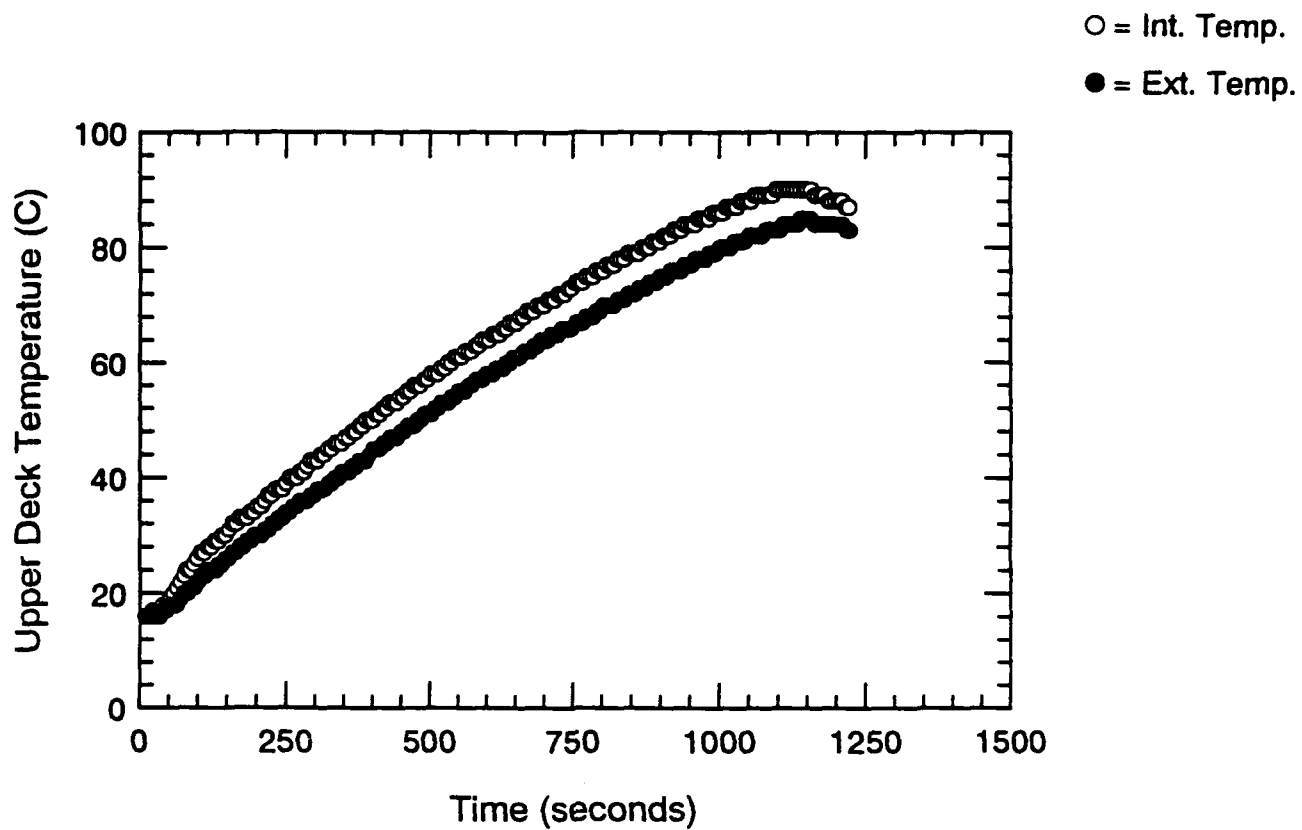


Figure A.58 Surface Thermocouple-Time Histories - S107

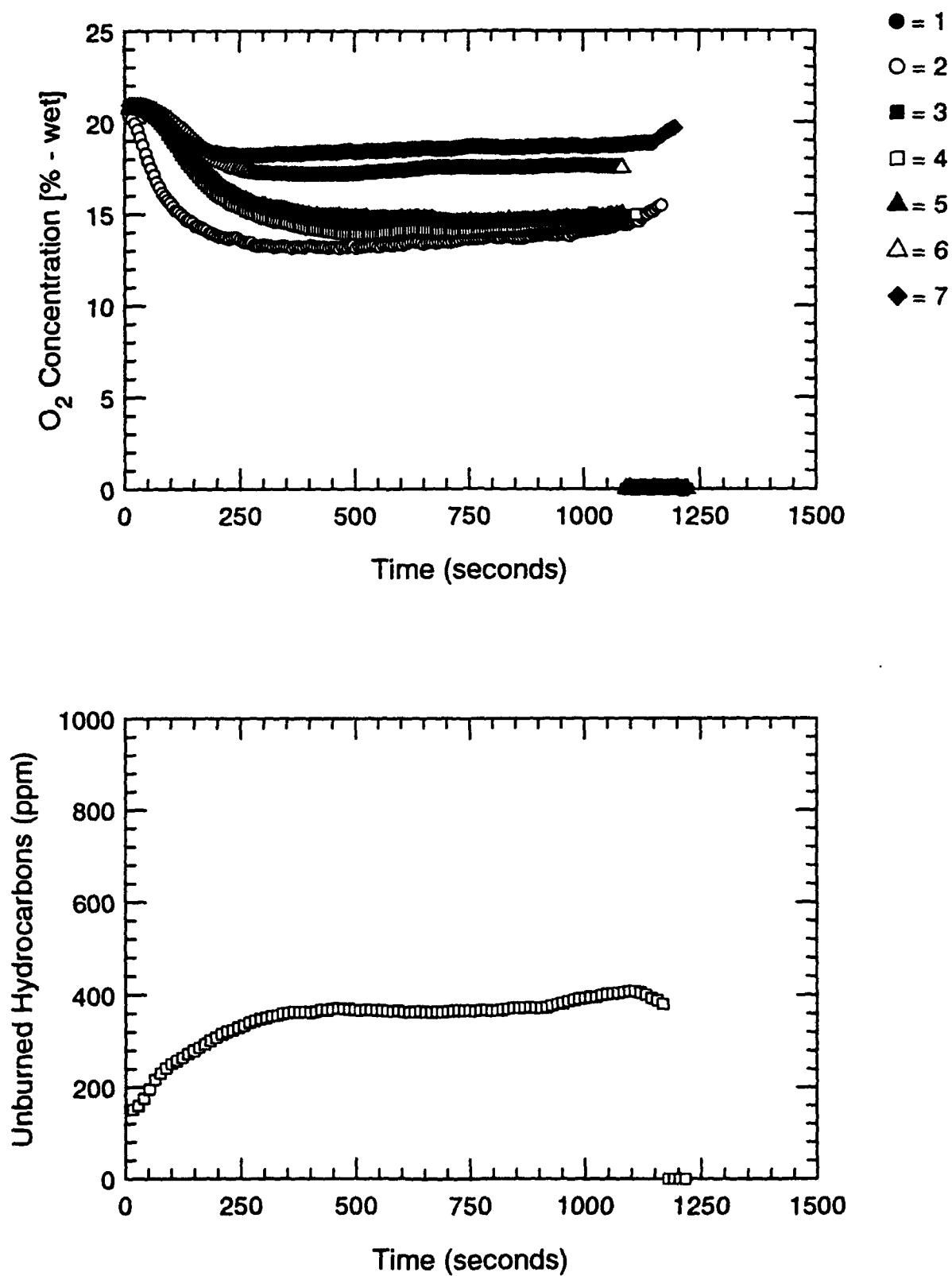


Figure A.59 Oxygen and Unburned HC Concentration-Time Histories - S107

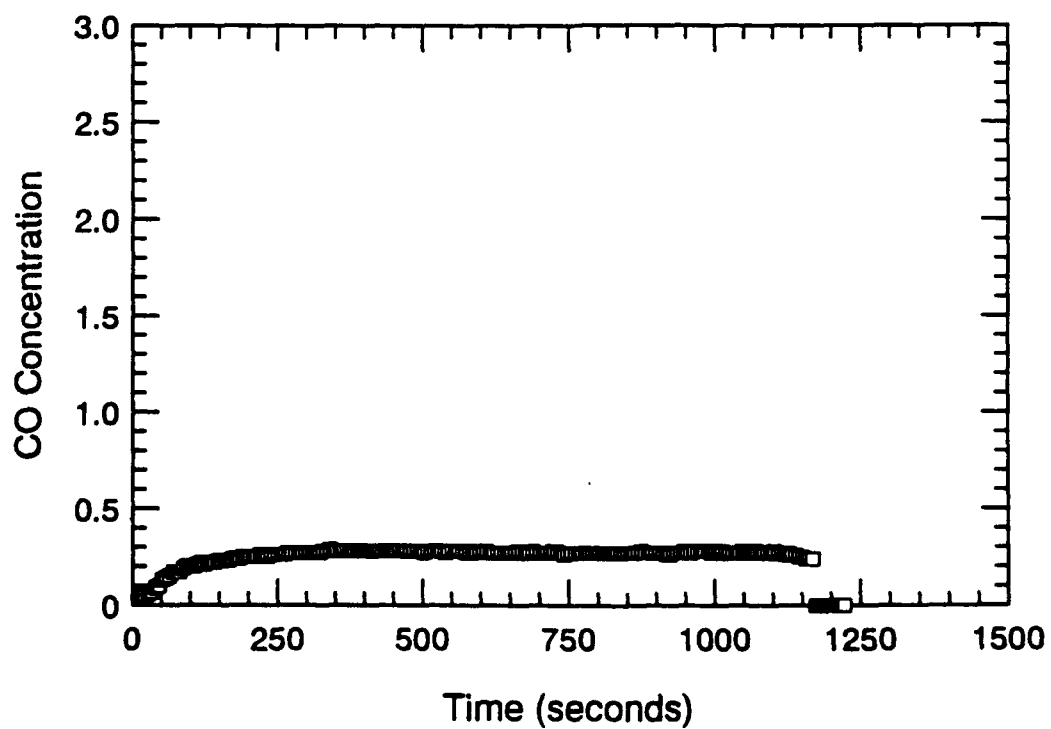
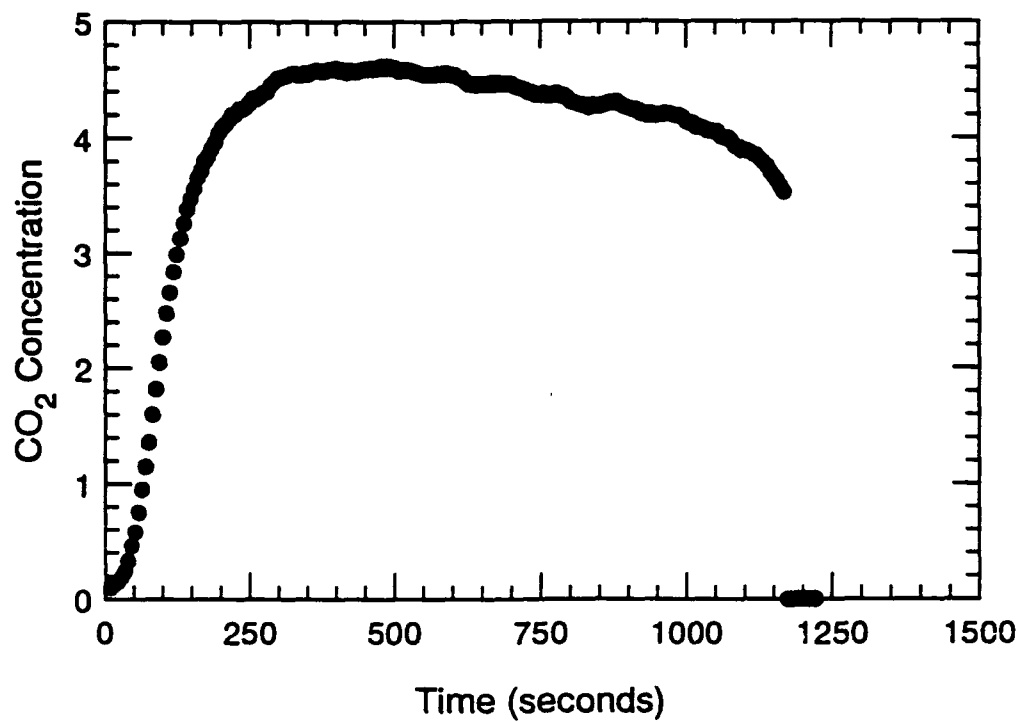


Figure A.60 CO₂ and CO Concentration-Time Histories - S107

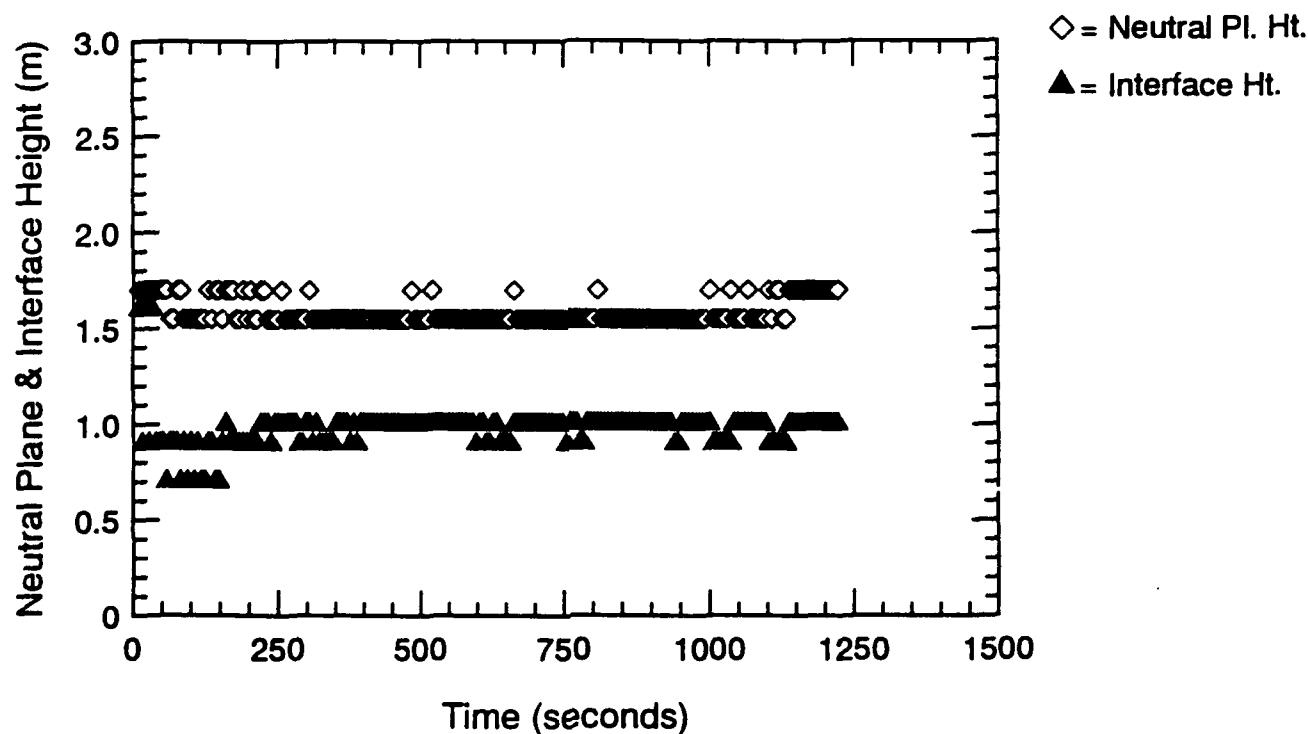
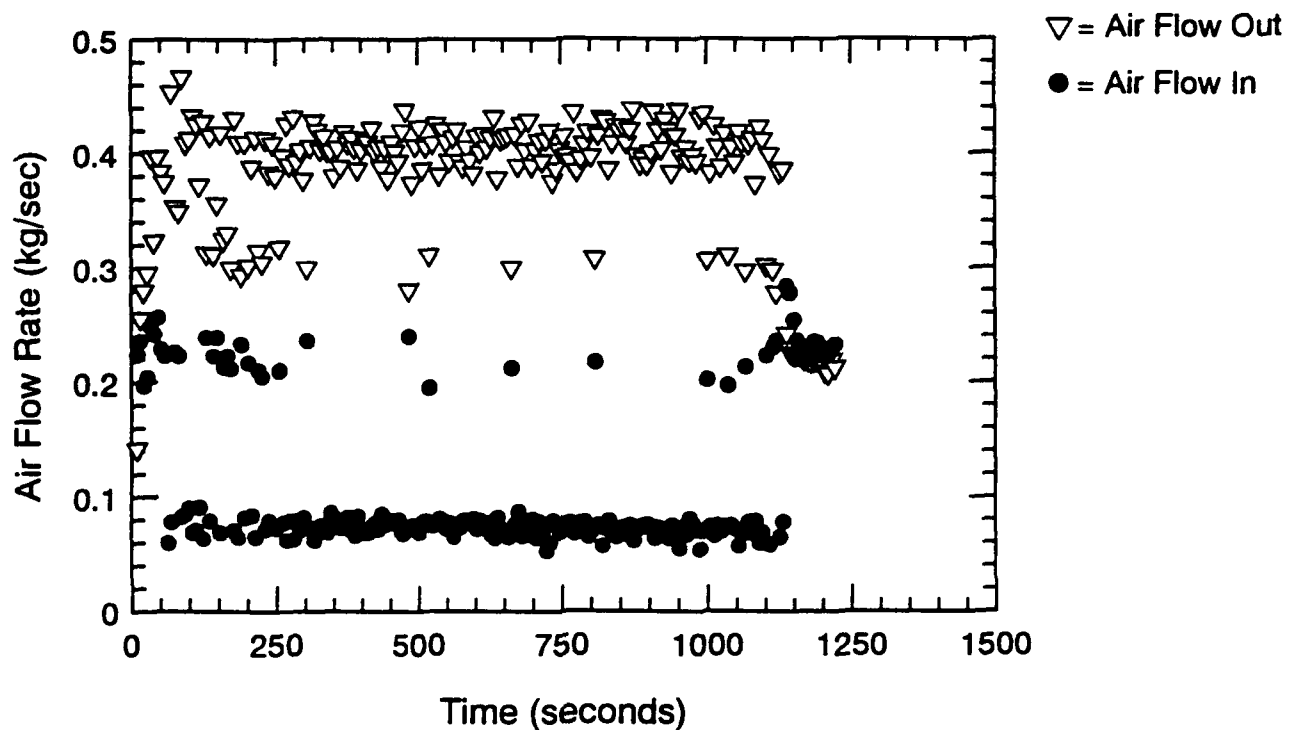


Figure A.61 Air Flow Rate, Neutral Plane & Interface Ht.-Time Histories - S107

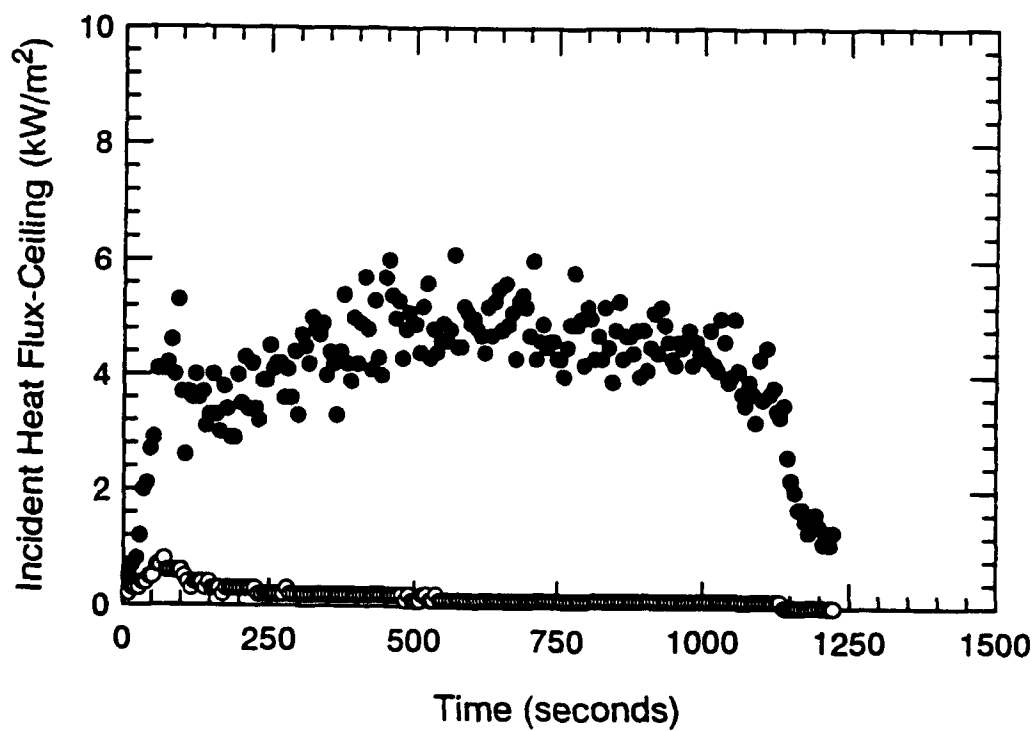
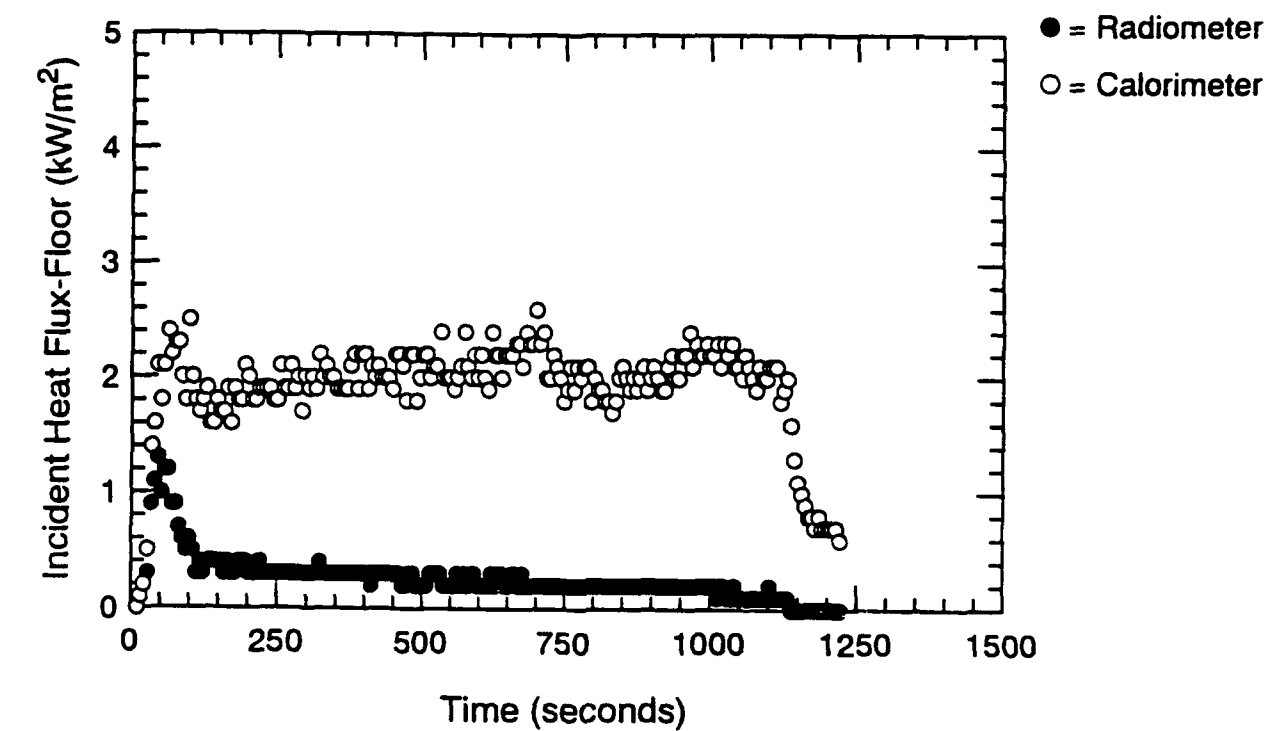


Figure A.62 Incident Heat Flux at Floor and Ceiling-Time Histories - S107

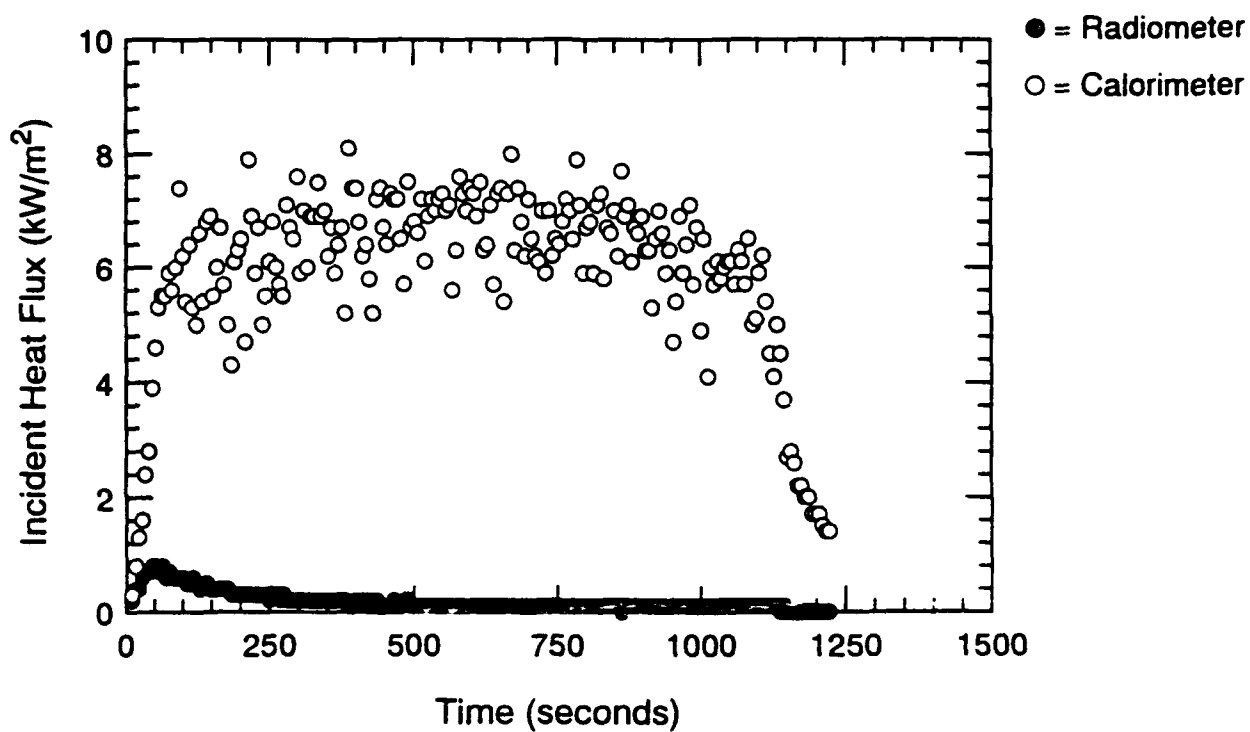


Figure A.63 Incident Heat Flux at Fwd. Bulkhead-Time Histories - S107

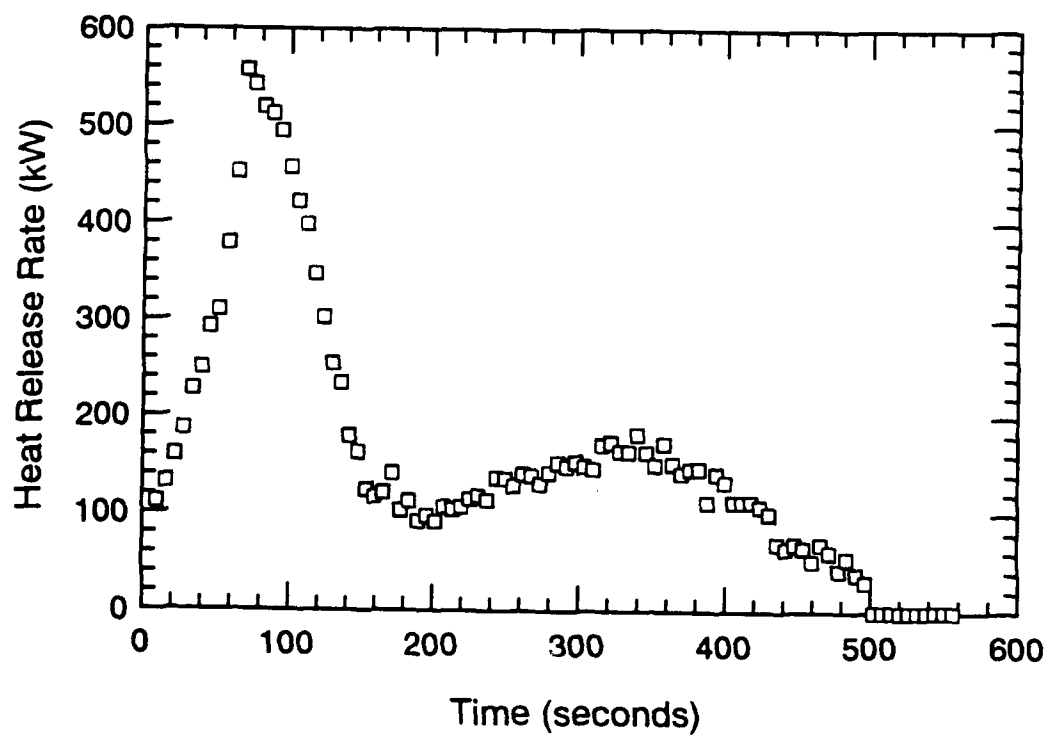
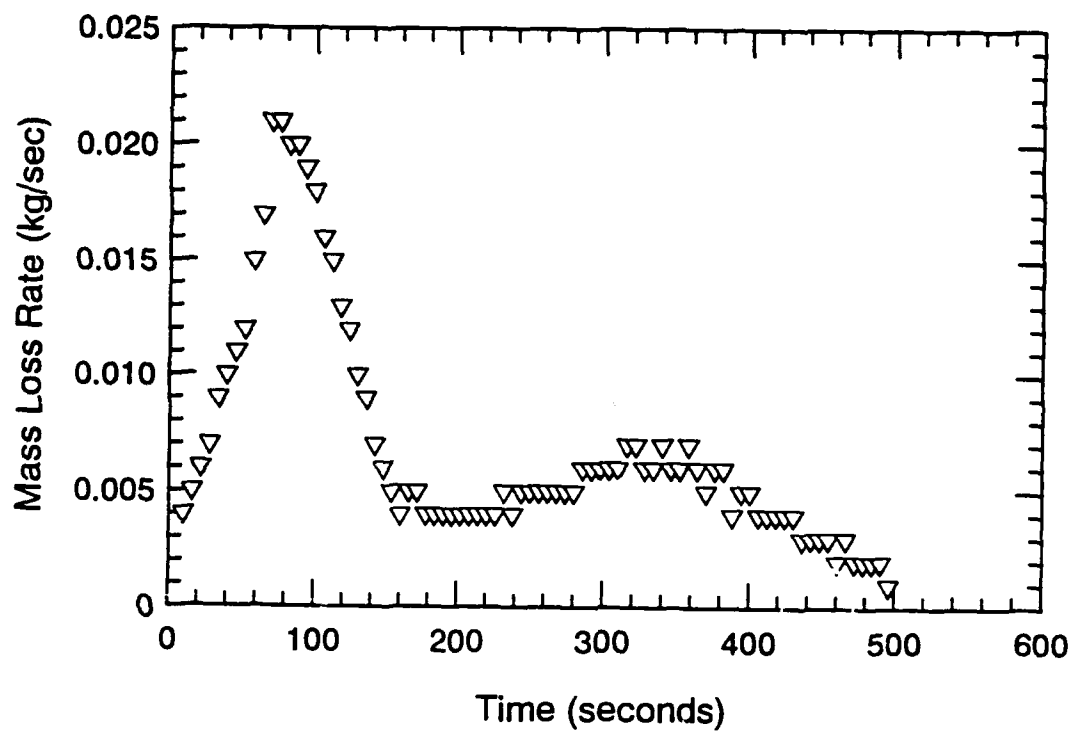


Figure A.64 Mass Loss Rate and Heat Release Rate-Time Histories - S108

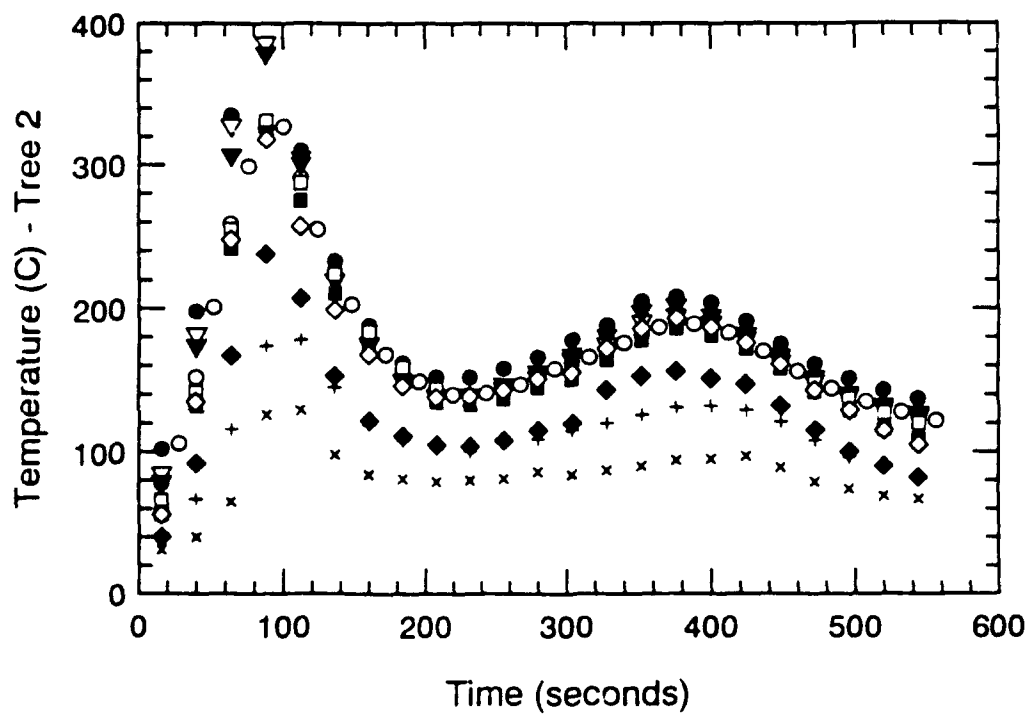
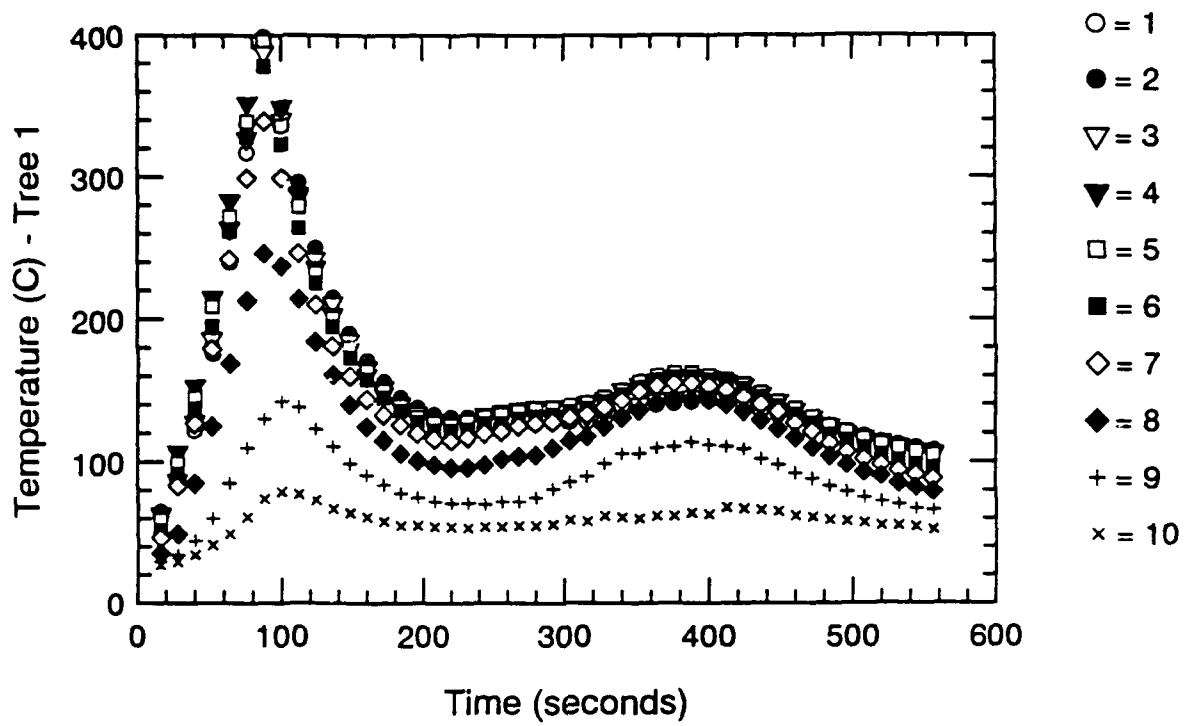


Figure A.65 Thermocouple Trees 1 & 2-Time Histories - S108

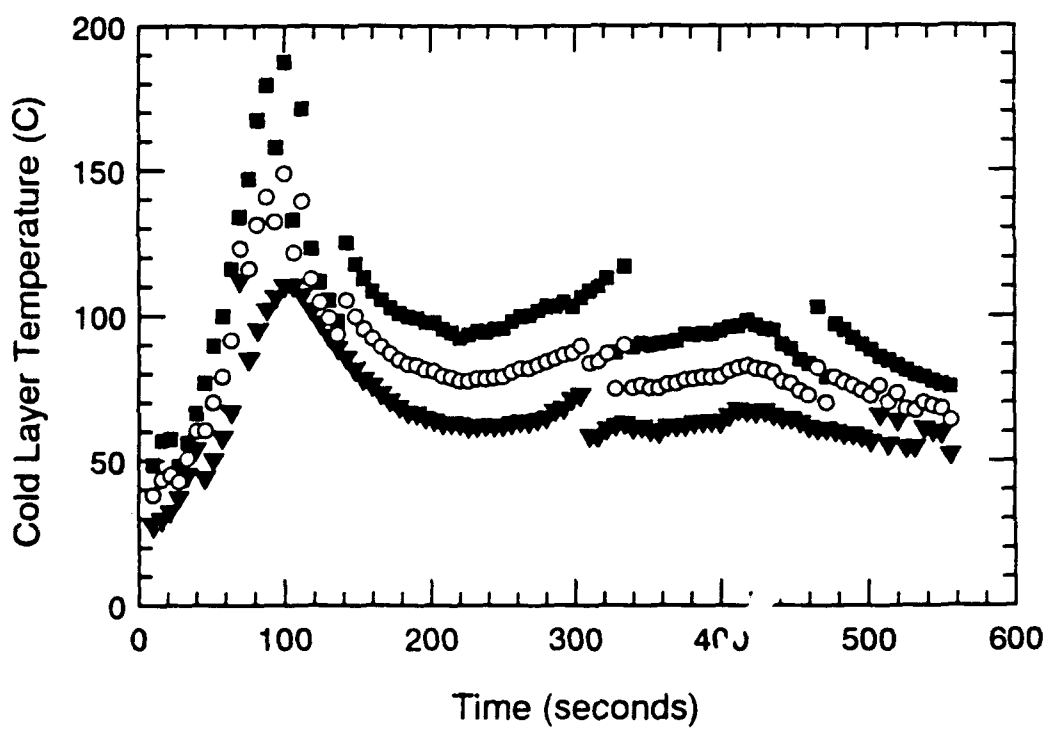
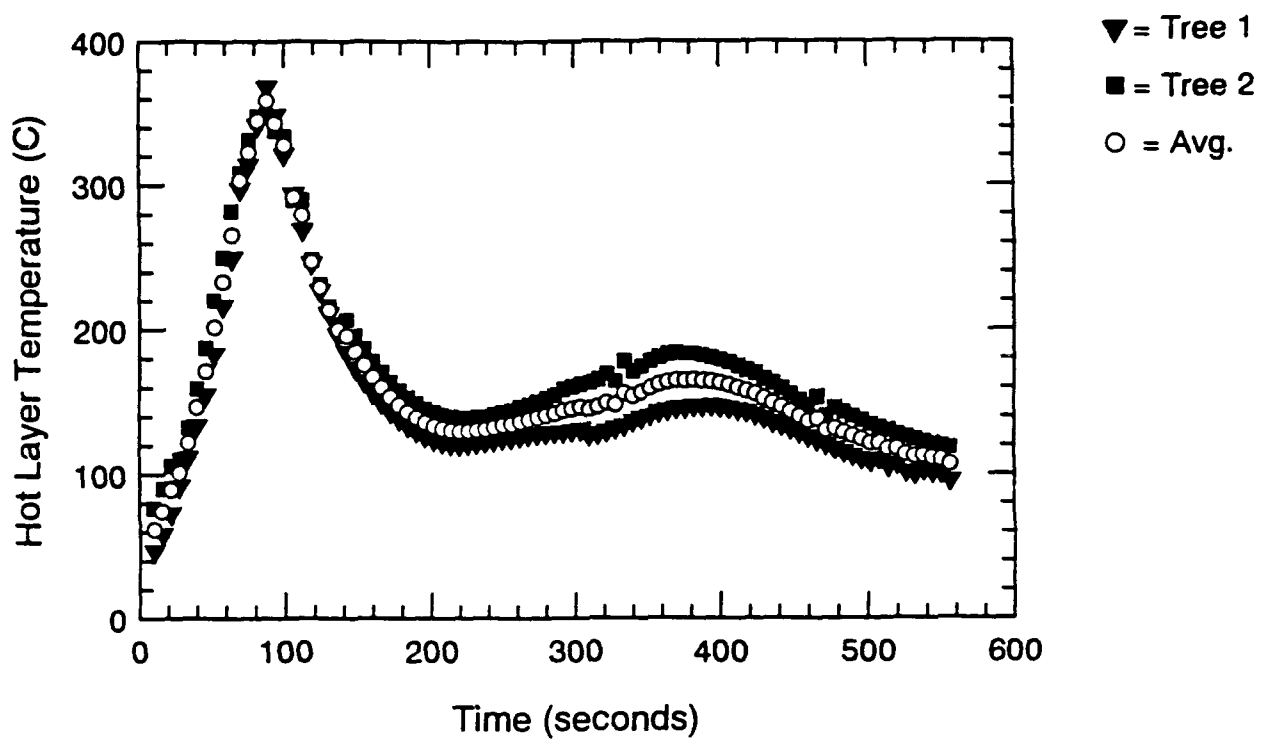


Figure A.66 Hot and Cold Layer Temperature-Time Histories - S108

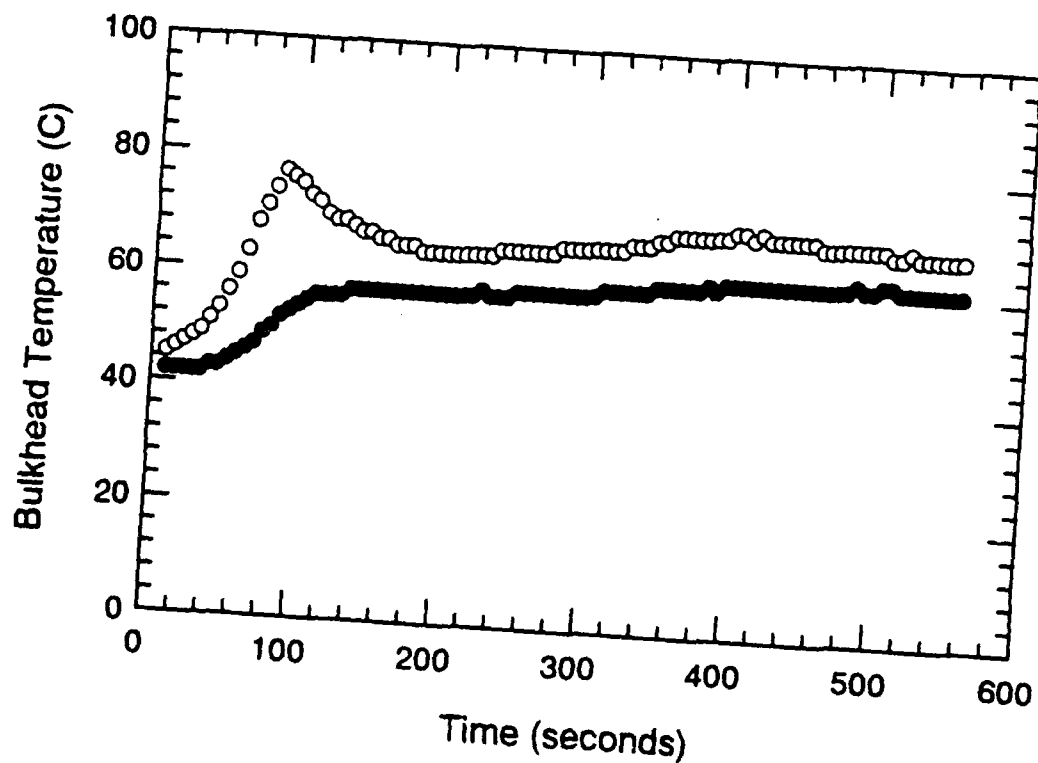
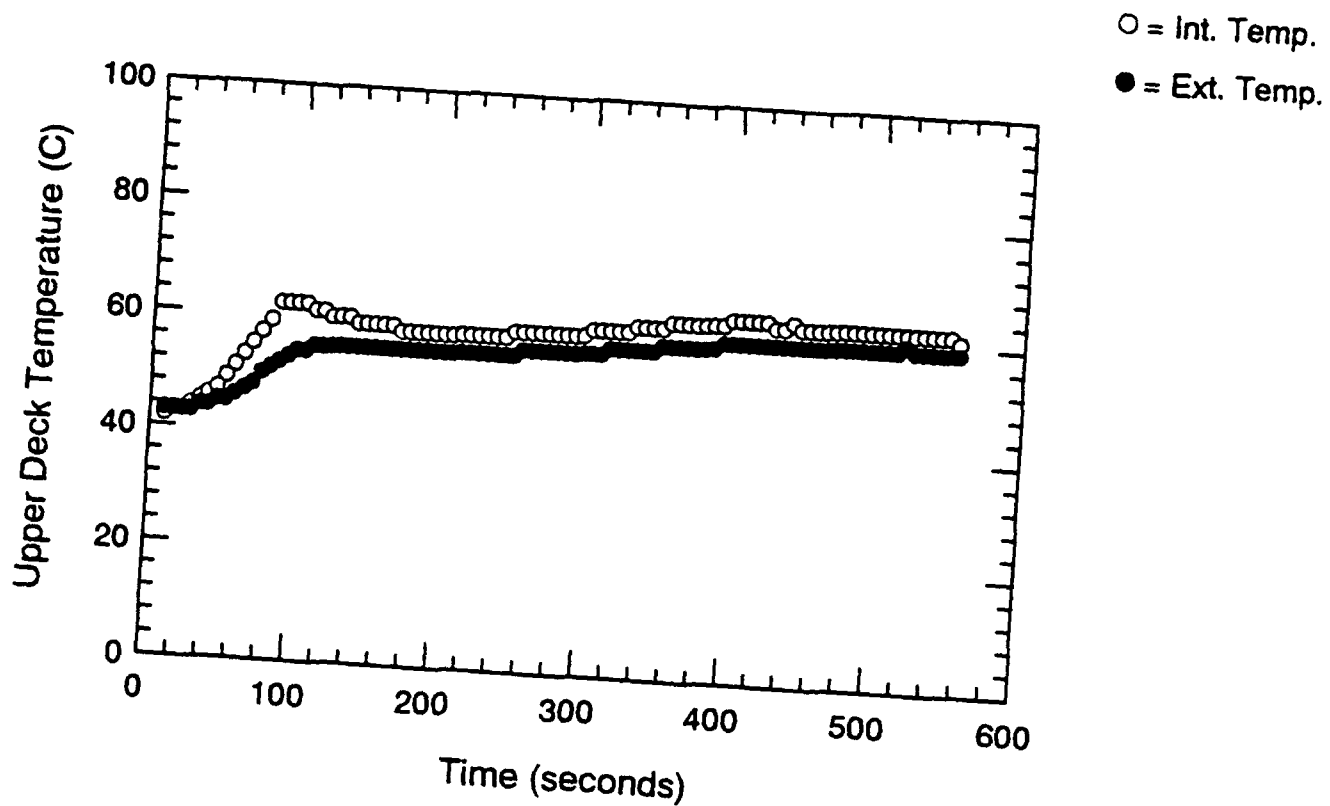


Figure A.67 Surface Thermocouple-Time Histories - S108

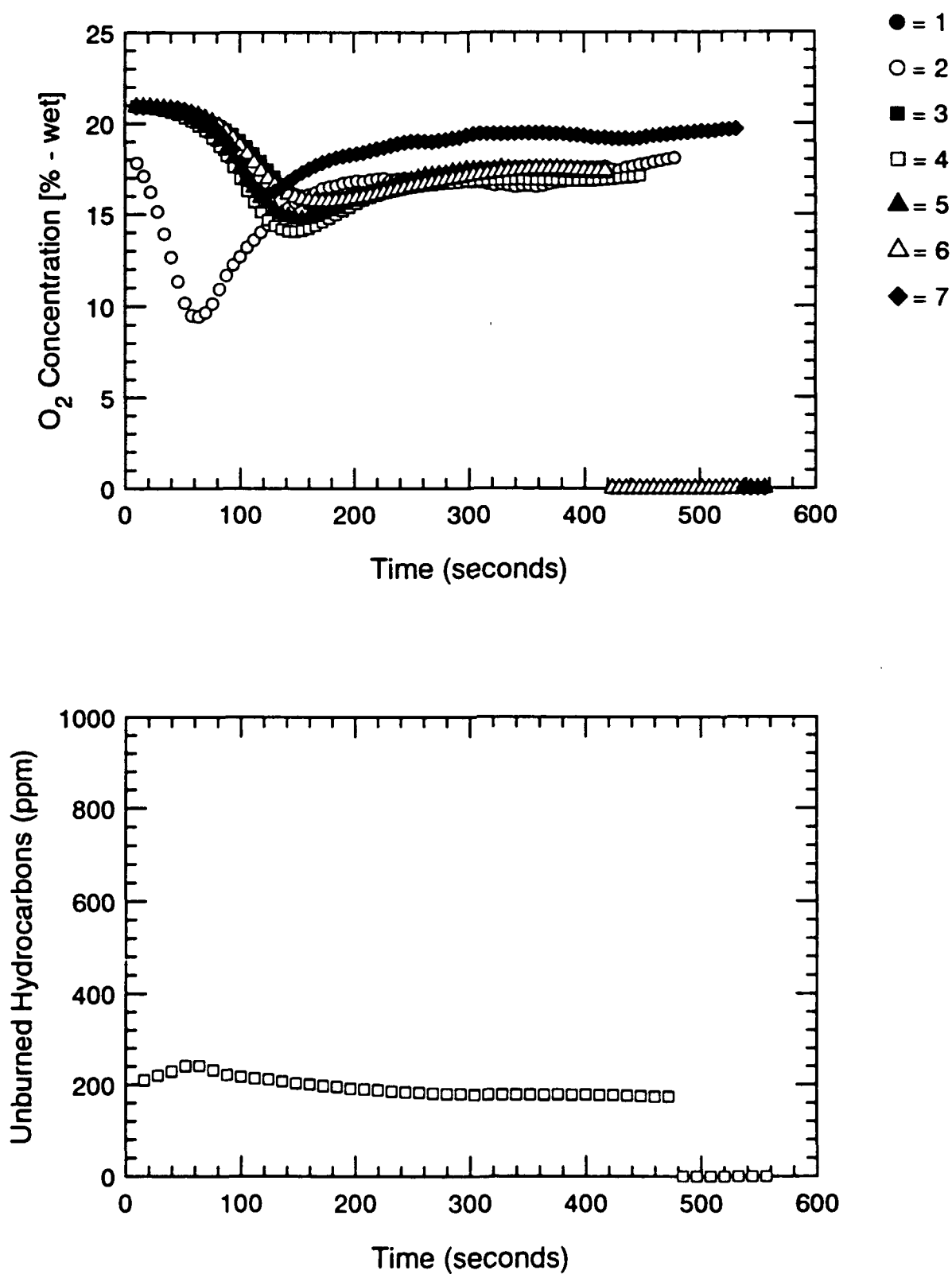


Figure A.68 Oxygen and Unburned HC Concentration-Time Histories - S108

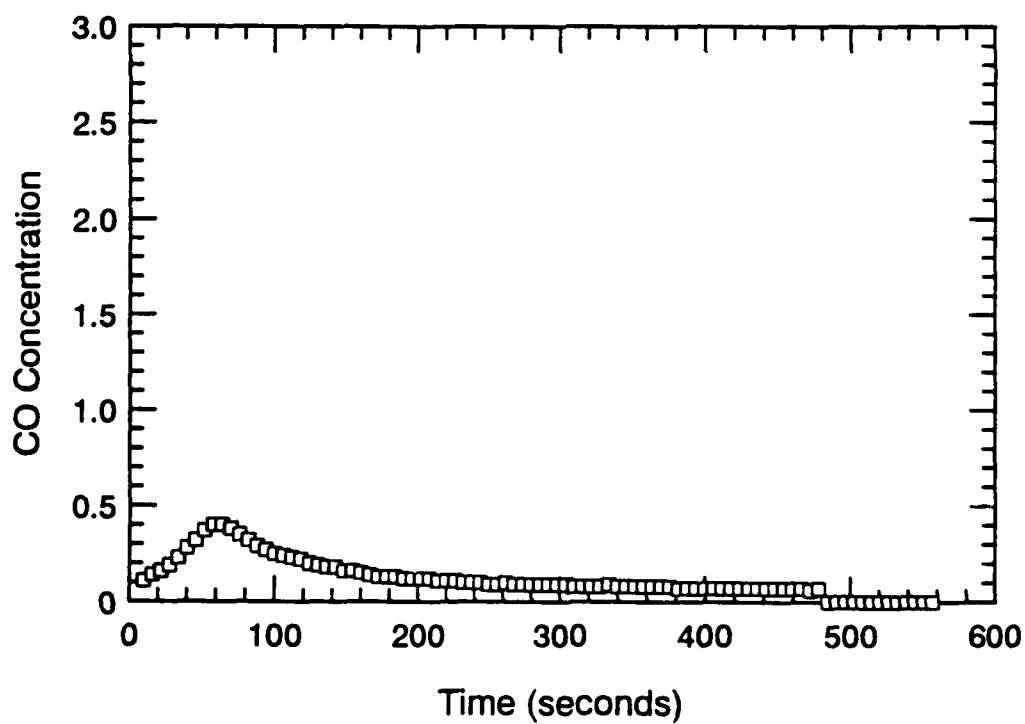
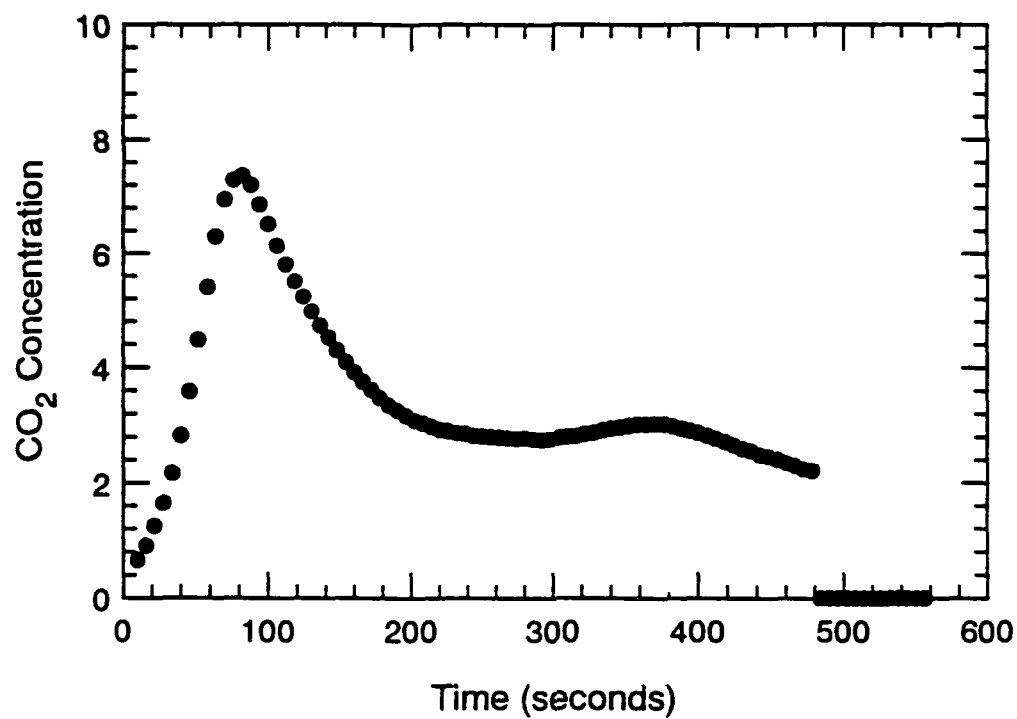


Figure A.69 CO₂ and CO Concentration-Time Histories - S108

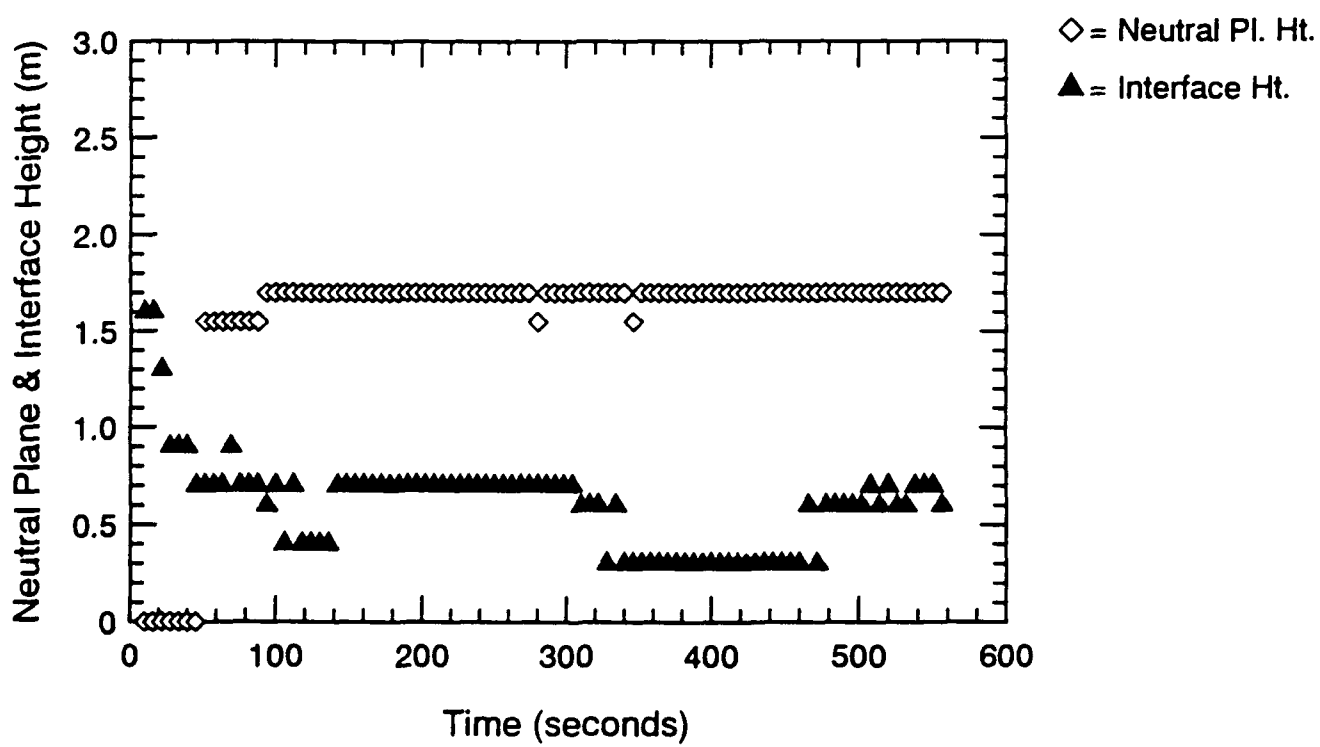
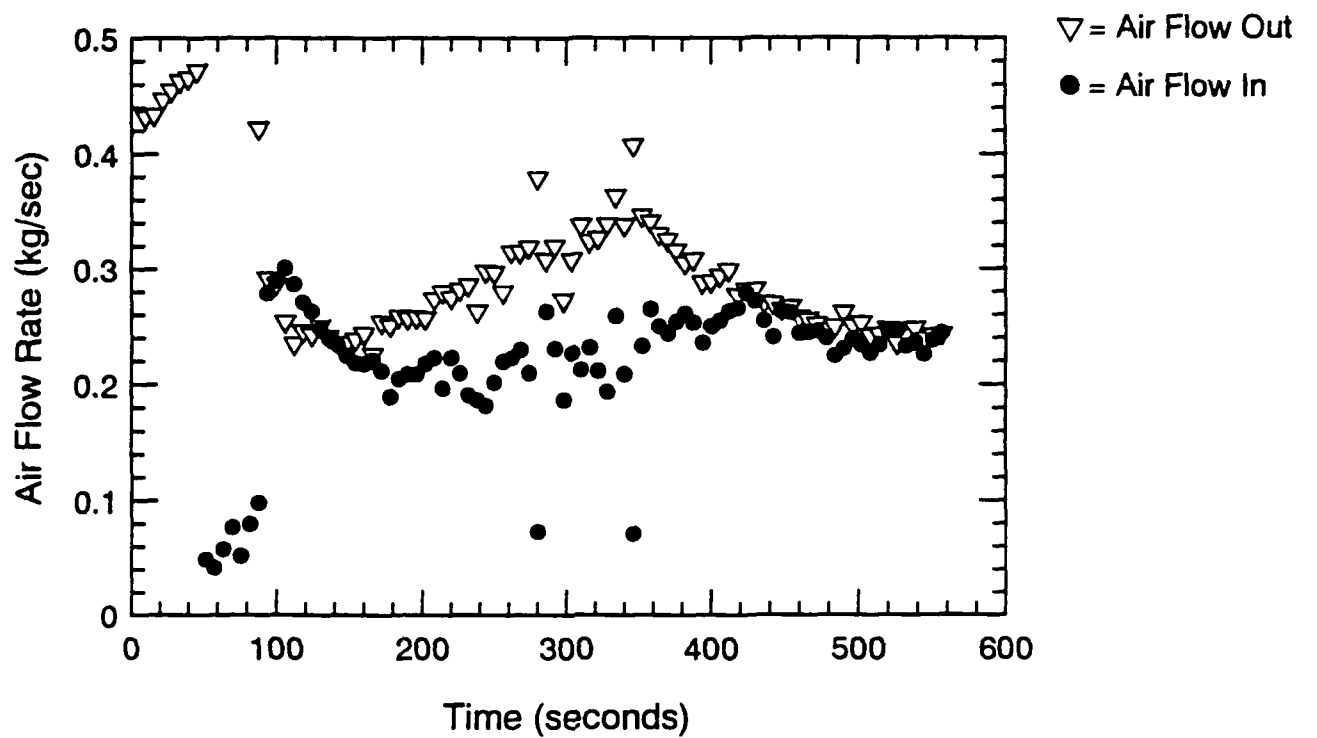


Figure A.70 Air Flow Rate, Neutral Plane & Interface Ht.-Time Histories - S108

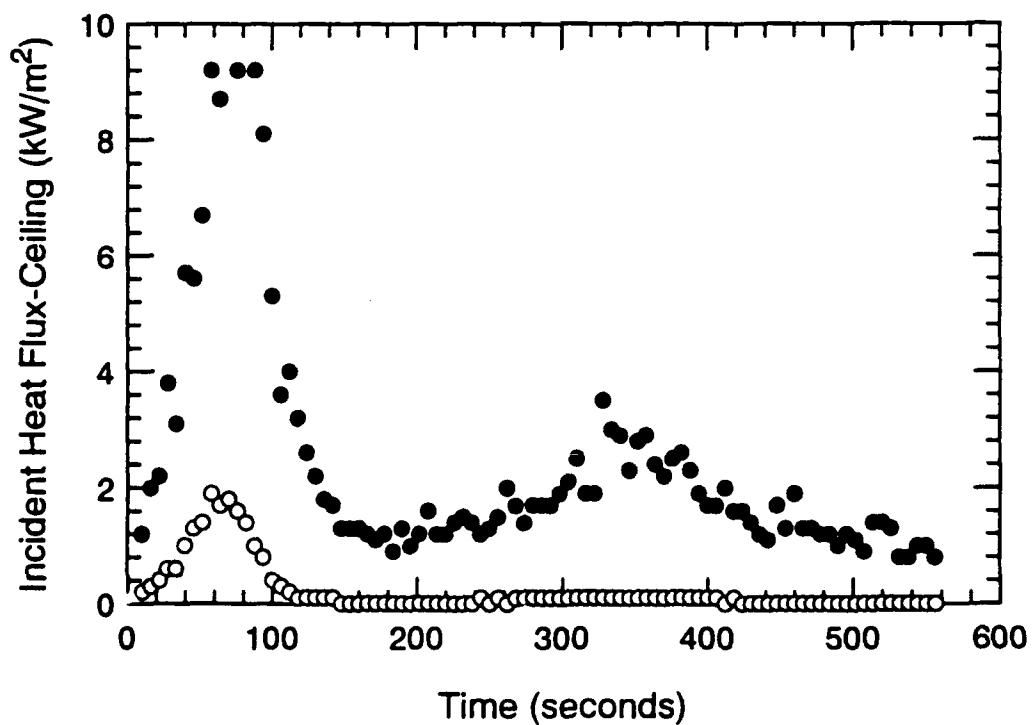
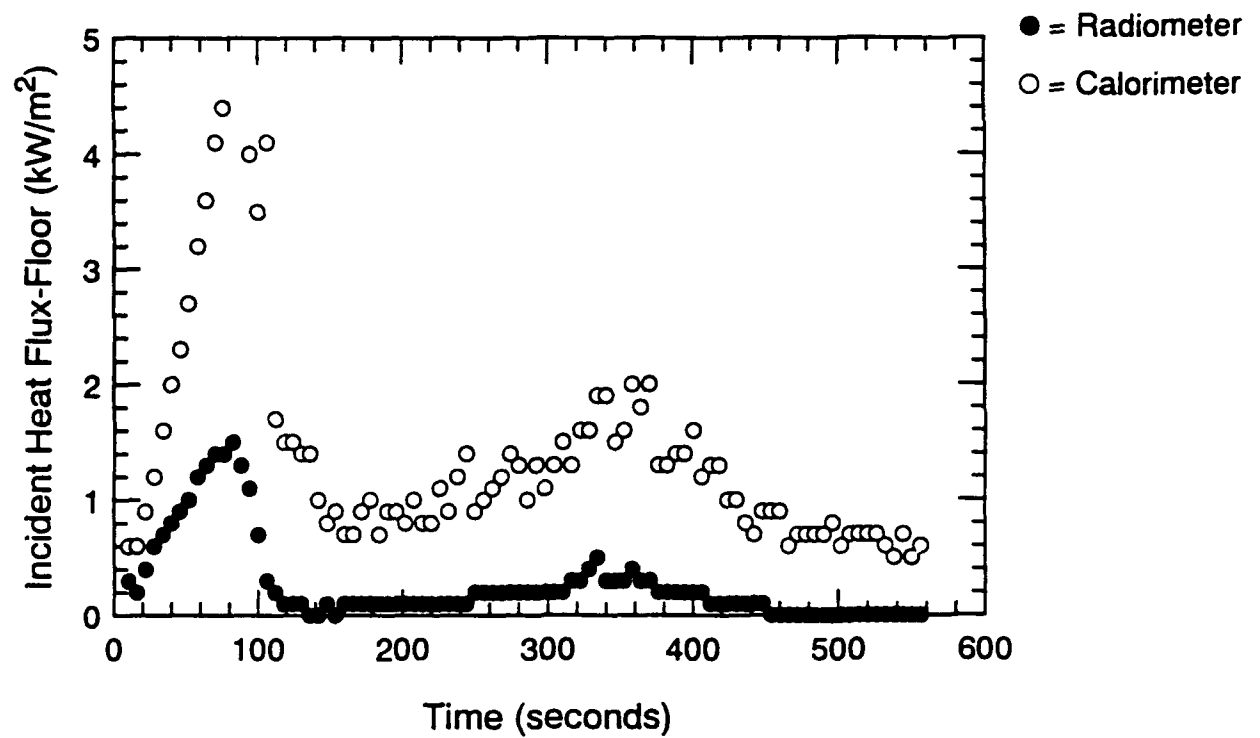


Figure A.71 Incident Heat Flux at Floor and Ceiling-Time Histories - S108

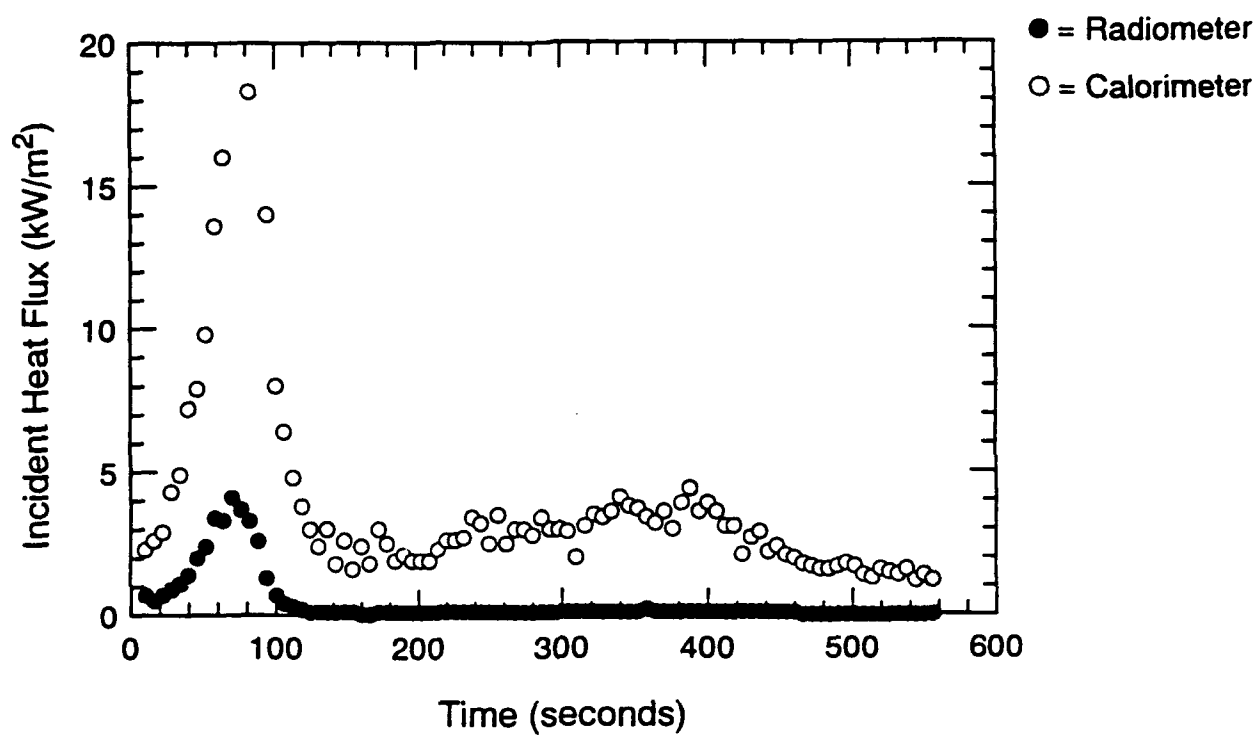


Figure A.72 Incident Heat Flux at Fwd. Bulkhead-Time Histories - S108

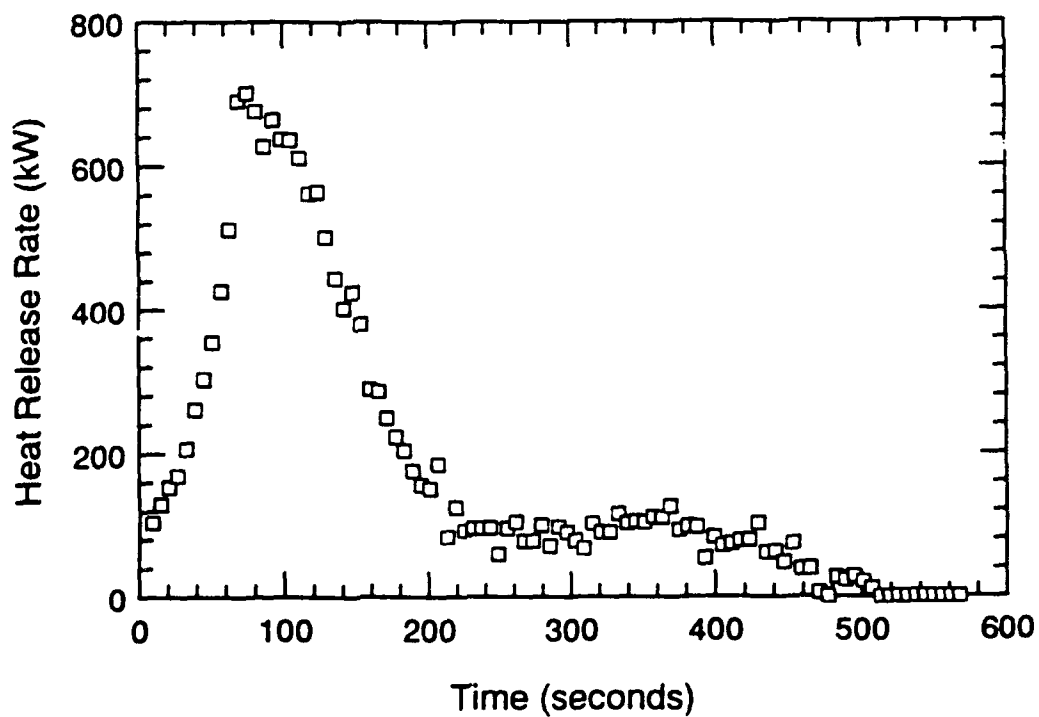
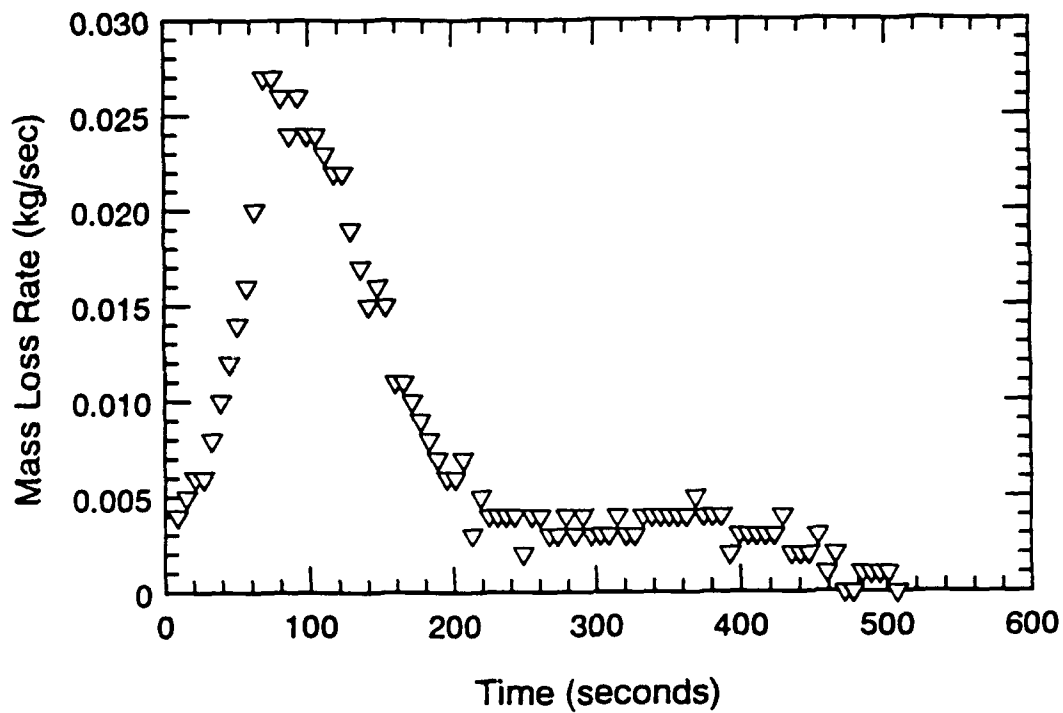


Figure A.73 Mass Loss Rate and Heat Release Rate-Time Histories - S109

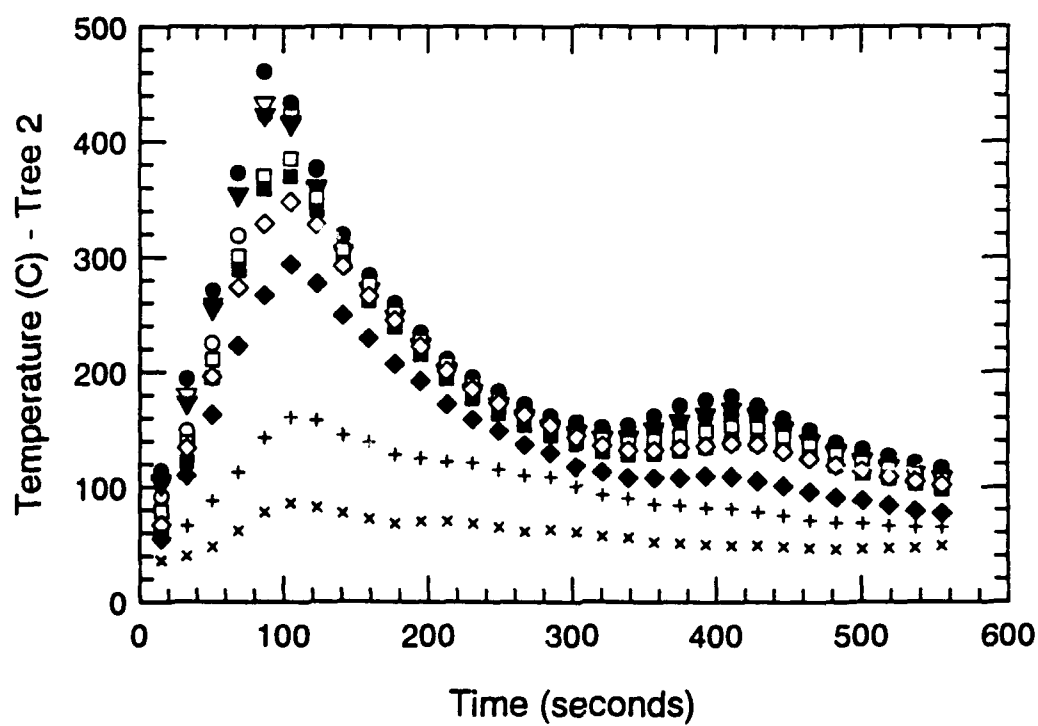
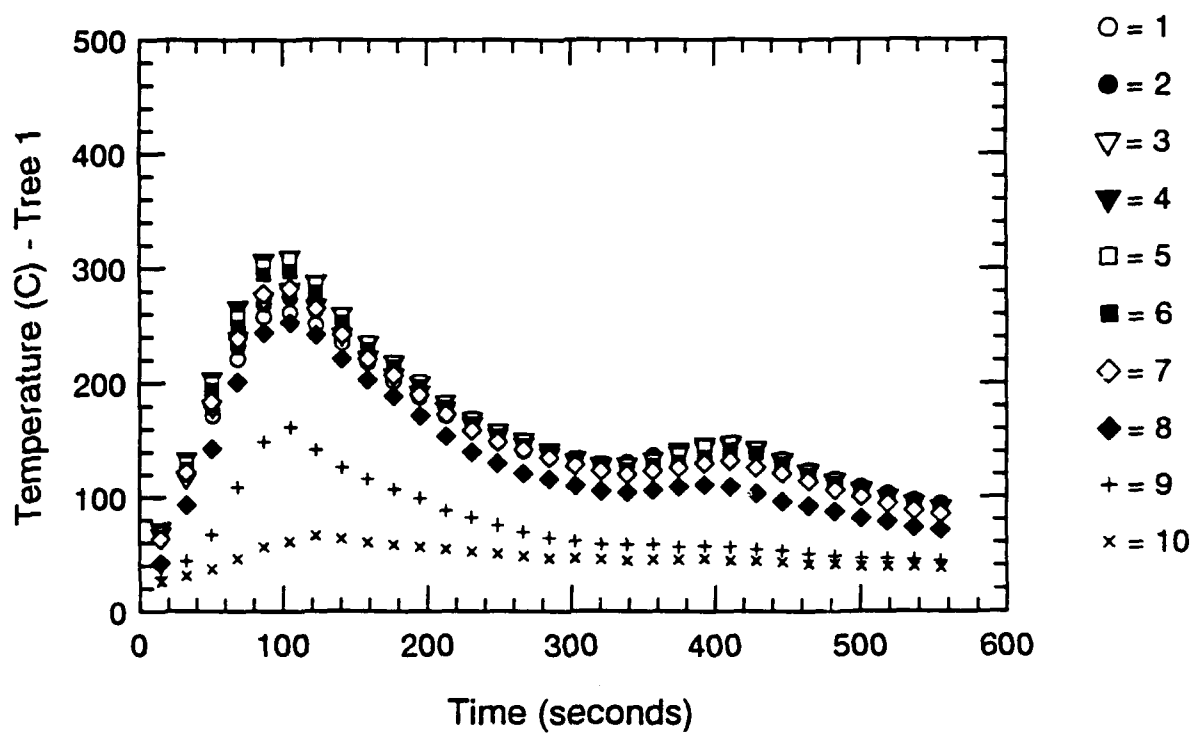


Figure A.74 Thermocouple Trees 1 & 2-Time Histories - S109

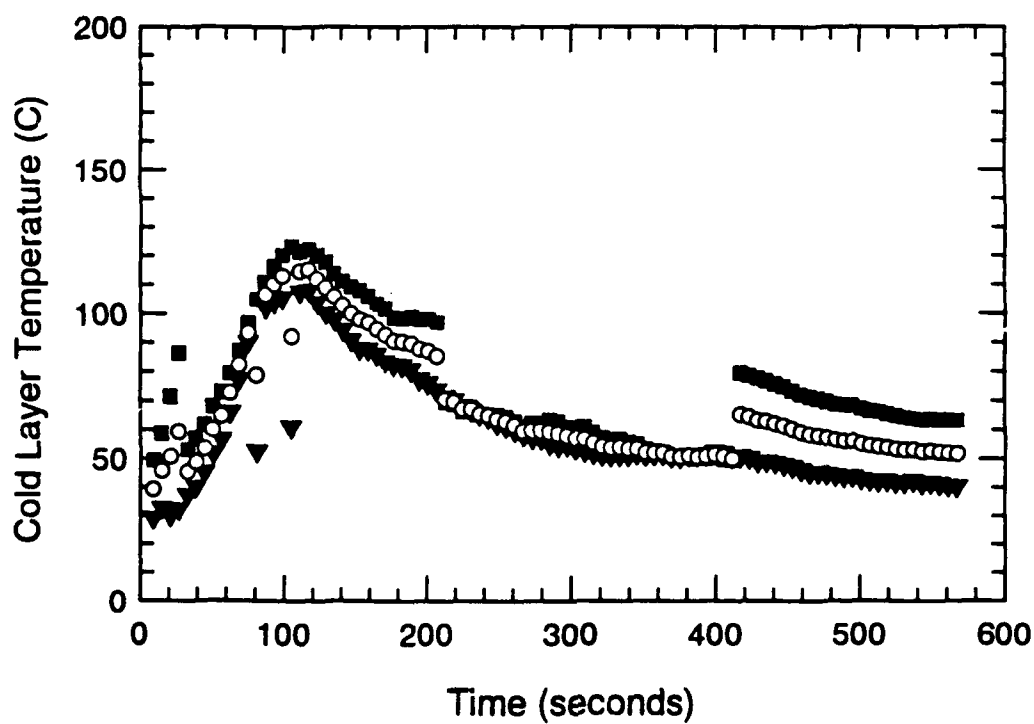
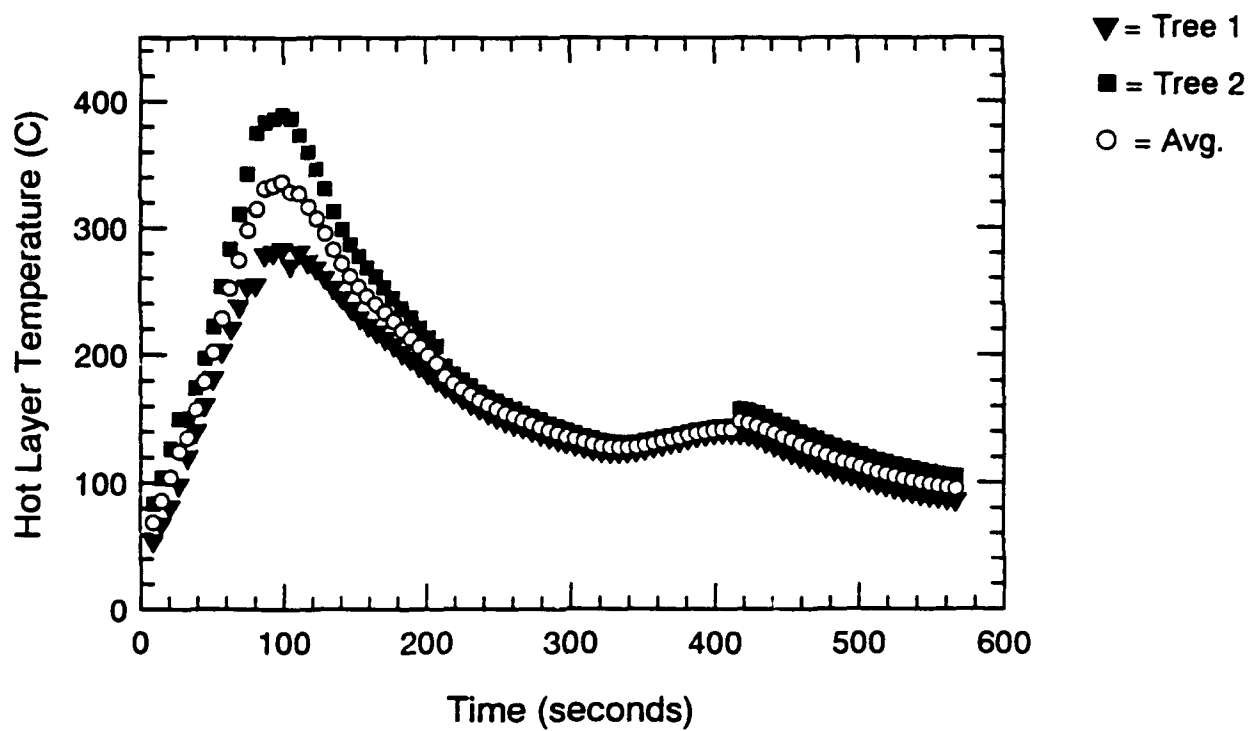


Figure A.75 Hot and Cold Layer Temperature-Time Histories - S109

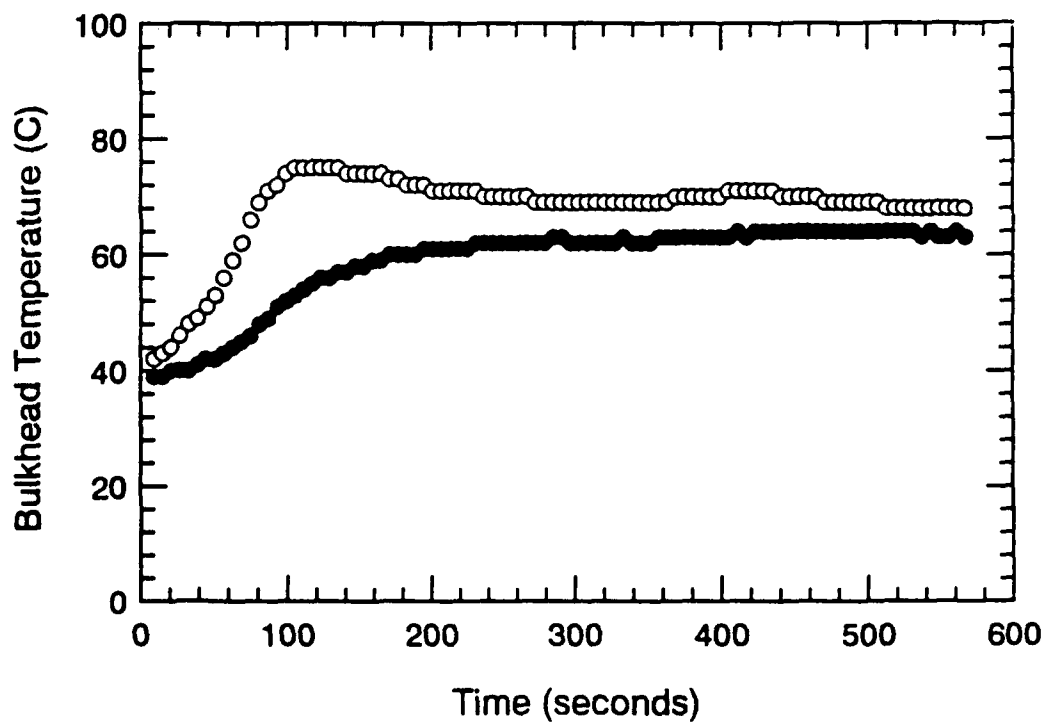
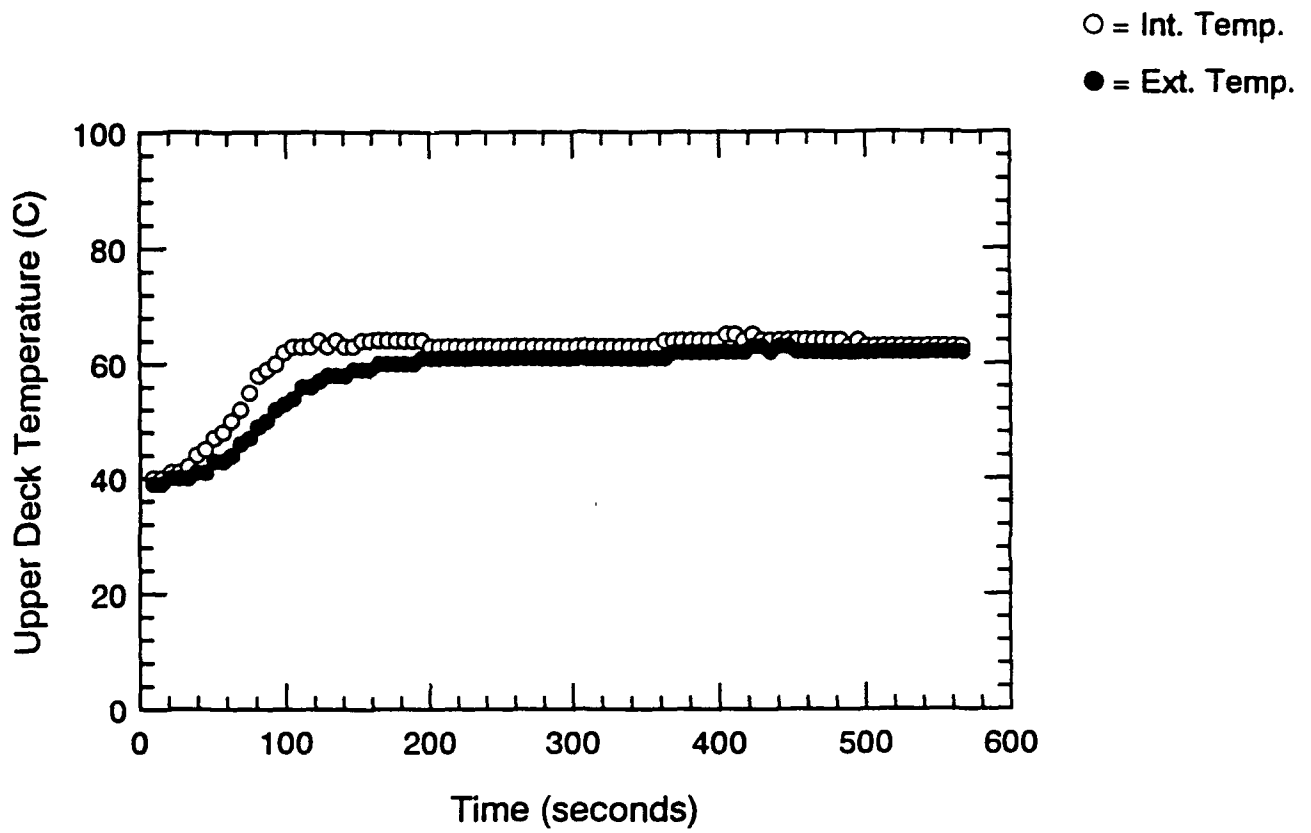


Figure A.76 Surface Thermocouple-Time Histories - S109

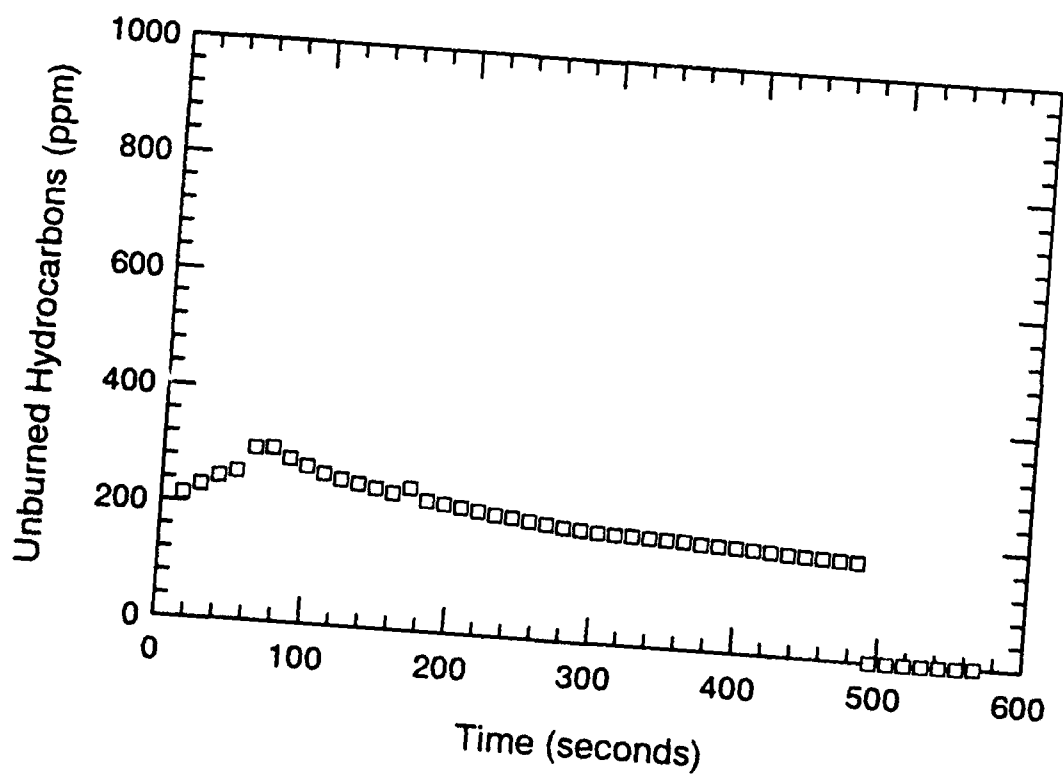
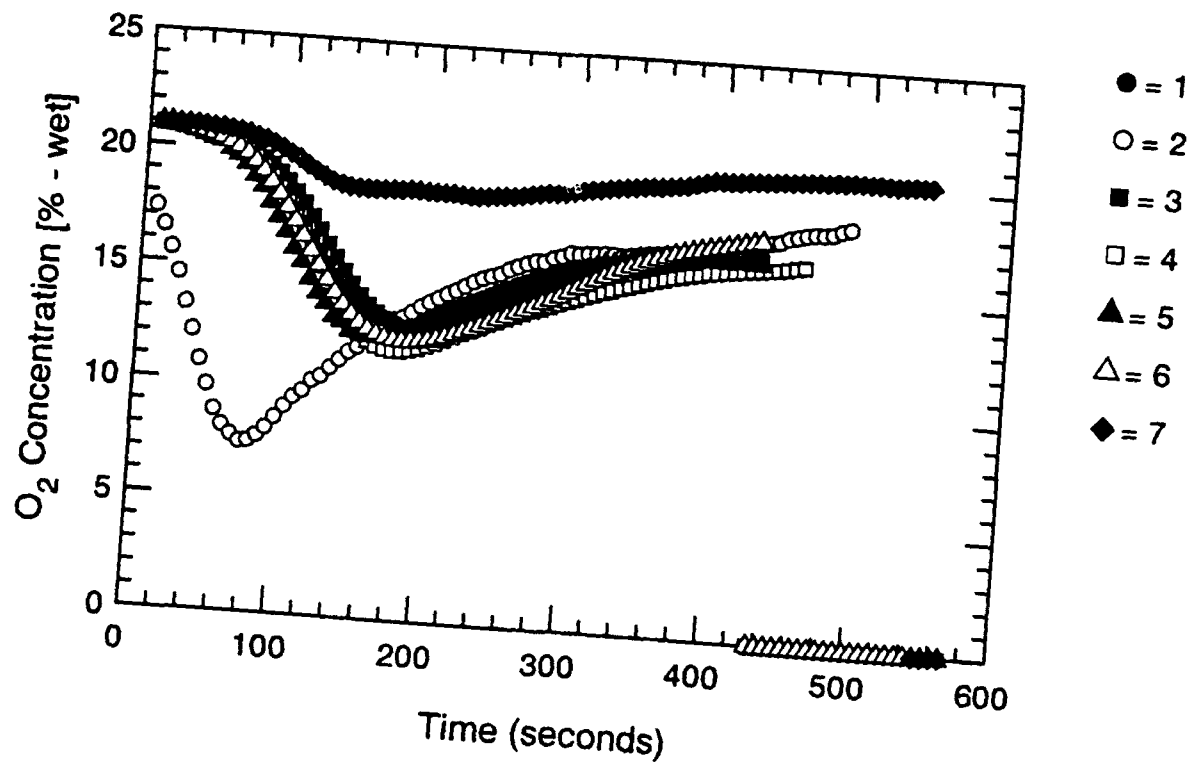


Figure A.77 Oxygen and Unburned HC Concentration-Time Histories - S109

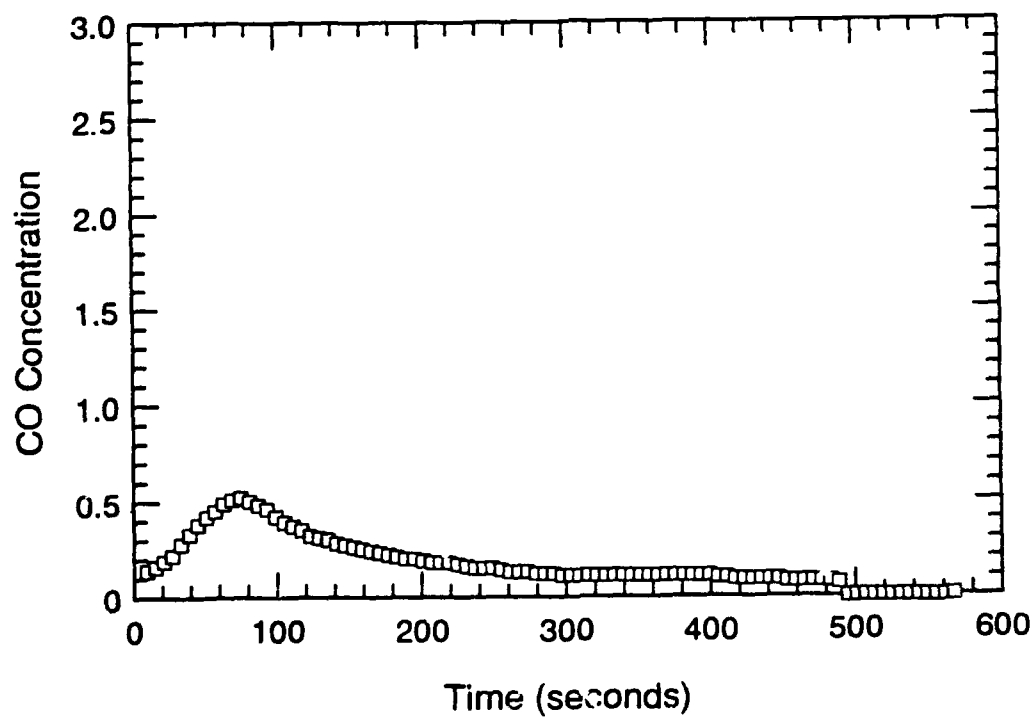
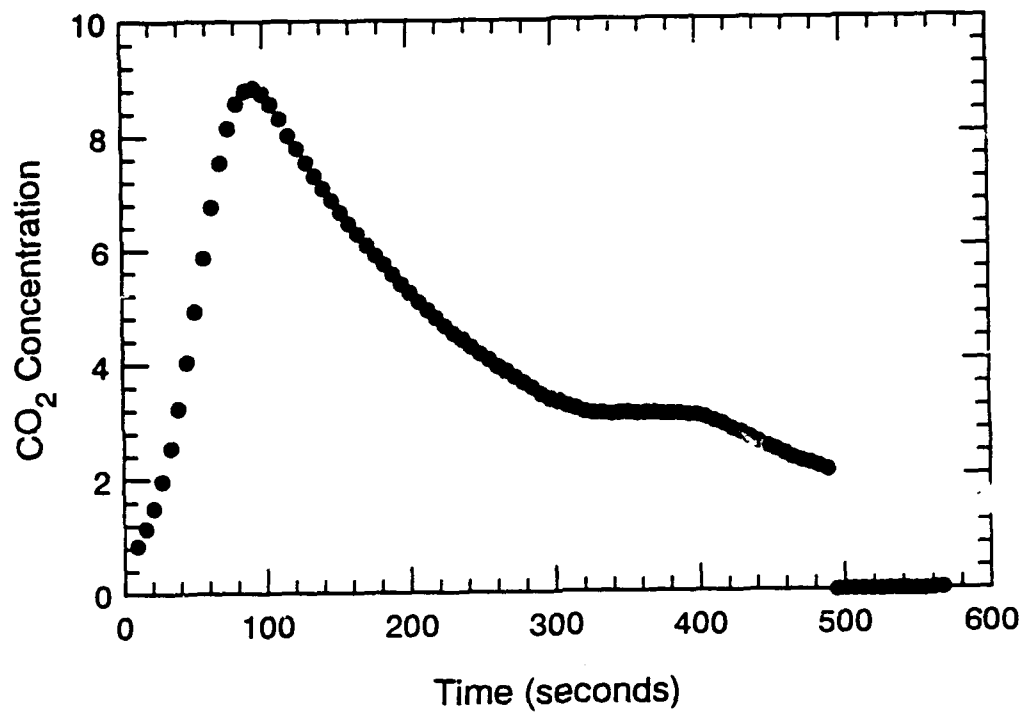


Figure A.78 CO₂ and CO Concentration-Time Histories - S109

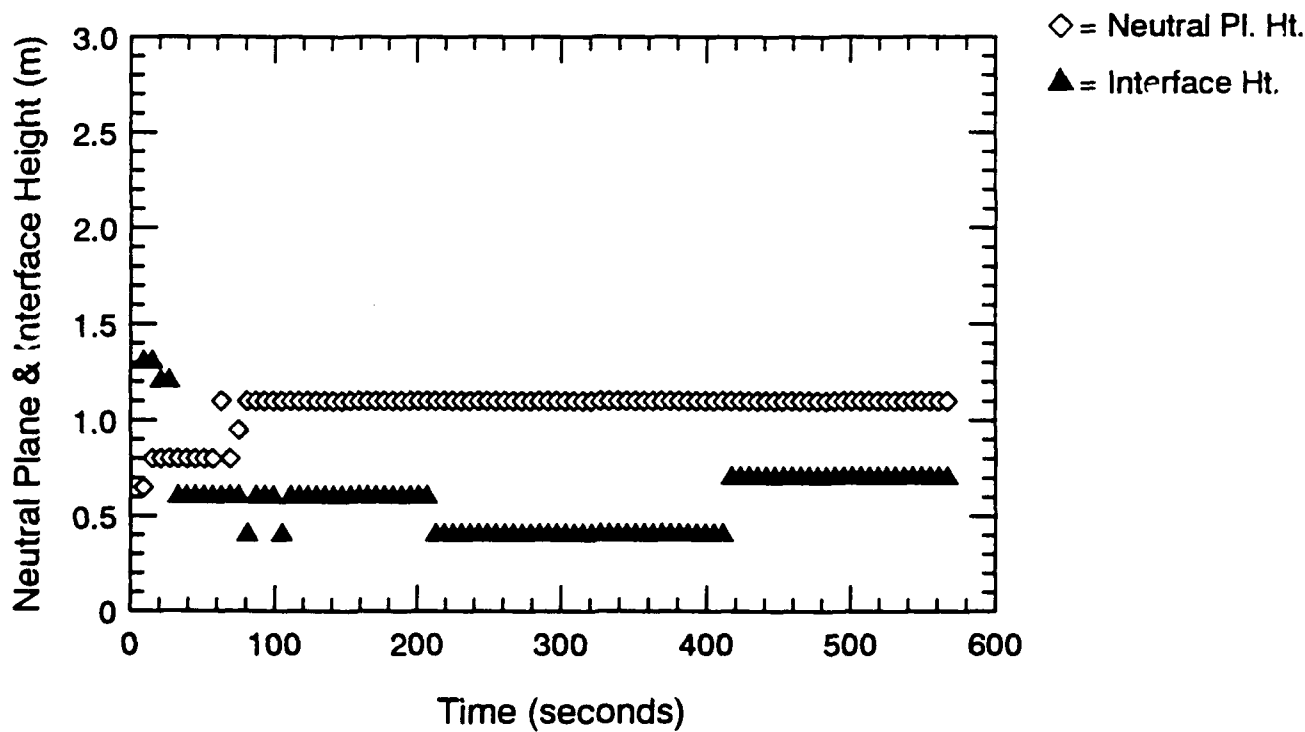
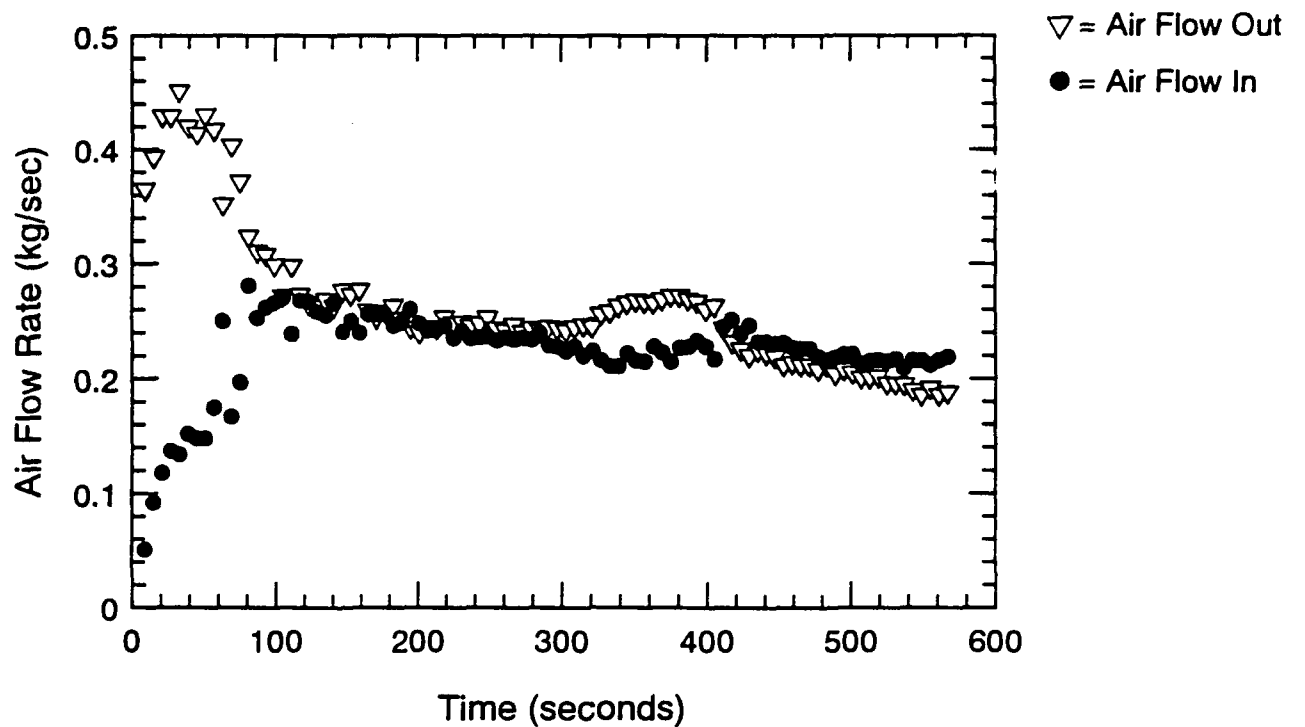


Figure A.79 Air Flow Rate, Neutral Plane & Interface Ht.-Time Histories - S109

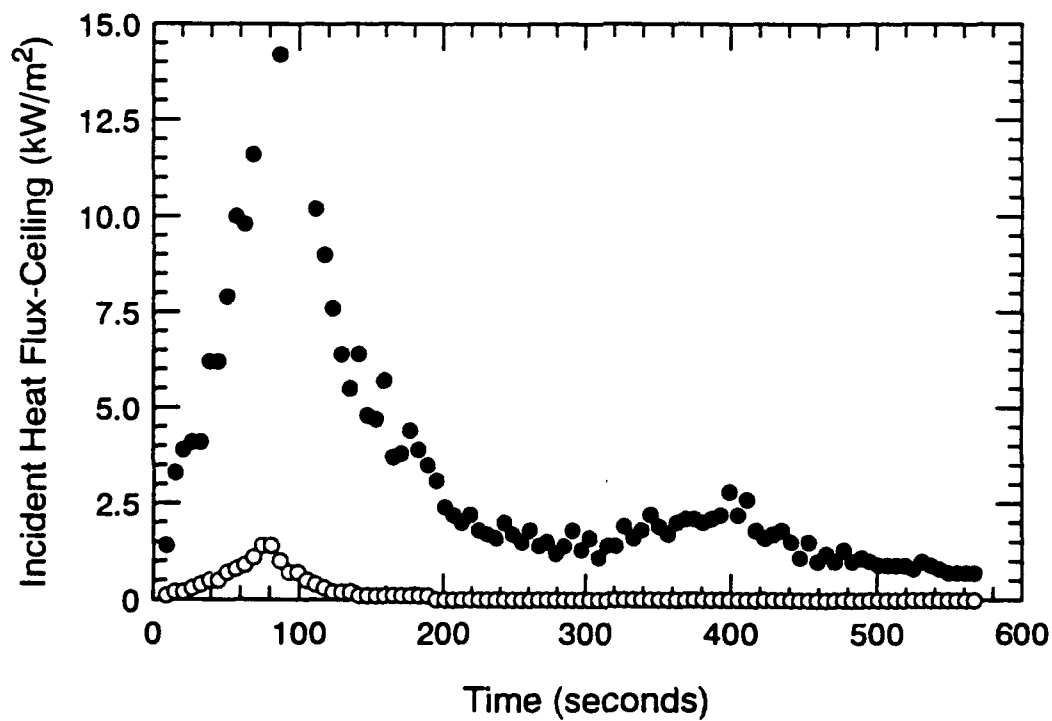
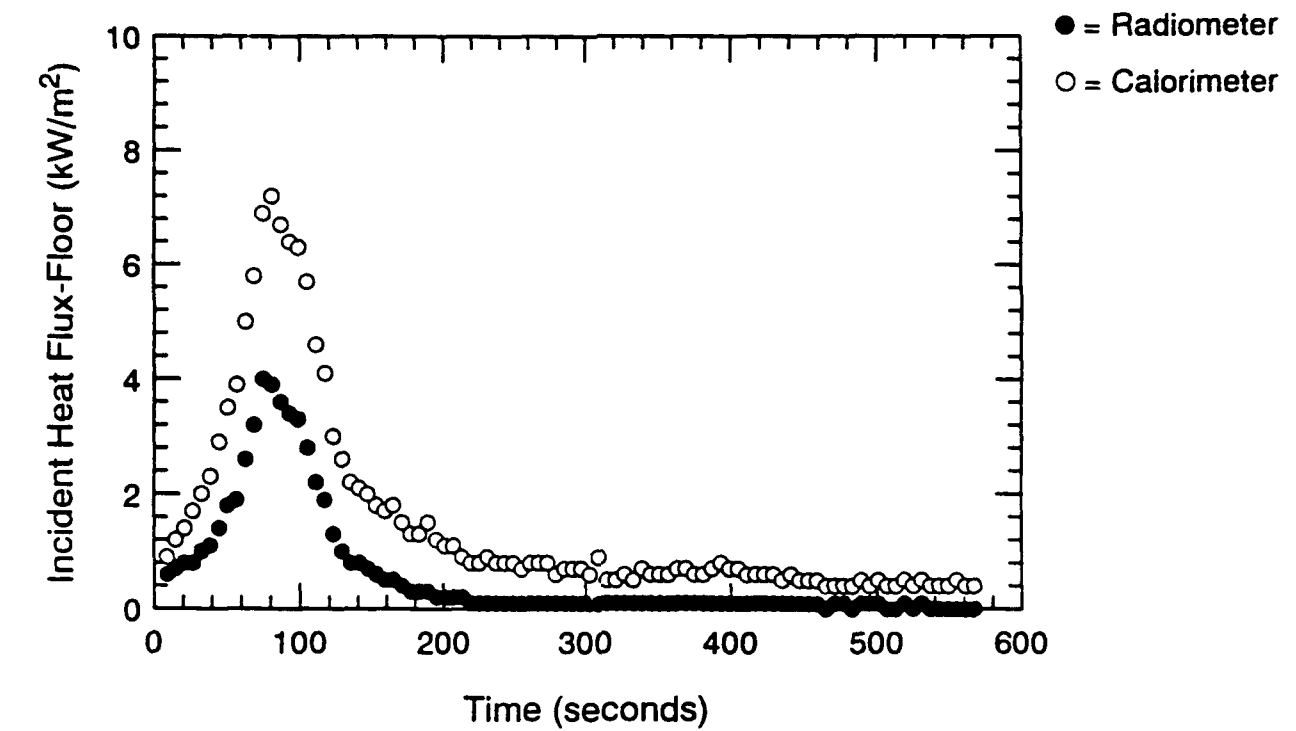


Figure A.80 Incident Heat Flux at Floor and Ceiling-Time Histories - S109

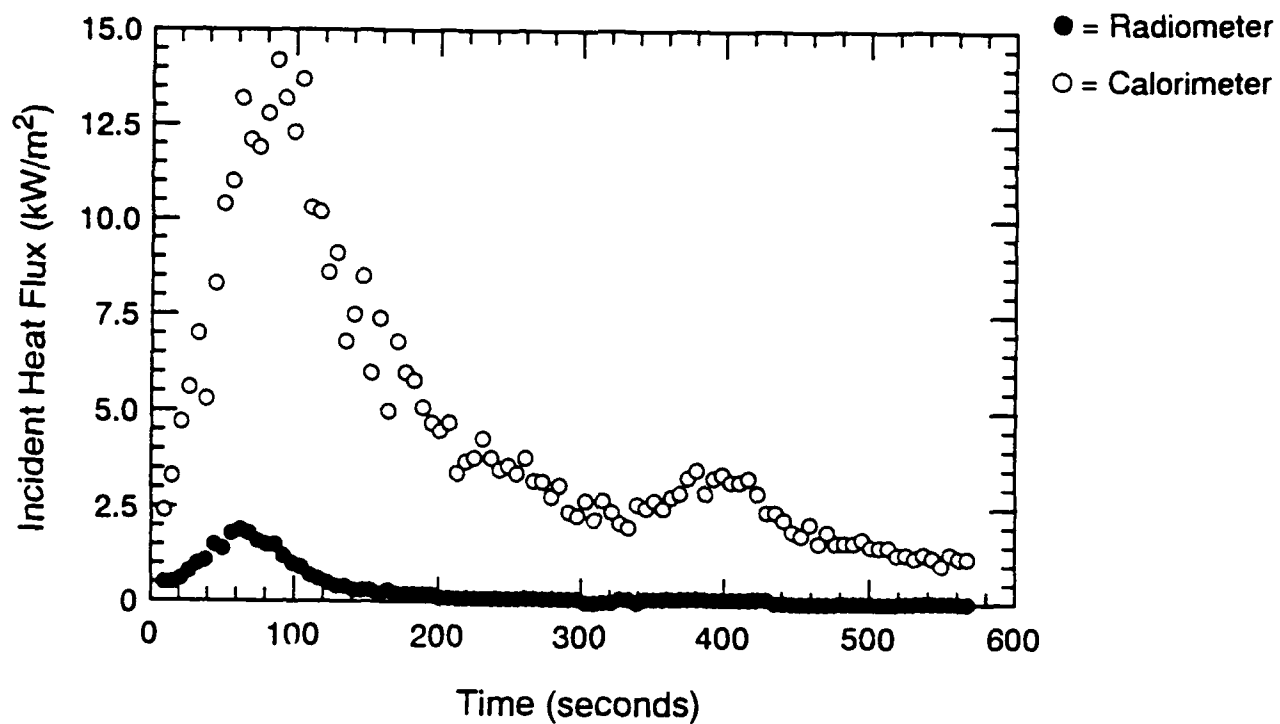


Figure A.81 Incident Heat Flux at Fwd. Bulkhead-Time Histories - S109

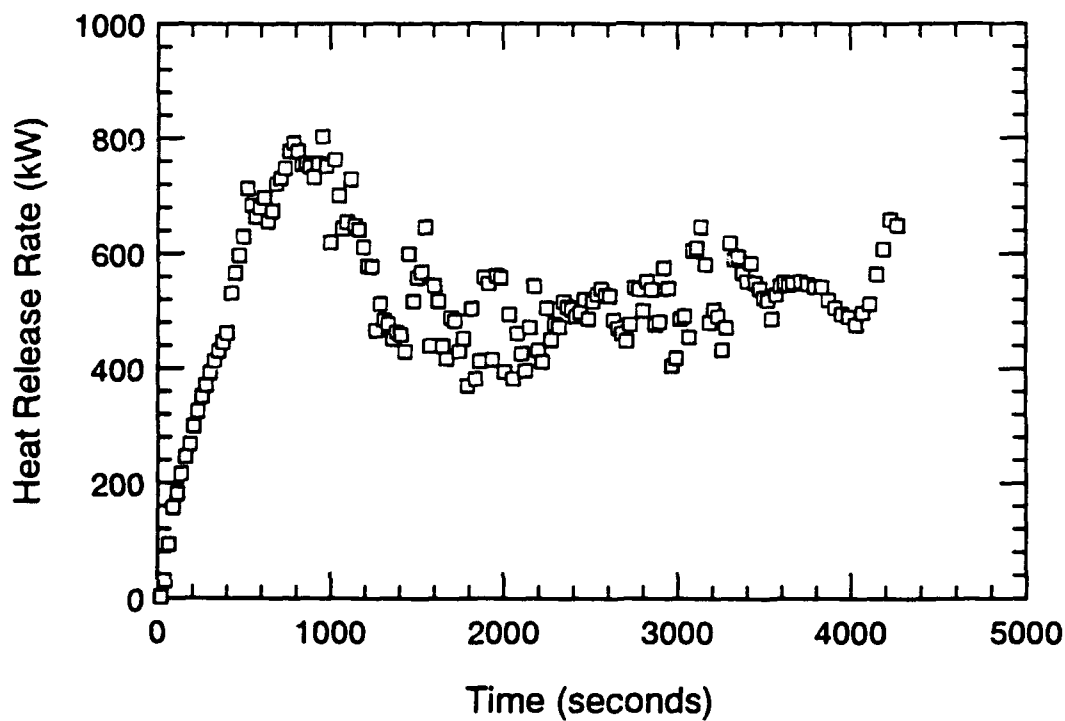
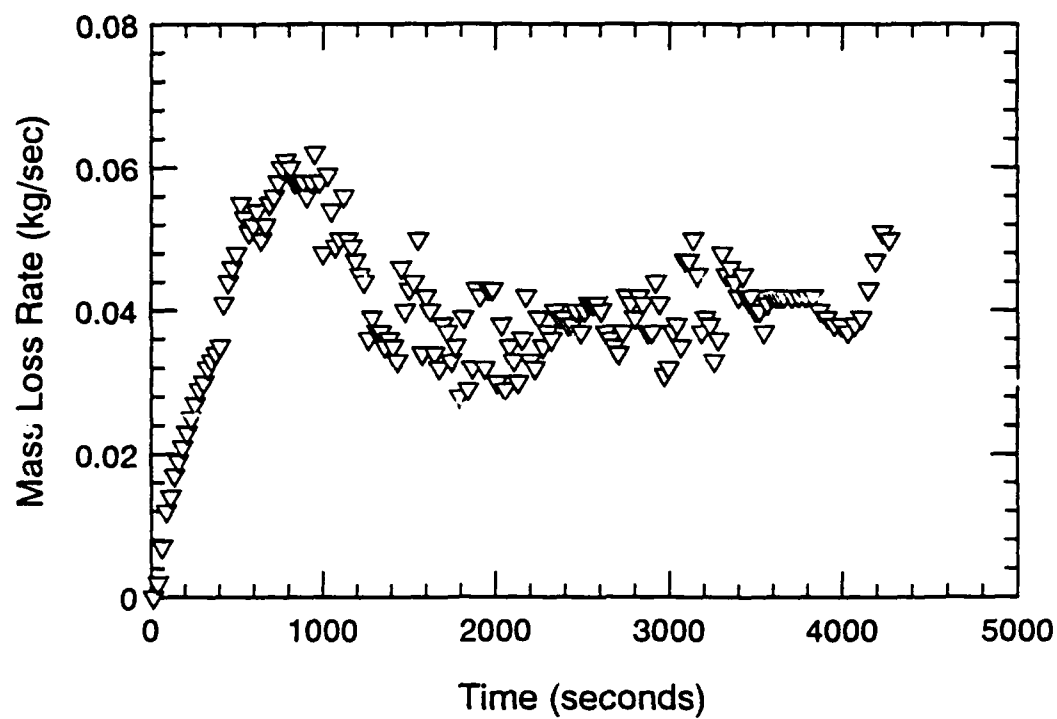


Figure A.82 Mass Loss Rate and Heat Release Rate-Time Histories - S110

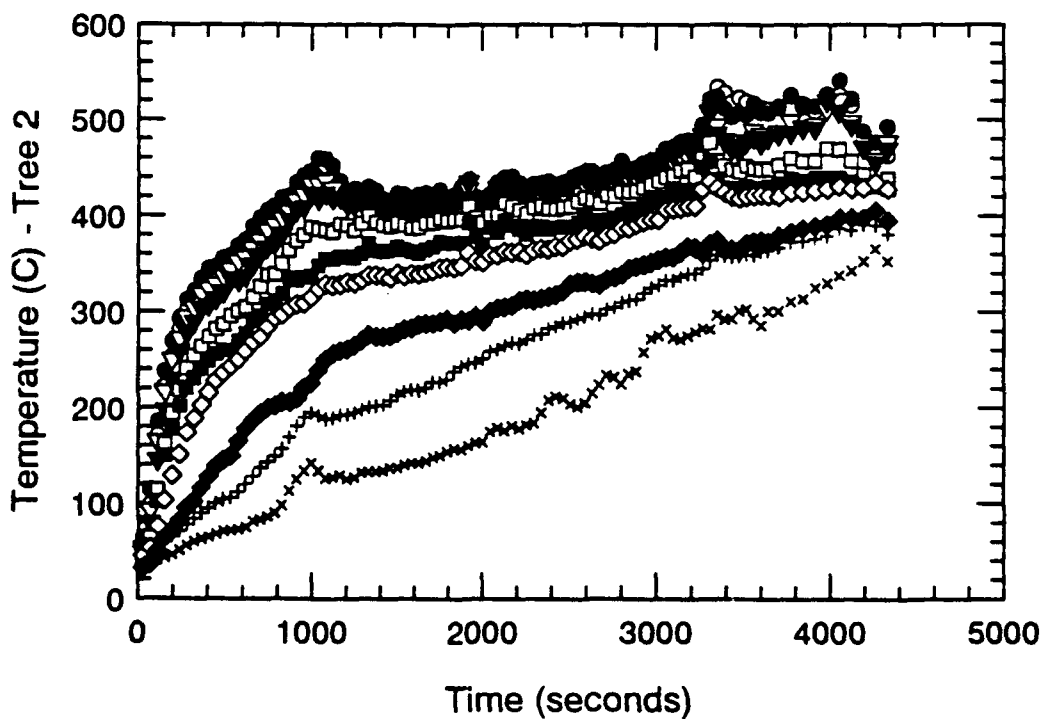
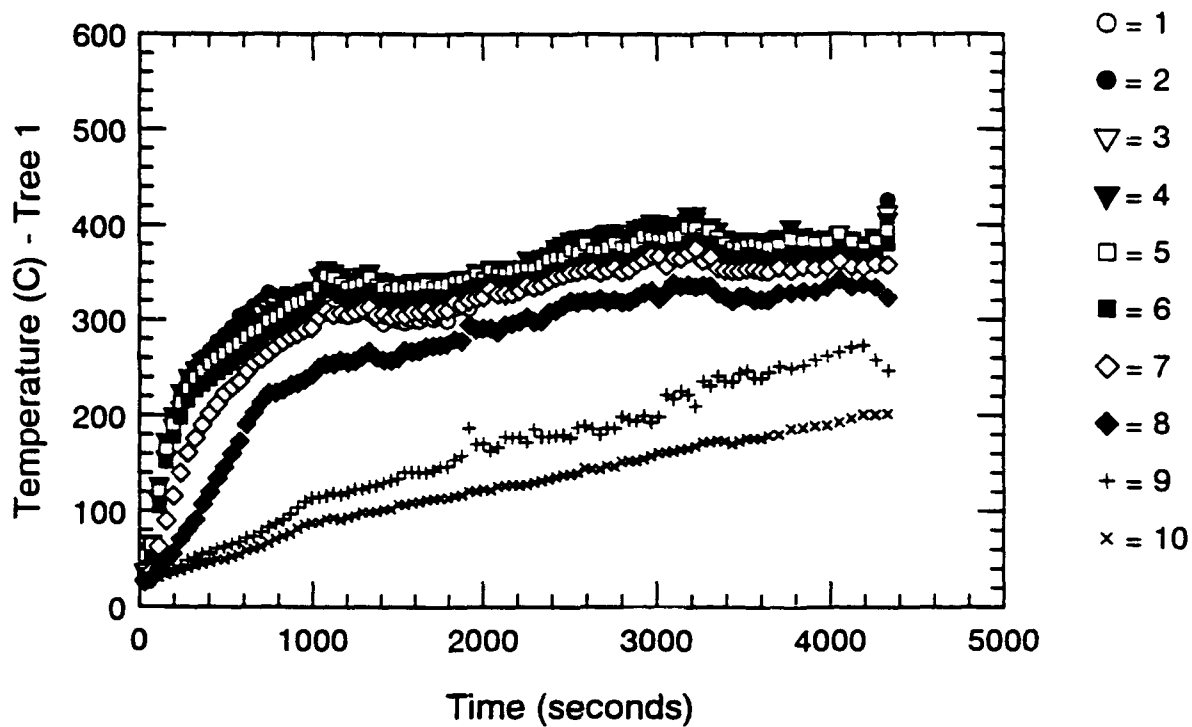


Figure A.83 Thermocouple Trees 1 & 2-Time Histories - S110

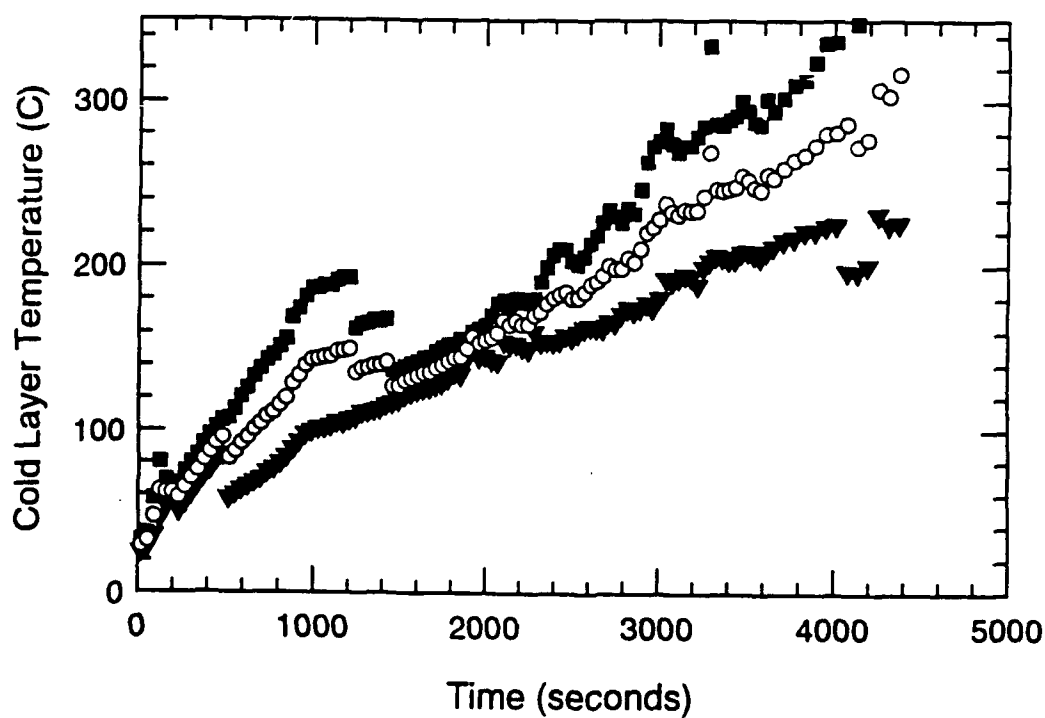
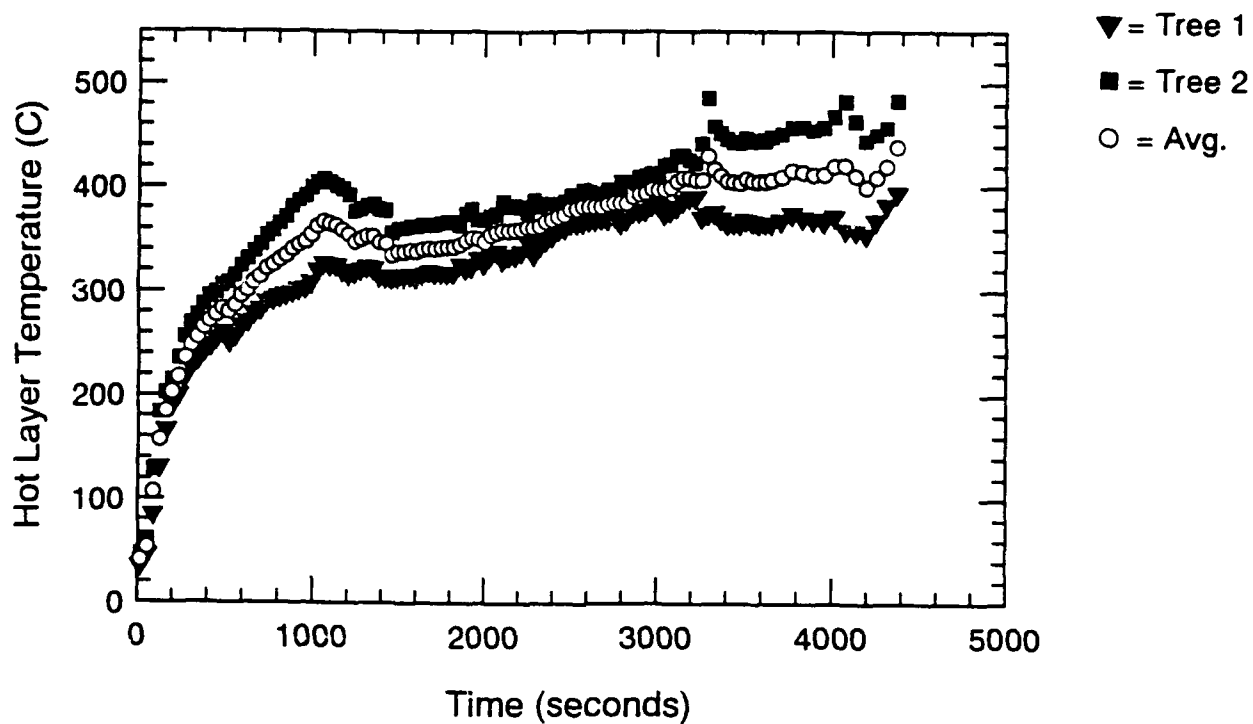


Figure A.84 Hot and Cold Layer Temperature-Time Histories - S110

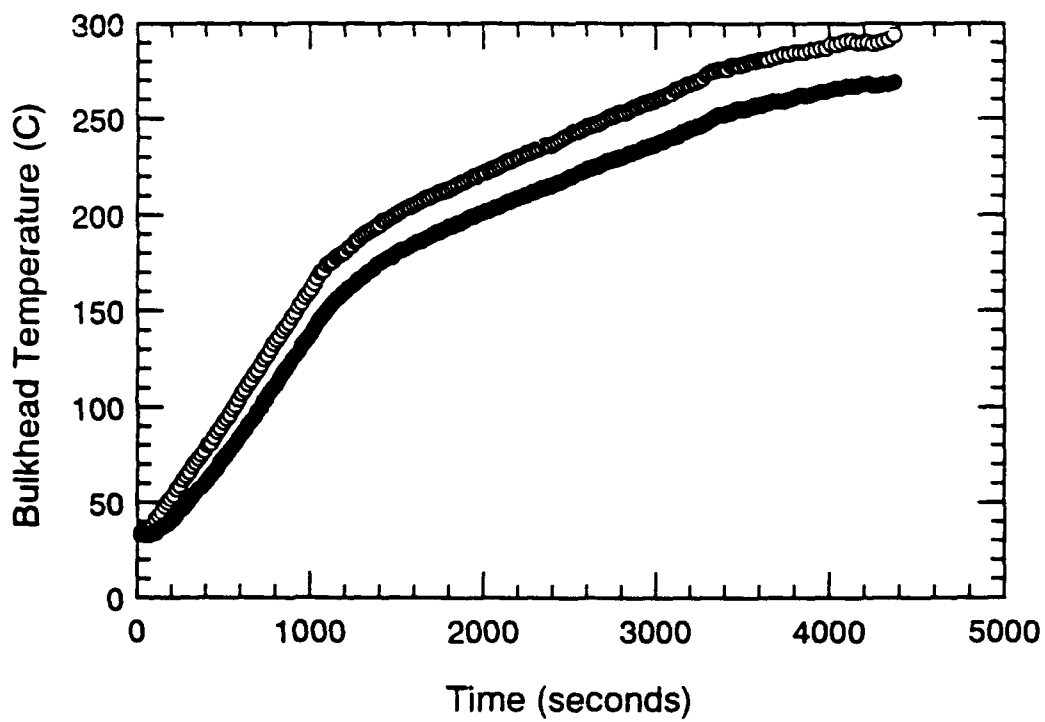
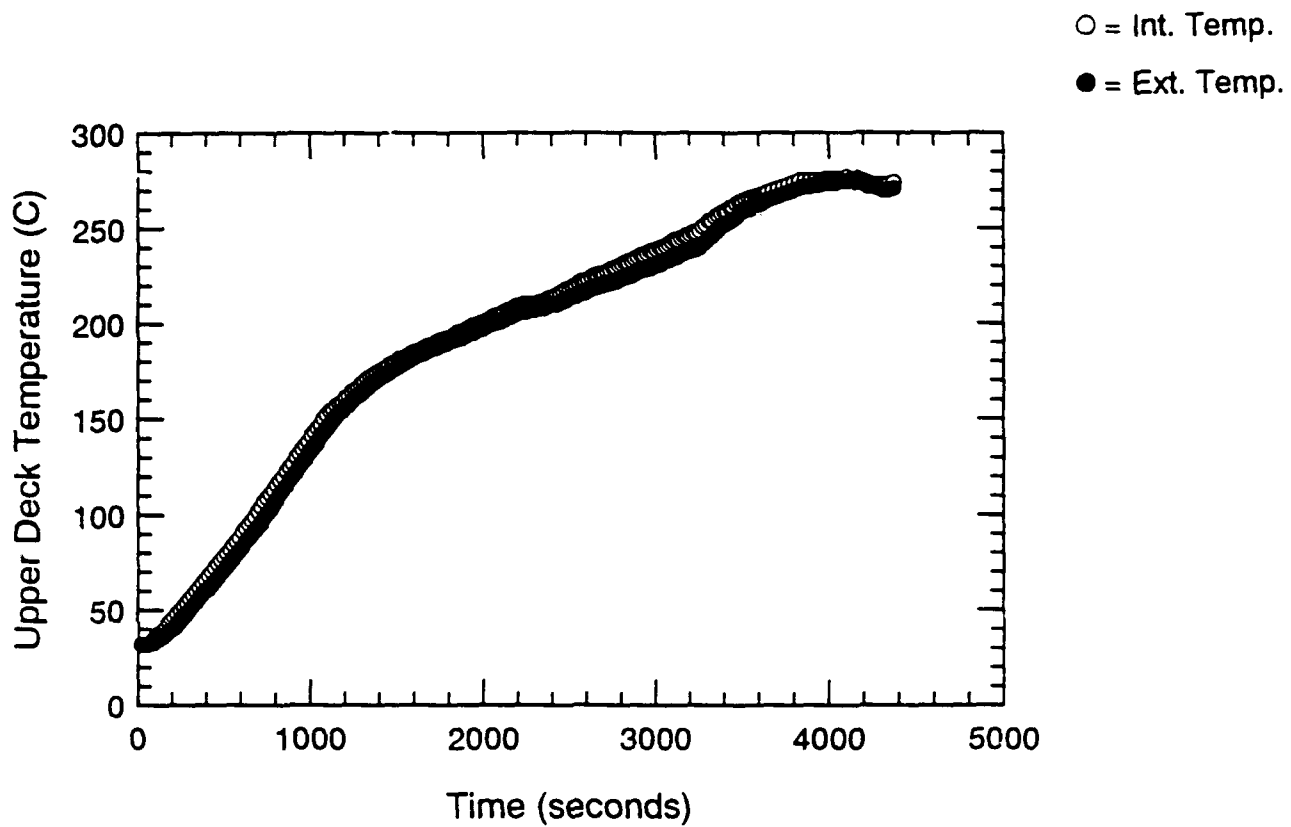


Figure A.85 Surface Thermocouple-Time Histories - S110

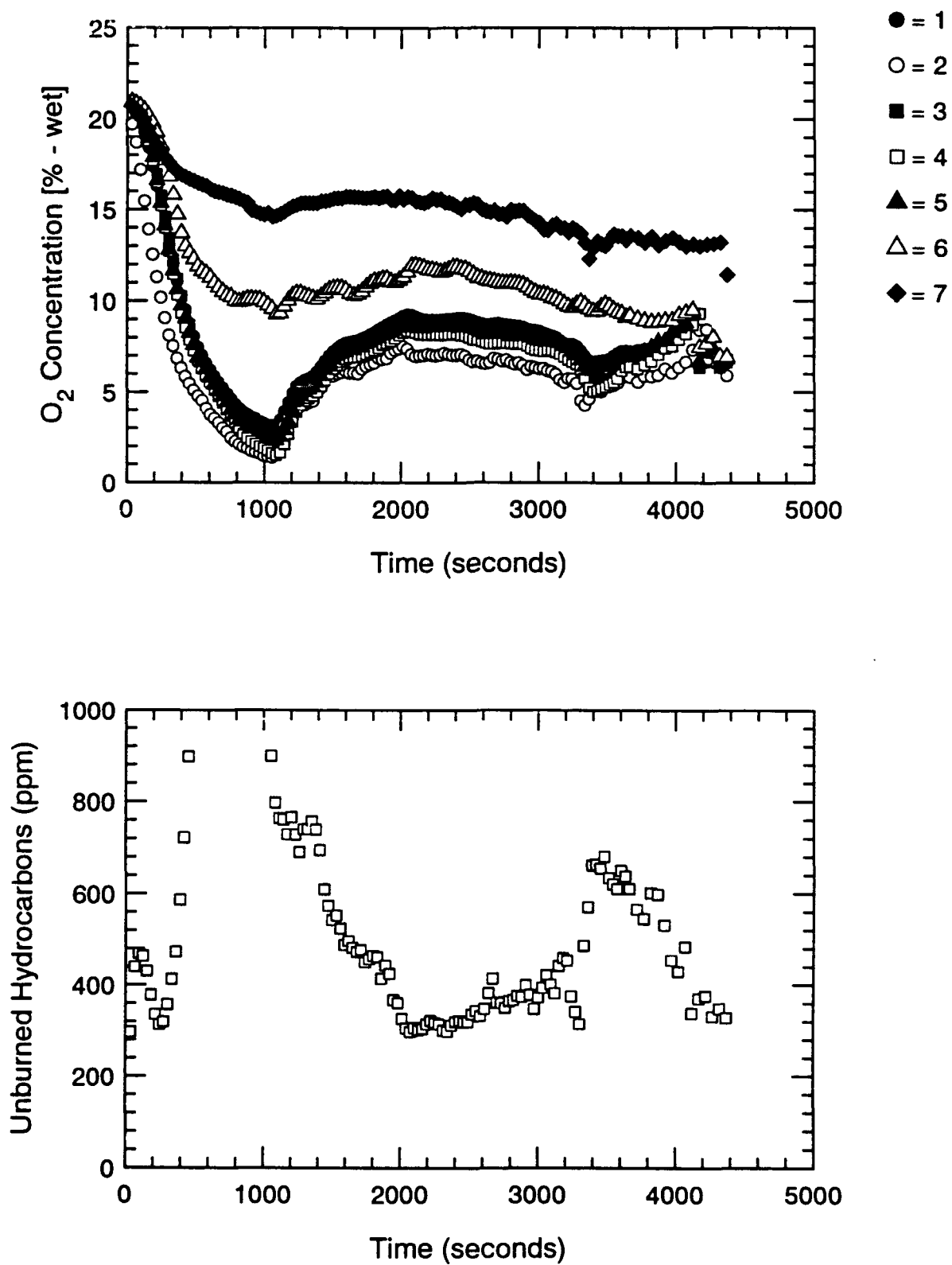


Figure A.86 Oxygen and Unburned HC Concentration-Time Histories - S110

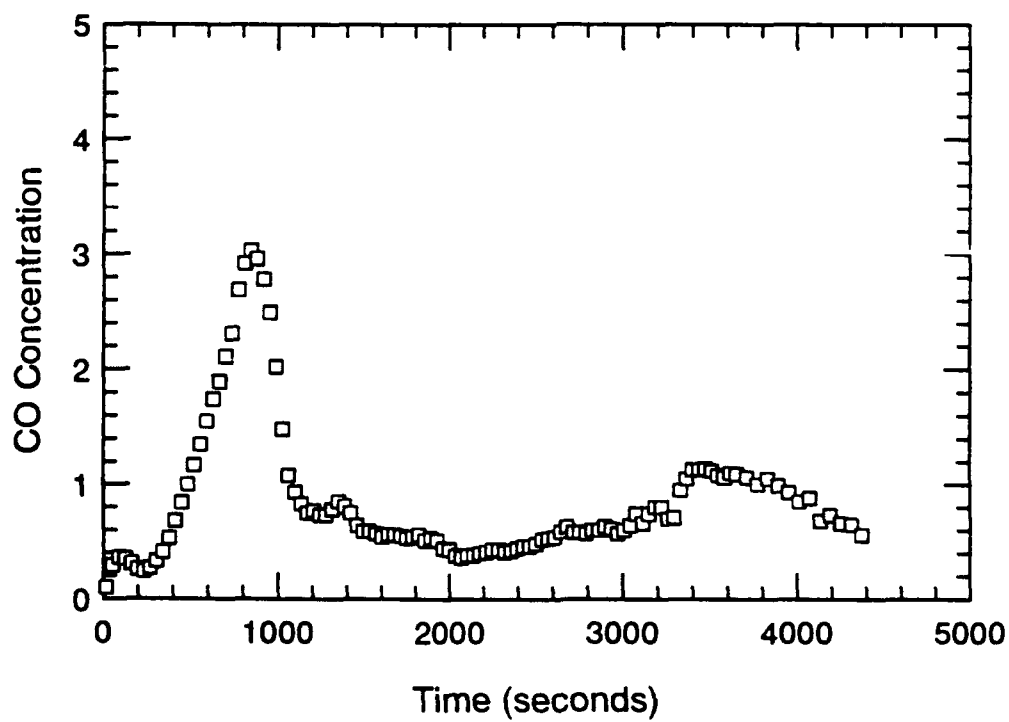
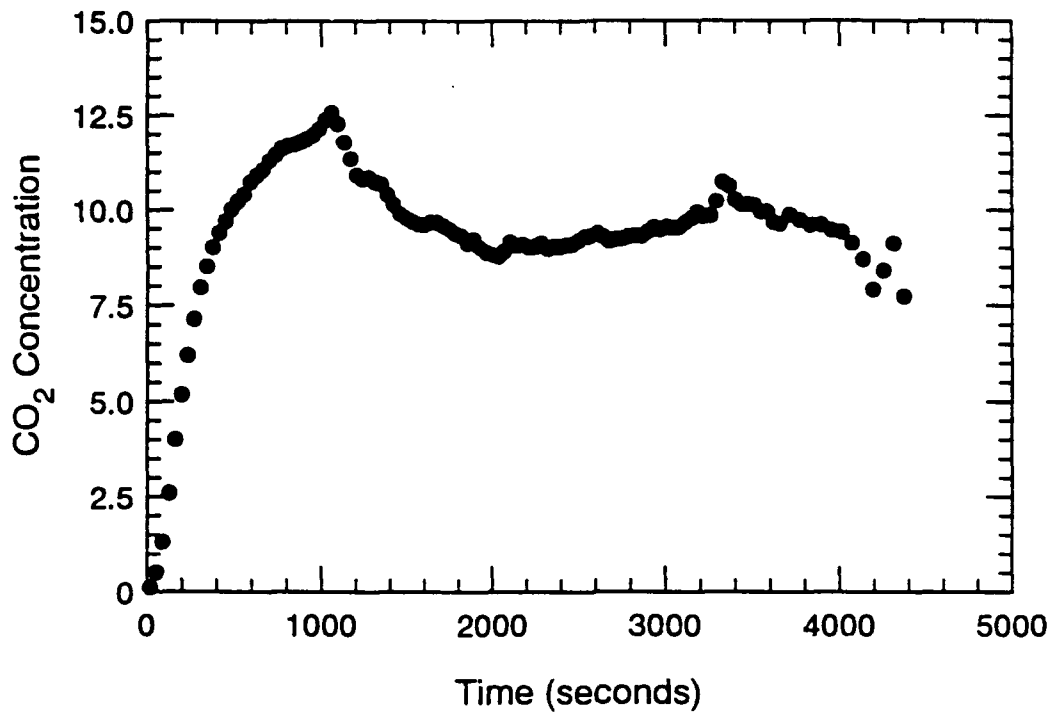


Figure A.87 CO₂ and CO Concentration-Time Histories - S110

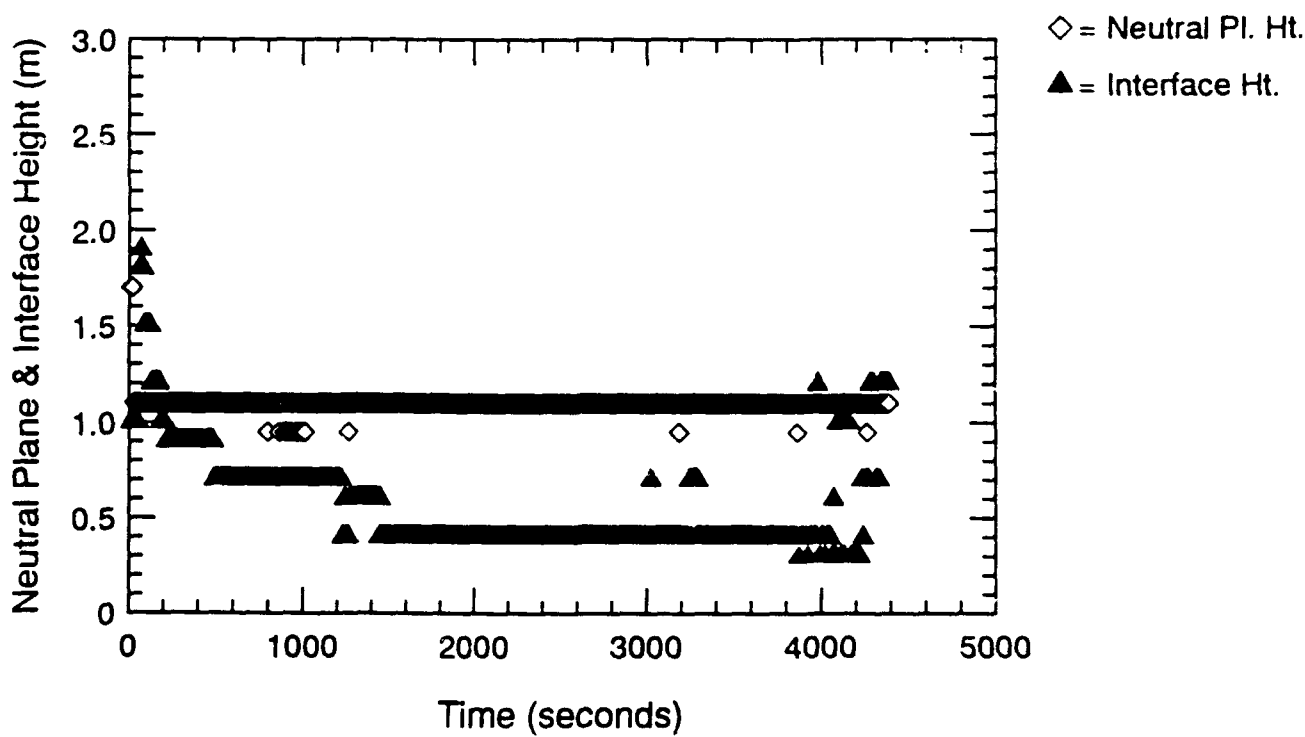
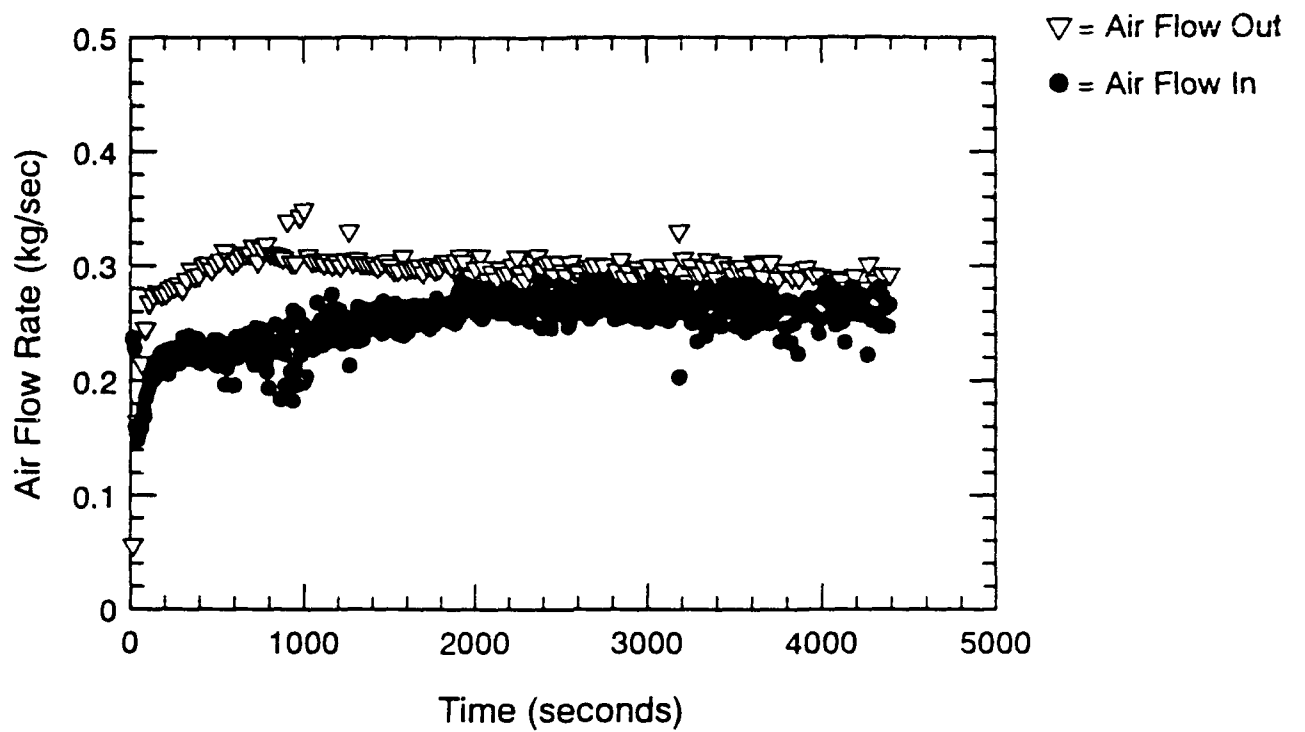


Figure A.88 Air Flow Rate, Neutral Plane & Interface Ht.-Time Histories - S110

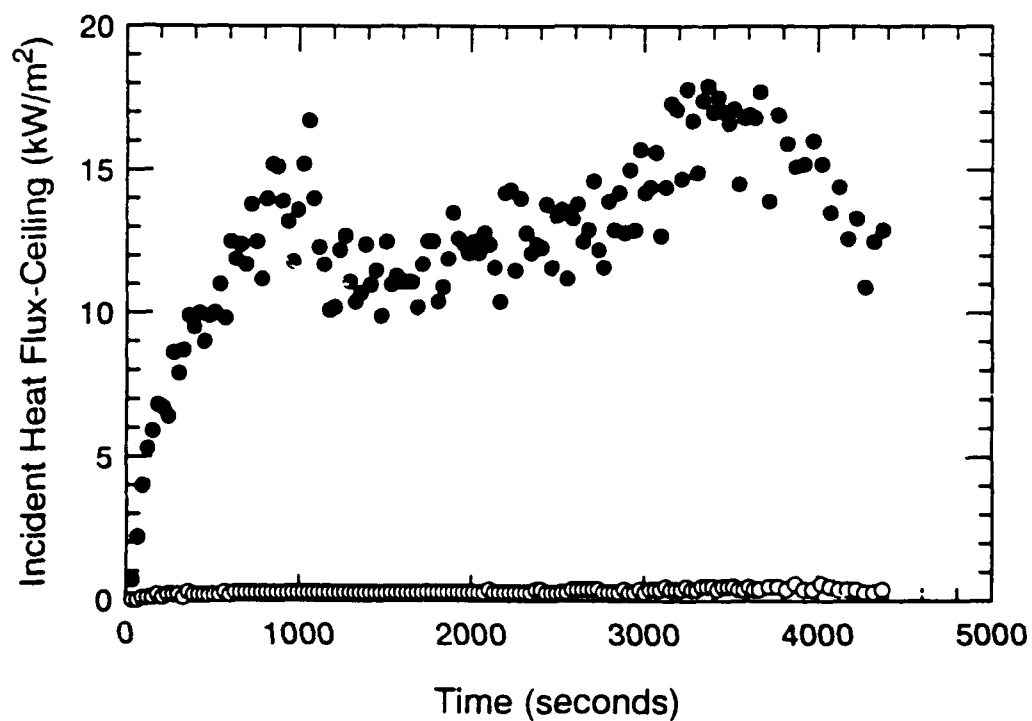
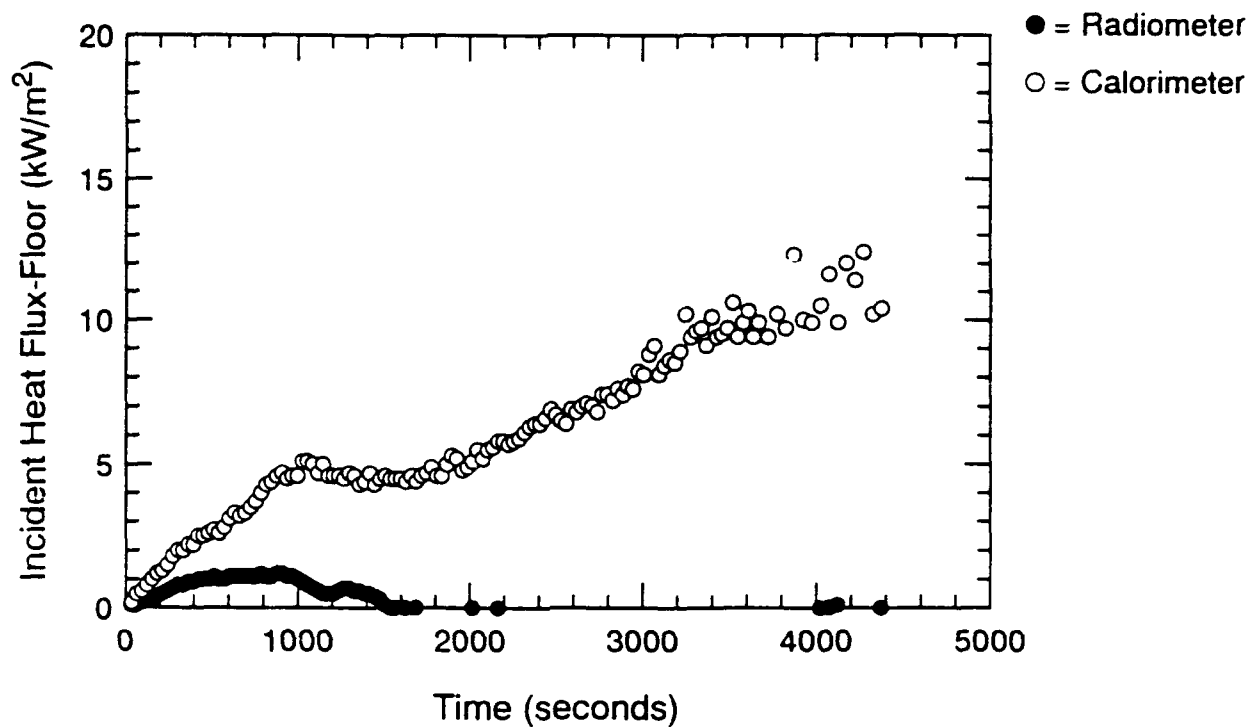


Figure A.89 Incident Heat Flux at Floor and Ceiling-Time Histories - S110

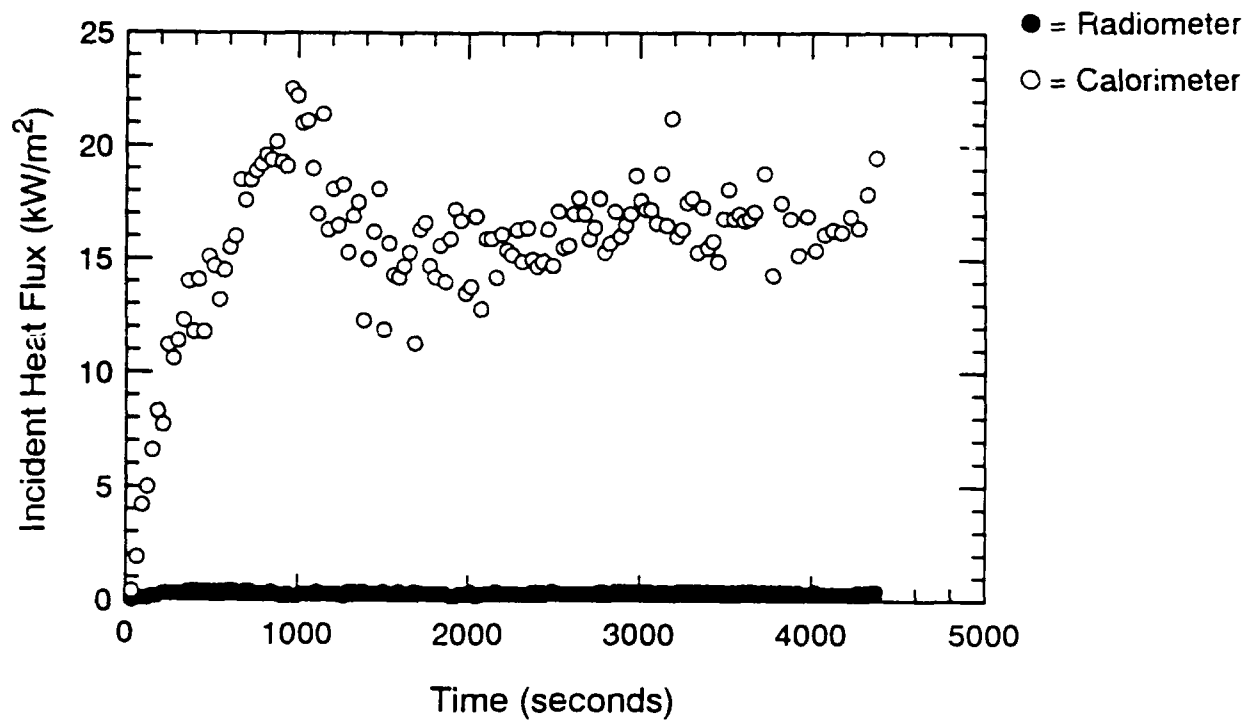


Figure A.90 Incident Heat Flux at Fwd. Bulkhead-Time Histories - S110

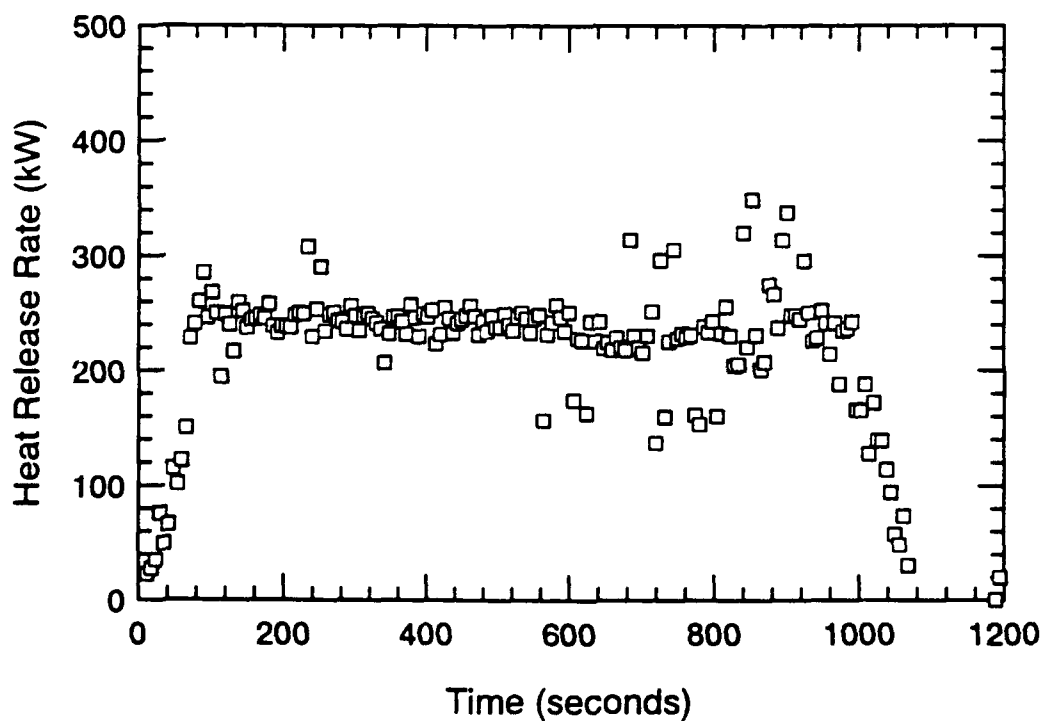
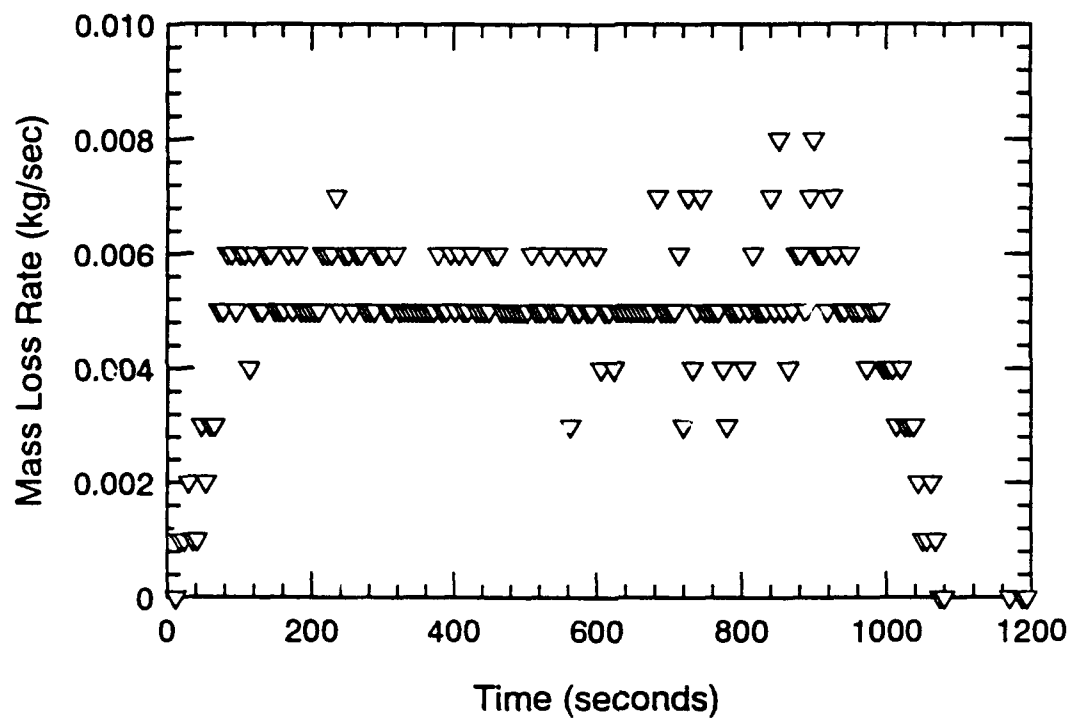


Figure A.91 Mass Loss Rate and Heat Release Rate-Time Histories - S111

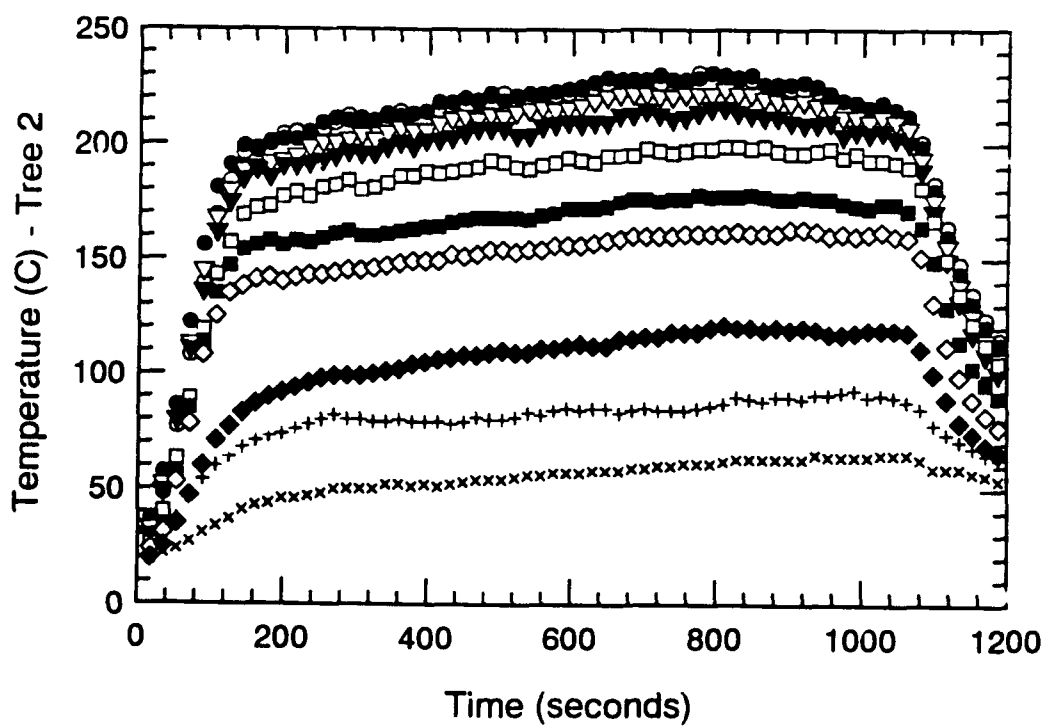
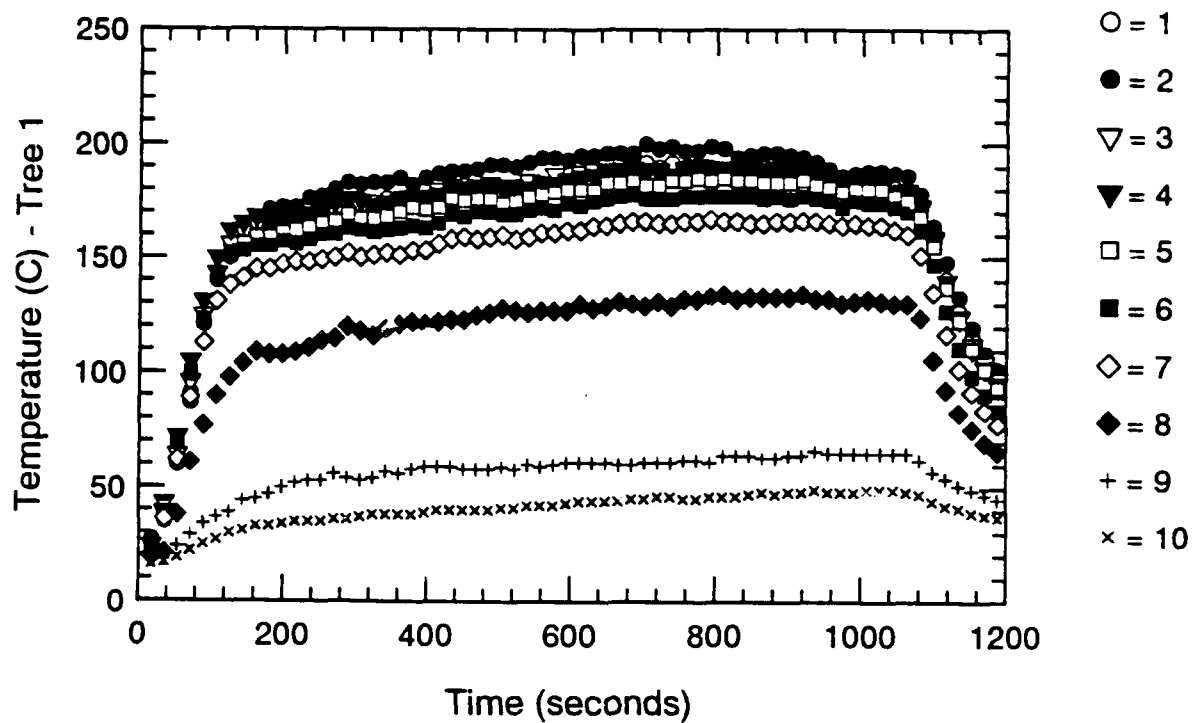


Figure A.92 Thermocouple Trees 1 & 2-Time Histories - S111

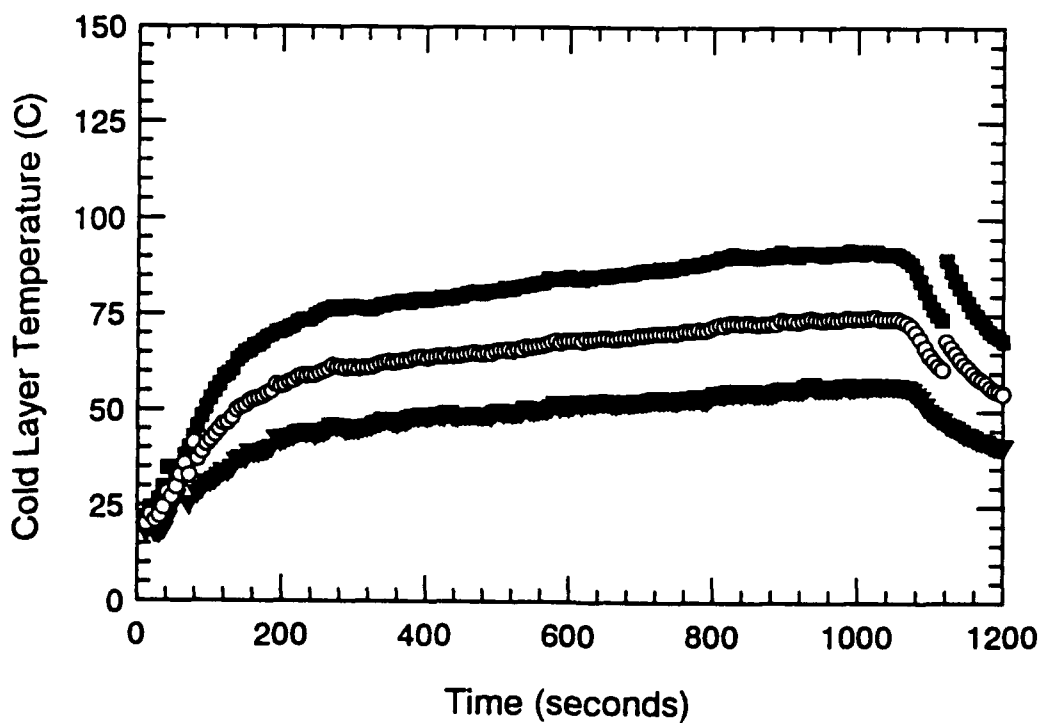
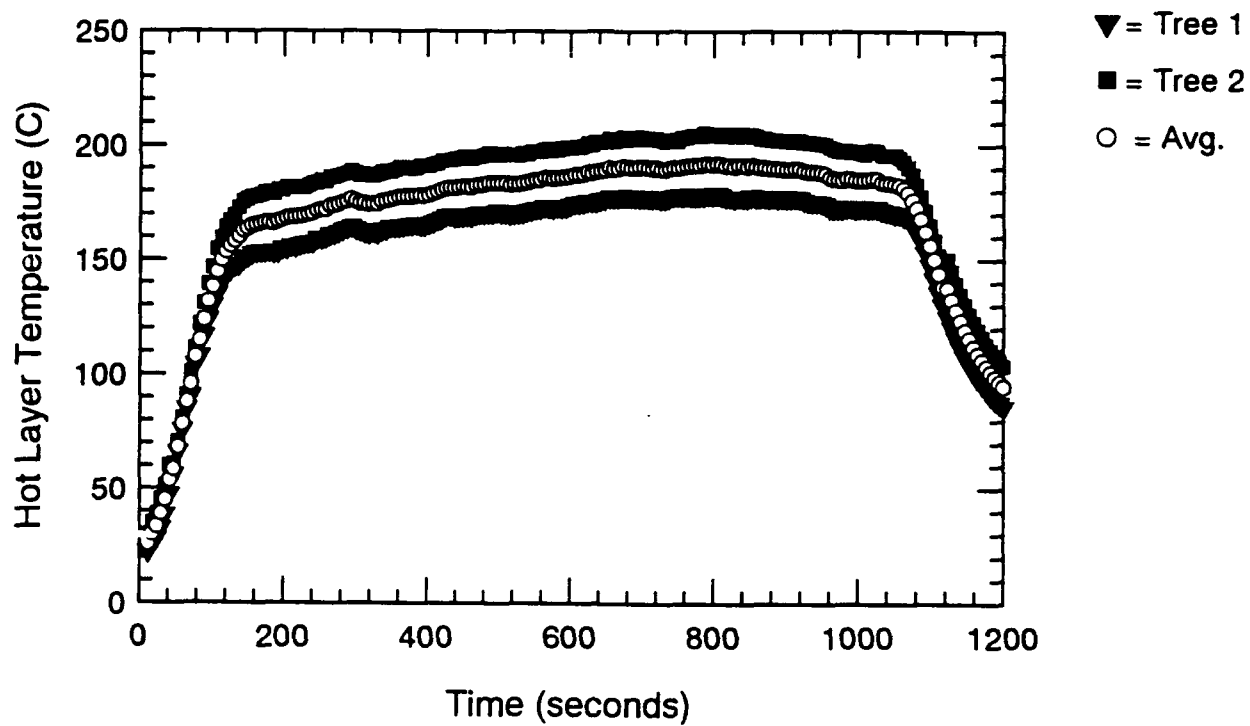


Figure A.93 Hot and Cold Layer Temperature-Time Histories - S111

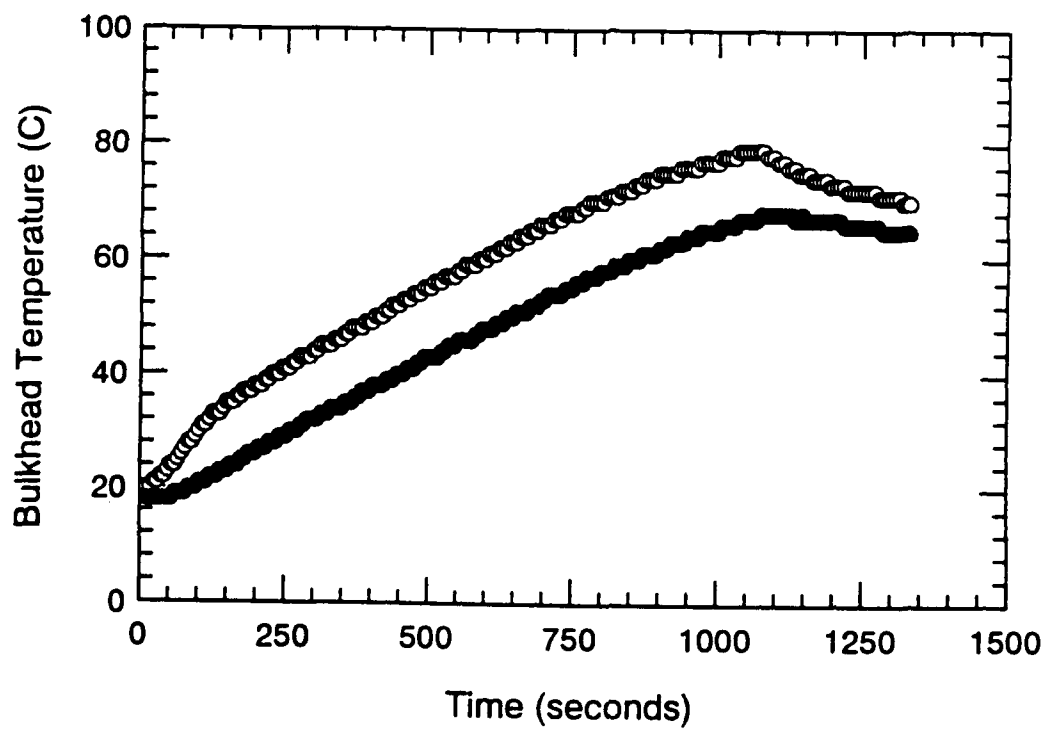
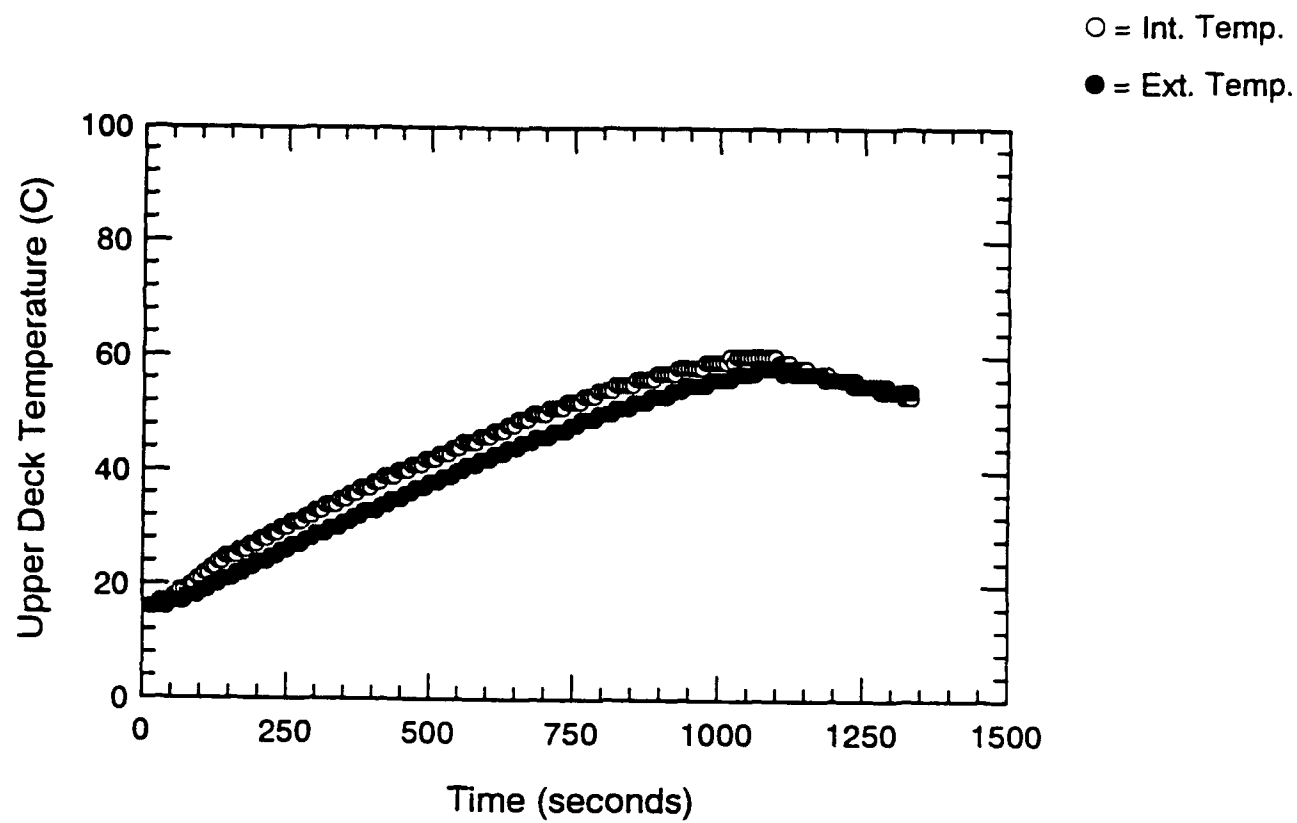


Figure A.94 Surface Thermocouple-Time Histories - S111

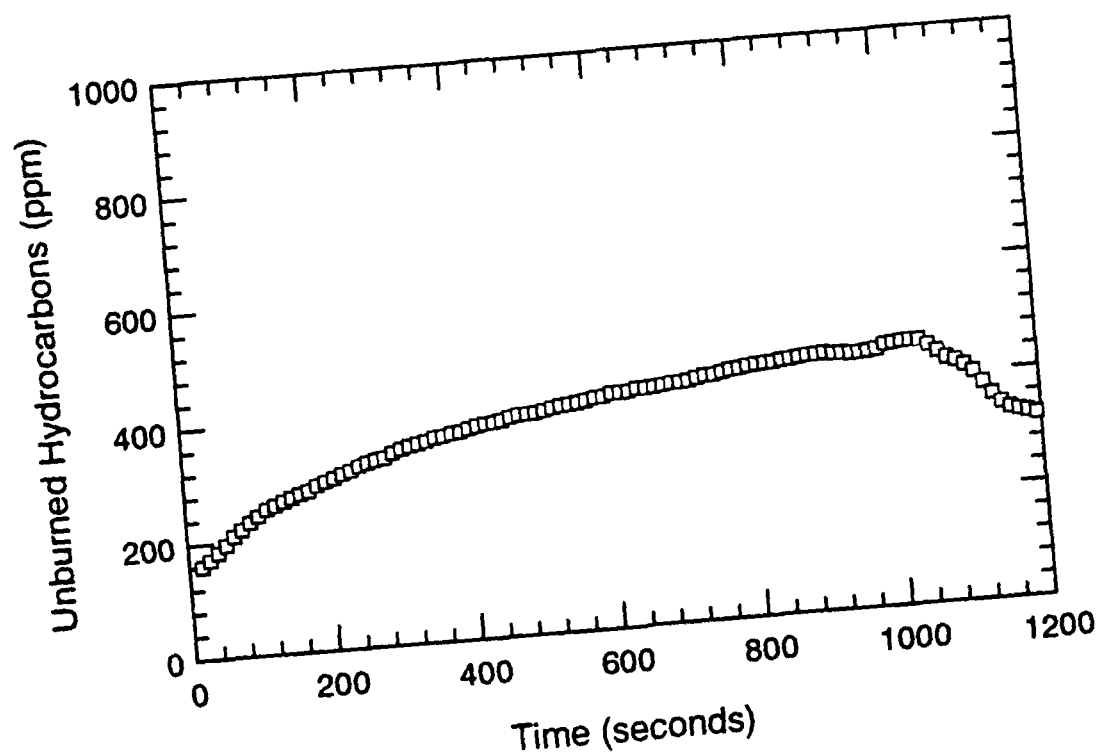
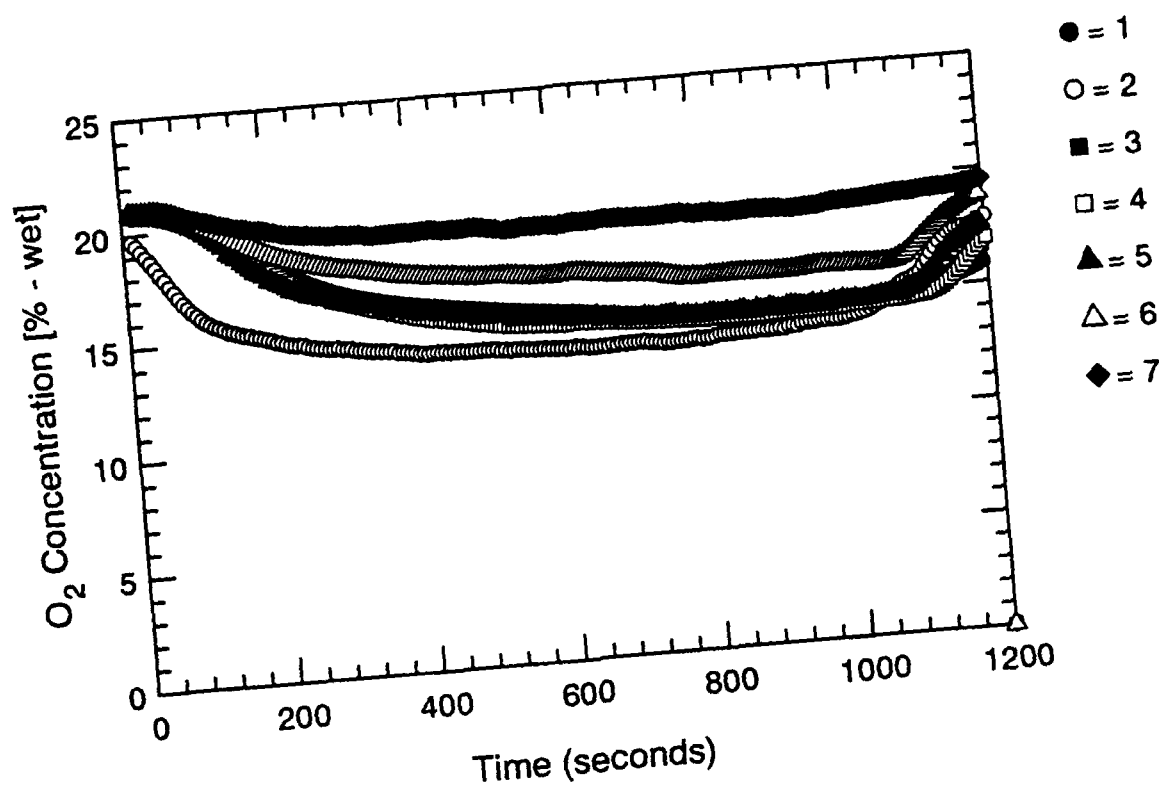


Figure A.95 Oxygen and Unburned HC Concentration-Time Histories - S111

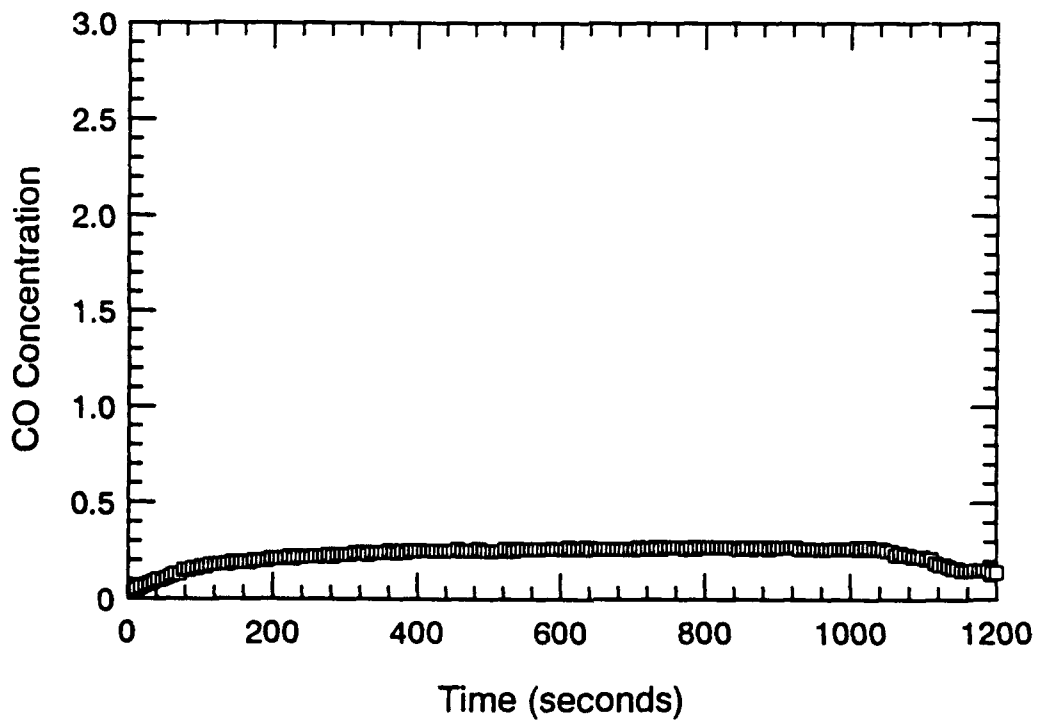
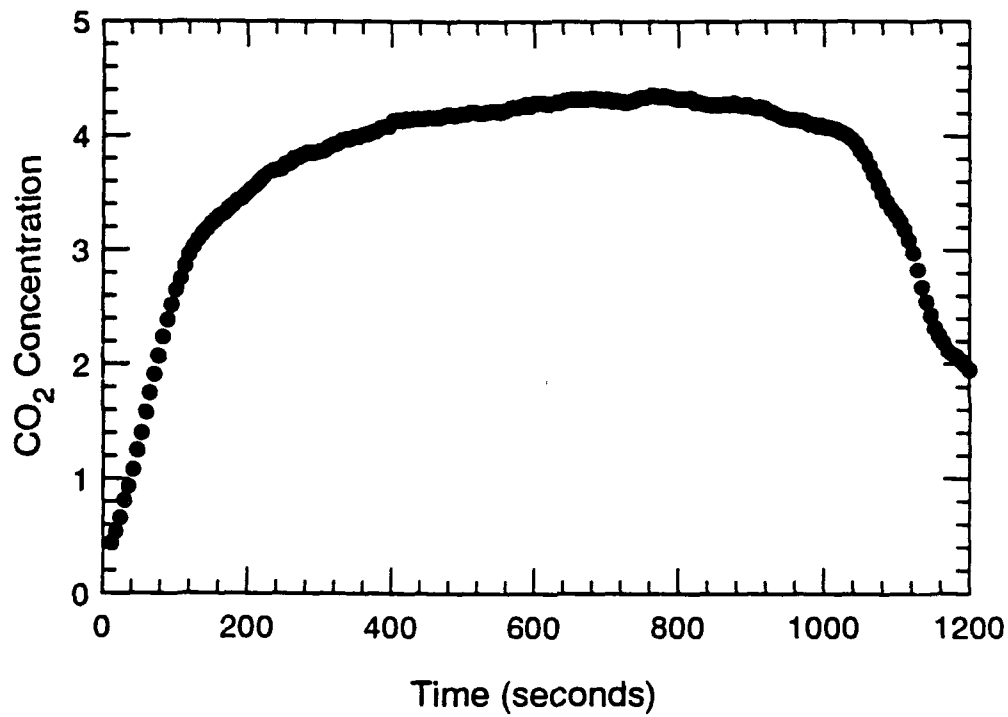


Figure A.96 CO₂ and CO Concentration-Time Histories - S111

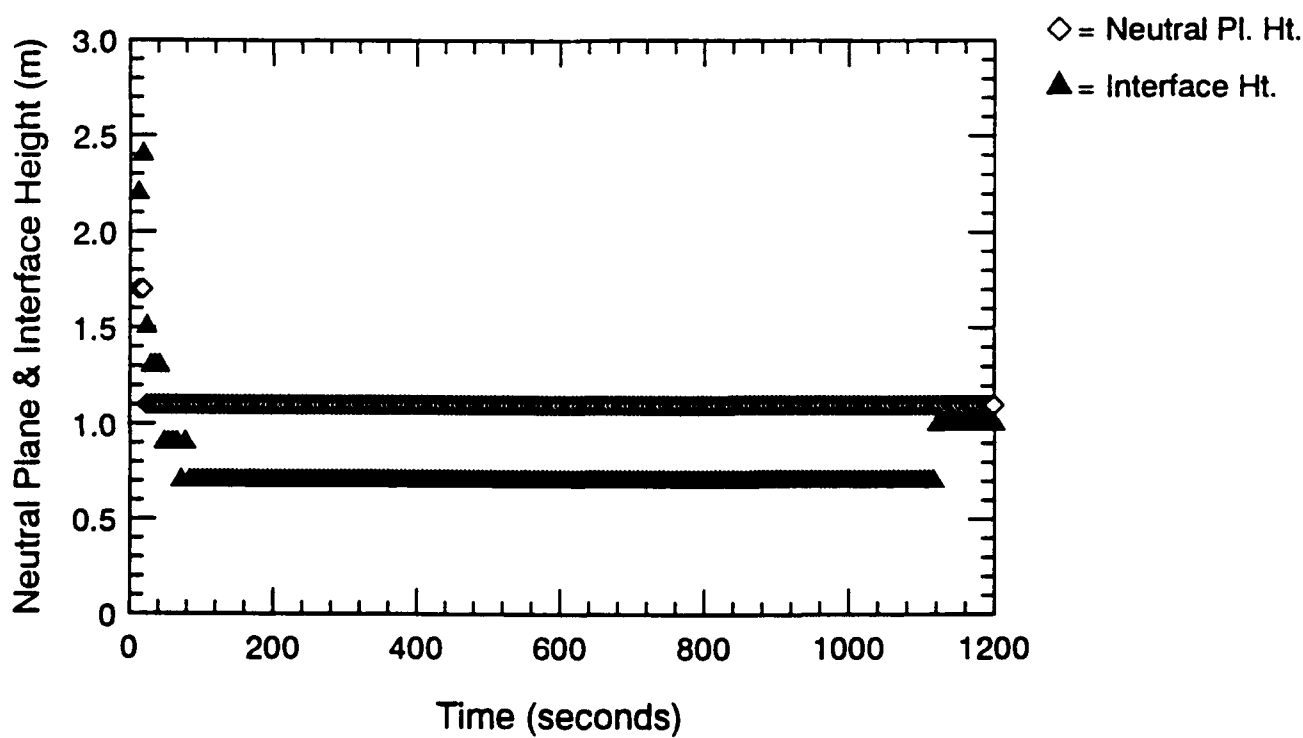
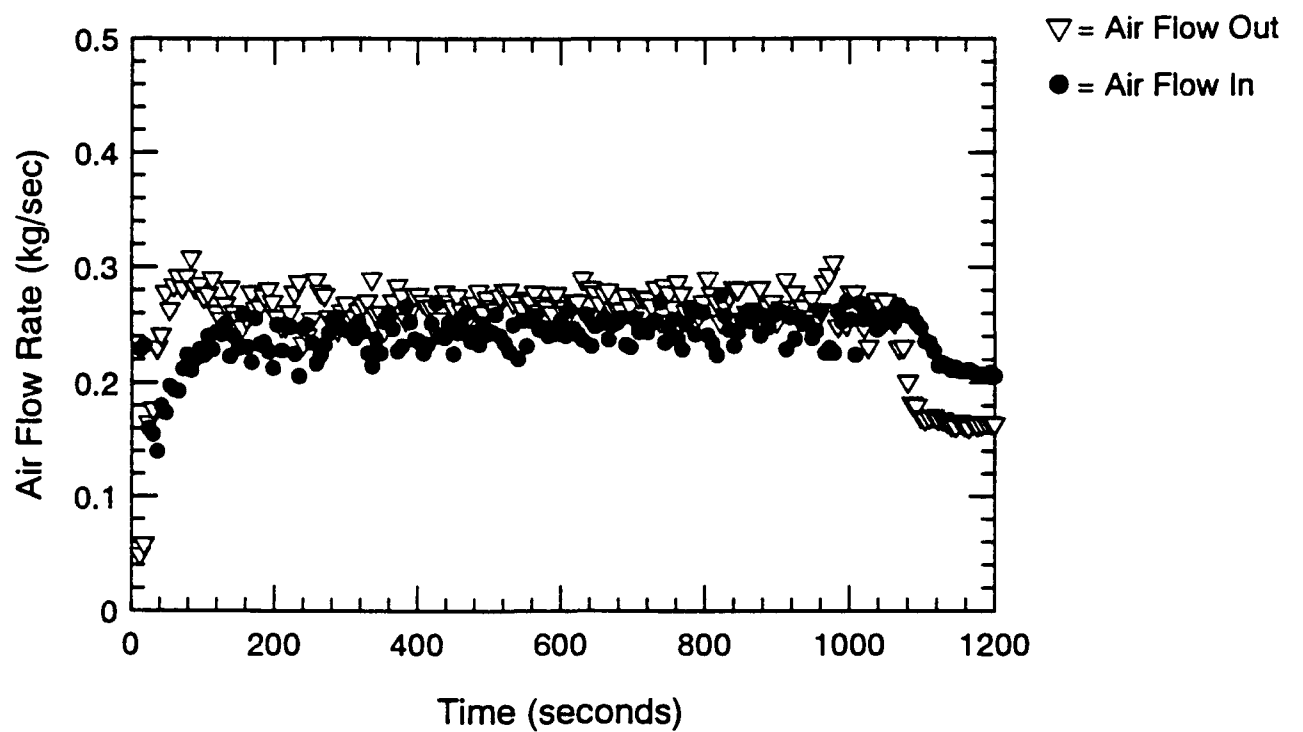


Figure A.97 Air Flow Rate, Neutral Plane & Interface Ht.-Time Histories - S111

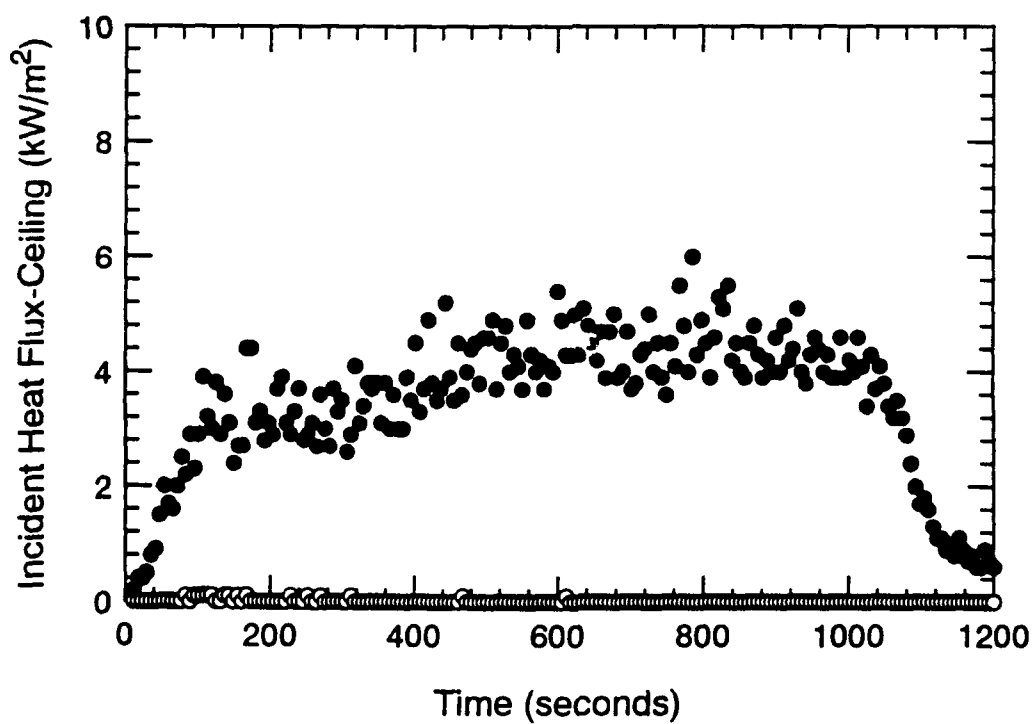
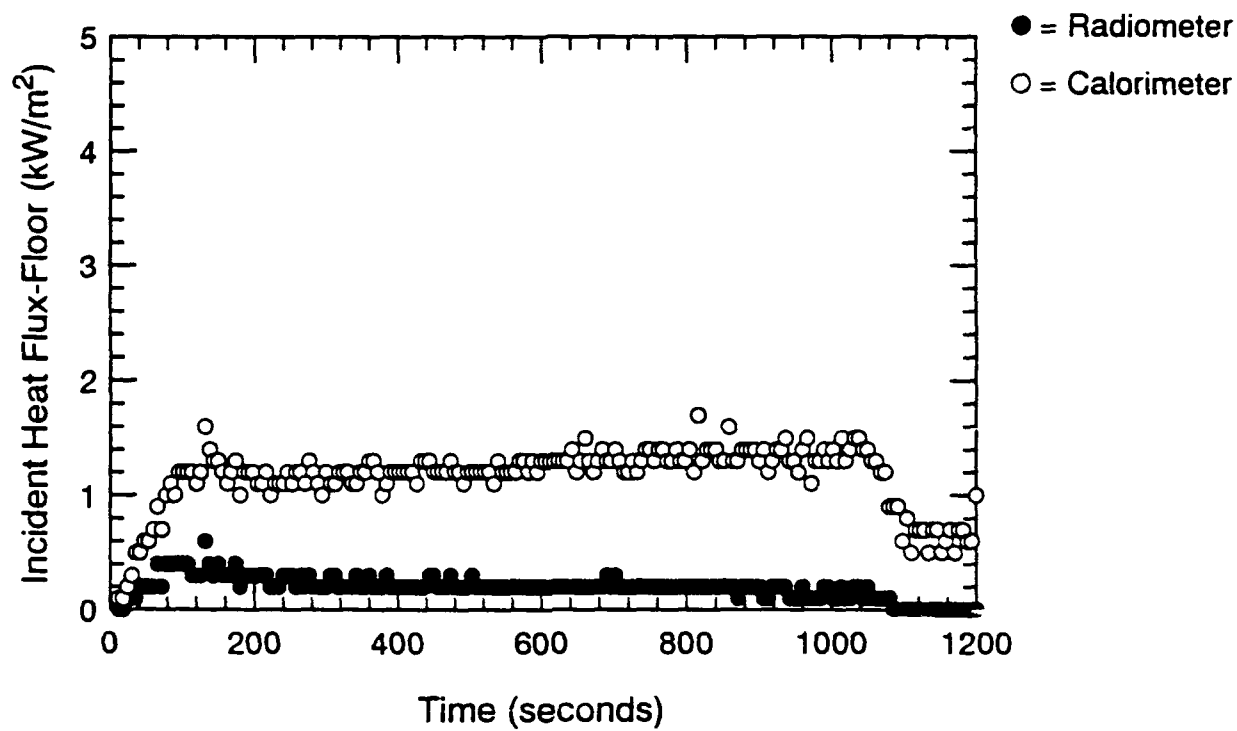


Figure A.98 Incident Heat Flux at Floor and Ceiling-Time Histories - S111

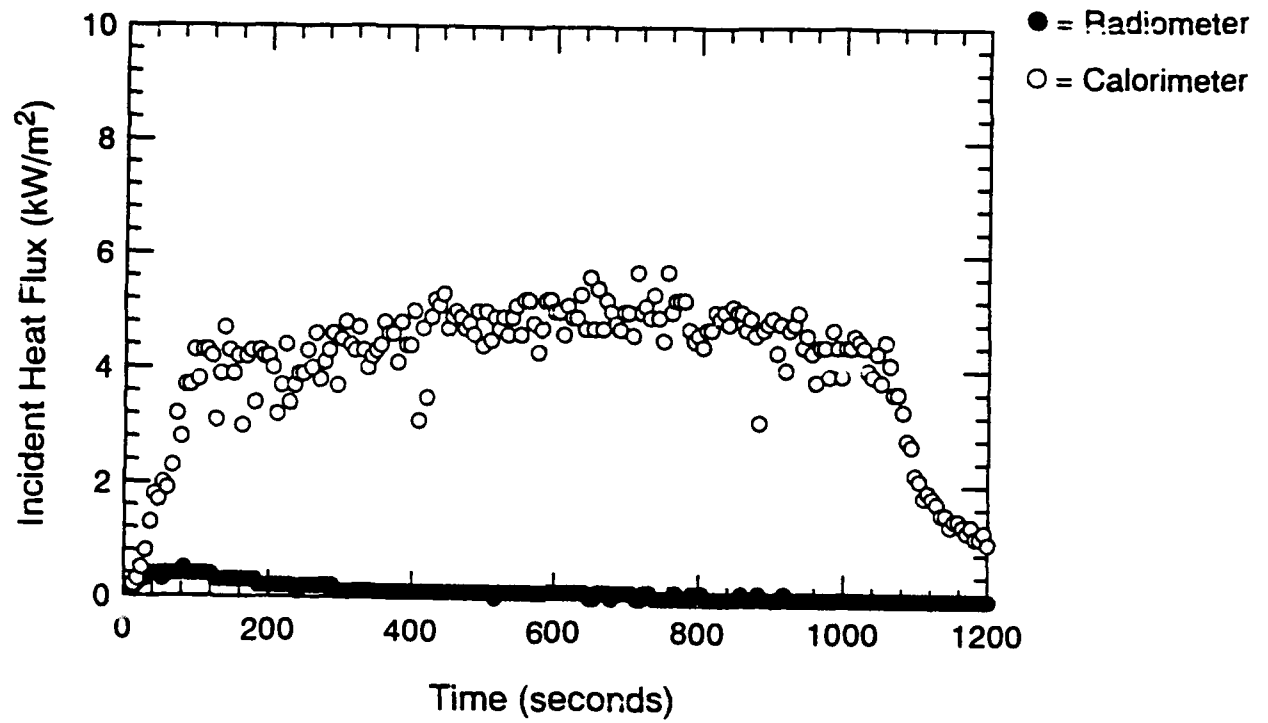


Figure A.99 Incident Heat Flux at Fwd. Bulkhead-Time Histories - S111

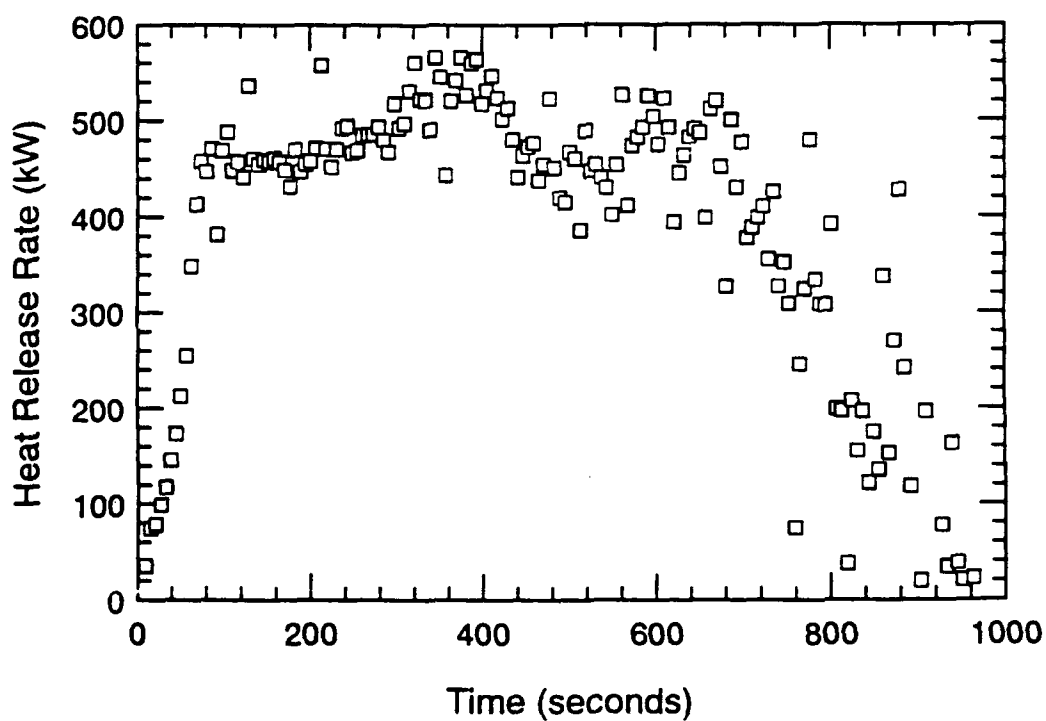
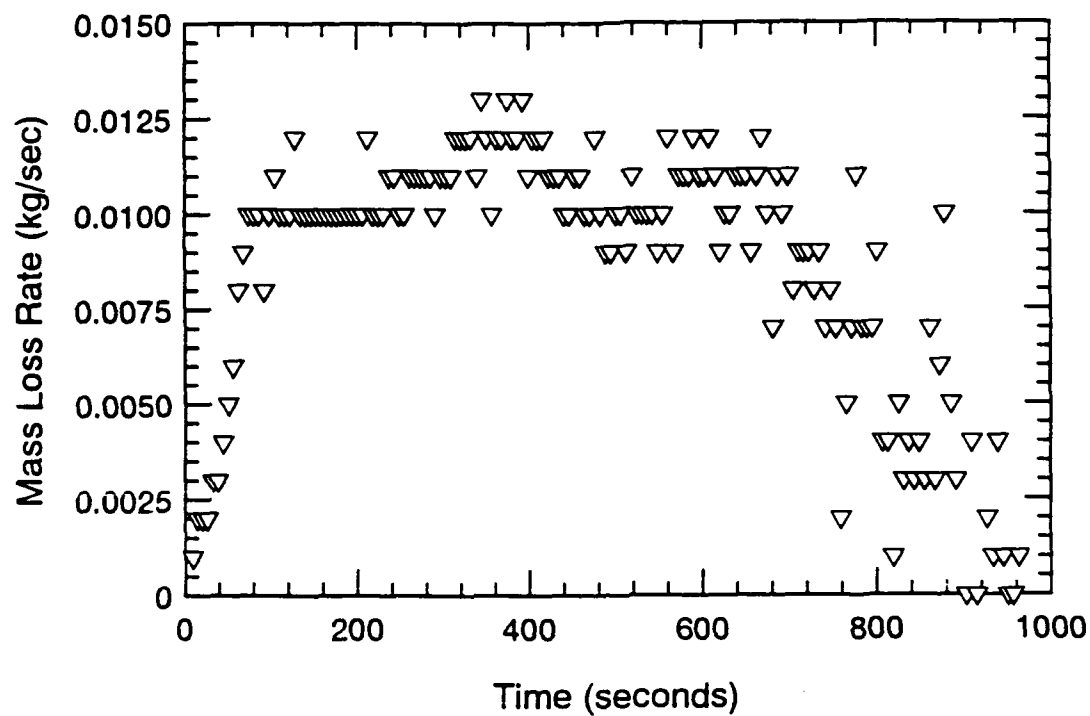


Figure A.100 Mass Loss Rate and Heat Release Rate-Time Histories - S112

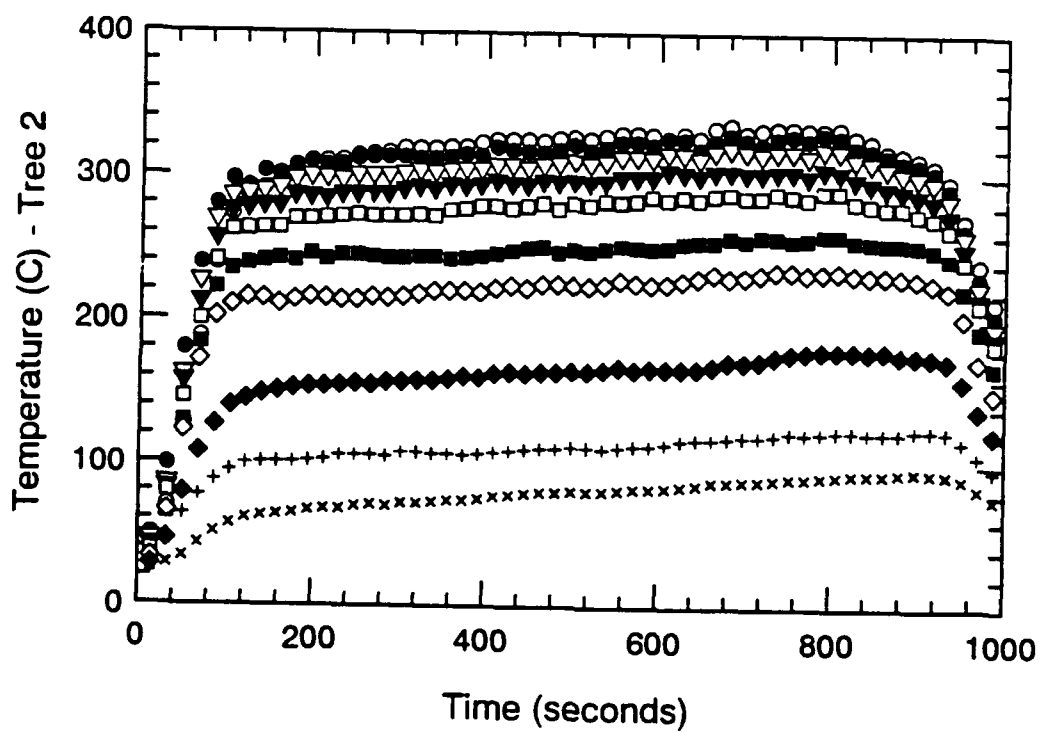
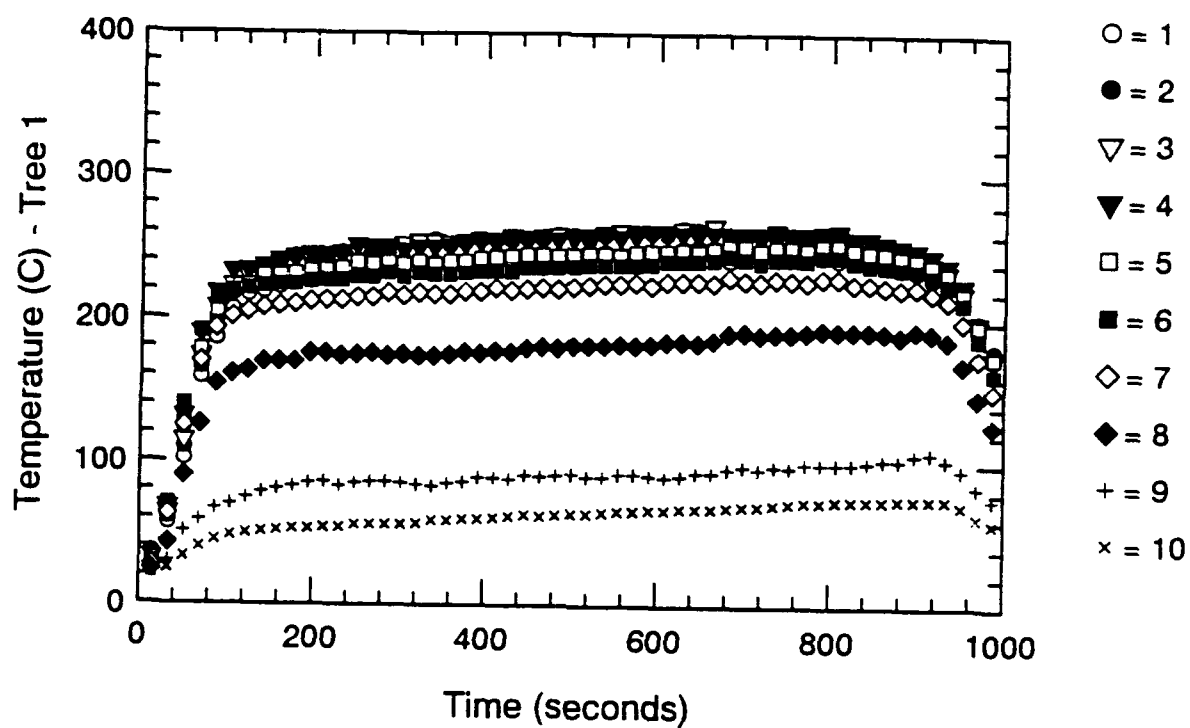


Figure A.101 Thermocouple Trees 1 & 2-Time Histories - S112

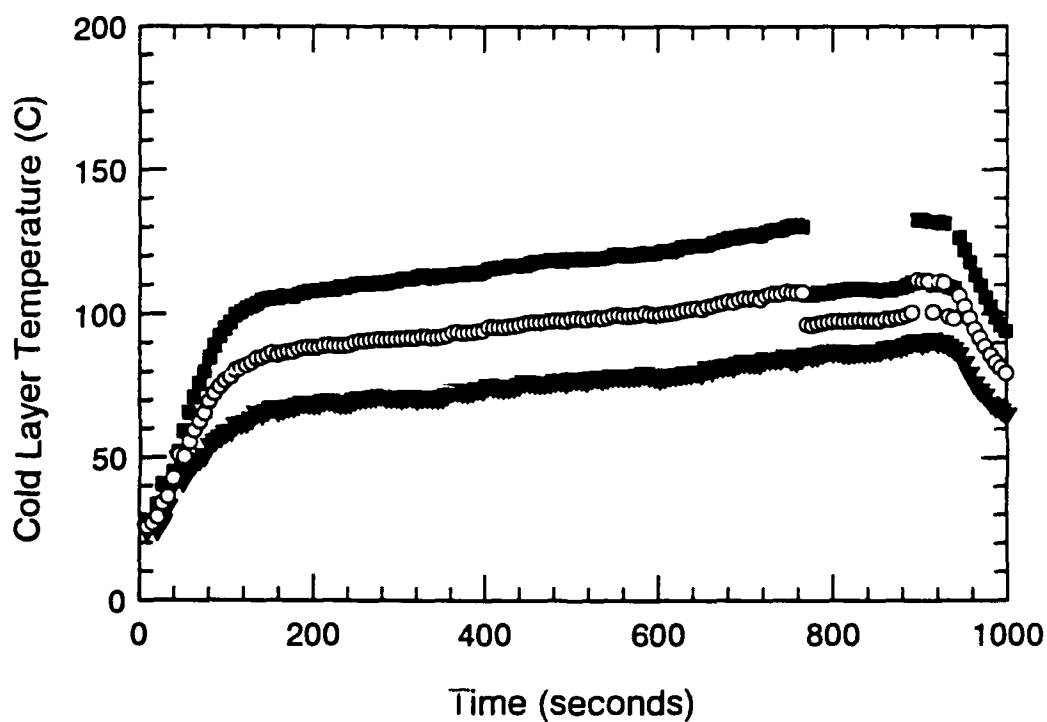
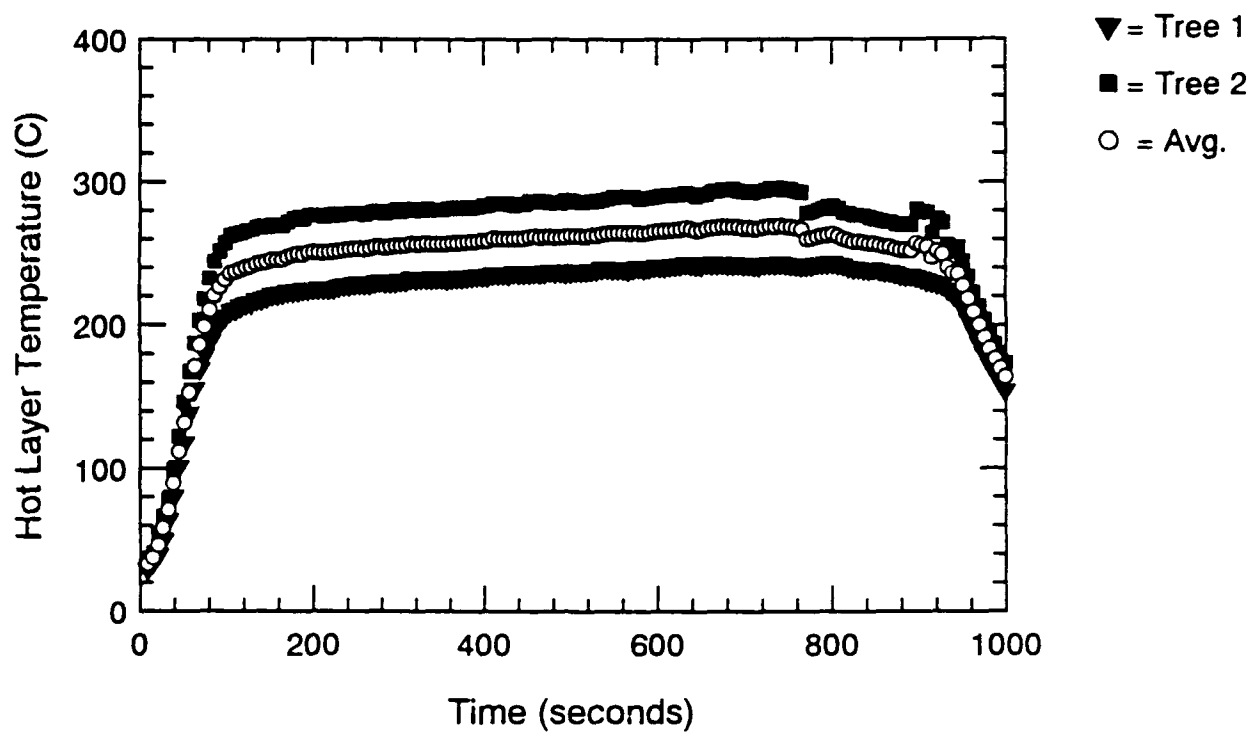


Figure A.102 Hot and Cold Layer Temperature-Time Histories - S112

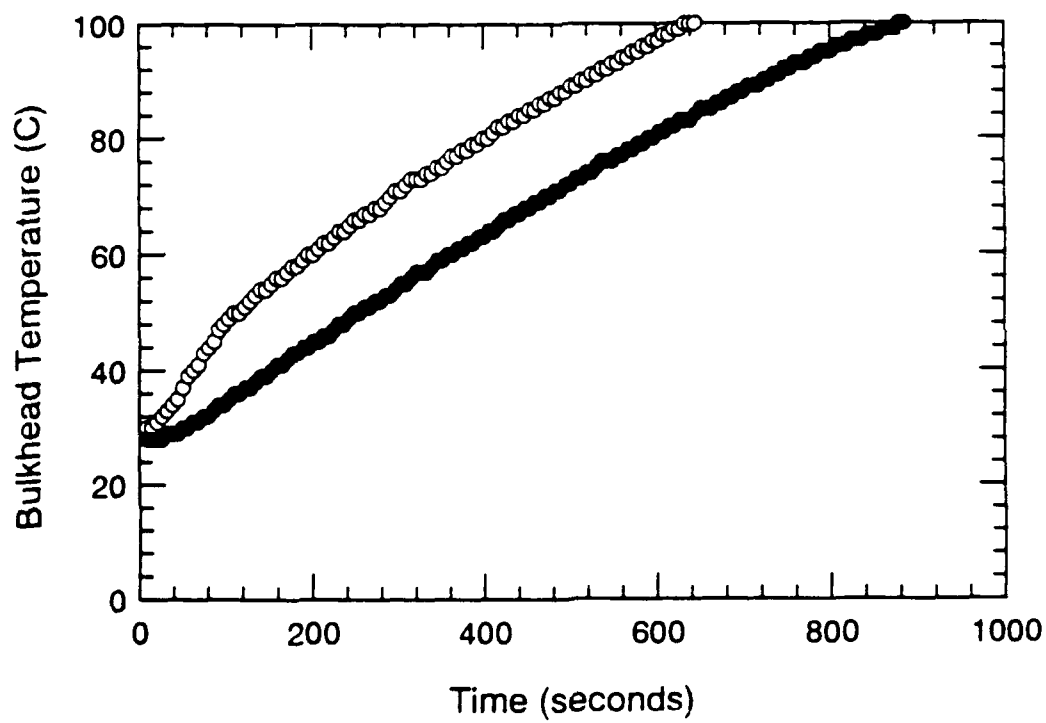
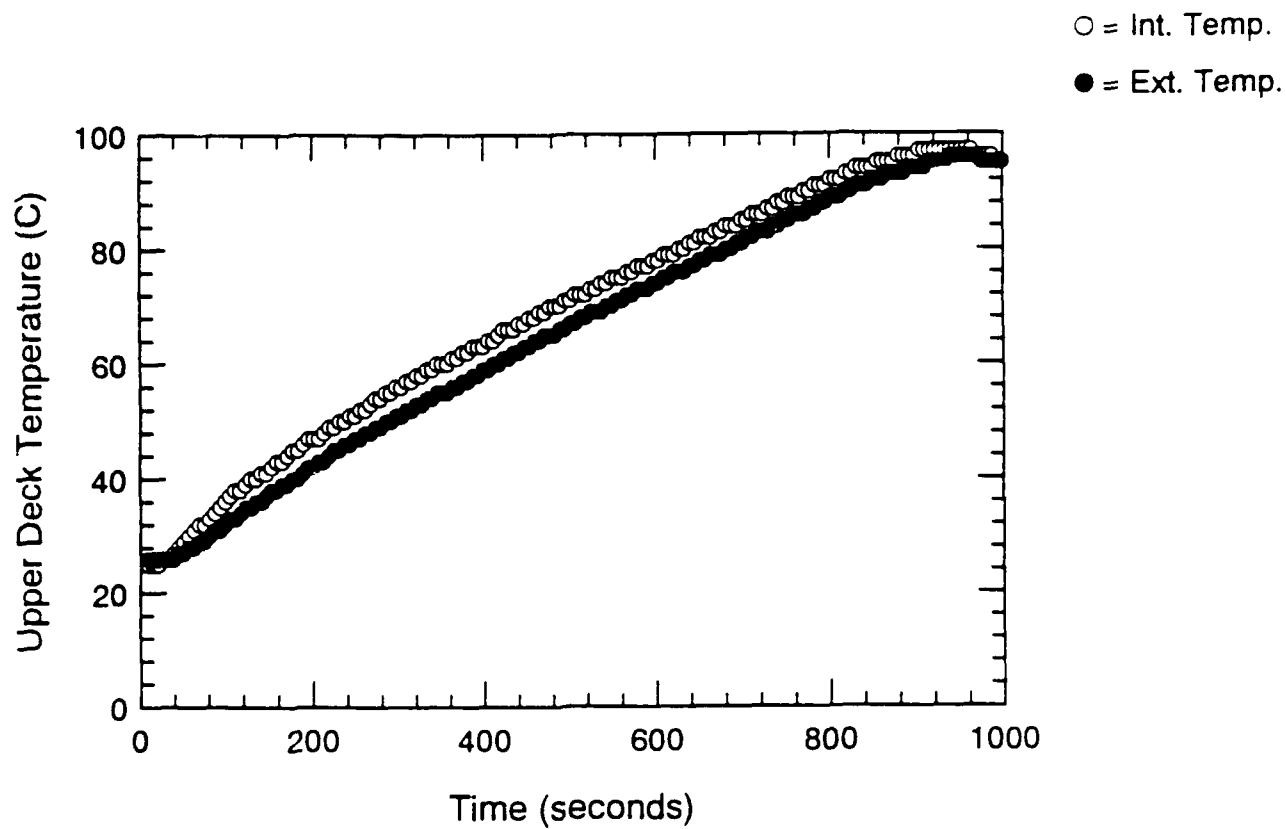


Figure A.103 Surface Thermocouple-Time Histories - S112

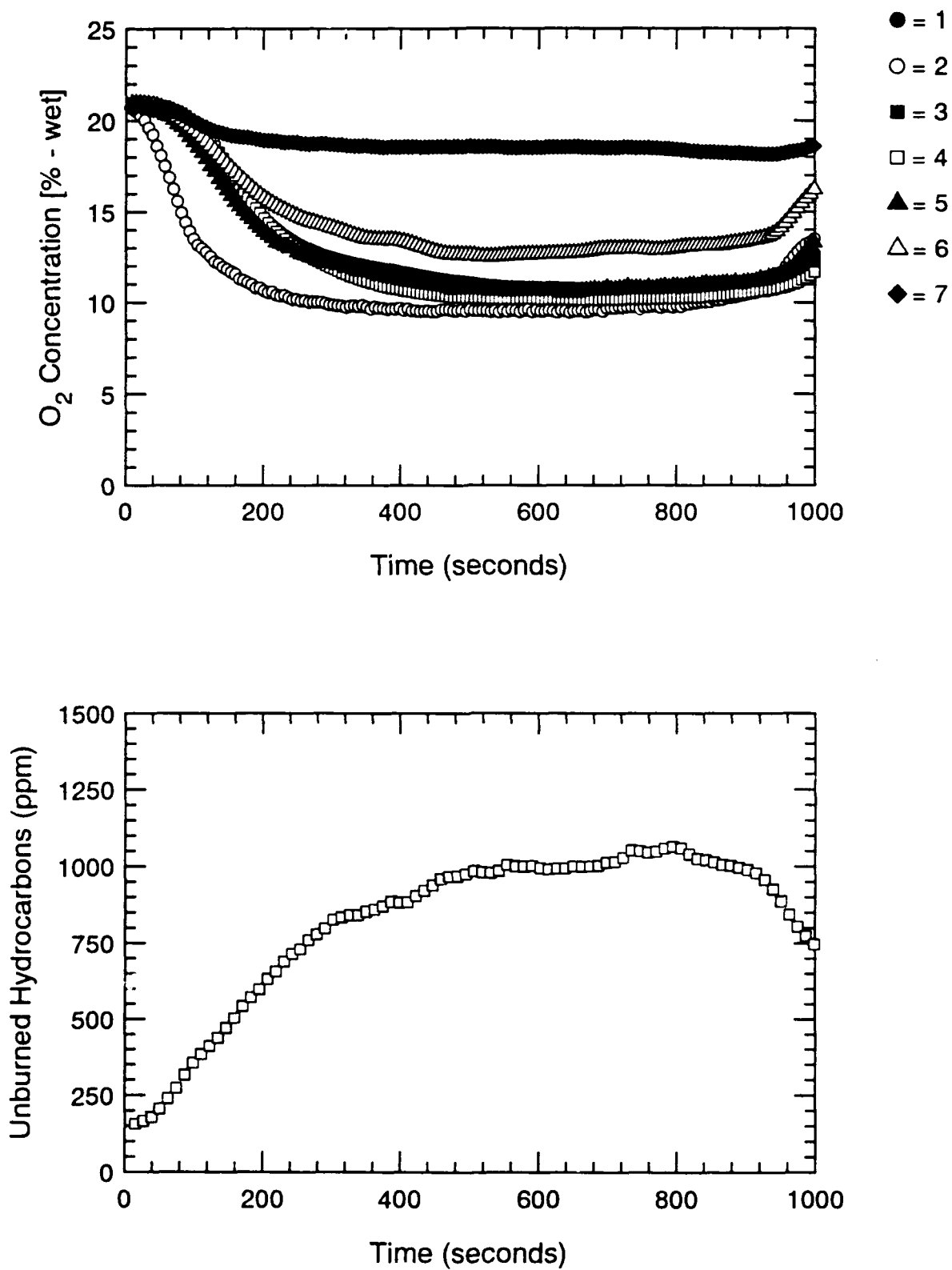


Figure A.104 Oxygen and Unburned HC Concentration-Time Histories - S112

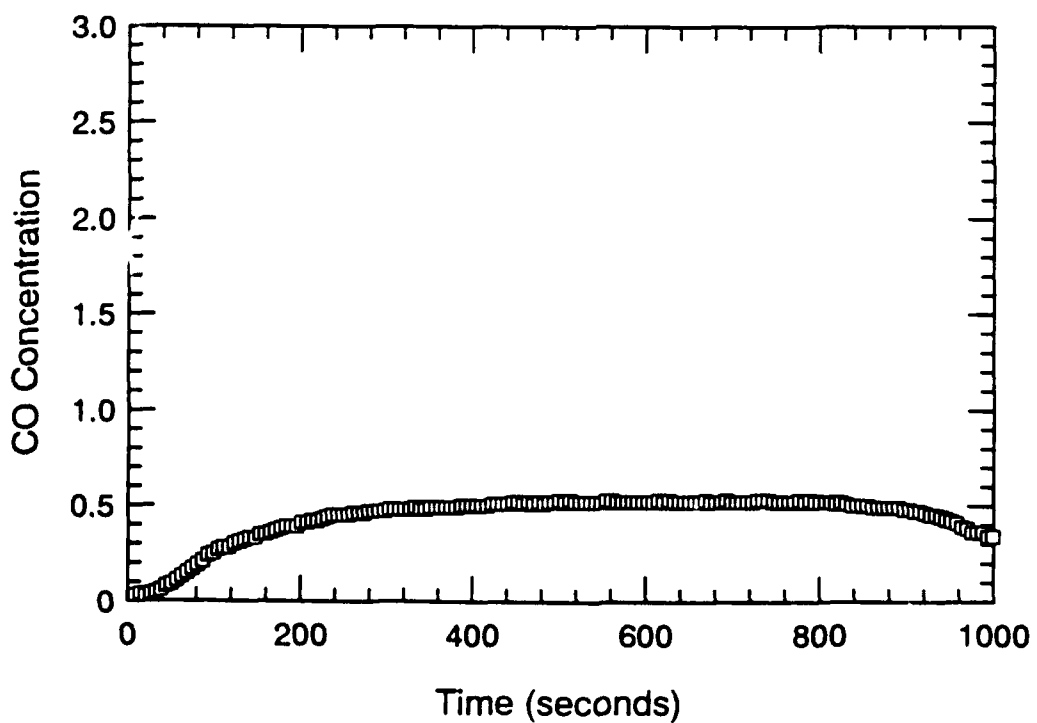
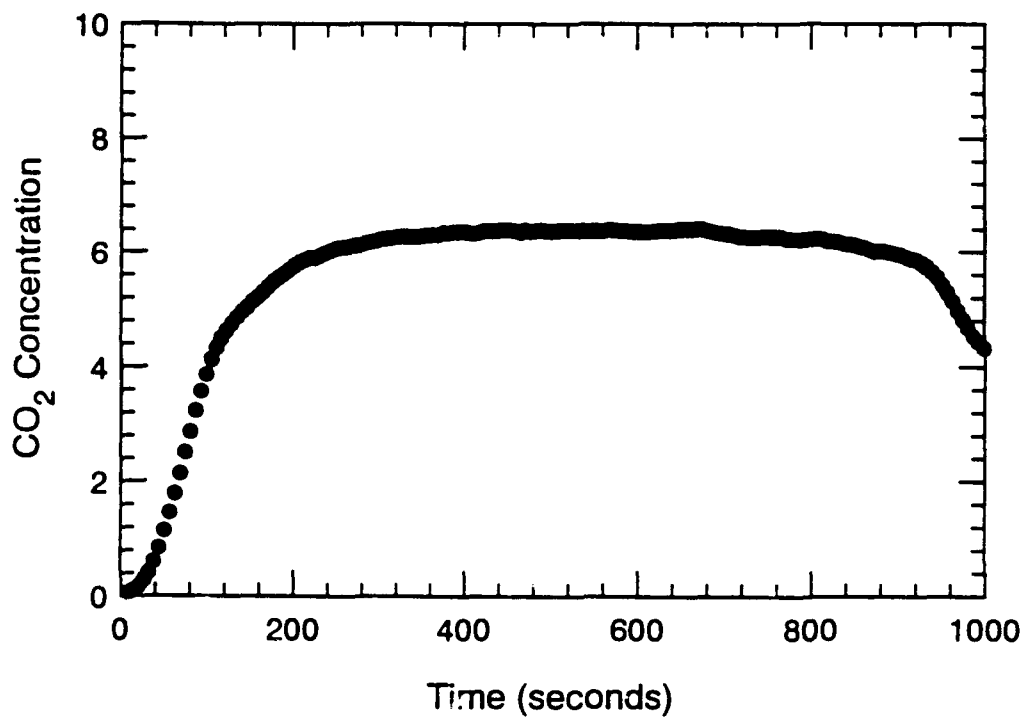


Figure A.105 CO₂ and CO Concentration-Time Histories - S112

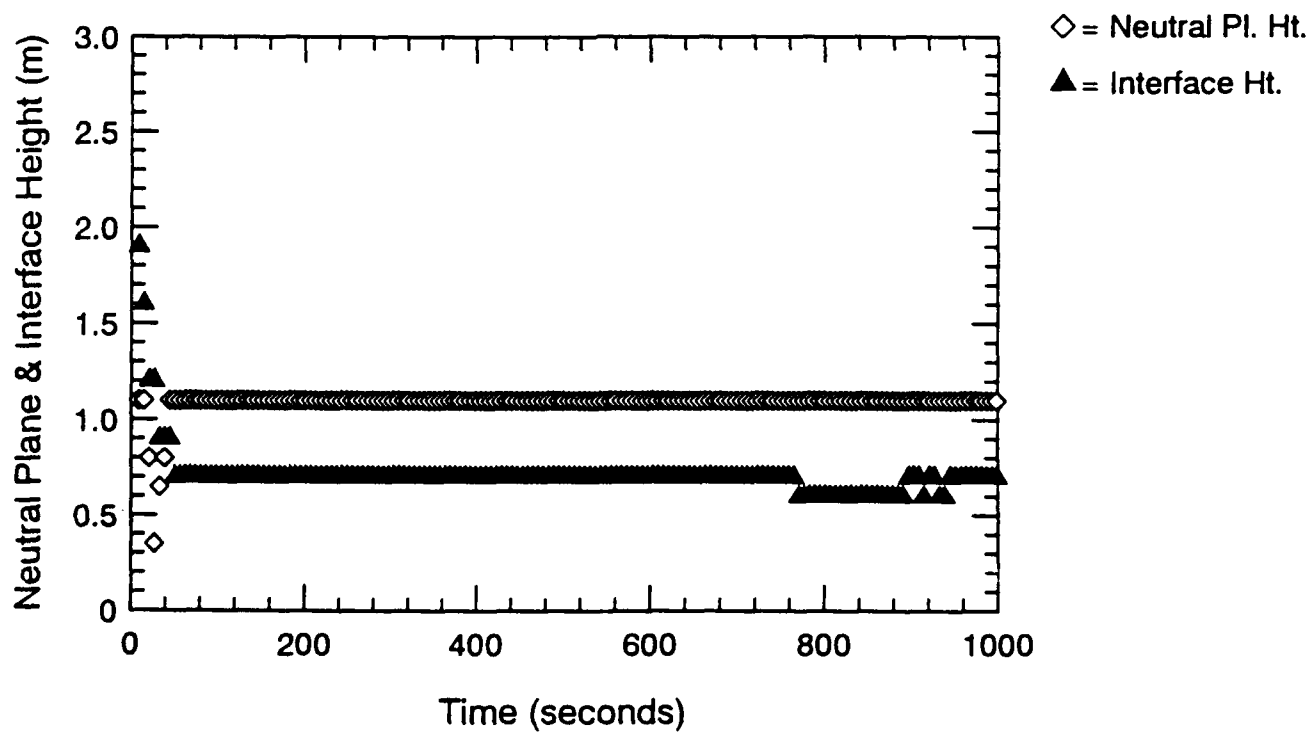
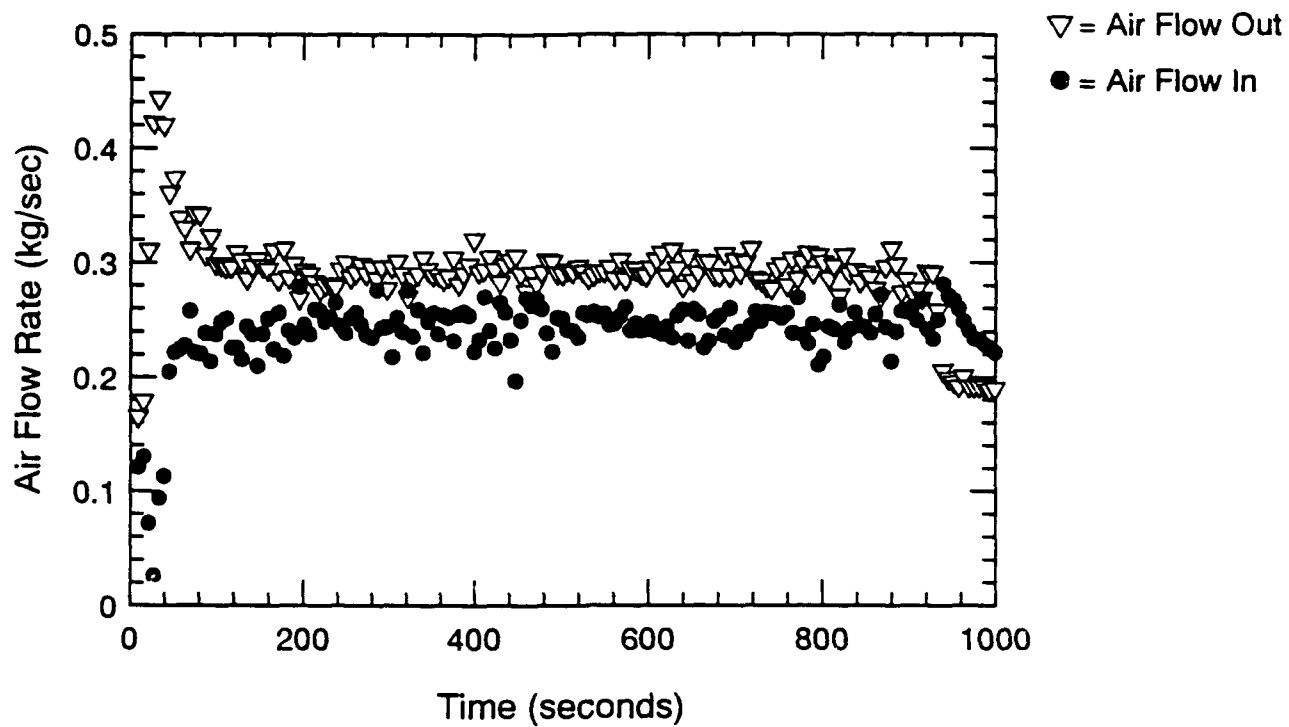


Figure A.106 Air Flow Rate, Neutral Plane & Interface Ht.-Time Histories - S112

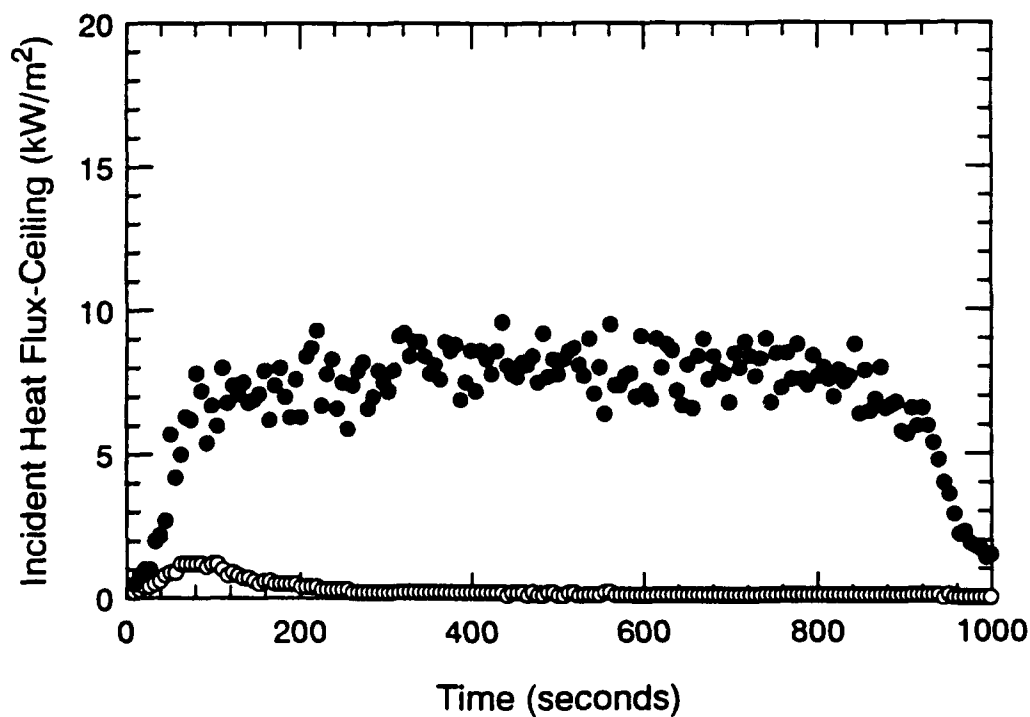
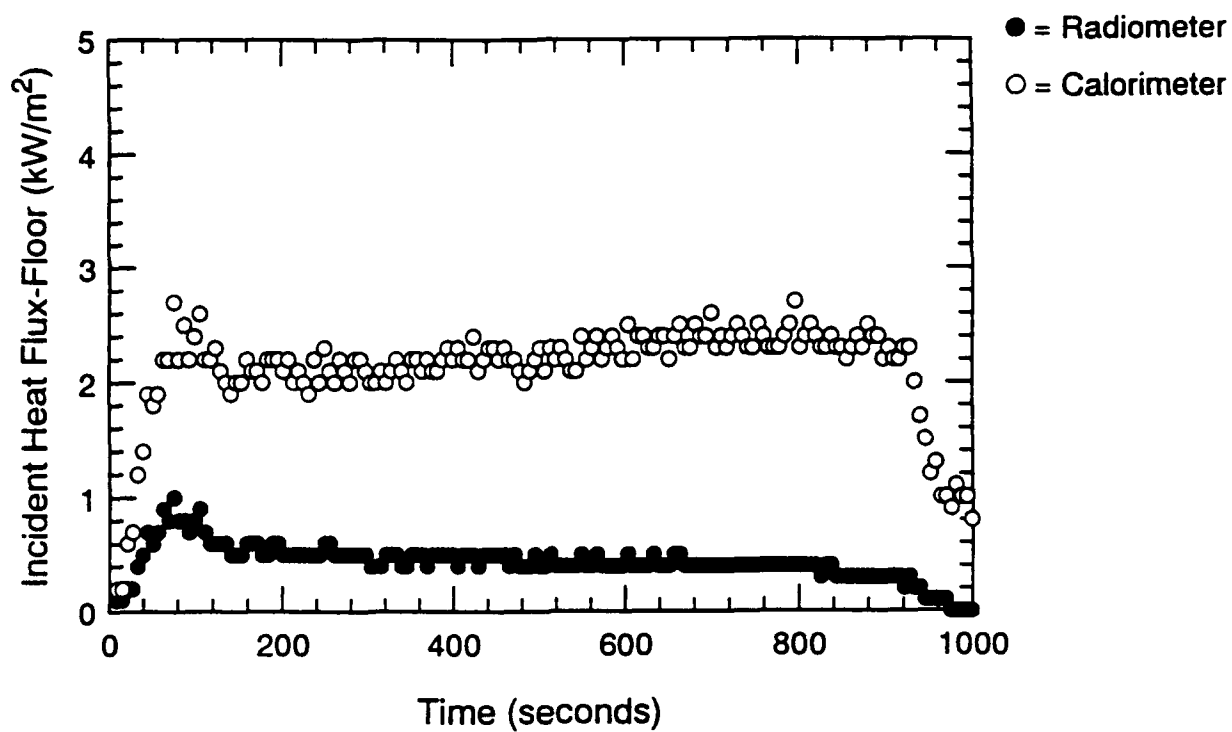


Figure A.107 Incident Heat Flux at Floor and Ceiling-Time Histories - S112

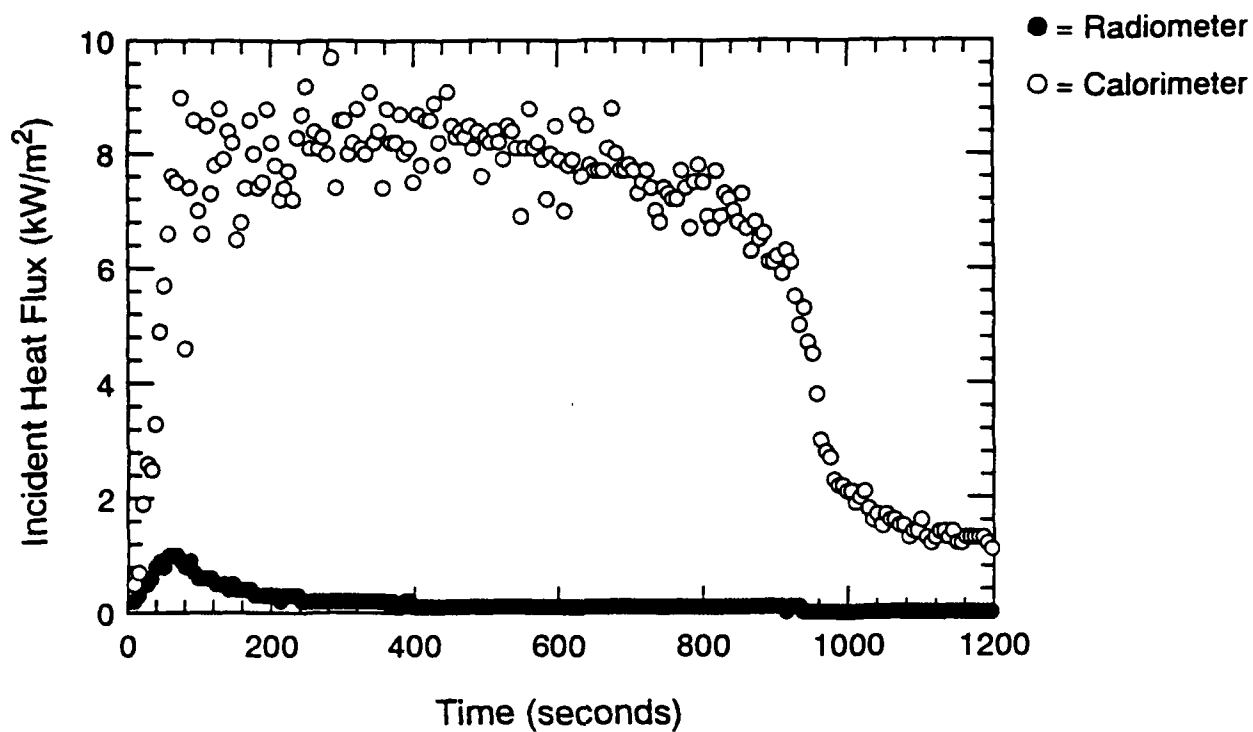


Figure A.108 Incident Heat Flux at Fwd. Bulkhead-Time Histories - S112

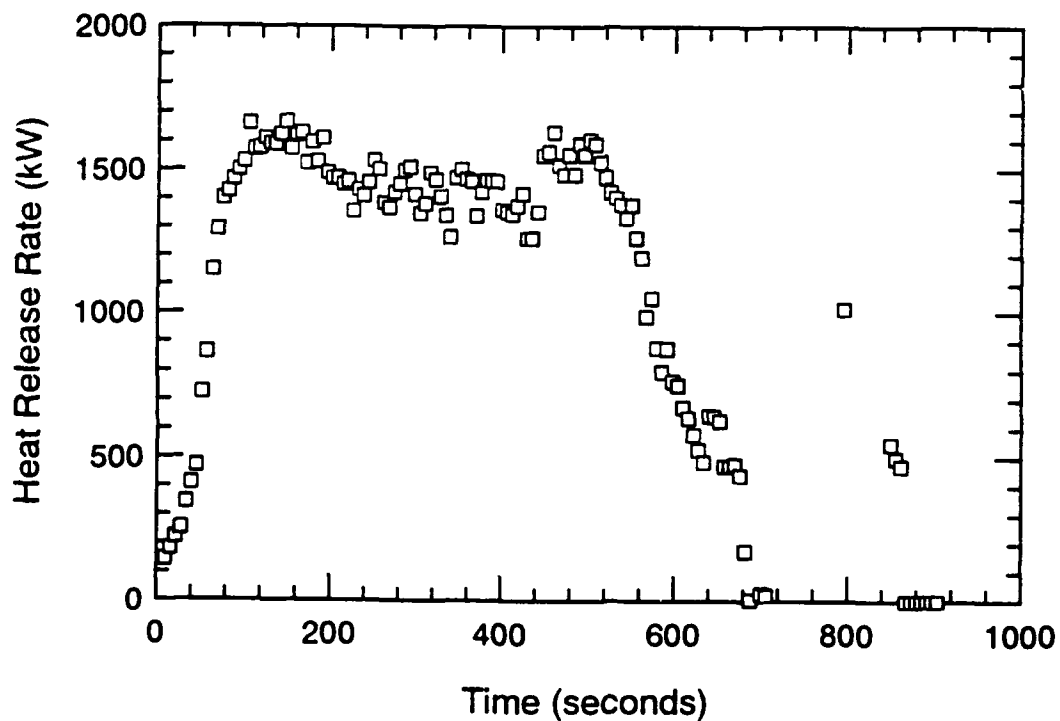
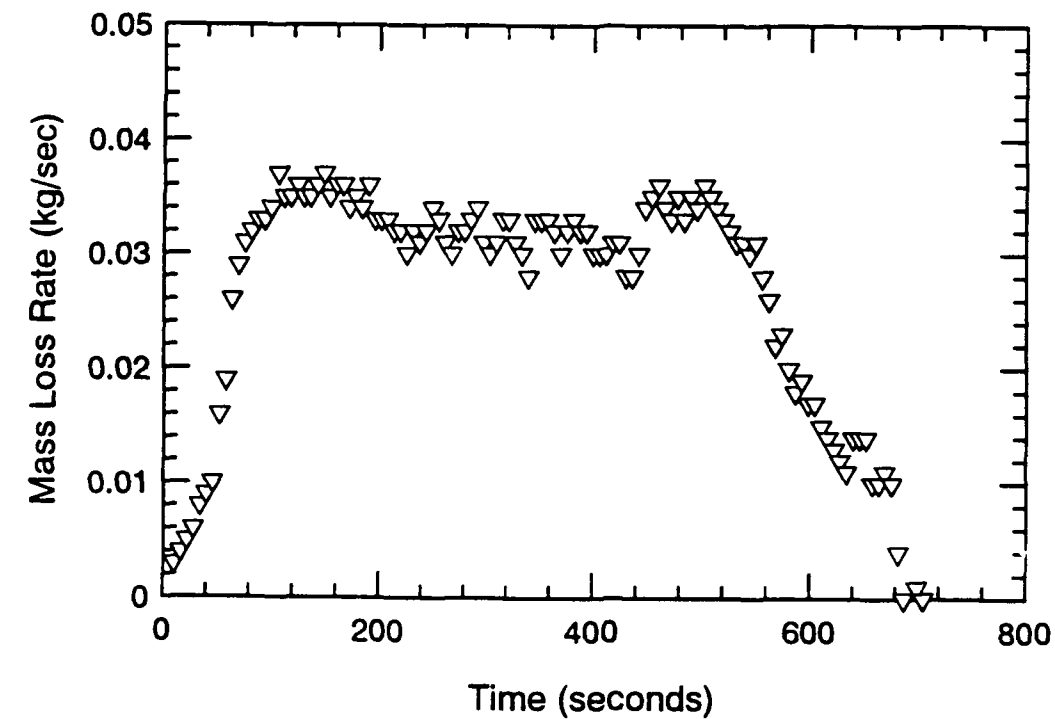


Figure A.109 Mass Loss Rate and Heat Release Rate-Time Histories - ADD1

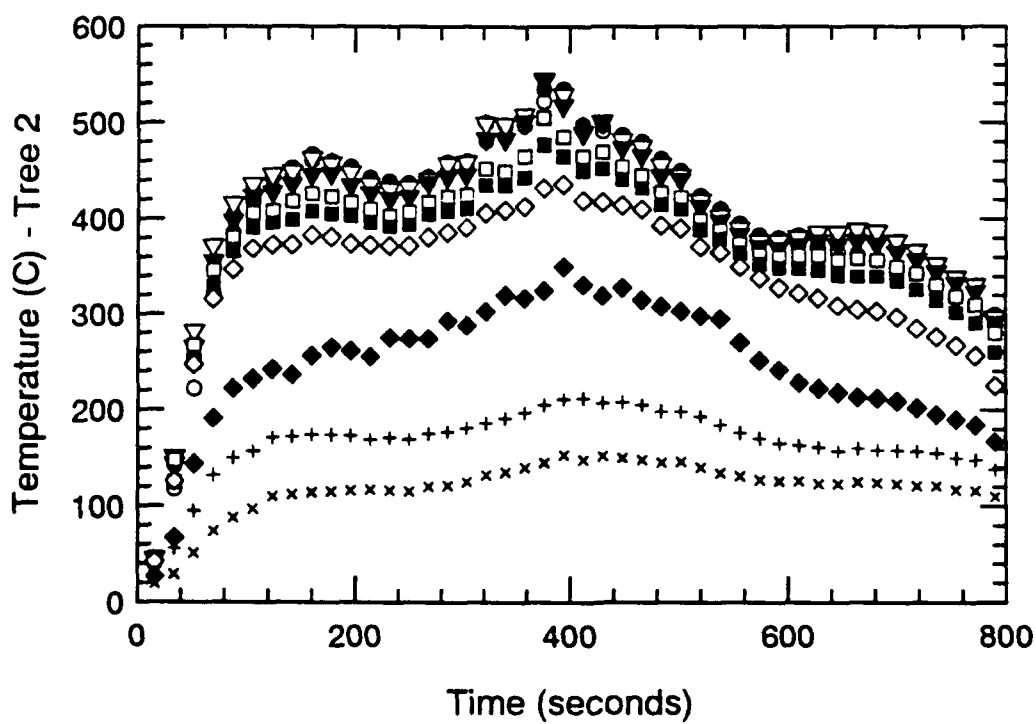
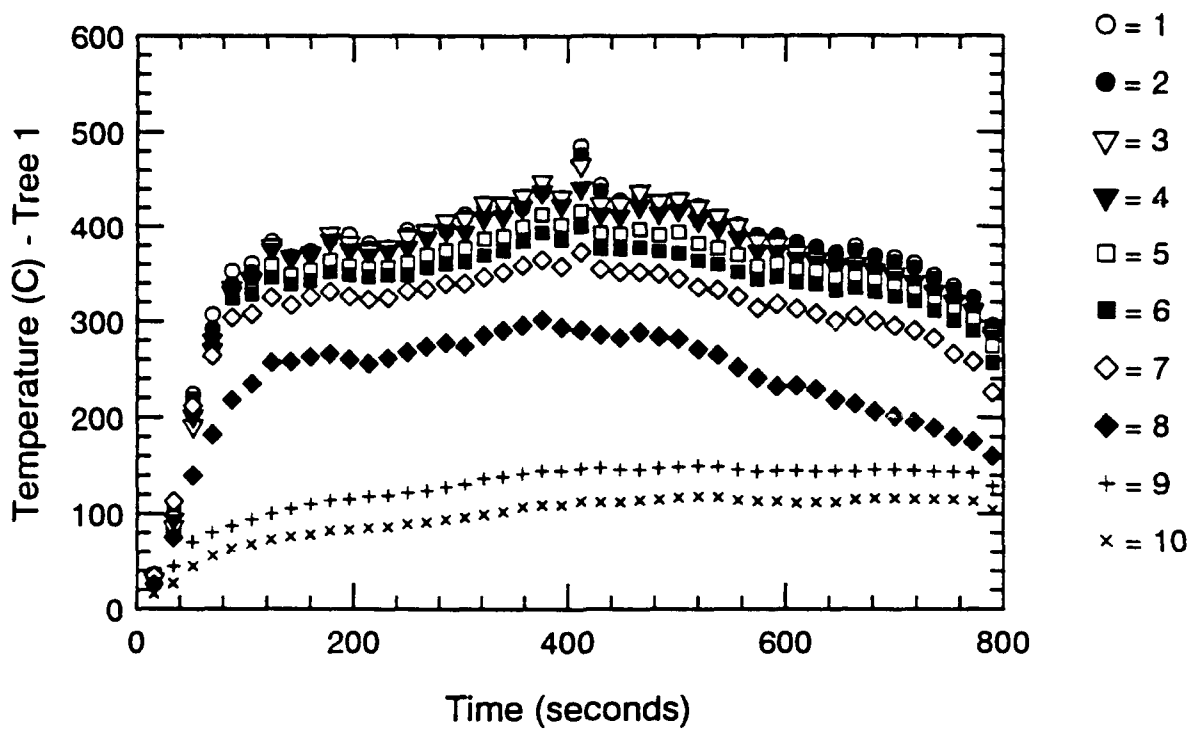


Figure A.110 Thermocouple Trees 1 & 2-Time Histories - ADD1

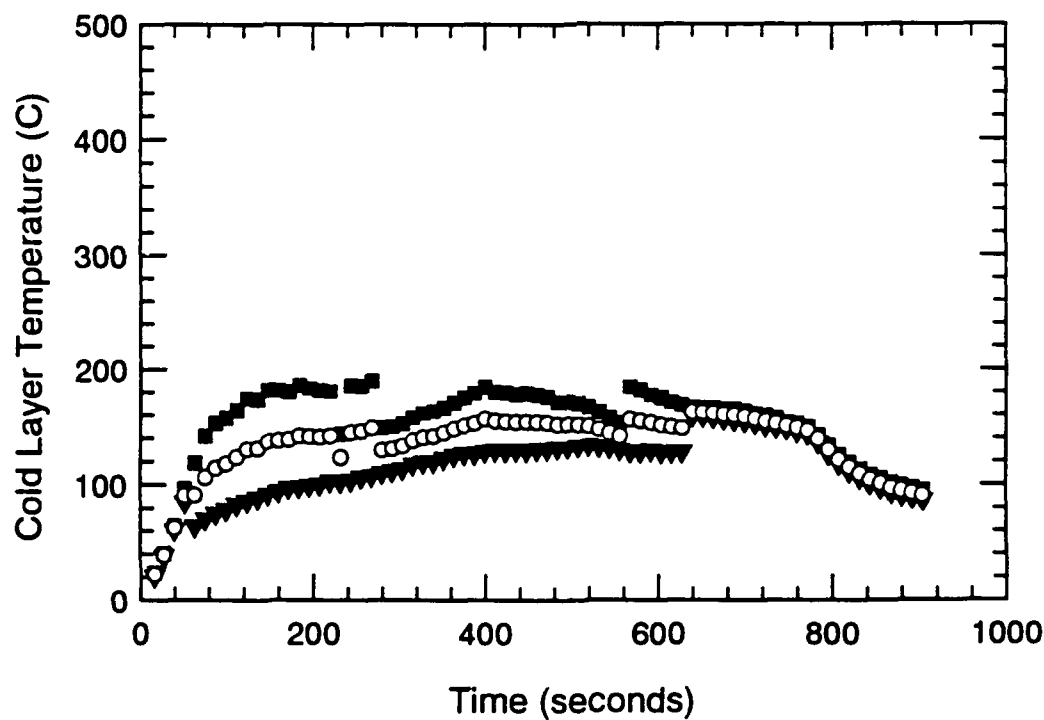
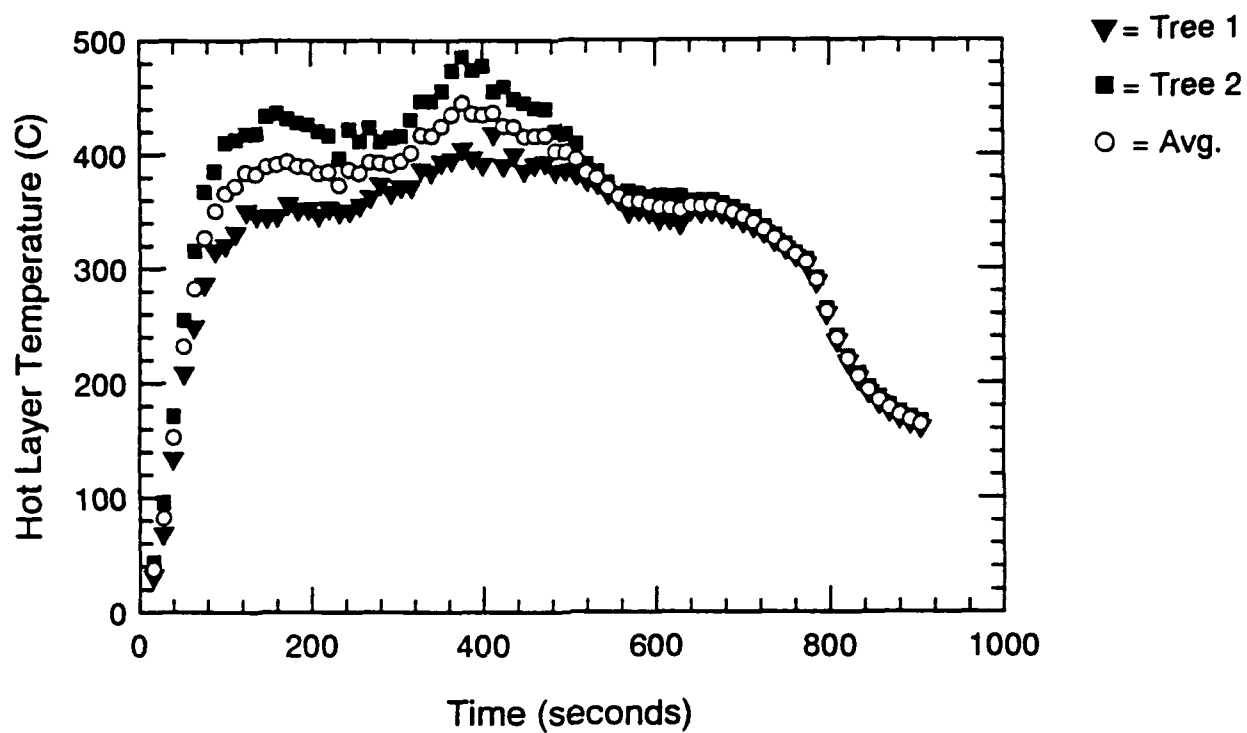


Figure A.111 Hot and Cold Layer Temperature-Time Histories - ADD1

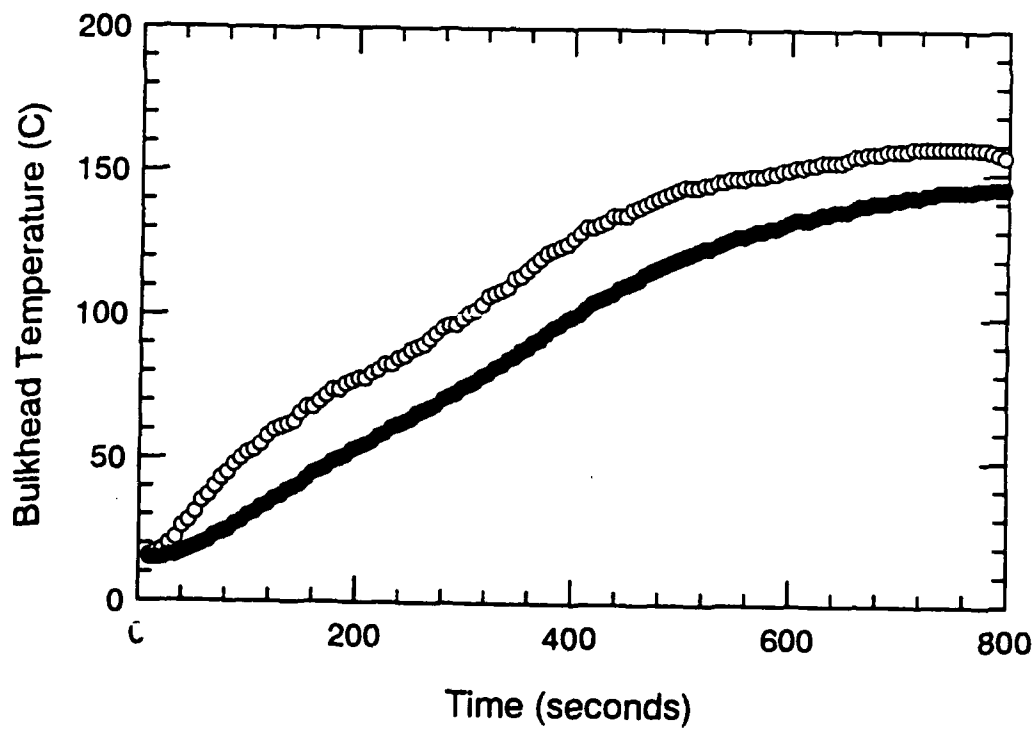
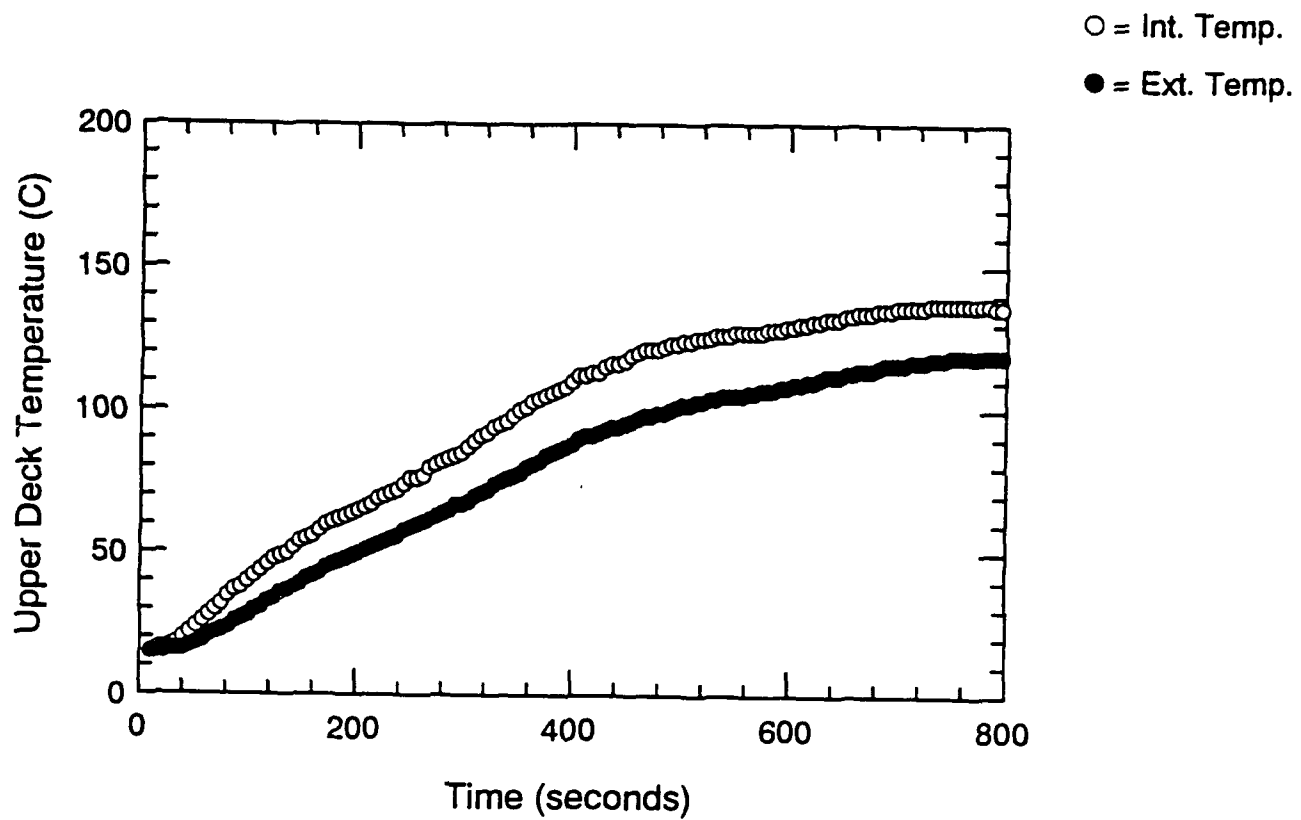


Figure A.112 Surface Thermocouple-Time Histories - ADD1

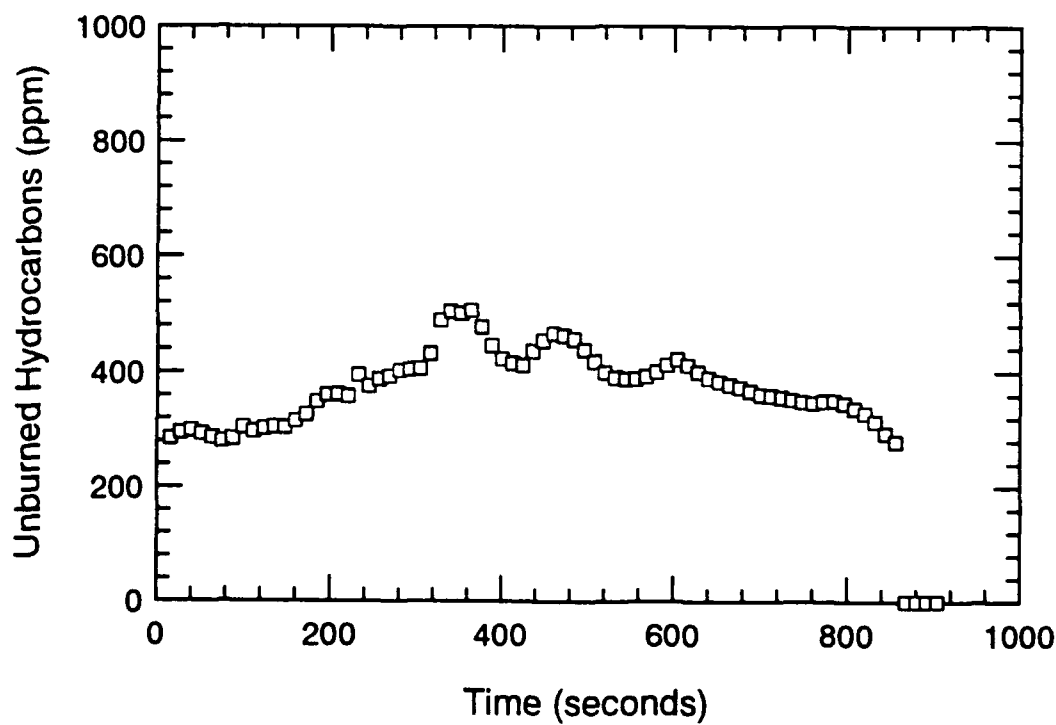
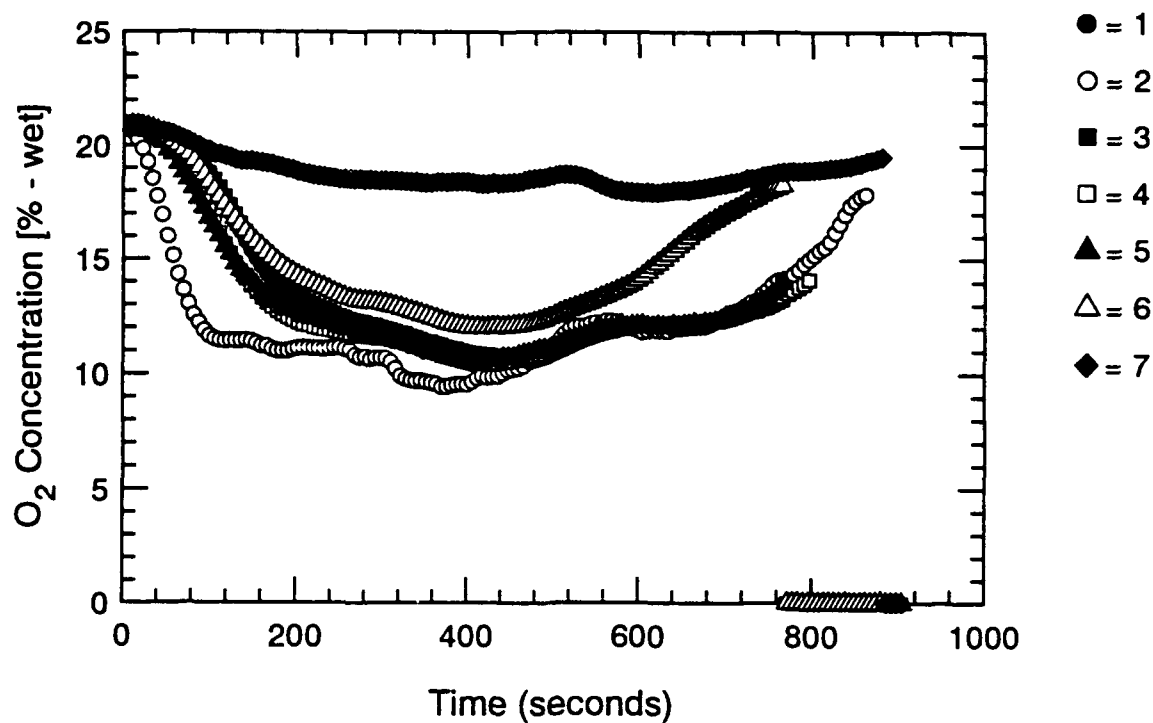


Figure A.113 Oxygen and Unburned HC Concentration-Time Histories - ADD1

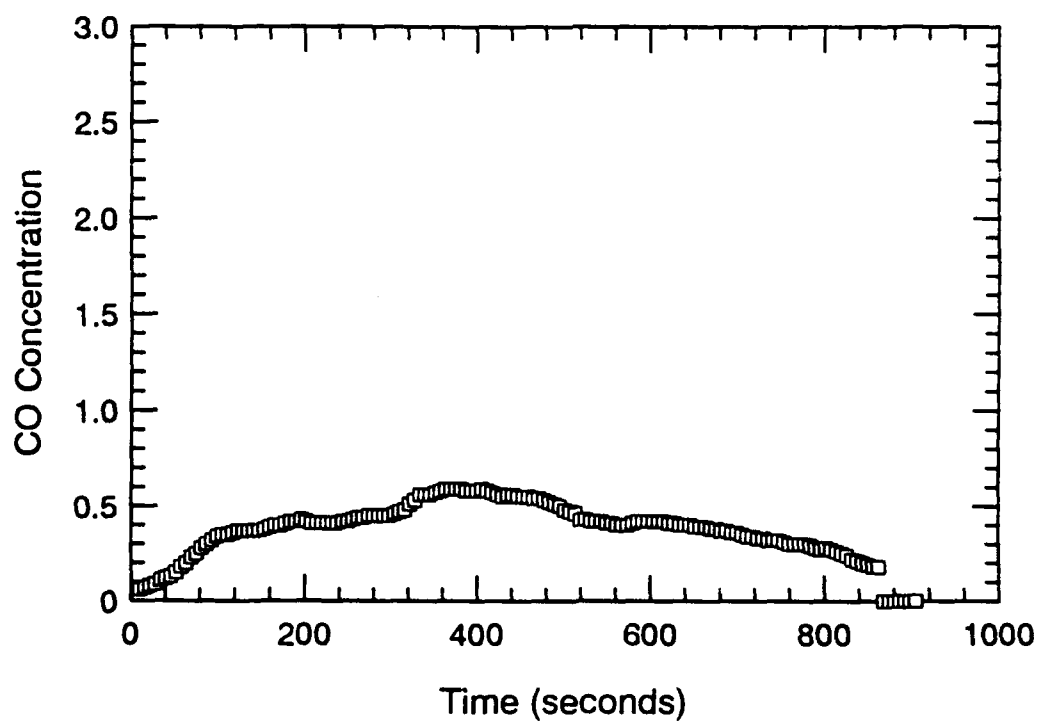
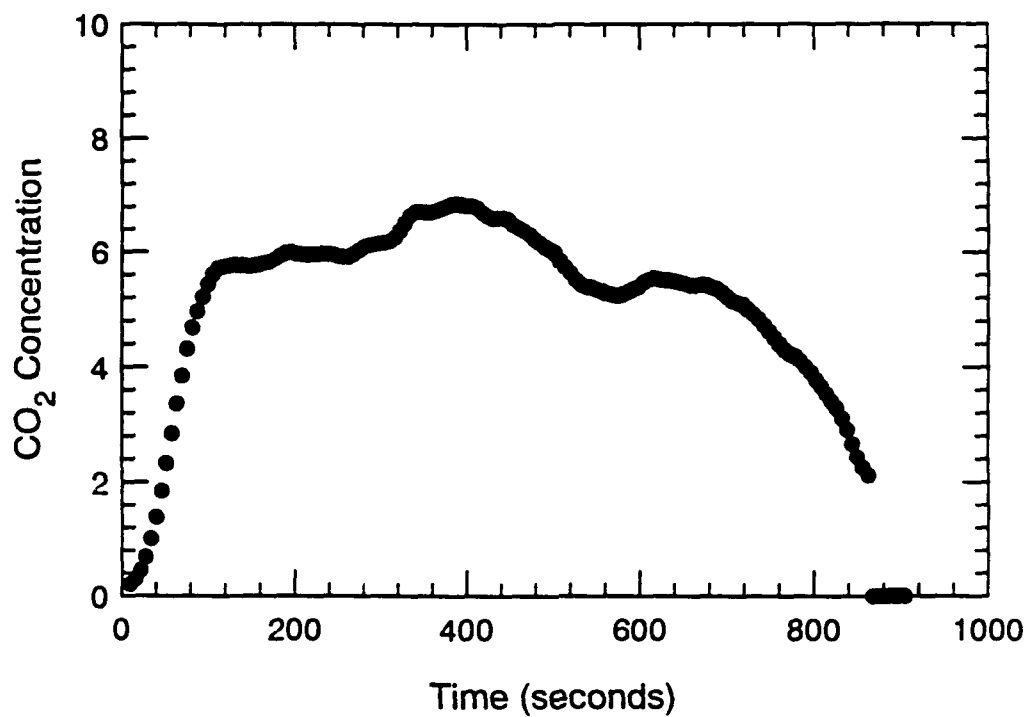


Figure A.114 CO₂ and CO Concentration-Time Histories - ADD1

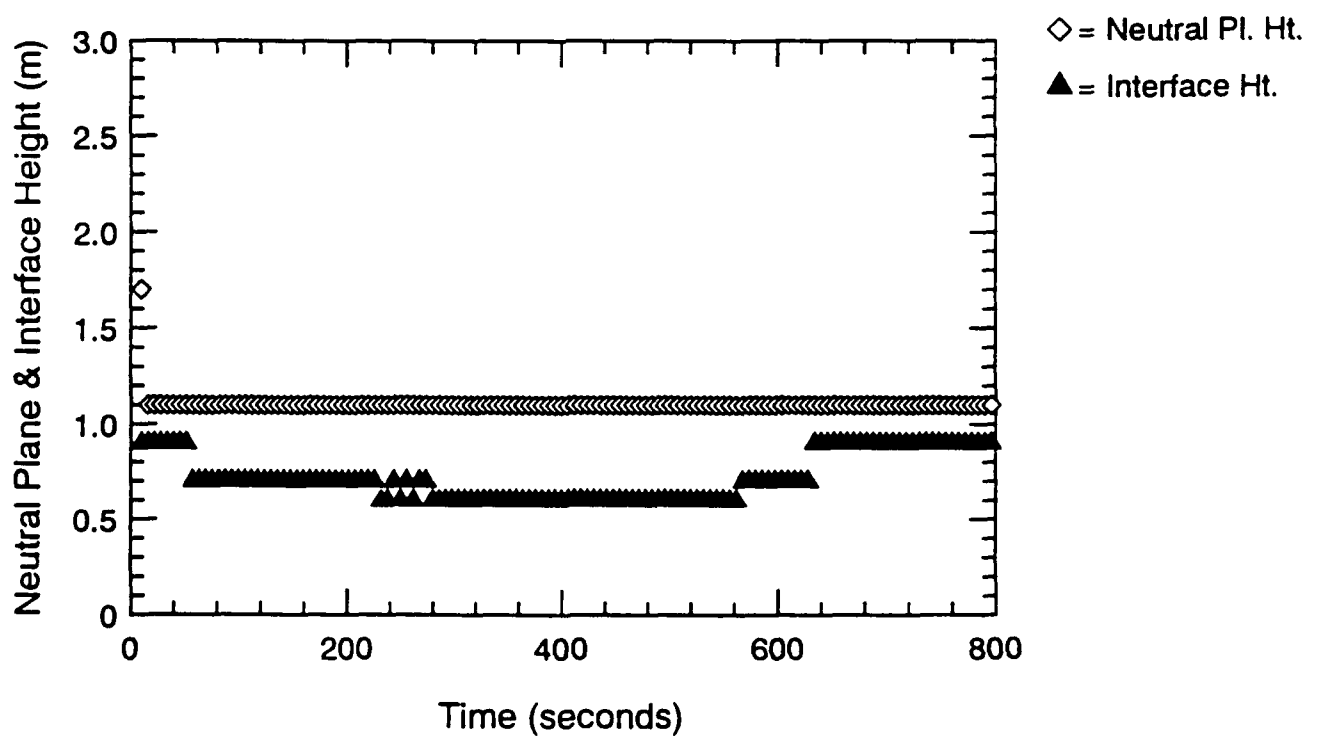
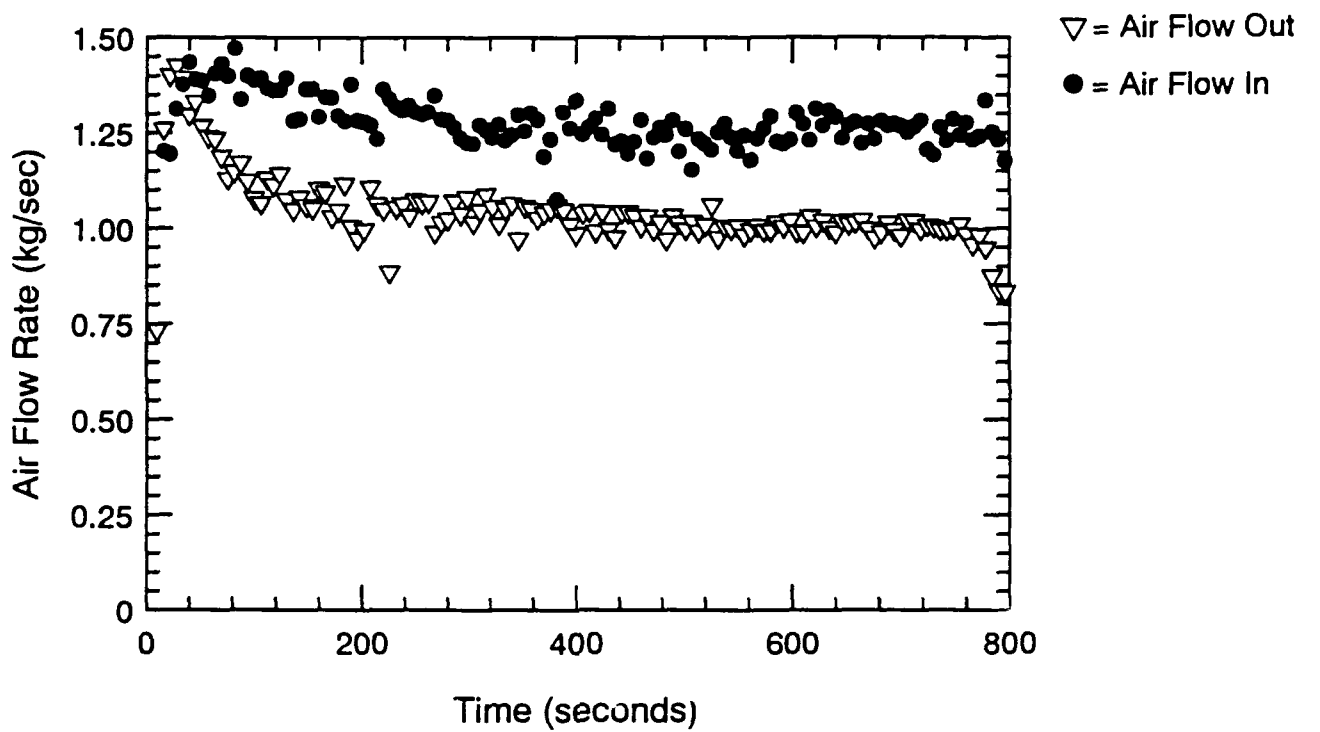


Figure A.115 Air Flow Rate, Neutral Plane & Interface Ht.-Time Histories - ADD1

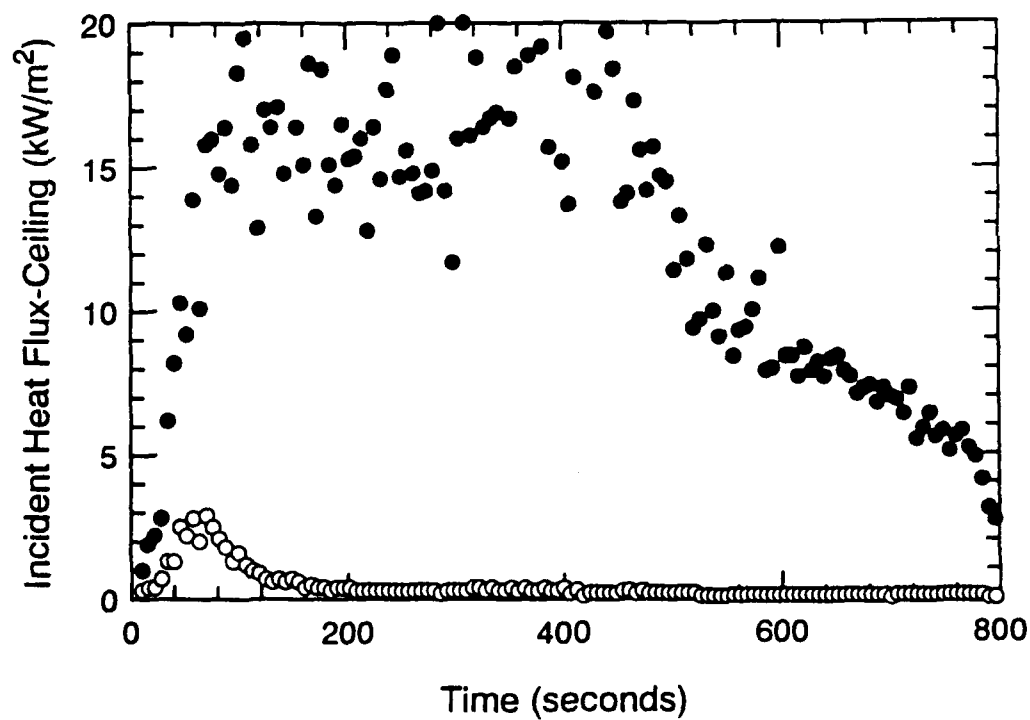
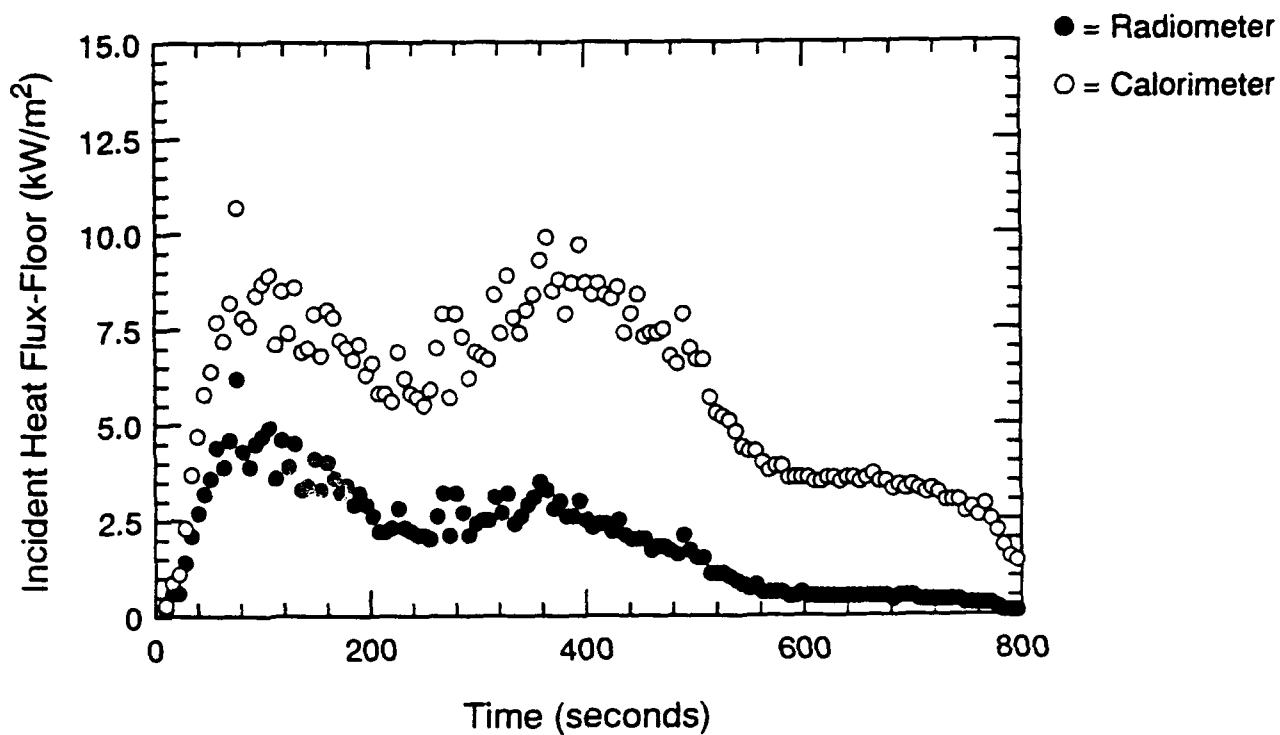


Figure A.116 Incident Heat Flux at Floor and Ceiling-Time Histories - ADD1

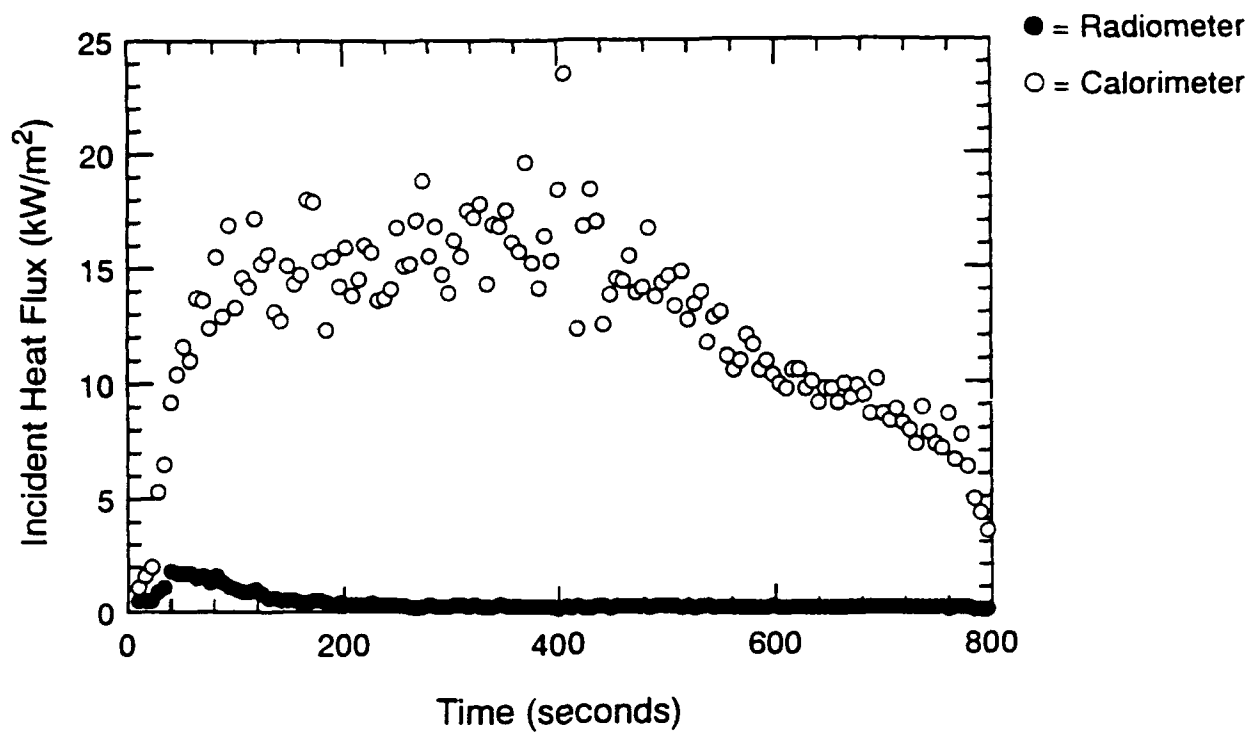


Figure A.117 Incident Heat Flux at Fwd. Bulkhead-Time Histories - ADD1

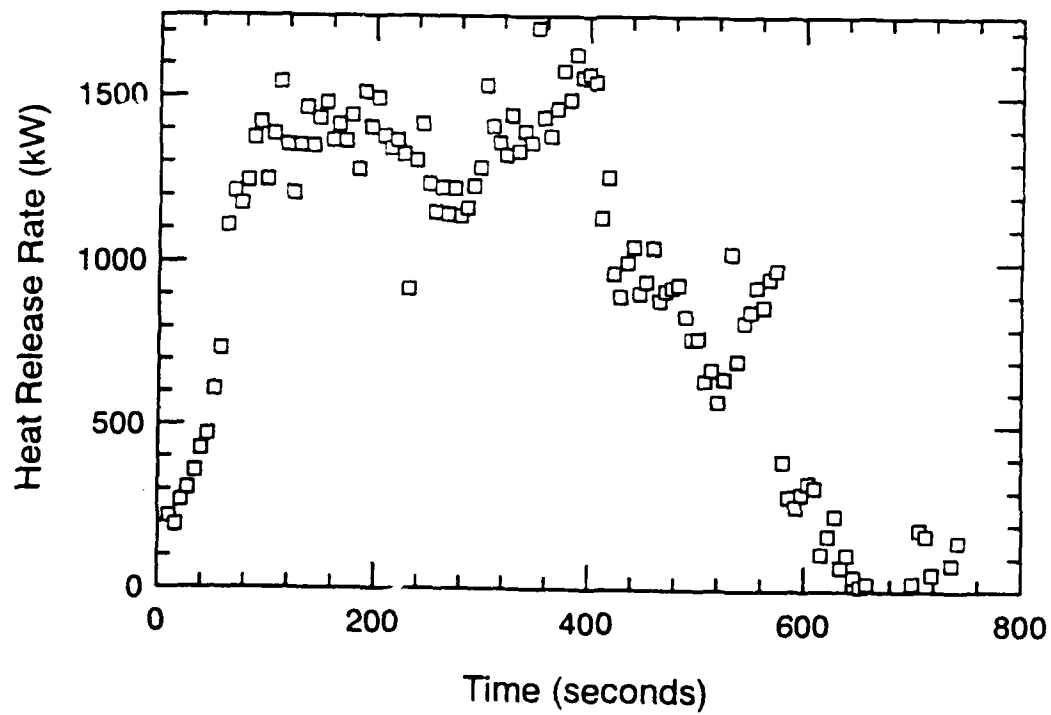
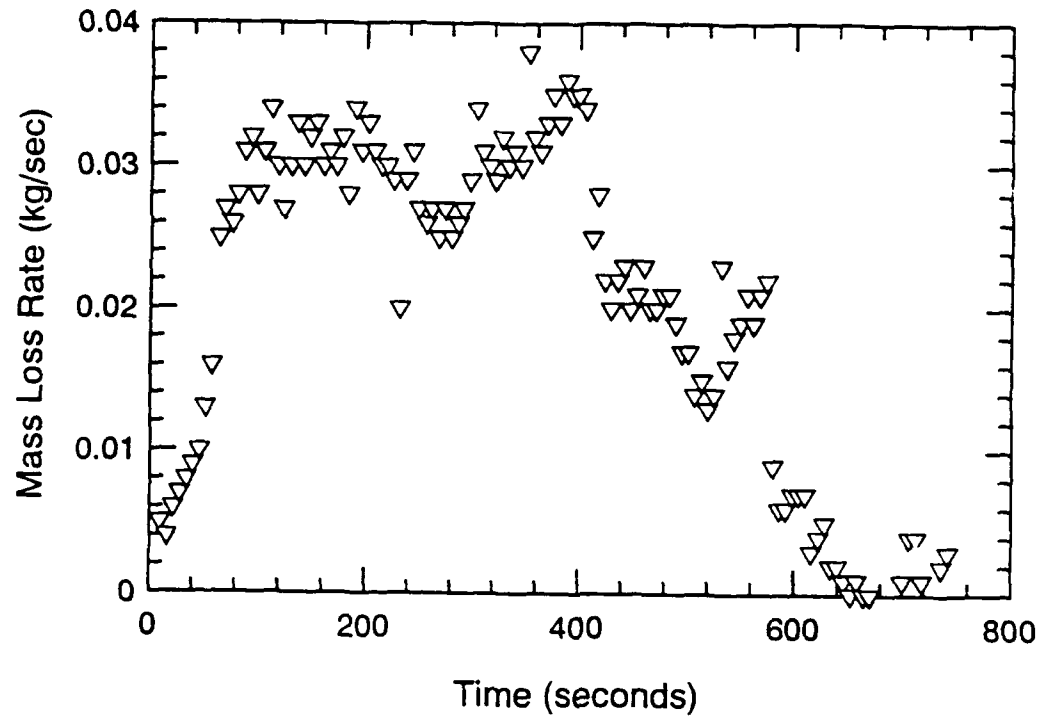


Figure A.118 Mass Loss Rate and Heat Release Rate-Time Histories - ADD2

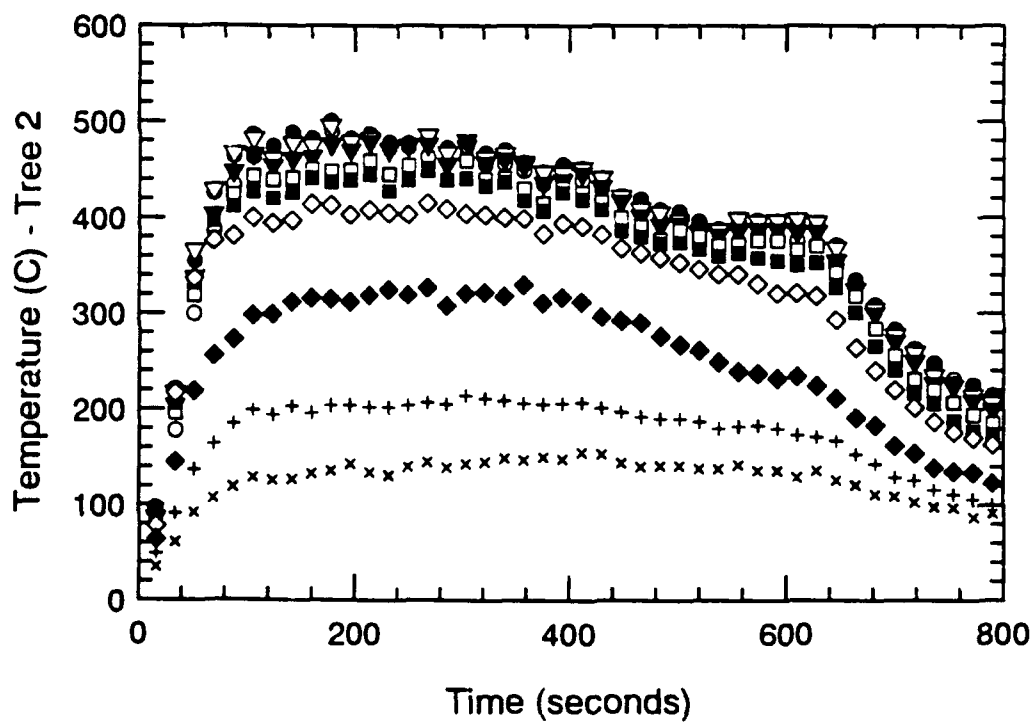
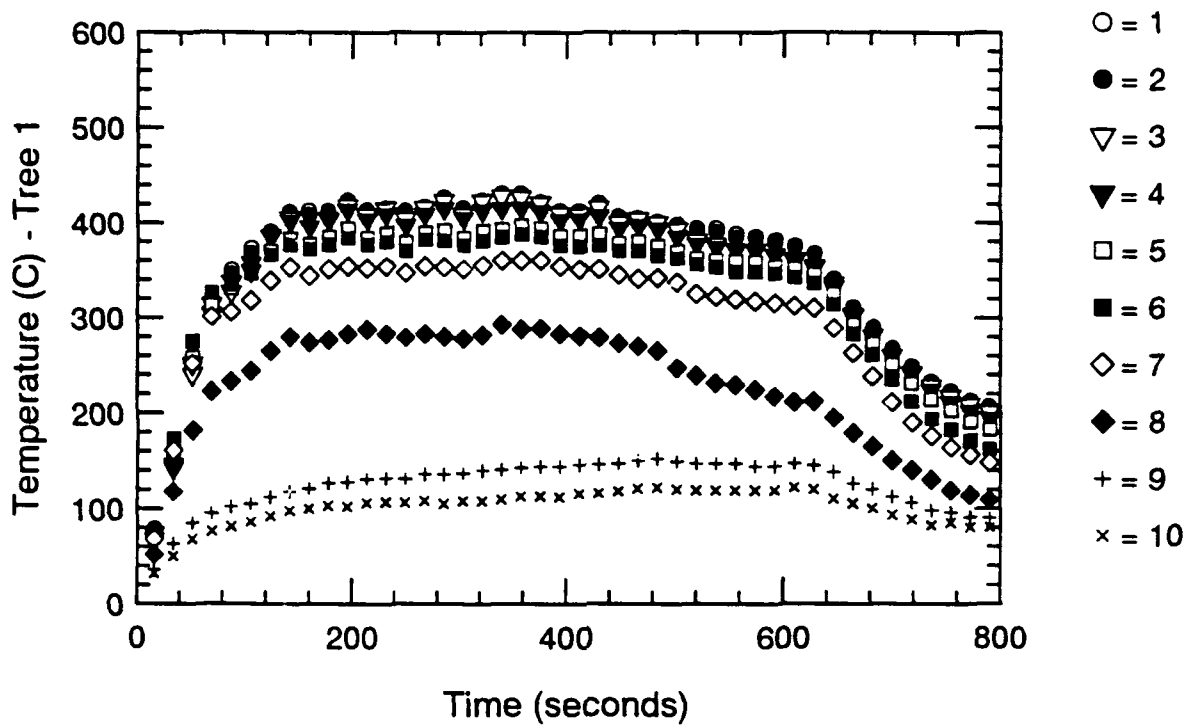


Figure A.119 Thermocouple Trees 1 & 2-Time Histories - ADD2

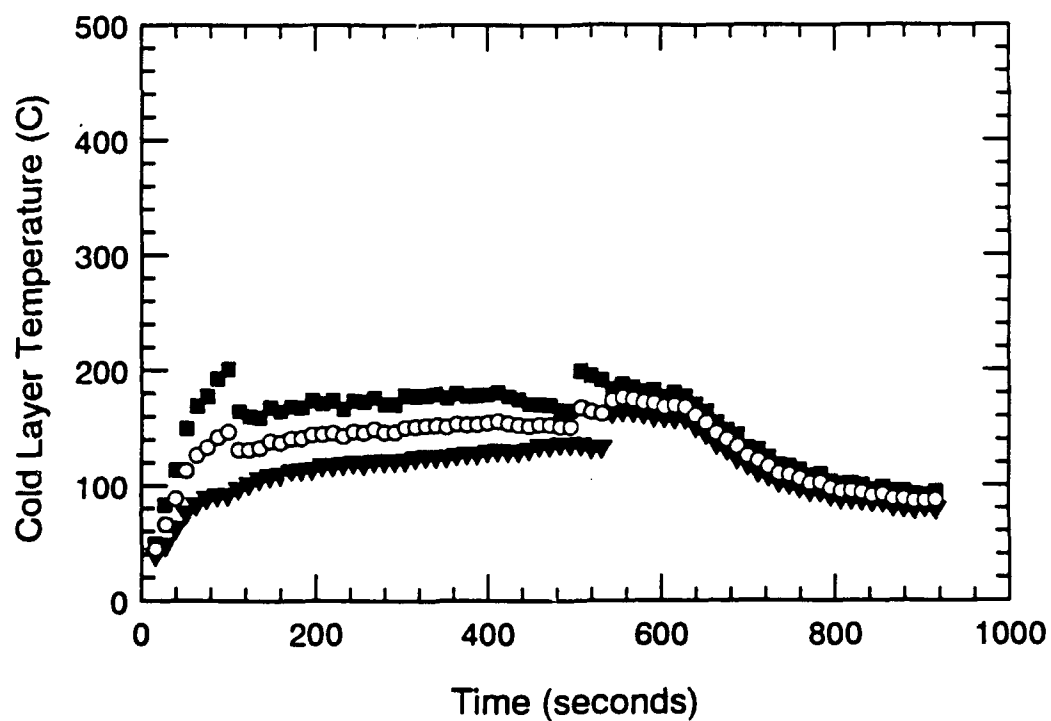
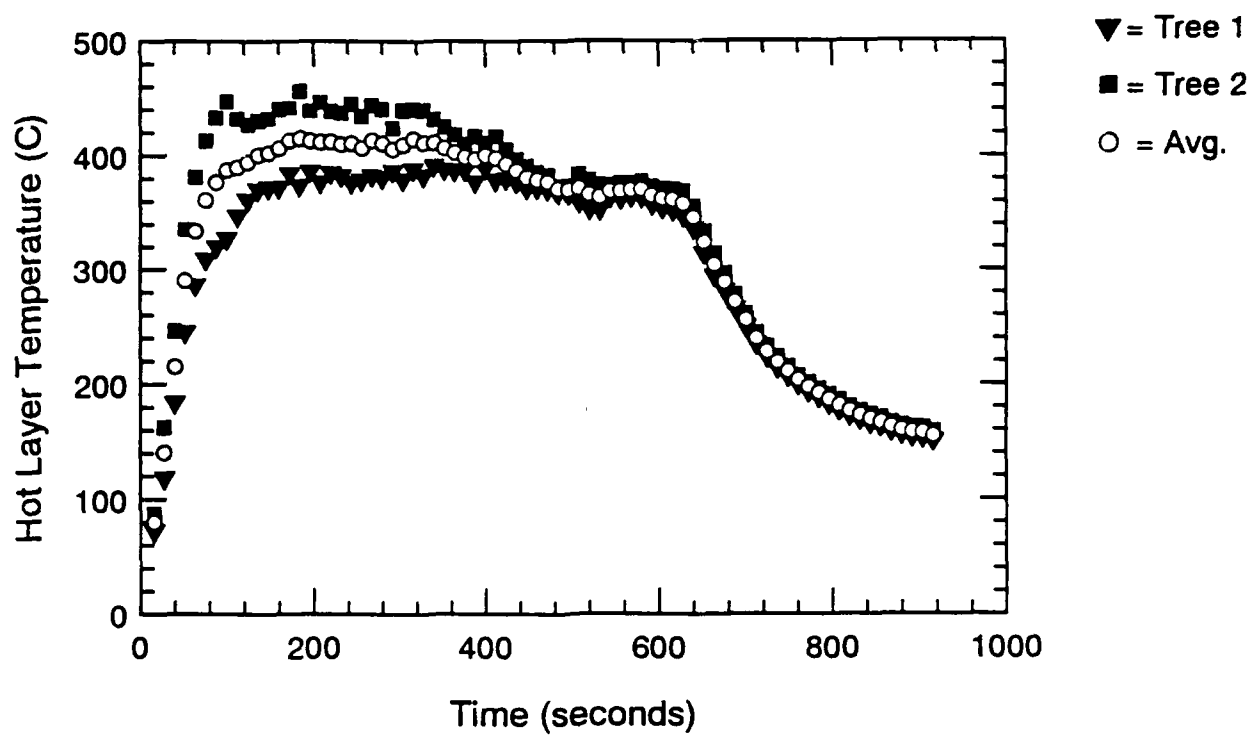


Figure A.120 Hot and Cold Layer Temperature-Time Histories - ADD2

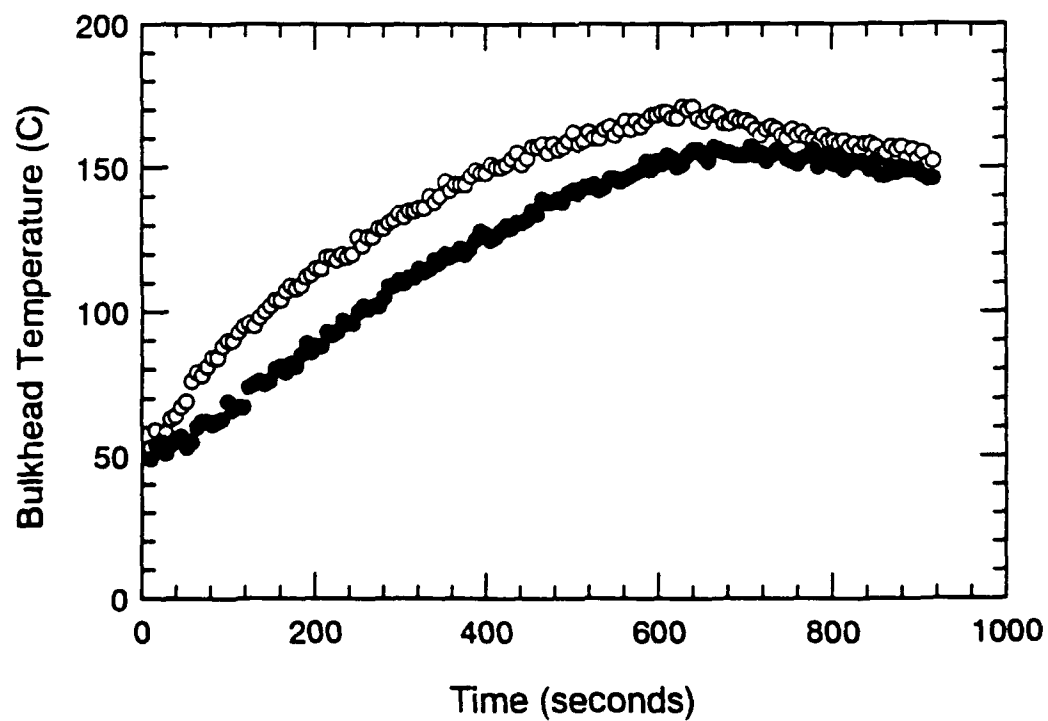
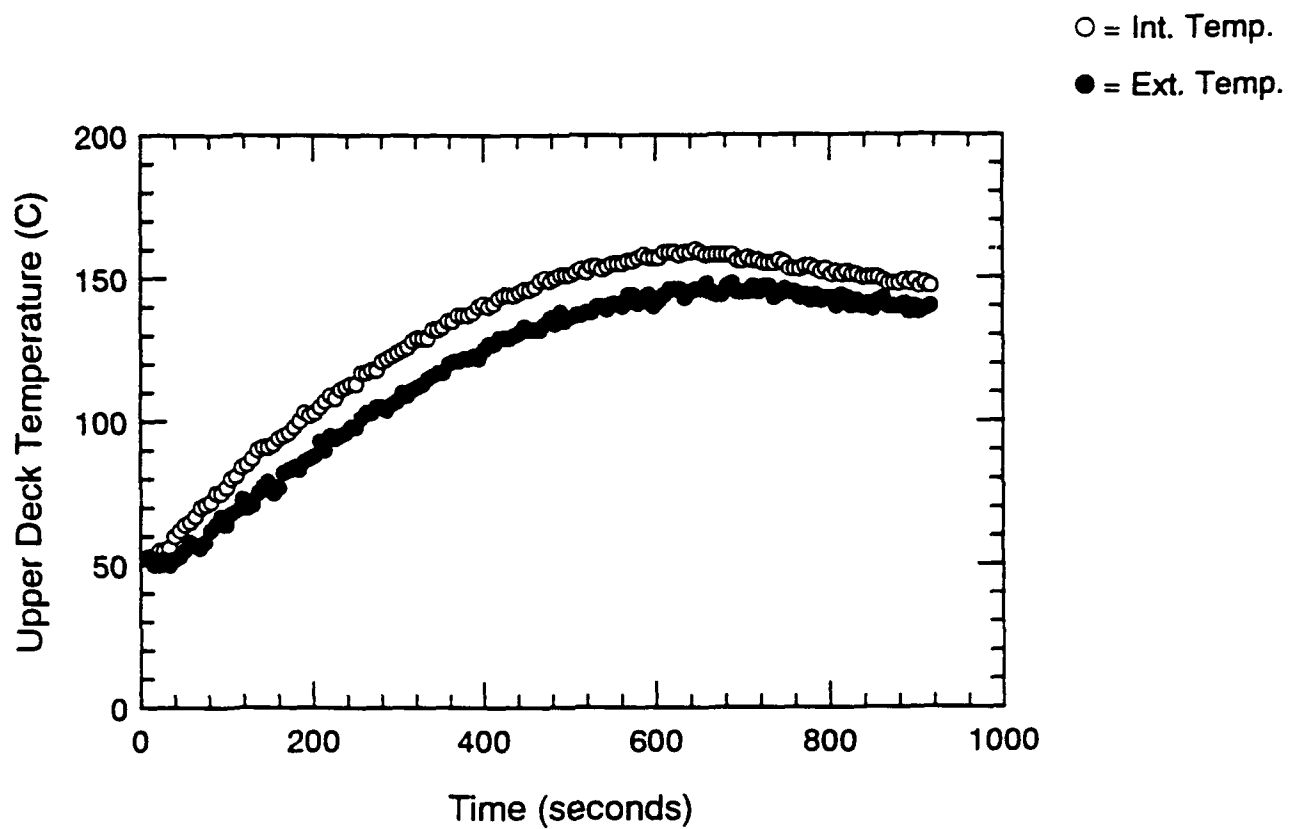


Figure A.121 Surface Thermocouple-Time Histories - ADD2

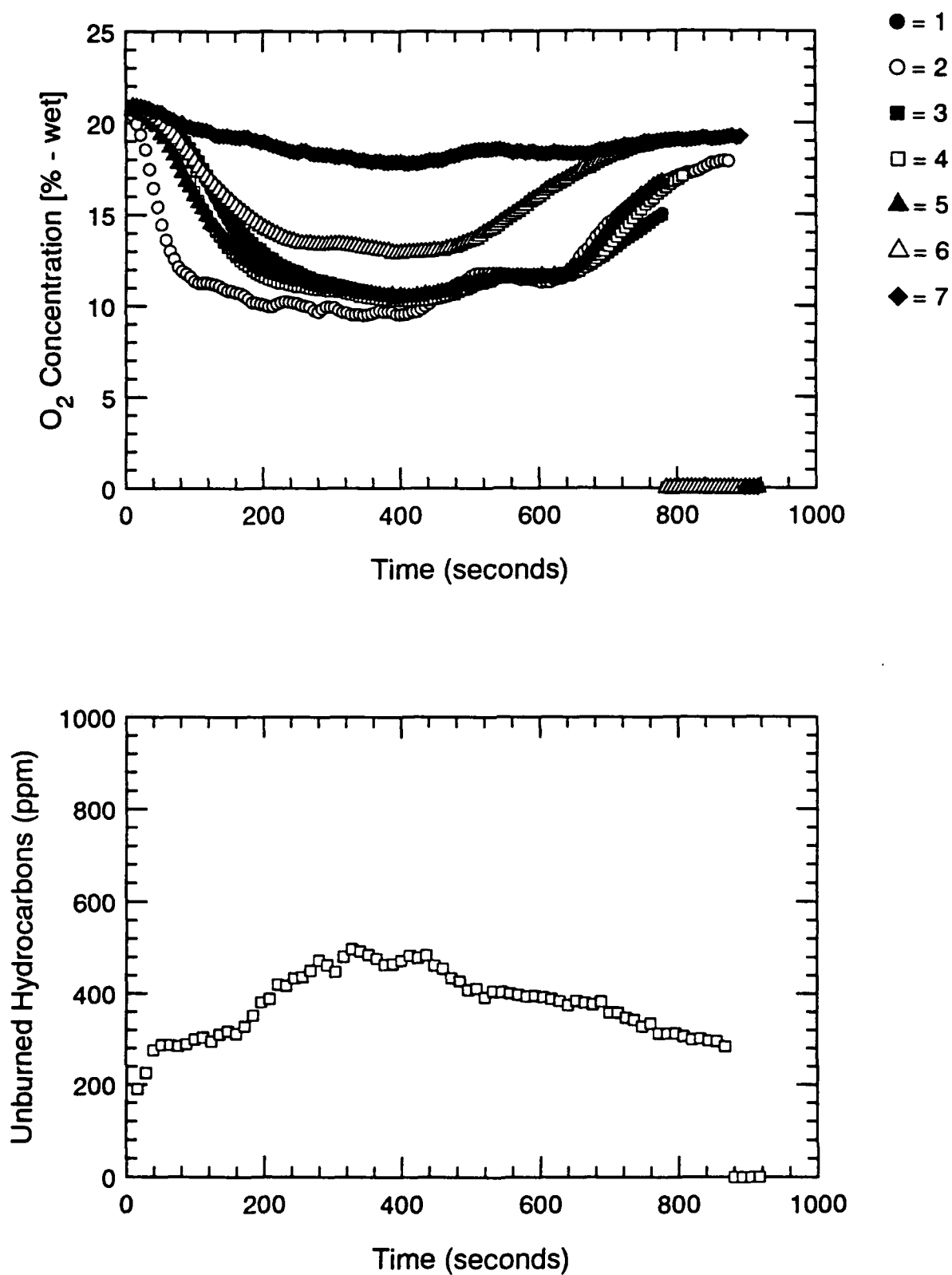


Figure A.122 Oxygen and Unburned HC Concentration-Time Histories - ADD2

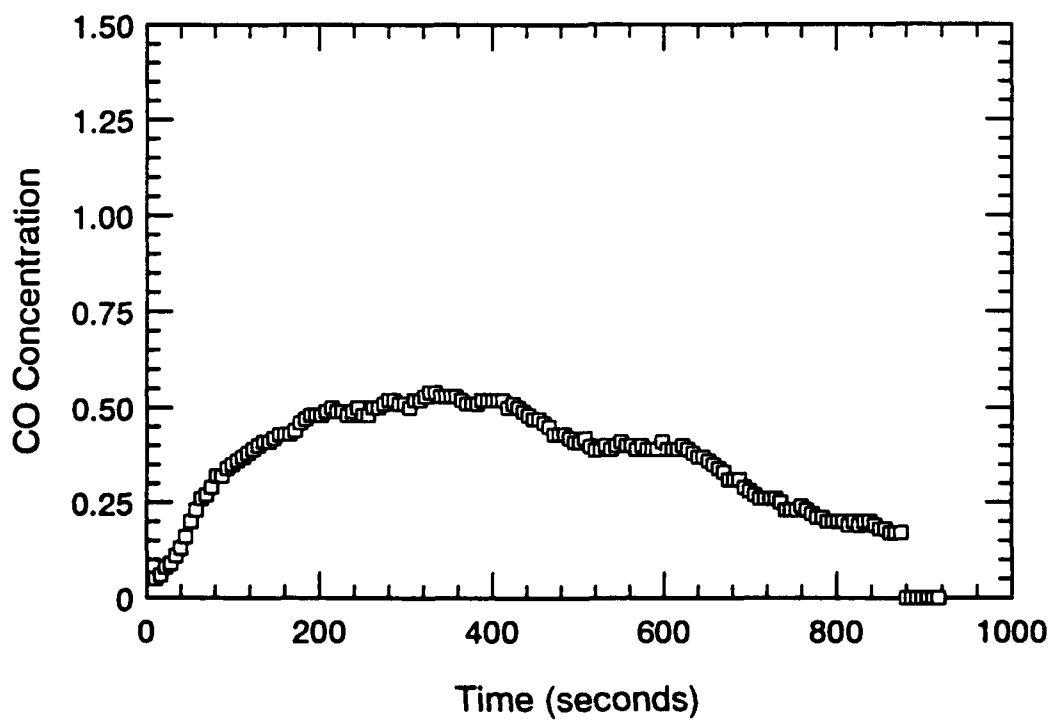
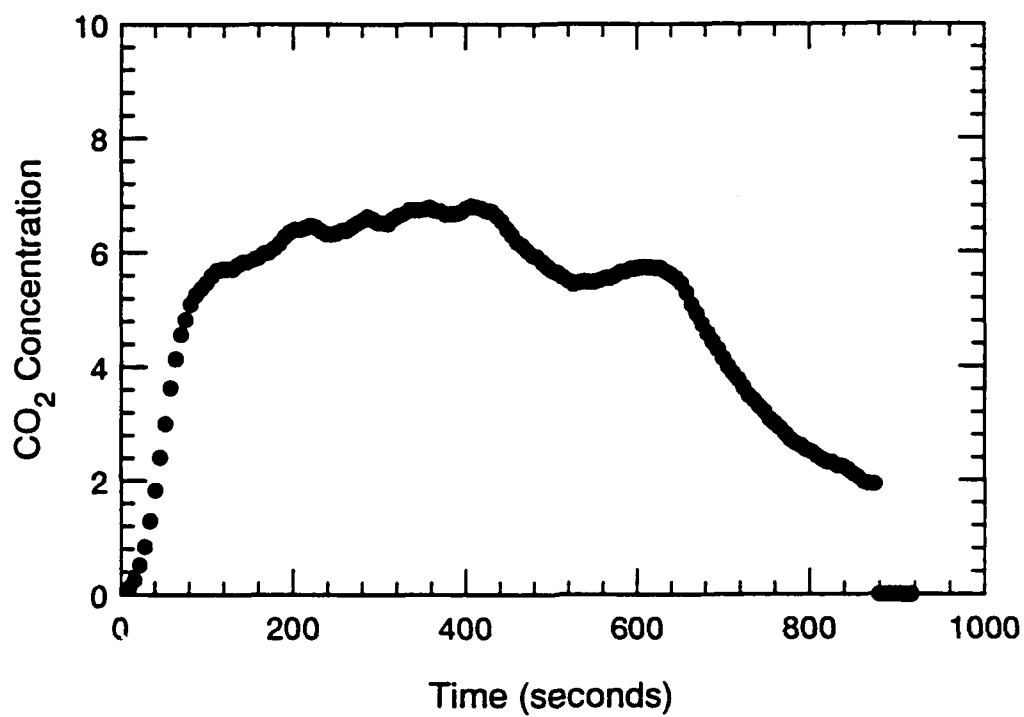


Figure A.123 CO₂ and CO Concentration-Time Histories - ADD2

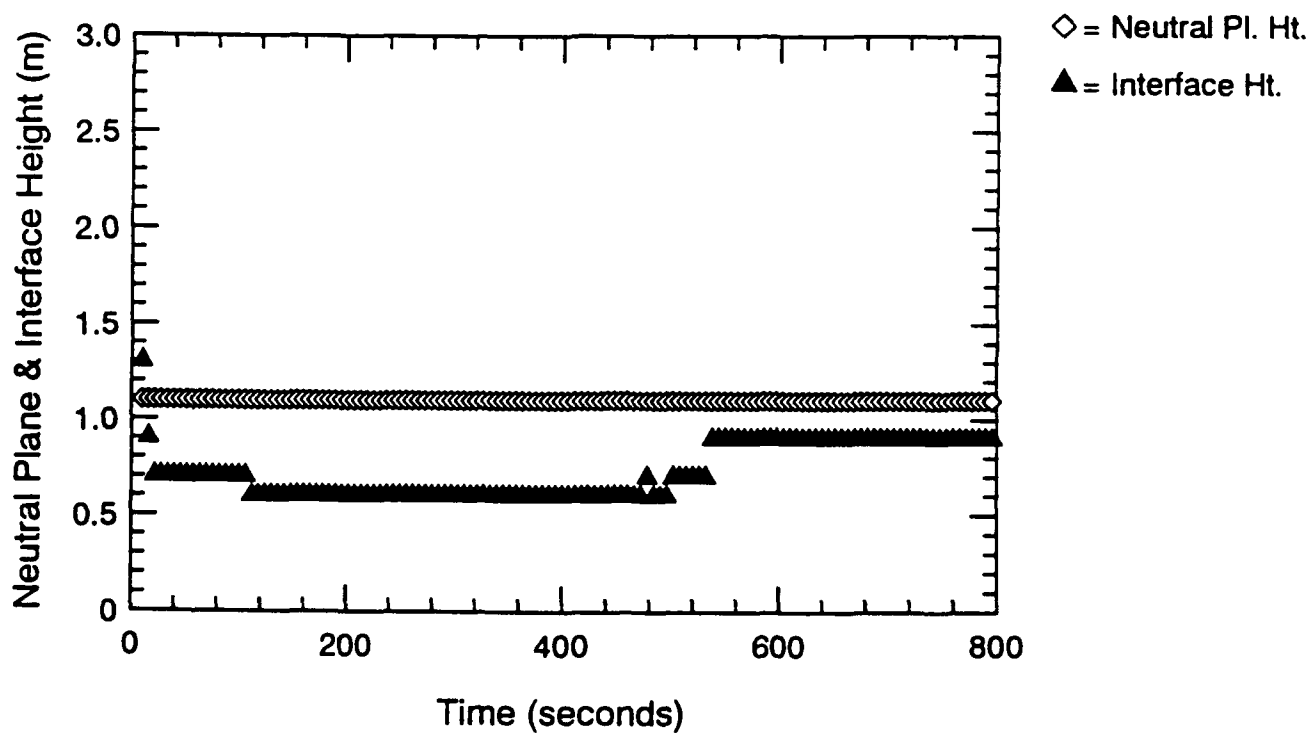
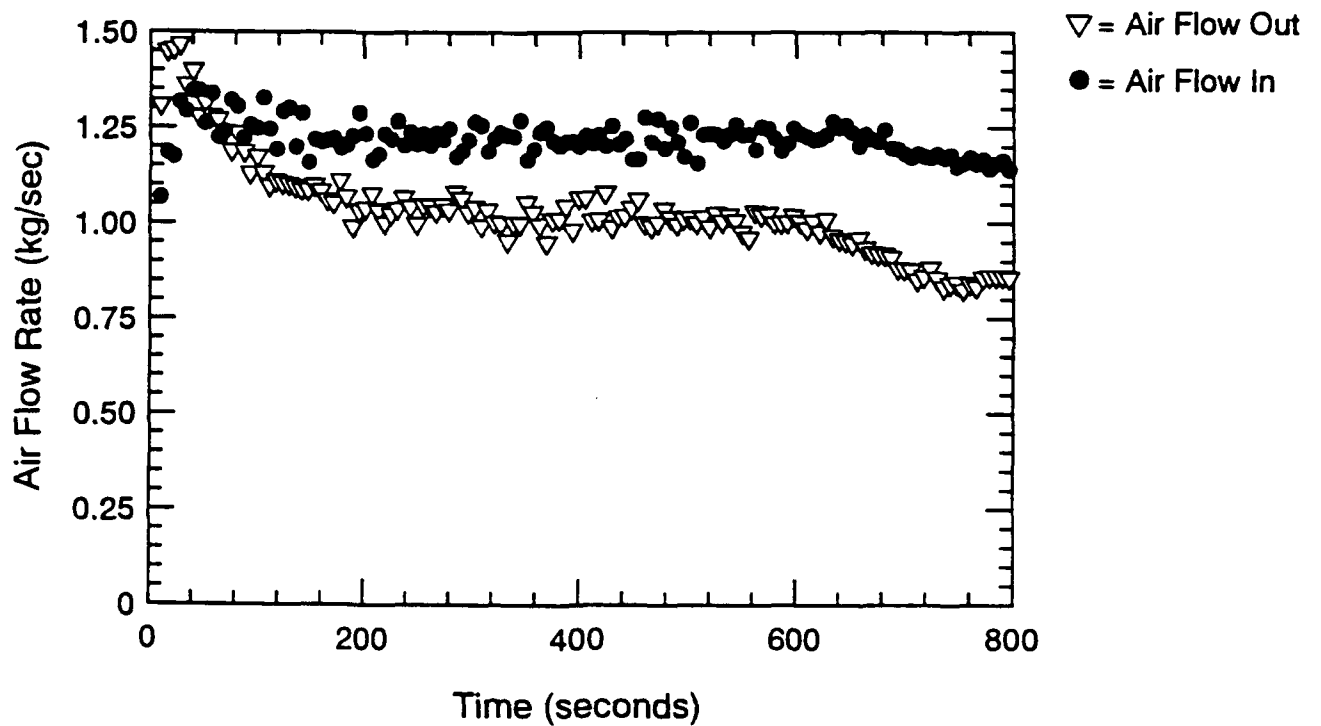


Figure A.124 Air Flow Rate, Neutral Plane & Interface Ht.-Time Histories - ADD2

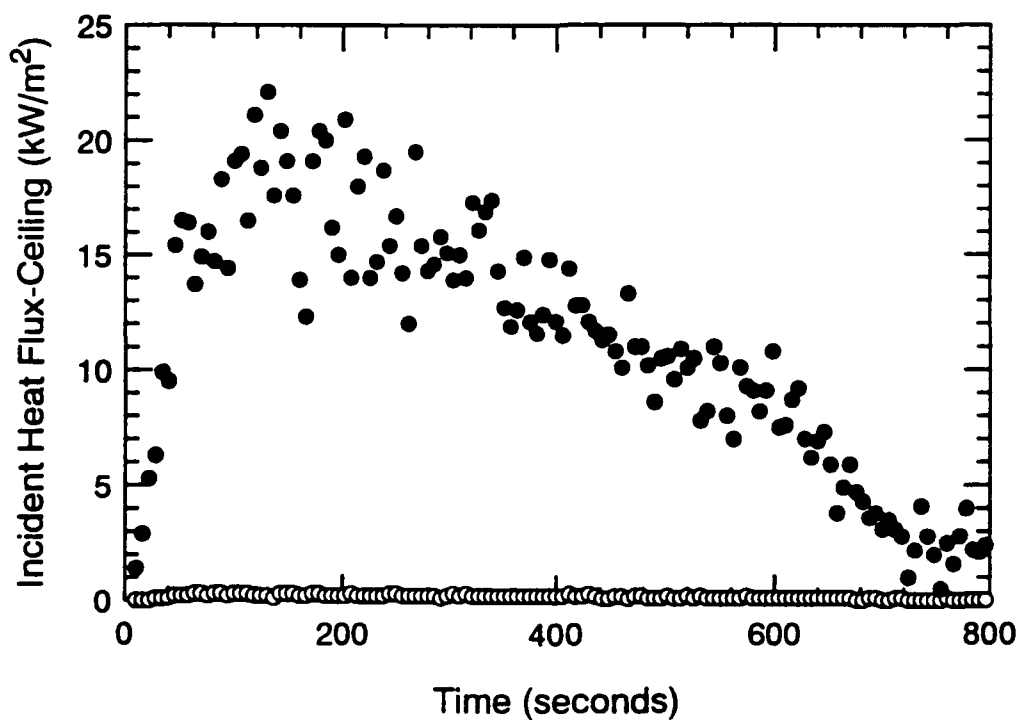
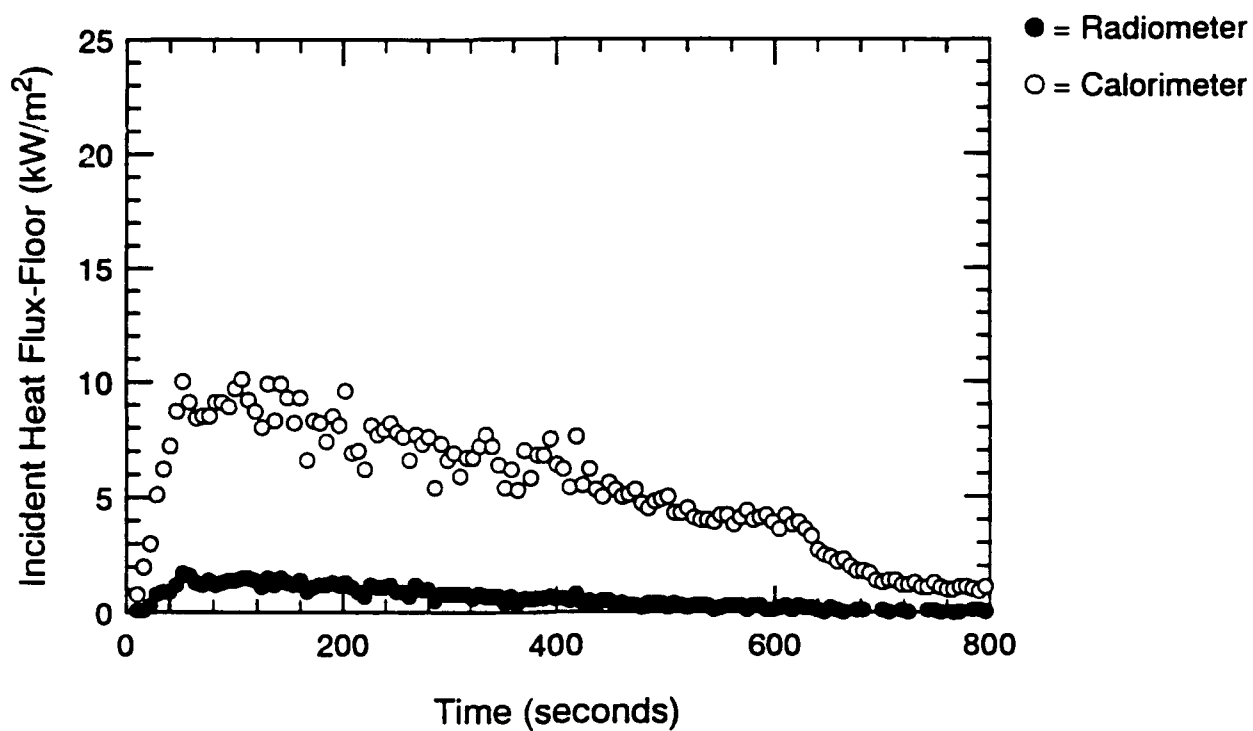


Figure A.125 Incident Heat Flux at Floor and Ceiling-Time Histories - ADD2

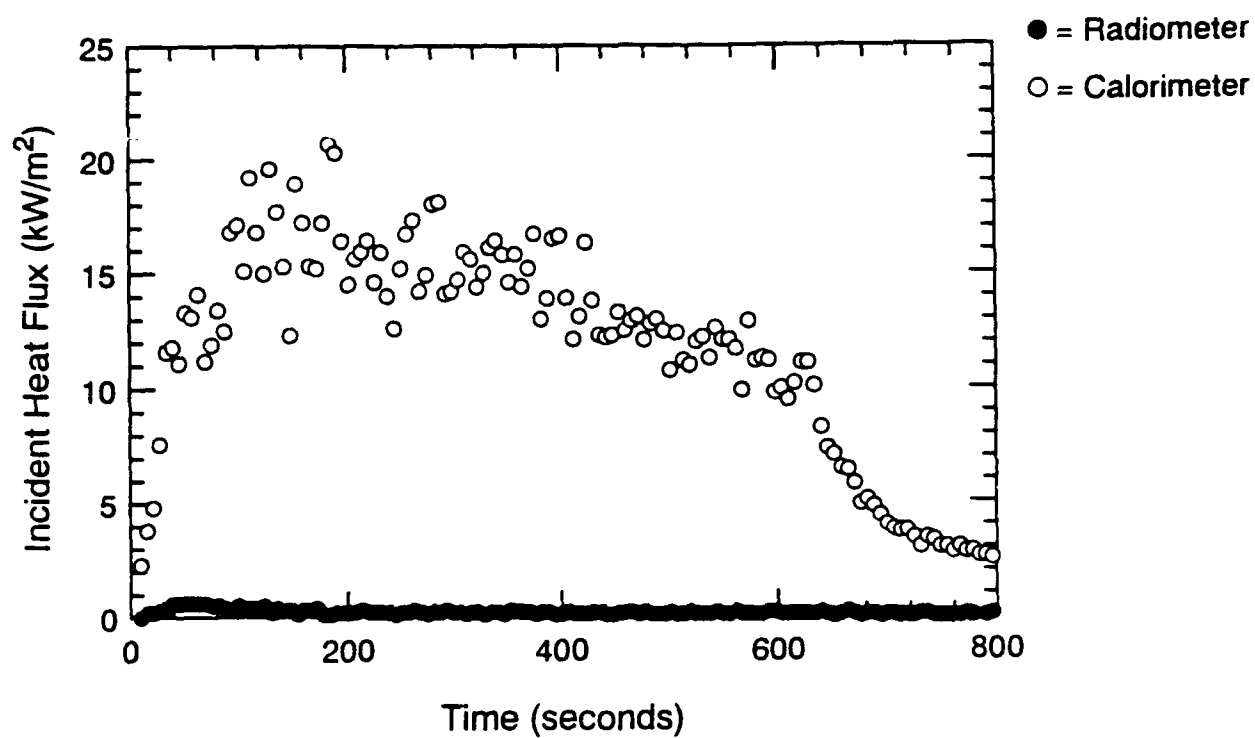


Figure A.126 Incident Heat Flux at Fwd. Bulkhead-Time Histories - ADD2

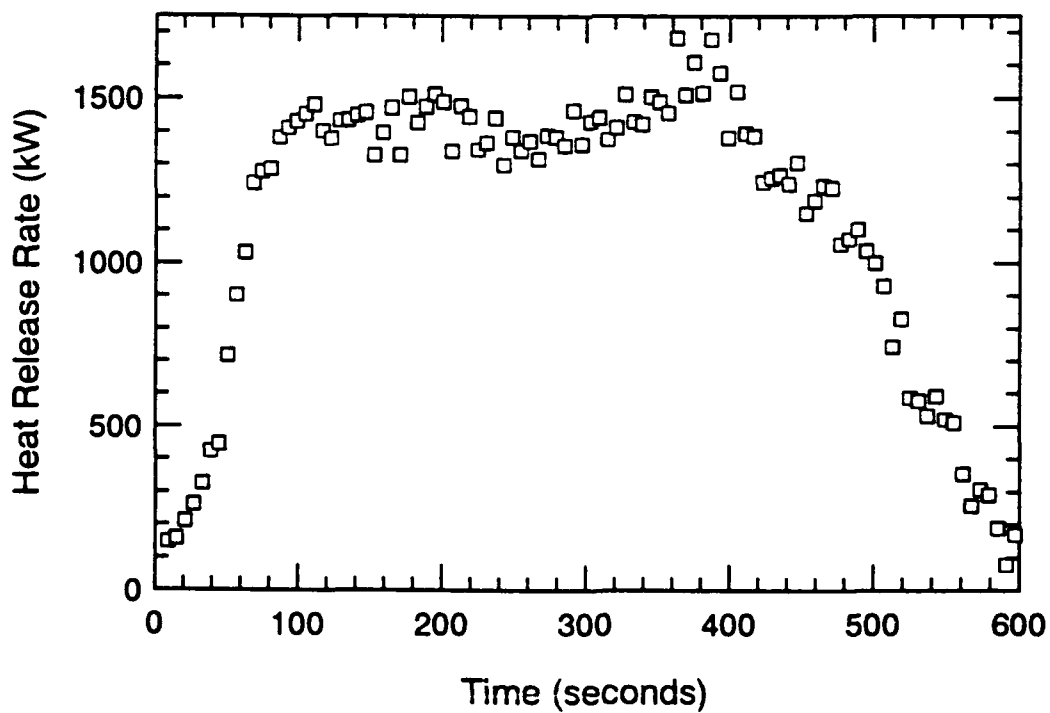
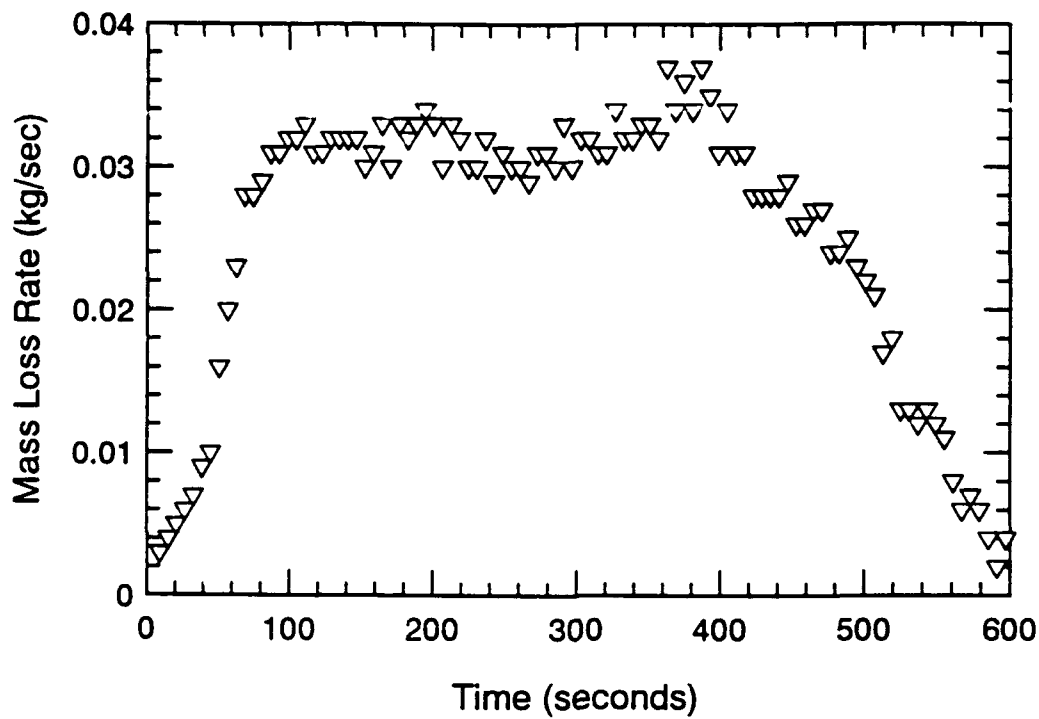


Figure A.127 Mass Loss Rate and Heat Release Rate-Time Histories - ADD3

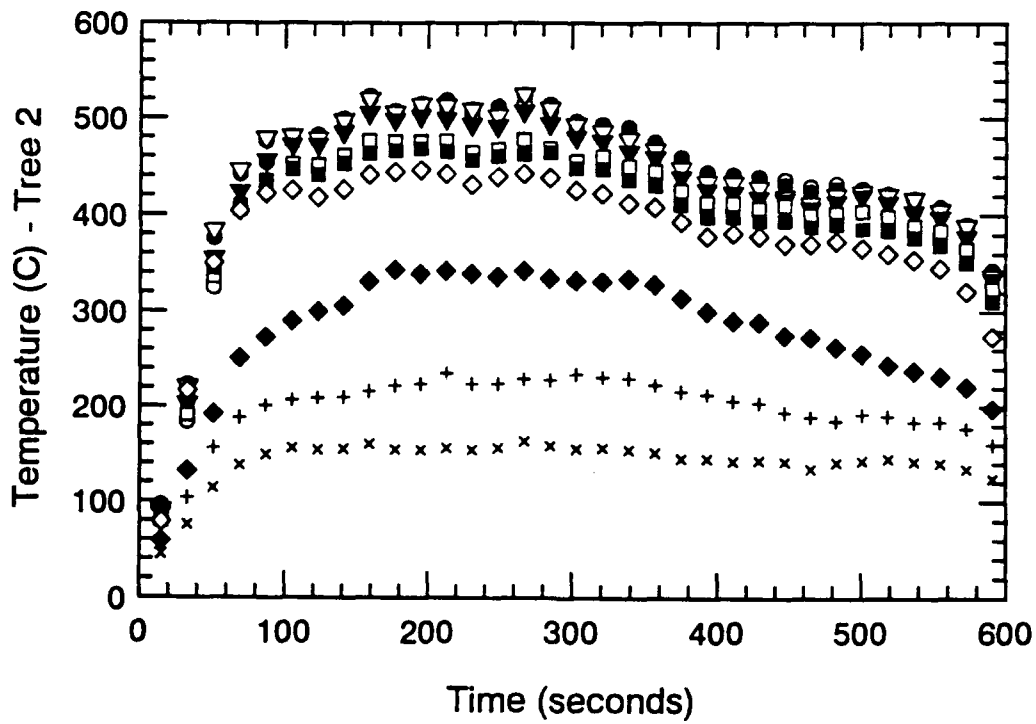
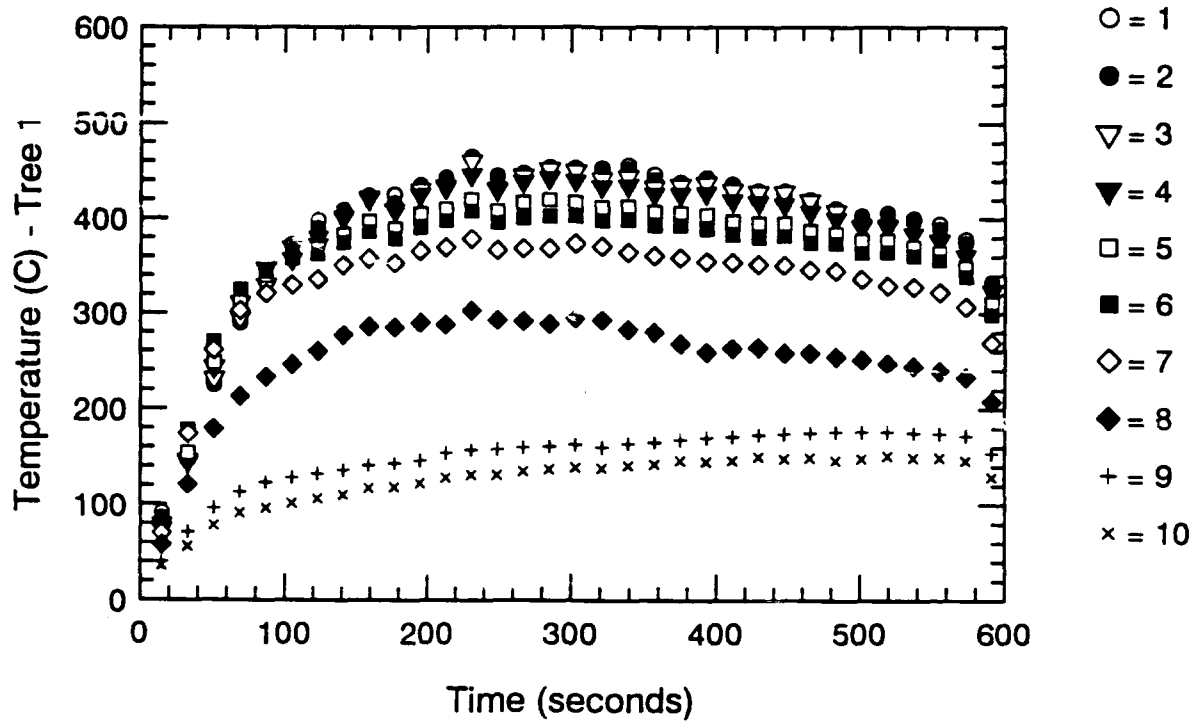


Figure A.128 Thermocouple Trees 1 & 2-Time Histories - ADD3

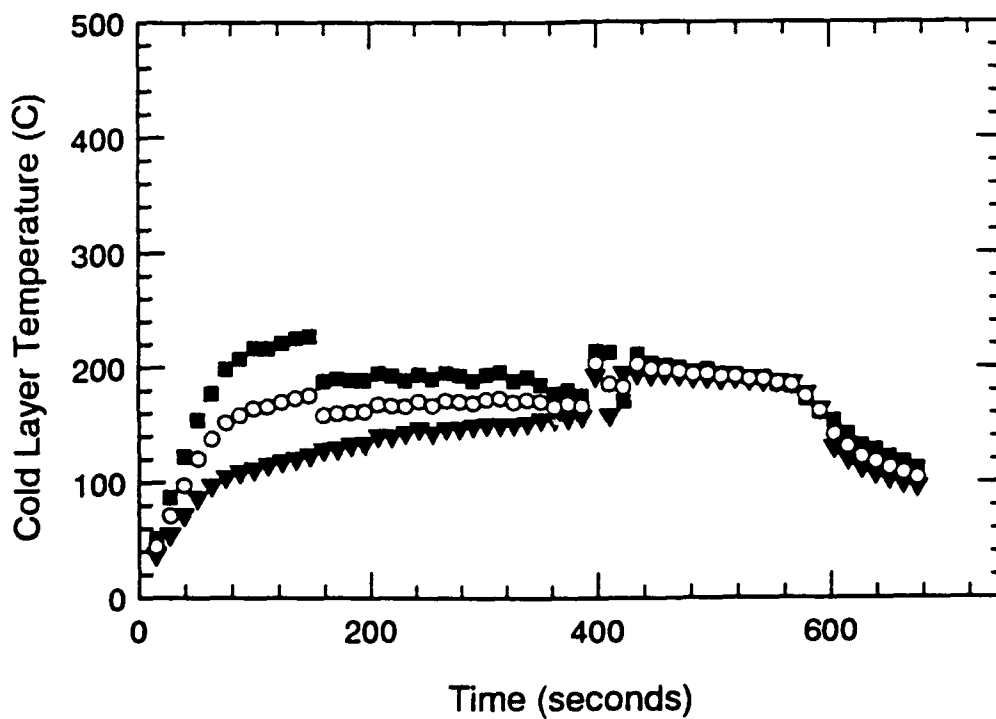
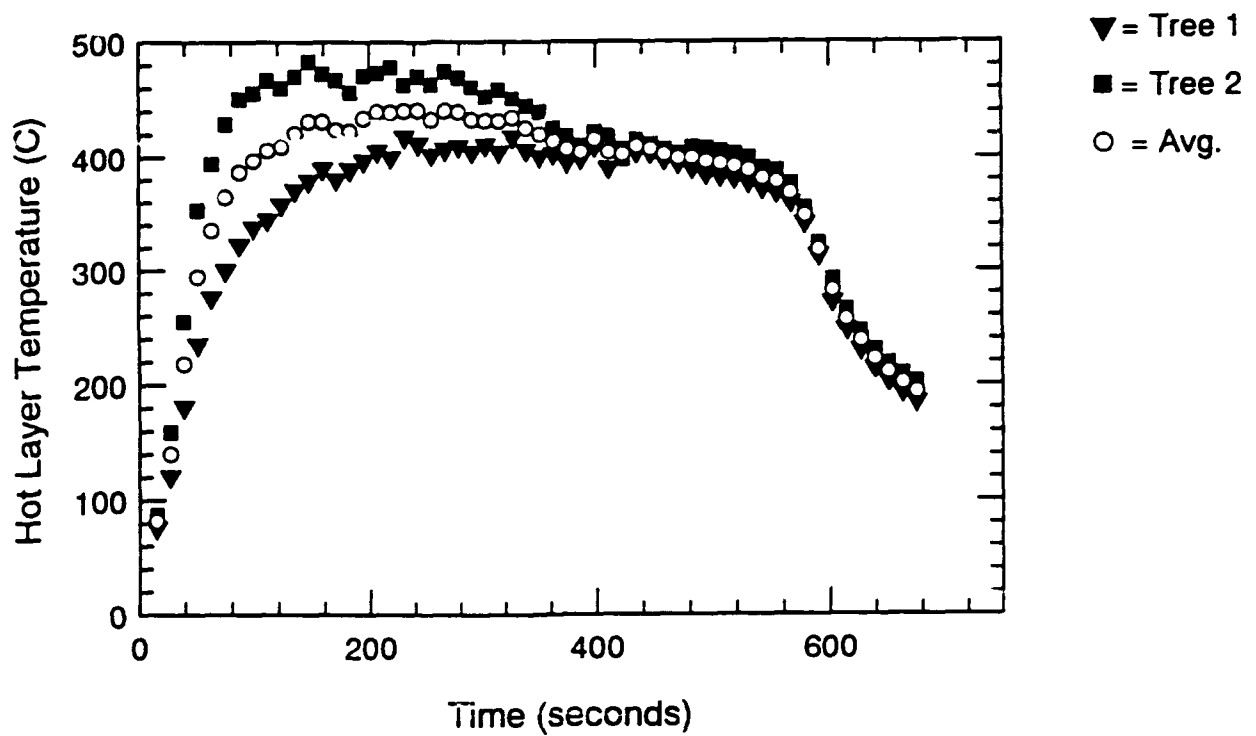


Figure A.129 Hot and Cold Layer Temperature-Time Histories - ADD3

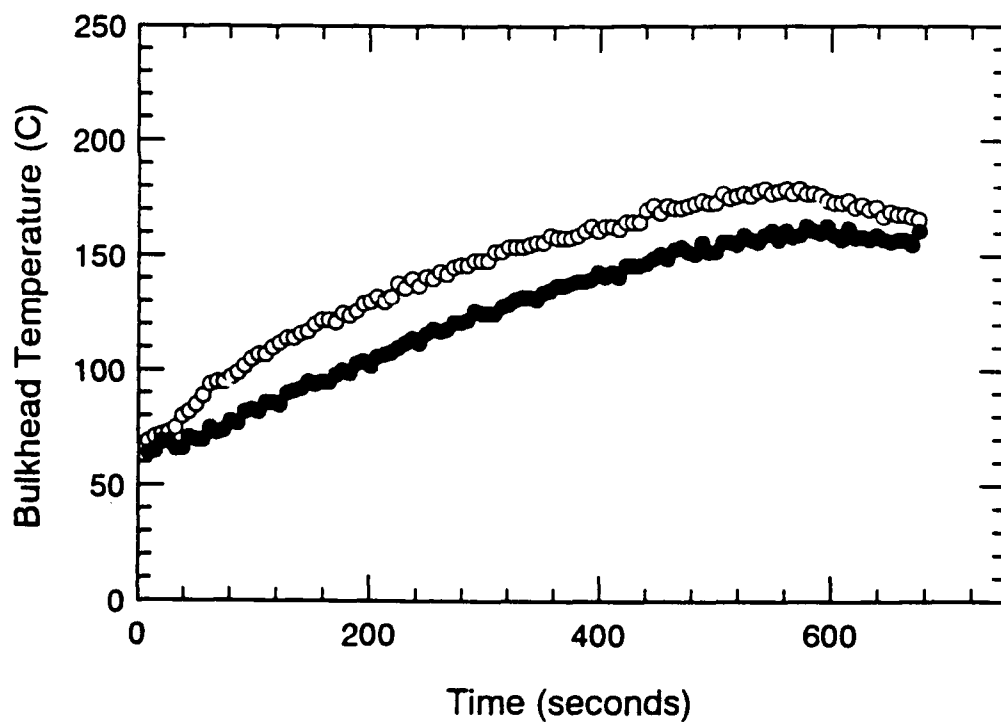
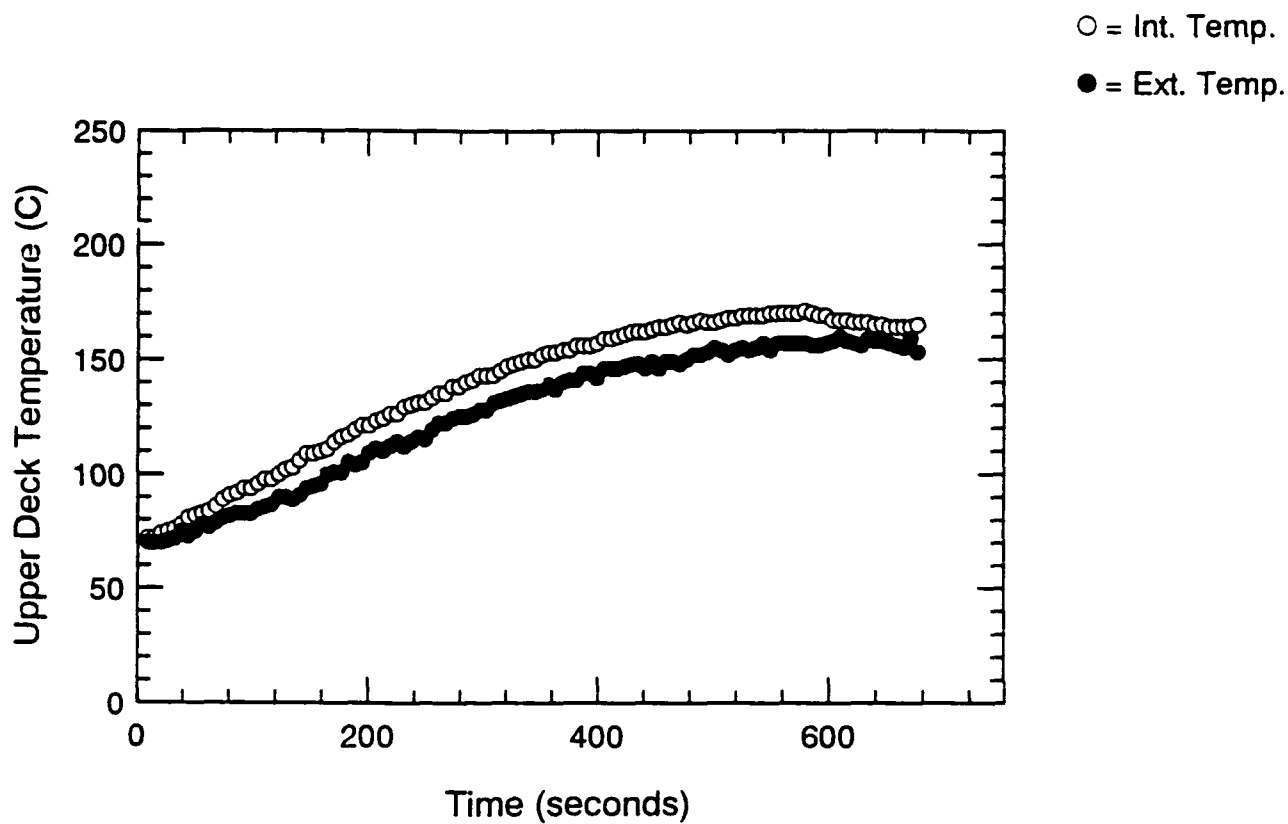


Figure A.130 Surface Thermocouple-Time Histories - ADD3

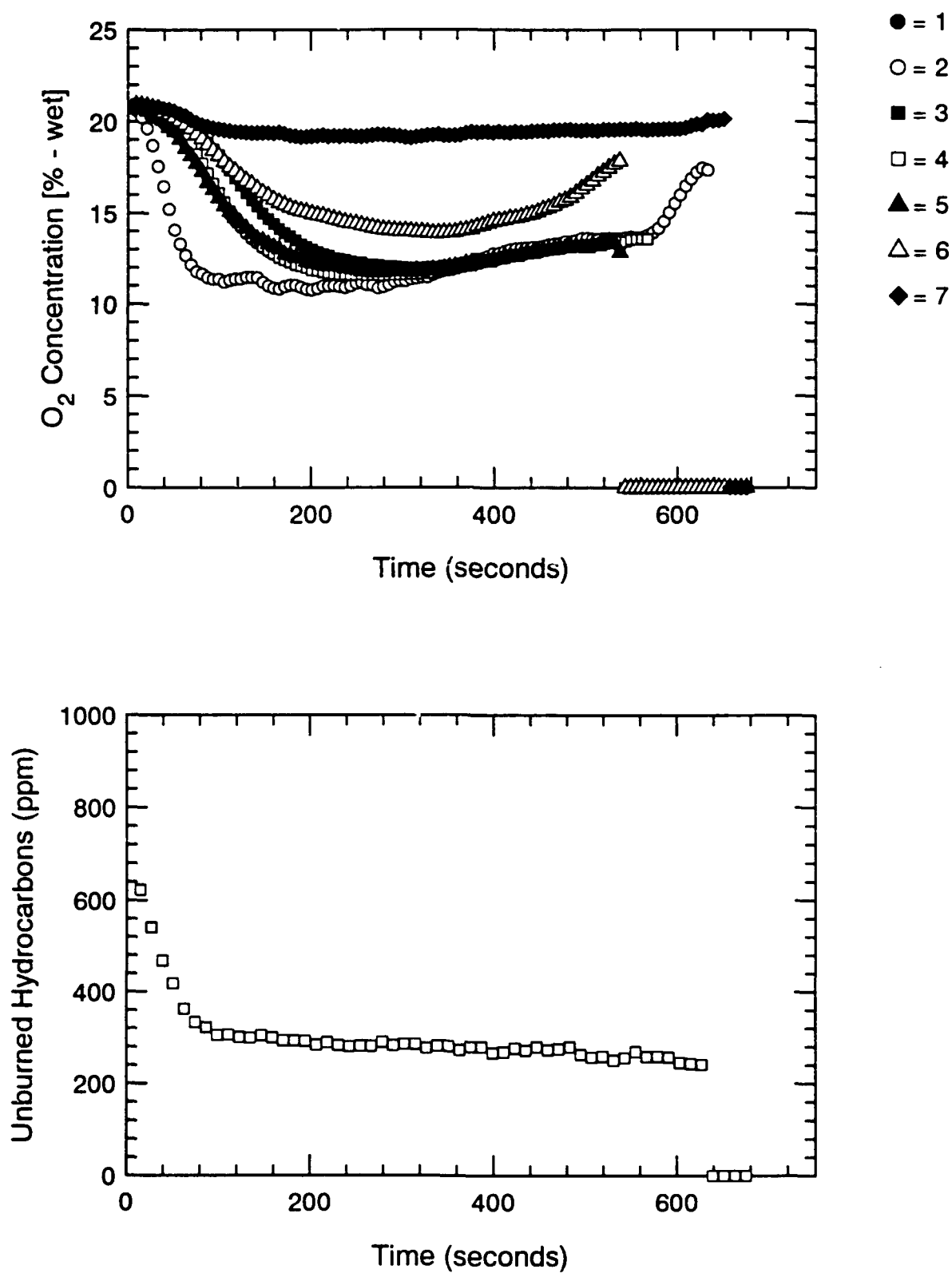


Figure A.131 Oxygen and Unburned HC Concentration-Time Histories - ADD3

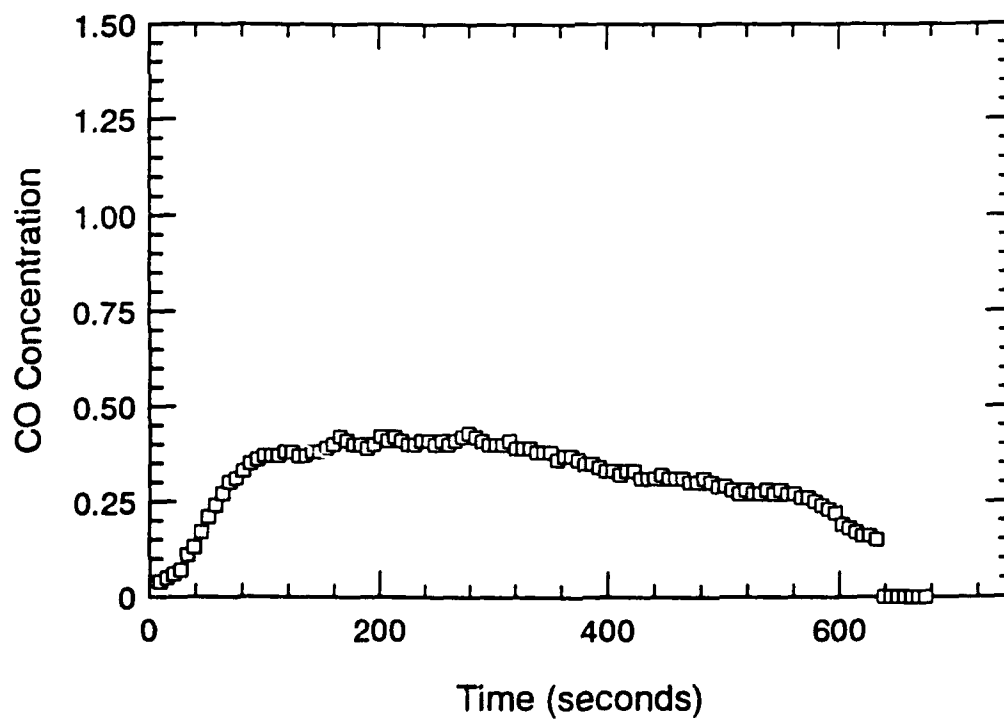
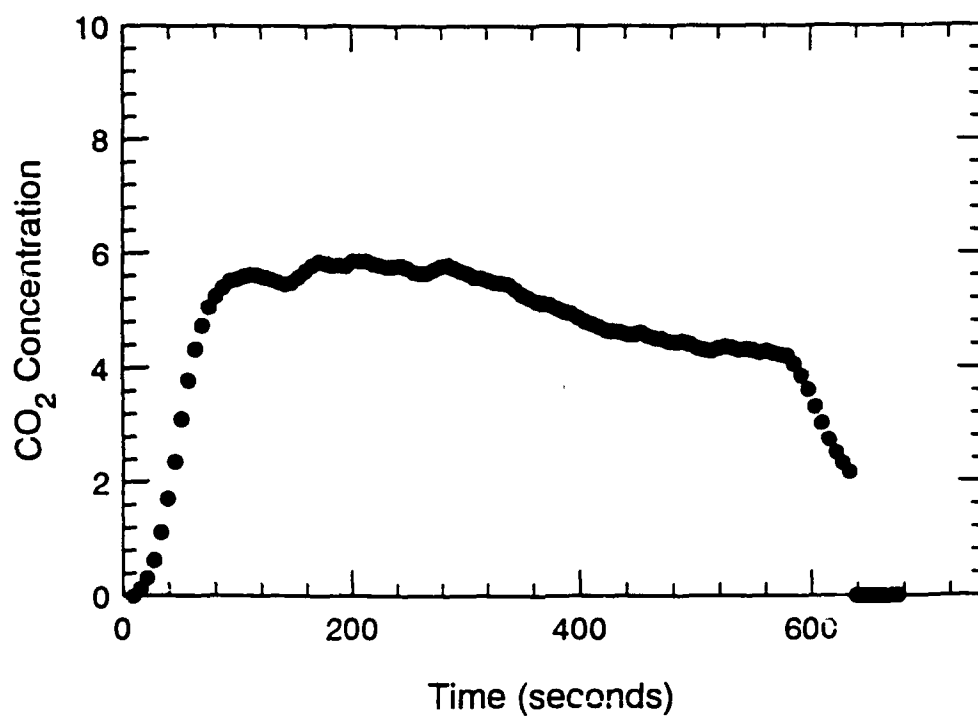


Figure A.132 CO₂ and CO Concentration-Time Histories - ADD3

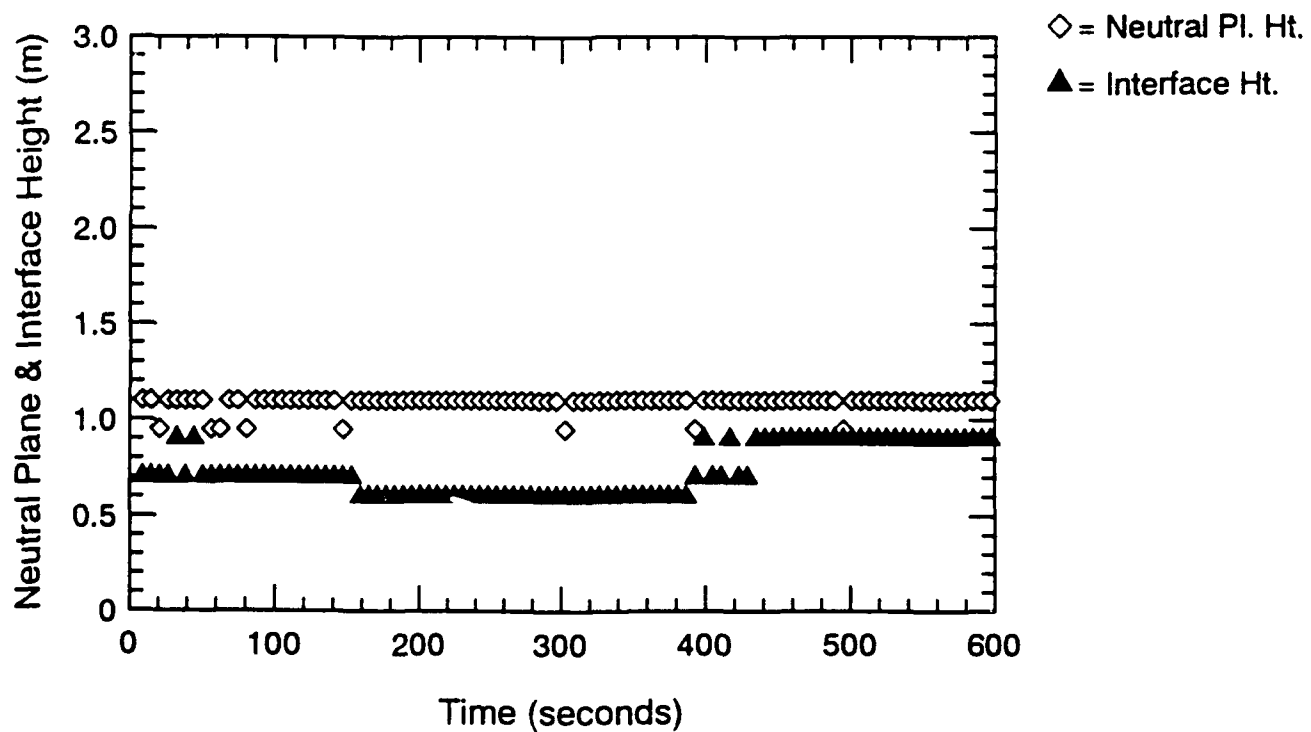
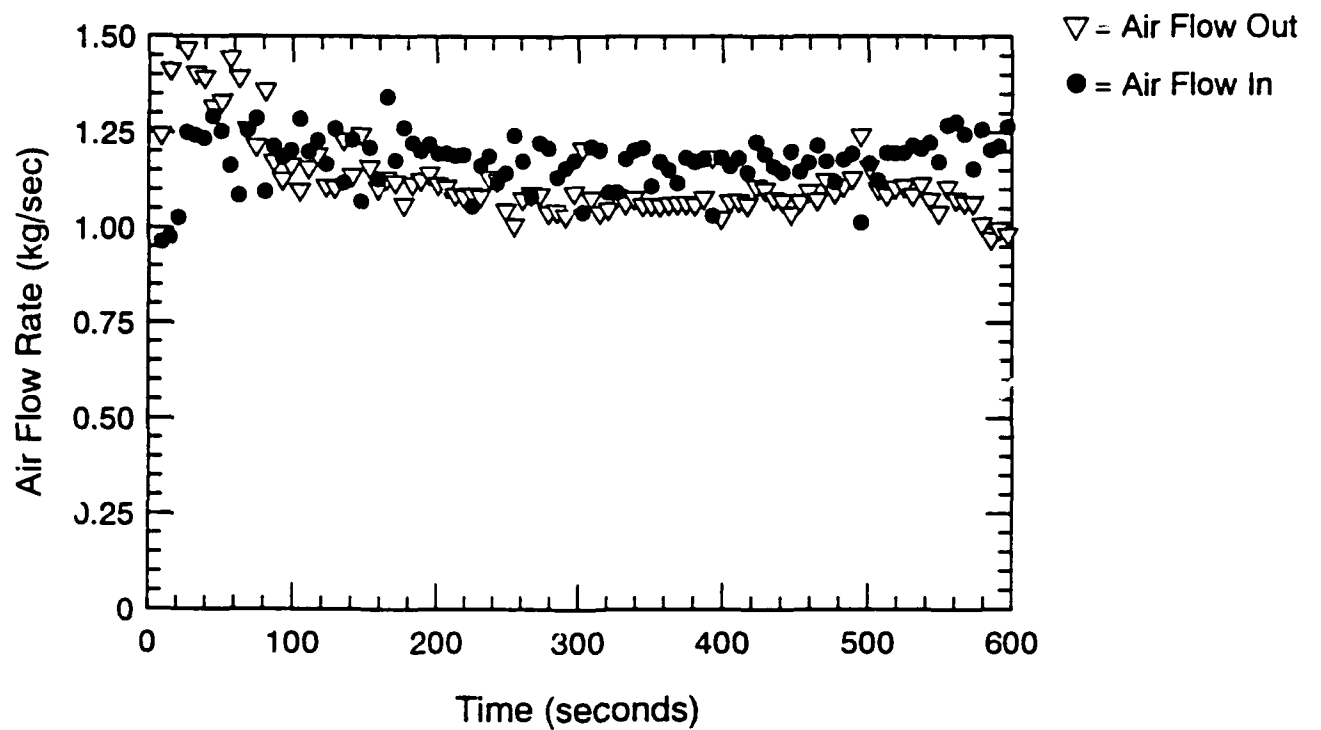


Figure A.133 Air Flow Rate, Neutral Plane & Interface Ht.-Time Histories - ADD3

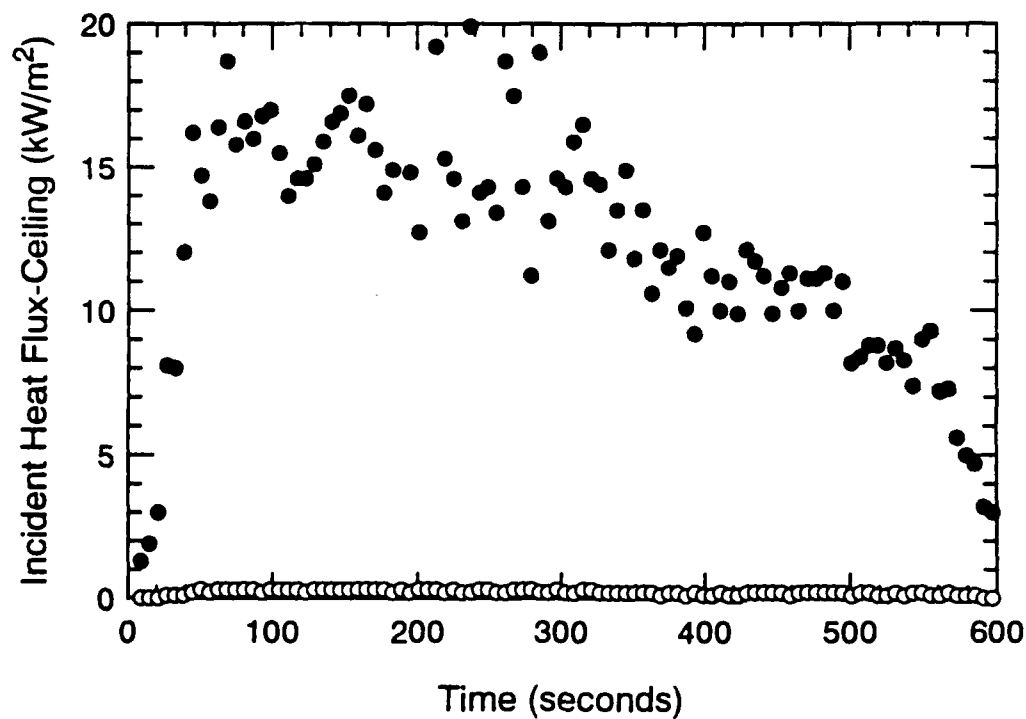
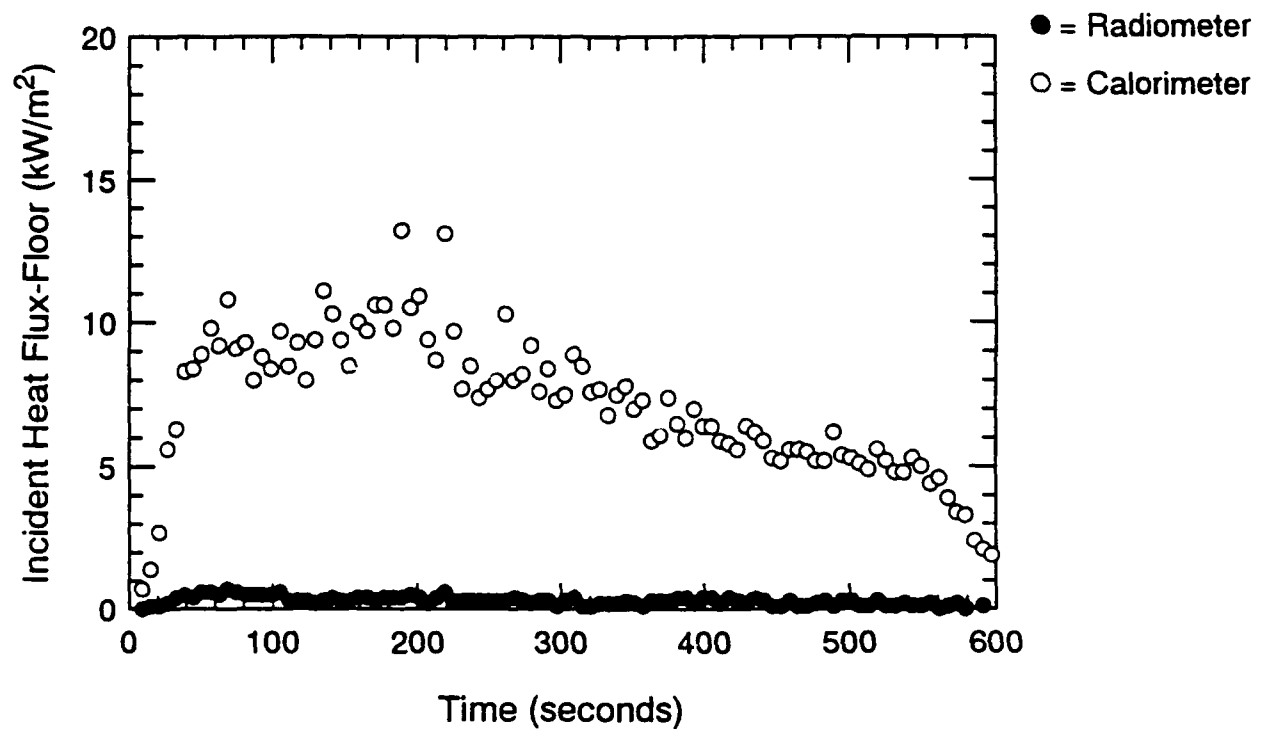


Figure A.134 Incident Heat Flux at Floor and Ceiling-Time Histories - ADD3

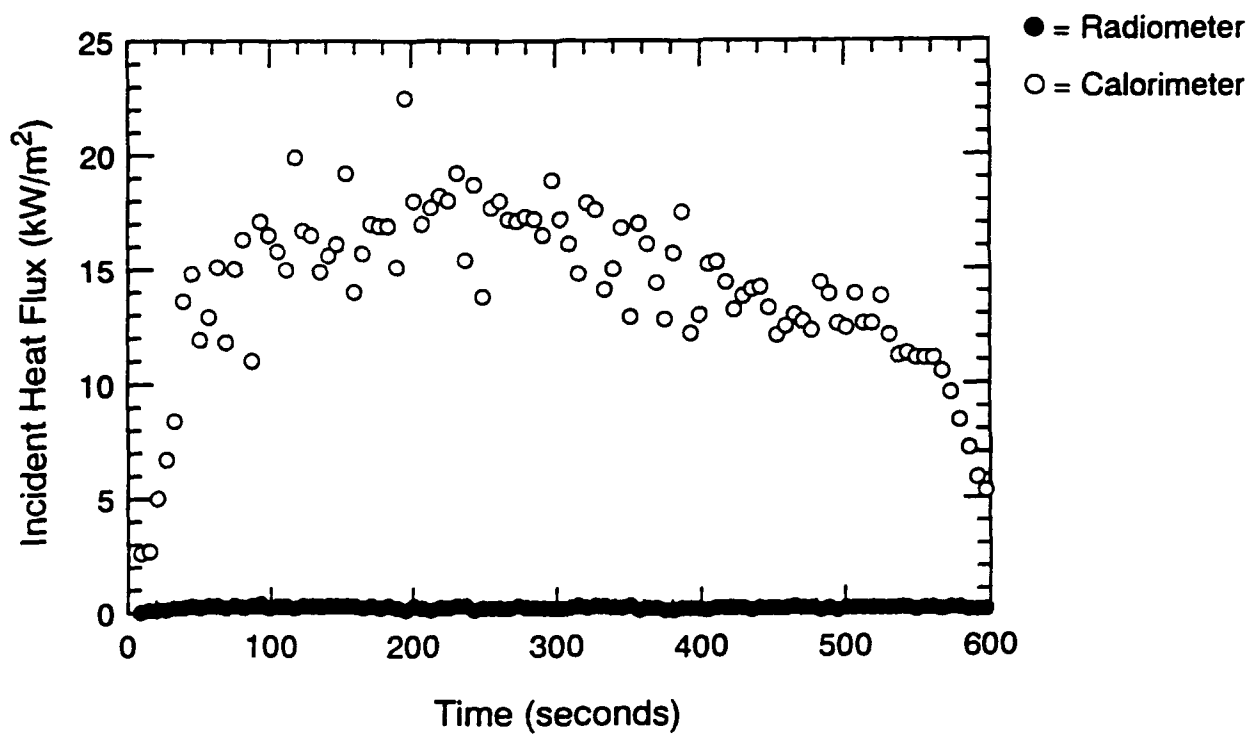


Figure A.135 Incident Heat Flux at Fwd. Bulkhead-Time Histories - ADD3

APPENDIX B. Series 2 Test Results

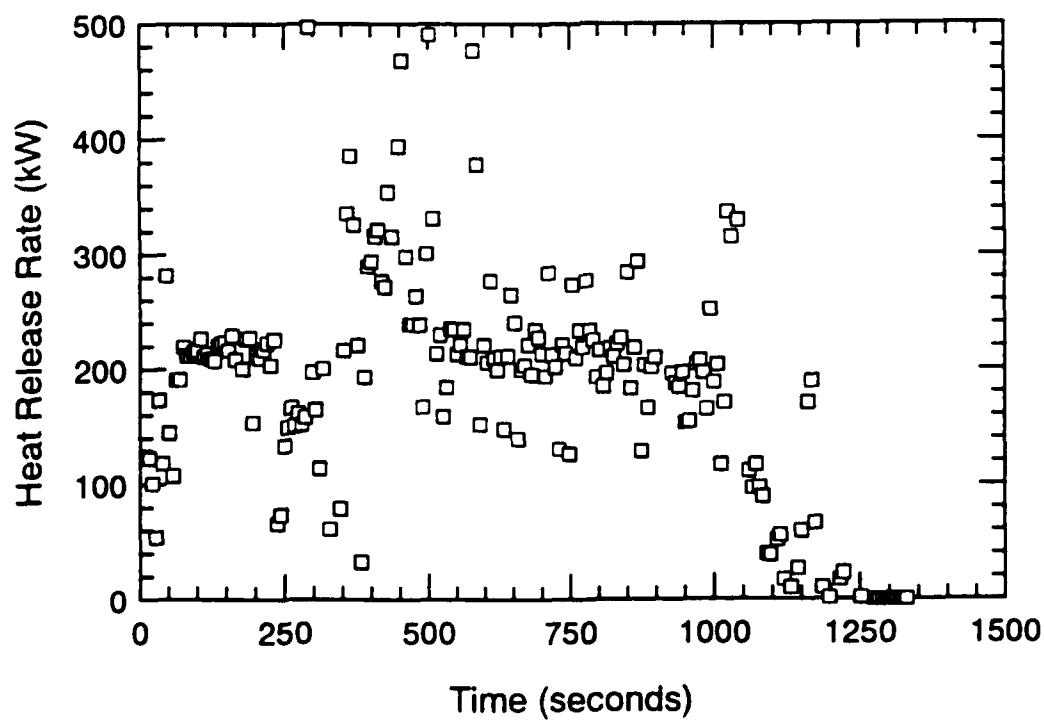
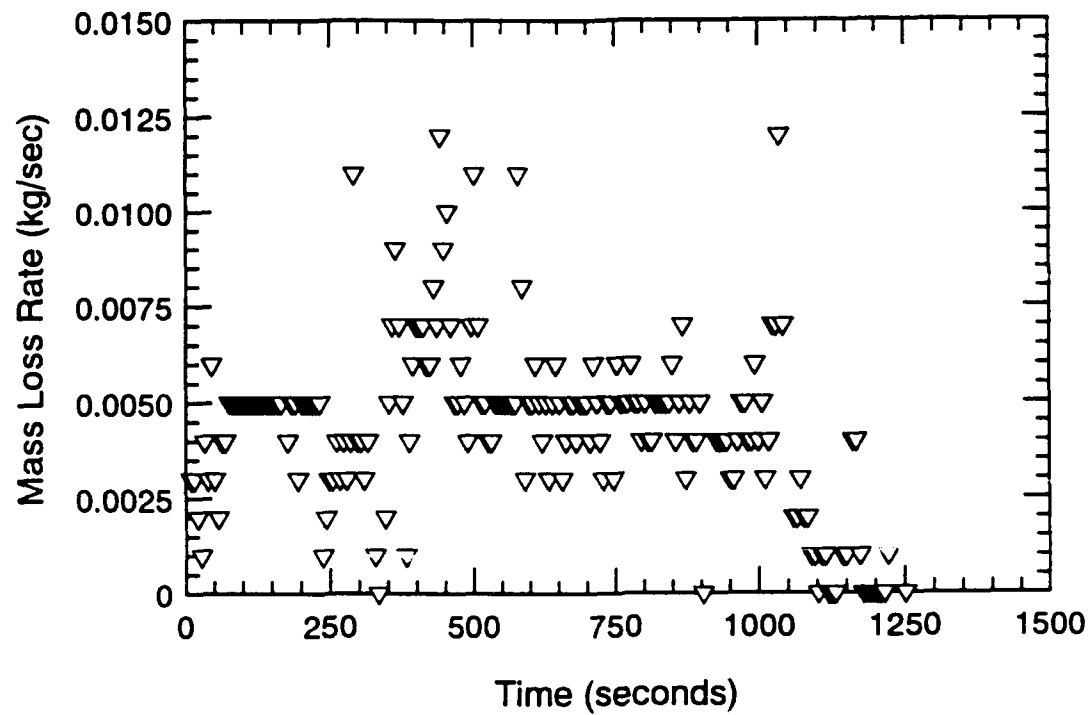


Figure B.1 Mass Loss Rate and Heat Release Rate-Time Histories - S201

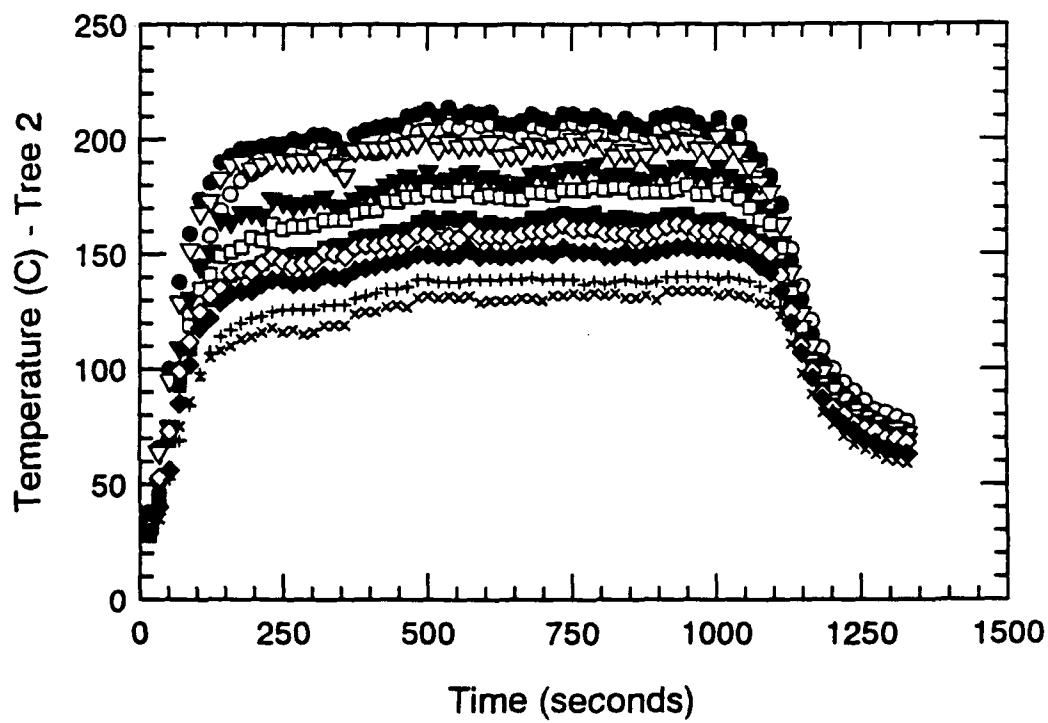
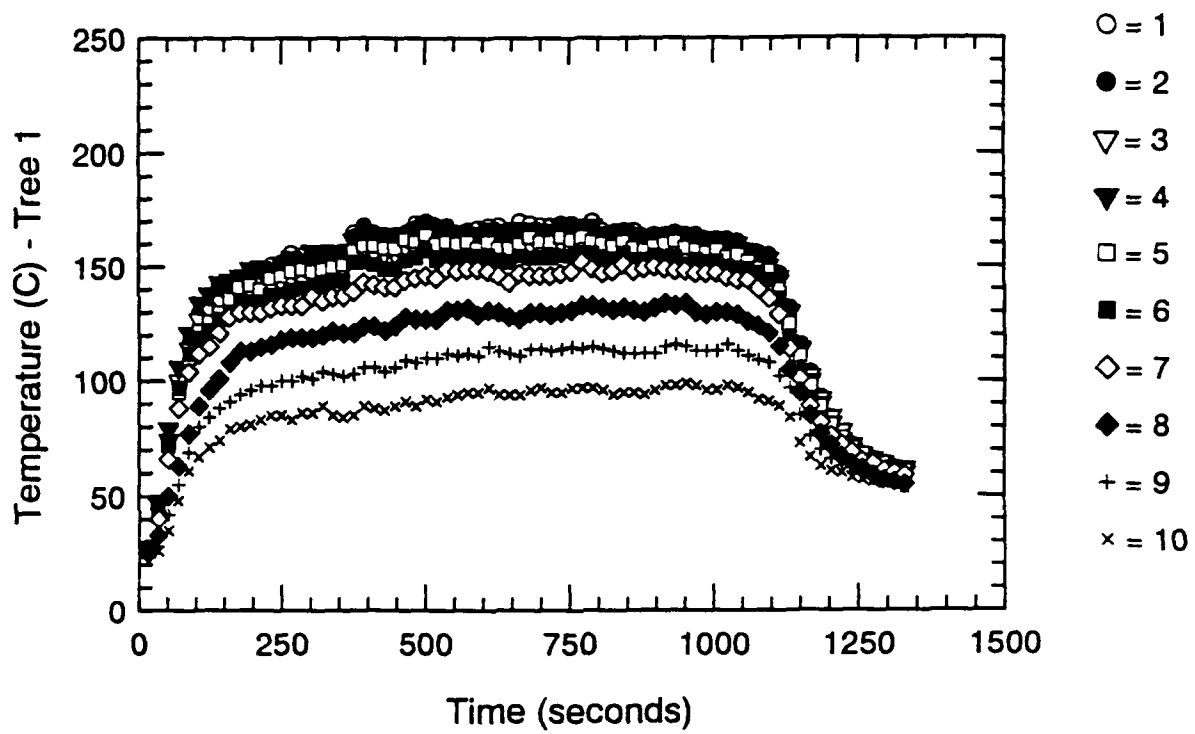


Figure B.2 Thermocouple Trees 1 & 2-Time Histories - S201

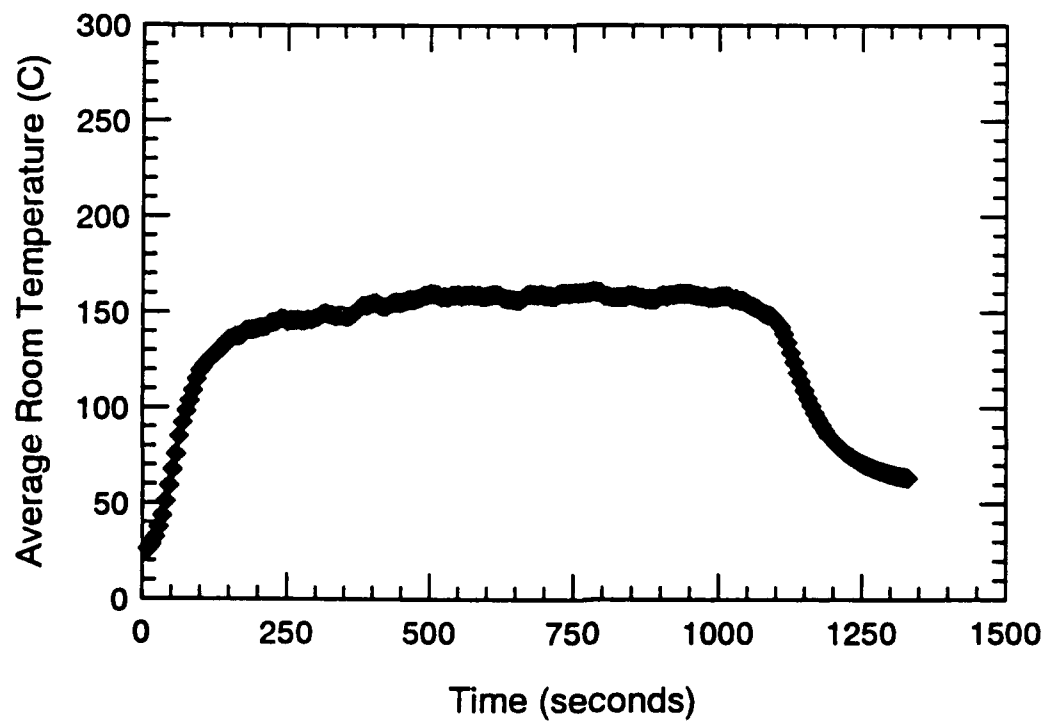
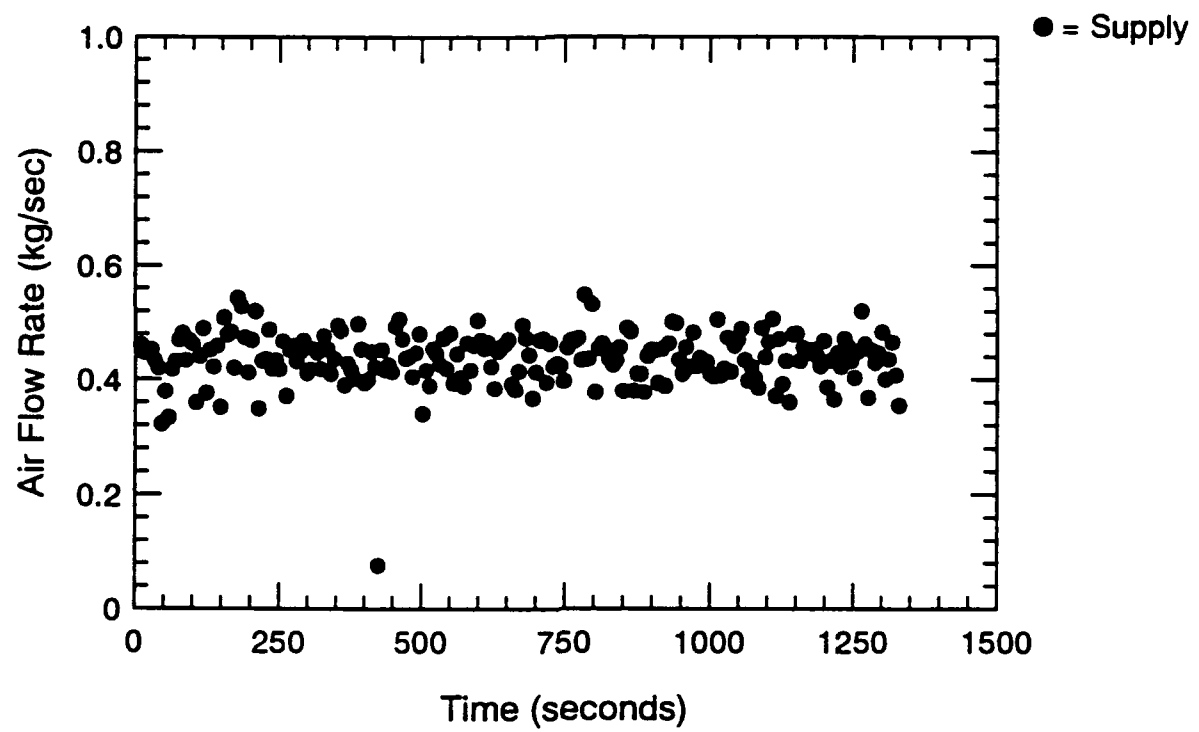


Figure B.3 Air Flow Rate and Avg. Temperature-Time Histories - S201

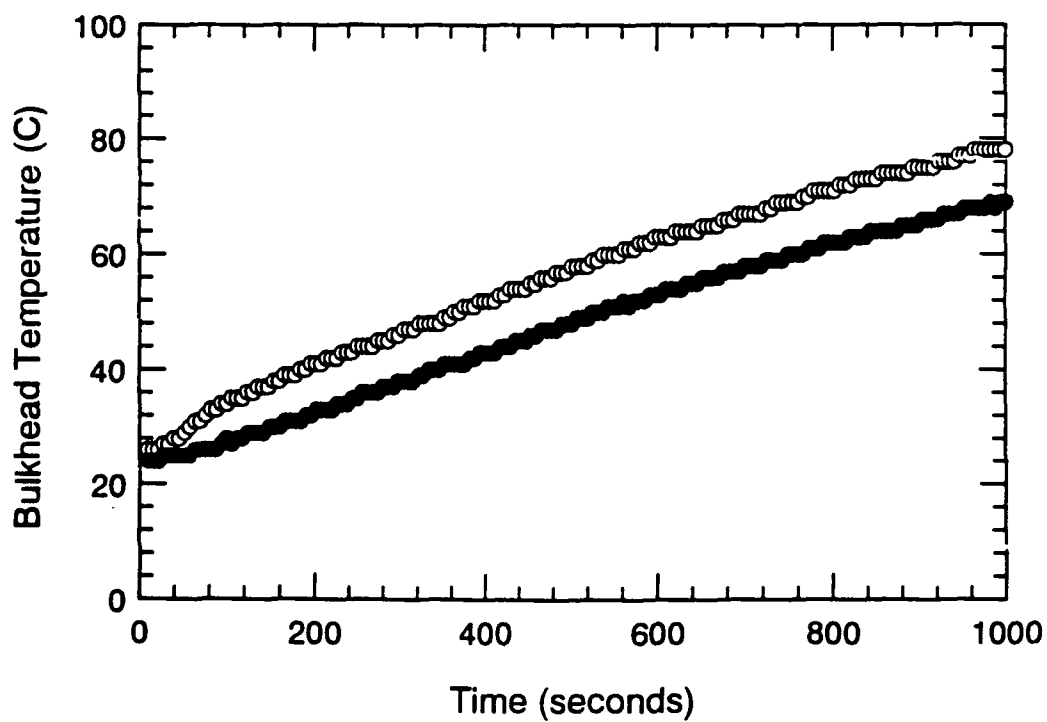
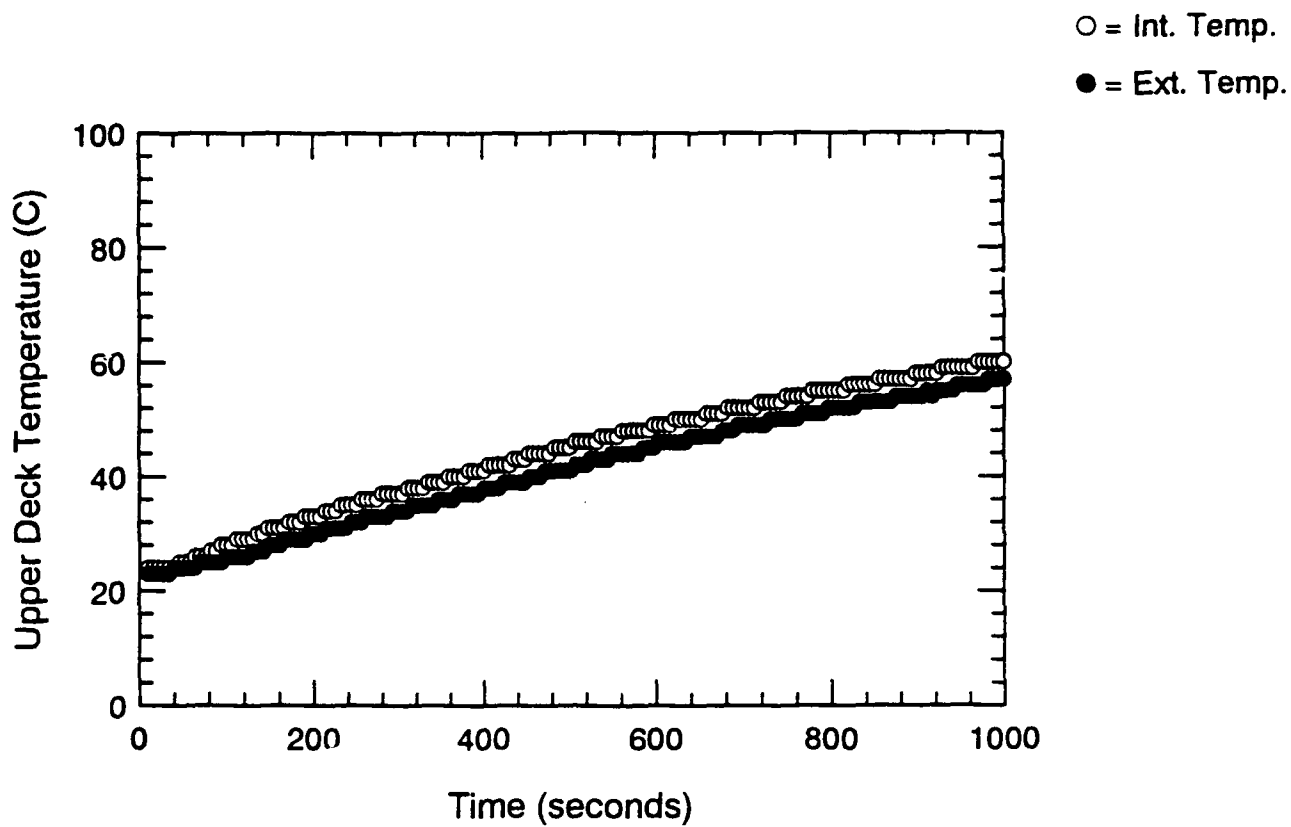


Figure B.4 Surface Thermocouple-Time Histories - S201

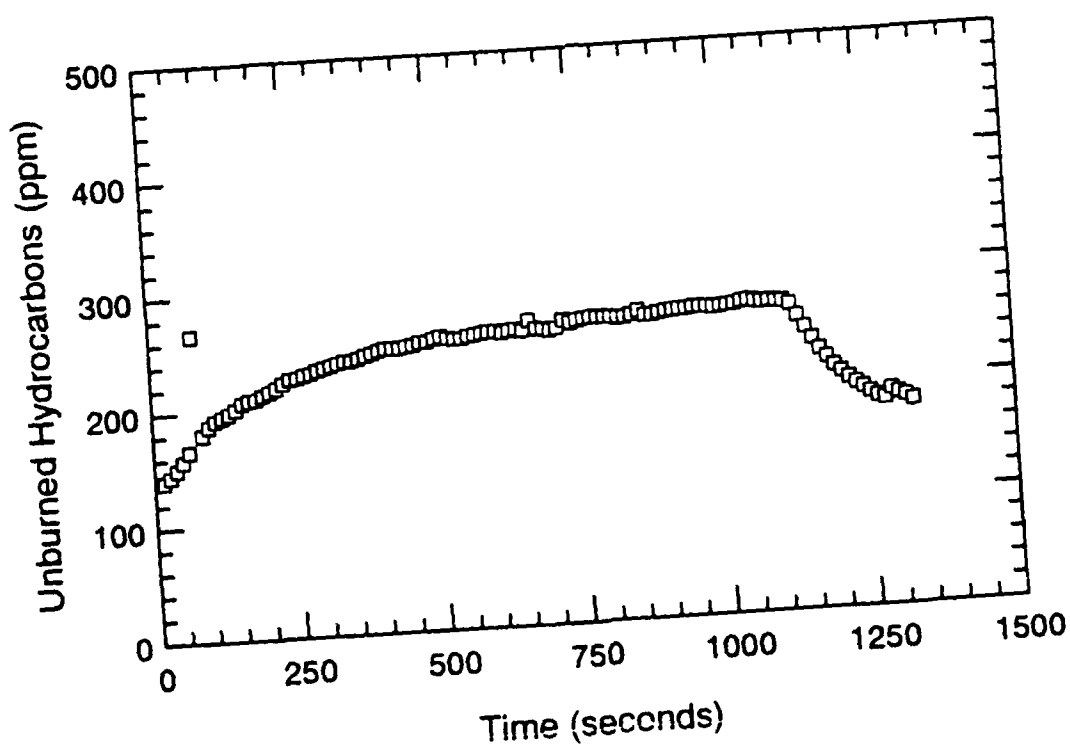
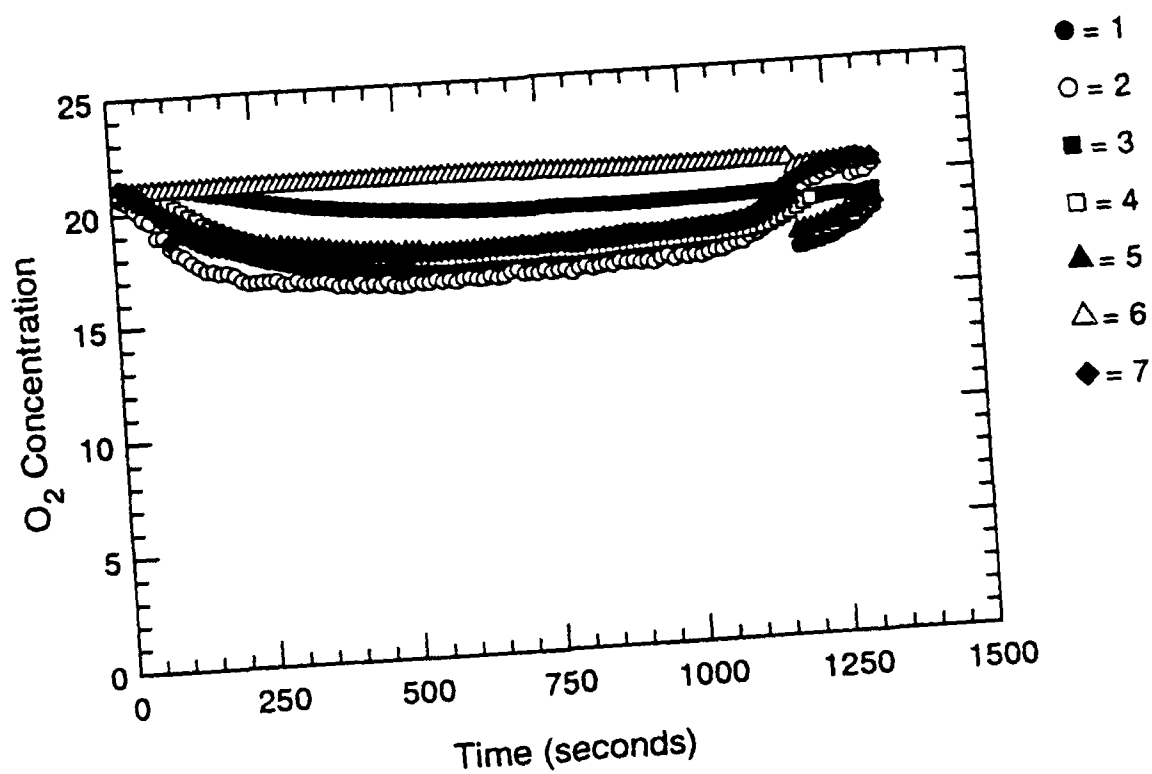


Figure B.5 Oxygen and Unburned HC Concentration-Time Histories - S201

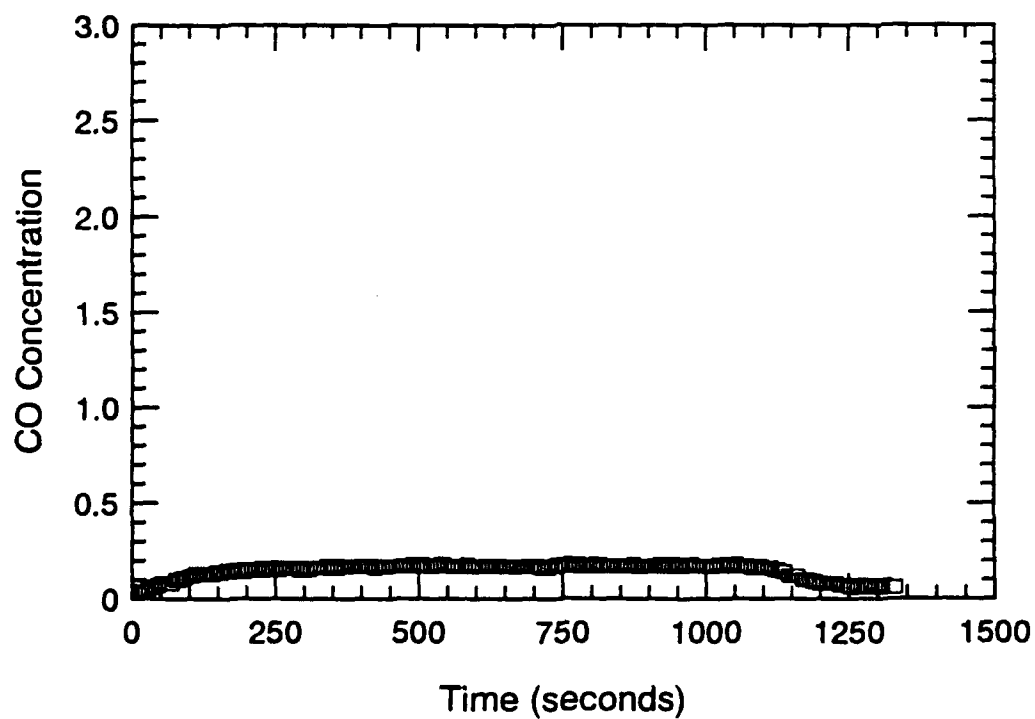
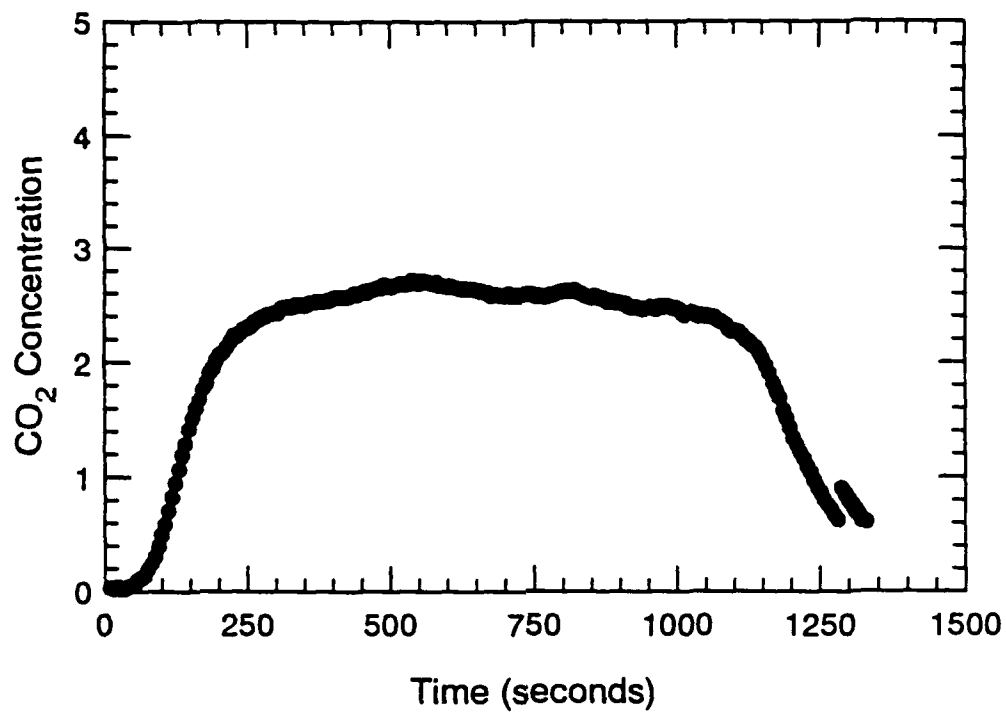


Figure B.6 CO₂ and CO Concentration-Time Histories - S201

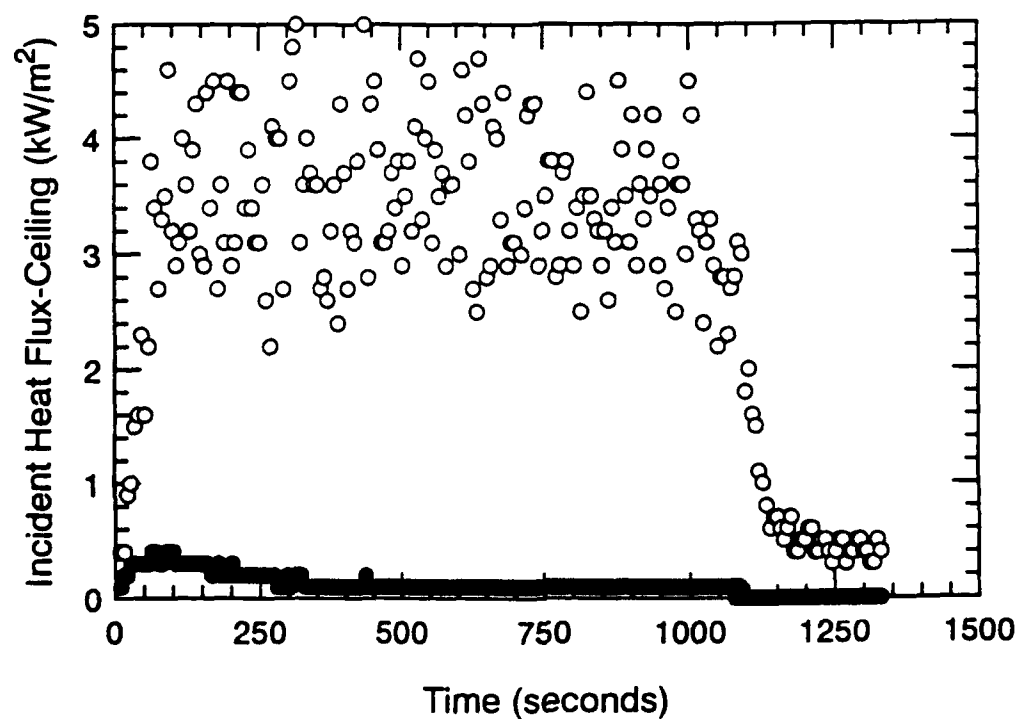
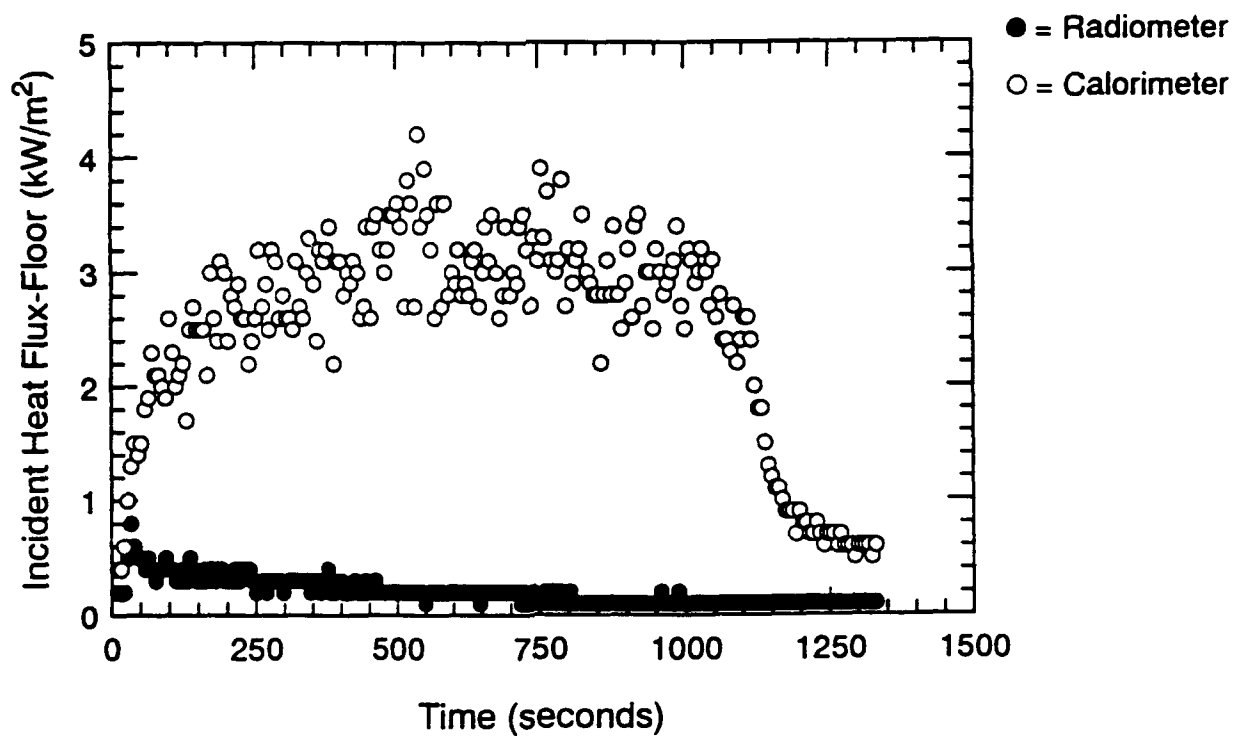


Figure B.7 Incident Heat Flux at Floor and Ceiling-Time Histories - S201

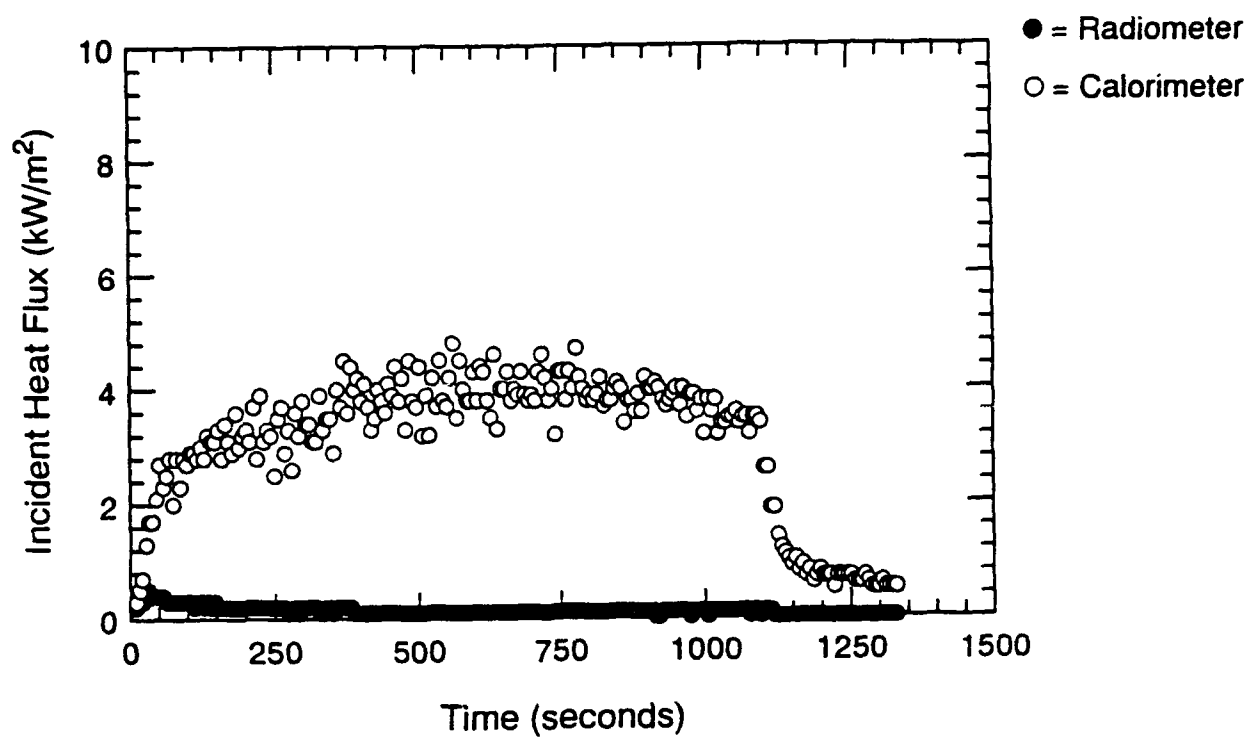


Figure B.8 Incident Heat Flux at Fwd. Bulkhead-Time Histories - S201

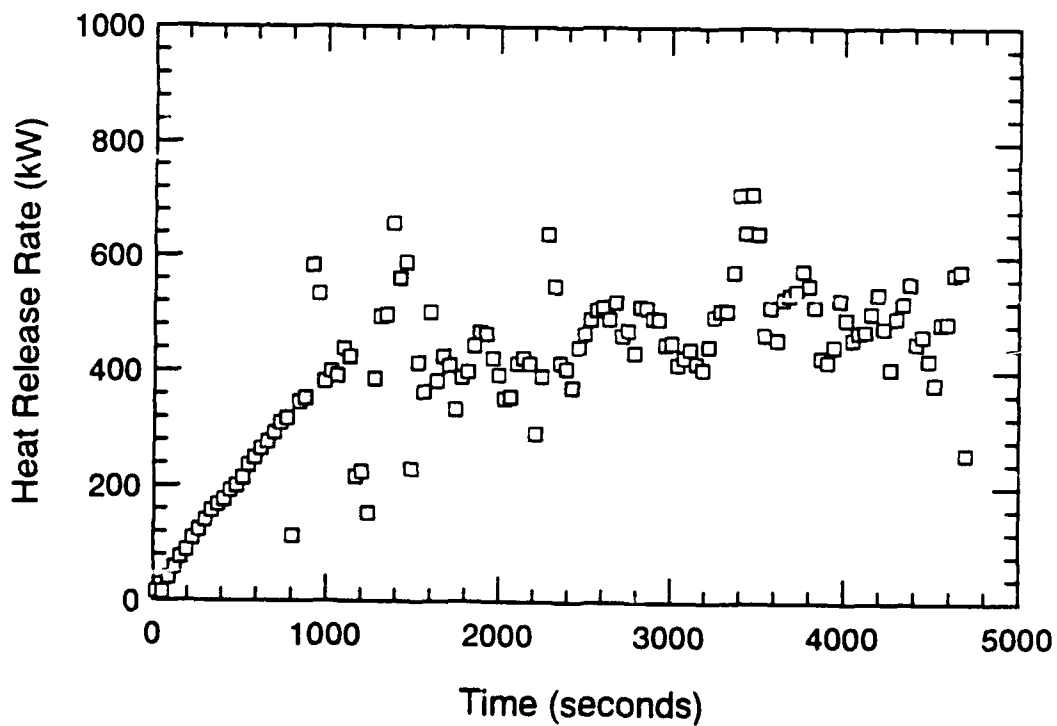
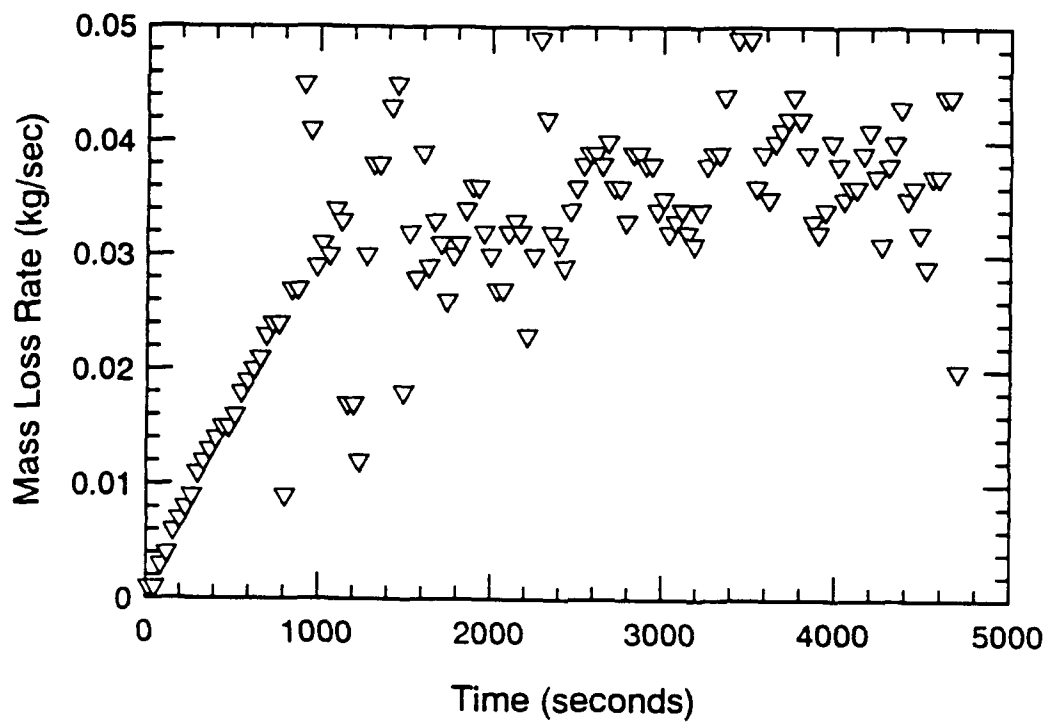


Figure B.9 Mass Loss Rate and Equivalence Ratio-Time Histories - S202

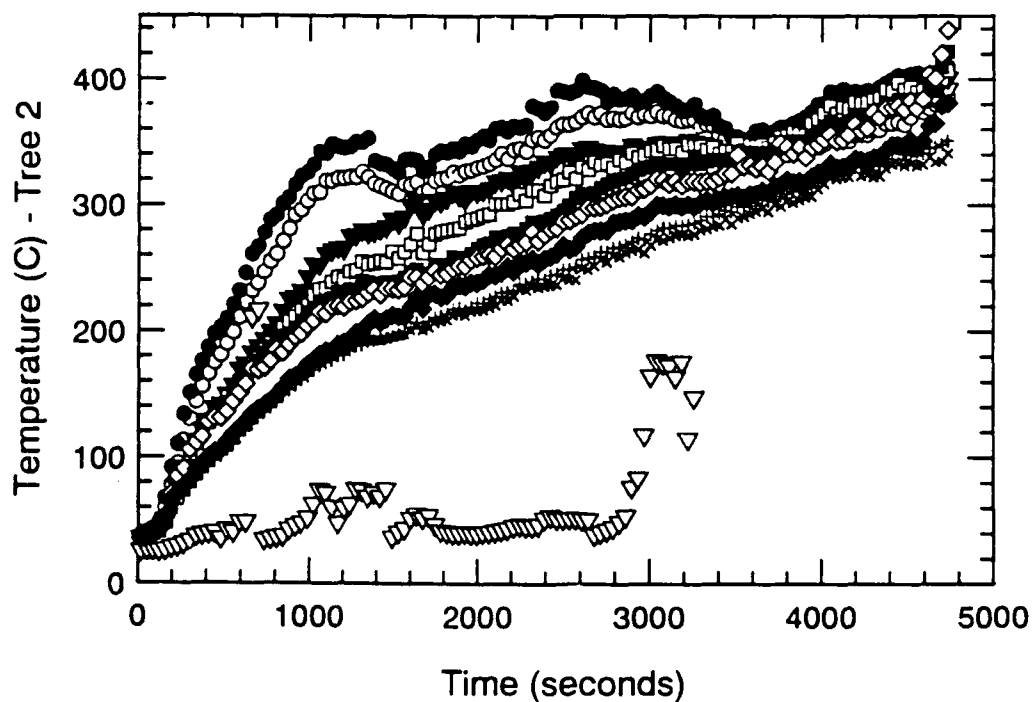
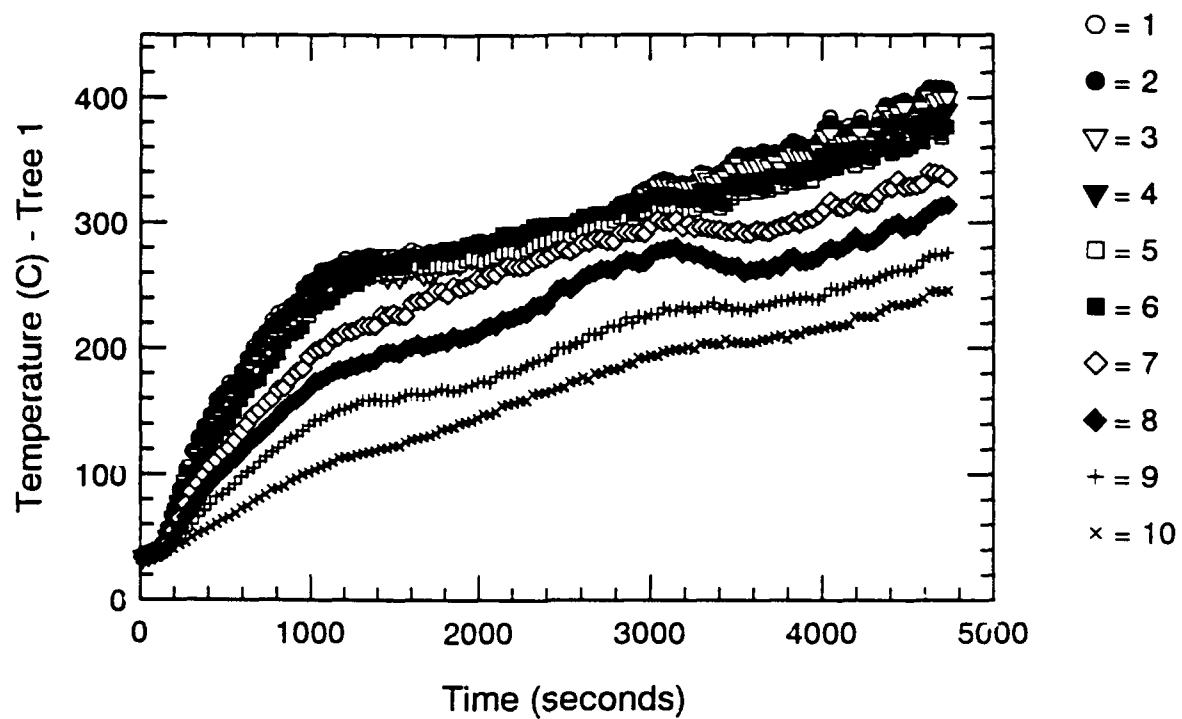


Figure B.10 Thermocouple Trees 1 & 2-Time Histories - S202

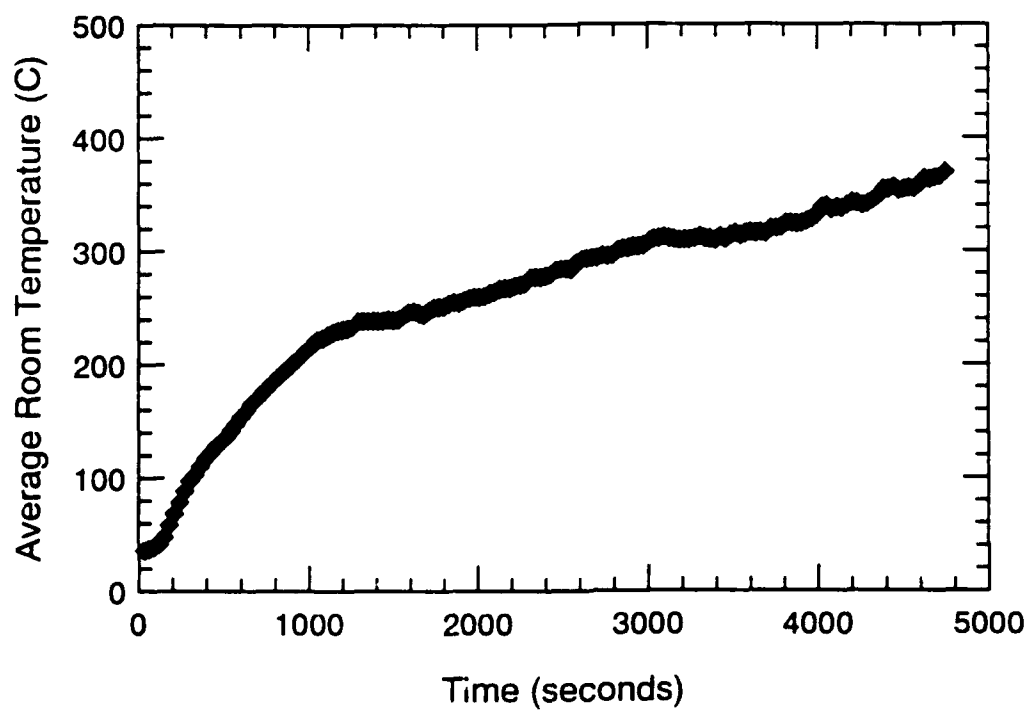
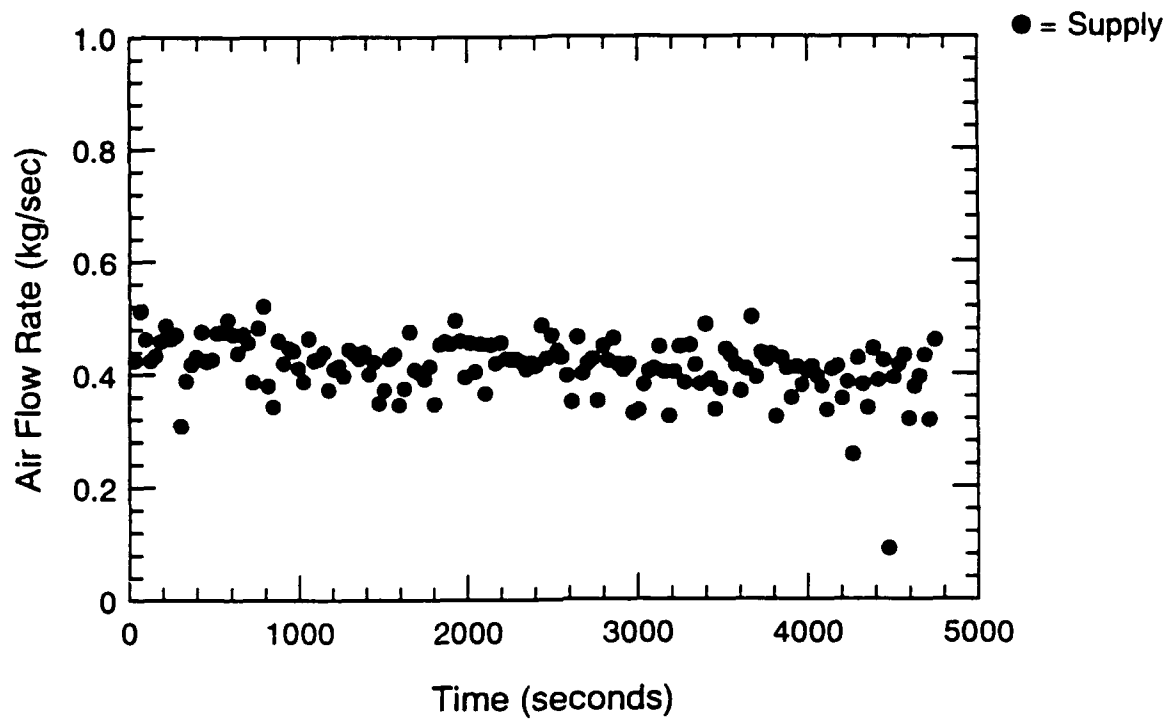


Figure B.11 Air Flow Rate and Avg. Temperature-Time Histories - S202

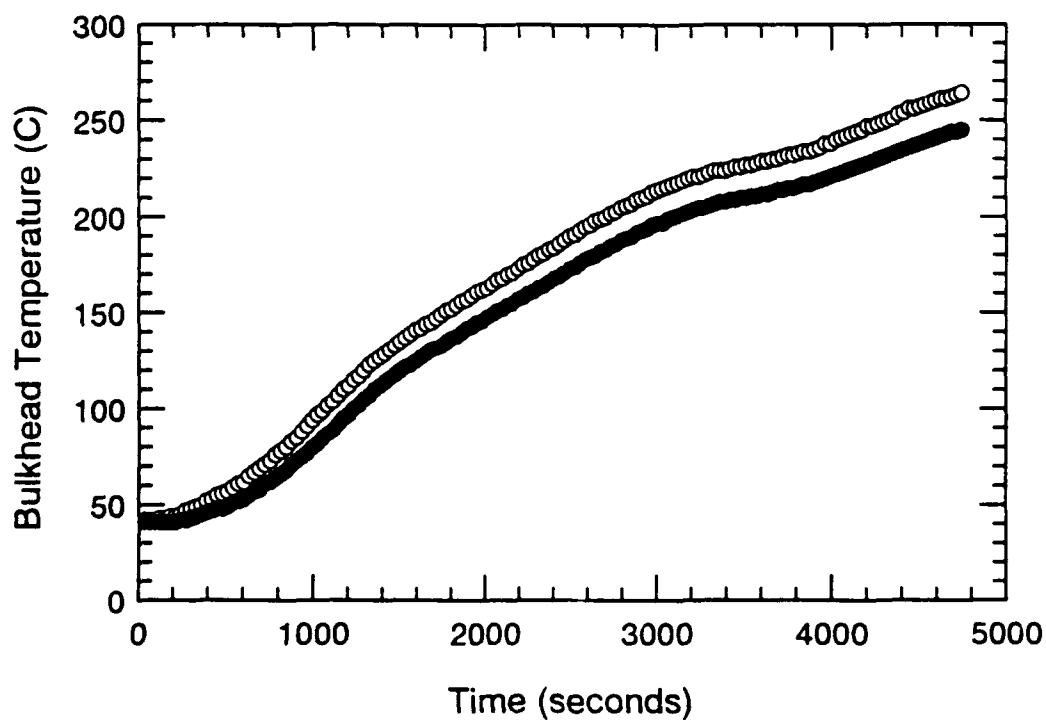
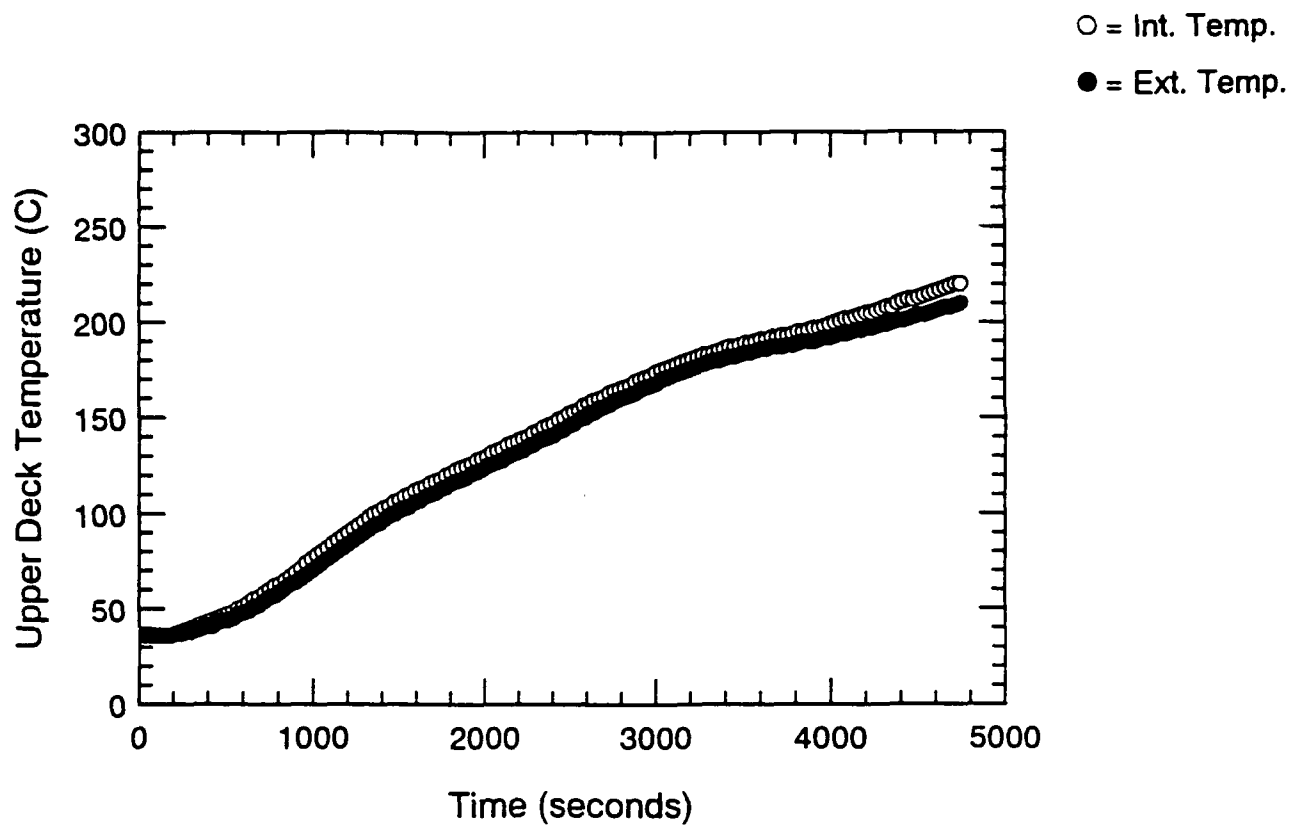


Figure B.12 Surface Thermocouple-Time Histories - S202

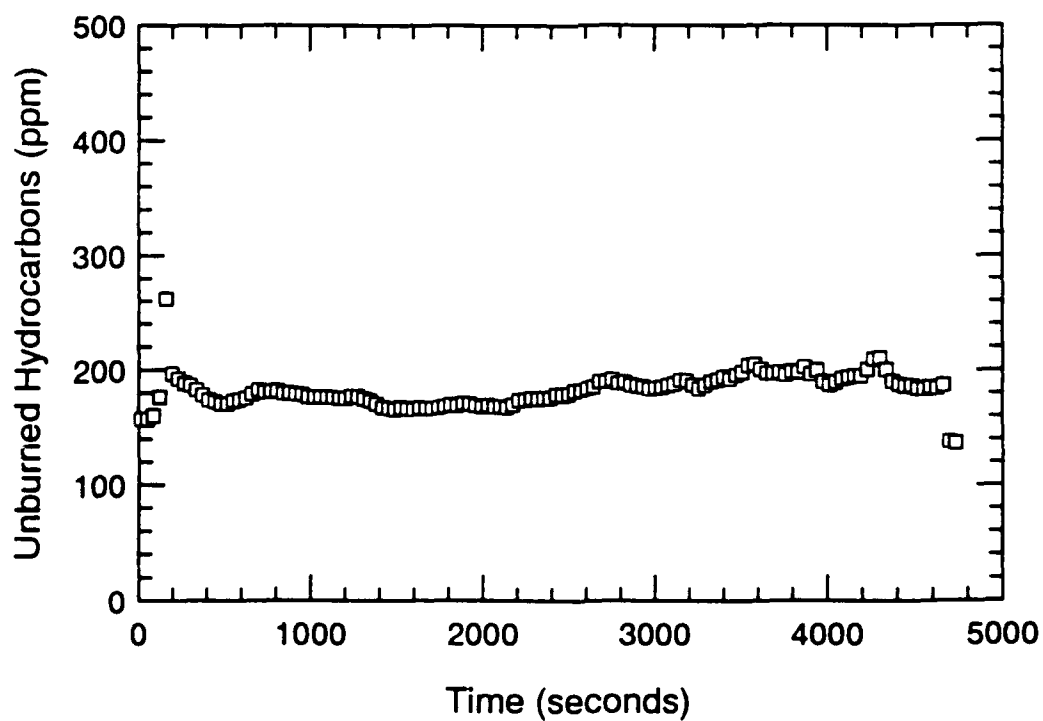
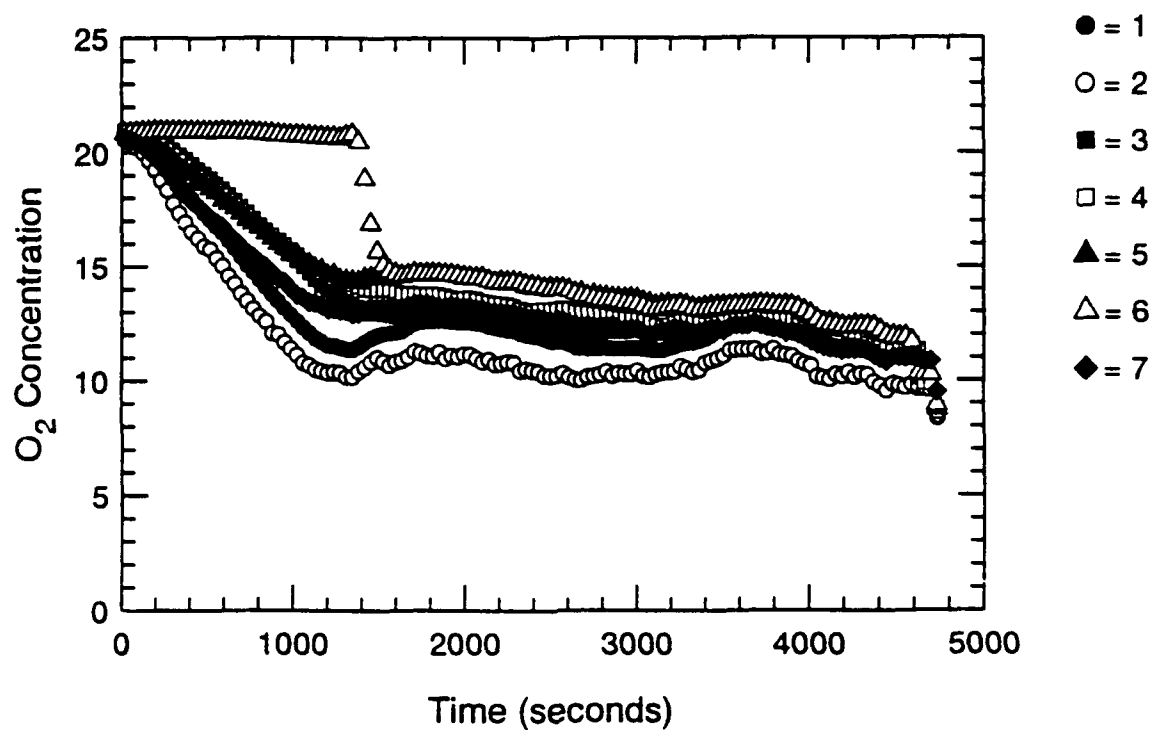


Figure B.13 Oxygen and Unburned HC Concentration-Time Histories - S202

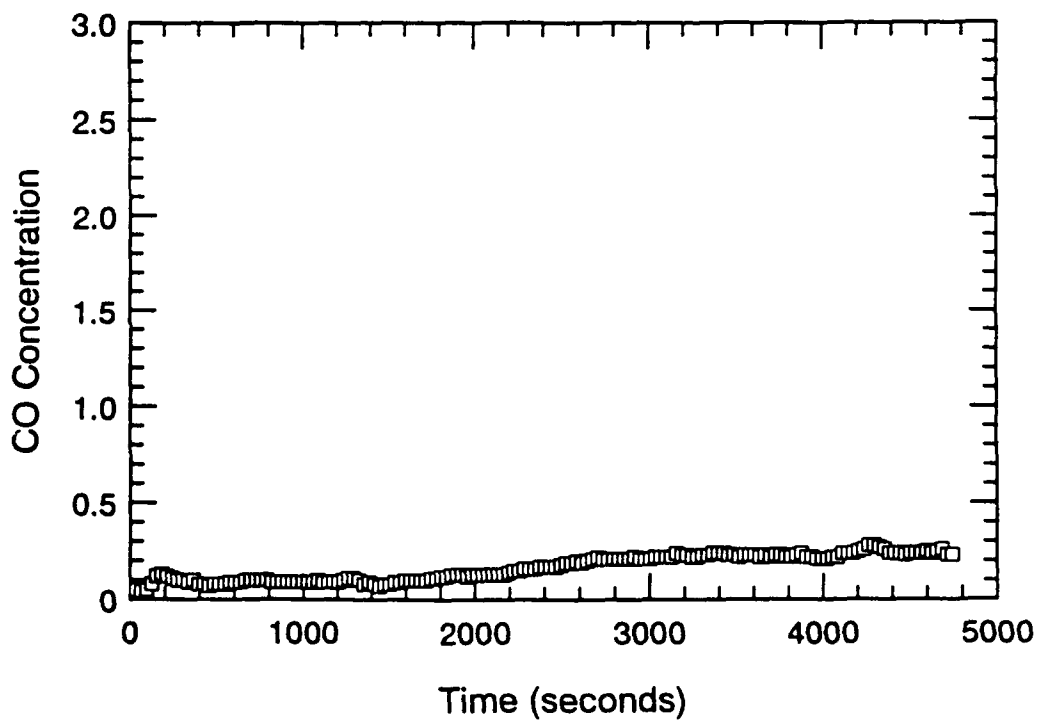
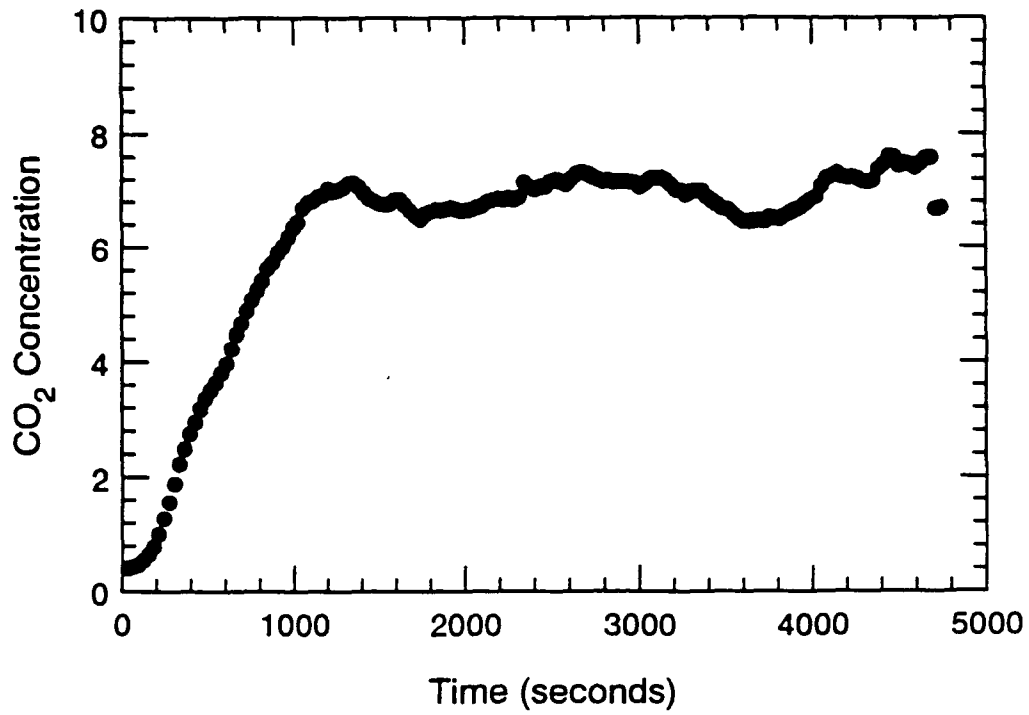


Figure B.14 CO₂ and CO Concentration-Time Histories - S202

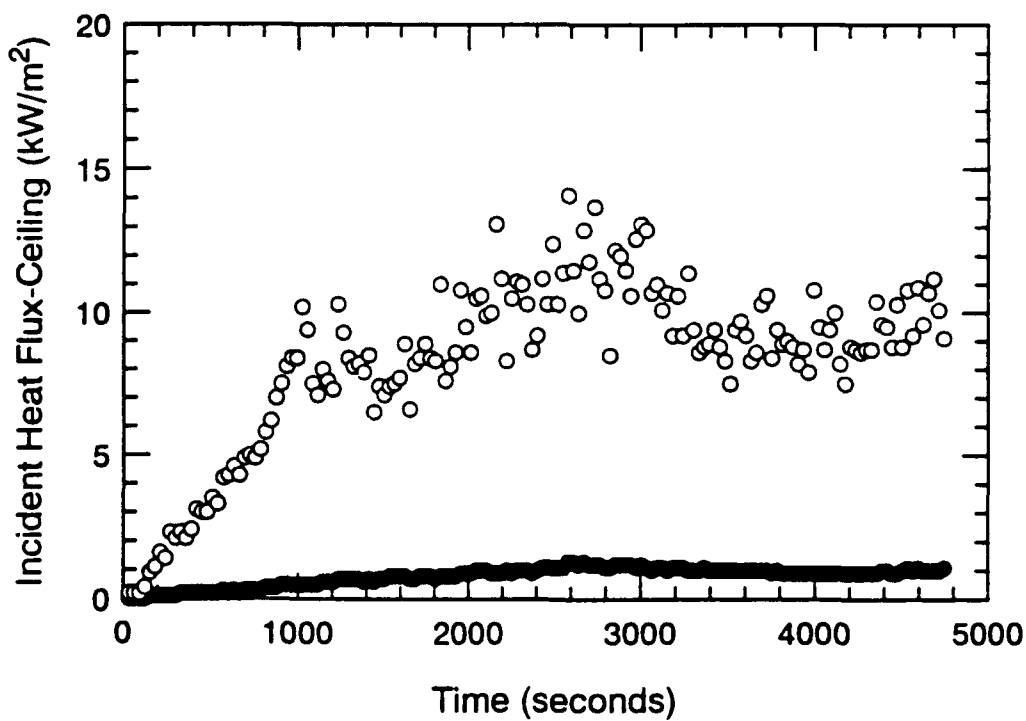
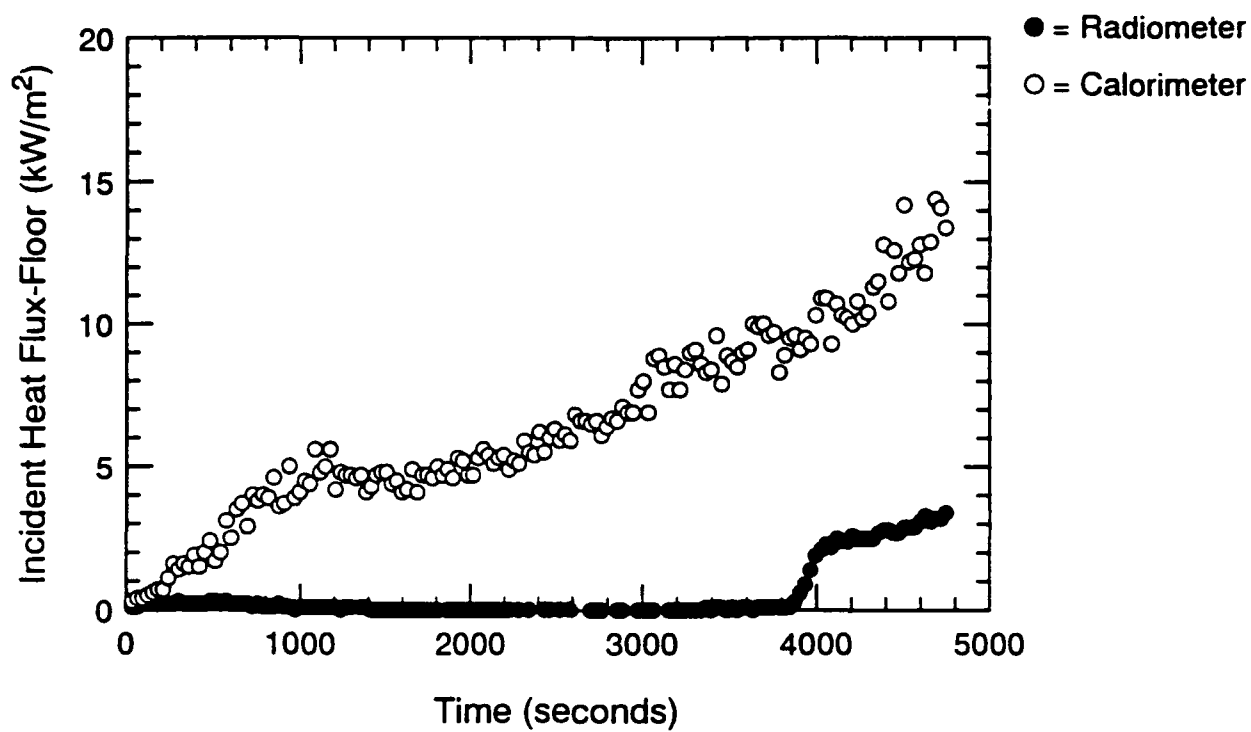


Figure B.15 Incident Heat Flux at Floor and Ceiling-Time Histories - S202

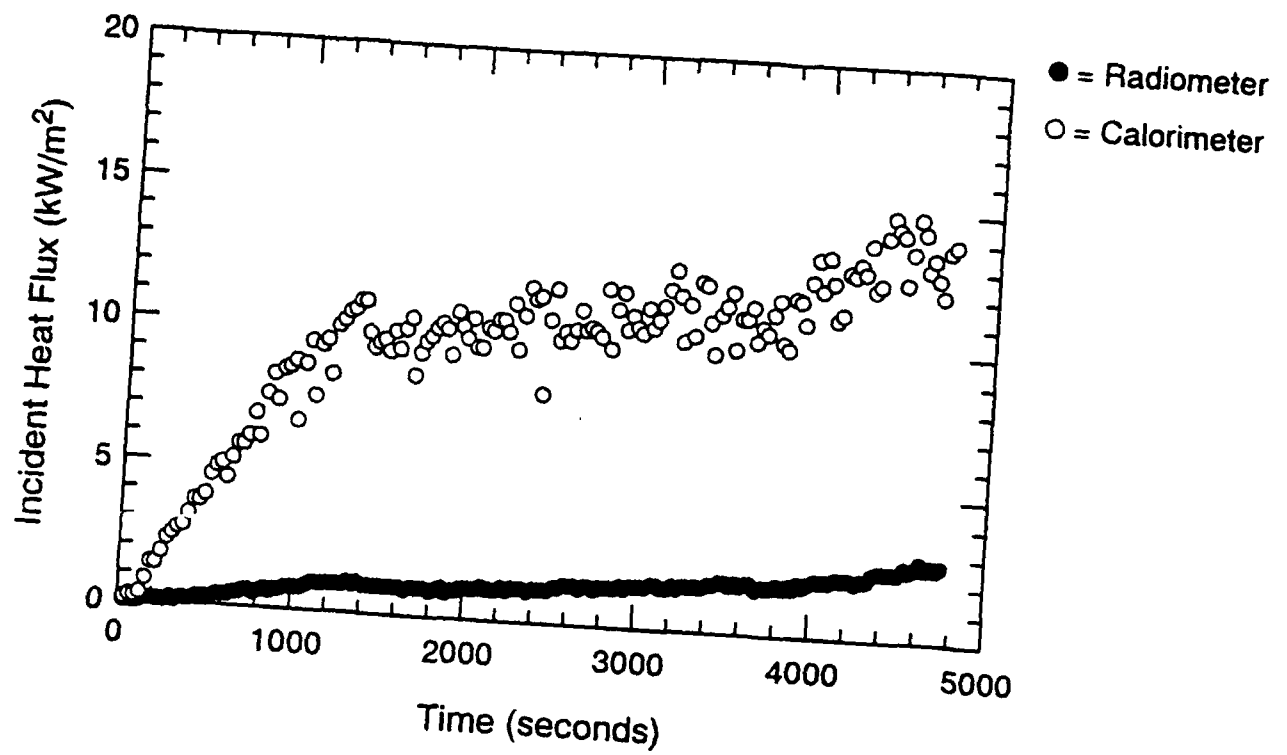


Figure B.16 Incident Heat Flux at Fwd. Bulkhead-Time Histories - S202

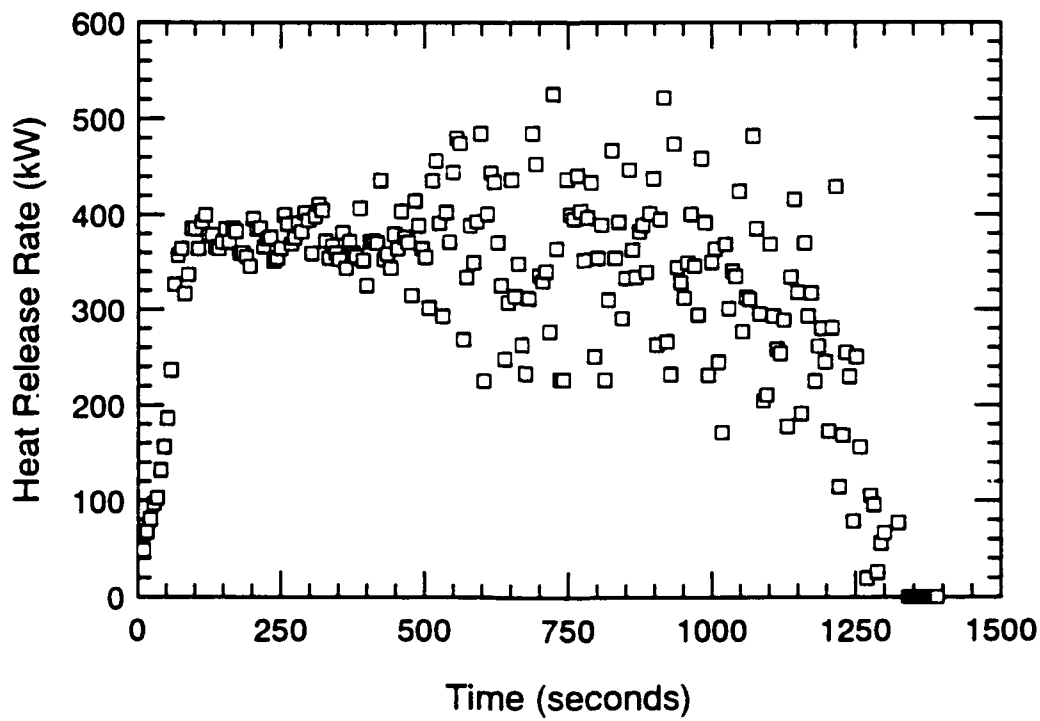
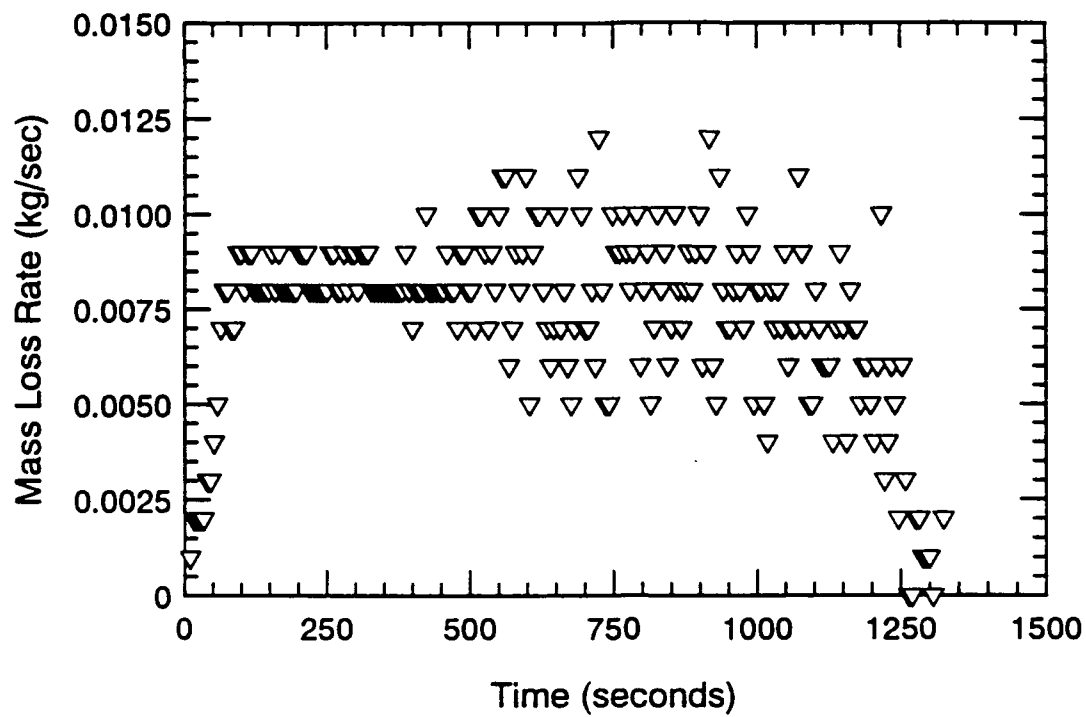


Figure B.17 Mass Loss Rate and Equivalence Ratio-Time Histories - S203

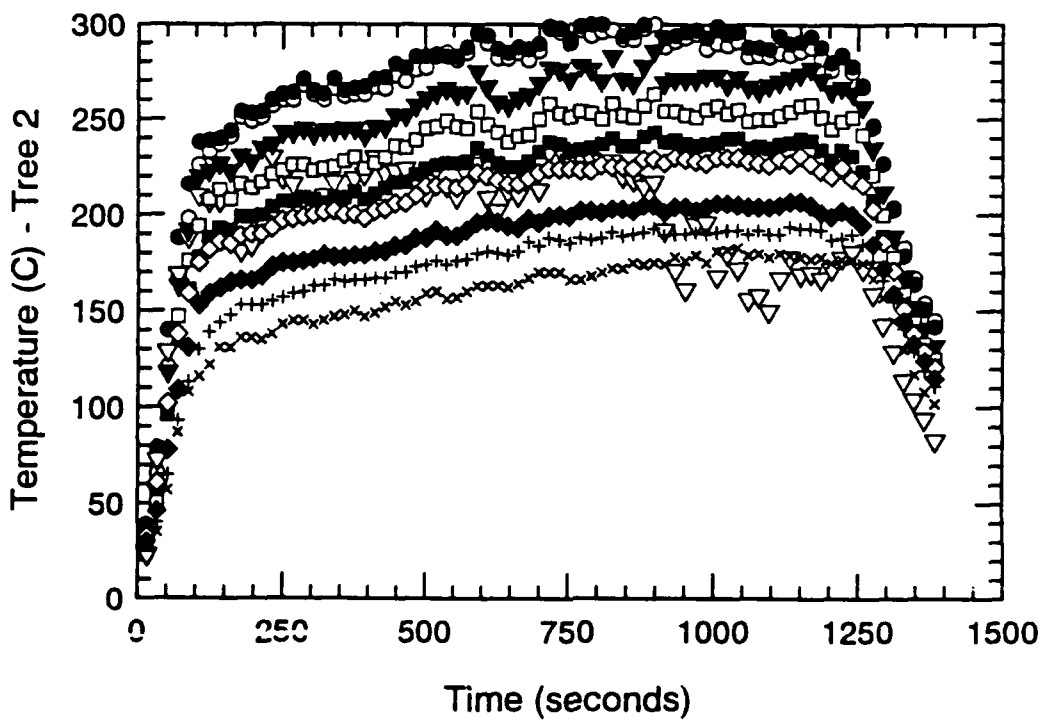
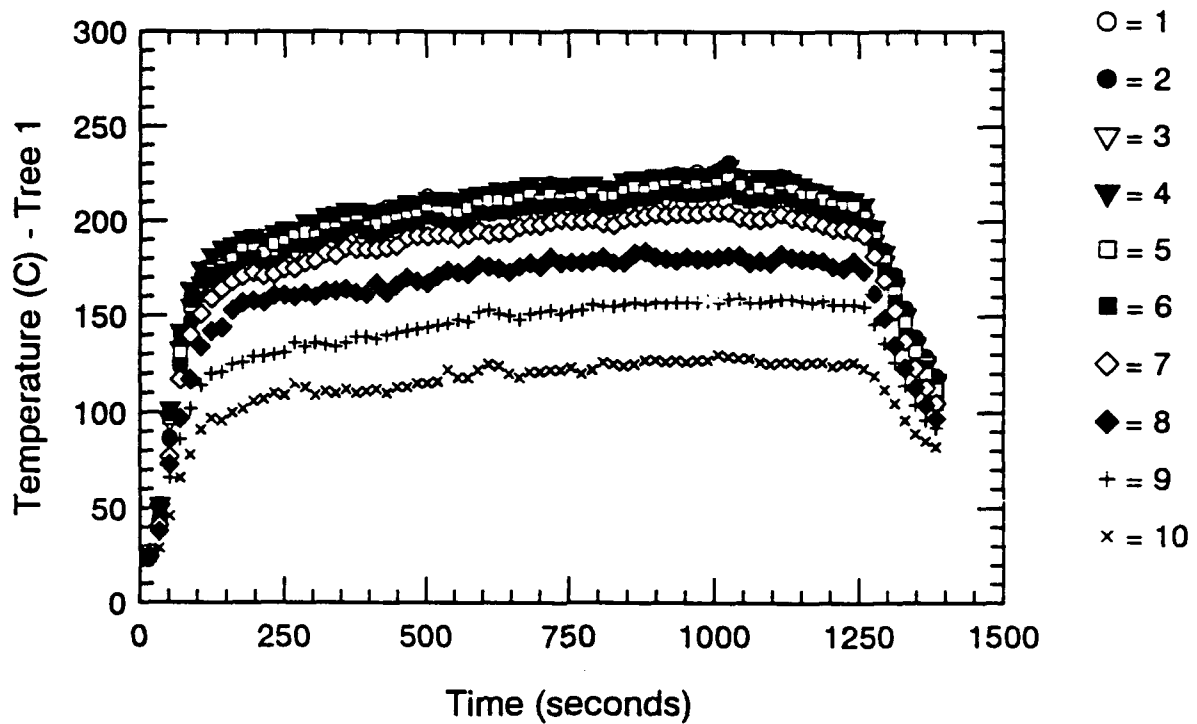


Figure B.18 Thermocouple Trees 1 & 2-Time Histories - S203

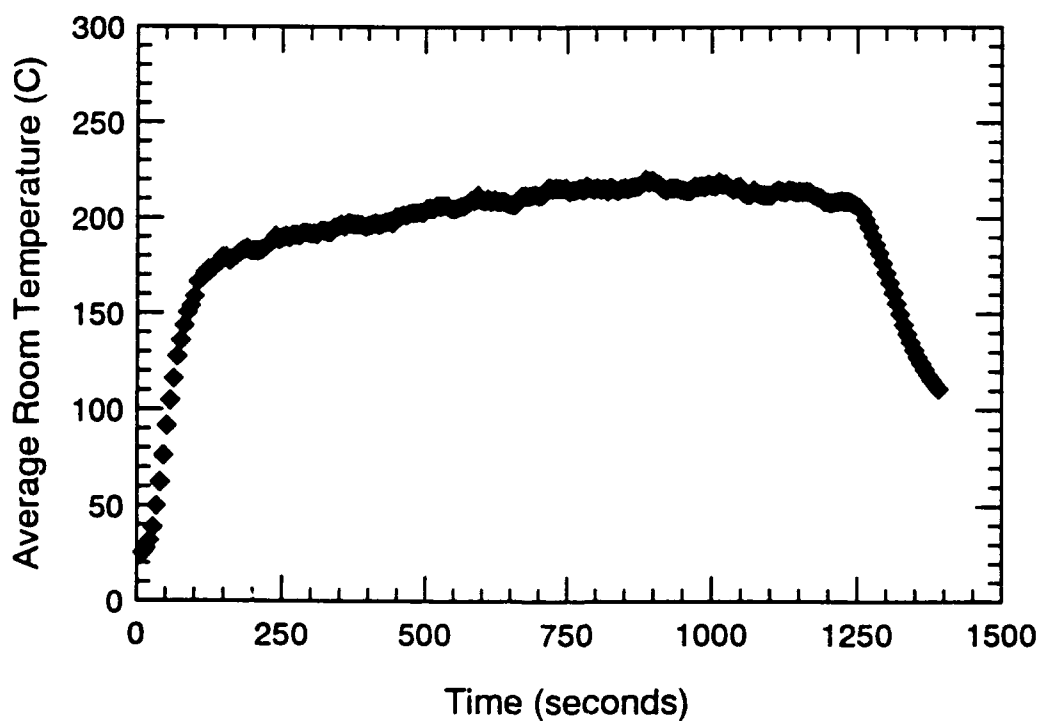
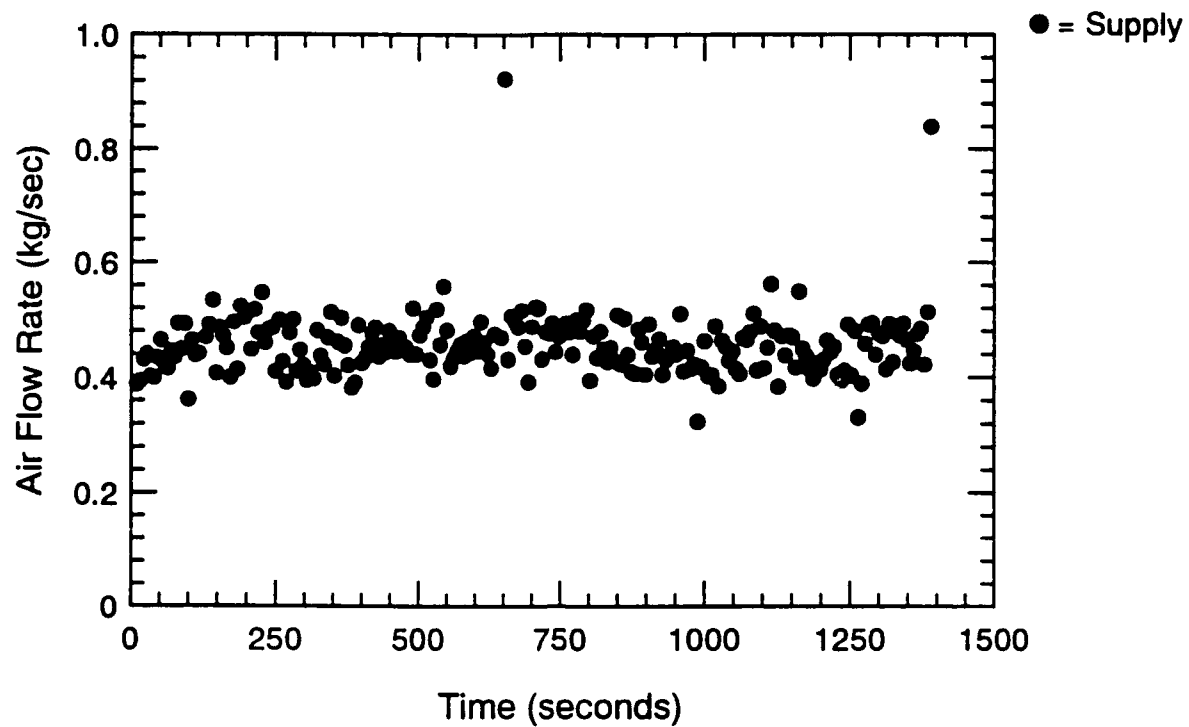


Figure B.19 Air Flow Rate and Avg. Temperature-Time Histories - S203

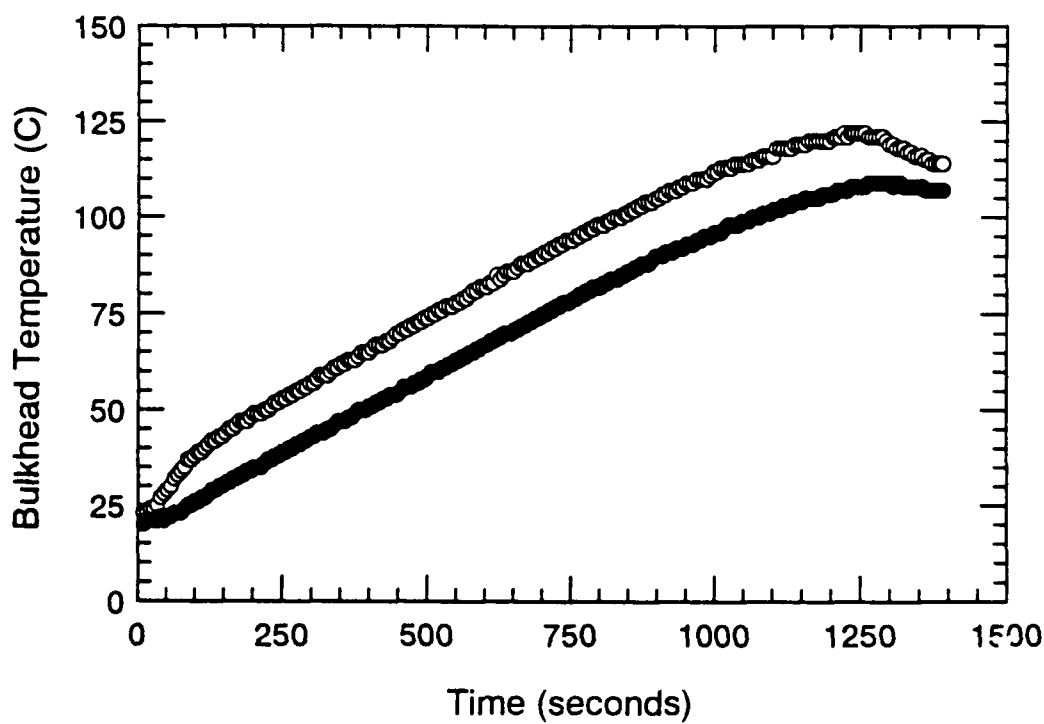
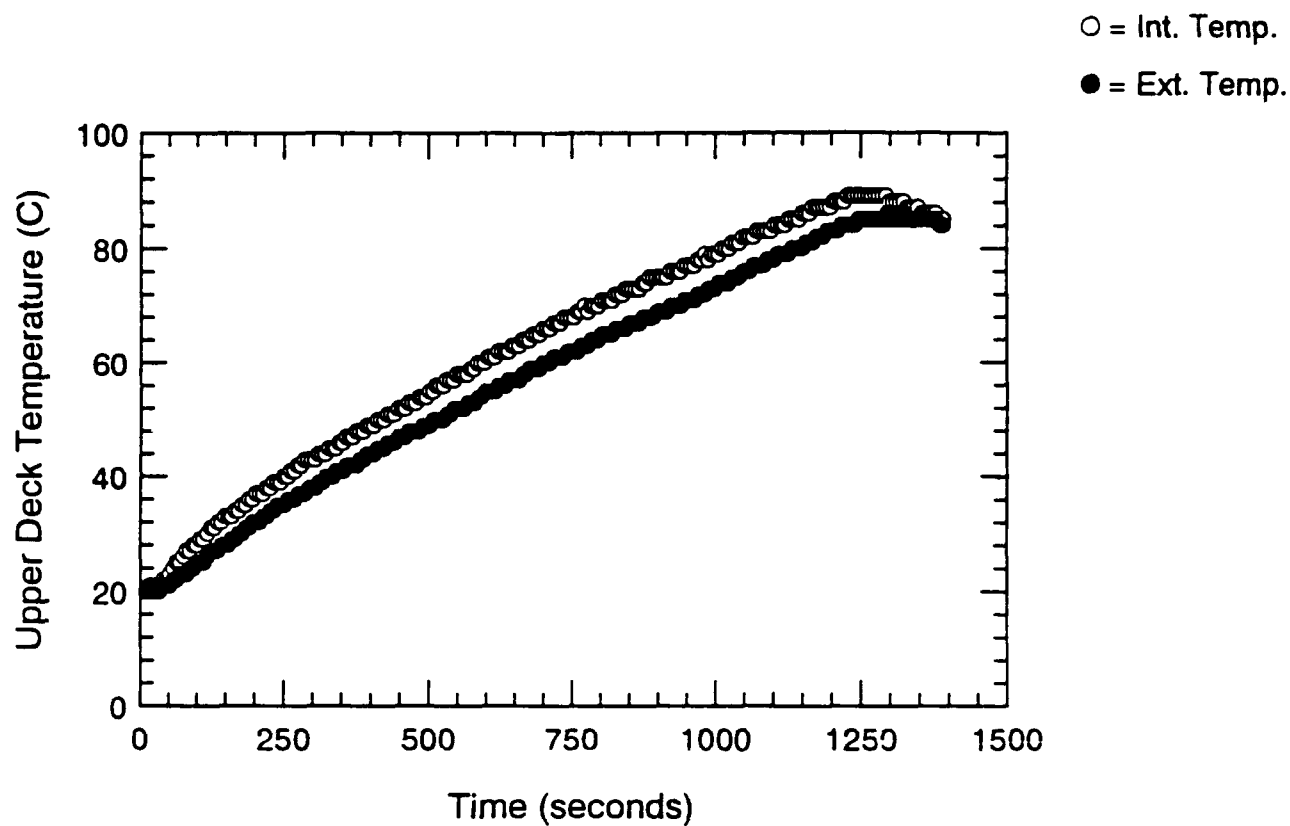


Figure B.20 Surface Thermocouple-Time Histories - S203

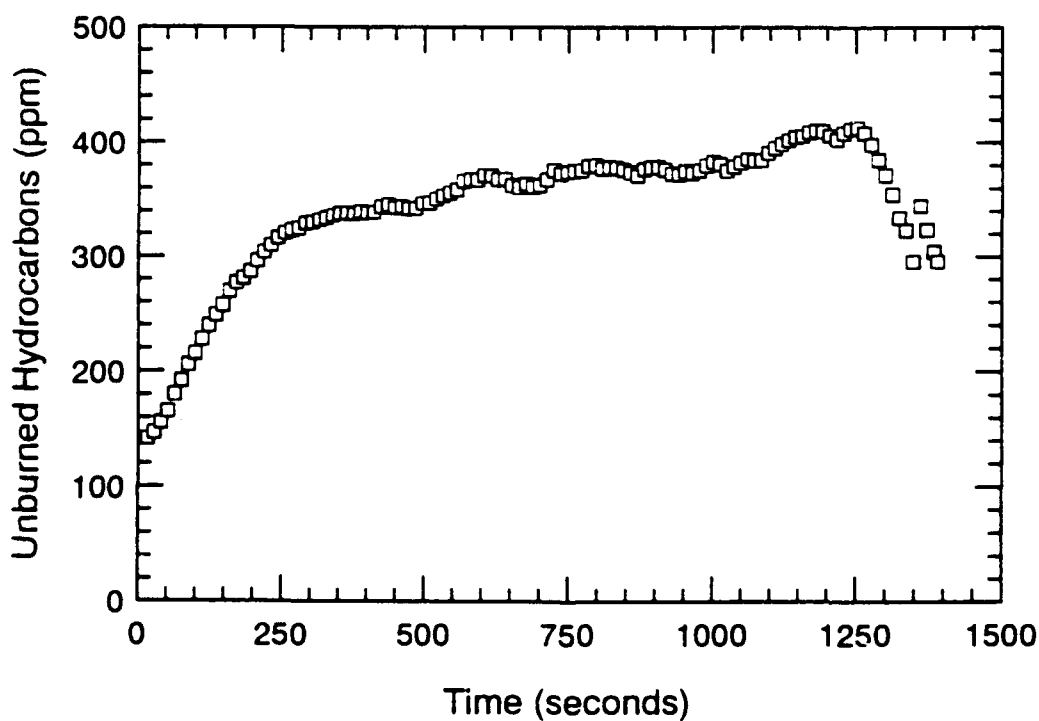
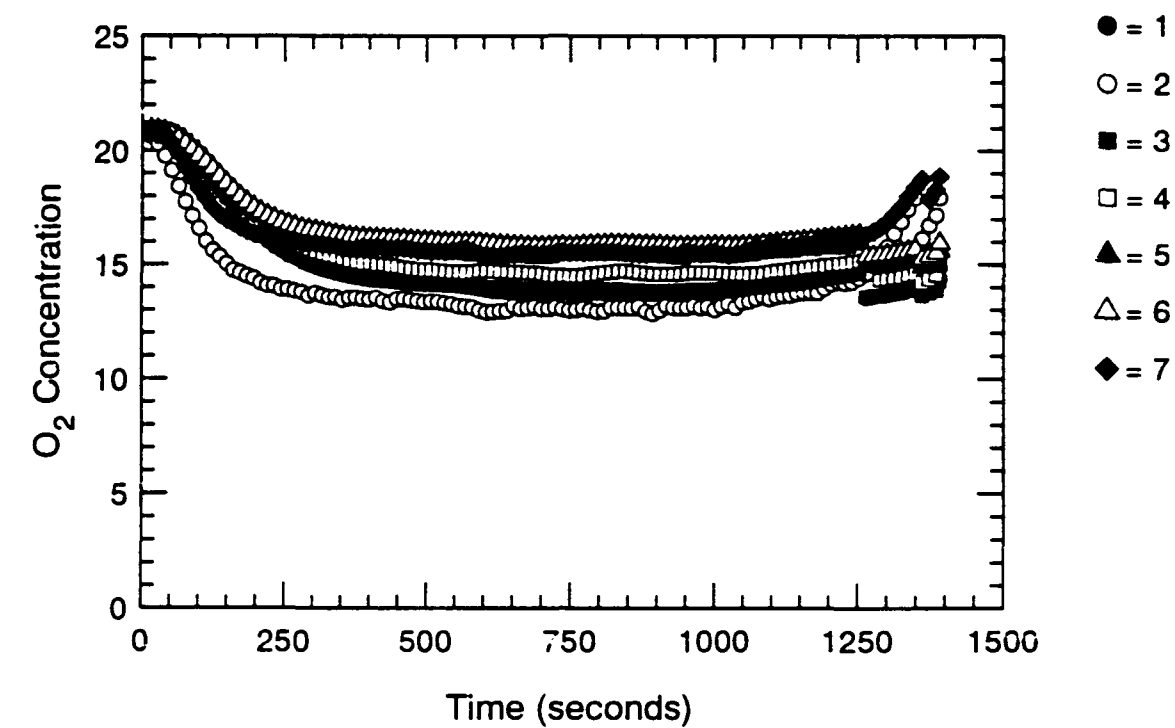


Figure B.21 Oxygen and Unburned HC Concentration-Time Histories - S203

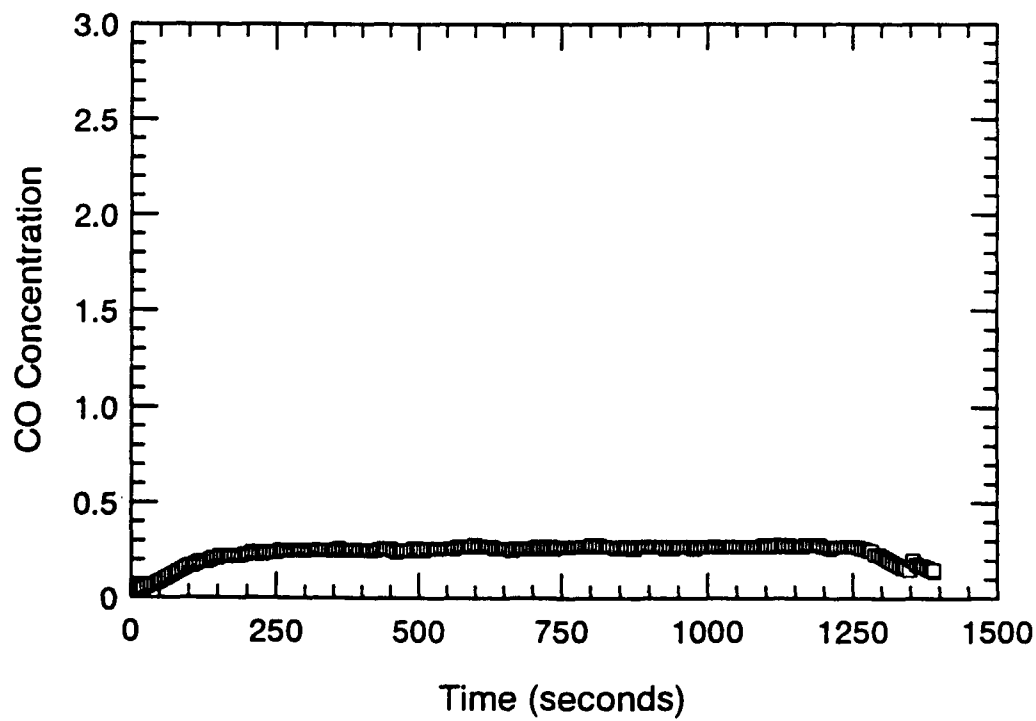
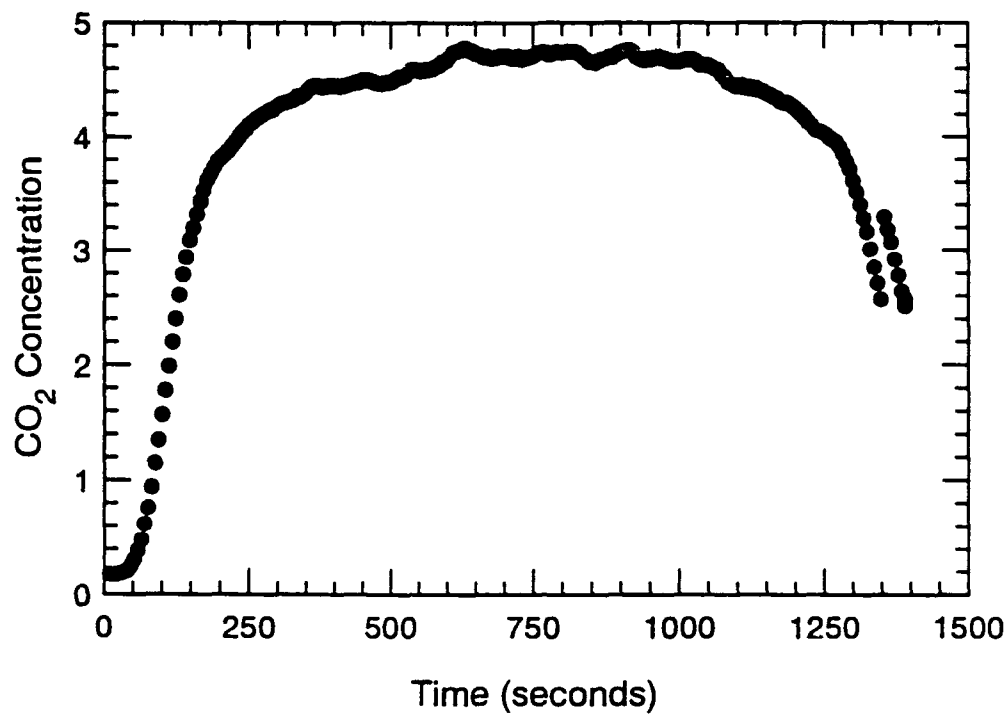


Figure B.22 CO₂ and CO Concentration-Time Histories - S203

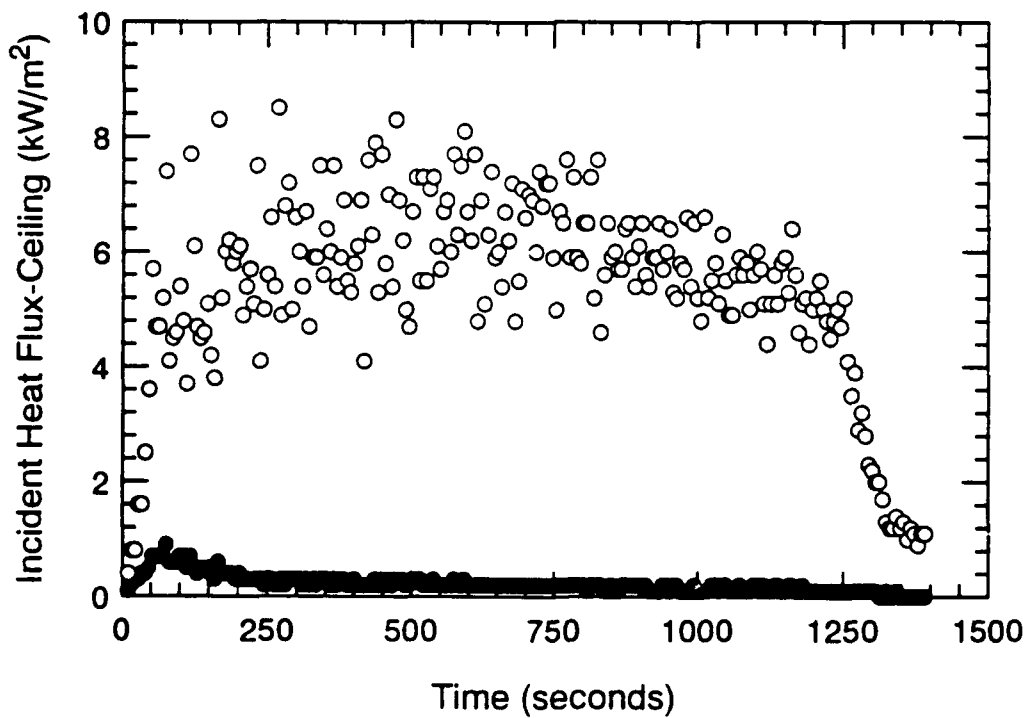
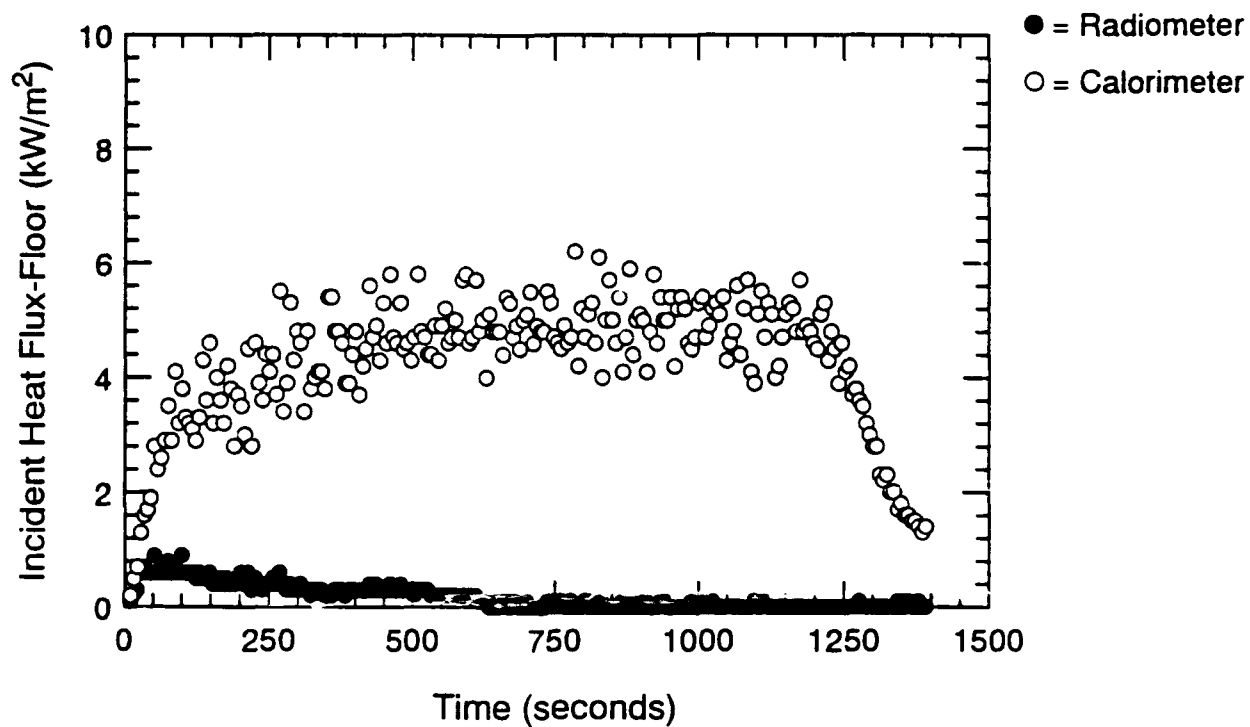


Figure B.23 Incident Heat Flux at Floor and Ceiling-Time Histories - S203

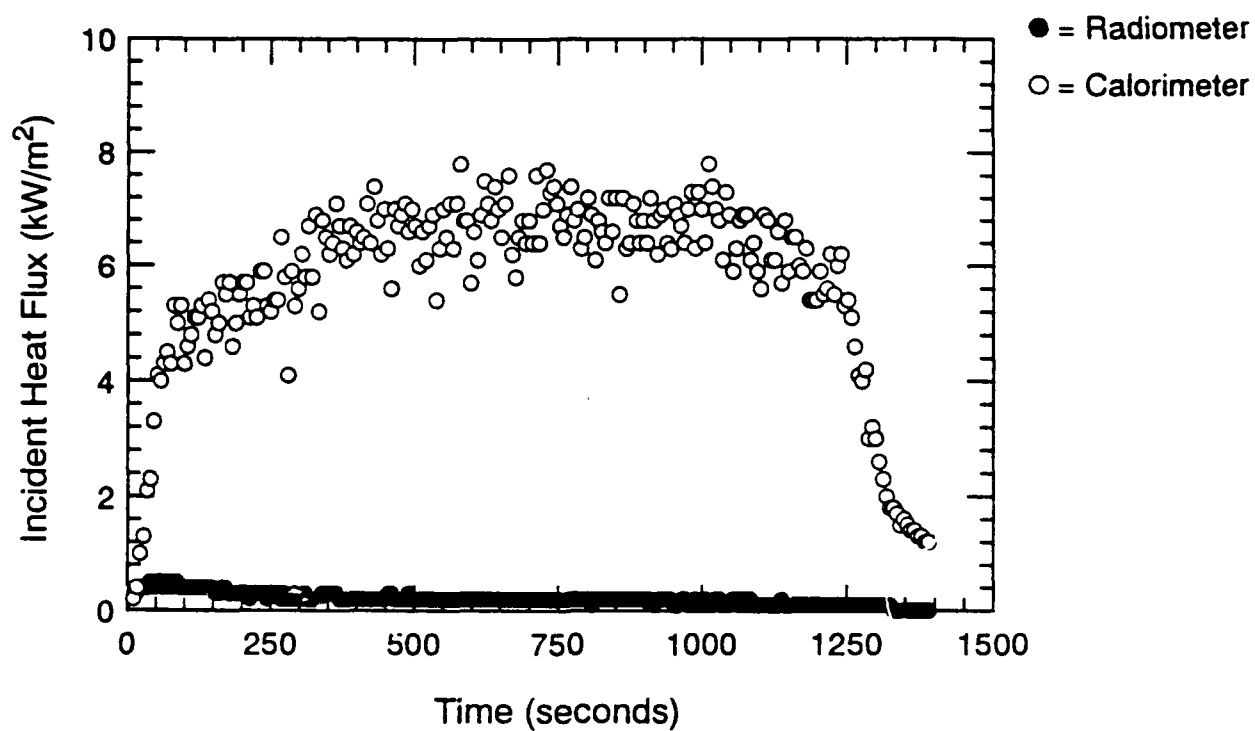


Figure B.24 Incident Heat Flux at Fwd. Bulkhead-Time Histories - S203

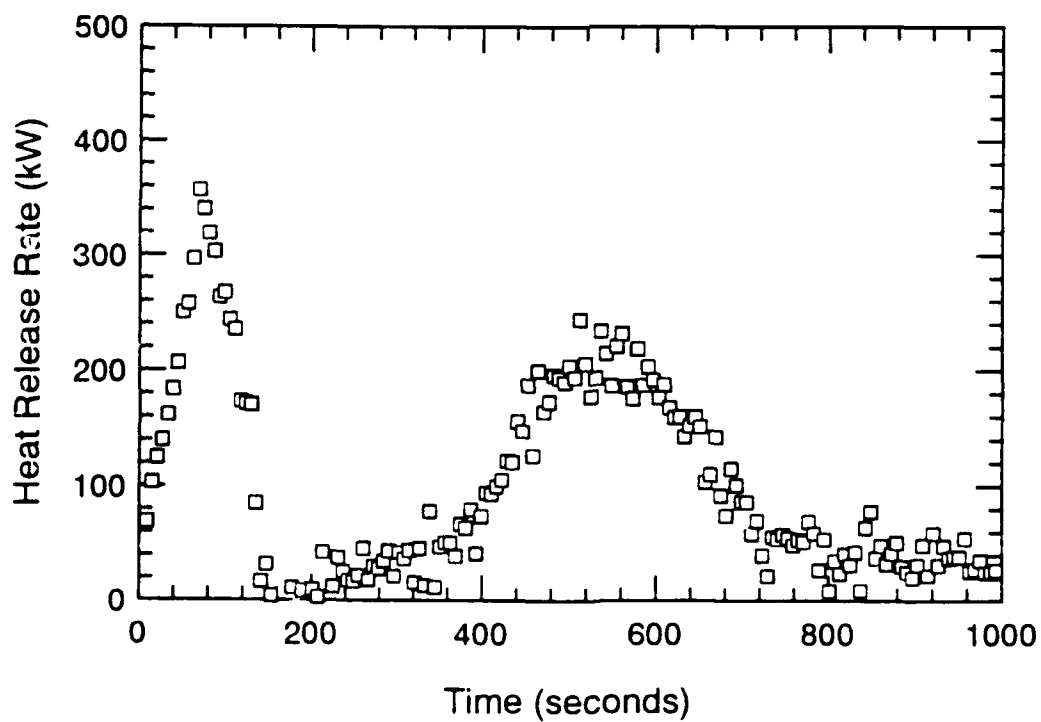
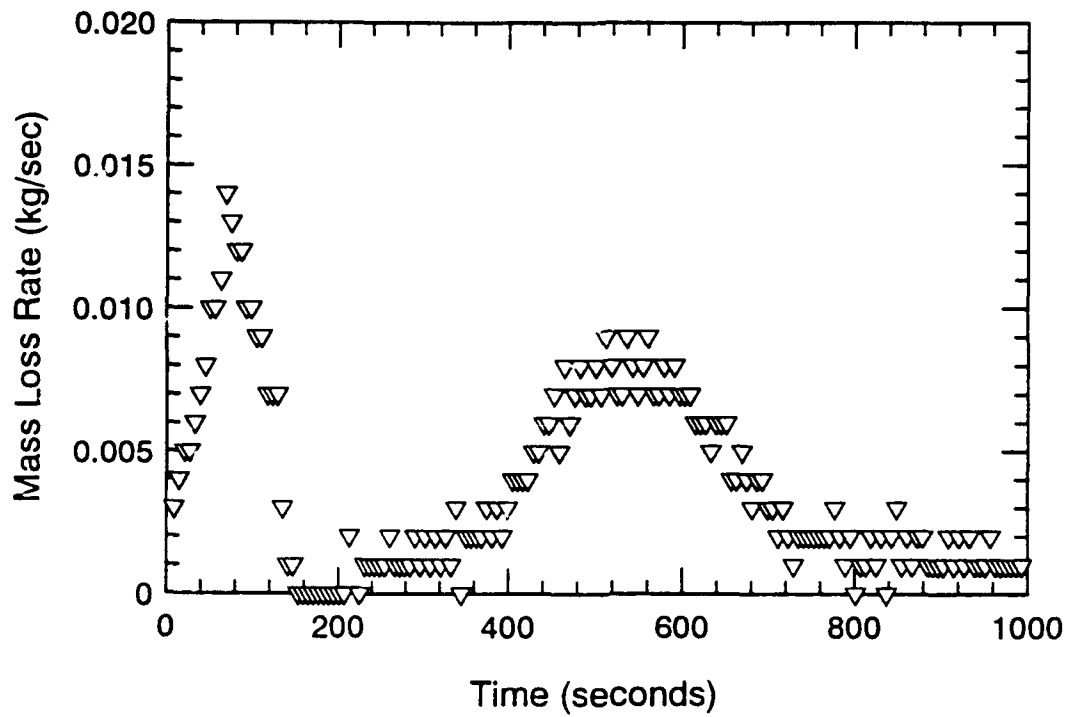


Figure B.25 Mass Loss Rate and Equivalence Ratio-Time Histories - S204

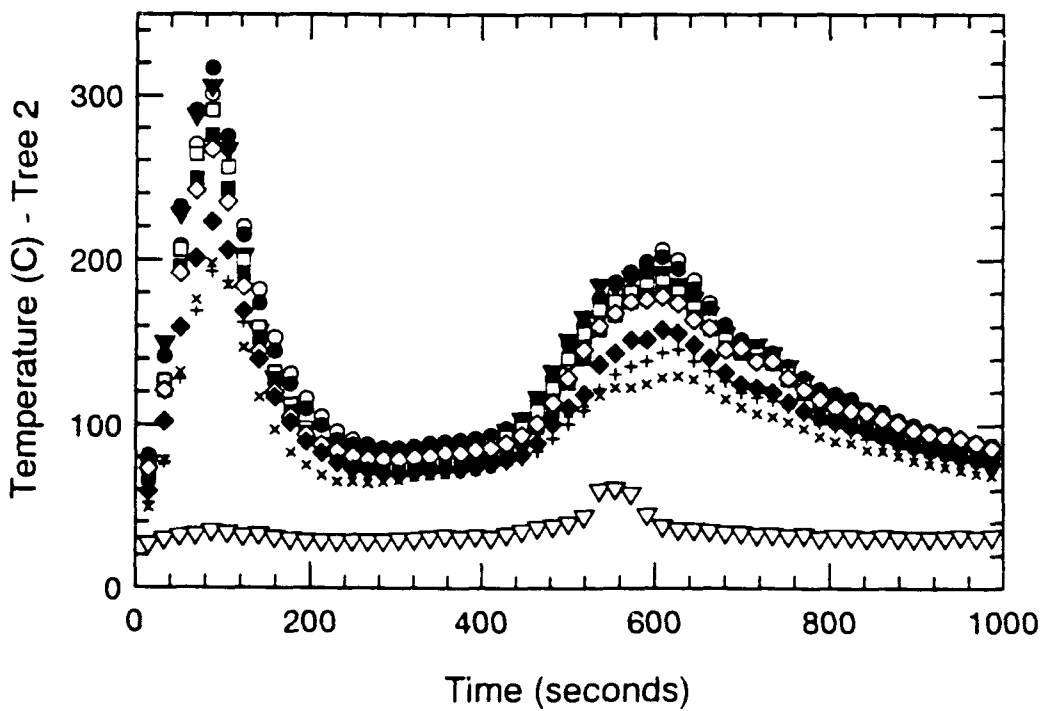
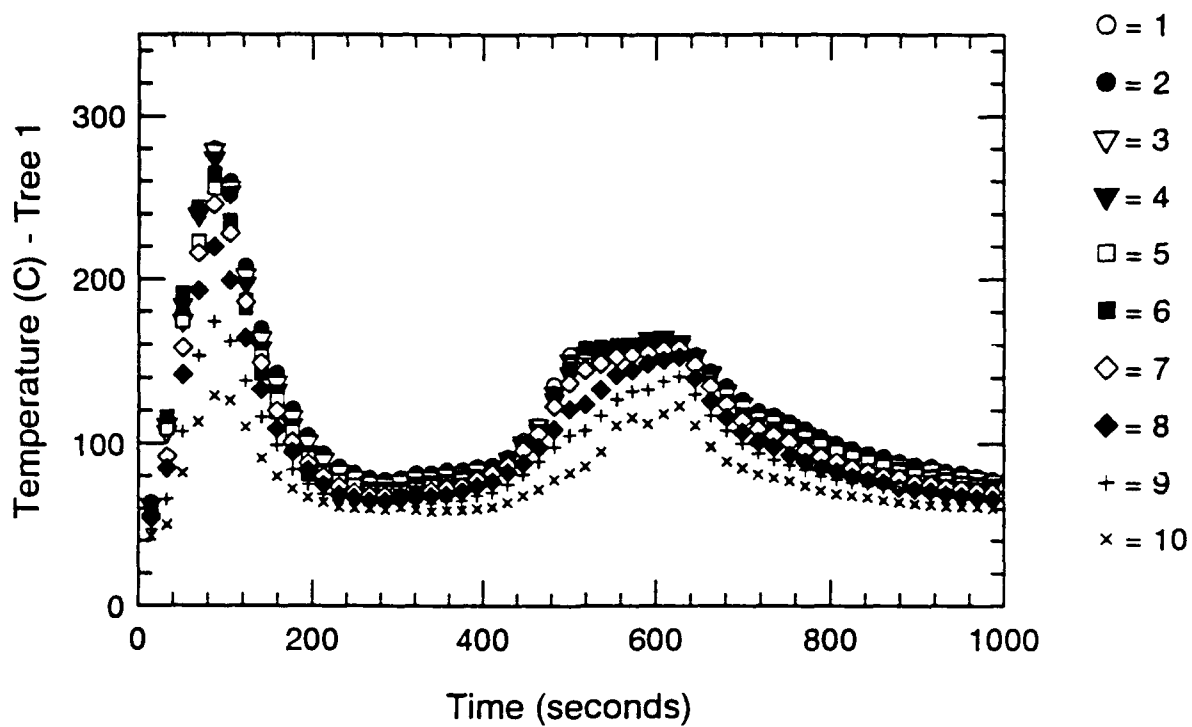


Figure B.26 Thermocouple Trees 1 & 2-Time Histories - S204

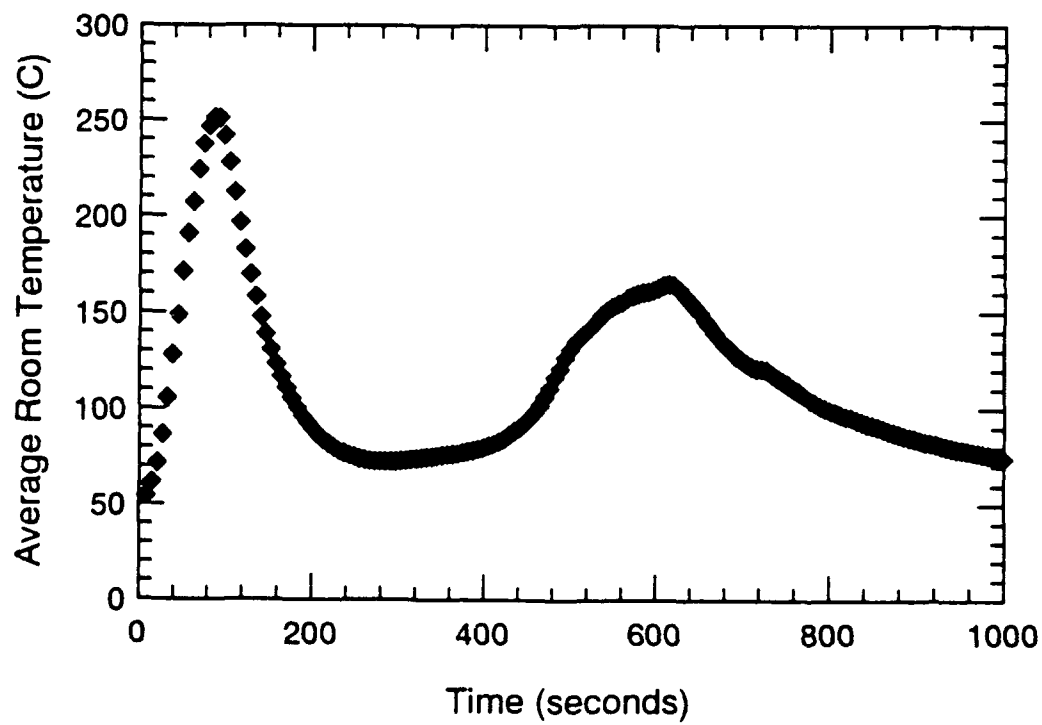
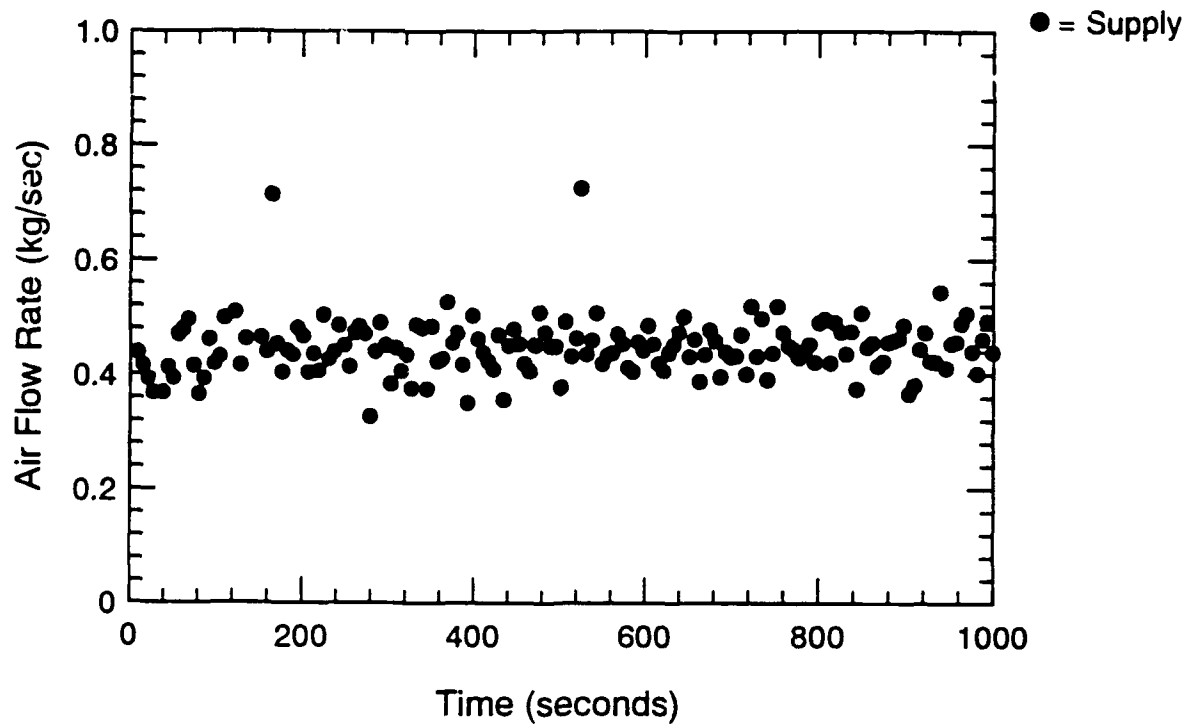


Figure B.27 Air Flow Rate and Avg. Temperature-Time Histories - S204

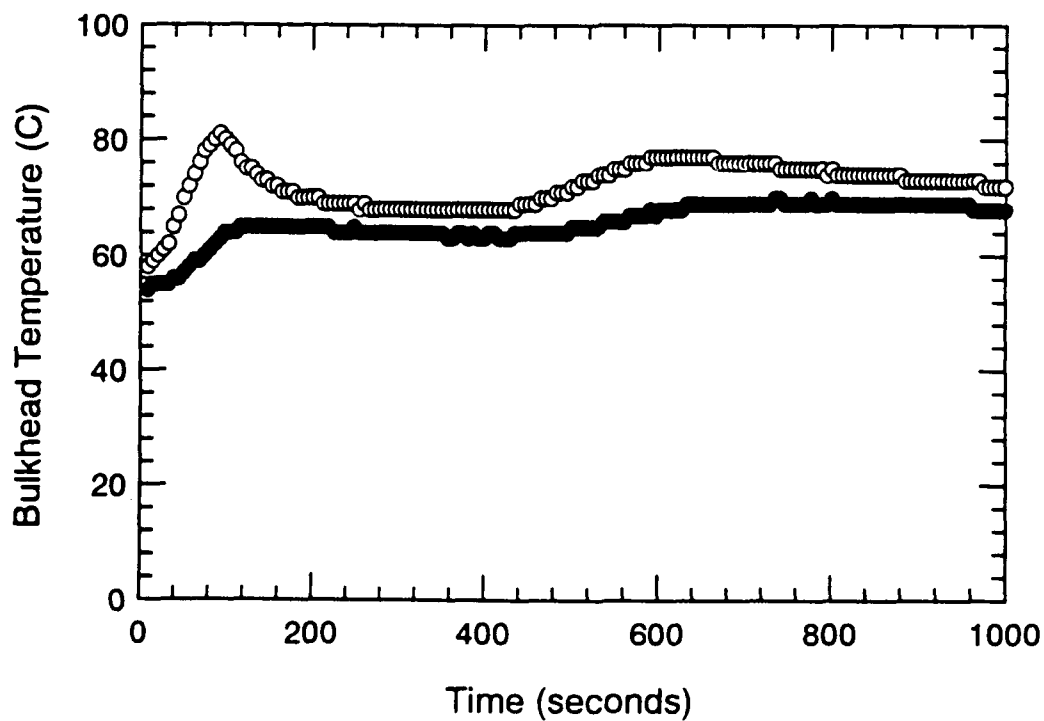
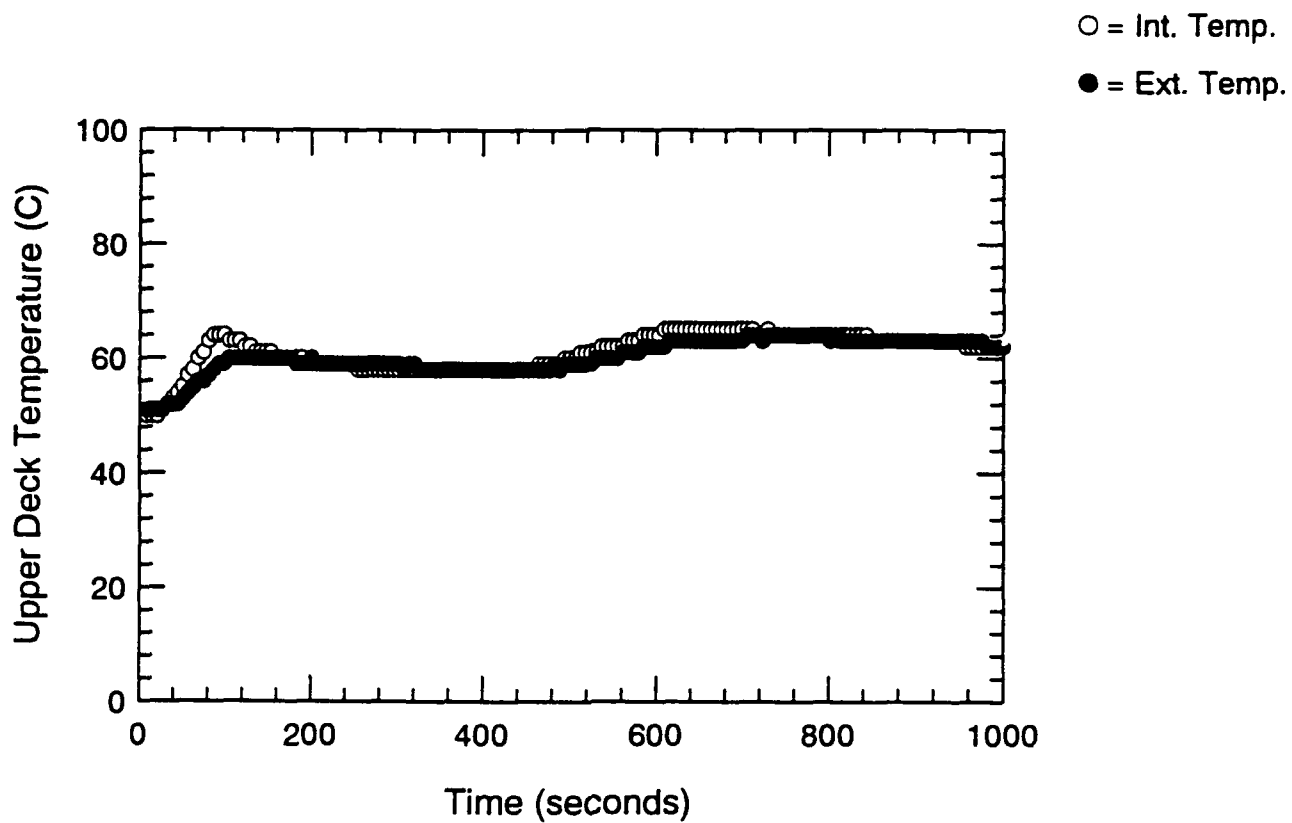


Figure B.28 Surface Thermocouple-Time Histories - S204

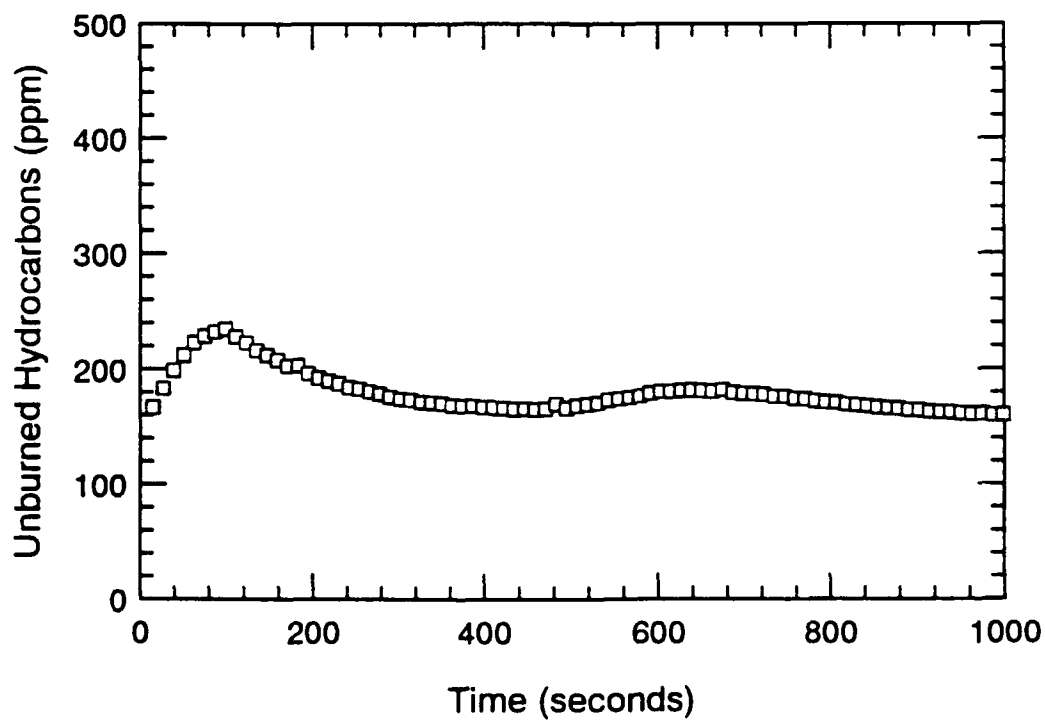
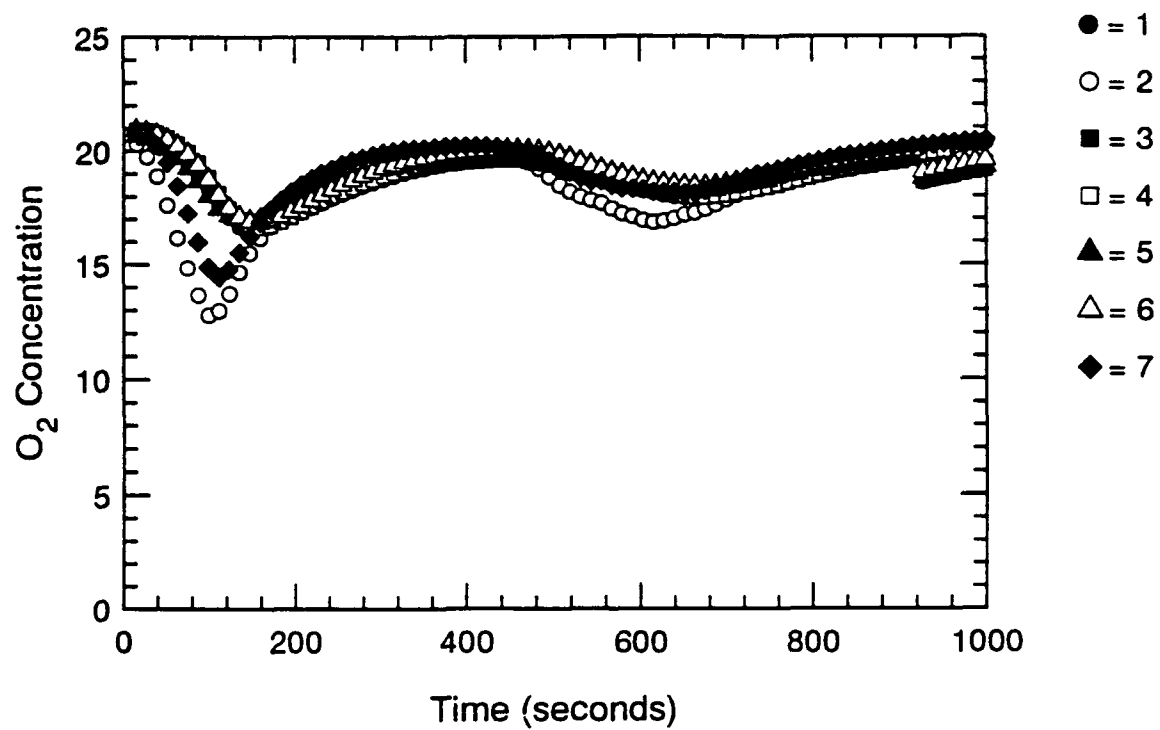


Figure B.29 Oxygen and Unburned HC Concentration-Time Histories - S204

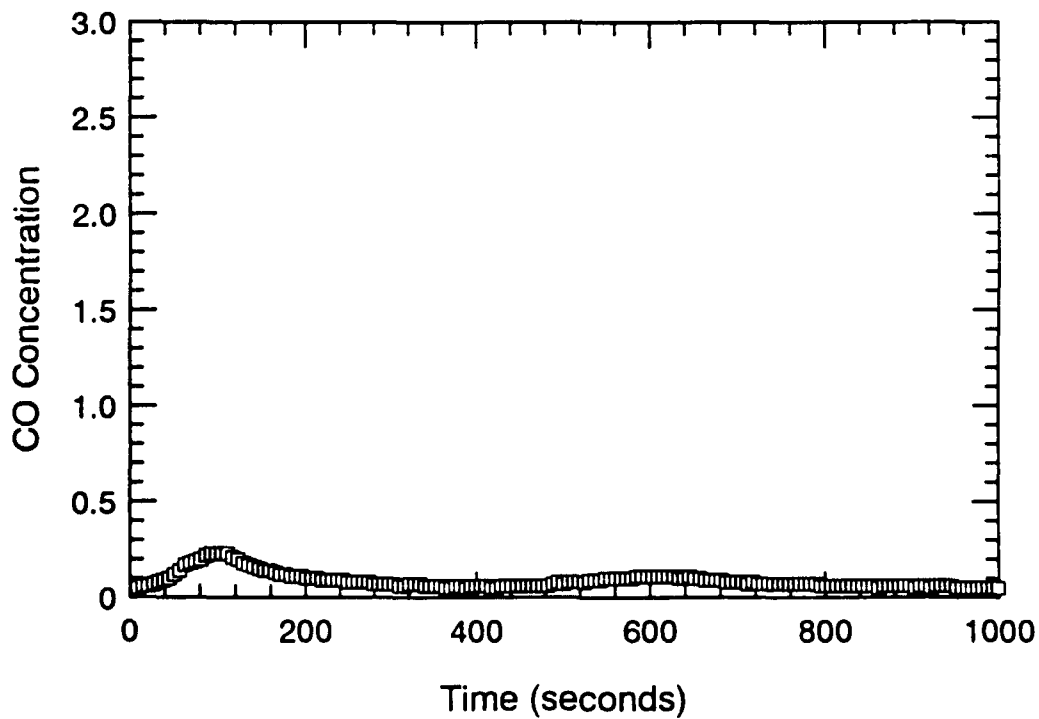
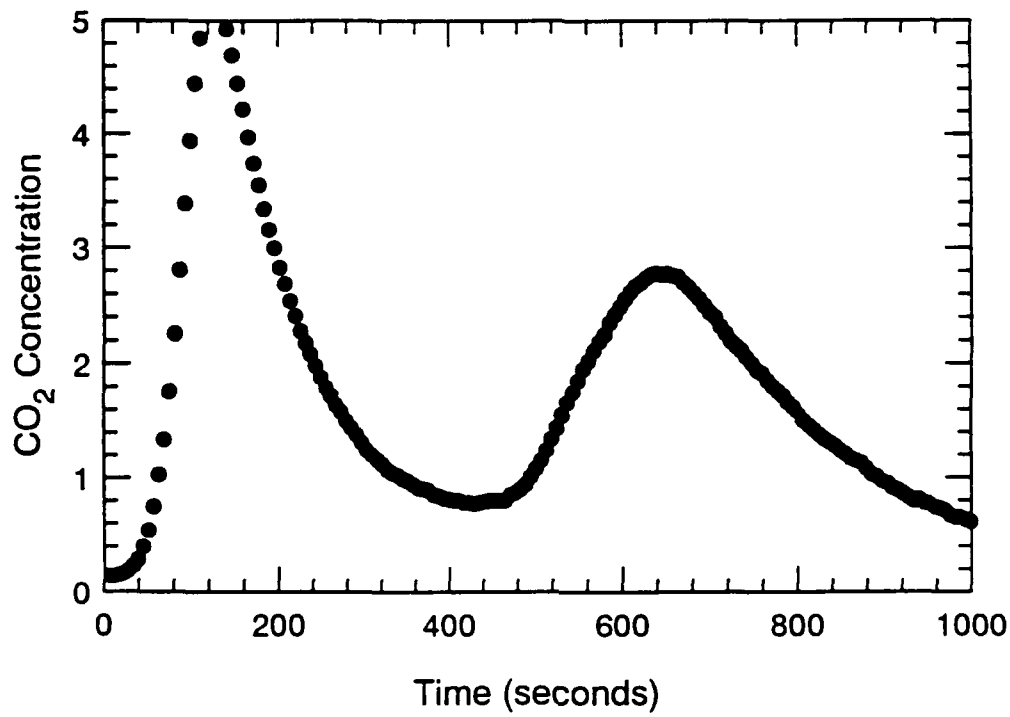


Figure B.30 CO₂ and CO Concentration-Time Histories - S204

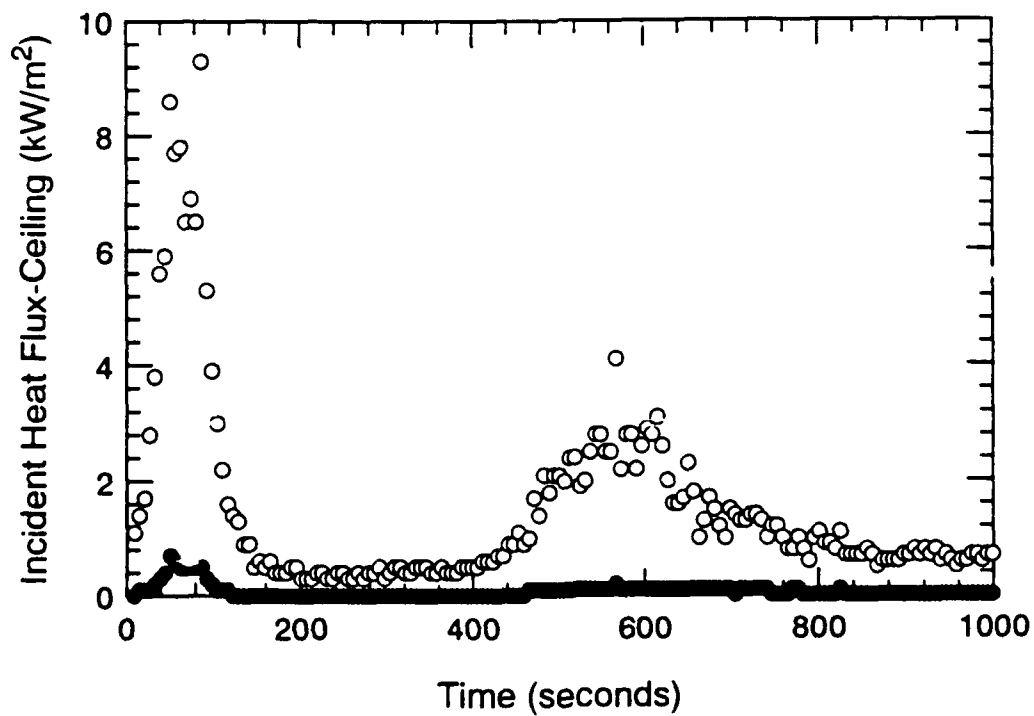
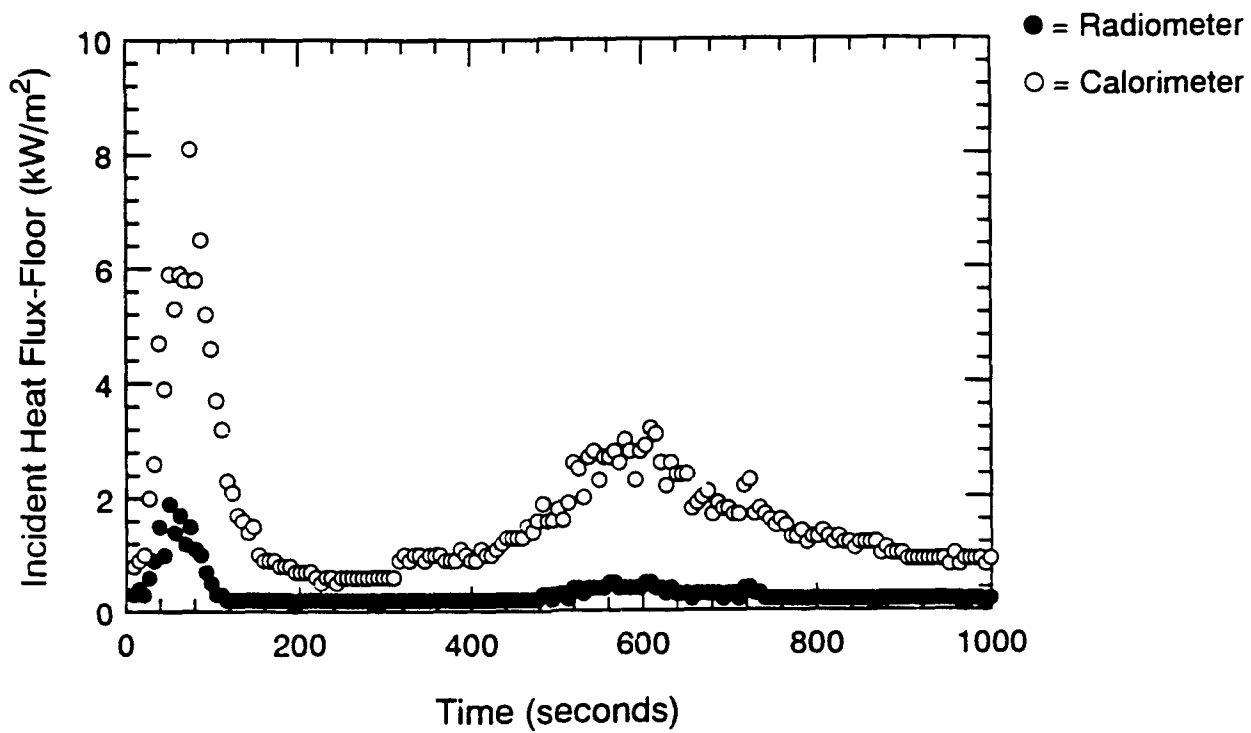


Figure B.31 Incident Heat Flux at Floor and Ceiling-Time Histories - S204

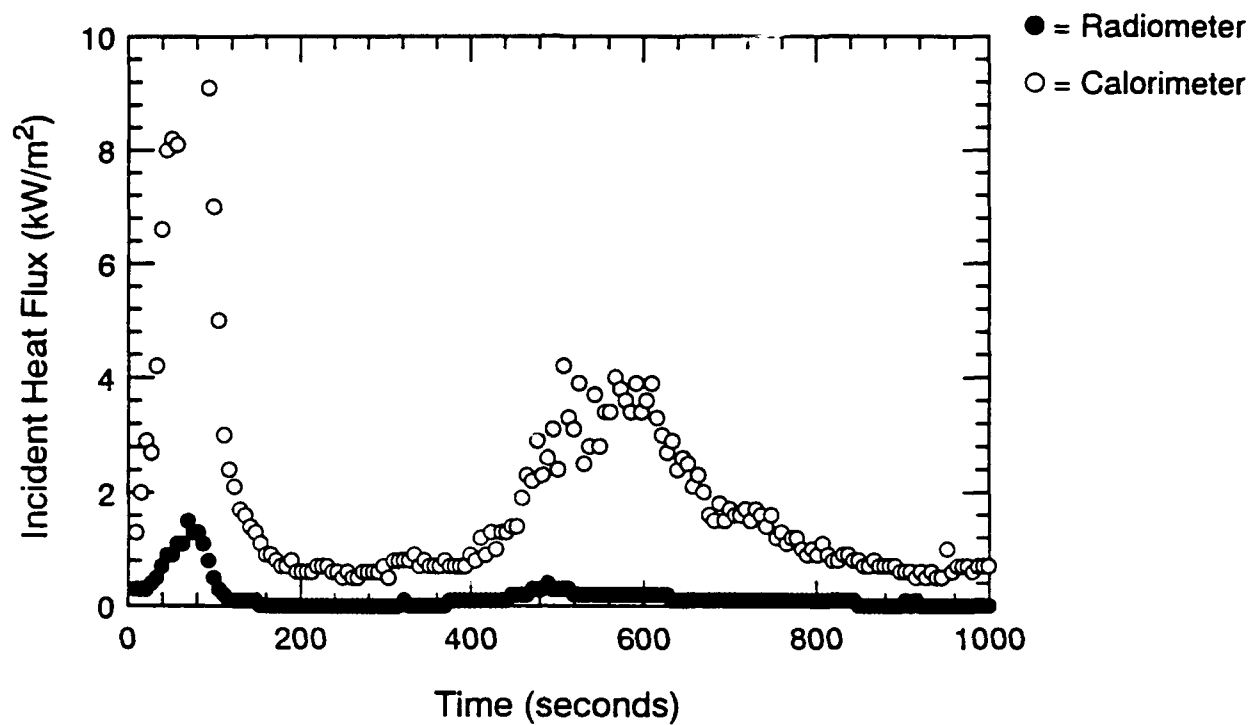


Figure B.32 Incident Heat Flux at Fwd. Bulkhead-Time Histories - S204

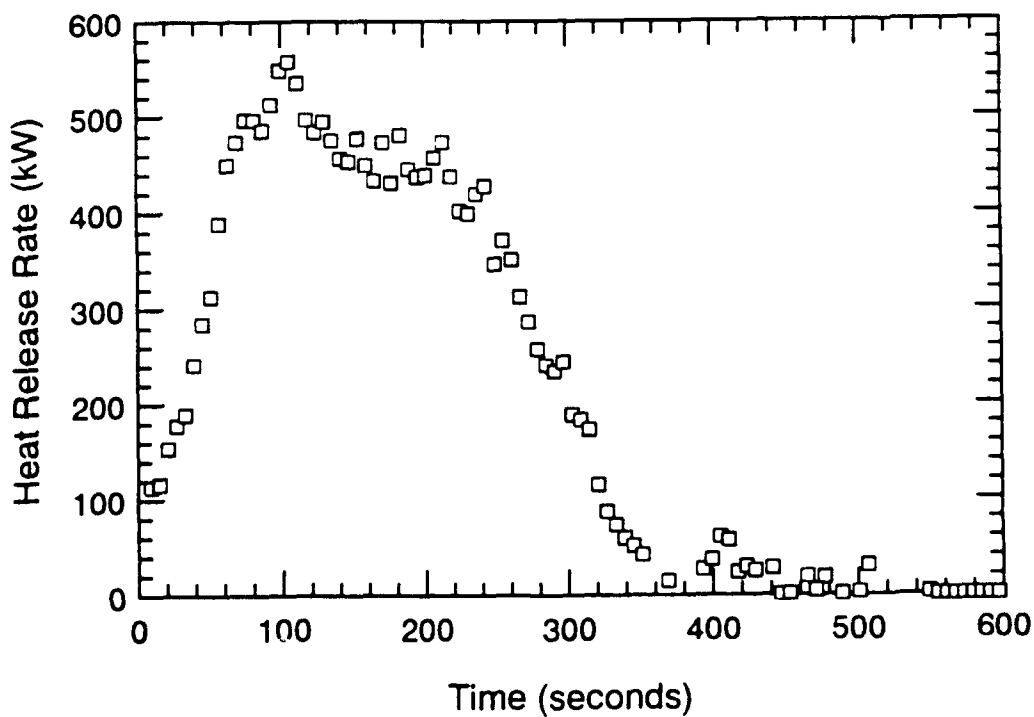
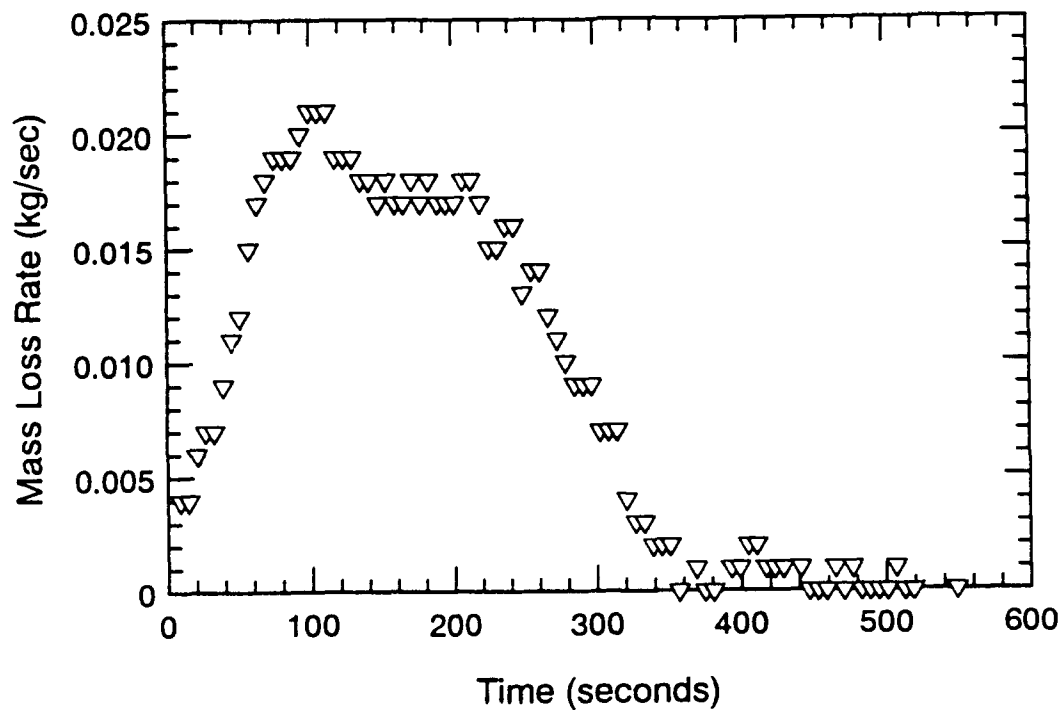


Figure B.33 Mass Loss Rate and Equivalence Ratio-Time Histories - S205

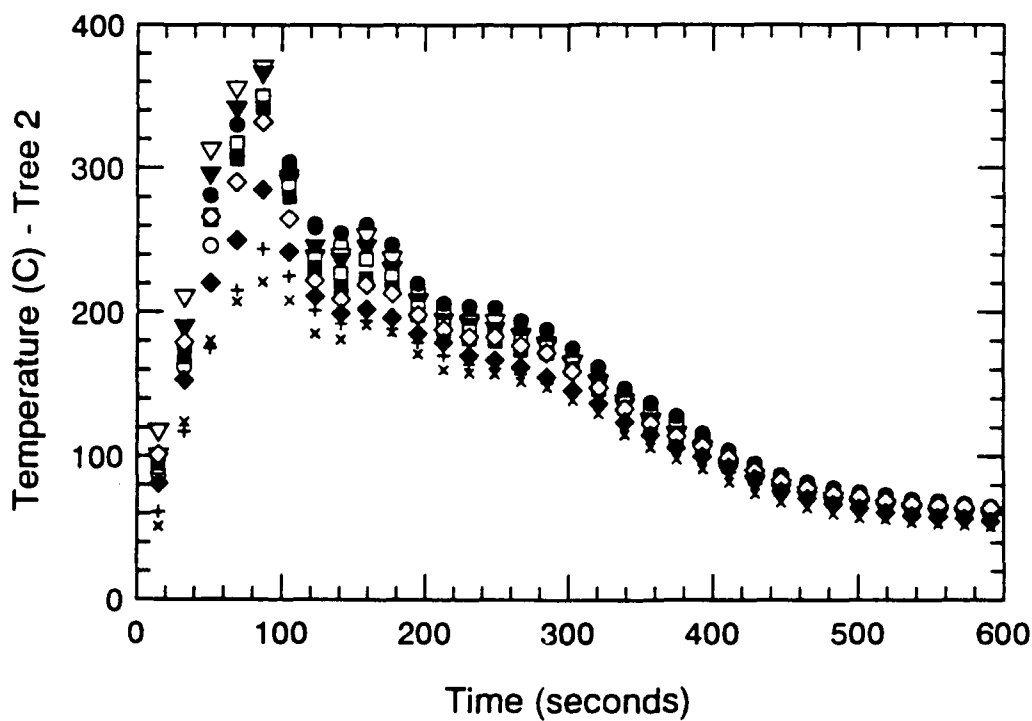
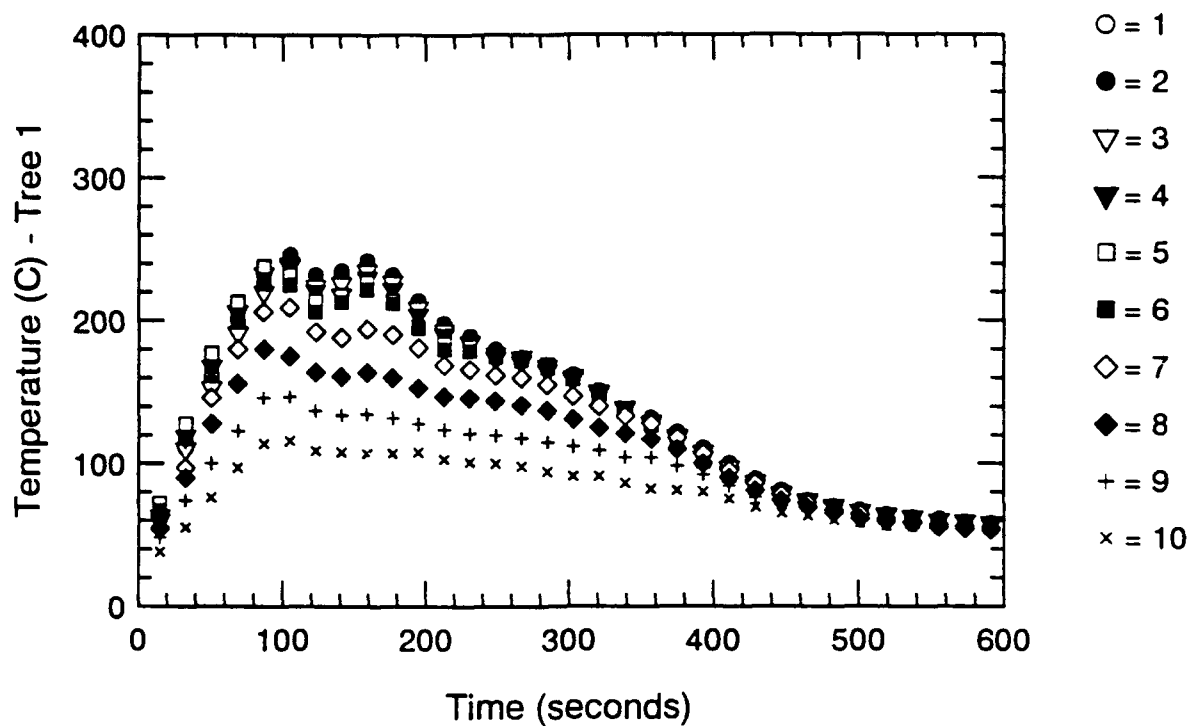


Figure B.34 Thermocouple Trees 1 & 2-Time Histories - S205

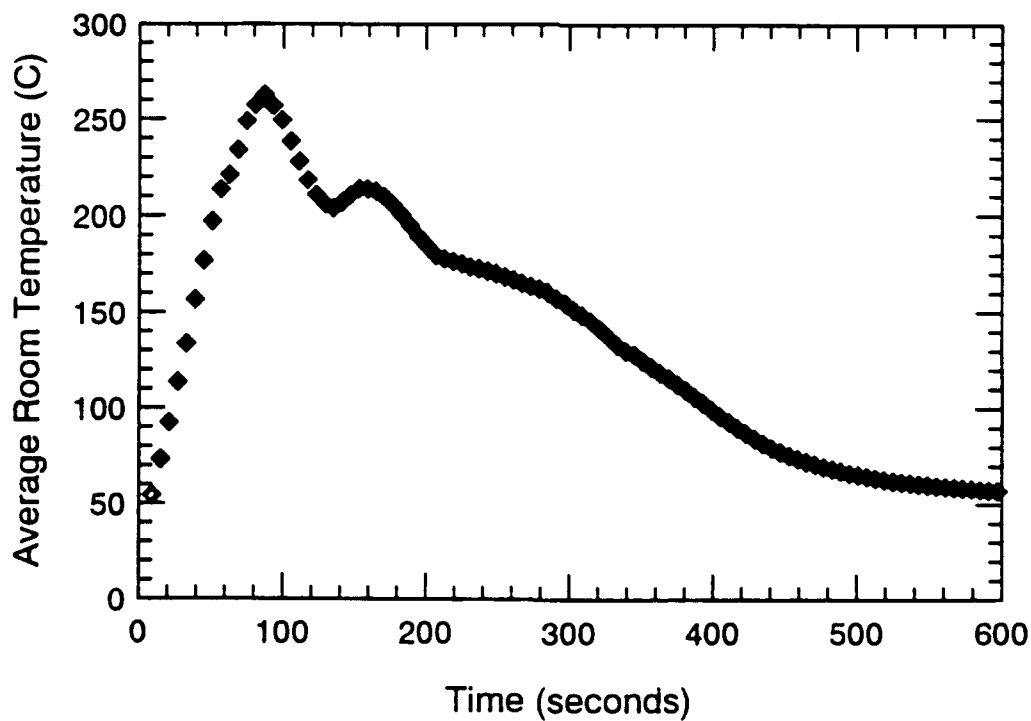
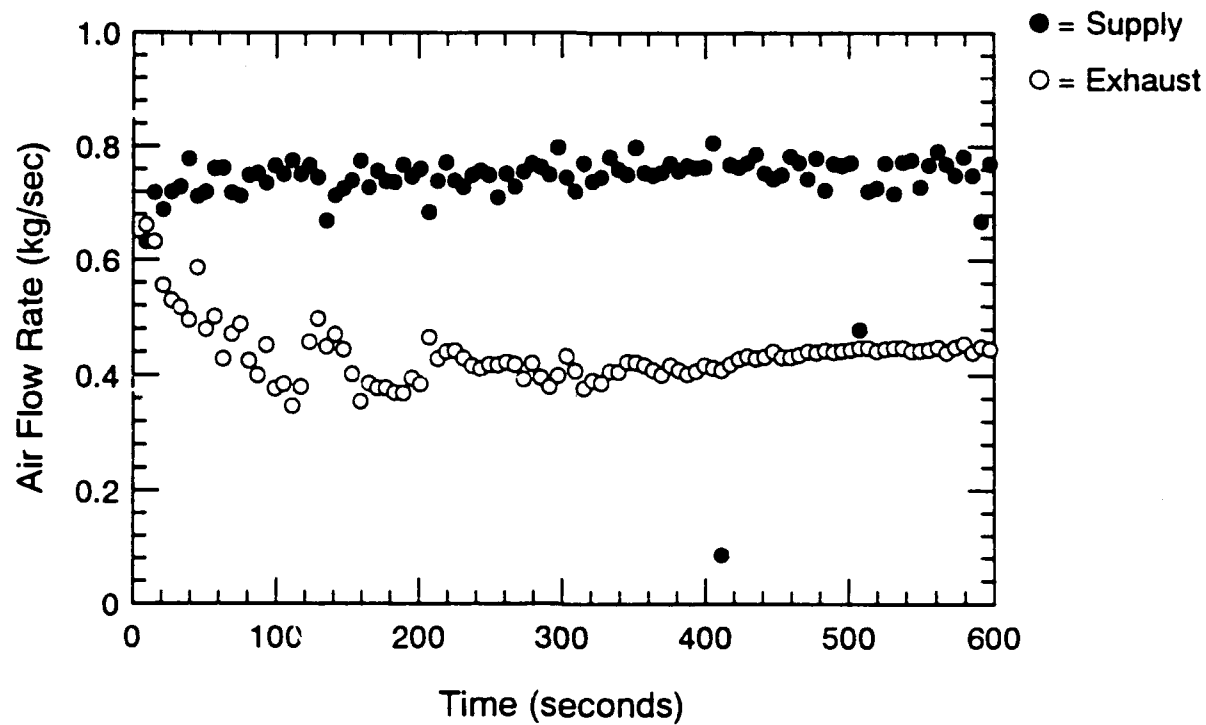


Figure B.35 Air Flow Rate and Avg. Temperature-Time Histories - S205

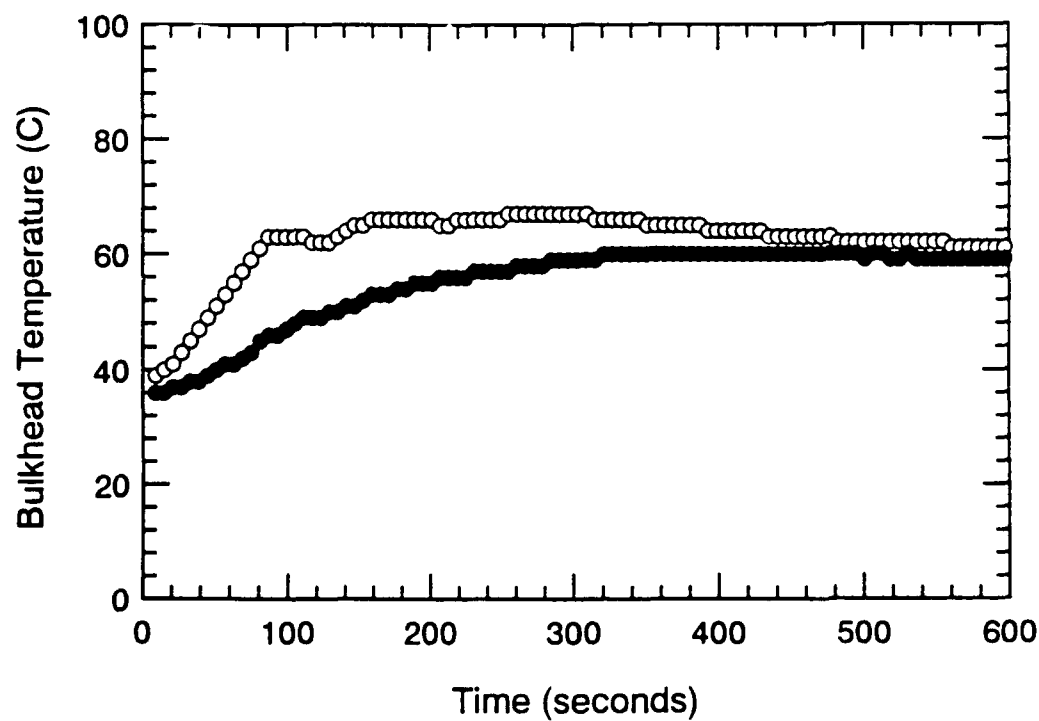
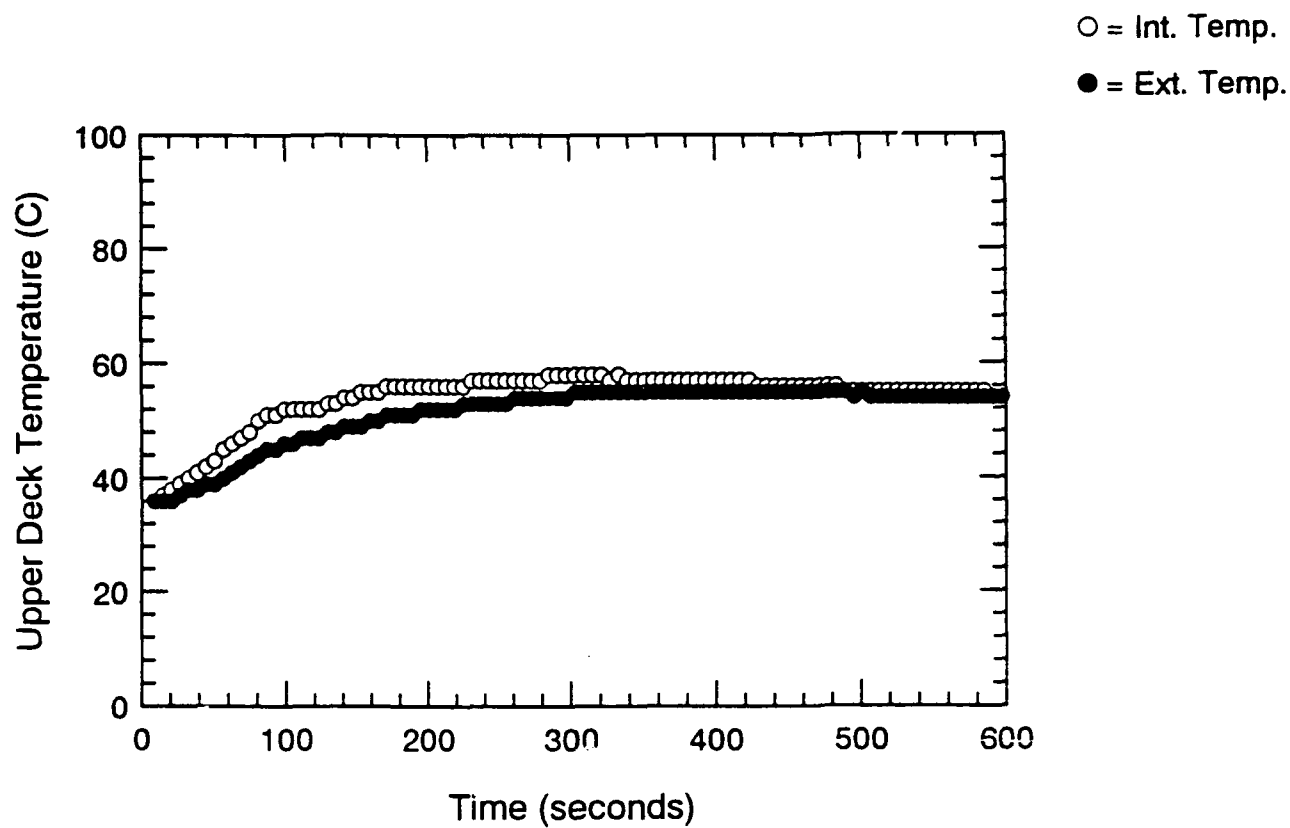


Figure B.36 Surface Thermocouple-Time Histories - S205

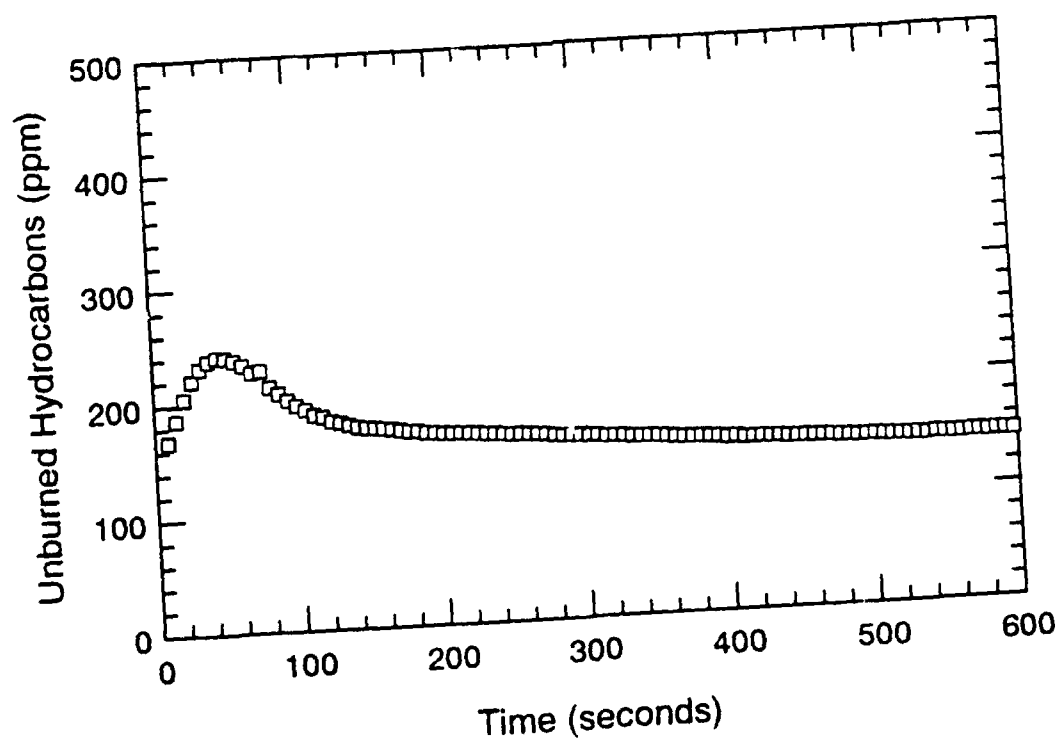
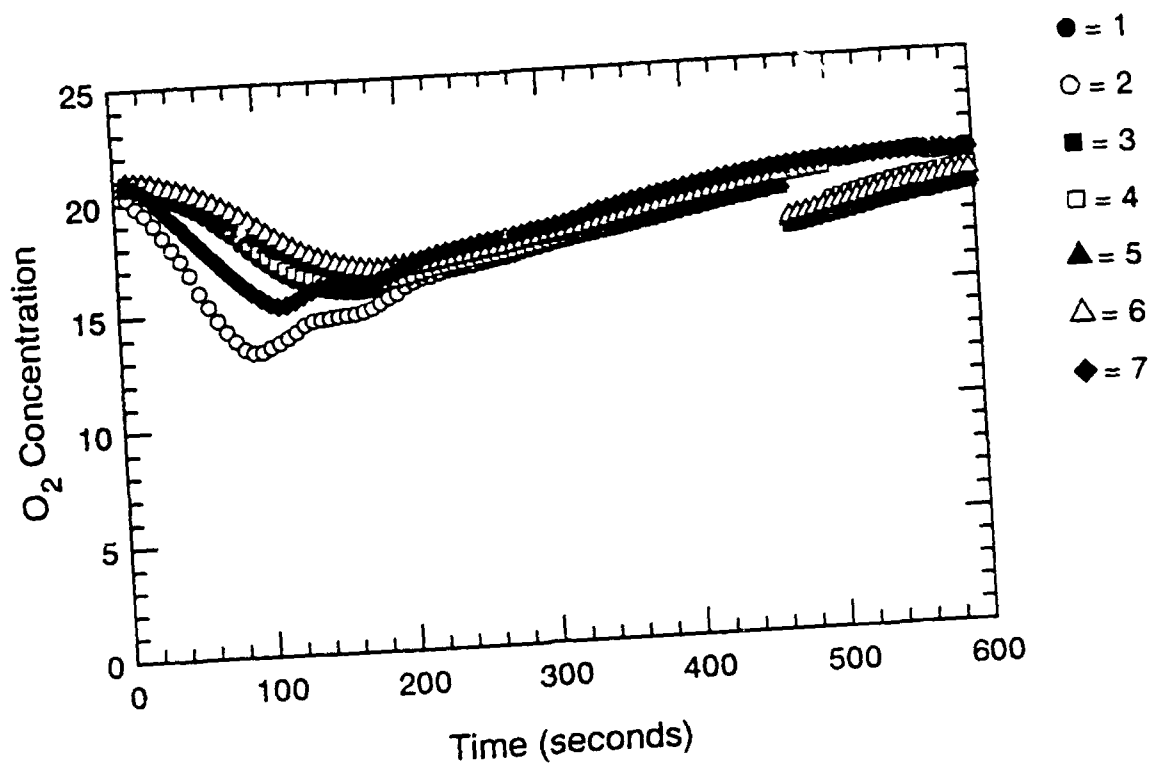


Figure B.37 Oxygen and Unburned HC Concentration-Time Histories - S205

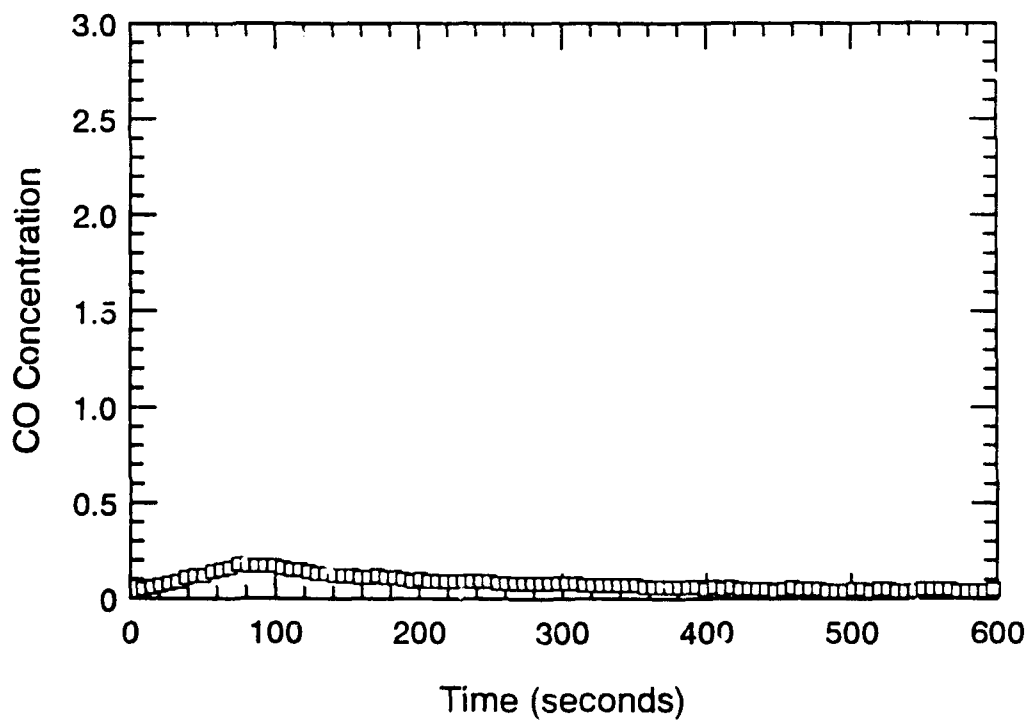
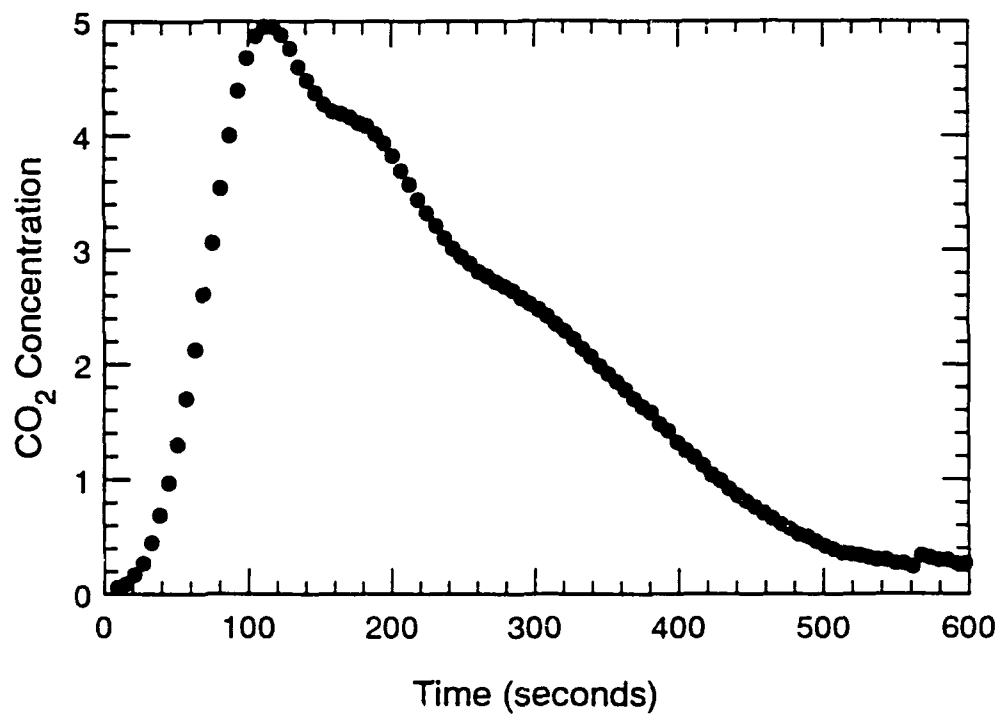


Figure B.38 CO₂ and CO Concentration-Time Histories - S205

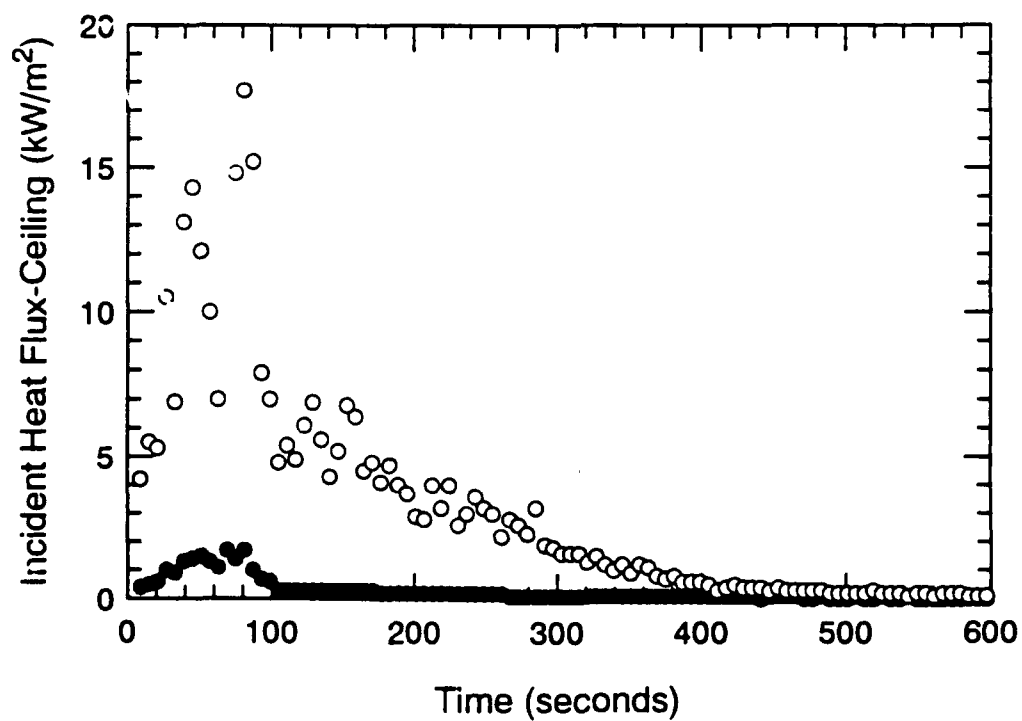
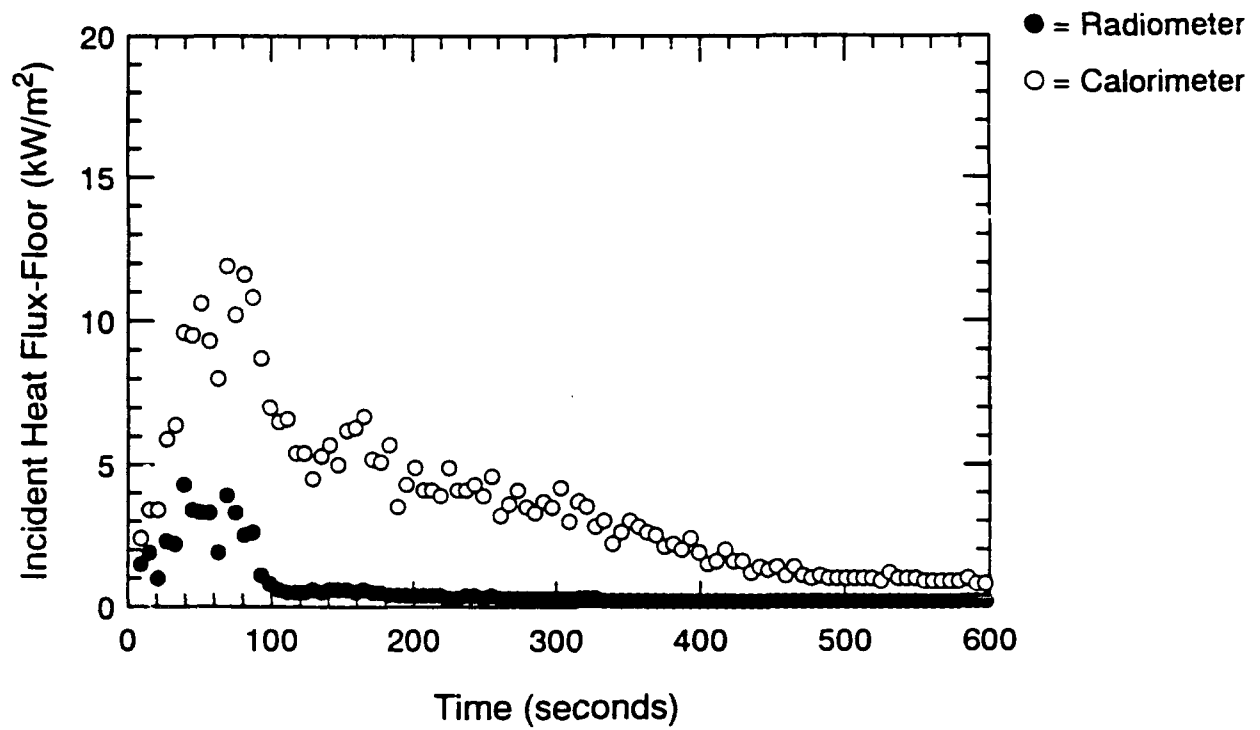


Figure B.39 Incident Heat Flux at Floor and Ceiling-Time Histories - S205

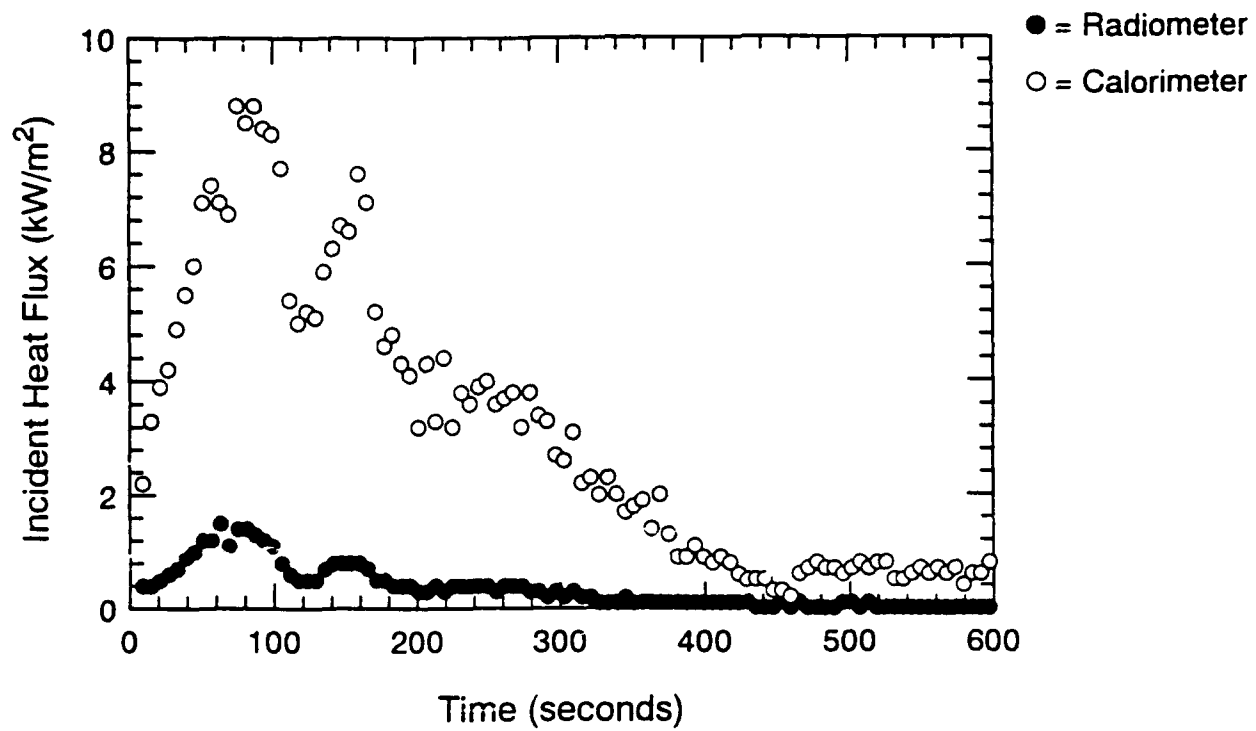


Figure B.40 Incident Heat Flux at Fwd. Bulkhead-Time Histories - S205

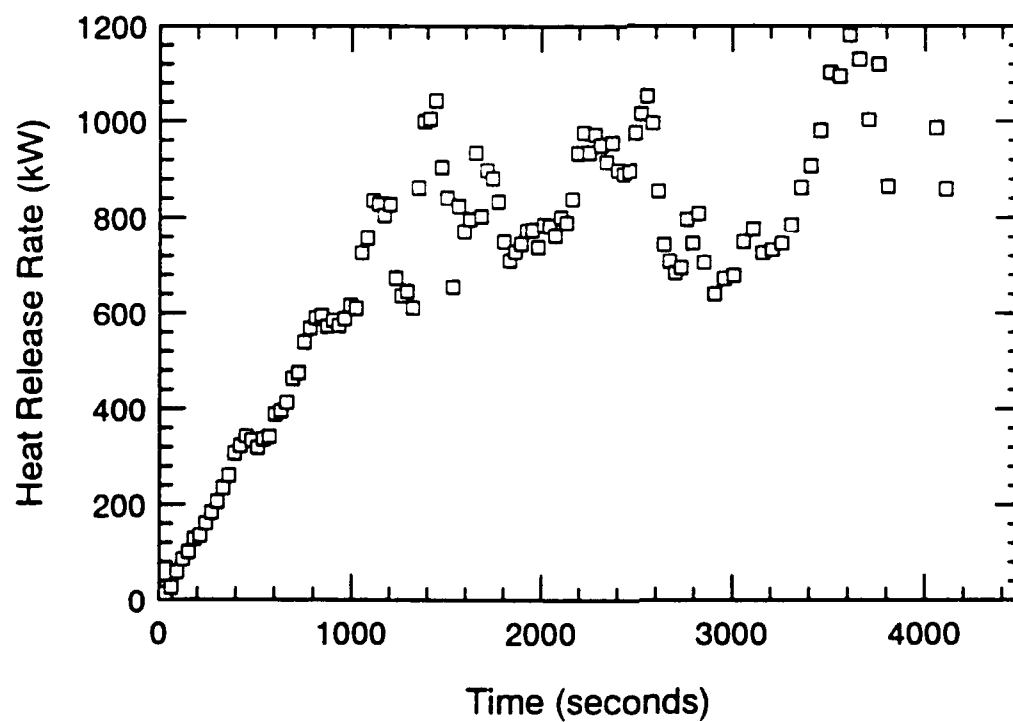
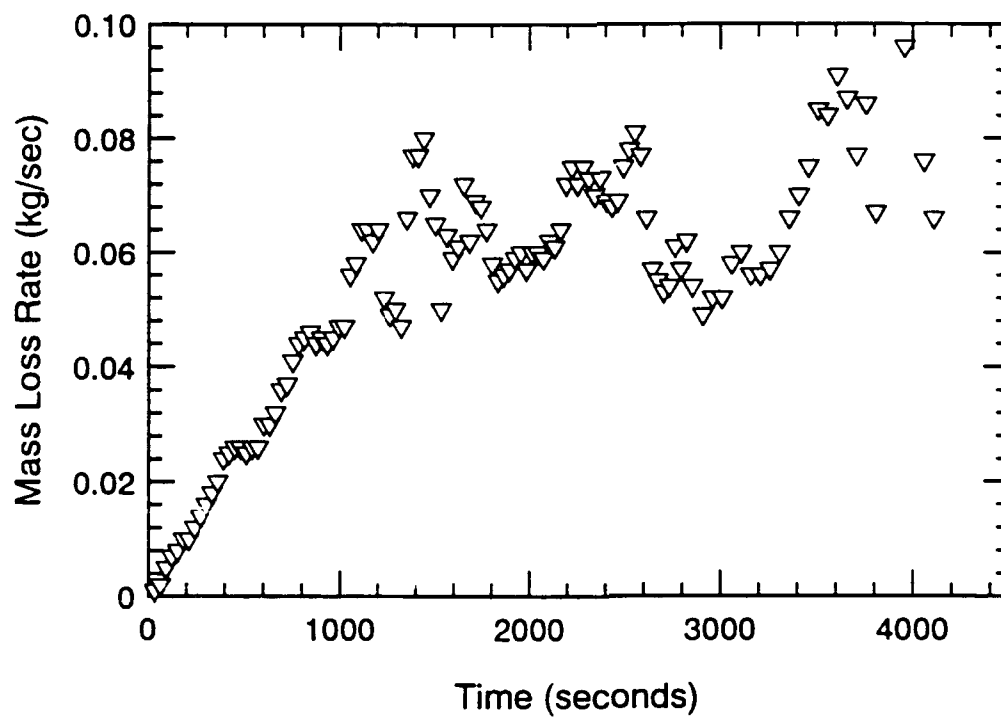


Figure B 41 Mass Loss Rate and Heat Release Rate-Time Histories - S206

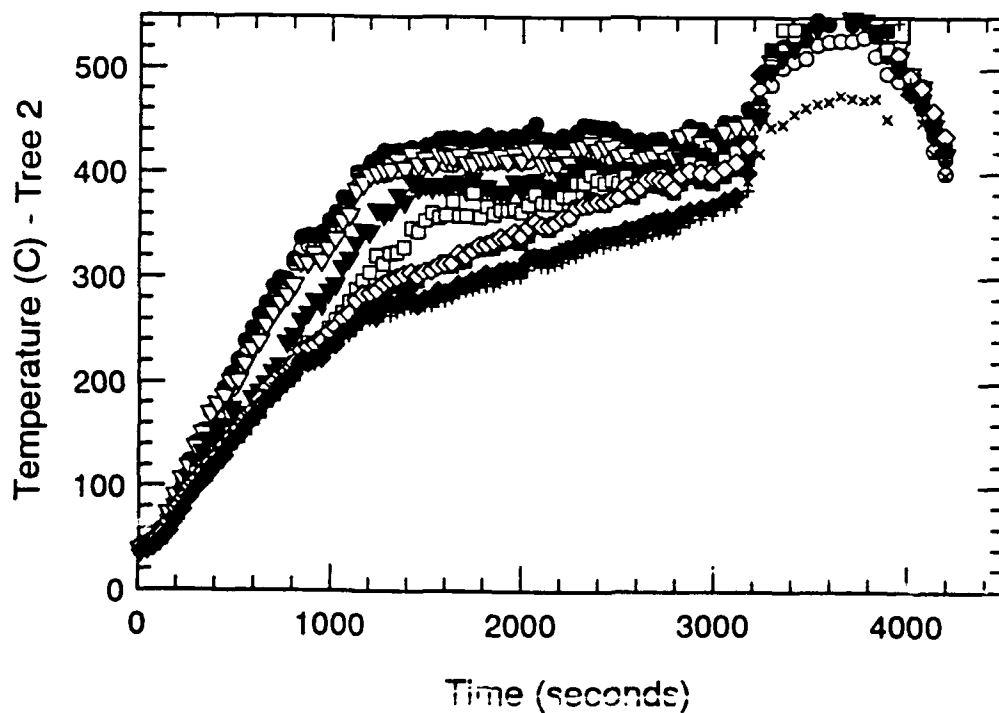
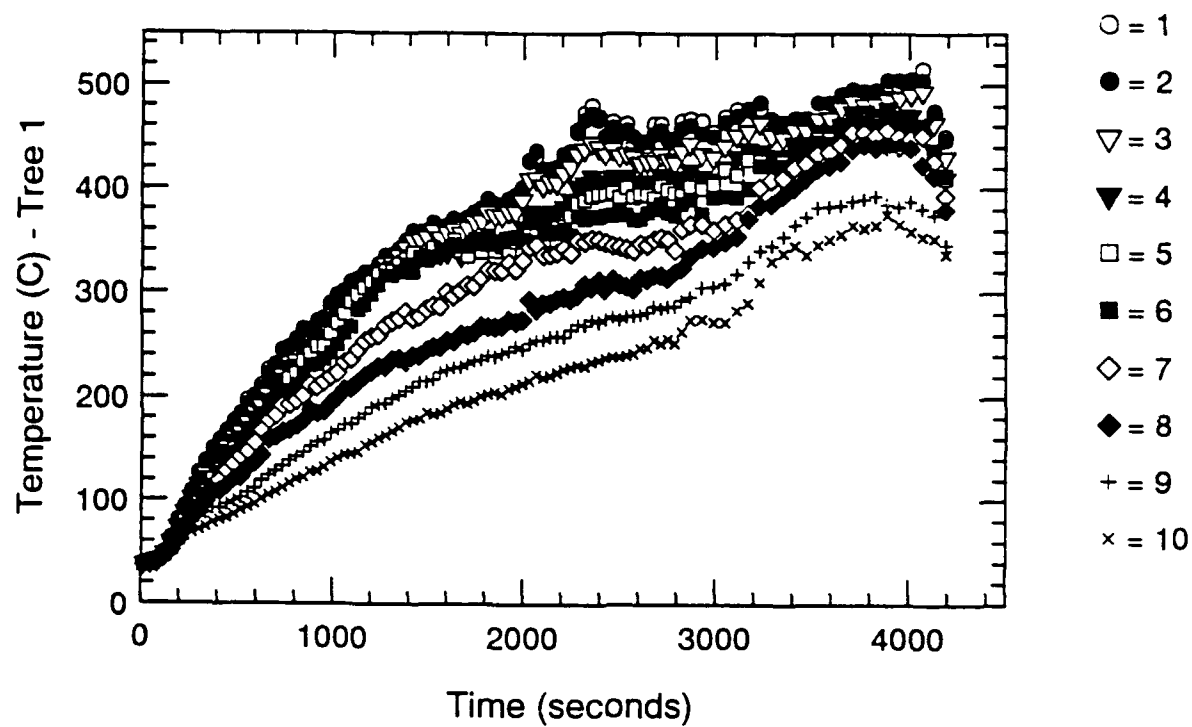


Figure B.42 Thermocouple Trees 1 & 2-Time Histories - S206

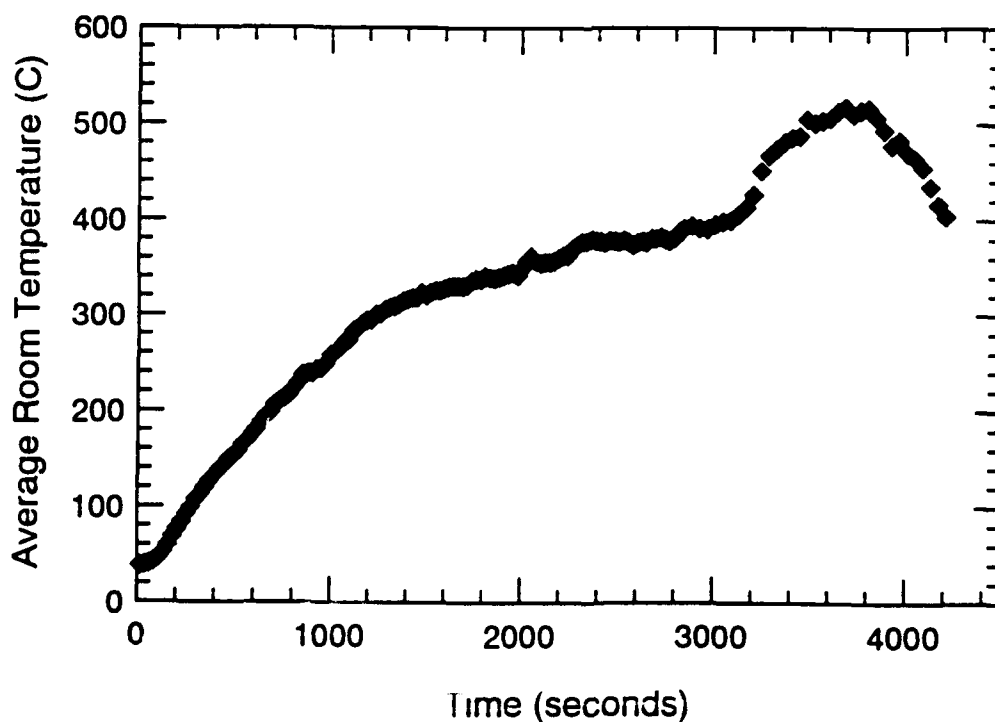
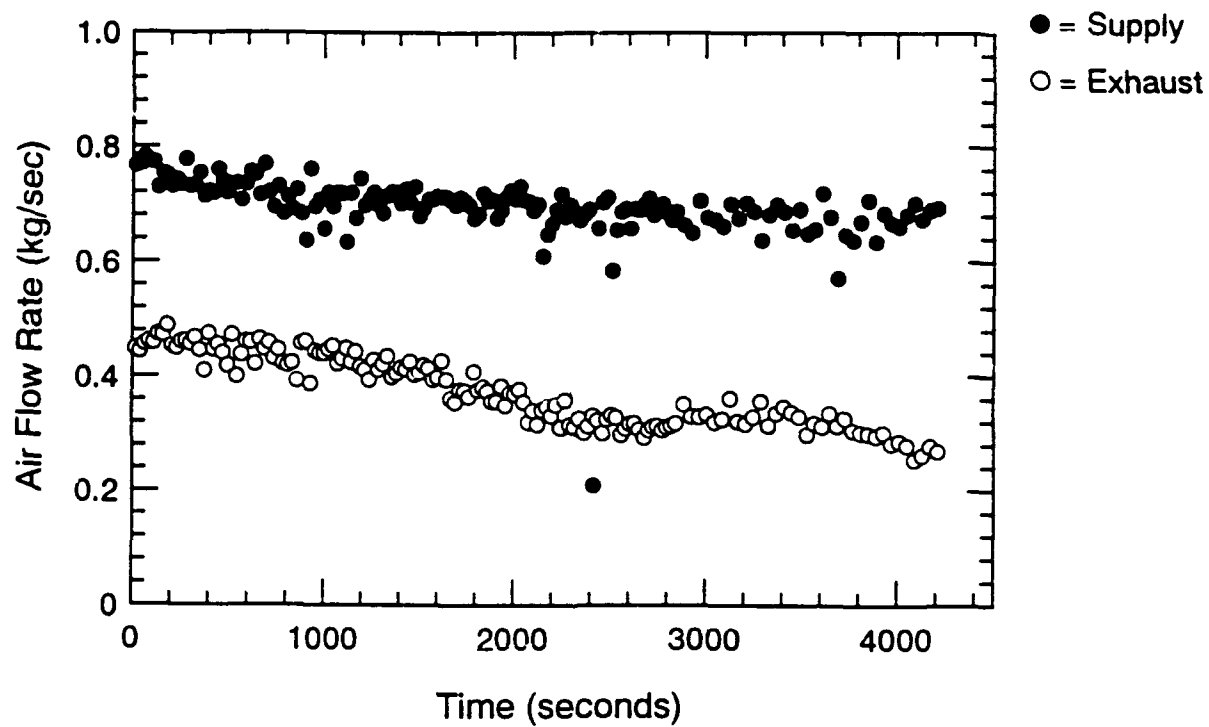


Figure B.43 Air Flow Rate and Avg. Temperature-Time Histories - S206

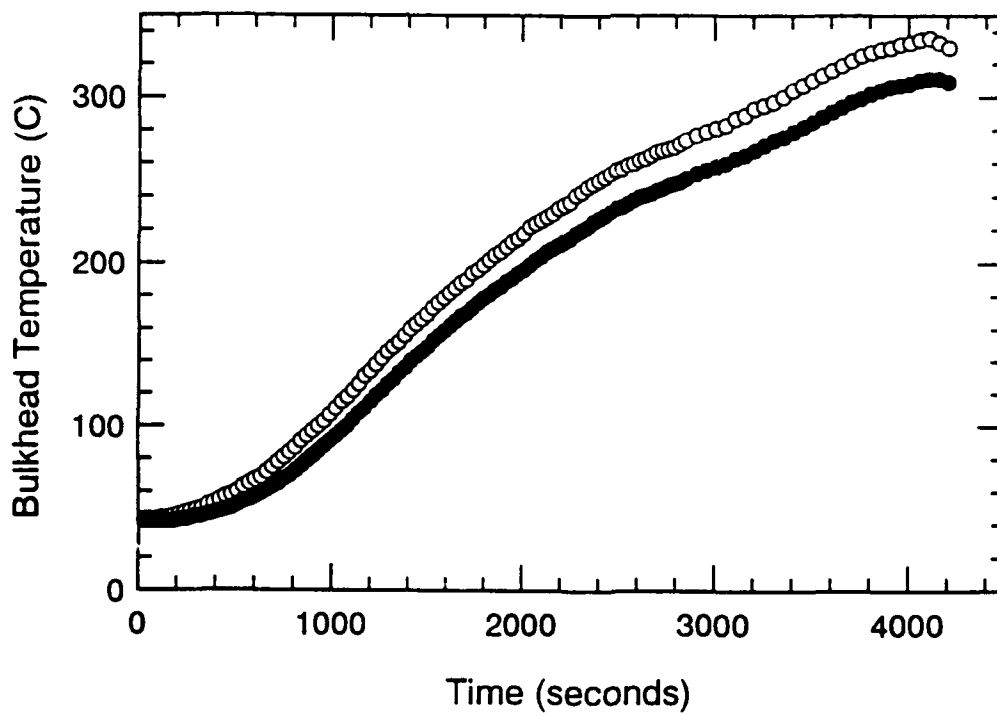
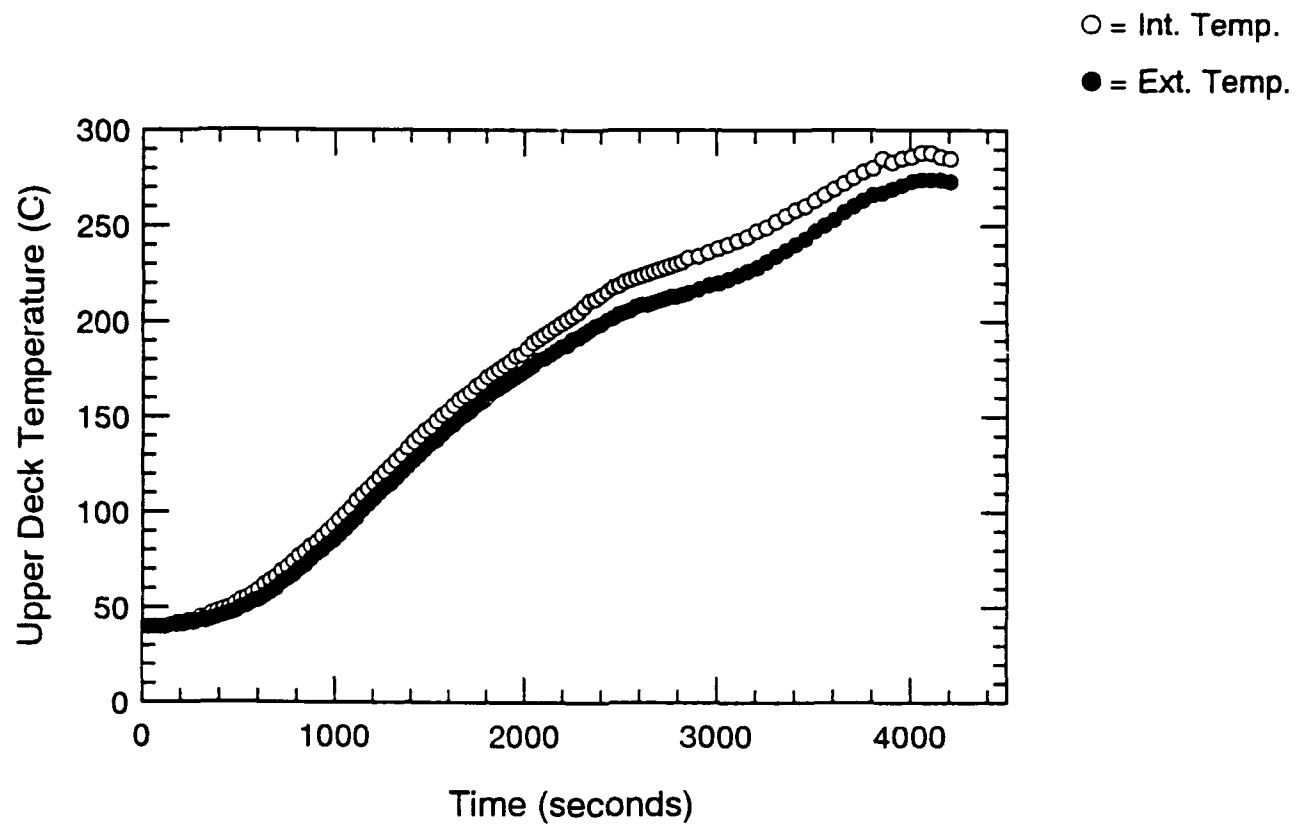


Figure B.44 Surface Thermocouple-Time Histories - S206

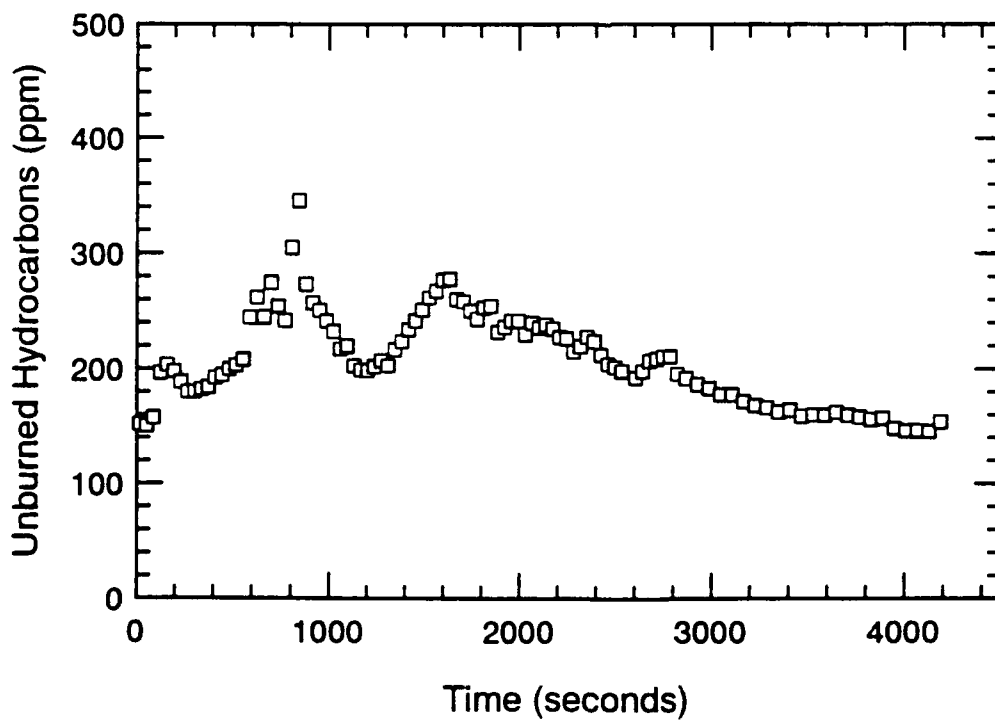
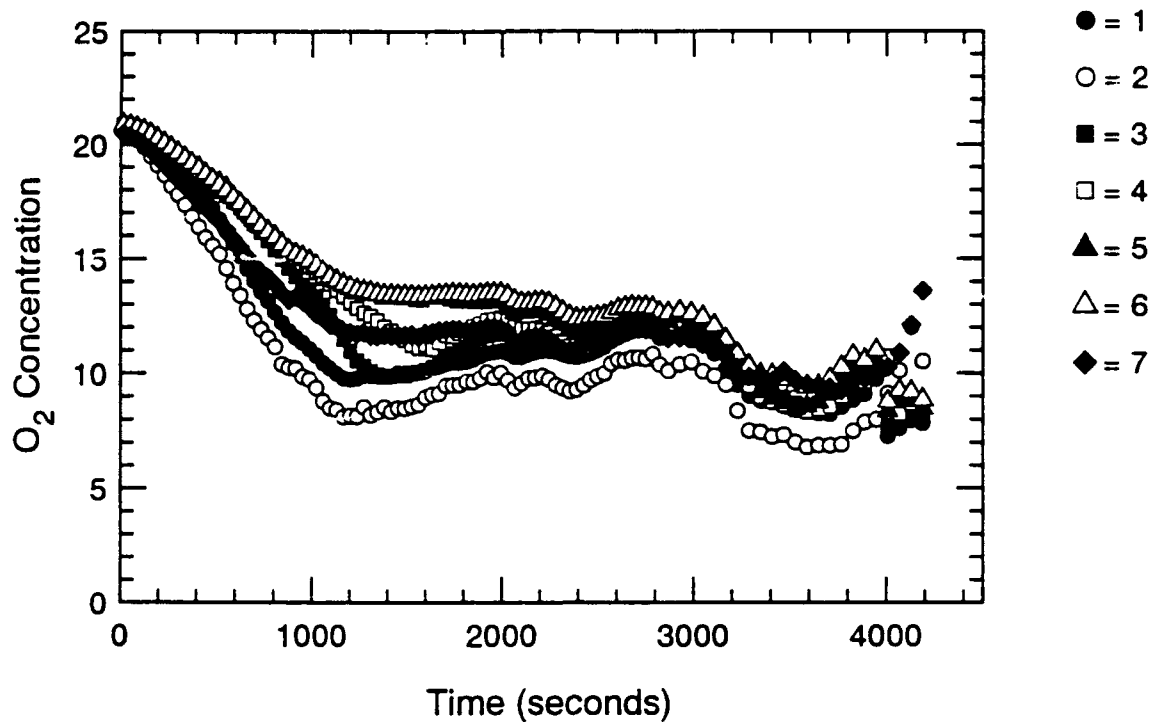


Figure B.45 Oxygen and Unburned HC Concentration-Time Histories - S206

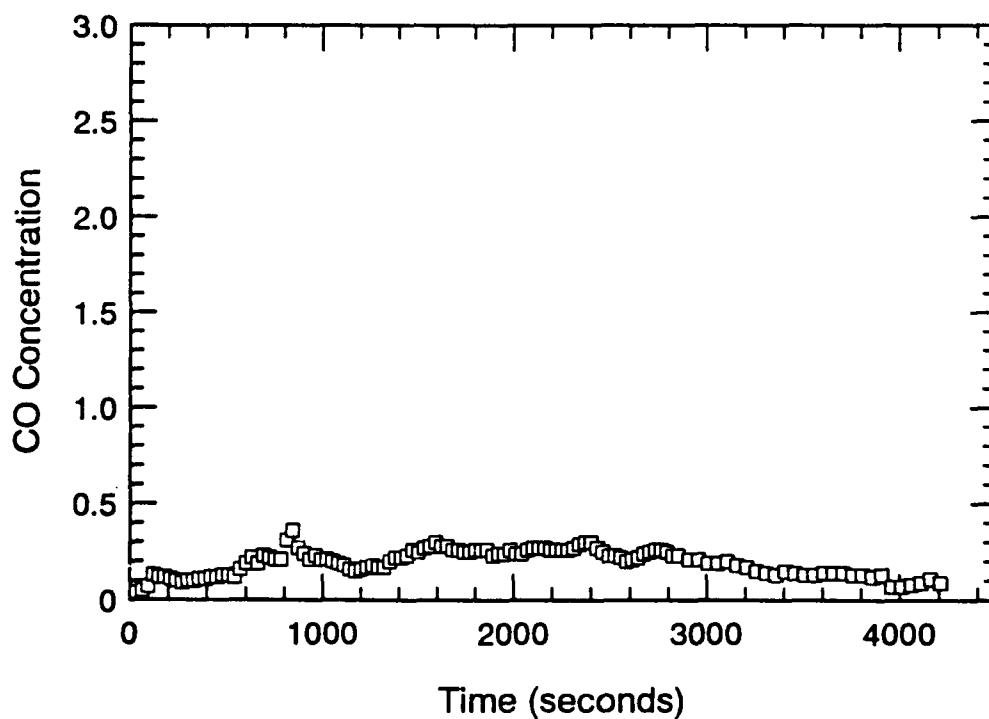
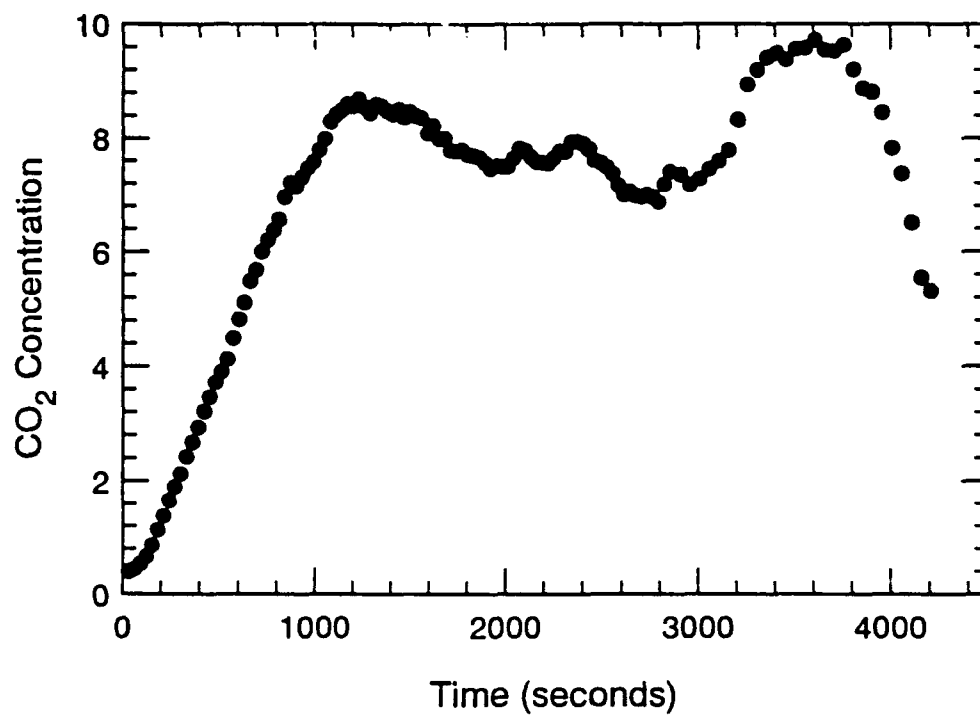


Figure B.46 CO₂ and CO Concentration-Time Histories - S206

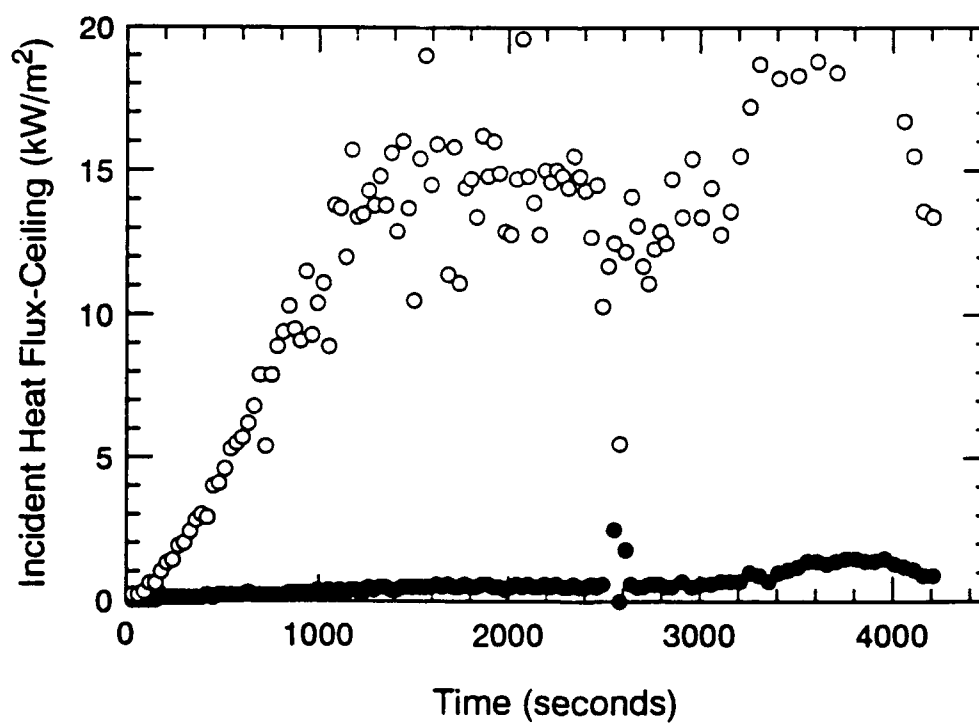
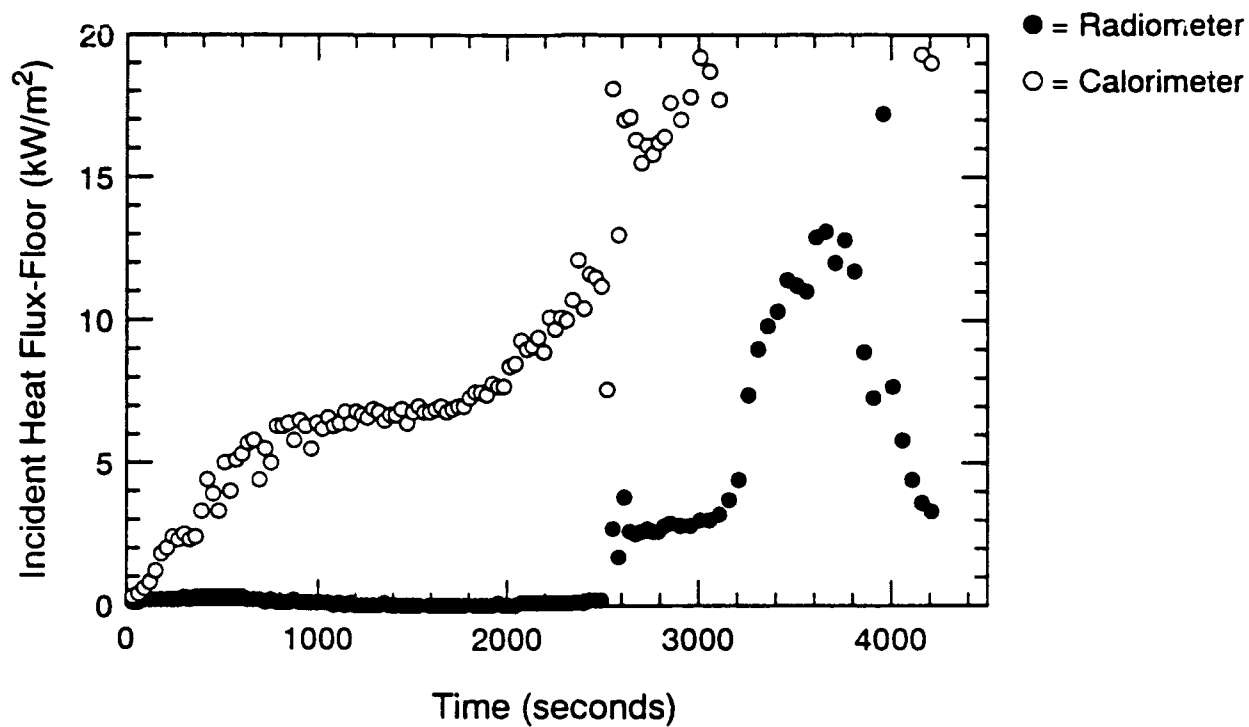


Figure B.47 Incident Heat Flux at Floor and Ceiling-Time Histories - S206

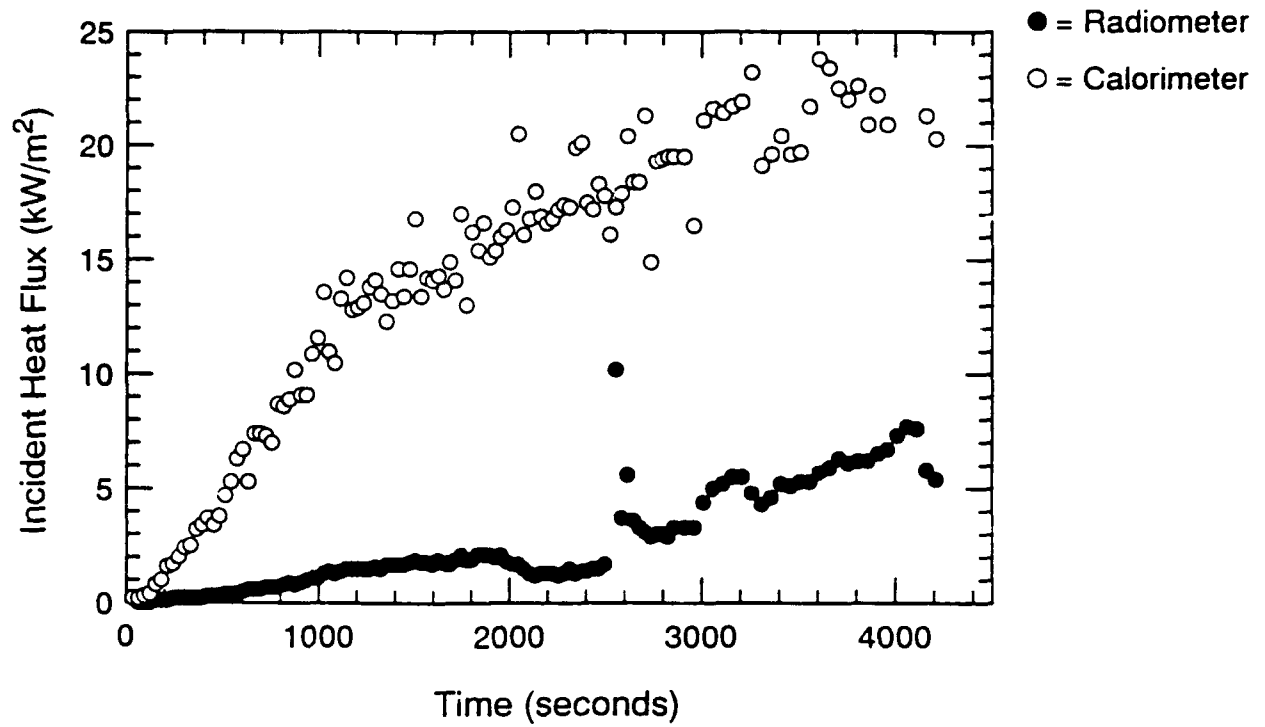


Figure B.48 Incident Heat Flux at Fwd. Bulkhead-Time Histories - S206

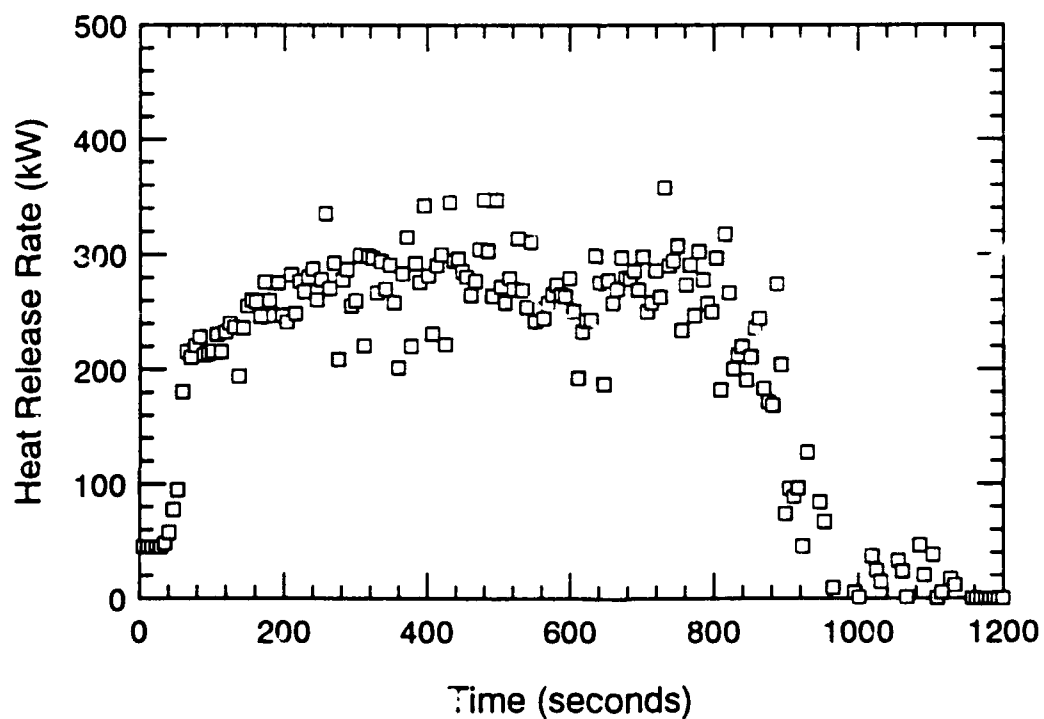
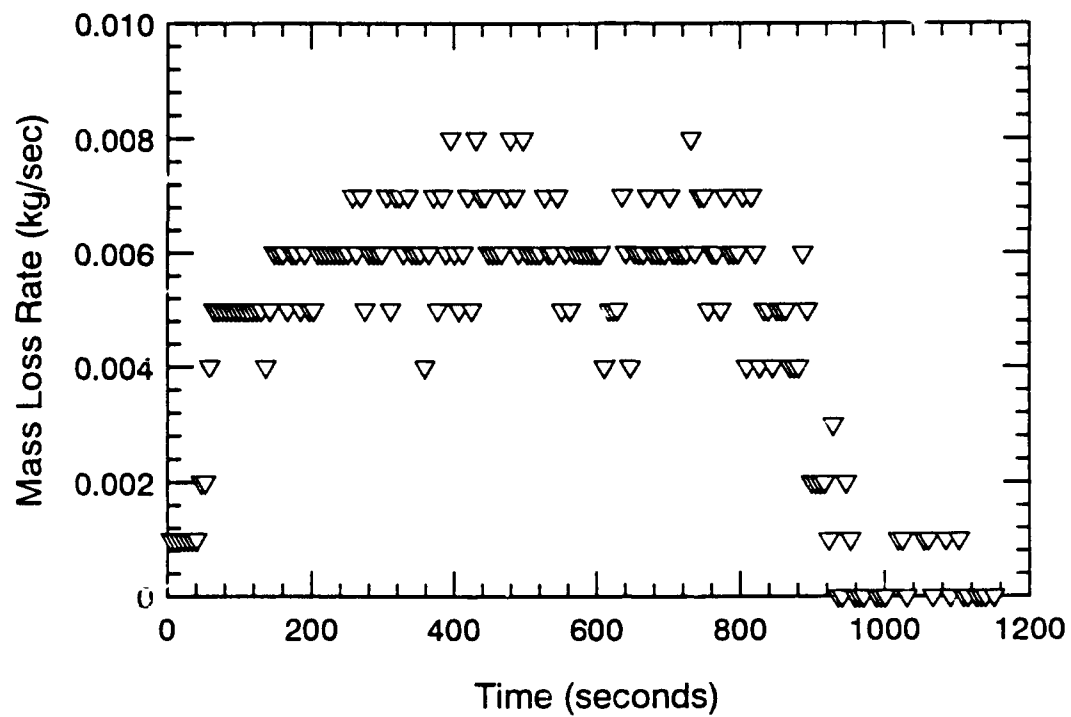


Figure B.49 Mass Loss Rate and Heat Release Rate-Time Histories - S207

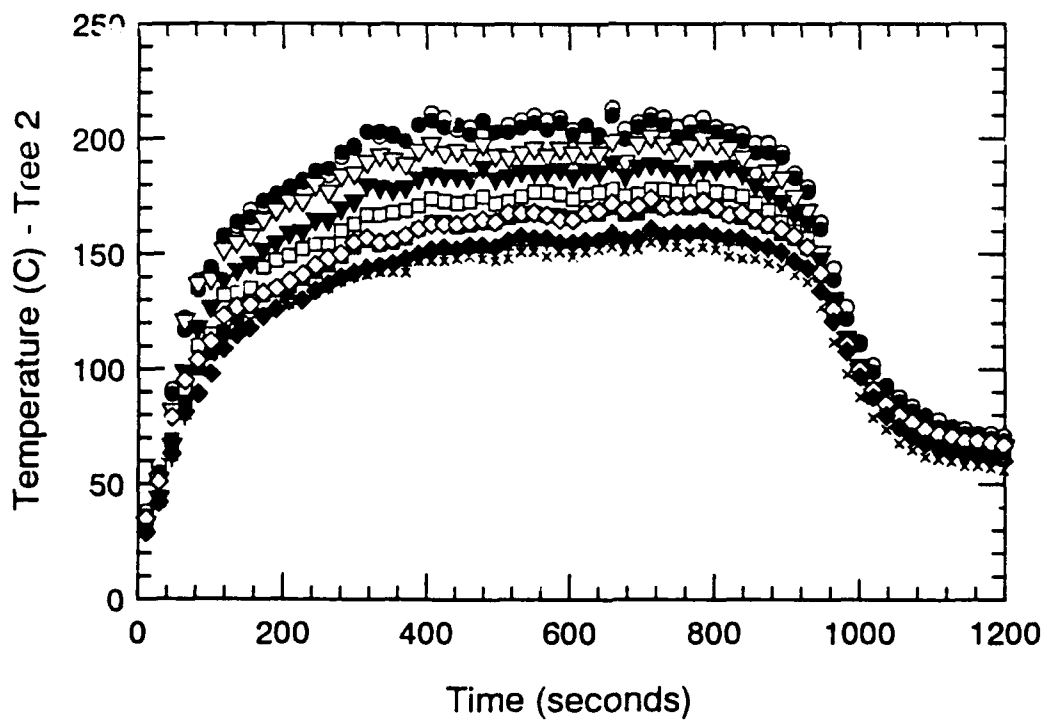
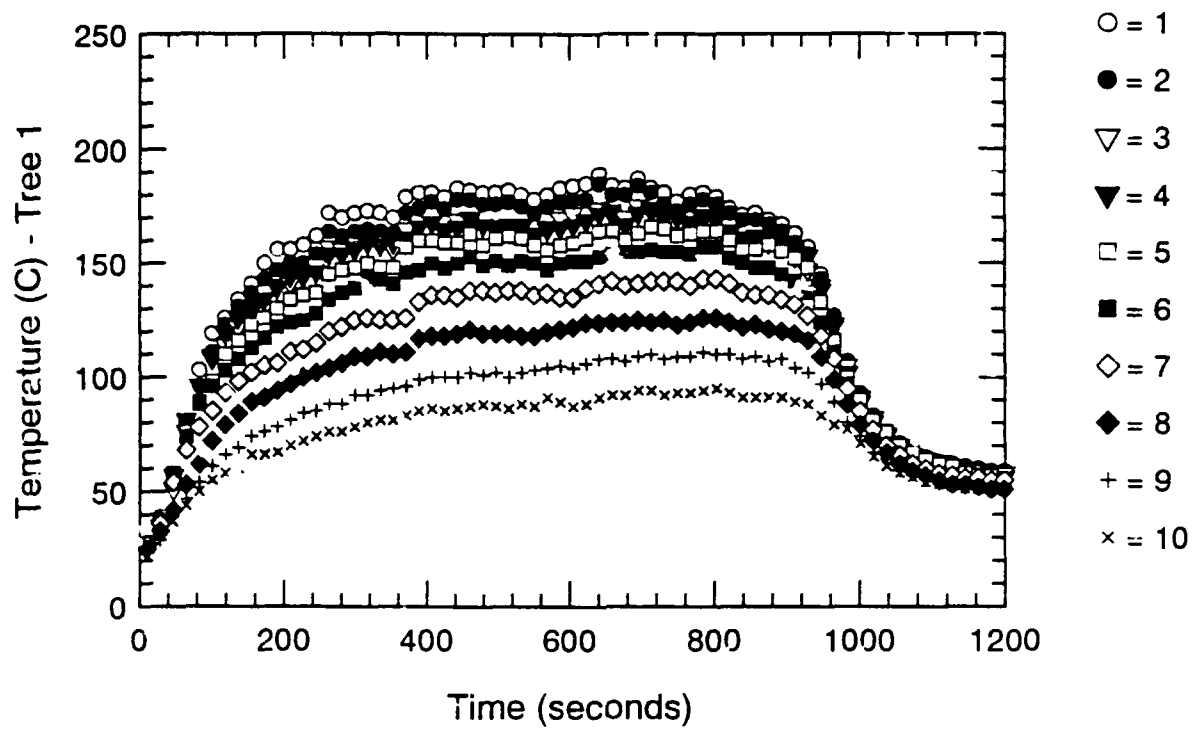


Figure B.50 Thermocouple Trees 1 & 2-Time Histories - S207

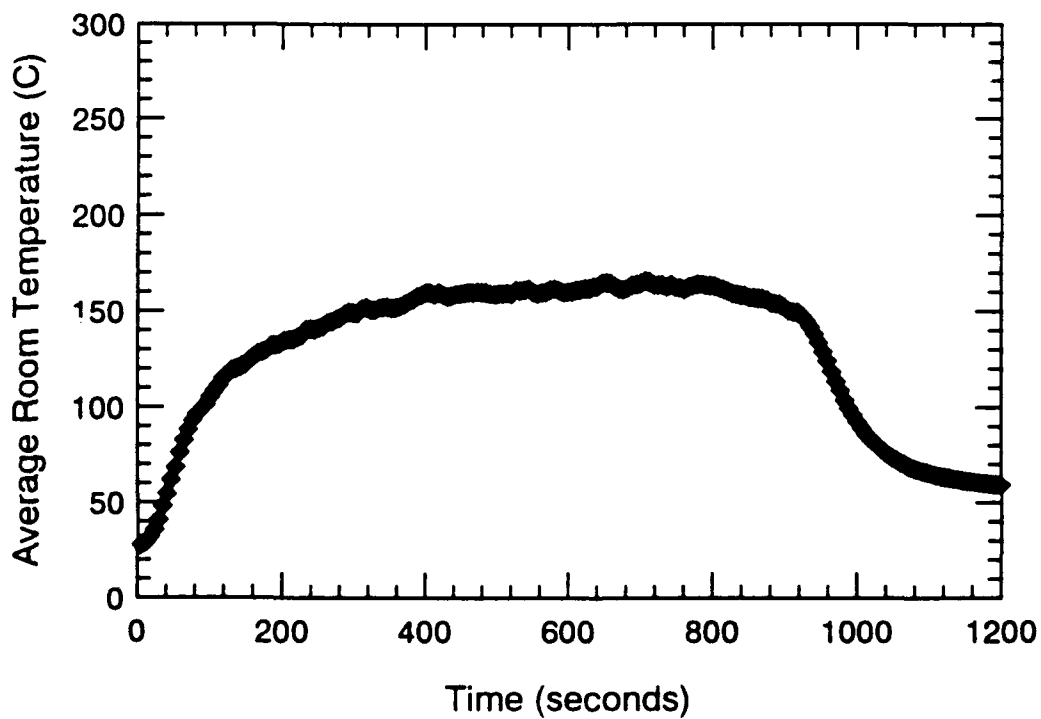
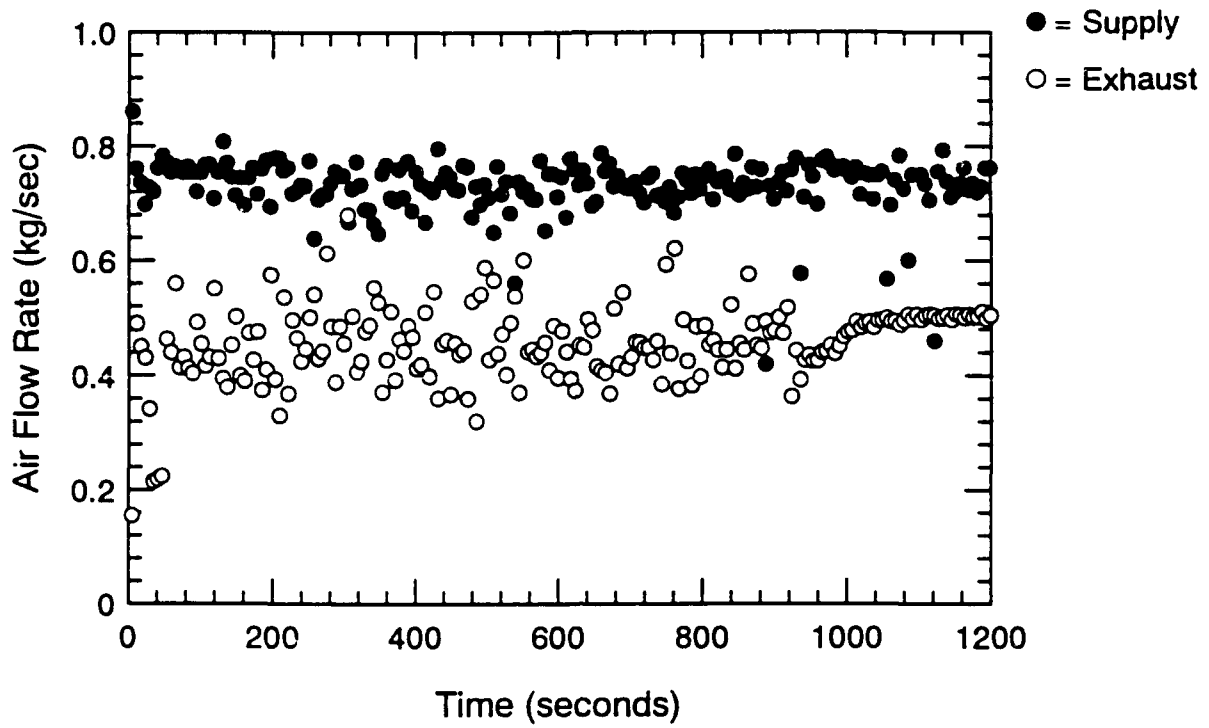


Figure B.51 Air Flow Rate and Avg. Temperature-Time Histories - S207

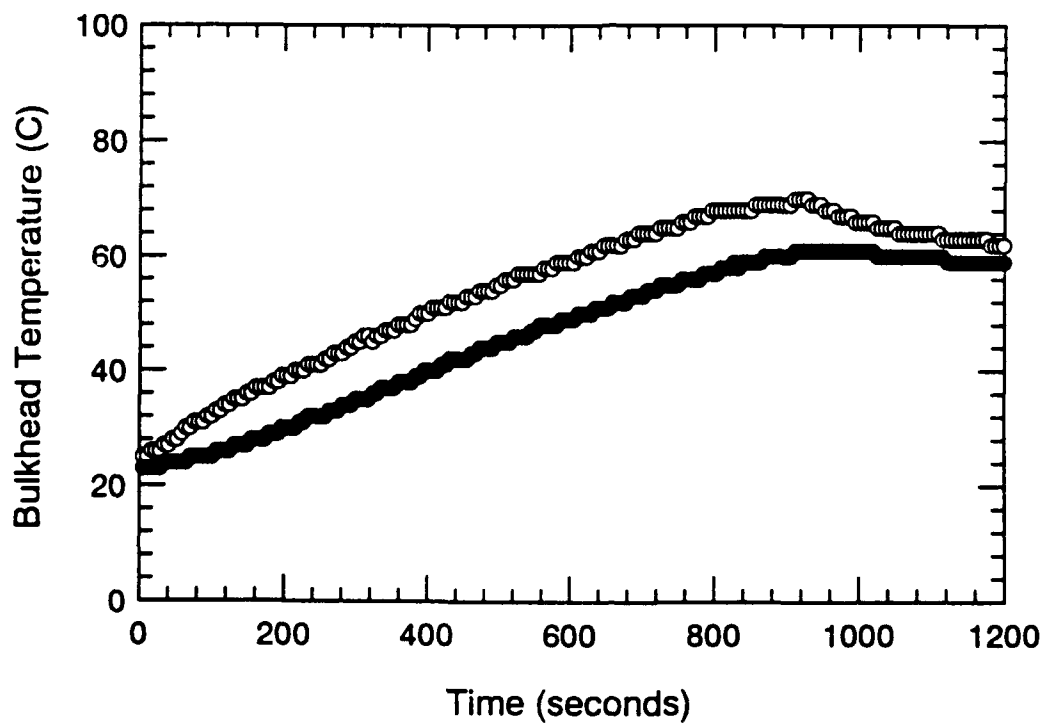
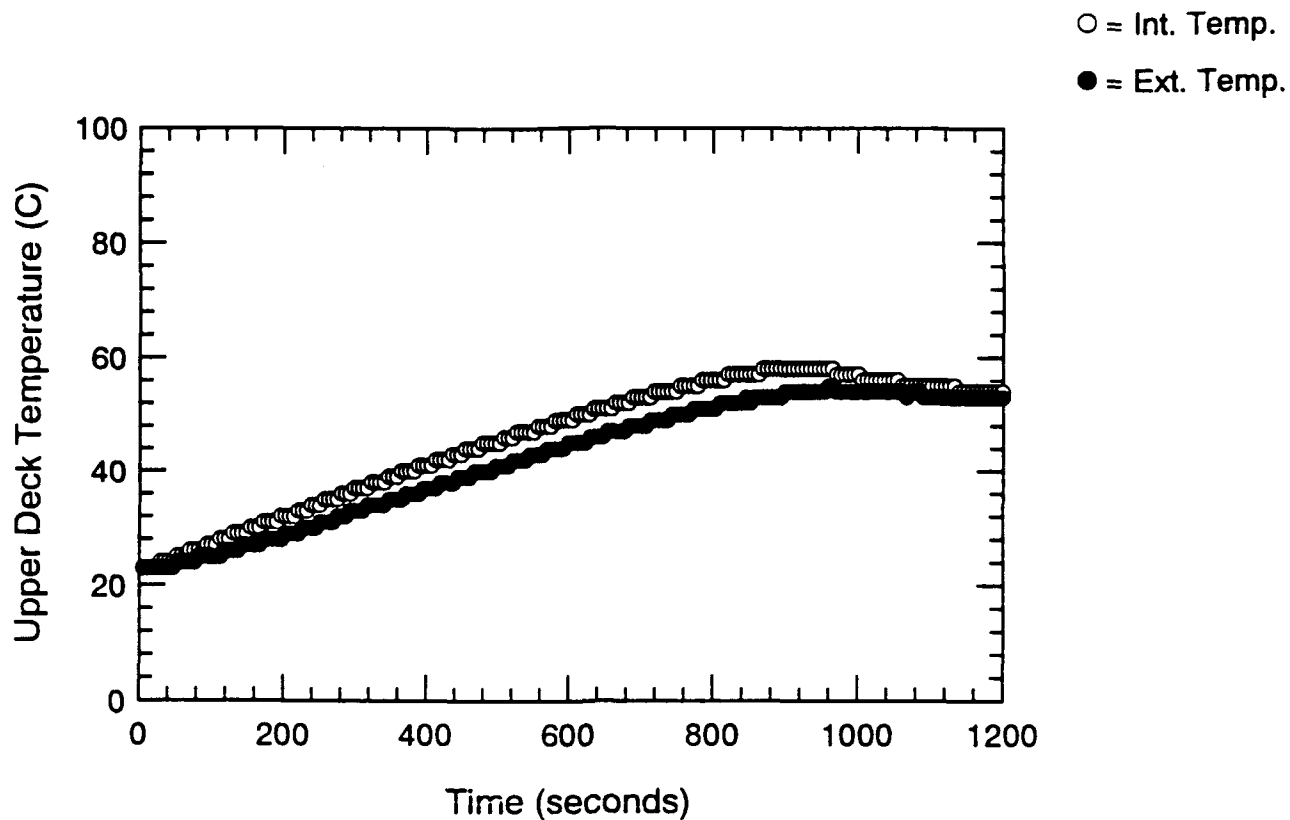


Figure B.52 Surface Thermocouple-Time Histories - S207

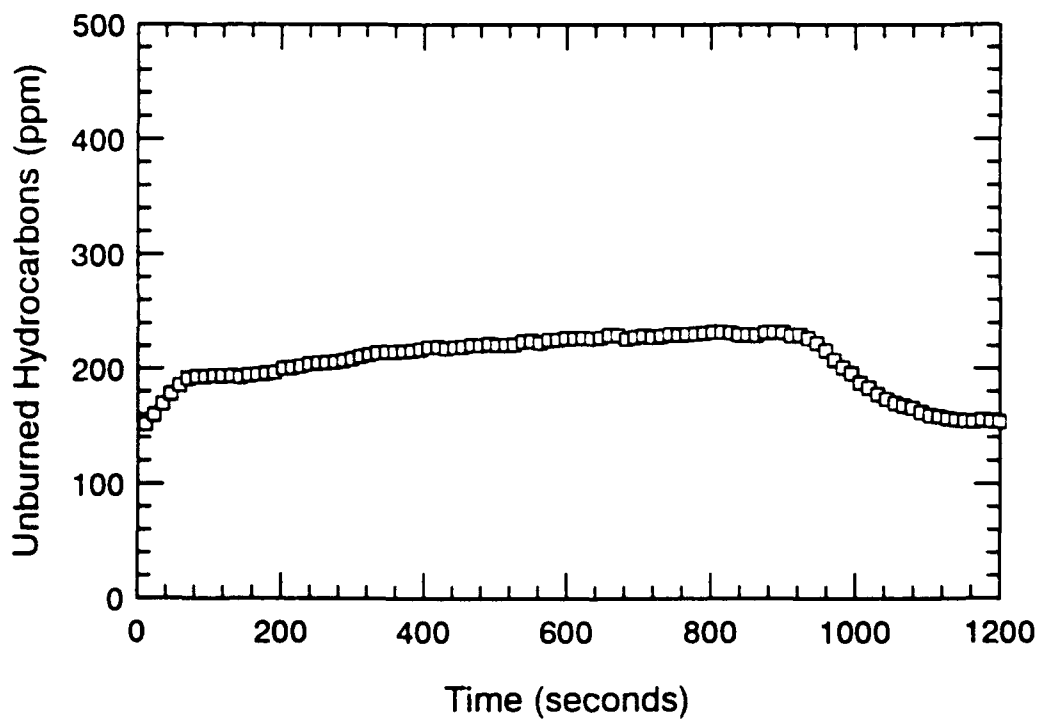
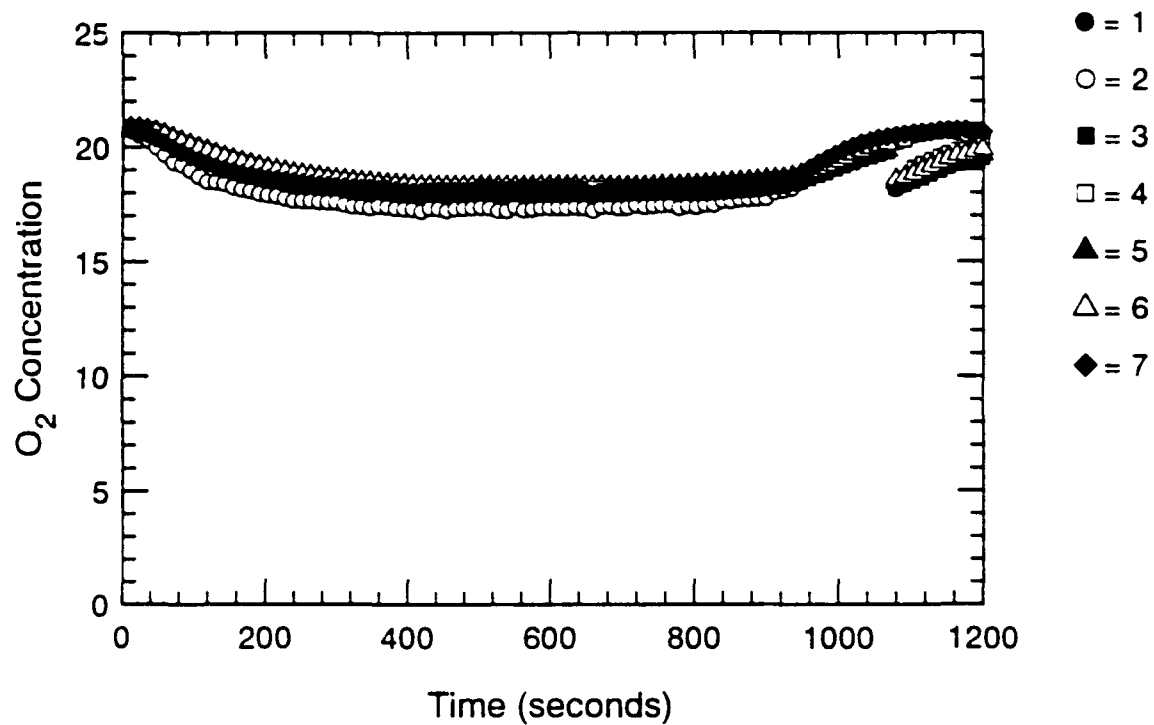


Figure B.53 Oxygen and Unburned HC Concentration-Time Histories - S207

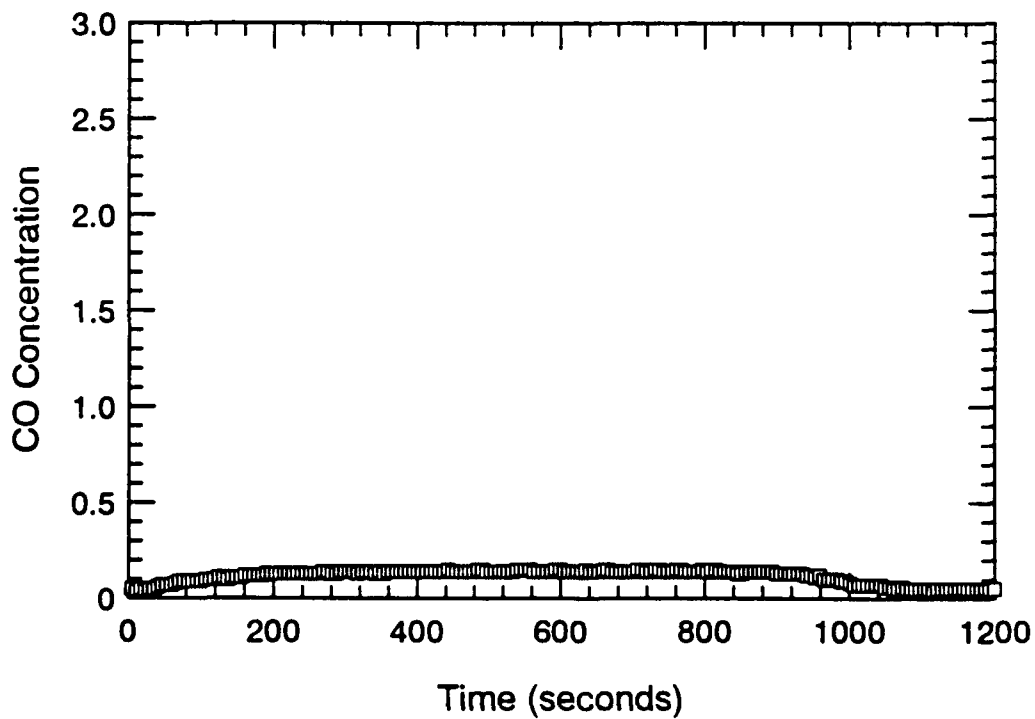
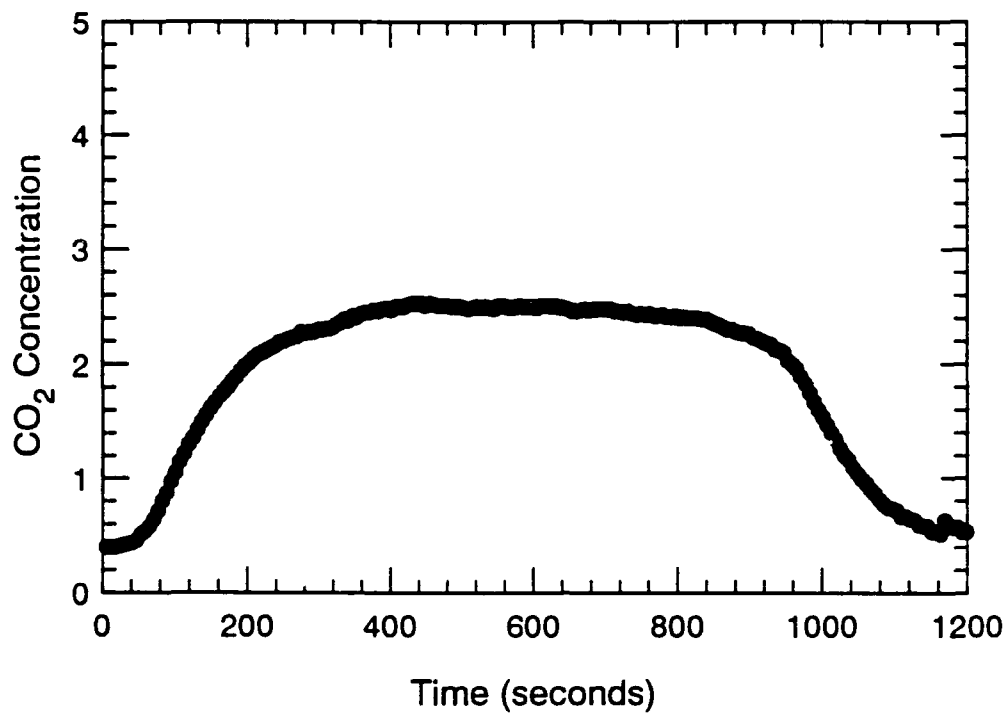


Figure B.54 CO₂ and CO Concentration-Time Histories - S207

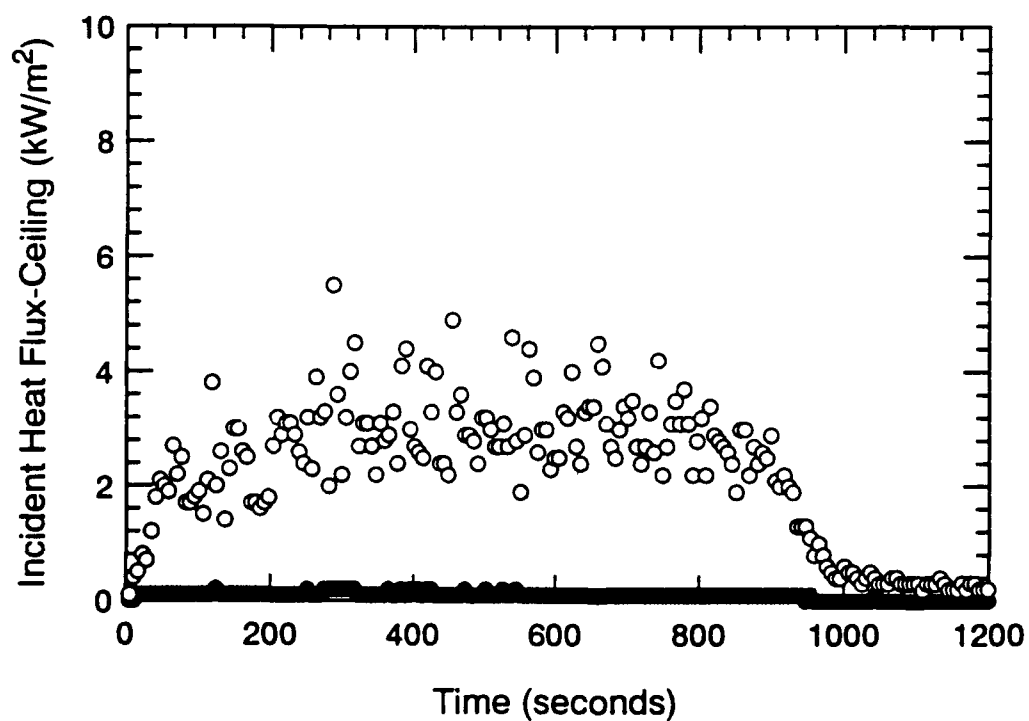
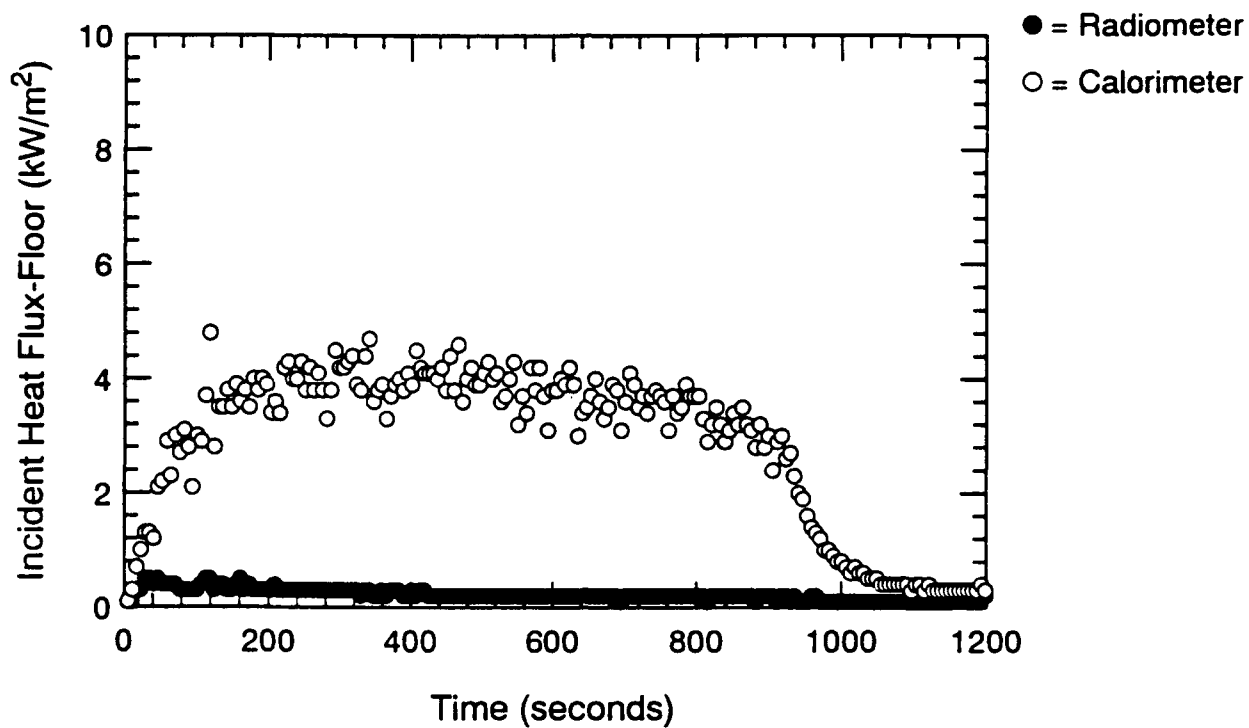


Figure B.55 Incident Heat Flux at Floor and Ceiling-Time Histories - S207

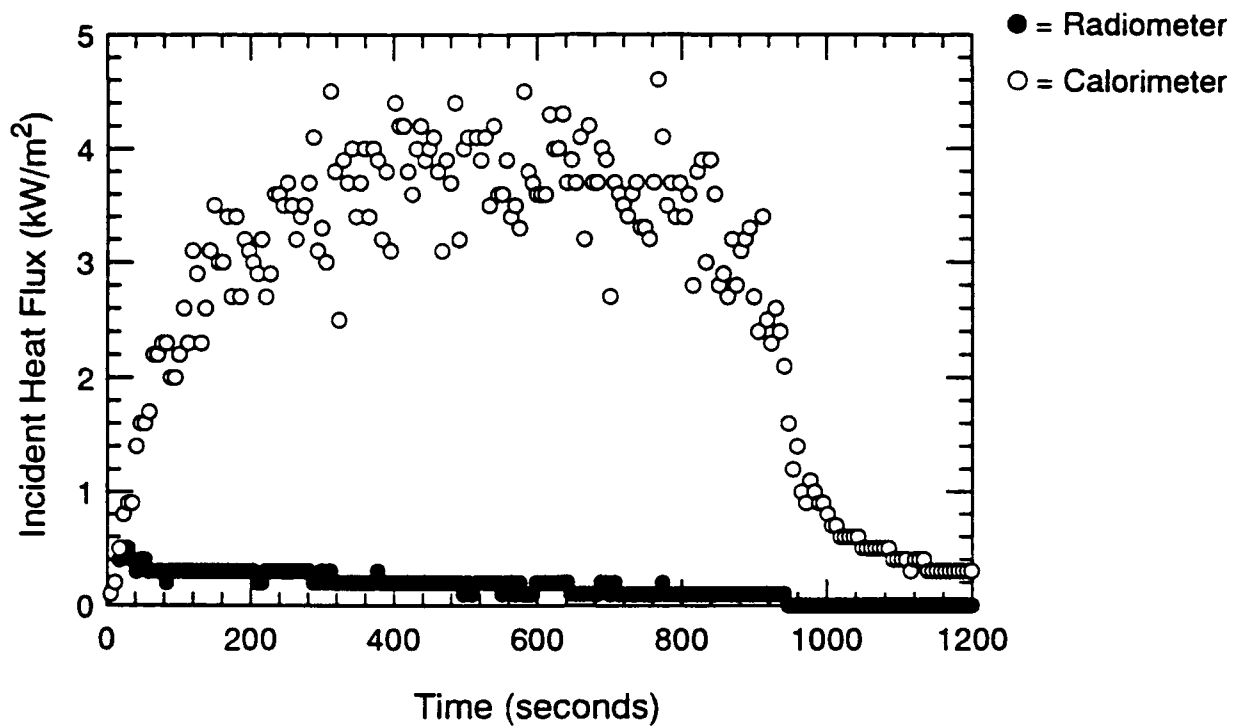


Figure B.56 Incident Heat Flux at Fwd. Bulkhead-Time Histories - S207

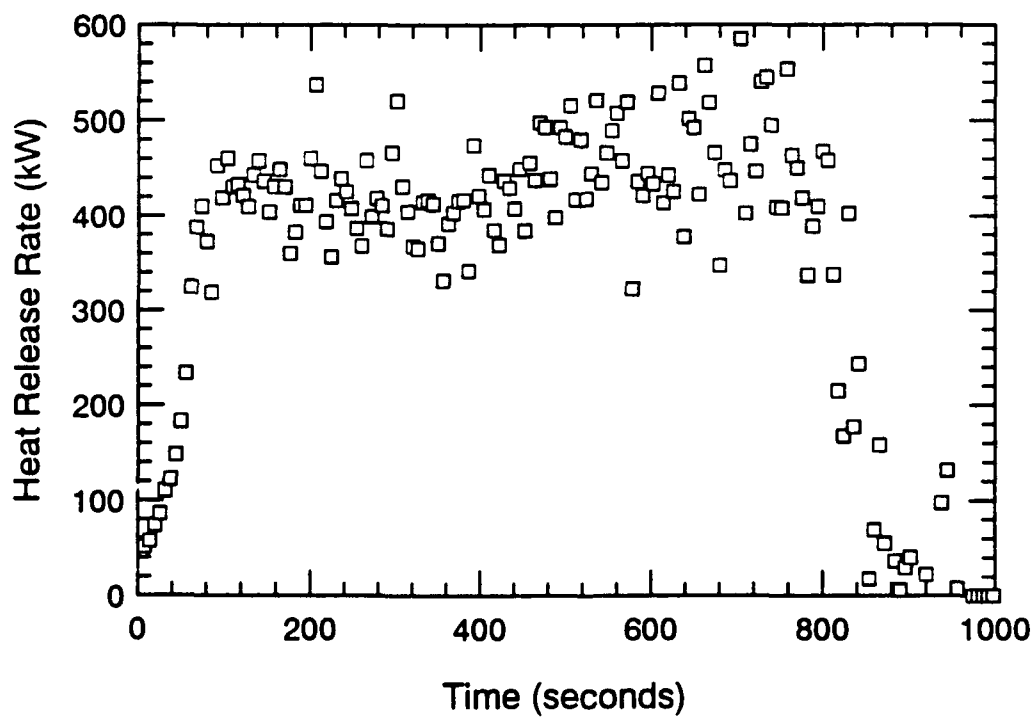
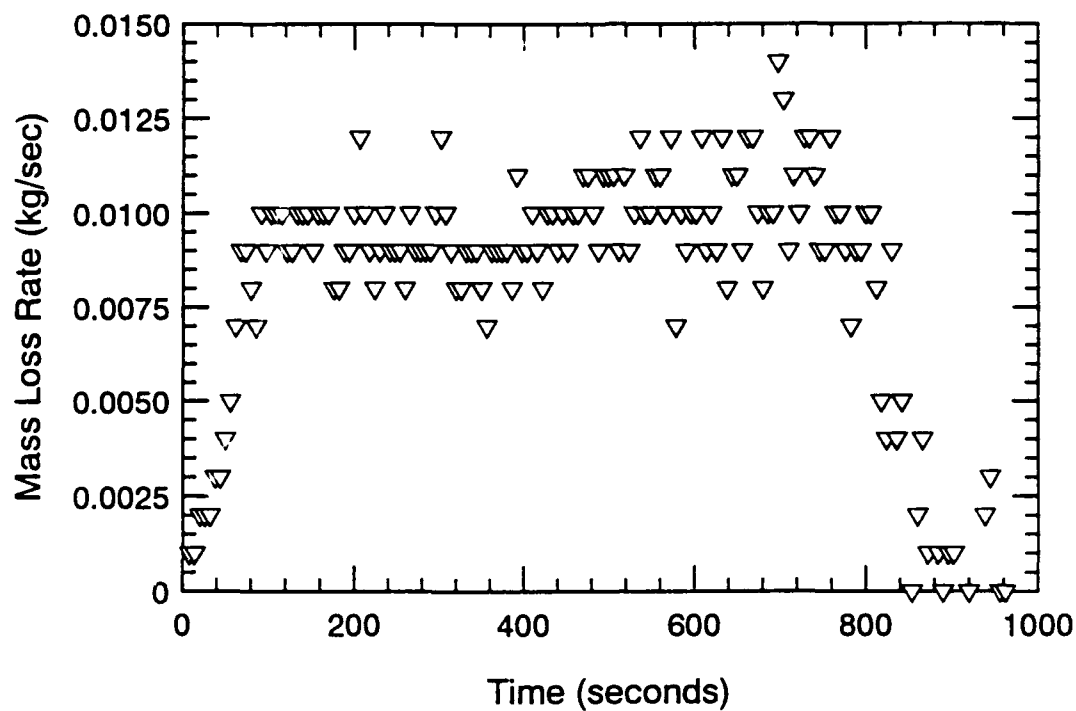


Figure B.57 Mass Loss Rate and Heat Release Rate-Time Histories - S208

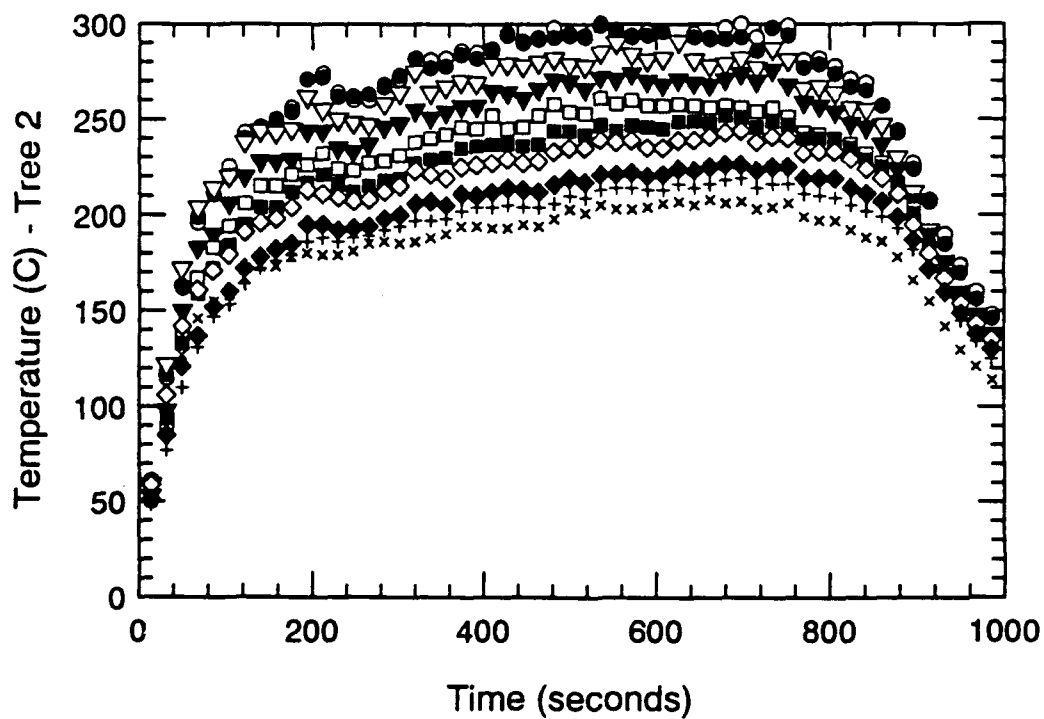
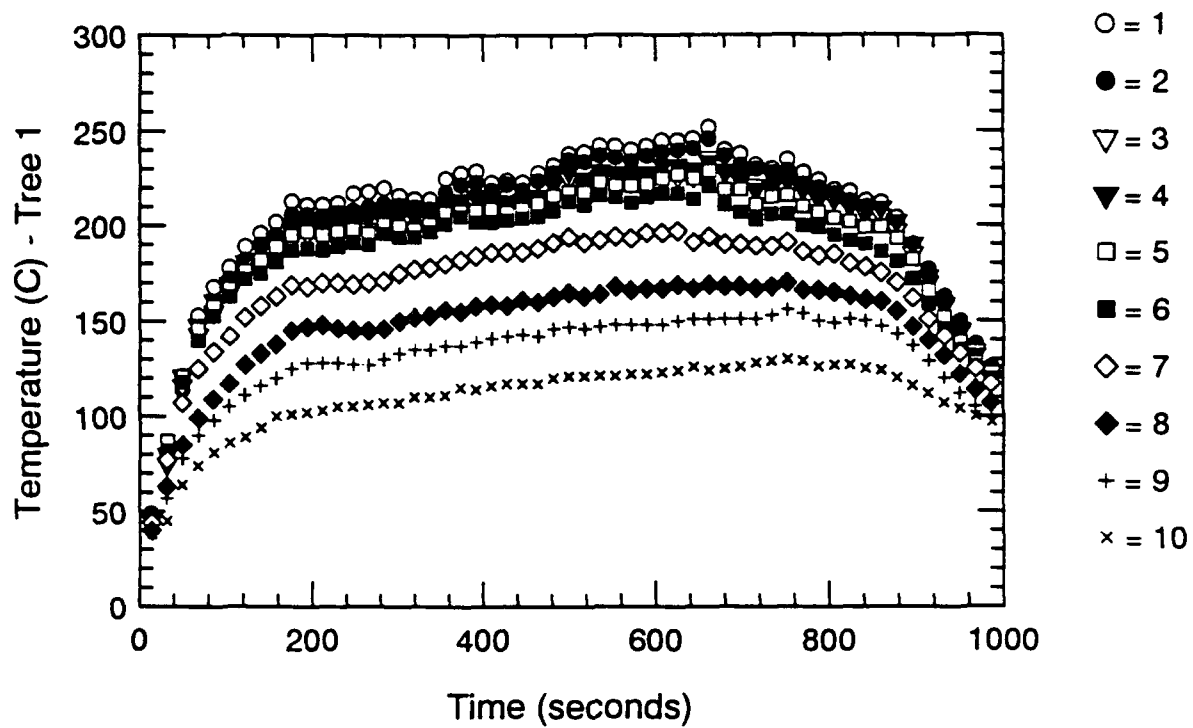


Figure B.58 Thermocouple Trees 1 & 2-Time Histories - S208

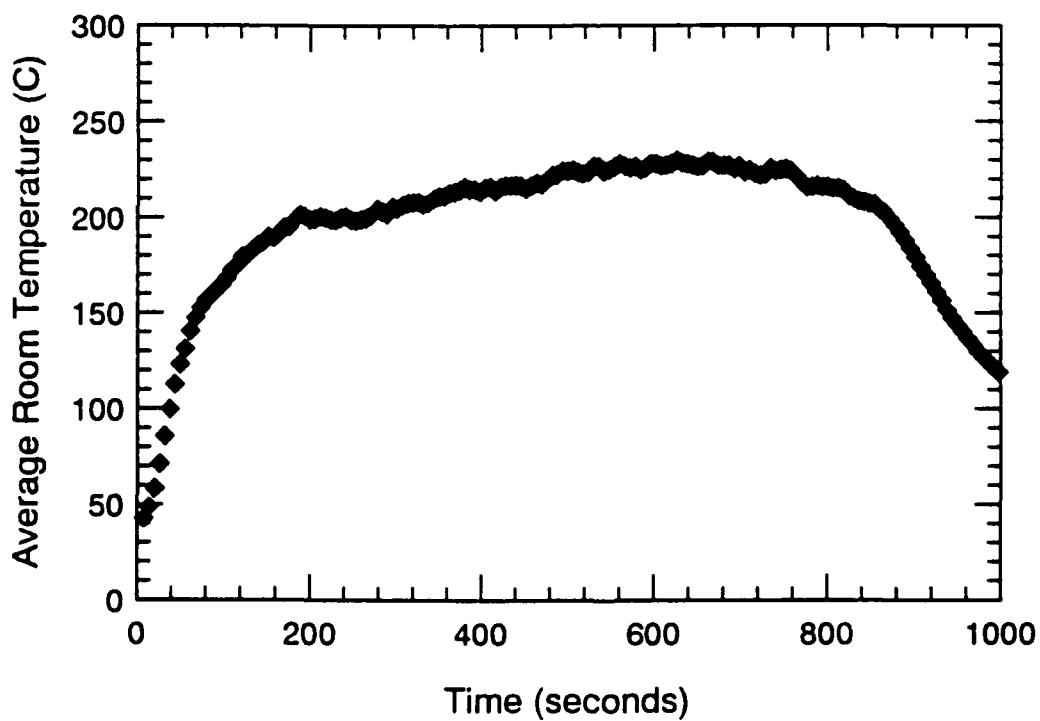
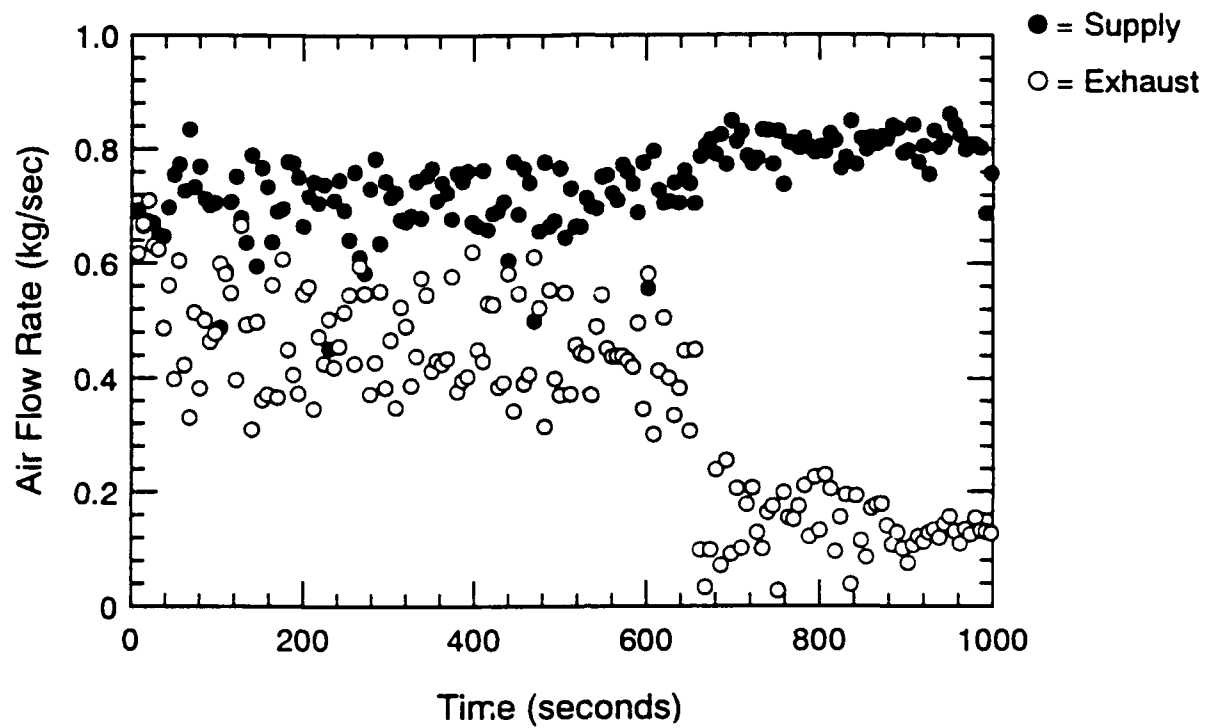


Figure B.59 Air Flow Rate and Avg. Temperature-Time Histories - S208

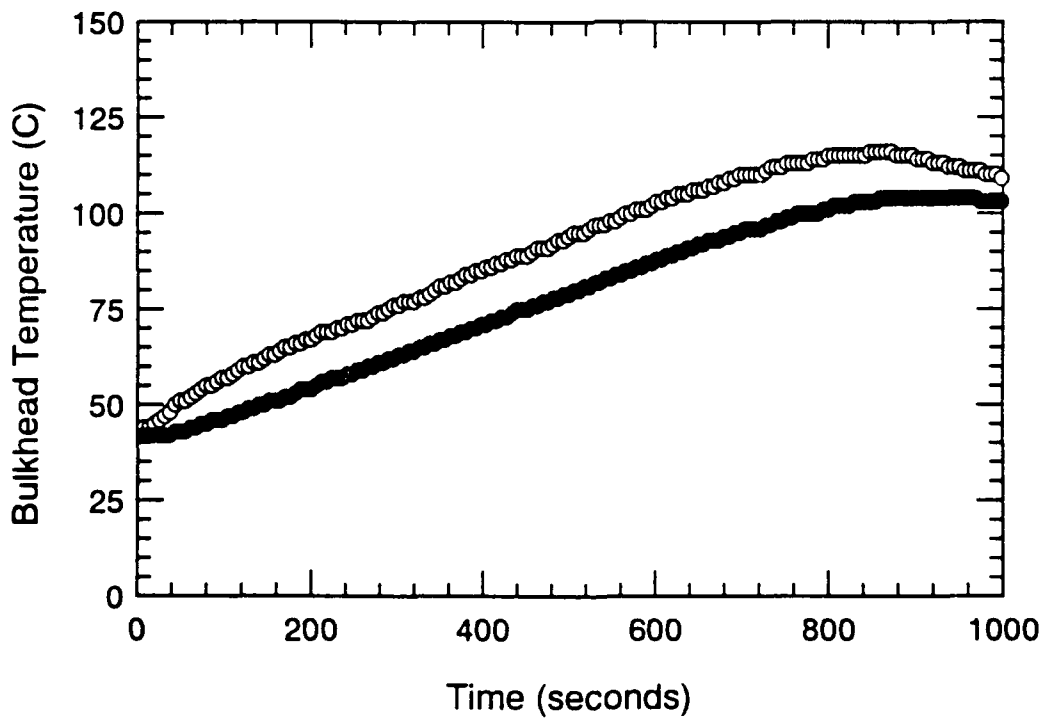
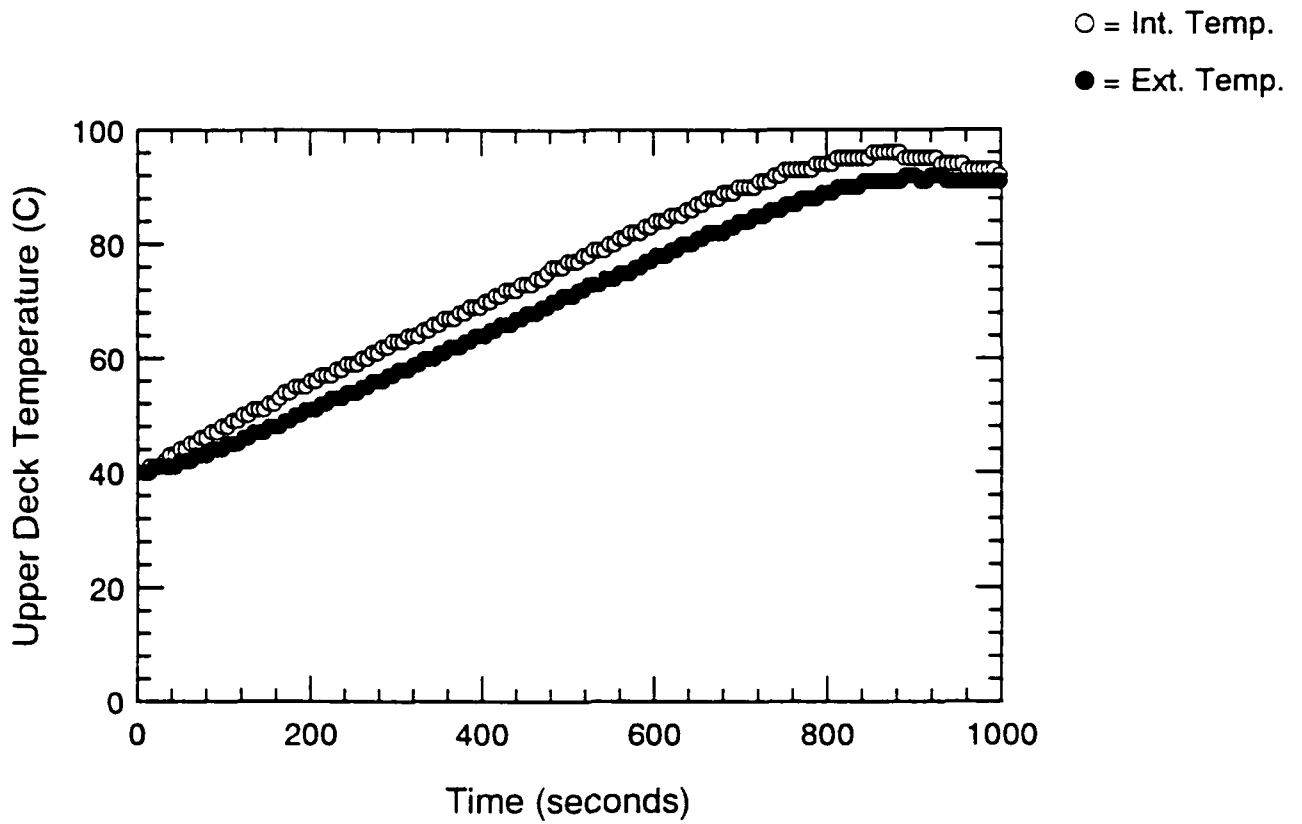


Figure B.60 Surface Thermocouple-Time Histories - S208

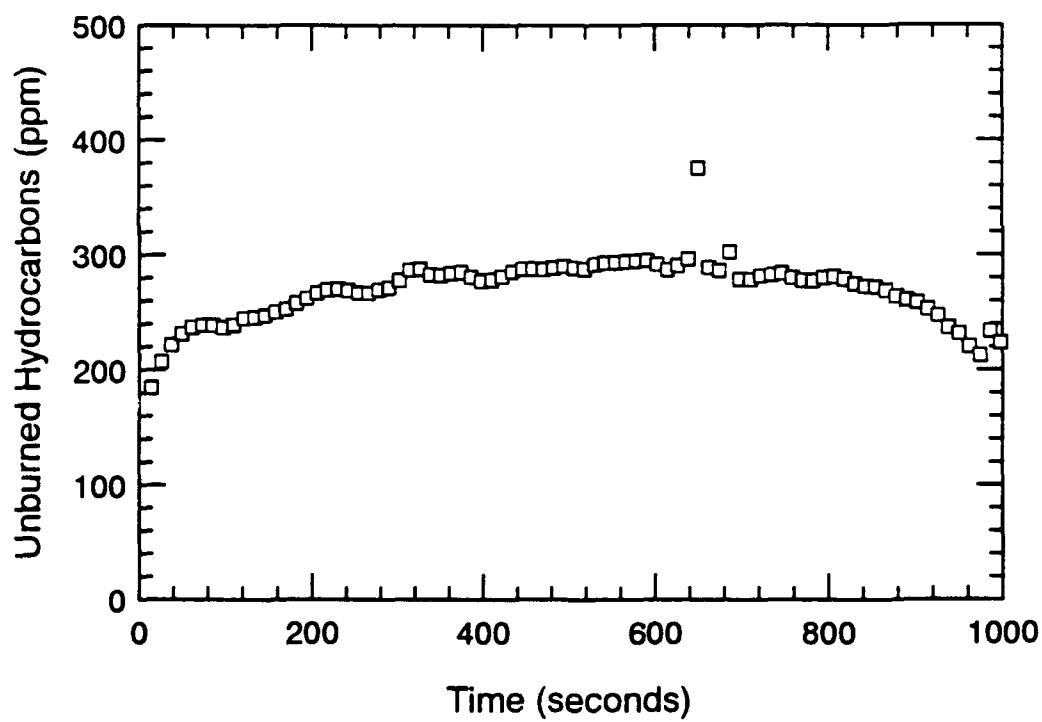
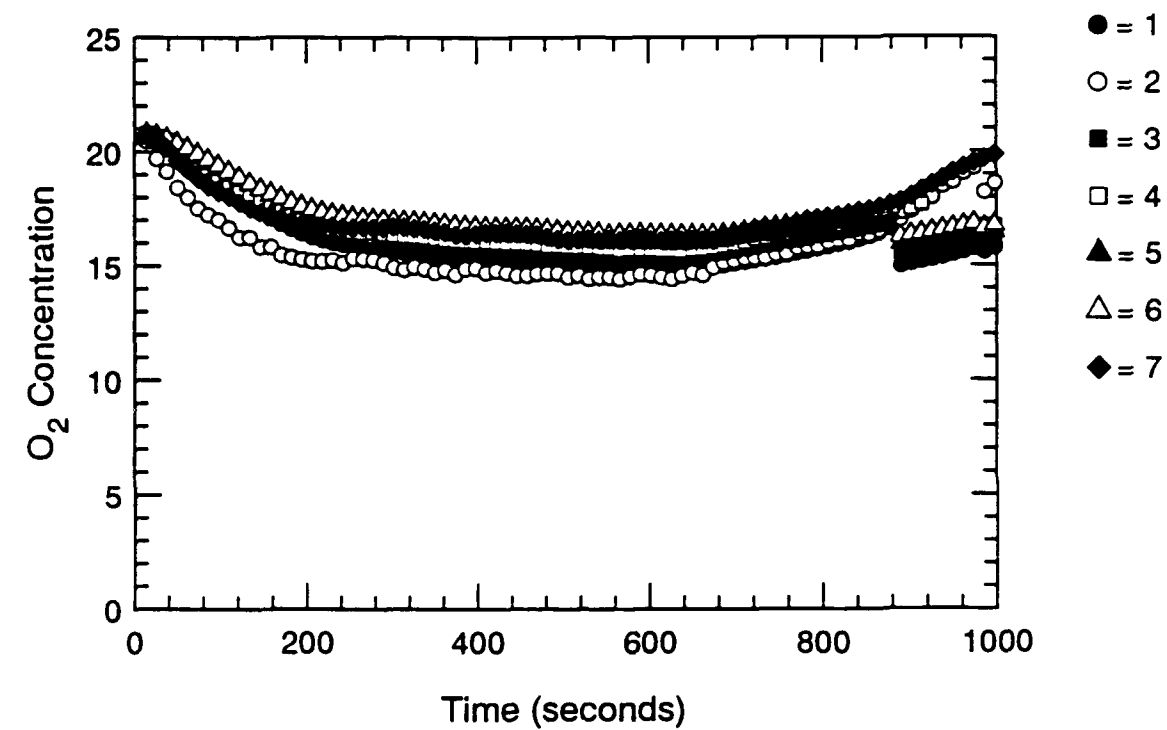


Figure B.61 Oxygen and Unburned HC Concentration-Time Histories - S208

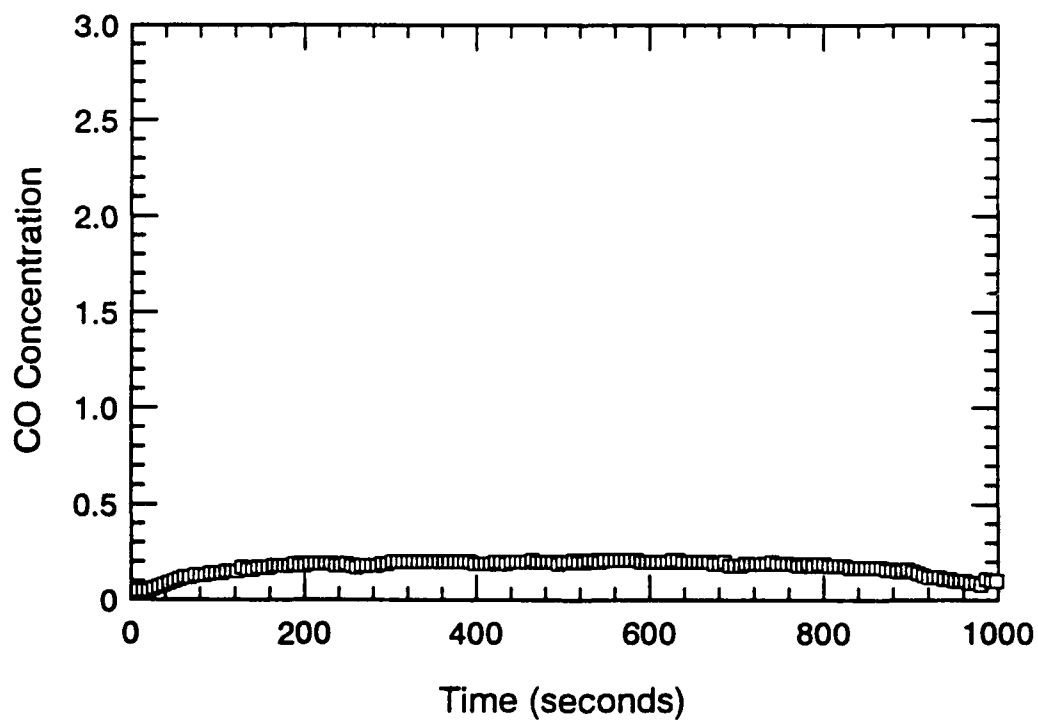
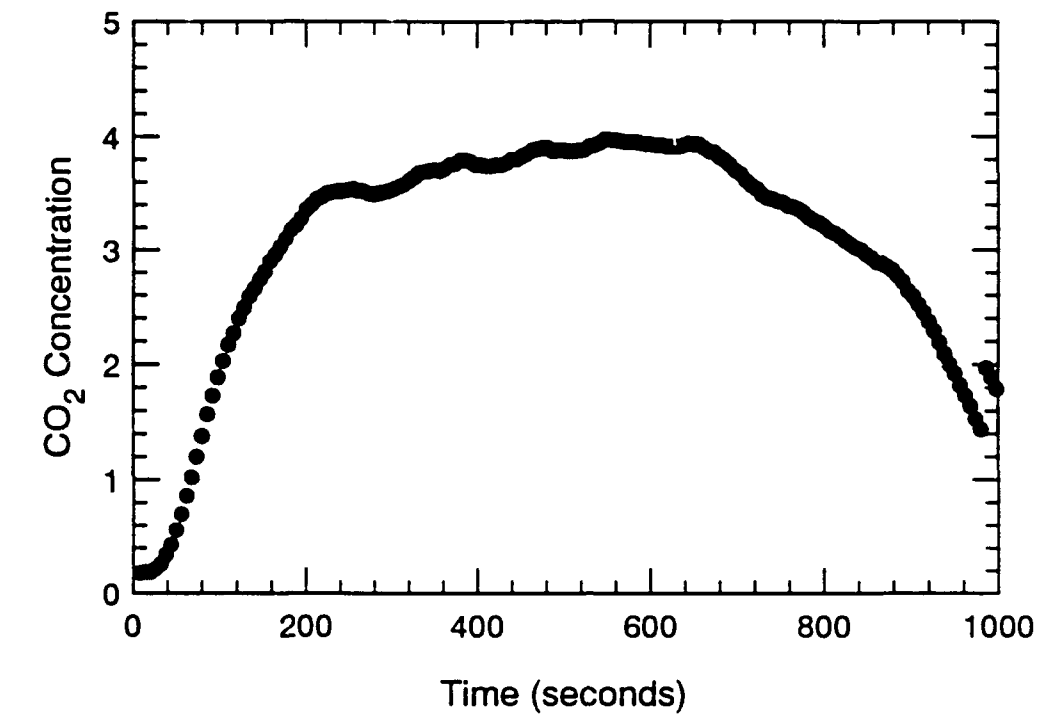


Figure B.62 CO₂ and CO Concentration-Time Histories - S208

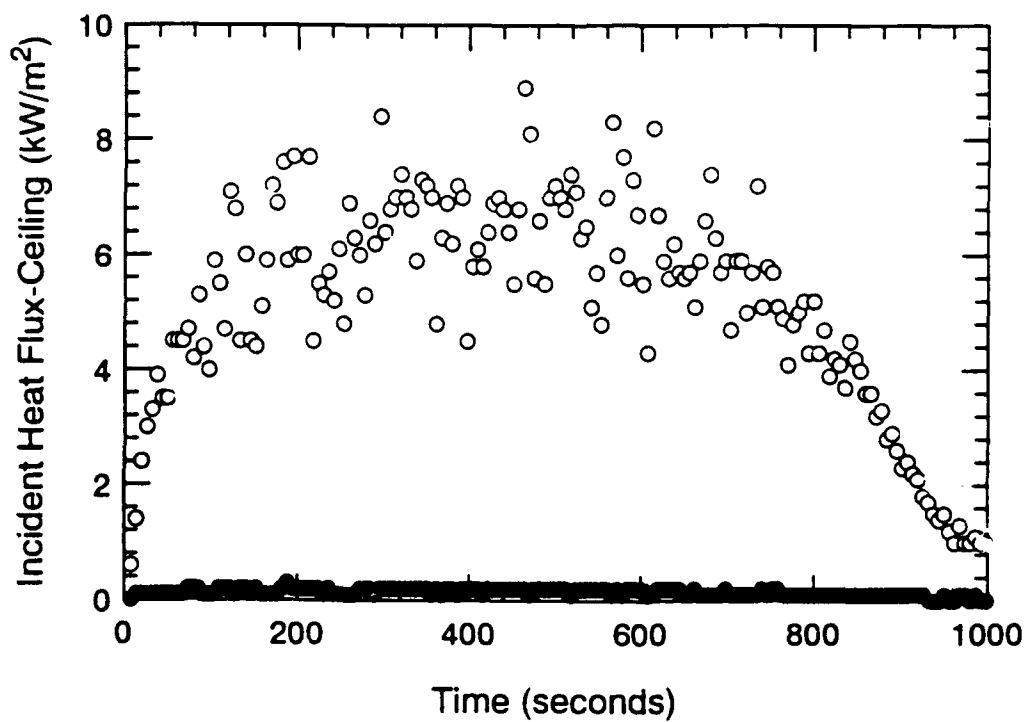
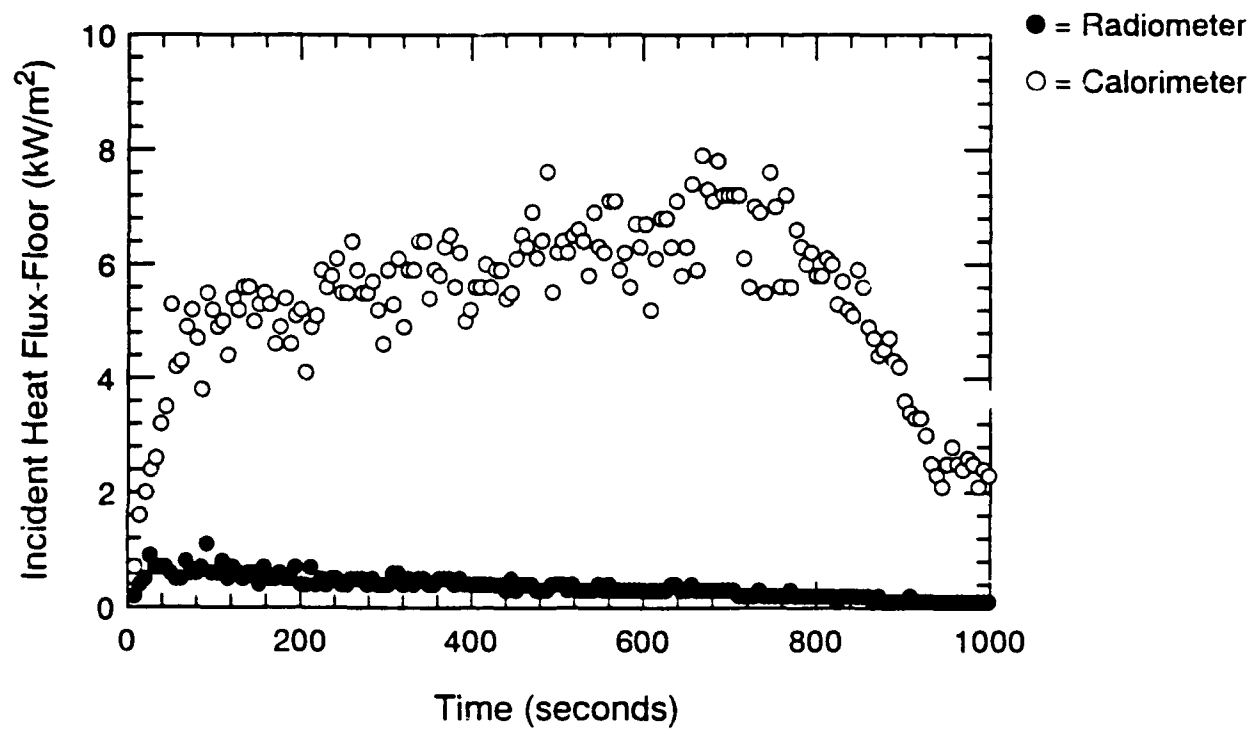


Figure B.63 Incident Heat Flux at Floor and Ceiling-Time Histories - S208

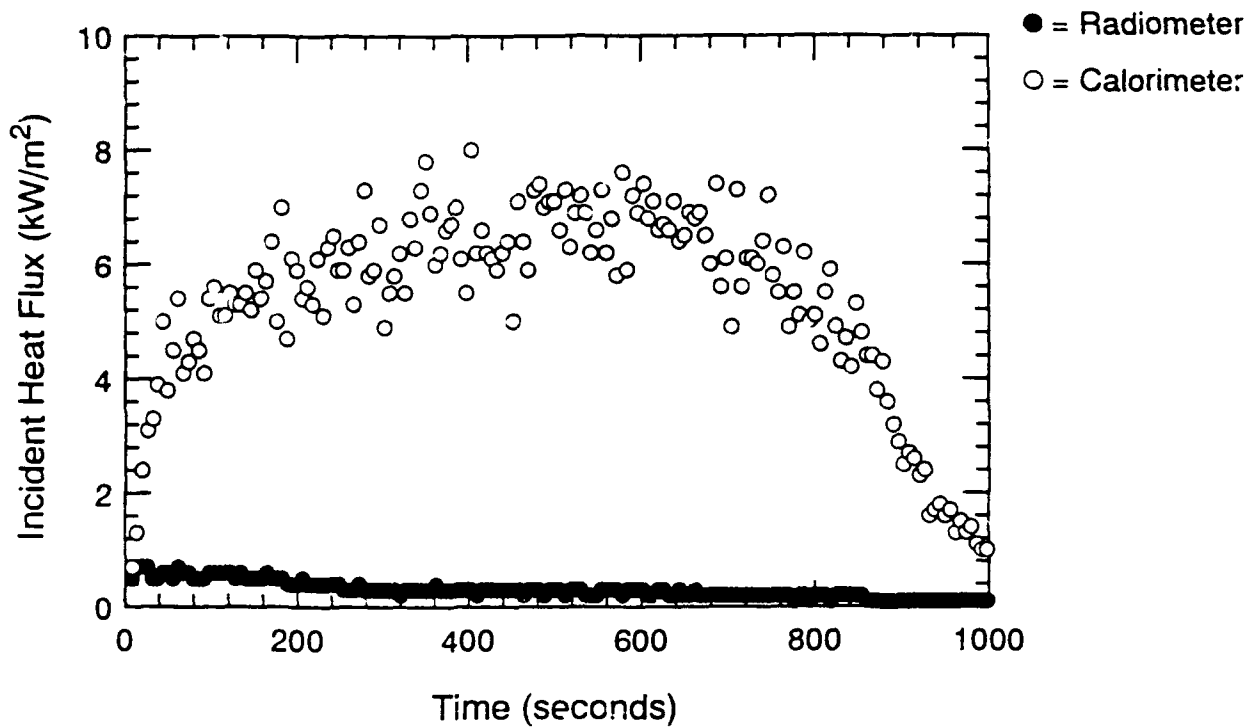


Figure B.64 Incident Heat Flux at Fwd. Bulkhead-Time Histories - S208

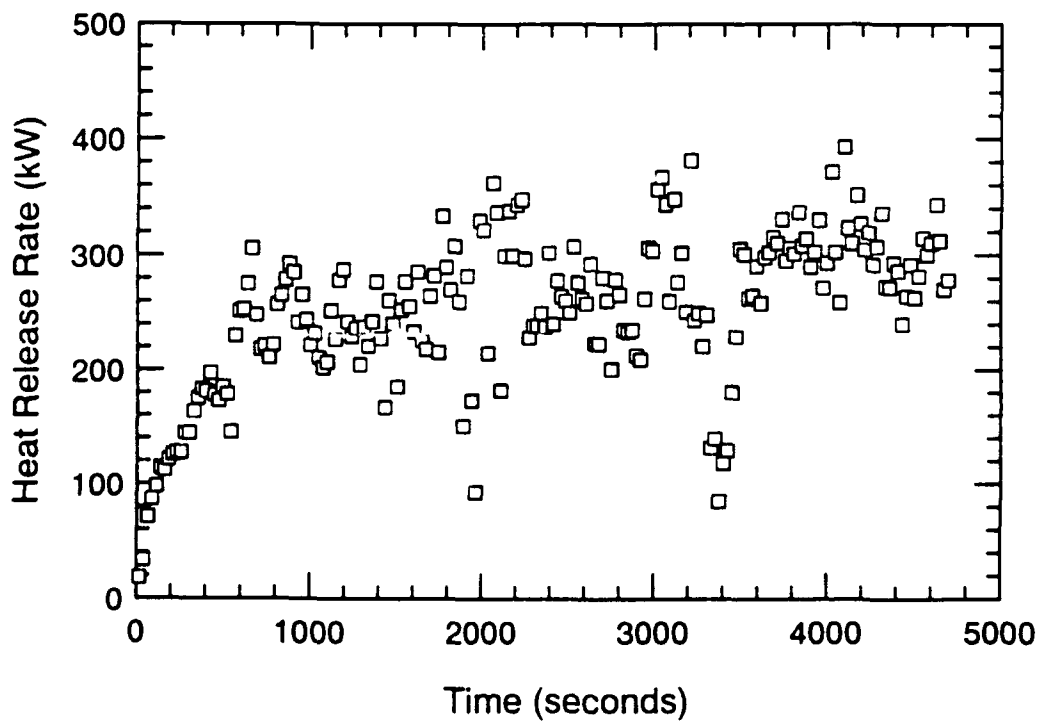
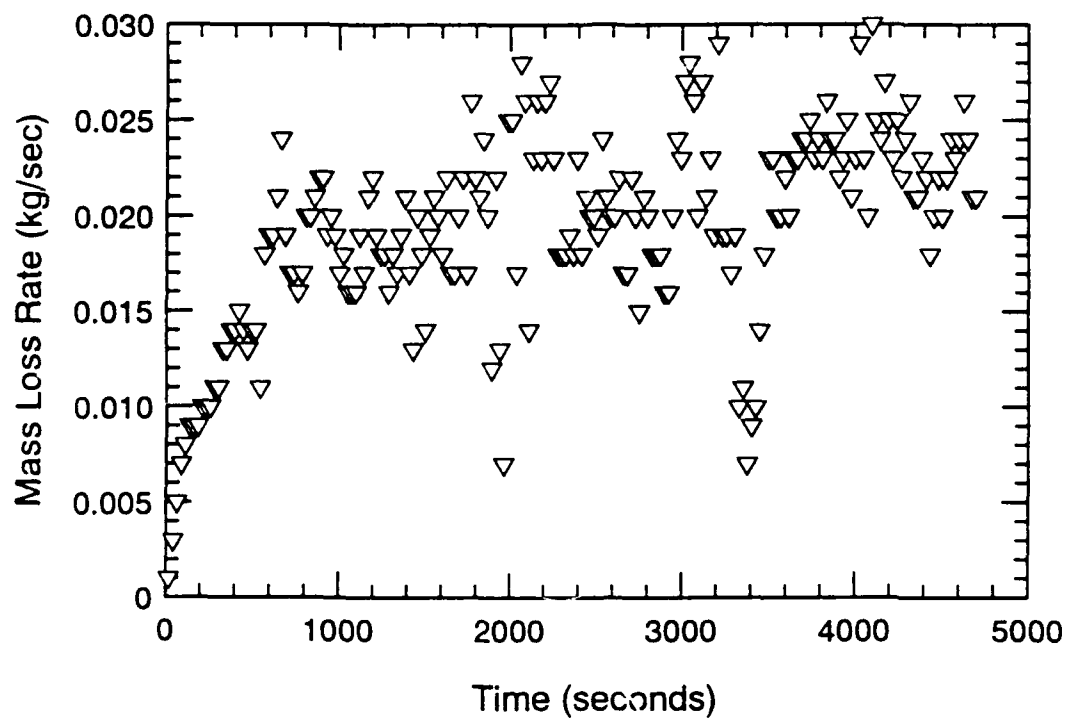


Figure B.65 Mass Loss Rate and Heat Release Rate-Time Histories - S209

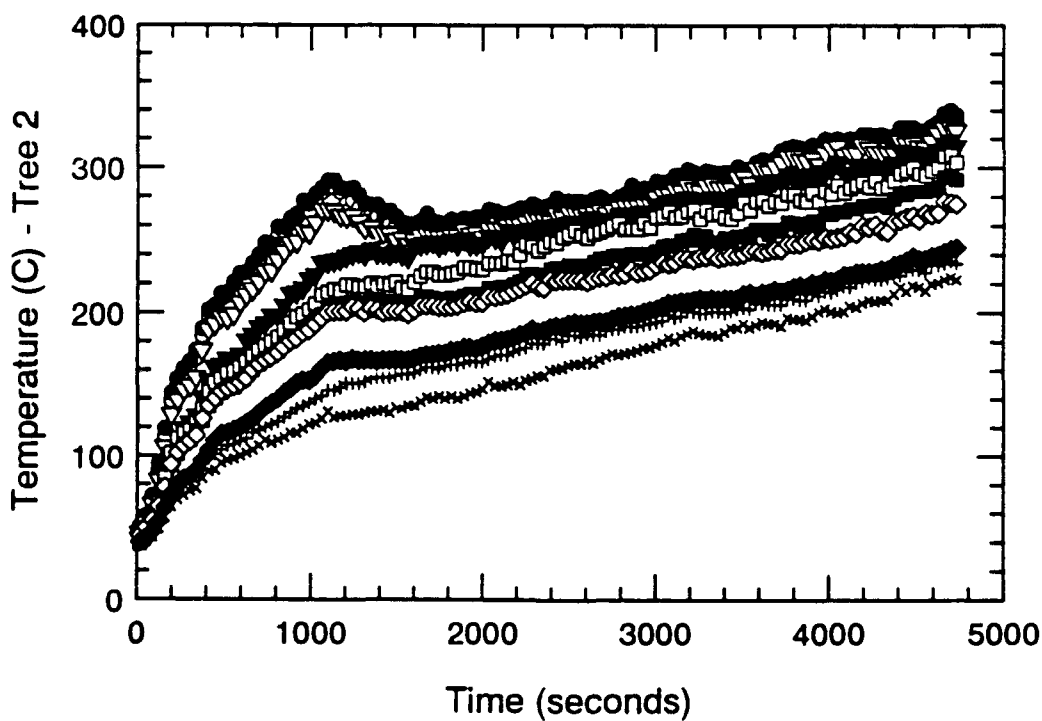
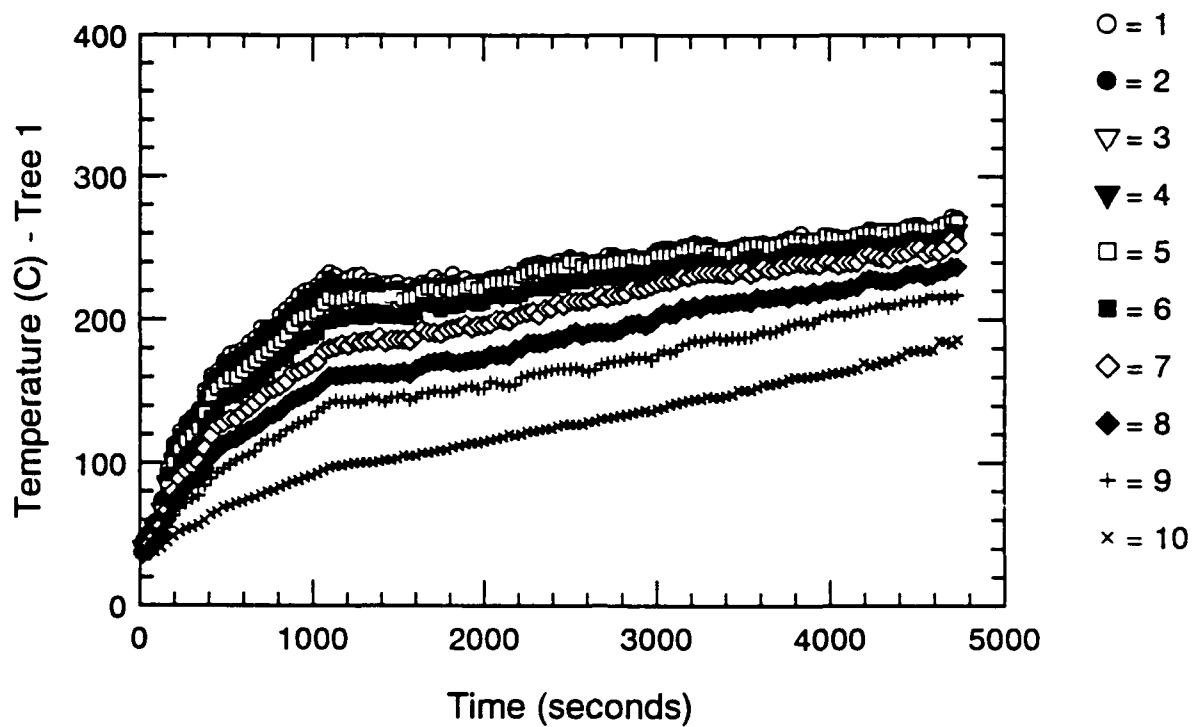


Figure B.66 Thermocouple Trees 1 & 2-Time Histories - S209

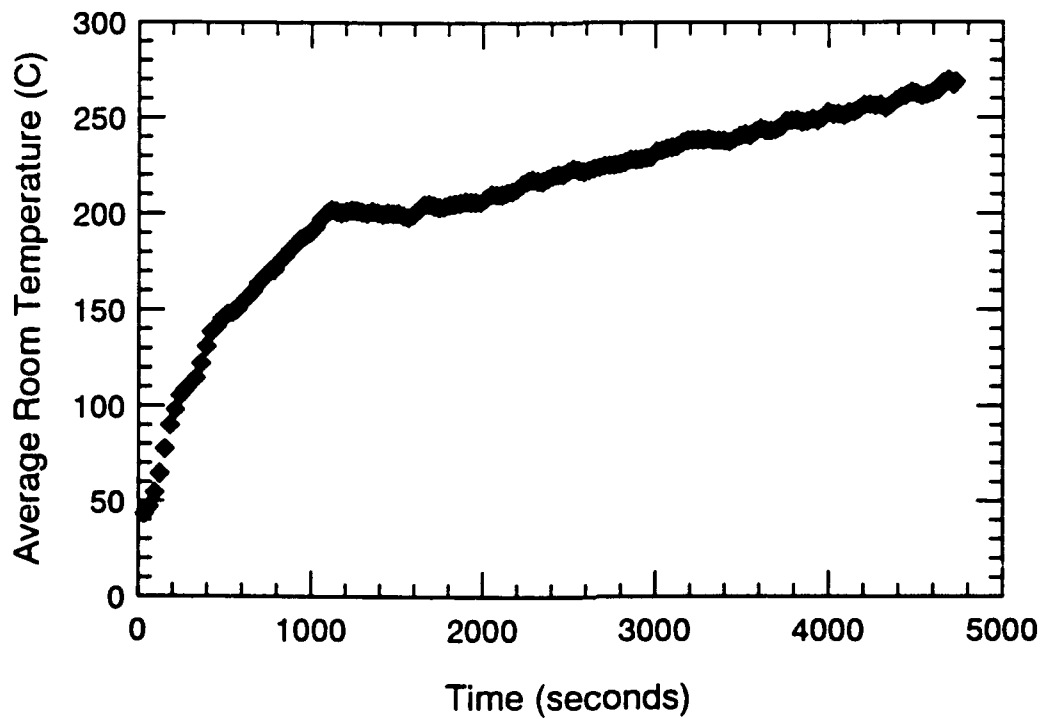
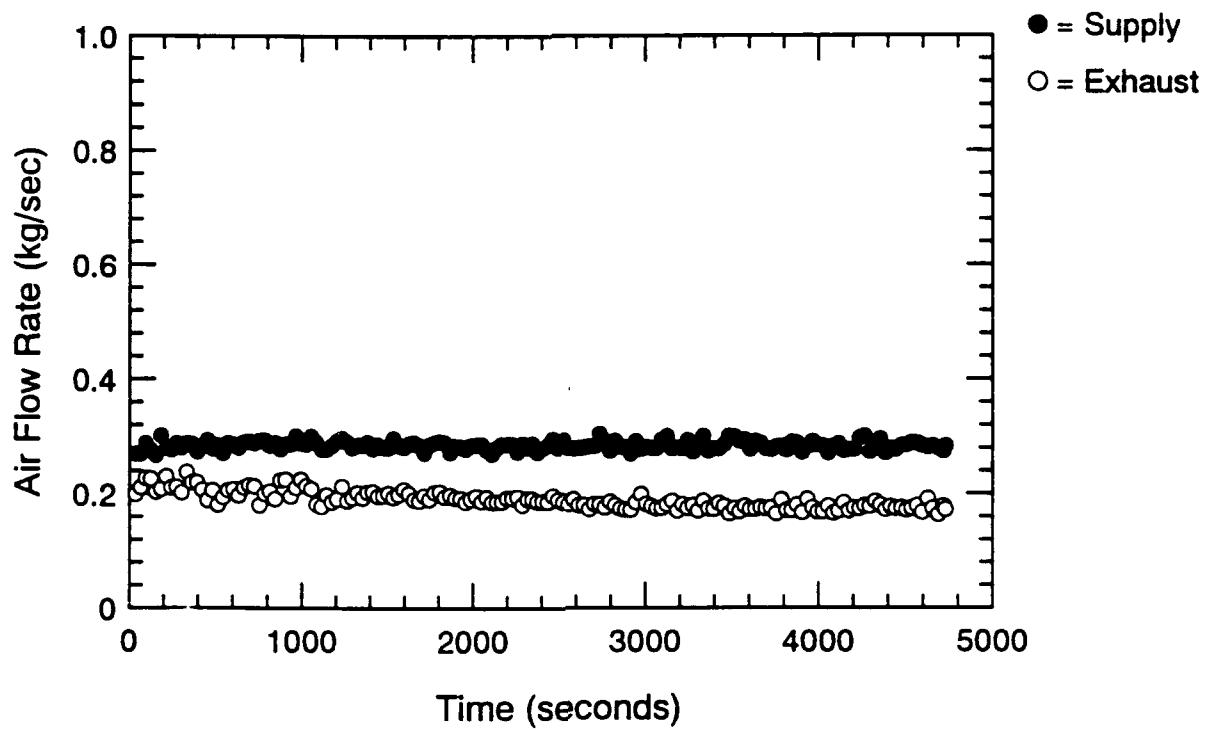


Figure B.67 Air Flow Rate and Avg. Temperature-Time Histories - S209

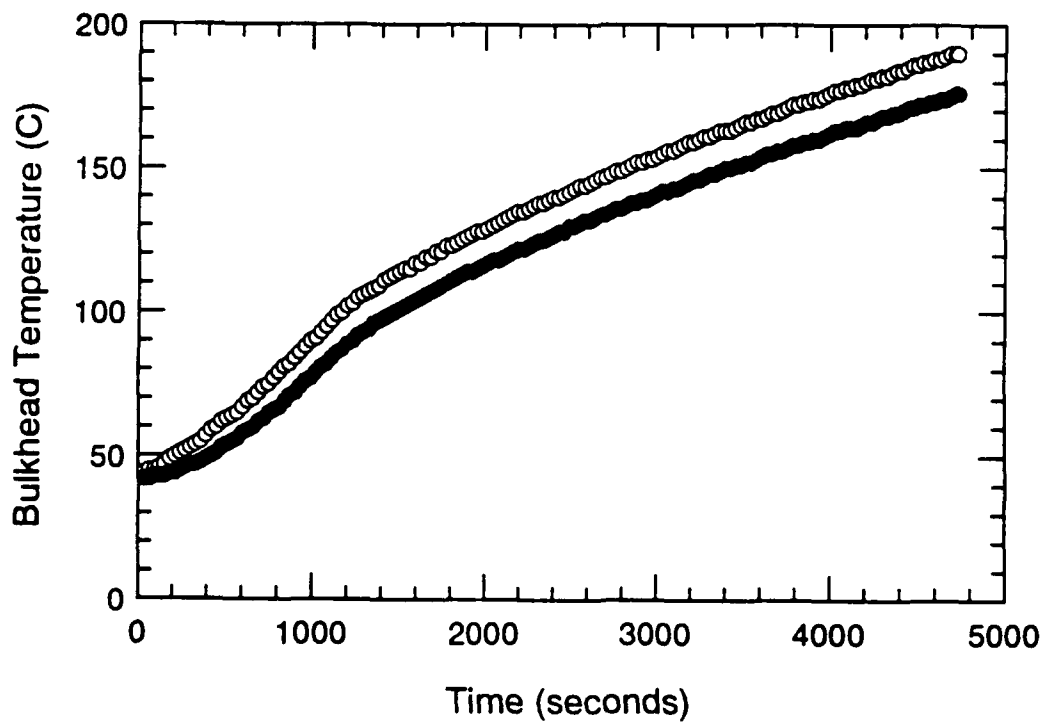
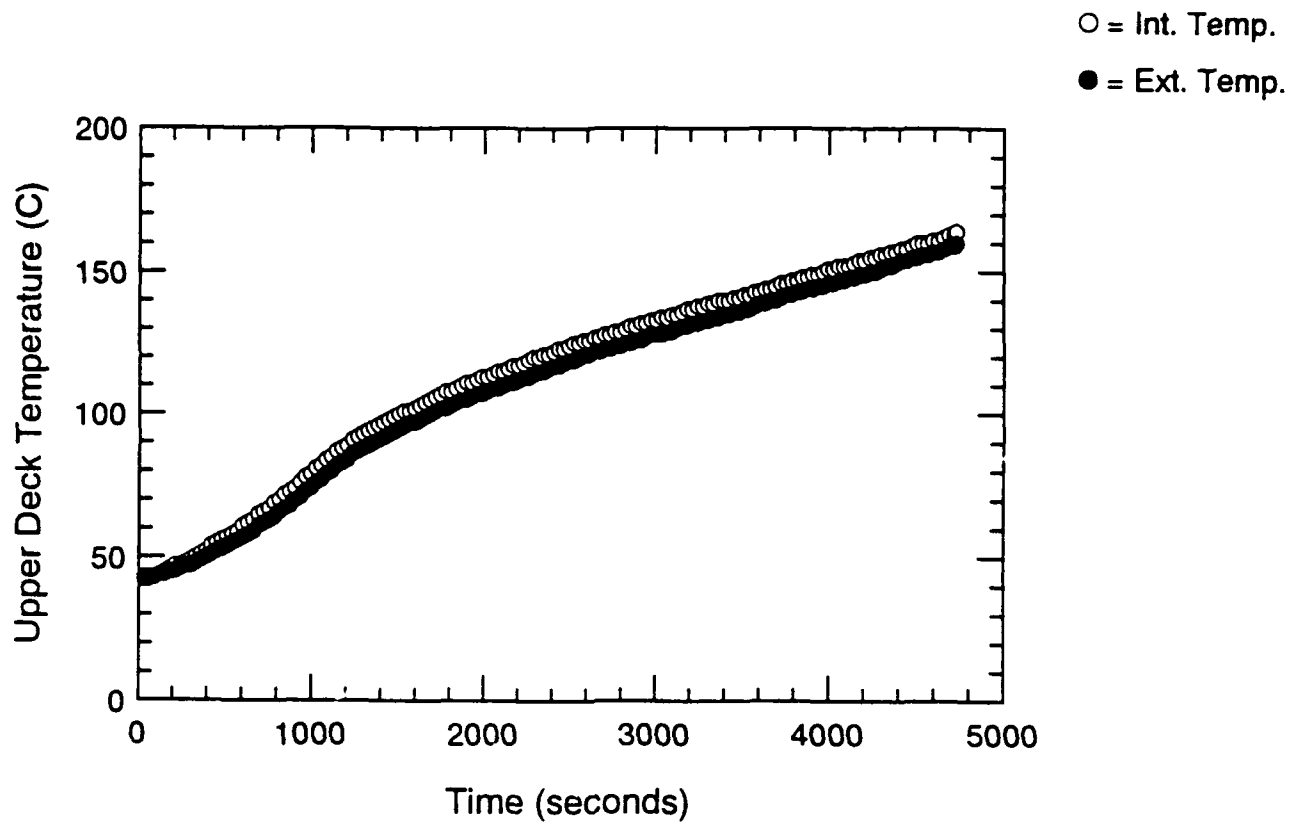


Figure B.68 Surface Thermocouple-Time Histories - S209

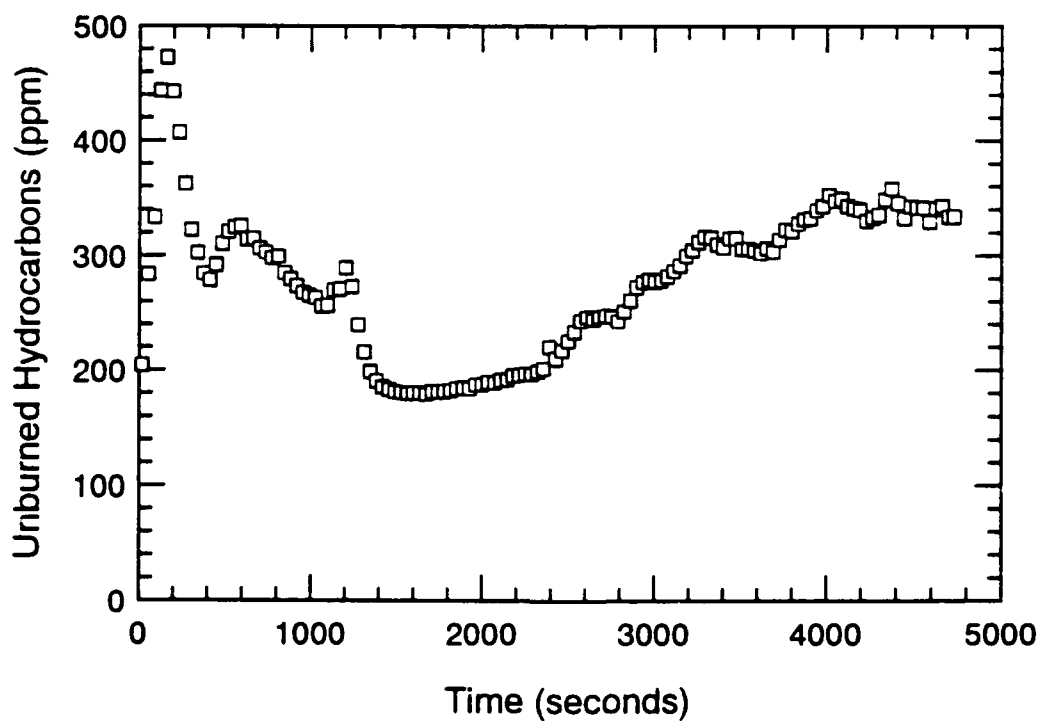
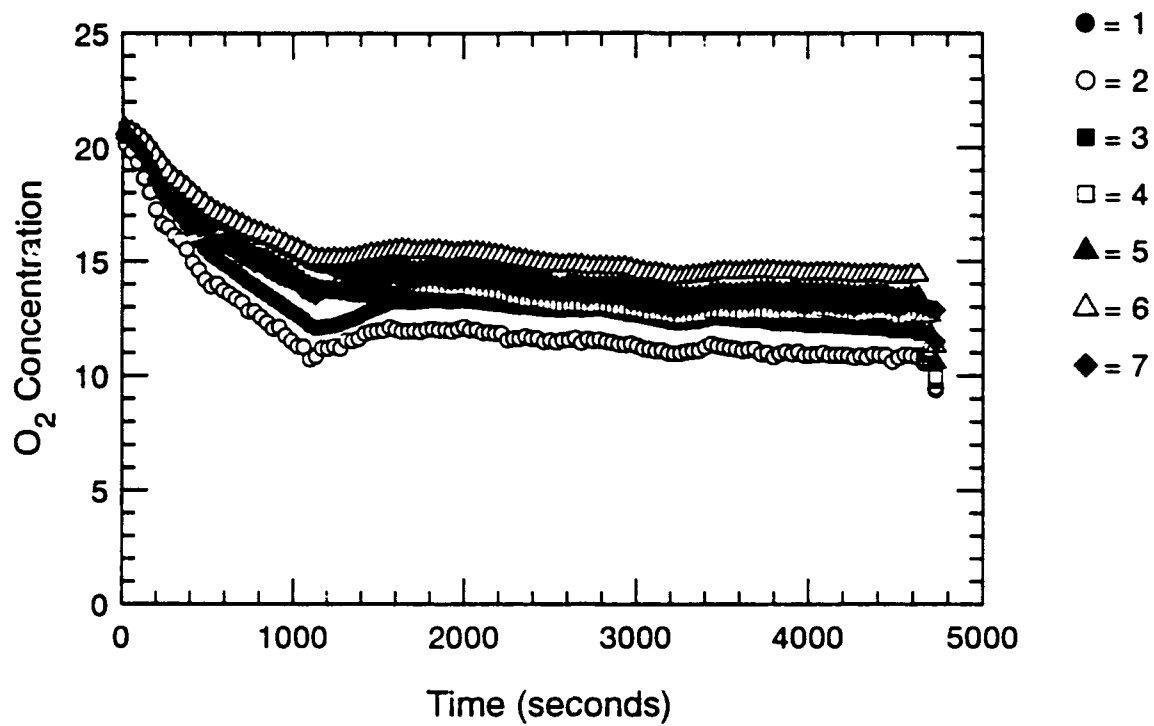


Figure B.69 Oxygen and Unburned HC Concentration-Time Histories - S209

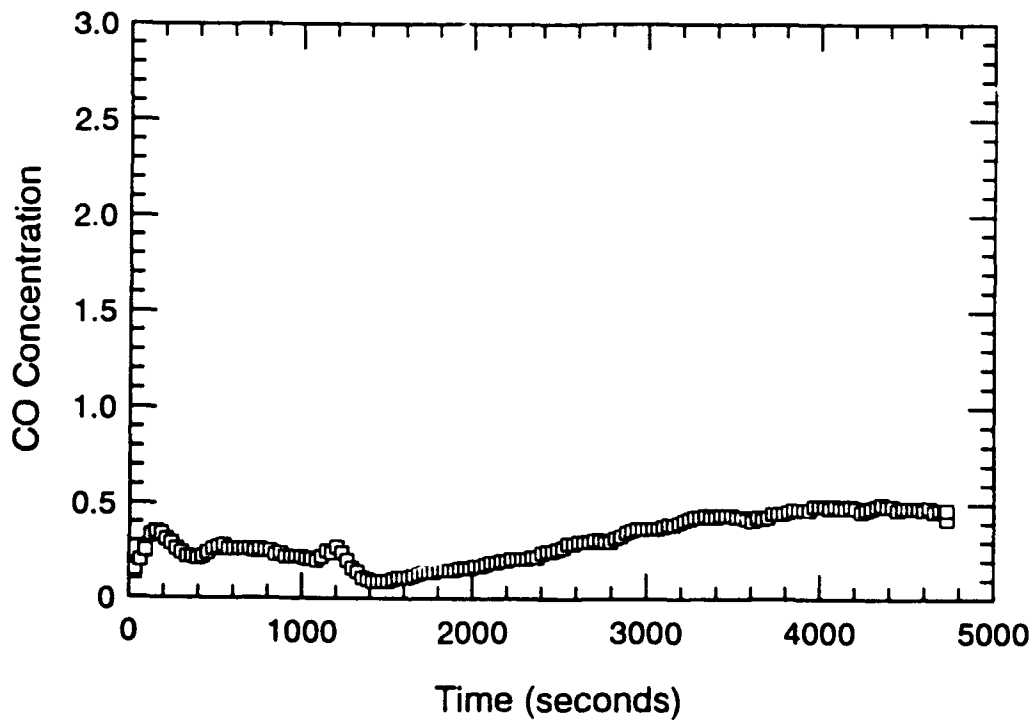
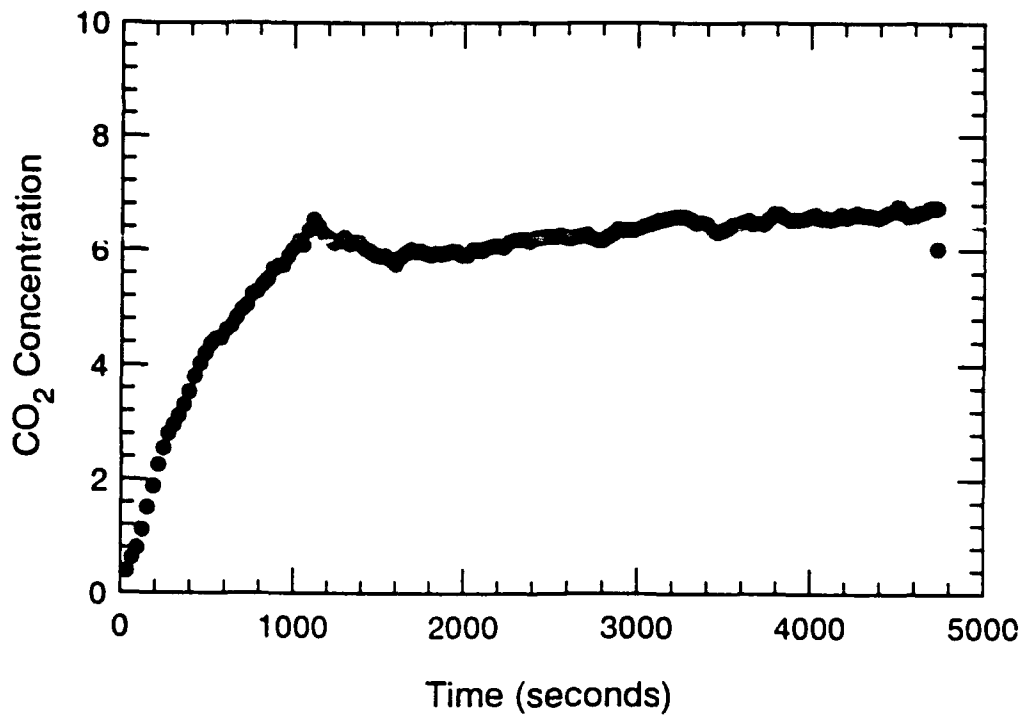


Figure B.70 CO₂ and CO Concentration-Time Histories - S209

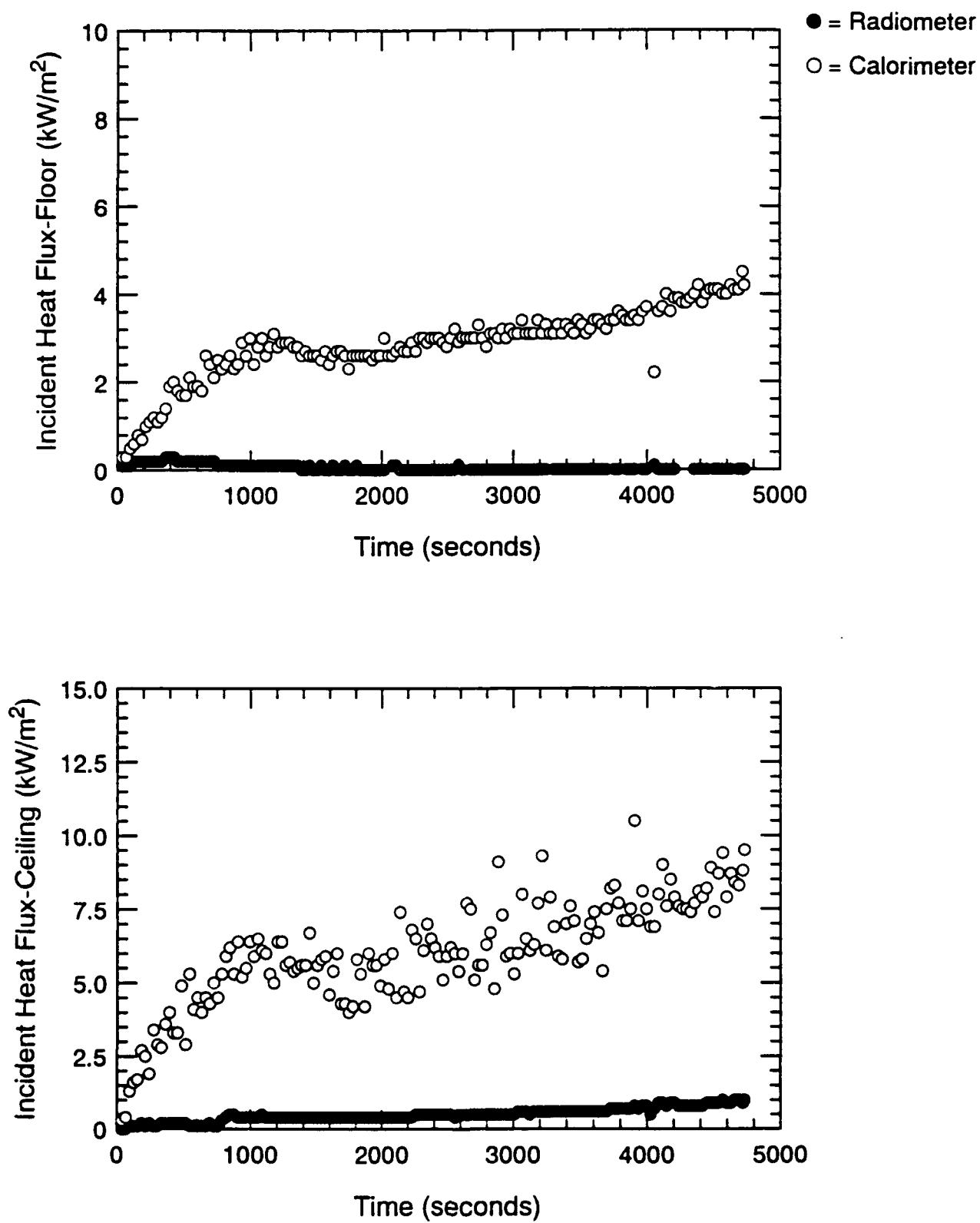


Figure B.71 Incident Heat Flux at Floor and Ceiling-Time Histories - S209

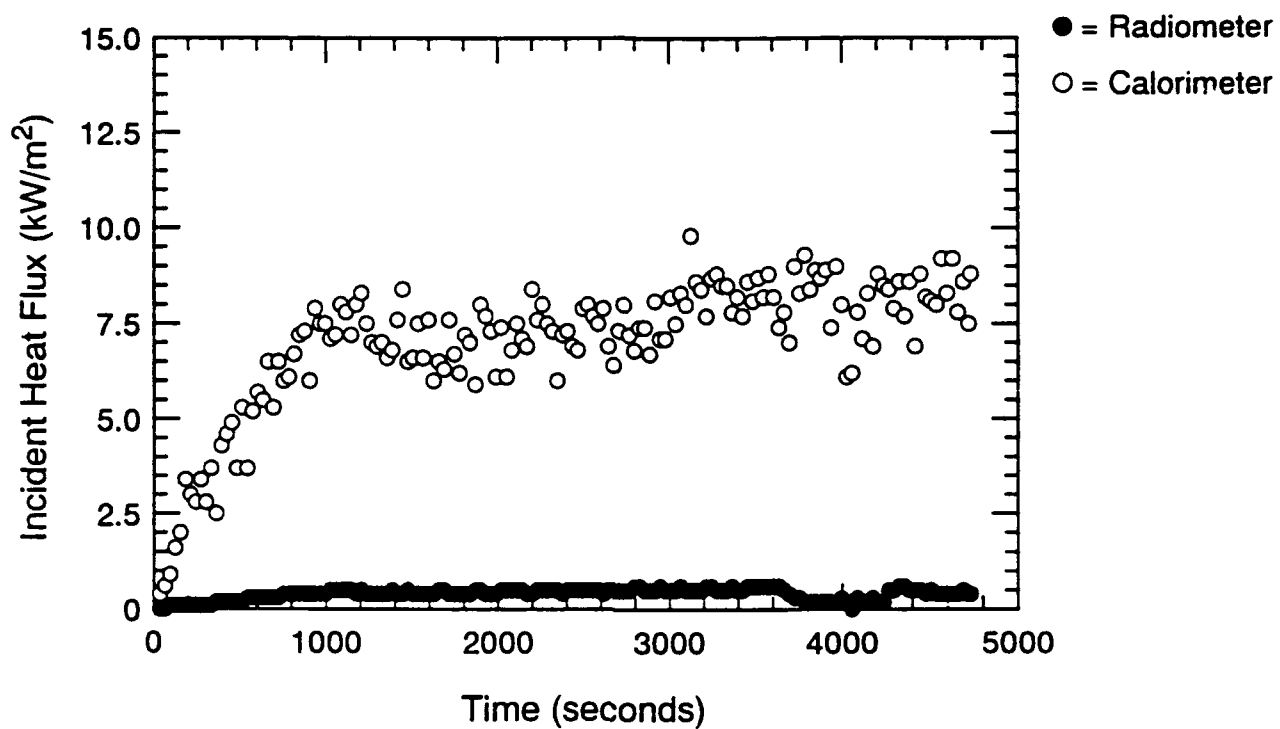


Figure B.72 Incident Heat Flux at Fwd. Bulkhead-Time Histories - S209

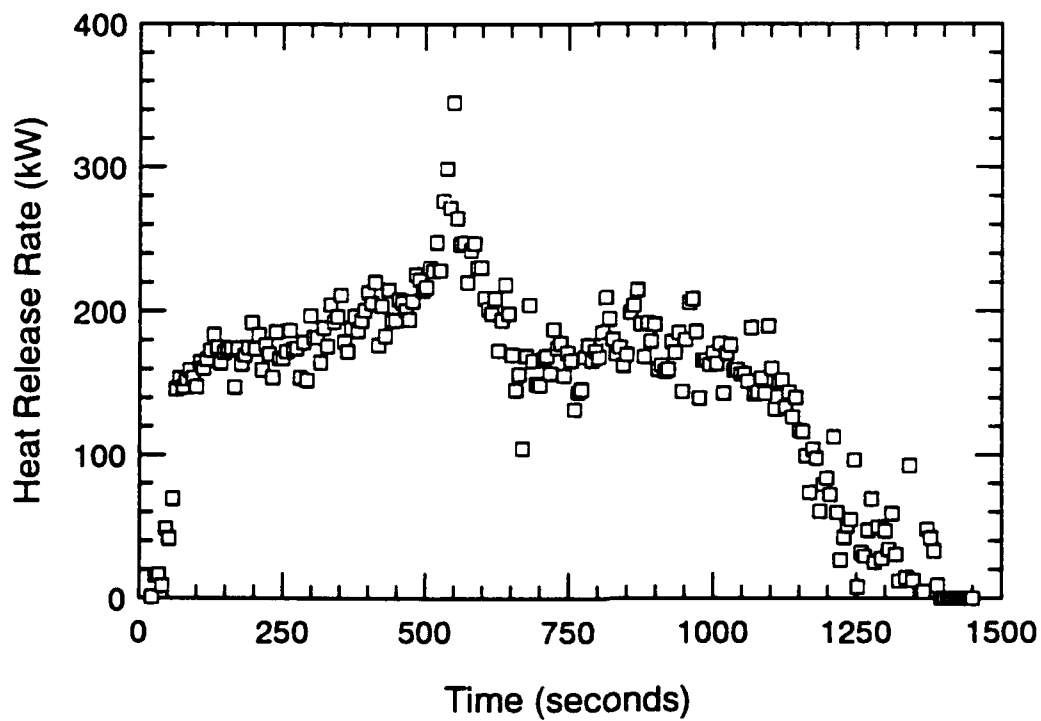
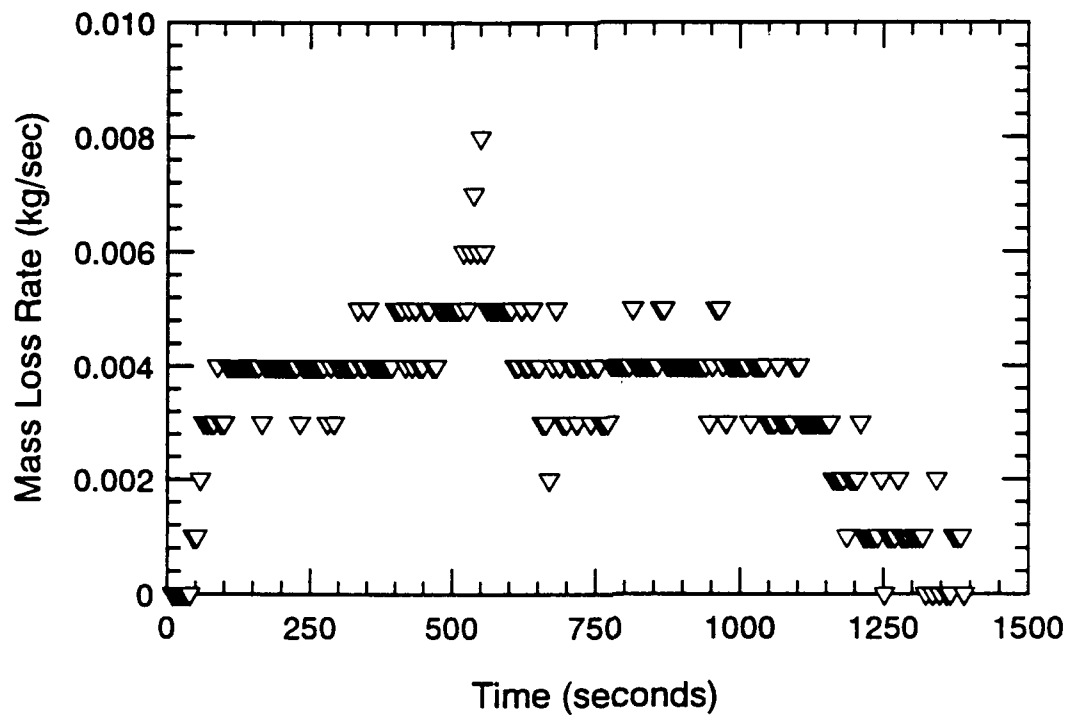


Figure B.73 Mass Loss Rate and Heat Release Rate-Time Histories - S210

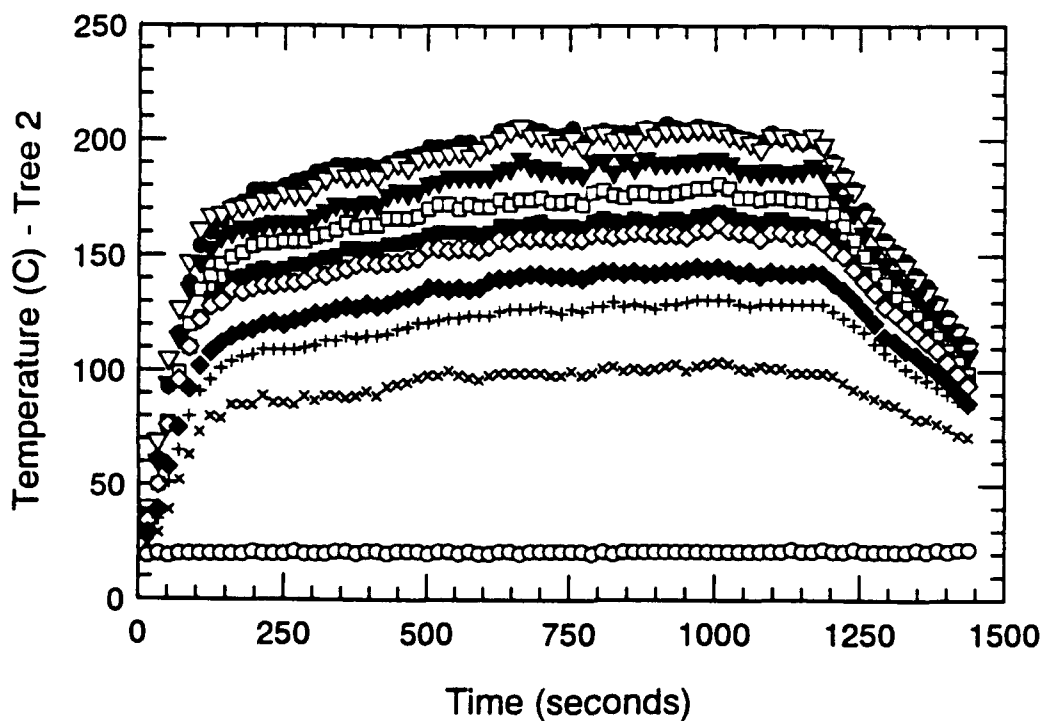
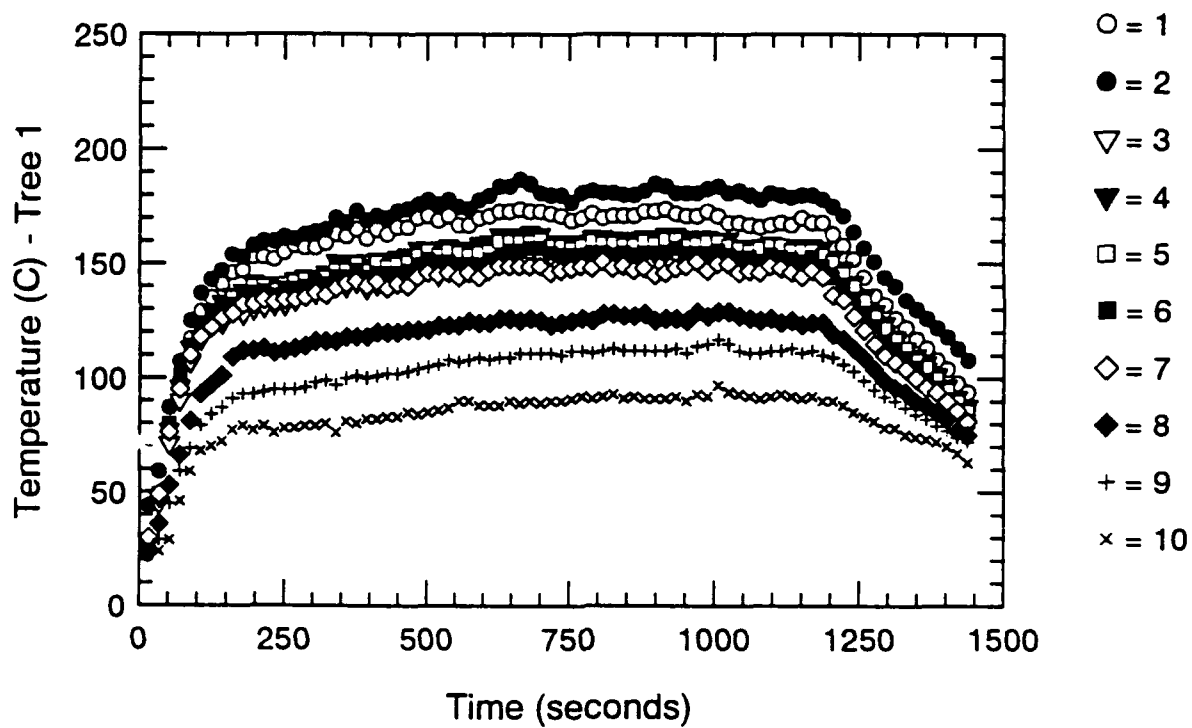


Figure B.74 Thermocouple Trees 1 & 2-Time Histories - S210

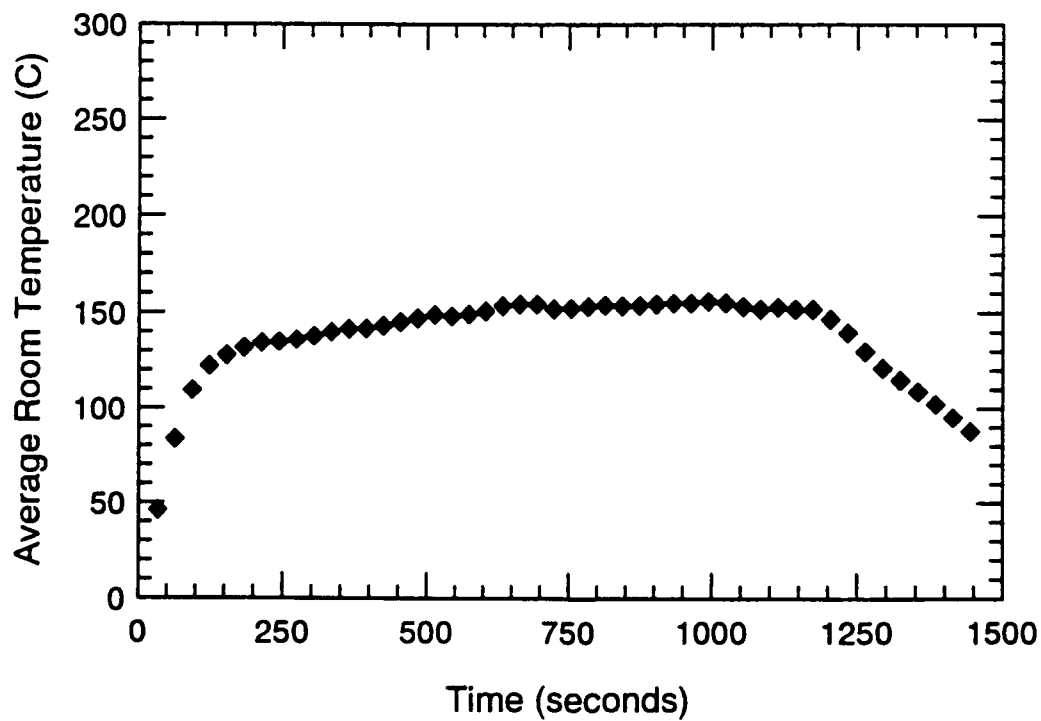
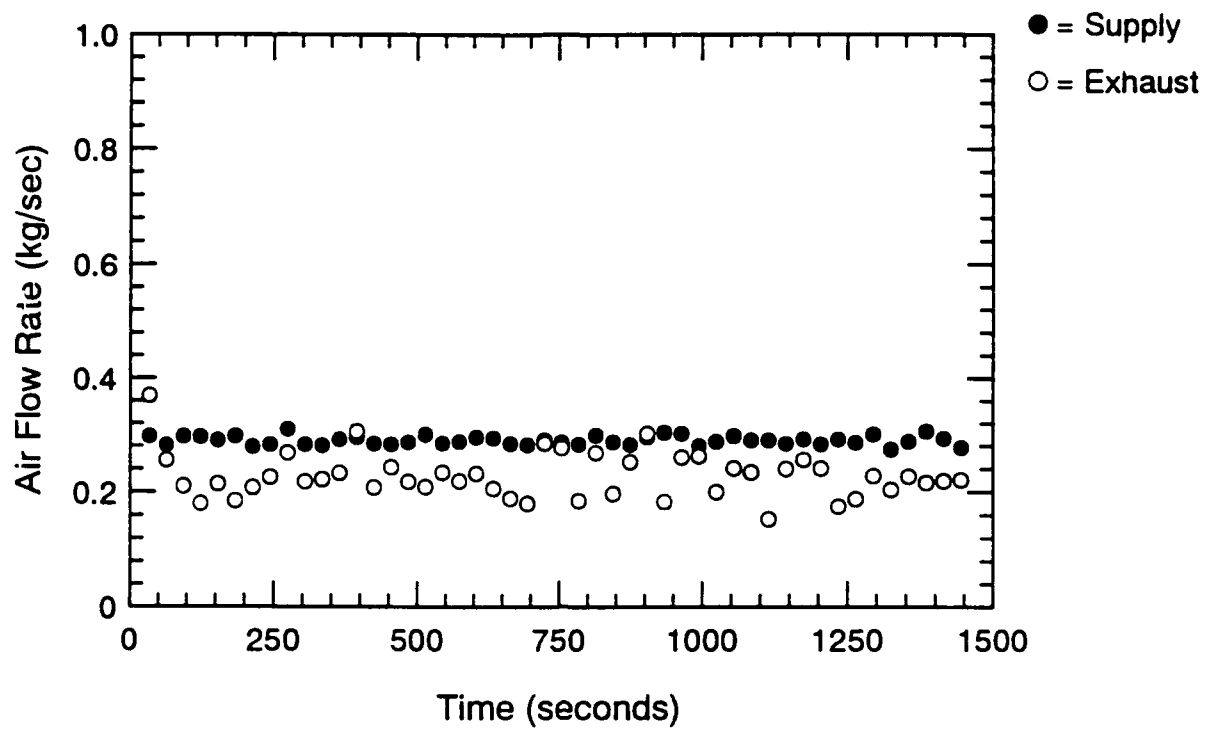


Figure B.75 Air Flow Rate and Avg. Temperature-Time Histories - S210

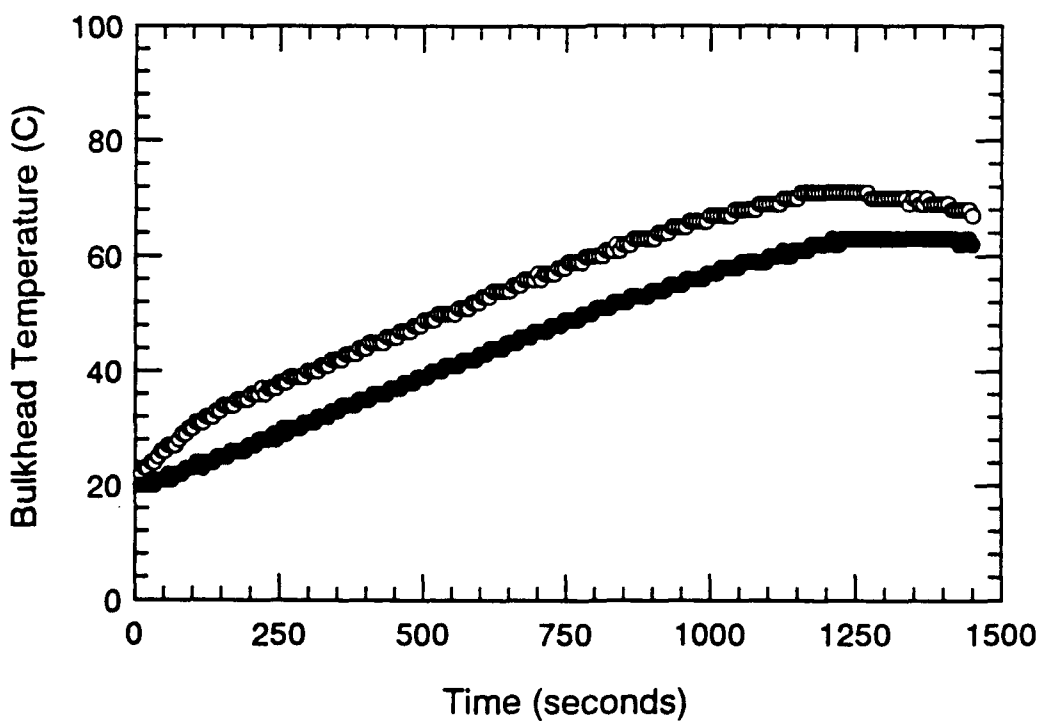
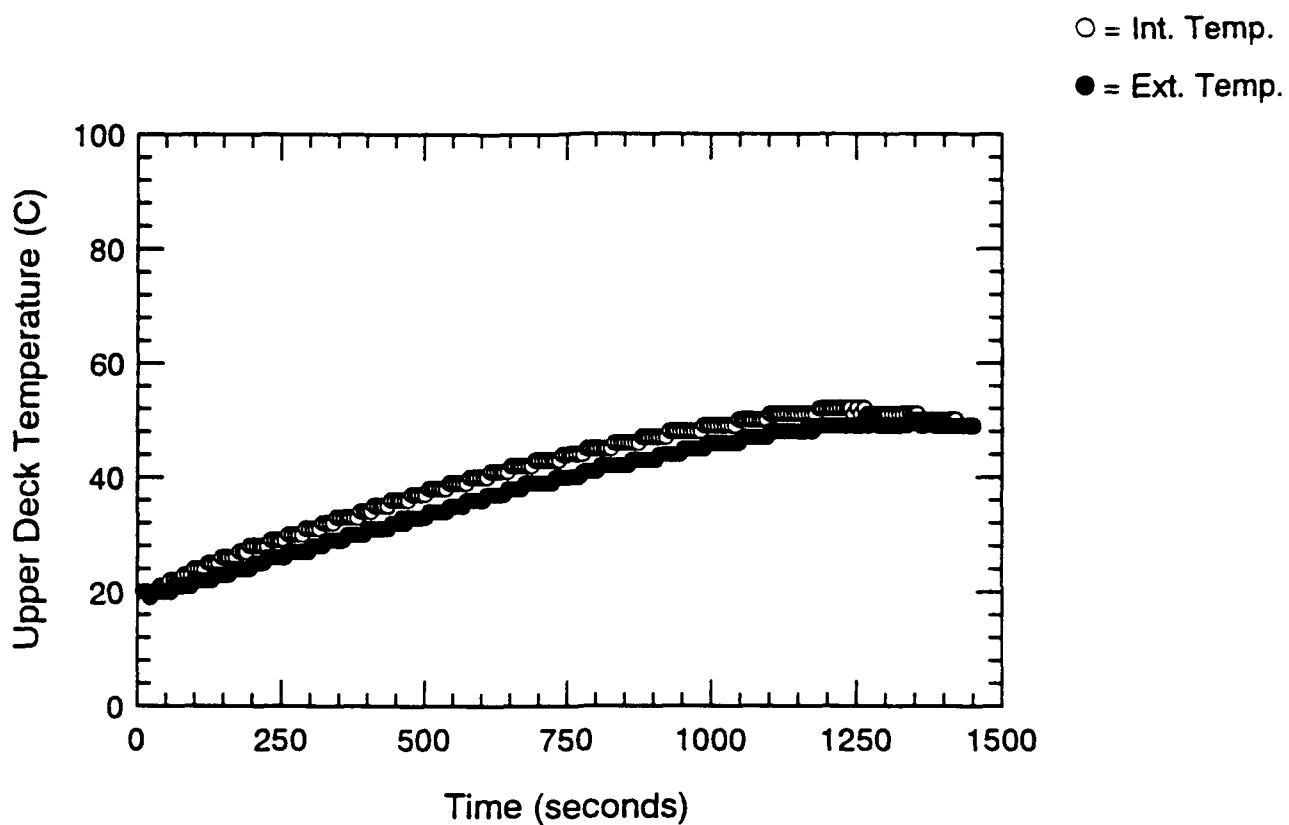


Figure B.76 Surface Thermocouple-Time Histories - S210

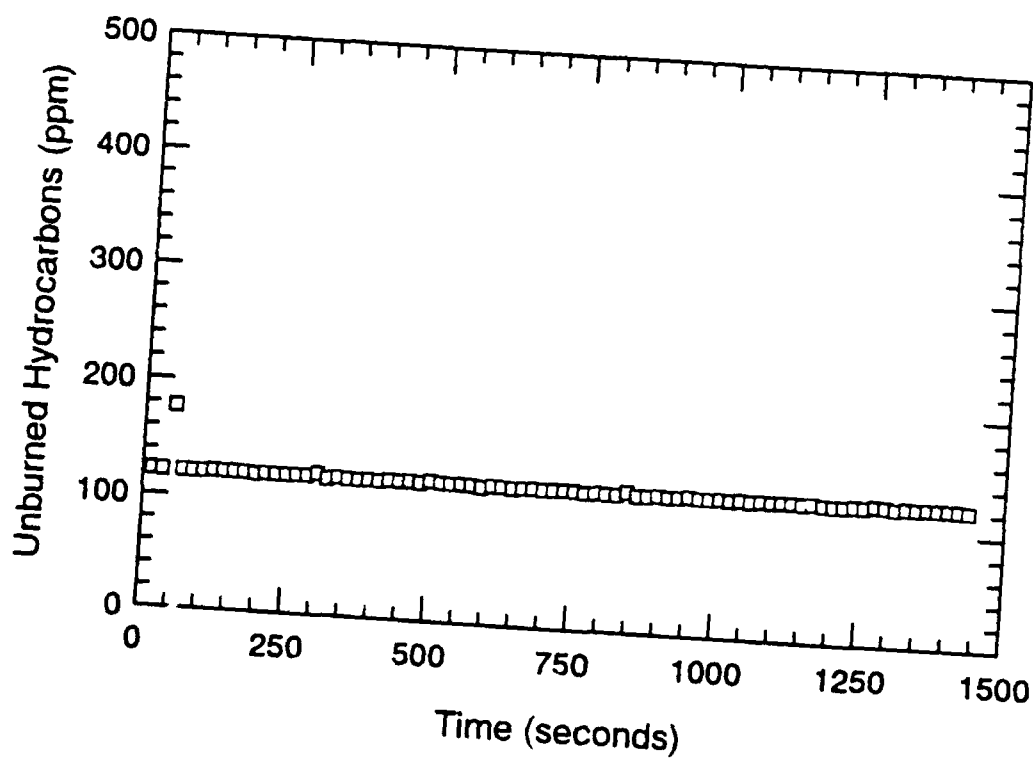
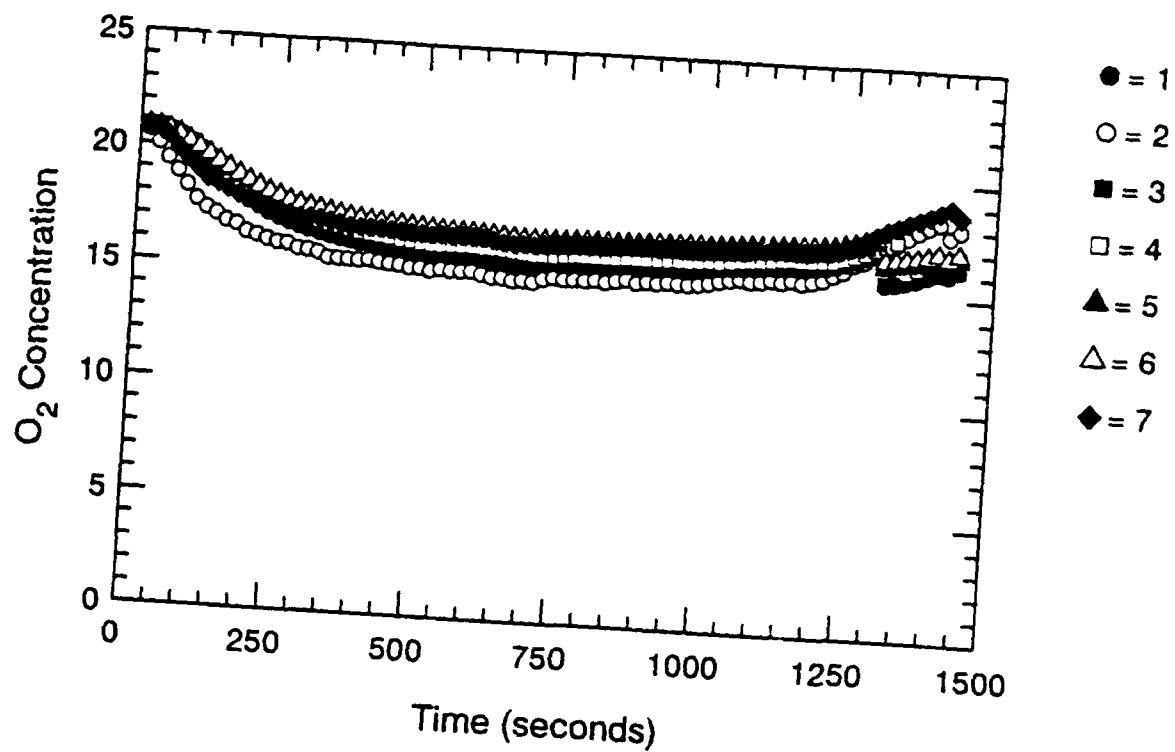


Figure B.77 Oxygen and Unburned HC Concentration-Time Histories - S210

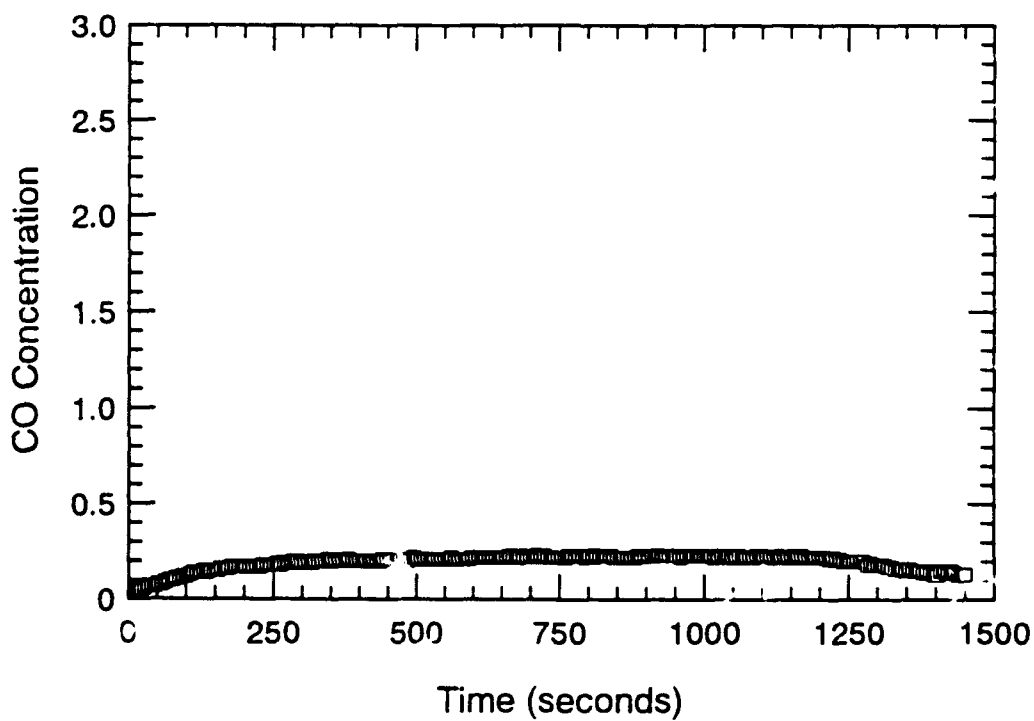
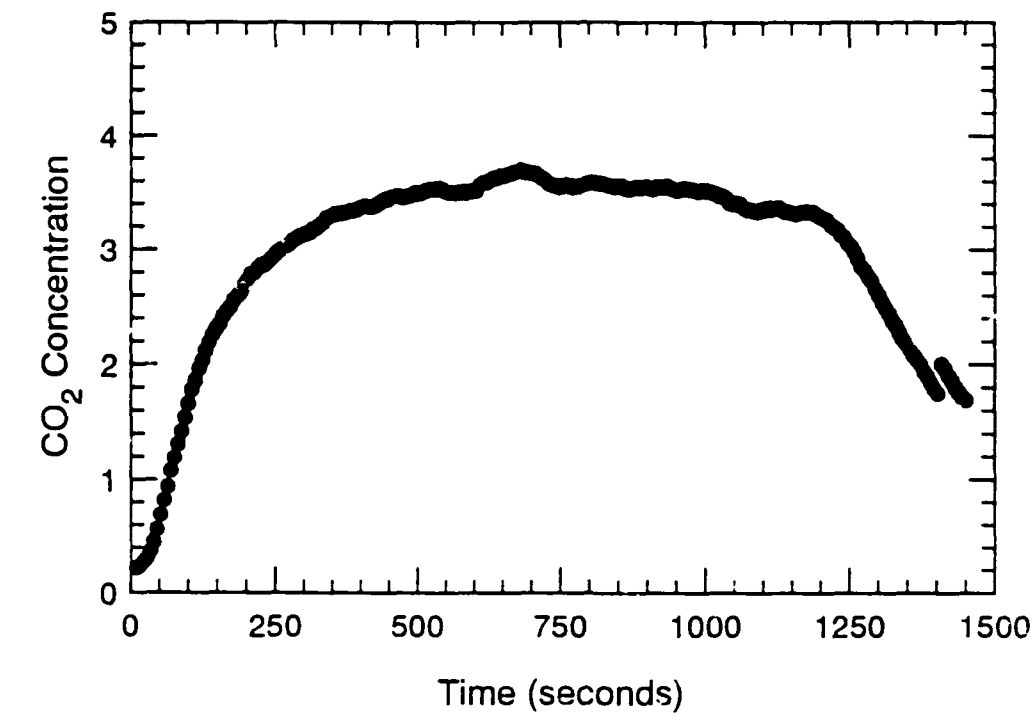


Figure B.78 CO₂ and CO Concentration-Time Histories - S210

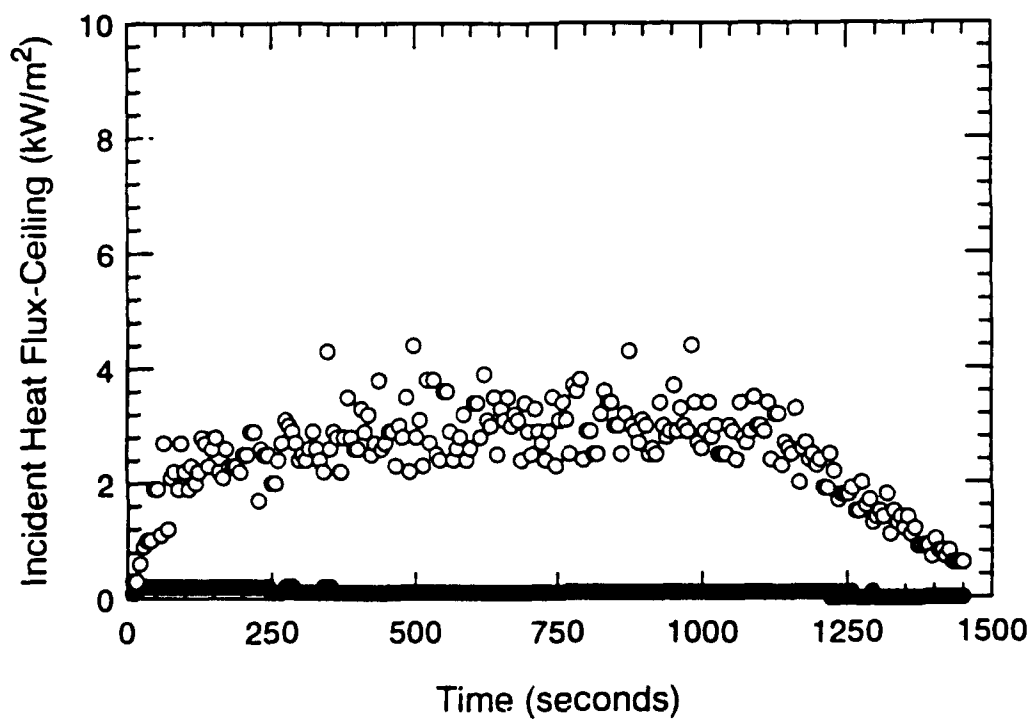
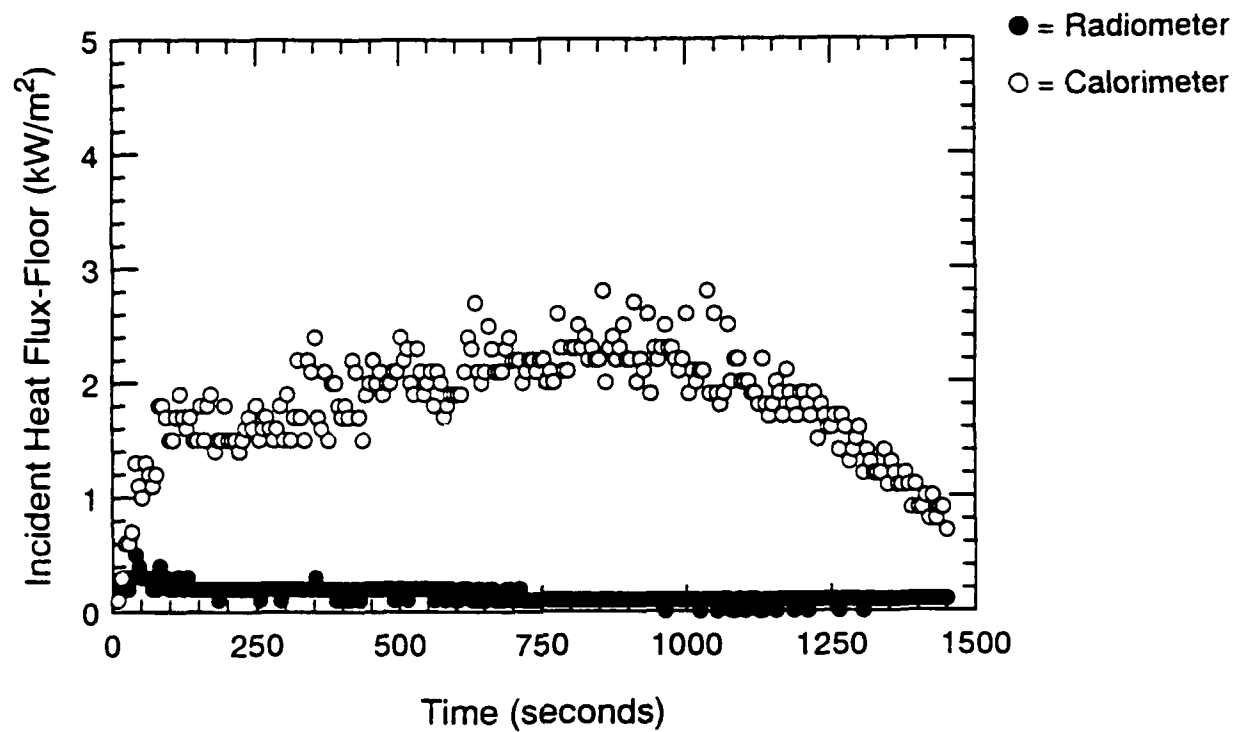


Figure B.79 Incident Heat Flux at Floor and Ceiling-Time Histories - S210

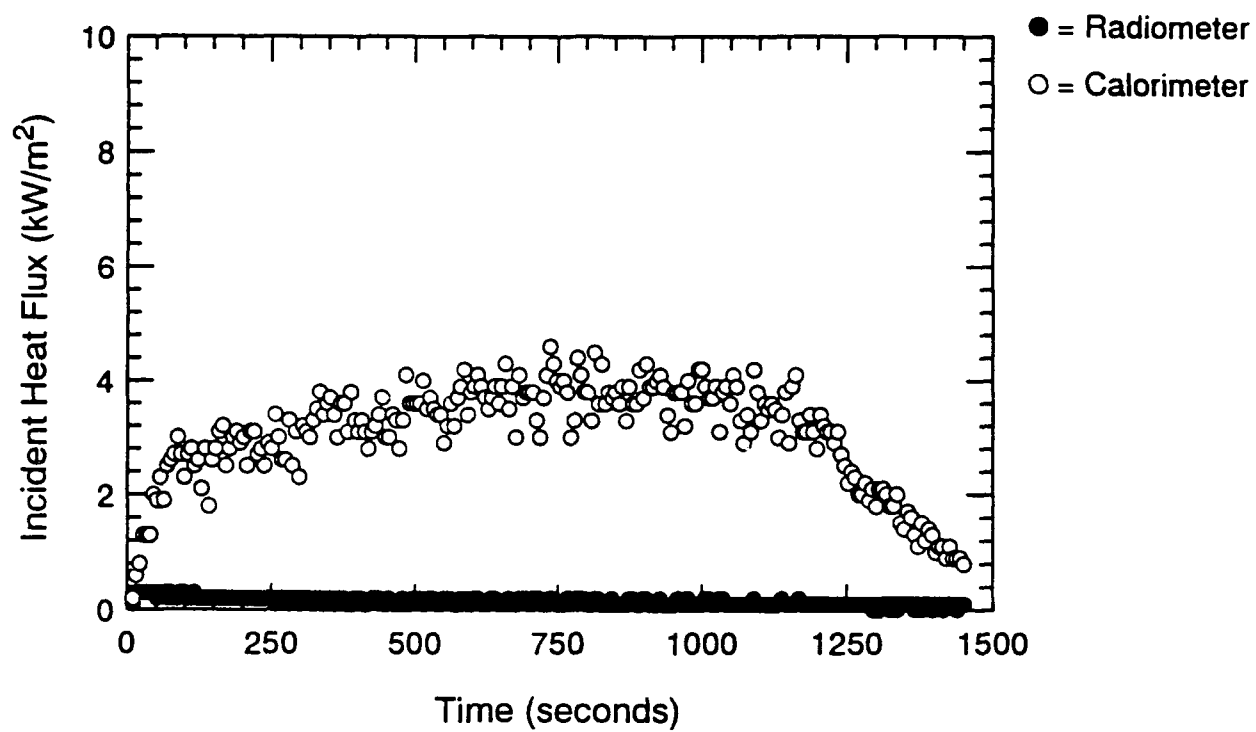


Figure B.80 Incident Heat Flux at Fwd. Bulkhead-Time Histories - S210

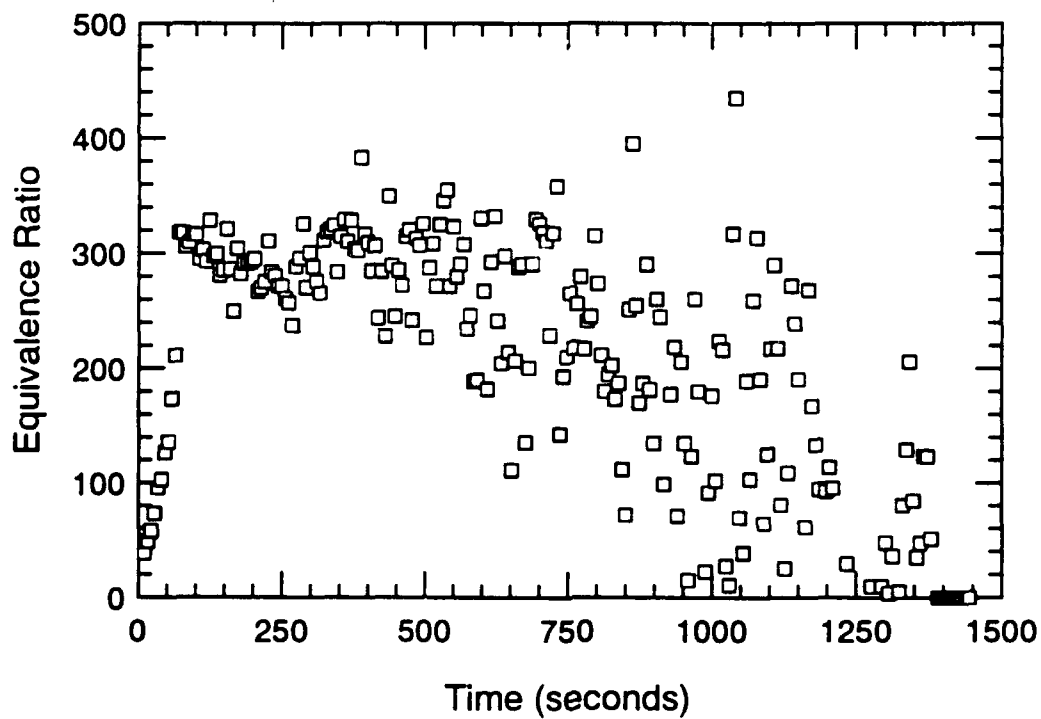
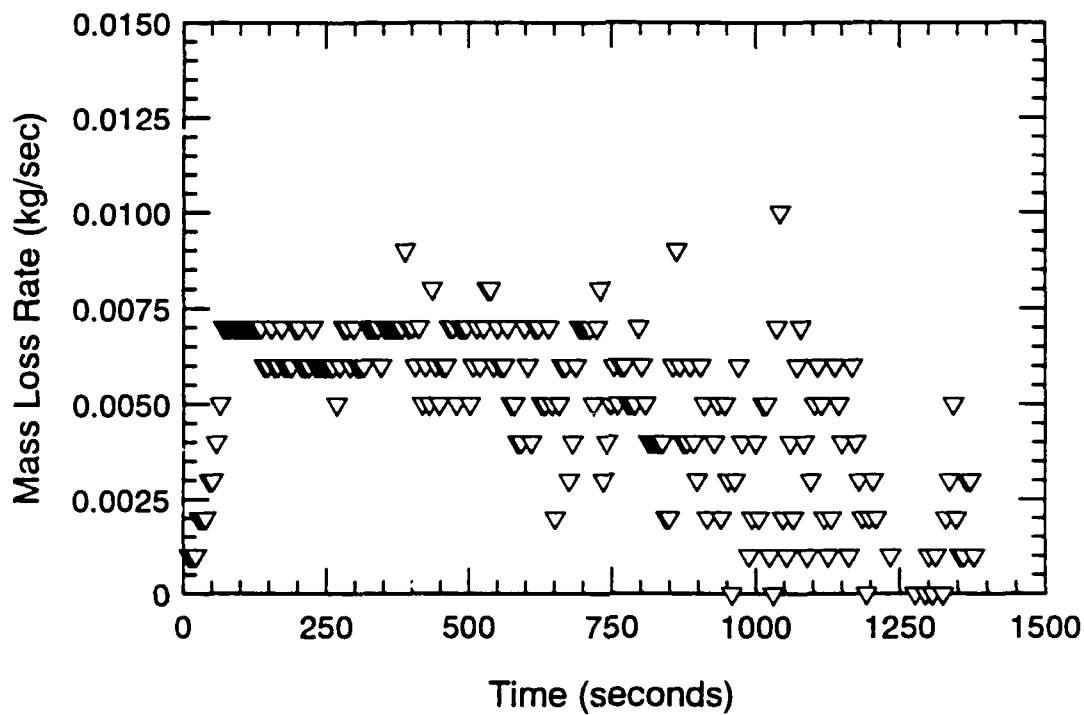


Figure B.81 Mass Loss Rate and Heat Release Rate-Time Histories - S211

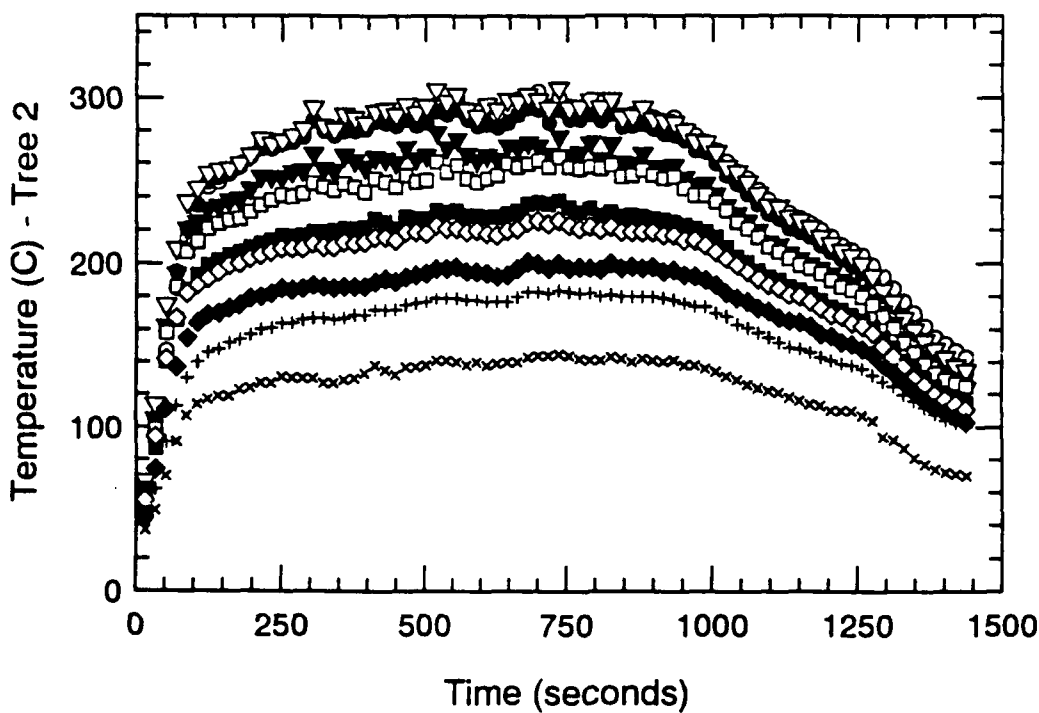
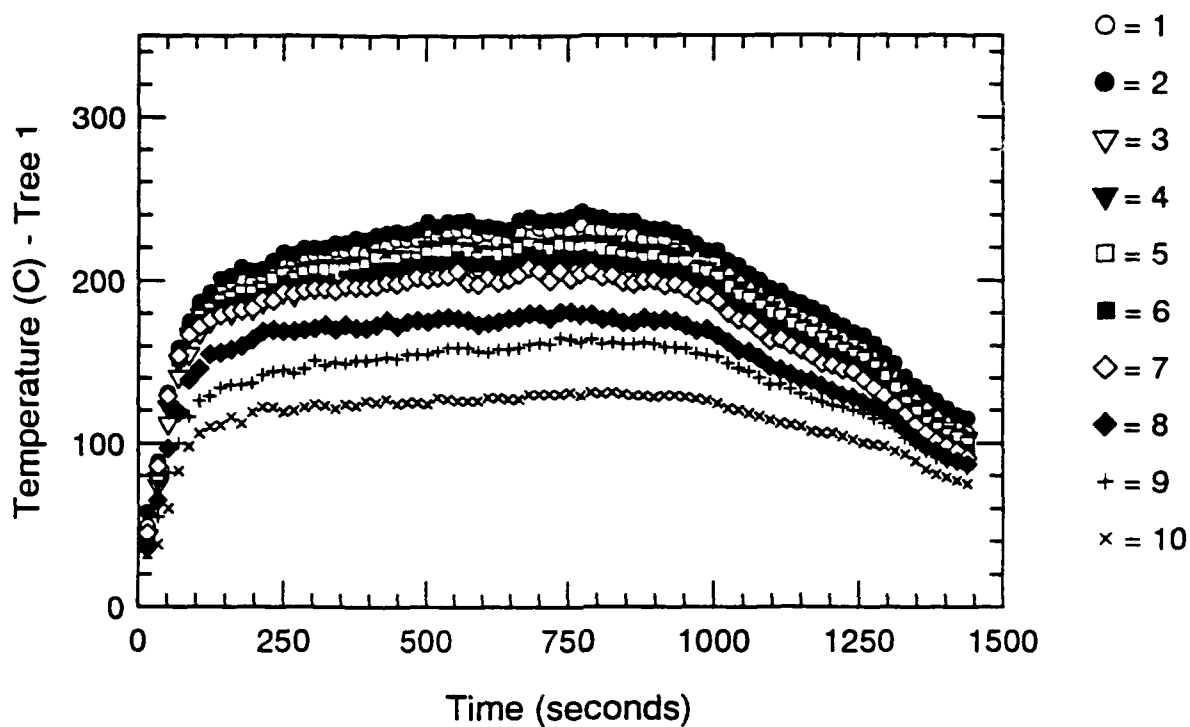


Figure B.82 Thermocouple Trees 1 & 2-Time Histories - S211

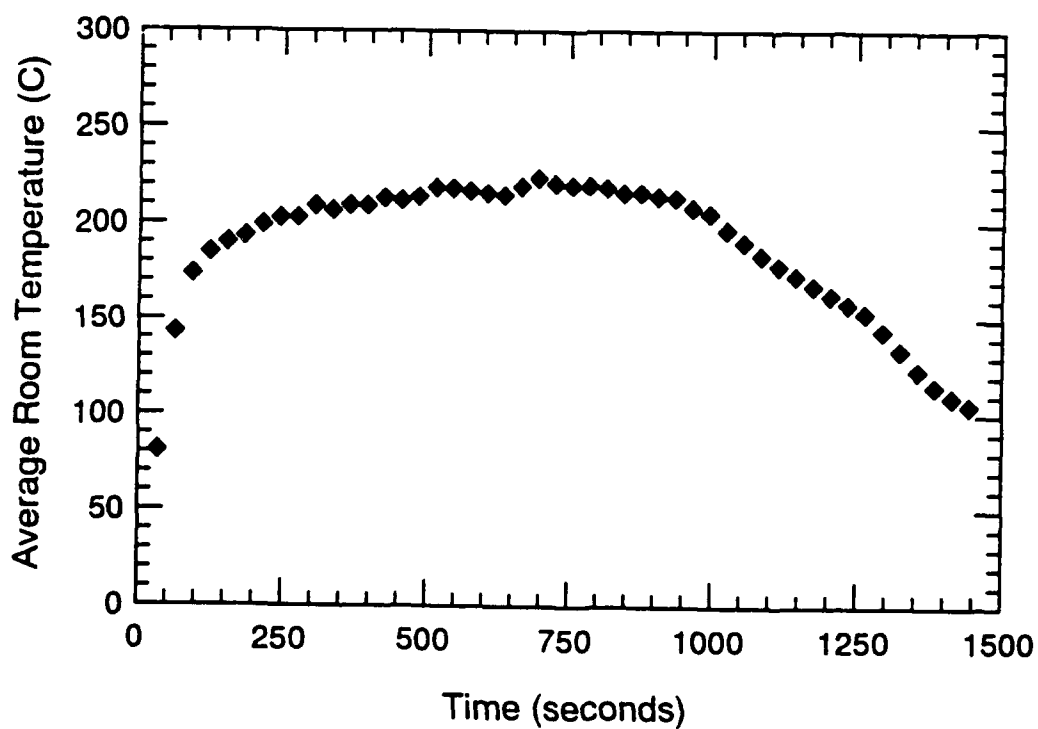
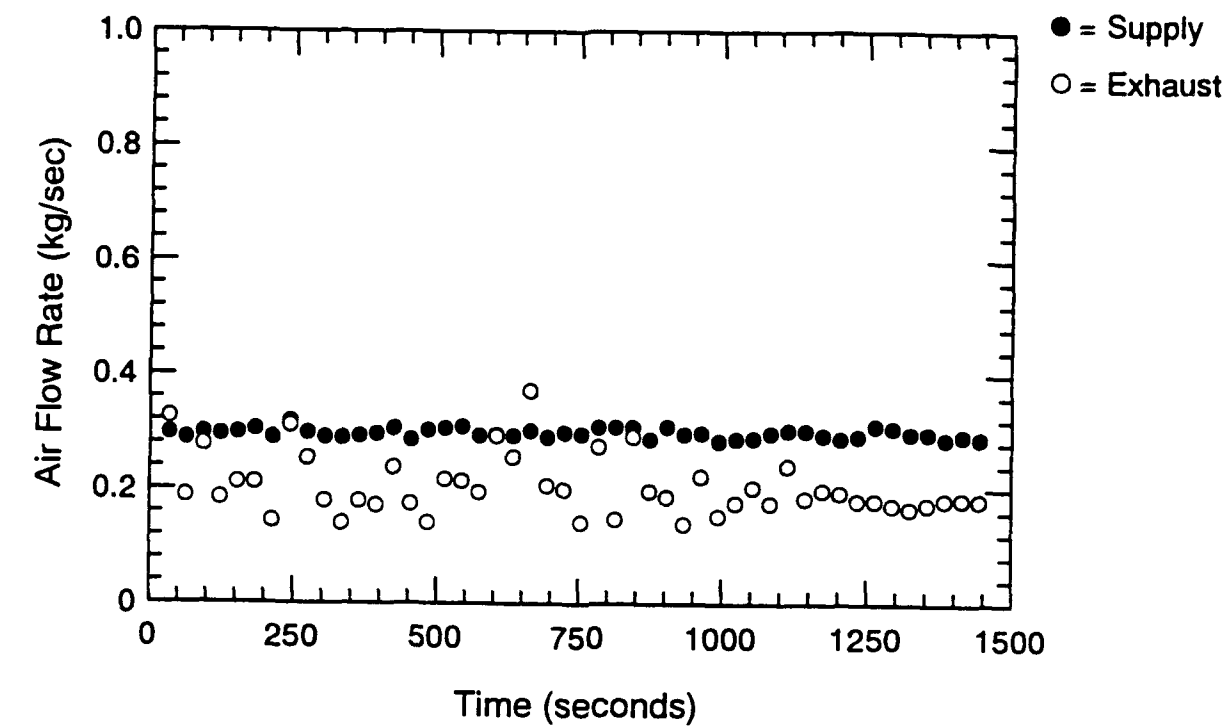


Figure B.83 Air Flow Rate and Avg. Temperature-Time Histories - S211

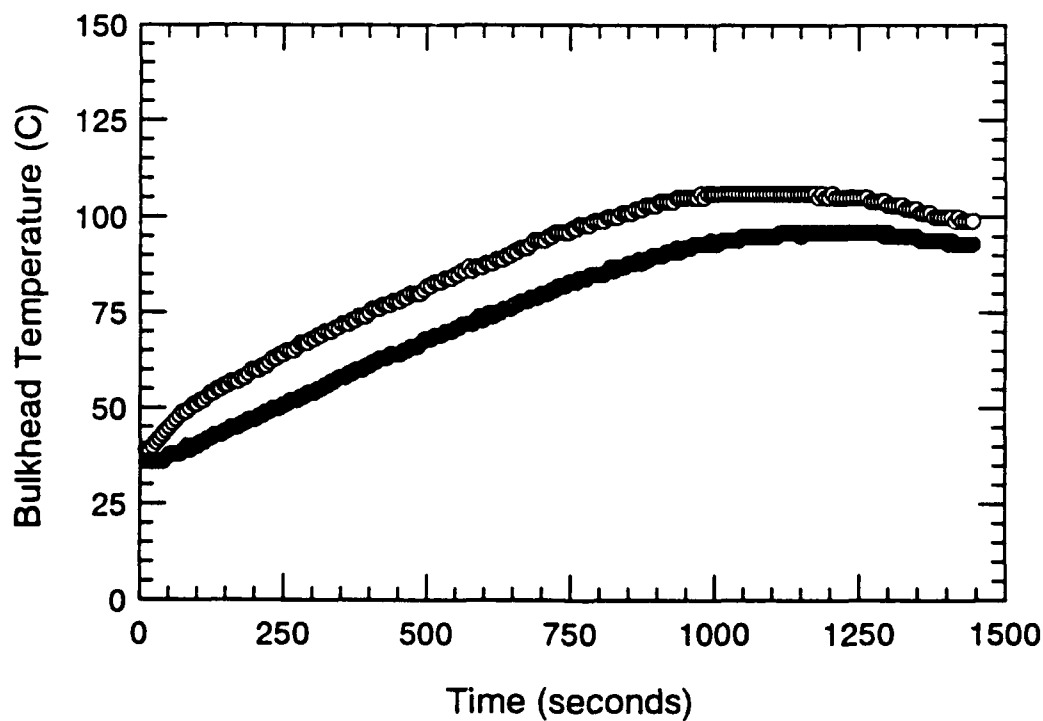
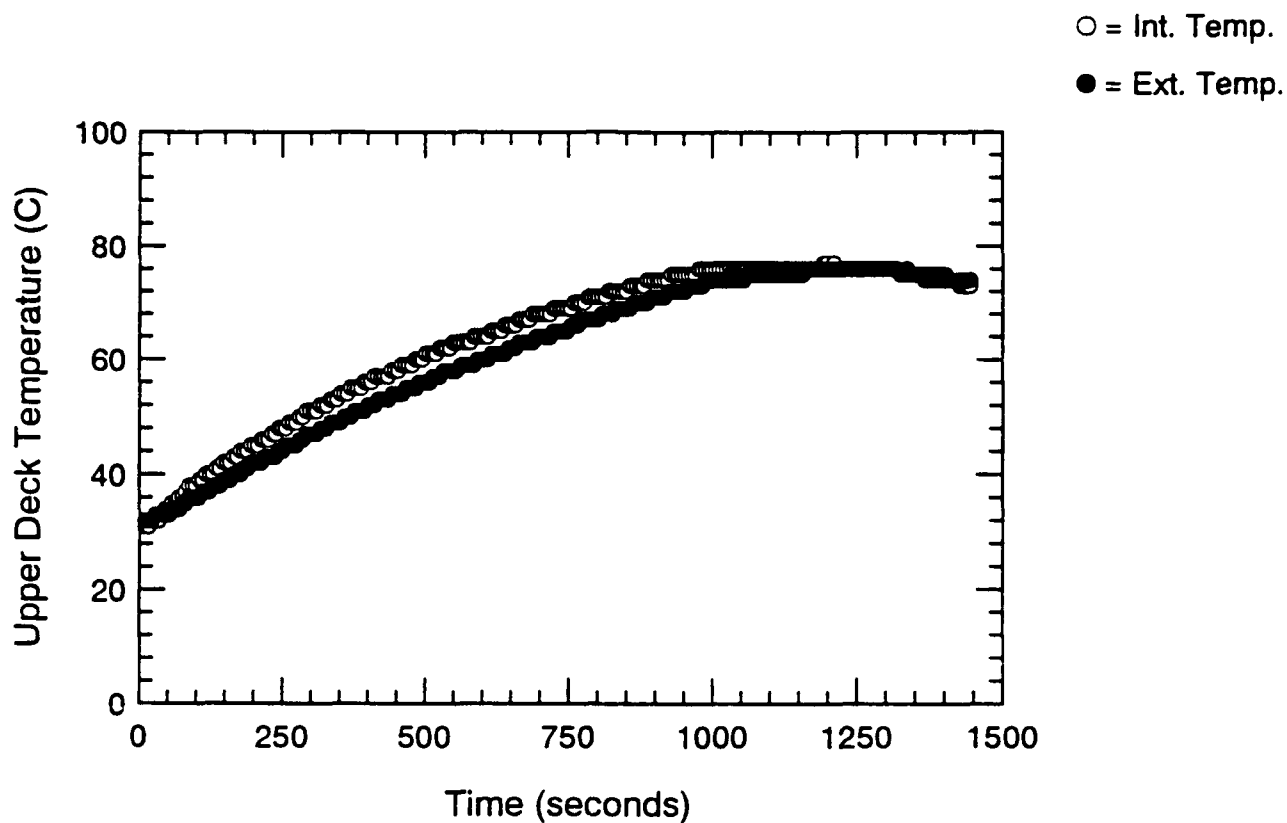


Figure B.84 Surface Thermocouple-Time Histories - S211

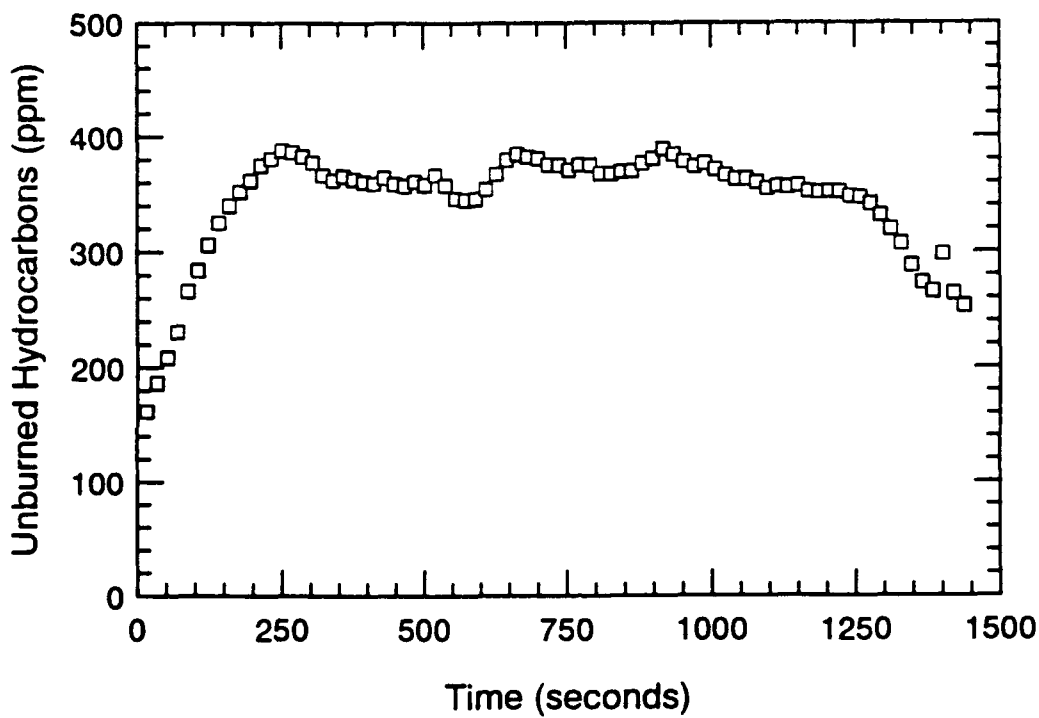
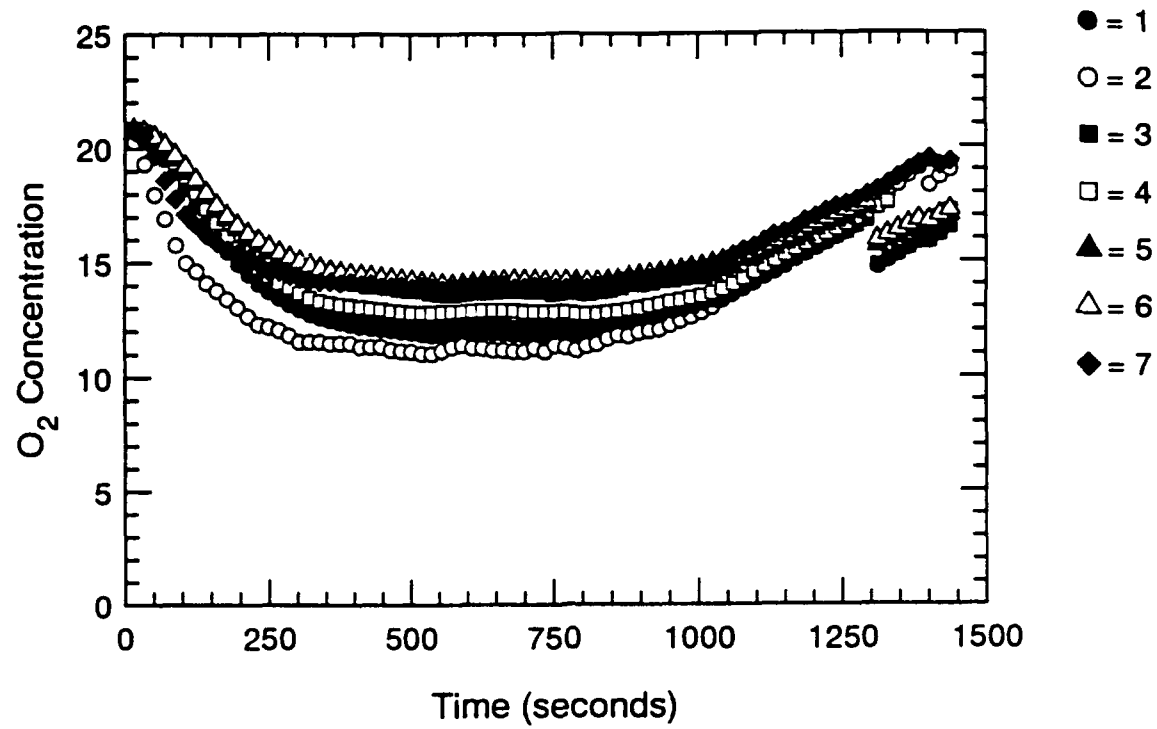


Figure B.85 Oxygen and Unburned HC Concentration-Time Histories - S211

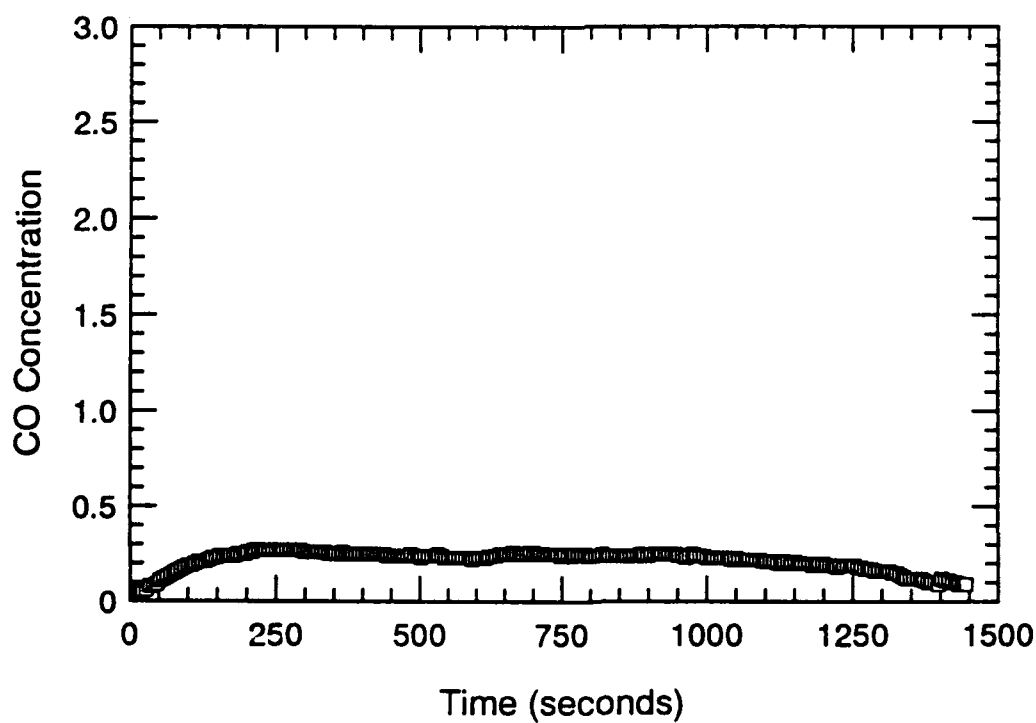
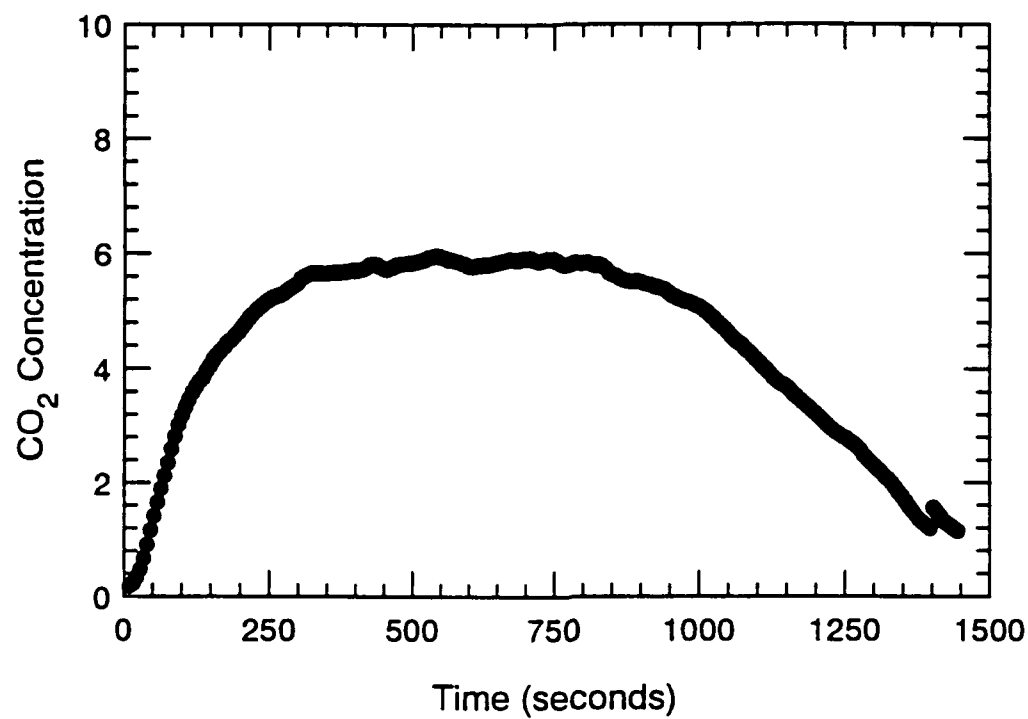


Figure B.86 CO₂ and CO Concentration-Time Histories - S211

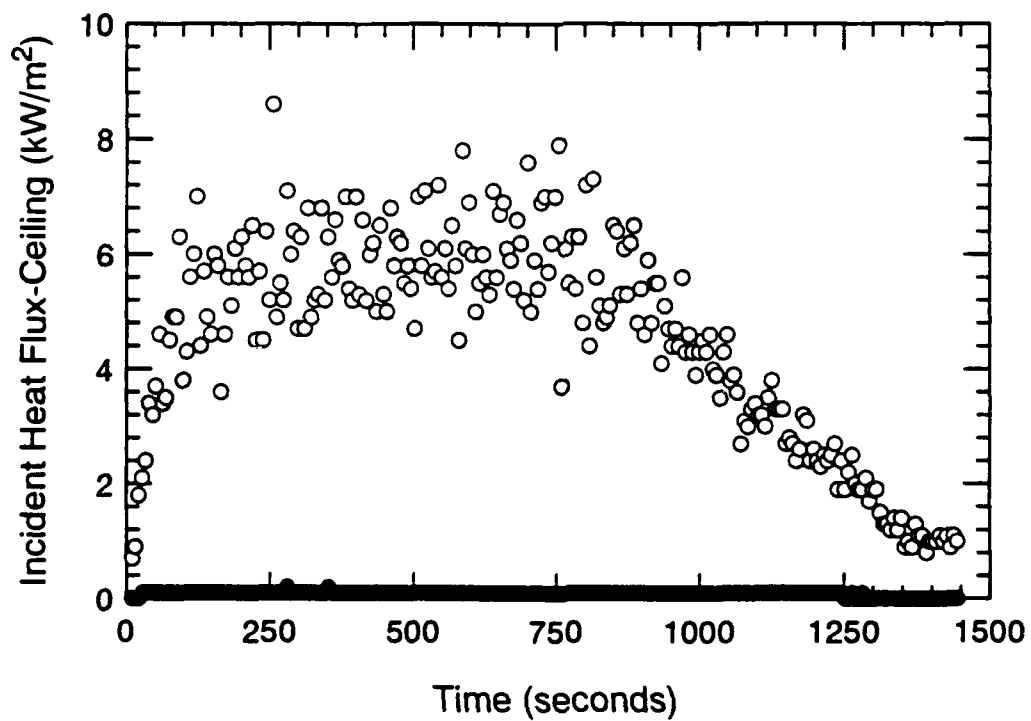
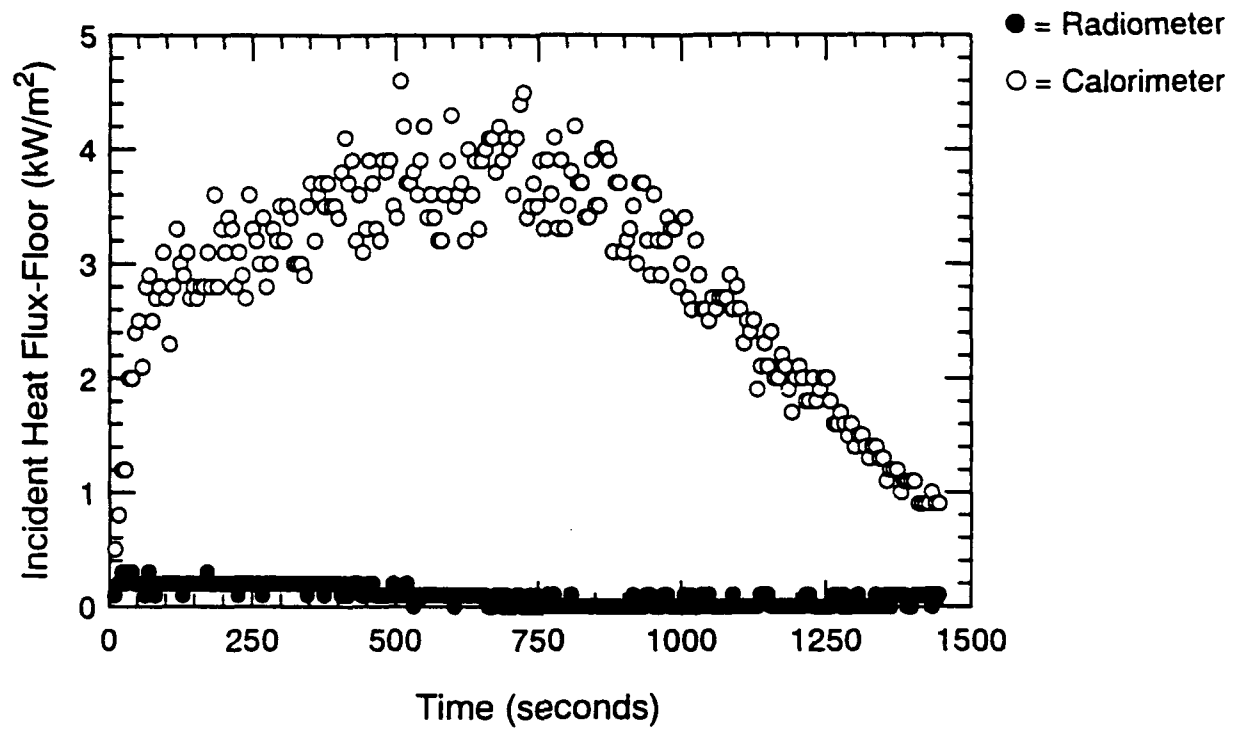


Figure B.87 Incident Heat Flux at Floor and Ceiling-Time Histories - S211

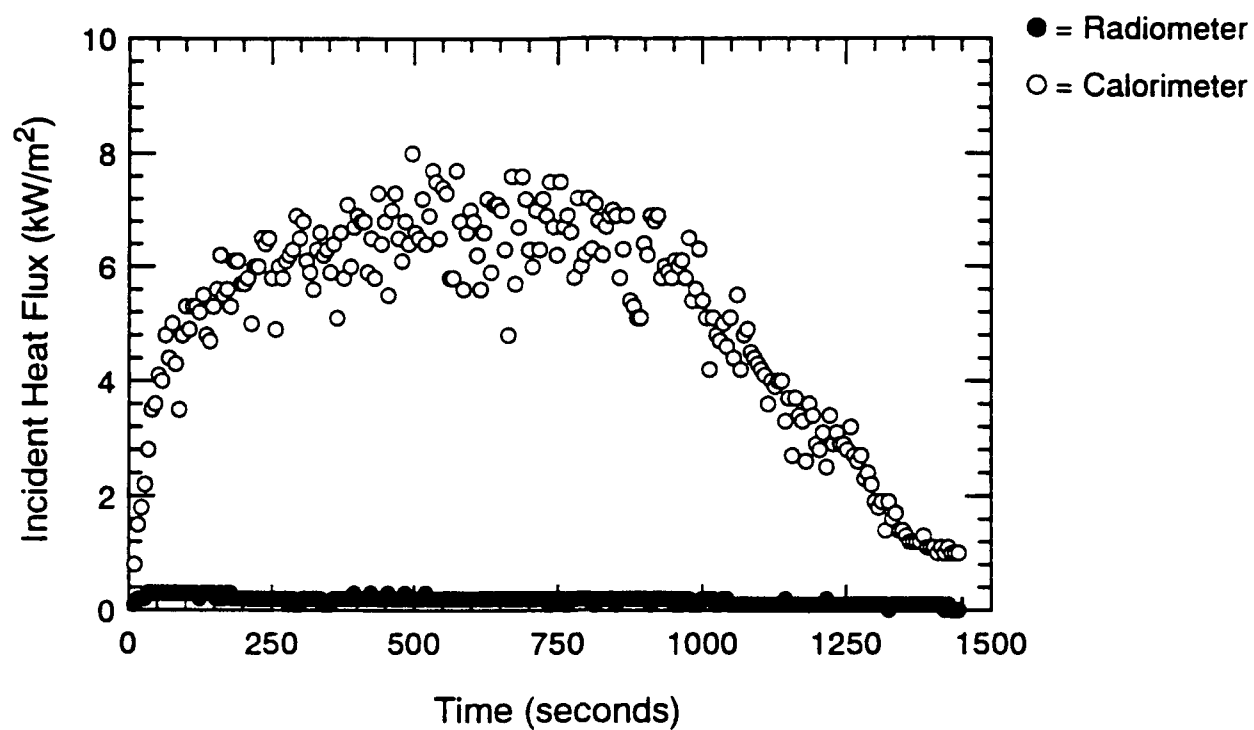


Figure B.88 Incident Heat Flux at Fwd. Bulkhead-Time Histories - S211

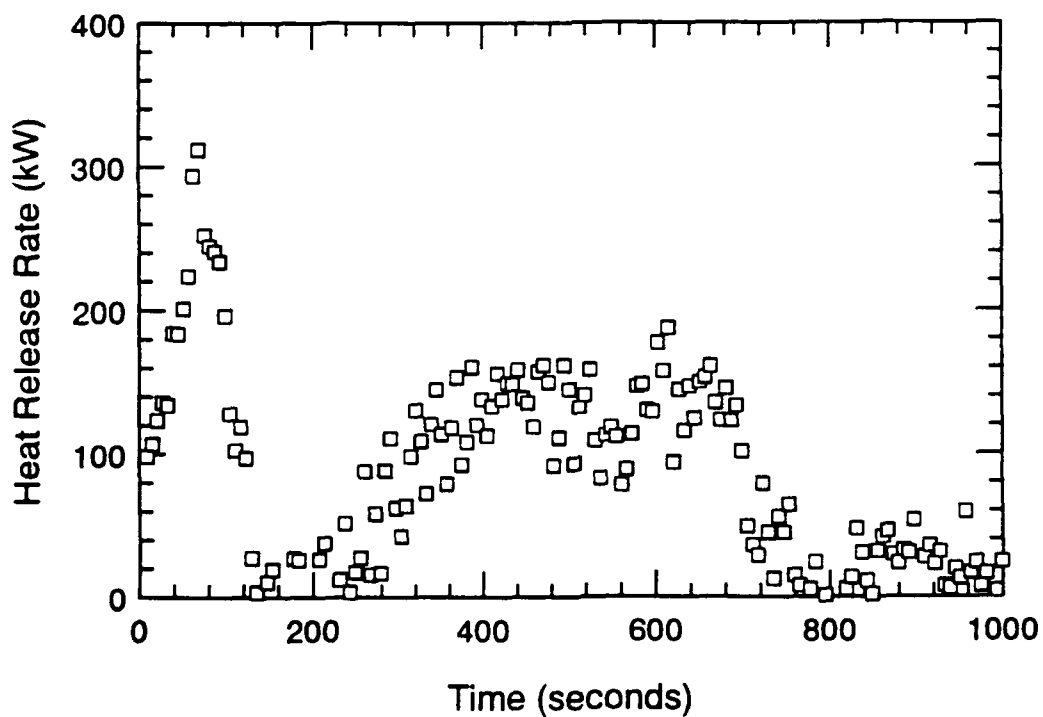
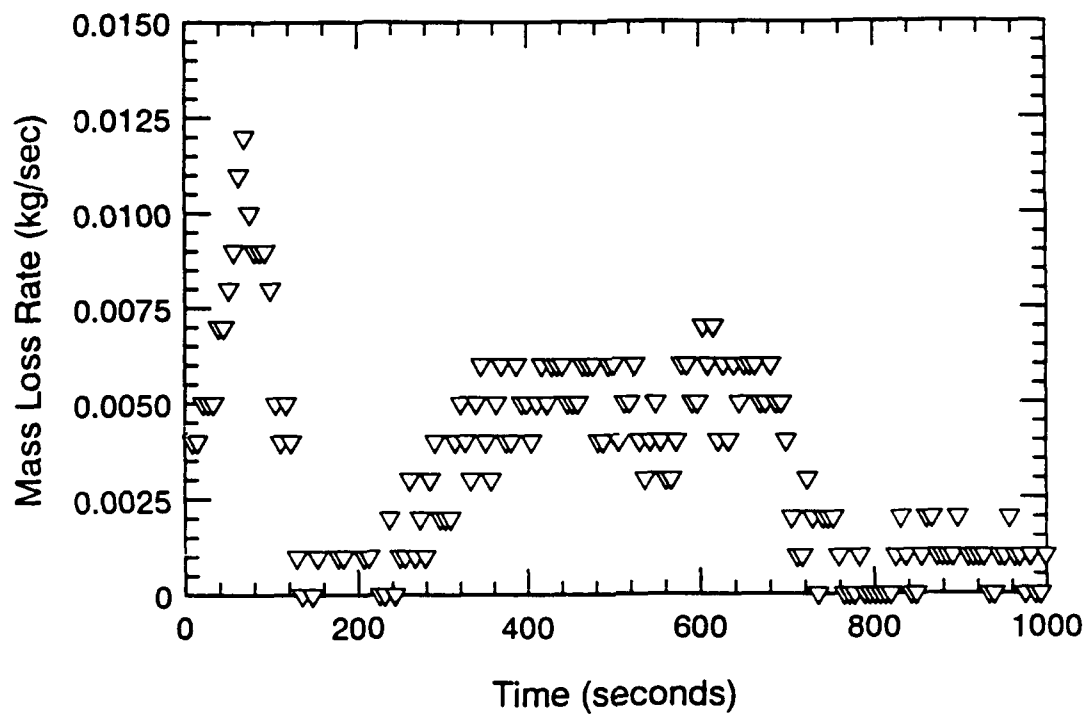


Figure B.89 Mass Loss Rate and Heat Release Rate-Time Histories - S212

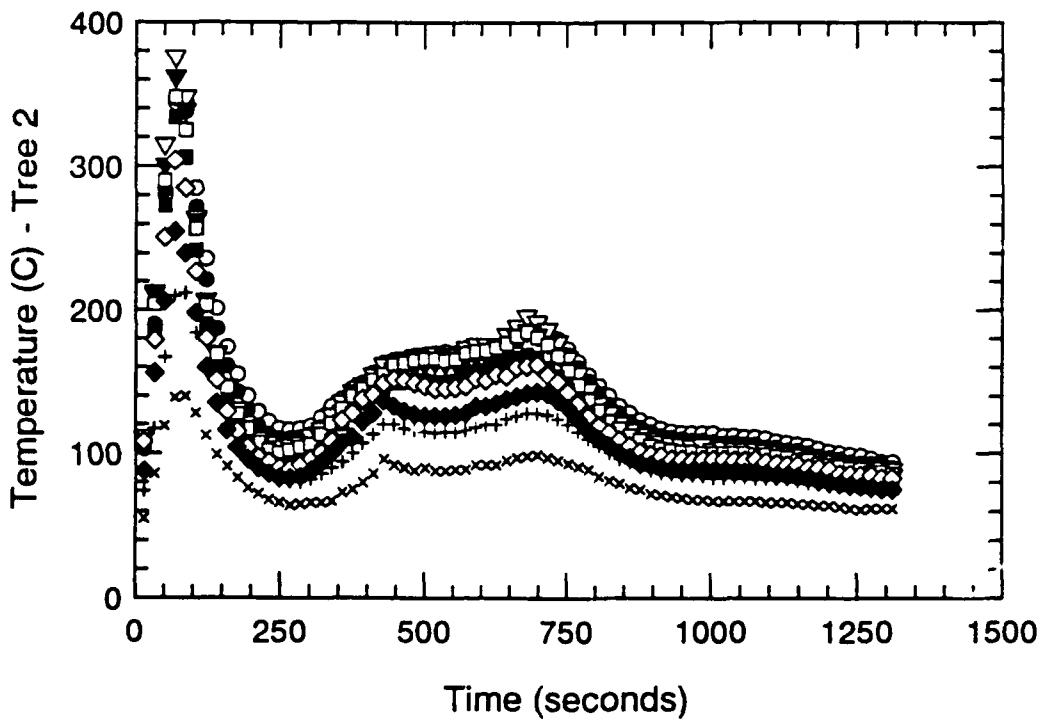
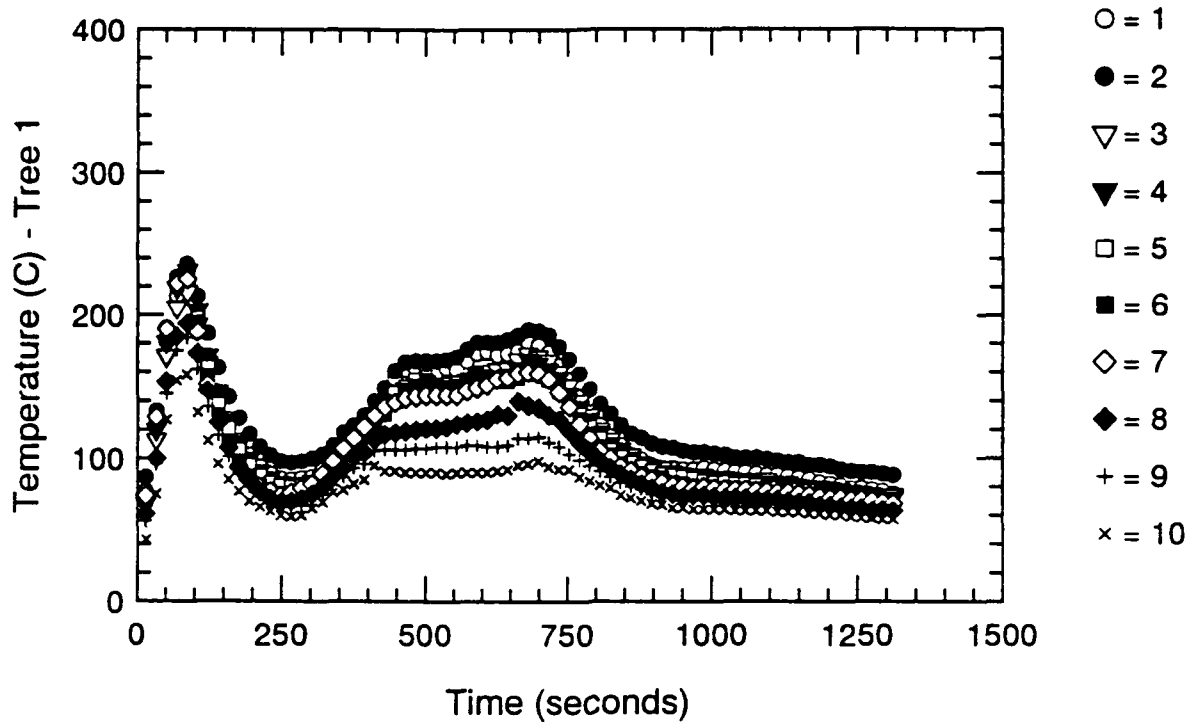


Figure B.90 Thermocouple Trees 1 & 2-Time Histories - S212

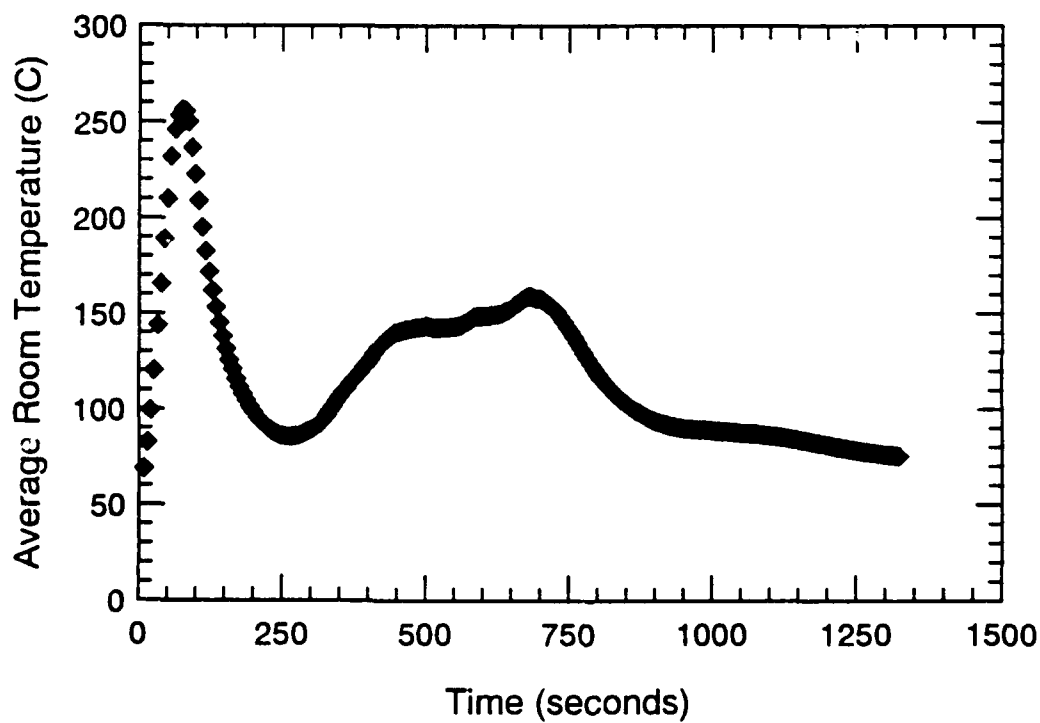
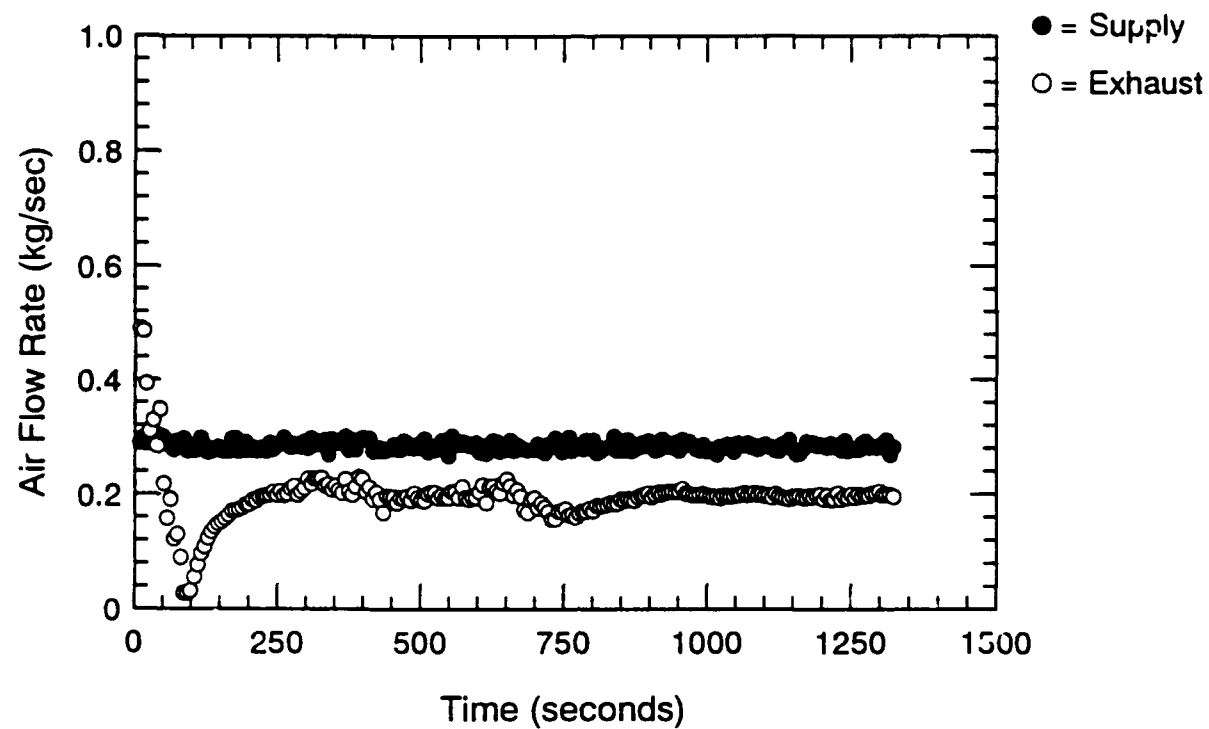


Figure B.91 Air Flow Rate and Avg. Temperature-Time Histories - S212

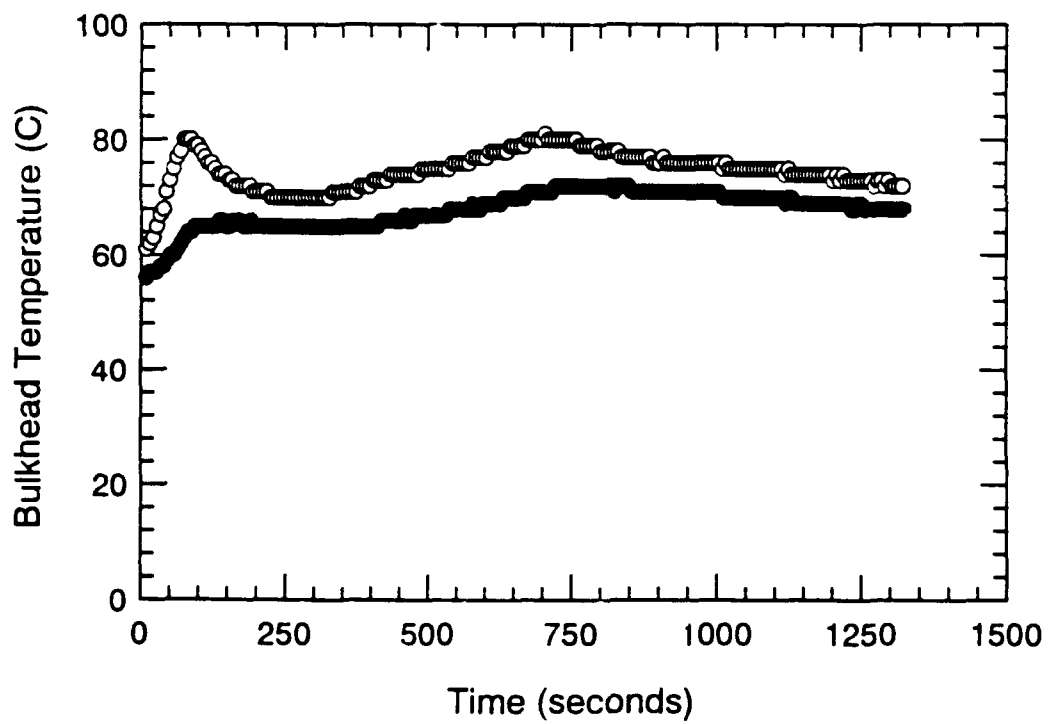
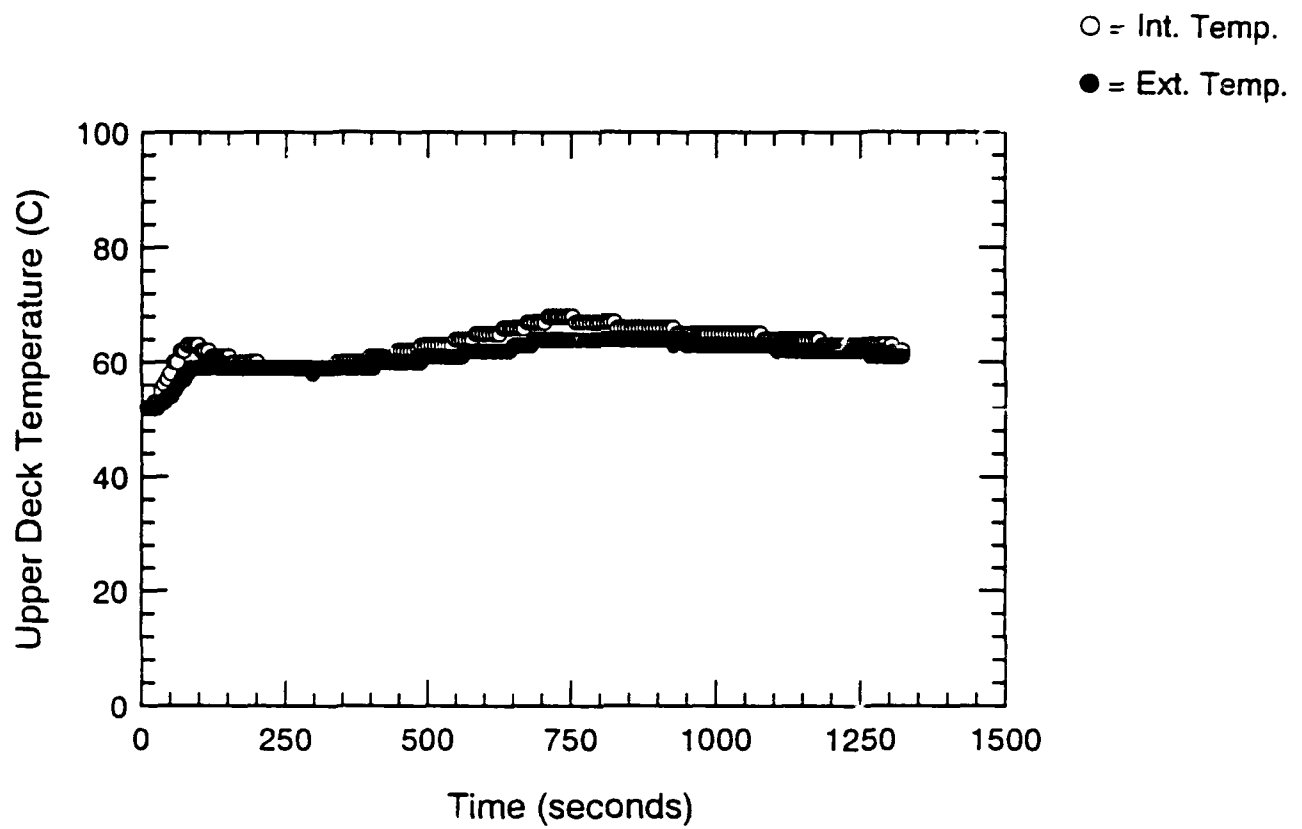


Figure B.92 Surface Thermocouple-Time Histories - S212

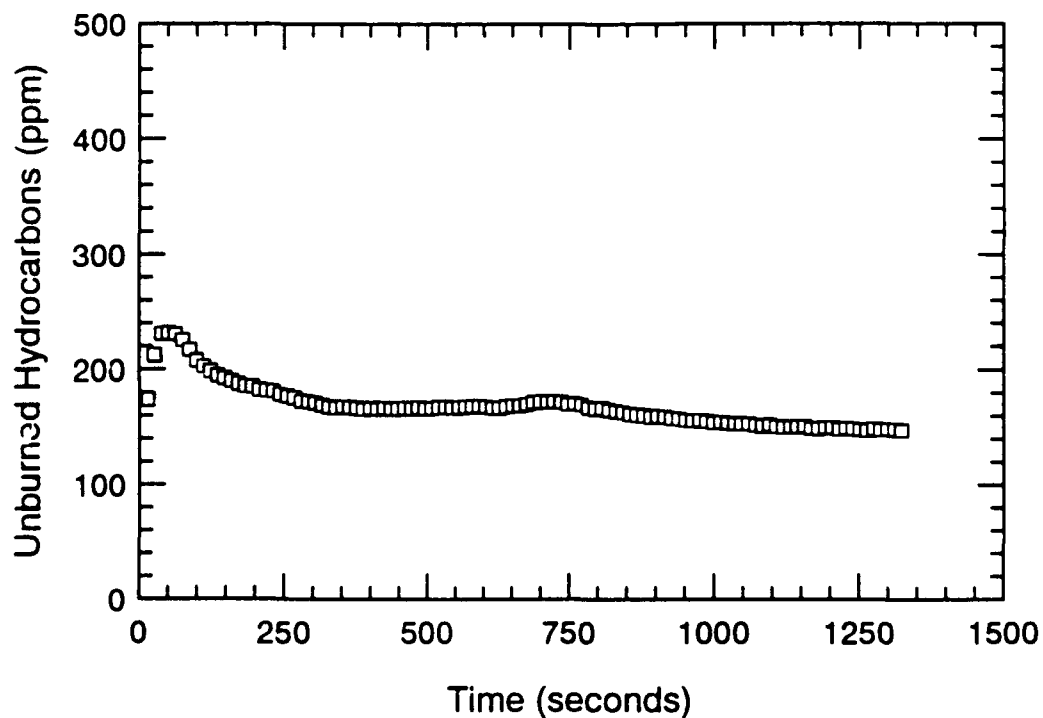
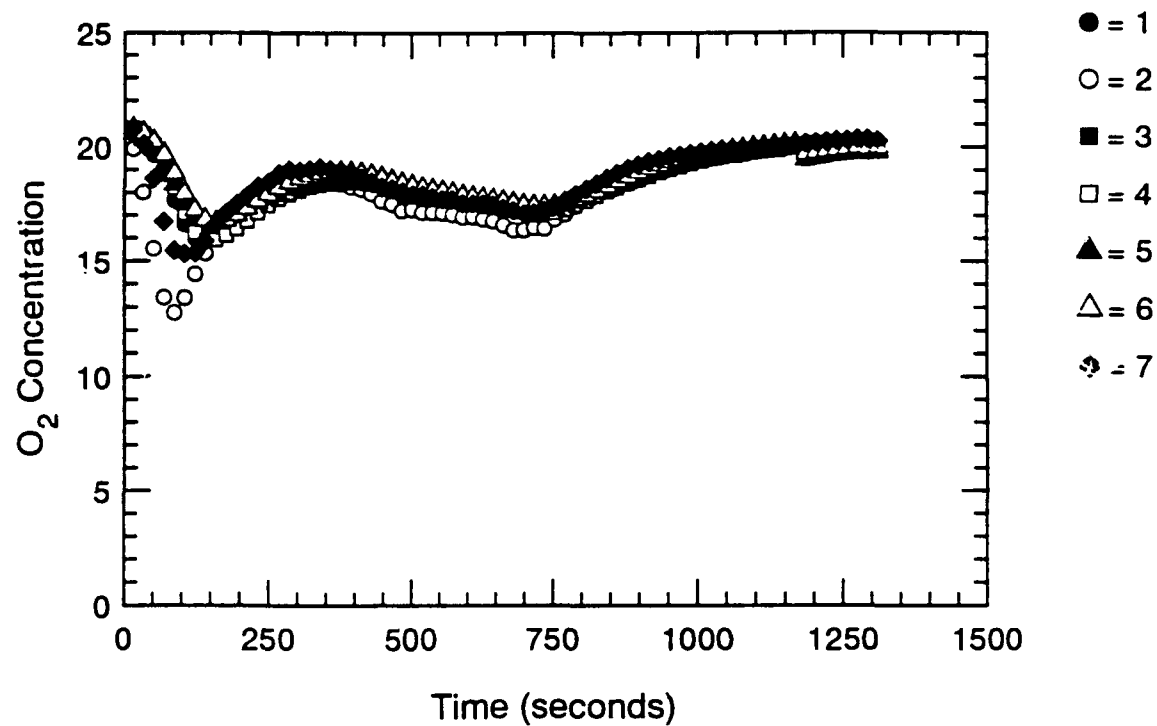


Figure B.93 Oxygen and Unburned HC Concentration-Time Histories - S212

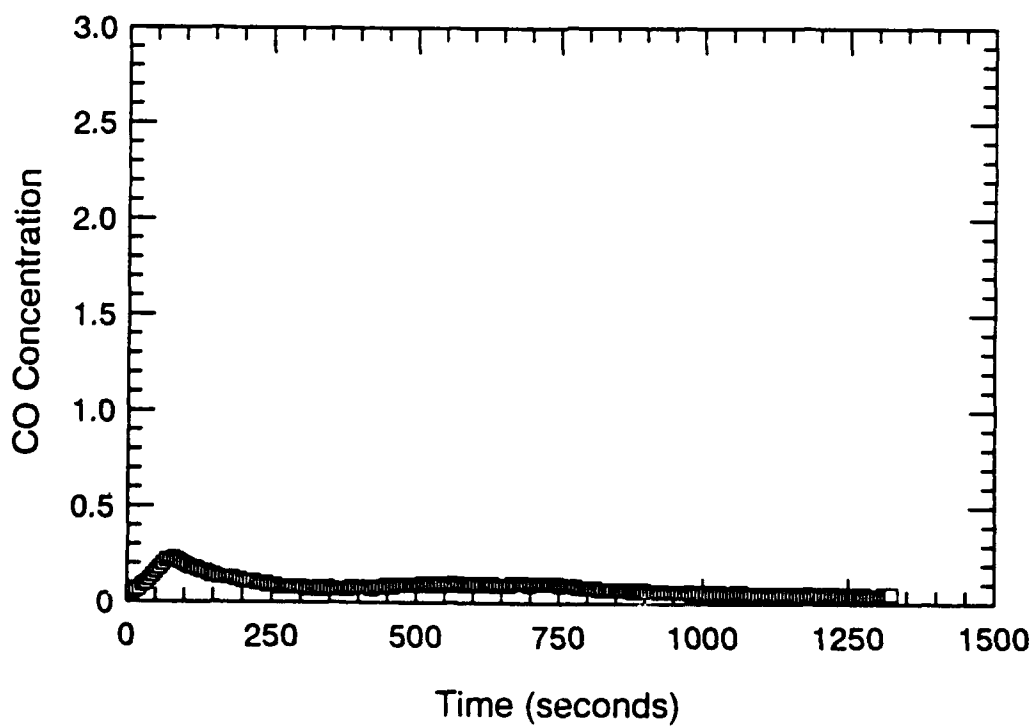
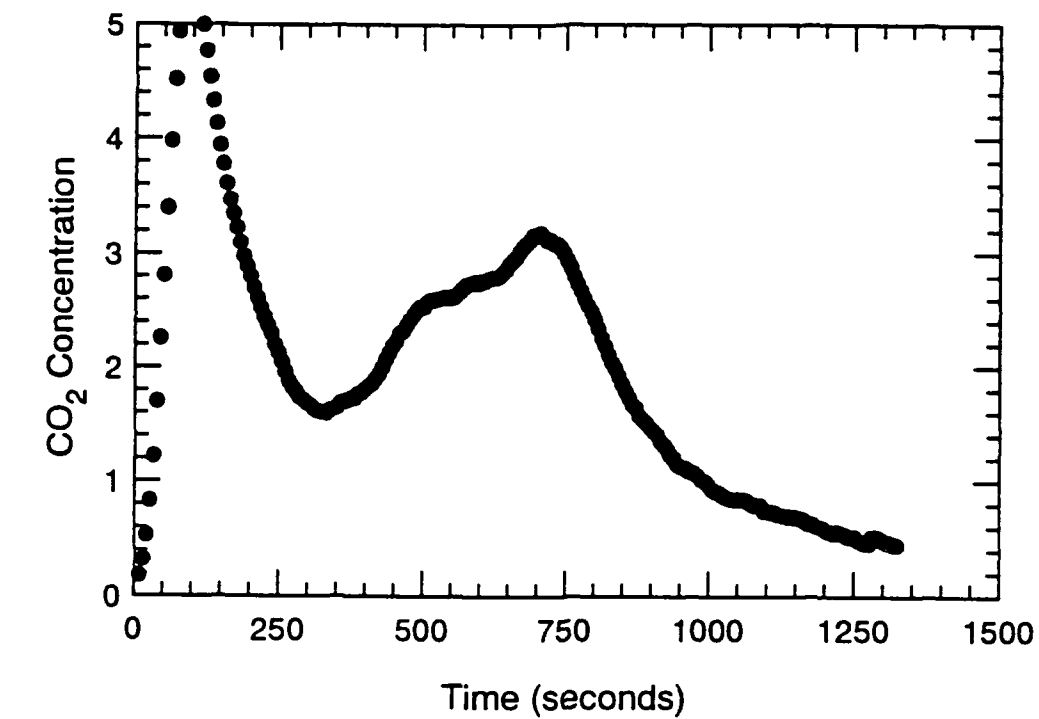


Figure B.94 CO₂ and CO Concentration-Time Histories - S212

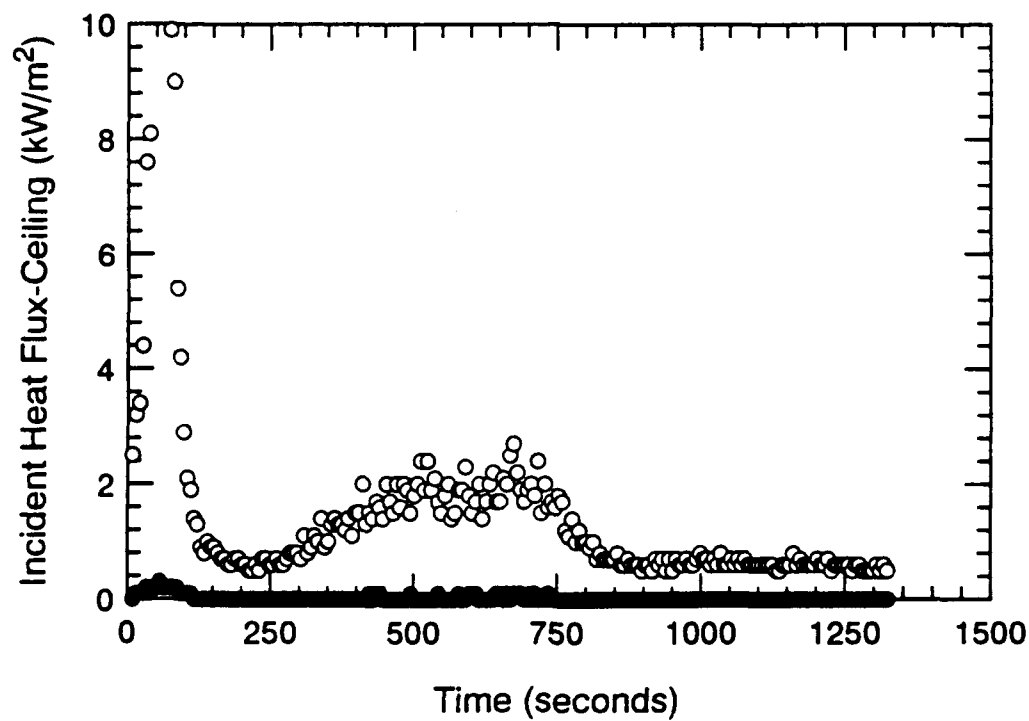
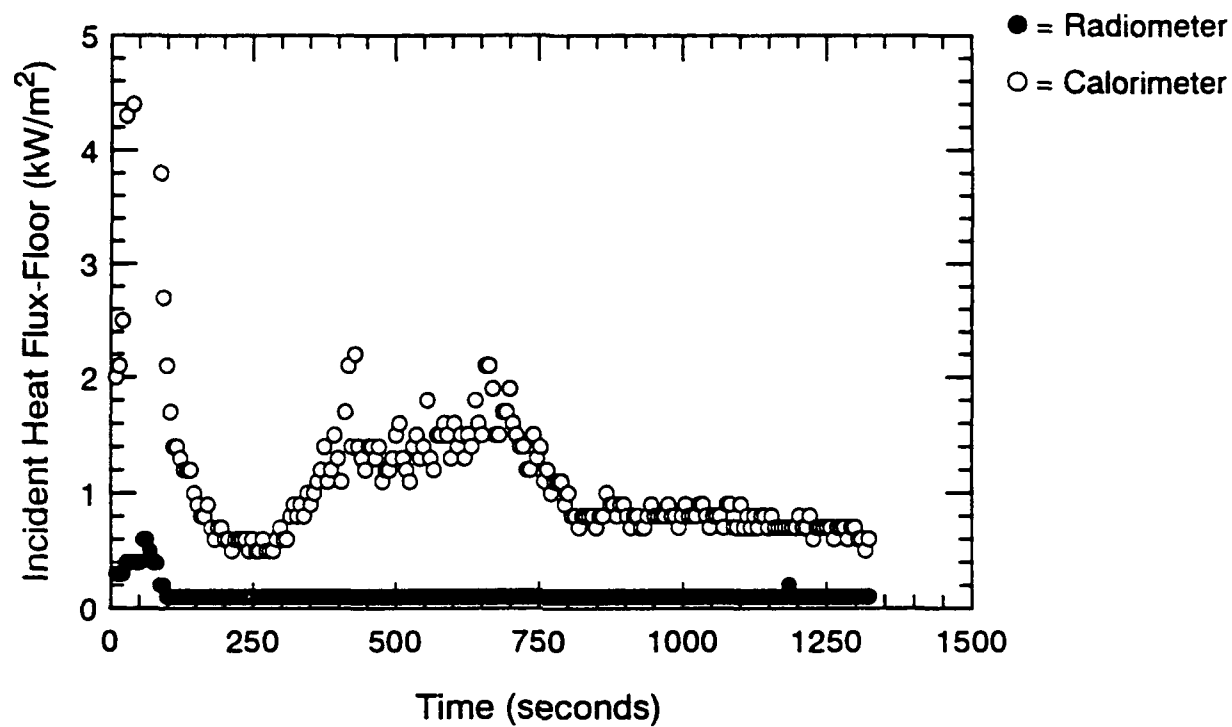


Figure B.95 Incident Heat Flux at Floor and Ceiling-Time Histories - S212

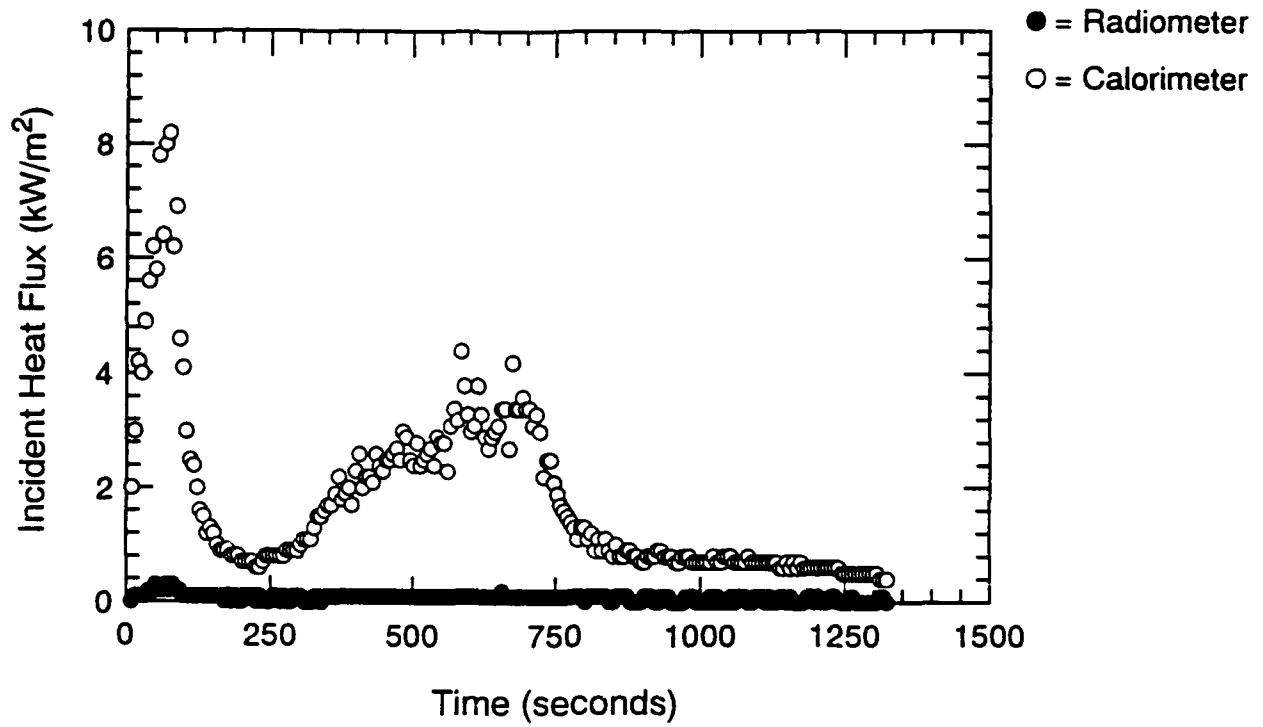


Figure B.96 Incident Heat Flux at Fwd. Bulkhead-Time Histories - S212

APPENDIX C. Series 1- Peatross/Beyler Temperature Prediction Method Results

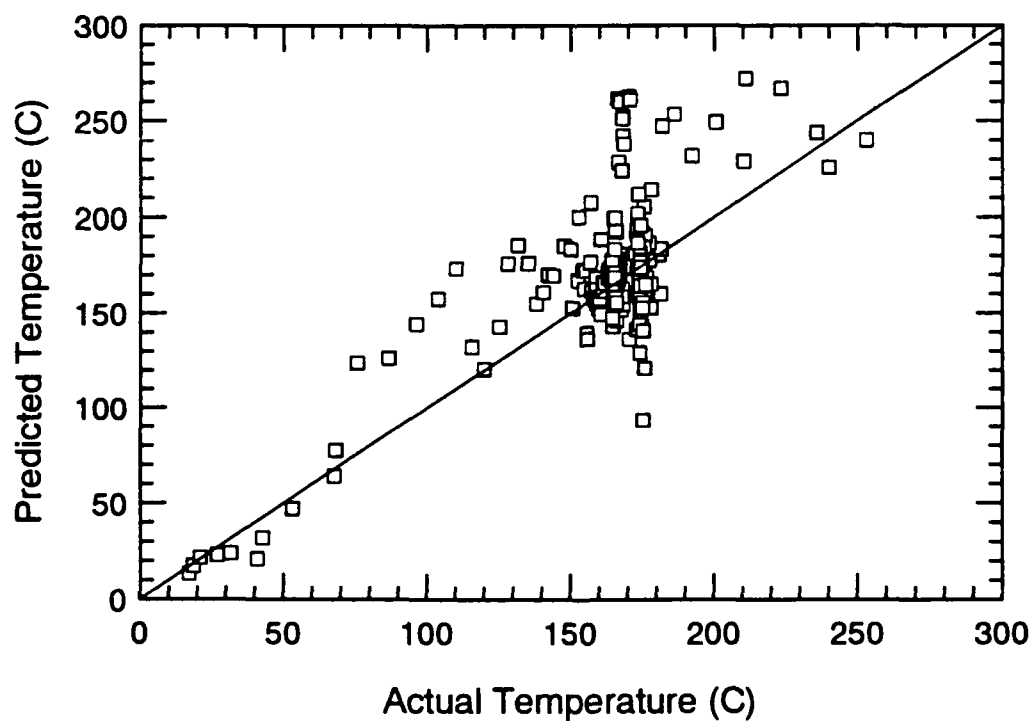
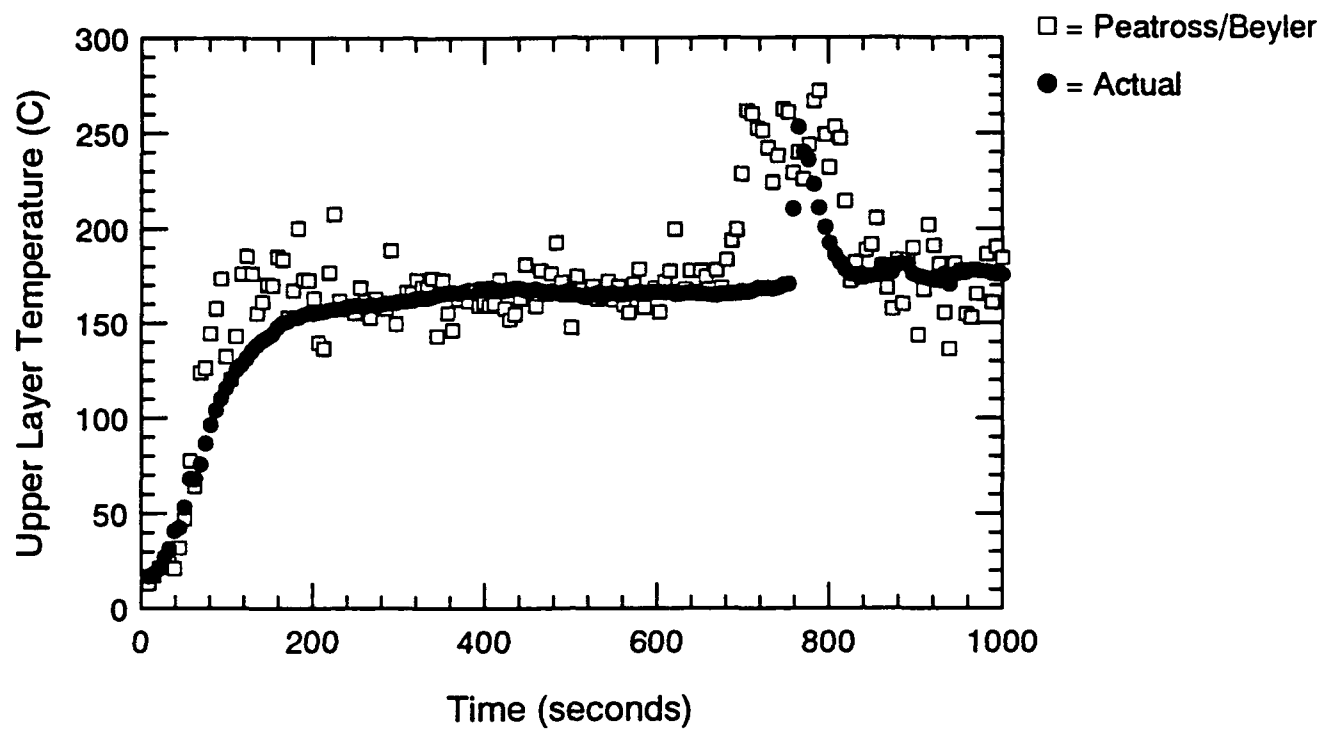


Figure C.1 Temperature Predictions Using Peatross/Beyler Method - S101

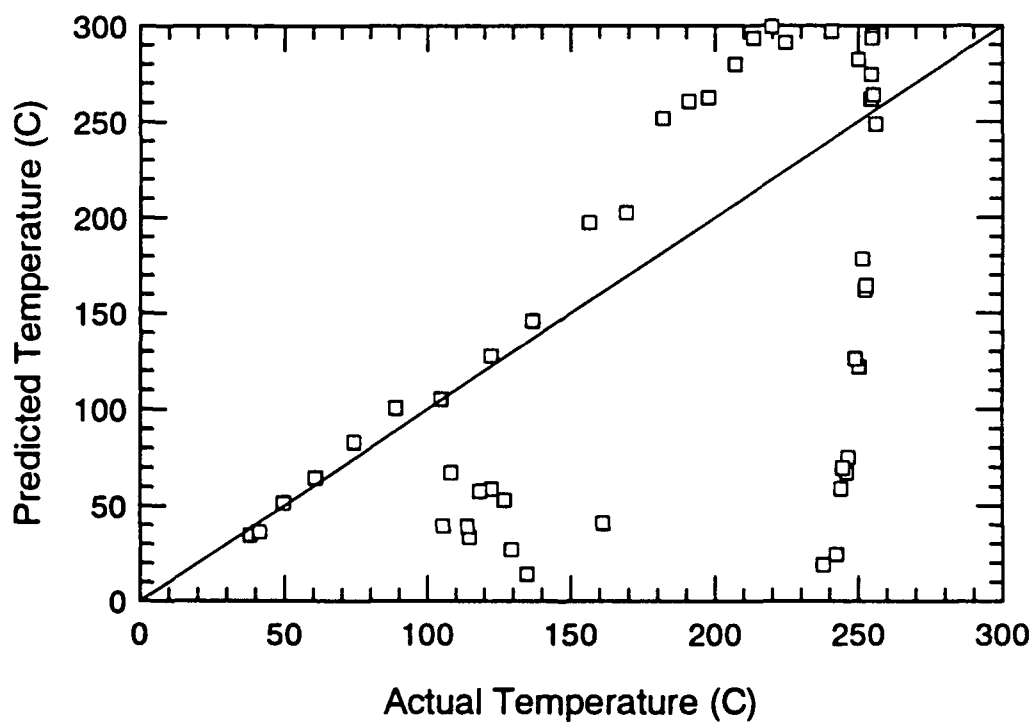
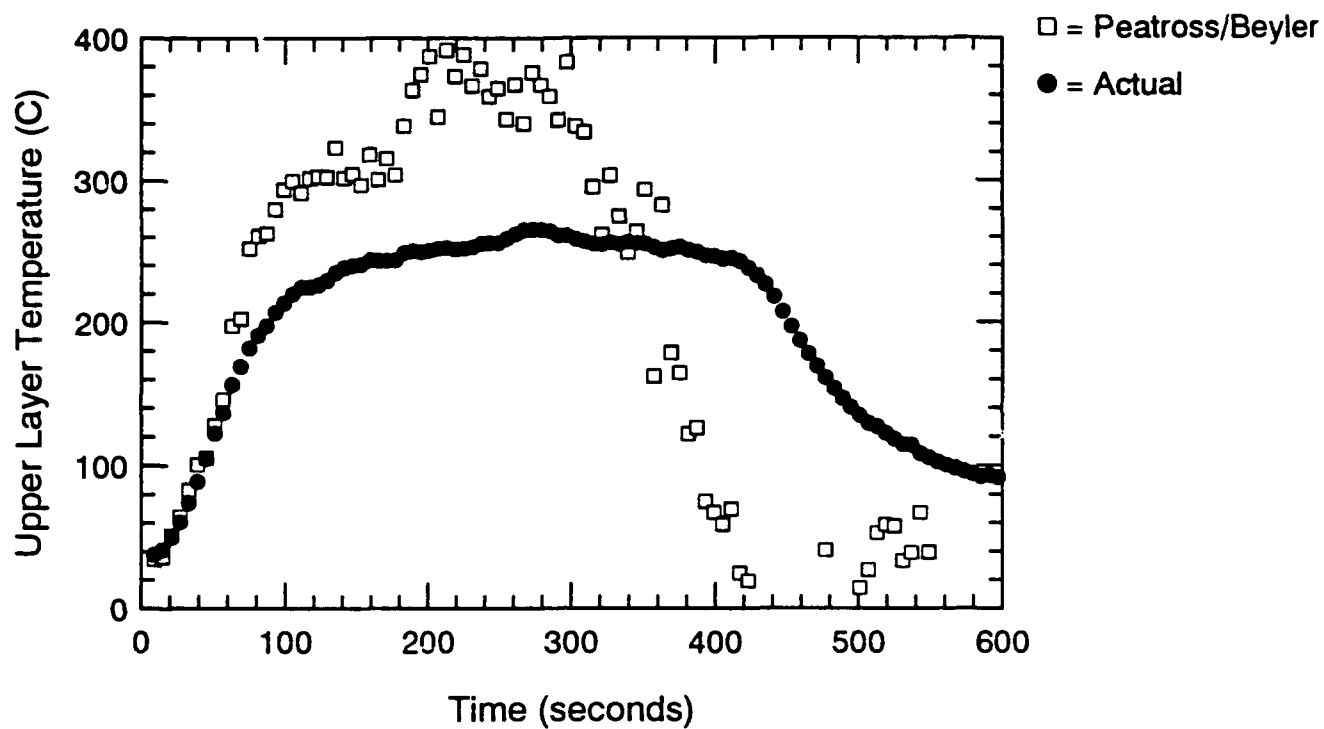


Figure C.2 Temperature Predictions Using Peatross/Beyler Method - S102

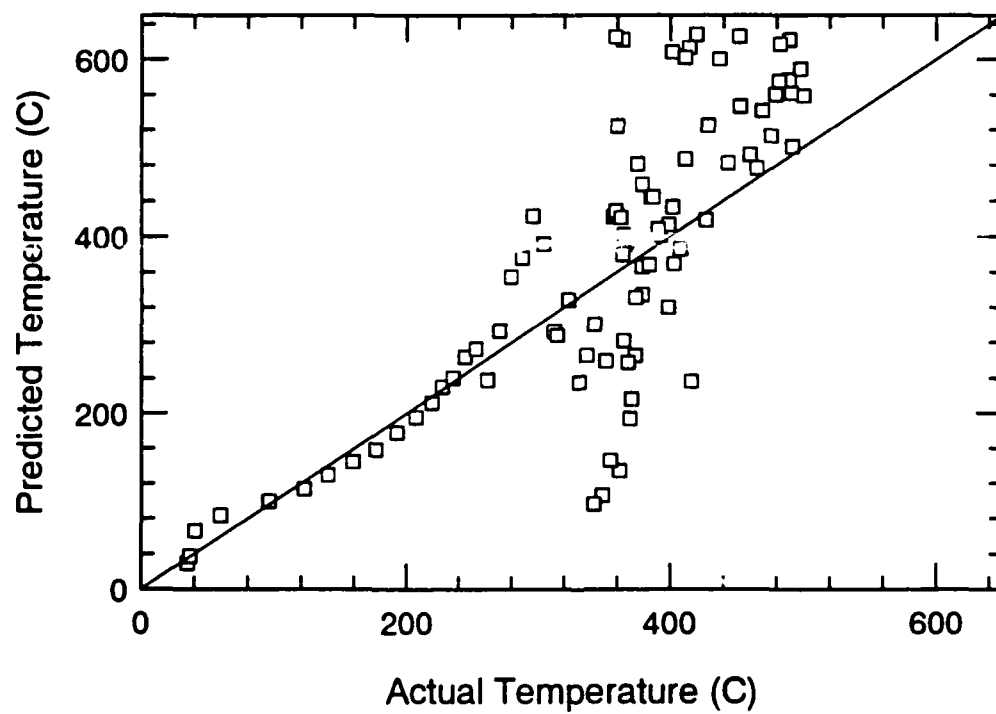
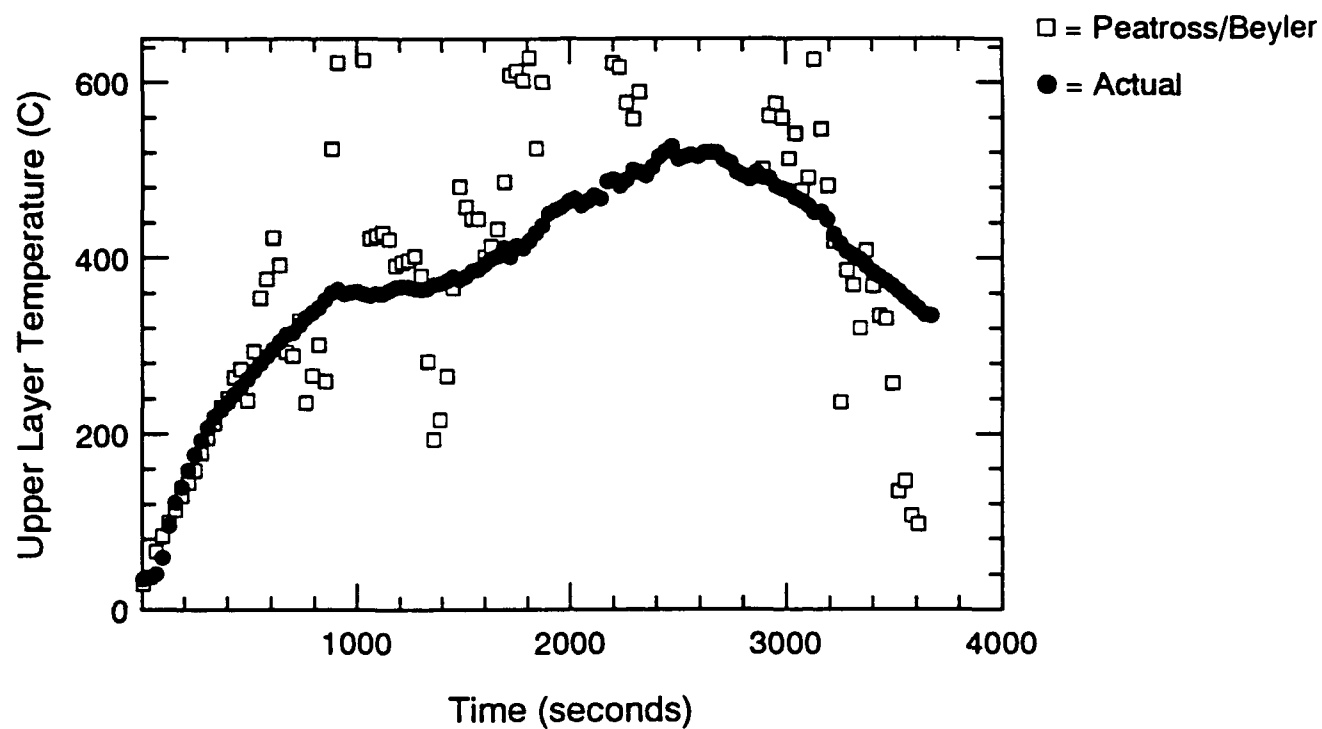


Figure C.3 Temperature Predictions Using Peatross/Beyler Method - S103

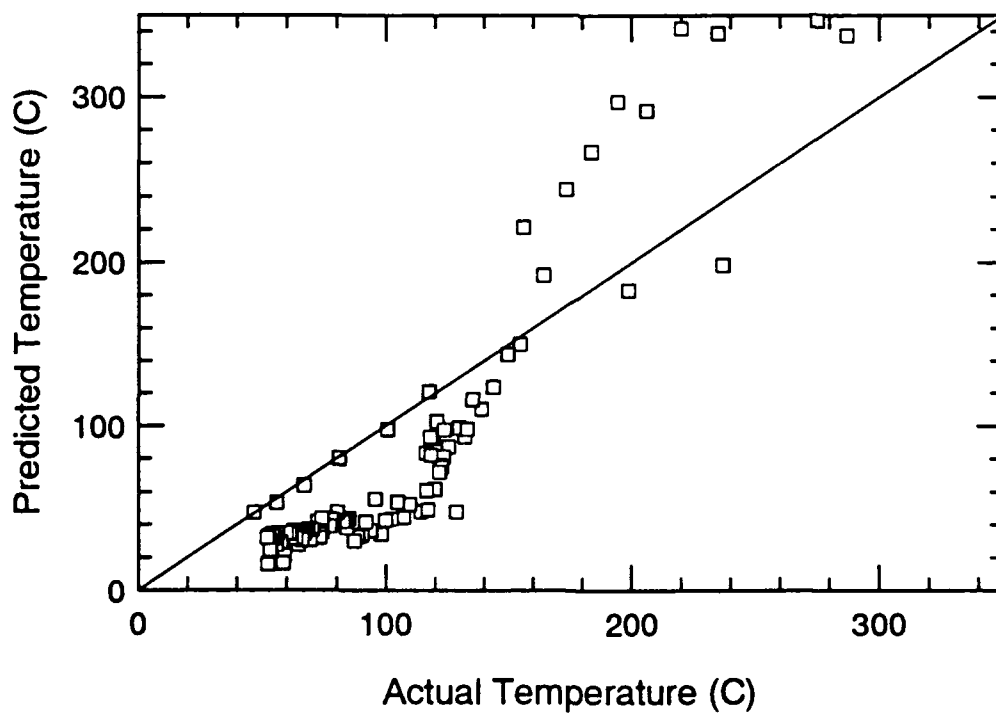
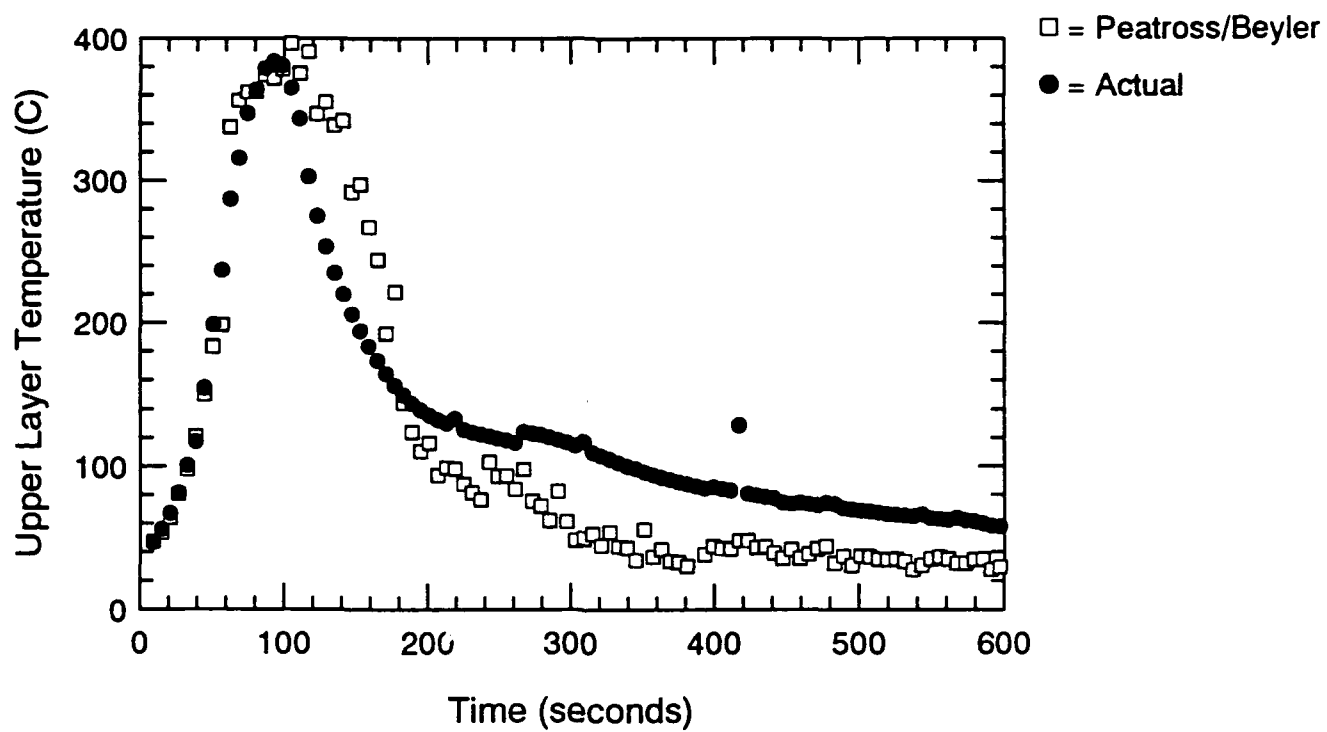


Figure C.4 Temperature Predictions Using Peatross/Beyler Method - S104

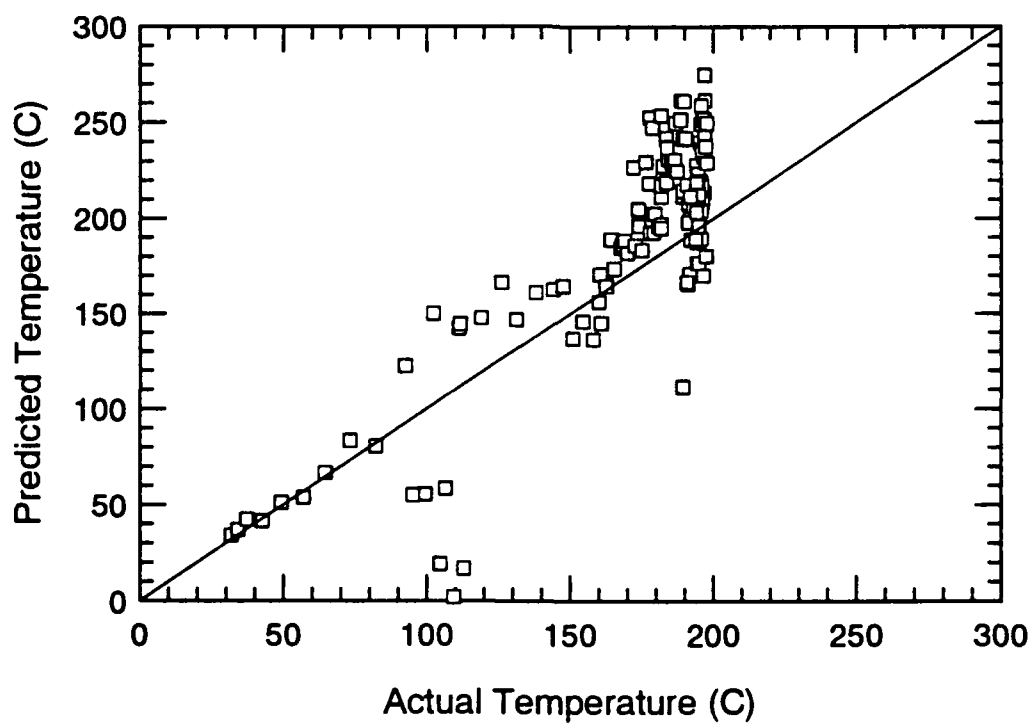
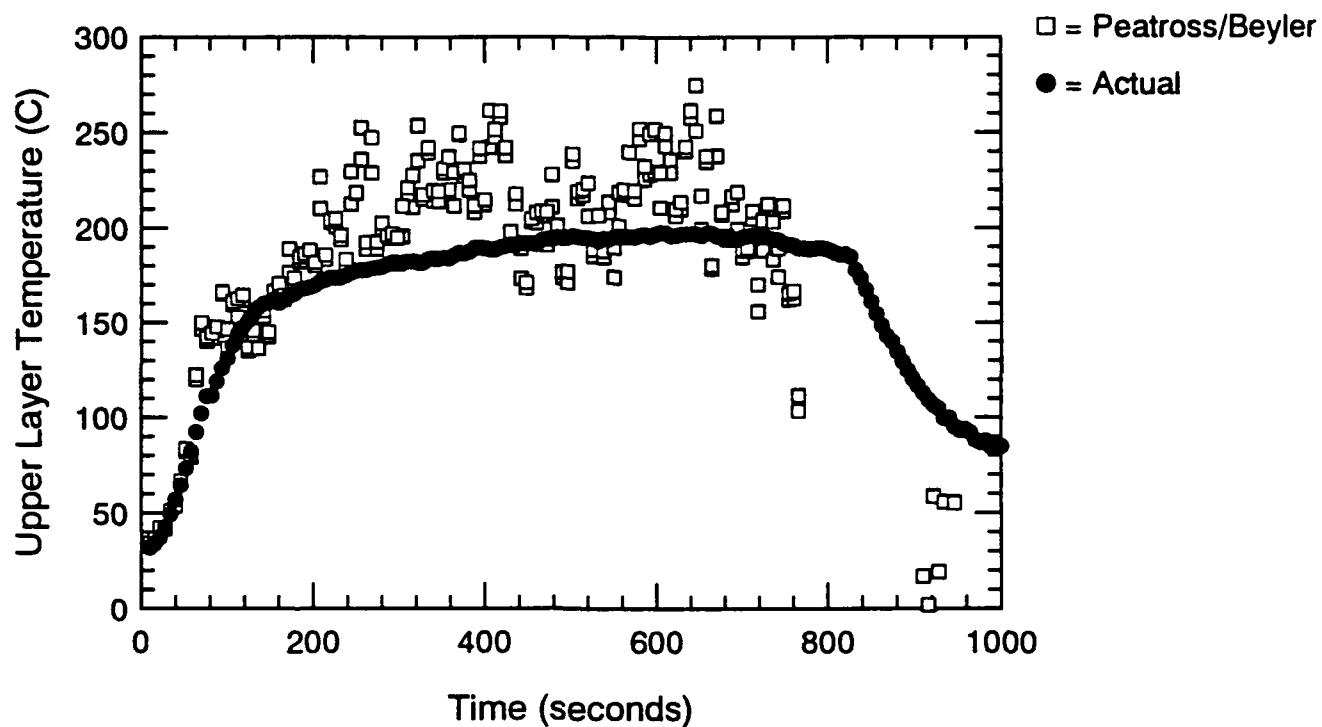


Figure C.5 Temperature Predictions Using Peatross/Beyler Method - S105

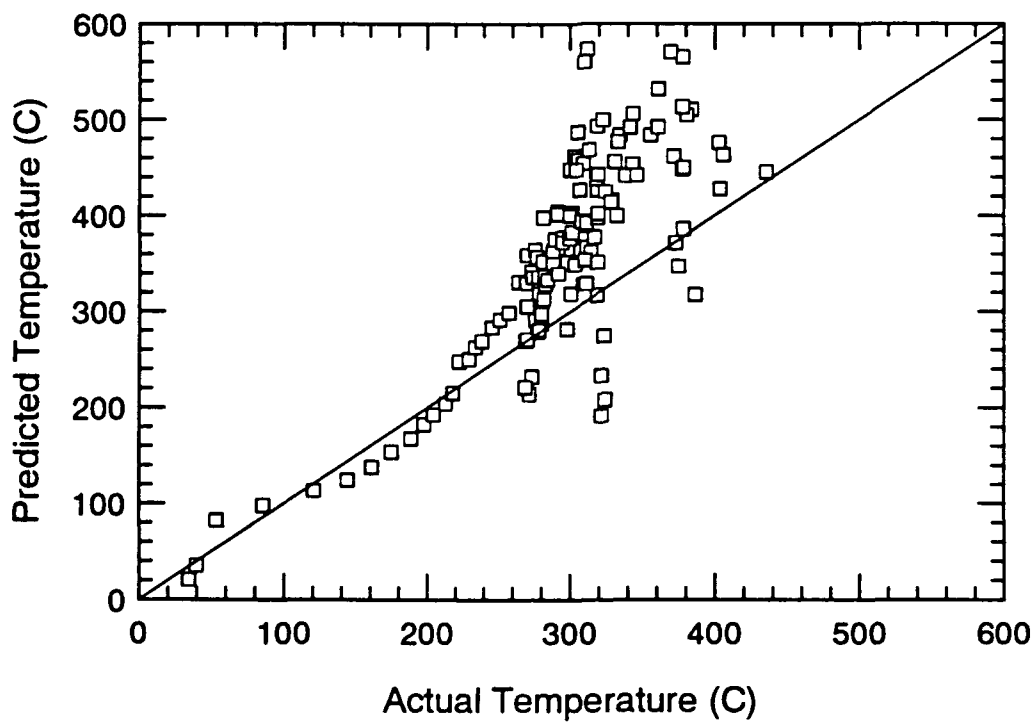
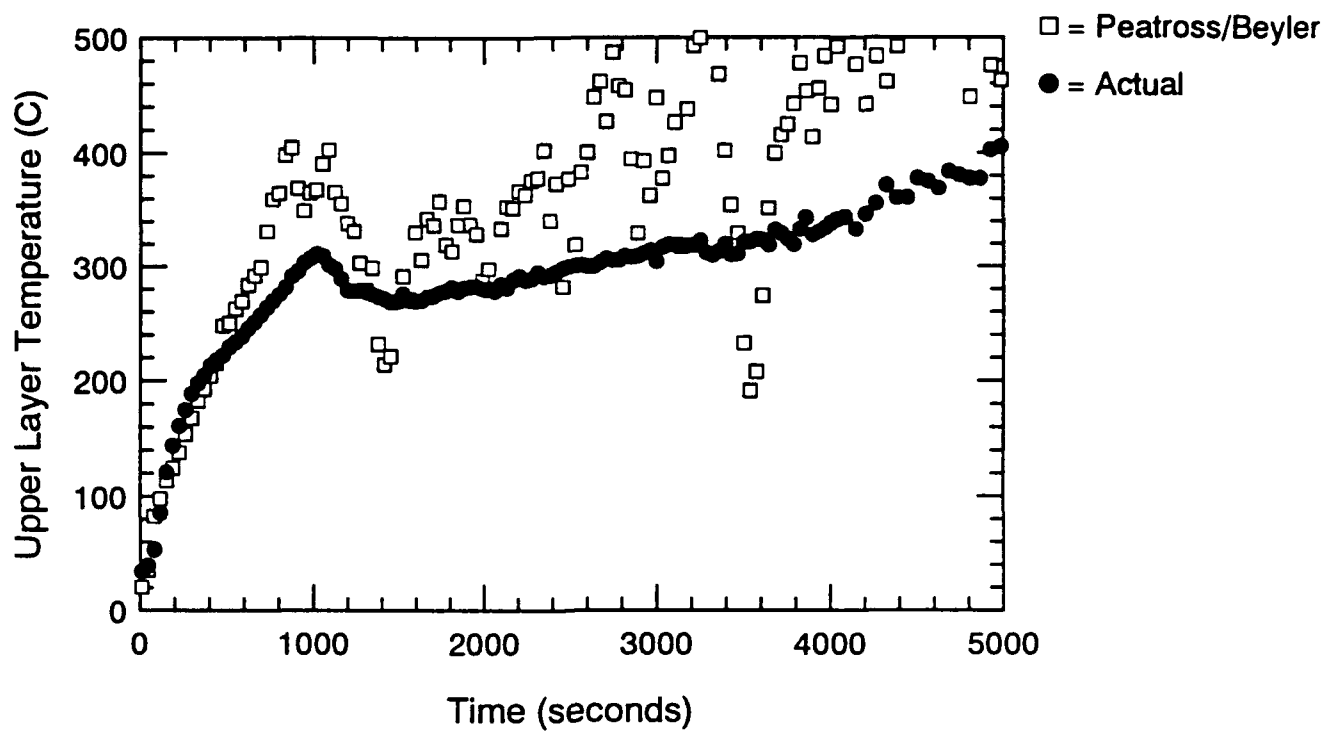


Figure C.6 Temperature Predictions Using Peatross/Beyler Method - S106

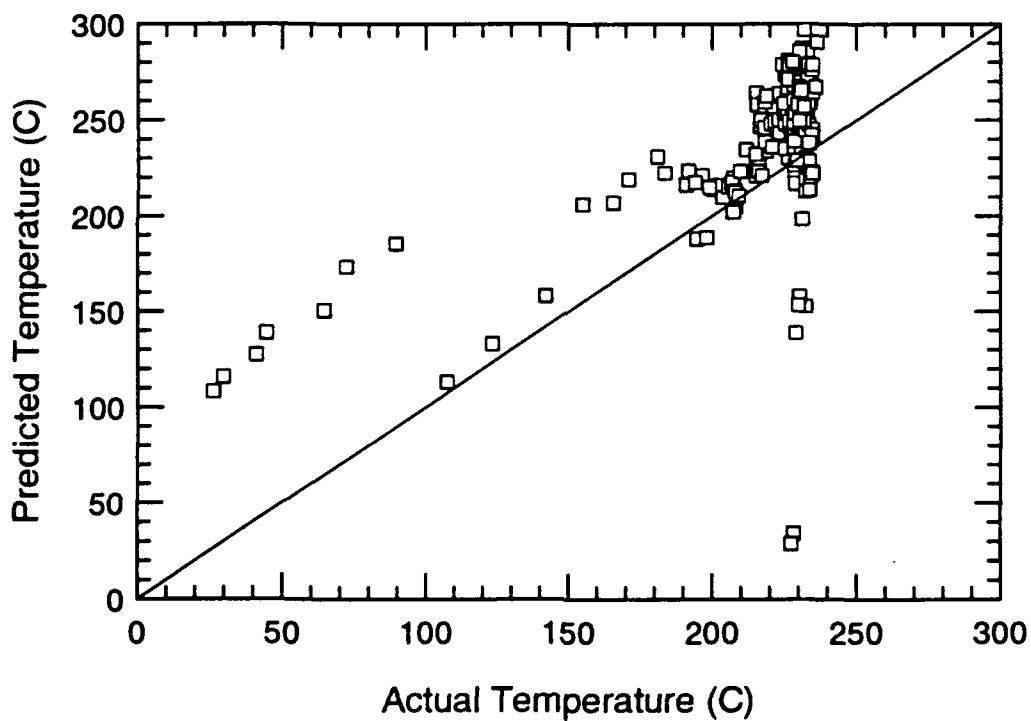
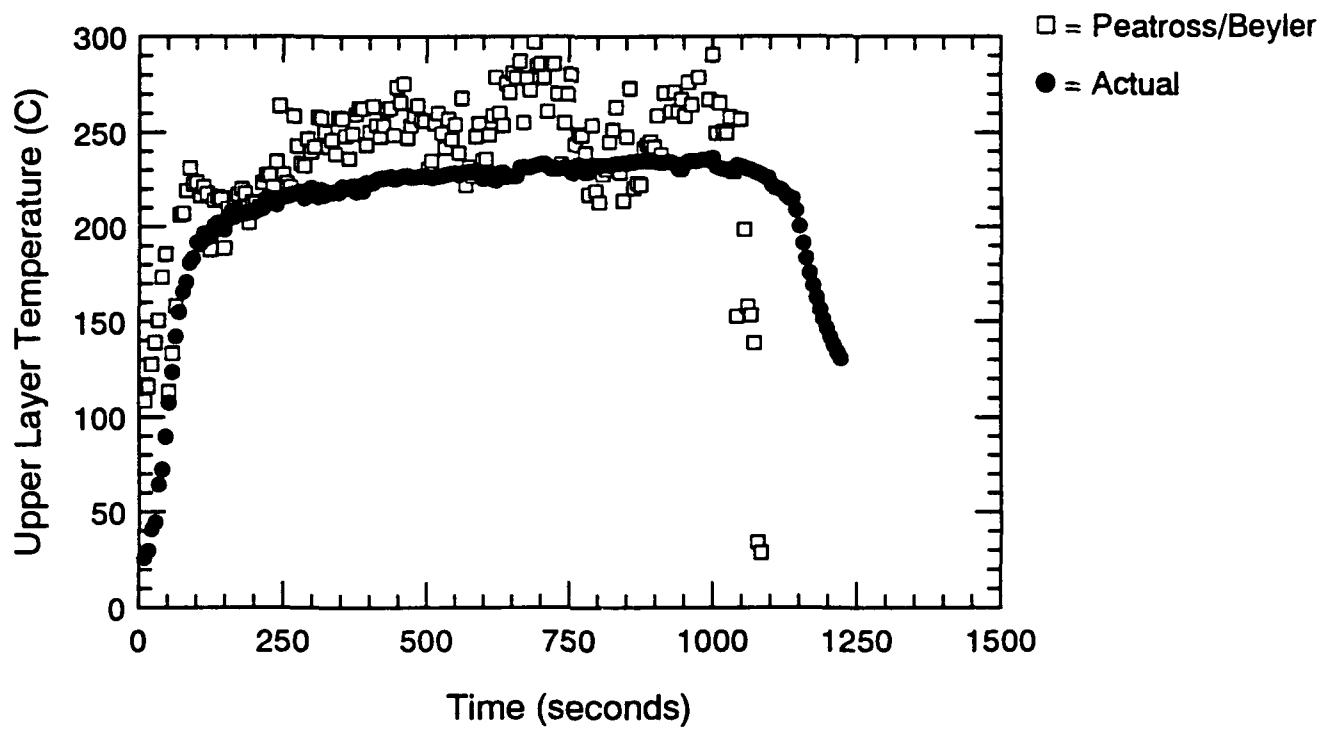


Figure C.7 Temperature Predictions Using Peatross/Beyler Method - S107

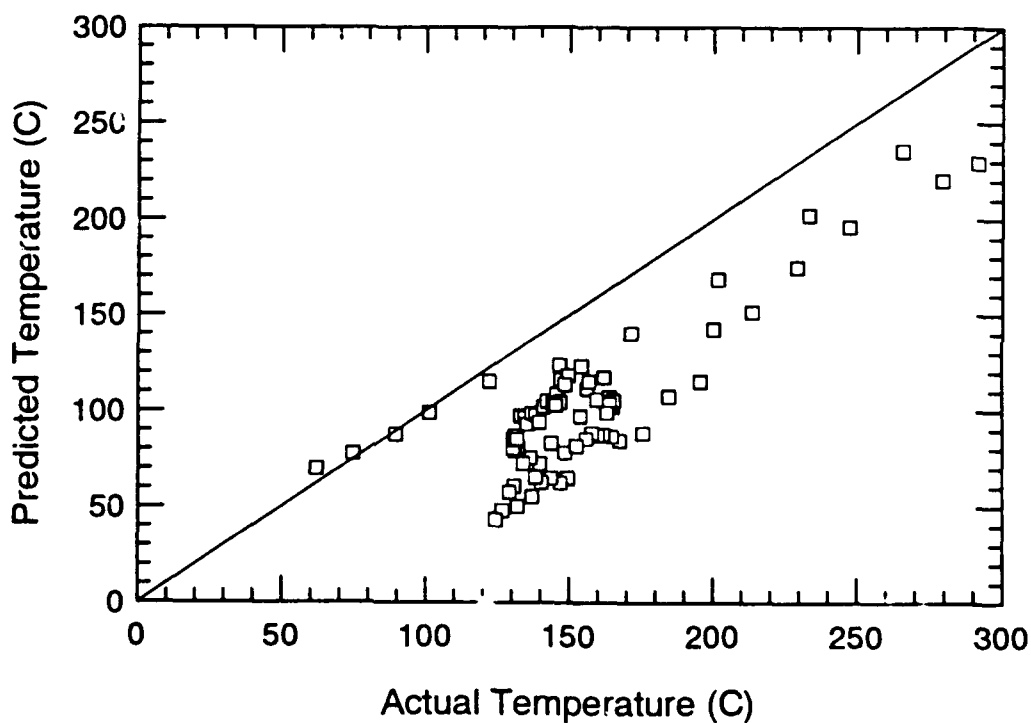
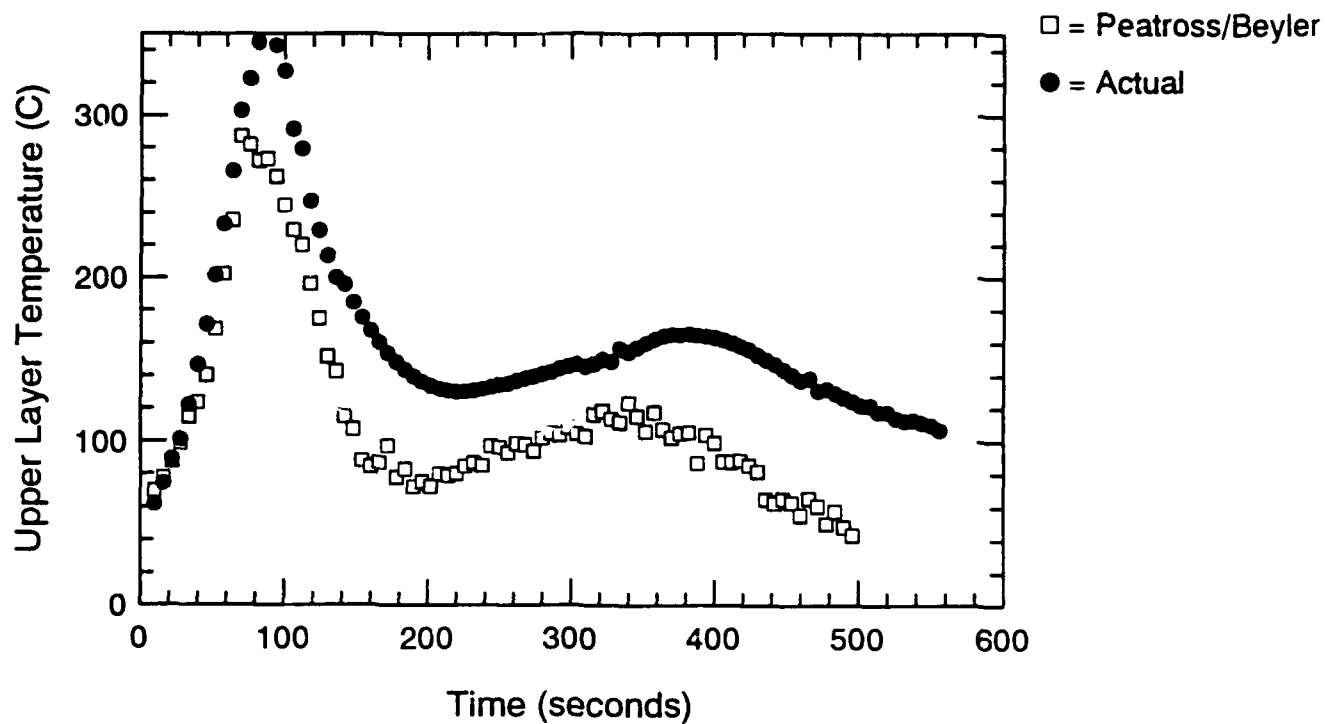


Figure C.8 Temperature Predictions Using Peatross/Beyler Method - S108

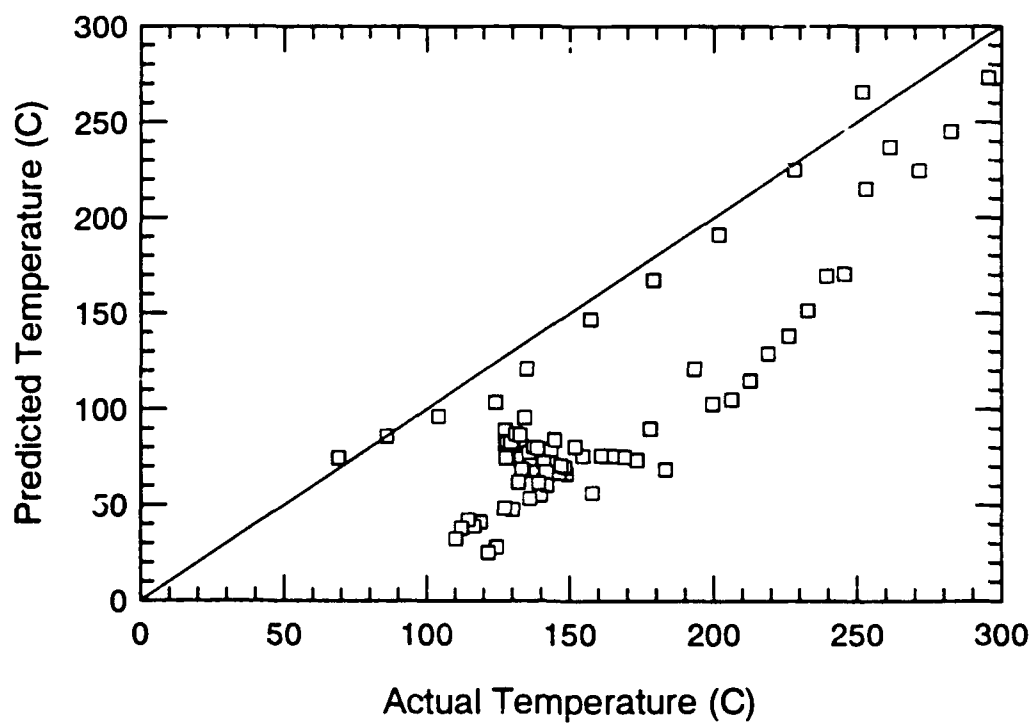
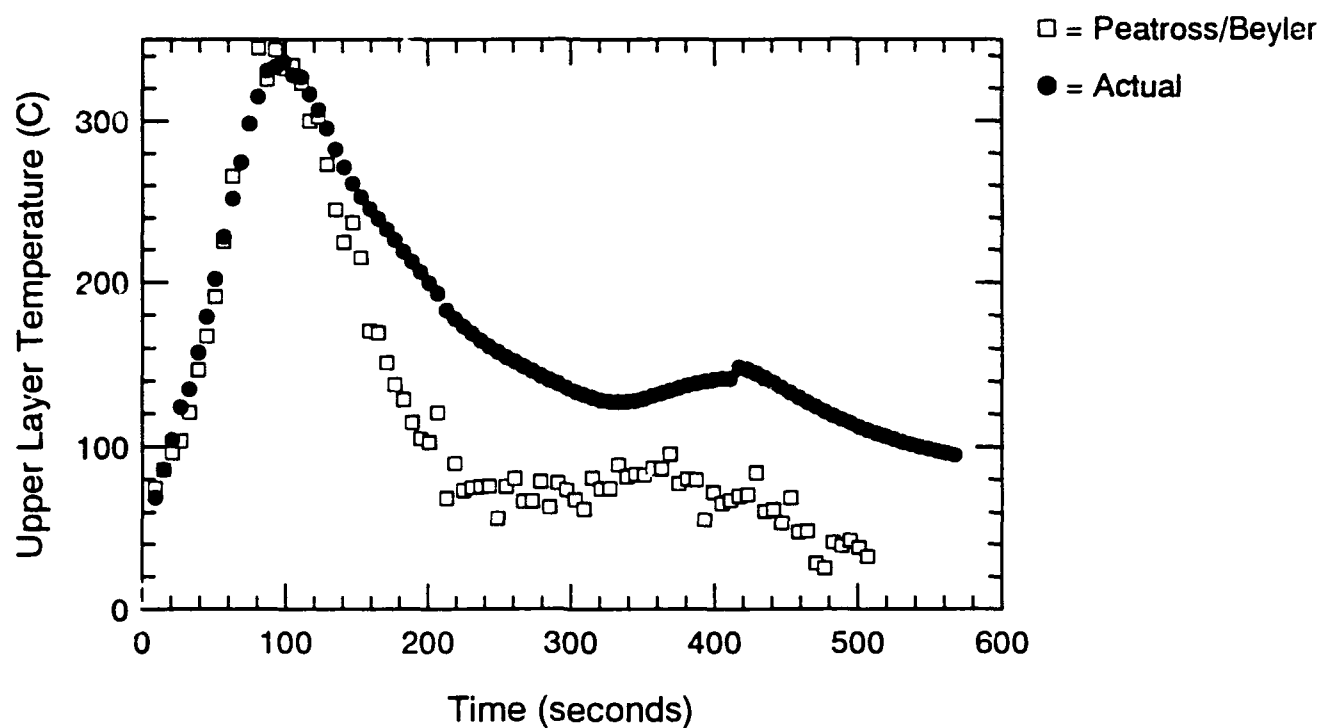


Figure C.9 Temperature Predictions Using Peatross/Beyler Method - S109

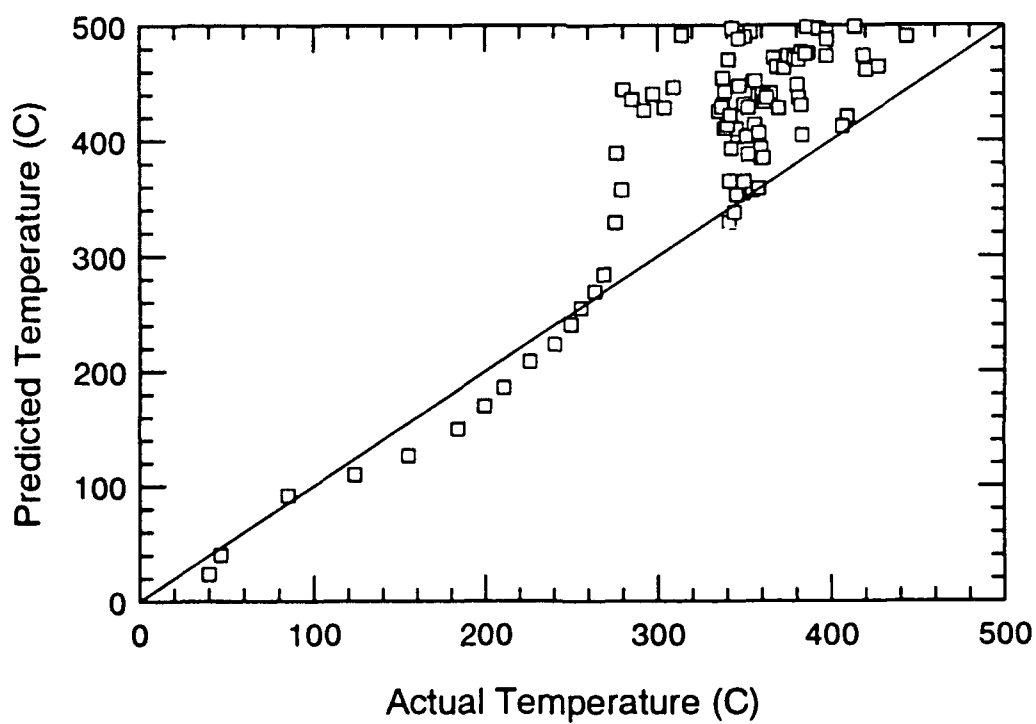
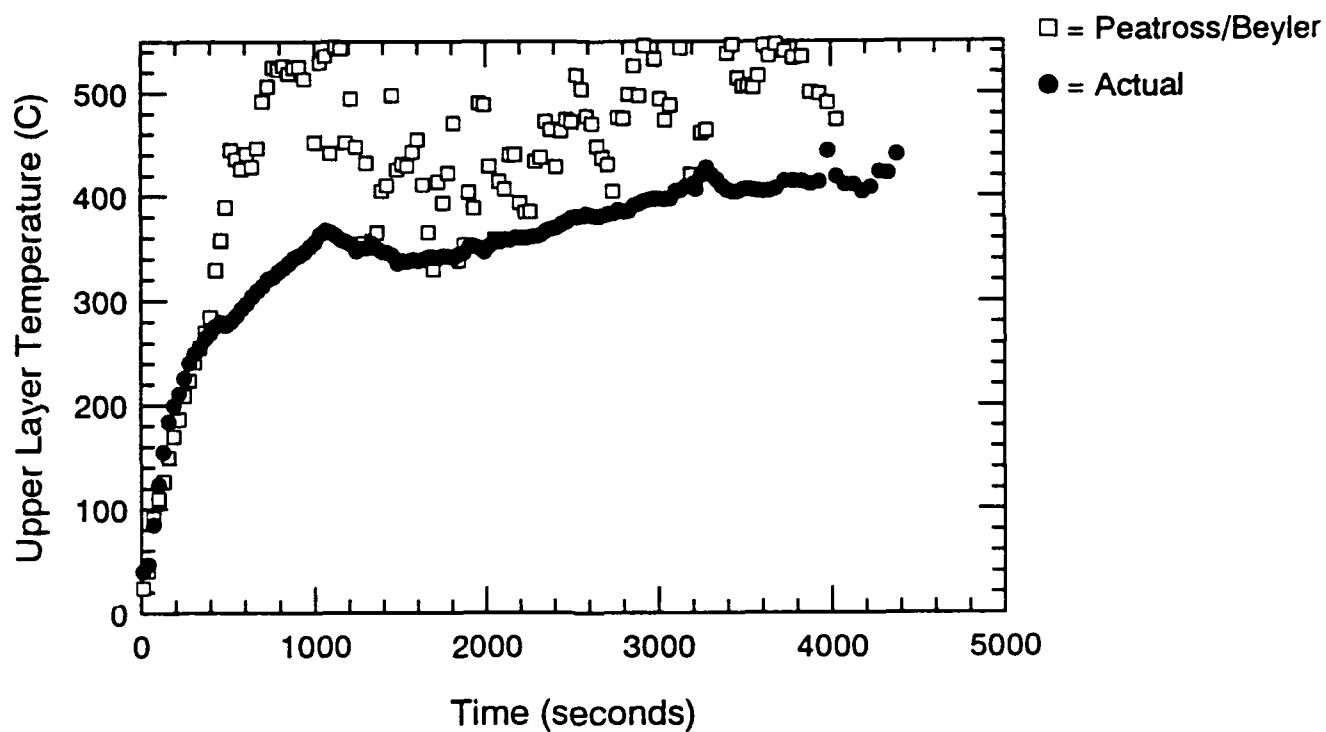


Figure C.10 Temperature Predictions Using Peatross/Beyler Method - S110

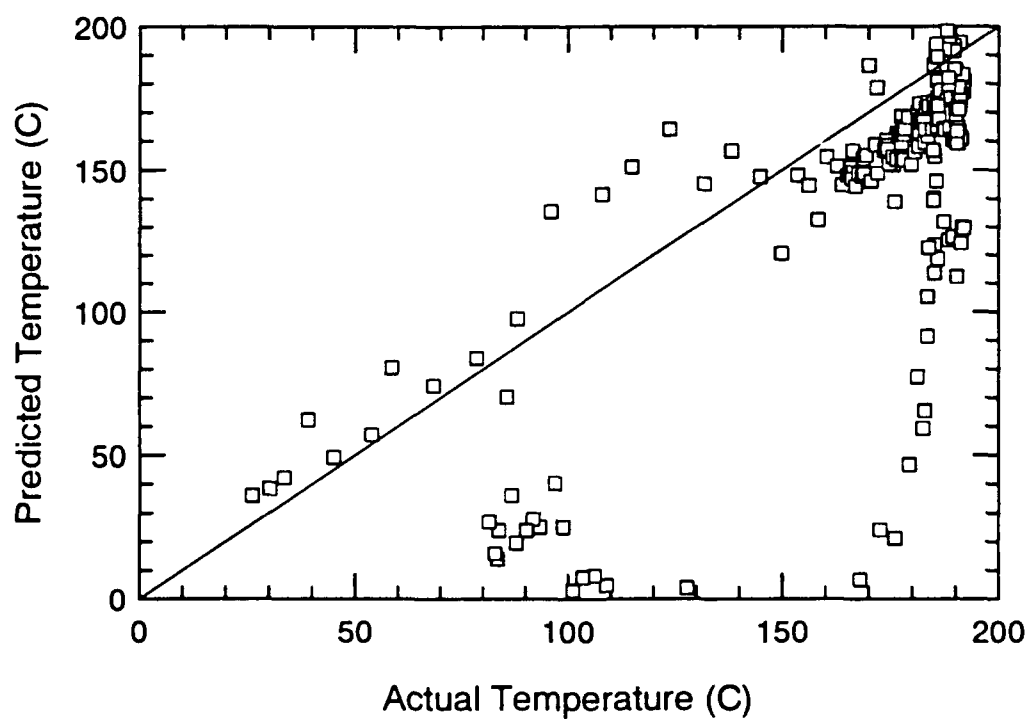
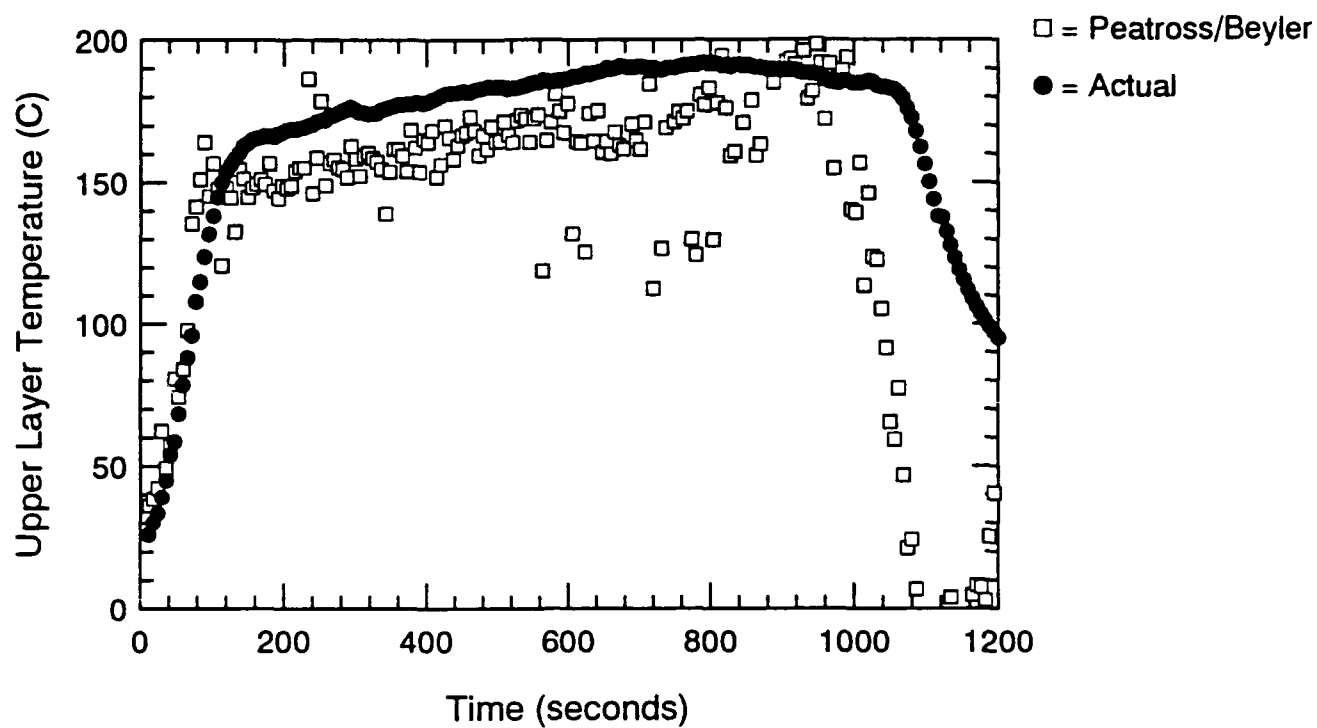


Figure C.11 Temperature Predictions Using Peatross/Beyler Method - S111

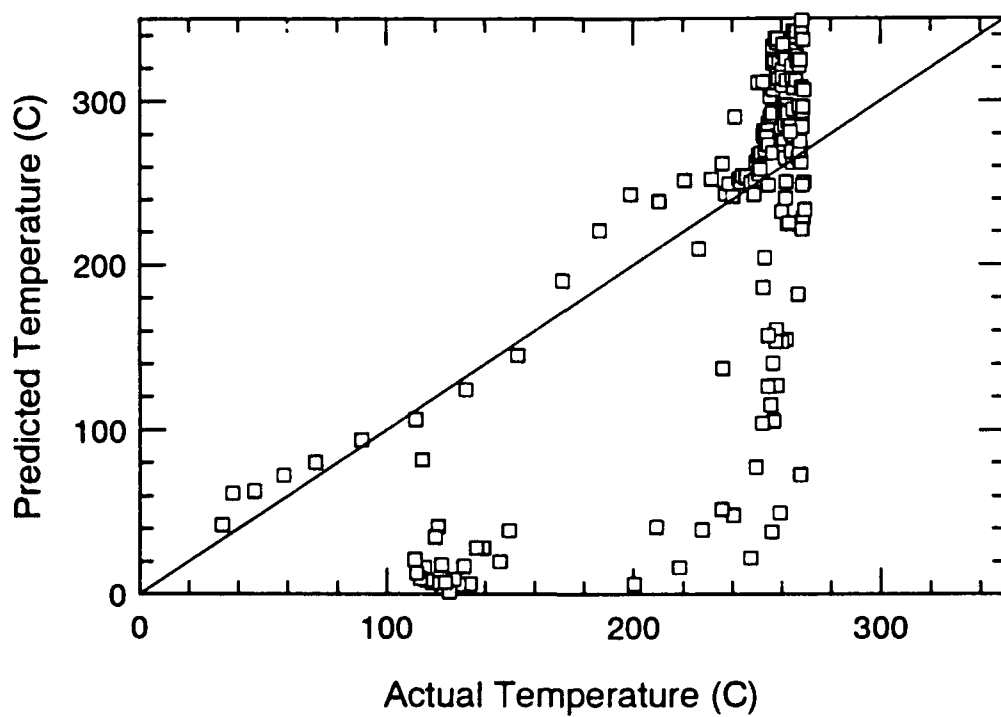
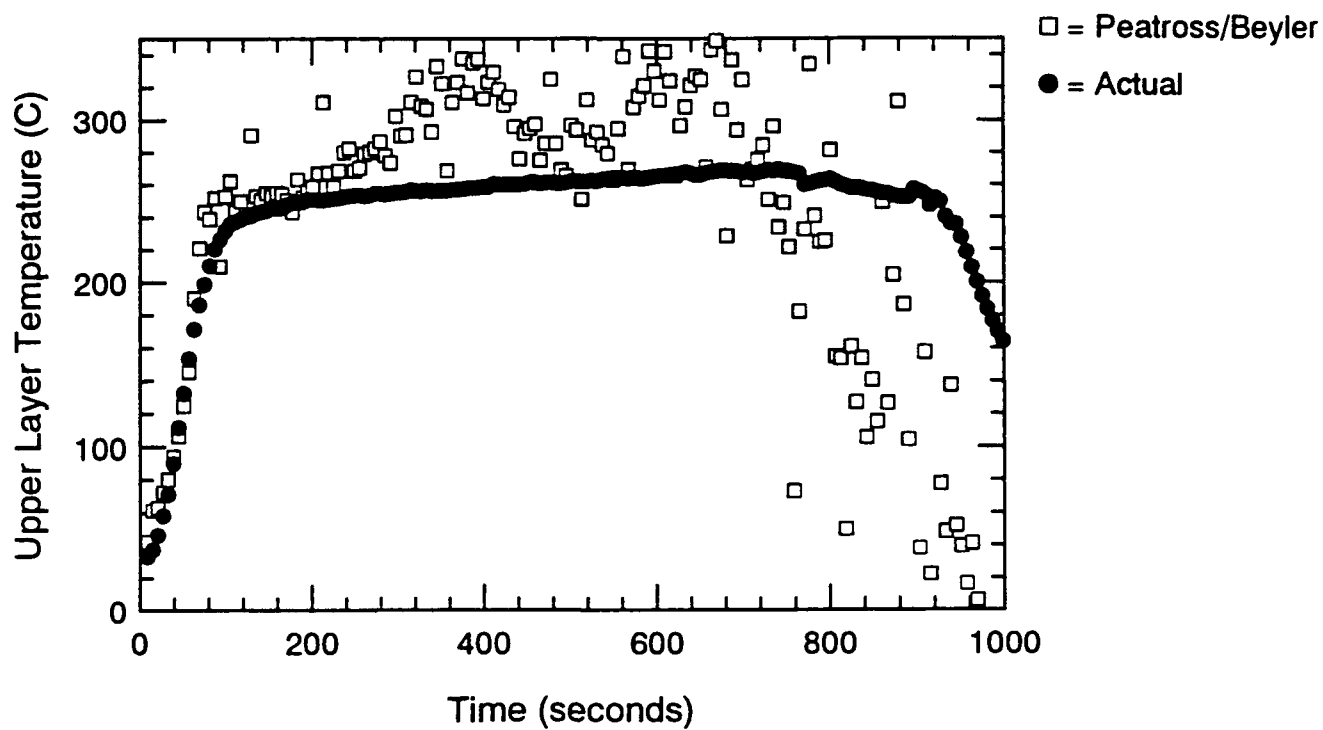


Figure C.12 Temperature Predictions Peatross/Beyler Method - S112

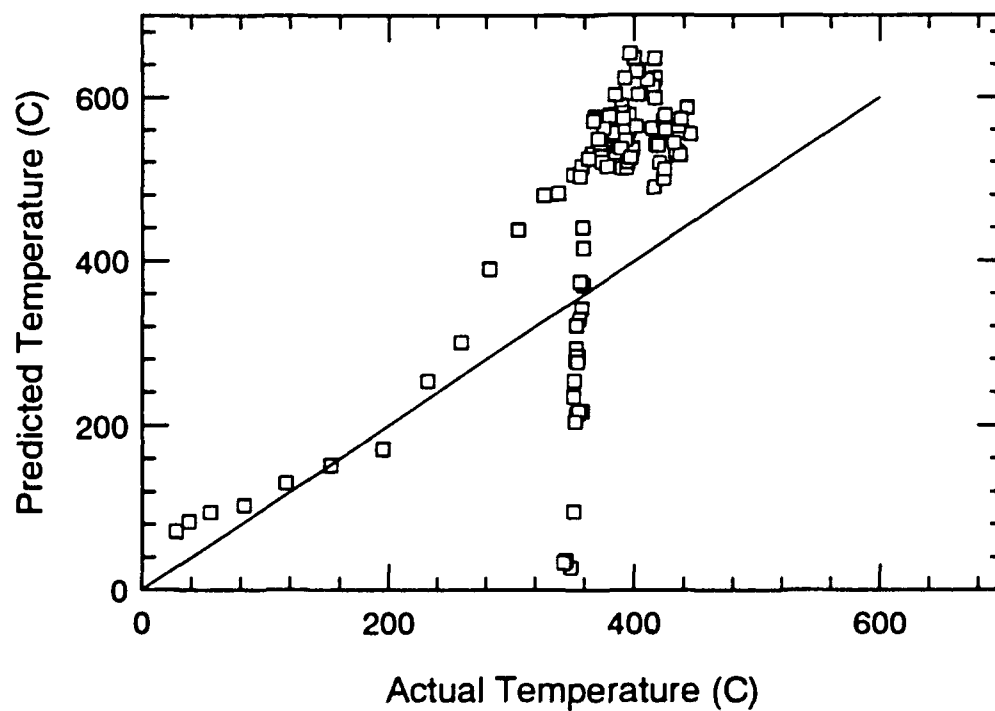
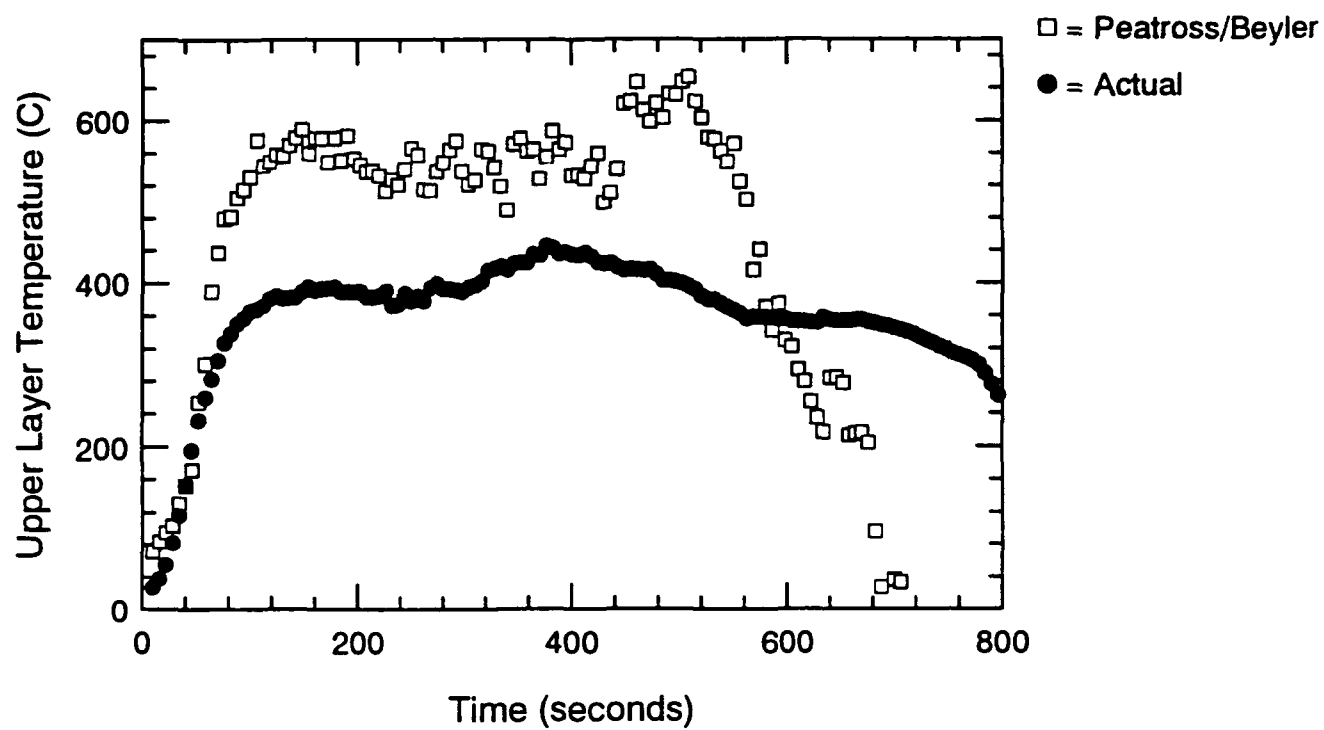


Figure C.13 Temperature Predictions Using Peatross/Beyler Method - ADD1

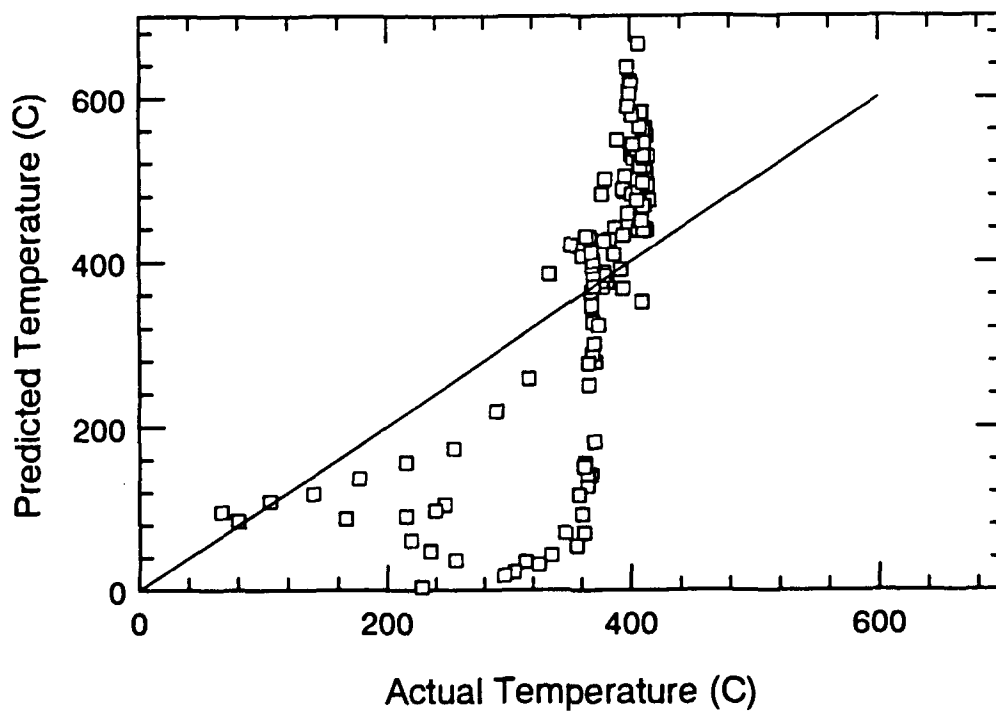
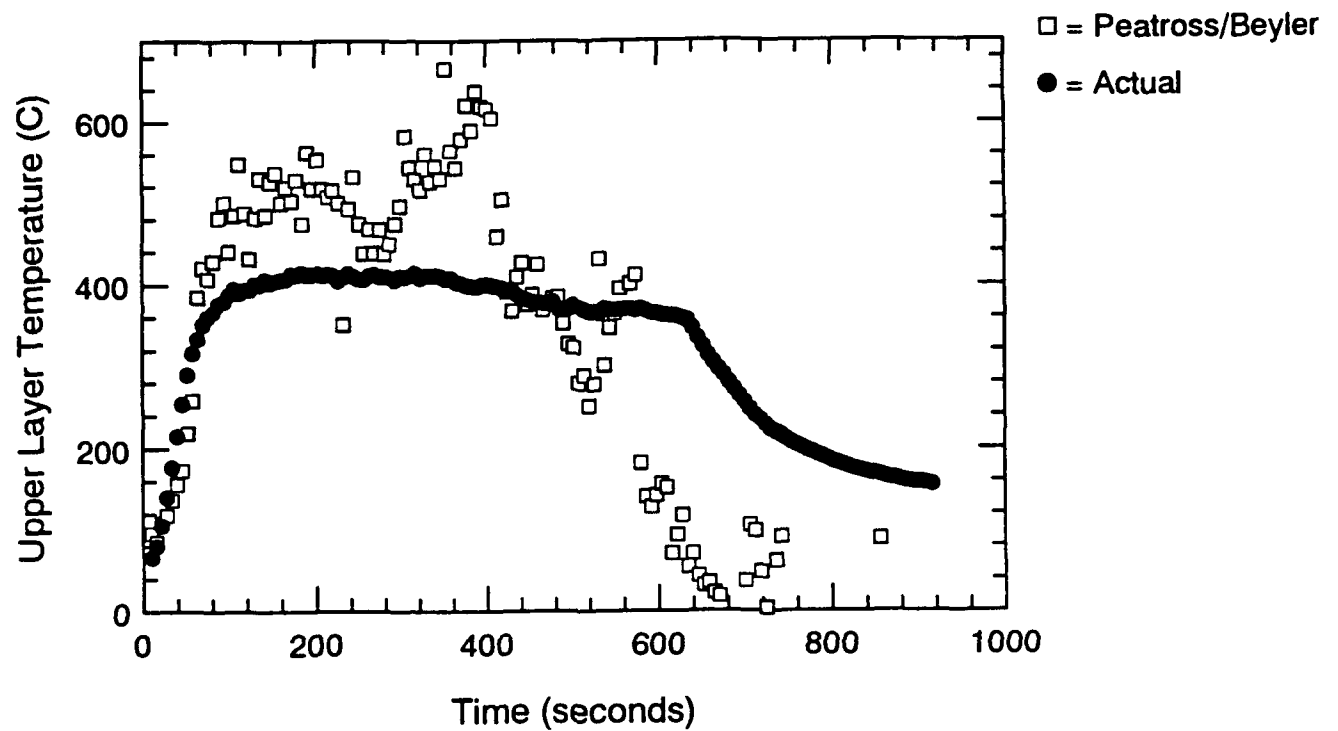


Figure C.14 Temperature Predictions Using Peatross/Beyler Method - ADD2

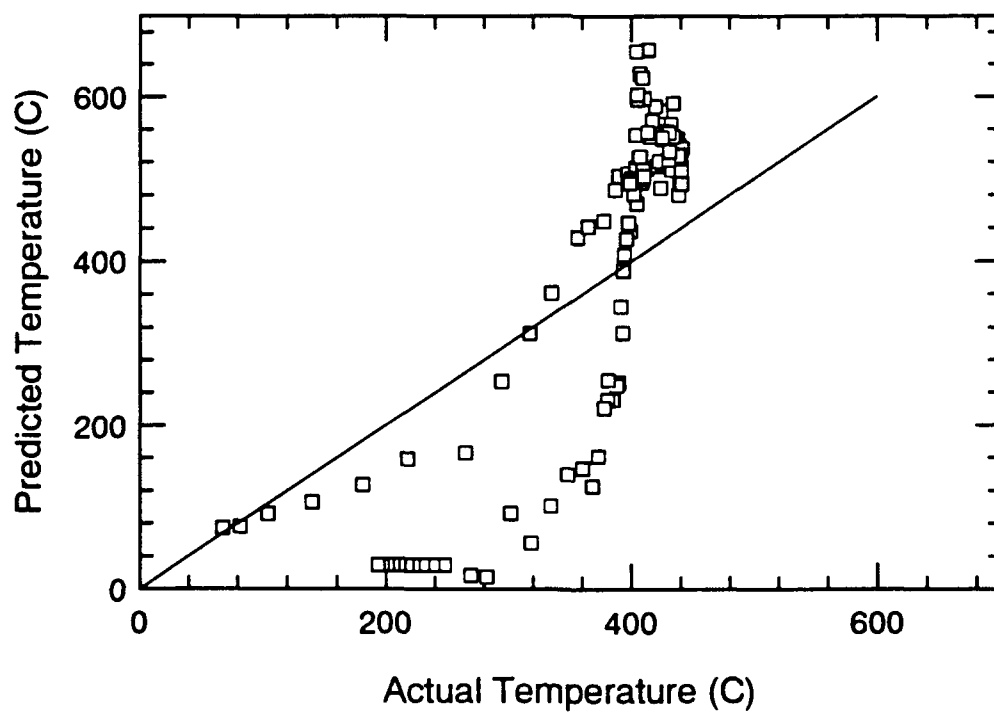
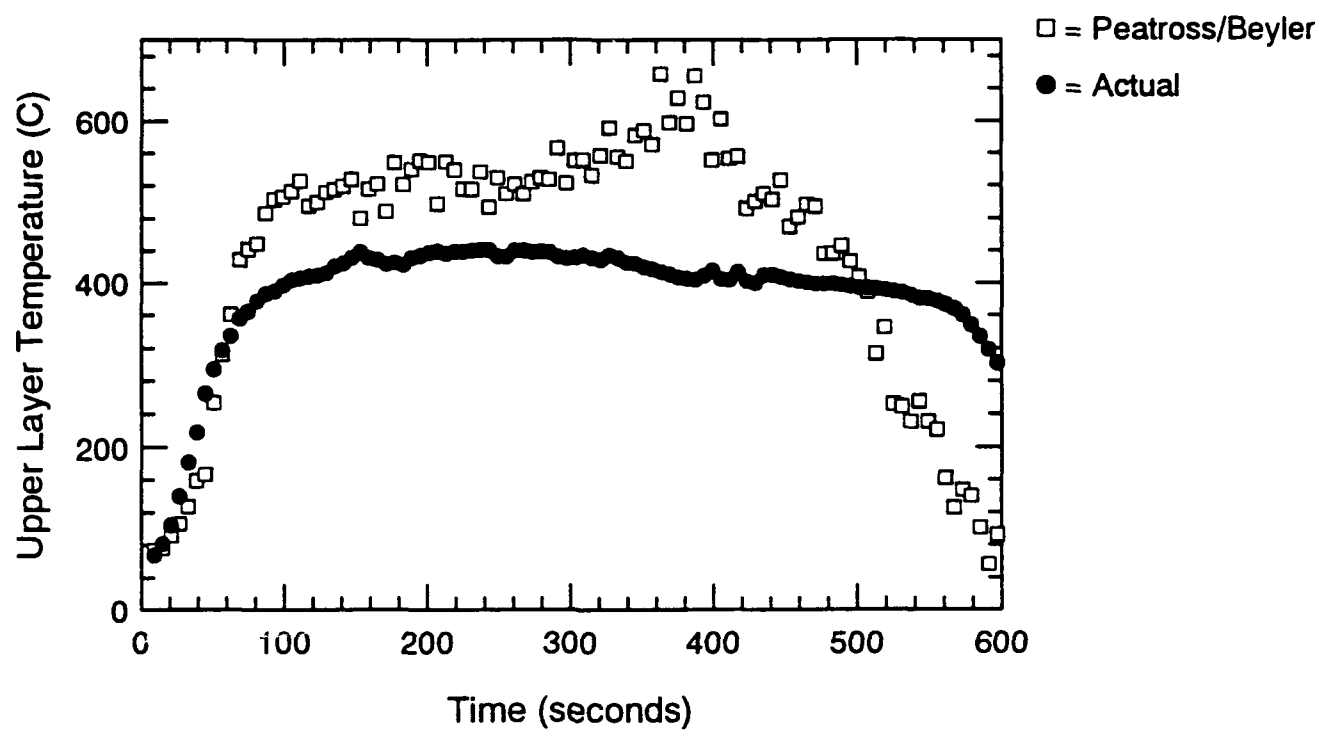


Figure C.15 Temperature Predictions Using Peatross/Beyler Method - ADD3

APPENDIX D. Series 2 - Peatross/Beyler Temperature Prediction Method Results

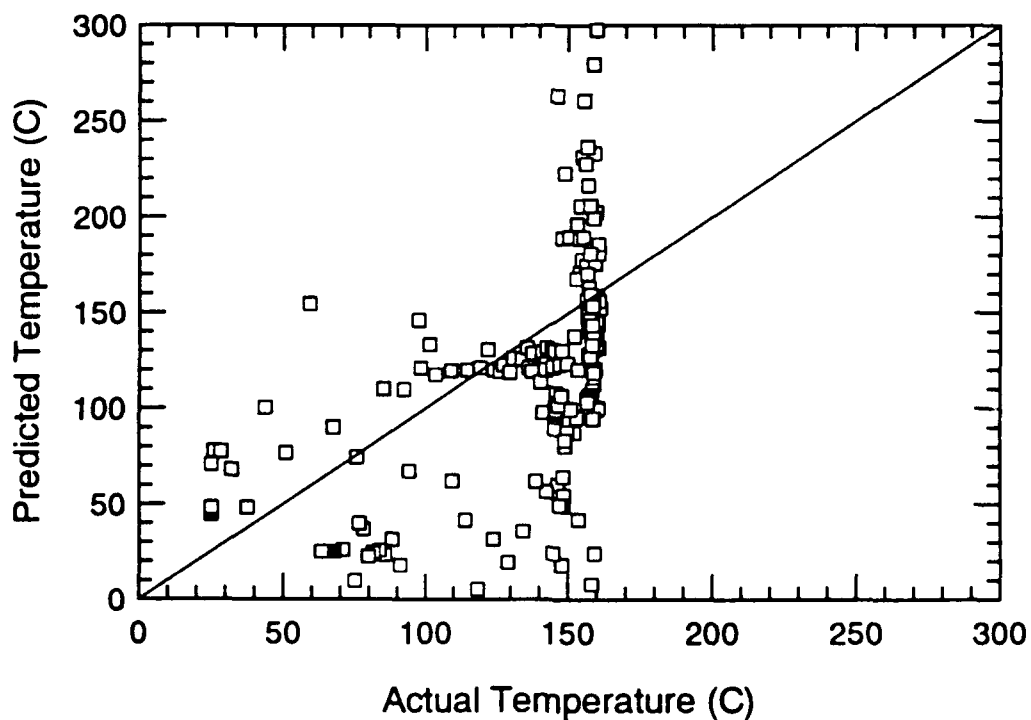
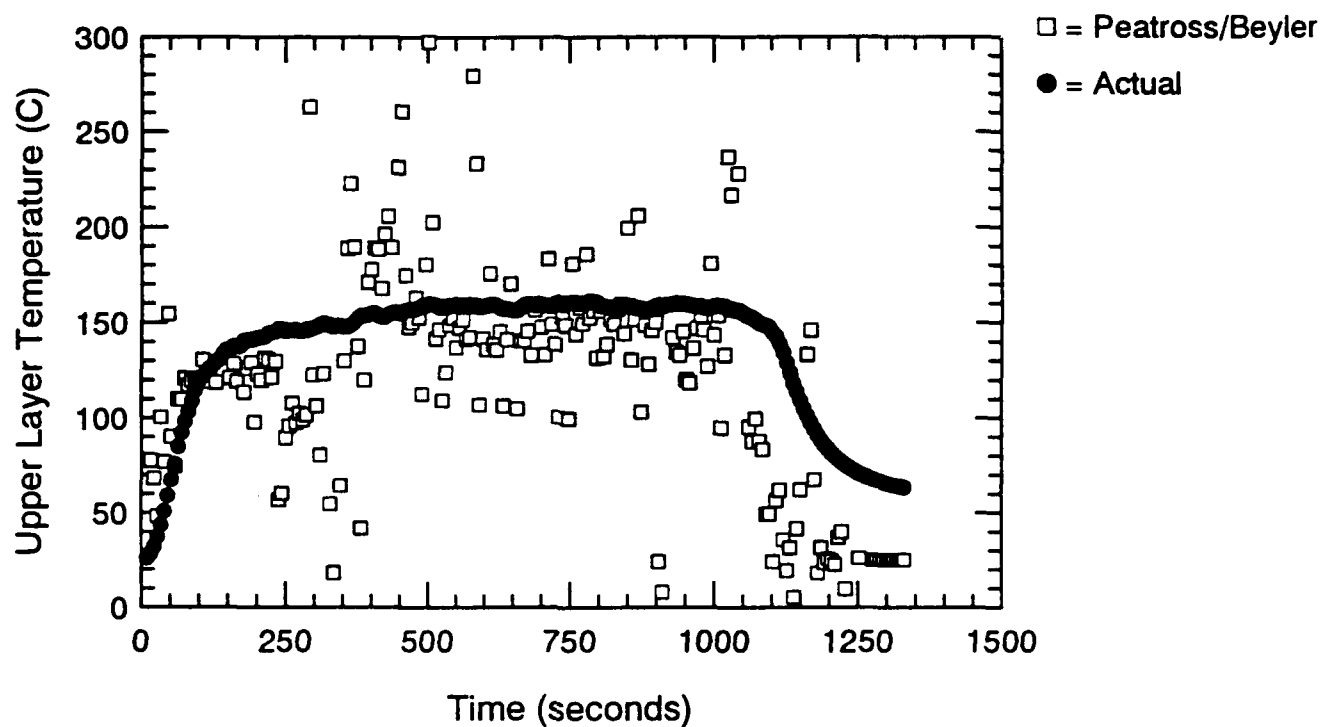


Figure D.1 Temperature Predictions Using Peatross/Beyler Method - S201

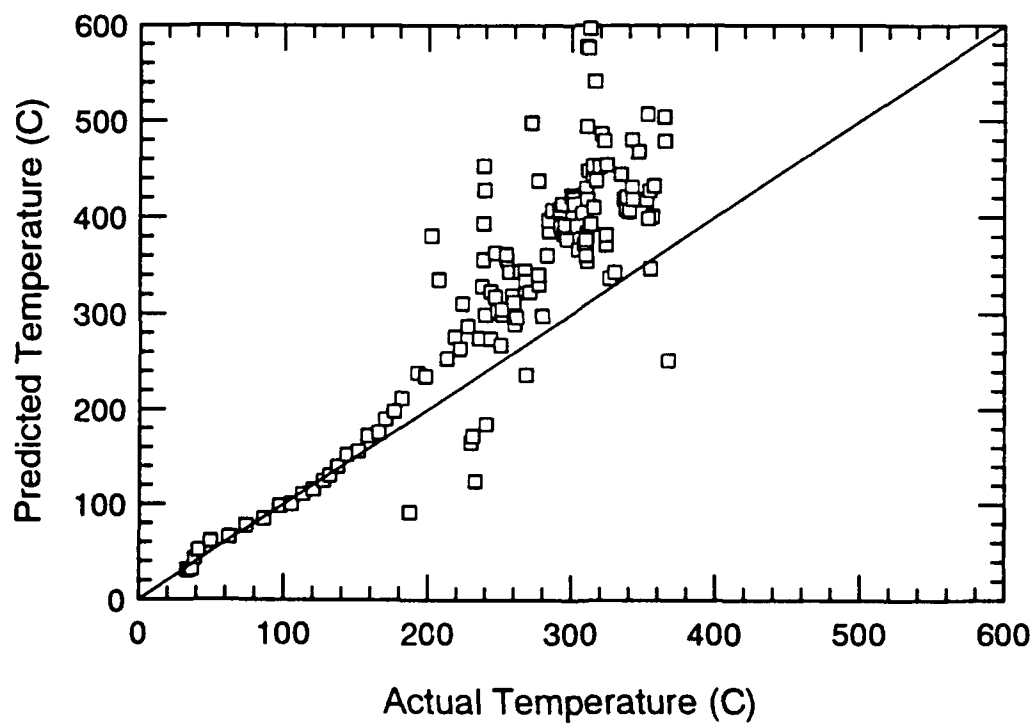
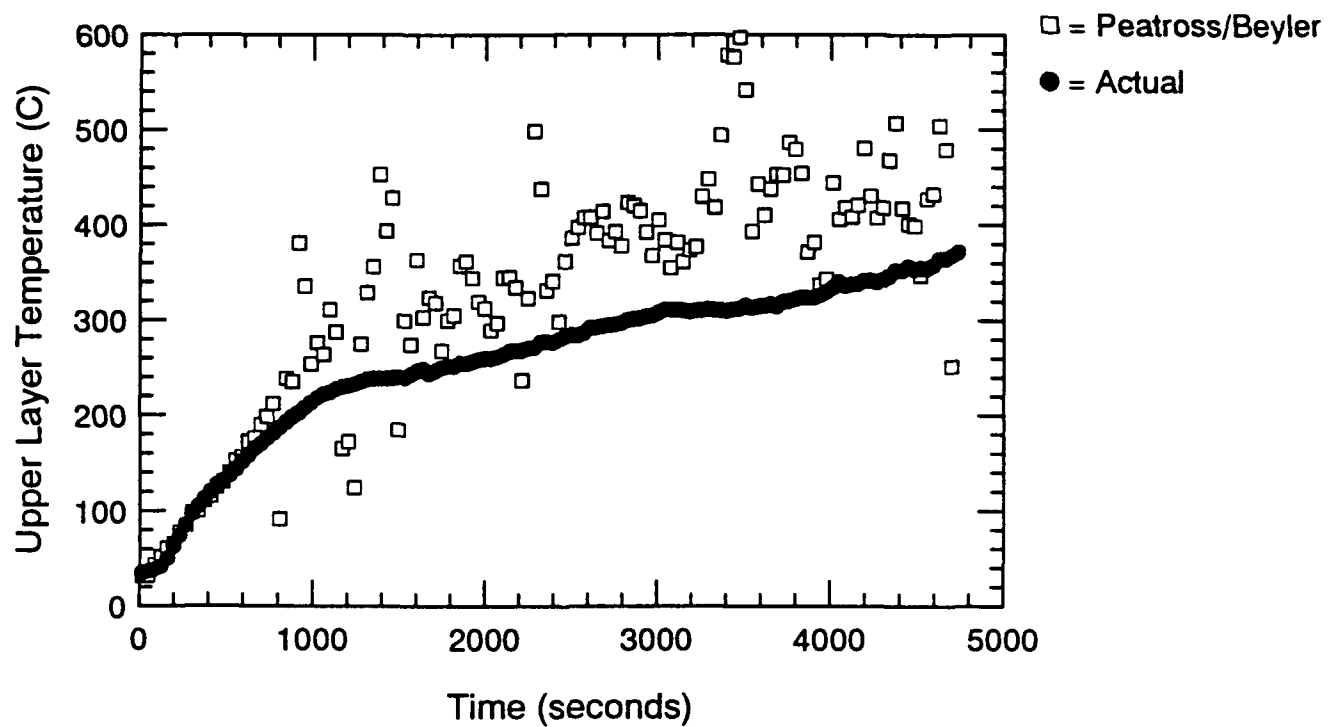


Figure D.2 Temperature Predictions Using Peatross/Beyler Method - S202

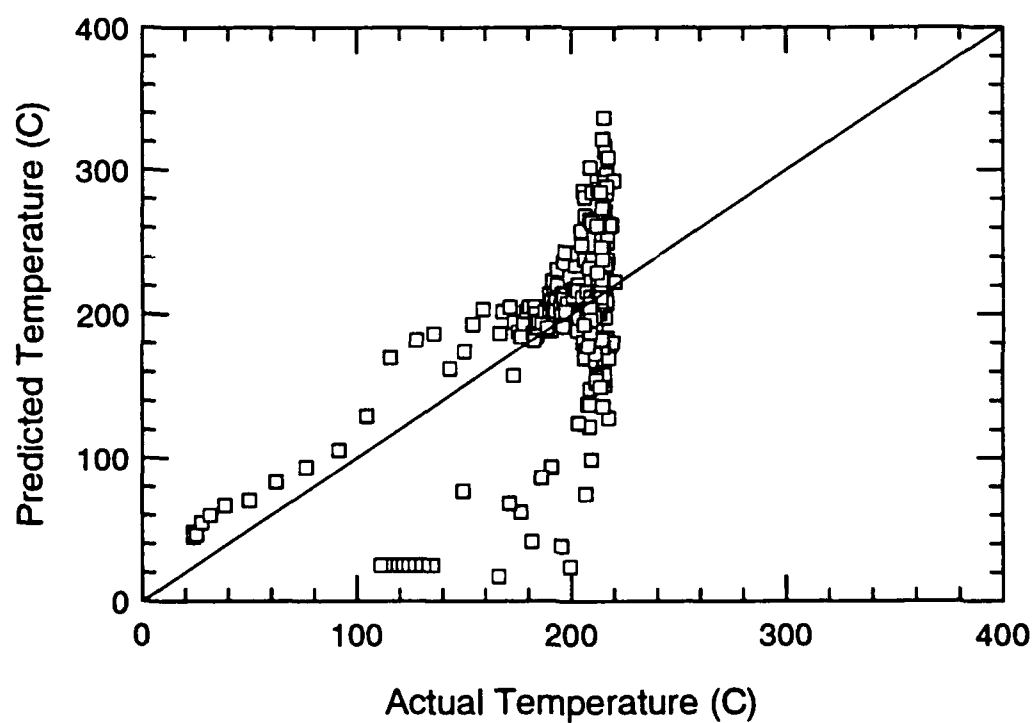
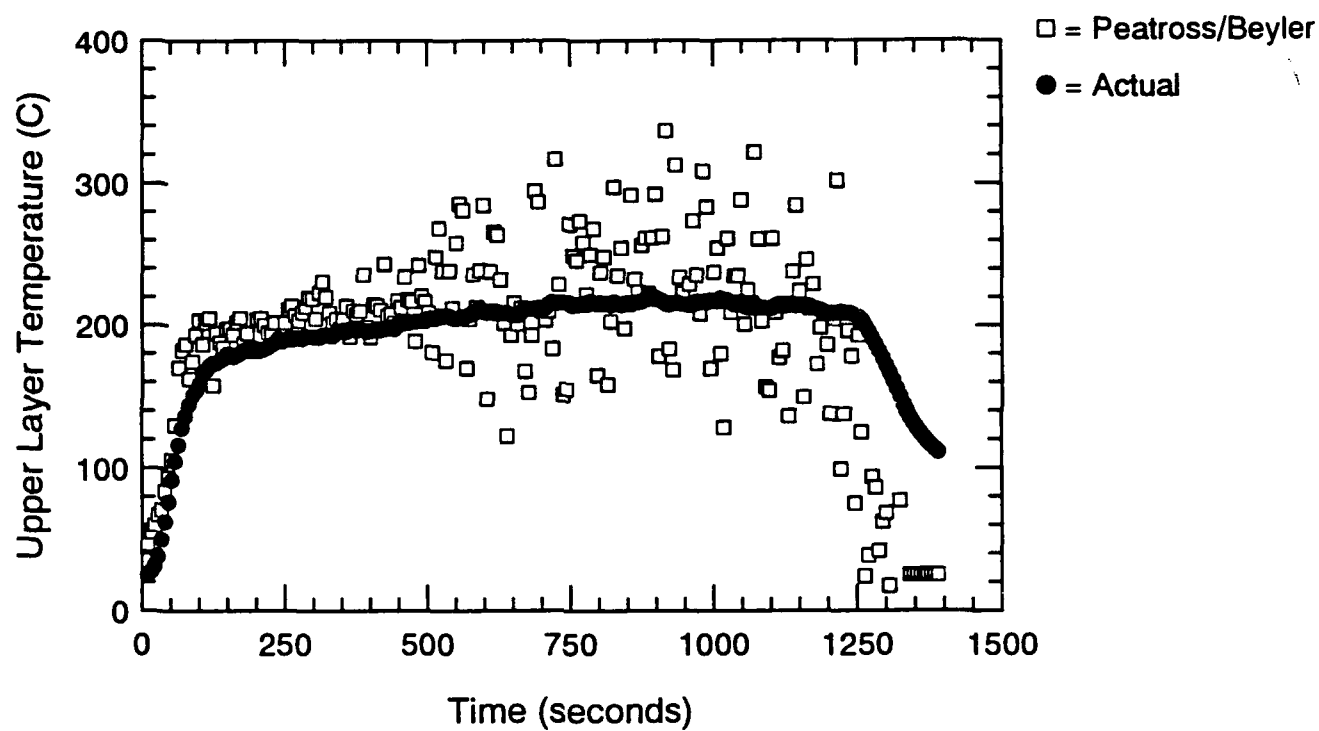


Figure D.3 Temperature Predictions Using Peatross/Beyler Method - S203

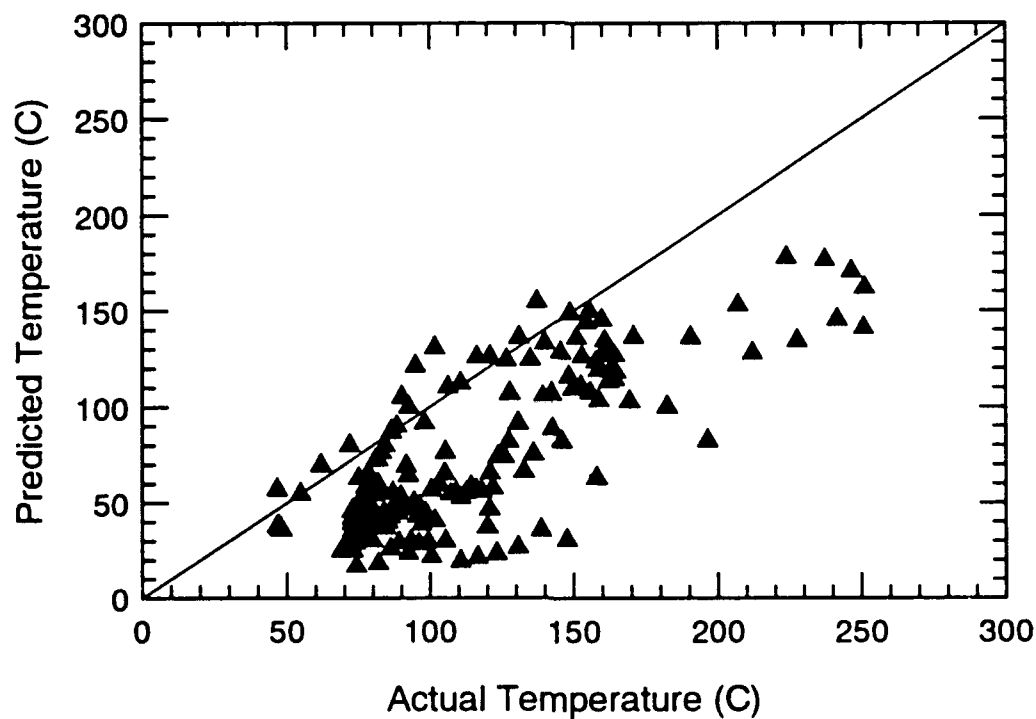
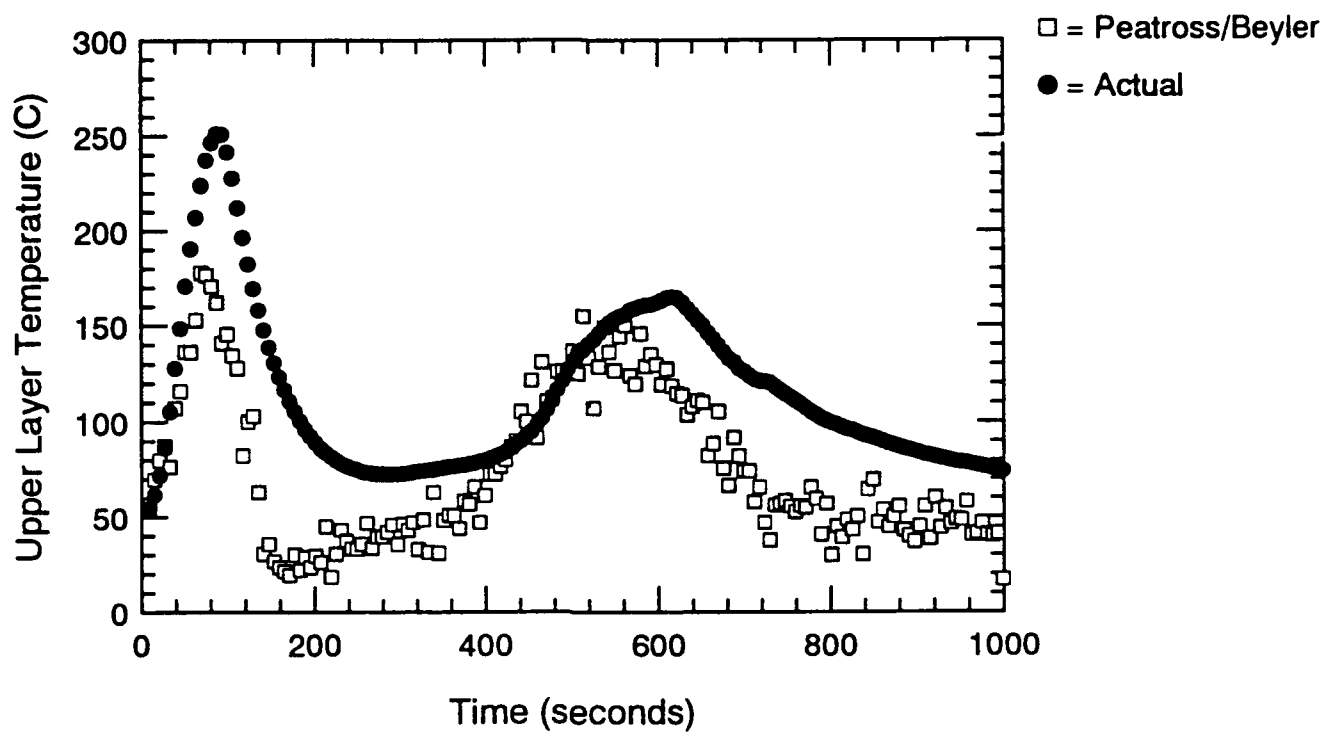


Figure D.4 Temperature Predictions Using Peatross/Beyler Method - S204

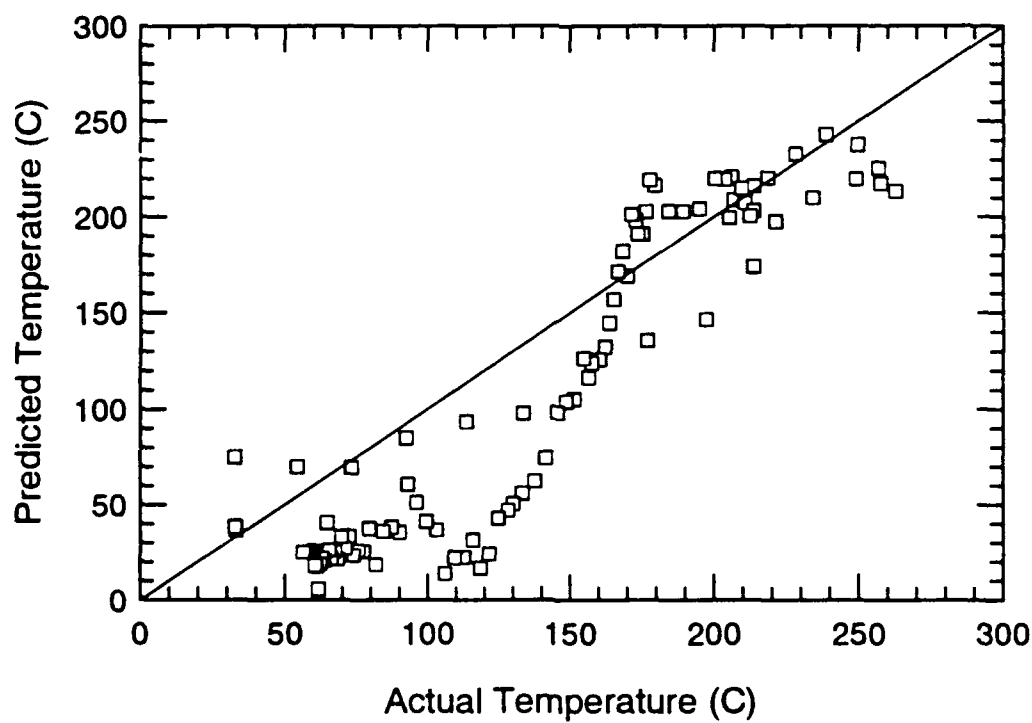
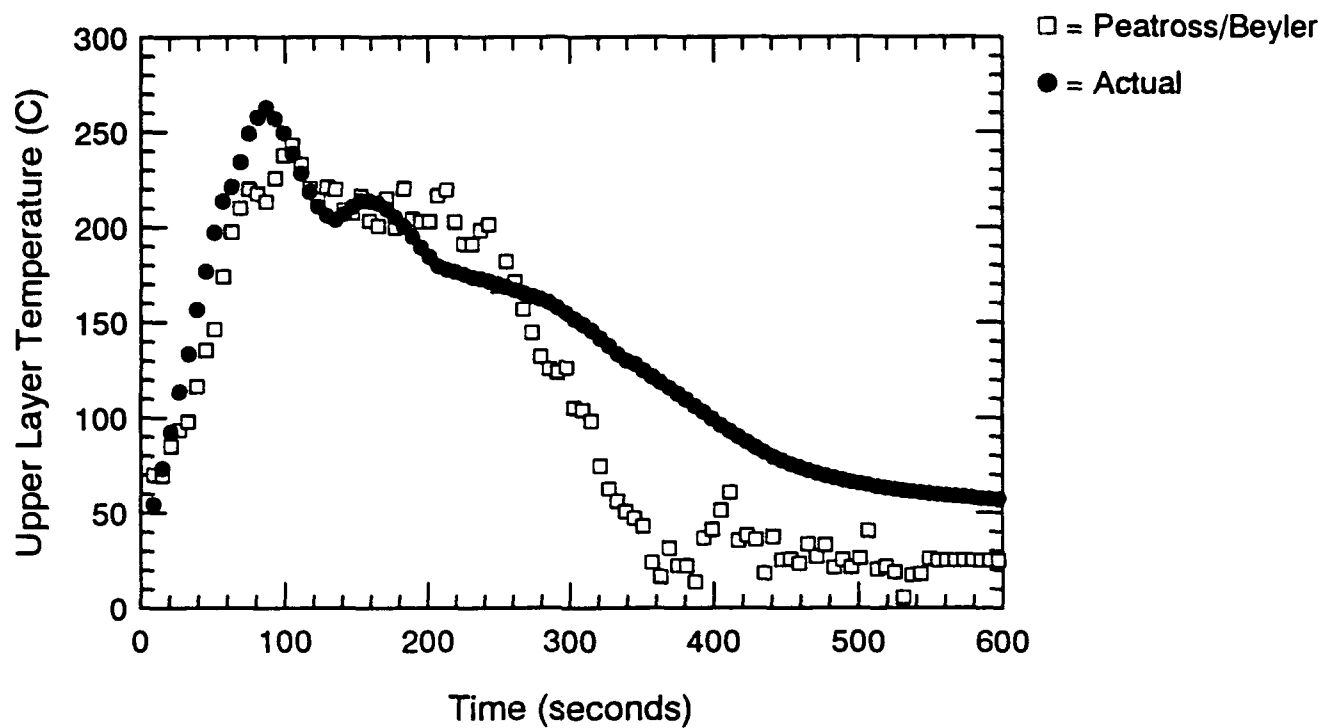


Figure D.5 Temperature Predictions Using Peatross/Beyler Method - S205

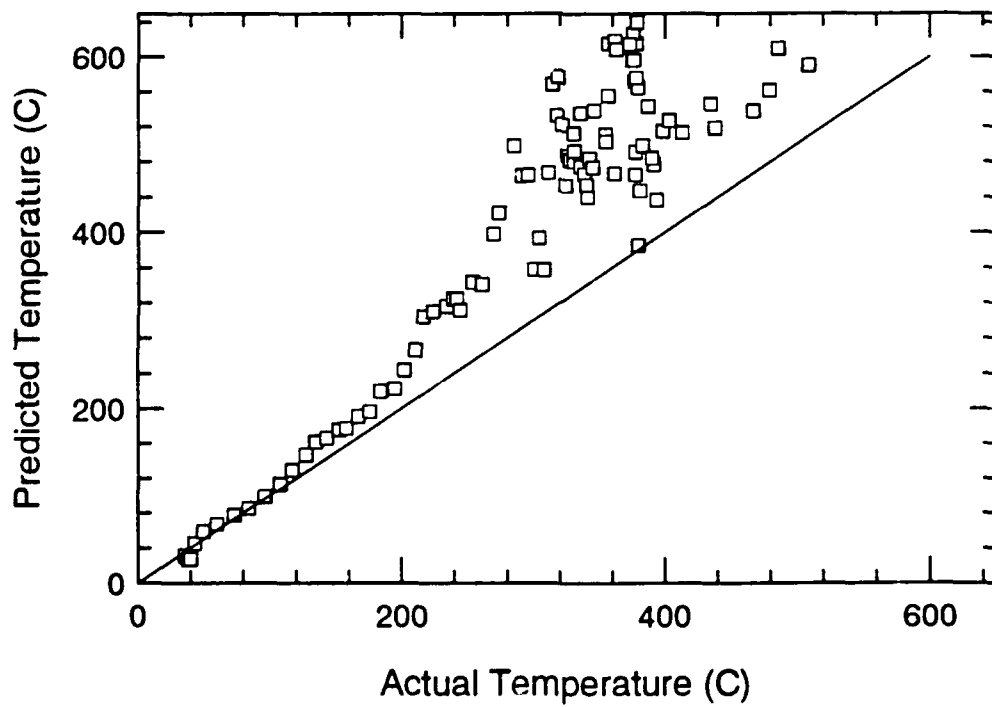
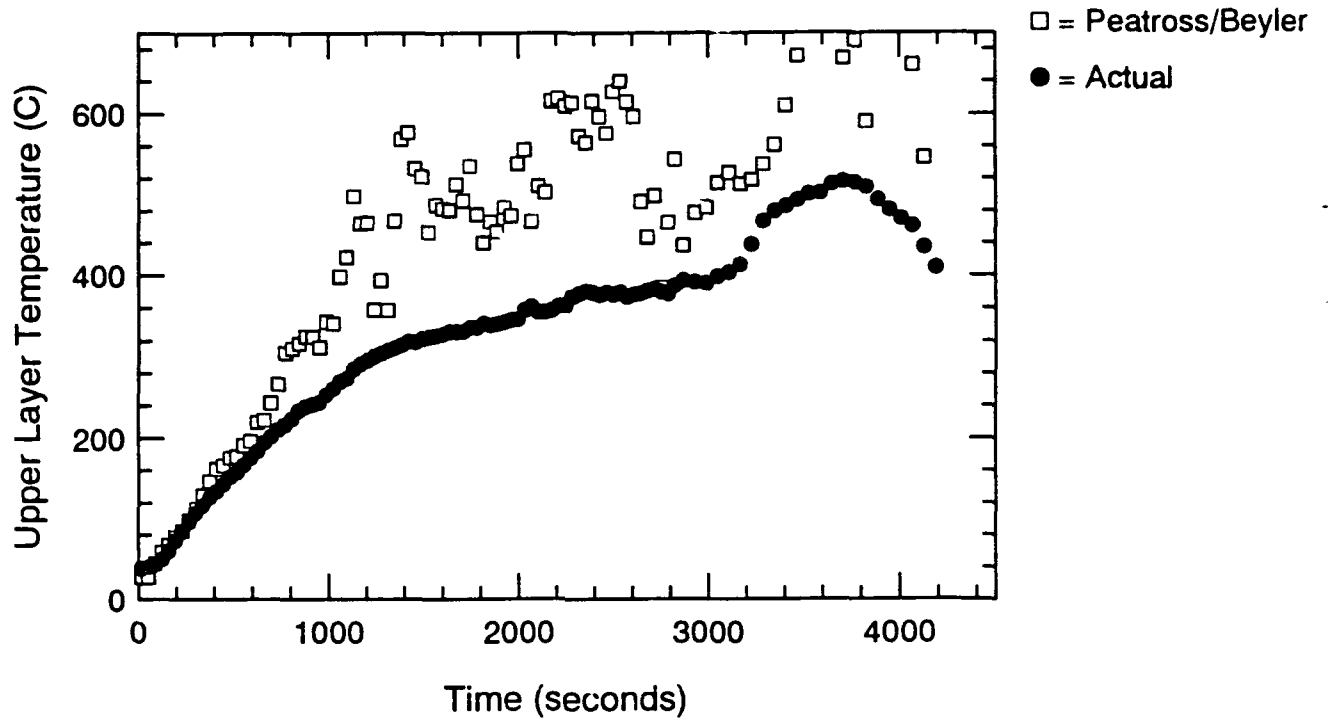


Figure D.6 Temperature Predictions Using Peatross/Beyler Method - S206

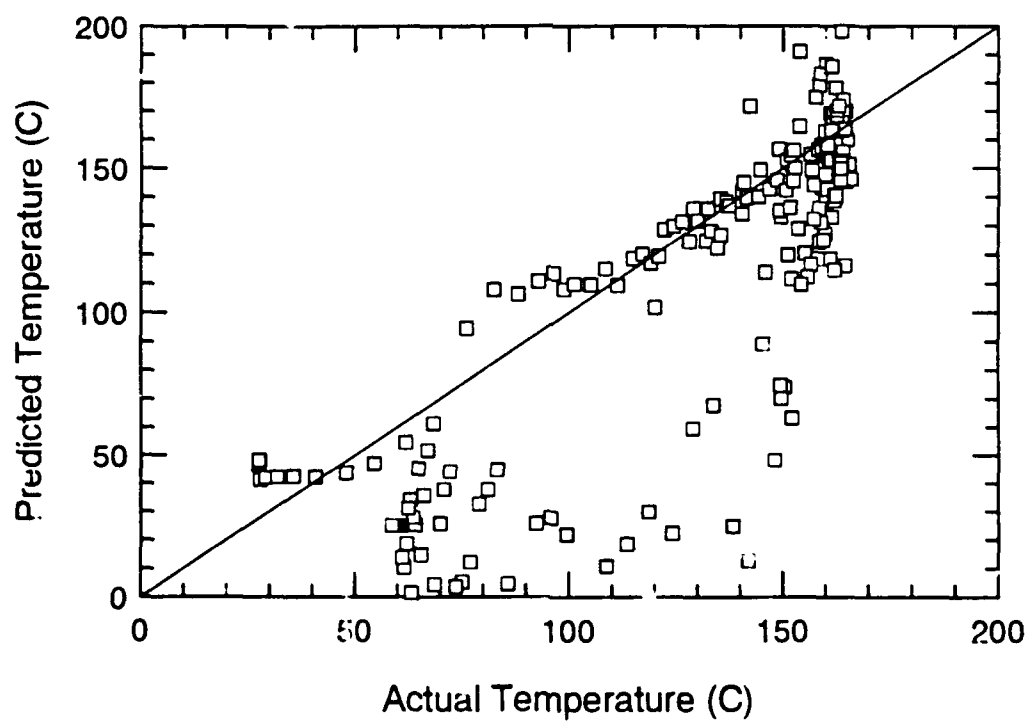
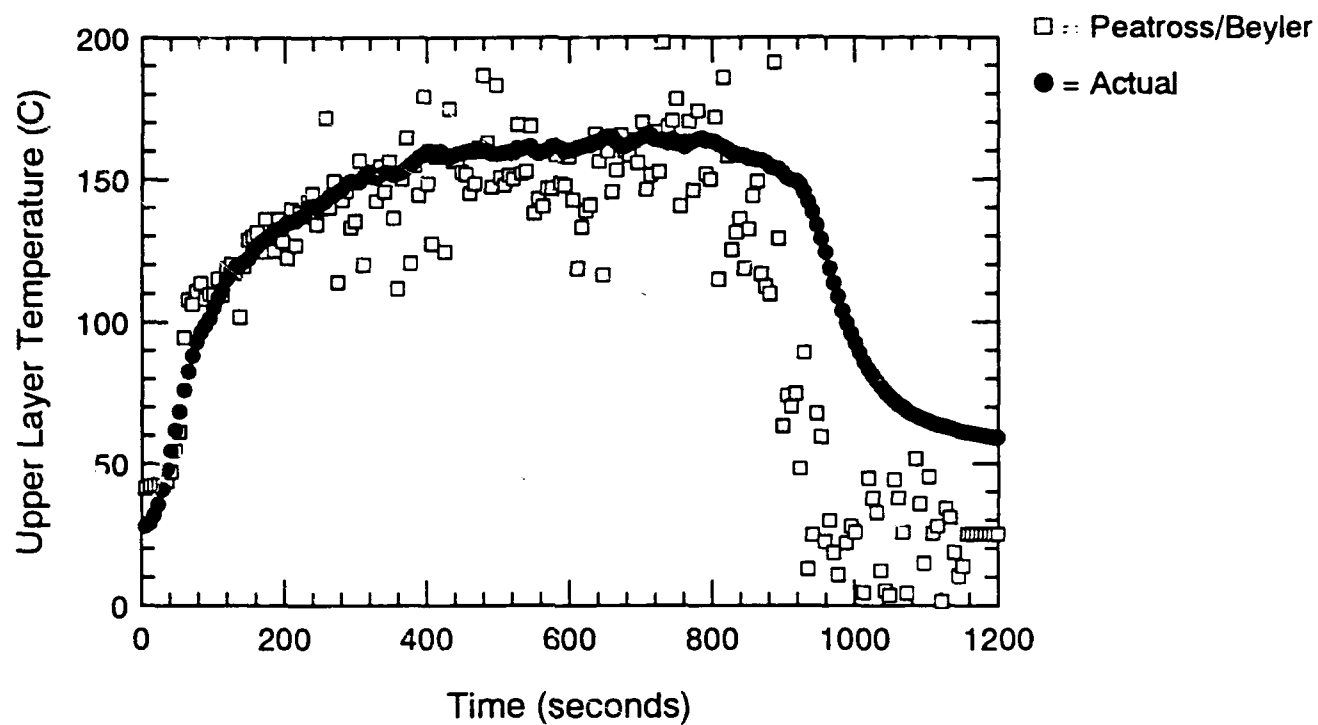


Figure D.7 Temperature Predictions Using Peatross/Beyler Method - S207

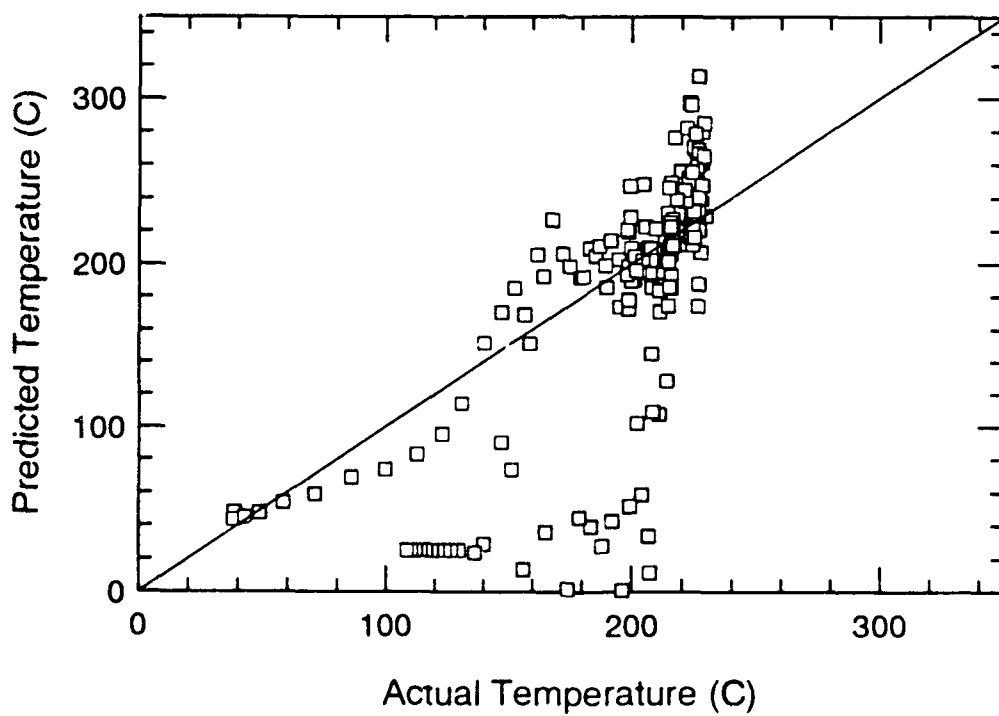
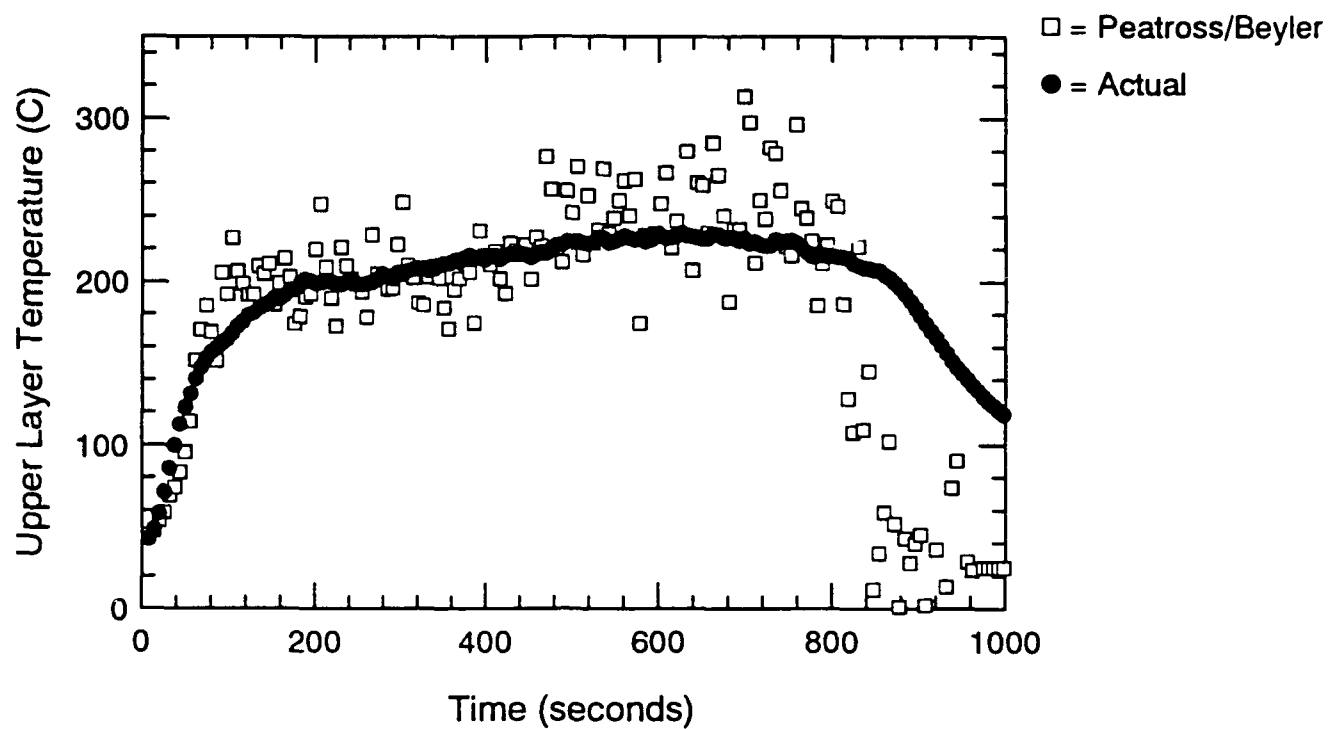


Figure D.8 Temperature Predictions Using Peatross/Beyler Method - S208

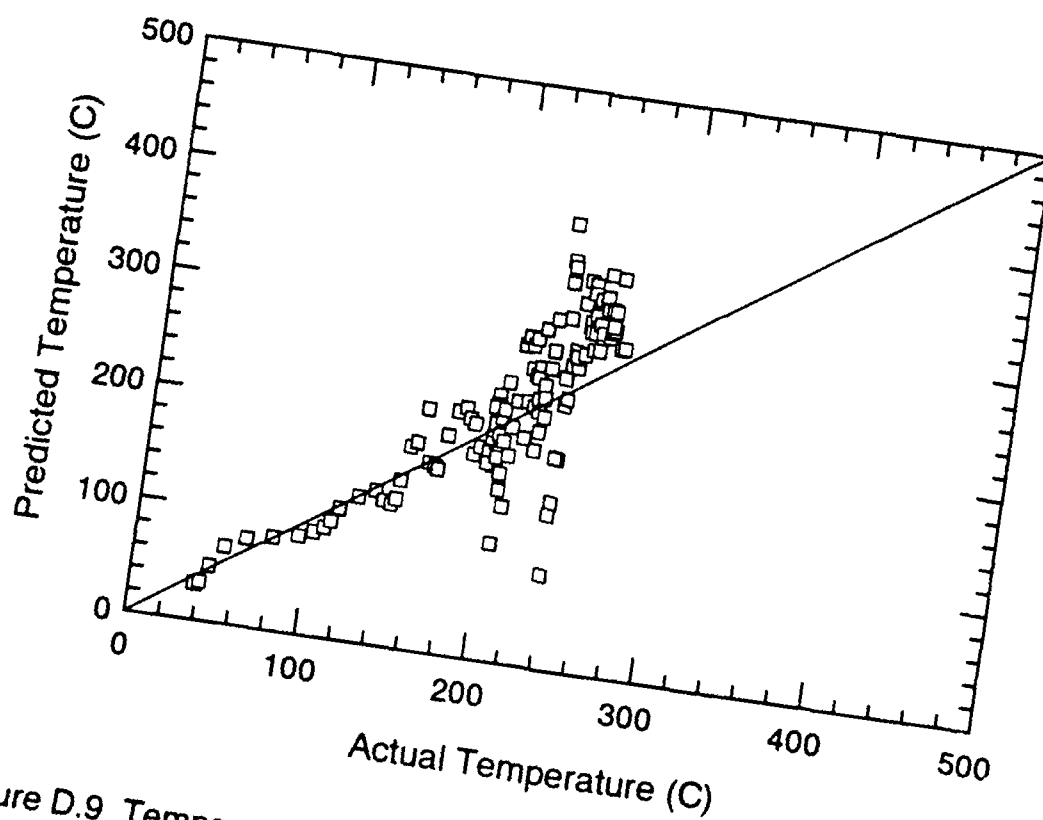
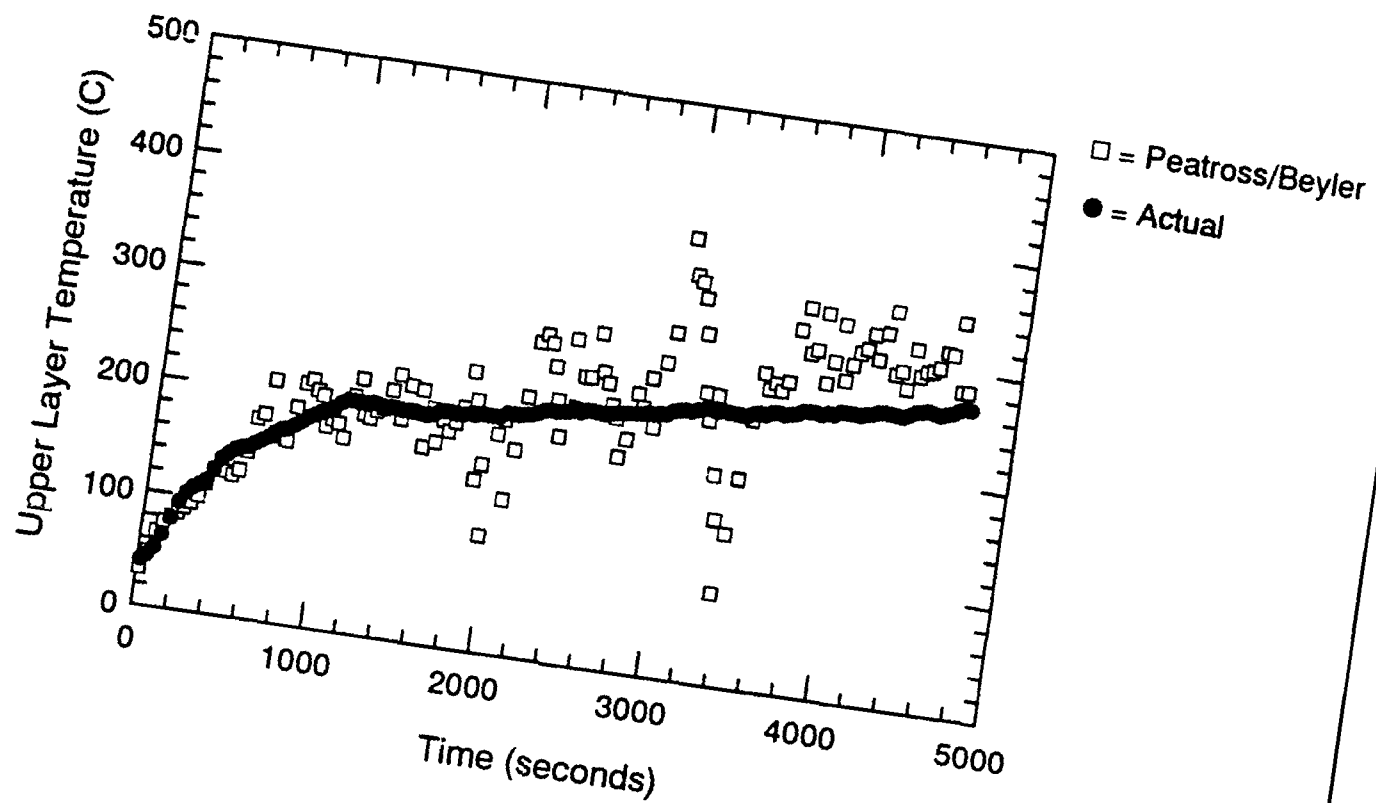


Figure D.9 Temperature Predictions Using Peatross/Beyler Method - S209

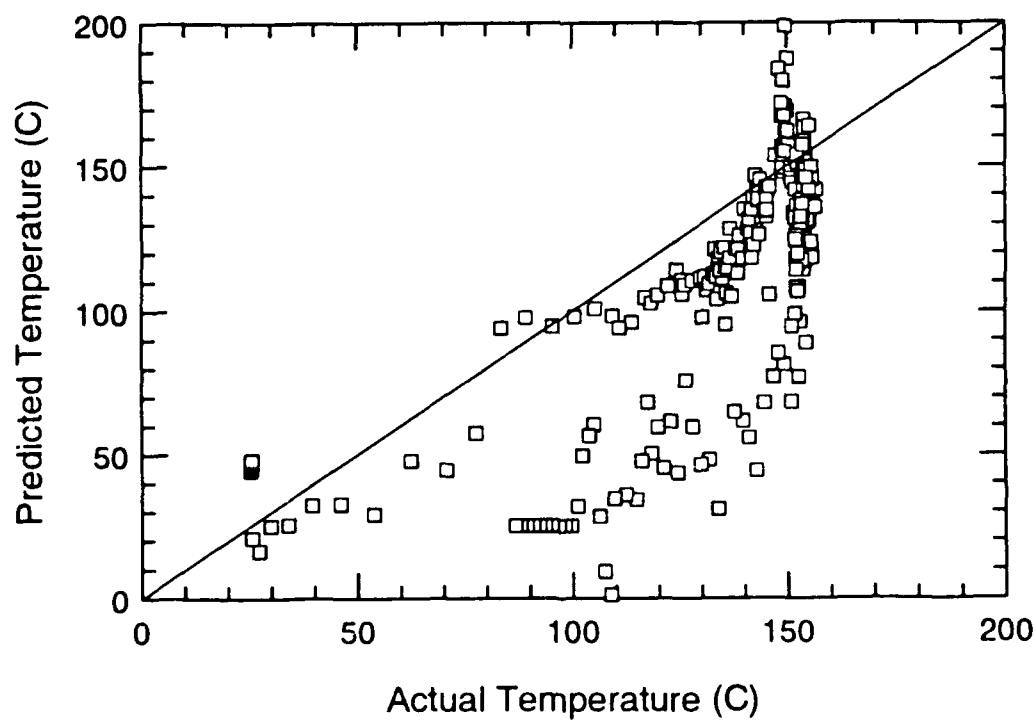
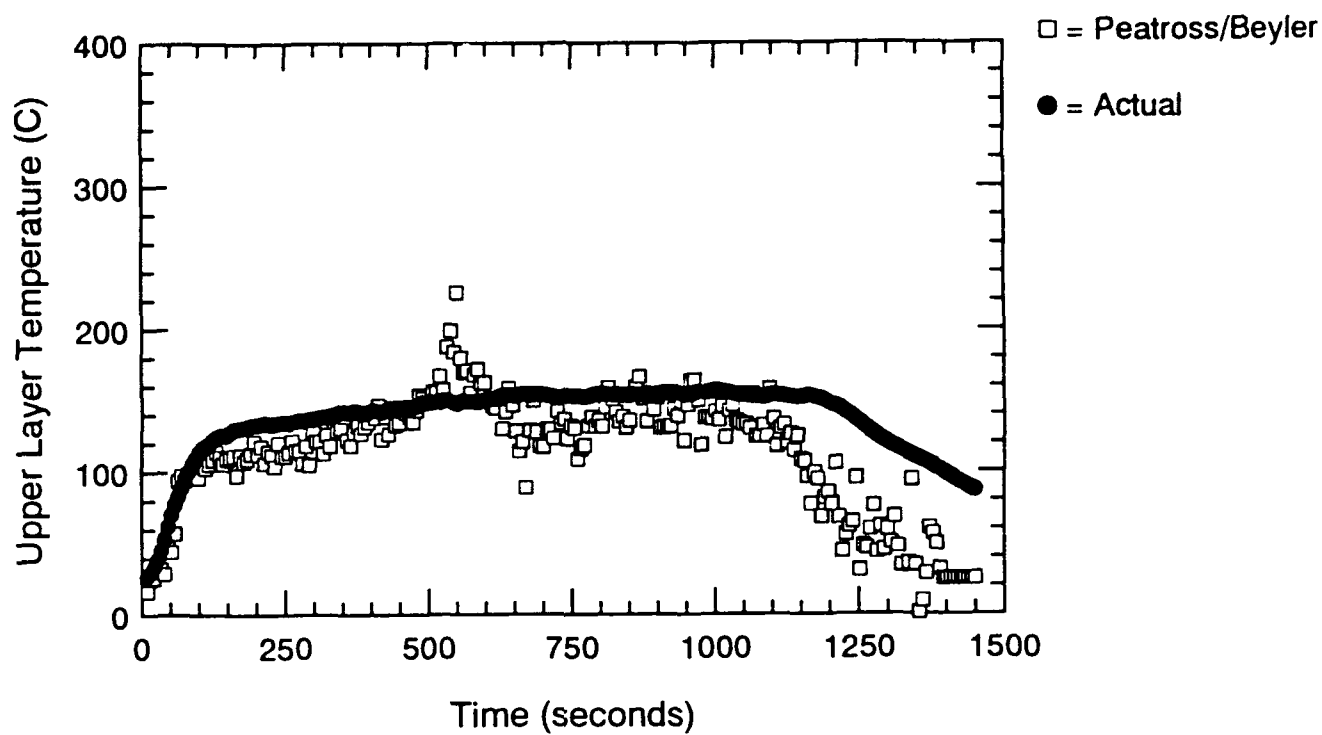


Figure D.10 Temperature Predictions Using Peatross/Beyler Method - S210

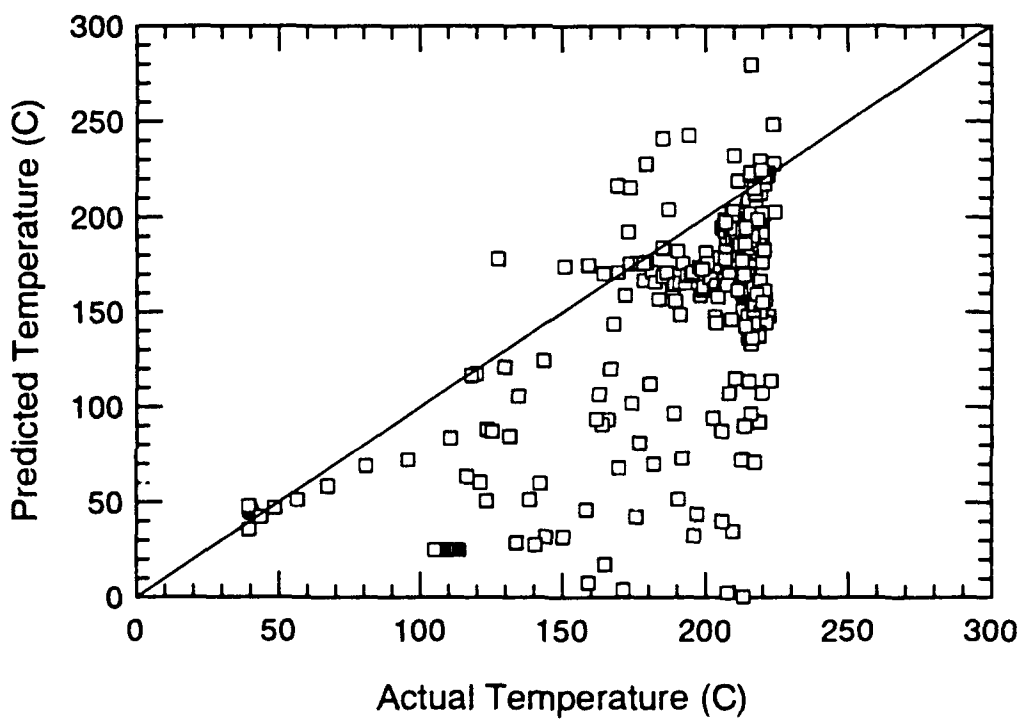
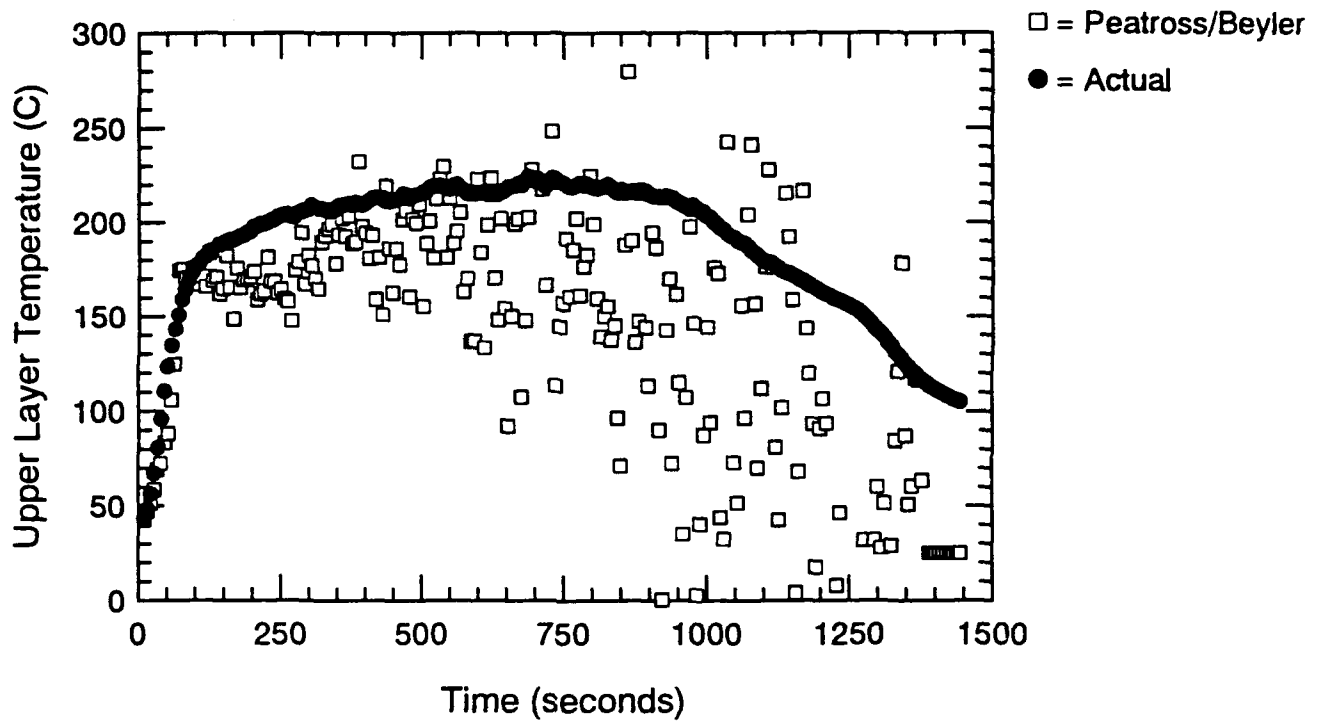


Figure D.11 Temperature Predictions Using Peatross/Beyler Method - S211

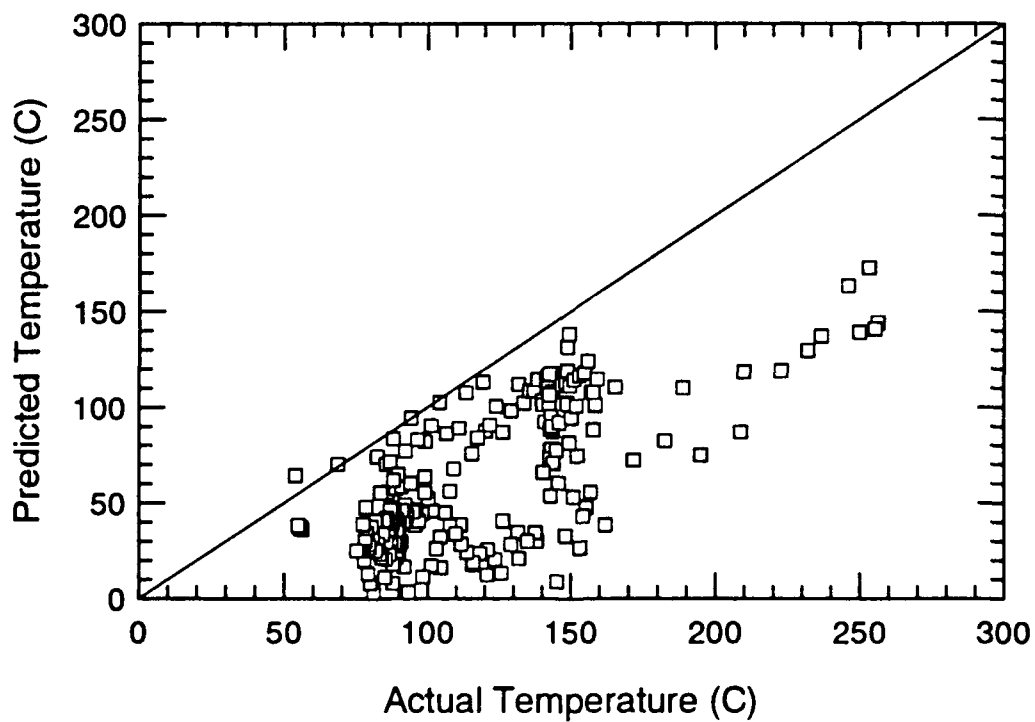
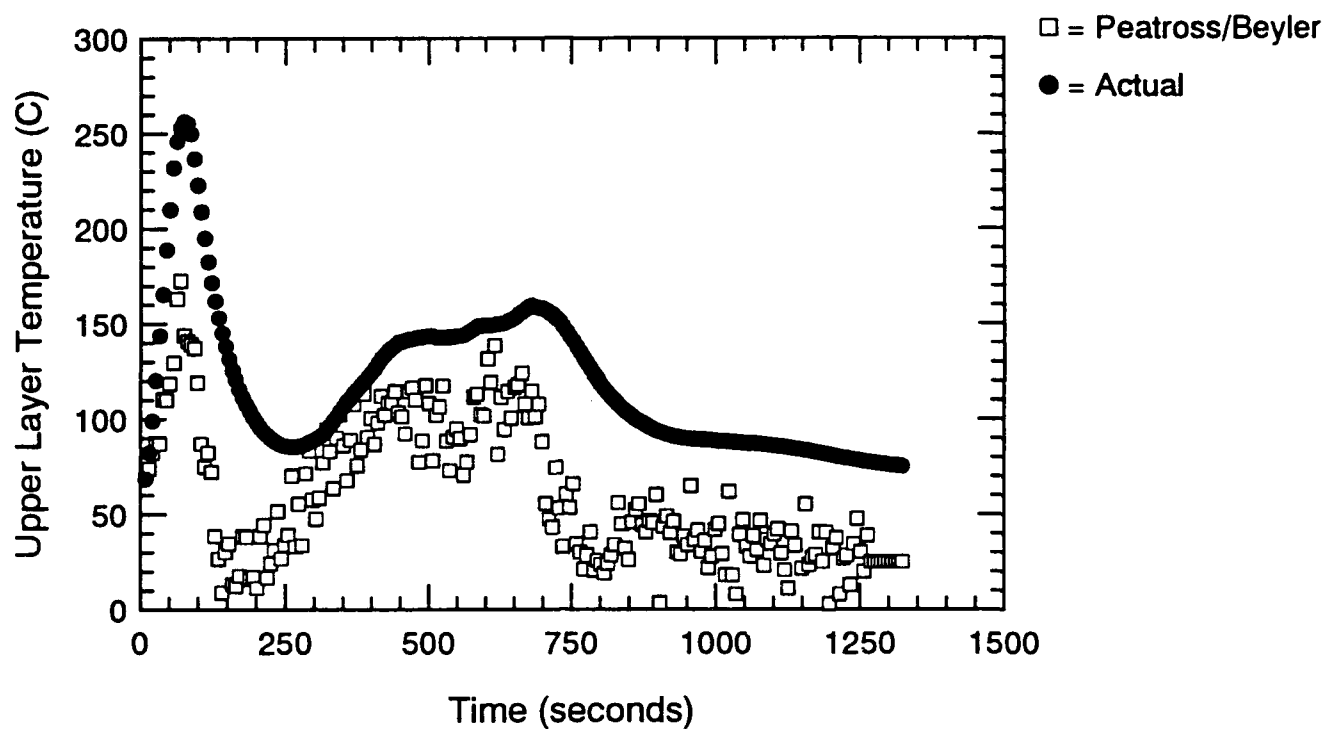


Figure D.12 Temperature Predictions Using Peatross/Beyler Method - S212

APPENDIX E. Deal/Beyler Layer Driven Vent Flow Rate Prediction Method Results

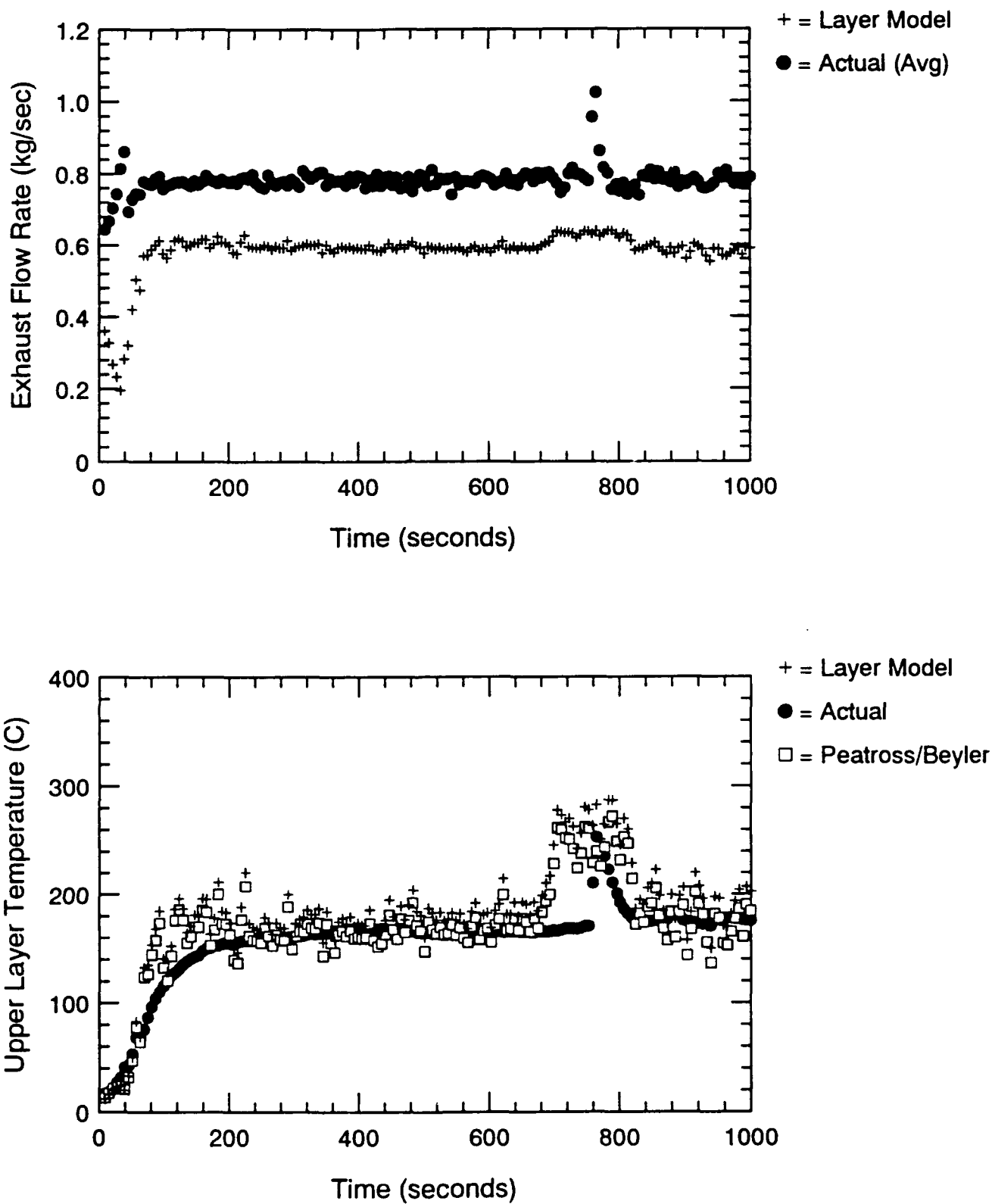


Figure E.1 Vent Flow and Temperature Predictions Using Deal/Beyler Layer Driven Model - S101

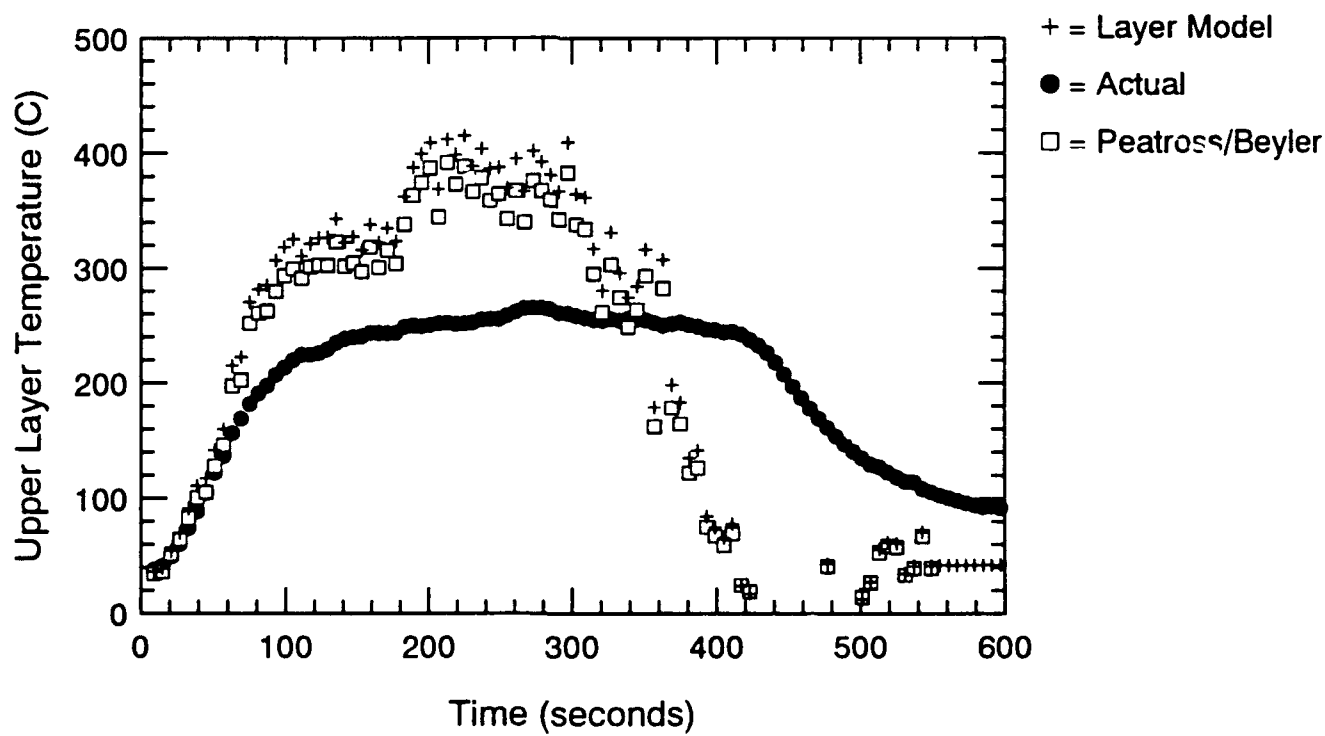
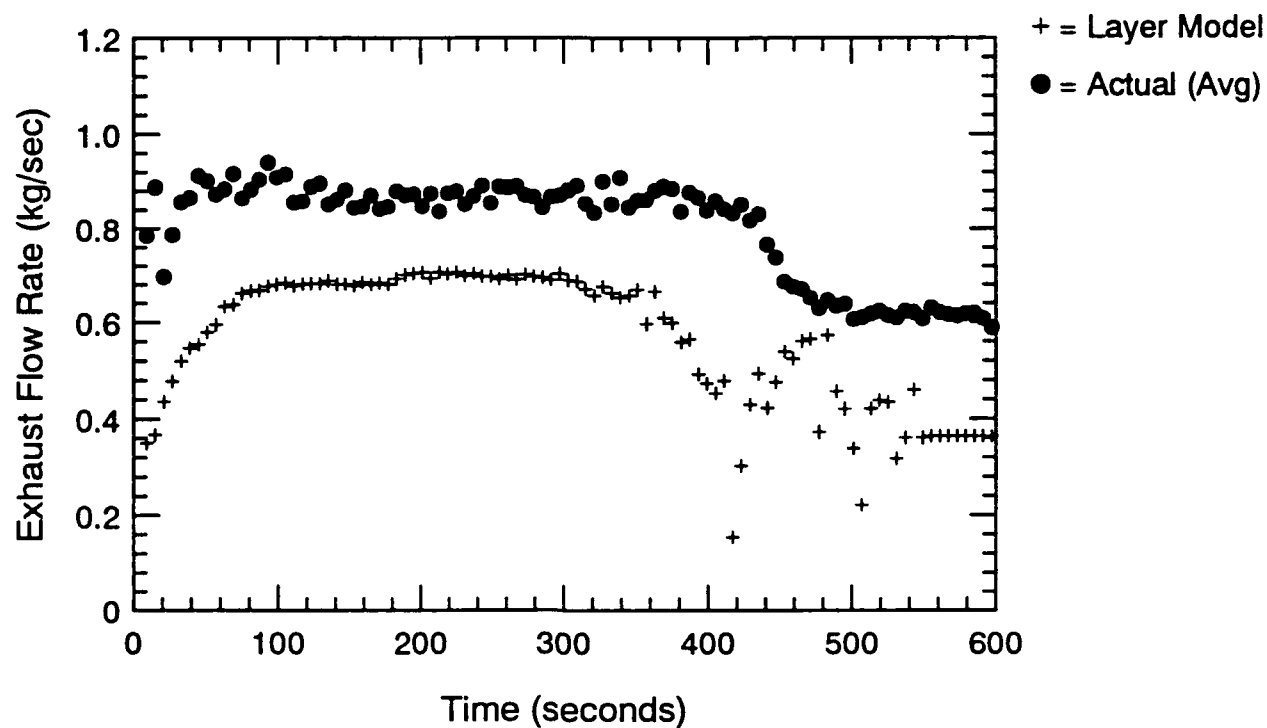


Figure E.2 Vent Flow and Temperature Predictions Using Deal/Beyler Layer Driven Model - S102

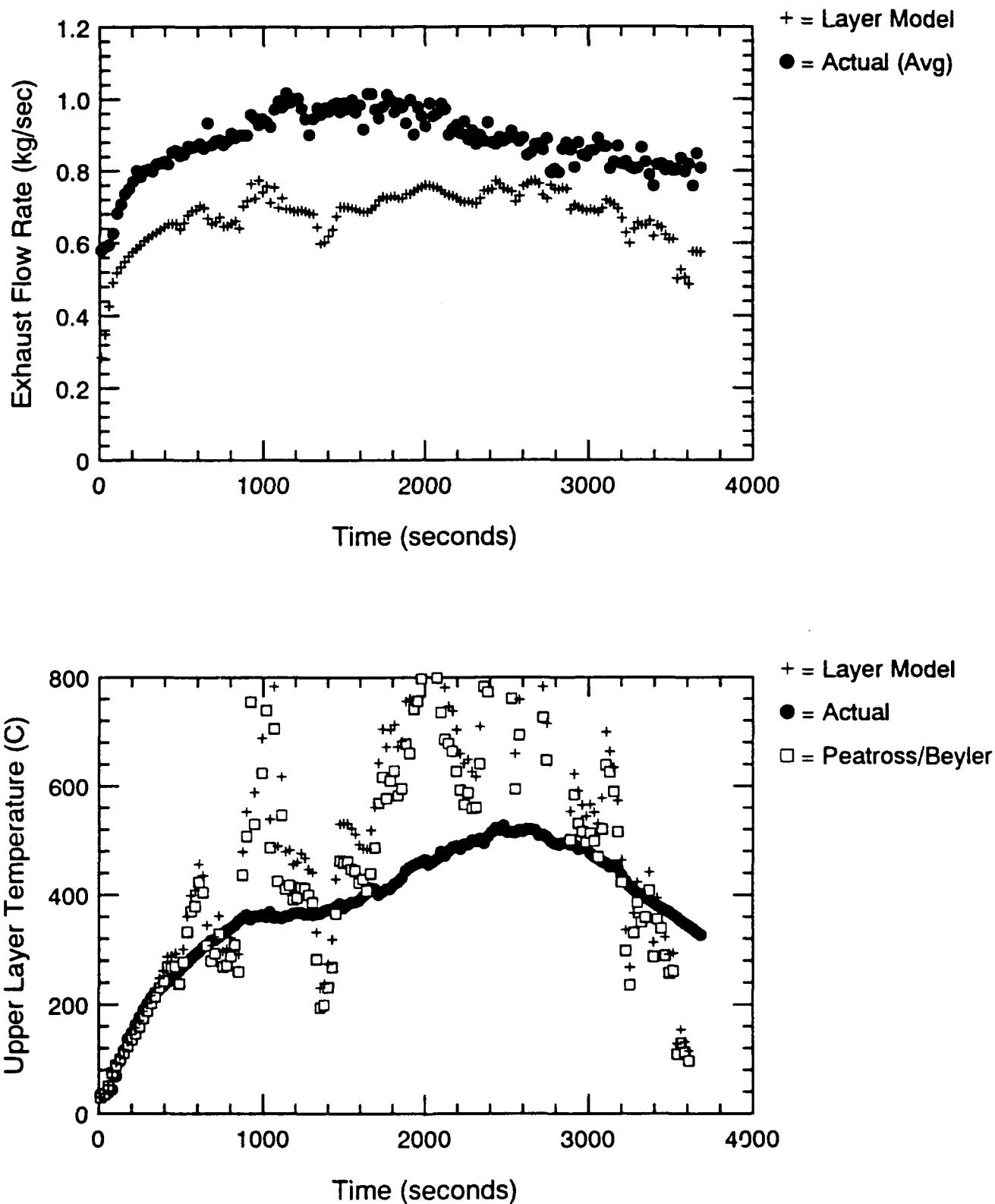


Figure E.3 Vent Flow and Temperature Predictions Using Deal/Beyler Layer Driven Model - S103

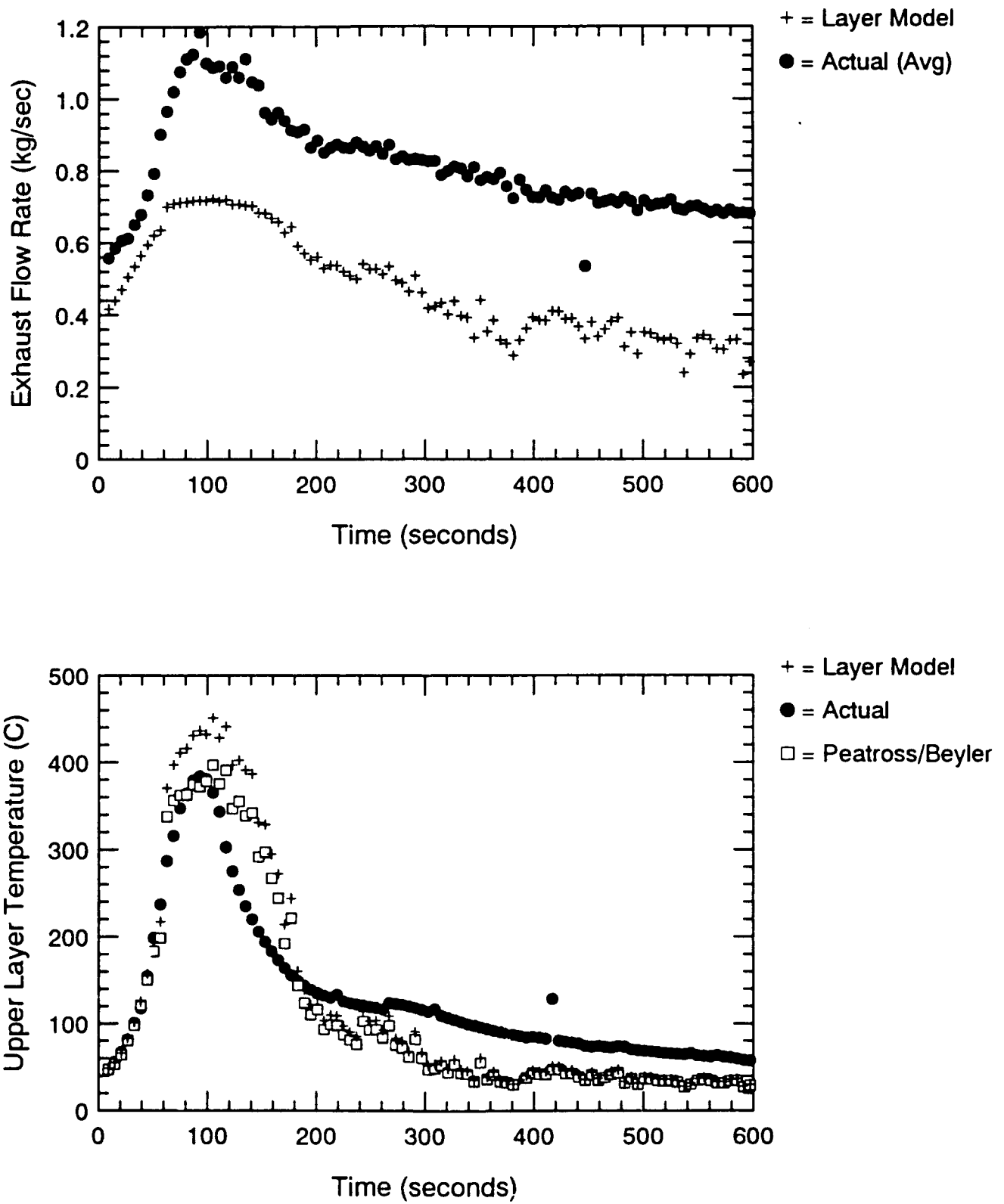


Figure E.4 Vent Flow and Temperature Predictions Using Deal/Beyler Layer Driven Model - S104

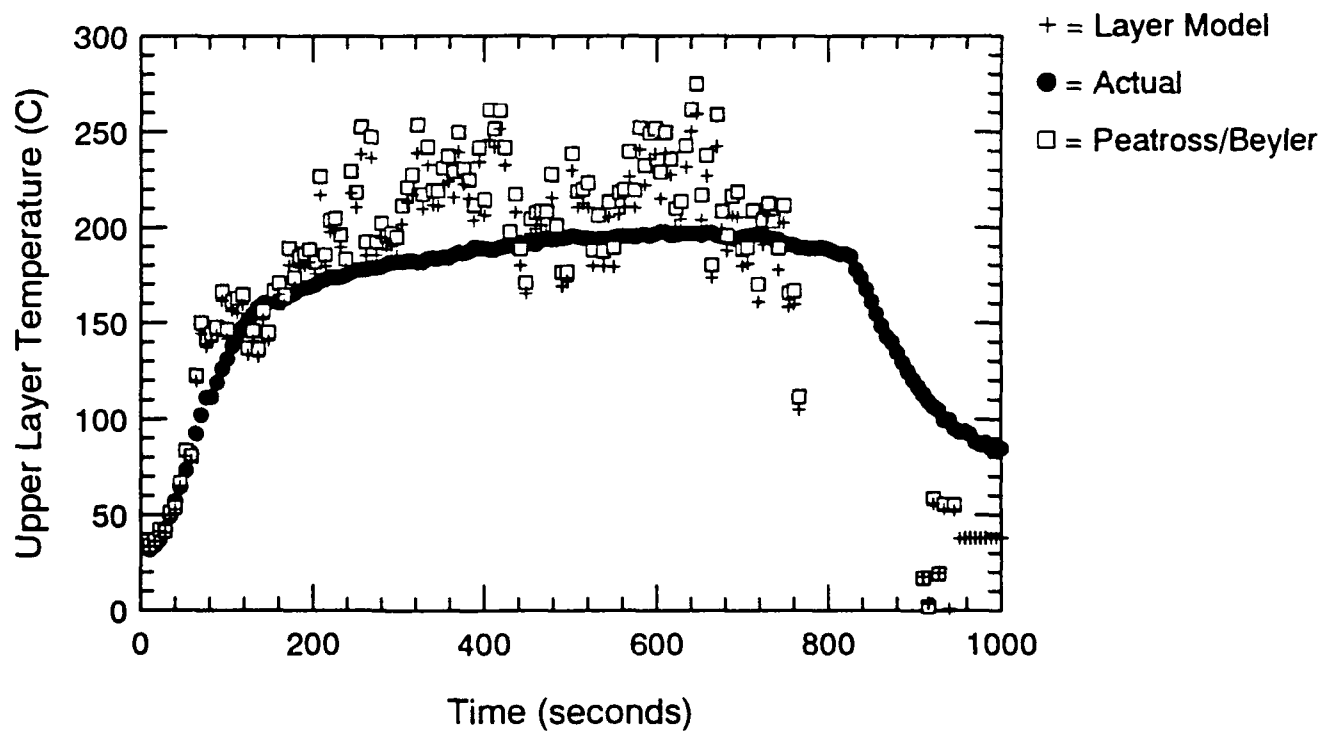
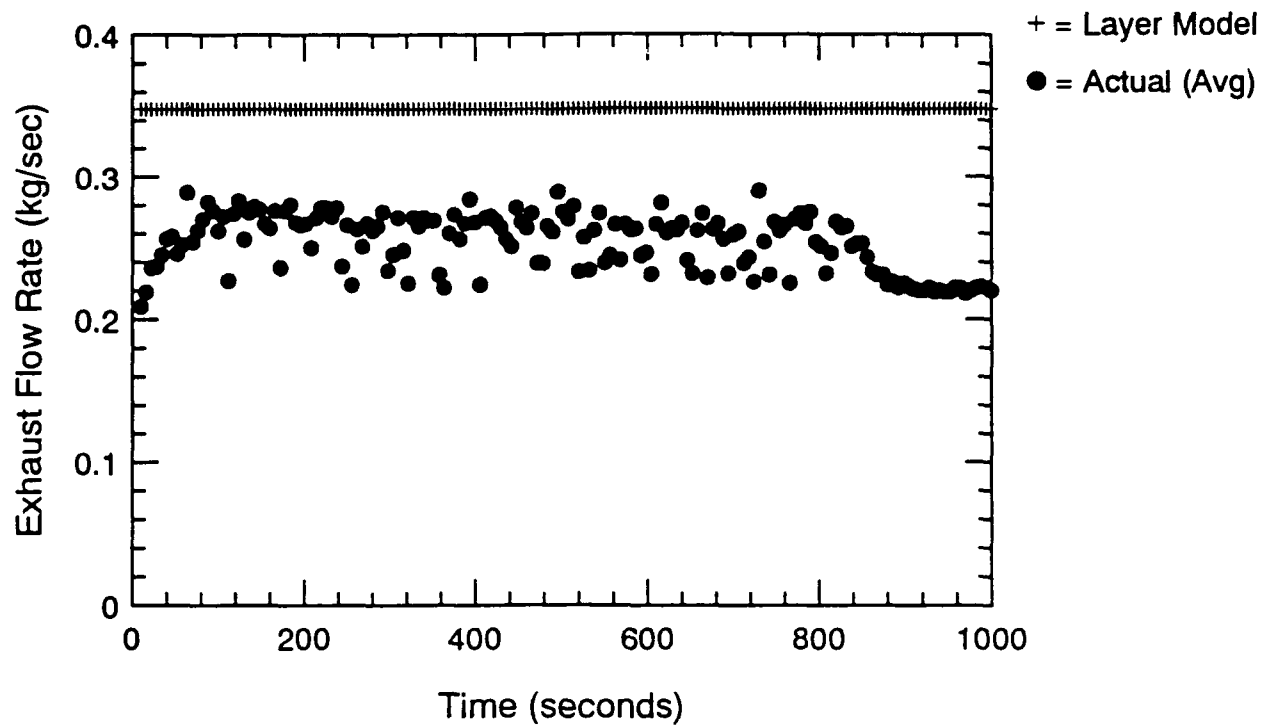


Figure E.5 Vent Flow and Temperature Predictions Using Deal/Beyler Layer Driven Model - S105

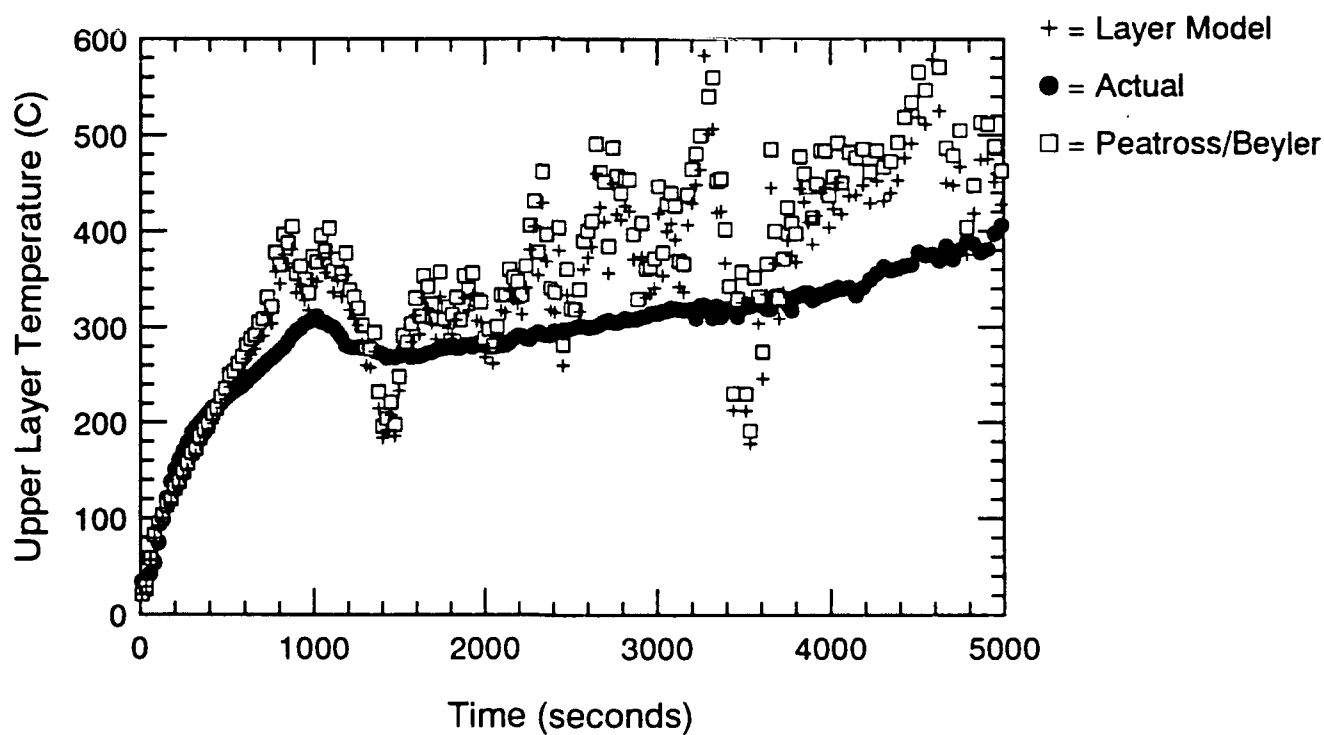
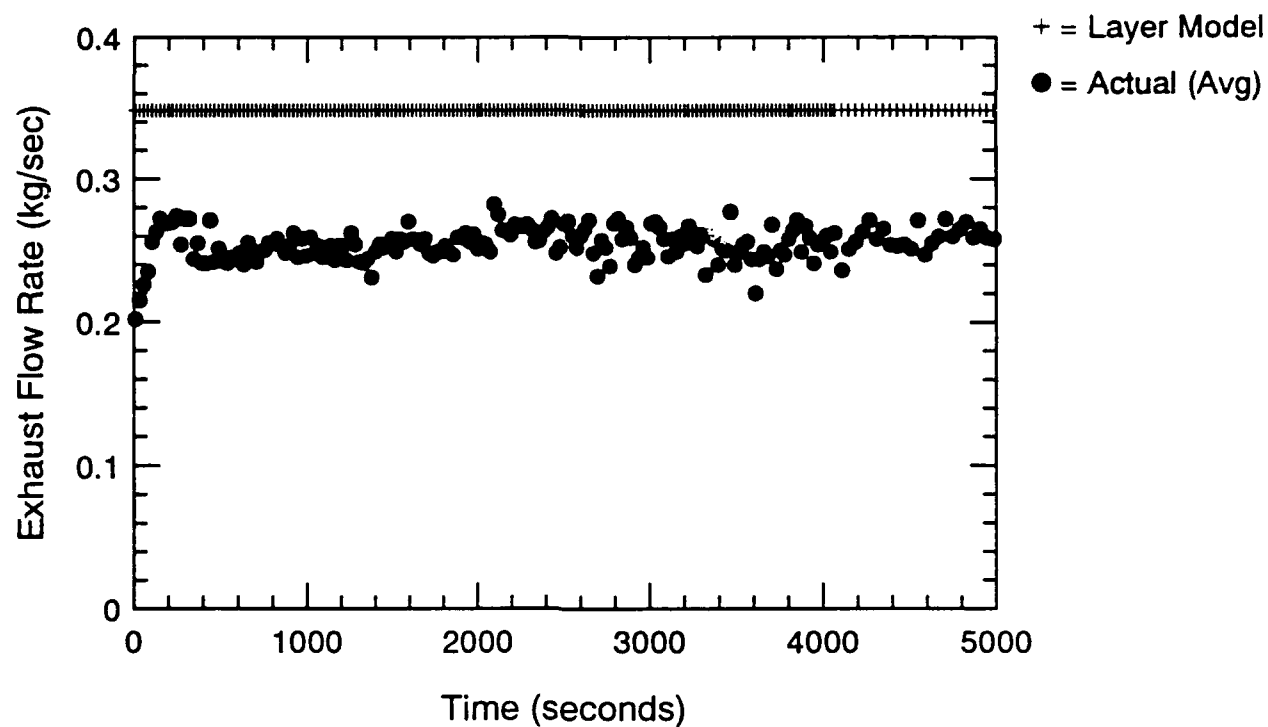


Figure E.6 Vent Flow and Temperature Predictions Using Deal/Beyler Layer Driven Model - S106

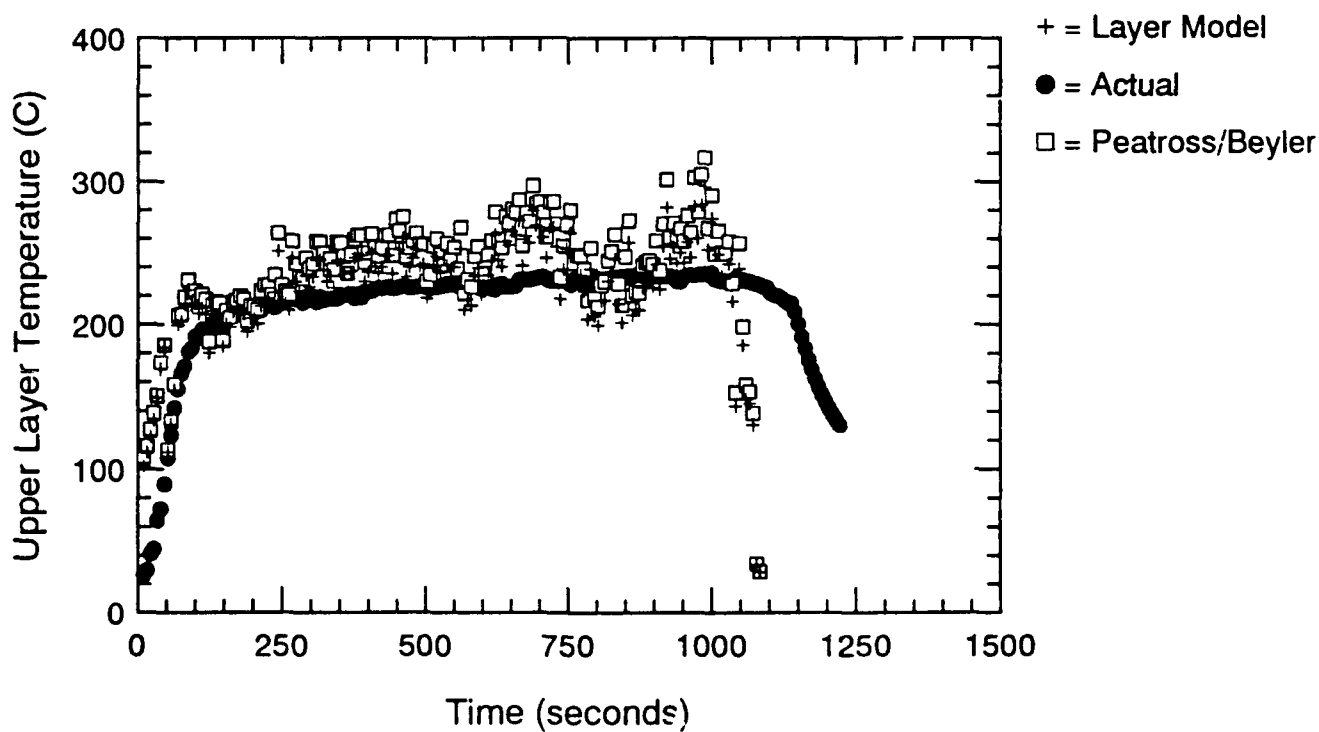
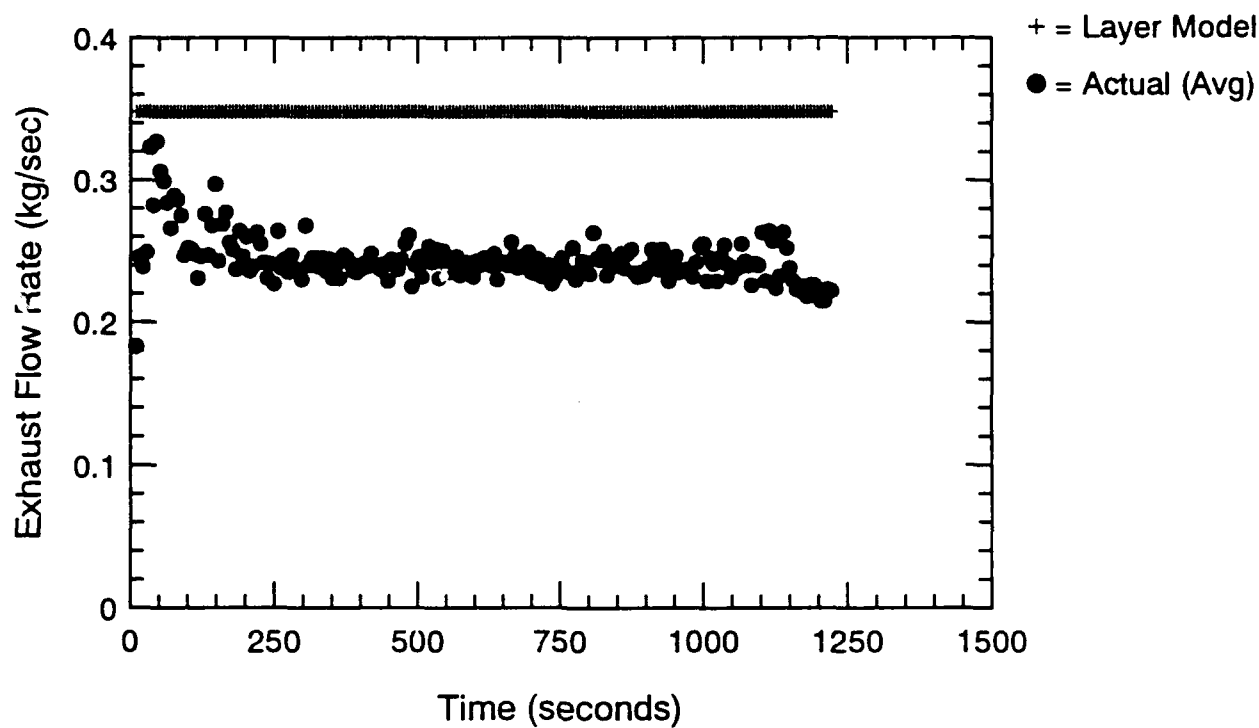


Figure E.7 Vent Flow and Temperature Predictions Using Deal/Beyler Layer Driven Model - S107

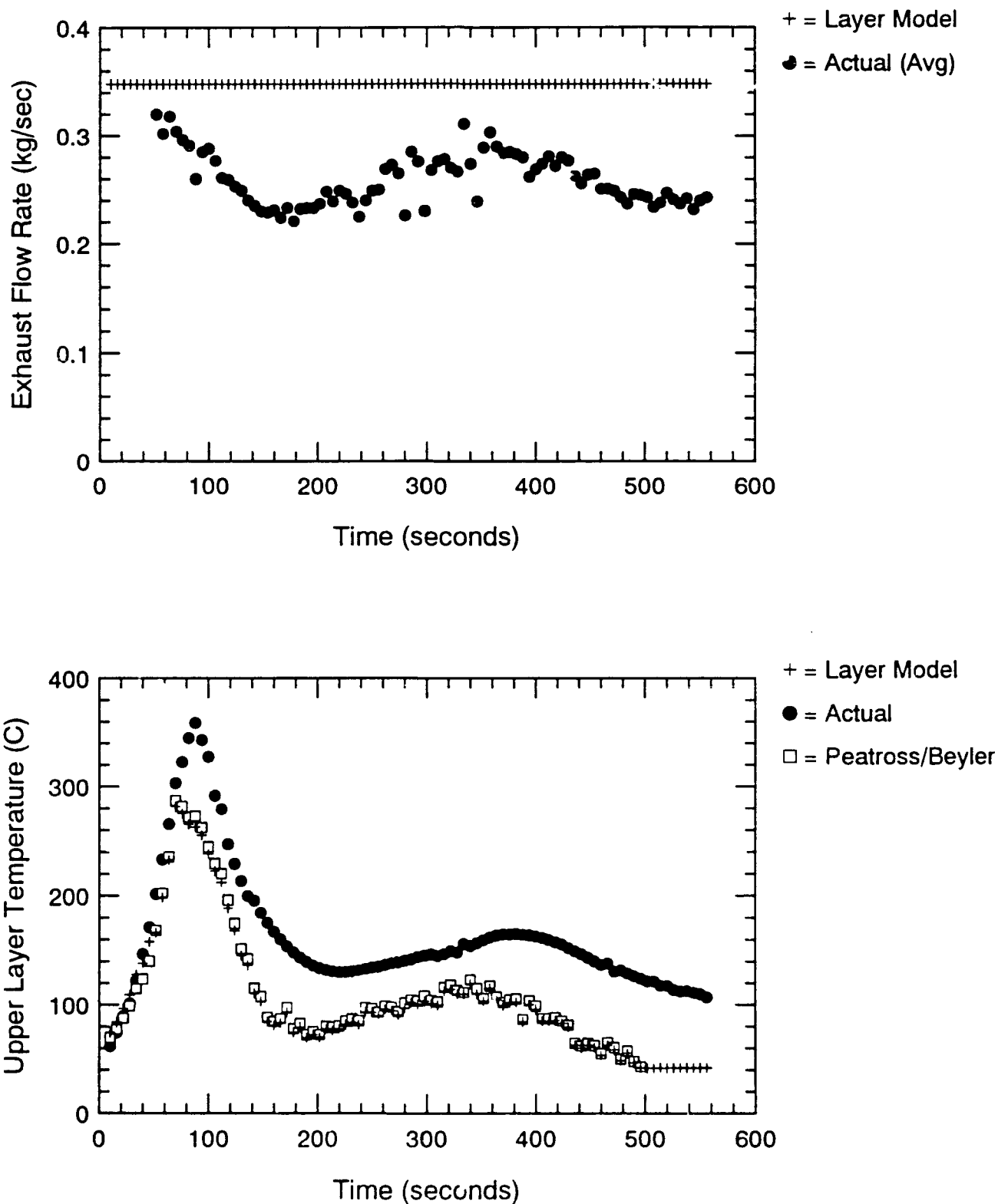


Figure E.8 Vent Flow and Temperature Predictions Using Deal/Beyler Layer Driven Model - S108

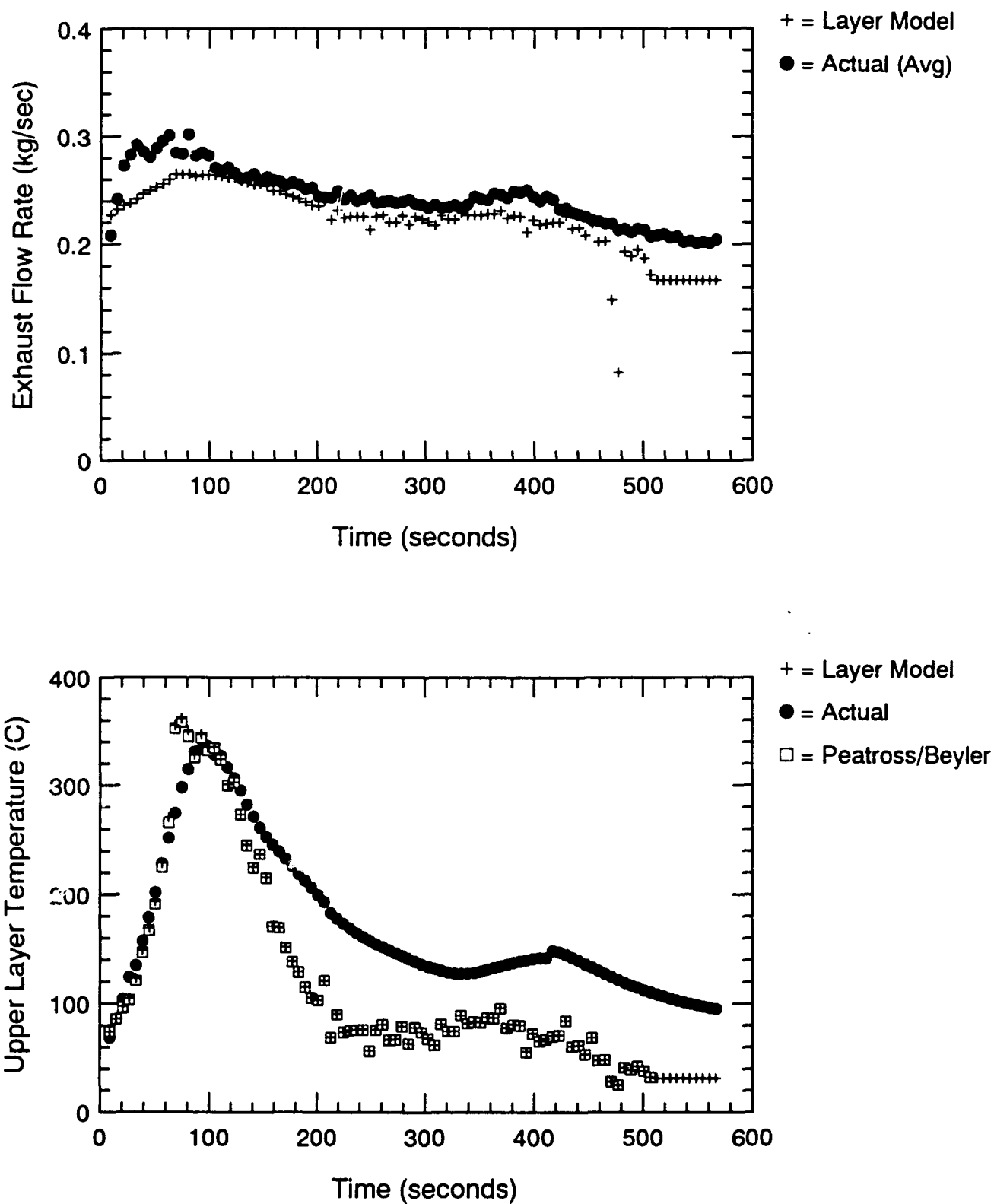


Figure E.9 Vent Flow and Temperature Predictions Using Deal/Beyler Layer Driven Model - S109

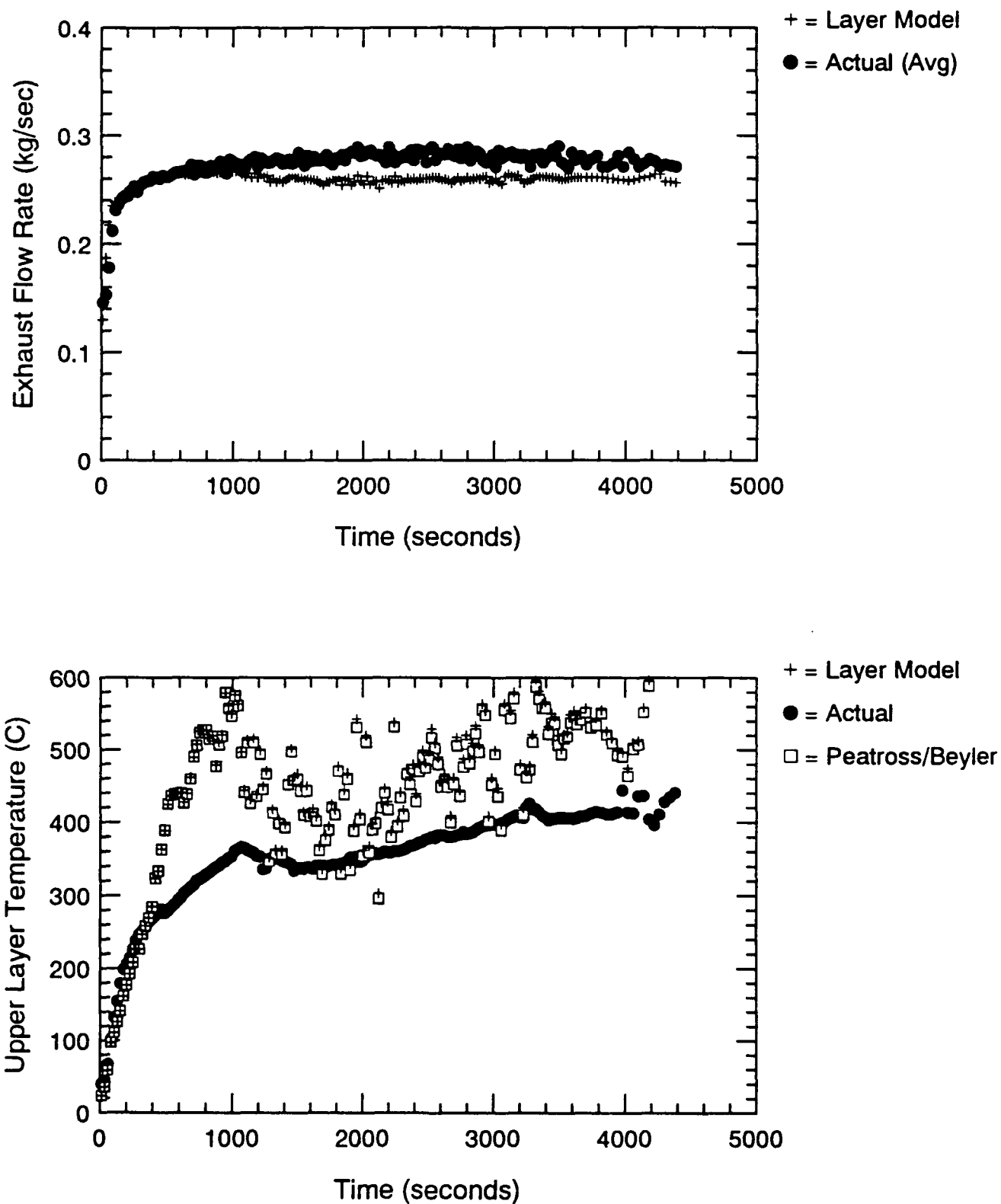


Figure E.10 Vent Flow and Temperature Predictions Using Deal/Beyler Layer Driven Model - S110

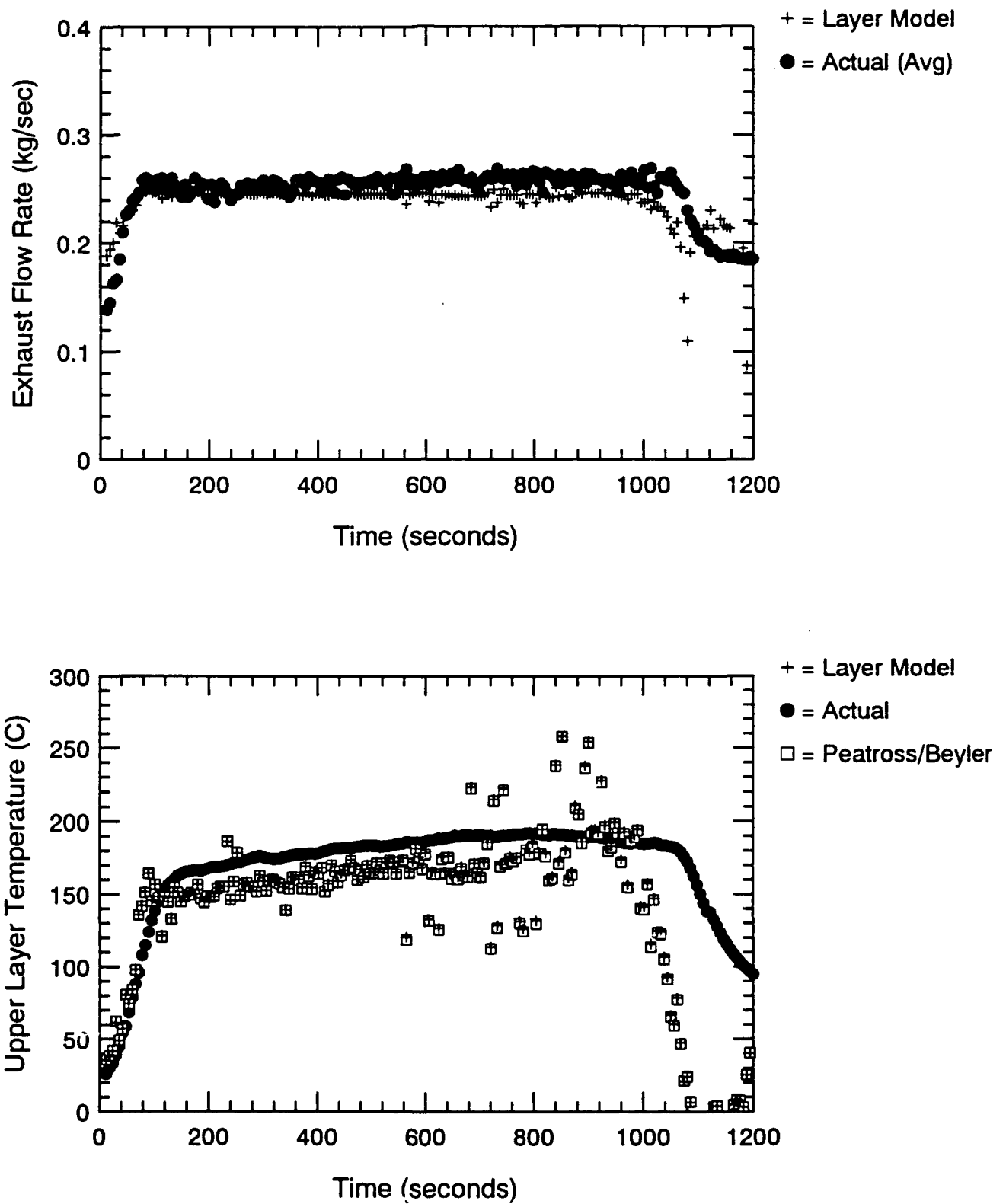


Figure E.11 Vent Flow and Temperature Predictions Using Deal/Beyler Layer Driven Model - S111

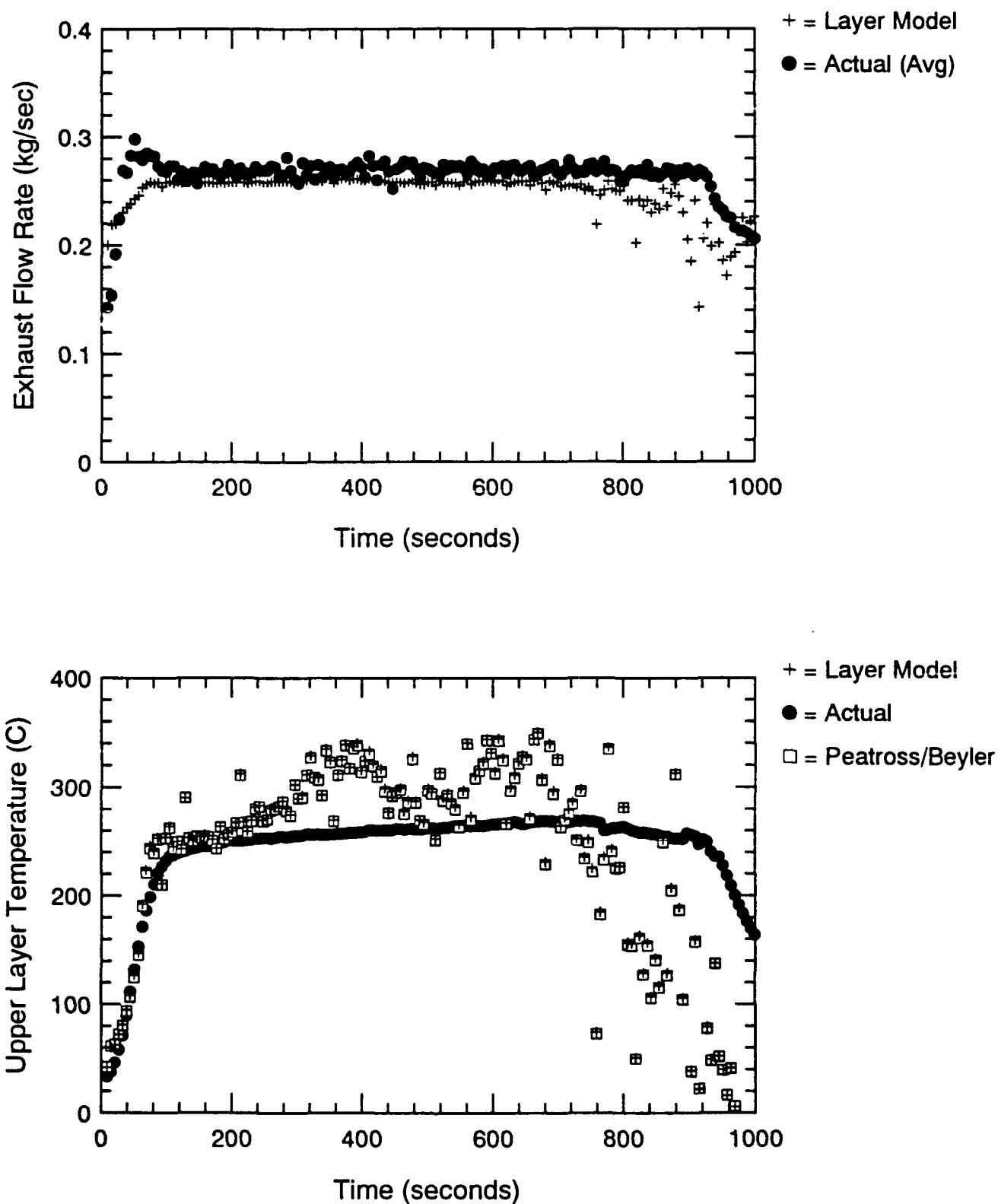


Figure E.12 Vent Flow and Temperature Predictions Using Deal/Beyler Layer Driven Model - S112

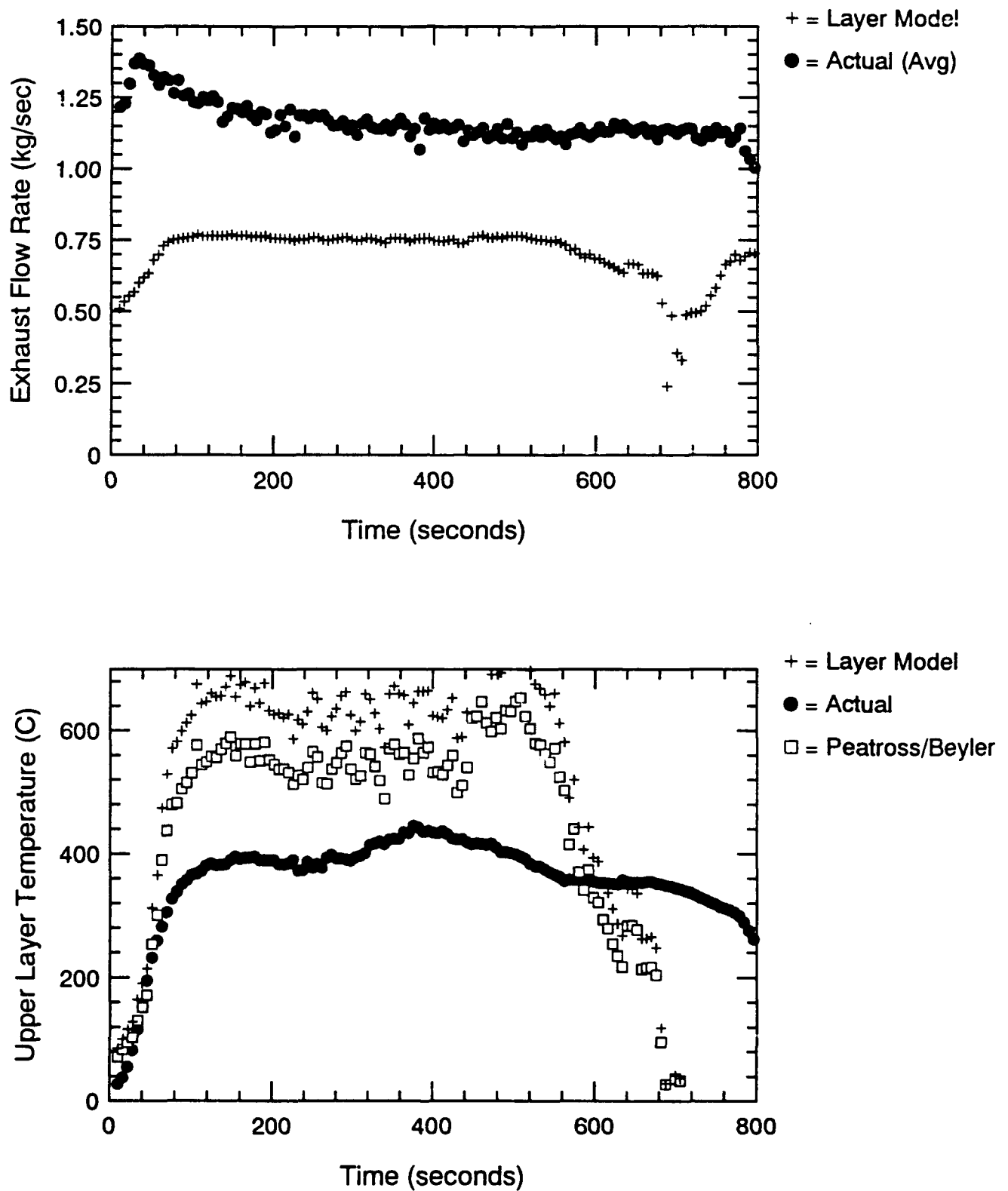


Figure E.13 Vent Flow and Temperature Predictions Using Deal/Beyler Layer Driven Model - ADD1

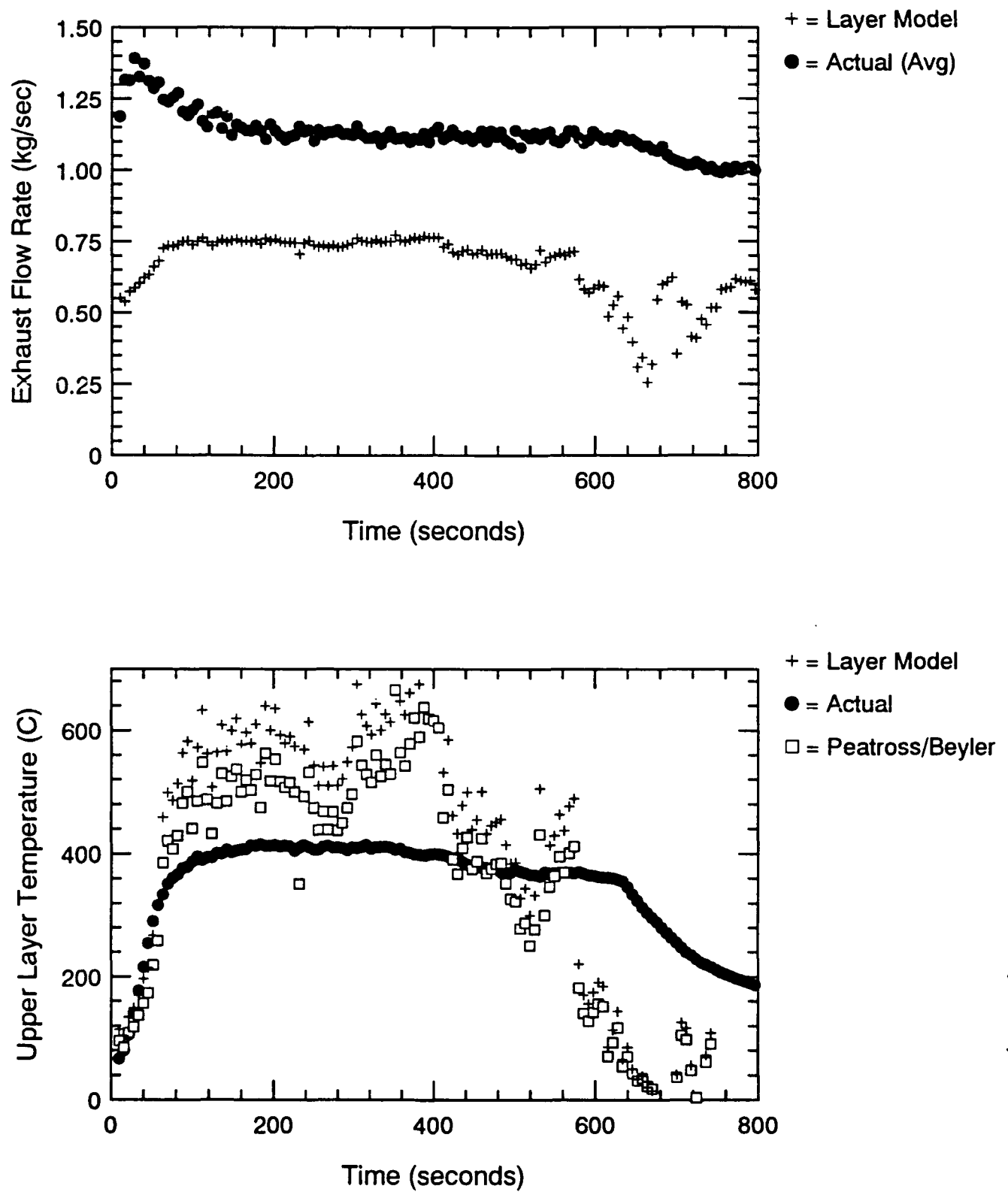


Figure E.14 Vent Flow and Temperature Predictions Using Deal/Beyler Layer Driven Model - ADD2

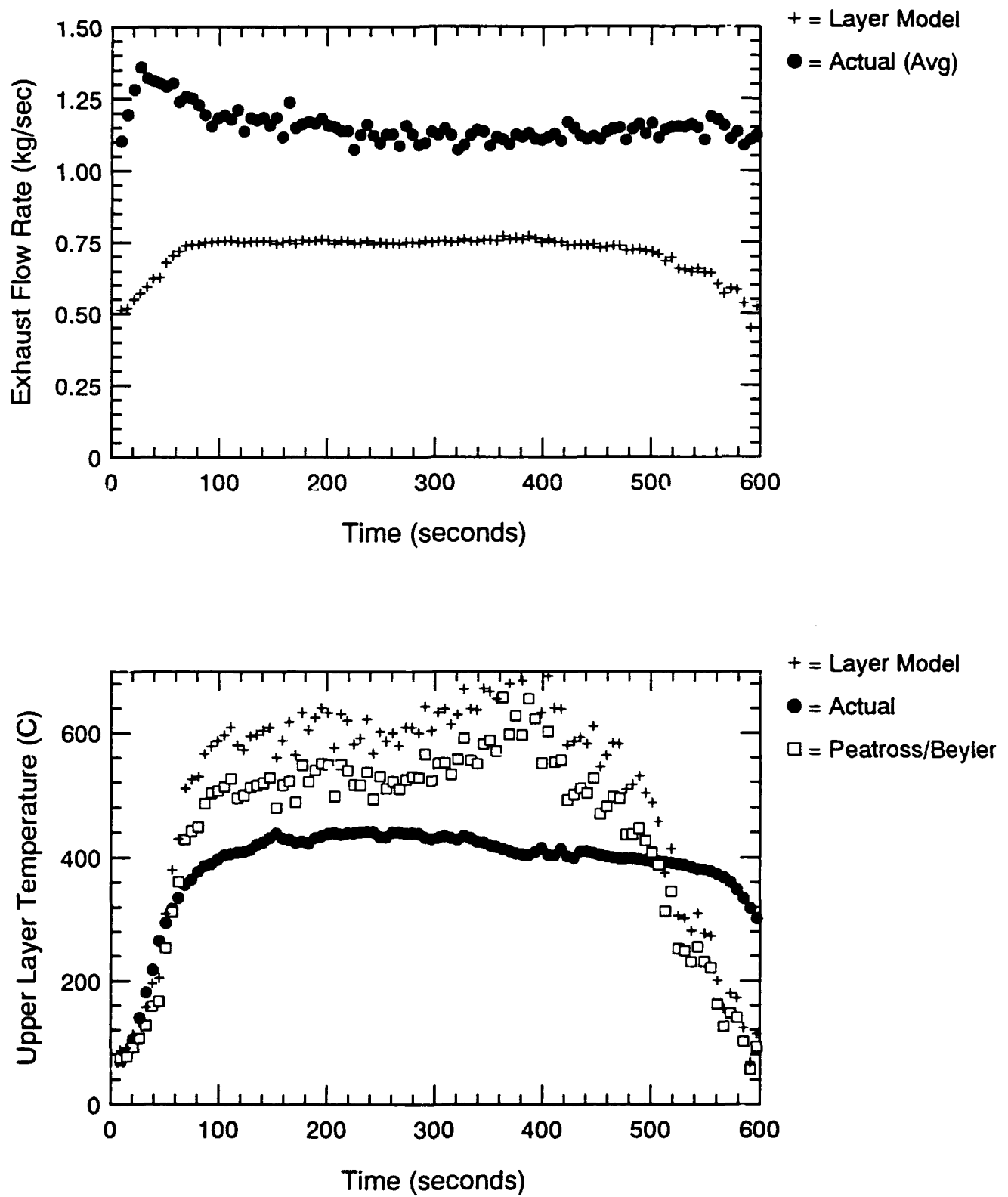


Figure E.15 Vent Flow and Temperature Predictions Using Deal/Beyler Layer Driven Model - ADD3

APPENDIX F. Mowrer Vent Flow Rate Prediction Method Results

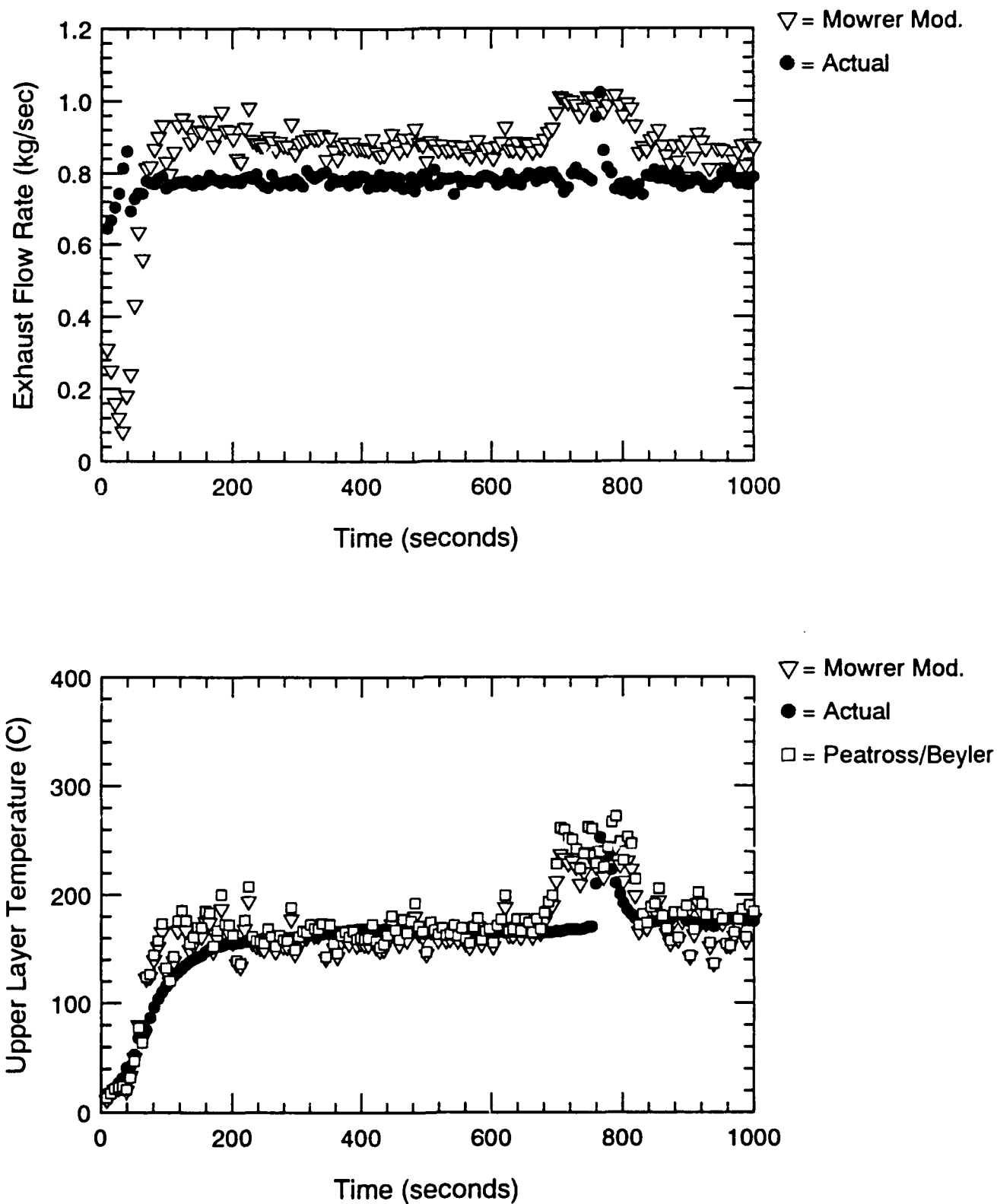


Figure F.1 Vent Flow and Temperature Predictions Using Mowrer Model - S101

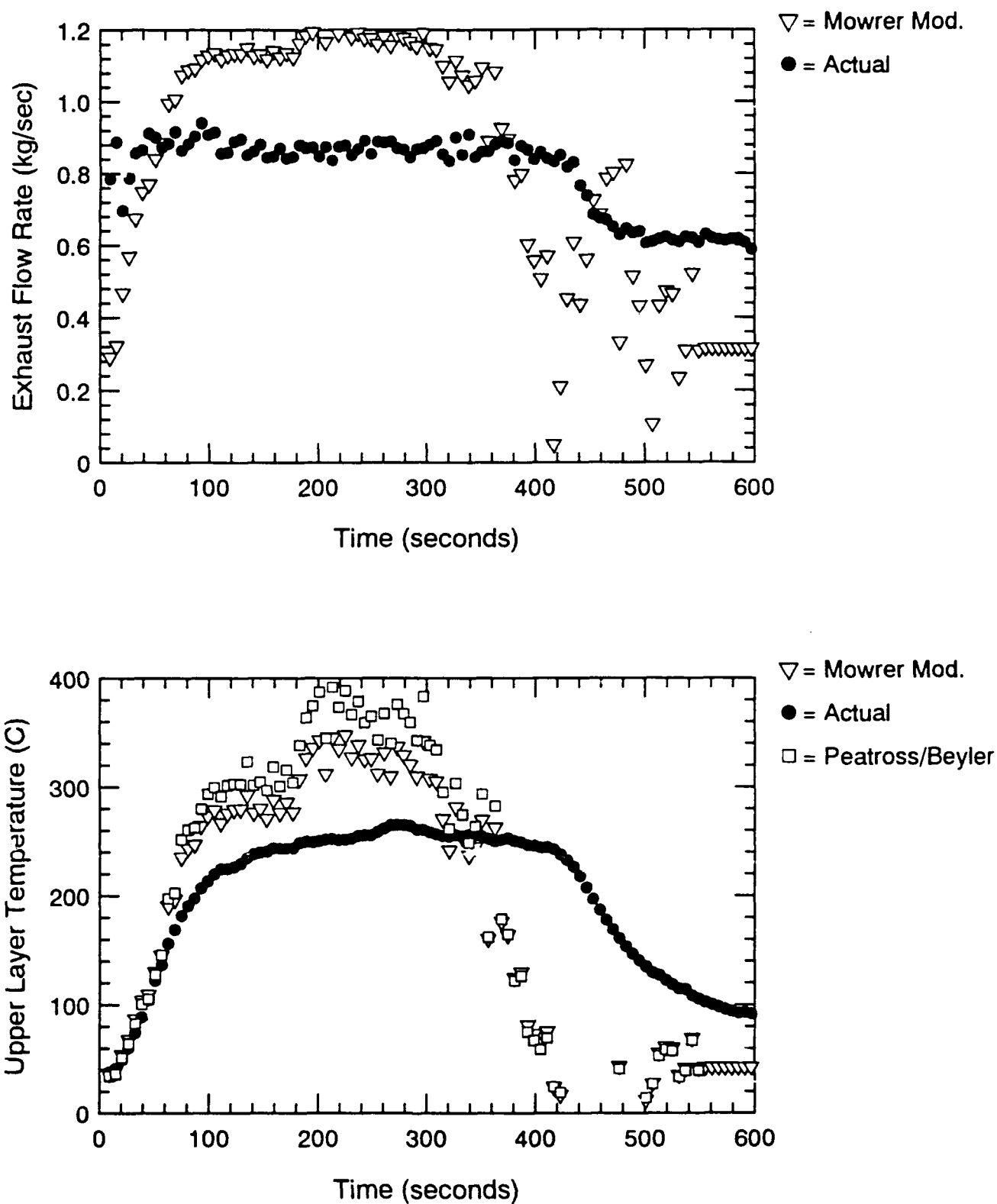


Figure F.2 Vent Flow and Temperature Predictions Using Mowrer Model - S102

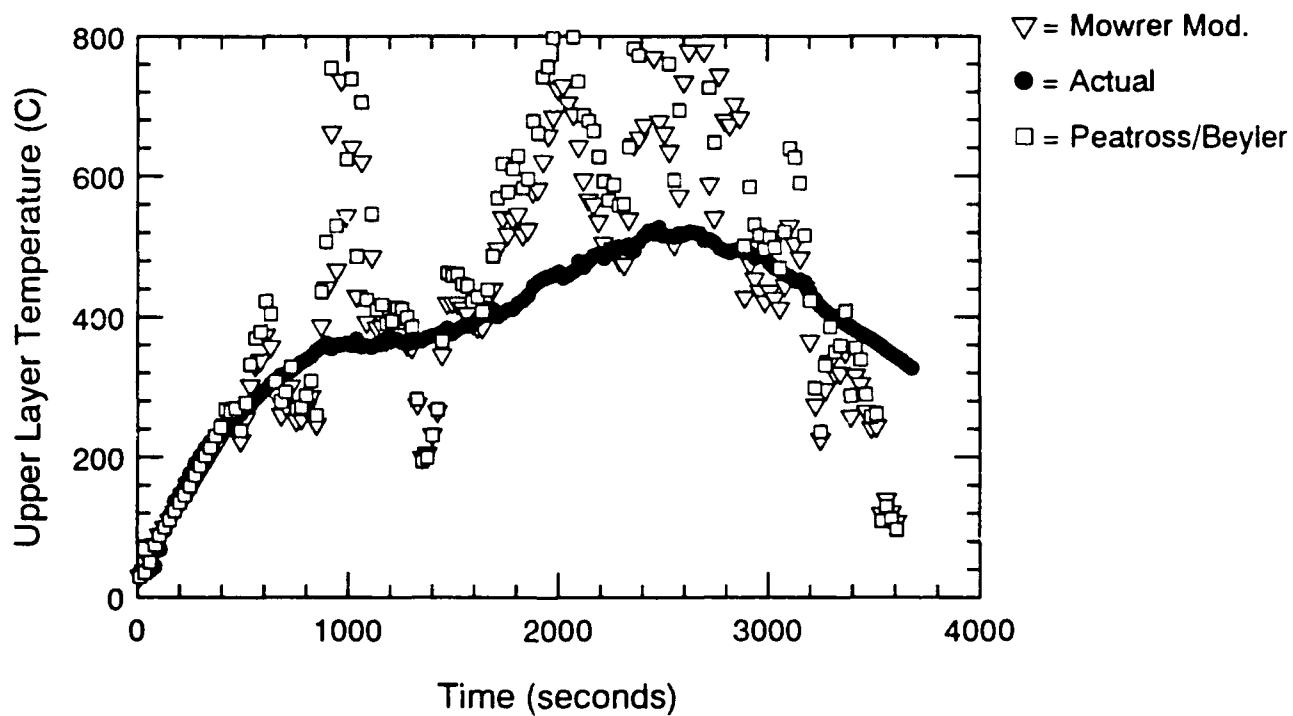
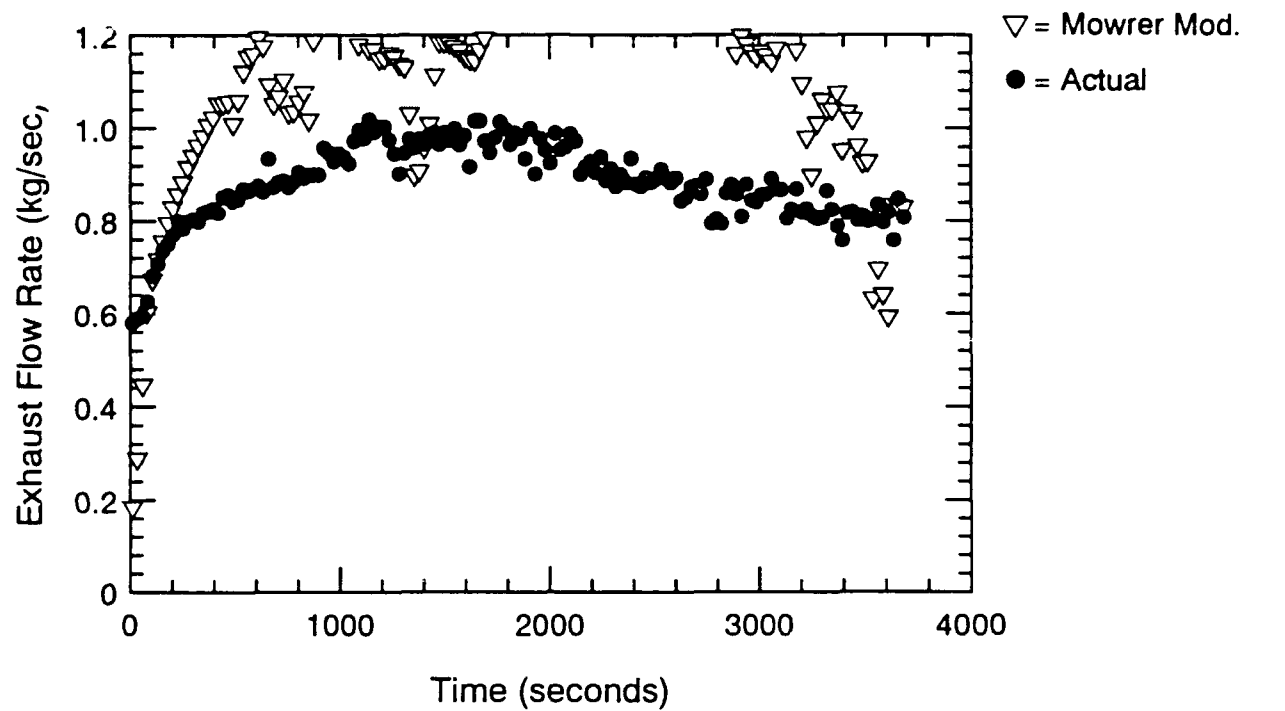


Figure F.3 Vent Flow and Temperature Predictions Using Mowrer Model - S103

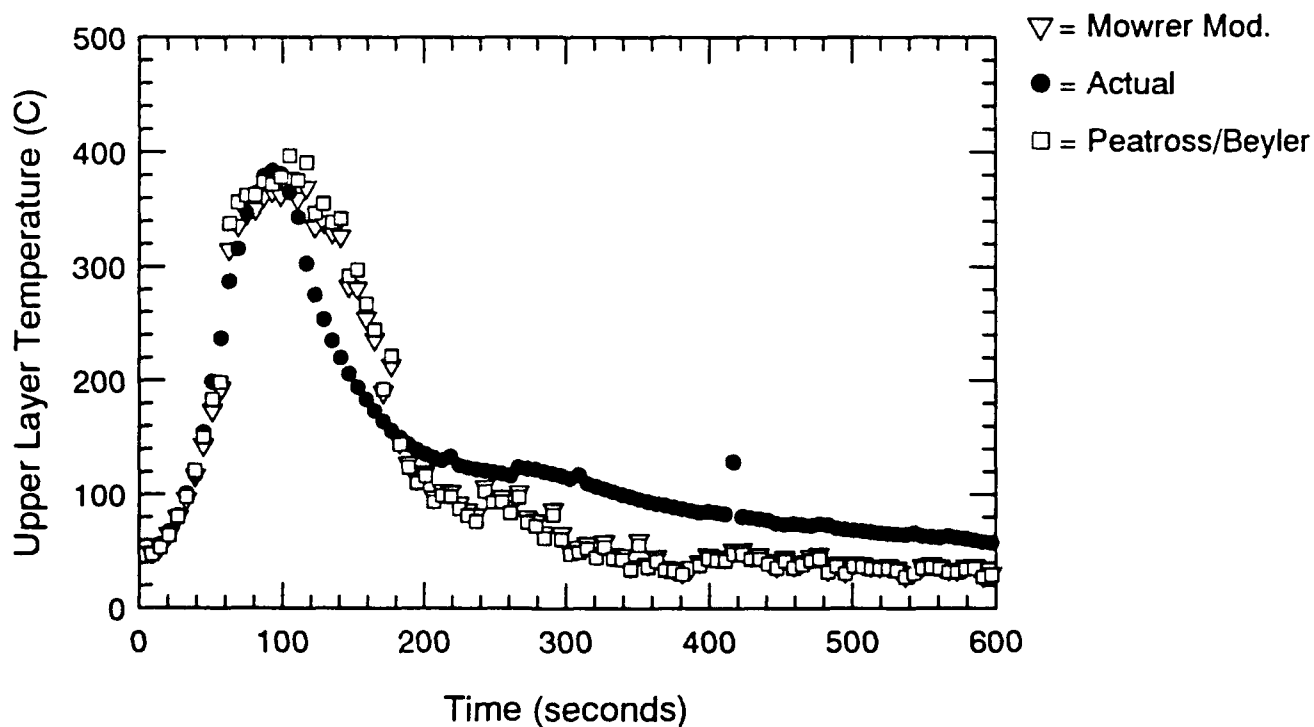
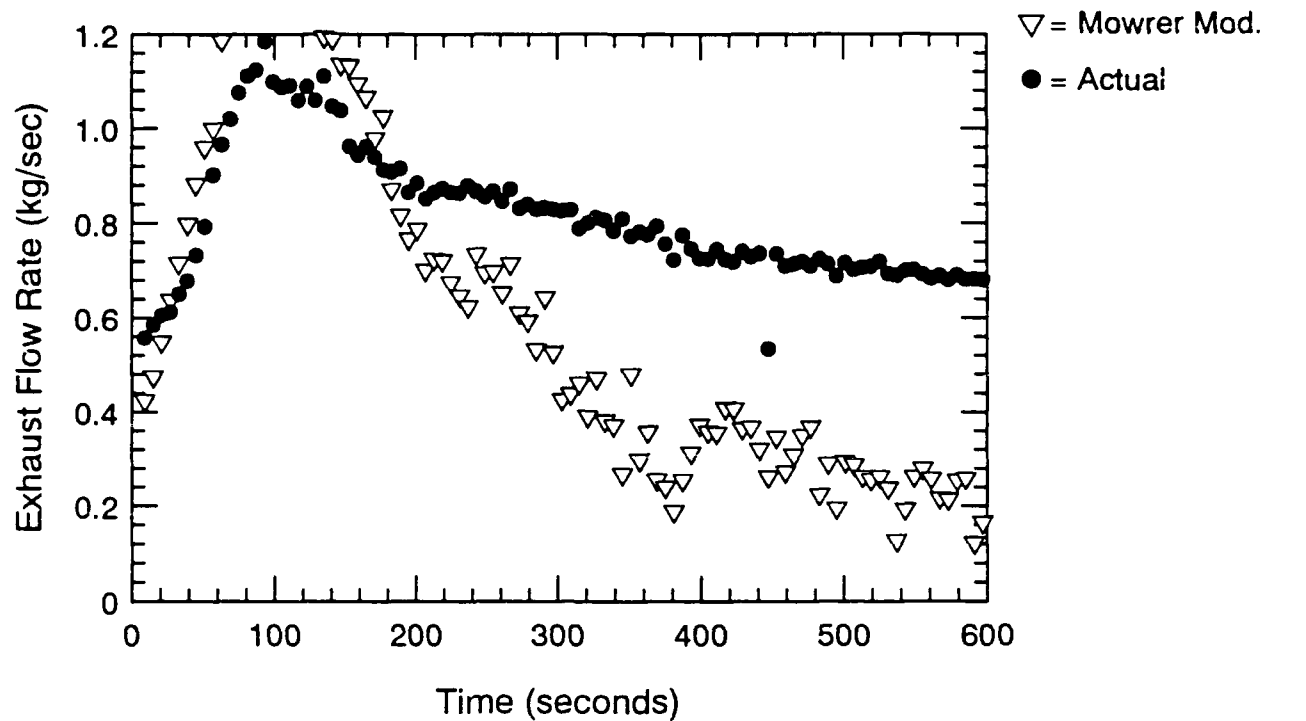


Figure F.4 Vent Flow and Temperature Predictions Using Mowrer Model - S104

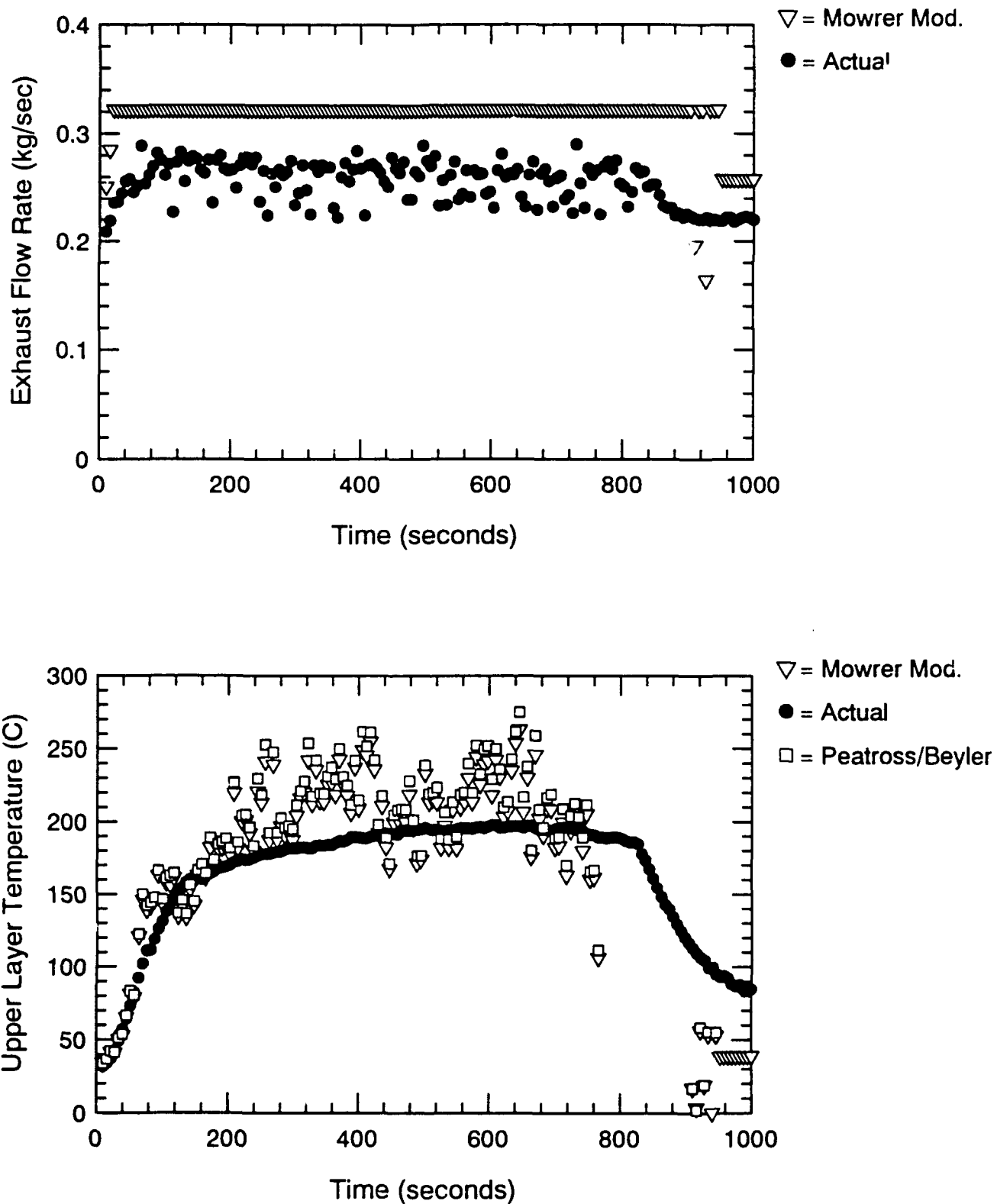


Figure F.5 Vent Flow and Temperature Predictions Using Mowrer Model - S105

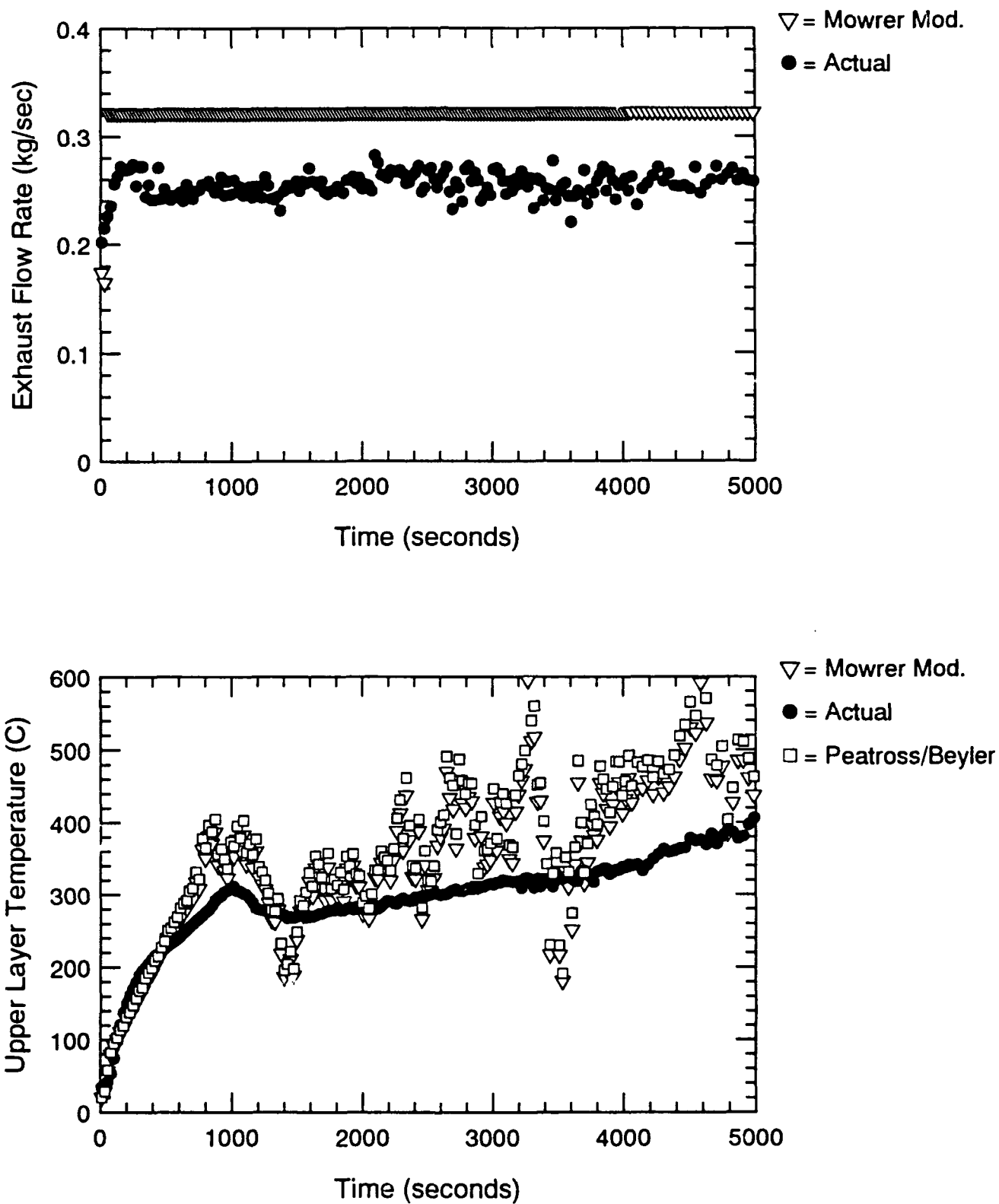


Figure F.6 Vent Flow and Temperature Predictions Using Mowrer Model - S106

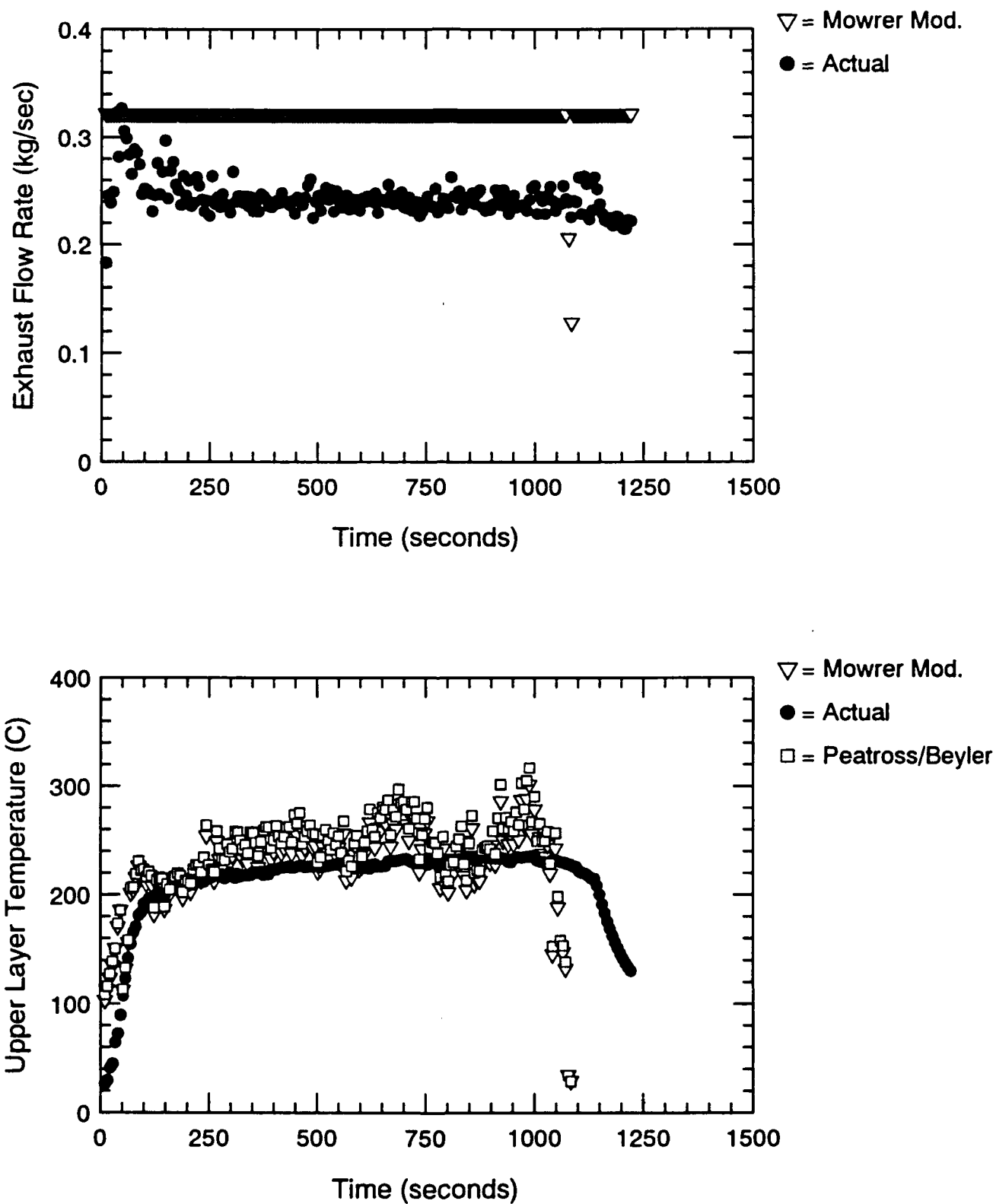


Figure F.7 Vent Flow and Temperature Predictions Using Mowrer Model - S107

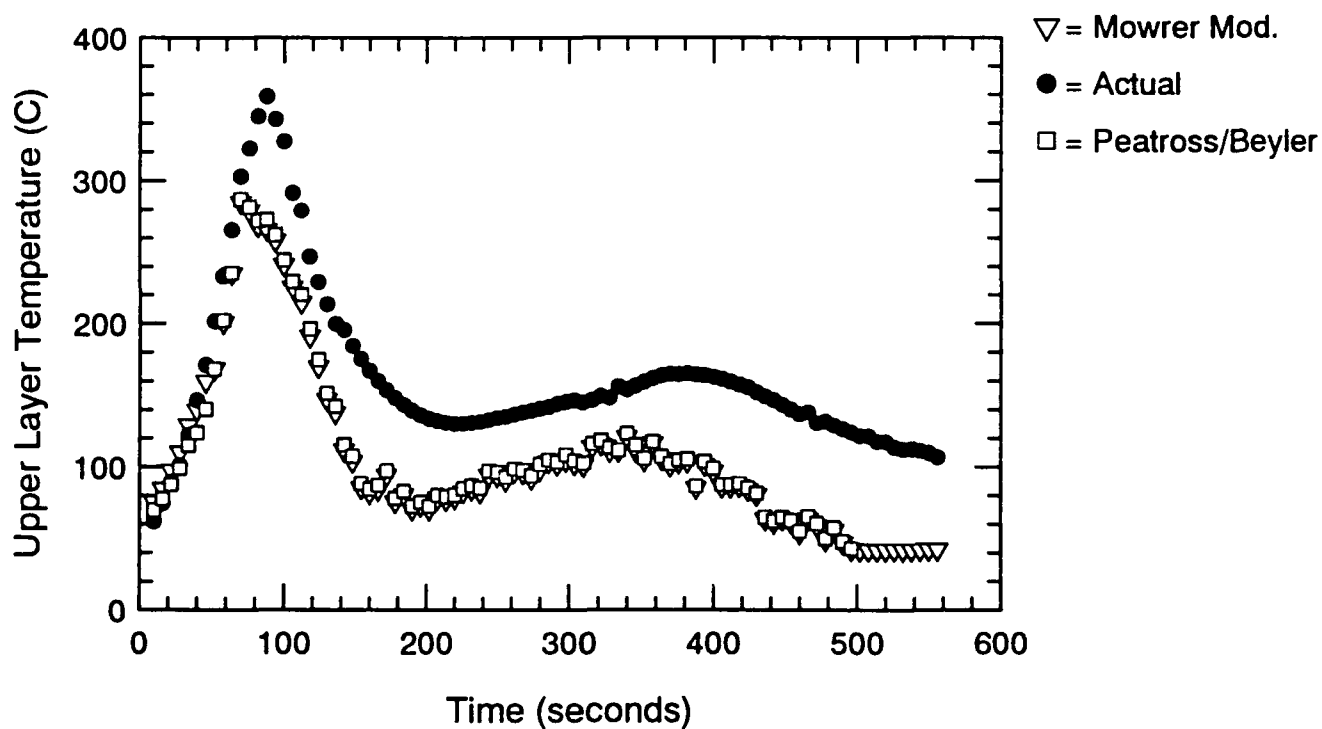
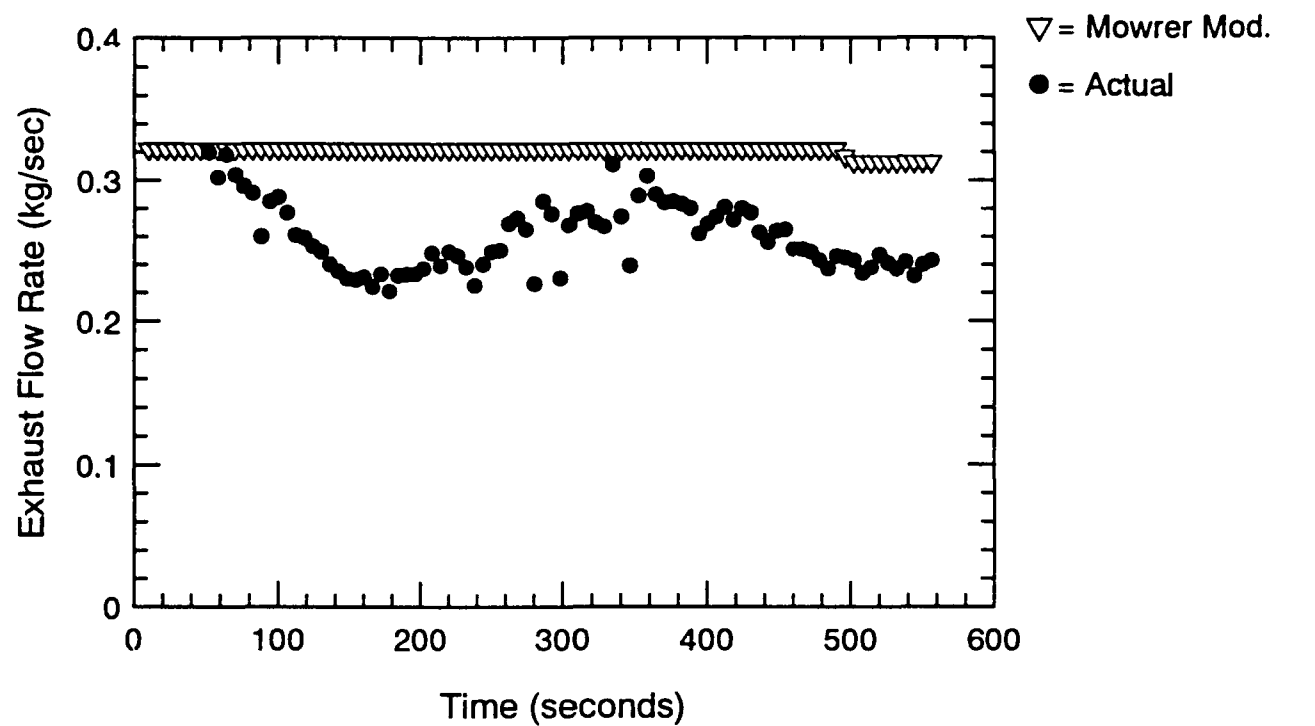


Figure F.8 Vent Flow and Temperature Predictions Using Mowrer Model - S108

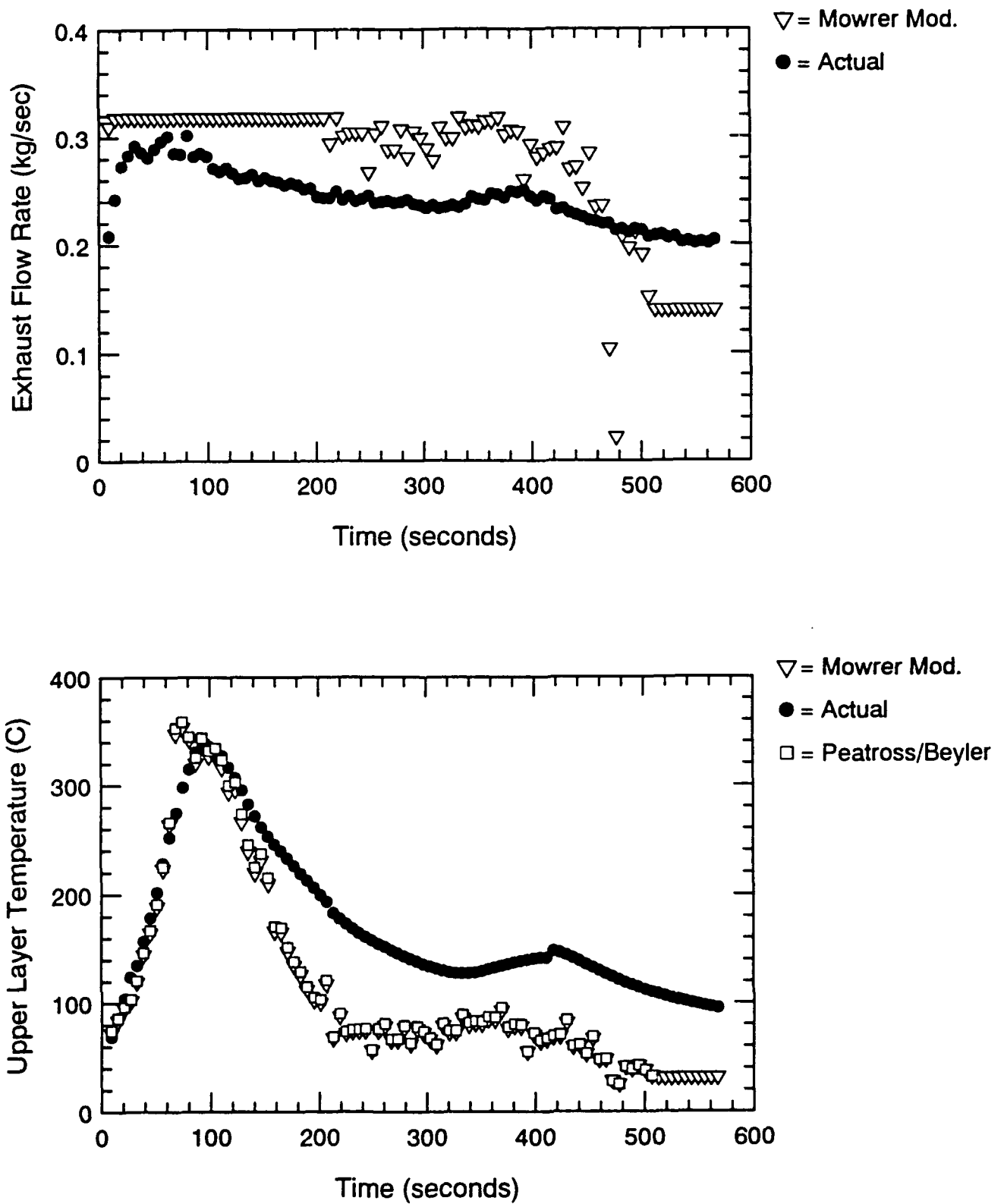


Figure F.9 Vent Flow and Temperature Predictions Using Mowrer Model - S109

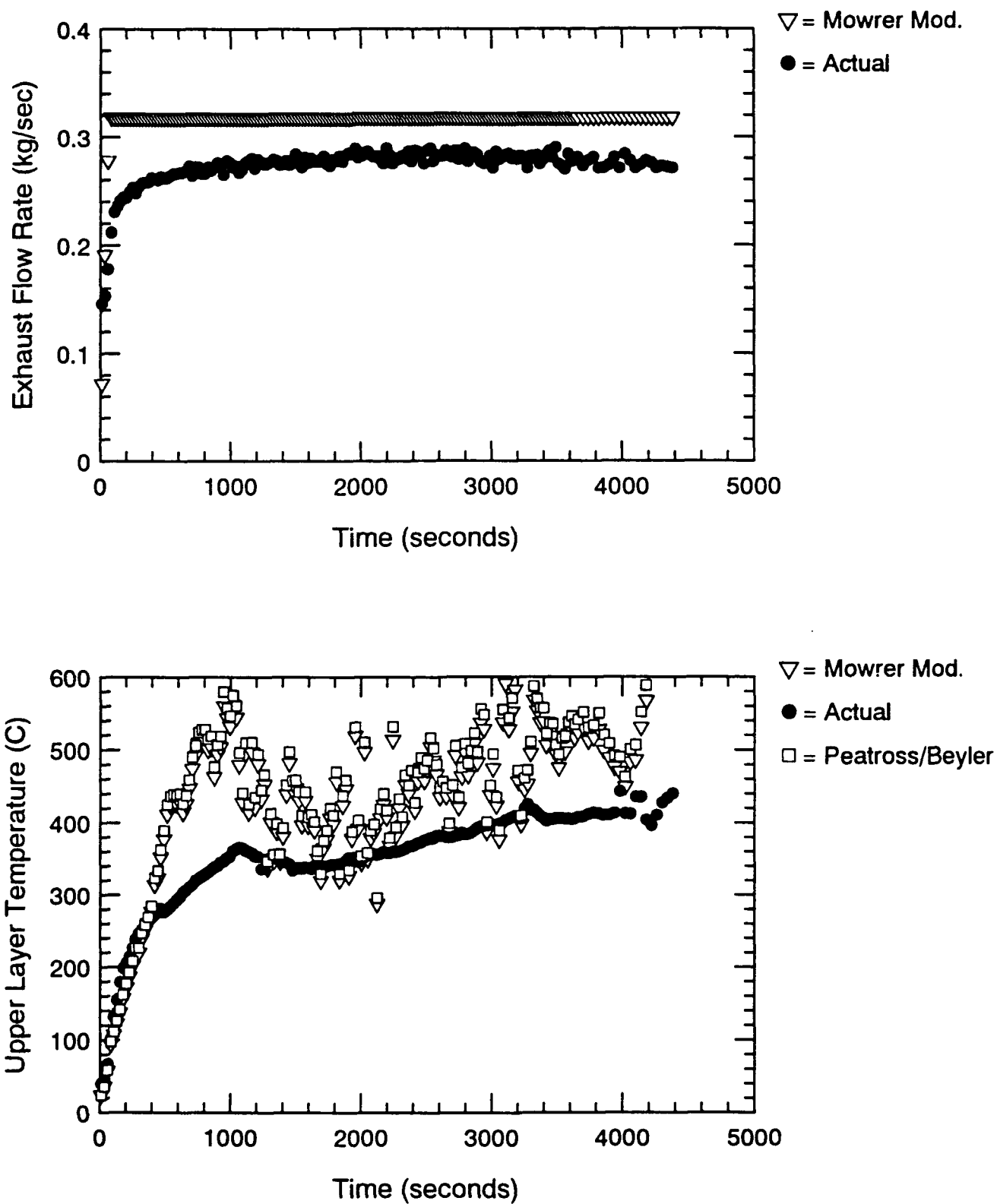


Figure F.10 Vent Flow and Temperature Predictions Using Mowrer Model - S110

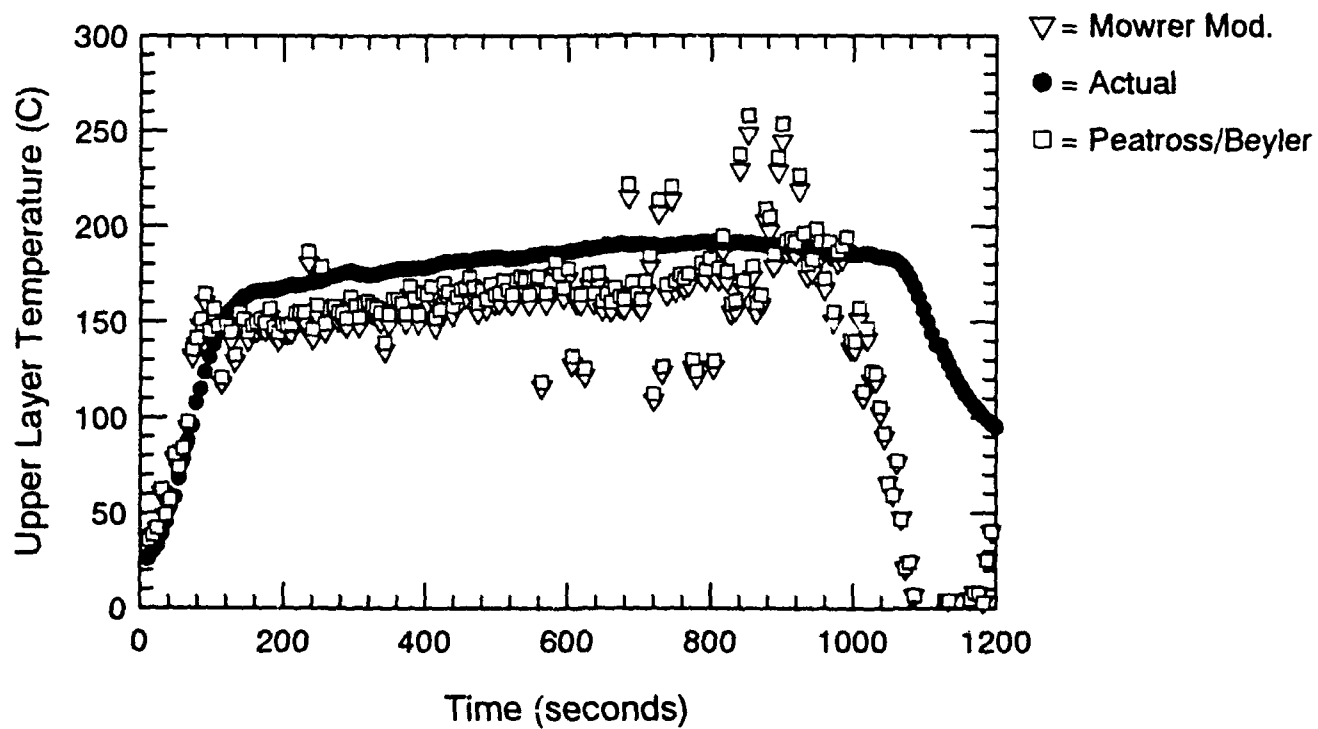
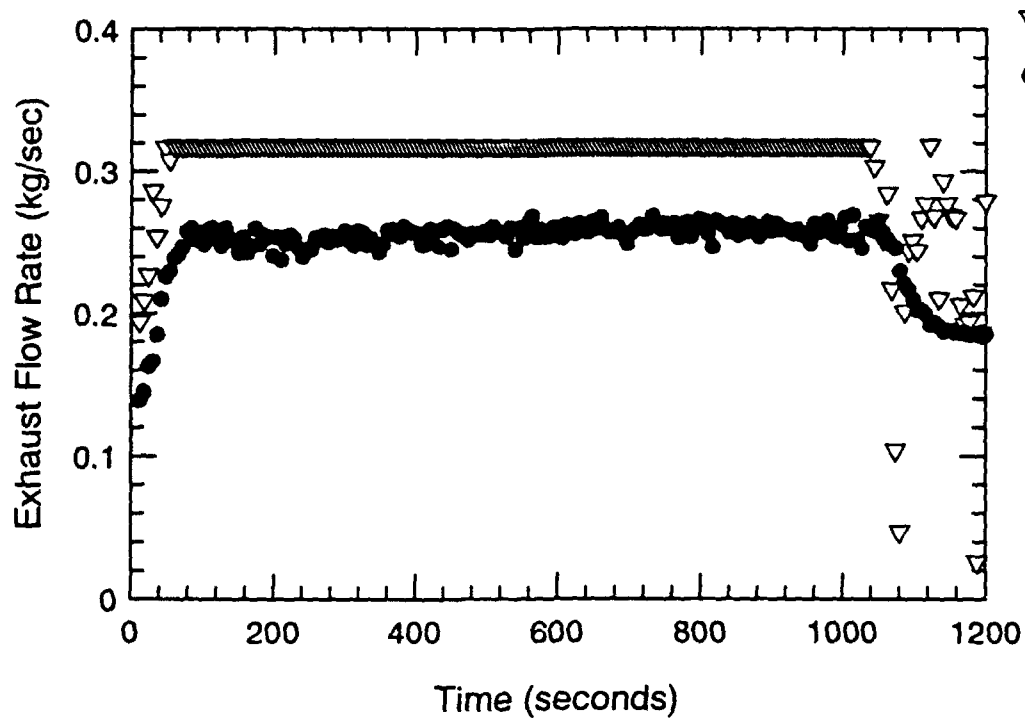


Figure F.11 Vent Flow and Temperature Predictions Using Mowrer Model - S111

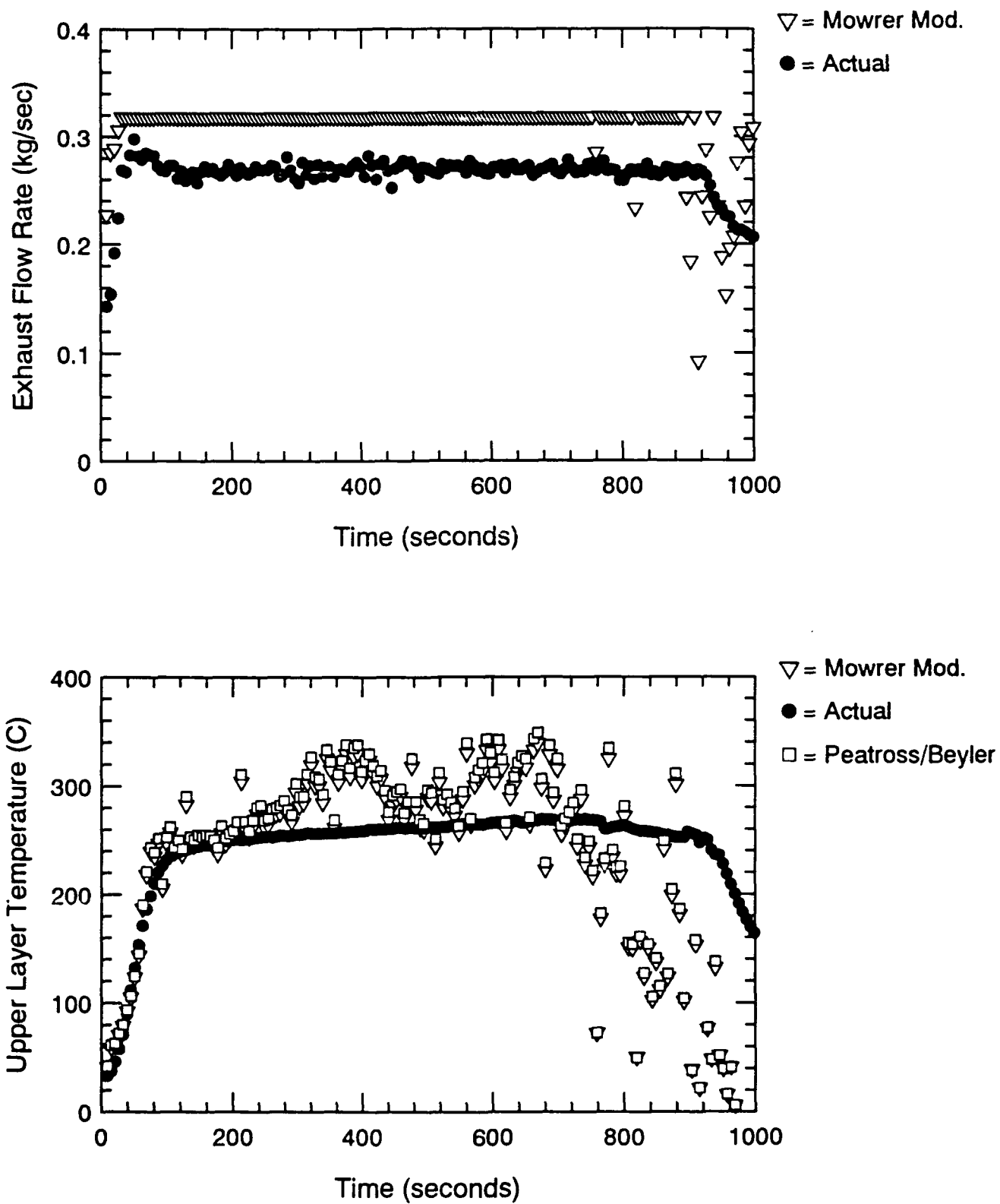


Figure F.12 Vent Flow and Temperature Predictions Using Mowrer Model - S112

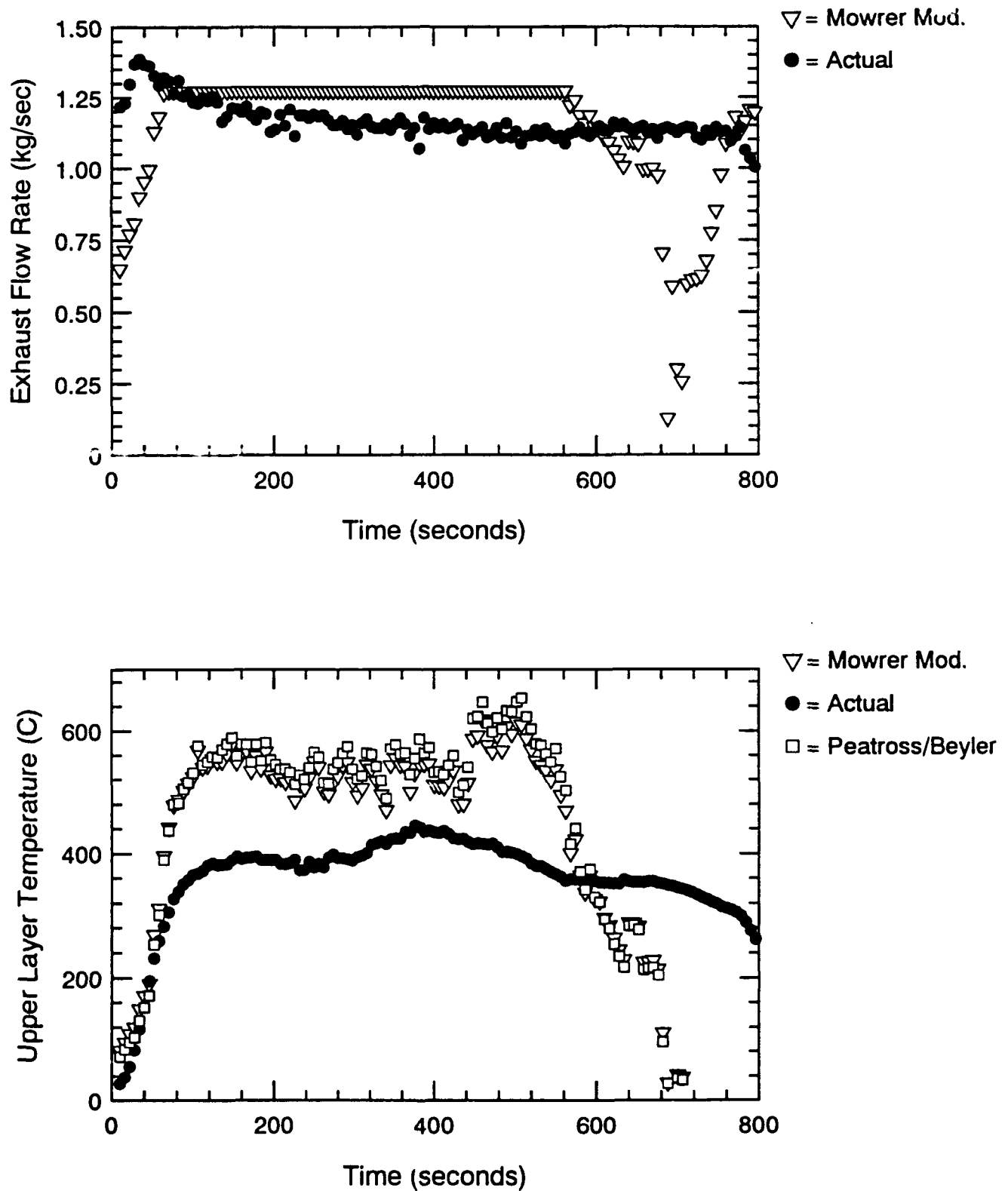


Figure F.13 Vent Flow and Temperature Predictions Using Mowrer Model - ADD1

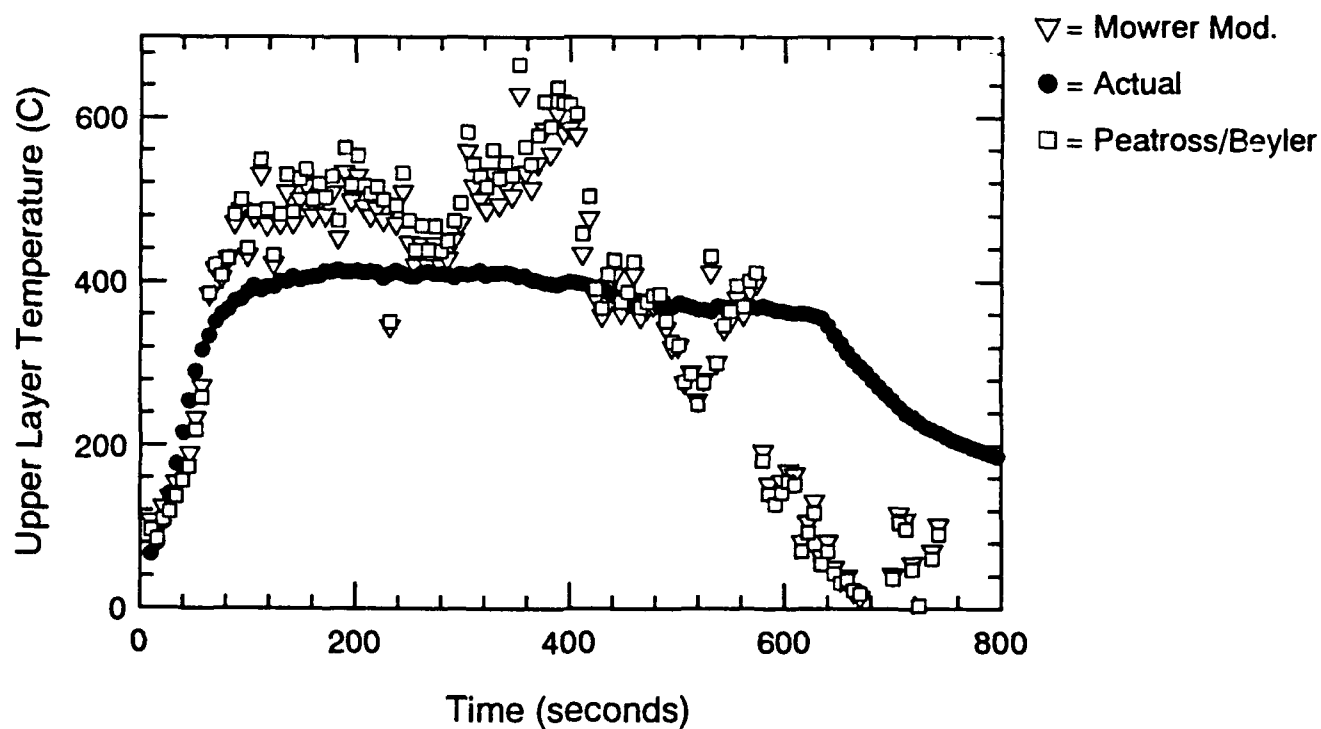
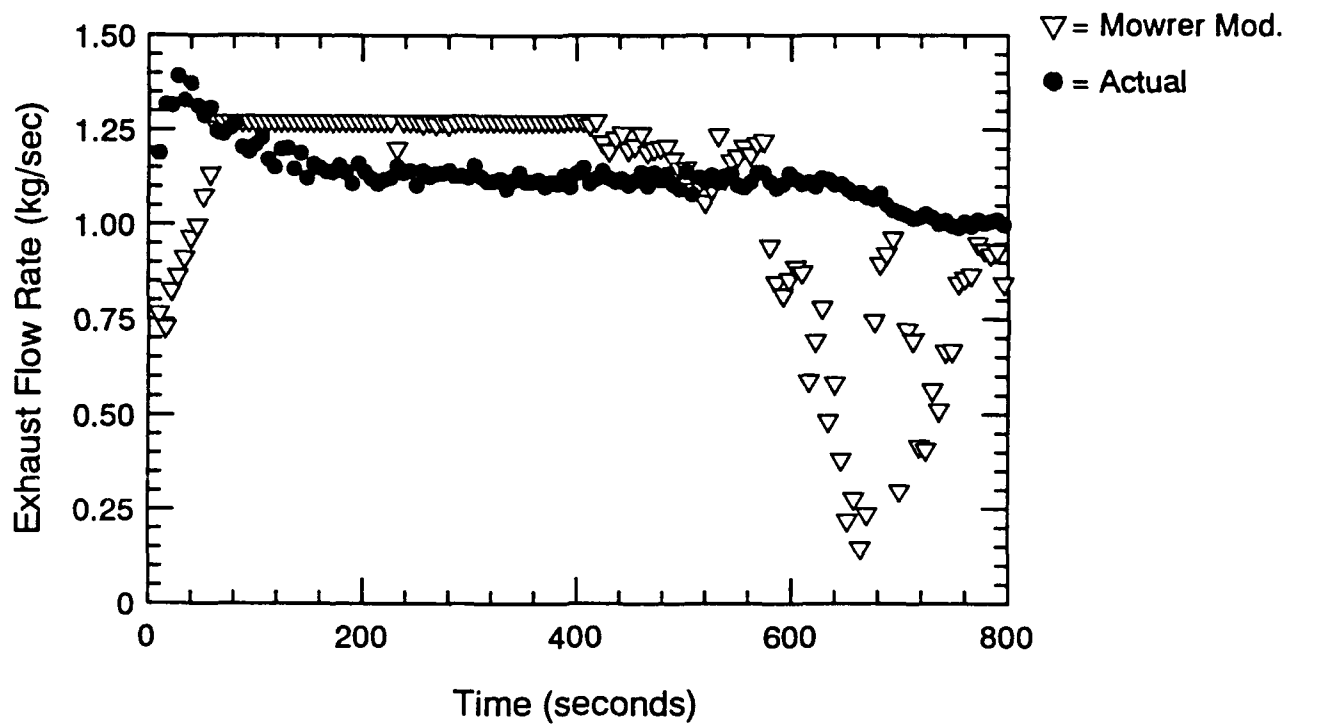


Figure F.14 Vent Flow and Temperature Predictions Using Mowrer Model - ADD2

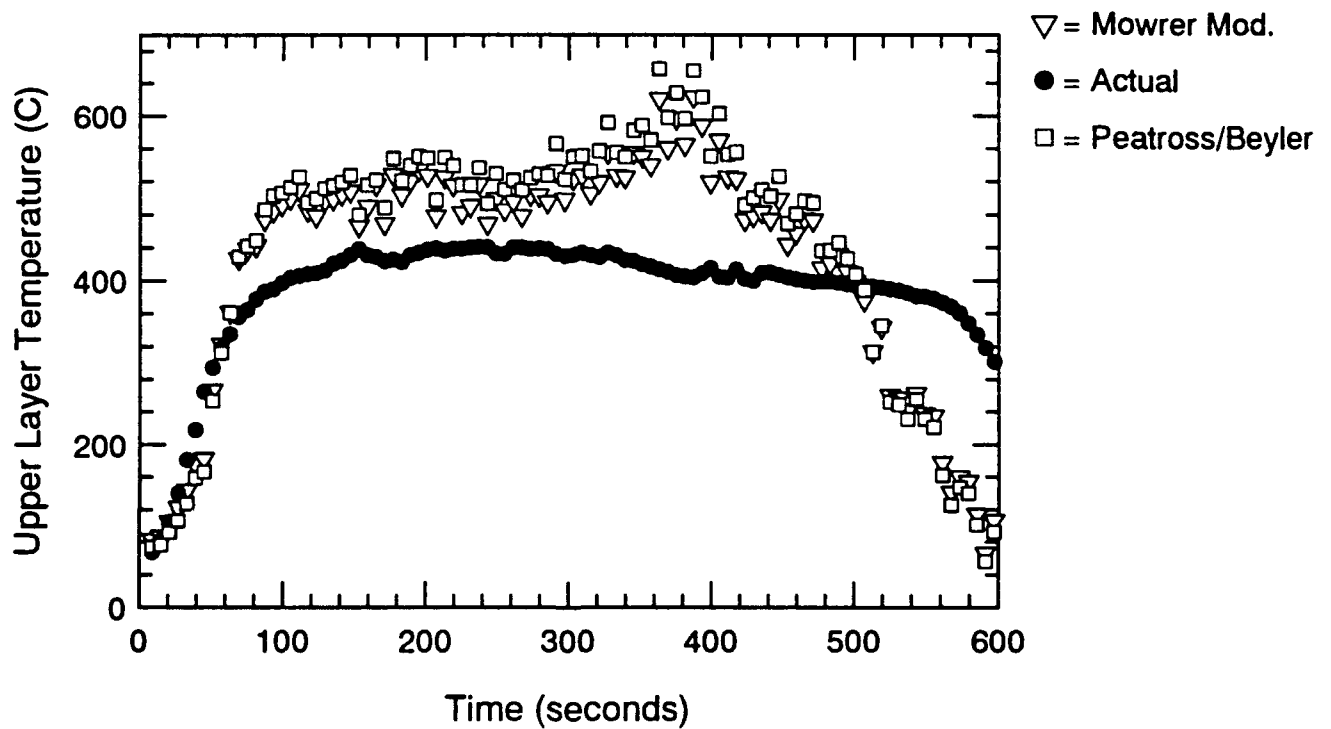
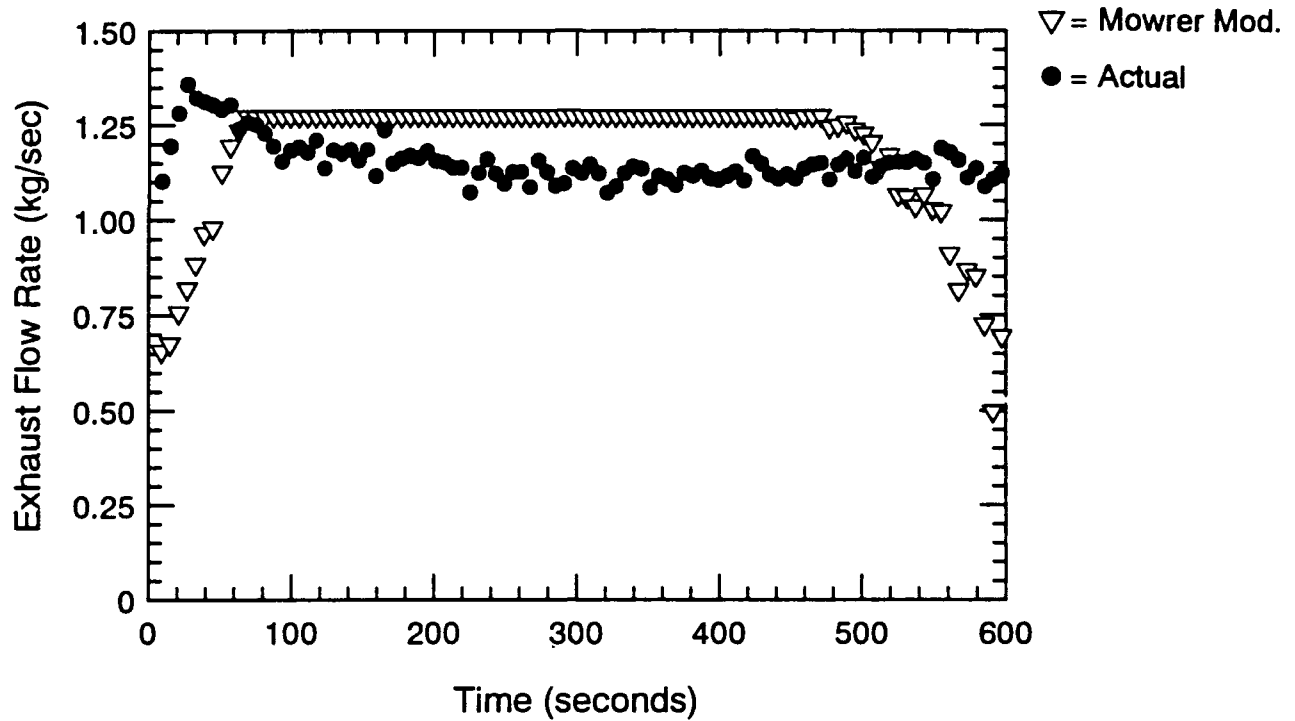


Figure F.15 Vent Flow and Temperature Predictions Using Mowrer Model - ADD3

APPENDIX G. MQH Temperature Prediction Method Results

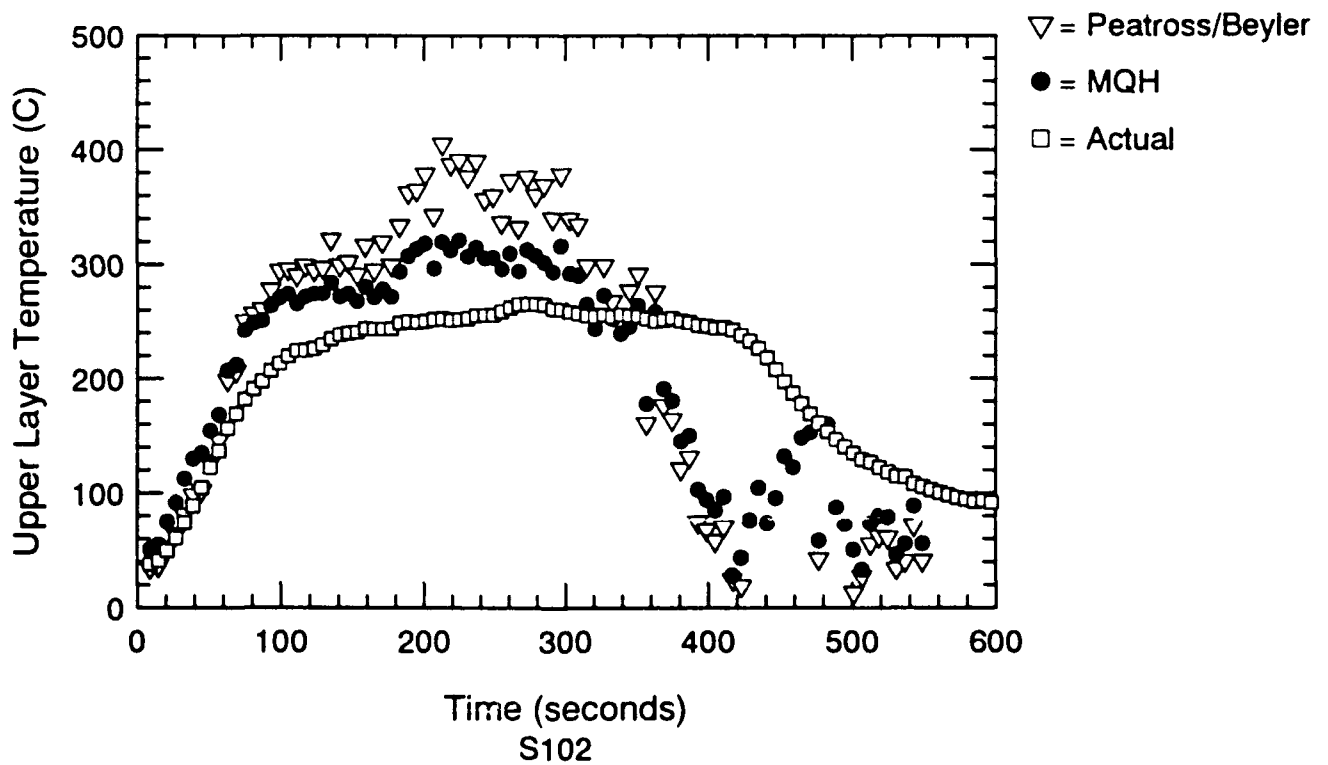
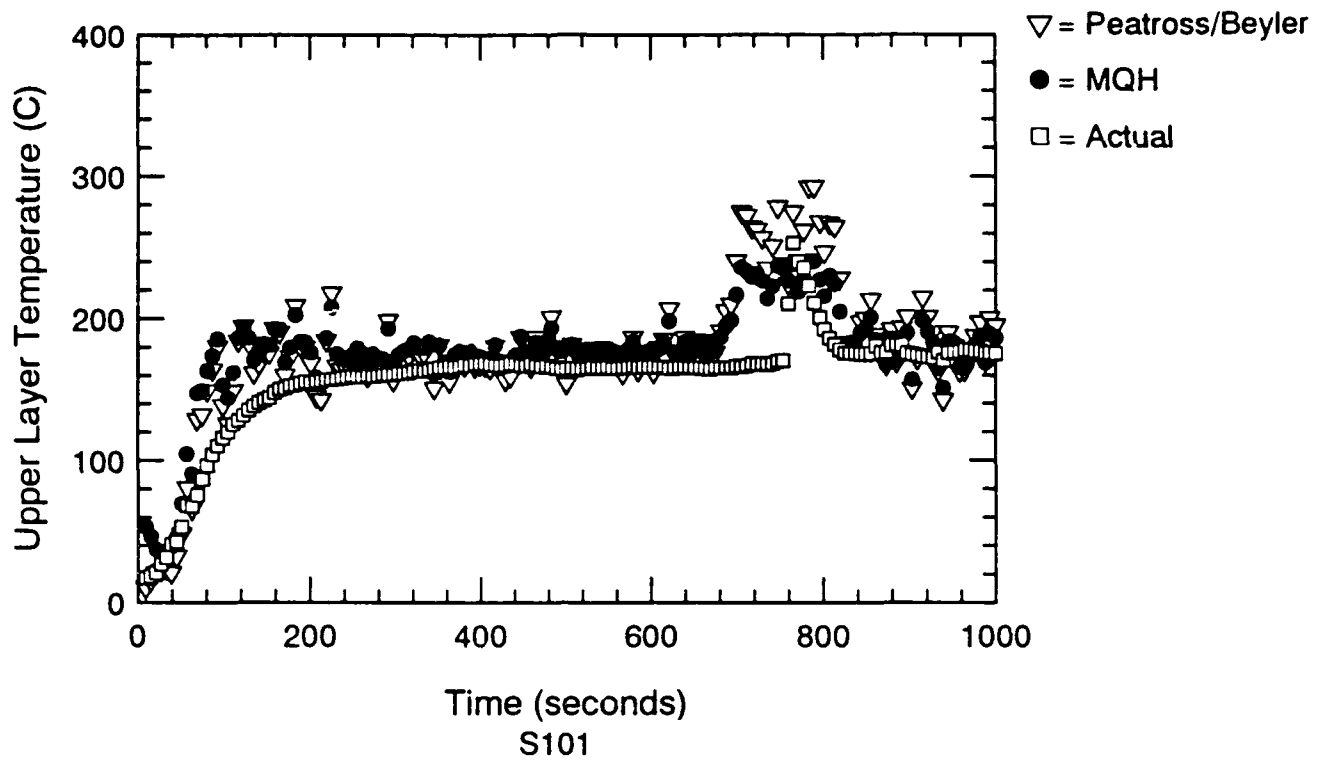


Figure G.1 Temperature Predictions Using MQH Method - S101 & S102

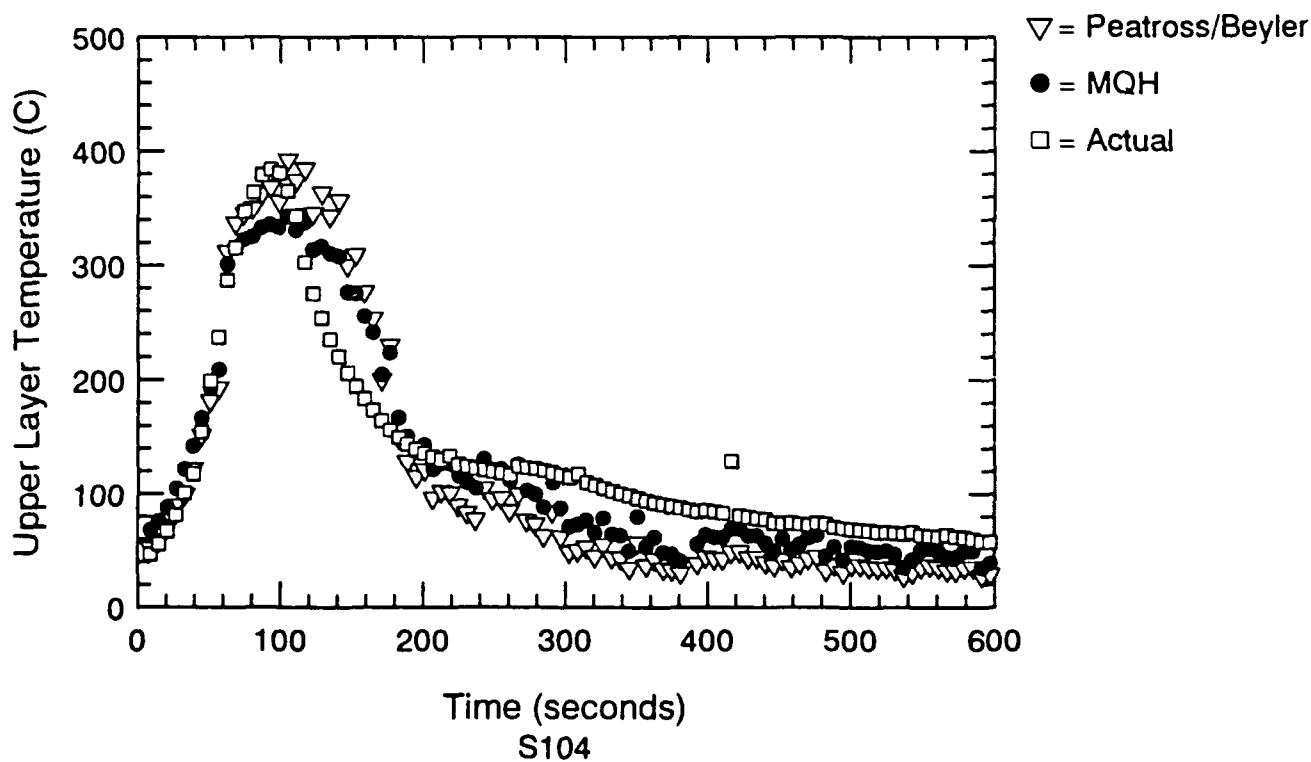
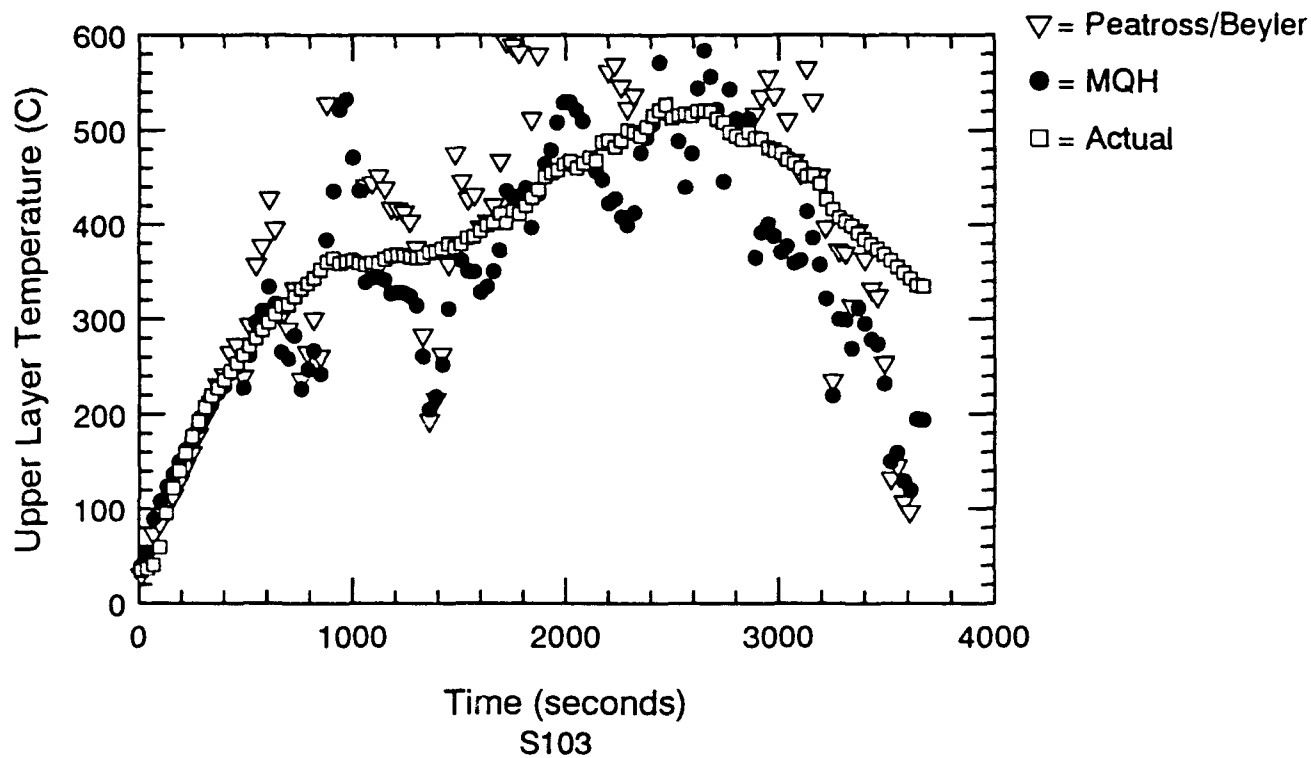


Figure G.2 Temperature Predictions Using MQH Method - S103 & S104

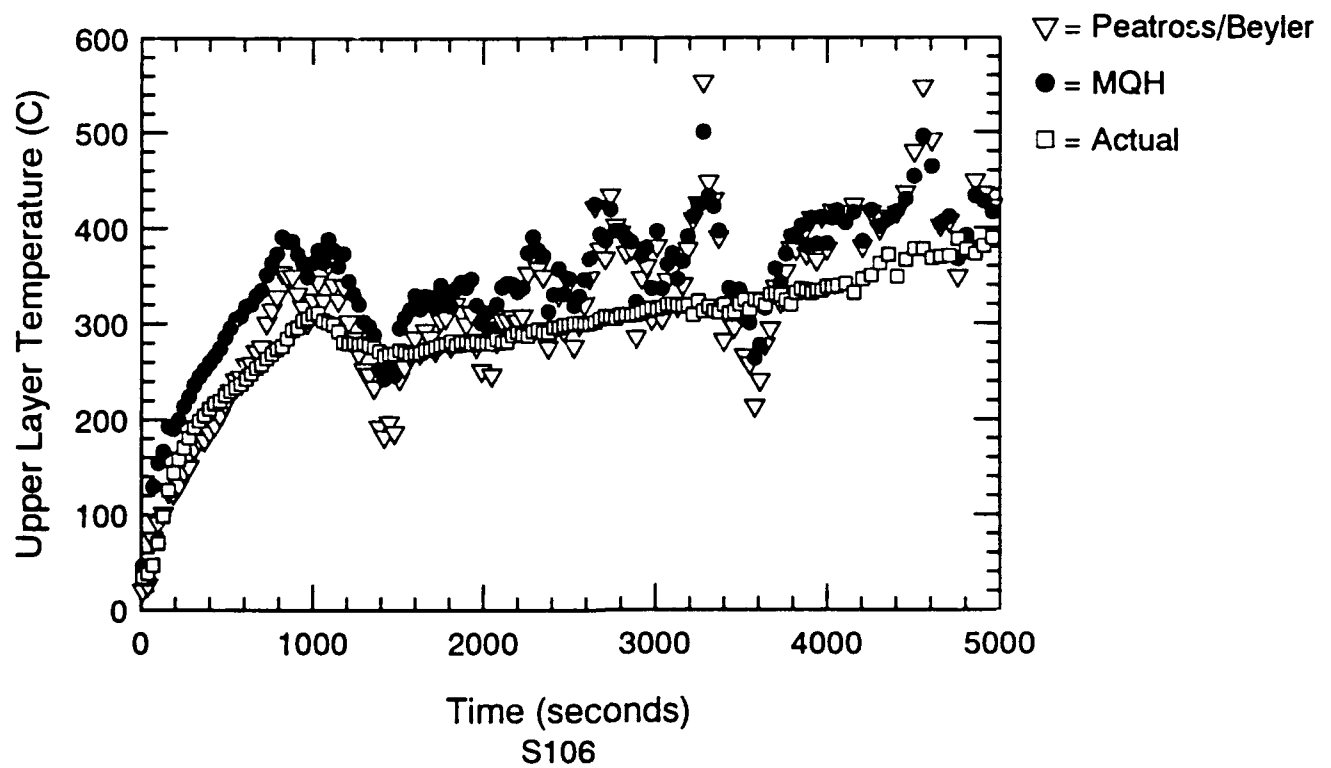
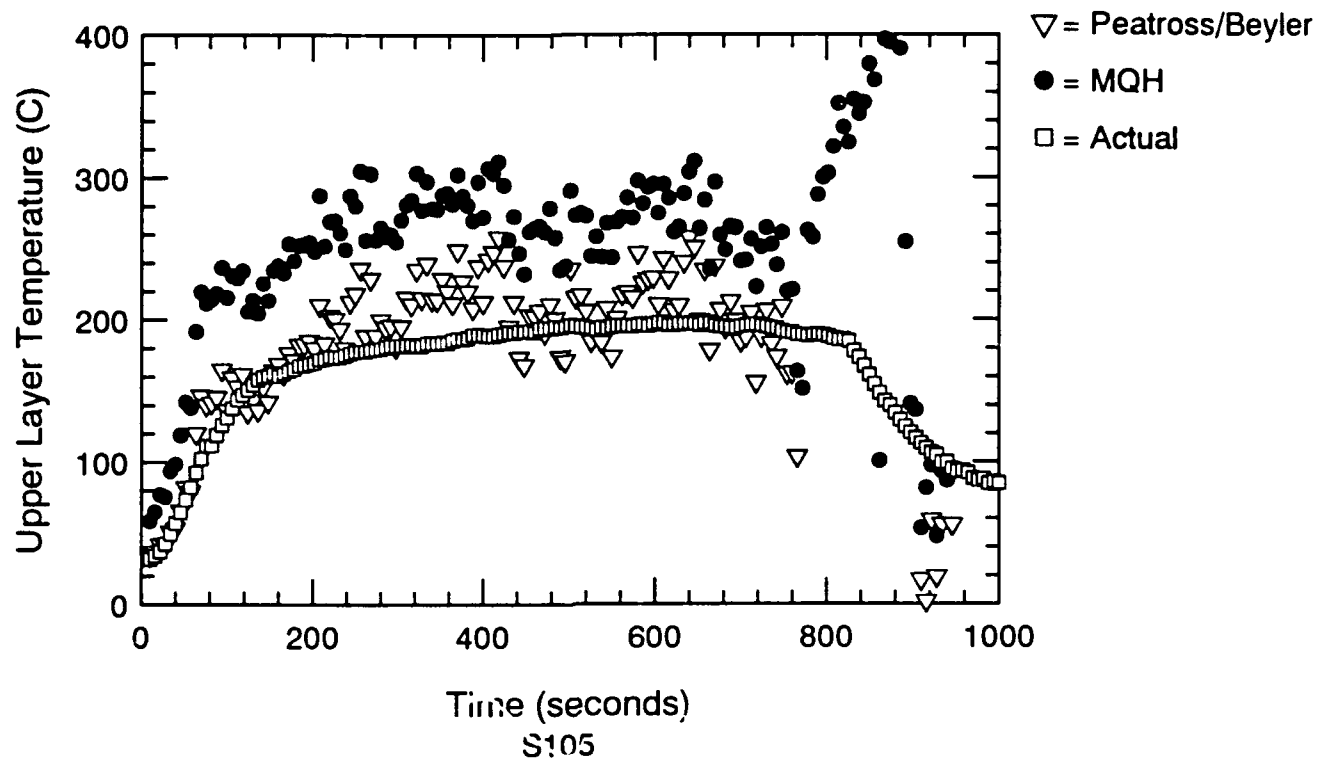


Figure G.3 Temperature Predictions Using MQH Method - S105 & S106

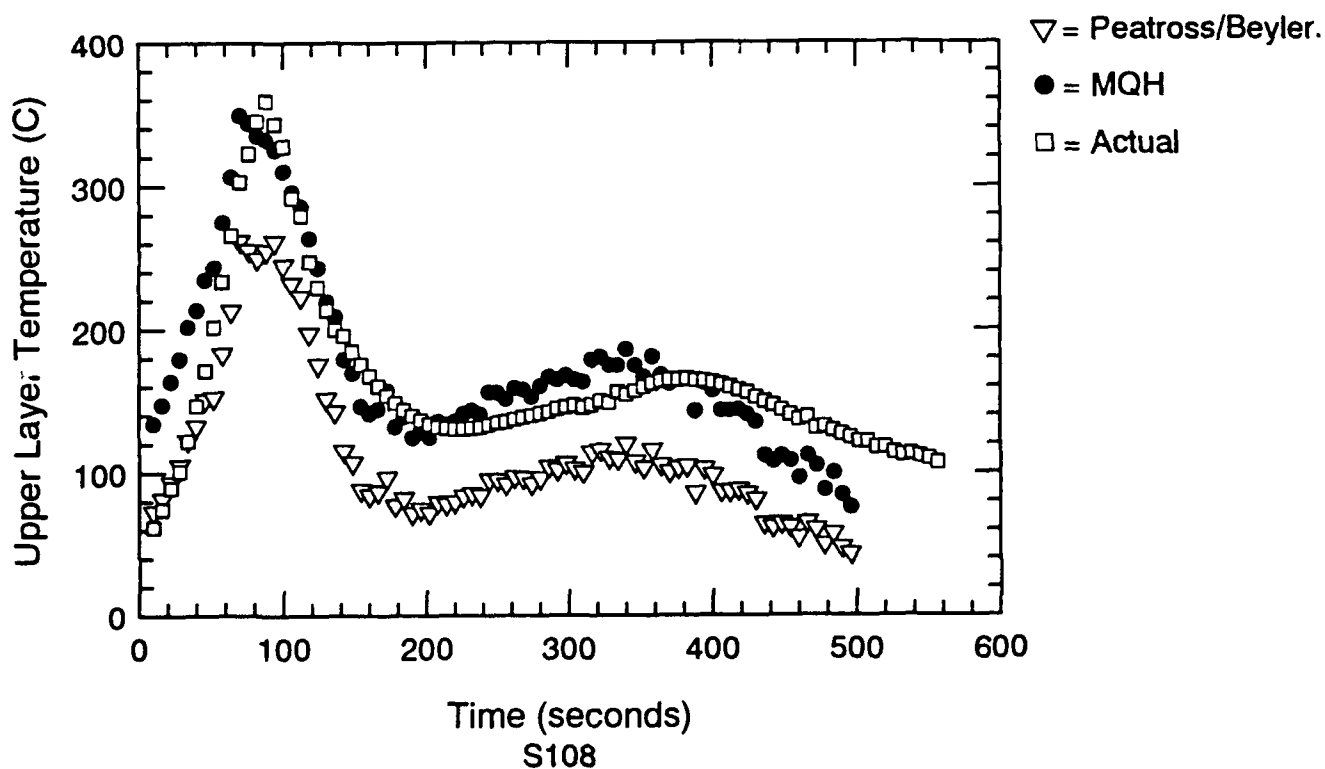
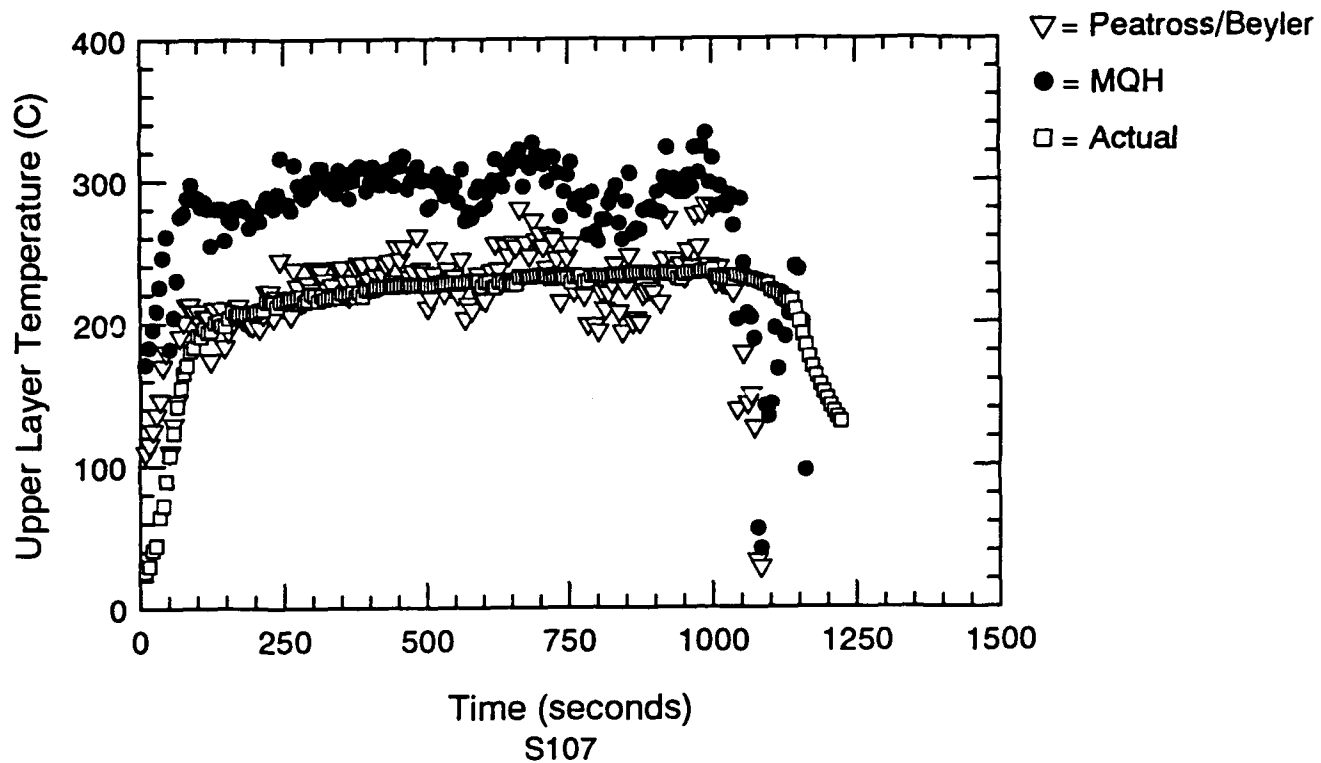


Figure G.4 Temperature Predictions Using MQH Method - S107 & S108

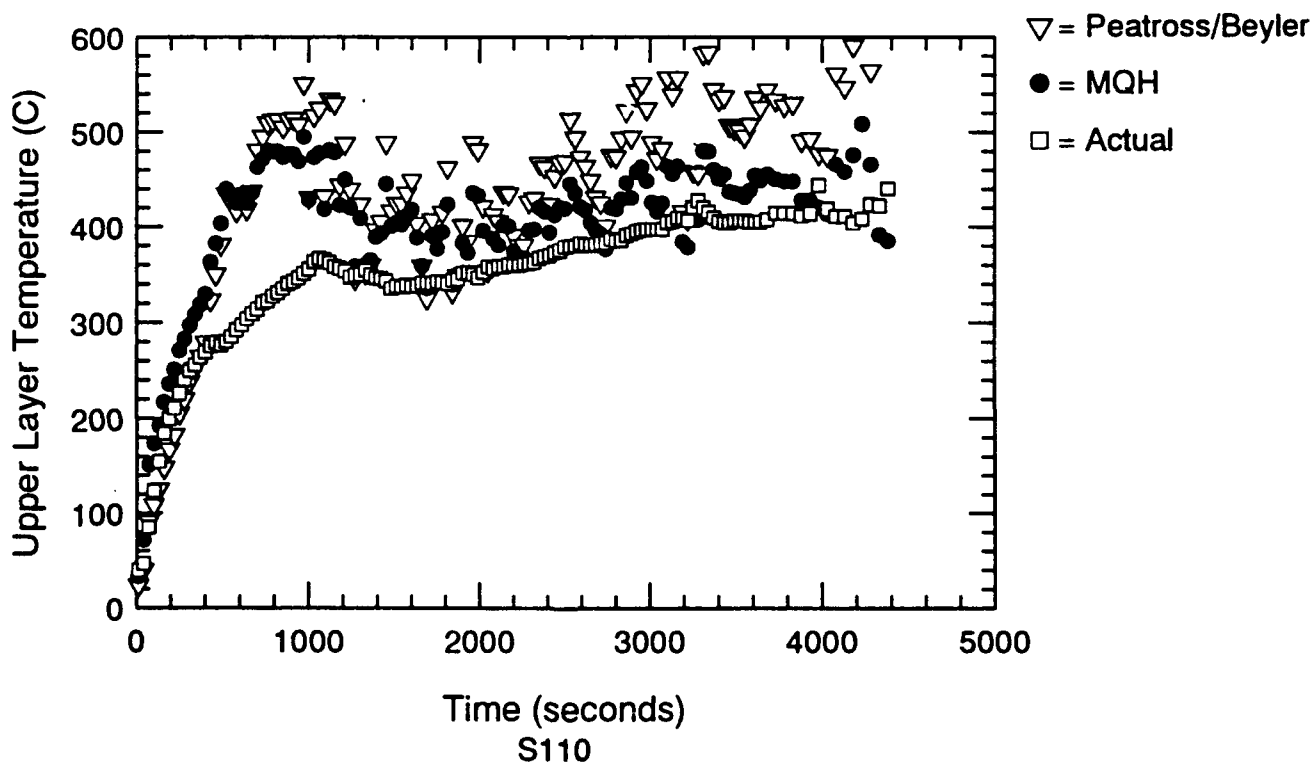
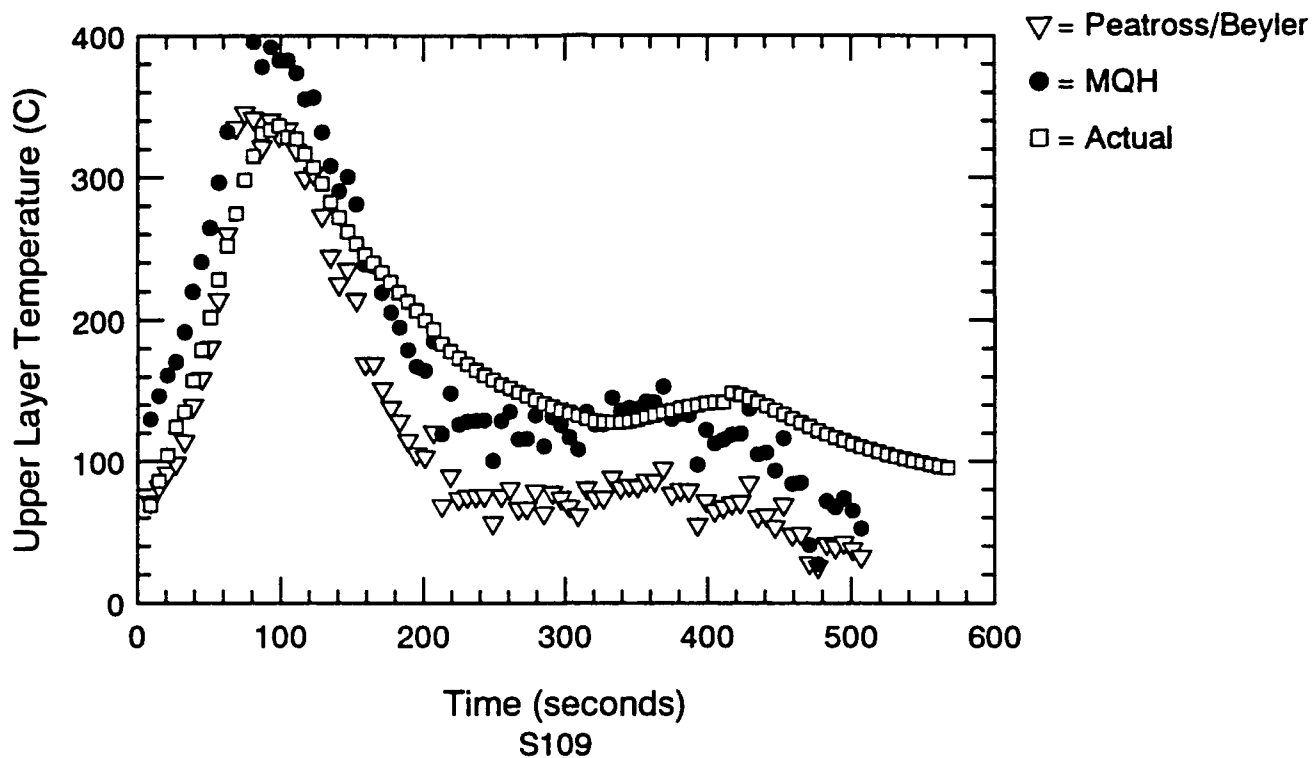


Figure G.5 Temperature Predictions Using MQH Method - S109 & S110

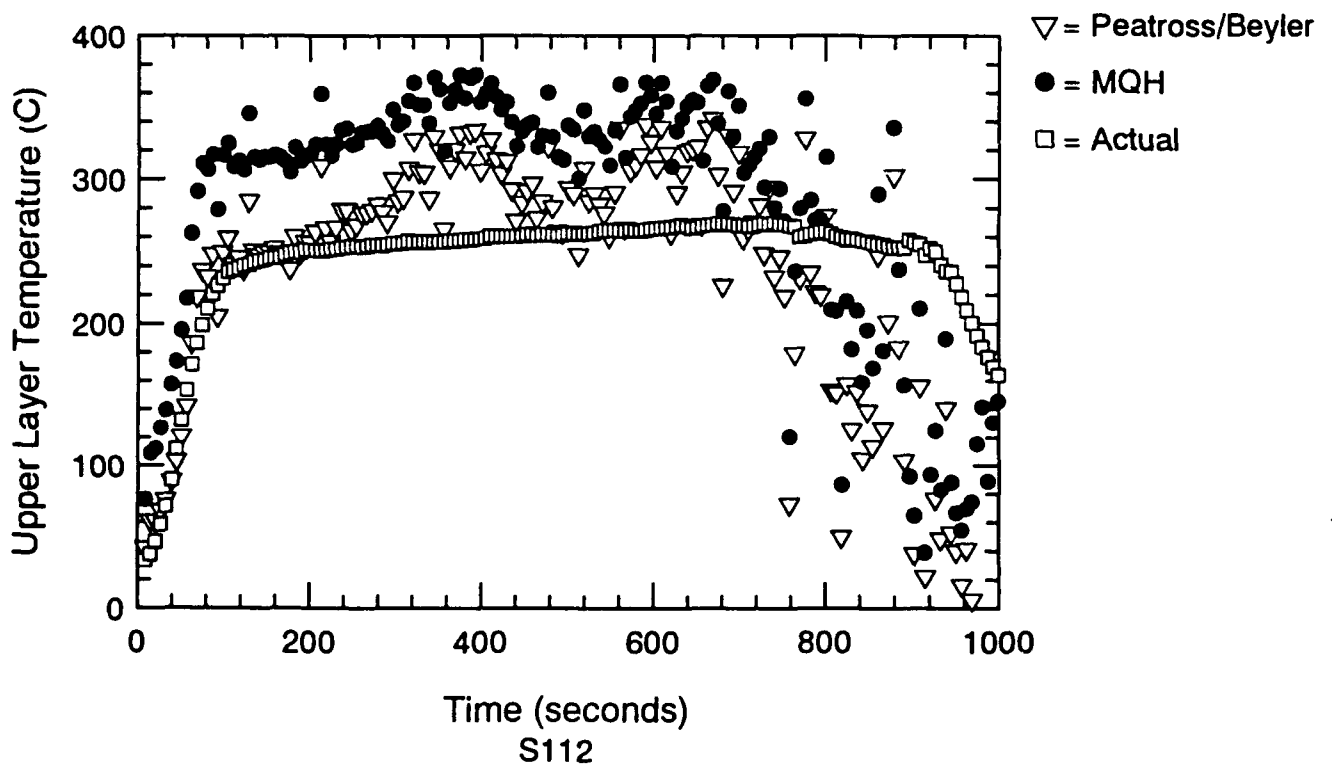
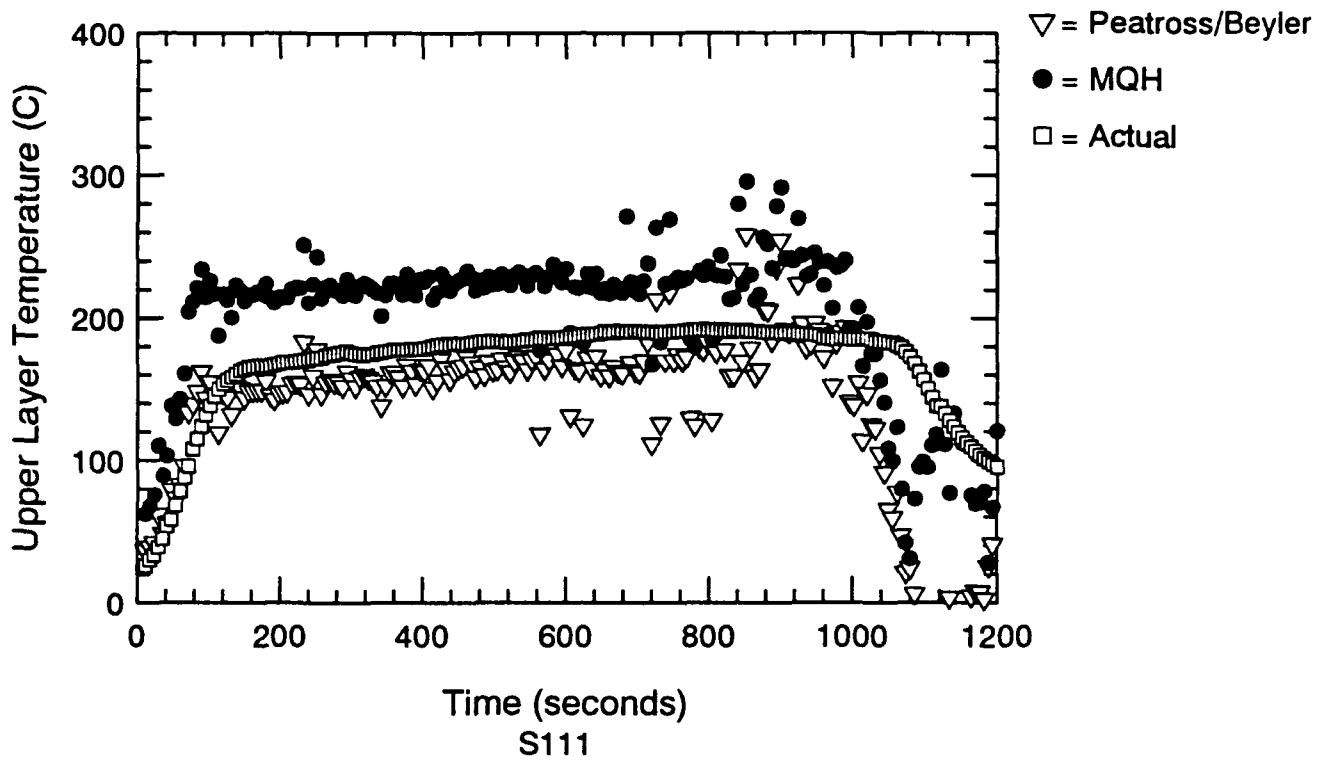


Figure G.6 Temperature Predictions Using MQH Method - S111 & S112

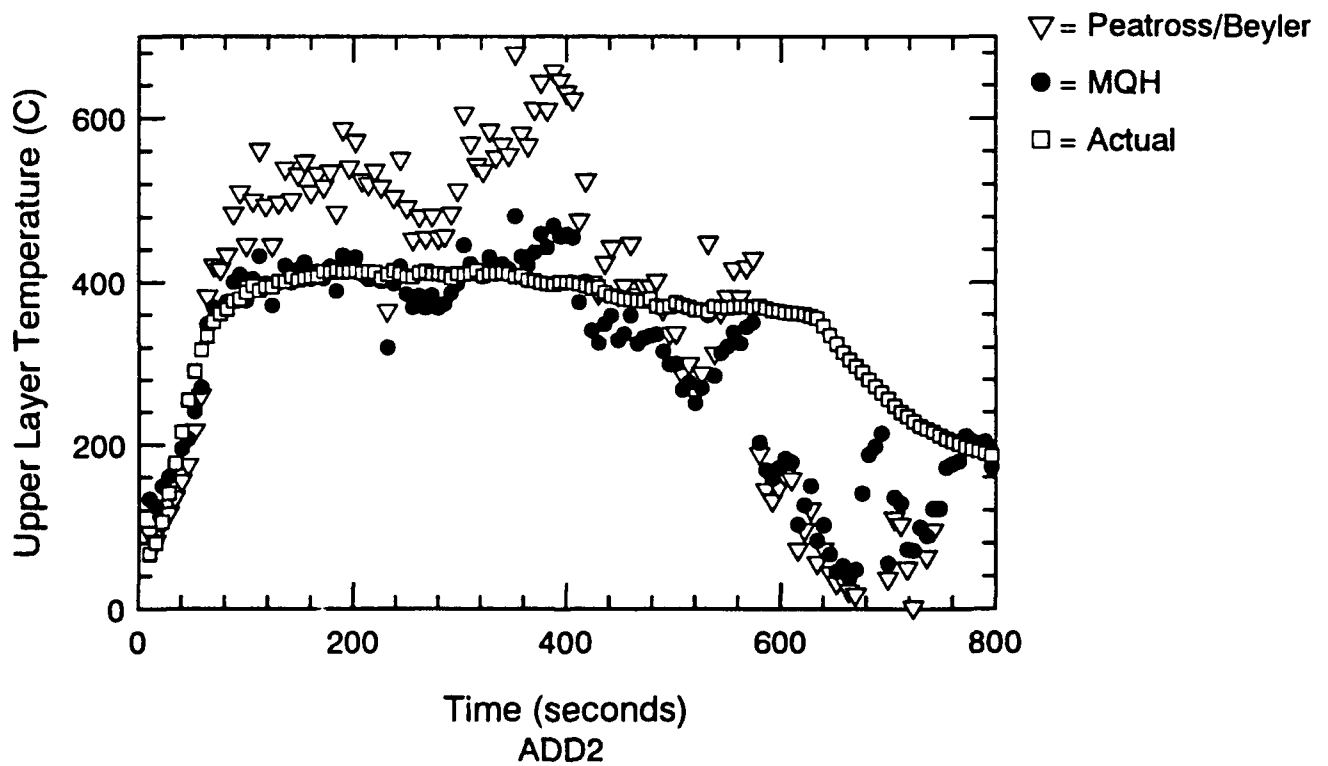
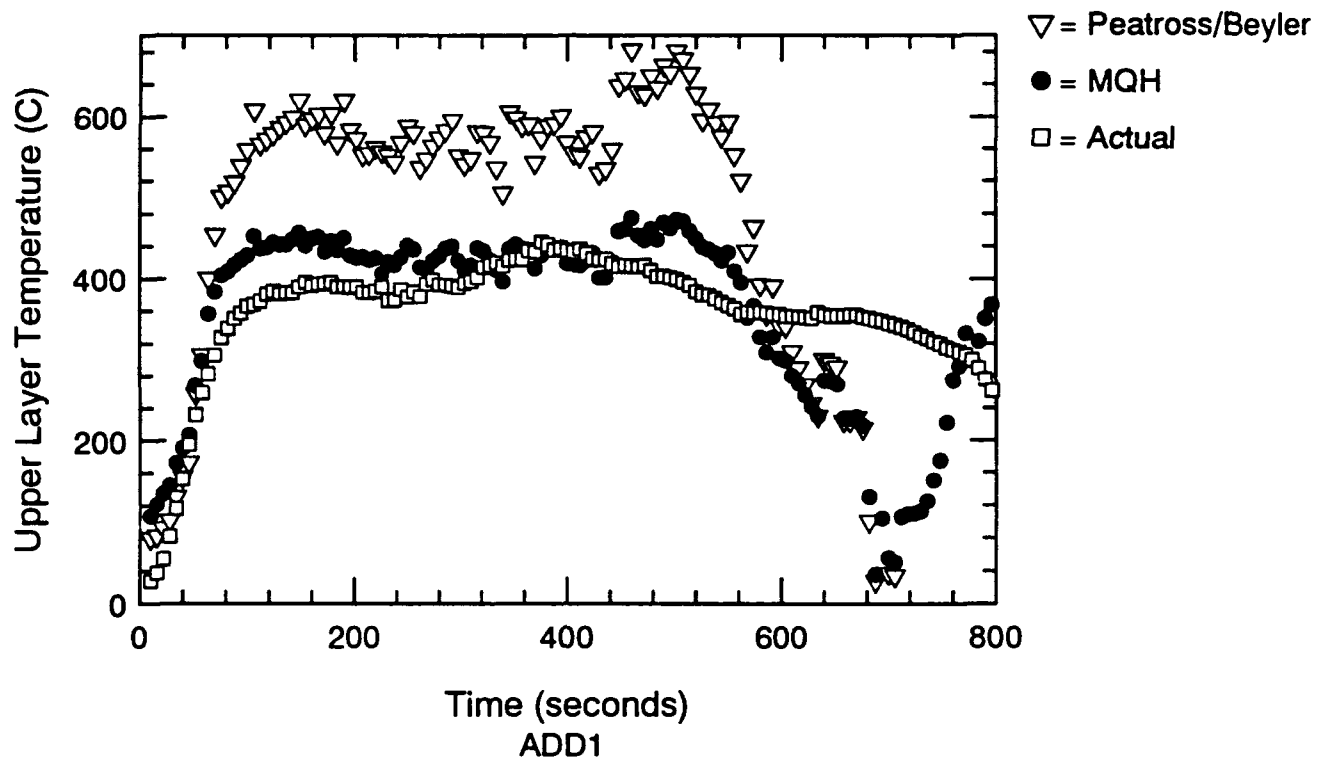


Figure G.7 Temperature Predictions Using MQH Method - ADD1 & ADD2

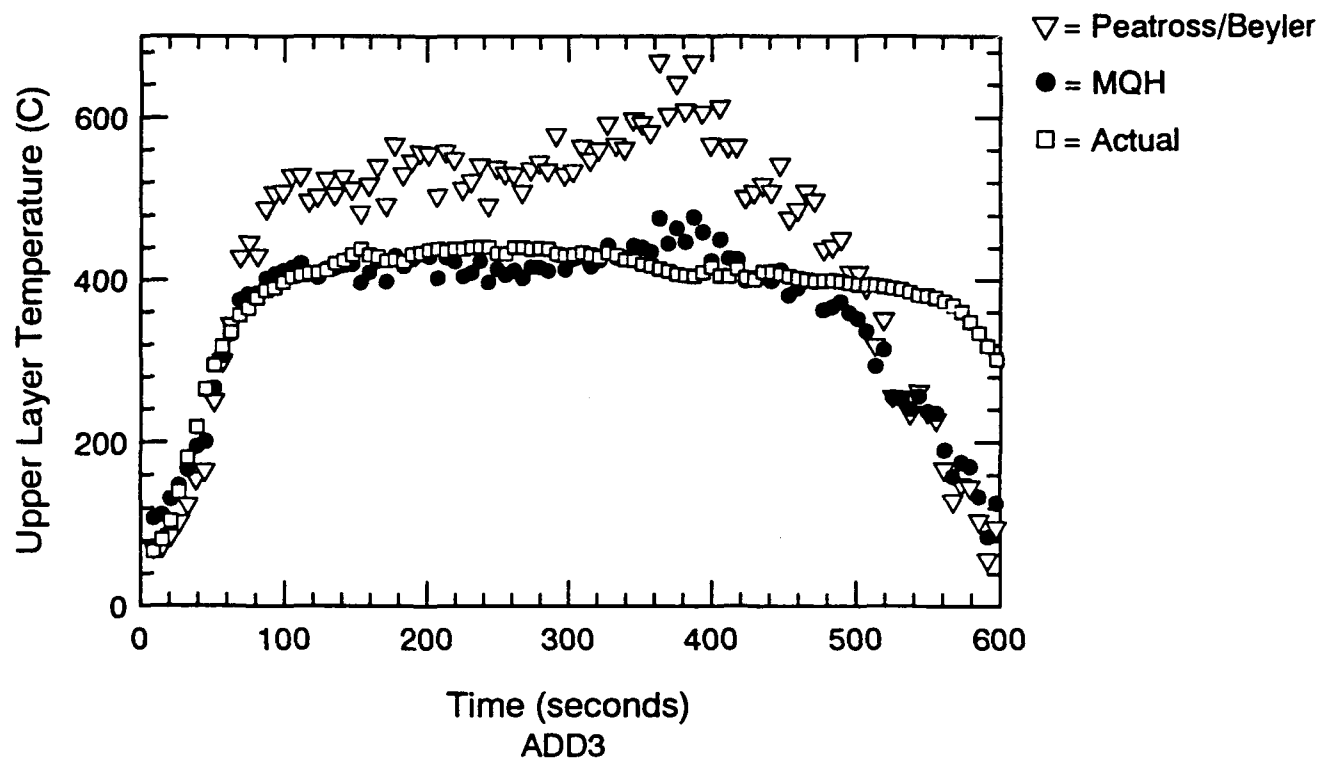


Figure G.8 Temperature Predictions Using MQH Method - ADD3

APPENDIX H. Barrier Temperature Predictions Using Peatross/Beyler Method

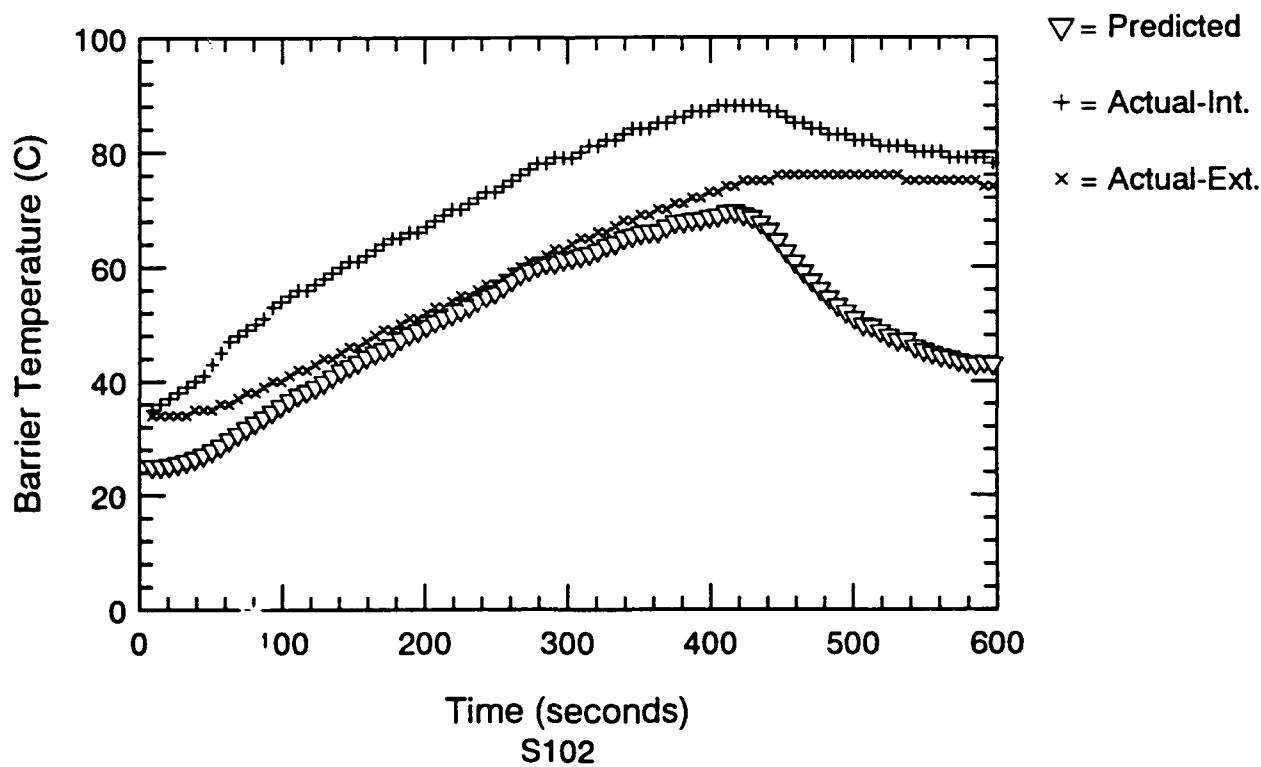
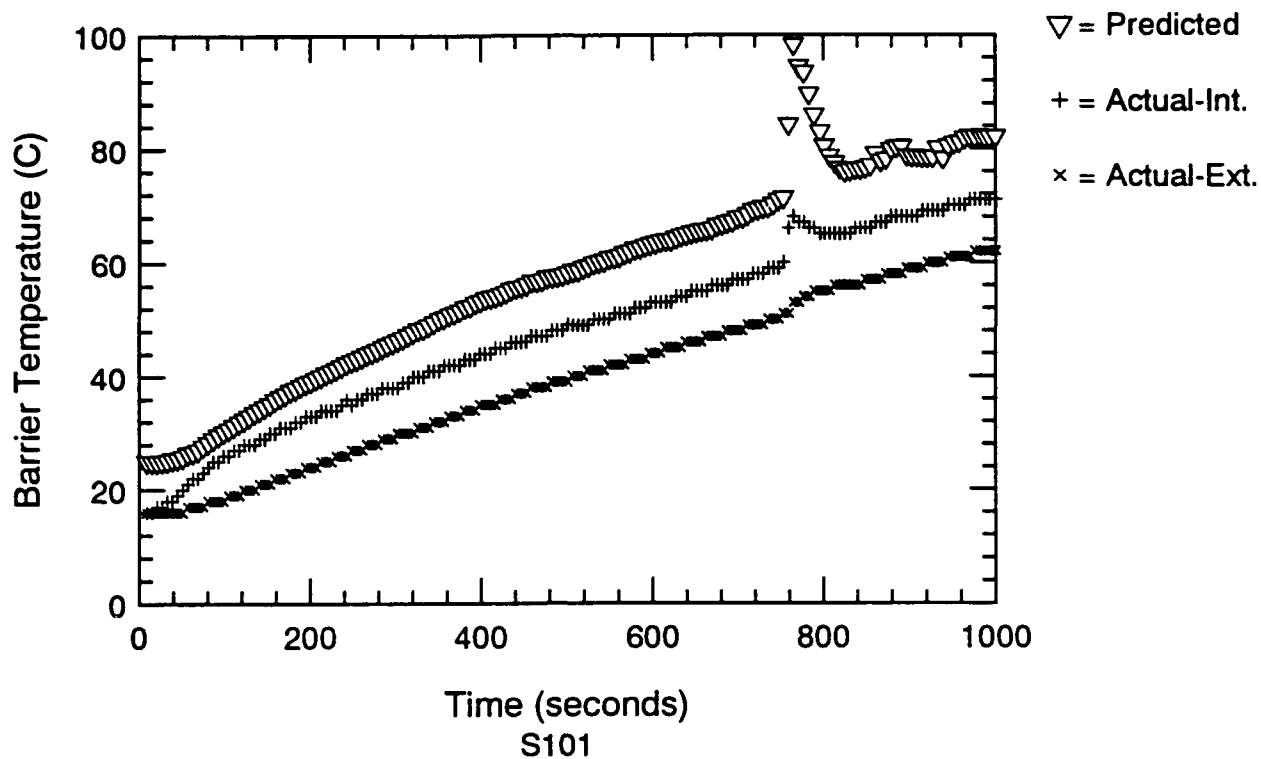


Figure H.1 Barrier Temp. Predictions Using Peatross/Beyler Method - S101 & S102

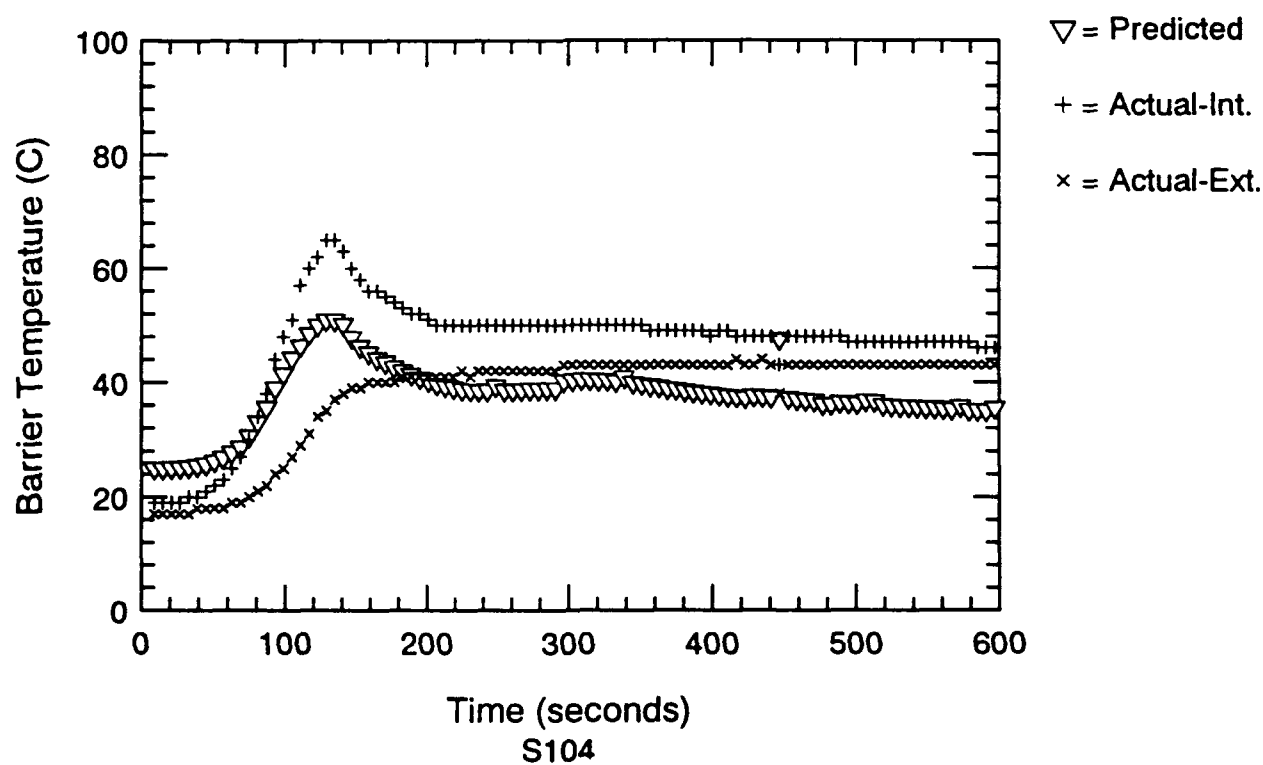
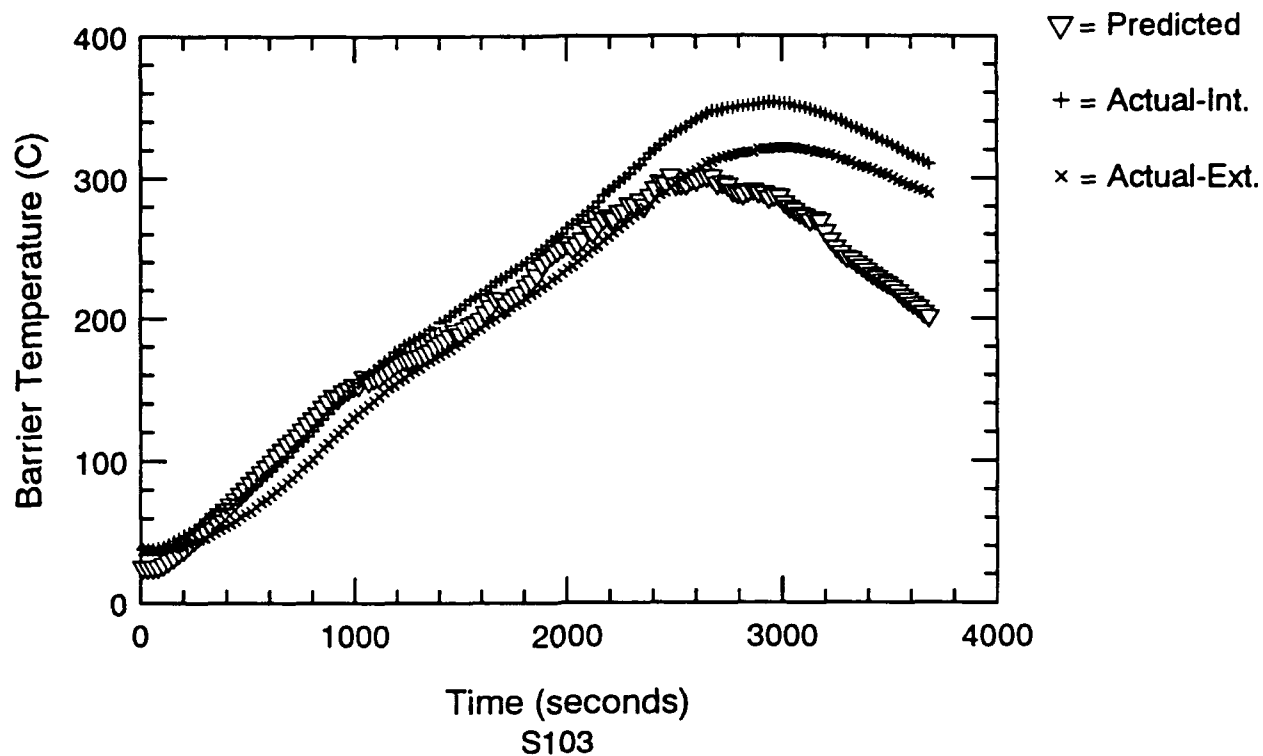


Figure H.2 Barrier Temp. Predictions Using Peatross/Beyler Method - S103 & S104

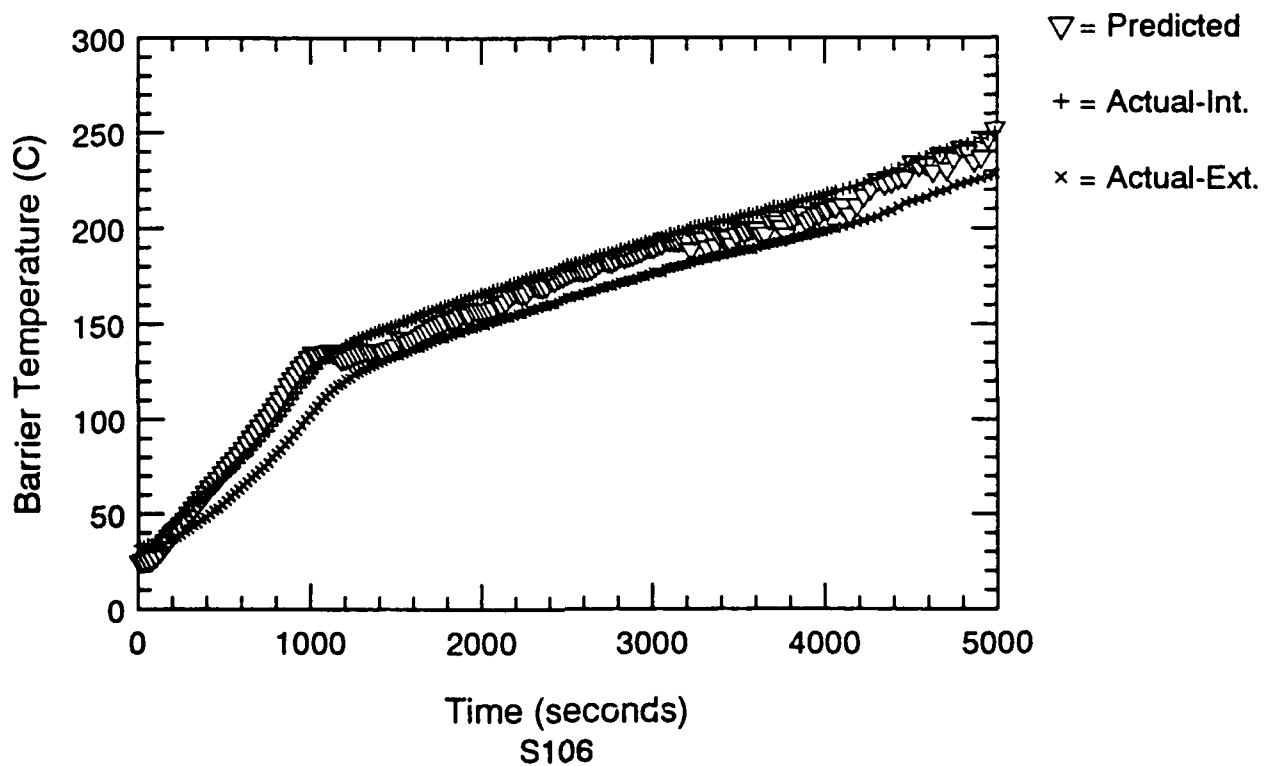
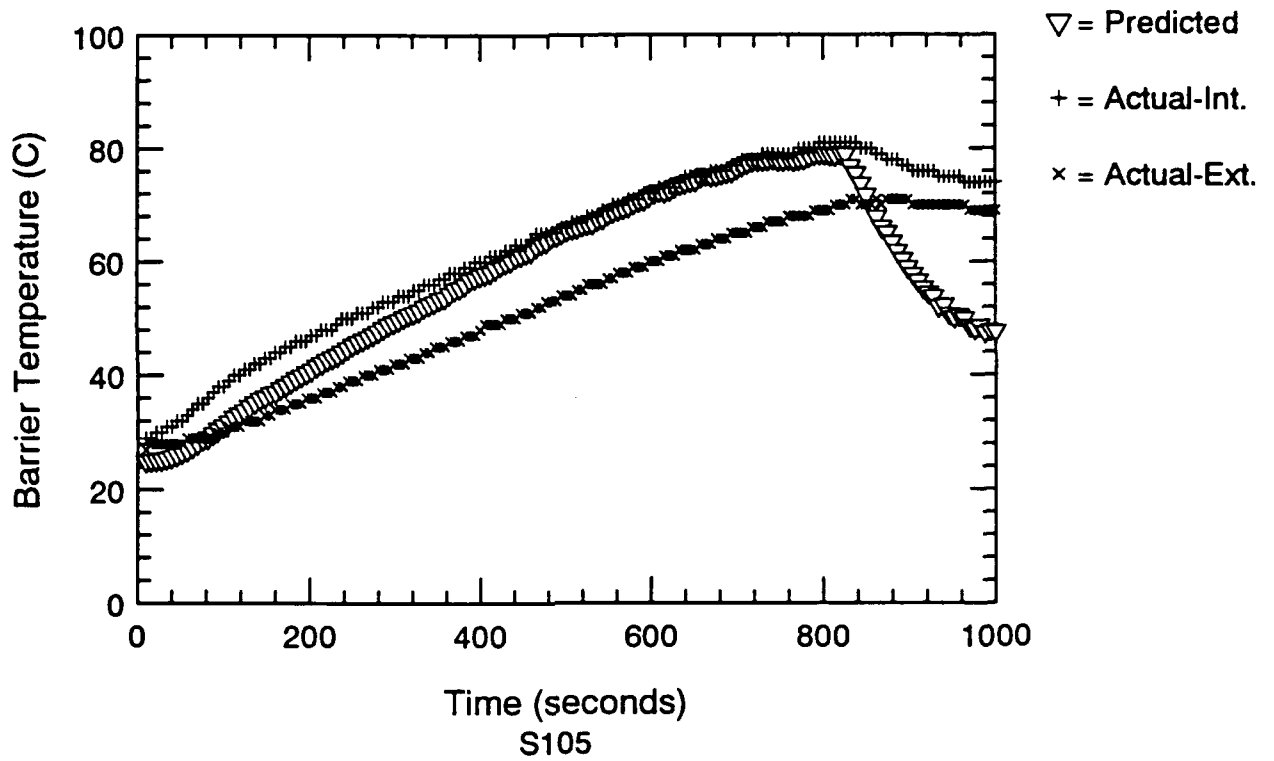


Figure H.3 Barrier Temp. Predictions Using Peatross/Beyler Method - S105 & S106

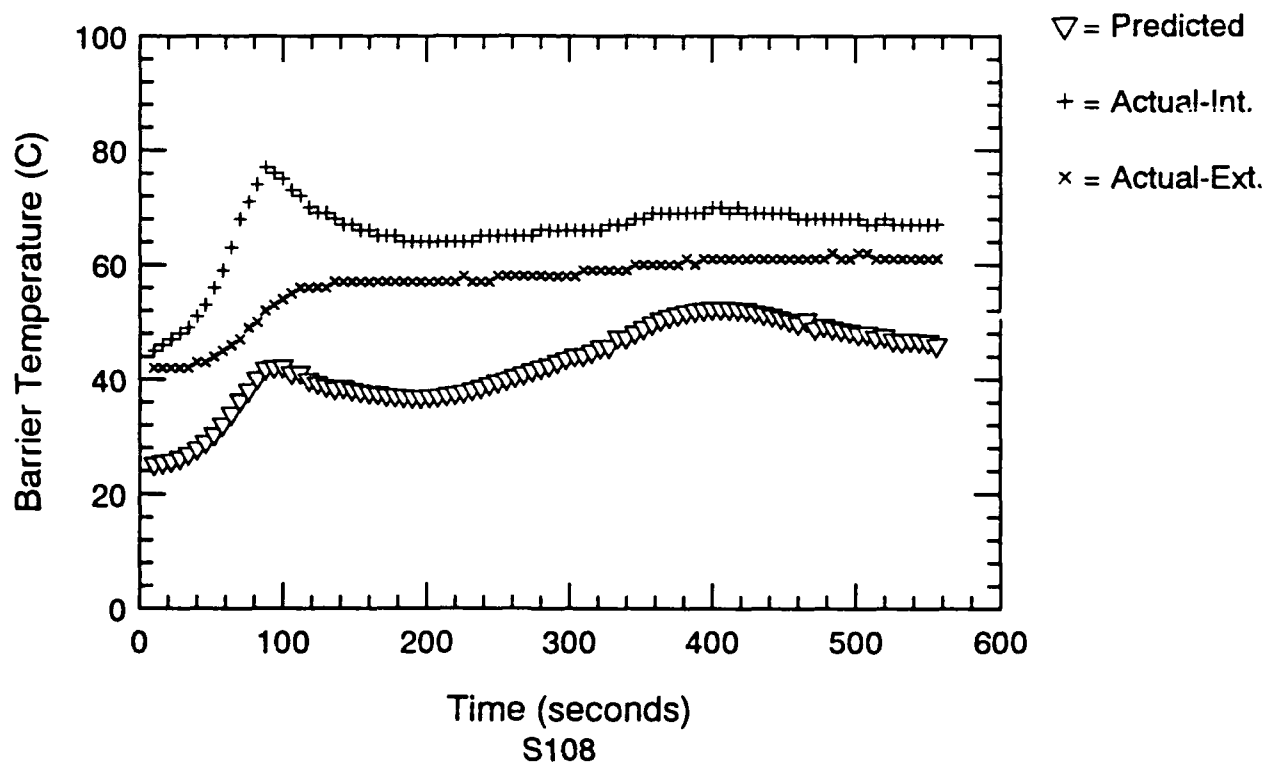
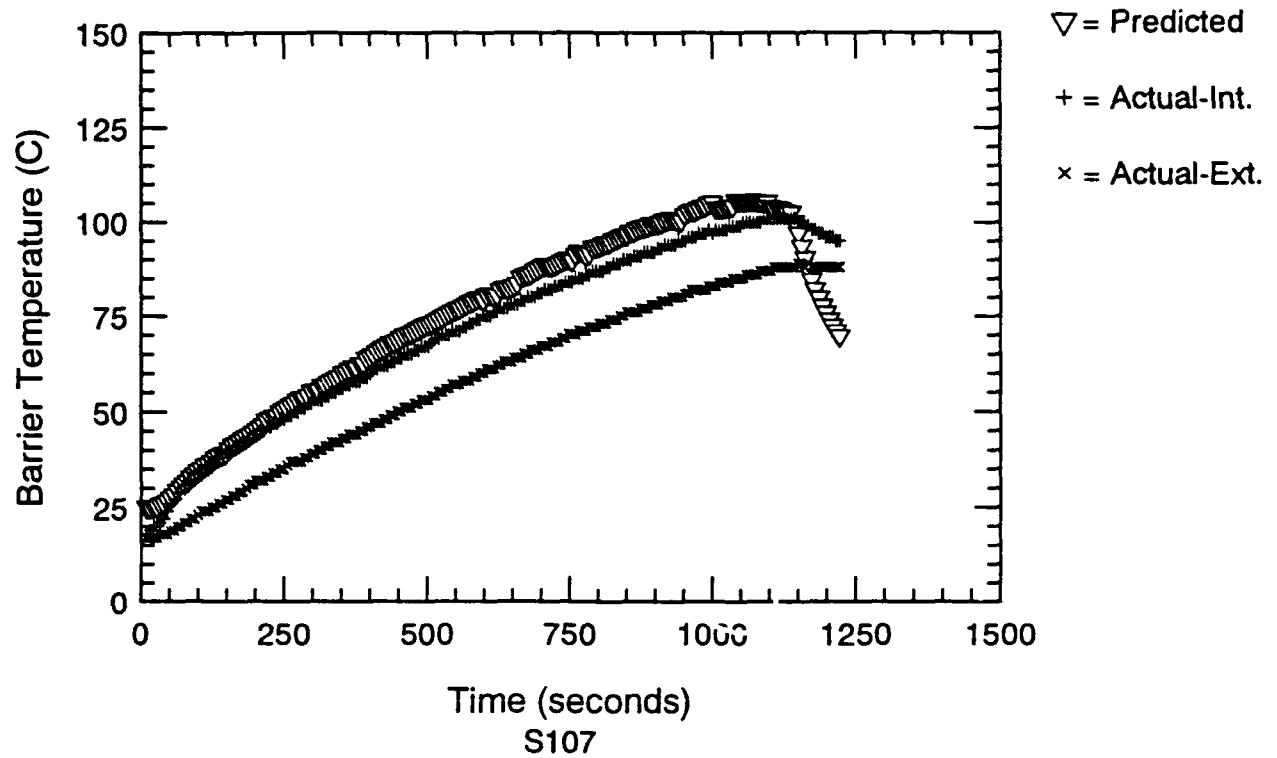


Figure H.4 Barrier Temp. Predictions Using Peatross/Beyler Method - S107 & S108

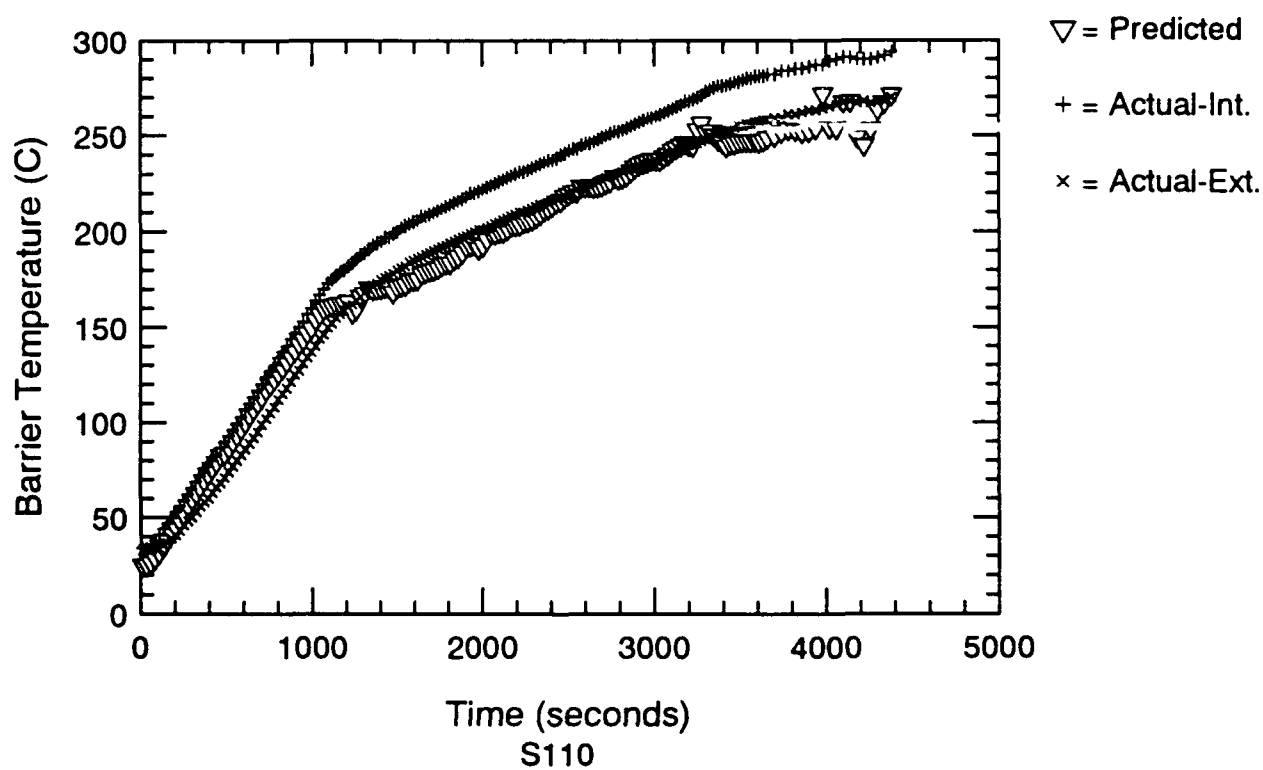
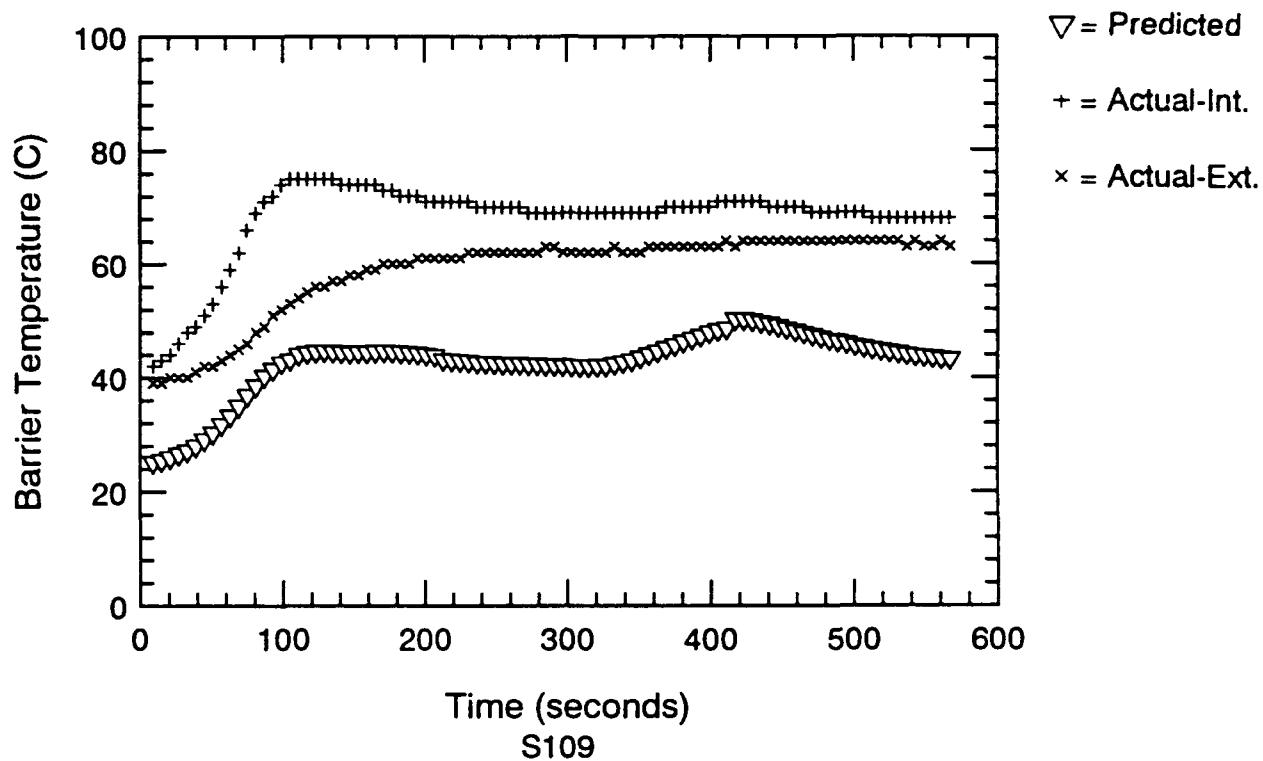


Figure H.5 Barrier Temp. Predictions Using Peatross/Beyler Method - S109 & S110

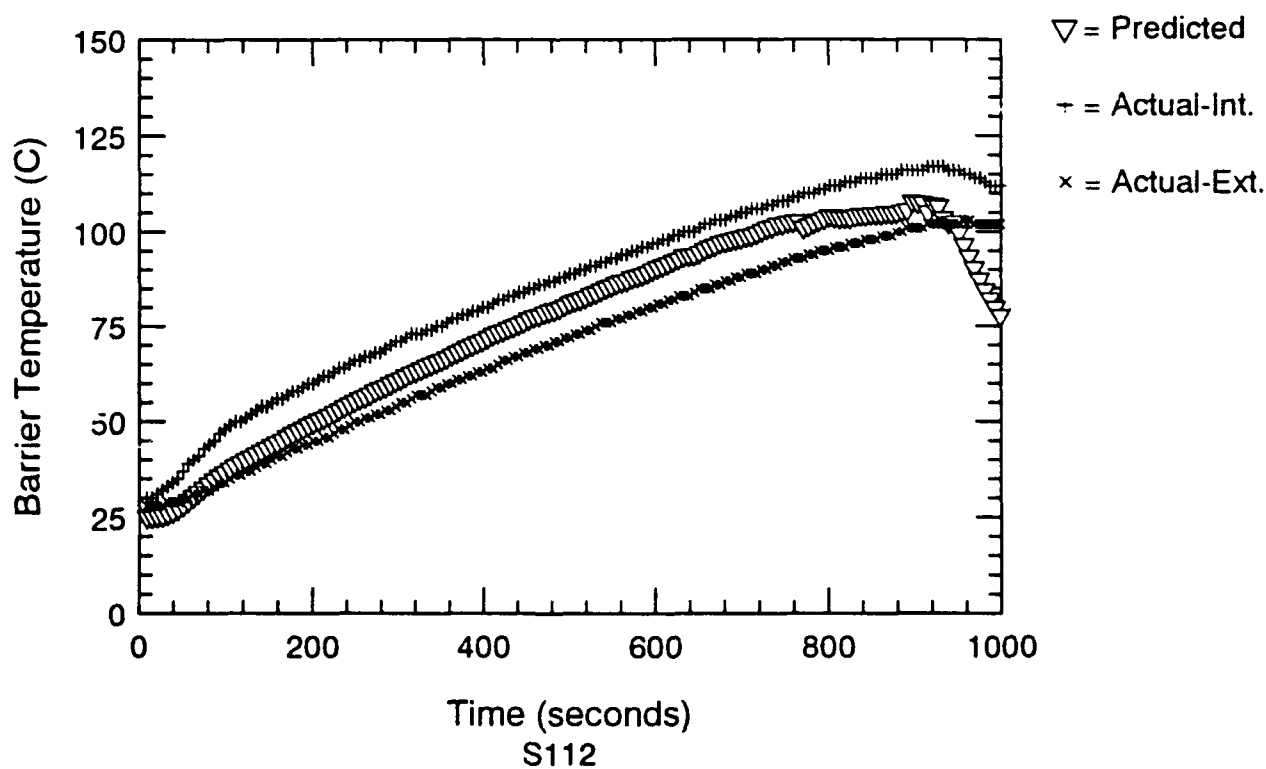
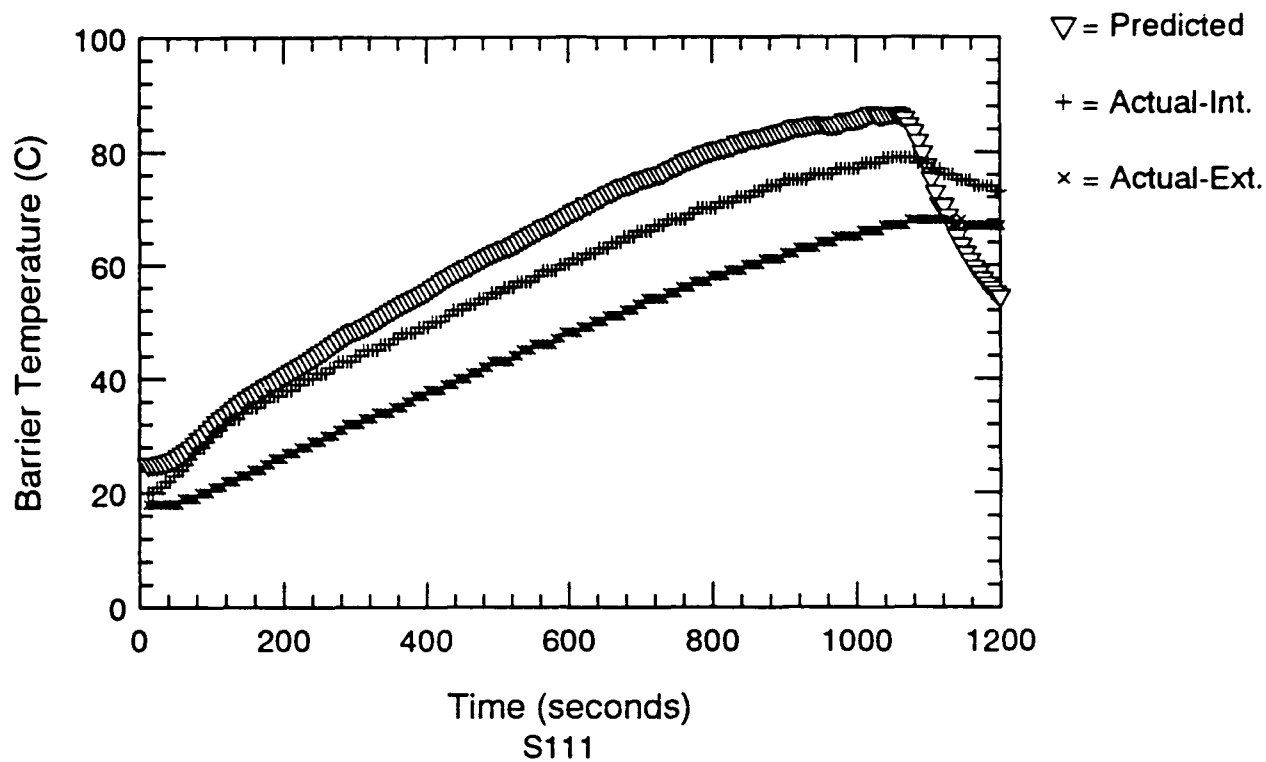


Figure H.6 Barrier Temp. Predictions Using Peatross/Beyler Method - S111 & S112

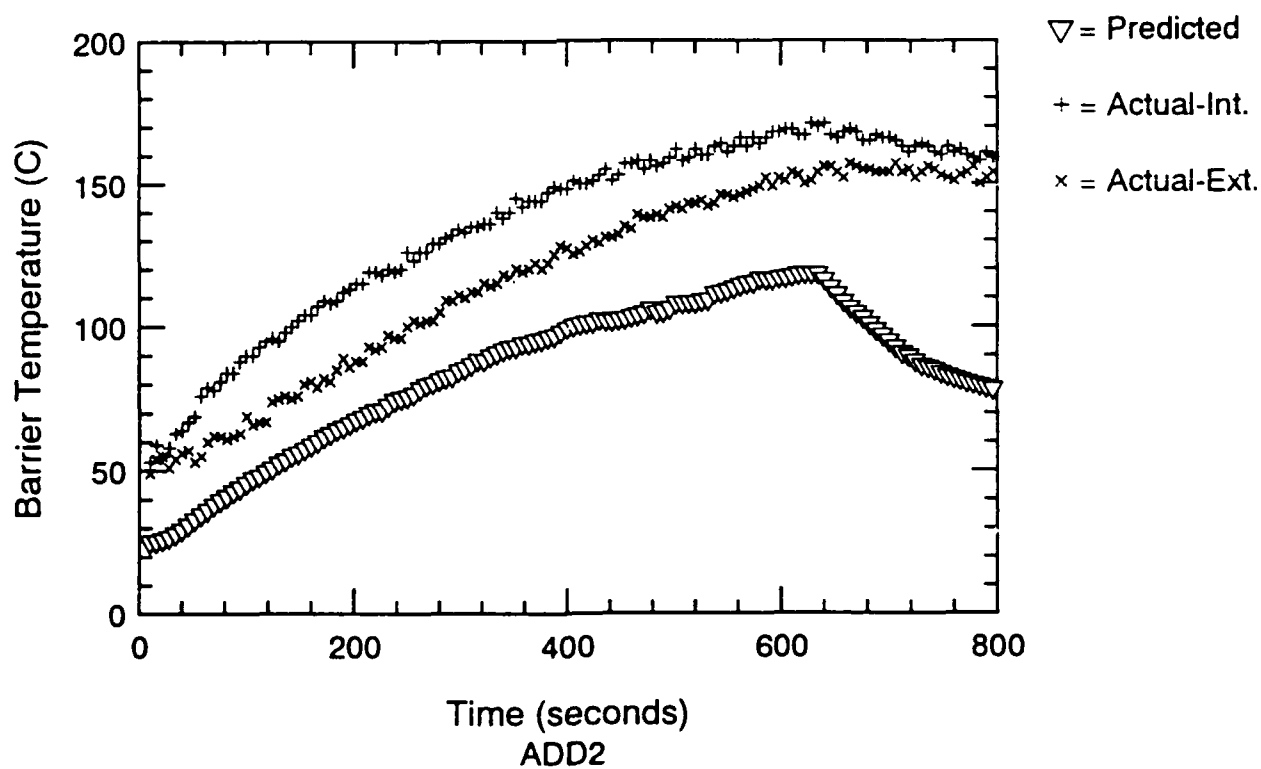
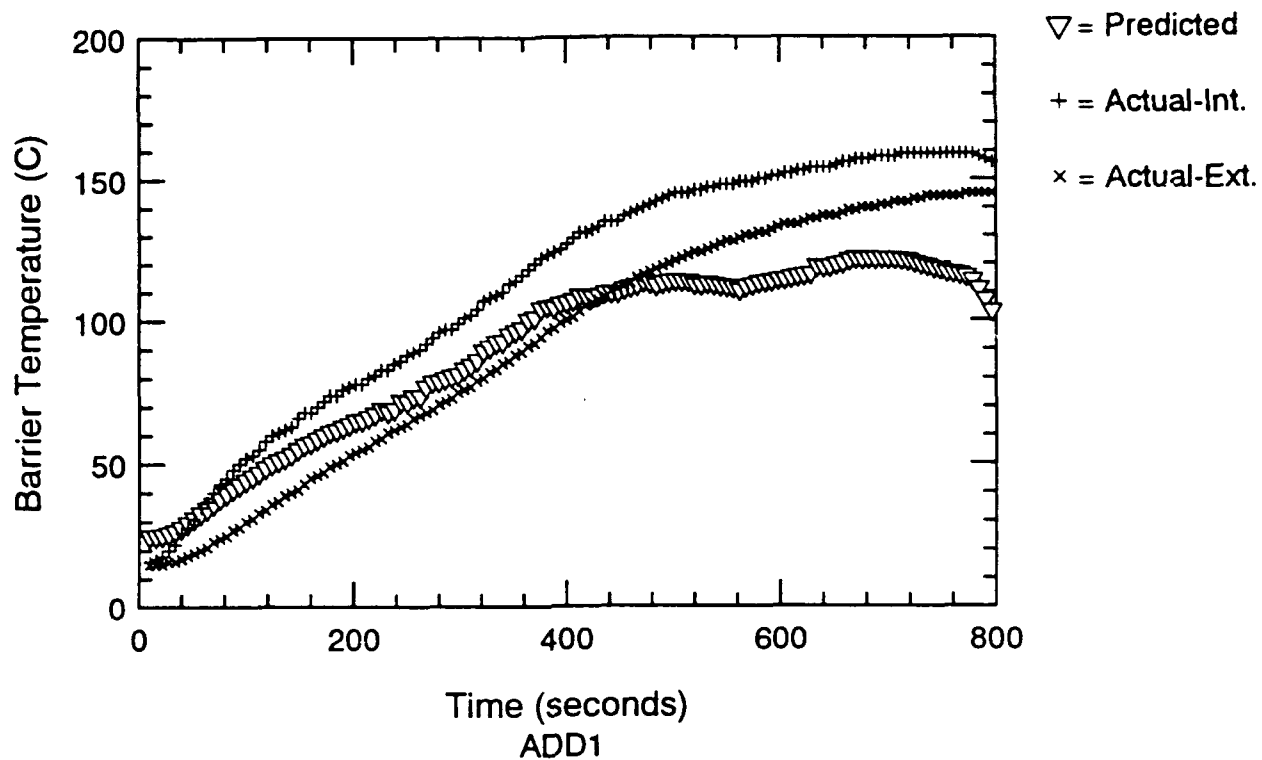


Figure H.7 Barrier Temp. Predictions Using Peatross/Beyler Method - ADD1 & ADD2

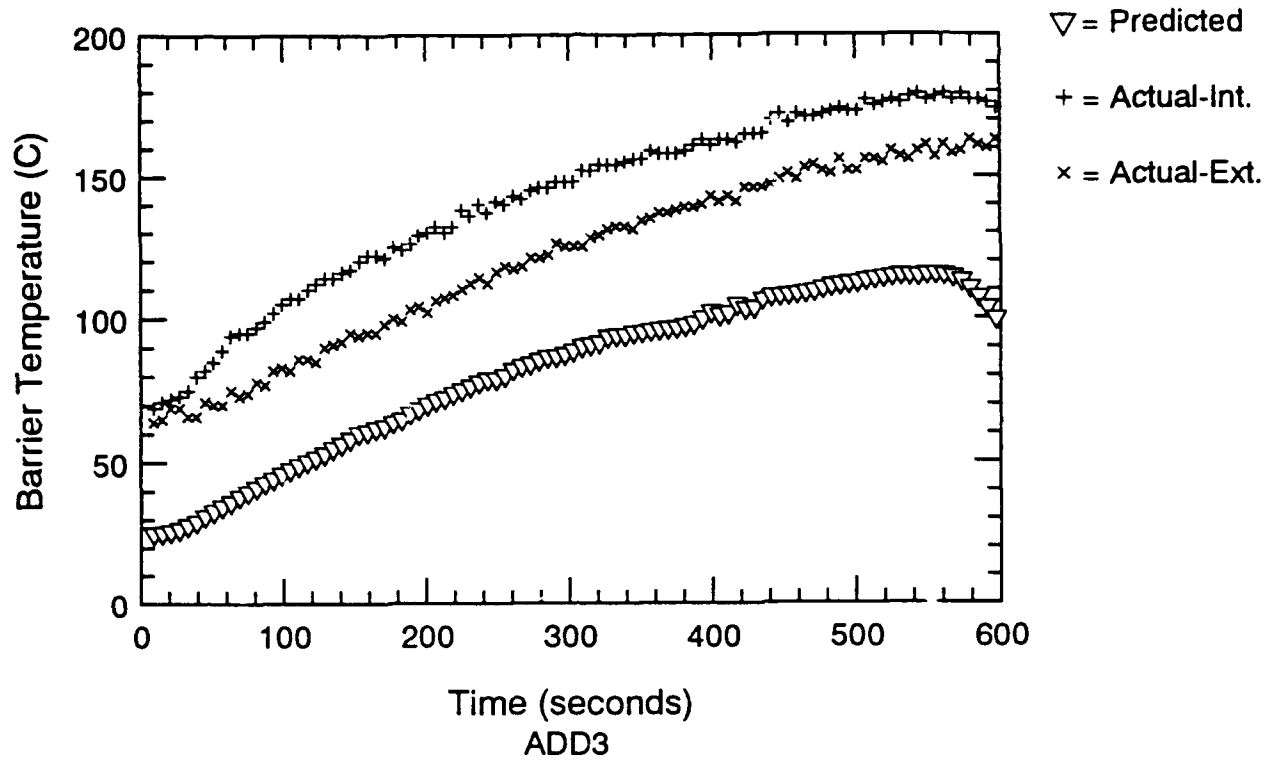


Figure H.8 Barrier Temp. Predictions Using Peatross/Beyler Method - ADD3

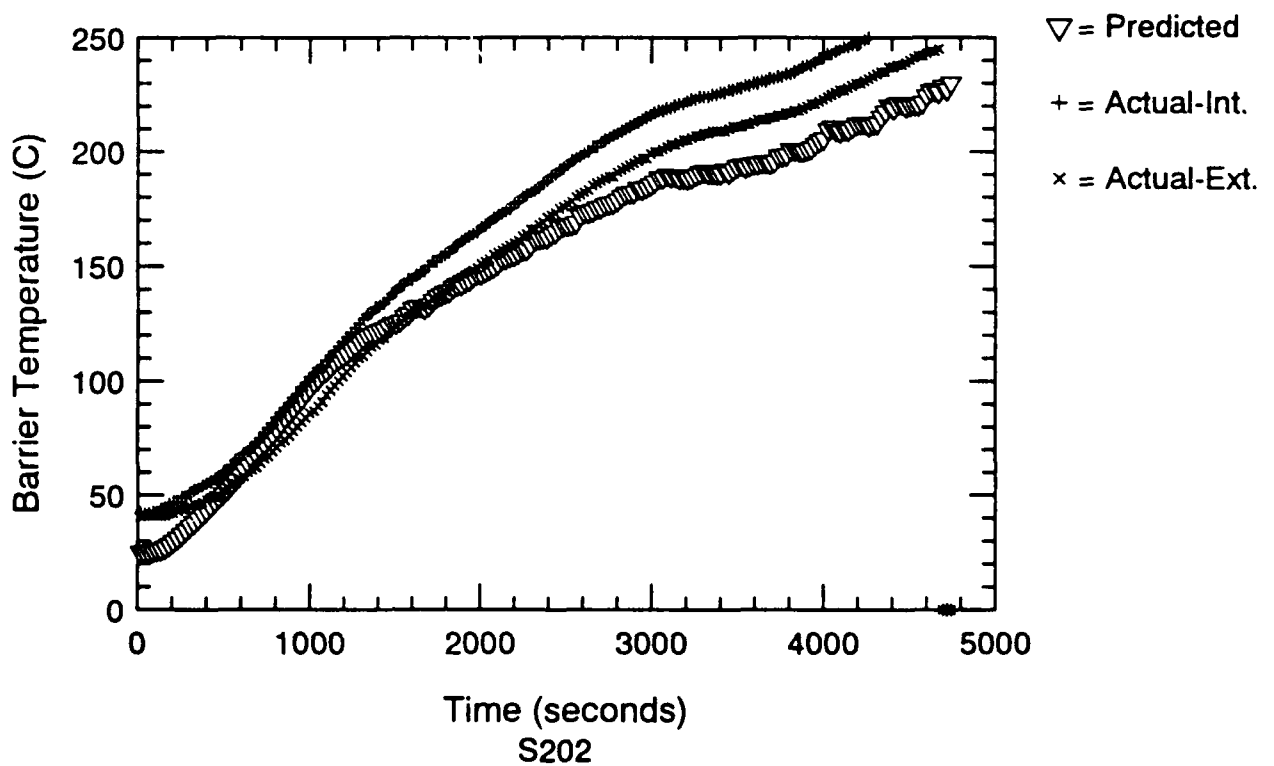
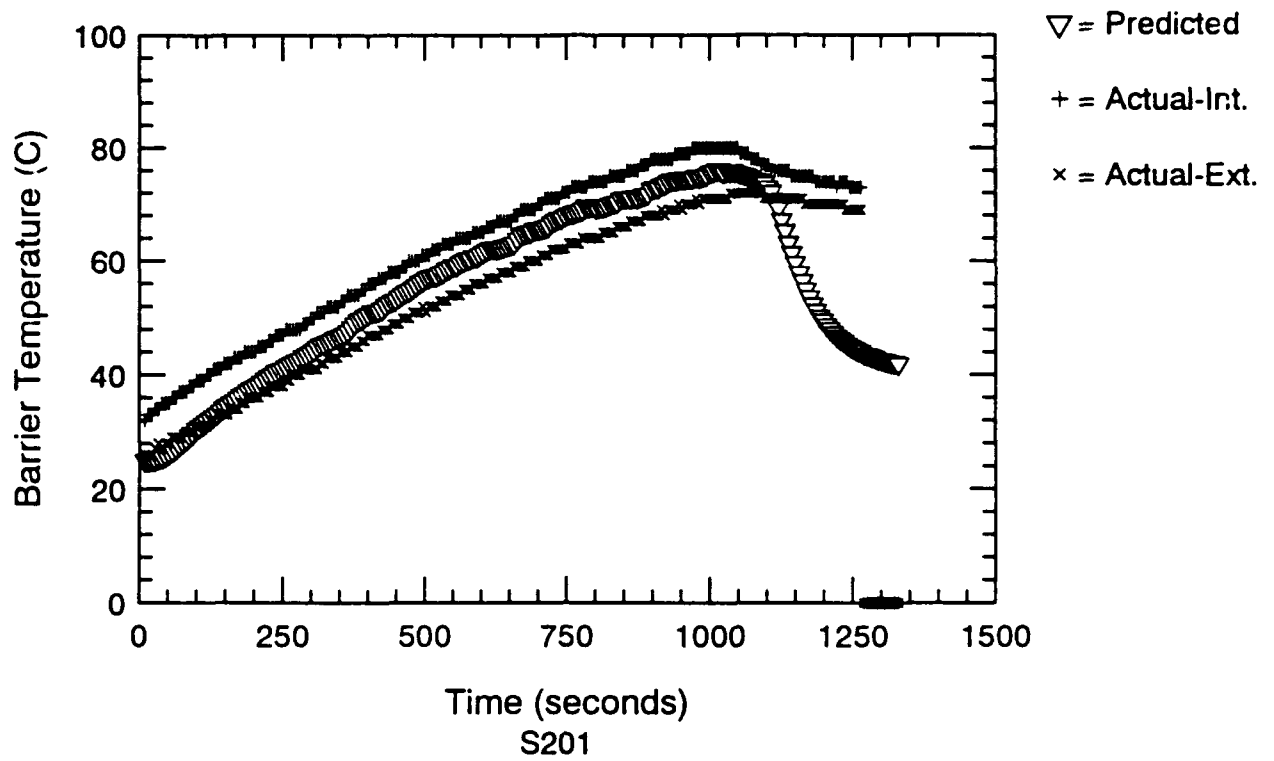


Figure H.9 Barrier Temp. Predictions Using Peatross/Beyler Method - S201 & S202

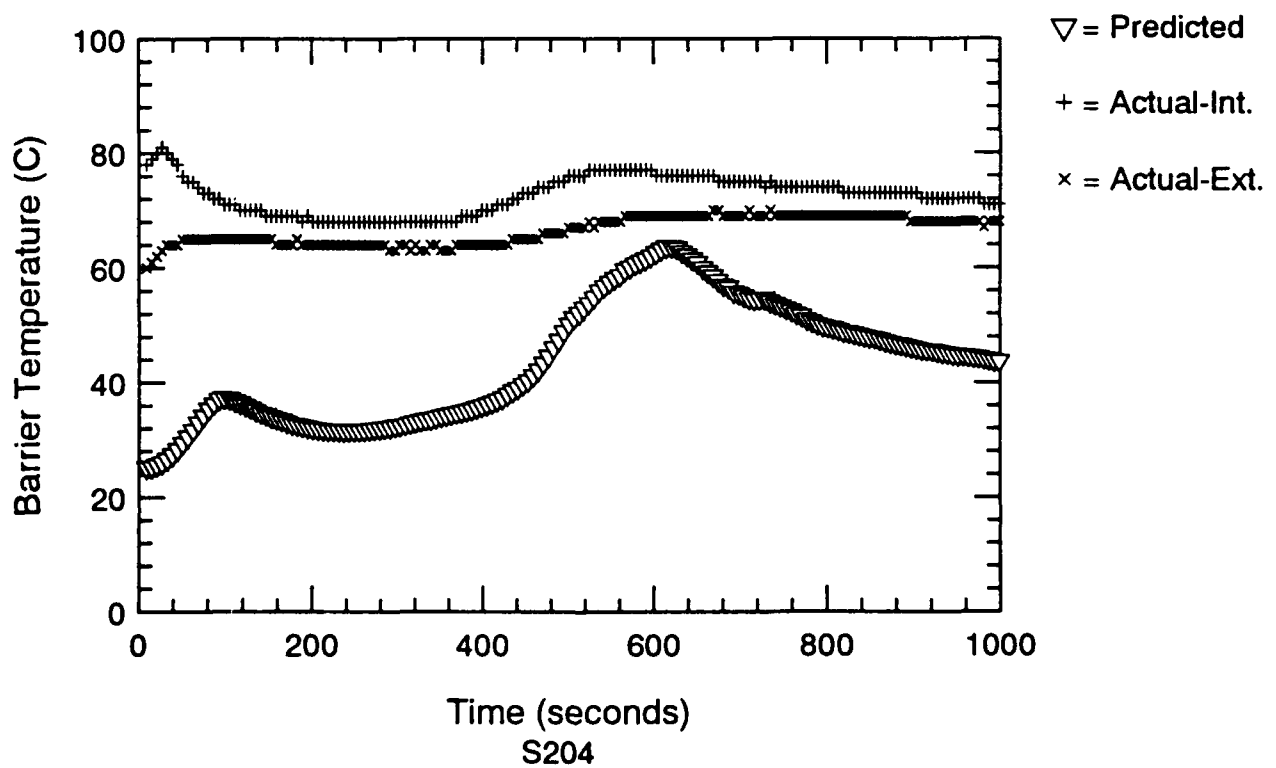
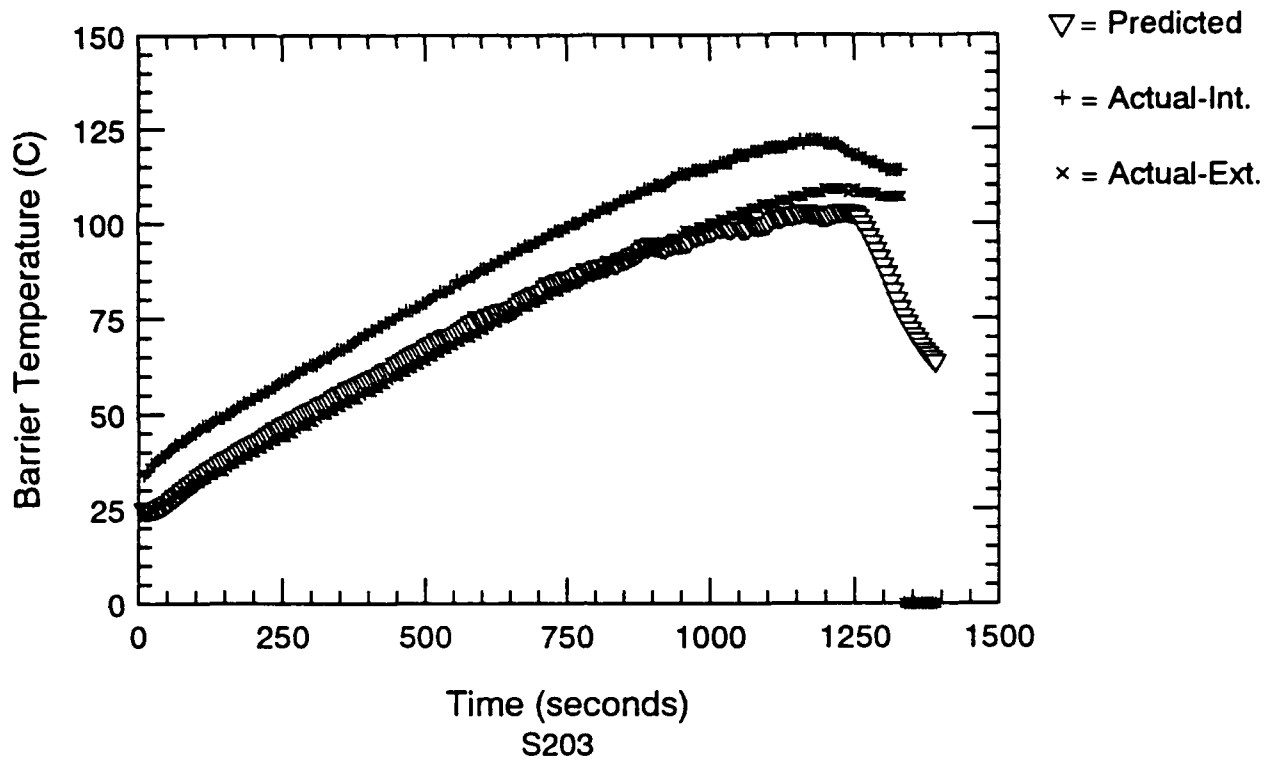


Figure H.10 Barrier Temp. Predictions Using Peatross/Beyler Method - S203 & S204

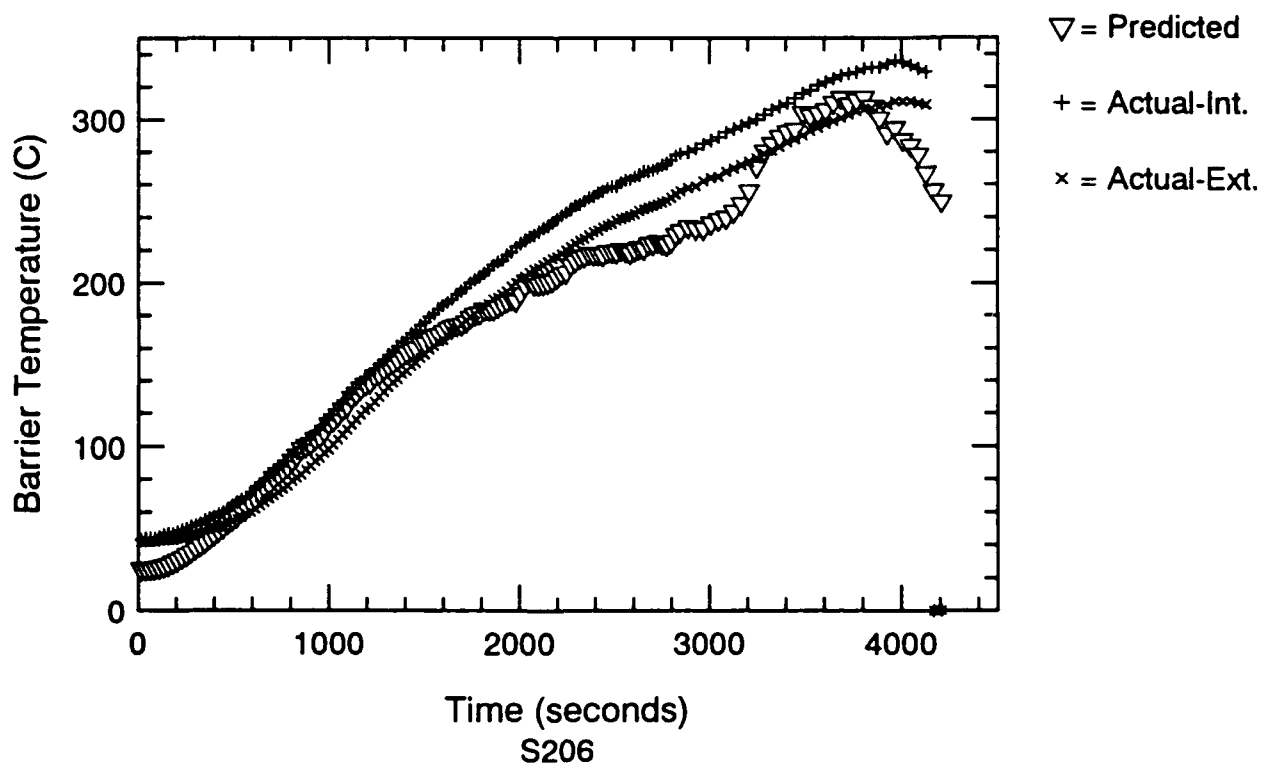
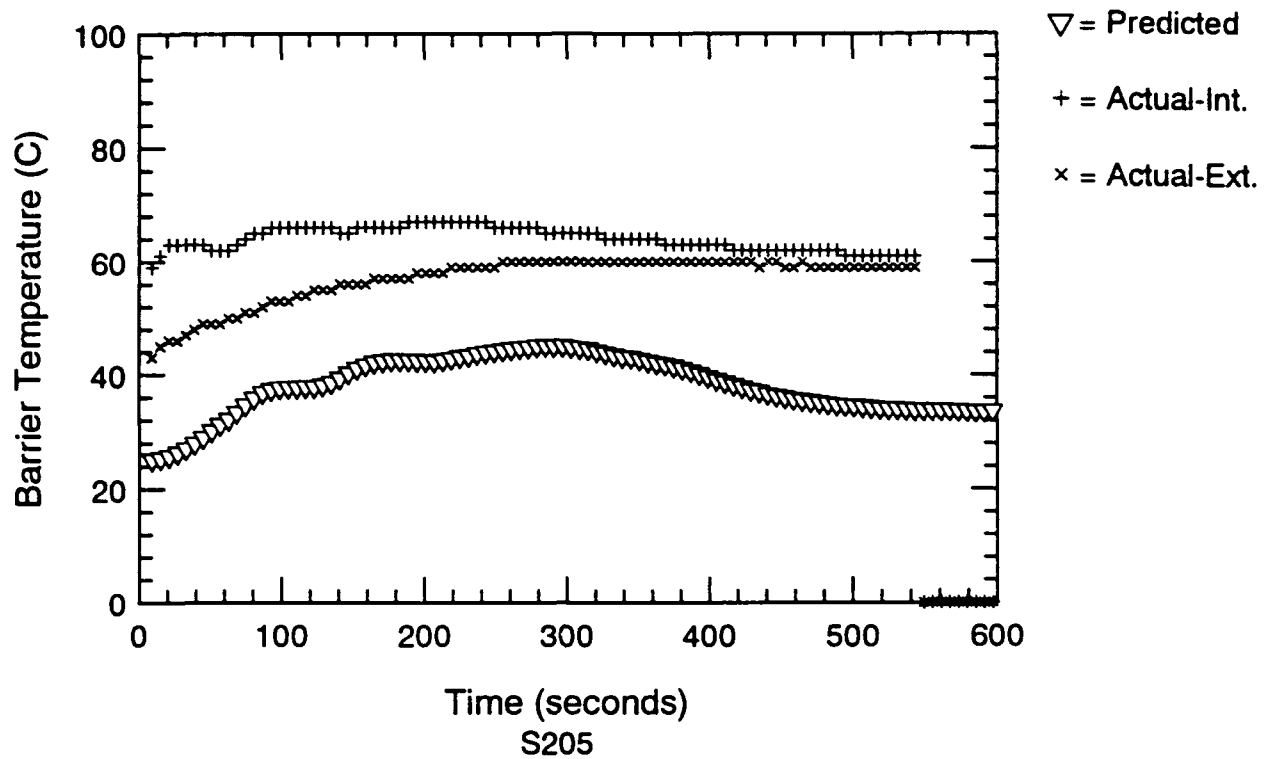


Figure H.11 Barrier Temp. Predictions Using Peatross/Beyler Method - S205 & S206

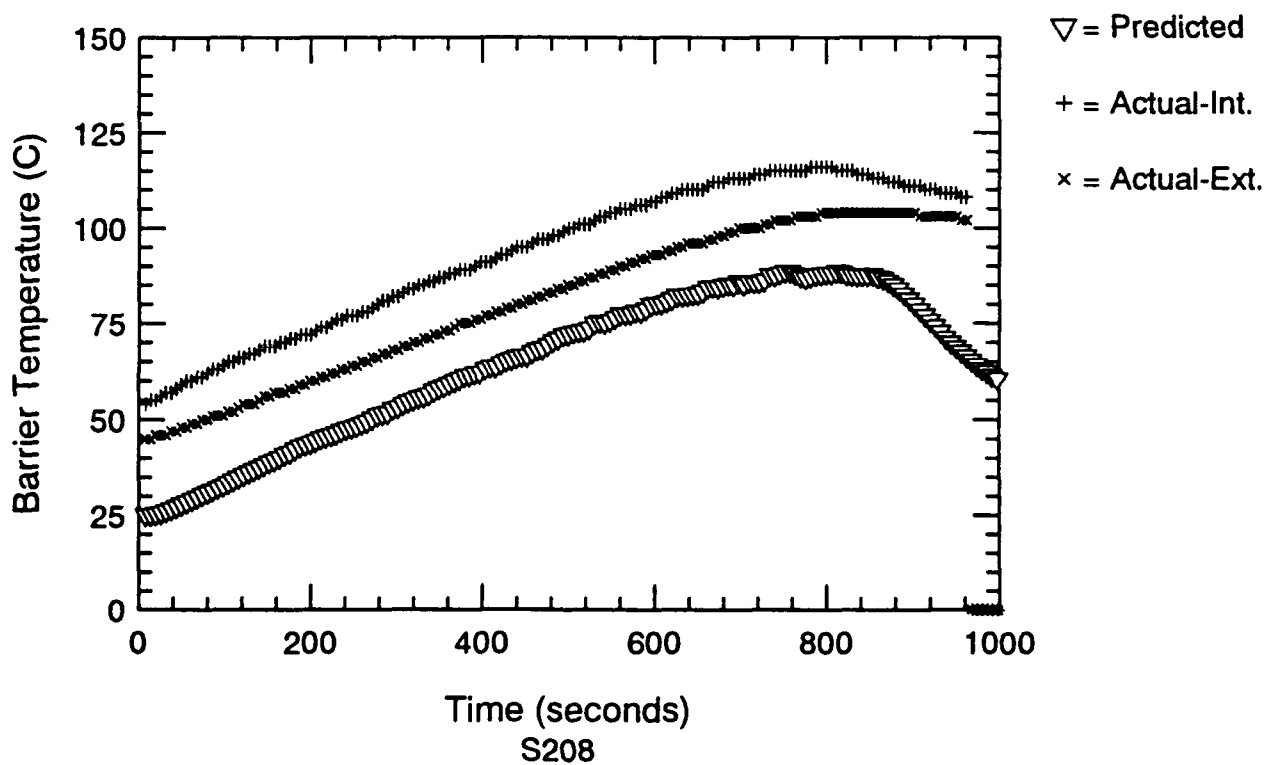
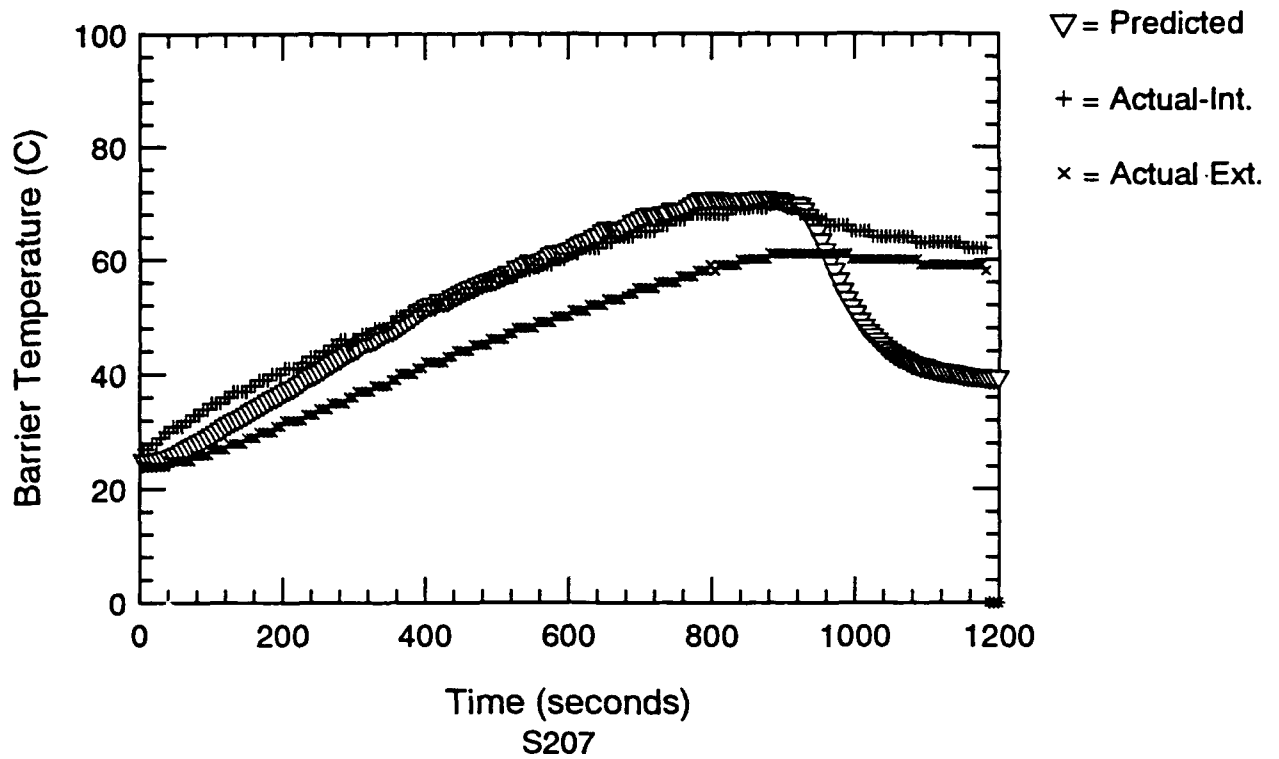


Figure H.12 Barrier Temp. Predictions Using Peatross/Beyler Method - S207 & S208

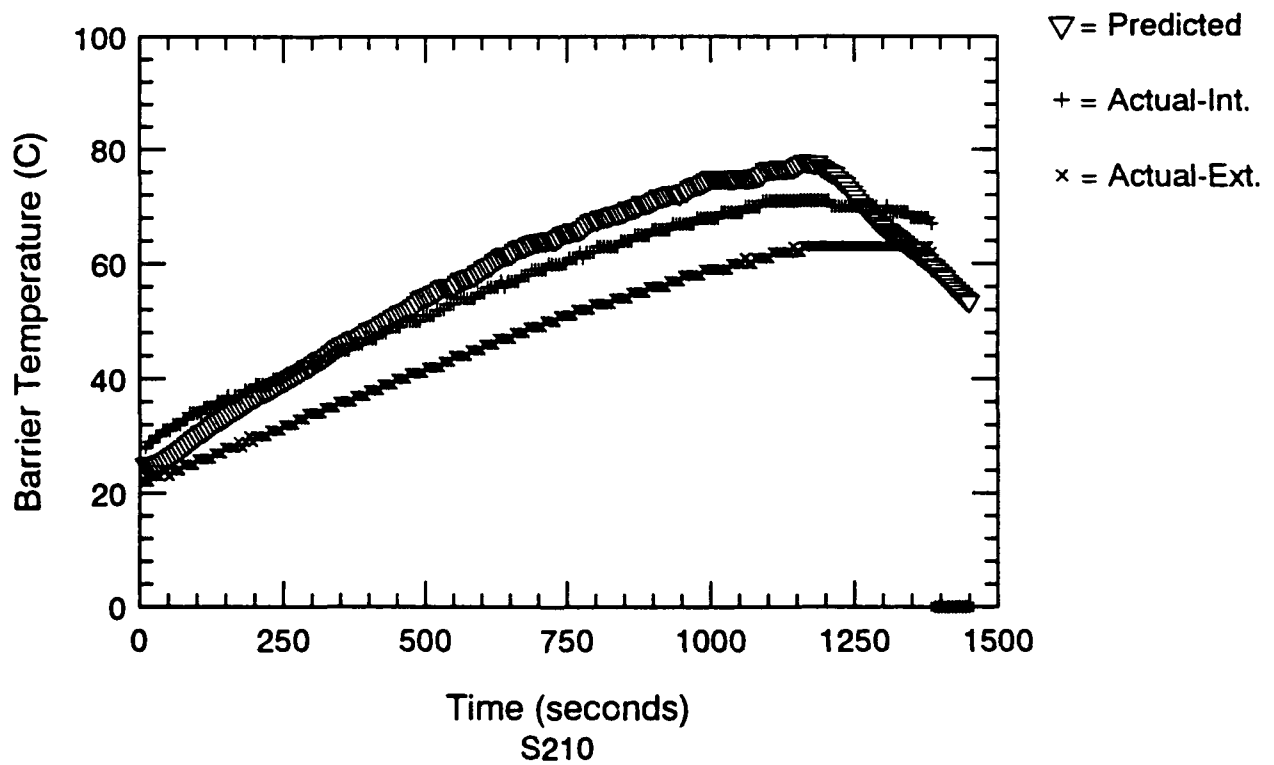
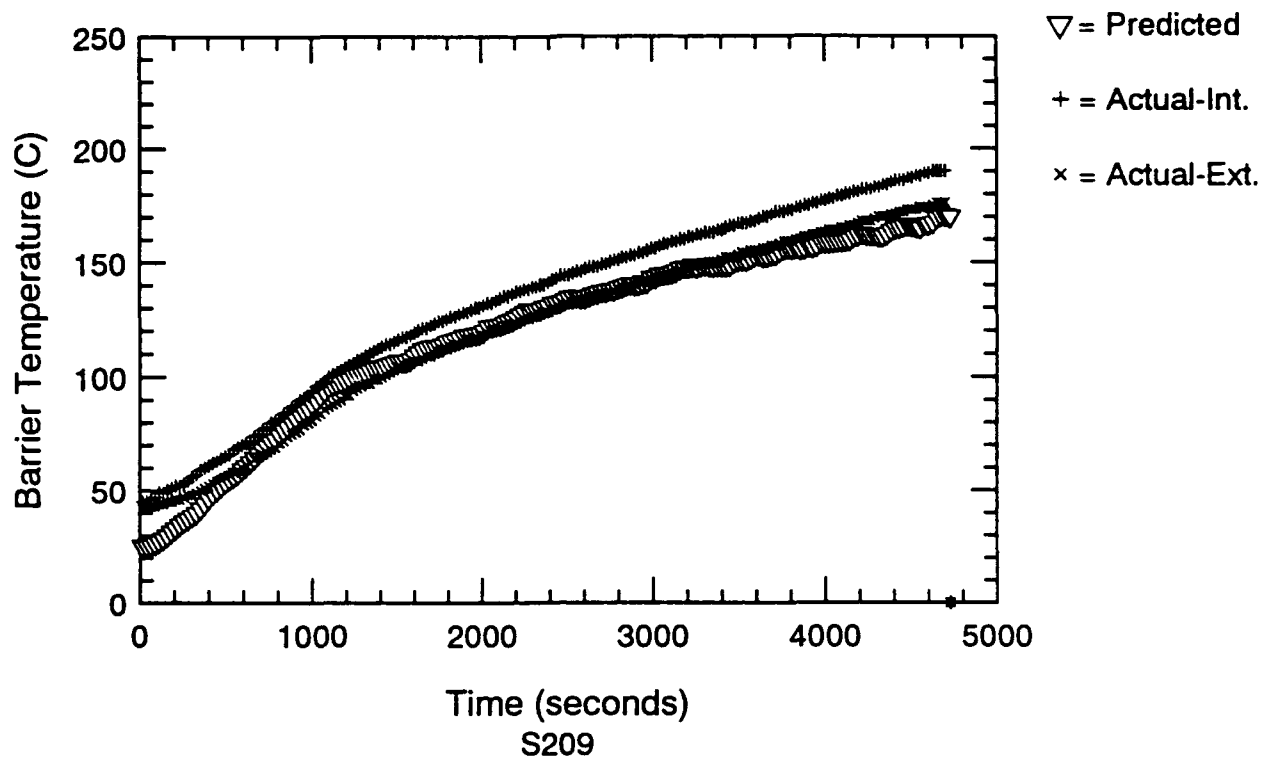


Figure H.13 Barrier Temp. Predictions Using Peatross/Beyler Method - S209 & S210

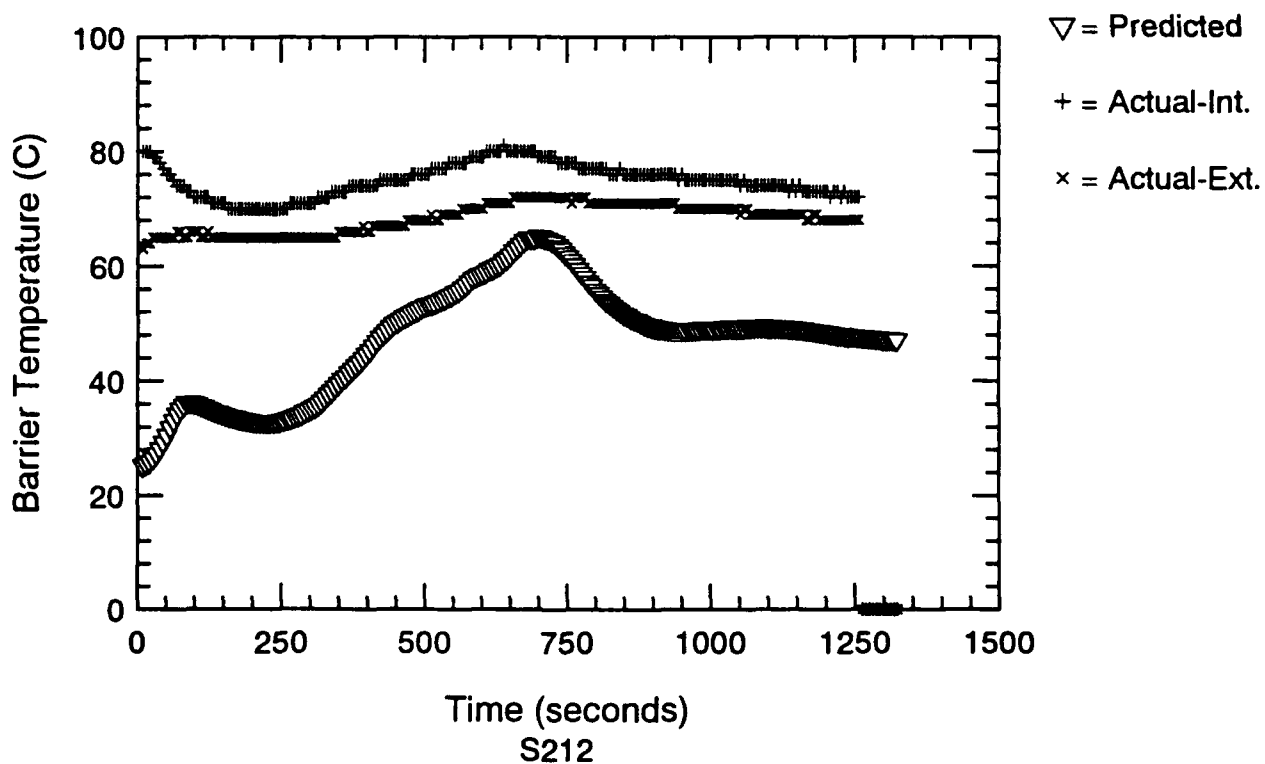
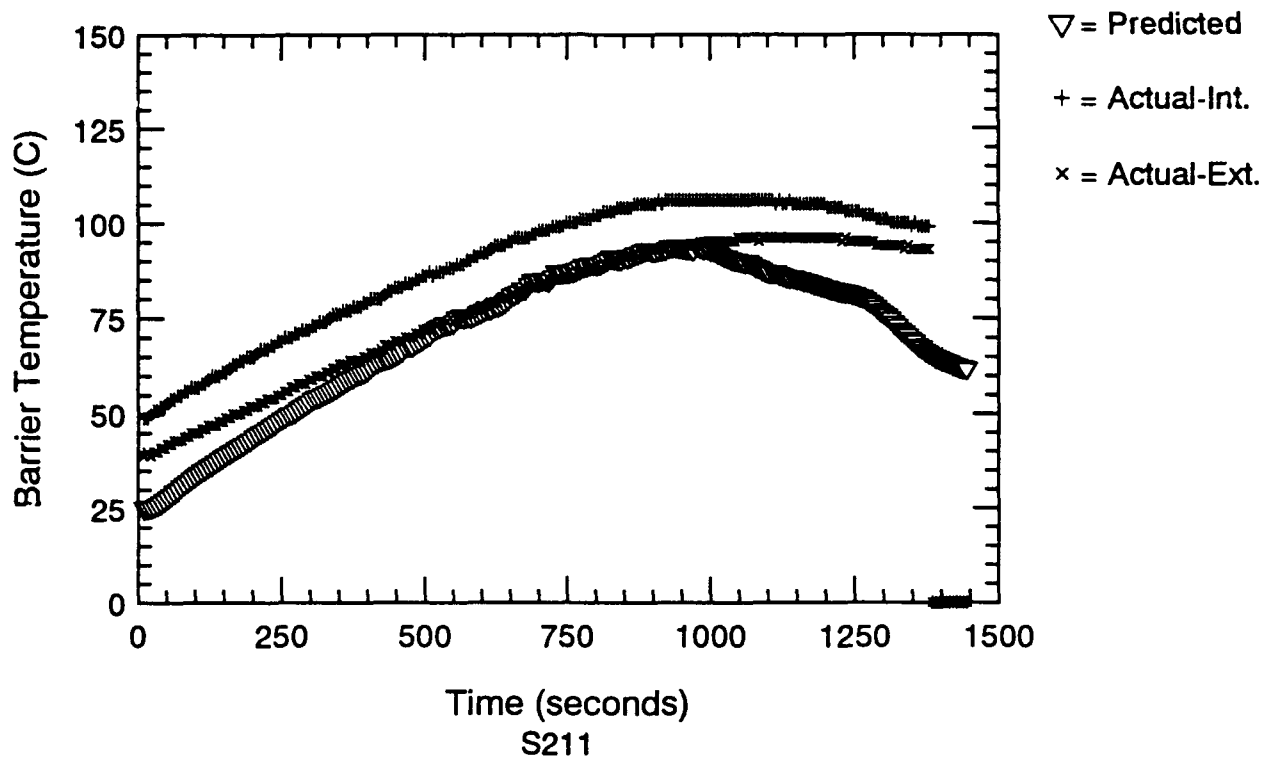


Figure H.14 Barrier Temp. Predictions Using Peatross/Beyler Method - S211 & S212